CRREL
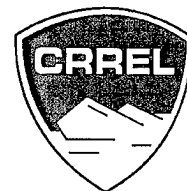
International Symposium on Physics, Chemistry, and Ecology of Seasonally Frozen Soils, Fairbanks, Alaska, June 10–12, 1997

I.K. Iskandar, E.A. Wright, J.K. Radke, B.S. Sharratt, P.H. Groenevelt, and L.D. Hinzman, Editors
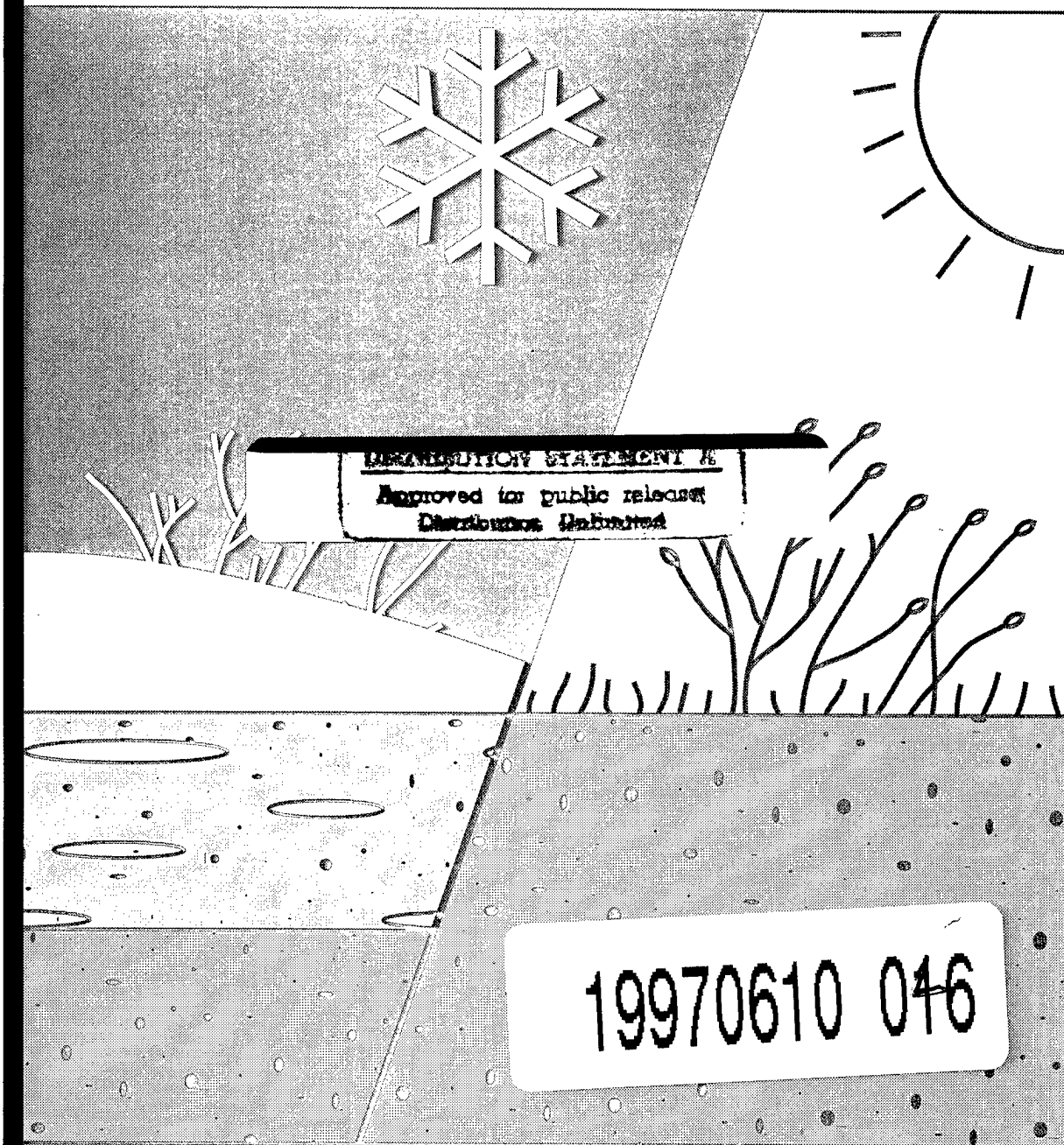
19970610 046

Proceedings of the

INTERNATIONAL SYMPOSIUM ON PHYSICS, CHEMISTRY, AND ECOLOGY OF SEASONALLY FROZEN SOILS, FAIRBANKS, ALASKA, JUNE 10–12,1997

I.K. Iskandar, E.A. Wright, J.K. Radke, B.S. Sharratt, P.H. Groenevelt, and L.D Hinzman, Editors

April 1997
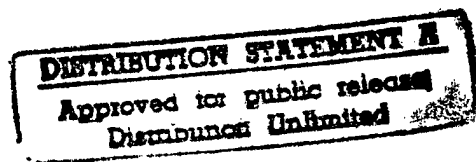
DTIC QUALITY INSPECTED 2

19970610 046

PREFACE

Freezing and thawing can have a profound influence on the stability, hydrology, chemistry and ecology of soils in the northernmost latitudes of the world. This symposium is the third to address the impact of freezing on the physical, chemical, or biological processes of managed ecosystems. The first symposium, *Freezing and Thawing Symposium*, was held on November 13, 1968, in New Orleans, Louisiana. All contributions to the 1968 symposium were from the United States. Nine presentations discussed the physical processes of frozen soils while one presentation dealt with biological processes as impacted by freezing. The second symposium, *Frozen Soil Impacts on Agricultural, Range, and Forest Lands*, was held on March 21–22, 1990, at Spokane, Washington. The 1990 symposium included 41 presentations given by scientists from Canada, Norway, Sweden, and the United States. Approximately 25% of the presentations dealt with simulation while other presentations discussed instrumentation, climatology, physics, and chemistry of frozen soils. The proceedings of the second symposium was published as CRREL Special Report 90-1.

Many advances in research have been made since these symposia, particularly in the simulation, biology, and chemistry of frozen soil systems. These advances have come from many countries. This symposium is an opportunity for scientists and engineers from around the world to meet and discuss frozen soil phenomena in managed ecosystems.

The sponsors of this symposium are:

> USDA Natural Resource Conservation Service
> USDA Agricultural Research Service
> > Office of Technology Transfer
> > National Soil Tilth Laboratory
> > North Central Soil Conservation Research Laboratory
> University of Alaska, Water Research Center
> University of Guelph, Department of Land Resource Science
> USA Cold Regions Research and Engineering Laboratory
> Soil Science Society of America
> The Organizing Committee consists of:

Co-Chairs:
> Dr. Jerry K. Radke
> USDA National Soil Tilth Laboratory, Ames, Iowa

> Dr. Brenton S. Sharratt
> USDA North Central Soil Conservation Research Laboratory, Morris, Minnesota

Program:
> Dr. Pieter Groenevelt
> Department of Land Resource Science, University of Guelph,
> Guelph, Ontario, Canada

Publications:
> Dr. I.K. Iskandar
> USA Cold Regions Research and Engineering Laboratory, Hanover, New Hampshire.

Coordinator:
> Dr. Larry D. Hinzman
> Water Research Center, University of Alaska, Fairbanks, Alaska

REVIEWERS AND AFFILIATIONS

G.M. Marion, USACRREL******
L.W. Gatto, USACRREL***
V.L. Cochran, USDA–ARS **
J.G. Davis, Colorado State University**
G.N. Flerchinger, USDA–ARS**
K.M. Hinkel, University of Cincinnati**
A.W. Hogan, USACRREL **
A.J. Palazzo, USACRREL**
C.L. Ping, University of Alaska**
C.H. Racine, USACRREL**
S.D. Sparrow, University of Alaska**
H.E. Allen, University of Delaware
S.A. Arcone, USACRREL
C.S. Benson, University of Alaska
E.C. Berry, USDA–ARS
P.B. Black, USACRREL
R.R. Blank, USDA–ARS
J.G. Bockheim, University of Wisconsin
J. Brown, International Permafrost Association
M.M. Burgess, Natural Resource Canada
E. Chamberlain, USACRREL
C.M. Cho, University of Manitoba
J.L. Clayton, USDA–USFS
C.M. Collins, USACRREL
J.H. Cragin, USACRREL
D.K. Dagesse, University of Guelph
A.T. DeGaetano, Cornell University
N.E. Derby, University of Minnesota
J.V. Drew, University of Alaska
M.M. Ellsbury, USDA–ARS
A.M. Fish, USACRREL
S.A. Grant, USACRREL
D.M. Gray, University of Saskatchewan
K. Henry, USACRREL
J.P. Hardy, USACRREL
L.E. Hunter, USACRREL
D.L. Kane, University of Alaska
B.D. Kay, University of Guelph
I. Kennedy, USDA–ARS

M.A. Kestler, USACRREL
D.C. Leggett, USACRREL
G.A. Lehrsch, USDA–ARS
L.C. Lewis, USDA–ARS
A.G. Lewkowica, University of Ottawa
M.J. Lindstrom, USDA–ARS
V.J. Lunardini, USACRREL
R. MacLean, University of Alaska
D.K. McCool, USDA–ARS
G.C. McIntosh, University of Minnesota
D.J. McKay, USACRREL
M.V. Mironenko, Vernadsky Institute
J.L. Nieber, University of Minnesota
K. O'Neill, USACRREL
M.W. Oswood, University of Alaska
S.I. Outcalt, University of Cincinnati
P.P. Overduin, York University
T. Pangburn, USACRREL
J.L. Pikul, Jr, USDA–ARS
C.M. Reynolds, USACRREL
K.E. Saxton, USDA–ARS
M.S. Seyfried, USDA–ARS
K. Shook, University of Saskatchewan
R.S. Sletten, University of Washington
E.J.A. Spaans, University of Minnesota
M. Stahli, Swedish University of Agricultural Sciences
R. Stottlemyer, USDA–USFS
J.M. Sullivan, Worcester Polytechnical Institute
V.R. Tarnawski, St. Mary's University
C. Tarnocai, Agriculture & Agri-Food Canada
K. VanCleve, University of Alaska
L.A. Viereck, University of Alaska
W.B. Voorhees, USDA–ARS
D.M. White, University of Alaska
D.E. Wilkins, USDA–ARS
J.D. Williams, USDA–ARS
J. Yarie, University of Alaska
S.C. Zoltai, Natural Resource Canada

---

*Number of papers reviewed

CONTENTS

Water and Solutes

Tillage, Management and Erosion

Snow

II. CHEMISTRY

Carbon

Nitrogen

Phosphorus

III. ECOLOGY

Pedology

Ecosystems

Biology

IV. MODELING AND REMOTE SENSING

Modeling

Remote Sensing

Summary and Discussion

INTRODUCTION

Physics, Chemistry, and Ecology of
Frozen Soils in Managed Ecosystems
An Introduction

B.S. SHARRATT[1], J.K. RADKE[2], L.D. HINZMAN[3], I.K. ISKANDAR[4], AND P.H. GROENEVELT[5]

ABSTRACT

Some of the world's most productive soils lie within cold regions. To enhance the productivity and quality of soil resources within these regions, knowledge must be advanced concerning the impact of freezing and thawing on soil properties and processes. The International Symposium on Physics, Chemistry, and Ecology of Seasonally Frozen Soils is a step toward broadening our knowledge of frozen soil processes. This paper emphasizes the physical nature of frozen soil and the importance of freezing and thawing to the transport of water and heat at the Earth's surface. We also discuss the chemistry and biology of the soil system as affected by freezing and thawing. Ascertaining changes in ecosystem structure and productivity in response to perturbations in climate or management depends primarily on the use of models; these models require the acquisition of new knowledge to better define linkages among the physical, chemical, and biological components in cold regions. New knowledge concerning the dynamics of the frozen soil system will allow global societies and industries to develop sustainable and environmentally-safe management systems.

Key words: Physical properties, freezing and thawing, land management, biology.

INTRODUCTION

In the vastness of the earth and the ecosystems that constitute the complexities of life, soil is a resource that sustains all terrestrial organisms which includes some 5.8 billion people. By the year 2050, this same resource will likely support over 9 billion people, or even perhaps our planet's carrying capacity of 10 billion people (Rogers, 1996). Only through wise management of the soil resource, along with continued strides in technology, will the quality of life be sustained for future generations.

Approximately 50% of the Earth's land mass is frozen at some time during the annual cycle, with 20% of the land underlain by permafrost (Fig. 1). Within this region of frozen soil lie some of the world's most productive, as well as least productive, soils (Visher, 1945). To enhance the productivity and quality of soil resources within this region, knowledge concerning soil freezing and thawing must be advanced to cope with new environmental constraints imposed upon land managers. In addition, new discoveries concerning frozen soil phenomena must be made at a rate that will further improve the productivity of soils to meet the needs of future generations. The International Symposium on Physics, Chemistry, and Ecology of Seasonally Frozen Soils is a step toward expanding that knowledge where new discoveries can be shared among nations and new ideas can be debated by multidisciplinary scientists.

The earth's ecosystems must be managed with skill and care to ensure that productivity and diversity are sustained amidst changes in climate as well as in government and industry philosophies. For example, the Canadians have recently reviewed their international and domestic policies for determining the appropriate responses to a changing climate (Jackson, 1992). Indeed, will our forest and agricultural industries cope with a 1 to 2°C global warming over the next 50 years (Bengtsson, 1994)? How will ecosystem productivity be affected as ecosystems move northward with global warming

---

[1] USDA, Agricultural Research Service, North Central Soil Conservation Research Laboratory, Morris, Minnesota 56267, USA
[2] USDA, Agricultural Research Service, National Soil Tilth Laboratory, Ames, Iowa 50011, USA
[3] University of Alaska, Water Research Center, Fairbanks, Alaska 99775, USA
[4] U.S. Army Cold Regions Research and Engineering Laboratory, 72 Lyme Road, Hanover, New Hampshire 03755-1290, USA
[5] University of Guelph, Department of Land Resource Science, Guelph, Ontario, N1G 2W1, Canada
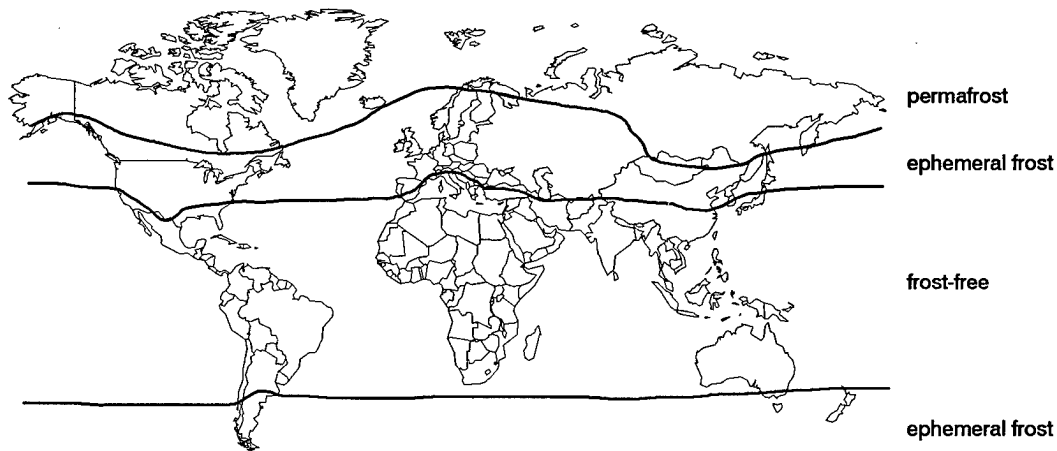
Figure 1. Latitudinal distribution of permafrost and seasonal frost as determined from climatic regions of Heintzelman and Highsmith (1973) and data of Nekrasov (1983).

(Bengtsson, 1994)? And, if world food supplies diminish and necessitate clearing northern forest for agriculture, will soils of northern regions sustain crop production? Although the answers to these questions may be uncertain, we must acquire new knowledge that will thwart the future calamities caused by man and weather. Research scientists and educators have an obligation to provide information about ecosystem adaptation and processes that will allow wise use of natural resources by all people.

Ecosystem diversity and productivity depend not only on land management, but also on processes within that ecosystem that are responsive to climate. Processes that occur in soils are largely governed by the surface energy balance, which is often difficult to predict due to the complexity of and interactions among exchange sites. These interactions are even more complex in cold regions where soils undergo cyclic freezing and thawing at the surface. The phase transition of soil water into ice affects the partitioning of available energy, with about 80 times more energy consumed or released during this phase transition as compare with either heating or cooling water. Freezing and thawing also exert forces within a soil that cause changes in structure and water and nutrient supplies. In addition, freezing and thawing cause physical degradation of organic substances and also changes in migratory patterns and physiology of soil biota.

The aim of this symposium is to identify those soil physical, chemical, and biological properties and processes of frozen soils that impact the productivity and diversity of managed ecosystems in cold regions. The following sections briefly discuss properties and processes characteristic of soils in cold regions. These sections do not cover the spectrum of changes that occur in freezing and

thawing soils; they do, however, illustrate the importance of such changes in managing ecosystems.

THE PHYSICAL NATURE OF FROZEN SOIL

The study of properties and processes that occur within the soil-atmosphere continuum enhance our capabilities to more effectively manage ecosystems for the preservation of water, air, and soil resources. It is near the soil surface where processes, such as freezing and thawing, are most dynamic and responsive to changes in climate and management.

Climatology

Processes at the soil-atmosphere interface are largely governed by radiative exchange and surface cover. It is in the realm of micrometeorology where interactions between energy exchange and surface cover are quantified to improve our understanding of physical characteristics that affect energy exchange and biota adaptation and diversity. Climatology also aids in differentiating regions of our planet according to criteria such as the depth of seasonal frost, freezing index, and snow cover (Wilson,1969). Indeed, temperature thresholds are useful for defining ranges of biota adaptation. In subarctic regions, for example, the adaptation of agricultural crops may be limited by soil temperatures as low as -30°C (Sharratt, 1993).

Frost heave

Visual manifestations of the forces exerted by soil freezing and thawing are perhaps most evident in subarctic or arctic regions where foundations of roads and buildings may be damaged by heaving and thaw consolidation. Likewise, in the midwestern

2

United States, alfalfa crops may succumb to desiccation due to heaving. Clayey and silty soils are prone to heave. It is the freezing process which results in a reduction in soil water potential, thus creating potential gradients that induce water flow from the unfrozen to frozen regions in the soil (Hoekstra, 1969). The formation of an ice lens due to water flow results in soil displacement; however this displacement may cause no permanent change in soil structure if the expanded structure collapses with the melting of the ice lens (Kay et al., 1985).

Soil structure

Strength and stability of soil structural units, or aggregates, affect processes such as root development as well as erosion. Loss of soil stability is of practical concern on hillslopes due to slippage and erosion. Changes in soil stability are influenced by biological activity, wetting and drying, and freezing and thawing. Freezing and thawing can enhance or diminish stability as structural bonds are created or disrupted by freezing (Bryan, 1971). In northern prairie ecosystems, freeze-drying is a disruptive force aided by wind that causes breakdown of clods formed by tillage or of soil aggregates (Fig. 2; Staricka and Benoit, 1995). Pore size and continuity are also affected by soil freezing. Indeed, creation of cleavage planes or macropores within the soil matrix due to freezing and thawing may allow for more rapid movement of water, chemicals (Iskandar, 1986), and air through the soil (Sharratt, 1997).
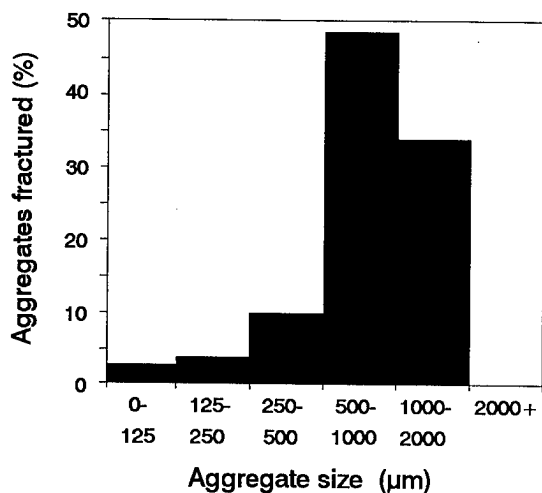
Figure 2. Sizes of aggregates fractured from moldboard plow furrow slices by freeze-drying during winter in Minnesota.

Simulation of soil physical processes

Although many processes and properties of soils are impacted by freezing and thawing, it is within the realm of simulation where this knowledge can be defined and assembled into a usable framework. These simulations provide insight into the complexity of the soil-atmosphere system and can be used to evaluate management criteria. Some examples include: 1) the SOIL model (Jansson, 1991) which was developed for forestry applications where soils are subject to freezing and thawing, 2) the SHAW model (Flerchinger and Pierson, 1991) which has been used in agricultural and rangeland applications where soils may have a sparse canopy cover and are subject to freezing and thawing, 3) the model developed by Bonan (1991) which mimics processes in the boreal forest where landscapes may be overlain by moss and underlain by permafrost, and 4) the Rigid Ice model (O'Neill and Miller, 1985) which is useful in engineering and environmental applications where an expanding soil matrix, caused by frost heave, may affect the integrity of structures (e.g. foundations, roots). Our ability to forecast ecosystem change in response to perturbations in climate or management depends profoundly upon these and other models. Therefore, improving simulations will require the acquisition of new knowledge to better define linkages among factors important in heat and water transport.

CHEMISTRY OF FROZEN SOILS

Clean water is a concern for all people. Many government bodies have established initiatives (e.g. the Canada Water Act authorized by the Canadian government in 1970 and the Clean Water Act approved by the US Congress in 1972) for restoring surface and ground waters. The long-term commitment by some nations to enhance water resources indicates the complexity of remediation for curtailing pollution. For example, pollutants can be transported within watersheds or fields by snowmelt runoff, but yet runoff is difficult to control or predict with our current technologies. Soil properties such as water content, pore ice content, infiltration rate, and hydraulic conductivity determine to some extent the potential for runoff. Indeed, soil freezing may be the leading cause of runoff in cold regions (Burwell et al., 1975). However, frozen soil may not always be a detriment to environmental quality as new technologies utilize frozen soil barriers to confine hazardous waste spills (Iskandar and Jenkins, 1985).

Movement of chemicals

Pore ice restricts vertical water flow within the soil profile. Water flow may thus be channeled downslope, carrying both chemicals and sediments. Soil freezing and thawing may also cause redistribution of chemicals within a soil profile (Panday and Corapcioglu, 1991). Osmotic potential gradients established as a result of solute exclusion during freezing contribute to water and chemical redistribution in the soil profile. Solutes may move upward in the soil profile as water migrates toward an advancing freezing front. However, the net movement of solutes over winter may be downward in the soil (Fig. 3) and will depend on infiltration and other hydrologic properties such as soil water content and conductivity. Freezing and thawing may affect the availability of plant nutrients or result in the precipitation of solutes, which occurs as solutes are excluded from ice. For example, Fine et al. (1940) found that cyclic freezing resulted in an increase in exchangeable potassium in expanding clays and a decrease in potassium in non-expanding clays.
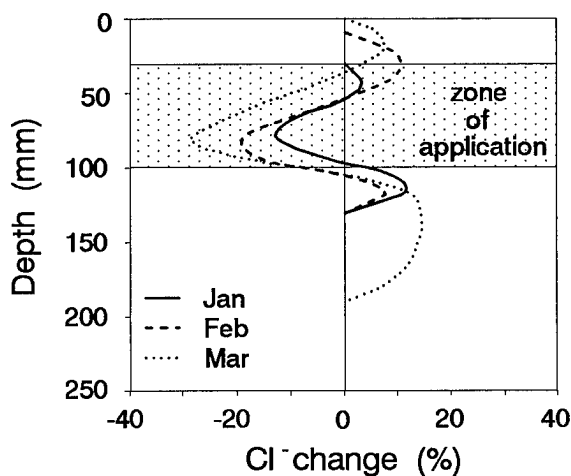
Figure 3. Changes in the distribution of fall-applied Cl⁻ within a clay loam during the 1993-1994 winter in Minnesota.

Soil gas exchange

The degradation of the atmosphere from undesirable constituents (e.g. nitrous oxide) is a concern for the well being of future generations. Many sources contribute to the degradation of the atmosphere, including soil. Decomposition of organic material by soil microorganisms results in evolution of carbon dioxide. Carbon dioxide fluxes may be minimal when the soil is frozen, but are accentuated in the early spring following thaw.

Indeed, Skogland et al. (1988) noted this release as a "respiratory burst". Methane also contributes to the degradation of the atmosphere. Perhaps the escape of methane to the atmosphere is most evident in northern regions where pore ice blockage, from snowmelt or saturated soils, inhibit oxygen diffusion (Clein and Schimel, 1995). Dise (1992) noted that methane fluxes from Minnesota peatlands during winter are 10 to 20% of the annual flux. The emission of another greenhouse gas, nitrous oxide, has been found to be twice as high during spring thaw compared to any other season (Christensen and Tiedje, 1990). Seasonal variations in gas flux from soil may not only be influenced by microbial activity, but also by physical changes in flow paths, especially the continuity of flow paths (Sharratt, 1997).

Simulation of chemical movement

Simulations have been developed to mimic the fate or movement of chemicals in seasonally frozen soils. Examples of these simulations include: 1) the ICE-1 model (El-Kadi and Cary, 1990). This model includes coupled water, heat, and solute transport in an unsaturated soil, 2) the SOILN model (Johnsson et al., 1987) which ascertains the fate of nitrogen in a soil subject to freezing and thawing, 3) the model by Panday and Corapcioglu (1994) which mimics the fate of contaminants (petroleum products) in frozen soils, and 4) the GWFREEZE model (Zukowski and Tumeo, 1991) which addresses solute transport in a freezing soil. These models portray processes within the soil matrix with known boundary conditions (chemical, temperature, and water). Therefore, to evaluate the impact of management on the movement of chemicals in soils, these models require either the use of existing data or a link to other models that mimic temporal variations in surface boundary conditions.

BIOLOGY OF FROZEN SOILS

The importance of soil biological processes to soil productivity is evidenced by the role of organisms in promoting the development of soil structure and in the decomposition of organic matter. Soil organisms are found in all regions of our planet and are suspected of residing in other planetary ecosystems within our solar system. Indeed, the ability of soil organisms to adapt to their environment is unique and tests our very theories of survival and adaptation under extreme environmental conditions.

Cellular organisms

Cells are the basic building blocks to life processes, therefore the survival of higher organisms depend upon the integrity of the cell. Turgid cells generally have a freezing point depression between 0 and -4°C (Levitt, 1972), although many cells remain unfrozen even at -10 to -15°C (Mazur, 1980). The cell wall membrane is vital for surviving low temperatures. The membrane blocks the penetration of extracellular ice and thereby prevents ice nucleation within the cell (Mazur, 1980). Nevertheless, cell membranes can be damaged mechanically or electrically due to charge redistribution during extracellular freezing (Korber, 1988). Many factors influence ice nucleation within the cell; these include temperature, rate of cooling, permeability of the wall membrane, and osmolality of the cell contents. The optimum cooling rate to avoid intracellular freezing varies with cell type (Korber, 1988), but slower rates generally repress cell freezing due to an increase in cell osmolality as water is expelled to extracellular regions. Slow freezing, however, can injure cells due to the "solution-effect", which is caused by a progressive increase in salt concentration around the cell wall (Mazur, 1980). Cells also undergo shrinkage during freezing due to the expulsion of intracellular water. This shrinkage may be greater than 50% and depends on cooling rate, external water potential, membrane permeability, and surface area to volume ratio of the cell (Korber, 1988).

Microorganisms

Like cells, microorganisms rely on the process of dehydration to avoid freeze injury. Dehydration appears to be an important conditioning process that occurs prior to and during freezing and that is promoted in drier soil. The importance of dehydration in survival of microbes is supported by Nelson and Parkinson (1978) who found that drier soils contribute to the greater survival of microorganisms at -22°C, and by Bartram (1916) who reported that drier soils enhance survival of bacteria and fungi when exposed to temperatures as low as -32°C. In addition to physiological changes, survival of microbes in frozen soil is also dependent on soil properties such as texture. Soil texture governs the amount of liquid water surrounding soil particles at subfreezing temperatures. It is this water film that serves as the ecological niche where microflora can avoid possible damage from ice crystals and find nutrients (Gilichinsky et al., 1995). Survival at sub-freezing temperatures is typically greater in fine-textured than in sandy soils due to the greater liquid water content. In contrast to survival, growth of microbes continues only to about -5°C, at which temperature the availability of free water diminishes (Clein and Schimel, 1995). Microbial activity, however, occurs at -6.5°C (Coxson and Parkinson, 1987.). Evidence of microbial activity in frozen soil was found: 1) under winter snowpacks where mineralization and nitrification contribute to surface water degradation (Rascher et al., 1987), 2) in subarctic ecosystems where C losses during winter approach 10 to 30% of the annual loss (Rascher et al., 1987), and 3) in tundra ecosystems where nearly all C and N loss occurs when the soil is frozen (Hobbie and Chapin, 1996).

Soil fauna

Dehydration may also be an important process for survival of fauna in frozen soil. Forge and MacGuidwin (1992) found that microfauna survival at temperatures of -4°C was lower at higher soil water potentials. They attributed the lower survival of a nematode in wet soil to lack of physiological changes prior to freezing as well as to injury caused by pore ice or to desiccation as a result of direct contact with pore ice. Macrofauna adaptation to freezing soil includes migrating to unfrozen regions within the soil profile as well as entering aestivation (Berry and Radke, 1995). Berry and Radke (1995) noted that survival at low temperatures is also dependent on faunal stage of development and species. For example, while immature and adult earthworms cannot tolerate temperatures much below 0°C (Berry and Radke, 1995), cocoons of earthworm can tolerate temperatures as low as -13.5°C (Holmstrup, 1994).

Plants

Survival of plants from low temperature exposure depends on both physiological changes that occur during the hardening process as well as on the amount of carbohydrates stored in crown and root tissues. Hardening of plants occurs over a wide temperature range; this range is from 15 to -5°C for alfalfa (Sharratt et al., 1986). The hardening process involves notable changes in the roots and crown, such as a decrease in total water content of the cell, structural changes in the protoplasm, and conversion of starch to sugar. (Smith, 1978). Despite these changes, plants such as legumes and grains cannot survive temperatures below -15°C. The physical nature of freezing soil also influences survival. Heaving can sever roots, thus promoting desiccation or disease infestation in plants. In addition, ice

5

lenses and sheets can cause lethal concentrations of respiratory products to accumulate in root and crown tissue. Seeds, unlike winterhardy plants, respire little and can survive extended periods of time in frozen soil; seeds of arctic lupine survived 10,000 years in permafrost in the Yukon Territory (Porsild et al., 1967).

CONCLUSIONS

Freezing and thawing is a process that affects soils in many regions of the world. To cope with issues related to a rising population and environmental quality, knowledge must be advanced concerning the impact of soil freezing on productivity and diversity of managed ecosystems. The International Symposium on Physics, Chemistry, and Ecology of Seasonally Frozen Soils is a step toward broadening our knowledge of frozen soil processes. The information embodied within the Proceedings of the Symposium represents some of the most recent advancements in the physiochemistry and biology of seasonally frozen soils. We believe this knowledge can be used in identifying new areas of research and in developing new simulations for the optimization of productivity and diversity of ecosystems. We also believe this information will be useful to all people who utilize the soil resource in cold regions and desire to find sustainable and environmentally-safe management systems.

REFERENCES

Bartram, H.E. 1916. The effect of natural low temperatures on certain fungi and bacteria. J. Agric. Res. 14:651-

Bengtsson, L. 1994. Climate of the 21st century. Agric. For. Meteorol. 72:3-29.

Berry, E.C. and J.K. Radke. 1995. Biological processes: relationship between earthworms and soil temperature. J. Minnesota Acad. Sci. 59(2):6-8.

Bonan, G.B. 1991. A biophysical surface energy budget analysis of soil temperature in the boreal forests of interior Alaska. Water Res. Res. 27:767-781.

Bryan, R.B. 1971. The influence of frost action on soil-aggregate stability. Trans. Inst. Br. Geog. 54:71-88.

Burwell, R.E., D.R. Timmons, and R.F. Holt. 1975. Nutrient transport in surface runoff as influenced by soil cover and seasonal periods. Soil Sci. Soc. Am. Proc. 39:523-528

Christensen, S. and J. Tiedje. 1990. Brief and vigorous N2O production by soil at spring thaw. J. Soil Sci. 41:1-4.

Clein, J.S. and J.P. Schimel. 1995. Microbial activity of tundra and taiga soils at sub-zero temperatures. Soil Biol. Biochem. 27:1231-1234.

Coxson, D.S. and D. Parkinson. 1987. Winter respiratory activity in aspen woodland forest floor litter and soils. Soil Biol. Biochem. 19:49-59.

Dise, N.B. 1992. Winter fluxes of methane from Minnesota peatlands. Biogeochem. 17:71-83.

El-Kadi, A.I. and J.W. Cary. 1990. Modelling the coupled flow of heat, water, and solute in freezing soils, including heave. Software for Engineering Workstations 6:48-51.

Fine, L.O., T.A. Bailey, and E. Truog. 1940. Availability of fixed potassium as influenced by freezing and thawing. Soil Sci. Soc. Am. Proc. 5:183-186.

Flerchinger, G.N. and F.B. Pierson. 1991. Modeling plant canopy effects on variability of soil temperature and water. Agric. For. Meteorol. 56:227-246

Forge, T.A. and A.E. MacGuidwin. 1992. Effects of water potential and temperature on survival of the nematode Meloidogyne hapla in frozen soil. Can. J. Zool. 70:153-1560.

Gilichinsky, D.A., S. Wagener, and T.A. Vishnevetskaya. 1995. Permafrost microbiology. Permafrost Periglacial Proc. 6:281-291.

Heintzelman, O.H. and R.M. Highsmith. 1973. World regional geography. Prentice Hall, Inc., New Jersey. 468 pp.

Hobbie, S.E. and F.S. Chapin, III. 1996. Winter regulation of tundra litter carbon and nitrogen dynamics. Biogeochem. 35:327-338.

Hoekstra, P. 1969. Water movement and freezing pressures. Soil Sci. Soc. Am. Proc. 33:512-518.

Holmstrup, M. 1994. Physiology of cold hardiness in cocoons of five earthworm taxa (Lumbricidae: Oligochaeta). J. Comp. Physiol. B 164:222-228.

Iskandar, I.K. and T.F. Jenkins. 1985. Potential use of artificial ground freezing for contaminant immobilization. In: Proc. Intern. Conf. on New Frontiers for Hazardous Waste Management. Pittsburgh, PA Sep 15-18, 1985 pp.128-137

Iskandar, I.K. 1986. Effect of freezing on the level of contaminants at uncontrolled hazardous waste sites. Part I. Literature review. CRREL SR 86-19, Hanover, NH

Jackson, C.I. 1992. Global warming: implications for Canadian policy. Climate Change Digest 92-01. Atmosphere Environment Service. 17 pp.

Jansson, P. 1991. Simulation model for soil water and heat conditions: Description of the SOIL model. Swedish University of Agricultural Sciences, Department of Soil Science Rep. 165. 73 pp.

Johnsson, H., L. Bergstrom, P. Jansson, and K. Paustian. 1987. Simulating nitrogen dynamics and losses in a layered agricultural soil. Agric., Ecosyst., Envir. 18:333-356.

Kay, B.D., C.D. Grant, and P.H. Groenevelt. 1985. Significance of ground freezing on soil bulk density under zero tillage. Soil Sci. Soc. Am. J. 49:973-978.

Korber, C. 1988. Phenomena at the advancing ice-liquid interface: solutes, particles and biological cells. Quart. Rev. Biophys. 21:229-298.

Levitt, J. 1972. Responses of plants to environmental stresses. Academic Press, New York. 697 pp.

Mazur, P. 1980. Limits to life at low temperatures and at reduced water contents and water activities. Origins Life 10:137-159.

Nekrasov, I.A. 1983. Dynamics of the cryolithozone in the northern hemisphere during the pleistocene. In: Permafrost - Proc. 4th Intl. Conf., Nat. Acad. Press, Washington, D.C., p. 903-906.

Nelson, L.M. and D. Parkinson. 1978. Effect of freezing and thawing on survival of three bacterial isolates from an arctic soil. Can. J. Microbiol. 24:1468-1474.

O'Neill, K. and R.D. Miller. 1985. Exploration of a rigid ice model of frost heave. Water Res. Res. 21:281-296.

Panday, S. and M. Corapcioglu. 1994. Theory of phase-separate multicomponent contaminant transport in frozen soils. J. Contaminant Hydrol. 16:235-269.

Panday, S. and M. Corapcioglu. 1991. Solute rejection in freezing soils. Water Res. Res. 27:99-108

Porsild, A.E., C.R. Harington, and G.A. Mulligan. 1967. Lupinus articus Wats. grown from seeds of Pleistocene age. Sci. 158:113-114

Rascher, C.M. C.T. Driscoll, and N.E. Peters. 1987. Concentration and flux of solutes from snow and forest floor during snowmelt in the West-central Adirondak region of New York. Biogeochem. 3:209-224.

Rogers, A. 1996. Taking Action. United Nations Environmental Programme, SMI Limited, Hertfordshire, England.

Sharratt, B.S. 1993. Freeze-thaw and winter temperature of agricultural soils in interior Alaska. Cold Reg. Sci. Tech. 22:105-111.

Sharratt, B.S. 1997. Tillage-induced air permeability modified by soil freezing. In: International Symposium on Physics, Chemistry, and Ecology of Seasonally Frozen Soils, Fairbanks, AK June 10-12, 1997 (this issue).

Sharratt, B.S., D.G. Baker, and C.C. Sheaffer. 1986. Climatic effect on alfalfa dry matter production. Part 1. Spring harvest. Agric. For. Meteorol. 37:123-131.

Skogland, T., S. Lomeland, and J. Goksoyr. 1988. Respiratory burst after freezing and thawing of soil: experiments with soil bacteria. Soil Biol. Biochem. 20:851-856.

Smith, D. 1978. Forage management in the north. Kendall/Hunt Publ. Co., Dubuque, IA. 237 p.

Staricka, J. and G. Benoit. 1995. Freeze-drying effects on wet and dry aggregate stability. Soil Sci. Soc. Am. J. 59:218-223.

Visher, S.S. 1945. Climatic maps of geologic interest. Geol. Soc. Am. Bull. 56:713-736.

Wilson, C. 1969. Climatology of the cold regions. II. Northern hemisphere. U.S. Army CRREL Monograph I-A3b. 168 pp.

Zukowski, M.D. and M.A. Tumeo. 1991. Modeling solute transport in ground water at or near freezing. Ground Water 29:21-25.

I. PHYSICS

The Seasonally Frozen Layer
Geotechnical Significance and Needed Research

P.J. WILLIAMS[1]

ABSTRACT

Geotechnical problems of frost damage to highways, buildings, and pipelines, have stimulated research into the mechanical and thermal properties of freezing ground. Agronomists have tended to emphasise chemical/physical interpretations. The microclimatological questions are also analysed in diverse ways. An historical review provides the background for an integrated study of the effects of freezing in relation to the soil microstructure..

The thermal properties, strength and deformation, transport phenomena, hydrologic and other characteristics of frozen ground are determined by the thermodynamic relations of the unfrozen water and ice. These relations are a consequence of the soil's porous nature and of the form and extent of particle surfaces. The microscopic structure of a freezing fine-grained soil is the origin of its particular bulk properties. This is the basis of research into more cost effective responses to the contamination of ground in cold regions and other current issues.

Key words: soil freezing, thermodynamics, microstructure, contamination

INTRODUCTION

The active layer is the term for the seasonally freezing and thawing layer in the permafrost regions. What goes on in the active layer dominates geotechnical engineering, agronomy and more too. Away from the permafrost we do not speak of an active layer although perhaps we should. Curiously, at a time when we are struck by how little freezing affects certain biological systems (frozen frogs and such like), we are realising that freezing has effects on soils so fundamental that they are second only to the origin of the material itself. These effects radically modify the soil's macro- and microstructure and properties. The thickness of the layer affected may be more than 5 meters (for example in Mid-Asia, Matveyev, 1989) although we usually think of seasonal freezing extending only a meter or two and much less in warmer places.

The agricultural soil scientist often uses the language of chemistry and that of physics in studying freezing soils, while the engineer uses that of mechanics. If we pull these approaches together and apply elementary thermodynamics we have a synthesis that is surely the heart of geocryology - the study of freezing ground.

FREEZING IN POROUS MEDIA

Nersessova's papers (1953-1957) on the quantities of unfrozen water present in frozen soils are a landmark. That not all the water in a soil froze exactly at 0°C, was inherent in Beskow's doctoral thesis and splendid monograph (Beskow 1935) and even in the ideas of Taber (1929) who first clearly set out what frost heave was: the migration of water into the freezing layers to give discrete layers of ice. Clearly there was a hydraulic gradient developed and this was due to the suction, or 'cryosuction' developed in the soil water. Taber and Beskow believed that the freezing point of the water was less than 0°C but only by a small amount and because of solutes and some effects of surface adsorption. Nersessova, however, established through calorimetric measurements of the 'apparent' heat capacity (ascribable largely to heat of fusion), that freezing in fine-grained soils took place

[1] Distinguished Research Professor, Geotechnical Science Laboratories, Carleton University, Ottawa, Ontario K1S 5B6, Canada

over a range of temperatures of several, even many, degrees below 0°C. There are thus significant quantities of water unfrozen within the frozen soil, Fig. 1.
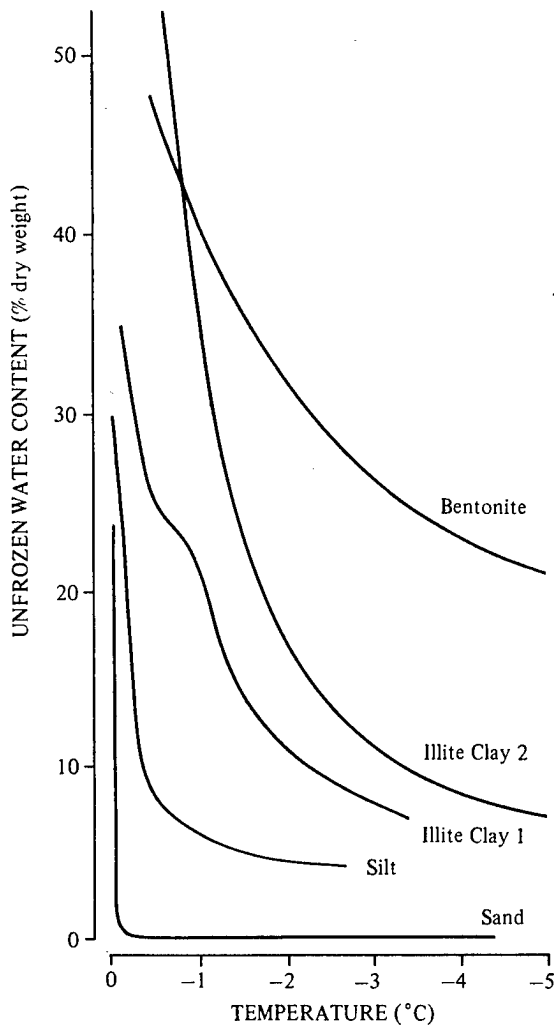
Figure 1. Unfrozen water contents of saturated soils as a function of temperature. The remainder of the pore space is filled with ice.

EXPLANATIONS FOR UNFROZEN WATER IN FROZEN SOIL

The capillary model:

The development of the suction (or 'cryosuction') and the depression of the freezing 'point' (actually a range of negative temperatures) is ascribed to the small size of the soil pores, which act as capillaries. Freezing can thus be compared to the drying of a soil. As water is replaced, whether by air, or by ice, the pressure of the water, p_w, falls, this constituting the suction (sometimes called tension, or negative pore

pressure). This pressure state follows from the confined interface (the meniscus) between the two phases and is proportional to its radius of curvature, which is often equated, with some approximation, with the radius, r, of the pore:

$$\text{suction} = p_1 - p_w = 2\,\sigma/r$$

where p_1 is pressure of air or ice and is surface tension air to water, or ice to water respectively.

There are objections to the analogy with unsaturated unfrozen soil. For example, ice being crystalline, does not have a curved interface towards the water, so the relation of curvature to pressures in the two phases may not be exactly as implied by the capillary equation. Certainly, the model only applies over a rather small temperature range, of 0° to -1°C or so, because at lower temperatures the water is present as an adsorbed layer around particles rather than occupying the pores which are filled, instead, with ice.

The adsorbed layer:

There is no doubt that water within a distance from the particle mineral surface of some molecular diameters and more, has modifications of its properties including a lowered freezing 'point'. Exactly how thick a layer is involved is uncertain but it seems that water remaining unfrozen below about -1°C is essentially within this adsorbed layer. Measurements of surface area of the particles can be used to predict unfrozen water content (Anderson and Tice 1972).

Thermodynamic models:

The suction or tension of the water in unfrozen soils, as the water content is reduced, was identified with the Gibbs free energy, in the classic paper of Schofield (1938). Schofield and Botelho da Costa (1938) pointed out the substantial depression of the freezing point to be expected on that account. Edlefsen and Andersen (1943), Everett (1961) and others (the present paper is not a comprehensive review of the literature) expanded upon this concept with its implications for the relation of freezing 'points' to the pressures of the water and ice. Fremond and Mikkola (1991) combined continuum mechanics and macroscopic thermodynamics in their model of frost heave and related effects.. Koopmans and Miller (1966) and Williams (1967) showed experimentally how the unfrozen water content-temperature relation in the frozen soil could be predicted from the suction-moisture content relation (the soil moisture characteristic curve) of the unfrozen soil.

The thermodynamic models are characterised by

their generality. They do not describe what is actually happening at the microscopic scale. Defay and Prigogine's (1951) approach to porous media describes the role of capillarity (surface tension and pore diameters). The remarkable study by Edlefsen and Anderson was entirely theoretical. They considered in terms of free energy, the effects of capillarity, of adsorption, of solute concentration and more. They also discussed the appropriate form of the 'generalised Clausius-Clapeyron' equation to be applied to soils (ultimately they favoured the wrong form).

The Clausius-Clapeyron equation provides a convenient picture of what happens in the freezing soil. Sometimes people talk of it as not describing correctly freezing within soils. Neither Clausius, the famous German thermodynamicist, nor Clapeyron, a French boiler maker, as far as I know had anything whatsoever to do with soils. The eponymous equation is quite fundamental, and deals with phase equilibria, in terms of pressure and temperature. Nothing we find out about soils is likely to disprove it: the problem is to find exactly how it applies in the complex soil system.

MECHANICS OF FREEZING SOILS

The Clausius-Clapeyron equation in the form:

$$T - T_0 = (P_w V_w - P_i V_i)T/L_f$$

(where V_i and V_w are the specific volumes of ice and water respectively, T is temperature, T_0 is the 'normal' freezing point 273.15 K, and L_f is the latent heat of fusion) helps us understand the mechanics of freezing soils. The pressure of the ice P_i leads to the (heaving) pressure that the soil exerts even though the expansive force of the ice is partly taken up by the resistance of the frozen soil (Williams and Wood 1985). The pressure (suction) P_w of the water is the cause of the migration of water to and into, the frozen ground and thus the frost heave.

A saturated (unfrozen) soil that loses moisture, becomes firmer (stronger). This is because, in engineering (soil mechanics) terms, the negative pore pressure u in the water, the suction, gives rise to a positive effective stress σ (σ is total stress) according to the classic equation (see e.g. Wu, 1981):
$$σ = σ - u$$
The frictional strength is proportional to the effective stress. A good illustration is the brick-like vacuum pack of coffee - low pressure inside, atmospheric pressure outside, the difference giving the

effective (or intergranular) stress. The same effect occurs when soils are frozen. The water content is reduced but not by evaporation or drainage. If the soil is compressible (prone to shrinkage) there will be a redistribution of water with segregation of ice (possibly such small segregations as not to be seen with the naked eye). The soil particles are pulled together by the suction of the unfrozen water and may be squeezed together by the thin layers of segregating ice. This consolidation effect, ascribable to the effective stress was demonstrated by Williams (1963), Chamberlain and Gow (1979) and others.

In the freezing of compressible, clay soils vertically aligned shrinkage cracks develop immediately below the frost line. Simply put this is a result of the cryosuction and effective stress. The cracks are subsequently favoured sites for ice formation, resulting in the orthogonal pattern of ice layers. When thawed the material breaks into cubes commonly some centimetres or more across. Othman and Benson (1993) relate the observed increased hydraulic conductivity following freeze-thaw to these structures and point out the cumulative effects of repeated freeze-thaw cycles. They refer to the structures as 'microstructure' but this term is best restricted to truly microscopic effects not visible in detail by the naked eye

The behaviour of the ice of course, also has an important role in the rheological properties.

Continuing heave
Frost heave is not limited to the moment of freezing nor, in the spatial sense, does it occur at the frost line (frozen soil boundary). The existence of the frozen fringe (Miller et al. 1975) without ice segregations is well-established. The understanding given by the thermodynamic models allows prediction of the hydraulic gradients (Burt and Williams, 1975) that exist along temperature gradients. As a consequence there can be a long term accumulation of ice ('continuing frost heave'). Smith and Patterson (1989) measured frost heave continuing over months, some 40cm within the frozen layer. The temperatures were between 0° and -0.5°C and the gradients were small, as in nature. But the ground was frozen and the cryosuctions are large at -0.5°C.

'Dynamic equilibrium' of freezing soils.
A key geotechnical issue for frozen soils is their hydrological, mechanical and strength properties at a degree or two below 0°C. The unfrozen water content is relatively high (except for exclusively coarse sand or gravel) and together with the stresses in the soil, is a function of temperature. This

constitutes a state of dynamic equilibrium (a term coined by Russian scientists). Figure 2 shows a diagram by Yershov (1991, 1997) representing the stresses in a freezing soil, taking into account many of the effects mentioned above. Whether this diagram is correct in the details, it demonstrates the complexity and the implications of these effects. In analysing freezing soils, we have to ensure that the laws of mechanics and thermodynamics are all met.
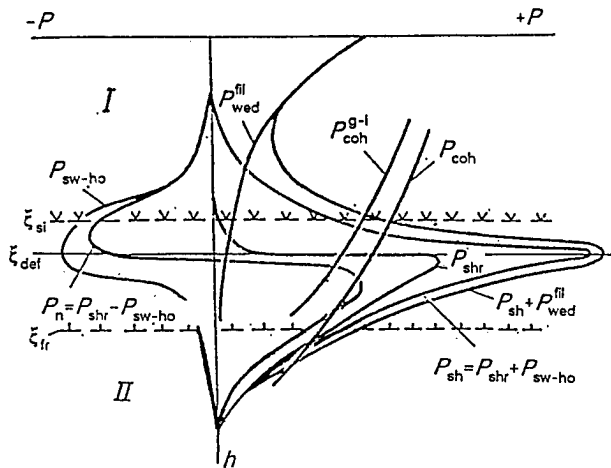
Figure 2. Development in freezing soil of stresses of shrinkage P_{shr}, swelling P_{sw}, heave P_{ho}, horizontal shear P_{sh}, and normal volumetric stresses P_n and thus the wedging P_{coh} pressure of film water P_{wed}^{fil}, local and cohesion at the boundary "soil-ice layer" P_{coh}^{g-i}; boundaries ξ_{fr}, ξ_{si}, ξ_{def} are those of freezing, visible segregated ice formation and change in deformation direction in the sample, respectively; I, II are frozen and thawed parts of the ground, respectively. (From Yershov 1997.)

SIGNIFICANCE OF SOIL MICROSTRUCTURE

There have been a number of largely descriptive studies of the microstructure of frozen and thawed soils by Harris (1983), Bunting (1983) and others. It is widely recognised that freezing modifies geotechnical properties but Pusch (1977, 1979) appears to be the first until very recently (except perhaps in Russia), to directly relate microstructure and unfrozen water content. He observed (using an electron microscope) that freezing of a remoulded clay resulted in aggregation of clay particles. The close packing of particles within the aggregates meant that the effective surface area of the clay was reduced and there was a corresponding reduction of unfrozen water content.
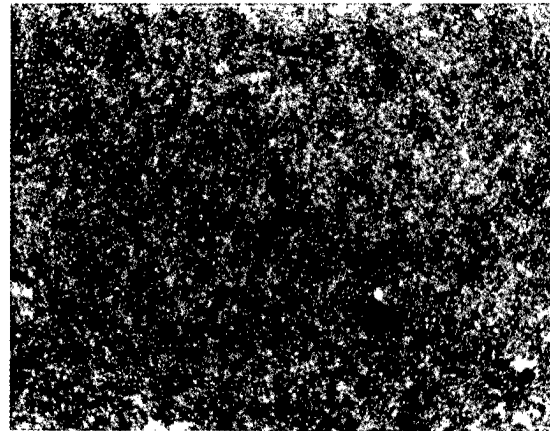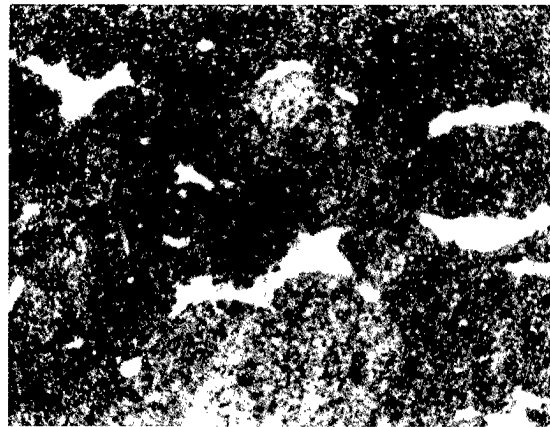
Figure 3. (a) Caen silt, optimum density, before freezing (b) after four freeze-thaw cycles (c) Moley clay lightly compacted before freezing (d) after four freeze-thaw cycles. The length of the frames corresponds to 13mm.

12
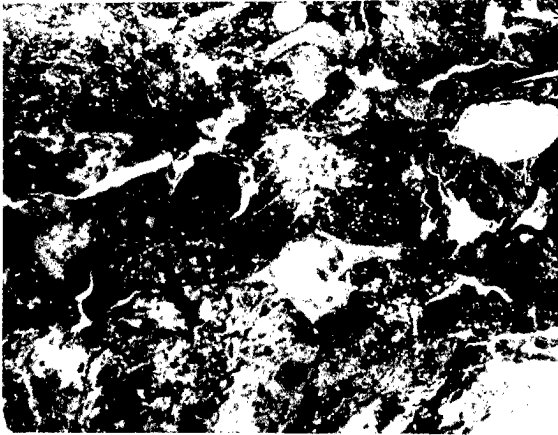
Figure 3(d) (see previous page)

Recently the microstructure of several soils have been studied in thin sections, prepared using resin impregnation (Van Vliet-Lanoë and Dupas, 1991), from samples exposed to freeze thaw cycles. The never-frozen soil (Figure 3(a)) has a poorly defined structure but a single freeze-thaw cycle produces a striking degree of aggregation of the particles. It is the effective stresses from the freezing process that cause the consolidation into aggregates. More detail is revealed in colour photographs which could not be reproduced.The large longitudinal pores (fig. 3(b)) are the sites of ice lens (big enough to be seen in the frozen samples by the naked eye). Some of the water in the lenses would have come from the proximal aggregates but some may have a more distant origin. The sample in Fig.3 (d) shows another common feature: the accumulation of iron deposits on the surface of aggregates. In some soils a sorting occurs, with fine particles accumulating above the aggregates or particles.

The modifications continued with successive freeze-thaw cycles but decreasingly. The temperature was lowered by the same amount in these subsequent cycles and the stress conditions developed, associated with the temperature dependent cryosuction, should have been similar. But it was established (White and Williams 1994) that there were significant differences in hydraulic conductivity, bulk density, frost heave and other properties after the succesive freeze-thaw cycles. Only after some ten cycles did there appear to be little further change.

Temperature has a decisive role for the properties of frozen soil. It is the size and geometry of voids, and particle sizes, however, that determine the conditions for the soil moisture and thus the soil-specific properties and behaviour at freezing temperatures. The microstructure accounts for the unfrozen water content (as a function of temperature) of a particular soil. In turn, the unfrozen water content determines the temperature dependent heat capacity of the frozen soil. The ice-water ratio is an important factor in the thermal conductivity. The hydraulic conductivity of newly thawed soil is determined by the pore structure and geometry, and in the frozen soil the configuration of the ice and water is also important. Movement of contaminants in freezing soils is related to the hydraulic conductivity. Strength and creep properties are also a function of the proportions of ice and water and of the partitioning of stress within the soil system. It seems that most properties of frozen soils can be traced back to their particular microstructure. We should not be surprised: after all, metallurgists found a century ago that the microstructure of metals explained many of their properties.

SOIL MICROSTRUCTURE - AN EXAMPLE OF ITS SIGNIFICANCE:

Consider the effects of adding a fluid contaminant, for example, diesel fuel, to ground subject to seasonal freezing. The microstructure on freezing, following contamination, Figure 4, is clearly different from that produced by freezing of the same soil when uncontaminated. We do not yet know how the modifications affect the unfrozen water content in this particular case. One suspects it is decreased. Thermal conductivity would be greater therefore. Heat capacity is difficult to assess immediately, since it depends on the slope of the unfrozen water content/temperature curve at each temperature. At any rate it will change and so will the thermal diffusivity (Williams and Smith, 1991).

The depth of the seasonally freezing and thawing layer will therefore change (the depth is also affected by the loss of vegetation through contamination). When thaw occurs, the soil structure will be even looser than in the uncontaminated but otherwise similarly treated material. Accordingly soil strength will be lower. The particular forms of surface flow and solifluction associated with tundra areas especially, are likely to be more prominent when large areas, such as the massive Komi oil spill in Russia, are considered. An all-important question is, how quickly will the spilled oil spread laterally and downwards into streams and ground water? So far only quite preliminary studies seem to have been made for freezing conditions. But it is clear that the microstructure of the soil in the frozen or thawed
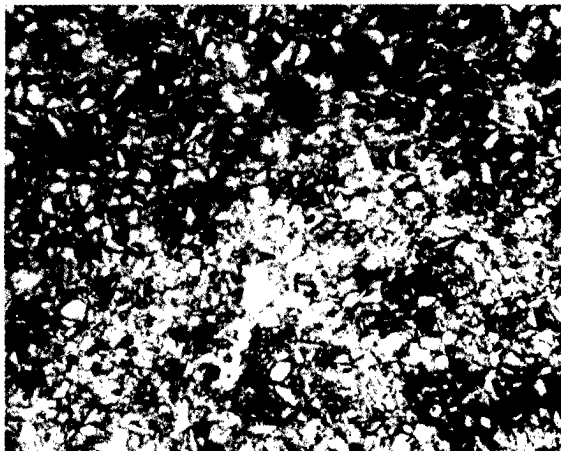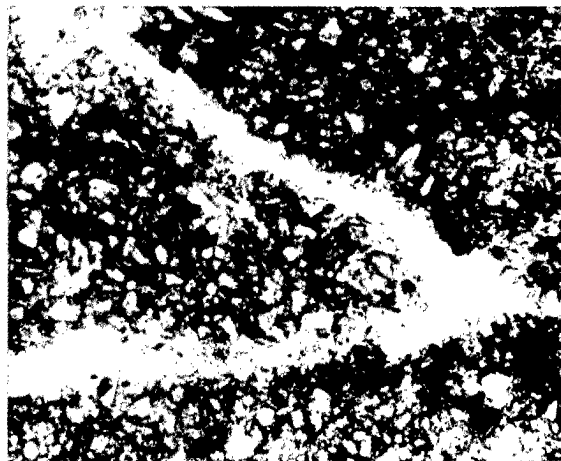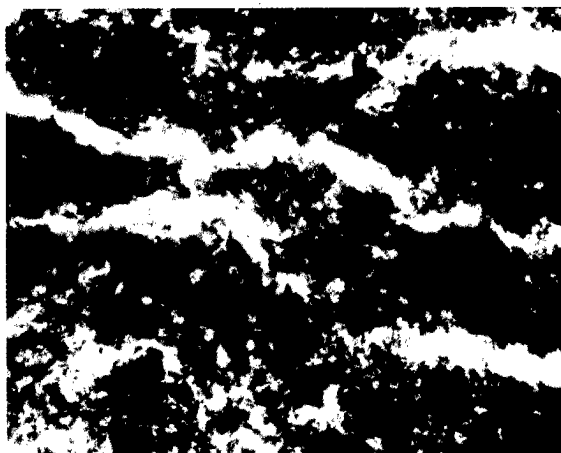
state, is crucial, together with the temperature.

We lack information about contaminant movement in ground, for example at -10°C. One suspects that, unlike for warmer freezing temperatures, it is small. The use of frozen soil as a contaminant barrier in permafrost areas requires that we know. At the other end of the temperature range are the effects in regions of warm or relict, permafrost. Here the contaminant-modified soil can lead to slightly higher mean temperatures sufficient to cause much deeper seasonal thawing and ultimately, loss of permafrost. In ice-rich soils there will be irregular subsidence and development of thermokarst terrain. Currently the role of remote sensing in detecting such changes of terrain as they develop, is being investigated (Williams et al., 1997). The problem of responding to oil spills in a cost-effective manner suggests studies along these lines will be expanded.

CONCLUSION

My intention has been to show through a historical overview, that studies of the soil microstructure are a rallying point for the diverse professional-technical approaches to the properties of freezing soils. The microscopic structure (including at the level of electron microscopy) provides the ultimate explanation of many of the properties and behaviour of freezing soils. Examples of the potential application of such studies include problems of contamination and remediation, the analysis of strength and creep, and the problem of stress corrosion cracking in pipelines. No doubt there is much also to be gained for cold regions agronomy through further studies of microstructure.

ACKNOWLEDGEMENT

REFERENCES

Anderson, D.M. and A.R. Tice. 1972. Predicting unfrozen water contents in frozen soils from surface area measurements. Highway Res. Rec. 393: 12–18.

Beskow, G. 1935. Tjälbildningen och tjällyftningen med särskild hänsyn til vägar och järnvägar. 242 pp. Statens väginstitut, Stockholm Meddelande 48. (Also translated into English: Tech. Inst. Northwestern Univ., Ill., Nov. 1947.)

Figure 4. (a) Caen silt, prior to freezing (b) after three freeze-thaw cycles (c) Caen silt contaminated with diesel fuel (10 parts per million), after three freeze-thaw cycles. Width of frames corresponds to 4.9 mm.

14

Bunting, B.T. 1983. High Arctic soils through the microscope: Prospect and Retrospect. Annals Amer. Assoc. Geographers, 73(4): 609–616.

Burt, T.P., and P.J. Williams. 1976. Hydraulic conductivity in frozen soils. Earth Surface Processes, 1(3): 349–360.

Chamberlain, E.J., and A.J. Gow. 1979. Effect of freezing and thawing on the permeability and structure of soils. Engineering Geology. 13: 73-92.

Defay, R., and 1. Prigogine. 1951. Tension superficielle et adsorption. Liége. Traité de Thermodynamique; conformement aux méthodes de Gibbs et de Donder. Editions Desoer. 295 pp.

Edlefsen, N.E., and A.B.C. Anderson. 1943. Thermodynamics of soil moisture. Hilgardia 15(2): 298 pp.

Everett, D.H. 1961. The thermodynamics of frost damage to porous solids. Trans. Faraday Society. 57(9): 1541–1551.

Fremond, M., and M. Mikkola. 1991. Thermomechanical modelling of freezing soil. Ground Freezing. 91. Yu and Wang (eds.) Balkema.

Harris, C., 1983. Vesicles in thin sections of periglacial soils from north and south Norway. *In* Proceedings Fourth Intern. Conf. on Permafrost. Fairbanks, Alaska. Washington D.C. 445–459.

Koopmans, R.W.R., and R.D. Miller. 1966. Soil freezing and soil water characteristics curves. Soil Sc. Soc. Am. Proc. 30: 680–685.

Matvayev, I.A. (Ed.). 1989. Atlas Sel'skogo Khozaystva Yakutskoy ASSR (Atlas of Agriculture of the Yakut ASSR). Moscow. Main Administration of Geodesy and Cartography of the Council of Ministers of the USSR. p. 27.

Miller, R.D., J.P. G. Loch, and E. Bresler. 1975. Transport of water and heat in a frozen permeameter. Soil Sc. Soc. Am. 39(6): 1029–1036.

Nenesova, Z.Z. 1953–1957. In: Materialy po laboratornym lssledovaniiam merzlykh gruntov. Institut Merzlotovedenia. (Izd.) Akad. Naul SSSR Moskva Sb. 1.2.3.

Othman, M.A., and C.H. Benson. 1993. Effect of freeze-thaw on the hydraulic conductivity and morphology of compacted clay. Can. Geotechnical Journal. 30: 236–246.

Pusch, R. 1977. Ice formation in clays with speedy reference to their microstructural constitution. *In* Proc. International Symposium Frost Action in Soils. Luleå, Sweden. 1: 137–142.

Pusch, R. 1979. Unfrozen water as a function of clay microstructure. Engineering Geology. 13: 157–162.

Schofield, R.K. 1935. The pF of the water in the soil. Third Intern. Congress Soil Sci. 2: 37–48.

Schofield, R.K, and J.V. Botelho da Costa. 1938. The measurement of pF in soil by freezing point. Agric. Sci. 28: 645–653.

Smith, M.W., and D.E. Patterson. 1989. Detailed observation on the nature of frost heaving at a field scale. Can. Geotechnical Journal. 26(2): 306–317.

Taber, S. 1929. Frost heaving. Journal of Geology. 37: 428–461

Van Vliet-Lanoë, B., and A. Dupas. 1991. Development of soil fabric by freeze/thaw cycles—Its effect on frost heave. Ground Freezing 91. Balkema, Rotterdam. 189–195.

White, T.L., and P.J. Williams. 1994. Cryogenic alteration of frost susceptible soils. Ground Freezing 94 (Ed. Fremond). Balkema. 17–24.

Williams, P.J. 1963. Suction and its effects in unfrozen water of frozen soils. *In* Proc. Permafrost Intern. Conf. N.A.S/N.R.C. Washington D.C. 225–229.

Williams, P.J. 1967. Properties and behaviour of freezing soils. Norwegian Geotechnical Institute. Publn. 72. 120 pp.

Williams, P.J., and J.A. Wood. 1985. Internal stresses in frozen ground. Can. Geotechnical Journal, 22(3): 413–416.

Williams, P.J., and M.W. Smith. 1991. The Frozen Earth. Fundamentals of Geocryology. 306 pp.

Williams, P.J., D.W. Riseborough, W.G. Rees, and T.L.White. 1997. Strategies for development of cost effective amelioration procedures for oil spills in cold regions. *In* Models for cold region contaminant hydrology. Ann Arbor Press.

Wu, T.N. 1981. Soil Mechanics. T.H. Wu. Worthington, Ohio, and Allyn and Bacon.

Yershov, E.D. 1990. 1997. General Geocryology. Nedra, Moscow. 550 pp. (in English: Cambridge Univ. Press, 1997).

Water and Ice

Freezing and Thawing Effects on Soil Water and Solute Movement in Repacked Soil Columns

J.K. RADKE[1] AND E.C. BERRY[1]

ABSTRACT

Overwinter freezing and thawing of soils causes movement of soil water and solutes in the soil profile. Experiments were conducted to measure the effects of freeze/thaw on soil water and solute movement in a Webster silt clay loam (fine-loamy, mixed mesic Typic Haplaqualls). PVC cylinders (0.13 m inside diameter and 1.2 m long) were packed with topsoil. Potassium bromide tracer was placed in the top 0.05 to 0.15 m soil layers in some of the columns. The soil columns were buried vertically in the field and exposed to the winter freeze/thaw conditions. Field columns were extracted throughout the winter and sectioned into 0.05 m layers. Each layer was analyzed for water content, bulk density, and electrical conductivity. Water moved upwards to the freezing zone carrying along some solutes. Electrical conductivity values verified the movement of solutes during the freeze/thaw periods. Bulk density changed abruptly due to expansion and compression of the soil matrix during freeze/thaw periods. Physical properties of thawed soil retained some of the changes caused by freezing and remained more variable compared to the properties of unfrozen soil.

Key words: Soil water, soil solutes, freeze-thaw, *Lumbricus terrestris*, soil structure

INTRODUCTION

Seasonally frozen soils occur over large areas of North America, Europe, and Asia (Sharratt et al. 1995). Freezing and thawing of agricultural soils impacts soil quality and productivity through physical (Radke and Berry 1995), chemical (Honeycutt, 1995), and biological (Berry and Radke 1995) changes. Freezing and thawing causes movement of water and solutes in the soil (Cary et al. 1979). Water moves upwards towards the frost layer to form ice layers or lenses thus depleting water from the soil below the frost layer. When the upward water flux is insufficient to satisfy the thermodynamic requirements, the freezing front moves downward and new ice lenses begin to form. A classic experiment (Taber 1930) demonstrated the formation of ice layers and soil heaving in a soil column with a standing water table near its bottom. Although it is more common for ice crystals or ice lenses to be observed in the field (Kay et al. 1985), ice layering can occur under the right field conditions.

As water freezes into ice crystals, soil aggregates are forced apart and pressure on the aggregates may compress or rupture them. An aggregative or disaggregative net effect on soil structure may occur depending on the soil, water content, and other conditions.

As ice crystals or lenses form, salt is excluded from the ice and an enriched region of solute develops at the edges of the ice (Cary et al. 1979). This increased solute concentration lowers the freezing point further (Fuchs et al. 1978). Thus, at any time, there may be varying amounts of ice and unfrozen solute throughout the frozen soil matrix (Dirksen and Miller 1966). This leads to many complex possibilities in regards to physical, chemical, and biological states and processes.

The objectives of this study were to 1) determine the movement of water and solutes and 2) monitor soil structural changes in repacked soil columns exposed to overwinter freezing and thawing in the field.

EXPERIMENTAL PROCEDURE

The soil column experiments were initiated in 1992 using 32 repacked soil columns. The experiment continued for the next three winters with 24 soil columns in the 1993-94 and 1994-95 seasons and 30 soil columns in the 1995-96 season.

Column Packing Procedure

Polyvinyl Chloride (PVC) Schedule 40 plastic cylinders (North American Corp., Wichita Falls, TX)[1], 13-cm diameter and 120-cm long, were packed with Webster silty clay loam (fine-loamy, mixed mesic Typic Haplaqualls) topsoil to bulk densities of

---

[1] *The USDA neither guarantees nor warrants the standard of the product, and the use of the name does not imply approval of the product to the exclusion of others that may be suitable.*

[2] USDA, Agricultural Research Service, National Soil Tilth Laboratory, 2150 Pammel Drive, Ames, Iowa 50011, USA

1.0, 1.2, or 1.4 g/cm³. The topsoil was passed through a 1.25 cm sieve. Measured weights of soil (at 5% gravimetric water content) were gently packed in successive 5-cm layers until the cylinder was full. Water was added to each of the 5-cm layers during packing to give specific gravimetric water contents in the soil columns with the lower water contents. The "high soil water content" columns were saturated from the bottom and allowed to drain to field moisture capacity. In soil columns with a bromide tracer treatment, KBr was added to the two layers from 5 cm to 15 cm below the soil surface to simulate an application of N fertilizer. Five adult *Lumbricus terrestris* (L.) earthworms were added at the top of selected soil columns. The top and the bottom of each soil column was covered with plastic bags to minimize water loss until the columns were installed in the field. Columns were stored at approximately 10°C until installation.

Field Installation of the Soil Columns

Soil columns were installed in a field (Webster silty clay loam soil) located just south of Ankeny, Iowa (41°43'N, 93°36'W) during early to mid-November. Several 15-cm diameter by 120-cm long PVC cylinders were installed in holes dug with a tractor-mounted post-hole digger to serve as casings for the soil columns. The casings were spaced 3 m apart. The soil columns were inserted into the casings so the top of the soil column was level with the surrounding field surface. The top gaps between casings and columns were packed with fiberglass insulation and then sealed with duct tape. The bottom of the soil columns were in contact with the field soil and the tops were open so water could move in and out of the columns.

Soil Sampling and Analyses

Soil columns were extracted from their casings in groups of four or five (depending on the number of treatments) at various times during the winter. Sampling intervals were approximately two-weeks depending on the weather (Figure 1). The unfrozen soil was removed from the bottom of the columns in 5-cm layers with a special positioning jig and a custom-made 13-cm diameter soil auger. The frozen portion of the soil was cut into 5-cm layers using a chop saw fitted with a coarse-cut, carbide-tipped blade after either cutting away the plastic cylinder from the soil or pressing the frozen soil out of the cylinder. The 5-cm layer consisting of the transition from frozen to unfrozen soil was separated into two sections and each processed separately. All layers were analyzed for gravimetric water content, bulk density, and electrical conductivity. Electrical conductivity was used to assess changes in Br⁻ concentration.
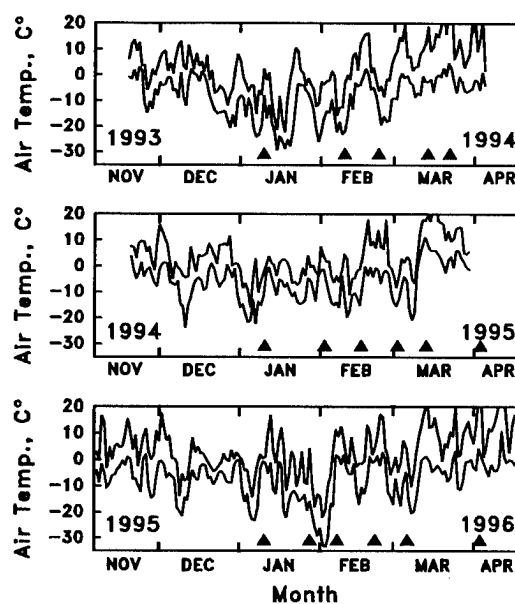
Figure 1. Daily maximums and minimums for three consecutive winters at Ankeny, Iowa. Triangles denote the sampling dates for each group of soil columns.

Weather Station Measurements

Six CRREL-type frost tubes (Ricard et al., 1976) were installed in the plot area. Soil temperatures at depths of 5, 10, 15, 25, 50, 75, and 100 cm, air temperature, solar radiation, and rainfall were recorded at the weather station located at the experimental site. Snow depth, density and water content were measured after each precipitation event or two to three times a week otherwise. Soil water in the field soil was monitored with five neutron access tubes and one Time Domain Reflectometry (TDR) profile array during the winters of 1994-95 and 1995-96. Weather station data will be used to calibrate the SHAW model (Flerchinger 1991 and Flerchinger and Saxon 1989) for predicting frost depth and the number of freeze/thaw cycles.

Experimental Layout

The arrangement of the soil columns in the field varied slightly from year to year and treatments varied each year. The 1992-93 field trial with 32 soil column columns provided information needed for refining the techniques and procedures used during the next three winters. Twenty-four soil columns were installed in the Ankeny field on 16 November 1993. All columns had a bulk density of 1.4 g/cm³ and a bromide tracer of 750 kg Br/ha (equivalent to approximately 130 kg N/ha) mixed into the 5 - 15 cm layer of soil. The treatment variables were initial water content and the presence or absence of earthworms (Table 1). Soil columns were extracted in groups of four (one from each treatment) on 1) 10 January 1994, 2) 11 January 1994, 3) 9 and 10

18

Table 1. Treatment ID codes and initial conditions and specifications for the three winters.

Trtmnt ID	Bulk Density	Water Content	Bromide Tracer	Number of Worms
	g cm⁻³ $g\,cm^{-3}$	$g\,g^{-1}$	-	#
1993-94				
HMB0	1.4	0.20	Yes	0
HMB5	1.4	0.20	Yes	5
HHB0	1.4	0.30	Yes	0
HHB5	1.4	0.30	Yes	5
1994-95				
MLB0	1.2	0.16	Yes	0
MHB5	1.2	0.30	Yes	5
MHB0	1.2	0.30	Yes	0
MH05	1.2	0.30	No	5
1995-96				
MHB0	1.2	0.30	Yes	0
MH05	1.2	0.30	No	5
LHB0	1.0	0.30	Yes	0
MLB0	1.2	0.16	Yes	0
LLB0	1.0	0.16	Yes	0

The first character of the treatment code represents a (H)igh, (M)edium, or (L)ow bulk density; second character -- high, medium, or low water content; third character -- bromide tracer or none; and fourth character -- number of earthworms added.

February 1994, 4) 22 and 23 February 1994, 5) 14 March 1994, and 6) 22 and 23 March 1994. The four columns sampled on 11 January 1994 were used for infiltration tests (data not presented here).

Another 24 soil columns were installed on 15 November 1994. These columns were packed to a bulk density of 1.2 g/cm³. A bromide tracer was used in three of the four treatments and the amount was reduced to 185 kg Br/ha. The treatment variables were initial water content, presence or absence of bromide tracer, and the presence or absence of earthworms (Table 1). These soil columns were extracted in groups of four on 1) 10 and 11 January 1995, 2) 2 and 3 February 1995, 3) 16 and 17 February 1995, 4) 2 and 3 March 1995, 5) 14 and 15 March 1995, and 6) 3 and 4 April 1995.

Thirty soil columns were installed on 9 November 1995. Bromide was used in 24 of the columns (4 of 5 treatments) at the reduced rate of 185 kg Br/ha. A fifth treatment had five earthworms and no bromide tracer. The treatment variables were bulk density and water content (Table 1). These soil columns were extracted in groups of five on 1) 10 - 12 January 1996, 2) 24 and 25 January 1996, 3) 7 and 8 February 1996, 4) 21 - 23 February 1996, 5) 6 and 7 March 1996, and 6) 3 and 4 April 1996.

Graphical and Statistical Analyses

Soil water content, bulk density, and electrical conductivity data were plotted as a function of depth for each soil column and visual comparisons were made. Two procedures were used to summarize the data. For Procedure 1, data from the 5-cm thick slices for each soil column were divided into two groups: the top portion of the soil column that was frozen at the time of sampling and the bottom unfrozen portion. The 5-cm section with both frozen and unfrozen portions was not included in the two groups and was analyzed separately. Occasionally, the first group would include thawed soil near the soil surface. Procedure 2 was similar to Procedure 1 except the two data groups were separated into 1) the top portion that was frozen at the time of sampling or any time before and 2) the bottom portion that had never froze. The transitional layer (if any) was analyzed separately. Data from all groups and for each procedure were analyzed using the Descriptive Statistics and ANOVA routines in CoStat (CoHort Software, Berkeley, CA).

RESULTS AND DISCUSSION

The three winters (1993-94, 1994-95, and 1995-96) had several cold and warm periods as illustrated by the maximum and minimum air temperatures at the experimental site (Figure 1). Generally, the depth of soil freezing increased through January and into February. Soil thawing often occurred above the frozen zone during the warm periods. Frozen soil depths at the time of sampling are shown in Figure 2. For the later samplings, only frost crystals were found in the partially thawed soil. The soil was always completely thawed for the last sampling period.

The earthworms had a difficult time moving vertically in the soil columns during the winter of 1993-94. Apparently, the earthworms were inhibited by the high bromide concentration in the 5 to 15 cm layer and did not tunnel deeply enough to survive the winter. Laboratory tests of worm sensitivity to bromide showed that the lower concentrations used in 1994-95 still affected their behavior. Earthworms placed in soil columns without the bromide tracer made tunnels twice as deep as and had a higher survival rate than those in the columns with bromide tracer. In the 1995-96 experiment, earthworms were placed only in soil columns with no bromide tracer and survived at a much higher rate, but the depth of observed earthworm tunnels were not as great as the 'no bromide' treatment in 1994-95. However, deeper tunnels may have been missed since this was not a priority observation during the sampling procedure.

The upward movement of soil water to the freezing layer was very apparent in all of the soil
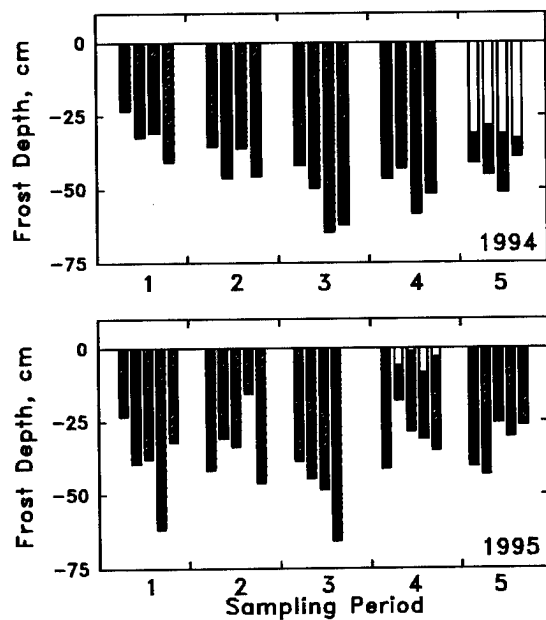
Figure 2. Measured frost depths for soil columns in 1994 and 1995. Black bars represent frozen soil and white bars represent unfrozen soil. Bar order for 1994 is MLB0, MHB5, MHB0, and MH05. Bar order for 1995 is MHB0, MH05, LHB0, MLB0, and LLB0.

Figure 3. Electrical conductivity, bulk density, and gravimetric soil water content for the HHB5 column sampled on January 10, 1994. The dashed line denotes the base of the frost layer in the column.

columns across all years. Abrupt changes in bulk density at the bottom of the frozen layer were often observed. Electrical conductivity measurements sometimes showed unexpected movement of bromide to deeper depths, apparently through preferential flow paths. The 1993-94 experiment showed very large variability in the measured parameters from soil column to soil column making it clear that the freezing process was quite random. This made treatment and other comparisons very difficult.

A typical set of the measured variables for the "wet, with worms" (Treatment HHB5) soil column sampled January 10, 1994 is shown in Figure 3. A higher soil water content is readily evident in the frozen zone. With both the tops and bottoms of the soils columns open, infiltration and evaporation are possible at the top and water exchange with the field soil can occur at the bottom. The change in bulk density at the freezing front is difficult to measure but very noticeable. Ice lens formation can cause great forces on the adjacent soil aggregates, either compacting them, crushing them, or forcing them apart. Lowered bulk densities are common in the frozen layer. The electrical conductivity shows a gradual movement of bromide down from the 5 - 15 cm enriched layer. The peak around the 70-cm depth indicates the possible preferential flow of bromide to this depth. It is possible that the path was an earthworm tunnel.

Two more sets of curves are shown in Figures 4 and 5 for the "wet, no worms, bromide" (MHB0)

treatment sampled January 11, 1995 and for the "1.2 bulk density, wet, worms, no bromide" (MH05) treatment sampled February 23, 1996. Figure 4 is similar to Figure 3 except showing a slightly greater freeze depth with no preferential flow of bromide. The soil column shown in Figure 5 was sampled
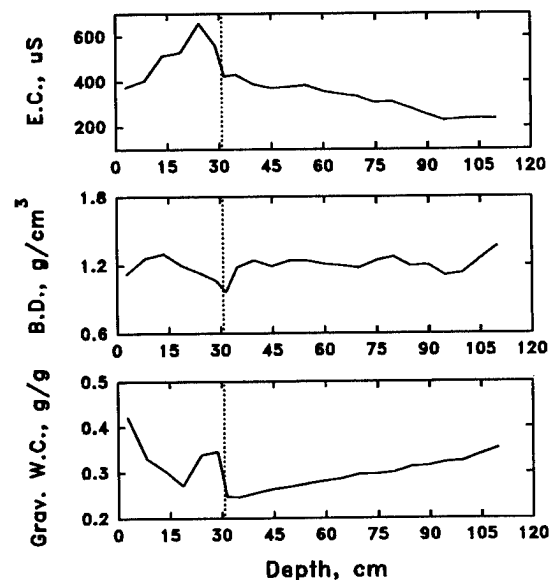
Figure 4. Electrical conductivity, bulk density, and gravimetric soil water content for the MHB0 column sampled on January 11, 1995. The dashed line denotes the base of the frost layer in the column.

20
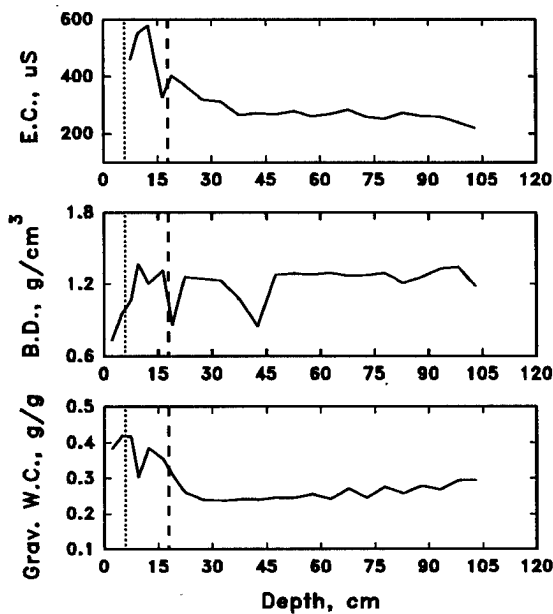
Figure 5. Electrical conductivity, bulk density, and gravimetric water content for the MH05 column sampled on February 23, 1996. The small-dash line denotes the base of the frost layer in the column, and the large-dash line denotes the bottom of the partially thawed region of the column.

later in the winter after the frozen layer had partially thawed leaving a shallow frozen layer near the surface and a layer of ice crystals approximately 6 to 16 cm deep. The bulk density shows a dip at approximately 45 cm -- possibly the maximum freeze depth.

Water contents in the frozen soil and in the soil below the frozen zone are summarized for the three winters (Table 2). Water contents were consistently higher in the frozen layer and had higher standard deviations. Treatment effects on water content were significant for the 1994-95 and 1995-96 winters in both the frozen and unfrozen zones. Treatment effects in 1993-94 probably were lost due to water movement in and out of the tops and bottoms of the columns. Water content change with sampling date was not significant except in the frozen zone in 1995-96. Comparing water contents in soil that was frozen at any time to the soil that was never frozen (Procedure 2) gave similar results. Water content over time (sampling date) was very highly significant for both the frozen and never frozen groups (data not shown). This likely reflects the upward movement of water into the freezing zone and the later redistribution of water after thawing (Sharratt 1995).

Soil bulk densities were always less in the frozen zone of the soil columns and the variability was greater in all cases, except one (Table 3). All of the columns were packed with uniform bulk densities from top to bottom. A slight increase in soil bulk density near the bottom of the columns could be due to settling by gravity, but except for initial bulk

Table 2. Treatment means and standard deviations of measured gravimetric water contents in the frozen (top) and unfrozen (bottom) portions of the soil by year and treatment. The Tukey least significant difference (lsd) and the treatment (Tmt) and sampling date (Date) significance levels are shown for each winter.

Trtmnt ID	'Frozen' Mean	'Frozen' Std. Dev.	'Unfrozen' Mean	'Unfrozen' Std. Dev.
			$g\ g^{-1}$	
Water Content 1993-94				
HMB0	0.282	0.0720	0.228	0.0092
HMB5	0.262	0.0592	0.233	0.0124
HHB0	0.294	0.0603	0.244	0.0132
HHB5	0.322	0.0471	0.248	0.0113
lsd	0.047	0.0400	0.020	0.0067
Tmt	ns	ns	ns	ns
Date	ns	ns	*	*
Water Content 1994-95				
MLB0	0.307	0.0676	0.234	0.0057
MHB5	0.352	0.0562	0.288	0.0109
MHB0	0.347	0.0608	0.286	0.0154
MH05	0.357	0.0447	0.290	0.0174
lsd	0.026	0.0346	0.021	0.0049
Tmt	**	ns	***	***
Date	ns	ns	ns	***
Water Content 1995-96				
MHB0	0.338	0.0705	0.258	0.0118
MH05	0.360	0.0549	0.242	0.0146
LHB0	0.398	0.0863	0.260	0.0192
MLB0	0.235	0.0535	0.151	0.0095
LLB0	0.319	0.0805	0.182	0.0033
lsd	0.052	0.0220	0.022	0.0124
Tmt	***	*	***	ns
Date	**	***	ns	ns

ns = not significant at 0.05
 * = significant at less than 0.05
 ** = significant at less than 0.01
*** = significant at less than 0.001

densities of 1.0 g cm^{-3}, bulk densities in the frozen zone decreased. Bulk densities decreased from the initial 1.4 g cm^{-3} throughout the soil columns in 1993-94, but the decrease was greater in the frozen zone. Treatment effects were significant for the 1993-94 and 1995-96 data analyzed by both Procedure 1 (Table 3) and Procedure 2 (data not shown). Treatments were not significant for the 1994-95 data.

Electrical conductivity values usually were

Table 3. Treatment means and standard deviations of measured bulk densities in the frozen (top) and unfrozen (bottom) portions of the soil by year and treatment. The Tukey least significant difference (lsd) and the treatment (Tmt) and sampling date (Date) significance levels are shown for each winter.

Trtmnt ID	'Frozen' Mean	'Frozen' Std. Dev.	'Unfrozen' Mean	'Unfrozen' Std. Dev.
		---gm cm^{-3}---		
Bulk Density 1993-94				
HMB0	1.301	0.2108	1.344	0.0953
HMB5	1.210	0.1978	1.369	0.0407
HHB0	1.315	0.1751	1.383	0.0418
HHB5	1.316	0.1312	1.373	0.0638
lsd	0.049	0.0743	0.041	0.0367
Tmt	**	ns	ns	*
Date	ns	ns	ns	*
Bulk Density 1994-95				
MLB0	1.147	0.1108	1.240	0.0459
MHB5	1.147	0.1129	1.242	0.5359
MHB0	1.164	0.1296	1.234	0.0452
MH05	1.135	0.1043	1.232	0.0380
lsd	0.031	0.0252	0.035	0.7568
Tmt	ns	ns	ns	ns
Date	***	***	ns	ns
Bulk Density 1995-96				
MHB0	1.204	0.0886	1.245	0.0394
MH05	1.067	0.2306	1.236	0.0480
LHB0	0.928	0.2203	1.156	0.0454
MLB0	1.117	0.1378	1.216	0.0568
LLB0	1.009	0.0447	1.083	0.0494
lsd	0.061	0.1034	0.049	0.0338
Tmt	***	**	***	ns
Date	ns	ns	ns	ns

ns = not significant at 0.05
* = significant at less than 0.05
** = significant at less than 0.01
*** = significant at less than 0.001

Table 4. Treatment means and standard deviations of measured electrical conductivities in the frozen (top) and unfrozen (bottom) portions of the soil by year and treatment. The Tukey least significant difference (lsd) and the treatment (Tmt) and sampling date (Date) significance levels are shown for each winter.

Trtmnt ID	'Frozen' Mean	'Frozen' Std. Dev.	'Unfrozen' Mean	'Unfrozen' Std. Dev.
		---µS---		
Electrical Conductivity 1993-94				
HMB0	721.1	145.24	625.1	90.19
HMB5	705.5	134.33	582.4	37.15
HHB0	541.4	107.35	424.2	22.99
HHB5	649.7	118.19	469.3	40.19
lsd	94.7	68.59	64.8	53.39
Tmt	**	ns	***	ns
Date	***	ns	***	ns
Electrical Conductivity 1994-95				
MLB0	409.0	74.60	443.7	49.76
MHB5	500.1	108.95	413.3	38.83
MHB0	520.2	119.09	393.2	46.52
MH05	393.3	85.41	382.2	41.17
lsd	71.9	34.95	57.3	16.46
Tmt	**	ns	ns	ns
Date	ns	ns	**	***
Electrical Conductivity 1995-96				
MHB0	365.3	107.79	295.1	34.02
MH05	429.0	139.09	312.3	36.24
LHB0	334.4	141.50	335.1	40.28
MLB0	310.8	107.06	323.1	32.70
LLB0	259.3	104.75	299.8	34.59
lsd	68.9	71.70	47.3	27.78
Tmt	***	ns	ns	ns
Date	ns	ns	**	ns

ns = not significant at 0.05
* = significant at less than 0.05
** = significant at less than 0.01
*** = significant at less than 0.001

greater in the top frozen portion of the soil columns where treatment effects were significant for all three winters (Table 4). Rapid movement of bromide to deeper depths in some of the soil columns was responsible for the variation. Initial analysis of the bromide data confirms this movement. The bromide results will be presented in another paper.

Earthworm tunnels were measured in the soil columns during the last two winters of the experiment. During 1994-95, bromide was either toxic or inhibited earthworm migration in the soil columns. Earthworm tunnels were limited to the top 45 cm of the columns containing bromide tracer but extended to 115 cm in the columns without bromide. The next year, the depth of earthworm tunnels increased with time as the earthworms migrated to stay below the frozen zone. The random variability of the measured soil properties made it difficult to sort out treatment effects, but earthworm tunnels may have provided preferential flow paths in some

22

cases. Laboratory studies with more controlled conditions are being conducted to answer some of these questions.

SUMMARY AND CONCLUSIONS

Water and solutes moved upward in the soil columns towards the advancing freezing front. Ice lens formation created pressure affecting soil structure and physical properties. Soil bulk density generally was decreased in the frozen zone with a higher variability, both while frozen and after thawing. Some compaction and fracturing of the soil occurred near the freezing front. During and after thaw, melted soil water equilibrated with the soil matrix and the salts were redistributed in the soil solution. Solute and water movement were unpredictable in several of the soil columns and likely were the result of preferential flow paths. These flow paths may have developed by a random fracturing of the soil matrix due to freezing and thawing. Or, earthworm burrows may have provided a channel. Movement of solutes and water after thawing depended on several factors including soil water content, rainfall and infiltration rates, and soil property changes.

ACKNOWLEDGMENTS

REFERENCES

Berry, E.C. and J.K. Radke. 1995. Biological processes: Relationships between earthworms and soil temperature. J. MN Acad. Sci. 59:(2):6-8.

Cary, J.W., R.I. Papendick, and G.S. Campbell. 1979. Water and salt movement in unsaturated frozen soil: principles and field observations. Soil Sci. Soc. Am. J. 43:3-8.

Dirksen, C. and R.D. Miller. 1966. Closed-system freezing of unsaturated soil. Soil Sci. Soc. Am. Proc. 30:168-173.

Flerchinger, G.N. 1991. Sensitivity of soil freezing simulated by the SHAW model. Trans. ASAE 34:2381-2389.

Flerchinger, G.N. and K.E. Saxon. 1989. Simultaneous heat and water model of a freezing snow-residue-soil system II. Field verification. Trans ASAE 32:573-578.

Fuchs, M., G.S. Campbell, and R.I. Papendick. 1978. An analysis of sensible and latent heat flow in a partially frozen unsaturated soil. Soil Sci. Soc. Am. J. 42:379-385.

Honeycutt, C.W. 1995. Soil freeze-thaw processes: Implications for nutrient cycling. J. MN Acad. Sci. 59:(2):9-14.

Kay, B.D., C.D. Grant, and P.H. Groenevelt. 1985. Significance of ground freezing on soil bulk density under zero tillage. Soil Sci. Soc. Am. J. 49:973-978.

Radke, J.K. and E.C. Berry. 1995. Studies on freezing and thawing soils in Iowa. J. MN Acad. Sci. 59:(2):19-26.

Ricard, J.A., N. Tobiasson and A. Greatorex. 1976. The field assembled frost gage. Technical note from Corps of Engineers, U.S. Army, Cold Regions Research and Engineering Laboratory, Hanover, NH.

Sharratt, B.S. 1995. Migration of water during winter in west central Minnesota soils. J. MN Acad. Sci. 59:(2):15-18.

Sharratt, B.S., K.E. Saxton, and J.K. Radke. 1995. Freezing and thawing of agricultural soils: Implications for soil, water, and air quality. J. MN Acad. Sci 59:(2):1-5.

Taber, S. 1930. The mechanics of frost heaving. J. Geol. 38:303-317.

Water Infiltration and Movement in Seasonally Frozen Soils

M. STÄHLI[1], P.-E. JANSSON[1], L.-C. LUNDIN[2] AND H. FLÜHLER[3]

ABSTRACT

Understanding surface runoff and water infiltration into a frozen soil caused by a melting snow cover is highly relevant for a number of environmental questions. The complex interactions between heat and water flows, as well as different scales, make it difficult to quantify field conditions. In the present study four small soil plots were investigated with regard to the water and heat dynamics during one winter season (1995/96). Profile measurements of soil temperature, liquid and total water content were used to test a one-dimensional deterministic model (SOIL). The model calculates the water flow in a frozen soil in two domains. The general agreement between the measurements and the simulated results was satisfactory, mainly with respect to the water budget in the topsoil during the three snowmelt events of the winter.

Key words: Snowmelt, infiltration, numerical model.

INTRODUCTION

The partitioning of water released from a melting snow cover into surface runoff and soil infiltration is a crucial topic for a number of environmentally relevant processes, such as erosion or solute leaching. It closely depends on the extent to which the underlying soil is frozen. There is experimental evidence for snowmelt infiltration into frozen soil, although the liquid soil water adsorbed by the particles is nearly immobile. Previous research has shown that the saturation of the soil has a strong influence on the amount of snowmelt infiltration (e.g., Kane and Stein 1983; Granger et al. 1984). It is mainly the partitioning of liquid water, ice and air in a frozen soil that regulates the infiltration. The concept of two flow domains, originally presented by

Lundin and Johnsson (1990), has recently been introduced into a one-dimensional soil water and heat model (SOIL; Jansson 1996). The model has earlier been used for studying soil frost in arable (e.g., Thunholm et al., 1989; Jansson and Gustafsson 1987), as well as forest soils (e.g., Jansson 1987). First applications of the two domain approach showed an improved prediction of the timing of runoff compared to the one domain approach (Stähli et al. 1996). Assessing a hydraulic conductivity is, however, difficult for the water moving through this second flow domain (Stadler et al. 1997). Another uncertainty is related to the amount of infiltrating water that refreezes while passing the frozen soil. Lundin et al. (1996) suggested an approach to calculate the heat transfer coefficient assuming the capillary soil to be a heat exchanger.

The main objective with this paper is to test the model and especially the validity of the two domain approach by using data from a small-plot experiment which was performed at Uppsala (central Sweden) during winter 1995/96.

MATERIALS AND METHOD

Model description

The SOIL model calculates water and heat fluxes in the soil-plant-atmosphere continuum in one dimension and includes processes of evapotranspiration, surface runoff, pipe drainage, soil freezing and snow dynamics. The basic equations for water and heat flow in the soil are the Richards equation (Richards 1931) and Fourier's law, respectively. A detailed description of the model can be found in Jansson (1996) or on the internet homepage http://www.mv.slu.se/bgf/soil.htm where it is also freely available.

[1] SLU, Department of Soil Sciences, P.O. Box 7014, 750 07 Uppsala, Sweden
[2] Uppsala University, Department of Earth Sciences, Norbyvägen 18 b, 752 36 Uppsala, Sweden
[3] ETH Zürich, Institute of Terrestrial Ecology, Grabenstasse 3, 8952 Schlieren, Switzerland

At below-zero temperatures, snow accumulation is considered to form a homogeneous snowpack with a certain water content and retention, and with a density-dependent heat conductivity. Soil freezing is treated similarly as drying, taking into account the partitioning of heat into a latent and sensible fraction.

Melting of the frozen soil usually coincides with snowmelt infiltration which, in the model, is calculated assuming two water conducting flow domains: firstly, the liquid water that is adsorbed by the particles (*low flow domain*), and secondly, the pore space which is air-filled at the start of the infiltration (*high flow domain*). When snowmelt infiltration occurs the water is firstly filling up the low flow domain and then entering the high flow domain. As soon as full saturation is reached the water is running of on the surface. Figure 1 illustrates this concept schematically.
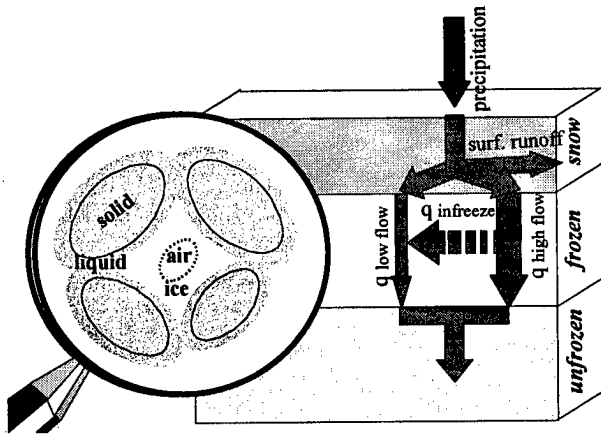
Figure 1. The concept of two-domain water flow in frozen soils.

The flow within the low flow domain is based on Darcy's law assuming the same hydraulic conductivity, k_w, as during unfrozen conditions (Mualem 1976):

$$k_w = k_s S_e^{(n+2+\frac{2}{\lambda})} \qquad (1)$$

where k_s = saturated hydr. conductivity (m s^{-1})
S_e = effective saturation (-)
n = tortuosity factor (-)
λ = pore size distribution index (-).

Since k_w decreases by several orders of magnitude when the temperature decreases below the freezing point, this water phase is nearly immobile at only few degrees below zero. For the flow in the high flow domain a unit gravitational gradient is assumed, and the hydraulic conductivity, k_{hf} is given as (Stähli et al. 1996)

$$k_{hf} = k_w(\theta_{tot}) - k_w(\theta_{ice} + \theta_{lf}) \qquad (2)$$

where θ_{tot} = total water content (m^3 m^{-3})
θ_{ice} = ice content (m^3 m^{-3})
θ_{lf} = water content in the low flow domain.

One major point in this two-flow domain approach is that water which infiltrates to the previously air-filled pores may freeze, depending on the temperature of the soil. In this process the heat released when water is freezing in the high flow domain causes melting of ice in the fine pores of the low flow domain. So, in fact, infiltration causes a redistribution of liquid water from the high to the low flow domain, $q_{infreeze}$, computed as

$$q_{inf\,reeze} = \alpha_h \frac{T}{L_{ice}} \Delta z \qquad (3)$$

where α_h = heat transfer coefficient (W m^{-1} °C^{-1})
T = soil temperature (°C)
L_{ice} = latent heat of fusion (J m^{-3})
Δz = thickness of layer (m).

At the lower frost boundary, the hydraulic conductivity, k_{wf} is reduced in order to prohibit an extensive water redistribution towards the freezing front:

$$k_{wf} = 10^{-fc_iQ} k_w \qquad (4)$$

where fc_i = impedance factor (-)
Q = thermal quality, i.e. the mass ratio of frozen water to total amount of water (-)

Experimental set-up

Four small lysimeters (2 x 2 m, 1.4 m depth) were constructed at Uppsala (central Sweden) and identically instrumented (Fig. 2): TDR probes and thermocouples were placed at six different levels (10, 17, 25, 35, 50 and 70 cm) to monitor profiles of liquid soil water content and temperature. A tube was installed vertically for measuring the total water content (ice + liquid) with the neutron probe. The fluctuations of the groundwater level were monitored with pressure transducers and used as indications of capillary water transport toward the frost boundary, as well as for percolation after snowmelt. A standard climate station was located next to the plots. All measurements were conducted automatically with a data logger system, except for the neutron probe readings and the snow depth measurements that were made manually.

25
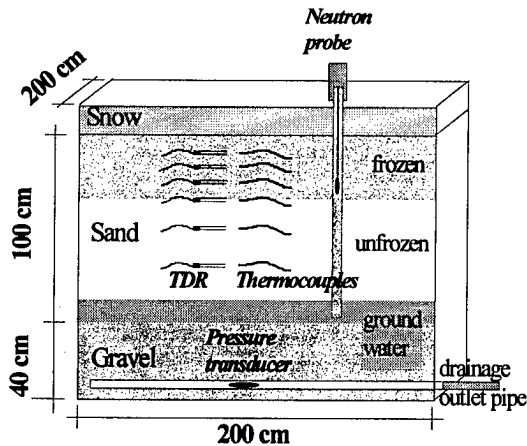
Figure 2. Sketch of the experimental set up for one of the small plots.

The soils used in this study were two different sands, one with a nearly uniform grain size of 0.06-0.2 mm (Baskarp), and one with a wider distribution including a clay content of 7% by weight (Nåntuna). The physical properties (Table 1) of these two soils were partly determined in situ (pF-curves, freezing point depression curve) and partly in a lab column (saturated hydraulic conductivity).

Table 1. Physical properties of the two soils.

	Baskarp	Nåntuna
Field saturation, θ_S	36 %$_v$	39 %$_v$
Air entry pressure, ψ_a	25 cm	4.2 cm
Pore size distribution index, λ	1.7	0.54
Wilting point, θ_{wilt}	4.0 %$_v$	1.5 %$_v$
Saturated hydraulic conductivity, k_S	0.01 cm min^{-1}	not determined

Model application

First, the model was roughly calibrated by adjusting the most sensitive parameters controlling the boundary conditions (snow, groundwater, lower thermal boundary). Then, a finer calibration was made by adjusting parameters which described the upwards flow to the lower frost boundary (eq. 4) and the freezing point depression curve. When a satisfying correspondence with the measurements had been achieved the sensitivity of the two parameters k_S and α_h was tested.

RESULTS

Measurements

In central Sweden, the winter 1995/96 was exceptional with respect to the climatic conditions (Fig. 3): low precipitation in combination with very low temperatures caused a deep and long lasting frost penetration. Only two short intermediate periods of thawing around 13 January and 28 February interrupted the frost from the end of November 1995 to the beginning of April 1996. Since the temperature in the first week of April raised to more than +10 °C, the final snowmelt was very rapid and occurred when the soil was still frozen at a depth of 20 to 80 cm.
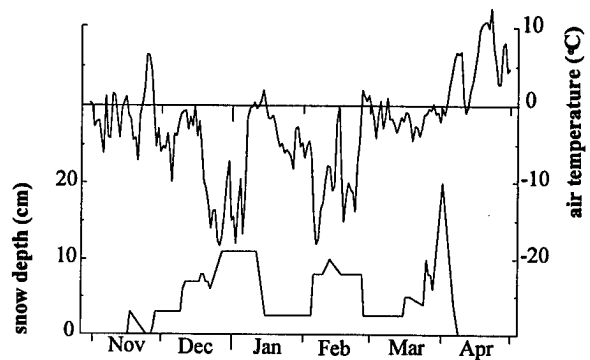
Figure 3. Air temperature and snow depth measured at the site (Nov. 1995 - April 1996).

Before freezing, the soils were well drained with a groundwater level between the 90- and 110-cm depth. The neutron probe and groundwater level measurements (Fig. 4) indicated steady capillary water transport towards the lower frost boundary until the end of February. Especially in the Baskarp sand, the water storage decreased considerably at 70-cm depth, and the groundwater level decreased correspondingly. This redistribution was facilitated by the properties of the soil and the low saturation in the upper part of the profiles. Effects of the two intermediate periods with above-zero temperatures were seen in the neutron probe measurements of the uppermost layer. No response to these two infiltration events was observed at the groundwater level, indicating that snow meltwater was entirely refreezing in the frost layer. In contrast, the final snowmelt caused a sudden response of the ground water level, almost one month before all frost had disappeared from the soils. This response was mainly due to the snowmelt infiltration and only in part due to melting of the frozen soil. An additional evidence for the water flow through the frozen soil was the rapid decrease of water content in the top of the profiles.

26
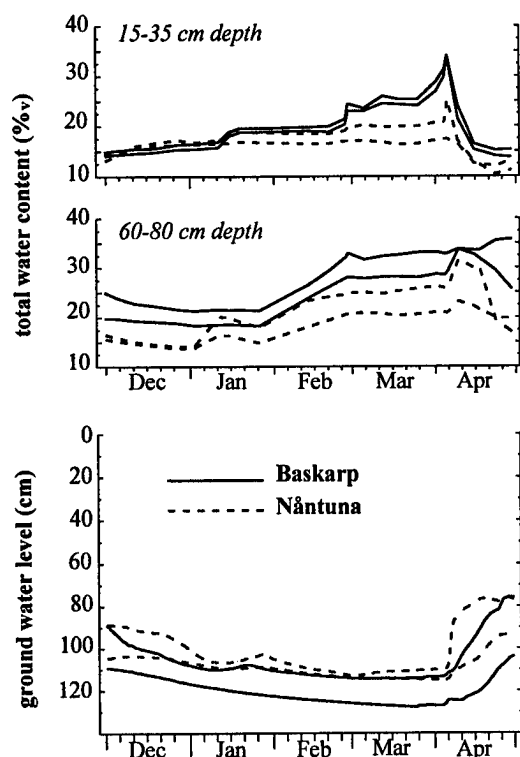
Figure 4. Groundwater level and total water content (10-30 cm, 40-60 cm) measured in the four small plots.

Whereas the two plots with Baskarp sand behaved similarly despite of slightly different initial conditions, the Nåntuna sand revealed considerable differences between the two plots. In the plot Nåntuna 1, the infiltrations were not reflected clearly in the neutron probe measurements of the topsoil. The reason for that was not obvious.

An attempt was made to quantify the water infiltrating during the three different melting periods (Table 2). The change of total water storage (ice and liquid) in the layers 0 to 20 cm and 20 to 40 cm was calculated from the neutron probe measurements. When comparing these results with the modeled infiltration rate, one should consider the significant uncertainty of the neutron probe method caused by the non uniform measurement volume and the difficulties with regard to the calibration procedure especially close to the soil surface.

In the Baskarp sand the amount of infiltrating snowmelt increased steadily from the first to the final infiltration. If we assume that all infiltrated water was

Table 2. Water budget at the soil surface

	dW_{tot}[1] 0-20 cm (mm) measured	dW_{tot}[1] 20-40 cm (mm) measured	surface infiltration (mm) simulated
Baskarp			
1st inf (13 Jan)	4	3	2
2nd inf (27Feb)	9	6	12
3rd inf (Apr)	13	18	41
Nåntuna			
1st inf (13 Jan)	5	1	
2nd inf (27 Feb)	2	1	
3rd inf (Apr)	7	5	

([1] dW_{tot} = change of total water storage)

refreezing in the top 40 cm, an assumption that might be a good approximation with regard to the solid soil frost, the measured water storage increase was comparable to the calculated infiltration (Table 2).

Regarding the second and third snow melt events, a clearly lower infiltration into the topsoil was measured in the Nåntuna sand. It can be speculated whether a part of the water ran off on the surface or penetrated to lower depths. In situ observations did not strengthen the assumption of extensive surface runoff.

Simulations

In the present article, only simulations for the Baskarp-sand are shown. The general correspondence of the simulated soil water and heat dynamics with the profile measurements was promising (Fig. 5). As an example, the root mean square error between simulated and measured soil temperature for the period January 1 to April 15 was 1.1 °C at 10 cm depth and 0.6 °C at 25-cm depth, and the coefficient of determination for the same period was around 0.7 at the same levels. To get this correspondence it was unconditionally necessary to establish the correct boundary conditions especially with regard to the heat. Obviously, the role of the snow cover was crucial, and this application confirmed - once again - that it is particularly delicate to model a thin snow cover of only a few centimeters.
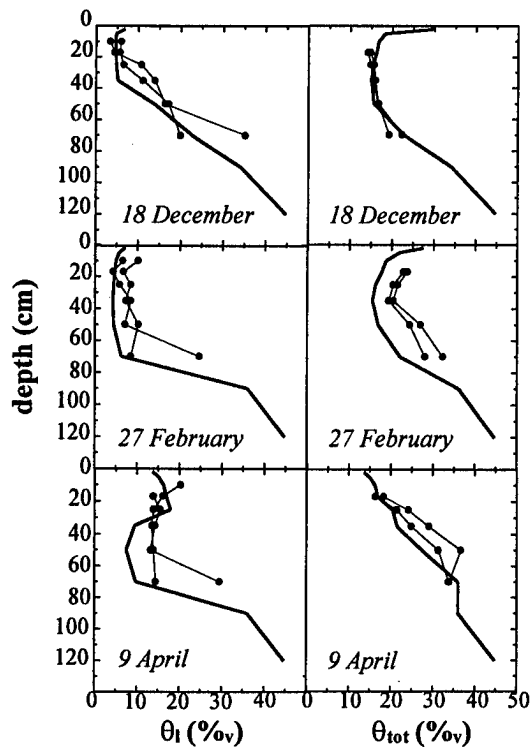
Figure 5. Depth profiles of liquid and total water contents at three stages of the winter (line: simulated; dots: measurements).

Figure 6. Sensitivity analysis of the heat transfer coefficient α_h (lines = simulation, dots = measurements).

Profiles of liquid and total water content are shown in figure 5 for an early, an intermediate and a late stage of the winter season. The soil moisture content at the start of freezing (18 December), which has been pointed out as a decisive factor for the infiltration later in the spring (e.g., Storey 1955), was very well represented by the model. Later in February, the model underestimated the total water content by approximately 5 %$_v$ in the uppermost 60 cm, which was probably caused by too slow of a capillary raise towards the freezing front. In that context, it should be mentioned that the impedance factor f_{ci} (eq. 4; in this study f_{ci} = 2) controlling the rate of upward water flow to the frost zone showed to be of minor sensitivity. This finding was in contrast to previous SOIL-model applications (e.g., Lundin 1990; Stadler et al. 1997) where a strong influence of f_{ci} on the total water content was concluded. The profiles of 9 April showed that the model succeeded to describe the water dynamics immediately after the final snowmelt. The water regime changed rapidly during these days inducing a complex combination of a raising ground water level, a still-existing ice body and infiltrating water. From the numerical point of view, these situations are the most difficult to handle.

A sensitivity analysis of the heat transfer coefficient α_h (eq. 3) was made where α_h was varied from 10 to 1000 W m^{-1} °C^{-1} (Fig. 6). The best agreement with measurements was achieved with α_h = 100 W m^{-1} °C^{-1}, especially what concerned infiltration in February. If a higher α_h-value was taken, the infiltrating snowmelt refroze entirely in the top 10 cm, which was not observed in reality. A lower α_h-value caused the snowmelt water to penetrated too deeply into the profile.

The sensitivity of the hydraulic conductivity was investigated as well. The default value of k_S = 0.01 cm min^{-1} was varied in a range from 0.1 k_S to 10 k_S. Liquid and total water content at 17-cm depth for the infiltration in February and April are shown in figure 7. Only minor differences resulted for the February period with respect both to the liquid and the total water content. But for the infiltration in April, changes in k_S exert a marked influence. With a small k_S, the water content increased too much in the uppermost layers followed by a delayed decrease. On the other hand, the infiltrating water passed the topsoil too rapidly when a large k_S-value was taken, and, thus, the water content was underestimated.

28
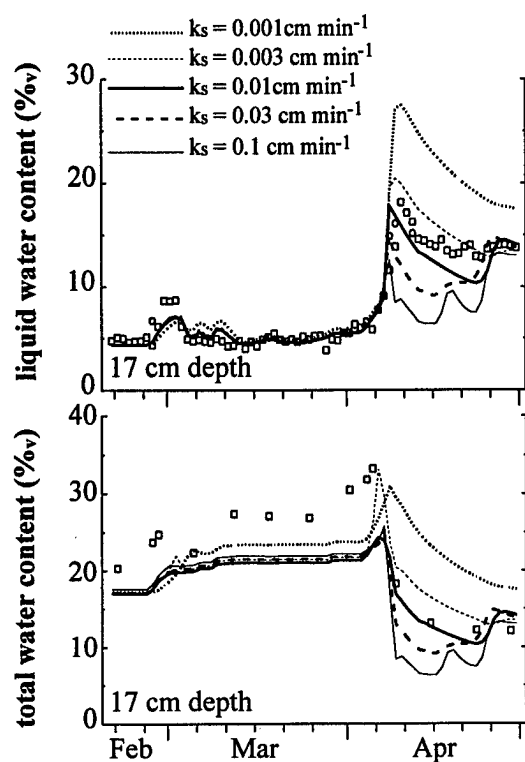
Figure 7. Sensitivity analysis of the saturated hydraulic conductivity k_S (lines = simulation, dots = measurements).

DISCUSSION AND CONCLUSIONS

The factors which control snowmelt infiltration into frozen soils have been identified in many earlier publications (e.g., Granger et al. 1984; Kane and Stein 1983; Johnsson and Lundin 1991). In principle, the mechanisms of infiltration are fairly well understood, and the difficulty due to the complex interaction between water and heat is recognized. However, the issue of quantifying the fluxes using mechanistic mathematical formulations and appropriate model structures has seldom been addressed. Possibly, this resulted from the lack of a suitable tool in combination with the few detailed data sets available. In this study we have tried to give a quantitative description of the mechanisms. It was demonstrated that a general agreement between model outputs and profile measurements was possible to obtain. However, limitations regarding the simulation of the water fluxes towards the lower frost boundary were discovered. The model performance for reproducing the three infiltration events of the winter was good with respect to the water budget in the topsoil. The two-flow domain model approach strongly depends on a reasonable estimation of the heat transfer coefficient a_h. For the Baskarp sand $a_h = 100$ W m^{-1} °C^{-1} gave the best fit.

Earlier studies by Stähli et al. (1996) and Stadler et al. (1997) confirmed this order of magnitude. It is obvious from eq. 3 that the soil temperature must be simulated very accurately to set appropriate values for a_h. In the present study this requirement was met: e.g., the deviations between measured and simulated soil temperatures at 17 cm averaged about 0.1 °C during the February infiltration (Stähli and Jansson 1996). In this context, the appropriate description of the freezing characteristic curve is crucial.

The model also showed a high sensitivity to the second essential parameter, k_S, especially during the final snowmelt event. It seems to be of a high priority to carry out in situ measurements of k_S and k_W (e.g., with the instantaneous profile method; Watson 1966) and to calibrate k_S for unfrozen conditions. Such site-specific data reduces the number of free parameters and will allow us to test the validity of the expression for the hydraulic conductivity in the high flow domain (eq. 2).

The simulations infer that no surface runoff occurred during the entire winter. Visual observations in situ confirmed this result. The main reasons were the very low saturation of the soil at the onset of freezing, the relatively low snowmelt rate and the zero-inclination of the surface. Future measurements on the small-plots with different boundary conditions will hopefully further improve our understanding of the infiltration behavior of the two sandy soils. The model, on the other side, allows us to extrapolate this knowledge to other soil types and to quantify the water fluxes.

REFERENCES

Jansson, P.-E. 1987. Simulated soil temperature and moisture at a clearcutting in central Sweden. Scand. J. For. Res. 2:127-140.

Jansson, P-E. 1996. Soil water and heat model. Technical description. Division of Agricultural Hydrotechnics. Internal report. Department of Soil Sciences, Swedish University of Agricultural Sciences, Uppsala.

Jansson, P.-E., and A. Gustafsson. 1987. Simulation of surface runoff and pipe discharge from an agricultural soil in northern Sweden. Nordic Hydrology. 18:151-166.

Granger, R. J., D.M. Gray, and G.E. Dyck. 1984. Snowmelt infiltration to frozen Prairie soils. Can. J. Earth Sci. 21:669-677.

Johnsson, H., and L.C. Lundin. 1991. Surface runoff and soil water percolation as affected by snow and soil frost. J. Hydrol. 122:141-159.

Kane, D.L., and J. Stein. 1983. Water movement into seasonally frozen soils. Water Resour. Res. 19:1547-1557.

Lundin, L.-C. 1990. Hydraulic properties in an operational model of frozen soil. J. Hydrol. 118:289-310.

Lundin, L.-C., and H. Johnsson. 1990. Modelling infiltration of snow melt water into frozen soils. p. 53-62. *in* G. Sigurdsson (ed.) Nordic Hydrologic Conference 1990, Kalmar, 29 July - 1 August 1990, NHP report no 26, Norrköping, Sweden.

Lundin, L.-C., M. Stähli, and P.-E. Jansson. 1996. A two domain theory for infiltration into a partially frozen soil. p. 321-330. *in* O. Sigurdsson, K. Einarsson, and H. Adalsteinsson (ed.) Nordic Hydrological Conference 1996, Akureyri, Iceland, 13-15 August 1996, vol. 1.

Mualem, Y. 1976. A new model for predicting the hydrologic conductivity of unsaturated porous media. Water Resour. Res. 12:513-522.

Richards, L.A. 1931. Capillary conduction of liquids in porous mediums. Physics. 1:318:333.

Stadler, D., H. Flühler, and P.-E. Jansson. 1997. Modelling snowmelt runoff from small forest plots with sloped, frozen soils. Submitted to Ecol. Model.

Stähli, M., P.-E. Jansson, and L.-C. Lundin. 1996. Preferential water flow in a frozen soil - a two-domain model approach. Hyd. Proc. 10:1305-1316.

Stähli, M. & P.-E. Jansson. 1996. Snowmelt infiltration into unsaturated frozen soil - a small plot study. p. 331-339. *in* O. Sigurdsson, K. Einarsson, and H. Adalsteinsson (ed.) Nordic Hydrological Conference 1996, Akureyri, Iceland, 13-15 August 1996, vol. 1.

Storey, H.C. 1955. Frozen soil and spring and winter floods. *In* Yearbook of Acriculture 1955. U.S. Dept. Agr., Washington, D.C.

Thunholm, B., L.-C. Lundin, and S. Lindell. 1989. Infiltration into a frozen heavy clay soil. Nordic Hydrology. 20:153-166.

Watson, K.K. 1966. An instantaneous profile method for determining the hydraulic conductivity of unsaturated porous materials. Water Resour. Res. 2:709-715.

Mechanics of Meltwater Movement
Above and Within Frozen Soil

J.M. BAKER[1] AND E.J.A. SPAANS[1]

ABSTRACT

The disposition of water that is released as snow melts in agricultural fields is of considerable importance with respect to flooding, solute transport, and recharge of soil moisture depleted during the previous growing season. We have made a broad range of measurements during the snowmelt season for several years at the University of Minnesota Agricultural Experiment Station in Rosemount, MN. In level portions of untilled fields the contribution of snowmelt to soil moisture recharge is generally small (less than 20% of overwinter liquid equivalent precipitation). Evaporation is also not a large sink for water from the snowpack; model estimates suggest it accounts for less than 20% of the overwinter precipitation. Most of the water released during snowmelt finds its way to low points within the field, resulting in the formation of large ephemeral ponds, which can form within a day to depths approaching 1 m. Infiltration is often almost as rapid, despite the presence of a frozen layer in the soil below.

Key words: snowmelt, infiltration, focused recharge, soil moisture.

INTRODUCTION

Late winter/early spring is a critical time of the hydrologic year in the Upper Midwest. Typically, nearly all of the precipitation that has fallen over the winter is still present in a snow and ice pack on the surface. As sun angle and daylength increase this pack begins to melt, but infiltration is inhibited by the diminished permeability of the frozen soil below.

This can result in runoff, which contributes to erosion, flooding, and contamination of surface waters with agricultural chemicals. Further, melt that does not infiltrate is not available to recharge soil moisture depleted during the previous growing season. Thus the disposition of water from the snowpack is of critical importance from both a hydrologic and agronomic standpoint.

MATERIALS AND METHODS

We have conducted detailed investigations of overwinter hydrometeorology for several years at the University of Minnesota Agricultural Experiment Station in Rosemount, MN, approximately 20 km south of St. Paul. The measurements are made in a 17 ha farm field, where the soil properties (texture, hydraulic conductivity, moisture retention, and albedo, among others) have been extensively characterized. At the scale of interest for typical erosion models, the field would be considered relatively level, and there is never off-site runoff. However, there is topographical variation within the field, with a maximum difference in elevation of approximately 3.5 m between the highest points in the field and the lowest points (Fig. 1). This terrain is typical of glacial outwash plains - level in a general sense, but

---

frequently punctuated with minor depressions in the landscape. The soils, Waukegan silt loam(fine-silty over sandy, mixed, mesic, Typic Hapludolls) in the upland areas interspersed with closely related Kennebec silt loam (fine-silty, mixed, Cumulic Hapludolls) in the depressions, are permeable when not frozen, and runoff during the growing season is rare.

During spring thaw, the situation is more complicated. We have made extensive measurements in an attempt to understand the processes involved. Soil water content is measured hourly at multiple depths at two sites, in an upland area and in one of the depressions, using automated, multiplexed time-domain reflectometry (TDR) systems (Baker and Allmaras, 1990; Spaans and Baker, 1996). When ice is present, the measured TDR travel time is primarily determined by the amount of liquid water. Under such conditions the TDR readings are used to compute liquid water content with a specific calibration developed by Spaans and Baker (1995). Soil temperature is measured at the same points using precision, individually calibrated thermistors.

Meteorological data are collected from a permanent mast in the center of the field, where fetch exceeds 180 m in all directions. These include temperature and humidity at 2 m, wind speed at four heights, incoming and reflected solar radiation, incoming and outgoing longwave radiation, infrared surface temperature, and snow depth, which is measured remotely with an ultrasonic proximity sensor suspended above the surface. This measurement is also made at the center of the depression, doubling as a measurement of pond depth following snowmelt. Precipitation is measured at a nearby point in the field where both a weighing gauge and a heated tipping bucket are installed within a Wyoming-type shield. Manual measurements made approximately weekly include snow density, total soil water by neutron moderation (measured both in the depression and in an upland location), and snow depth at multiple points by visual observation.

Data are reported from three consecutive winters: 1993-94, 1994-95, and 1995-96. In the first winter,

the previous crop had been maize, and the field was chisel-plowed and disked following harvest. In 1994, following soybeans, the field was only lightly cultivated with a tandem disk. In 1995 alfalfa was planted in August following an oats crop, so there was no fall tillage. The three winters provide a cross section of sorts; 1993-94 was much colder and snowier than average (Table 1), 1994-95 was much warmer than average with very little snow, and 1995-96 was near normal in both respects.

RESULTS & DISCUSSION

Table 2 shows the overwinter change in soil water content in the upland portion of the field for each year, derived from neutron probe measurements. The changes are only a fraction of the precipitation received during the period and retained in the snowpack prior to melt. Superficially, the reason for this is that during snowmelt, much of the water that is released flows to the depressions, where it ponds initially before ultimately infiltrating.

These ponds are a common feature of the landscape in the upper Midwest for a brief period each spring. They can be quite large (1 ha or more) and surprisingly deep (some we have measured at the Rosemount Experiment Station approach 1 m), but they are also quite ephemeral, sometimes disappearing as rapidly as they form. Figure 2 shows plots of pond depth for all three years for the depression shown in the southwest corner of the field shown in Figure 1. As mentioned earlier, these three winters were very different, and soil surface conditions were different in each year as well. Under the circumstances, it is remarkable that the three plots are so similar. Even more remarkably, TDR data and soil temperature measurements clearly show that in the first two cases, the soil beneath the pond still contained a substantial layer of frozen soil at the time the pond disappeared, and indeed did not completely thaw for several more weeks. In 1996, the last indications of ice in the soil disappeared on the same day that the pond did, but the profile still clearly contained ice during much of the infiltration.

32

Table 1. Summary of weather for the winters of 1993-94, 1994-95, and 1995-96. Numbers in parentheses are departures from normal, where normals are 20 year averages.

Month	1993-94		1994-95		1995-96	
	mean temp, °C	snowfall, mm	mean temp, °C	snowfall, mm	mean temp, °C	snowfall, mm
November	-0.8 (-1.4)	196	+3.3 (+2.7)	157	-2.6 (-3.2)	168
December	-5.4 (+2.4)	114	-4.2 (+3.7)	165	-7.2 (+0.7)	409
January	-15.3 (-4.1)	617	-7.5 (+3.7)	107	-12.1 (-0.9)	368
February	-10.4 (-2.6)	305	-7.1 (+0.8)	53	-7.8 (+0.6)	30
Season	-8.0 (-1.4)	1232 (+330)	-3.9 (+2.7)	482 (-420)	-7.4 (-0.9)	975 (+70)
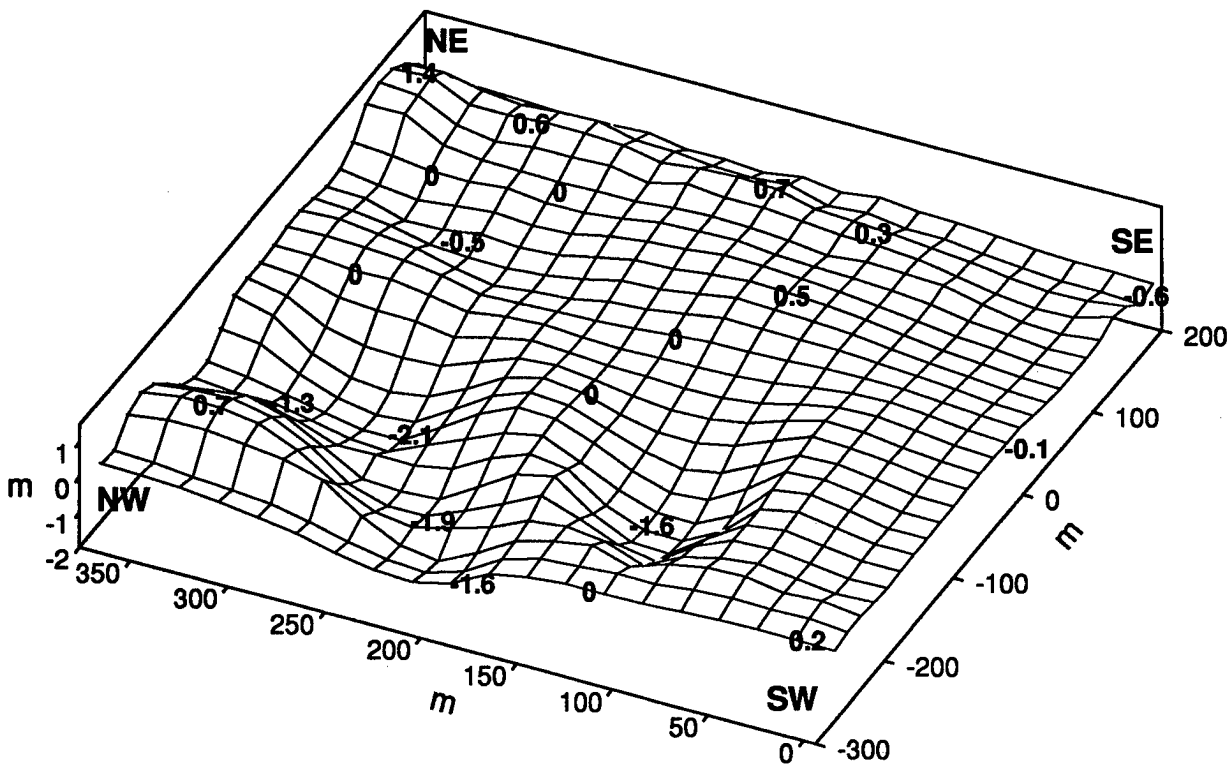
Figure 1. Topographic map of the experimental site at Rosemount, MN. Dimensions are in m, as are the point elevations, which are referenced to the elevation of the center of the field where the instrument mast is located.

Table 2. Changes in soil water content of the root zone (0.1 to 1.1 m depth) over winter, computed from neutron probe readings made just before the soil profile began freezing and just after all snow has melted.

Year	start date	end date	precip, mm (LWE)	Δ soil water, mm	recharge efficiency, %
1993-94	Dec. 2	Mar. 14	64	10.1	15.9
1994-95	Nov. 30	Mar. 17	48	16.6	34.6
1995-96	Dec. 1	Mar. 19	87	22	25.3

Precipitation totals represent liquid water equivalent precipitation measured between the two dates. Recharge efficiency is the change in soil water divided by the precipitation in the period, multiplied by 100.
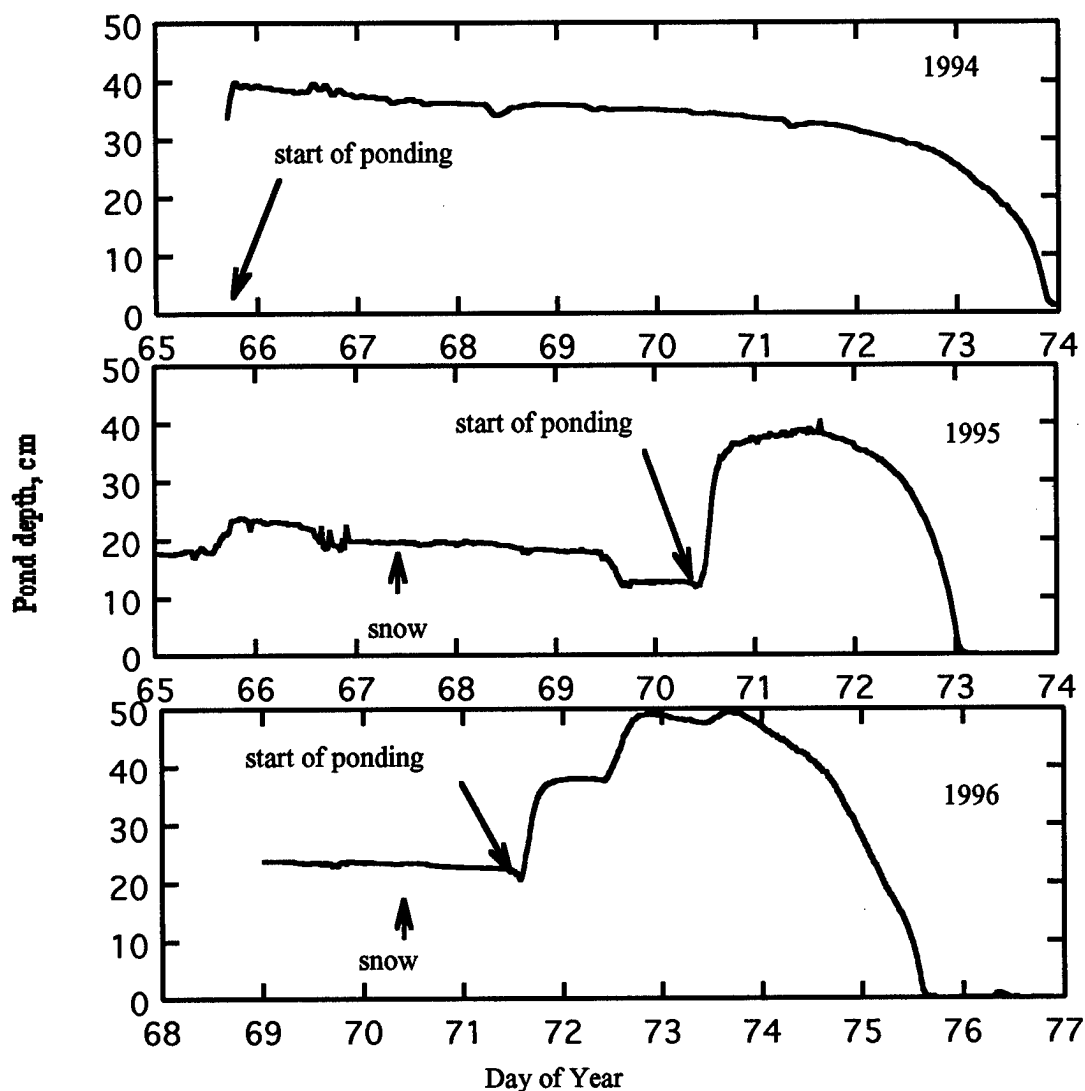
Figure 2. Depth of ponding as a function of time following spring snowmelt. A. Spring 1994. B. Spring 1995. C. Spring 1996.

Infiltration rates calculated from changes in pond depth and knowledge of the basin topography reveal maximum infiltration rates in each case approaching the measured saturated hydraulic conductivity of the soil (~0.3 m day^{-1}), despite the persistent presence of a frozen soil layer 20-40 cm thick.

Two questions present themselves:
1. Why is initial infiltration of snowmelt sufficiently inhibited to cause runoff and ponding?
2. How does the ponded water subsequently infiltrate so rapidly if the soil profile is not completely thawed?

Initial snowmelt infiltration

The ensuing discussion assumes that the soil profile beneath the snowpack is frozen at the time spring snowmelt begins, which is typically the case in Minnesota. When the snowpack begins to melt, the released water, at a temperature of 0 °C, percolates downward. As it comes in contact with matter at lower temperature it will release heat by refreezing. The heat released during refreezing must either be consumed in downward conduction to the colder soil below, conduction upward toward a cooling surface (as occurs when the sun goes down), or in increasing the heat content (temperature) locally.

If the transport of heat by the percolating water to the zone of refreezing is matched by heat transport away from it, ice will accumulate. If delivery slows relative to heat removal then freezing will proceed upward; conversely if the balance is shifted by an increase in convective heat transfer (and/or conduction) from above or a decrease in downward transport away from the freezing zone then there must be some combination of remelting, downward water movement, and/or lateral water movement to bring the system back to balance. If the delivery of heat to the frozen zone so far exceeds transport away from it that all ice melts, then infiltration of meltwater continues downward until either a new equilibrium between regelation and heat flow is established, all water is absorbed or transported

through the profile (cessation of latent heat supply), or the soil is completely unfrozen (cessation of latent heat consumption).

What we have observed in the upland areas of agricultural fields during the initial stage of snowmelt is the formation of ice or ice-rich layers at or near the soil surface. This dramatically reduces infiltrability so that as the snow continues to melt, at least a portion of the additional water travels laterally toward depressional areas, where it accumulates. The lensing is generally very thin (on the order of 1 mm), but it doesn't require a very thick layer of ice or frozen saturated soil to induce lateral flow of meltwater.

Pond infiltration

After pond formation subsequent heat, supplied primarily by solar radiation, causes thawing of the upper boundary of the frozen soil and downward movement of the zone of regelation. Since the profile was initially unsaturated, this infiltration and ice formation takes place in the larger (previously air-filled) pores. Eventually a point is reached when conduction away from the freezing front is no longer sufficient to sustain new ice formation, so these larger pores transport water into the unfrozen subsoil below. In 1994 this occurred nearly a week after pond formation, because the weather following initial snowmelt became cold and cloudy for several days before a return of warm weather and higher net radiation occurred. In the other two years, sustained warm, sunny weather during and following snowmelt caused the ponds to disappear as rapidly as they formed.

In two of the three years this drained the pond without thawing the soil; evidently there can be local thermal disequilibrium. That is, large, water-transmitting pores and cracks are (or become) temporarily water-filled but ice-free while the smaller pores within peds remain frozen, and hence at a lower temperature. Even more remarkably, this situation can persist for many hours while an entire pond drains.

CONCLUSIONS

We conclude that runoff of snowmelt is a common and nearly inevitable occurrence if the soil beneath is initially frozen. The melt is the water source, and the frozen soil below is the heat sink for the lens formation that creates the impeding layer of runoff-inducing ice. The infiltration of the ponds that are thus formed in depressions within each field depends on further heat input, but thawing of the entire profile is not a prerequisite. Rapid infiltration can occur prior to the disappearance of ice from the soil, but the mechanisms involved remain a matter of conjecture.

REFERENCES

Baker, J.M., and R.R. Allmaras. 1990. System for automating and multiplexing soil moisture measurement by time-domain reflectometry. Soil Sci. Soc. Am. J. 54:1-6.

Spaans, E.J.A., and J.M. Baker. 1995. Examining the use of time domain reflectometry for liquid water content measurement in frozen soil. Water Resour. Res. 31:2917-2925

Spaans, E.J.A., and J.M. Baker. 1996. The soil freezing characteristic: Its measurement and similarity to the soil moisture characteristic. Soil Sci Soc. Am. J.60:13-19.

Some Details of the Ice Lens Formation Mechanism at the Bottom of a Seasonally Freezing Layer in a Permafrost Zone

S.E. GRECHISHCHEV[1] AND O.V. GRECHISHCHEVA[1]

ABSTRACT

A one-dimensional physico-chemical mathematical model of ice lens growth at the bottom of seasonally thawing layer (STL) in a permafrost area is proposed and used. The new details of ice lens formation mechanism are discussed. Conditions of ice lens growth in the STL inside and near the ground dams and their stability are considered for climate and geotechnical conditions of Yamal Peninsula.

Key words: Ice lens, mathematical model, seasonally thawing layer, permafrost, embankments.

Physical processes in freezing - thawing of silty soils in a seasonally thawing layer (the STL) can result in formation of subsoil ice layers. The type of ice formation due to freezing from above in the winter is called seasonal heaving. There is also the freezing of the STL from below, which under certain conditions causes formation and then long-term growth of an ice interlayer or layer of a higher icecontent on a bottom of the STL (long-term heaving) - on top of upper boundary of permafrost. This layer has received the name "transitive." The transitive layer for the first time was identified by V.K.Yanovskyi, and its geosystematical importance was established and investigated by (Shur 1989). Due to its high icecontent, it performs a thermal "protection" of cryogenic geosystems.

The transitive layer can be formed on slopes and in embankments (see Fig.1a). In this case, except for general long-term heaving, there is the danger of loss of stability of soils on slopes or on slopes of an embankments in the case of the approach of a summer with anomalously high thawing of soils, which can form an ice interlayer. Then the surface of sliding will look as shown on Figure 1b. The cohesion on this
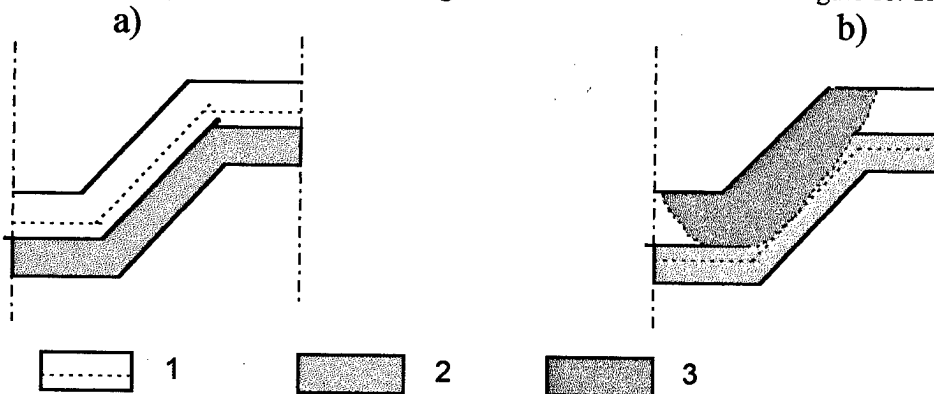
Figure 1. Sheme of growth of an ice interlayer - "transitive" layer (a) and possible destruction (b) of embankment and its soil basis: 1 - bottom of STL - top border of a frozen ground, 2 - longterm-growing an interlayer of ice, 3 - sliding block of a slope.

[1] Moscow Department, Institute of Earth Cryosphere, Vavilov Street 30/6, Room 85, Moscow 117982, Russia

surface, where it passes a thawing interlayer, will be practically equal to zero, and pore pressure will be increased. That is, the STL begins as though it is "floating" on spreading surface. To it, in particular, occur such phenomena as slide-flows, which with a certain periodicity cover large areas on slopes of Yamal and Ghydan Peninsulas. Their movement occurs on very flat slopes (1-1.5 degree).

It is of interest to study this phenomenon with help of mathematical modeling. It can allow us to realize some new theories of the functioning of cryogenic geosystems, and also essentially to add to geotechnical accounts of stability of slopes and embankments in the North by the forecast of high ice-content "transitive" layer growth.

It is known that in soil the interlayers of segregated ice will be formed due to cryogenic migration of moisture to a freezing front. The following equations of a water freezing kinetics in large and thin pores on freezing front were obtained (Grechishchev at al. 1980, 1984)

$$\dot{m}_i = R \cdot \left[\frac{L \cdot (T_0 - T_B)}{T_0} - \Delta v \cdot (p_B - p_a) \right] , \qquad (1)$$

$$\dot{m}_s = BR \cdot \left[\frac{L \cdot (T_0 - T_B)}{T_0} - \Delta v \cdot (p_B - p_a) - v_i \cdot \sigma_B^{ef} \right], (2)$$

$$\Delta v = v_i - v_w , \qquad (3)$$

where $\dot{m}_s$ and $\dot{m}_i$ = speed of a water freezing in
        thin and large pores accordingly (kg/m²s)
L = heat of phase transition of water in (J/kg);
T_0 = temperature of phase balance of ice with
        water at atmospheric pressure (K);
B = empirical kinetic factor (dimensionless);
R = empirical kinetic factor (kg²/m² s J);

T_B = temperature of a freezing front, (K);
σ_B^{ef} = effective stress in skeleton of a thawed
        soil on a freezing front (Pa);
p_B = pore pressure on freezing front (Pa);
p_a = atmospheric pressure (Pa).

Expressions (1) and (2) show that speeds of a water freezing and condition of its thermodynamic equilibrium on a freezing front in pores of the different size are nonsimilar. Therefore, if in large pores already ice was formed and there filtration has stopped, at the same time the thin pores remain not frozen, and through them a flow of water is possible, its freezing is described by expression (2). According to this expression, the freezing of a water flow through thin pores (if those exist) is controlled by temperature, pore pressure and effective stress in soil skeleton normaly to the freezing front surface. For example, the increase of stress in the skeleton, as it follows from equation (2), is capable of actually stopping freezing in thin pores. Then the freezing of a soil will occur only in large pores according to equation (1), and the formation of a cryogenic flow of water becomes impossible since its freezing stops.

Kinetic factors B and R are determined by practical consideration and, irrespective of soil, are constants.

Equations (1) and (2) determine driving forces of cryogenic migration of a moisture. They are mainly described below, at a one-dimensional mathematical model of formation and growth of an ice interlayer when the STL freezes from below.

Initial moment of time τ is τ_s - end of a summer or beginning of autemn -winter period. At this moment the STL is maximum and equal - H_{th} .
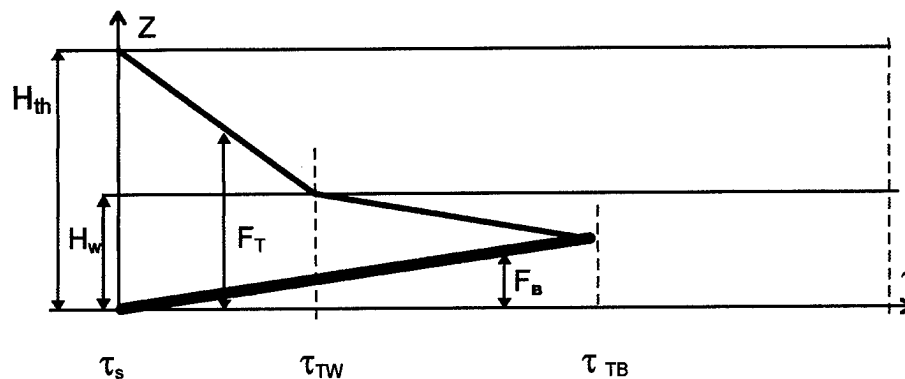
Figure 2. Schematic structure of one-dimensional area of model

Directed upwards coordinate Z will be counted from the STL bottom. In the bottom part the STL a zone of a water-saturated soil is allocated by thickness H_w. The soils, laying above this zone, are sapposed to be water-unsaturated. The STL freezing occurs from above (coordinate of the bottom of upper frozen layer - F_T) and from below (coordinate of the top surface of lower frozen layer -F_B). Characteristic moments of time: are τ_{TW} - contact of the top freezing with top surface of a water-saturated zone, and τ_{TB} - complete freezing a STL.

At this model the following simplifications are entroduced:

• Independence of a temperature field on mass-exchange in unfrozen soil;
• Quasi-stationary distribution of temperature inside layers which are freezing from above and from below;
• Undeformability of unfrozen soils of the STL (as the external loads are away, and the seasonal cycles of a freezing and thawing were carried out already as a minimum 2 -3 times and STL soils are consolidated under the own weight) and, as a consequence, quasi stationary of pore pressure distribution in unfrozen soil;
• Linear approximation of the unfrozen water content dependence on frozen soil temperature.

The system of equations of model consists of equations expressing (a) heat balance, (b) mass balance, (c) equilibrium, (d) continuity, and (e) physical conditions.

Initial temperature of the STL is equal to 0 °C.

The freezing from below occurs due to action of a cold flow from permafrost, which is expressed by a following equation:

$$q_t(\tau) = \frac{t_0 \cdot \sqrt{\lambda_{f2} \cdot C_{f2}}}{\sqrt{\tau \cdot \pi}} \cdot \left(1 + \frac{0.6 \cdot H_{th}\sqrt{C_{f2}}}{\sqrt{\lambda_{f2} \cdot \tau_s}}\right) \quad , \quad (4)$$

$$\tau \geq \tau_s \quad ,$$

where q_t = thermal flow;
t_0, λ_{f2} and C_{f2} = temperature, factors of a heat conductivity and heat capacity of spreading permafrost;
τ = time.

The equation (4), according to A.V.Pavlov (1975), is in good accordance to a naturel data in period of autumn-winter freezing of STL.

Freezing the STL from above occurs under action of cooling of a surface, occurring a constant speed in average, that results in following linear dependence of a freezing depth on time

$$F_T(\tau) = H_{th} - (\tau - \tau_s) \cdot \sqrt{\frac{\overline{\lambda} \cdot \dot{T}_s}{\overline{Q}}} \quad , \quad (5)$$

wher $\overline{\lambda}$, $\overline{Q}$ = factor of a heat conductivity and latent heat of phase transitions on the average for frozen from upper parts;

$\dot{T}_s$ = average speed of soil surface temperature decreasing in theperiod of autumn-winter freezing of STL, °C/s , which is pozitive.

Moisture balance on surface of a lower freezing front of STL:

$$q_w = (w_0 - w_u) \cdot \dot{m}_s - \left(1 - \frac{v_w}{v_i}\right) \cdot w_u \cdot \dot{m}_i, \quad (6)$$

$$q_w \geq 0 \quad ,$$

where q_w = moisture flow to freezing front (or speed of a heaving of the STL from below);

w_0 = initial moisture content ;

w_u = unfrozen water content.

Equation (6) expresses the fact that the whole moisture flow, moving from the STL to border of the bottom freezing through thin pores, will transform to ice minus the flow of opposite direction, which will be formed due to expansion of freezing water in large pores.

The unfrozen water contents:

$$W_u = \begin{cases} W_0 \cdot \left(1 - \frac{\Delta T_{ef}}{\Delta t_{cr}}\right) & , \quad \Delta T_{ef} < \Delta t_{cr} \quad , \quad (7) \\ 0 & , \quad \Delta T_{ef} \geq \Delta t_{cr} \quad , \end{cases}$$

$$\Delta T_{ef} = (T_0 - T_B) - T_0 \cdot \frac{\Delta v \cdot (P_B - P_a)}{L} \quad , \quad (8)$$

$$\Delta T_{ef} \geq 0 \quad ,$$

where Δt_{cr} = fixed temperature of a complete freezing of unfrozen water (is taken with "plus", °C) it is nominated on the basis of linear approximation of an initial part of unfrozen water curve, received experimentally, or very approximately from Table 1, made on the basis of published data.

Table 1. Δt_{cr} for some soils.

Soil type	Δt_{cr}
Sand	0,003 ÷ 0,3
Silt	0,2 ÷ 1,2
Loam	0,8 ÷ 2,0
Clay	1,5 ÷ 3,5

The equation (7) is a linear approximation of dependence of the unfrozen moisture contents on temperature.

The conditions of mechanical equallibrium are expressed by the following equations:

$$\sigma_B^{ef} + p_B = p_a + \overline{p} \cdot g \cdot H_{th} , \qquad (9)$$

$$p_{Hw} = \begin{cases} p_a , & F_T > H_w , \\ p_a + \overline{p}_f \cdot g \cdot (H_{th} - F_T) , & F_T < H_w , \end{cases} \qquad (10)$$

where $\overline{p}$, $\overline{p}_f$ = average of soil density for the whole STL and for its frozen part accordingly;

p_{Hw} = pore pressure on top border of a water-saturated layer.

Equation (9) expresses the fact that the complete vertical stress on surface of a freezing from below consists of atmospheric pressure and weight of upper material. Expression (10) states, that pressure from above on pore moisture in the unfrozen part of a water-saturated layer is equal to atmospheric pressure so long as the freezing from above has not reached surface of a water-saturated zone. After that the pore pressure becomes equal to the sum of an atmospheric pressure and a weight of the upper frozen part of soil. The occurrence of such a cryogenic pressure head proves to be true by direct natural scaled measurements (see Fig.3).

H, m
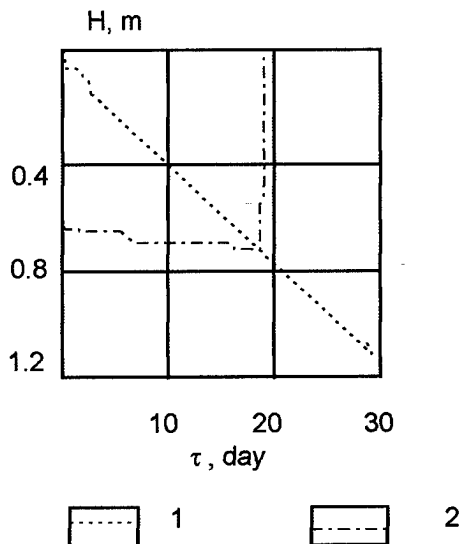
Figure 3. Change of piezometer level of soil water for the period of a freezing of STL (v.Amderma).
1 = lower boundary of a soil freezing, 2 = level of water in piezometer, H = depth from surface, τ = time from beginning of a soil freezing from above.

Conditions of balance (9) and (10) together with (2) permit an important peculiarity of segregated ice growth on the STL bottom. They mean that at the beginning of an autumn freezing the whole load from they own weight of the STL on the bottom is on the soil skeleton and according to equation (2) speed of a STL heaving q_s from freezing from below approximately proportional to the following expression:

$$q_s \sim \frac{L \cdot (T_0 - T_B)}{T_0} - v_i \cdot \overline{p} \cdot g \cdot H_{th} . \qquad (11)$$

After that, as the freezing from above will reach a water-saturated zone of the STL, the speed of a heaving becomes approximately proportional to another expression

$$q_s \sim \frac{L \cdot (T_0 - T_B)}{T_0} - (v_i - v_w) \cdot \overline{p} \cdot g \cdot H_{th} . \qquad (12)$$

As v_i more than 10 time exceeds a difference $(v_i - v_w)$, then comparison of last two expressions shows, that after close of the top freezing with water-saturated zone the opportunity of an ice segregation in transitive layer sharply increases.

The estimated accounts on developed model were carried out for climatic and soil conditions of Central Yamal. Permafrost conditions and the properties of soils were set approximately. Water-saturation of STL was varied. As a first approach, results of one-dimensional acounts to slopes and embankment are used, as their watersaturation greatly varies from above to downwards.

Estimated accounts (about 40 numerical experiments) permit allocation of the following peculiarities of ice-segregation in transitive layer.

Ice interlayers in sand are not formed. Maximum icesegregation is in silts and loams, wich coincides to well known natural scaled data.

The lower (~ 0,5 W/m²) and upper (~ 40 W/m²) limits of a thermal flow downwards,which are critical on condition of growth of ice interlayers on bottom of STL exist. It is obvious that a thermal flow less than ~ 0,5 W/m² has no sufficient capacity for lifting of weight of STL. At thermal flow greater 40 W /m², the freezing goes with too large speed, and the filtration has no time to give an appreciable contribution to ice saturating. Usual thermal flow downwards in natural conditions varies from 1,5 up to 3,5 W/m².

In the majority of cases, growth of segregated ice lenss on the bottom of the STL begins after close of the top freezing with surface of water-saturated part of the STL. There is the critical thickness of a water - saturated layer equal about 20-25 cm, at which (and smaller) this layer freezes from below earlier, than it is reached with a freezing from above consequently it

40

does not give the contribution in ice segregation for reasons mentioned above.

The usual thickness of an annual ice-segregation in transitive layer in silt and loam could be equal to the first millimeters (up to one centimeter).

For climatic conditions of central Yamal and local soils, which can be used for embankments, the formation of ice interlayers in the top part of an embankment is impossible. However at the lower parts of slopes of embankments, especially in bottom part with increase of moisture, and silt and clay contents in soils (practically for all Yamal silts and loams), there is the probability of formation and growth of ice interlayers.

There is a problem of the danger of ice in soil interlayers, if they are formed. The stability of embankments made from local materials requires decisions questions on thickness and site of interlayers, about opportunity of their long-term growth and about statistical distribution of warm / cold and damp / dry summers.

REFERENCE

S.E.Grechishchev, L.V.Chistotinov, Yu.L.Shur. 1980. Cryogenic physico- geological processes and their forecast . Ed. Nedra, Moscow, Russia.

S.E.Grechishchev, L.V.Chistotinov, Yu.L.Shur. 1984. Fundamentals of modeling of cryogenic physico - geological processes. Ed. Nauka , Moscow, Russia.

A.V.Pavlov. 1975. Heat Exchange of ground with atmosphere in northern and moderate latitudes of territory USSR. Yakutiya edition., Yakutsk, Russia.

Yu.L.Shur. 1989. Thermokarst and structure of the top horizons of frozen soils. Ed. Nauka, Moscow, Russia.

Elevation and Latitude Impacts on
Soil Temperature and Duration and
Distribution of Frost and Snowfall in Colorado

J.G. DAVIS[1]

ABSTRACT

The Colorado Climate Center operates a network of 150 weather stations scattered throughout the state of Colorado (USA). The stations have been operating for up to a five-year period, and data from each location from 1992-1995 was utilized. Elevation had a much greater impact than latitude or longitude on soil temperature and freezing and snowfall parameters within the state of Colorado. Regression of soil temperature with air temperature was significant at each location; however, the regression equations varied from site to site. The first fall frost was more strongly correlated with both the length of the frost-free period and the number of thaws (in both spring and fall) than was the last spring frost. The first fall frost is an important variable because, if it arrives early, yield quality can be damaged. The number of thaw cycles was greater in the spring than in the fall at all elevations. The freezing and thawing action in the spring can have a significant effect on crop stand establishment and winter hardiness of perennials.

Key words: Elevation, latitude, longitude, frost, snow

INTRODUCTION

Wide climatic variations occur within short distances in Colorado (Berry 1977). For example, the difference in annual average temperature between Pike's Peak and Las Animas (150 km apart) is approximately the same as that between Iceland and southern Florida. Average annual snowfall varies from nearly 750 cm at Cumbres Pass to less than 63 cm at Manassa in only a 50 km distance. Elevation ranges from 1021 m to 4399 m in Colorado. Forty-three percent of the land area of the state is at elevations less than 1800 m, 44 % ranges from 1800-3000 m, and 12 % lies at elevations greater than 3000 m (Siemer 1977).

In general, temperature declines and precipitation increases with increasing elevation; however, slope orientation, wind direction, and local air movements modify this general trend to create increased variability (Berry 1977). Air temperature generally declines 2 C for every 300 m elevation increase; however, air temperatures in Colorado are determined primarily by solar radiation (Siemer 1977). Precipitation and snowfall usually increase with elevation, but this is not always the case. For example, in the eastern plains, precipitation increases towards the east although the elevation declines. In addition, the percentage of precipitation due to snowfall tends to increase with elevation.

Soil temperature has been monitored at depths down to 3 m in Fort Collins, Colorado, since 1890 (Doesken 1996). Near the soil surface, soil temperatures follow air temperatures quite closely. As depths increase, soil temperature lags behind air temperature changes, and the annual range of soil temperatures diminishes. At 0.6 m deep, the seasonal cycle lags behind the surface by two to three weeks, but at 3 m deep, the temperatures lag by nearly three months of the surface temperatures. The greater the depth, the less temperature change on a daily basis. In addition, snowcover moderates the fluxes in soil temperature (Doesken 1996). When there is no snowcover, frost penetrates deepest.

---

[1] Department of Soil and Crop Sciences, Colorado State University, Fort Collins, Colorado 80523-1170, USA

The objective of this study was to evaluate the influence of latitude, longitude, and elevation on frost dates, length of frost-free period, the number of thaw cycles in the spring and fall, number of snowfall events, days of snow cover, and soil temperature in Colorado. Prediction of soil temperature from air temperature at varying elevations, latitudes, and longitudes was explored. These relationships will be used to draw conclusions regarding predictability of freezing temperatures and implications for crop management.

METHODS

Data from 150 weather stations across the state of Colorado were collated from years 1992-1995 for use in this study (see website for the Colorado Climate Center at http://www.nstl.gov/frozen). Latitude, longitude, and elevation was noted for each weather station (range is given in Table 1). Minimum soil temperature was measured at 5 cm deep in 1995 at three of the 150 locations.

The date of the last spring frost (air temperature ≤ 0 C) and the first fall frost were determined and utilized to calculate the length of the frost-free period. The number of spring thaw cycles (periods with air T > 0 C from 1st January to the last spring frost) were counted as were the number of fall freeze-thaw cycles (periods with air T > 0 C from the first fall frost to 31st December). In addition, the number of snowfall events were counted and grouped as spring (before last spring frost), summer (during frost-free period), and fall (after first fall frost); everyday with snowfall was considered a snowfall event. The days of snow cover were also counted and grouped into spring, summer, and fall snow cover.

All measured variables were correlated (Pearson correlation) with latitude, longitude, and elevation and correlated with one another. Elevations were divided into five categories (<1433 m, 1433-1961 m, 1962-2133 m, 2134-2484 m, > 2484 m) for determination of trends; each category has approximately 100 data points.

RESULTS

All of the measured variables were correlated with elevation at the p<0.01 significance level (Table 2). The large numbers of data points increases the potential for significant correlation. The correlation coefficients were highest with elevation as compared

with latitude and longitude in every case. The highest correlation coefficients were for the date of the first fall frost and the length of the frost-free period as related to elevation. The date of the first fall frost, the number of spring thaw cycles, the number of spring snowfall events and days of spring snow cover, and the number of fall snowfall events and days of fall snow cover were significantly correlated with both latitude and longitude as well as elevation. Latitude was related to the number of fall thaw cycles, and longitude was related to the last spring frost and the length of the frost-free period, the number of summer snowfall events, and the days of summer snow cover.

As elevation increased, the date of the last spring frost became later, the date of the first fall frost became earlier, and the length of the frost-free period declined (Fig. 1). At the highest elevation, the average frost-free period was only 44 days. The number of thaw cycles in both spring and fall declined with increasing elevation up to 2134 m and then increased with elevation (Fig. 2). There were more thaw cycles in the spring than in the fall at all elevations. The number of snowfall events increased with elevation whether in the spring, summer, or fall (Fig. 3). The days of snow cover also increased with elevation regardless of season (Fig. 4). At any elevation range, there were more snowfall events and days of snow cover in the spring than in summer or fall. The fall had more days of snow cover than the summer, but the number of snows (including hail) was higher in the summer than the fall in three out of five of the elevation groupings.
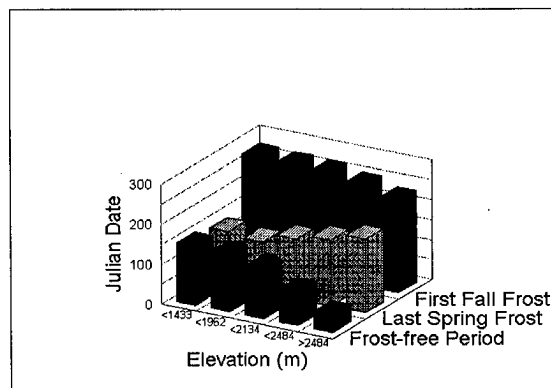
Figure 1. Impact of elevation on frost dates and length of the frost-free period.
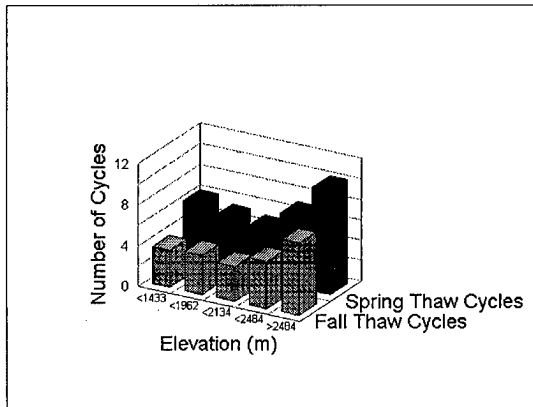
Figure 2. Number of thaw cycles as a function of elevation.
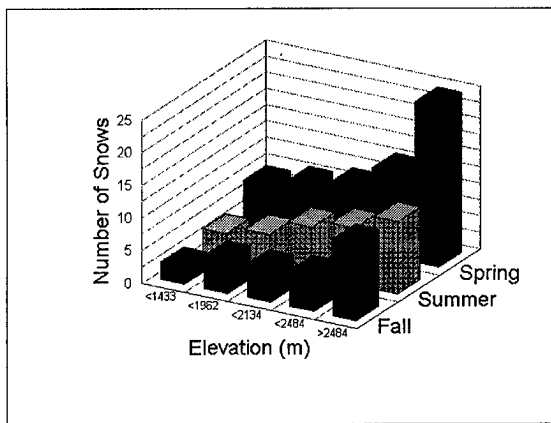
Figure 3. Number of snowfall events as a function of elevation.
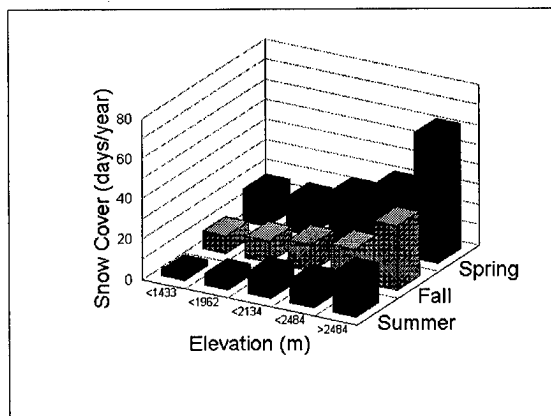
Figure 4. Impact of elevation on the days of snow cover.

The date of the first fall frost was much more strongly correlated (r = 0.91) with the length of the frost-free period than the date of the last spring frost (r = -0.32) was (Table 3a). The number of thaw cycles in both the spring and the fall was more strongly correlated with the length of the frost-free period than with the date of the last spring frost or first fall frost; however, the relationship between the number of thaw cycles and the date of the first fall frost was considerably stronger than with the date of the last spring frost. The number of snowfall events was also most strongly correlated with the length of the frost-free period, regardless of season. The analysis of the days of snow cover revealed a similar pattern.

The number of fall thaw cycles was significantly correlated (r = 0.56) with the number of spring thaw cycles (Table 3b). The number of spring snowfall events was more strongly correlated with the number of spring thaw cycles than the number of fall thaw cycles, and the reverse was true for the number of fall snowfall events. The number of summer snowfall events was not strongly correlated with either number of thaw cycles. The days of snow cover had similar correlations as the number of snowfall events.

The number of snowfall events in each season was highly correlated with the number of snowfall events in the other seasons of the same year (Table 3c). The days of snow cover in any particular season was strongly correlated with the number of snowfall events in that season (r ranges from 0.72 to 0.80), although it was also strongly correlated with the number of snowfall events in other seasons. Lastly, the days of snow cover in any season were strongly correlated with the days of snow cover in the other seasons of the same year (Table 3d). Three soil temperature monitoring sites were located in agricultural areas to represent a range in latitude, longitude, and elevation (Table 4). Burlington and Fruita are both of low elevation and similar latitude, but Burlington is in the eastern Colorado plains near the Kansas border, and Fruita is on the West Slope near the Utah border. Center is of moderate longitude, but it is located at considerably higher elevation and lower latitude than the other sites.

Soil temperature was consistently lower in Center and higher in Burlington throughout the year (Figure 5). In fact, soil temperature never declined to 0 C in Burlington, but in Center soil temperature was below 0 C for about 100 days or nearly one-third of the year. Soil temperatures at Fruita were below zero for a period less than half as long as in Center.

Soil temperature was regressed against daily maximum, minimum, and average air temperatures for a full year at each of the three monitoring sites (Table 5). At all three locations, the regression with minimum air temperature had the highest R^2 values, and maximum air temperature had the lowest R^2 values. The soil temperature prediction equations based on minimum air temperature are nearly identical for Fruita and Center, but the equation for Burlington had a much greater intercept and a flatter slope (Figure 6).

Figure 6. Prediction of minimum soil temperature at 5 cm depth from minimum air temperature in Burlington, Center, and Fruita, Colorado.
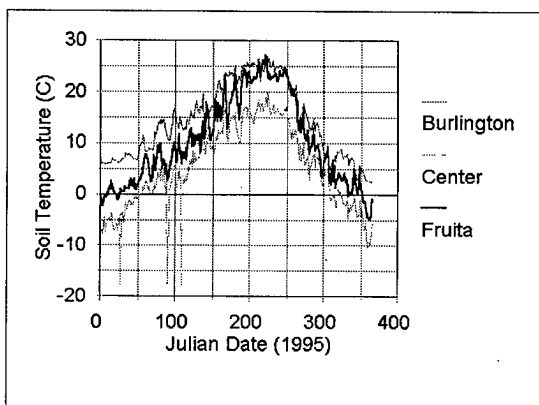
Figure 5. Soil temperature as a function of the Julian date in Burlington, Center, and Fruita, Colorado in 1995.
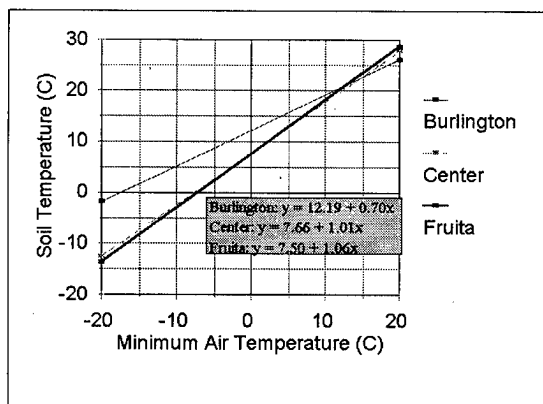
Figure 6. Prediction of minimum soil temperature at 5 cm depth from minimum air temperature in Burlington, Center, and Fruita, Colorado.

DISCUSSION

Elevation had a much greater impact than latitude or longitude on freezing and snowfall parameters within the state of Colorado. However, the range in elevation was much greater (maximum/minimum = 3.40) than the range in latitude (maximum/minimum = 1.11) or longitude (maximum/minimum = 1.07). In addition, there is a longitudinal relation with elevation because the Rocky Mountains bisect the state into lower elevation sections on both the east and west sides of the mountains. This relationship is revealed in correlations of latitude and longitude with elevation. The correlation of longitude with elevation was highly significant (p<0.01 with an r = 0.33), but latitude was not correlated significantly with elevation (r = 0.05).

The first fall frost is an important variable because if it arrives early, yield quality can be damaged. The first fall frost was more strongly correlated with both the length of the frost-free period and the number of thaws (in both spring and fall) than was the last spring frost. Therefore, the date of the first fall frost can have a large impact on crop productivity, regardless of the elevation.

The number of thaw cycles was greater in the spring than in the fall at all elevations. In addition, the number of snowfall events and the days of snow cover were significantly correlated with the number of thaw cycles in that season. The number of spring thaws was related to the number of fall thaws, and both were highly correlated with the length of the frost-free period. The interaction between elevation and thaw cycles showed that the number of thaw cycles was least at moderate elevations (1962-2133m). The freezing and thawing action in the spring can have a significant effect on crop stand establishment and winter hardiness of perennials.

Soil temperature followed a trend with elevation. The soil temperature at Center was less than that at Fruita which was less than that at Burlington. However, Center lies at an elevation nearly 1000 m greater than Fruita, and Fruita is only about 100 m higher than Burlington. Even though Fruita and Burlington have nearly the same elevation and latitude, there was a large difference in soil temperature from the eastern plains of Burlington to the western plateau where Fruita is located. Prediction equations would predict minimum soil temperature to reach 0 C when minimum air temperature is -17.4, -7.6, and -7.1 C in Burlington, Center, and Fruita, respectively. It is surprising that the prediction equations for Fruita and Center were

45

similar while Burlington's equation was far different.

References
Berry, J.W. 1977. A climatic summary for Colorado. pp. 37-38 In E.G. Siemer (ed.) Colorado climate. Colorado State University; Fort Collins, CO.

Doesken, N. 1996. Temperatures down in the soil. Colorado Climate 19(2):14-17.

Siemer, E.G. 1977. Colorado climate. Colorado State University; Fort Collins, CO.

Table 1. Locations of weather stations.

	Latitude	*Longitude*	*Elevation (m)*	*Precipitation (cm)*	*Snowfall (cm)*
Minimum	37 5	102 7	1033	18	50
Maximum	41 0	109 2	3511	100	1000

Table 2. Correlation coefficients of frost and snow variables related to latitude, longitude, and elevation (* means the correlation is significant at $p \leq 0.05$; ** means the correlation is significant at $p \leq 0.01$).

	Latitude	*Longitude*	*Elevation*
Julian Date of Last Spring Frost	0.006	0.11*	0.27**
Julian Date of First Fall Frost	-0.15**	-0.17**	-0.66**
Frost-free Period (days)	-0.09	-0.32**	-0.80**
Number of Spring Thaw Cycles	0.24**	-0.18**	0.42**
Number of Fall Thaw Cycles	0.24**	-0.02	0.43**
Number of Snowfall Events			
Spring	0.19**	0.12**	0.57**
Summer	-0.06	0.29**	0.41**
Fall	0.20**	0.15**	0.47**
Days of Snow Cover			
Spring	0.20**	0.12**	0.54**
Summer	-0.08	0.32**	0.45**
Fall	0.19**	0.11*	0.43**

Table 3. Correlation coefficients of frost and snow variables (* means the correlation is significant at $p \leq 0.05$; ** means the correlation is significant at $p \leq 0.01$).

A.

	Julian Date of Last Spring Frost	Julian Date of First Fall Frost	Frost-free Period (days)
Julian Date of First Fall Frost	-0.24**		
Frost-free Period (days)	-0.32**	0.91**	
Number of Spring Thaw Cycles	0.10*	-0.45**	-0.48**
Number of Fall Thaw Cycles	0.10*	-0.41**	-0.43**
Number of Snowfall Events			
Spring	0.17**	-0.53**	-0.58**
Summer	0.11*	-0.26**	-0.32**
Fall	0.13**	-0.40**	-0.42**
Days of Snow Cover			
Spring	0.17**	-0.46**	-0.53**
Summer	0.14**	-0.31**	-0.39**
Fall	0.13**	-0.33**	-0.39**

B.

	Number of Spring Thaw Cycles	Number of Fall Thaw Cycles
Number of Fall Thaw Cycles	0.56**	
Number of Snowfall Events		
Spring	0.62**	0.48**
Summer	0.04	0.11*
Fall	0.37**	0.66**
Days of Snow Cover		
Spring	0.58**	0.48**
Summer	0.06	0.18**
Fall	0.34**	0.65**

Table 3. Correlation coefficients of frost and snow variables (* means the correlation is significant at p≤0.05; ** means the correlation is significant at p≤0.01). (continued)

C.

	Number of Snowfall Events		
	Spring	Summer	Fall
Number of Snowfall Events			
Summer	0.42**		
Fall	0.60**	0.36**	
Days of Snow Cover			
Spring	0.77**	0.39**	0.56**
Summer	0.42**	0.72**	0.41**
Fall	0.49**	0.34**	0.80**

D.

	Days of Snow Cover	
	Spring	Summer
Days of Snow Cover		
Summer	0.50**	
Fall	0.67**	0.50**

Table 4. Location of soil temperature measurement sites.

Site	Latitude	Longitude	Elevation
Burlington	39 18	102 16	1271 m
Center	37 45	106 7	2338 m
Fruita	39 9	108 44	1378 m

Table 5. R-Square values for daily soil temperature predictions from maximum, minimum, and average air temperature values (* means the correlation is significant at p≤0.05; ** means the correlation is significant at p≤0.01).

Site	Average Air Temperature	Maximum Air Temperature	Minimum Air Temperature
Burlington	0.71**	0.56**	0.82**
Center	0.89**	0.79**	0.89**
Fruita	0.91**	0.75**	0.92**

Investigation of Water-Rock Interactions
in the Apsat River Basin

D.D. BALDANOVA[1], D.B. RADNAYEVA[1],
AND S.V. BORZENKO[1]

ABSTRACT

We determined the peculiarities of formation of natural water geochemical characteristics and secondary products of weathering in relation to the composition of primary rock. In 1988 and 1989, hydrochemical sampling was performed in the Apsat River basin located in the Kodar-Udocan District. The variation of pH values, of ionic strength of solution, and of Kurlov's formula are reported. The secondary mineral stability fields were found from Helgeson's diagrams. In 1988 the secondary products of weathering rocks were leonhardite, gibbsite and kaolinite. In 1989 the secondary minerals were mainly leonhardite and gibbsite, and on some samples of water, the secondary mineral kaolinite was noted. In 1988 certain samples of waters were saturated by quartz. Waters of 1989 were not saturated by quartz. Free and aggressive carbon dioxide quantities, stability on saturation indexes for calcium carbonate were determined.

Key words: Water-rock interaction, secondary products of weathering, natural waters.

INTRODUCTION

Vernadskii (1960) showed the great geological importance of the water-rock-gas-organic substance system for evolution of earth crust processes and phenomena. The physicochemical theory of mineral formation (Korjinskii 1982) and theoretical basis of simulation in geochemistry (Helgeson 1968, Karpov 1981) makes it possible to interpret developments of earth crust weathering profiles under different hydrothermal conditions. It has been shown by Shvartzev (1995), that a water-rock system satisfies principal demands of synergetics. The main premise of self-organization of the water-rock systems is their non-equilibrium-equilibrium character, determining formation of increasingly new mineral phases and geochemical types of the water. The new water structures are capable to perceive, appreciate and convey information.

In our work from the viewpoint of water–rock interactions we determined the peculiarities of formation of natural water geochemical characteristics and secondary products composition in relation to primary rock under permafrost conditions.

METHODS

In the summer of 1988 and 1989 hydrochemical sampling was performed in the Apsat River basin. In 1988, 100 samples of water were taken; in 1989, 25 samples were taken. Total chemical analyses of macrocomponents were made.

Karl Zeiss Jena AAS-3 atomic-absorption pectrophotometer was used to determine calcium, magnesium, potassium, sodium and sulfate ions by use of the most sensitive resonance lines and an air-acetylene flame.

The formula of Kurlov was found for each sample (Nikanorov and Posokhov 1985). Figures of percentage by ion concentration in gram equivalents per meter squared are given in this paper. Here the sum of cations is equal to 100%, and the sum of anions is equal to 100%.

As mineralization of waters was low and it was assumed that effects of association and hydration ions were unessential, activity coefficients of ions were calculated by the Debye-Huckel equation.

RESULTS AND DISCUSSION

The Apsat River basin, located in the Kodar-Udocan District of the North Transbaikal region, is

[1] Institute of Natural Resources, P.O. Box 147, 26, Butina st., Chita, Russia, 672090

formed from rocks of granitic, sand boulder pebble and coal-bearing gravelly conglomerate formations. In granitic formations, the predominant minerals are plagioclase, K-feldspar, biotite, muscovite, and quartz. The accessory minerals are fluorite, galena, sphalerite, chalcopyrite, molybdenite, wolframite, sheelite, cassiterite, ortite, and zircon-cryolite-pyroclore.

In the mountainous Transbaikal region unfavorable groundwater forming conditions are due to development of permafrost, which serves as a waterproof screen for rainfall, and also to steep slopes promoting intense surface flow. The permafrost has mainly continuous extension. Their depth is as great as 1200–1300 m and decreases to 25–600 m in valleys and intermountain depressions (Bogomolov 1969).

Natural waters in the Apsat River basin are represented by above permafrost level waters. Fresh waters are predominant with mineralization up to 50 g/m³; in rare cases, water mineralization is higher. According to chemical analyses data of 1988, most of the Apsat River natural waters belong to calcium hydrocarbonate, calcium sulfate, and hydrocarbonate types. Negligible amounts of the fluoride hydrocarbonate and hydrocarbonate sulfate water types are observed in fields of rocks enriched by fluorite and sulfide minerals. The variation of pH values were from 5.39 to 8.32, of ionic strength of solution— from 0.0002 to 0.009, of mineralization—from 9 to 120 g/m³, of Kurlov's formula:
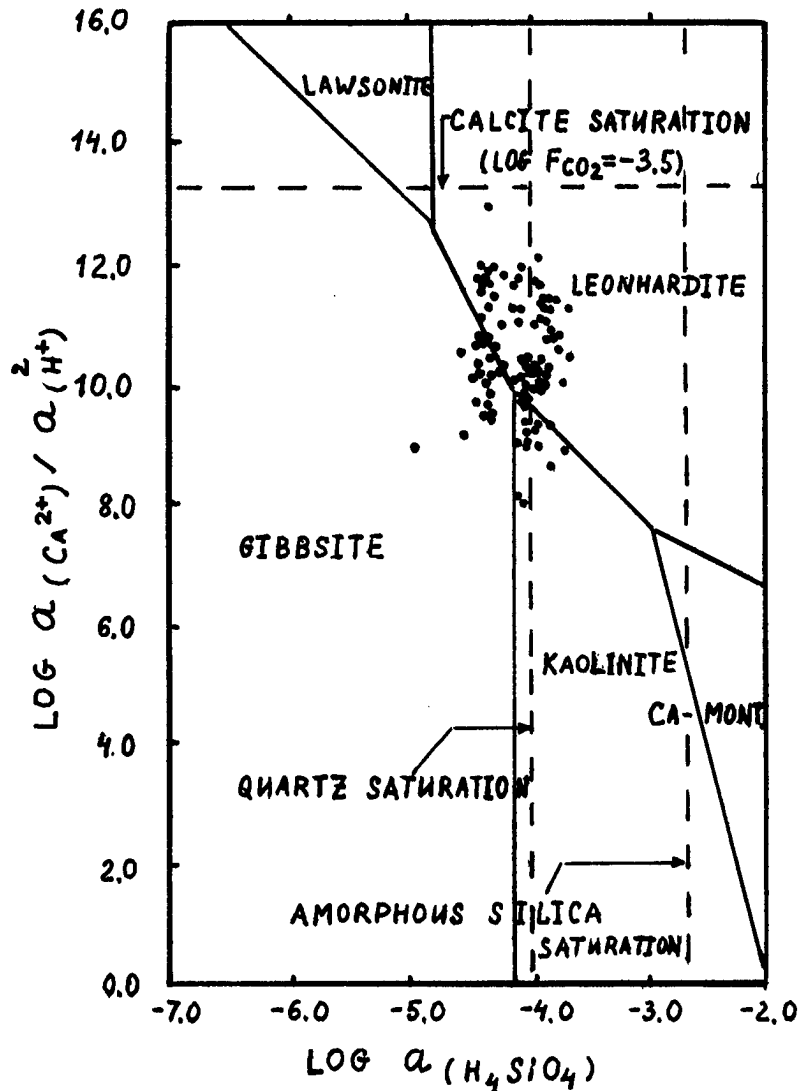
Figure 1. The system HCl-H_2O-Al_2O_3-CaO-CO_2-SiO_2 at 25°C. Water activity data of 1988 are plotted by points.

50

$$\frac{HCO_3\ 23\text{-}96\ SO_4\ 0\text{-}75\ F\ 0\text{-}28\ Cl\ 0\text{-}11}{Ca\ 46\text{-}84\ Na + K\ 4\text{-}35\ Mg\ 6\text{-}32}.$$

According to 1989 chemical analyses the composition of waters can be considered as calcium hydrocarbonate, sulfate hydrocarbonate, hydrocarbonate sulfate and sulfate types. Negligible amounts of fluoride hydrocarbonate, and sulfate hydrocarbonate types are noted. The limits of variation of pH values were from 4.78 to 7.86, of ionic strength from 0.0006 to 0.03, of mineralization—from 20 to 2350 g/m^3, of Kurlov's formula:

$$\frac{HCO_3\ 1\text{-}99\ SO_4\ 0\text{-}99\ Cl\ 0\text{-}47\ F\ 0\text{-}33}{Na + K\ 3\text{-}89\ Ca\ 8\text{-}82\ Mg\ 2\text{-}56}.$$

To find stability fields of secondary minerals, activities of ions were calculated and plotted on Helgeson's activity diagrams (Fig. 1–3). The water activity diagram of 1988 (Fig. 1) showed leonhardite, kaolinite and gibbsite as secondary products of weathering. In 1988 certain samples of waters were saturated by quartz. For 1989 it was concluded that the secondary products of weathering were mainly gibbsite and leonhardite, and in a few samples of water analyses
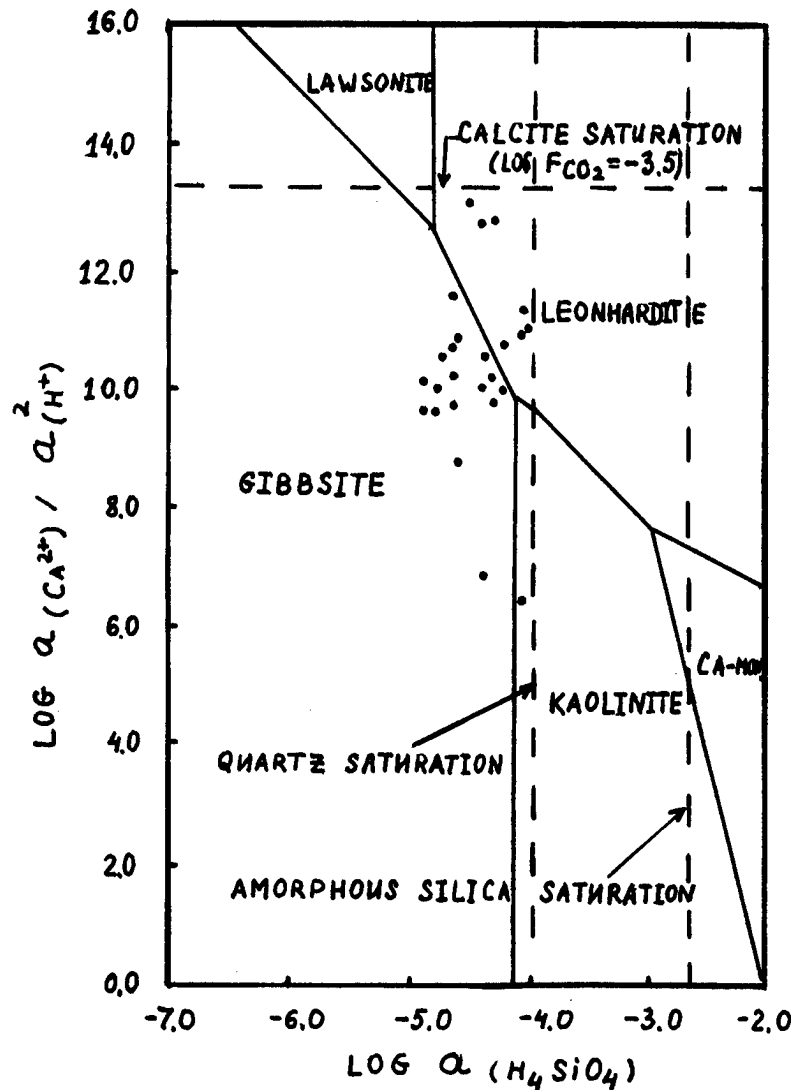
Figure 2. The system $HCl\text{-}H_2O\text{-}Al_2O_3\text{-}CaO\text{-}CO_2\text{-}SiO_2$ at 25°C. Water activity data of 1989 are plotted by points.
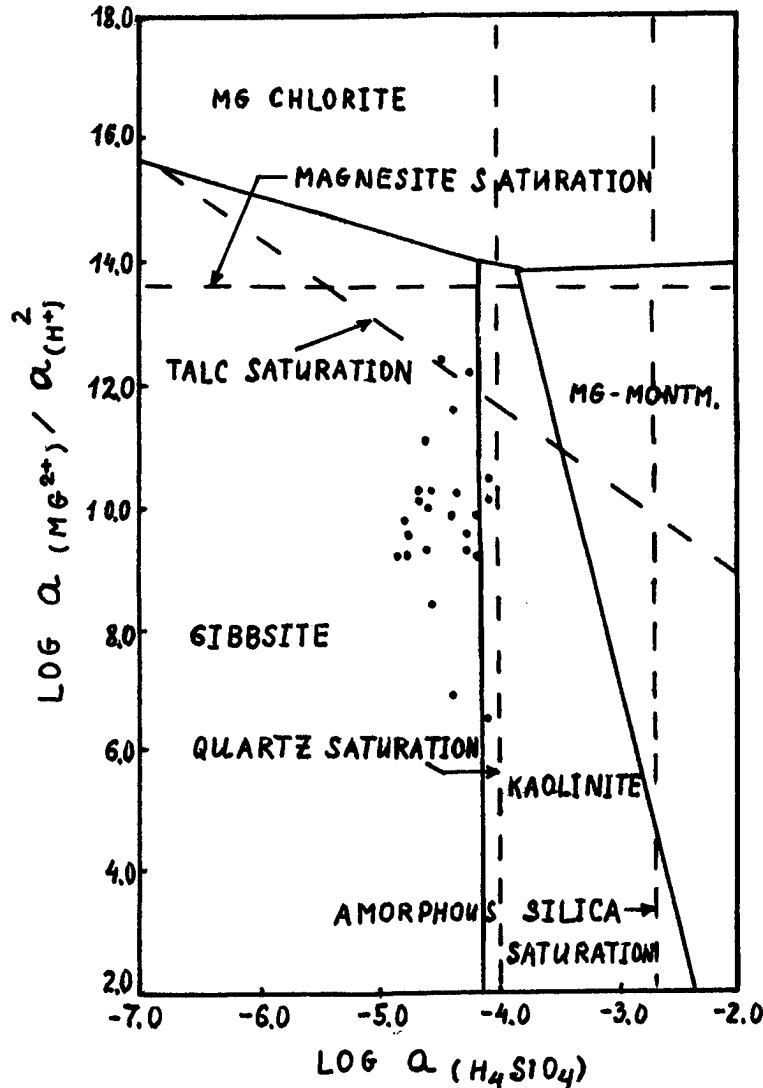
Figure 3. The system $HCl-H_2O-Al_2O_3-MgO-CO_2-SiO_2$ at 25°C. Water activity data of 1989 are plotted by points.

kaolinite was noted. Waters of 1989 were not saturated by quartz (Fig. 2 and 3).

In order to evaluate water reactivity to rocks, free and aggressive carbon dioxide quantities, and stability on saturation indexes for calcium (J) were estimated.

Free and aggressive carbon dioxide quantities varied in 1988 from 1.3 to 141 and from 1.3 to 100.4 g/m^3, in 1989 from 1.2 to 32.9 and from 0.1 to 30.9 g/m^3, respectively.

In 1988 values of the saturation indexes for calcium carbonate varied from -0.7 to -5.2 and it demonstrated water aggressiveness and ability to dissolve calcite.

In 1989 values of the saturation indexes for cal-

cium carbonate varied from 1.0 to –4.9. It should be recognized that water in some samples exceeded saturation by calcium carbonate (J>0), but in other samples water had the ability to dissolve calcite (J<0).

CONCLUSIONS

From the viewpoint of interactions in a water–rock system, our results show that certain changes have occurred in granitic rocks in the Apsat River basin. In 1988 the secondary products of weathering rocks were leonhardite, gibbsite and kaolinite. In 1989 the secondary minerals were mainly leonhardite and gibbsite and for some samples of water ka-

olinite was noted. In 1988 certain samples of waters were saturated by quartz. Waters of 1989 were not saturated by quartz. Furthermore, in 1989 natural waters characteristics were changing from lowering hydrocarbonate types to increasing hydrocarbonate sulfate, and sulfate types.

ACKNOWLEDGMENTS

REFERENCES

Bogomolov, N.S., V.M. Stepanov, and A.A. Shpak. 1969. Hydrogeological formation of different age intrusive rocks. p. 116–143. *In* N.I. Tols-tykhin (ed.) Hydrogeology of USSR. Vol. 21. Nedra, Moscow, Russia.

Helgeson, H.C. 1968. Evaluation of irreversible reactions in geochemical processes involving minerals and aqueous solutions. I. Thermodynamic relations. Geoch. Cosmochim. Acta 32: 853–877.

Karpov, I.K. 1981. Physicochemical simulation in geochemistry. Nauka, Novosibirsk.

Korjinskii, D.S. 1982. Theory of metasomatic zonality. Nauka, Moscow.

Nikanorov, A.M., and E.V. Posokhov. 1985. Hydrochemistry. Gidrometeoizdat, Leningrad.

Shvartzev, S.L. 1995. Problem of self-organization of water-rock geological system. Geologiya i geophyzica 4: 22–29.

Vernadskii, V.I. 1960. Selected works. Vol.4. Academy of Sciences of USSR, Moscow.

Water and Heat

Heat and Water Regimes of Soil for the Winter–Spring Period
Experiment and Modeling

Ye. M. GUSEV[1]

ABSTRACT

A set of mathematical physically based models describing a soil water regime over the winter-spring period is considered. It includes models for soil freezing, water migration to the freezing zone from the underlying unfrozen zone, soil temperature profiles before and during the spring snowmelt, water infiltration into frozen soil, soil thaw and its heating after snow-cover loss. The models were created on the basis of the integral balance method what allows one to combine the physical basis of models with simple mathematical formulations. The calculated dynamics of soil freezing depth, soil temperature and moisture profiles, the total amount of infiltrated water, and daily runoff were verified against the observations. The results of field investigations by the author and measurements of water-balance stations situated in the forest and forest-steppe zones of the European part of the Former Soviet Union were used to validate model simulations.

Key words: Soil freezing and thawing, soil temperature and moisture, winter-spring period, infiltration, surface runoff.

INTRODUCTION

Infiltration of snow meltwater into frozen soil and soil water storage during the period of spring snow melt are very important processes of soil water formation. The infiltration rate and the amount of infiltrated water are determined from soil moisture and soil thermal conditions at the beginning of snowmelt and water yield. Hydrologic and thermal regimes prior to spring melt are the result of dynamic hydrologic and thermal processes which occurred throughout the winter. Therefore, in the present work an attempt is made to construct a set of mathematical physically based models describing the soil water regime for the winter-spring period. To attain this goal it was necessary to study the following processes: (1) soil freezing with water migration to freezing zone from underlying unfrozen zone, (2) formation of soil temperature distribution before and during the spring snowmelt, (3) water infiltration into frozen soil, (4) soil thawing and warming after the snow-cover loss. We will consider the theoretical basis of modeling these processes and its experimental validation following Gusev (1985, 1988, 1989, 1993) and Gusev et al. (1992).

THEORY

Calculation of soil freezing depth with consideration of water migration to the freezing boundary

The problem of calculation of the dynamics of soil freezing depth was solved on the basis of the integral balance method both with respect to the heat balance (more exactly, enthalpy) and with respect to the water balance (Gusev 1988). The essence of this method (Goodmen 1967) lies in the approximating the vertical distribution of characteristics of soil hydro-thermal regime (for example, soil temperature T or moisture W) by polynomials as functions of the vertical coordinate z. These polynomials contain unknown, time-varying coefficients which are finding from the boundary conditions by employing

[1] Institute of Water Problems, Russian Academy of Sciences, Novobasmannaja st. 10, Box 231, Moscow 107078, Russia

balance equations in an integral form.

The approximation of the vertical temperature distribution (Figure 1a) was taken just as in Gusev (1988). Here T_S , T_{SR} and T^* are the temperatures (°C) respectively of snow surface, soil surface and soil at a depth where seasonal temperature fluctuations fade away; ξ is the soil freezing depth (m); h is the depth of snow cover (m); σ is the time-varying depth of penetration (m) (Gusev 1985), characterising the region of a noticeable change in the soil temperature since the start of freezing.
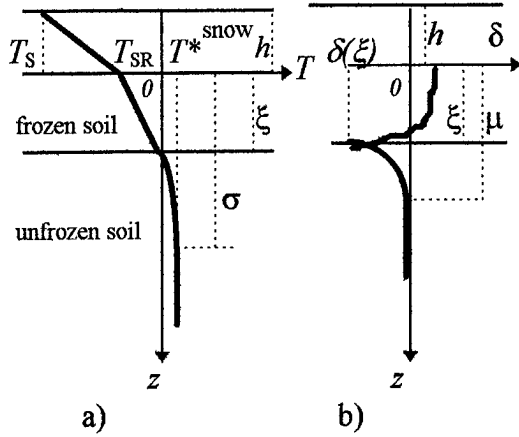
Figure 1. *Schematic vertical distribution of soil temperature (a) and increment of soil moisture (b) during the period of soil freezing in snow cover, frozen and unfrozen zones of soil.*

We note also that hereafter the characteristics related to snow cover, frozen zone of soil, and its unfrozen zone will have the subscripts 1, 2 and 3, respectively. In result we arrive at the following equation for the dynamics of the freezing front (Gusev 1988):

$$L^* \frac{d\xi}{dt} = q_F - q_H \quad , \qquad (1)$$

$$L^* = \lambda_I \rho_w \left[W_\xi - u^* \right] + \frac{c_2 |T_{sr}|}{2} \quad , \qquad q_F = -k_2 \frac{T_s}{\xi + \eta} \quad ,$$

$$q_H = \frac{2 k_3 T^*}{\sqrt{9/4 \xi^2 + 12 \cdot a_3 (t + t_0) - 3/2 \xi}} \quad ,$$

$$\eta = h \frac{k_2}{k_1} \quad , \qquad a_3 = \frac{k_3}{c_3} \quad ,$$

where t is a time (s) (here, $t=0$ means the beginning of freezing); ρ_w is the water density (kg m^{-3}); u^* is the content of unfrozen water (m^3 m^{-3}); c_2 is the effective heat capacity of the frozen zone (J m^{-3}); k is the thermal conductivity (W m^{-1} °C^{-1}); a is the thermal diffusivity (m^2 s^{-1}); t_0 is a parameter (s) reflecting the influence of the period preceding the period of soil freezing on the soil temperature profile (Gusev 1985); q_F is upward heat flux to the snow surface (W m^{-2}); q_H is a heat flux into frozen zone of soil from unfrozen zone (W m^{-2}); λ_I is the heat of water-ice transformation (J kg^{-1}) at 0°C, and W_ξ is the mean moisture in frozen zone (m^3 m^{-3}).

It has been shown in Gusev (1988), that

$$W_\xi \xi = W_0 \xi + \overline{\delta} \xi - \int_0^t j(\xi) dt \quad , \quad \overline{\delta}(\xi) = \frac{1}{\xi} \int_0^\xi \delta(\xi) d\xi \quad , \quad (2)$$

where δ is the deviation of the moisture from its initial value W_0 (m^3 m^{-3}); j is a water flow into frozen zone from unfrozen zone (m s^{-1}) (Figure 1b).

According to (Gusev 1988)

$$\overline{\delta}(\xi) = \frac{\int_0^t j(\xi) dt}{1/3 (\mu - \xi) + \xi} \quad , \qquad (3)$$

$$\mu - \xi = \sqrt{9/4 \xi^2 + 12 \cdot a_3 (t + t_0)} - 3/2 \xi \quad , \qquad (4)$$

$$j(\xi) = \begin{cases} k_0 \dfrac{T_s}{\xi + \eta} \quad , \quad W_0(\xi) + \overline{\delta}(\xi) > u^* \\[3mm] \dfrac{2D[u^* - W_0(\xi)]}{\mu - \xi} \quad , \quad W_0(\xi) + \overline{\delta}(\xi) \le u^* \end{cases} \quad , (5)$$

where $\mu-\xi$ is the depth of zone of the depression of the moisture content (m) (Figure 1b); D is the diffusion coefficient of soil water (m^2 s^{-1}); k_0 is the coefficient of thermal hydraulic conductivity (m^2 s^{-1} °C^{-1}). We will formulate a scheme for calculation of the soil freezing depth and changes in moisture content in frozen zone, resulting from water migration from the unfrozen zone.

The freezing depth ξ is calculated with a certain time step (for example 10 days) by means of a recursion formula analogous to that given in Gusev (1988) and based on solving eq.(1). The calculation of ξ at every time step is carried out twice. At first, the moisture content at the previous time step is used as W_ξ (at the beginning of the calculations the initial

56

moisture content is used) to calculate ξ-value which, in its turn, is used to determine W_ξ for the given time step by eqs. (2)-(5). Then the freezing depth ξ is recalculated to be refined using a new value of W_ξ.

Temperature profile of frozen zone before spring snowmelt

The next problem is to calculate the temperature profile in frozen soil before the period of spring snowmelt. This is necessary because the rate of infiltration of melted snow into frozen soil and the total amount of infiltrated water depend, to a large extent, on the soil thermal conditions at the beginning of snowmelt. Here, it is assumed that we can neglect the changes in the position of freezing depth and snow cover height just before the spring snowmelt. The problem was solved by using parabolic approximation of temperature profiles in snow and frozen soil. The method allows us to obtain the expression for temperature profile in frozen soil as a function of the vertical coordinate z (m) (Gusev 1993):

$$T(z) = \widetilde{T}_2 + C_{(2)} z^2 - \frac{k_1}{k_2} \frac{C_{(2)}\xi^2 - C_{(1)}h^2}{y} z -$$
$$-\frac{C_{(2)}\xi^2 h + C_{(1)}h^2 \xi \frac{k_1}{k_2}}{y} \quad , \quad y = \frac{k_1}{k_2}\xi + h \qquad (6)$$

$$\widetilde{T}_2 = \frac{k_1}{k_2} T_s \frac{\xi - z}{y} \quad ,$$

$$C_{(i)} = F_{(i)} \int_0^{t_w} \frac{\partial T_{sn}}{\partial \tau}\left[A_{(i)} e^{\widetilde{p}(t_w - \tau)} + B_{(i)} e^{\widetilde{q}(t_w - \tau)}\right] d\tau \quad ,$$

$$A_{(i)} = \frac{\widetilde{p} + d_{(i)}}{\widetilde{p} - \widetilde{q}} \quad , \quad B_{(i)} = \frac{\widetilde{q} + d_{(i)}}{\widetilde{q} - \widetilde{p}} \quad , \quad (i) = 1, 2 \quad ,$$

$$F_{(1)} = \frac{2}{3}\frac{\left(1 + \frac{h}{y}\right)}{h^2} \quad , \quad F_{(2)} = -\frac{3}{2}\frac{k_1}{k_2}\frac{1}{\xi y} \quad ,$$

$$d_{(1)} = 6a_2 \frac{1 + \frac{k_1}{k_2}\frac{\xi}{y}}{\left(1 + \frac{h}{y}\right)\xi^2} \quad , \quad d_{(2)} = -6a_1\frac{1}{h^2} \quad ,$$

where t_w is the duration of winter period (s), $\widetilde{p}$ and $\widetilde{q}$ are the roots of the following quadratic equation:

$$r^2 + r\widetilde{E} + \widetilde{Q} = 0 \quad , \quad \widetilde{Q} = a_1 a_2 \frac{36}{\xi^2 h^2} \quad ,$$

$$\widetilde{E} = 3\left[a_2\left(1 + 3\frac{k_1}{k_2}\frac{\xi}{y}\right)\Big/\xi^2 + a_1\left(1 + 3\frac{h}{y}\right)\Big/h^2\right] \quad .$$

Between the beginning of snowmelt and the beginning of water yield of thawed snow there is a small period during which some additional transformation of the temperature profile takes place. These changes can be also simulated by using the integral heat balance method (Gusev 1989, 1993). All the above allows us to obtain the temperature distribution in soil just before spring water yield denoted as $T_{in}(z)$ (°C).

Infiltration of water into soil during snow melt

The numerical model is based upon the following conceptual model (Gusev 1989). Snow meltwater infiltrated into frozen soil increases the temperature of its wetted part approximately up to 0°C. Part of the water in this case freezes; while the remaining part (assuming a high enough conductivity of the frozen soil layer) moves downward and moistens the underlying soil layers.

We will assume that the moisture profile at the boundary of the wetted and unwetted zones of the soil has a stepped form. Such an assumption proves to be correct when describing infiltration into unfrozen soil (various modifications of the Green-Ampt model (Green and Ampt 1911)), since a sharp decrease in hydraulic conductivity of soil resulting from a decrease in its water content leads to the formation of soil moisture profile of the shockwave type. In the case of frozen soil, a reduction of hydraulic conductivity at the infiltration front is intensified by freezing a portion of the water. As a result, a moisture wave propagates down the soil profile with a sufficiently distinct moistening front (i.e. the infiltration column). In this case, the differential equation of moisture transport in the soil has a well-known form:

$$q_0 = K\left(1 + \frac{H}{z_0}\right) \quad , \qquad (7)$$

where q_0 is the water flow (m s^{-1}); H is the effective capillary potential of the soil (m); K is the average hydraulic conductivity of the wetted zone (m s^{-1}) and z_0 is position of the infiltration front (m). As a first approximation we can consider that the integral

parameters K and H depend on the average content of liquid water in the wetted part of the soil u ($m^3\,m^{-3}$) and on its average ice content I ($m^3\,m^{-3}$). They are connected with the total soil moisture content W ($m^3\,m^{-3}$) by the following equation:

$$W = \frac{\rho_I}{\rho_W} I + u \qquad , \qquad (8)$$

where ρ_I and ρ_W are the densities of ice and water (kg m^{-3}), respectively.

An estimation of u and I is needed for calculating the infiltration rate q_0. This calculation is related to the solution of the problem on soil heat regime during water infiltration into frozen soil.

This problem can be also solved using the integral balance method. In the given case, the equations for the heat (enthalpy) balance of wetted and unwetted frozen soil are used. The result of the approximate solution of the given problem can be represented in the following form (Gusev 1989):

$$\Delta I(t) = \begin{cases} \dfrac{B(t)}{\rho_I \lambda_I z_0(t)} & , \quad z_0(t) > 0 \\ 0 & , \quad z_0(t) = 0 \end{cases} \quad , \quad (9)$$

$$B(t) = -\int_0^t k_2 \left[\left. \frac{dT_{in}}{dz} \right|_{z=z_0} + \frac{2T_{in}(z_0)}{\tilde\sigma(t) - z_0(t)} \right] exp\left(\frac{12 a_2 t}{\xi^2} \right) dt ,$$

$$\tilde\sigma(t) = -2z_0(t) + \sqrt{9z_0^2(t) + 12 a_2 t} \quad , \quad (10)$$

where $\Delta I = I - I_0$ is the average change of ice content in wetted zone; I_0 is the initial ice content in frozen soil ($m^3\,m^{-3}$) and $t=0$ means the beginning of water yield during snowmelt.

Adding to eq.(9) the equation of water transfer in the wetted zone eq.(7), the equation of dynamics of the depth of penetration eq.(10), and the water balance equation of the wetted zone we get

$$\int_0^t (q_0 - K_n) dt = z_0 \left(\frac{\rho_I}{\rho_w} \Delta I + u - u_0 \right) , \quad (11)$$

where $K_n = K(u_0, I_0)$ is the hydraulic conductivity of the soil ahead of the infiltration front (m s^{-1}) as a function of initial values of u_0 and I_0 (the technique of estimation of u_0 and I_0 is presented in Gusev (1989)). Thus we obtain a system of four

equations in five unknowns $I(t)$, $u(t)$, $q_0(t)$, $z_0(t)$, and $\tilde\sigma(t)$. To close this system it is necessary to have one more equation. In the case of fulfilment of the condition

$$I + u \le p^* \quad , \qquad (12)$$

where p^* is the effective soil porosity (with consideration of the proportion of pores occupied by entrapped air), the equation

$$q_0 = J_0 \quad , \qquad (13)$$

where J_0 is the rate of water yield of snow (m s^{-1}), can be used. If condition eq.(12) is violated, the closing equation is

$$I + u = p^* \qquad (14)$$

In this case $q_0 < J_0$ (the soil surface is flooded and the formation of runoff occurs).

The solution of the system of eqs. (7), (9) - (11) and (13) or (14) for the given time moments (for example, with a daily time step) allows the calculation of the dynamics of infiltration rate and the amount of infiltrated water as well as the soil temperature distribution in the unwetted zone (as it was mentioned above the soil temperature in wetted zone is equal to $0°C$).

The functions $K(u,I)$ and $H(u,I)$ can be calculated by Gusev (1989).

Soil thawing out and heating after the snow-cover loss

It is convenient to distinguish two typical stages in soil heating after snow-cover loss. The first is directly related to thawing of frozen soil. The second is connected with heating of soil after its thawing out. For the first stage the behaviour of the upper thawing boundary ξ_{th} (m) can be described (Gusev et al. 1992) by

$$\xi_{th} = \sqrt{\int_0^t \frac{2k_3 T_{sr}^2(\tau)}{L^{**}} d\tau} \quad , \qquad (15)$$

$$L^{**} = \lambda_I \rho_w \left[W_{th} - u^* \right] + \frac{c_3 |T_{sr}|}{2} \quad ,$$

where W_{th} is the moisture of the thawed zone ($m^3\,m^{-3}$) and the time moment $t=0$ corresponds to snow-cover loss.

58

The parameterization of the soil heating on the base of the integral heat balance method allows one to describe the temperature distribution in the soil after the end of its thawing by set of two parabolic functions (Gusev et al. 1992).

EXPERIMENTAL VERIFICATION

Soil freezing and water migration to the front of freezing from underlying unfrozen soil

Verification of simulated values of the soil freezing depth and the increment of soil moisture in frozen zone during the cold season against observations was carried out using measurements of the Moscow Water-Balance Station from 1972 to 1981 and the Bolkhov Water-Balance Station from 1976 to 1984. The thermo-physical parameters of the soil and snow cover required for the calculations

were estimated by Gusev (1985) using the data given in Kalyuzhnyi and Pavlova (1981) and Pavlova and Golitsyna (1974). The special technique was developed for determining parameters D and k_0 (Gusev 1988). The values of all parameters were obtained for the regions where the mentioned water-balance stations are situated.

The results of comparison between the calculated and observed soil freezing depth and soil moisture increment in frozen zone for the Moscow Water-Balance Station are given in Figure 2.

Soil temperature distribution

A comparison between the observed and calculated soil temperature profiles $T(z)$ was carried out by using measurements from the Nizhnedevitsk Water-Balance Station and results of field experiments carried out by the author at the Kursk Biosphere Station. At these stations a special research of soil heat regime was carried out. Soil temperature were obtained by means of electrical thermistors located at different horizons in the soil profile. Some examples of the agreement between the calculations and measurements are shown in Figure 3.

a)

b)

Figure 2. Comparison between calculated and measured data on the dynamics of soil freezing depth (a) and changes in soil moisture of frozen zone (b) for the Moscow Water-Balance Station.
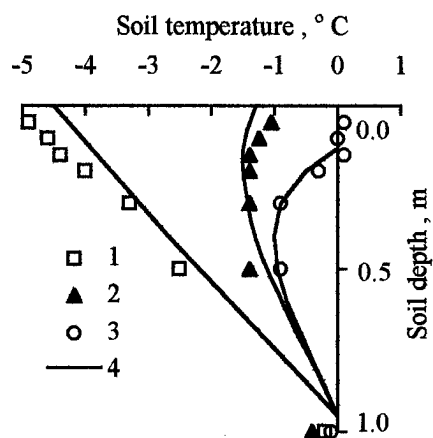
Figure 3. The dynamics of modeled and measured soil temperature distributions at the Kursk Biosphere Station in 1980. 1-3 = measurements on 25 March, 31 March and 2 April, respectively; 4 = calculations on the same dates. Water yield of melting snow begins on April 1.

Water infiltration into frozen soil and surface runoff

The described method for the calculation of infiltration rate and surface runoff was tested against the measurements from the Moscow Water-Balance Station and from the field experiments conducted by

the author at the Kursk Biosphere Station. The calculated and observed runoff hydrographs were compared for two sites at the Moscow Water-Balance Station from 1971 to 1983 and for four sites at the Kursk Biosphere Station from 1979 to 1985. As the initial information for the calculation we used the data on (a) soil freezing depth, obtained by frostmeters, (b) height and density of snow, (c) dynamics of the air temperature (daily values) for the period (about a month) preceding the beginning of snowmelt, and (d) dynamics of water yield based on measurements of precipitation and changes in water equivalent snow depth.

The values of thermo-physical parameters of the soil $u*$, k, c were taken from Kalyuzhnyi and Pavlova (1981), Pavlova and Golitsyna (1974) with taking into account the available data on the soil moisture and density (averaged over the uppermost 30-cm soil layer) from the stations.

The soil hydro-physical parameters for calculating functions K and H for the Moscow Water-Balance Station were estimated on the basis
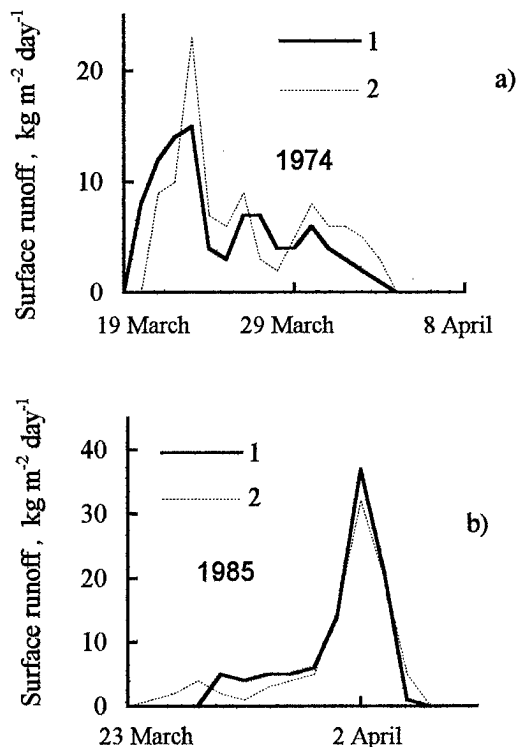
of results of special investigations of infiltration into thawed soil conducted at this station in 1961. These parameters for the Kursk Biosphere Station were taken from Gusev (1981) and Yasinskiy (1982).

Figure 4 gives some examples of comparison between the calculated and measured surface runoff hydrographs. The agreement between the calculations and observations can be considered as satisfactory, especially if we take into account the accuracy of estimation of the initial data and thermo- and hydro-physical parameters of the system. The coefficient of correlation between the calculated and measured values of the surface runoff is equal to 0.95 and their standard deviation is 13 mm (Figure 5).
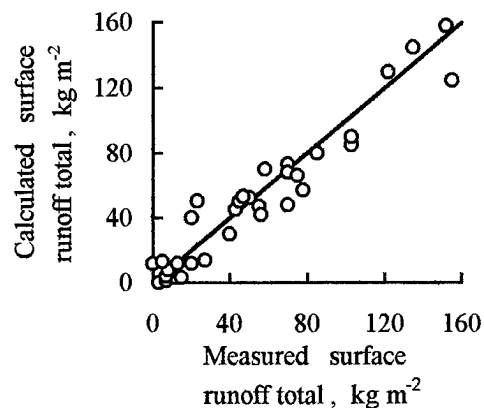
Figure 5. Comparison between calculated and measured total amount of overland surface runoff during the period of snowmelt for runoff-measuring sites at the Moscow Water-Balance and Kursk Biosphere Stations.

Soil heat regime after snow cover loss

A comparison between the calculated and observed data on characteristics of soil heat regime was carried out using the results of the author's field experiments at the Kursk Biosphere Station. Ice content measurements were conducted with TET-2 resistance thermometers at various depths of soil during 1989. Besides that, the frostmeters were used to observe the lower and higher boundary of frozen zone. The data on the thermo-physical parameters of the soil were also taken from Kalyuzhnyi and Pavlova (1981) and Pavlova and Golitsyna (1974) taking into account the available data on the soil moisture and density from the stations. The data on mean daily air temperatures were taken from the nearest meteorological station.

Figure 6 gives a comparison between the calculated and measured mean daily soil temperature at different depths.

Figure 4. Calculated (1) and measured (2) surface runoff hydrographs from different sites at the Moscow Water-Balance (a) and Kursk Biosphere (b) Stations.
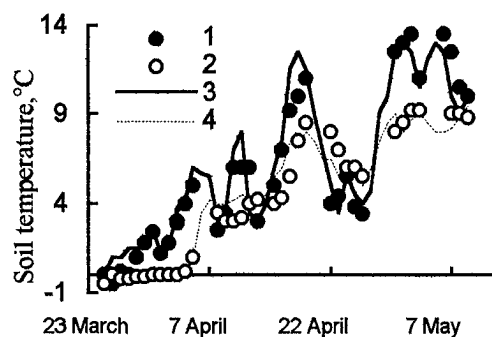
Figure 6. Dynamics of measured (1, 2) and calculated (3, 4) mean daily soil temperature for bare soil at depth of 0.1 (1, 3) and 0.4 (2, 4) m, respectively.

CONCLUSION

The presented models describing the processes of soil freezing, water migration to frozen zone from underlying unfrozen zone, formation of soil temperature profile before the period of snowmelt, water infiltration into frozen soil, soil thawing out and heating after snow-cover loss show that the models are suitable for the calculation of characteristics of the heat and water regimes of soil during the winter-spring period with satisfactory accuracy. These models may be used for estimating the efficiency of various methods of soil water regime management, for optimizing snow amelioration, for forecasting the spring surface runoff, etc.

ACKNOWLEDGMENTS

REFERENCES

Goodmen, T. 1967. Application of the integral methods in nonlinear problems of nonsteady-state heat transfer. p. 41-96. *In* Problems of Heat Transfer. (in Russian). Atomizdat, Moscow, USSR.

Green, W.H. and Ampt, G.A. 1911. Studies on soil physics. I. The flow of air and water through soils. J. Agr. Sci. 4: 1-24.

Gusev, Ye.M. 1981. Experimental investigation of infiltration under pressure. p.195-205. *In* S.V.Nerpin (ed.) Physics of Soil Water. (in Russian). Nauka, Moscow, USSR.

Gusev, Ye.M. 1985. Approximate numerical calculation of soil freezing depth. (in Russian). Meteorol. Hydrol. 6: 94-102.

Gusev, E. M. 1988. Simplified calculation of soil freezing depth with consideration of water migration to the freezing boundary. Water Resources 15 (1): 9-17.

Gusev, E.M. 1989. Infiltration of water into soil during melting of snow. Water Resources 16 (2): 108-122.

Gusev, Ye.M. 1993. Formation of soil water regime and resources for the winter-spring period. (in Russian). Fizmatlit Publishing Company, Nauka Publishers, Moscow, Russia.

Gusev, Ye.M., Busarova, O.Ye., Shurkhno, A.A. and Yasinskiy, S.V. 1992. Effects of straw mulch on the thermal conditions in soil after snow-cover loss. Eurasian Soil Sci. 24 (8): 12-23.

Kalyuzhnyi, I.L. and Pavlova, K.K. 1981. Formation of meltwater losses. (in Russian). Hydrometeoizdat, Leningrad, USSR.

Pavlova, K.K. and Golitsyna, E.F. 1974. Thermal properties of soil in thawed and frozen states. (in Russian). Transactions of Hydrological State Institute 214: 123-133..

Yasinskiy, S.V. 1982. Spatial nonuniformity of soil hydraulic conductivity at saturation for arable and virgin lands in the central forest-steppe zone. (in Russian). Meteorol. Hydrol. 10: 113-115.

Erosion and Crop Response to
Contour-Ripped Planted-Wheat in
Seasonally Frozen Soil of the Pacific Northwest

J.D. WILLIAMS[1], D.E. WILKINS[1], AND W.F. SCHILLINGER[2]

ABSTRACT

Soil erosion in the dryland farming region of the Pacific Northwest occurs predominantly in conjunction with low intensity rainfall falling on thawing soil. Fields susceptible to erosion under these conditions have long, steep slopes and minimal green or residue cover. These conditions are common to winter wheat-summer fallow cropping practices. We review here literature discussing the conservation practice of contour ripping frozen soil planted to winter wheat in the Pacific Northwest. This practice breaks slope length by opening channels through the frozen soil and plow pan. The channels detain water on the slope, reducing runoff and erosion, and allow infiltration, increasing water stored in the soil profile. Contour ripping serves as an effective erosion control without significant deleterious effects to crop yield or pathogen infestation. However, the conservation effectiveness decreases rapidly with each storm following contour trenching; and conditions of steep slopes or shallow soil however, caution must be used with the prescription and application of this conservation treatment.

Key words: Frozen soil erosion, summer fallow-winter wheat, steep slopes, low intensity rainfall, conservation tillage

INTRODUCTION

Seasonally frozen soils combined with cultural tillage practices create conditions that lead to 90% of the erosion in the inland Pacific Northwest farm region occurring on less that 20% of the landscape during 1% of the year (McCool et al. 1976). Rainfall on frozen soil, with or without snow cover, or rapid snowmelt on frozen soil create the most damaging flood and erosion events in this region. These events are exacerbated by mechanical fallow practices and long, steep slopes with minimal green or residue cover following fall seeding. One of the most effective conservation methods developed in recent years is contour ripping, which entails the creation of

deep channels, 300-600 mm deep spaced 3-6 m depending on slope and soil depth, in planted wheat (Wilkins et al 1991, Pikul et al. 1996, Schillinger and Wilkins 1996). Contour ripping is accomplished using shanks up to 1 m long and 50 mm wide; equipment specifically for this use has been developed by farmers/producers (Harold Clinesmith, pers. com., Benge, Washington 1988), and by researchers (Wilkins et al. 1991).

Contour ripping serves two major conservation functions: firstly it shortens slope length of impermeable frozen soil, and secondly it increases infiltrability on the slope by creating flow pathways through the concrete frost that typically forms in this cropping system (Pikul et al. 1992). Contour channels are created shortly after fall seeding or during the first frozen soil event sufficiently deep to support the equipment. Moderately recharged soil water and surface soil with good structure are ideal conditions for contour ripping immediately after seeding (Schillinger and Wilkins 1996). This set of conditions increases the likelihood that contour channels will remain open longer through the winter. Unfortunately, in September and October the top 50 mm of soil is often dry and dust-mulched as a result of rod-weeding. Under these soil conditions, contour channels are prone to filling with loose, unconsolidated material.

Contour ripping is an effective soil and water conservation method as demonstrated by research in the Pacific Northwest (Wilkins and Zuzel 1994, Wilkins et al. 1996, Schillinger and Wilkins 1996) and eastern Montana (Pikul et al. 1996), and by producer/farmer experience. Harold Clinesmith has used this technique for some years on his farm and found it extremely effective. Figures 1 and 2 show Mr. Clinesmith's ripper and the confluence of two, similar small watersheds. Mr. Clinesmith has observed, in 47 years of farming, similar runoff and erosion from these watersheds. However, the watershed to the right was contour ripped the year of Figure 2, halting runoff. Trench spacing specifications are available to optimize time and equipment requirements (Pikul et al. 1996). Field-

---

Figure 1. Contour ripper used for soil and water conservation by farmer/ producer, Harold Clinesmith, of Benge, Washington.
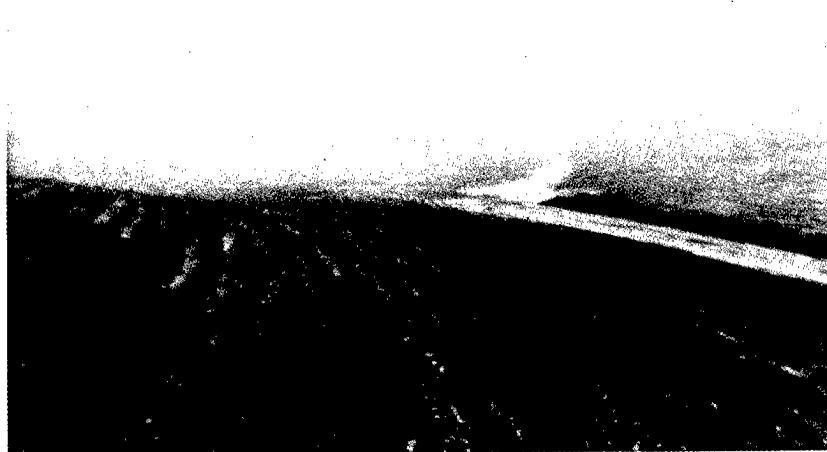
Figure 2. Confluence of two similar watersheds on Mr. Clinesmith's property. The one to the right was contoured ripped, halting runoff.

scale crop yield, crop disease, and weed infestation were not negatively influenced by contour ripping (Wilkins et al. 1991, Schillinger and Wilkins 1996, Wilkins et al. 1996).

Contour ripping is a successful conservation treatment, and contributes an important tool to the triad of mechanical, chemical, and biological methodologies necessary for successful winter wheat production and soil and water conservation The purpose of this poster is to examine the relationship

between the time of contour ripping with the general effectiveness of the treatment, and present conditions under which contour ripping should not be used.

METHODS, RESULTS AND DISCUSSION

We examined data presented by Schillinger and Wilkins (1996) and Wilkins et al. (1996. Comparisons between ripped and nonripped fields

63

revealed a decreased effectiveness of contour ripping to reduce runoff after a single rain or frozen soil event. Eroded soil filled the contour trenches in 1993, and the soil was not transported any further downslope (Wilkins et al. 1996). Contour trenches, in effect, change source or transport zones into deposition zones and decrease the number of rills (Table 1). This effect is demonstrated by the change in soil erodibility index (ratio of soil loss in the tilled treatment to the control) in the winter of 1995 by Schillinger and Wilkins (1996) (Fig. 3). With each subsequent frozen soil and runoff event, the erosion ratio (ripped:non-ripped) increased, indicating diminished erosion control effectiveness in the ripped treatment.

Table 1. Soil loss from 24 Jan.-28 Feb. 1995.

Tillage	Change in rills (no. per plot)	Soil loss (t ha^{-1})
Control	2.2	6.5
Ripped	-0.8	-0.2
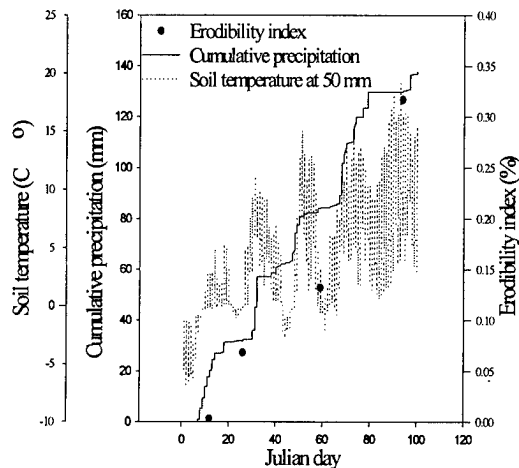
Figure 3. Daily range in soil temperature, cumulative precipitation, and erodibility index for ripped and control treatments (Schillinger and Wilkins 1996).

Our experience shows that contour ripping is most effective in a well structured soil with moderately high soil moisture immediately after seeding or during the first frozen soil event of the season. Channels ripped under these conditions provide a open channel into the soil profile capable of providing an infiltration pathway for water

flowing over frozen soil. Soil freeze/thaw events occur from 1 to 7 times per year in the Pacific Northwest (Zuzel 1986). Schillinger and Wilkins (1996) measured soil loss following four freeze/thaw rain events (Fig. 4). Soil loss doubled from the first to last event in the control treatment, but increased 20 times in the ripped treatment, although it never reach the level of soil loss in the control.
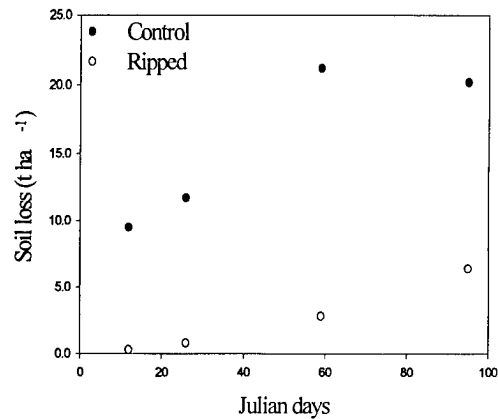
Figure 4. Soil loss from control and ripped treatments following rain on frozen soil events (Schillinger and Wilkins 1996).

Ripping in frozen soil requires additional power, but decreases the possibility of loose, unconsolidated soil quickly filling the trenches. Slopes up to 52% are farmed in the Pacific Northwest. Conservatively 7% of the most erodible cropland is on slopes greater than 20 % (Johnson and Makinson 1988). For safety reasons, we do not recommend contour trenching on slopes greater than 20% when the soil is frozen. Care must be taken, of course, to rip the trenches on the contour to prevent formation of concentrated flow or development of piping in the soil. Contour ripping does not provide effective erosion control without sufficiently deep soil for additional soil water storage. Contour trenching into shallow soil might lead to profile saturation and soil loss through mass movement. Producers should be aware of impermeable or clay layers in deeper soils that create conditions ideal for rotational slumping associated with increased soil water. Soil moisture increases within 1 m of ripped contour trenches and is believed responsible for increased grain yields adjacent to the trenches (Schillinger and Wilkins 1996). However, in dry winters that occur occasionally in the Pacific

64

Northwest and regularly in the upper Great Plains (Pikul pers. comm.), we would expect no enhancement of soil moisture.

CONCLUSION

Research and farmer/producer experience support the use of contour ripped channels for soil and water conservation in seasonally frozen soils. Application of this conservation tool will enhance soil and water conservation, despite a gradual filling in of the trenches with subsequent storm events throughout the winter. On many summer fallow-winter wheat farms in the Pacific Northwest, the risk of accelerated soil erosion or yield loss is low if the precautions outlined above are considered.

REFERENCES

Johnson, D. R., and A. J. Makinson. 1988. Soil survey of Umatilla County, Oregon. USDA-SCS. 398 p.

McCool, D. K., M. Milan, R. I. Papendick, and F. L. Brooks. 1976. Erosion research in the dryland grain region of the Pacific Northwest. Pages 50-59, *In* Soil Erosion: Prediction and Control. Soil Cons. Soc. Am., Ankeny IA.

Pikul, J. L., Jr., D. E. Wilkins, J. K. Aase, and J. F. Zuzel. 1996. Contour ripping: A tillage strategy to improve water infiltration into frozen soil. J. Soil & Water Cons. 51(1): 76-83.

Pikul, J. L., Jr., J. F. Zuzel, and D. E. Wilkins. 1992. Infiltration into frozen soil as affected by ripping. Trans ASAE 35(1): 83-90.

Schillinger, W. F., and D. E. Wilkins. 1996. Deep ripping seeded wheat fields to improve water infiltration and reduce soil loss. J. Soil & Water Cons. (in press).

Wilkins, D. E., and J. F. Zuzel. 1994. Tillage to enhance water infiltration through frozen soil. Pages 459-464, *In* Proceedings of 13th International Conference, International Soil Tillage Research Organization Vol. I, H.E. Jensen, P. Schjonning, S. A. Mikkelsen, and K. B. Madsen (eds), 24-29 July 1994, Aalborg, Denmark.

Wilkins, D. E., J. F. Zuzel, J. L. Pikul, Jr., and R. W. Smiley. 1991. Tillage tool for enhancing water infiltration through frozen soil. Pages 393-398, *In* Proceedings of the National Symposium, Preferential Flow, T. J. Gish and A. Shirmohammadi (eds), 16-17 December 1991, Chicago IL. Published by ASAE, St. Joseph MI.

Wilkins, D. E., J. F. Zuzel, and J. D. Williams. 1996. Tilling seeded wheat fields for erosion control. 17 July 1996 ASAE Annual International Meeting, Phoenix AZ.

Zuzel, J. F. 1986. Probability distributions of rain on seasonally frozen soils. Pages 237-244, *In* Cold Regions Hydrology Symposium, July 1986, American Water Resources Association.

Model COLD
Validation and Application for
Modeling Annual Dynamics of Soil Water

Ye. M. GUSEV[1] AND O.N. NASONOVA[1]

ABSTRACT

Model package COLD, describing the processes of formation of the soil heat and water regime during the cold season, is presented. It includes three independent analytical models: FRED (FREezing Depth), which simulates variations of soil freezing depth, SOT (SOil Temperature), calculating the vertical profile of soil temperature before the spring snow melt, and MIR (Melting, Infiltration, Runoff), simulating the spring snowmelt with subsequent infiltration and surface runoff. COLD was validated for the forest-steppe zone of Russia using agrometeorological data from 1955 to 1988. After that, COLD was incorporated into a package ANDY_SWASH (ANnual DYnamics of Soil WAter Stores for Homogeneous areas), which was also validated using the above-mentioned data. Verification of simulated water storage in the 1-m soil layer against observations in various non-forested ecosystems shows good agreement.

Key words: Soil freezing, soil temperature, snow cover, snow melt, infiltration.

INTRODUCTION

Many vital processes in the middle and high latitudes of the Earth show a clear seasonal course. In particular, biomass production of terrestrial systems of green plants takes place during warm season. However, water supply of the plants is affected not only by hydrometeorological conditions of the growing season, but also by the amount of snow, accumulated on the soil surface, and by its partitioning between surface runoff and infiltration into the soil during snowmelt.

This paper describes the development and validation of a model simulating the hydrothermal processes occurring during the winter-spring period on a local scale. When modelling, the main emphasis was made on analytical methods.

Using an analytical mathematical formalism usually requires distinguishing the main aspects of phenomena and neglecting secondary details. The difficulty is that during different intervals of the cold season different hydrothermal processes dominate. Consequently, it is impossible to develop a general, simple and convenient analytical model for a whole cold season. It is necessary to divide it into several periods with prevalence of some kind of the processes to develop a model for each period and then to link them into one package.

In our opinion it is appropriate to divide a cold season into three periods: (1) period of soil freezing, connected with penetration of zero-isotherm into the soil, (2) pre-spring period with relatively small variations of current soil freezing depth and snow height, together with near-zero air temperature, and (3) the period of spring snowmelt. Each period has a separate analytical model, description and validation of which has been detailed in a number of publications (Gusev 1988, 1989, 1993). Principal advantages of the models are that, being physically based and well provided with parameters, they have relatively simple mathematical algorithms and require standard meteorological data as forcing factors. Here, these models were linked as individual blocks into one general package COLD.

[1] Institute of Water Problems, Russian Academy of Sciences, Novaya Basmannaya 10, Box 231, Moscow 107078, Russia

MODEL DESCRIPTION

The model package COLD, describing the hydrothermal processes on a local scale, includes the following three independent analytical models: model FRED (FREezing Depth), SOT (SOil Temperature), and MIR (Melting, Infiltration, Runoff).

It should be noted that the main elements of each model are universal; i.e., suitable for calculating the dynamics of soil water content in different natural zones. However, when linking the models into the package, we have used some empirical relations and parameterizations appropriate to the steppe and forest-steppe zones. That is why the given version of COLD is suitable only for these zones. Besides that, to simplify the scheme it was assumed that the increment of soil water supply from snow melting occurs only in spring; i.e., possible short periods of winter thawing were neglected.

Now we shall briefly describe all the models of the package separately. For convenience all mathematical symbols are systematized in an Appendix.

Modelling the dynamics of soil freezing depth (model FRED)

The soil freezing depth ξ at the time step t_i can be calculated as (Gusev 1988):

$$\xi(t_i) = -\eta(t_i) - \frac{q_H(t_{i-1})\Delta t}{L^*} +$$

$$+\sqrt{[\xi(t_{i-1})+\eta(t_i)]^2 - \frac{2k_2 T_{sn}\Delta t}{L^*} + \left[\frac{q_H(t_{i-1})\Delta t}{L^*}\right]^2}, \quad (1)$$

$$L^* = \lambda_1 \rho_w (W - u^*) + \frac{c_2|T_s|}{2}, \quad (2)$$

$$q_H = \frac{2k_3\tilde{T}}{\sqrt{2.25\xi^2 + 12 \cdot a_3(t_i + t_0) - 1.5\xi}}, \quad (3)$$

$$\eta = h\frac{k_2}{k_1}, \quad a_3 = \frac{k_3}{c_3},$$

where parameter t_0 is the influence of a period prior to freezing, in our calculations it is taken to be 10 days (Gusev 1993), and the snow temperature T_{sn} is assumed to be equal to the air temperature T_2. Snow depth is determined by the following expression:

$$h = S / \rho_1 . \quad (4)$$

Snow density ρ_1 is calculated following Yosida (1955). Snowpack S (in SI units) is obtained from

$$S(t_i) = \begin{cases} S(t_{i-1}) + \alpha P(t_i)\Delta t & T_2 \le 0 \\ S(t_{i-1}) - \frac{k_m T_{sn}}{1 - \varepsilon_w}\Delta t & T_2 > 0 \end{cases} . \quad (5)$$

Here, $\varepsilon_w = 110 / \rho_1 - 0.11$ (Kuchment et al. 1983) is water holding capacity of snow. The empirical factor α was found to be equal to 0.7 from observational data of the water balance station Nizhnedevitskaya (forest-steppe zone, the Voronezh region, Russia).

Snow thermal conductivity k_1 can be calculated using an empirical relation (Abels 1892) rewritten in SI units as:

$$k_1 = 2.9 \cdot 10^{-6} \rho_1^2 . \quad (6)$$

The soil surface temperature is calculated as:

$$T_s = T_{sn}\xi / (\xi + \eta) . \quad (7)$$

The outputs of the model include soil freezing depth, snow depth and snow density at the end of every time step being equal to 10 days. The values of these quantities at the end of the cold season are used by the model SOT.

Formation of the vertical profile of soil temperature at the beginning of snowmelt (model SOT)

This model is necessary because the rate of infiltration of thawed snow into frozen soil and the total amount of infiltrated water depend, to a large extent, on the soil thermal conditions at the beginning of snowmelt. The model simulates formation of the vertical profile of soil temperature $T_{in}(z)$ and calculates the mean value of soil temperature in the frozen zone T_{mn} at the mentioned moment. The quantity T_{mn} greatly affects the content of unfrozen water in the frozen soil which, in its turn, influences the infiltration rate of thawed snow.

The problem of calculating the vertical profile of temperature in the frozen zone has been solved in Gusev (1993) using the integral balance method (Goodman 1967). The main idea of the method is to approximate the vertical distribution of soil temperature by a polynomial in the vertical coordinate z with indeterminate, time-dependent coefficients, which are found using the heat balance

equation in the integral form and the boundary conditions.

As shown in Gusev (1993), the typical vertical profile of soil temperature in winter usually has a linear character (Figure 1a). In spring, before snowmelt, the nonlinear component in the vertical distribution of temperature within both snow and soil zones dominates (Figure 1b). So, the
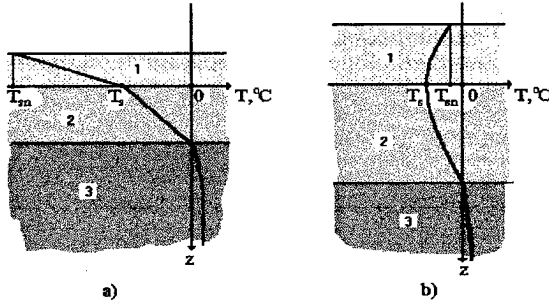
Figure 1. Schematic profiles of the soil and snow temperatures: (a) in winter, (b) in pre-spring period; 1 - snow, 2 - frozen soil, 3 - unfrozen soil.

temperature profile in frozen soil for this period allows the following parabolic approximation:

$$T_{in}(z) = \beta_1 z^2 + \beta_2 z + \beta_3 \quad . \qquad (8)$$

Here, β_1, β_2 and β_3 are functions depending on the dynamics of temperature of the land surface $T_{sn}(t)$, on the duration of winter t_w, on the quantities k_1, k_2, ξ, h and on the thermal diffusivities of snow $a_1 = k_1 / (c_1 \rho_1)$ and frozen soil $a_2 = k_2 / c_2$. Model SOT calculates numerical values of β_1, β_2 and β_3 at the onset of snowmelt. The theoretical basis of calculating these quantities has been described in (Gusev 1993).

Upon integrating eq. (8) with respect to z, we obtain the mean temperature of frozen zone T_{mn} at the beginning of the snowmelt period. This value is used in the next model, model MIR.

Modelling spring runoff and infiltration of thawing snow into the soil (model MIR)

The infiltration rate q_0 can be written as:

$$q_0 = \overline{K}\left(1 + \overline{H} / z_0\right) \quad , \qquad (9)$$

$$\overline{K} = \frac{1}{z_0}\int_0^{z_0} K dz \quad , \quad \overline{H} = \int_{\phi(z_0)}^{\phi(0)} K / \overline{K} d\phi \quad , \quad (10)$$

where $\overline{K}$ is the average hydraulic conductivity of the moist zone, $\overline{H}$ is effective capillary potential of the soil, $z=0$ corresponds to the earth's surface, and $z=z_0$ is the depth of the infiltration front.

To a first approximation we assume that $\overline{K}$ and $\overline{H}$ depend on the average contents of liquid water u and ice I in wet soil and can be computed by Gusev (1989) as follows:

$$\overline{K}(u,I) = K_0\left(\frac{u - u_s}{p - u_s}\right)^4 \frac{1}{(1 + 8 \cdot I)^2} \quad , \quad (11)$$

$$\overline{H}(u,I) = H_0 \frac{1 + 8 \cdot I}{1 - I / p^*} \cdot \frac{u - \tilde{u}_n}{p^* - I - \tilde{u}_n} \quad . \quad (12)$$

Here, u_s approximately can be set to be equal to the amount of unfrozen water for the temperature -5°C (Kalyuzhnyi and Pavlova 1981). Effective soil porosity can be estimated by Gusev (1993):

$$p^* \approx p \cdot (1 - 0.1 \cdot W_0 / p) \quad , \qquad (13)$$

where W_0 is initial total soil moisture before the beginning of snowmelt.

Therefore, to calculate the infiltration rate we need the values of u and I which are connected with the total water content W by the following relation:

$$W = I \cdot (\rho_I / \rho_w) + u \quad . \qquad (14)$$

The ice content is calculated as:

$$I = I_0 + \Delta I \quad , \qquad (15)$$

where ΔI is the ice content increment during infiltration, and I_0 is the ice content in the frozen zone before snow melting, which is related to the initial value of the total soil moisture W_0 by relation:

$$I_0 = (W_0 - \tilde{u}_n)(\rho_w / \rho_I) \quad . \qquad (16)$$

The quantity $\tilde{u}_n$ is calculated by Gusev (1989):

$$\tilde{u}_n = \begin{cases} u^* & T_{mn} \leq T^* \qquad (17) \\ u^* + (W_0 - u^*)\dfrac{Q_T}{Q_{T0}} & T_{mn} > T^*, \; Q_T \leq Q_{T0} \\ W_0 & T_{mn} > T^*, \; Q_T > Q_{T0} \end{cases}$$

68

where $u*$ and $T*$ are the parameters of the relation between the amount of unfrozen water in frozen soil and its temperature. Their sense becomes clear from Figure 2. Typical values of $u*$ and $T*$ for chernozem soil are equal to 0.23 m^{3}m^{-3} and -0.1°C, respectively (Kalyuzhnyi and Pavlova 1981). The quantities Q_T and Q_{T0} are determined as:

$$Q_{T0} = \lambda_I \rho_w (W_0 - u^*) , \quad Q_T = 2k_2 \frac{|T^*|}{0.25\xi} \Delta\tau . \quad (18)$$

Here, $\Delta\tau$ is the time interval between the beginning of snowmelt and the moment at which the relation

$$|T_s| \approx |T_{sn}| / \left(1 + \frac{h}{\xi}\frac{k_2}{k_1}\right) < |T^*| . \quad (19)$$

is fulfilled.
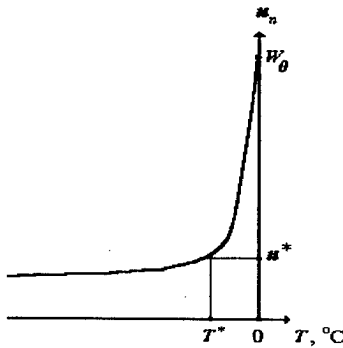
Figure 2. Dependence of amount of unfrozen water in the frozen soil u_n on soil temperature T.

It should be noted that the processes affecting the rate of infiltration basically take place in the uppermost 20-30 cm soil layer. That is why here we use the total soil moisture averaged over the top 20 cm. It is connected with the mean available moisture of the 1-m soil layer W_a by equation:

$$W_0 = 1.24 \cdot W_a + 0.115 , \quad (20)$$

which was derived from standard data from the agrometeorological station Petrinka (forest-steppe zone, the Kursk region, Russia) on average soil moisture in 1-m and 0.2-m soil layers under different agricultural crops from 1955 to 1988.

The increment of ice content ΔI is obtained from the solution of the problem on soil heat regime during the snowmelt period (Gusev 1989):

$$\Delta I(t_i) = \begin{cases} \dfrac{B(t_i)}{\rho_I \lambda_I z_0(t_i)} & z_0(t) > 0 \\ 0 & z_0(t) = 0 \end{cases} , \quad (21)$$

$$B(t_i) = -\sum_{i=1}^{t_i} k_2 \left[\frac{dT_{in}}{dz}\bigg|_{z=z_0} + \frac{2T_{in}(z_0)}{\sigma(t_i) - z_0(t_i)} \right] \cdot e^{-\frac{12a_2 t}{\xi^2}\Delta t} ,$$

where σ, the penetration depth (the depth of a noticeable change of soil temperature resulting from the infiltration of liquid water), is calculated as:

$$\sigma(t_i) = -2z_0(t_i) + \sqrt{9z_0^2(t_i) + 12a_2 t} . \quad (22)$$

By combining eqs.(9), (21) and (22) with the water balance equation for wet soil

$$\int_0^t (q_0 - K_n)dt = z_0\left(\Delta I(\rho_I / \rho_w) + u - \tilde{u}_n\right) \quad (23)$$

(where $K_n = K(\tilde{u}_n, I_0)$ is the coefficient of hydraulic conductivity of the soil ahead of the infiltration front) we obtain the system of four equations in five unknown quantities: $\Delta I(t)$, $u(t)$, $q_0(t)$, $z_0(t)$ and $\sigma(t)$. To close the system, it is necessary to use the fifth equation:

$$q_0 = J_0 , \quad \text{if} \quad I + u \le p^* , \quad (24)$$

otherwise the closing equation is as follows:

$$I + u = p^* . \quad (25)$$

In this case $q_0 < J_0$ (the earth's surface is flooded and surface runoff occurs).

Solution of the described system of equations allows one to calculate the dynamics of infiltration rate and the total amount of infiltrated water during the period of spring snowmelt. The time step of MIR is equal to 1 day. The use of a smaller time step can be explained by the fact that the rate of hydrothermal processes during the spring snowmelt is much higher than during the soil freezing.

VALIDATION OF THE MODEL COLD

Data and parameters

The model package COLD was validated using the following standard records from the agrometeorological station Petrinka (forest-steppe

69

zone, the Kursk region, Russia) from 1955 to 1988 at the same spatial resolution as the model has: (i) soil hydrophysical parameters, such as field capacity and porosity; (ii) diurnal agrometeorological data on air temperature at 2 m and precipitation, and (iii) the water storage in the 1-m soil layer measured on different agricultural fields (winter and spring wheat, winter rye, barley, buckwheat, corn, grass).

In addition, we used data on water stores in the 1-m soil layer for fallow from 1955 to 1973 obtained in the Central-Chernozem State Forest-Steppe Reserve (Gertsyk 1979) situated not far from the Petrinka.

Some heat and hydrophysical parameters of the soil for the package COLD, namely, u_s, u^*, T^*, $\tilde{T}$, k_2, k_3, c_2, c_3, were obtained on the basis of the results of investigations given in (Kalyuzhnyi and Pavlova 1981) while taking into account the type of soil (typical chernozem), typical fresh snow density, typical soil moisture in the winter period (which is usually close to the field capacity) and soil density.

The temperature coefficient of snowmelt k_m was obtained from the field measurements of snowpack in the Kursk region. Its value being close to $5.8 \cdot 10^{-5}$ kg m^{-2} s^{-1} °C^{-1} is recommended in the literature (Apollov et al. 1974). The values of hydraulic conductivity at saturation K_0 and maximum value of effective capillary potential H_0 for the given type of soil were estimated on the basis of field experiments (Gusev 1981, Yasinskii 1982).

The main problems are connected with the provision of the model with the following parameters: hydraulic conductivity at saturation K_0 and the dependence of unfrozen water in frozen soil on soil temperature $u_n(T)$ for obtaining u^*, T^* (Figure 2) and u_s (which is connected with u^*). Available information on these parameters, which have the most influence on the increment of soil water storage during snowmelt, is very limited.

Results and discussion

Outputs of the package COLD include available soil water storage in the uppermost 1-m soil layer in spring, at the beginning of warm season (V_{sp}). Calculated values of V_{sp} for different agricultural crops were verified against values measured in different agricultural fields. Their comparison is depicted in Figure 3. The root mean square deviation between simulated and measured values is equal to 21.6 kg m^{-2} which is only twice as large as the error of measurements of water storage in the 1-m soil layer (Mastitskaya 1959). This disagreement was expected because COLD does not take into account

the winter thawing; i.e., all accumulated snow is assumed to melt only in spring.
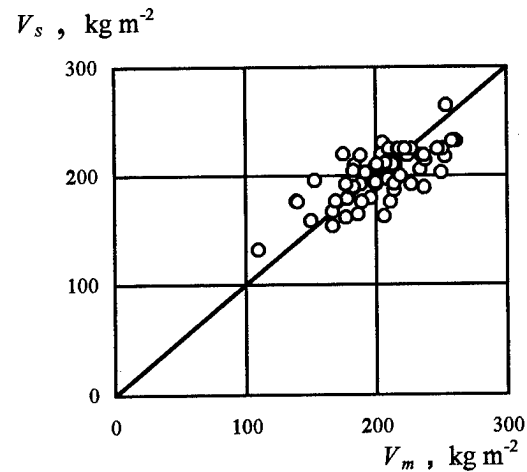
Figure 3. Comparison of measured V_m against simulated V_s available (calculated as the difference between total water storage and plant wilting point) water storage in the 1-m soil layer in spring at the end of the cold season using programme COLD.

Calculated by COLD, available soil water storage can be used as an input value for the model VAST (Vegetation-Atmosphere-Soil Transfer scheme), describing the processes of heat and water exchange within a soil-vegetation-atmosphere system during the warm period (Gusev and Nasonova 1997). Combining COLD and VAST into one package, named ANDY__SWASH (ANnual DYnamics of Soil WAter Stores for Homogeneous areas), gives us an opportunity to simulate soil water variations continuously throughout a year, and year by year.

For validation of the whole package ANDY_SWASH we performed simulations for different types of the land surface (fallow, agricultural crops, grassland). Simulated values of available water storage in the 1-m soil layer, V_s, were compared with corresponding measured values, V_m. Some results of comparison are depicted in Figure 4, which shows annual and interannual variation of simulated V_s and measured V_m soil water storage. All the simulations were run continuously over a number of years.

The comparison of simulated and measured dynamics shows that the simulations give reasonable descriptions of soil water variation for the warm season in the studied region with a continental climate. The root mean square error of the calculations is equal to 25, 30, and 33 kg m^{-2} for fallow (18 years, 131 points), grassland (12 years,
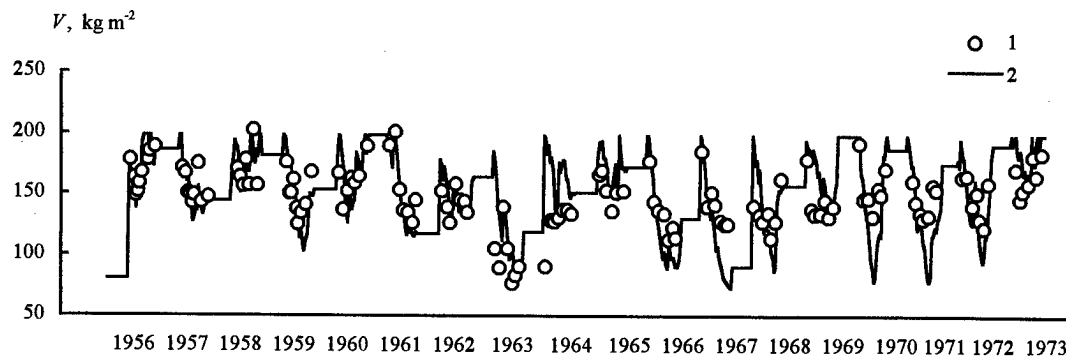
Figure 4. Interannual variation of measured (1) and simulated (2) available water storage V in 1-m soil layer below fallow.

256 points) and agricultural crops (49 years-locations, 570 points), respectively. Such errors can be considered as satisfactory.

CONCLUSION

Three models describing hydrothermal processes over the cold season of a year were linked into the package named COLD. Validation of the package shows that it is suitable for calculating annual and interannual variations of soil water storage in different agro- and non-forested ecosystems of the forest-steppe zone with satisfactory accuracy. The root mean square error of the calculations of the water storage in the 1-m soil layer does not exceed 33 kg m^{-2}, which is in satisfactory agreement with the accuracy of field measurements at agro-meteorological stations of the Former Soviet Union.

The package COLD together with the model VAST provides a basis for estimating the efficiency of various methods of soil water regime management, for calculating water use and regimes of irrigation, for optimizing snow amelioration, for forecasting the consequences of "dry" agriculture, and, in particular, soil mulching by plant remains.

ACKNOWLEDGMENT

REFERENCES

Abels, H. 1892. Beobachtungen der taglichen periode der temperatur im schnee und bestimmum des warmeleitungsvermogens des schnees als function sciner dichtigkeit. (in German). Rep. Meteorolog. 16(1):1-53.

Apollov, B.A., G.P. Kalinin, and V.D. Komarov. 1974. Course of hydrological forecasts. (in Russian). Gidrometeoizdat, Leningrad, USSR.

Gertsyk, V.V. 1979. The materials of many-years chernozem water content observations in Central Chernozem reserve. p. 73-229. (in Russian). *In* V.A. Ryabov (ed.) Materials of stationary research for the components of forest-steppe preserved biogeocoenoces. Climate, soil moisture and phytophenology. Gidrometeoizdat, Leningrad, USSR.

Goodman, T.R. 1967. Application of integral methods in nonlinear problems of nonstationary heat exchange. p. 41-96. (in Russian). *In* P.L. Kirillov (ed.) Problems of heat exchange. Atomizdat, Moscow, USSR.

Gusev, Ye.M. 1981. Experimental research of infiltration. p. 195-205. (in Russian). *In* S.V. Nerpin (ed.) Physics of soil water. Nauka, Moscow, USSR.

Gusev, E. M. 1988. Simplified calculation of soil freezing depth with consideration of water migration to the freezing boundary. Water Resources 15(1): 9-17.

Gusev, E.M. 1989. Infiltration of water into soil during melting of snow. Water Resources 16(2): 108-122.

Gusev, Ye.M. 1993. Formation of regime and resources of soil water during winter-spring period. (in Russian). Fizmatlit, Nauka, Moscow, Russia.

Gusev, Ye.M., and O.N. Nasonova. 1997. Modelling annual dynamics of soil water storage for agro- and natural ecosystems of the steppe and forest-steppe zones on a local scale. Agric. For. Meteor.

(in press)

Kalyuzhnyi, I.L., and K.K. Pavlova. 1981. Formation of thawed snow runoff losses. (in Russian). Gidrometeoizdat, Leningrad, USSR.

Kuchment, L.S., V. N. Demidov, and Yu.G. Motovilov. 1983. Formation of river runoff. Physical-mathematical models. (in Russian). Nauka, Moscow, USSR.

Mastitskaya, S.B. 1959. About a method for determination of soil moisture in different soil-climatic zones. (in Russian). Trans. Central Inst. of Prognosis 88: 57-75

Yasinskii, S.V. 1982. Spatial variability of soil hydraulic conductivity at saturation for arable and virgin soil in the Central Forest-Steppe. (in Russian). Meteorol. Hydrol. 10: 113-115.

Yosida, Z. 1955. Physical studies on deposited snow. Contrib. Inst. Low Temp. Sci., Sapporo, 7: 19-74

APPENDIX: List of mathematical symbols

a_1 thermal diffusivity of snow ($m^2 s^{-1}$)

a_2 thermal diffusivity of frozen soil ($m^2 s^{-1}$)

a_3 thermal diffusivity of unfrozen soil ($m^2 s^{-1}$)

c_1 specific heat capacity of ice ($J\,kg^{-1}{}^{\circ}C^{-1}$)

c_2 heat capacity of frozen soil ($J\,m^{-3}\,{}^{\circ}C^{-1}$)

c_3 heat capacity of unfrozen soil ($J\,m^{-3}\,{}^{\circ}C^{-1}$)

g acceleration due to gravity ($m\,s^{-2}$)

h snow depth (m)

H_0 maximum effective capillary potential of the soil ($J\,kg^{-1}$)

I soil ice content ($m^3 m^{-3}$)

I_0 ice content in the frozen soil before snow melt ($m^3 m^{-3}$)

J_0 the rate of water yield of snow ($kg\,m^{-2}\,s^{-1}$)

k_m temperature coefficient of snow melting ($m^{-2}\,kg\,s^{-1}\,{}^{\circ}C^{-1}$)

k_1 thermal conductivity of snow ($W\,m^{-1}\,{}^{\circ}C^{-1}$)

k_2 frozen soil thermal conductivity ($W\,m^{-1}\,{}^{\circ}C^{-1}$)

k_3 thermal conductivity of unfrozen soil ($W\,m^{-1}\,{}^{\circ}C^{-1}$)

K hydraulic conductivity of the moist soil ($W\,m^{-1}\,{}^{\circ}C^{-1}$)

K_0 saturated hydraulic conductivity of the moist soil ($kg\,m^{-2}\,s^{-1}$)

K_n hydraulic conductivity of the soil ahead of the infiltration front ($kg\,m^{-2}\,s^{-1}$)

p soil porosity (dimensionless)

p^* effective soil porosity (with the exception of pores occupied by entrapped air) (dimensionless)

P precipitation rate ($kg\,m^{-2}\,s^{-1}$)

q_0 infiltration rate ($kg\,m^{-2}\,s^{-1}$)

q_H conductive heat flux from underlying unfrozen zone to the front of freezing ($W\,m^{-2}$)

S snowpack ($kg\,m^{-2}$)

t time (s)

t_0 parameter characterizing the influence of a period prior to freezing on freezing depth formation (s)

t_w duration of winter (s)

T air temperature (°C)

T_{in} soil temperature profile before snowmelt (°C)

T_{mn} mean soil temperature in frozen zone before snowmelt (°C)

T_s soil surface temperature (°C)

T_{sn} snow surface temperature (°C)

T_2 air temperature at a reference height (here, at 2 m) (°C)

T^* temperature parameter in relation between the amount of unfrozen water in frozen soil and its temperature (Figure 2) (°C)

$\widetilde{T}$ soil temperature at the depth where seasonal temperature variations are damped out (°C)

u volumetric content of liquid water in wet soil during snowmelt ($m^3 m^{-3}$)

u_s static soil water ($m^3 m^{-3}$)

u^* minimum amount of unfrozen water in frozen soil ($m^3 m^{-3}$)

$\widetilde{u}_n$ volumetric initial content of unfrozen water in frozen soil before snowmelt ($m^3 m^{-3}$)

V available soil water storage in 1-m soil layer ($kg\,m^{-2}$)

V_{sp} available soil water storage in 1-m soil layer at the beginning of warm season ($kg\,m^{-2}$)

W volumetric total soil water content ($m^3 m^{-3}$)

W_a volumetric available soil moisture in the 0.2-m soil layer ($m^3 m^{-3}$)

Y surface runoff ($kg\,m^{-2}\,s^{-1}$)

z vertical coordinate (m)

z_0 position of infiltration front (m)

Δt time step of calculations (s)

ε_w water holding capacity of snow (dimensionless)

λ_I heat of water-ice transformation at 0°C ($J\,kg^{-1}$)

ρ_I ice density ($kg\,m^{-3}$)

ρ_w water density ($kg\,m^{-3}$)

ρ_1 snow density ($kg\,m^{-3}$)

ρ_{10} density of fresh snow ($kg\,m^{-3}$)

σ penetration depth (m)

ξ soil freezing depth (m)

ψ matric potential of soil water ($J\,kg^{-1}$)

Model for the Dynamics of Characteristics of Spatial Variability of Soil Freezing Depth

Ye.M. GUSEV[1] AND O.Ye. BUSAROVA[1]

ABSTRACT

In the present work we attempt to create a model describing the dynamics of formation of soil freezing depth variability, taking into account the spatial variability of the main factors influencing this process, the height of snow cover and the soil moisture. The proposed model allows us to calculate the variation of the area-averaged soil freezing depth and its standard deviation for areas with intermediate linear size ranging from several tens of meters up to several tens of kilometres. This model was validated using standard records of the agrometeorological and water-balance stations located in the Kursk region (forest-steppe zone, Russia), and experimental studies carried out by the authors at the Kursk Biosphere Station.

Key words: Soil freezing depth, soil moisture, snow cover, spatial variability.

INTRODUCTION

One of the most distinguishing features of natural objects (natural and agricultural ecosystems, biomes, etc.) is a pronounced spatial heterogeneity of their geophysical parameters, which in its turn produces a noticeable spatial variability in relevant characteristics of the heat and moisture regime of soil. This fact necessitates the construction of dynamic-stochastic models for the processes of heat and water exchange in soil, when we need to describe the heat and water exchange between the underlying surface and the atmosphere, as well as the formation of the water and heat regime of objects having a large spatial scale. These models must combine both: (a) physical determinism of natural processes, which is the basis for different advanced dynamic models for the formation of the hydrothermal regime of soil (they are used in hydrology, agrometeorology, and crop forecasts), and (b) stochastic character of the spatial distribution of soil parameters or hydrometeorological factors governing the above regime.

The necessity to solve such a problem is conditioned by at least two circumstances. The first is a nonlinear character of a number of relationships between various hydrometeorological characteristics, soil parameters, and indices of the soil hydrothermal regime entering the dynamic equations for the water and heat exchange in soil. By virtue of this, the area-averaged characteristics of the hydrothermal regime of soil cannot always be obtained by way of a simple substitution of the mean values of forcing data or landsurface parameters in dynamic equations (which is possible in the case of linear equations). The second circumstance is that the information on the area-averaged values of certain characteristics with significant spatial variability is often inadequate to solve the problem under consideration.

The characteristic linear size of a region or a cell of the calculation grid in two-dimensional hydrological models or the models of general circulation, which require the consideration of the inner spatial heterogeneity, lies in the range of 1-100 km. Such objects are usually assigned to intermediate or mesoscale ones in accordance with the frequently used classification of spatial scales (for example, in the international projects deal with biospheric aspects of the hydrological cycle, with

intercomparison of land-surface parameterization schemes, et al.).

Recently, there appeared models describing the heat and moisture regime of soil during the warm half year for large-scale, spatially heterogeneous objects (e.g., Entekhabi and Eagleson 1989). Among them is, in particular, the mesoscale model, which we elaborated for describing the variation of soil water storage during the vegetation period (Gusev et al. 1995). This model takes into account the spatial variation of atmospheric precipitation, leaf area index of the vegetation cover, and spring soil water storage. The statistical characteristics of spatial distribution of the latter parameter are considered in such models as the given initial quantities. At the same time, they themselves are the consequence of heterogeneity of both the autumn soil water storage and the spatial variability of its spring refill. As for the spatial distribution of the total amount of spring water infiltration into soil, it strongly depends on the spatial heterogeneity of the soil freezing depth and the depth of snow cover (Gusev 1993). Hence, the combination of physical determinism of hydrological processes and stochastic character of spatial distribution of some landsurface parameters becomes an important problem for the cold period too.

The goal of the present work is to create the dynamic-stochastic model of the soil freezing variation taking into account the spatial variability of the main factors influencing this process.

THEORY

The proposed dynamic-stochastic model of soil freezing depth calculates its mean value and variability characteristics for a relatively large-scale heterogeneous object (a field, farm, region, cell of a grid of a climatic or hydrological model). The solution of this problem, which presents a certain stage for the subsequent assessment of the spring refill of the soil water storage (hydrological aspect of the problem), may also be important by itself when we assess the spatial variability of hibernation feasibility of winter crops (agrometeorological aspect) (Palagin 1981).

The methodological basis for the solution of the problem in hand is the spatial averaging of the dynamic equations for soil freezing, which are valid for a relatively small homogeneous area. We used the equations for the dynamics of the soil freezing depth, which were obtained and published by one of

the authors of this paper (Gusev 1993). One of the versions of such equations looks as follows:

$$\xi(t) \approx \xi_0(t) + k_S F_2(t) h(t),\qquad(1)$$

$$\xi_0(t) \approx A F_1(t),\qquad A \approx \sqrt{2 \frac{k_S}{\lambda(W - W_{un})}},$$

where $\xi(t)$ is the depth of soil freezing at a moment t; W, W_{un}, and k_S are respectively the total moisture in frozen soil, content of unfrozen water in it, and its thermal conductivity; $h(t)$ is the height of snow cover at the current moment; λ is the heat of fusion of ice transformation; F_1 and F_2 are functions mainly depending on the dynamics of air temperature, dynamics of the snow cover height during the cold period, and the thermal conductivity of snow. We don't represent here the expressions for these functions (they are given in [Gusev 1993]), since for further analysis we only need general notation of the relationship of the quantities ξ, W, k_S, and h, which is reflected in Eq.(1). Exact expressions for the functions F_1 and F_2 are unnecessary.

The analysis of field data on the thermal conductivity of soils of different types (see, for example, (Kalyuzhnyi and Pavlova 1981)) shows that the first approximation for the dependence of k_S on soil moisture content may be expressed as:

$$k_S \approx \alpha + \beta W\qquad(2)$$

where α and β are the approximation parameters; and for soil moisture contents in the winter season (they are close to the soil field capacity), this expression may be simplified:

$$k_S \approx \beta W.\qquad(3)$$

From Eq.(1), with consideration of Eq.(3) it follows that the height of snow cover and the soil moisture are the principal characteristics having essential spatial variability and thus determining the spatial variability of freezing depth. The parameters W_{un} and β, depending on the density and mineral composition of soil, also vary; but there is virtually no information on their variability, and their influence on the variability of ξ is likely to be much less than that of variations in W and h.

The criterion which determines the spatial scale of the applicability of the dynamic-stochastic model for soil freezing proposed below is the spatial variation of air temperature. The model becomes inapplicable for areas within which the spatial

74

diversity of air temperature is noticeable. This condition is usually met by objects with a linear size not exceeding 10-100 km.

The main, and evidently sufficient (in the framework of this study), characteristics of a random variable are its two statistical characteristics: mean and standard deviation. This leads to the next, more restricted problem: to construct, using Eqs. (1) and (3), the system of equations describing not the variation of a "point" value of freezing depth, but that of its area-averaged value $\bar{\xi}$ and standard deviation σ_ξ within the limits of the area considered (hereafter, the dash above the relevant variable means its spatial average). In this case, the necessary source information is also presented by the area-averaged values of the variables W and h and their standard deviations.

The averaging of Eq.(1) with consideration of Eq.(3) leads to the following expression for $\bar{\xi}$

$$\bar{x} = \overline{AF_1} + \overline{k_S h F_2} = \overline{AF_1} + \overline{k_S} F_2 \bar{h} \approx$$
$$\approx (1 - \frac{C_{VW}^2}{4}) A(\overline{W}) F_1 + \overline{k_S} F_2 \bar{h} \approx \qquad (4)$$
$$\approx A(\overline{W}) \cdot F_1 + \overline{k_S} F_2 \bar{h} \ ,$$
$$C_{VW} = \frac{\sigma_W}{\overline{W}} = \frac{\sqrt{\overline{(\overline{W} - W)^2}}}{\overline{W}} \ ,$$

where σ_W is the standard deviation of the values of the soil moisture for an object considered. Neglect of the quantity $\frac{1}{4} C_{VW}^2$ in Eq.(4) is explained by the fact that the order of its usual values in winter is about 10^{-2}.

Thus, the freezing depth, averaged over a given area, may be calculated from the equation of the dynamics of freezing for a uniform area (not necessarily in the form of Eq.(1)) using the area-averaged values of W and h.

Let us derive the equation of σ_ξ variation. Subtracting Eq.(4) from Eq.(1), we obtain an expression for the assessment of the deviation of freezing depth from its average value. If we raise the obtained equation to a power 2 and average it over the area considered, then, with the absence of correlation between k_S and h, we get the following expression for σ_ξ

$$\sigma_\xi^2 = \sigma_A^2 F_1^2 + \overline{k_S}^2 F_2^2 \sigma_h^2 + \overline{h}^2 F_2^2 \sigma_k^2 \ , \qquad (5)$$

where σ_A, σ_h, σ_k are the standard deviations of the parameter A, snow cover height, and thermal conductivity of frozen soil, respectively.

Rewriting Eq.(5) in terms of Eqs.(1) and (3), we have:

$$\sigma_\xi^2 \approx \sigma_{\xi W}^2 + \sigma_{\xi h}^2 \ , \qquad (6)$$
$$\sigma_{\xi W}^2 = \left\{ \frac{1}{4} \bar{\xi}_0^2 \left(\frac{W_1}{\overline{W} - W_{un}} \right)^2 + (\bar{\xi} - \bar{\xi}_0)^2 \right\} C_{VW}^2 \ ,$$
$$\sigma_{\xi h}^2 = (\bar{\xi} - \bar{\xi}_0)^2 C_{Vh}^2 \ ,$$
$$C_{Vh} = \frac{\sigma_h}{\overline{h}} \ ,$$

where $\bar{\xi}$ and $\bar{\xi}_0$ are the freezing depths averaged over the area with the presence of snow cover and without it, respectively. The quantities $\sigma_{\xi W}^2$ and $\sigma_{\xi h}^2$ are the contributions the total dispersion σ_ξ^2 associated with the spatial variability of soil moisture and snow cover height, respectively.

It follows from Eq.(6) that a calculation method for the estimation of $\bar{\xi}$ and $\bar{\xi}_0$ is needed for the assessment of σ_ξ. In principle, we may use Eq.(4), but it is not convenient because of cumbersome calculations of the functions F_1 and F_2 (Gusev 1993). Therefore, we use here another method for calculating the average values of freezing depths, which is also discussed in (Gusev 1993). It is based on the equation for the rate of the freezing front movement:

$$\lambda^* \frac{d\bar{\xi}}{dt} = q_f - q_{un}, \qquad (7)$$
$$\lambda^* = \lambda \rho_W (\overline{W} - W_{un}) + \frac{C_S |T_S|}{2}, \qquad T_S = \frac{T_{sn} \bar{\xi}}{\bar{\xi} + H} ,$$
$$q_f = -\frac{\overline{k_S} T_{sn}}{\bar{\xi} + H}, \qquad H = \frac{\overline{k_S}}{k_{sn}} \bar{h} ,$$
$$q_{un} = \frac{2 k_{un} T^*}{\sqrt{2,25 \cdot \bar{\xi}^2 + 12 a_{un} (t + t_0) - 1,5 \cdot \bar{\xi}}} .$$

Here, q_f is the heat flux from the freezing front into the frozen zone, q_{un} is the heat flux from the unfrozen zone to the freezing front, T_{sn} is the

10-day mean temperature of snow surface (hereafter, all values of temperature are given in °C), generally taken equal to the air temperature at a measurement height (here, at 2 m), T_S is the temperature of soil surface, T^* is the temperature of soil at the depth where the seasonal variations of temperature fade out; C_S is the heat capacity of frozen soil, k_{un} and a_{un} are respectively the thermal conductivity and the thermal diffusivity of unfrozen soil, k_{sn} is the thermal conductivity of snow, ρ_W is the density of water, t_0 is the parameter accounting for the autumn cooling of soil until the air temperature steadily falls below 0°C (for central regions of the European part of Russia, this time may approximately be to a 10-day period [Gusev 1993, Pavlov 1975]).

The solution of Eq.(7) leads to a recurrence formula for calculating the freezing depth at the moment t_2, with its known value at the moment t_1 and with the 10-day step $\Delta t = t_2 - t_1$:

$$\bar{\xi}(t_2) = -H(t_2) - \frac{q_{un}(t_1)\Delta t}{\lambda^*(t_2)} + \qquad (8)$$

$$+\sqrt{\left[\bar{\xi}(t_1) + H(t_2)\right]^2 - \frac{2\bar{k}_S T_{sn}\Delta t}{\lambda^*(t_2)} + \left[\frac{q_{un}(t_1)\Delta t}{\lambda^*(t_2)}\right]^2}$$

The thermal conductivity of snow is calculated by the empirical Abels (1892) formula, which relates its value in cal/(s cm grad) with the snow density ρ_{sn} in g/cm^3:

$$k_{sn} = 0.0068\rho_{sn}^2 \qquad (9)$$

As for the dynamics of snow density, it is described by the following empirical recurrence equation (Yosida 1955), using a 10-day time step:

$$\rho_{sn}(t_2) = \rho_{sn}(t_1)\{1 + \frac{\rho_{sn}(t_1)\bar{h}}{\rho_W} \cdot$$
$$\cdot exp[0.08\frac{T_{sn}}{2} - 21\cdot\rho_{sn}(t_1)]\} . \qquad (10)$$

Here, the snow and water densities are also given in g/cm^3, $\bar{h}$ is given in cm.

The value $\bar{\xi}_0$ is also calculated by using Eq.(8), under condition of $\bar{h}(t) \equiv 0$.

EXPERIMENTAL VALIDATION

The proposed method was verified for three objects of different spatial scales. The first object was an agricultural field in the region of the Kursk Biosphere Station, the second one was the area of the Nizhnedevitsk Water-Balance Station, and the third one was the Kursk region. All objects are situated in the forest-steppe zone of Russia. The representative linear scales for these objects are 10^{-1}, 10^1, and 10^2 km, respectively. Hence, the working capacity of the model was verified for objects having the spatial linear scale in the range of approximately from several tens meters up to several tens kilometres.

To compare the calculated values of the freezing depth with experimental ones, we used the relevant measurement data obtained by the Danilin freezometers. In the region of the Kursk Biosphere Station, the measurements of freezing depths and snow cover heights were conducted by the authors of this paper during the winter 1979-1980, using 25 freezometers together with the pertinent snow stakes installed in an agricultural field. For the Nizhnedevitsk Water-Balance Station, we used the data of standard observations made with the help of 23 freezometers and snow stakes placed in different ecosystems within the area of the Station during the winter periods 1975-1976 and 1977-1978. For the Kursk region, we used the observation data from nine meteorological stations for the winter seasons 1954-1955 and 1956-1957.

The soil at all the objects is typical chernozem. Its thermophysical parameters are taken from Kalyuzhnyi and Pavlova (1981) with consideration of information available at the stations on the density and moisture of soil. The temperature T^* is estimated according to the data on the temperature of ground waters occurring below the soil surface by 10-15 m.

The quantities $\bar{h}$ and σ_h, necessary for calculations, are assessed from the of snow-measuring observations. $\bar{W}$ is determined from the observation data on the soil moisture in different sites of the areas under consideration: data of standard measurements of soil moisture at agrometeorological stations of the Kursk region and the Nizhnedevitsk Water-Balance Station, as well as data of the neutron moisturemeters used at three points in a field at the Kursk Biosphere Station.

The assessment of σ_W in the frozen layer of soil is based on the following considerations. In Verigo and Razumova (1973) there are estimations

of accuracy of standard measurements of the soil water storage in a 1-m soil layer for objects of different spatial scale in the steppe and forest-steppe zones of Russia. These errors are: 14 kg/m^2 for an agricultural field, 17 kg/m^2 for a farm (size of farm is about that of a water-balance station), 25 kg/m^2 for an administrative district (region). They define the measurement accuracy for the soil moisture averaged over a 1-m soil layer. σ_{WM} for the above objects is equal to 0.014, 0.017, and 0.025 m^3/m^3, respectively. Since the standard measurements of soil water storage in a 1-m soil layer is essentially based on the measurements of moisture in the consequent 10-cm layers and the errors of measurements in different layers may be considered as independent random values, the quantity σ_W in Eq. (6) may approximately be estimated as

$$\sigma_W = \sigma_W(\overline{\xi}) \approx \frac{\sigma_{WM}}{\sqrt{\overline{\xi} + 0.1}}, \qquad (11)$$

where $\overline{\xi}$ is expressed in meters.

The step-by-step use of Eqs. (6) - (10) and (11), with the given information on the 10-day mean values of air temperature and the dynamics of the quantities $\overline{h}$ and σ_h, allowed us to calculate the dynamics of the characteristics $\overline{\xi}$ and σ_ξ at the chosen objects for the indicated winter seasons and then to compare the results with those we got from observations.

Figure 1 shows the calculated and observed data on the dynamics of both the mean values of the freezing depths and their standard deviations for certain winter seasons. Figure 2 presents a general comparison of the calculated and measured values of the above characteristics for the three objects considered. The root-mean-square errors of the calculations are equal to 0.063 m for the mean depth of freezing and 0.061 m for its standard deviation.

DISCUSSION OF RESULTS

Analysis of the results shows that the total dispersion of freezing depth σ_ξ^2 is due mainly to the variability of the snow cover height $\sigma_{\xi h}^2$ (about 70-90%). This fact is apparently conditioned by the relatively rugged terrain of the forest-steppe zone, in
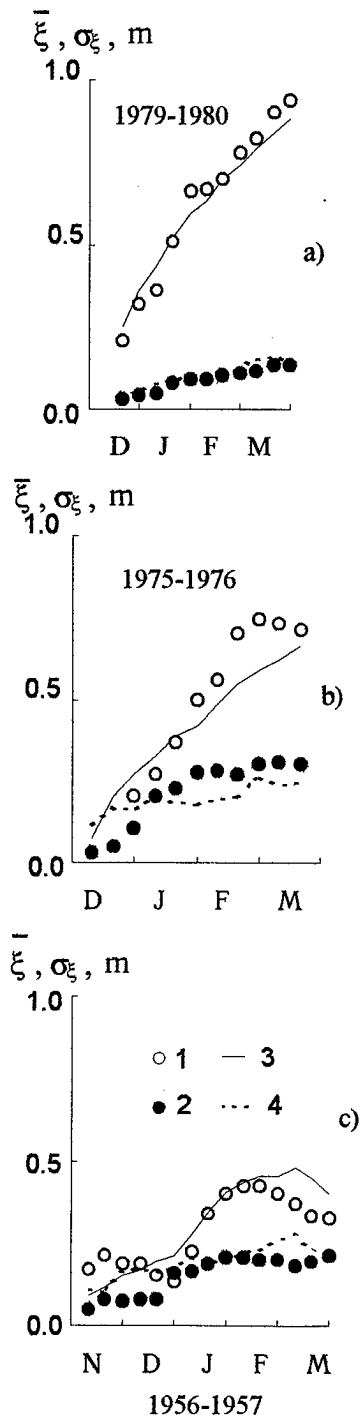
Figure 1. Variation of the measured (1, 2) and calculated (3, 4) mean values of soil freezing depth(1, 3) and values of its standard deviations (2, 4) for an agricultural field at the Kursk Biosphere Station (a), for the Nizhnedevitsk Water-Balance Station (b), and for the Kursk region (c).

77

ξ_c , m

1.0

0.5

0.0

0.0   0.5   1.0

ξ_m , m

a)

$\sigma_{\xi c}$, m

0.4

0.2

0.0

0.0   0.2   0.4

$\sigma_{\xi m}$, m

b)

ξ , m

1.2

0.8

0.4

0.0

0   0.5   1

P

a)

—— 1

□ 2

.... 3

○ 4

ξ , m

1.5

1.0

0.5

0.0

0   0.5   1

P

b)

ξ , m

1.2

0.8

0.4

0.0

0   0.5   1

P

c)
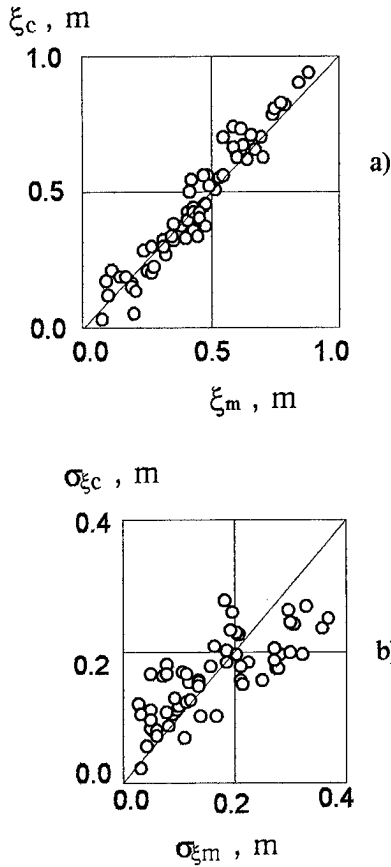
Figure 2. Comparison between calculated and measured values of the area-averaged depth of soil freezing (a) and its standard deviation (b). Here $\overline{\xi}_m$, $\sigma_{\xi m}$ and $\overline{\xi}_c$, $\sigma_{\xi c}$ are the measured and calculated values of the above characteristics, respectively.

which the considered objects are situated. In the case of a more smoothed relief or smaller quantities of snow supply, the mentioned ratio may change due to increasing the component $\sigma^2_{\xi W}$.

The assumption of a certain type of distribution function of freezing depth for an object under consideration allows us to construct such functions for definite dates using the obtained characteristics $\overline{\xi}$ and σ_ξ for these same dates. In this case, the method proposed here enables one to simulate not only the dynamics of the two statistical characteristics of the spatial distribution of soil freezing depth but its distribution function as well. In particular, by virtue of the non-negativity of the distribution function of this characteristic by the
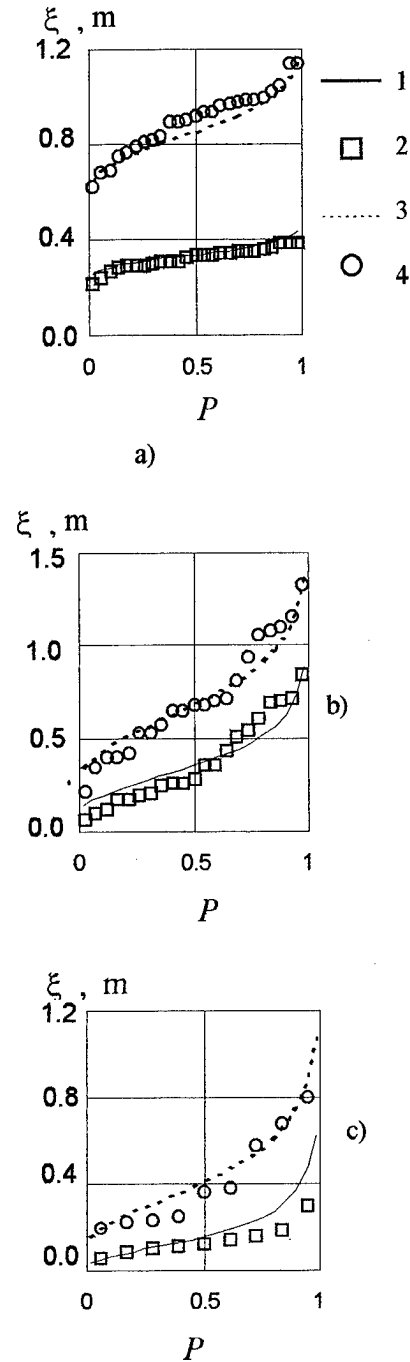
Figure 3. The calculated (1, 3) and empirical (2, 4) integral functions of distribution P for the soil freezing depth in an agricultural field at the Kursk Biosphere Station (a) on January 1, 1980 (1, 2) and March 31, 1980 (3, 4), at the Nizhnedevitsk Water-Balance Station (b) on January 18, 1976 (1, 2) and March 18, 1976 (3, 4), and in the Kursk region (c) on December 18, 1956 (1, 2) and February 18, 1957 (3, 4).

78

range of ξ values, we may try to approximate the gamma-distribution, for example. Some of the functions in this way and their comparison with similar empirical functions are presented in Figure 3. Both theoretical and experimental data are indicative of the increasing spatial variability with the increasing scale of an object. Thus, for the winter seasons here discussed, the average winter season coefficient of variation of freezing depth $C_{V\xi} = \dfrac{\sigma_\xi}{\overline{\xi}}$ is respectively equal to 0.16 ± 0.01 for the Kursk Biosphere Station, 0.58 ± 0.07 for the Nizhnedevitsk Water-Balance Station, and 0.52 ± 0.07 for the Kursk region. These data show that the degree of variability of soil freezing depth remains virtually unchanged when the linear scale of objects increases from 10 up to 100 km. So we may suppose that even the objects of a linear size of about 10 km (for example, water balance stations) are likely to incorporate a set of elementary ecosystems reflecting to a considerable extent the specific character of a larger area. This fact reinforces the possibility of using (for the first approximation) the integral curves of distribution of the soil freezing depth, obtained from the survey data of this depth in a certain limited area typical of the topography and landscape for a given geographical region, for the entire area under consideration (Appolov et al. 1974).

The above results of comparison of the calculated and observed data allow us to conclude that the proposed mesoscale dynamic-stochastic model for soil freezing depth produces satisfactory results in both cases – when describing the dynamics of its area-averaged values or the characteristics of its spatial variability.

ACKNOWLEDGMENTS

REFERENCES

Abels, H. 1892. Beobachtungen der taglichen periode der temperatur im schnee und bestimmum des warmeleitungsvermogens des schnees als function seiner dichtigkeit. (In German). Rep. Meteorol., Bd. XYI, No 1: 1-53.

Appolov, B.A., G.P. Kalinin, and V.D. Komarov. 1974. Hydrological forecasting. (In Russian). Hydrometeoizdat, Leningrad, USSR.

Entekhabi, D. and P.S. Eagleson. 1989. Landsurface hydrology parametrization for atmospheric general circulation models: Inclusion of subgrid scale spatial variability and screening with simple climate model. Rept. MIT Dept. Civil Engineering, N 325. Cambridge, US.

Gusev, Ye.M. 1993. Formation of soil water regime and resources for the winter-spring period. (In Russian). Fizmatlit publishing company, Nauka publishers, Moscow, Russia.

Gusev, Ye.M., O.Ye. Busarova, and O.N. Nasonova. 1995. Modelling evapotranspiration and soil water dynamics for inhomogeneous regions. p.285-288. In Proceedings of the second international study conference on GEWEX in Asia and GAME, 6th - 10th March, Pattaya, Thailand.

Kalyuzhnyi, I.L., and K.K. Pavlova. 1981. Formation of meltwater losses. (In Russian). Hydrometeoizdat, Leningrad, USSR.

Palagin, E.G. 1981. Mathematical modelling of agricultural meteorological conditions of winter crop hibernation. (In Russian). Hydrometeoizdat, Leningrad, USSR.

Pavlov, A.V. 1975. Heat exchange between soil and atmosphere in northern and middle latitudes of the USSR Area. (In Russian). Siberian division of the Akad. sci. of the USSR, Yakutsk, USSR.

Verigo, S.A., and L.A. Razumova. 1973. Soil moisture. (In Russian). Hydrometeoizdat, Leningrad, USSR.

Yosida, Z. 1955. Physical studies on deposited snow: thermal properties. p.19-74. In Contrib. inst. low temp. Sci., Hokkaido Univ., Ser. A, N 27, Sapporo, Japan.

Influence of Water and Heat Dynamics on Solifluction Movements in a Periglacial Environment in the Eastern Alps (Austria)

Ph. JAESCHE[1], H. VEIT[2], H. STINGL[3], AND B. HUWE[1]

ABSTRACT

Solifluction movements are closely linked to the development and melting of ground ice. Soil thermal and hydraulic conditions during thaw consolidation are regarded as crucial for understanding gelifluction processes. We set up a field station in the periglacial altitudinal belt of the Austrian Alps, 2650 m a.s.l., to investigate the dependency of solifluction movements on the ground thermal and hydraulic regimes. Automatic measurement devices included solifluction meters for the observation of subsurface soil displacement, heave meters, as well as TDR, tensiometers and thermistors. Preliminary results demonstrate that ground freezing and frost heave continued throughout the winter. Additional ground ice accumulated during early snowmelt events. The onset of strong gelifluction in response to ground thaw was recorded at a high temporal resolution. The importance of climatic control on solifluction was supported by the results of annual surface marker observations.

Key words: Periglacial, solifluction, frozen soil

INTRODUCTION

Solifluction is the slow downslope movement of soils in periglacial environments, including the effect of frost creep as a consequence of frost heave, and gelifluction, which describes the slow flowage of saturated soil over frozen material (Harris 1981, Williams and Smith 1989).

Observations of solifluction are widespread in various periglacial environments. They mainly reveal a strong regional variability in movement rates (cf., Harris 1981, Frenzel 1993) which can be explained through a set of easily measured factors such as topography, soil texture and vegetation. Only a few reports exist on temporal variability in solifluction, and analysis of controling conditions is scarce (cf., Matthews and Berrisford 1993).

Site factors and climatic conditions influence the soil thermal and hydraulic regimes and especially control the development and duration of ground ice. This is important for solifluction processes as it is generally assumed that gelifluction follows spring snowmelt and subsequent thaw of ground ice. Recently, laboratory simulations of solifluction have been undertaken (Harris et al. 1995). However, it is not yet proven by field data when exactly solifluction occurs, nor how soil water and temperatures concurrently behave.

A study was initiated in 1994, in a high alpine periglacial environment in Austria affected by solifluction, to investigate the interrelations between solifluction activity and local soil water and heat regimes using an automatic monitoring system. This paper presents preliminary results of ground freezing in winter 1995 and subsequent findings on solifluction activity in summer 1996.

SITE DESCRIPTION

The "Glatzbach" study area is situated in the Austrian "Hohe Tauern" mountain range (eastern central Alps), south of the "Großglockner" peak (Veit et al. 1995). The site is at elevations between 2640-2680 m a.s.l. and covers an area of about 50 x 100 m. Inclination increases from 10° at the north

facing to 20° at the east facing side. A steep moun-
tain ridge of bare rock at about 2700 m strongly
shades the site especially during winter. The mean
annual air temperature is about -2°C. Small soliflu-
ction lobes, only a few meters long with faces about
10-50 cm high, have developed on a fossil soliflu-
tion sheet which covers almost the whole slope.
Vegetation is heterogeneous with associations of
closed alpine grass heath developed next to debris
almost devoid of vegetation. Petrographically, the
area is characterized as a mixed zone of geomor-
phologically weak and easily weathering, calcareous
mica schists and phyllites.

Two solifluction lobes, about 50 m apart, were
instrumented. Soils show a high stone content (>2
mm) of 38-50 % by weight. The texture of the fines
(<2 mm) is a sandy loam (clay <5 %, silt 30-35 %),
and thus the soils are highly frost susceptible and
prone to gelifluction (Harris 1981). The liquid limit
is between 20-23 % and the plasticity index about 4-
6 %. At lobe 2, stone and silt contents slightly
increase below 60 cm and the plasticity index in-
creases to 11 %, indicating the change from recently
transported material to the buried solifluction sheet.

METHODS AND INSTRUMENT DESIGN

Automatic monitoring devices were set up in
1995 in duplicate to investigate soil thermal and
hydraulic regime. The individual components are
described below. Data acquisition was accomplished
by two field data loggers (DL-2, Delta-T). Logger
and battery were protected by a waterproof box. A
weather station was set up to record rainfall, wind,
atmospheric humidity and temperature. Although
electronic problems may have caused erroneous
(±1%) absolute values for temperature, the data are
useful for interpretation of air temperature changes.

Information about spatial and annual variation of
solifluction activity was obtained from observations
of 150 surface markers. The markers, 20-cm-long
PVC rods, were distributed irregularly on the whole
slope in 1994 and measured again in August 1995
and 1996.

Subsurface movements and frost heave

During the last decade, subsurface solifluction
movements have been measured using non-destruc-
tive methods such as strain-gauge sensors (e.g.,
Matsuoka and Moriwaki 1992) and inclinometer
access tubes (e.g., Price 1991). These devices require
either the presence of personnel at the site, or are
inadequate if strong vertical gradients of soil move-

ment or shearing occurs. Thus, an automatically
recording solifluction meter with independently
moving subsurface markers was constructed similar
to that of Lewkowicz (1992), which transforms soil
movements into potentiometer resistance changes.

The solifluction meter consists of a stainless-steel
casing (10 x 10 x 76 cm), in which 5 potentiometers
(AL 1710, Megatron) are mounted at 10-cm vertical
spacing. The box is anchored 2 m deep in the ground
by metal pipes (Fig. 1). The solifluction displace-
ments of five markers (∅ 2 cm), buried 50 cm
downslope at depths between 10 and 50 cm, are
transmitted to the potentiometers by nylon strings.
To minimize the effect of possible turbulent soil
movements, the strings are guided in small metal
tubes. The instrumentation cannot measure retro-
grade movements during ground thaw, but these
were expected to be negligible compared to the high
solifluction movements at the site (Veit et al. 1995).
Only a small pit of about 25-cm diameter was neces-
sary for installation of the box. The small tubes were
inserted into a narrow slit, and the markers were
buried in a hole only the size of their diameter. Each
string was then tightened and the pit refilled. The
soil was so plastic that the slit closed by itself within
minutes and good contact of the markers with the
surrounding soil was guaranteed.

Frost heave was measured using linear motion
transducers (WGO 20100, Megatron, 100 mm). The
potentiometer was encapsulated in an aluminum
tube and fixed to an above-ground metal bar that
stabilized the solifluction meter (Fig. 1). A heavy
steel/PVC-block was attached to the moveable axis
and rested upon the ground, so it could follow the
ground motions perpendicular to the surface. Similar
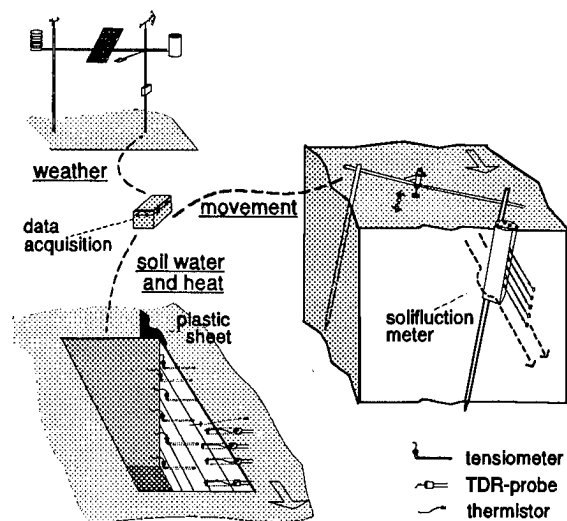
Figure 1. *Automatic measurement devices.*

devices were used in studies on solifluction by Smith (1987) and Matsuoka (1994).

Soil thermal and hydrologic regime

Soil temperatures were measured with thermistor probes (Fenwal 10 kΩ) inserted at 10 (lobe 1) and 8 (lobe 2) depths between 1 and 120 cm below surface. Volumetric soil water content in the unfrozen soil, or unfrozen water content θ_{uf} in the frozen soil, was registered at 6 depths between 10 and 90 cm using TDR-probes (TRIME MUX-6 & P2Z, IMKO). The probes had two rods of 16-cm length. The same signal processing was applied for both unfrozen and frozen conditions (cf., Stein and Kane 1983, Hayhoe and Bailey 1985), although it is recognized that

some authors have developed specific calibration functions for frozen soil measurements (Perfect and Kay 1993). Pressure transducer tensiometers were used to record matric potential as long as the soil remained unfrozen (10 at each plot, vertical spacing 10 cm).

All probes were installed horizontally into undisturbed soil, about 40-50 cm behind the side wall of a 1.2 x 0.9 m pit (Fig. 1). The pit was refilled with soil to minimize its influence on the thermal regime. A plastic sheet was left in place on the side wall to prevent lateral water flow between disturbed and undisturbed soil and to avoid influences on downslope subsurface water flow.
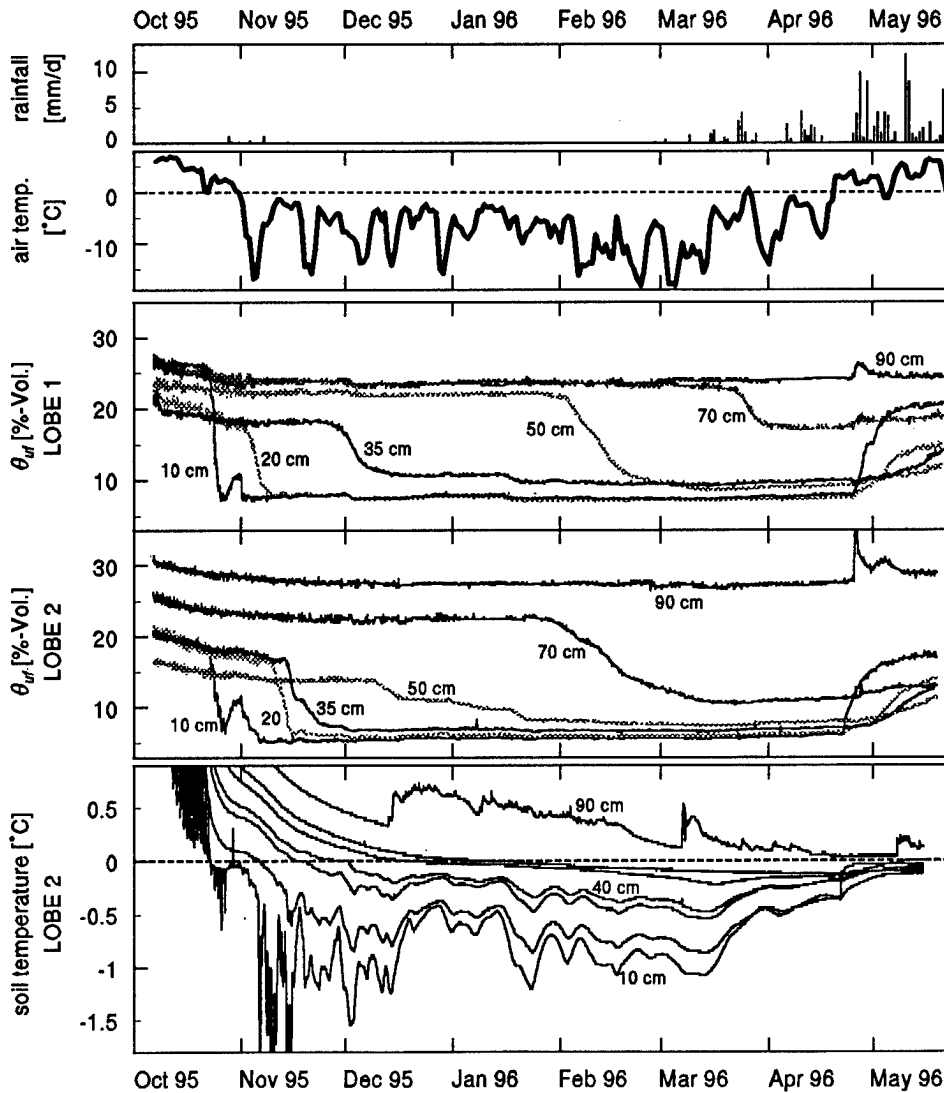
Figure 2. Winter 1995/96 soil temperatures (lobe 2), unfrozen water contents (lobes 1 and 2), air temperatures and rainfall

RESULTS AND DISCUSSION

Ground freezing during winter 1995/1996

Water and temperatures generally showed comparable behavior at both observed lobes (Fig. 2). Before the onset of freezing in the middle of October, soils were rather dry. Tensions ranged from 15 kPa (suction) at the lowest probe to 25 kPa at 10 cm depth. At both lobes, moisture content varied between 20 and 27 % by volume, generally increasing with depth. However, lobe 2 had significantly higher values at 90 cm depth, which are attributed to differences in soil texture, and lower values at 50 cm, that may reflect this probe's installation in backfilled soil.

Penetration of the 0°C isotherm into the ground started around October 20. It first affected the top 10 cm only, as can be seen in the abrupt unfrozen soil water content (θ_{uf}) changes at both 10-cm TDR probes. Following a short partial thaw, freezing recommenced after a sharp drop in air temperature on November 1 and finally the 0°C isotherm reached a depth of about 80 cm at both lobes. The rate of freezing during late 1995 was higher at lobe 2 than at lobe 1. Temperatures indicated for 90 cm on lobe 2 are probably due to erroneous signal processing, as lobe 1 temperatures at greater depths show a continual decline. TDR measurements confirm the frost penetration, showing resultant reductions of θ_{uf} to values between 5 and 15 % by volume. Increasing water tensions below the frozen layer were measured until tensiometers froze. When this happened, for example, at depths of 50 and 60 cm, tensions at both sites had reached values of 50 kPa. Only probes below 80 cm "survived" frost action: they measured lowest values towards the end of March, between 51 and 54 kPa at lobe 1, and 40 kPa at lobe 2. The timing of ice formation, as deduced from both temperature and water content measurements, does not correspond exactly. This may be due to inaccuracies of (horizontal) probe installation and to local

variability, as spacing between thermistors and TDR-probes is approximately 0.7 m.

Significant soil heaving started as soon as the ground began to freeze (Fig. 3). Shading by the nearby mountain ridge affects lobe 1 more than lobe 2, so the former started to heave 8 days earlier. During one week, each lobe showed diurnal frost heave to a maximum of 2 mm per day, then began to heave continuously until the end of April. Subsurface soil markers were not affected by diurnal frost heaving and no movements were recorded with the solifluction meters during the winter except at depths between 20 and 40 cm (Fig. 4a). Here, total movement of 1-3 mm may relate to local ice lensing following installation disturbance.

Frozen ground warming during late winter 1996

Air and soil temperatures began to increase in March, but θ_{uf} remained unchanged. Air temperature became positive after April 18, initiating snow melt, and on April 24 it rained. The same day on lobe 1, soil temperatures as well as θ_{uf} at 10 cm and subsequently at all depths started to increase. Gradients to a depth of 50 cm were inverted, eventually leading to near isothermal conditions with the highest values of θ_{uf} near the surface (Fig. 2, Fig. 5 stars to squares). Similar changes were observed at lobe 2 three days earlier.

Both sites also showed accelerated surface heave following the rain on April 24 (Fig. 3): During the next 11 days, heave of 1.6 cm occurred at lobe 1 and of 2.0 cm at lobe 2. A similar resurgence in heave rates under snowcover was observed by Smith (1987). Additionally, the solifluction meter recorded small displacements of the upper three subsurface markers at lobe 1 and of the 10-cm marker at lobe 2, starting 3 days after pronounced surface heaving occurred (Fig. 4a, squares). These movements reflect heaving of the markers, not downslope movements.

Increased air temperatures and the rain event led to drainage of water from the snow pack, which had
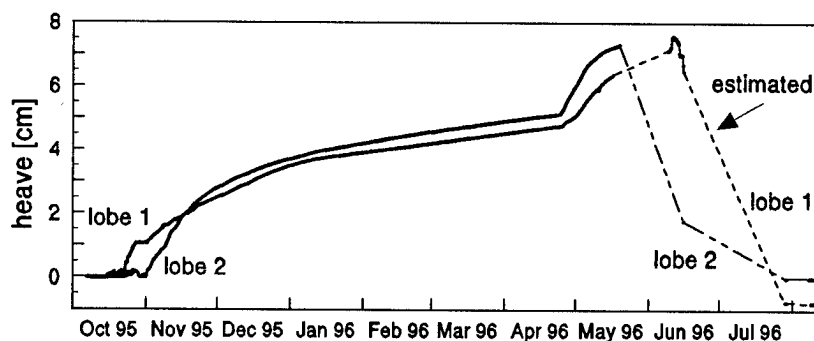
Figure 3. Frost heave and thaw consolidation at lobes 1 and 2 perpendicular to the ground.
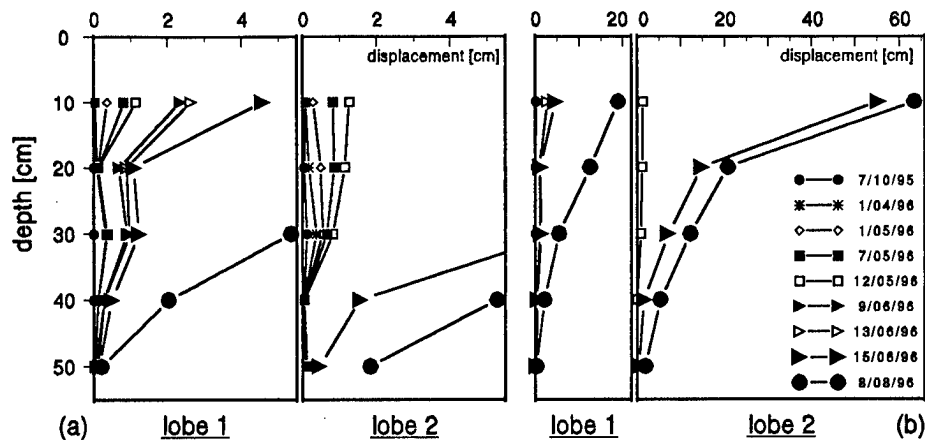
Figure 4. Solifluction meter records at lobes 1 and 2: (a) small (heave) movements during winter 1995/96, (b) large (gelifluction) movements during summer ground thaw. Note differences in displacement scales.

covered the area until the beginning of June. The water infiltrated and immediately refroze, increasing soil temperatures and corresponding θ_{uf} (Kane and Stein 1983, Hayhoe and Bailey 1985, Stein et al. 1994, Stadler et al. 1997). The infiltration capacity was reduced, ponded water formed a saturated layer at the snow-soil-interface, and basal ice may also have developed, increasing the heat content of the underlying soil as well (Marsh and Woo 1984).

TDR measurements at 90 cm depth showed volumetric water content increases of 2.5 % and 9 % respectively on April 24 at both sites. This effect is confirmed by readings from all the remaining tensiometers below 80 cm depth which fell to values between 1 and 7 kPa within one day. Thus, water must have partially percolated through the entire frozen soil without refreezing. Stadler et al. (1997) present similar observations for an alpine forest soil.

The movements of all subsurface markers down to 40 cm depth continued while the ground remained frozen (Fig 4a, small triangles). Surface soil heave at lobe 1 reached a total of 7.6 cm on June 11. Due to technical problems, only a few continuous data could be gathered after May 15. At lobe 2, maximum frost heave and ground thaw were completely missed, but were partially recorded at lobe 1.

Ground thawing in summer 1996

A visit to the site on June 7 showed that lobe 2 was just becoming bare, while lobe 1 was still covered by approximately 30 cm snow. One week later on June 15, the snow had retreated to the highest parts of the slope. By that time at lobe 2, temperatures throughout the profile exceeded 2.5°C and volumetric water contents were greater than 26 %.

Subsurface displacements of 55 cm in the top layer and of 15 and 7 cm at greater depths had occurred (Fig. 4b). However, the heave gauge had dropped to only 1/3 of its maximum elevation (> 7.4 cm; Fig. 3), despite the ground being obviously thawed.

At lobe 1 in the top 20 cm, significant increases of θ_{uf} within one day were recorded after June 10, when soil temperatures rose to values above 0°C. The heave gauge indicated accelerating settlement of 12 mm (16 %) within the next 5 days. Most importantly, the solifluction meter measured increasing displacement of the 10-cm marker by 2 cm during June 13-15 (Fig. 4a). The greatest gelifluction movements were recorded in the afternoons: 4-5 mm within 4 hours each.

At the beginnng of August, when the next readings were successfully stored, both lobes were completely thawed and resettled. Water contents had equalized throughout the profile, being higher than before freezing (Fig. 5). Negative heave values recorded in August represented a lower surface level, as site inspection proved. Solifluction of all subsurface markers resulted in movement profiles showing declining rates with soil depth (Fig. 4b). Excavation of vertical subsurface rod markers in the same area in 1989 had indicated similar profiles on the most active lobes (Veit et al. 1995). Total 1995-96 displacements at 10 cm depth were 19.0 cm (lobe 1) and 63.4 cm (lobe 2). These data compare well with mean movements of surface markers situated within 2 m at the same lobes (Table 1). Considering the strong movement of the nearest marker only, some influence of solifluction meter installation on soil movement at these locations may be supposed (Smith 1992).
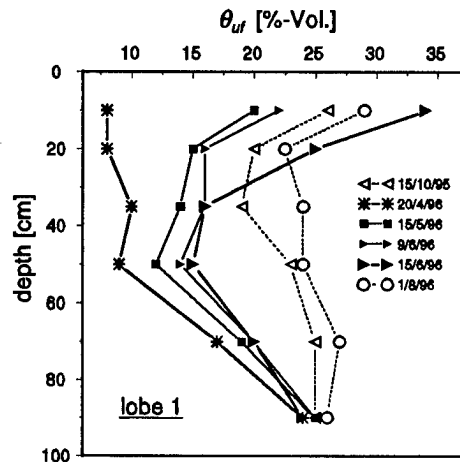
Figure 5. Unfrozen water content profiles at lobe 1 during winter 1995/96.

Local and annual variability of solifluction

Surface movements at the site show an extreme local heterogeneity which reflects spatial differences in microrelief, vegetation cover and stone content. The highest displacement rates (> 60 cm) were observed in regions that have only a sparse vegetation cover, and during snowmelt received enhanced surface runoff from snow patches upslope. Lobes densely covered by vegetation were largely inactive.

The average of all point movements is 14.8 cm in 1994-95 and about twice as high in 1995-96 (27.2 cm). Almost every single marker showed stronger movements in the second year. These rates are much higher than any previously reported, except those observed in the same area in the years 1985 to 1989 by Veit et al. (1995). They reported mean displacements between 8 and 22 cm in the years 1986 to 1989, and the greatest value was measured 4 years after marker installation. Other than at the solifluction meter, site disturbance during installation seems not to control surface marker movements in the following years. Annual fluctuations were explained by varying climatic conditions. Veit et al. (1995) consider differences in autumn air temperatures and especially the date of snow cover onset to be the most important factors, both of which greatly influence the depth of winter frost penetration. Furthermore, low temperatures after snowmelt in summer result in a larger number of gelifluction days. Our observations support this hypothesis, as in both 1994 and 1995, the winter snow cover developed exceptionally late and frost penetrated very deeply into the ground.

CONCLUSIONS

The new system for continuous recording of soil movements and thermal and hydrological regime, applied for the first time in a field study concerned with solifluction movements, produced valuable results. Extremely strong gelifluction movements were recorded, while the accompanying measurements showed the slow, simultaneous melt of ground ice. Annual variations of solifluction movements are climatically controlled.

Other work has stressed the importance of high water availability for ice lensing in autumn as the main requirement for strong solifluction, especially for frost creep (Harris 1981, Williams and Smith 1989). However, our observations indicate fairly dry soil conditions during freeze-up (compare also Smith 1988). Measurements performed during a period of warmer weather before snow cover ablation proved that additional ground ice formation near the soil surface occurred at that time, a possibility suspected earlier by Smith (1987) and Stein et al. (1994). This increased the total amount of soil heave and thus potential soil creep movements. More importantly, the higher ice contents promoted gelifluction by: (i) increasing the water supply from in-situ melting ice lenses, (ii) enhancing lateral subsurface and surface water flow over densely frozen ground, and (iii) retarding ground thaw, thus extending the time during which gelifluction can occur. These findings stress the importance of particular meteorological events for solifluction.

Future work will include modeling of the soil thermal and hydraulic regimes to analyze their inter-relations with solifluction rates, for example by identifying the number of days with soil conditions that promote solifluction. Such work is complicated by

Table 1. Annual downslope movement rates at lobes 1 and 2, measured 10 cm below the surface by solifluction meters, and at nearby surface markers.

	Lobe 1		*Lobe 2*	
	94/95	*95/96*	*94/95*	*95/96*
	Movement (cm/a)			
Solifluction meter (10 cm depth)	---	19.0	---	63.4
Next surface marker	11.8	36.7	25.3	85.2
Next 3 surface markers (avg.)	14.8	32.2	35.5	61.4

lateral surface and subsurface water flow. Additional analysis is needed of the regional distribution of solifluction, considering topography and other local factors, and of the interrelations with snowmelt and concurrent surface runoff patterns.

ACKNOWLEDGEMENT

REFERENCES

Frenzel, B. 1993. Solifluction and climatic variation in the Holocene. G. Fischer, Stuttgart.

Harris, C. 1981. Periglacial mass-wasting: A review of research. Geoabstracts, Norwich.

Harris, C., M. Gallop, and J.-P. Coutard. 1995. Laboratory simulation of periglacial solifluction: significance of porewater pressures, moisture contents and undrained shear strengts during soil thaw. Permafr. Perigl. Processes 6:293-311.

Hayhoe, H.N. and W.G. Bailey. 1985. Monitoring changes in total and unfrozen water content in seasonally frozen soil using time domain reflectometry and neutron moderation techniques. Water Resour. Res. 21:1077-1084.

Kane, D.L. and J. Stein. 1983. Water movement into seasonally frozen soils. Water Resour. Res. 19:1547-1557.

Lewkowicz, A.G. 1992. A solifluction meter for permafrost sites. Permafr. Perigl. Processes 3:11-18.

Marsh, P. and M. Woo. 1984. Wetting front advance and freezing of meltwater within a snow cover, 1, Observations in the Canadian Arctic. Water Resour. Res. 20:1853-1864.

Matsuoka, N. 1994. Continuous recording of frost heave and creep on a Japanese alpine slope. Arctic & Alpine Res. 26:245-254.

Matsuoka, N. and K. Moriwaaki. 1992. Frost heave and creep in the Sor Rondane mountains, Antarctica. Arctic & Alpine Res. 24:271-280.

Matthews, J.A. and M.S. Berrisford. 1993. Climatic controls on rates of solifluction: variation within Europe. p. 363-382. *In* B. Frenzel (ed.) Solifluction and climatic variation in the Holocene. G. Fischer, Stuttgart.

Perfect, E. and B.D. Kay. 1993. Hydrological properties of frozen soil. p. 767-781. *In* M.R. Carter (ed.) Soil sampling and methods of analysis. Lewis Publishers, Boca Raton.

Price, L.W. 1991. Subsurface movement on solifluction slopes in the Ruby Range, Yukon Territory, Canada - A 20-year study. Arctic & Alpine Res. 23:200-205.

Smith, D.J. 1987. Frost-heave activity in the Mount Rae Area, Canadian Rocky Mountains. Arctic & Alpine Res. 19:155-166.

Smith, D.J. 1988. Rates and control of soil movement on a solifluction slope in the Mount Rae area, Canadian Rocky Mountains. Z. Geomorph. N. F. 71:25-44.

Smith, D.J. 1992. Long-term rates of contemporary solifluction in the Canadian Rocky Mountains. p. 203-221. *In* J.C. Dixon and A.D. Abrahams (eds.) Periglacial Geomorphology. John Wiley, New York.

Stadler, D., M. Bründl, H. Wunderli, A. Auckenthaler, and H. Flühler. 1997. Field measurements of water transport in frozen soils. Journal of Hydrological Processes (accepted for publication).

Stein, J. and D.L. Kane. 1983. Monitoring the unfrozen water content of soil and snow using time domain reflectometry. Water Resour. Res. 19:1573-1584.

Stein, J., S. Proulx, and D. Lévesque. 1994. Forest floor frost dynamics during spring snowmelt in a boreal forested basin. Water Resour. Res. 30:995-1007.

Veit, H., H. Stingl, K.-H. Emmerich, and B. John. 1995. Zeitliche und räumliche Variabilität solifluidaler Prozesse und ihre Ursachen. Eine Zwischenbilanz nach acht Jahren Solifluktionsmessungen (1985-1993) an der Meßstation "Glorer Hütte", Hohe Tauern, Österreich. Z. Geomorph. N. F. 99:107-122.

Williams, P.J. and M.W. Smith. 1989. The frozen earth. Cambridge Univ. Press, New York.

Crystallization Heat of Soil Water

E.G. STAROSTIN[1] AND A.M. TIMOFEEV[1]

ABSTRACT

A method has been devised to find experimentally
crystallization heat of soil water. This method was
used for determination of crystallization heat of water
in clays. The results obtained show that crystalliza-
tion heat of soil water at low moisture is much dif-
ferent from that of volume water. The calorimetric
tests in determining unfrozen water show that an ef-
fect of the difference is much evident. For example
in clay samples examined the amount of unfrozen
water is 20 - 30% less at -10^0C using the values
of crystallization heat of soil water, compared with
the ones for volume water.

Key words: bound water, unfrozen water, crystalliza-
tion heat.

INTRODUCTION

The phase state of water in dispersion media at
temperatures below 0^0C arouses considerable interest
of researchers. The point is that presence of unfrozen
water in dispersion media plays an important role in
processes of heat and mass transfer and is one of the
main factors determining the formation of almost all
the most crucial physical and mechanical properties
of the media mentioned. Crystallization heat of bound
water is considered to be one of the main characteris-
tics determining the phase state of water in dispersion
media at temperatures below 0^0C.

Notwithstanding the fact that a great number of
investigations on phase state of water in dispersion
media have been conducted there is not yet a unified
point of view concerning crystallization heat of
bound water in dispersion media (Efimov, 1986).

To estimate the value difference in heat of water -
ice phase transition for bound and volume water it is
enough to compare their evaporation heat (Brovka,
1991). The estimation of this kind suggests that
within the temperature range between 0^0C and -25^0C
the mentioned difference in values of phase transition
heat may be up to 10%.

On the other hand, even on conducting the calo-
rimetric measurements (Efimov, 1985) let alone
mathematical modeling (Permiakov, 1989) there is
used the constant value equal to crystallization heat
of volume water at atmospheric pressure as crystalli-
zation heat of bound water.

This is Kirchgoff's equation more often used
(Gavriliev, 1970, Ershov et al, 1979, Stepanov and
Timofeev,1994) to describe crystallization heat of
bound water regarding enthalpy difference of volume
water and ice.

$$h_w - h_i = L_w^{\ 0} + (c_w - c_i)(t_f - t_e), \qquad (1)$$

where h_w and h_i - enthalpy of water and ice, respec-
tively, at t_f temperature; c_w and c_i - heat capacity of
water and ice, respectively; t_f - water freezing tem-
perature; $L_w^{\ 0}$ - crystallization heat of bound water at t_e
$= 0^0$C.

To deduce the phase state equation of bound wa-
ter there is used the following one in paper (Ivanov,
1969)

$$\frac{dL_w}{dt} = (c_i - c_w) + \frac{L_w}{t} - L_w \cdot \frac{\partial ln\,(v_i - v_w)}{\partial t}, \qquad (2)$$

[1] Institute of Physics and Engineering Problems of the North, Oktyabrsaya Street 1, 677891, Yakutsk, Russia

where L_w - crystallization heat of water; v_w and v_i - volumes of water and ice.

The equation determines the variations in crystallization heat of volume water along the line of water - ice phase equilibrium under changes of external pressure.

The expressions (1) and (2) describe the phase transitions of volume water and ignore the energy state of bound water. The usage of these expressions suggest that the difference between the crystallization heat of volume water and that of bound water is not significant and might be neglected.

At the phase transition temperature the bound water and ice are in equilibrium, and crystallization heat comes out to the enthalpy difference of bound water and ice at a given temperature

$$L_{bw} = h_{bw} - h_i, \qquad (3)$$

where L_{bw} - crystallization heat of bound water; h_{bw} - enthalpy of bound water; h_i - enthalpy of ice.

If one knows the enthalpy of bound water and ice at t_e temperature, he can write down the expression as

$$L_{bw} = h_{bw}^0 - h_i^0 + (c_{bw} - c_i) \cdot (t_f - t_e), \qquad (4)$$

where h_{bw} and h_i - enthalpy of bound water and ice, respectively, at t_e temperature; c_{bw} and c_i - heat capacity of bound water and ice, respectively; t_f - freezing temperature of bound water.

Although the formula is given in some papers (Brovka, 1991, Efimov, 1985, 1986, Chistotinov, 1975), it is not generally used in practice.

The point is that there is no evidence on the bound water enthalpy entering into the formula.

EXPERIMENTAL METHOD

Experimental determination of the bound water crystallization heat in dispersion systems is based on the calorimetric method and lies in the following.

Let us have two systems consisting of dispersion medium - unfrozen water - ice which differ from each other only by the total water amount. At temperature low enough one can assume

$$H_2 = H_1 + h_i (m_2 - m_1), \qquad (5)$$

where H_1 and H_2 - enthalpy of the first and second systems, respectively, at t_s temperature; h_i - specific ice enthalpy at t_s temperature; m_1 and m_2 - the total mass of water in the first and second systems, respectively.

Condition (5) means that the unfrozen water amount at a given temperature (supposedly, lower than -25^{0}C) does not depend on the overall water content in the system.

Let us consider the same systems at $t_e = 0^0$C, at which the overall water in the systems is in the liquid phase. With $\Delta m = m_2 - m_1$ that is a small enough value one can write down

$$H_2^0 = H_1^0 + h_{bw}^0 (m_2 - m_1), \qquad (6)$$

where H_1^0 and H_2^0 - enthalpy of the first and second systems, respectively, at t_e temperature; h_{bw}^0 - partial enthalpy of bound water at t_e temperature; m_1 and m_2 - total mass of water in the first and second systems, respectively.

Subtracting (6) term - by - term from (5) one will get

$$H_2^0 - H_2 = H_1^0 - H_1 + (h_{bw}^0 - h_i) \cdot (m_2 - m_1), \qquad (7)$$

Hence,

$$h_{bw}^0 - h_i = \frac{(H_2^0 - H_2) - (H_1^0 - H_1)}{(m_2 - m_1)}, \qquad (8)$$

It should be mentioned that h_{bw}^0 has been determined at t_e temperature, while h_i - at t_s temperature.

For the ice enthalpy we have

$$h_i = h_i^0 + c_i (t_s - t_e), \qquad (9)$$

where h_i^0 - enthalpy of ice at t_e temperature; c_i - ice heat capacity.

The usage of the expression (9) in the case considered proposes that ice being generated in the systems mentioned above has the same heat capacity as that of free ice.

Substituting (9) in (8) we have

$$h_{bw}^0 - h_i^0 = \frac{(H_2^0 - H_2) - (H_1^0 - H_1)}{(m_2 - m_1)} + c_i (t_s - t_e). \qquad (10)$$

Enthalpy differences $H_2^0 - H_2$ and $H_1^0 - H_1$ are readily found experimentally, for example, during adiabatic heating the systems from t_s up to t_e using the constant - power heat sources.

Expression (10) does not determine crystallization heat of bound water at t_e temperature as ice and bound water are not in equilibrium at this temperature. It should be hence taken into account that

88

$h_{bw}^0 - h_i^0$ represents the enthalpy difference of bound water and ice within the range of overall moisture content from m_1 to m_2.

Having divided the investigated area of overall moisture content changes into a number of intervals one should again conduct the experiments to determine the enthalpy difference for each interval. The data obtained make it possible to express the enthalpy difference $h_{bw}^0 - h_i^0$ as a function of overall moisture content.

Phase transition heat for water may be obtained by substituting this function in expression (4).Thus crystallization heat of bound water depends both on temperature and overall moisture content.

RESULTS AND DISCUSSION

A number of experiments have been carried out to determine crystallization heat of bound water in clay using the method described. Enthalpy difference of bound water and ice at 0^0C was being found during the experiment.

In fig. 1 there is shown a dependence of $h_{bw}^0 - h_i^0$ value entering in formula (4) on moisture for the clay sample.

$h_{bw}^0 - h_i^0, kJ/kg$
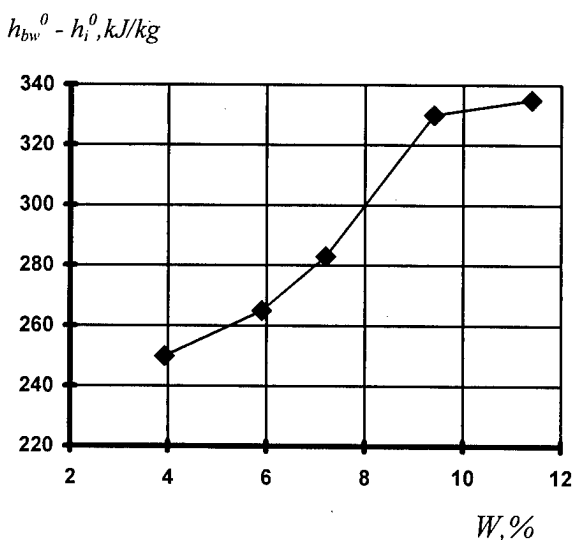
Fig. 1. Dependence of enthalpy difference $h_{bw}^0 - h_i^0$ of bound water and ice on moisture W.

Dependence of crystallization heat on overall moisture content as expected is significant for hygroscopic moisture. In the area of elevated temperature when moisture of clay sample exceeds the maximum hygroscopic one crystallization heat is equal to phase transition heat of volume water within the experimental error.

As enthalpy difference $h_{bw}^0 - h_i^0$ is a function of overall moisture content of the dispersion system, then crystallization heat depends as well on overall moisture content.

It must be noted though for a particular dispersion system that one can obtain the expression for crystallization heat depending on temperature from formula (4) provided the unfrozen water function is known.

Freezing temperature is determined by chemical potential value of bound water and ice while crystallization heat is characterized by enthalpy difference.

As there is no clear dependence between chemical potential and enthalpy while considering the dispersion systems with different scelet material, porosity etc., then one cannot mark the pronounced dependence between crystallization heat and phase transition temperature of bound water. So crystallization heat of bound water as a function of overall moisture content and temperature should be determined for a particular dispersion system.

During the experiment there was conducted the determination of unfrozen water amount in a sample using the method of steady heat supply (Stepanov and Timofeev, 1994), that may be considered as modification of a calorimetric method and supposes the usage of crystallization heat of water in calculations.

$W_{uf}, \%$
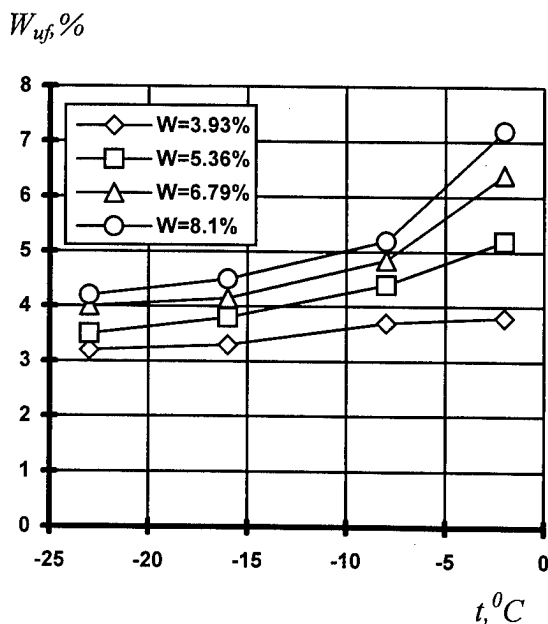
Fig. 2. Dependence of unfrozen water amount W_{uf} on temperature t in a clay sample at different moisture W (the experimental results are processed according to formula (1))

On the basis of experimental results there has

been evaluated unfrozen water content in a sample at different initial moisture. In fig. 2 there are shown the curves of unfrozen water using the equation (1) in calculations.

In fig. 3 there are shown the same curves using formula (4).

In this case the enthalpy difference $h_{bw}^{0} - h_{i}^{0}$ is approximated by a function obtained as a result of data processing shown in fig. 1.

$W_{uf}, \%$
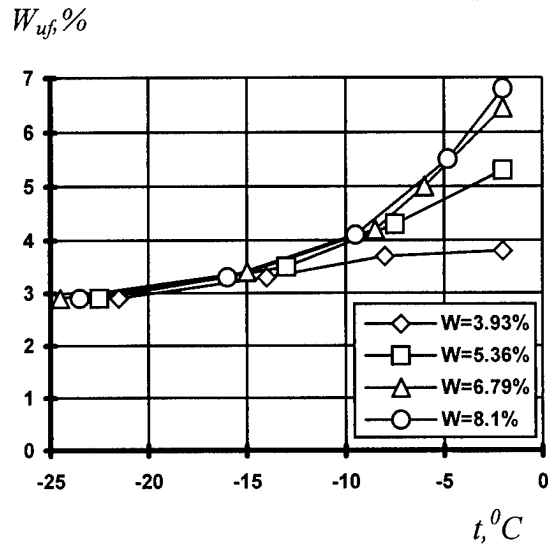
Fig. 3. Dependence of unfrozen water amount W_{uf} on temperature t in a clay sample at different moisture W (the experimental results are processed according to formula (4))

The results obtained show that crystallization heat of bound water at small moisture values differs greatly from that of volume water. In calorimetric tests on determination of unfrozen water amount the effect of this difference is clearly pronounced. Comparing figures 1 and 2 shows that in clay samples tested the unfrozen water amount is 20 - 30 % less at about -10°C using the values of bound water crystallization heat, compared with the case when values of volume water crystallization heat are used.

CONCLUSIONS

The determination method of crystallization heat makes it possible to find crystallization heat of water as a function of overall moisture content and temperature.

The investigations show that in hygroscopic moisture area the bound water crystallization heat differs greatly from that of volume water. This should be taken in account in calorimetric investigations of unfrozen water in soils.

REFERENCES

1. Brovka G. P. 1991. Heat and mass transfer in natural dispersion systems under freezing down. - Minsk.: Nauka i Tekhnika. - 192 p.

2. Chistotinov L. V. 1975. Something of thermodynamics of unfrozen water in soils. - In paper: Geocryological investigations. Issue 87: 24-39. Moscow.

3. Ershov E. D., Akimov Ju. P., Cheverov V. G. Kuchukov E. Z. 1979. Phase composition of moisture in frozen rocks. - Moscow: MSU. - 190 p.

4. Efimov S. S. 1985. On temperature dependence of water crystallization heat. - J. of Engineering Physics, v. 49, N 4: 658 - 664.

5. Efimov S. S. 1986. Moisture of hygroscopic materials. - Novosibirsk: Nauka. - 160 p.

6. Gavriliev R. I. 1970. Determination of temperature dependence of specific effective heat capacity in freezing down soils as well as unfrozen water amount inside them by a single test. In paper.: Determination methods of rocks thermal properties: 16-24. Moscow: Nauka.

7. Ivanov N. S. 1969. Heat and mass transfer in frozen rocks. - Moscow: Nauka. - 240 p.

8. Permiakov P. P. 1989. Identification of parameters of heat and moisture transfer mathematical model in frozen soils. - Novosibirsk: Nauka - 88 p.

9. Stepanov A. V., Timofeev A. M. 1994. Thermal properties of dispersion materials. - Yakutsk. - 124 p.

Optimization of Soil Mineralogical Composition
for Predicting Soil Thermal Conductivity

V.R. TARNAWSKI[1], B. WAGNER[2], J. WEBBER[3], AND L. PETTIPAS[4]

ABSTRACT

This paper reveals details of further improvement to a unified model for the prediction of thermal properties of soils having log-normal grain size distributions. Computer optimization of the default data of minerals' occurrence in soils has improved predictions by about 14%. The computer package developed (*TheHyProS*) is based on modified existing predictive models (De Vries, Campbell, etc.) and allows quick estimation of thermal conductivity, specific heat, and hydraulic properties over a full range of moisture content and over a temperature range of -30° to 95°C. A user-friendly interface allows for either default or self-entered modes of input. The default mode allows a soil selection from 12 available USDA textural classes. Reasonable assumptions concerning soil composition and compaction are made allowing use of the program by users with little soil physics knowledge. The self-entered mode requires data concerning bulk density, porosity, mineralogical composition and thermal properties of mineralogical components, grain size characteristics, and mass fractions of sand, clay and silt. Estimation of *field conditions* (i.e., expected soil moisture range, thermal conductivities, and specific heats under normal field conditions in a moderate climate) is also provided. Graphs and data may be viewed from within the program, or exported to many word processors or graphing packages.

Key words: soils, thermal and hydraulic properties, thermal conductivity, hydraulic conductivity.

INTRODUCTION

Knowledge of soil thermal and hydraulic properties is of major importance in current research and development efforts utilizing computerized techniques for the design of engineering ground structures such as pipelines, high voltage buried transmission lines, underground radioactive waste disposal facilities, ground heat storage, cold stores, etc. Computer simulation of heat and/or moisture flow in unsaturated soils has become a basic standard practice due to its tremendous power of predicting long-term performance, its augmenting capacity, and low cost. Reliable estimates of thermal and transport properties of soils are generally difficult to obtain, partly because of their high variability in the field, and partly because measuring procedures are time-consuming, expensive and error prone. The available data are generally fragmentary and unreliable. A review of recent literature shows that the ability to fully describe the simulated system does not keep pace with modern modeling expertise. Unfortunately, it is very difficult to identify a single predictive model of soil properties that could be applied successfully to all soils encountered in the field. Therefore, the main objective of this paper is to disclose some details of further improvement of a predictive unified computer model.

SURVEY OF PREDICTIVE MODELS

A review of recent literature demonstrates that a great deal of effort has been expended on the development of predictive models (Tarnawski and Wagner, 1992, 1993, 1996a, 1996b; Misra et al.,

1995; Ingersoll, 1988; Sundberg, 1988; Pande and Gori, 1987).

Misra et al. (1995) developed a theoretical model of thermal conductivity that attempts to take into account the microstructure of the soil. Heat transfer was assumed to occur in the regions of inter-particle contact of randomly arranged arrays of identical spheres. The resulting equation accounts for the presence of moisture at low contents, and shows a linear dependence of thermal conductivity on dry density.

Ingersoll (1988) developed analytical expressions for thermal conductivity and diffusivity which considered the following factors: porosity, water content, conductivity, specific heat, and density of solid matter, water and air. It was found that conductivity increases with water content, attaining a maximum value at saturation. However, the diffusivity showed a maximum at some intermediate moisture content. Ingersoll stated that although the model did not directly account for the soil type, the values of the porosity, moisture content, and conductivity of solid matter should reflect the given soil type.

Sundberg (1988), using a self-consistent approximation (every phase is surrounded by an effective medium with an effective thermal conductivity), developed a theoretical model predicting the effective thermal conductivity of soils and rocks, i.e., combination of the transport properties of separate solid and fluid phases, based on the effective continuous media approximation. To extend the self-consistent theory for soils, a correction factor (thermal contact resistance between grains of mineral soil, sandstone and limestone) was introduced. The model also accounts for vapour diffusion, unfrozen and frozen conditions including the unfrozen water content. Good results compared to experimental data of 600 soils and a number of crystalline and sedimentary rocks were reported.

Pande and Gori (1987) presented a theory for estimating the effective thermal conductivity. The results seem quite promising. However, inaccuracies occur for the degree of saturation values between 0.2-0.3 .

A critical review of other important predictive models of soil thermal conductivity was given by Tarnawski and Wagner (1992, 1993). In general, theoretical and semi-empirical models do not cover all types of soils encountered in the field and often do not produce satisfactory results. Few models make good predictions of the thermal properties of soils above and below the freezing point of soil moisture. A model by de Vries (1963) is probably the most suitable to be fully computerized and extended to soil hydraulic property estimation.

UNIFIED MODEL FUNDAMENTALS

The computer package named Thermal and Hydraulic Properties of Soils (*TheHyProS*) is based on the upgraded version of two well-known models by De Vries (1963) and Campbell (1985). According to the De Vries model the effective thermal conductivity of soil can be obtained from the following relation:

$$\lambda = \frac{\theta_w \lambda_w + \sum_{1}^{N} k_i \theta_i \lambda_i + k_a \theta_a \lambda_a}{\theta_w + \sum_{1}^{N} k_i \theta_i + k_a \theta_a} \quad (1)$$

where λ = thermal conductivity of the soil system; θ = volumetric fraction of the component; k = ratio of average temperature gradient of a soil component to average temperature gradient in soil water; a = air; w = water; i = soil solid component including ice; N = number of individual soil solid components

The k_i are calculated from:

$$k_i = \frac{1}{3} \sum_{abc} \left[1 + \left(\frac{\lambda_i}{\lambda_w} - 1 \right) g_i \right]^{-1} \quad (2)$$

where: a, b, c are axes of rotated ellipsoid; $a = b = n^*c$; n is a shape value; g_i are shape factors of the ellipsoids ($g_a = g_b$; $g_c = 1 - 2g_a$).

The shape factor, g_a, was calculated according to relations provided by Neiss (1982), and the shape value, n, was selected on the basis of data given by Dixon and Weed (1989), Neiss (1982), and De Vries (1963). Soil mineralogical composition strongly influences the type of soil and its thermal properties and therefore plays an important role in the computer prediction of thermal conductivity of soils (Tarnawski and Wagner, 1993). Consequently, *TheHyProS* offers two options regarding the use of soil mineralogical composition: a default or user input data. The default option is based on the fact that soils mainly consist of quartz, feldspar, calcite, clay minerals, and mica, which were roughly estimated based on the occurrence of these minerals in the soil environment (Table 1).

The mineral mass fractions of any soil whose mass fractions of separates are known can be

obtained using the data from this matrix. An example of calculating the mass fraction of quartz (m_q) in a soil is given below:

$$m_q = m_{q\text{-}cl} * M_{cl} + m_{q\text{-}si} * M_{si} + m_{q\text{-}sa} * M_{sa} \quad (3)$$

where: $m_{q\text{-}cl}$, $m_{q\text{-}si}$, $m_{q\text{-}sa}$, = mass fractions of quartz in clay, silt, and sand respectively; M_{cl}, M_{si}, M_{sa}, = mass fraction of clay, silt, and sand respectively.

A similar calculation has been performed for the mass fraction of any soil mineral (e.g., quartz, feldspar, calcite, clay minerals, and mica which are considered in this paper).

Table 2 shows the default data for textural classes of soils which is used in *TheHyProS* when the standard soil types option is selected. *TheHyProS* also offers a so called "self-entered option" which provides the possibility of considering soils with any desired mass fractions and mineral characteristics.

Some important features appended to the original De Vries model are as follows: a soil system can be composed of up to a maximum of 26 different minerals (user defined input) whose mass fraction, thermal conductivity, density, shape, and specific heat have to be known; a general relation is applied for the prediction of the mineralogical composition of soil separates; soil water is assumed to be a continuous medium of a soil system (Neiss,1982);and soil water hydraulic relations (*pF* - curve) are used for evaluation of the apparent thermal conductivity of soils (water vapor migration) at low moisture contents and obey a model proposed by Campbell (1974). In addition the new unified model is based on the following assumptions: hysteresis of the *pF* curve and change of structure due to freezing and thawing process is neglected, the grain size distribution is log-normal, soil mineral particles are uniform in distribution and shape, isotropic thermal conductivity of soil minerals, additive mode of heat transfer by conduction and convection, rigid soil matrix (no frost heave or thaw compression), soil moisture is pure water, and no osmotic or gravitational effects. Other details of the unified model were published by Tarnawski and Wagner (1992, 1993, 1996a, 1996b).

MODEL ENHANCEMENT

The unified model however, has some dilemmas associated with the use of the mineralogical composition of soils which might influence the prediction of thermal conductivity of soils.
One problem is related to uncertainties in the default

values of thermal conductivity of fine minerals (i.e., clay minerals, mica). The thermal conductivities of these minerals have not been measured due to very small particle sizes, and therefore have been adopted from larger minerals and rocks data. According to Robertson (1988), values of thermal conductivities for these minerals range from 0.4 to 3.4 W/m/K. Another problem is that the thermal conductivity of any soil is calculated using the same default data of soil mineralogical composition which was roughly estimated based on the occurrence of minerals in the soil environment (Table 1). It is also important to note that there is a lack of comprehensive data on the mineralogical composition of a large variety of different soil types. Therefore, it was necessary to carry out a preliminary computer optimization of the default matrix. The optimizing process includes varying the default input data of thermal conductivities and the occurrence of minerals in soils with continuous comparison of computer predictions with experimental data. This task has been performed on a personal computer and the following steps were used:

(i) Default mineral compositions are varied within a range of only $\pm$ 10% from the present default values (to avoid any equivocal results) with a step of 1% for each of the basic minerals. The best match with experimental data provides the optimal values for default mineral compositions.

(ii) The first step has been repeated five times to get more accurate results. A large amount of experimental thermal conductivity data for a wide variety of soils has been used in order to obtain default results that can be applied to basically any soil. For example, Kersten's (1949) data of 19 soils (unfrozen and frozen) contains 1011 points of measurements.

RESULTS AND COMPARISONS

A special computer program has been developed to carry out the task of optimizing the default input data of thermal conductivity of soil minerals. New computer predictions are compared with experimental data (all Kersten's soils) and a global solution (matrix) has been obtained (Table 3). Using the initial default matrix (trial 1) a new set of default values was obtained (trial 2). These values were used as defaults to obtain an improved matrix (trial 3). The overall prediction error for each soil decreased with any new trial up to 6. The average error was basically the same for trials 5 and 6. Therefore, results
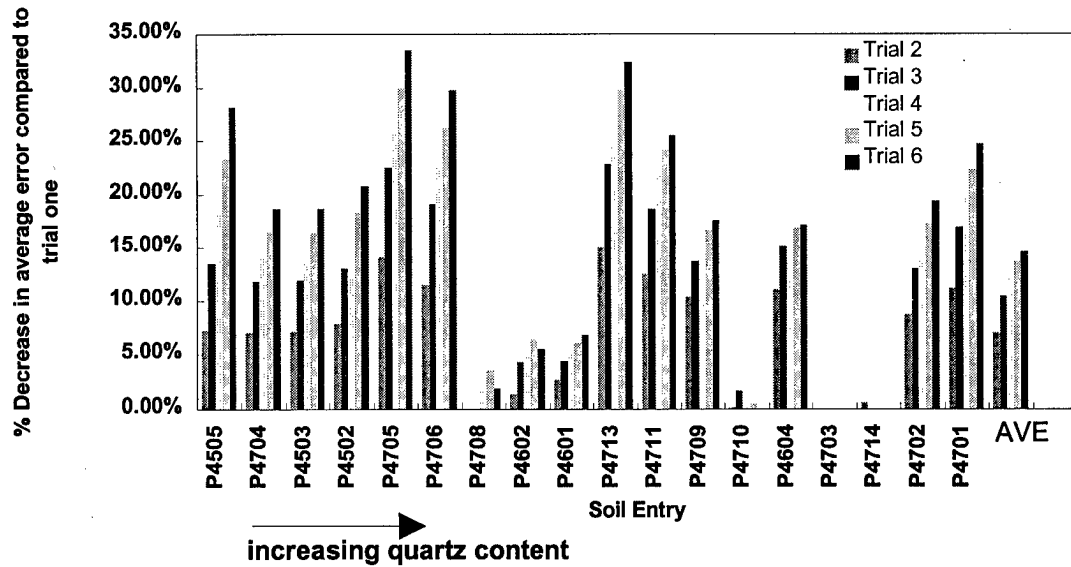
Fig. 1. Percent change of average error using optimal matrix for Kersten's soils

obtained from trial 5 were considered as the global matrix.

An extensive computer testing has been performed comparing new predictions (global matrix) with experimental data and an average error was calculated for each of Kersten's soil under investigation:

$$\Delta\lambda_{ave} = \Sigma\ err_i\ /\ n \qquad (4)$$

where $err_i = (\lambda_{com} - \lambda_{exp})/\ \lambda_{exp}$; error of each soil data entry λ_{com} = computed thermal conductivity; λ_{exp} = experimental thermal conductivity; n = number of soils entries processed.

The above percentage error changed when the matrix values were adjusted (trials 1-6). Therefore, the so called error percentage change was introduced:

$$\Delta\lambda_{ch} = 100*(\Delta\lambda_n - \Delta\lambda_1)/\Delta\lambda_n \qquad (5)$$
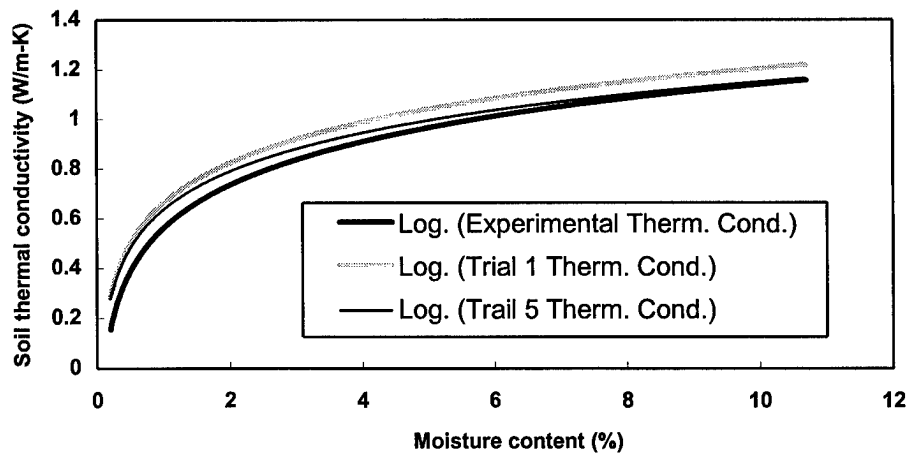
Fig. 2 Thermal conductivity of Fairbanks Sand (P4709)simulation and experimental results by Kersten, 1949

94
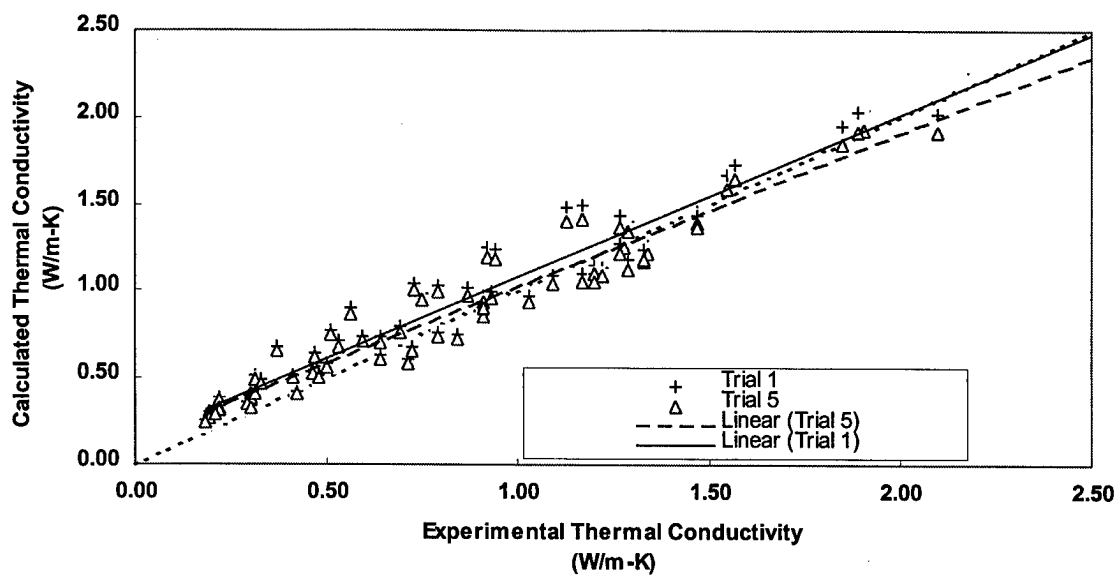
Fig. 3 Thermal conductivity of Fairbanks Sand (calculated vs. experimental data by Kersten 1949)

where $\Delta\lambda_n$ = new average % error of each soil data entry and $\Delta\lambda_1$ = trial one average % error of each soil data entry. Fig 1 shows the percent change of average error for all of Kersten's soils. The higher the percentage decrease error the better the results of the optimization. Two soils, P4703 (crushed quartz) and P4714 (fine crushed quartz) did not show any improvement from trial 2 to trial 6 and prediction results become worse. Therefore, the use of a matrix from trial 2 would be appropriate.

Figure 2 and 3 shows the improvement in thermal conductivity prediction of Fairbanks sand (P4709) vs. experimental data. In a low moisture content region (0 to 1%) the difference between results obtained from a trial 1 and a trial 5 is negligibly small. This indicates that the model predictions in that region have not been improved by the use of a new global matrix. When the soil moisture content is higher the prediction results obtained from the trial 5 follow very well the experimental data. Fig. 3 shows a linear least square fit of calculated results for trial 1 and trial 5. The values of the R-squared and a standard error are about the same (0.9377; 0.123) for trial 1 and 5, respectively. The prediction error for all soil types has been reduced by 7, 10.5, 12.5, and 13.8% for trial 2, 3, 4, and 5 with respect to trial 1, respectively. A similar trend can also be seen for other soils.

CONCLUSIONS

The use of the new global matrix shows a clear trend for improvement for all soil types under investigation. The preliminary analysis shows that the average prediction error for all soil types has been reduced by about 14% for trial 5 with respect to trial 1. Due to excessive computing times the gravel mineralogical composition was not optimized. The results obtained also identify another problem, i.e., still relatively large error at low soil moisture content. This is likely due to the assumption that water is a continuous medium, which is not valid at low moisture contents. A lack of complete and reliable data for soils with low moisture contents would also have some effect on the optimal matrix. Although these results have shown a certain improvement, they are preliminary and more rigorous optimization needs to be done.

ACKNOWLEDGMENTS

Table 1. Mass fractions of minerals in the soil separates (default matrix)

Type of mineral	Clay	Silt	Sand	Gravel
Quartz	0.05	0.40	0.88	0.65
Feldspar	0.05	0.30	0.10	0.25
Calcite	0.00	0.05	0.00	0.10
Clay minerals	0.80	0.15	0.00	0.00
Mica	0.10	0.10	0.02	0.00

Table 2 Default mass fraction data for textural classes of soils

Soil texture	Clay, M_{cl} Mass fraction	Silt, M_{si} Mass fraction	Sand, M_{sa} Mass fraction	Gravel M_{gr} Mass fraction
	-	-	-	-
Sand	0.04	0.04	0.92	0.00
Loamy sand	0.05	0.11	0.82	0.00
Sandy loam	0.12	0.20	0.68	0.00
Loam	0.12	0.44	0.44	0.00
Silty loam	0.12	0.70	0.18	0.00
Silt	0.07	0.86	0.07	0.00
Sandy clay loam	0.34	0.12	0.54	0.00
Clay loam	0.34	0.33	0.33	0.00
Silty clay loam	0.34	0.55	0.11	0.00
Sandy clay	0.55	0.05	0.40	0.00
Silty clay	0.55	0.40	0.05	0.00
Clay	0.70	0.15	0.15	0.00

Table 3. Mass fractions of minerals in the soil separates - new global matrix

Type of Mineral	Clay	Silt	Sand	Gravel
Quartz	0.05	0.35	0.80	0.65
Feldspar	0.05	0.25	0.10	0.25
Calcite	0.00	0.05	0.00	0.10
Clay minerals	0.88	0.15	0.00	0.00
Mica	0.02	0.20	0.10	0.00

REFERENCES

Campbell, G.S. 1974. A simple method for determining unsaturated conductivity from moisture retention data. Soil Science, 117: 311-314.

Campbell, G.S. 1985. Soil physics with basic. Amsterdam: Elsevier.

De Vries, D.A. 1963. Thermal properties of soils. In *Physics of the plant environment*. W.E.Van Wiik (Ed.), North-Holland Publishing Company, Amsterdam, 210-235.

Dixon, J.B., and S.B. Weed. 1989. Minerals in soil environments , 2nd ed., Soil Science Society of America, Madison, Wisconsin, pp.1244.

Ingersoll, J.G. 1988. Analytical determination of soil thermal conductivity and diffusivity. Journal of Solar Energy Engineering, 110:306-312.

Kersten, M.S. 1949. Thermal properties of soils. University of Minnesota. Bulletin No. 28, vol. LII, No. 21, pp. 225.

Misra, A., B. R. Becker and B.A. Fricke. 1995. A theoretical model of the thermal conductivity of idealized soil. HVAC&R Research, 1:81-96.

Neiss J. 1982. Numerische Simulation des Wärme- und Feuchtetransports und der Eisbildung in Böden. Fortschriftt-Berichte der VDI-Zeitschriften, Reihe 3, Nr. 73.

Pande, R.N. and F. Gori. 1987. Effective media formation and conduction through unsaturated granular materials. Int. J. Heat Mass Transfer. 30:993-1000.

Robertson, E.C. 1988. Thermal properties of rocks. U.S. Department of Interior. Geological Survey. Open-File Report 88-441. 106pp.

Sundberg, J. 1988. Thermal properties of soils and rocks (Ph.D thesis). Chalmers University of Technology and University of Göteborg, 310 pp.

Tarnawski, V.R., and B. Wagner. 1992. A new computerized approach to estimating the thermal properties of unfrozen soils. Canadian Geotechnical Journal, 29: 714-720.

Tarnawski, V.R., and B. Wagner. 1993. Modeling the thermal conductivity of frozen soils. Cold Regions Science and Technology, 22:19-31.

Tarnawski, V.R., and B. Wagner. 1996a. On the prediction of hydraulic conductivity of frozen soils. Canadian Geotechnical Journal, 33: 176-180.

Tarnawski, V.R., and B. Wagner. 1996b. Computer evaluation of thermal and transport properties of unsaturated soils. *In Proceedings of the 2nd European Thermal-Sciences and 14th UIT National Heat Transfer Conference*, Rome, Italy, May 29-31, pp. 345-350.

Modeling the Magnitude and Time Dependence of Nonconductive Heat-Transfer Effects in Taiga and Tundra Soils

S.I. OUTCALT[1], K.M. HINKEL[1], L.L. MILLER[1], AND F.E. NELSON[2]

ABSTRACT

A fully implicit finite-difference model of conductive heat transfer, incorporating temperature-dependent apparent thermal diffusivity and fusion effects, was employed to model the thermal field in freezing and thawing soils. Hourly temperature time series from thermistors at eight levels in the near-surface soil were available from three sites in Alaska. Using 3-hr averages, the simulated temperature was subtracted from the observed temperature for each level. These residuals indicate the relative magnitude and time-dependence of nonconductive heat transport. The temporal pattern of residuals suggests that the thermal field in midwinter most closely fits the conductive model. Negative residuals early in summer appear to result from the combined effects of evaporative cooling and upward migration of cooler water. These processes reduce the mean annual ground temperature by about 1°C in the middle region of the active layer. Conversely, residuals are positive during the zero-curtain and the snowmelt periods.

Key Words: Alaska, frozen ground, modeling, soil temperature

BACKGROUND

A variety of methods have been employed over the past decade to demonstrate the nature, time-dependence, and magnitude of nonconductive heat transport effects in freezing and thawing soils. Procedures include calculating apparent thermal diffusivity (ATD) using finite-element methods (McGaw et al. 1978, Hinkel et al. 1990) and analyzing thermal and chemical time series using fractal geometry and spectral analysis (Outcalt and Hinkel 1992, 1996, Hinkel and Outcalt 1993, 1994, 1995). The various techniques produced consistent results, and suggest seasonally dependent nonconductive heat transport due to vertical water advection and vapor transport.

In the active layer above permafrost, four thermal regimes are generally discernible during the annual cycle (Outcalt et al. 1997, Outcalt and Hinkel 1996). Each regime is characterized by a suite of operative heat-transfer processes. The "active layer regime" (AL) develops in summer, when the thawed zone is thickening. This is a period when conduction tends to dominate, but nonconductive heat-transfer processes may significantly affect the thermal evolution of the active layer. The thawed soil zone is cooled by internal evaporation and the upward migration of colder water from the thaw front toward the zone of evaporation near the surface (Outcalt and Nelson 1985). Infiltration of precipitation is also important during this period (Hinkel et al. 1993, Hinkel and Nicholas 1995).

As the active layer refreezes from the surface downward in autumn and early

winter, the lower part of the unfrozen zone becomes isothermal near 0°C, often for several months. This phenomenon is known as the *zero-curtain effect* (Sumgin et al. 1940); we refer here to the period during which this effect dominates as the "zero curtain regime" (ZC). Although heat conduction cannot occur across an isothermal zone, water and water vapor migrate vertically across the unfrozen layer in response to osmotic gradients, transporting both sensible and latent heat upward (Outcalt et al. 1990). This regime is therefore dominated by nonconductive heat-transfer and phase change effects.

As subfreezing temperatures penetrate to depth during mid- to late winter, the active layer freezes and the "freezing regime" (FR) commences. Once the pathways between soil pores become blocked with ice, movement of water and water vapor is restricted and conduction dominates.

When the snow melts in spring, moisture typically migrates downward. The transfer of both mass and sensible heat alters the bulk soil-thermal properties and disrupts the thermal field. Rapid warming of the frozen soil toward the melting point is characteristic of the "snowmelt regime" (SM). As the soil thaws in early summer, the AL regime begins the cycle again.

These divisions are based on the dominant heat transfer process, so the regime patterns are known from other analyses (Outcalt et al. 1990, Hinkel and Outcalt 1994, 1995). However, none of these methods give a good estimate of the thermal magnitude of nonconductive effects.

THE MODEL

Measurements of temperature in the mineral soil at Barrow, Alaska, were collected by McGaw et al. (1978), and estimates of ATD were derived using a finite-difference method. Because ATD is temperature dependent in soils (Farouki 1981), the estimates were fitted to a polynomial to obtain a temperature-dependent ATD value across the temperature range of 0°C to -6°C. The ATD rose from a small value just below 0°C to a value of $6 \times 10^{-6} m^2 s^{-1}$ at -6°C. Above 0°C and below -6°C, the value of $6 \times 10^{-6} m^2 s^{-1}$

was used, making the model extremely simple and conservative. Observed temperatures from the upper and lower probes were used as boundary conditions, and the model was initiated with the first measured thermal profile at all probe levels. The internal node values were estimated using a fully implicit finite-difference model, in which the new thermal vector is estimated by Gaussian elimination applied to the tri-diagonal matrix and the current thermal vector (Press et al. 1989). The model makes a simple adjustment for unequal node spacing during the calculation of the temperature-dependent Fourier modulus.

THE DATA SETS

Three data sets of soil temperature, containing measurements collected at eight levels over the annual cycle, were used for this analysis (Fig. 1). Two data sets were collected from sites in the discontinuous permafrost region of central Alaska. Located within the taiga at the Caribou/Poker Creeks Research Watershed near Fairbanks, Alaska, one site experiences only seasonal frost due to water seepage (Site A; Fig. 1a), while the other is underlain by permafrost (Site B; Fig. 1b). Probes were arrayed vertically at 7-cm intervals at both taiga sites, from near the surface (1 cm) to a depth of 50 cm. The time series from these taiga sites extend from mid-August 1992 to mid-August 1993.

The third site, located near Barrow, is in the continuous permafrost zone. The data set was collected from unconsolidated sediments below tundra within the Barrow Environmental Observatory. Probe levels had the same spacing as the taiga sites to a depth of 29 cm, but the lower three probes are at 50, 75 and 100 cm. The record extends from mid-August 1994 to mid-August 1995. However, midwinter temperatures descended below the lower limit of the data system (-22°C) at Barrow, so this period was excluded. The Barrow time series was therefore broken into two subsets, corresponding to periods in which *cooling* (10 Aug-22 Nov 1994) and *warming* (29 Mar-25 Aug 1995) dominated. The hourly observations were abstracted to form time
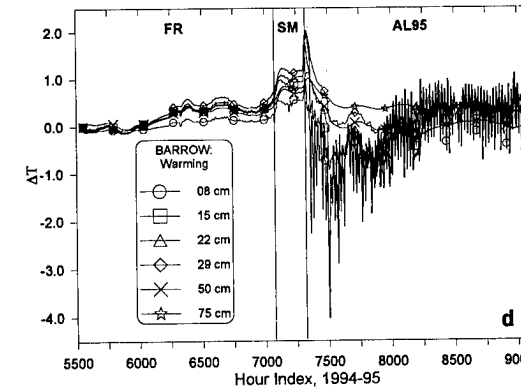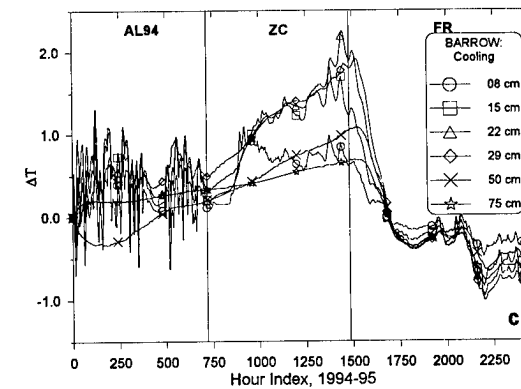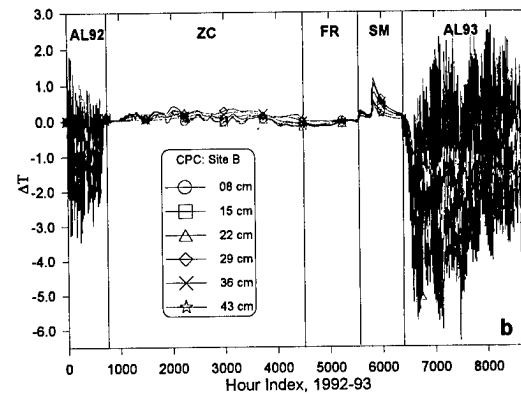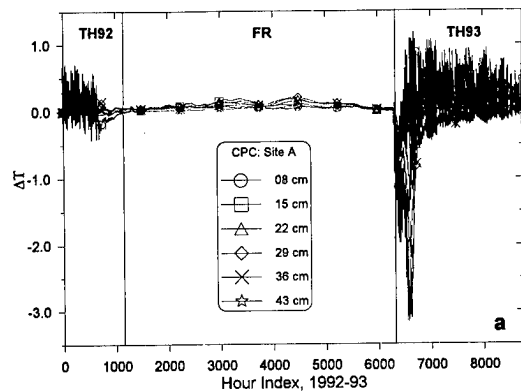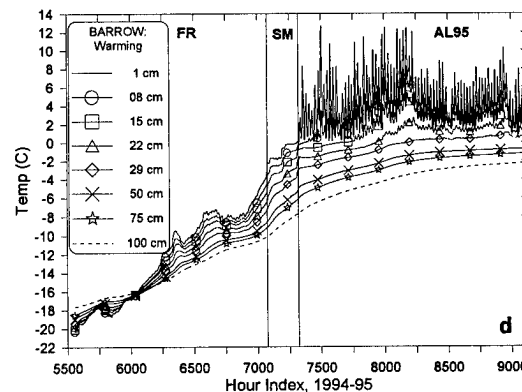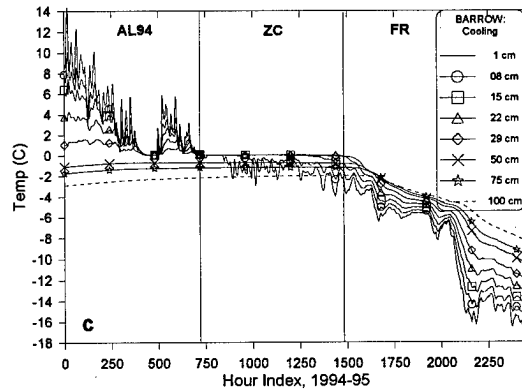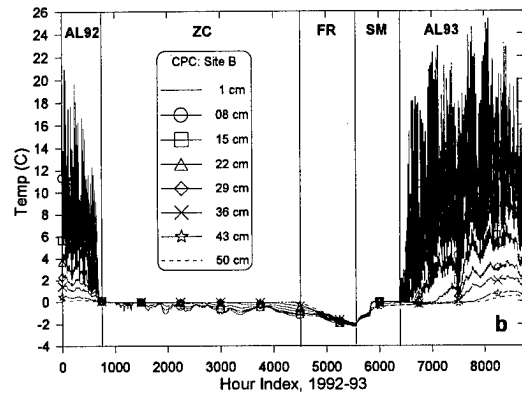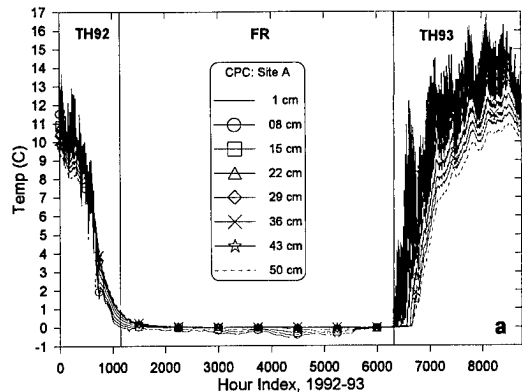
Figure 1. Temperature traces for taiga sites without (a) and with permafrost (b) for mid-Aug 1992 to mid-Aug 1993, and Barrow during cooling (c: 10 Aug-22 Nov 1994) and warming (d: 29 Mar-25 Aug 1995).

Figure 2. Time series of residuals (ΔT °C) derived from subtracting simulated soil temperatures from observed temperatures for the three sites shown in Fig. 1. The upper and lower traces are not shown.

100

series of 3-hour average temperatures at all three sites.

Thermal data from the three sites are presented in Figure 1. Vertical dividing lines were added to explicitly delimit thermal regime transitions. At the taiga seasonal frost site (Fig. 1a) only two regimes occurred: the midwinter soil (freezing/thawing) **FR** regime and the summer thaw or **TH** regime. At both permafrost sites (Site B and Barrow), the **TH** regime is replaced by the **AL** regime, which indicates summer thawing of the active layer.

THE SIMULATIONS

Graphs of the simulated time series appear generally similar to the observed time series. Deviations can best be observed by plotting differences between corresponding values in the two time series. Figure 2 displays "residuals" obtained by subtracting simulated from observed values. These plots represent an estimate of the magnitude and time-dependence of nonconductive effects. The general pattern indicates that residuals are minimized at all sites during the **FR** regime and maximized during the **TH/AL** regimes. Because traces from the upper and and lower probes were used as a boundary condition, they would plot as a straight line at $0°C$ on the ΔT axis and were therefore deleted.

The graphs of Figure 2 are quite complex. A final figure was therefore constructed showing residual traces for the two middle nodes at 22 and 29 cm. These represent departures of simulated values from the empirical record at probe levels most distant from the constraining boundary levels, and are shown in Figure 3.

Four significant results, evident from Figure 3, can be discerned from these simulations. At each of the sites, the **FR** regime appears to be governed by conductive processes with only weak nonconductive heat transfer effects present. During operation of the **FR** regime, the soil at depth is no longer directly coupled to the atmosphere due to the presence of snow cover, which strongly attenuates the amplitude of thermal fluctuations reaching the soil surface. Furthermore, pore ice inhibits
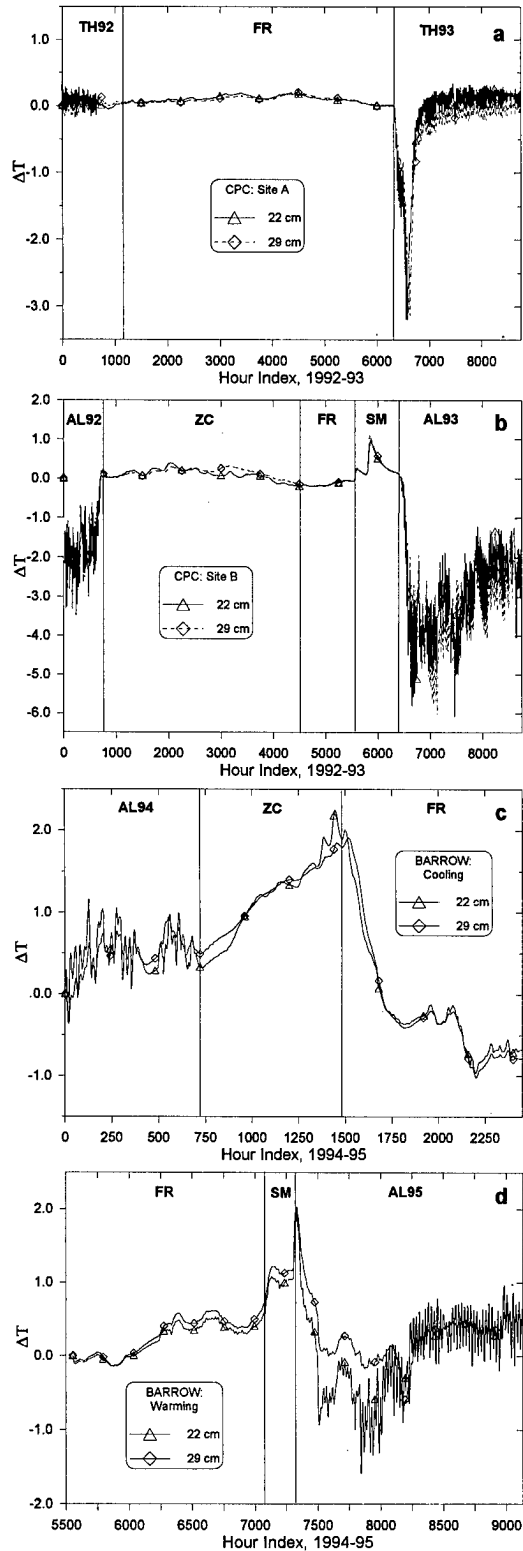
Figure 3. As in Fig. 2, but for the intermediate 22- and 29-cm probe levels. Note the change in the scale of the Y axis (ΔT °C).

101

migration of water and water vapor in the soil column, and this effect becomes more pronounced with colder subfreezing temperatures as residual water is converted to ice.

Near the onset of the **TH** and **AL** regimes at the taiga sites, observed temperatures are much colder than the simulations, yielding negative residuals. The steep cooling at the beginning of the **TH** regime at the seasonal frost site (Fig. 3a) ends once thawing of the winter subfreezing zone is complete. This pattern of negative residuals persists through both **AL92** and **AL93** regimes at the taiga permafrost site (Fig. 3b). At the tundra permafrost site (Fig. 3c and 3d), residuals tend to be negative during the early **AL** regime but become positive in late summer. Negative residuals occur when the soil cools by evaporation or is cooled by the advection of cold water from the base of the thawing active layer. These processes were added to conduction in a thermal model that successfully simulated the observed thermal regime in 0.5 m of peat covering the ice core of a palsa (Outcalt and Nelson 1985). This cooling effect is maximized during the period of high sun when evaporation is most effective, and diminishes as the active layer thickens later in summer.

The **ZC** regime at the tundra site (Fig. 3c) is a period of positive anomalies, indicating strong nonconductive effects which do not diminish until well into the **FR** regime. These warmer-than-modeled temperatures result from the release of latent heat. Although fusion effects were incorporated into the model, energy is also released by condensation of water vapor near the upper frost front (Outcalt et al. 1990).

The large positive residual associated with the **SM** regime appears at both permafrost sites (Figs. 3b & 3d), and reflects rapid downward movement of meltwater, generated at the surface, into the soil. The flux of warmer water raises the soil temperature to the ice point over a very short time and hastens thawing of the active layer in spring.

A crude estimate of the cumulative effects of nonconductive heat-transfer processes was obtained by calculating the
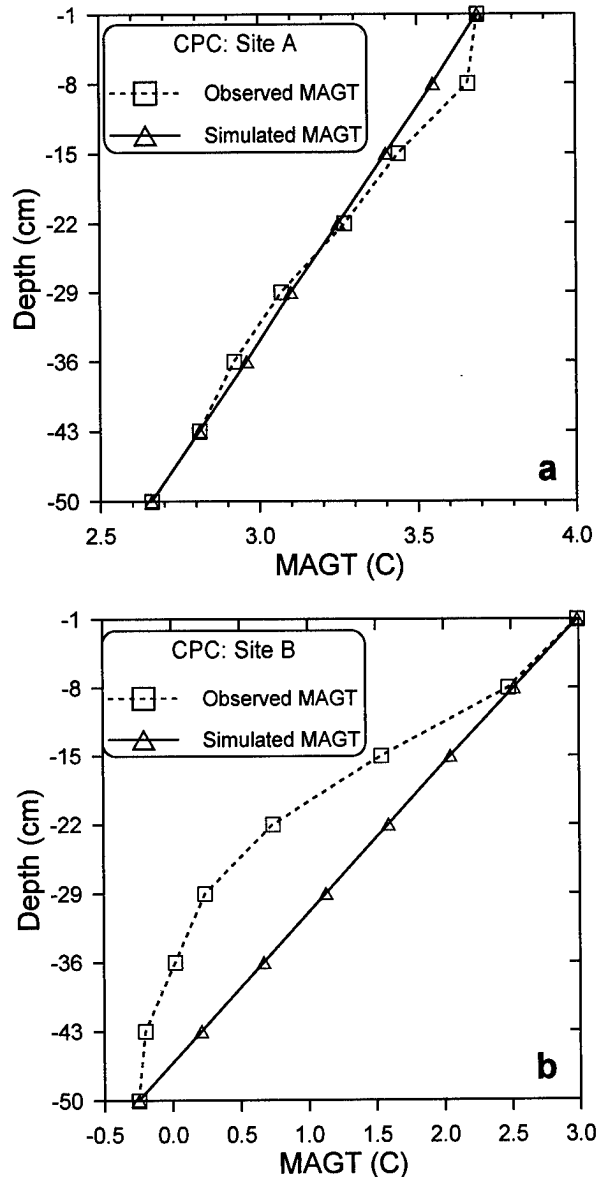
Figure 4. Observed (dashed) and simulated (solid) mean annual ground temperature (MAGT) at taiga sites shown in Figs. 1a and 1b. Note difference in X axis scale.

mean annual ground temperature (MAGT) for each probe level at the taiga site. Simulated MAGT plots as a straight line, with values decreasing with depth (Fig. 4). At Site A, the observed and simulated MAGTs are very similar. Thus, despite high-frequency, seasonally dependent variations in the residuals, the saturated soil generally behaves as a conductive system.

Conversely, nonconductive heat-transfer processes have a considerable impact in the active layer above permafrost at Site B. Here, observed MAGTs are cooler than simulated, by as much as 1°C, near the center of the active layer. Negative residuals occur primarily during the **AL** regime, as the thaw front is penetrating downward. Evaporative cooling and upward advection of cooler water from the base of the thawed zone have a measurable effect on the MAGT at this location.

CONCLUSIONS

The use of "residuals," as outlined in this paper, is a powerful tool for documenting and exploring the relative magnitude and regime dependence of nonconductive heat transfer processes.

The **TH** regime in seasonal frost terrain, and the **AL**, **ZC**, and **SM** regimes in soils underlain by permafrost, all display characteristics that are not typical of a conductive heat-transfer system. Negative residuals are prominent early in the **TH** and **AL** regimes but diminish later in summer. Cooling in early summer probably results from internal evaporative cooling in the near-surface soil, and from advection of cold water moving upward toward the region of evaporation. At the taiga permafrost site, the cooling is sufficient to lower the MAGT by about 1°C in the middle region of the active layer.

Positive residuals characterize the **ZC** and **SM** regimes. Condensation in the upper unfrozen active layer retards cooling during the **ZC** regime, while infiltration of snow meltwater causes rapid soil warming in spring (**SM**). Conversely, small residuals occur only during the **FR** regime, indicating that the temperature field can be success-fully modeled using conductive heat transfer theory incorporating the effects of fusion.

ACKNOWLEDGMENTS

REFERENCES

Farouki, O. T. 1981. Thermal properties of soils. CRREL Monograph 81-1, U.S. Army Cold Regions Research and Engineering Laboratory, Hanover, 136 pp.

Hinkel, K. M., and J. R. J. Nicholas. 1995. Active layer thaw rate at a boreal forest site in central Alaska. Arctic and Alpine Research, **27**: 72-80.

Hinkel, K. M., and S. I. Outcalt. 1993. Detection of nonconductive heat transport in soils using spectral analysis. Water Resources Research, **29**: 1017-1023.

Hinkel, K. M., and S. I. Outcalt. 1994. Identification of heat-transfer processes during soil cooling, freezing and thaw in Central Alaska. Permafrost and Periglacial Processes, **5**: 217-235.

Hinkel, K. M., and S. I. Outcalt. 1995. The detection of heat-mass transfer regime transitions in the active layer using fractal geometry. Cold Regions Science and Technology, **23**: 293-304.

Hinkel, K. M., S. I. Outcalt, and F. E. Nelson. 1990. Temperature variation and apparent thermal diffusivity in the refreezing active layer, Toolik Lake, Alaska. Permafrost and Periglacial Processes, **1**(4): 265-274.

Hinkel, K. M., S. I. Outcalt, and F. E. Nelson. 1993. Near-surface summer heat-transfer regimes at adjacent permafrost and non-permafrost sites in central Alaska. *In* Proceedings, 6th International Conference on Permafrost. South China University of Technology Press, Wushan Guangzhou, People's Republic of China, pp. 261-266.

McGaw, R. W., S. I. Outcalt, and E. Ng. 1978. Thermal properties of wet tundra soils at Barrow, Alaska. *In* Proceedings, Third International Conference on Permafrost. National

Research Council of Canada, Ottawa, pp. 47-53.

Outcalt, S. I., and K. M. Hinkel. 1992. The fractal geometry of thermal and chemical time series from the active layer, Alaska. Permafrost and Periglacial Processes, 3(3): 315-322.

Outcalt, S. I., and K. M. Hinkel. 1996. Thermally-driven sorption, desorption, and moisture migration in the active layer in central Alaska. Physical Geography, 17: 74-90.

Outcalt, S. I., and F. E. Nelson. 1985. A model of near-surface coupled flow effects on the diurnal thermal regime in a peat-covered palsa. Archives of Meteorology, Geophysics, and Bioklimatology, Series A, 33: 345-354.

Outcalt, S. I., F. E. Nelson, and K. M. Hinkel. 1990. The zero-curtain effect: heat and mass transfer across an isothermal region in freezing soil. Water Resources Research, 26: 1509-1516.

Outcalt, S. I., K. M. Hinkel, E. Meyer, and A. J. Brazel. 1997. Applications of Hurst rescaling to geophysical serial data. Geographical Analysis, in press.

Press, W. H., B. P. Flannery, S. A. Teukolsky, and W. T. Vetterling. 1989. Numerical Recipes in C: The Art of Scientific Computing. Cambridge University Press, Cambridge, 735 pp.

Sumgin, M. I., S. P. Kachurin, N. I. Tolstikhin, and V. F. Tumel'. 1940. Obshchee Merzlotovedenie [General Permafrostology]. Moscow: Academiia Nauk SSR.

Soil Temperature and Seasonal Thaw
Controls and Interactions in Floodplain Stands
Along the Tanana River, Interior Alaska

P.C. ADAMS[1] AND L.A. VIERECK[1]

ABSTRACT

At the Bonanza Creek Experimental Forest Long-Term Ecological Research (BNZ-LTER) site, we are monitoring a number of climate and vegetation parameters, including air and soil temperatures, seasonal thaw, canopy cover and organic layer thickness on the Tanana River floodplain. Monitoring sites are located within successional forest stands resulting from silt-bar deposition in five successional stages. In this paper we show differences in soil temperature and seasonal rate and depth of thaw that have developed as a result of the successional change in the vegetation. Year-to-year variability in environmental parameters is also shown to have an effect on the soil microclimate. Important factors in determining the soil temperature profile and rate of thaw are organic layer thickness, canopy cover, and snow depth.

Key words: Boreal forest, succession, soil temperature, thaw depth, permafrost.

INTRODUCTION

Soil temperature changes with successional stage in forest stands on the active floodplain of the Tanana River near Fairbanks, Alaska. These changes result from a number of factors that also change during the successional sequence, some as the result of the direct changes in ecosystem structure and function and some as the indirect result of related environmental changes. In addition, both soil temperature and the rate of annual thaw of the seasonal frost vary considerably from year to year within the same site. Factors that influence soil temperature and the thaw rate of seasonal frost include changes in forest floor organic layer thickness, canopy cover, soil moisture, snow deposition and its seasonal timing, and air temperature.

As part of the Bonanza Creek Experimental Forest Long-Term Ecological Research (BNZ-LTER) Program we monitor a number of climatic parameters, including air temperature, soil temperature, snow cover, and seasonal thaw, in five successional stages of forest development on the Tanana River floodplain. Additionally, we have described structural characteristics of the vegetation in these successional stages. Previous studies have documented a number of changes that directly affect soil temperatures, seasonal thaw, and the formation of permafrost across this floodplain successional sequence (Van Cleve et al. 1991, Viereck et al. 1993).

This study examines factors contributing to the observed soil temperatures and seasonal rate and depth of thaw across the successional sequence and through time. We show how these environmental variables are affected by development of a forest floor layer and by canopy structure interacting with air temperature and snowfall. We also consider the importance of year-to-year variability in air temperature and snow depth.

THE SUCCESSIONAL STAGES

Twelve stages of forest development in this area have been described in some detail (Viereck 1989). For the LTER study we selected five points in the floodplain successional sequence that we designated as "turning points," where we felt that rapid

vegetation change was resulting in dramatic changes in the associated stand environments (Van Cleve et al. 1996). These five successional stages, where we are presently monitoring soil temperature and other environmental factors along with their LTER site designation are described in Table 1. Detailed descriptions of these stages can be found in Viereck et al. (1993), Viereck (1989) and Van Cleve et al. (1996). Figure 1 shows the relationship of the sites where we are measuring environmental parameters to the total floodplain successional sequence. This cross section indicates the buildup of the organic layer with time, as well as the development of permafrost in the later stages of succession. The parent material at these sites, alluvial deposits, remains relatively constant (Van Cleve et al. 1991), although the texture varies from coarse to finer material with repeated fluvial deposition and increasing surface height.

One of the most important changes that takes place in the successional sequence is the development of a forest floor layer. In the earlier stages where deciduous shrubs and trees dominate, leaf litter accumulates to a depth of 5–10 cm, and is frequently buried by silt from flooding. As spruce begin to become dominant in the canopy, feathermosses invade the forest floor and begin to develop an O2 forest layer, an organic horizon in which the original form of most plant material cannot be recognized with the naked eye. Flooding and siltation occur less frequently and the organic layer increases to as much as 15–20 cm in the mature white spruce stands. In the black spruce stands a forest floor organic layer becomes well developed and persistent.

Table 1. Description of five successional stages and six monitoring sites

FP1A   Open willow stage comprised of seven species of *Salix*, and rapidly developing into an alder (*Alnus tenuifolia*) stand (5–15 years of age during the course of the 10 year study).

FP2A   Young closed balsam poplar (*Populus balsamifera*) stand with a dense but decadent tall shrub layer of alder (20–30 years of age).

FP3A   Closed mixed balsam poplar–white spruce (*Picea glauca*) stand where the 50-to 60-year old white spruce are currently reaching through the canopy and replacing the 80-year old balsam poplar.

FP4A   Closed mature (150- to 200-year old) white spruce stand with a well developed forest floor of feathermosses.

FP5A   Two open black spruce (*Picea mariana*)
and   stands on older terraces of the river.
FP5C   These two stands are nearly identical in vegetation structure. FP5A, located on an island, lacks permafrost whereas FP5C, on a terrace on the south side of the Tanana, is underlain with permafrost with a shallow active layer.

Another significant change during succession that affects soil temperature is the canopy cover. The deciduous canopy of willows, alders and balsam poplar offers a cooling effect on air and soil temperatures during summer months but is not
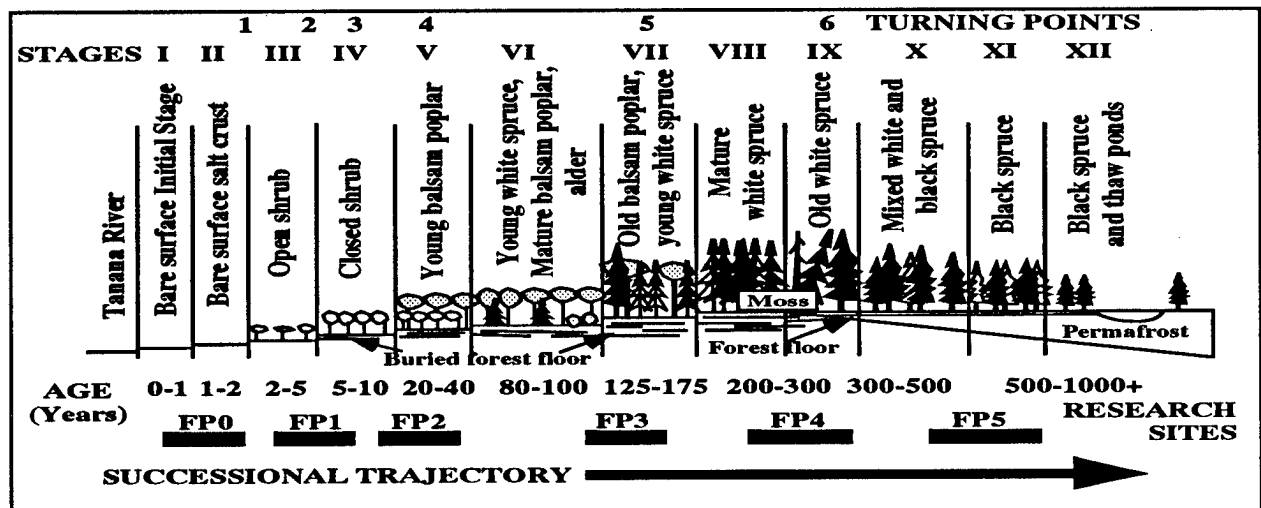
Figure 1. Primary succession on depositional terraces on the Tanana River floodplain. LTER research sites and vegetation type used in this paper are: FP1A–Open willow, FP2A-Balsam poplar/alder; FP3A–Balsam poplar/white spruce, FP4A-White spruce, FP5A and FP5C–Open black spruce.

106

effective in the winter. In contrast, the spruce canopy dramatically mediates air temperatures all year, as well as playing a major role in snow interception in winter months. As a result, there is significant variability in snow cover from one successional stage to another. Both the mediation of air temperature and the reduction in snow cover may contribute to lower winter soil temperatures. The effect of the canopy is reduced in the open low-growing black spruce stands.

METHODS

Environmental data used in this study were obtained from the LTER monitoring sites within the five successional stages on the Tanana River floodplain (Fig. 1). Measurements at the second replicate of black spruce (FP5C) were initiated because permafrost at FP5A, a site with similar vegetation and organic cover, is discontinuous or intermittent.

Air and soil temperatures are measured and recorded hourly by electronic data loggers at each of these locations. Initially, three replications of soil temperature thermistors were installed at 10- and 20-cm depths at each site. In 1993 these were replaced by a single set of six thermistors at 5-, 10-, 20-, 50-, 100-, and 200-cm depths. Monthly and annual air and soil temperatures are derived from daily mean temperatures.

Depth to the frozen layer is measured with a steel probe inserted into the ground at 10 points at each site. Seasonal frost is recorded as "out" when the depth to frost is greater than 245 cm. These measurements are made weekly at each site until the seasonal thaw is greater than 245 cm at all 10 points. Average depth of thaw for each date of measurement is the mean of the 10 values or mean of those values which are less than 245 cm. Average depths of thaw for all the years of measurement were obtained for each site by determining thaw depths for common dates at 10-day intervals through interpolative methods, and averaging those depths by common date. The date that seasonal frost is "out" is the average date among the years of measurement that the depth of thaw first exceeded 245 cm.

Organic layer thickness was determined from soil profiles taken at four locations at each site in the five successional stages. Although a leaf layer of 1- to 2-cm has recently begun to develop at the youngest successional stage, there has been no measurable change in the organic layer thickness at the other sites during the course of this study.

Snow depth at each site is measured only once or twice during the winter, although equivalent measurements are made at the two main LTER weather stations weekly throughout the winter. Long-term snow depth and snow water content are measured monthly at the Natural Resources Conservation Service (NRCS) official snow course, and are a part of that agency's permanent record.

RESULTS

Variability Among Successional Stages

Significant changes in average soil temperatures occur with succession on these floodplain sites (Fig. 2). Soil temperatures are greatest in the younger successional stages and decrease through succession. An exception is that soils at the balsam poplar/white spruce site (FP3A) are colder and warm more slowly than at the white spruce site (FP4A). Also the seasonal soil temperature patterns at the two black spruce sites (FP5A and FP5C) are quite different, with temperatures at FP5C showing little seasonal fluctuation at shallow depths, and remaining frozen below 50 cm. This pattern is displayed at 20 and 100 cm depths in Figure 2. Although soil temperature changes are dampened with increasing depth,
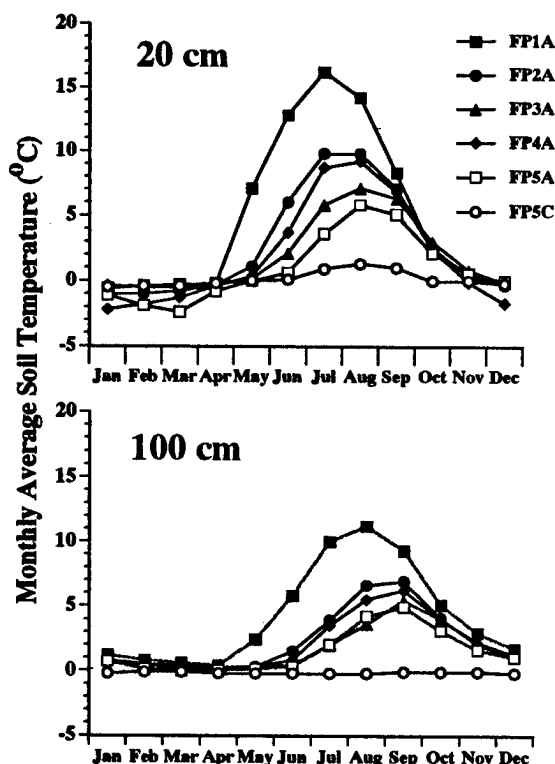
Figure 2. Monthly average soil temperature (1992–1996) measured at 20 cm and 100 cm depths at 6 sites in 5 successional stages (Table 1).

107

similar patterns exist at the other measured depths of 5-, 10-, 50-, and 200-cm.

Differences in soil temperature are reflected in the seasonal thaw rates of soils at these successional sites (Fig. 3). Soils at the willow site (FP1A) thaw quickly each spring, and the date of complete thaw averages more than a month earlier than at the balsam poplar/alder site (FP2A), the next earliest site to thaw completely. Complete thaw at the later successional sites occurs only in some years, and the average date is reflected in Figure 3. There is limited seasonal thaw at the black spruce permafrost site (FP5C). At the white spruce site (FP4A), a gravel surface exists somewhere between 170 and 180 cm deep which complicates the determination of the depth of thaw. The seasonal thaw is complete at this depth. Similar to the seasonal soil temperature patterns, the thaw rates at the balsam poplar/white spruce site (FP3A) are slower than those at the later successional white spruce stages.

Figure 4. Average canopy cover (%) by species at 6 sites in 5 successional stages (Table 1).

Figure 3. Depth of thaw (average for 1989–1996) at 6 sites in 5 successional stages (Table 1). The graph represents average depth of thaw at 10-day intervals, including the average date that seasonal frost melted completely (> 245 cm)
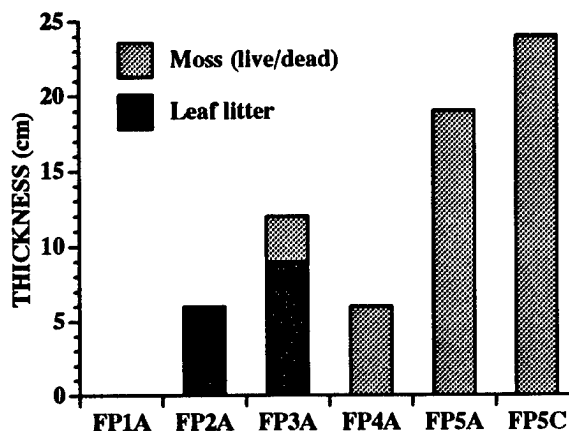
Figure 5. Organic layer thickness (cm) by type of organic material at 6 sites in 5 successional stages (Table 1).

A number of structural changes that may account for these soil temperature differences occur with succession. Canopy cover and type develop from no tree cover in the willow stage through primarily deciduous trees in the poplar and poplar/spruce stage, and reaches a maximum in mature white spruce stands (Fig. 4). Finally, the cover is reduced significantly in black spruce stands. Organic layer thickness changes from none in initial willow stages through heavy leaf layers to deep moss in the spruce stands (Fig. 5).

These structural changes result in differences in air temperature of less than a degree during the summer months (Fig. 6). The greatest differences occur during the winter months when the black

spruce permafrost site (FP5C) is the coldest at -26° C and the white spruce stand (FP4A), the warmest, averages -21.8° C. Differences in snow depth at the successional sites, when expressed as a percent of the snow depth recorded at the LTER weather station with no canopy cover, clearly reflect the variability in canopy cover (Fig. 7). Snow depth decreases most dramatically with increasing white spruce cover (FP3A and FP4A), while the depth in the open black spruce stands (FP5A and FP5C) decreases with increasing canopy density.

Temporal Variability

Significant temporal variability exists in these environmental parameters within the period of measurement. The monthly average soil temperatures, for example, are dramatically colder at all sites at the end of 1995 and throughout 1996 than any year since 1990. This general pattern is
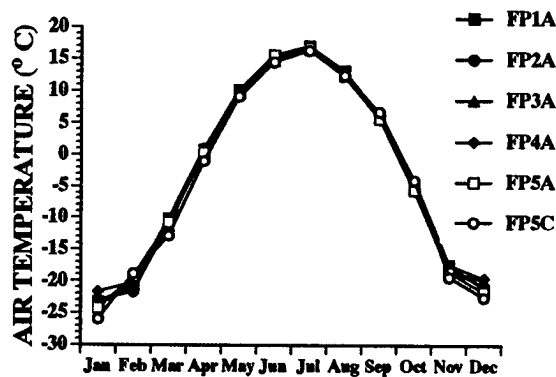
Figure 6. Average monthly air temperature (° C) from 1989 through 1996 at 6 sites in 5 successional stages (Table 1).
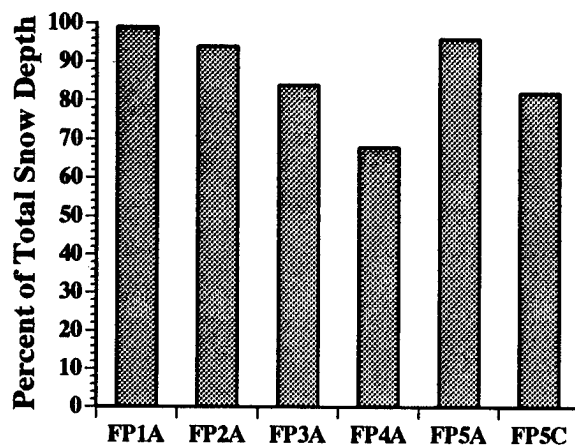
Figure 7. Snow depth shown as the percent of the snow depth measured at the LTER2 weather station without a canopy at 6 sites in 5 successional stages (Table 1)

Figure 8. Monthly average soil temperature at a balsam poplar/white spruce stand (FP3A) measured at 20 cm and 100 cm depths from 1992 through 1996.
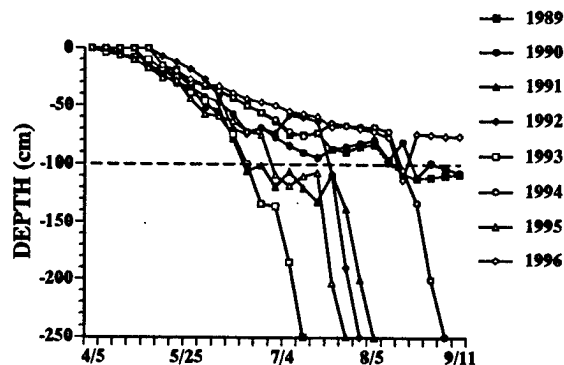
Figure 9. Depth of thaw at a balsam poplar/white spruce stand (FP3A), for 1989 through 1996.

illustrated in Figure 8 which shows the annual variability in soil temperature at the balsam poplar/white spruce (FP3A) stand. Similarly, 1996 was the first year since 1990 that the seasonal frost did not go out at all 10 probe points at the balsam poplar/white spruce site (FP3A) (Fig. 9). At most sites the complete thaw consistently occurred earliest in 1993, a record warm year in interior Alaska.

Snow depth varies greatly from year to year, as illustrated by the long-term snow record from the NRCS snow course (Fig. 10), showing the maximum snow depth in BCEF since 1968. Snow depth in 1991, at 151 cm, was the greatest ever recorded in interior Alaska and 1993, at 101 cm, was well above average. The maximum depth in 1996, 58 cm, was close to average but most of the snowfall did not occur until February. Figure 11 shows snow depth by month since the 1988–1989 snow year. In this figure

it is apparent that 1996 is unusual in the sparse snowfall early in the season. The snow depth was well below normal during the 1995–1996 snow year until February, when a near-record snowfall resulted in a normal maximum for the year.

Mean annual air temperature also varied considerably from year to year. During the period of the study mean annual temperatures at the adjacent LTER floodplain weather station varied from -0.9° C in 1993 to -4.3° C in 1990. Annual variability in air

109
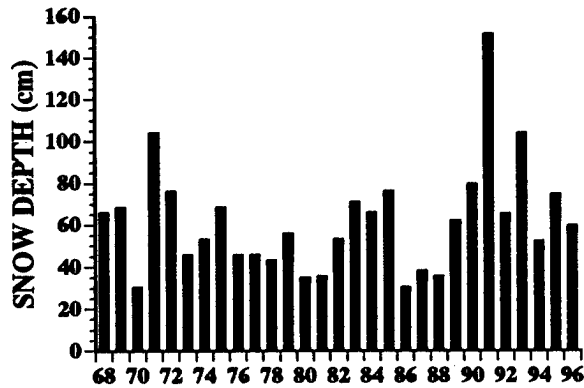
Figure 10. Annual maximum snow depth at the Bonanza Creek Experimental Forest official NRCS snow course from 1968 to the present.

Sep Nov Jan Mar

Oct Dec Feb Apr
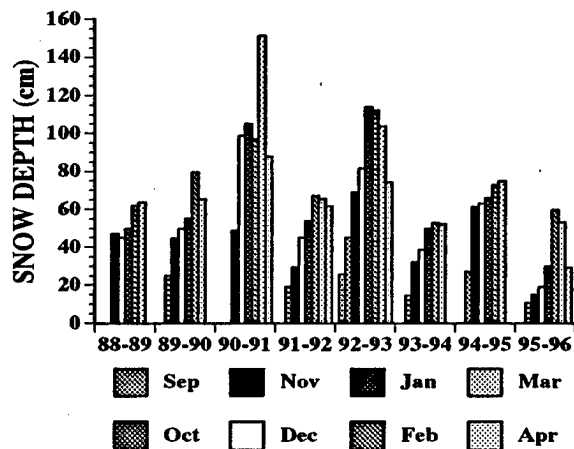
Figure 11. Monthly snow depth since September 1988 at the Bonanza Creek Experimental Forest official NRCS snow course. This figure shows the seasonal variability in snow accumulation.

temperature for the balsam poplar–white spruce stand (FP3A), is shown by monthly mean temperatures (Fig. 12). The other floodplain sites show similar air temperature patterns among years. The coldest and shortest summer was 1992 when both early spring (April and May) and late summer (September and October) air temperatures were at or near record cold for those months. The warmest year, 1993, had monthly mean temperatures only slightly above that of other years of the study.

SUMMARY AND CONCLUSIONS

The recording of long-term measurements of environment and vegetation changes in successional stands at the BNZ-LTER sites on the floodplain of the Tanana River can be used to demonstrate some of the controls on soil temperature in the boreal
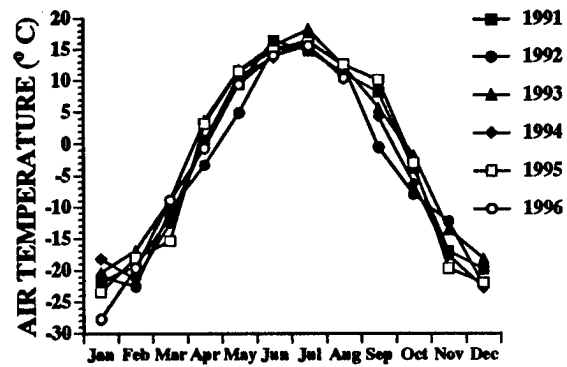
Figure 12. Monthly average air temperature (° C) at, a balsam poplar/white spruce stand (FP3A) for 1991 through 1996.

forest. The value of the long-term observations at the LTER sites is that we can begin to see correlations between some of these variables only after several years of data collection. Fortunately, during the period of our study we have experienced a record heavy snow year (1990–91), an exceptionally short snow-free season (1992), and a year in which significant snowfall was delayed until after the end of January (1995–96).

Bonan (1989, 1992), using data from BCEF and other boreal forest sites, developed a model to predict depth of thaw based on climate, topography, soil type, organic layer thickness, and forest canopy. He found that the moisture content, thickness of the organic layer and thus its thermal conductivity, as predicted from his model, had a significant effect on depth of seasonal thaw of the active layer. He did not use snow as one of the variables in his model, although the influence of snow on ground thermal regimes has been recognized (Smith 1975).

Our study on the Tanana River floodplain, with no topographic relief, shows that soil temperature decreases and seasonal thaw is delayed as forest succession proceeds. Of special significance is the change in canopy cover from deciduous shrubs and trees to a closed canopy of spruce. Simultaneously with the development of the spruce canopy, there is an increase in the forest floor organic layer thickness and a decrease in annual maximum snow depth. During the period of our study, annual variation in air temperature had little effect on soil temperature but variation in snow depth, especially during the early winter months, resulted in colder soil temperatures even though air temperatures during the same period were not correspondingly lower. This within-season variability in snow cover had the greatest temporal effect on soil temperatures in our study. The lack of snow through January of 1996,

coupled with a prolonged cold spell that month, resulted in the cold soil temperatures and delayed thaw in the spring and summer of 1996.

Climate warming within the boreal forest zone may complicate the study of long-term changes in soil temperatures and depth of thaw with succession. Osterkamp and Romanovsky (1996) have suggested that global climate warming may be resulting in warmer soil temperatures as well as the melting of permafrost in some regions of Alaska. The development of lower soil temperatures and permafrost through succession, as we have documented in this paper, may be affected by the series of warmer years that have been experienced in the Fairbanks area since 1975 (Viereck and Adams 1990, Juday 1993). A longer record of observations may be needed to confirm the effects of a changing climate regime.

Our results show the complexity of the interactions of both the environment and forest floor and stand structure characteristics in determining soil temperature, rate of thaw, and presence or absence of permafrost in forested stands on the floodplain of the Tanana River. Long-term measurements, such as those taken at the LTER sites, are needed to develop an understanding of the interactions of vegetation and the environment and to serve as both input to developing forest ecosystem models and to provide verification of existing models.

ACKNOWLEDGMENTS

REFERENCES CITED

Bonan, G.B. 1989. A computer model of the solar radiation, soil moisture, and soil thermal regimes in boreal forests. Ecological Modelling 45: 275–306.

Bonan, G.B. 1992. Soil temperatures as an ecological factor in boreal forests. p. 126–143. In: H.H. Shugart, R. Leemans, and G.B. Bonan (ed.) A systems analysis of the global boreal forest. Cambridge University Press, Cambridge, UK.

Juday, G.P. 1993. Baked Alaska? Scientist examines temperature trends. Agroborealis 25(2): 10–14.

Osterkamp, T.E. and V.E. Romanovsky. 1996. Characteristics of changing permafrost temperatures in the Alaskan arctic. Arctic and Alpine Research 28(3): 267–273.

Smith, M. W. 1975. Microclimatic influences on ground temperatures and permafrost distribution, Mackenzie Delta, Northwest Territories. Can. J. Earth Sci. 12: 1421–1438.

Van Cleve, K., F.S. Chapin III, C.T. Dyrness, and L.A. Viereck. 1991. Element Cycling in Taiga Forests: State-Factor Control. BioScience 41(2) 78–88.

Van Cleve, K., L.A. Viereck, and C.T. Dyrness. 1996. State factor control of soils and forest succession along the Tanana River in interior Alaska, USA. Arctic and Alpine Research 28(3): 388–400.

Viereck, L.A. 1989. Flood-plain succession and vegetation classification in interior Alaska. p. 197–203. Proc. Land classification based on vegetation: Applications for resource management, Moscow, ID. Nov. 17–19 1988. USDA–FS Gen. Tech. Rep. INT–257. Ogden UT.

Viereck, L.A. and P.C. Adams. 1990. Variation in microclimate among sites and changes of climate with time in Bonanza Creek Experimental Forest. In Proc. Long-term ecological research workshop into climate variability and ecosystem response, University of Colorado, Aug 21–23, 1988. USDA-FS Gen. Tech. Rep. SE–65 Asheville, NC.

Viereck, L.A., C.T. Dyrness, and M.J. Foote. 1993. Overview of vegetation and soils of the floodplain ecosystems of the Tanana River, interior Alaska. Can. J. For. Res. 23(5): 889–898.

Water and Solutes

Frozen Soil Effects on Depression Focused
Water and Solute Movement

N.E. DERBY[1] AND R.E. KNIGHTON[1]

ABSTRACT

A tracer study was initiated in November 1993 to monitor solute movement through the vadose zone into the shallow ground water. Granular potassium chloride (KCl) was surface applied to two areas overlying subsurface drains and to one area instrumented with soil solution samplers and ground water monitoring wells. One of the subsurface drain tracer plots was located on level ground while the other two sites were in small topographic depressions. The applied tracer was found to move rapidly to the shallow ground water under the depressional areas after infiltration of spring snowmelt in 1994. Excessive rainfall events were also responsible for the rapid transport of the applied chloride tracer. The findings of this study indicate that, under certain conditions, it may be necessary to delineate areas of a field based on topography to be integrated into a site-specific farming plan.

Key words: Depression focused recharge, tracer, chloride.

INTRODUCTION

Agriculture has long been named as a major contributor to non-point source pollution of ground water resources. In areas of predominantly sandy soils and shallow water tables, the risk of ground water contamination is increased due to the high hydraulic conductivities of the soil and close proximity of the contaminant to the ground water, respectively. With the advent of fertilizer and irrigation Best Management Practices (BMPs) and site-specific variable rate technology, more emphasis is being placed on field variability. One area that needs to be investigated further is the spatial variability of ground water recharge and subsequent contamination relative to ground surface topography.

It is theorized in this study that in agricultural fields, previously thought of as primarily non-point sources of pollution, areas exist that act as point sources of ground water contamination.

In 1971, Lissey measured the vertical potential gradient in topographic depressions to study the ground water flow patterns. These areas were classified as depression-focused recharge, discharge, or transient areas. In the depressional areas, most of the water available for spring recharge came from snowmelt runoff that ponded due to frozen soils. This water infiltrates as the soils thaw causing these areas to act as focal points for recharge, resulting in a ground water mound (Knuteson et al., 1989; and Lissey, 1971). Similarly, Freeze and Banner (1970) found that recharge in the spring was focused in depressions because infiltration was prohibited due to the frost lens and ran off into depressions until the frost lens thawed and the snow melt could infiltrate. As a result, many portions of an area formerly considered a recharge area may never receive direct infiltration to the ground water, but recharge would be depression focused. In a lowland versus upland study conducted by Delin and Landon (1993), applied water and agricultural chemicals reached deeper depths and were found at higher concentrations in the lowland area. Schuh and Klinkebiel (1994) also found highly variable recharge due to surface micro-topography variability.

Closely related to focused recharge is the process of preferential flow, as depression-focused recharge

[1] North Dakota State University, Department of Soil Science, P.O. Box 5638, Fargo, North Dakota 58105, USA

may be viewed as preferential flow on a field scale. Preferential flow is the general term used to describe rapid flow of water and solutes through the root zone to the water table by some means other than idealized piston flow. It is this preferential flow that has the ability to bring surface applied chemical rapidly and directly to the ground water with little or no degradation (Kladivko et al., 1991). In the case of small depressions, ponded water takes with it any mobile chemicals, and sometimes immobile chemicals, as it infiltrates. If the ground water is shallow enough, the chemicals may reach the ground water before they can be degraded or a crop can utilize them. It is depression-focused preferential flow of this nature that will be investigated in this project.

In order to investigate the phenomenon mentioned above, tracer material was applied to the soil surface and its movement monitored through the unsaturated zone and into the ground water. A distinction was made between areas which are relatively flat and those areas that are topographic depressions. The objectives of this study are:

1) Investigate the occurrence of depression focused recharge and the spatial variability of solute movement to a shallow water table aquifer due to depression focused infiltration.

2) Investigate the possibility of rapid, preferential flow to subsurface drains during intense rainfall/irrigation or other recharge events focused in topographic depressional areas.

MATERIALS AND METHODS

General site description

A field-scale study of Best Management Practices for irrigation and nitrogen fertilizer use on corn was initiated in 1990 near Oakes, ND (Steele et al., 1992). A primary objective of the study is to develop BMPs and to determine the impacts of those BMPs on ground water quality in the shallow aquifer underlying sandy soils typical of the Oakes Test Area. The study area comprises approximately 56 ha of the NW1/4, Sec.29, T.130 N, R.59 W in Dickey County, North Dakota. It is instrumented with lysimeters, wells, and subsurface drains to monitor soil leachate and ground water quality. The study is funded by the U.S. Bureau of Reclamation, operated by NDSU Departments of Soil Science and Agricultural Engineering, and farmed by Hokana Farms (Herman Meyer, landowner).

Data collected from the BMP site, the subsurface drains in particular, showed that nitrate nitrogen concentrations increased sharply after an excessively large rainfall event. A number of hypotheses have

surfaced about the occurrence, one of which is the existence of preferential flow in such situations.
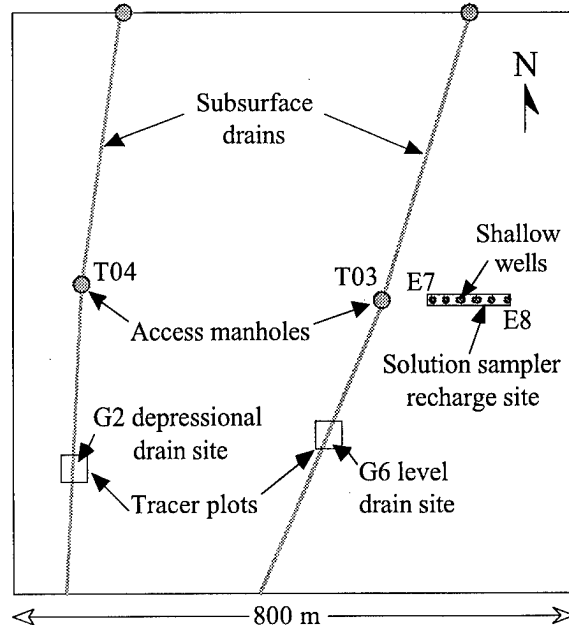
Figure 1. Plan view map of recharge sites on BMP quarter.

As a result of these prior observations, three tracer sites (Fig. 1) were chosen in the BMP field to investigate the possible occurrence of depression focused recharge and preferential flow. One site is located in a depressional area and is instrumented to monitor tracer concentrations of the soil solution and ground water. The other two sites are positioned directly over subsurface drains, one in a depressional area and one at a relatively flat area.

Potassium chloride (KCl) was used as a tracer as no KCl fertilizer had been applied to the field since the project was initiated in 1990. Also, ground water chloride levels had been monitored previously for four years, establishing a good background concentration.

Solution sampler site

One area chosen for the study of depression focused recharge is located on the "E" transect line between grid points E7 and E8 (Fig. 1) with the bottom of the depression at E7.6. The instrumentation at the site traverses a small topographic depression with points E7 and E8 located approximately on the ridges of the depression. A profile view of the instrumentation and ground surface topography at this site is included in Fig. 2. The elevation above mean sea level at the solution sampler site ranges from 398.07 m at E8 to 397.03 at

E7.6, a difference of only 1.04 m. The vertical scale has been exaggerated to show detail.
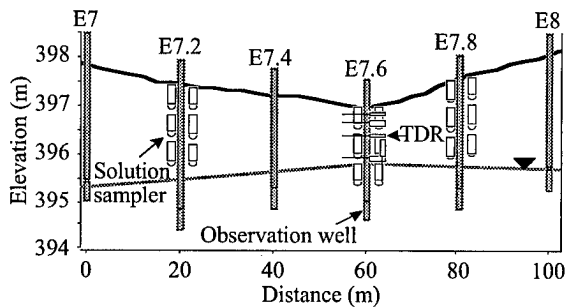
Figure 2. Cross section view of instrumentation installed at solution sampler site.

Granular potassium chloride (KCl) as 0-0-60 bulk fertilizer was surface broadcast at a rate of 448.4 kg ha^{-1} along the "E" transect between E7 and E8 on 11/10/93. The area receiving tracer was 6.1 m X 100 m, encompassing the wells E7, E7.2, E7.4, E7.6, E7.8, and E8. The KCl was mechanically incorporated with a disk immediately after application to a depth of approximately 10 cm. Total material applied to the 0.06 hectare strip was 67.5 kg, resulting in application of 224.2 kg ha^{-1} of both K$^+$ and Cl$^-$. Final tracer concentration in the top 15 cm of the soil after application was approximately 100 mg Cl$^-$ kg^{-1}, assuming a bulk density of 1.45 g cm^{-3}.

The ground water observation wells used for this study were installed by the U.S. Bureau of Reclamation in the fall of 1992. The wells were screened at a depth of 0-0.9 m below the existing water table elevation. The elevation above mean sea level of the top of the well casing and the length of pipe was recorded to allow for later measurement of water table elevation relative to the top of pipe elevation.

Soil solution samplers were constructed and installed on 9/29/93 at grid locations E7.2, E7.6, and E7.8 to monitor the tracer concentration in the soil solution. The solution samplers consisted of a 100-KPa porous ceramic cup attached to a 30-cm length of 5-cm diameter PVC pipe. A two-holed rubber stopper was inserted into the opposite end of the pipe. Two plastic tubes were inserted through the rubber stopper. One tube extended just below the bottom of the rubber stopper and was used as an air entry tube. The other tube extended into the ceramic cup at the bottom of the solution sampler and served as a solution extraction tube.

The final solution sampler installations consisted of three samplers, 0.3, 0.9, and 1.5 m deep, to the

west and three samplers to the east of each well at E7.2, E7.6, and E7.8. All plastic vacuum lines for each site were run through a section of plywood to hold the lines off the ground and keep the lines in order.

A Campbell Scientific CR10 datalogger was installed at E7.6 to log soil moisture, soil temperature, soil tension, and precipitation on an hourly basis. Soil moisture was measured via time domain reflectometry (TDR) at depths of 15, 30, 61, and 91 cm. One measurement was also recorded as an average moisture between 91 and 137 cm. This was accomplished by horizontal placement of the 15, 30, 61, and 91 cm TDR wave guides and vertical placement of one wave guide starting at 91 cm. Wave guides consisted of two 45-cm long, 0.3175-cm-diameter stainless rods soldered to a 75-300 ohm balun.

Soil temperature was measured using copper/constantan thermocouples at depths of 7.6, 15.2, 22.8, 30.5, 61.0, 91.4, 122.0, and 152.4 cm below the soil surface. Soil tension was measured with six tensiometers installed at depths of 15, 30, 61, 91, 122, and 152 cm below the soil surface.

Soil solution samples were taken once prior to tracer application in 1993 and approximately weekly the following spring. During an expected recharge event, samples were taken more frequently. The method of sample extraction involved creating a partial vacuum (70 KPa) in the solution sampler with a vacuum pump and allowing them to extract soil water over the course of a few hours up to one day, depending on the soil moisture status. When the soil solution was to be extracted from the samplers, a vacuum pump was used to pull the water which had collected through the ceramic cup, directly into a sample collection vessel attached in-line with the vacuum pump.

Water samples were taken from the shallow wells at the E transect solution sampler recharge site on roughly the same schedule as from the solution samplers. Peristaltic pumps were used to draw a sample from the screened section of the well. The water samples from each well were subsampled for chloride analysis.

Subsurface drain recharge sites

To supplement the solution sampler site, tracer material was applied to two areas overlying two subsurface drains on the BMP field (Fig. 1). One area was located just north of the G transect and west of G6 over the drain south of access manhole T03. This area was relatively level with no obvious topographic depressions. The other site was located over the drain

to the south of access manhole T04 in a slight depression south of grid point G2. Each plot was 0.09 ha in area measuring 30.5 m X 30.5 m.

The subsurface drains underlying the plots are constructed of 15-cm corrugated plastic drain line. The drain line under the plot at G2 is approximately 2.4 m below the ground surface and flows from south to north. The drain line located under the tracer plot near G6 is approximately 3 m below ground surface and also flows from south to north.

Access manholes designated T03 and T04 are located in-line to the north of the tracer plots. The manholes consist of a section of concrete culvert that serves as a connection point for two lengths of subsurface drain.

Granular potassium chloride (KCl) as 0-0-60 bulk fertilizer was surface broadcast to the 0.9 ha area at the same rate and in the same fashion as on the solution sampler plot.

Automated waste water samplers were installed at drain access manholes T03 and T04. The sampler was programmed to take a 500-ml sample of the drainage at 6-h increments for 6 days after the program was started. The samplers were only used during periods of intense rainfall, irrigation and during the spring thaw. During periods when no recharge was expected, the drains were sampled manually on a weekly basis. Manual samples were collected by lowering a stainless steel bucket into the access manhole to get a grab sample. Flow rates through the subsurface drains were measured and recorded every two hours with data logging flow meters.

RESULTS AND DISCUSSION

Solution sampler depression focused recharge site

The measurements and analysis results from samples taken at the E transect depression focused recharge site during the project are included and discussed below. The primary area of interest is the spatial and temporal variation of the applied tracer material.

Soil physical properties

Soil cores were taken at E7.2, E7.6, and E7.8 for particle size analysis. The cores were divided into 15-cm increments down to 152 cm. The particle size analysis was done by the Soil and Water Characterization Laboratory at NDSU. The results of the analysis and textural class of the samples are included in graphical form in Fig. 3.
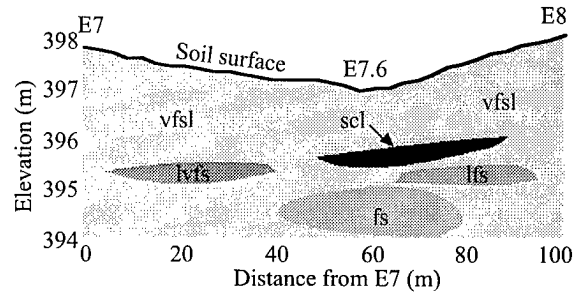
Figure 3. Soil profile textural classes at E transect recharge site.

The soil at the E transect recharge site was found to be predominately very fine sandy loam (vfsl) with a thin layer of heavier textured sandy clay (scl) at 61-76 and 76-91 cm at E7.6 and E7.8, respectively. The profile at E7.6 graded to fine sand at 107 cm with a maximum of 92.9% sand. Total sand ranged from 56.9 to 92.9% while the percent silt ranged from 4.0 to 26.0% and the clay ranged from 3.1 to 20.5%.

Soil hydraulic conductivity at 25 and 75 cm was measured with a compact constant head permeameter (Amoozegar, 1992) at E7, E7.6, and E8. The average K_{sat} measured at the 25-cm depth was 4 cm h^{-1} while the average at the 75 cm depth was 2.2 cm h^{-1}. The measurements were quite variable; however, the soil at the bottom of the depression consistently had a lower conductivity than the surrounding soils on the slopes and ridges of the depression. This is presumably due to movement of finer soil particles into the depression with runoff water over the years. In general, the variation in tracer movement and ground water recharge is not explained by variation in soil physical properties at the solution sampler site.

Chloride in soil solution and ground water

The spatial and temporal distribution of the applied chloride tracer material in the soil solution was found to be highly variable at the E transect recharge site. Chloride in the soil solution prior to tracer application was relatively low. During the following spring, chloride concentrations varied greatly.

Solution sampler and observation well chloride data for E7.2, E7.6, and E7.8 are shown as time series contours in Figures 4a, 4b, and 4c, respectively. Included in each of the figures is the concentration contour by date, the sampling locations for each date, water applications, water table elevation, and date of tracer application. The data represented at the solution sampler locations are average values from the two samplers at each depth.

116

The location of each sample is indicated by a small circle in the figures. For each of the three time series contours, the missing data from pre-tracer application through the winter are shown as a continuation of the initial conditions.
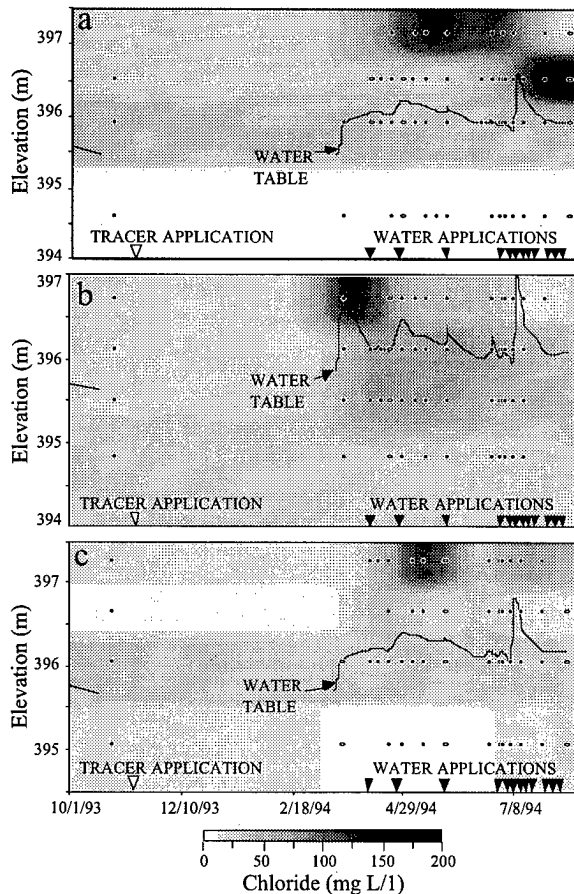
Figure 4. Chloride concentration and water table elevation at E7.2 (a), E7.6 (b), and E7.8 (c).

Figure 4a is the time series contour for chloride concentration at E7.2. As indicated by the plot, chloride tracer was transported to the top solution sampler (0.3 m) early in the year and then was moved to the 0.9 m depth following a 12-cm rainfall event in early July, 1994. No chloride fluctuations were observed deeper than 0.9 m or in the ground water at any time during the study at E7.2. This site does not exhibit focused recharge solute transport characteristics, as is indicated by the lack of chloride movement during the period of spring thaw.

The time series chloride data for E7.6 are shown in Fig. 4b. The chloride at E7.6 is seen to move rapidly to 0.3 m, the water table at the time, and then appears to dissipate to deeper into the ground water as time progresses. The initial rapid transport of

chloride corresponded to the spring thaw, when snowmelt accumulations are infiltrating at the bottom of the small depression. The large rainfall event in July did not result in an increase in chloride at the 0.3 m sampler. This would indicate that the majority of the applied tracer had already been moved past that depth. The close proximity of the water table to the soil surface in the depression is also a major factor in the rapid movement of chloride to the ground water.

Chloride at E7.8 is seen to move only to the 0.3-m depth midway through the study. Another increase in chloride is observed in July (Fig. 4c). These data suggest that the majority of the tracer chloride was moved past 0.3 m by Darcian flow and remained between the 0.3 and 0.9 m for the duration of the study. The intense rainfall then moved remaining chloride in a second pulse.

The collection and subsequent infiltration of snowmelt is the main factor influencing the travel time of surface applied chloride to greater depths. As sites E7.2 and E7.8 are on the sides or near the ridge of the depression, they receive less water for recharge than E7.6 which is at the bottom of the depression. In the bottom of the depression, the tracer is seen to move rapidly to the shallow ground water while on the ridges, the tracer remains near the surface. Only after several months and an extremely large rainfall event does some tracer move to an intermediate depth on one of the ridges.
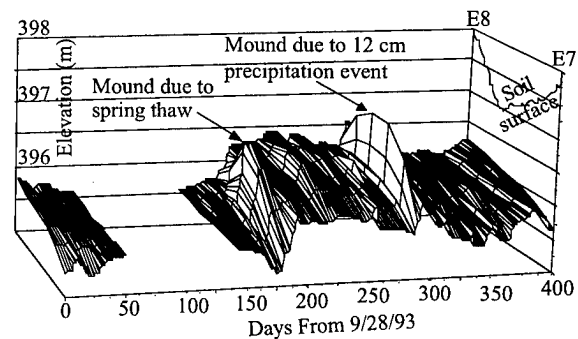
Figure 5. Water table elevations at E transect recharge site.

Water table elevation

Water table elevations were measured at each shallow well in the E transect recharge site when water samples were collected. The water table elevation relative to the soil surface is indicated in Fig. 5 for all wells, E7 through E8. The ground surface elevation line has been imposed on the vertical axis. A dramatic rise in water table was measured after the spring thaw of 1994. This mound

117

was caused by the infiltration of ponded water, which had collected in the depression as the snow melted but the underlying soil remained frozen. The water table was also very responsive to rainfall and irrigation events for all sites, especially at E7.6. In all instances, a ground water mound was formed under the depression at E7.6 after a water application. In a matter of days, the mound would recede, resulting in an increase in water table elevation in the adjacent wells.

The most dramatic indication of ground water recharge is seen after a 12-cm rainfall event in early July 1994. After this event, the water table rose to the soil surface in the depression at E7.6. The resulting mound caused dramatic increases in water table elevation in the adjacent wells also.
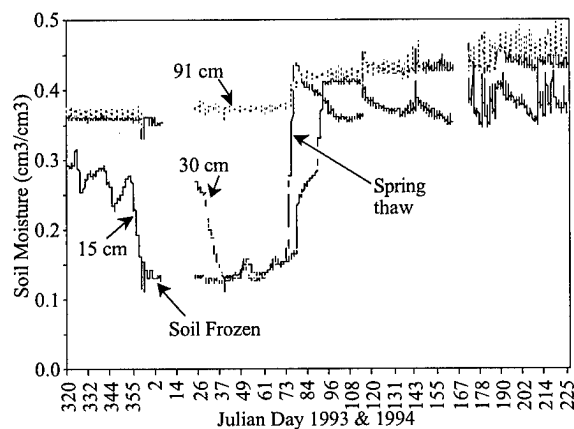
Figure 6. Soil moisture at E transect recharge site.

Soil moisture

Figure 6 is a plot of soil moisture at 15, 30, and 91 cm at E7.6. As TDR measures only liquid water and not frozen water, the plot can be used to determine if the soil is frozen or thawed. The time at which the soil thaws in the spring of 1994 is very evident by the sharp increase in liquid soil water. This trend is seen at both the 15- and 30-cm depths. The peak corresponds temporally to the formation of the ground water mound observed in the spring and with the rapid movement of applied chloride to the ground water at E7.6. Water applications are also evident throughout the season and are indicated by the smaller peaks in soil moisture.

The soil moisture measured at 91 cm does not fluctuate significantly throughout the season. This wave guide was very near the water table or in the ground water for the duration of the study and hence measured few changes in volumetric soil water.

Soil temperature

A plot of soil temperatures at 15, 30, and 122 cm at E7.6 is included in Fig. 7. Soil temperatures indicate the time at which the soil thawed in 1994. The temperature at 15 cm increased above 0°C on Julian day 76, 1994. This corresponds to the increase in liquid soil moisture on the same day as discussed above and is another indication of when the water ponded over the previously frozen soil rapidly infiltrated in the depression focused recharge event.
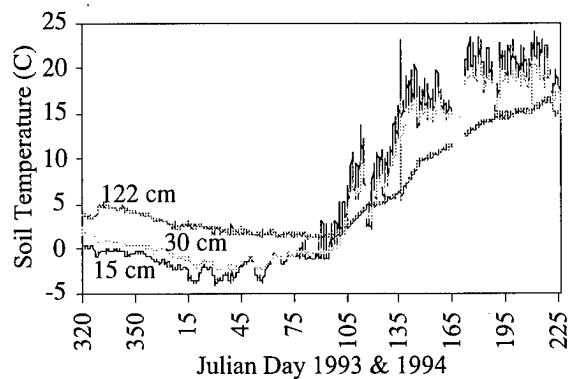
Figure 7. Soil temperature at bottom of depression.

Subsurface drain recharge sites

Chloride concentration in the drain effluent has been monitored approximately monthly since 1990. An average background concentration of approximately 9 mg Cl⁻ L⁻¹ had been measured at both access manholes prior to this experiment. The subsurface drain under the level or upland tracer plot sampled at access manhole T03 showed a slight increase in effluent chloride in April 1994 (Fig. 8a). The slight increase in chloride can be seen near the end of April with no other significant chloride peaks occurring throughout the remainder of the study period. Figure 8a also indicates that the increase in chloride concentration follows the same trend as the increase in drainage flow rate.

The results from the depressional site differ from the T03 site in that a large chloride spike was observed in the spring of 1994 in mid April. The T04 drain data for the study period is included in Fig. 8b. This shows that the chloride spike occurs after the spring thaw when the drain flow rates increase from ground water recharge. This also corresponds to the time period when the liquid soil water and the soil temperature increased at the solution sampler depression site. The increase in flow rate at this depressional site is much greater than the

flow increase measured at the level drain site. This indicates that the water collected in the depression, where the tracer chloride was applied, is contributing a great deal to the increased flow of that subsurface drain.
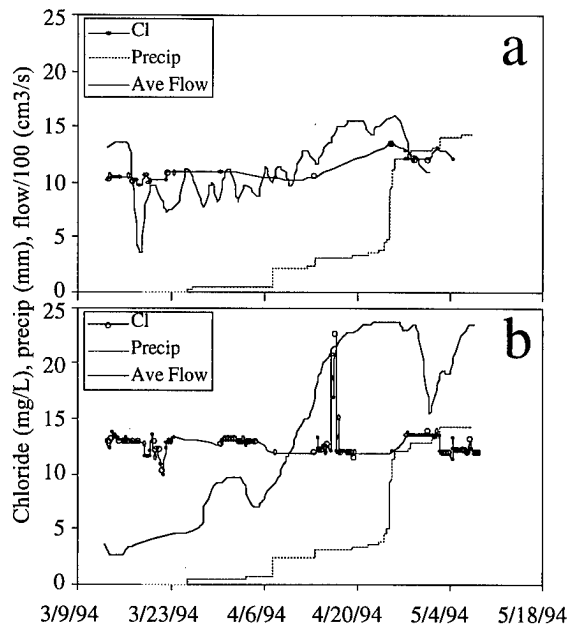
Figure 8. Drain flow, chloride concentration, and cumulative precipitation at a) T03 and b) T04.

The amount of chloride moved during the 24 h period when the spike was observed was calculated by subtracting the average background concentration of 9 mg L^{-1} from the measured concentrations and using the corresponding flow data. We calculated that 1.94 kg of chloride was moved in the 24 h period, accounting for 9.2 percent of the 21 kg of chloride applied on the plot. Although this is a relatively small amount of the total applied tracer, it is important to note that the depression was responsible for focusing the recharge in this area. In situations where a small amount of material is considered to be hazardous in ground water, this process becomes even more important.

CONCLUSIONS

Prior research has indicated that ground water recharge occurs at the topographically high areas on the landscape and the depressional areas are normally considered discharge sites. This research project has indicated that, at times, recharge is focused at the topographic depressions. Immediately following

spring thaw, when snowmelt previously ponded over frozen soil suddenly infiltrates, surface applied chemicals can be moved rapidly to shallow ground water. Also, in periods of intense rainfall, solutes in the upper soil layers can be transported to the ground water.

This study has demonstrated that a surface applied mobile tracer material leaches to the ground water much more rapidly under topographic lows than on higher or level portions of the field. Findings of this nature are important in that certain areas of a field can be designated as potential hot spots for ground water contamination. These areas can be integrated into a site-specific management plan and chemical applications can be altered accordingly.

REFERENCES

Amoozgar, A. 1992. Advances in measurement of soil physical properties: Bringing theory into practice. SSSA Special Publication no. 30.

Delin, G.N. and M.K. Landon. 1993. Effects of focused recharge on the transport of agricultural chemicals at the Princeton, MN Management Systems Evaluation Area, 1991-1992. U.S. Geological Survey open-file report 93-42.

Freeze, R.A. and J. Banner. 1970. The mechanism of natural ground water recharge and discharge: 2. Laboratory column experiments and field measurements. Wat. Resour. Res. 6:138-155.

Kladivko, E.J, G.E. van Scoyoc, E.J. Monke, K.M. Oates, and W. Pask. 1991. Pesticide and nutrient movement into subsurface tile drains on a silt loam soil in Indiana. J. Environ. Qual. 20:264-270.

Knuteson, J.A., J.L. Richardson, D.D. Patterson, and L. Prunty. 1989. Pedogenic carbonates in a calciaquoll associated with a recharge wetland. Soil Sci. Soc. Am. J. 53:495-499.

Lissey, A. 1971. Depression-focused transient ground water flow patterns in Manitoba. Geol. Assoc. Can. Spec. Pap. 9:333-341.

Schuh, W.M. and D.L. Klinkebiel. 1994. A study of water and contaminant movement to the Carrington aquifer. *In* Proceedings of North Dakota Water Quality Symposium, March 30-31, 1994. Fargo, North Dakota.

Steele, D.D, E.C. Stegman, L.D. Prunty, and R.E. Knighton. 1992. Overview of a field study of best management practices for improved irrigation and fertilizer use efficiencies. *In* Proceedings of North Dakota Water Quality Symposium, March 25-26, 1992. Bismarck, North Dakota.

Land-Slide Induced Changes in the
Chemical Composion of Active-Layer Soils and
Surface-Water Runoff, Yamal Peninsula, Russia

M.O. LEIBMAN[1] AND I.D. STRELETSKAYA[1]

ABSTRACT

Saline marine deposits are widely distributed at Yamal Peninsula. Slope processes such as active-layer detachments and retrogressive thaw slumps are characteristic of Central Yamal. They produce specific impact on chemical composition of the surface and underground (active layer) runoff. Removed matter as well as exposed surface are subjected to washing out of water-soluble salts and insoluble particles. Upper permafrost: ice-bonded deposits or massive ground are exposed to seasonal thaw and washed by surface and active-layer water. Depending on the ice type, different elements and ions get into the runoff and drainage system. The impact of water-soluble salt redistribution within the newly formed active layer on the active-layer runoff is considered as well. Peaks of concentration correlate with the peaks of active-layer detachment activity.

Key words: Permafrost, active layer, runoff, chemical composition, substance transfer.

INTRODUCTION

The process of the substance redistribution in permafrost areas differs from that outside permafrost areas and depends on the depth of seasonally thawed layer, rate of thaw and cycles and intensity of the surface denudation. The chemical elements distribution in the active layer and uppermost permafrost slope deposits has been discussed (Leibman and others 1993; Leibman 1996).

It seems obvious that active-layer soils are less saline compared with upper permafrost due to washing that lasted thousands of years. But active natural periglacial processes on slopes (active-layer detachments and retrogressive thaw slumps), as well as thermoerosion, characteristic of the area under investigation expose and subject to destruction upper permafrost layers. These layers bear more water-soluble salts, micro-elements, heavy metals and lenses of cryopegs than the removed cover deposits contain. Permafrost table may be exposed by human activity as well. Thus substance from permafrost gets into the active-layer water on both undisturbed and post-disturbed areas and changes the chemical composition of the surface water recharged from the surface and subsurface runoff. The authors suggest that the natural disturbances such as the landslides and natural substances such as water-soluble salts can serve as a reference pattern for (a) substance transfer affected by man-made active-layer detachments and removals, and for (b) artificial contributions into the chemical composition of the removed matter. That is why study of natural chemical distribution pattern can be used in future for study of pollutants transfer.

Thus, recent landslides in Central Yamal Peninsula near the Se-Yakha river (Fig. 1) were considered an additional source of substance in the runoff. Some aspects of the interrelations between the landslides, the active-layer chemical composition and the surface and subsurface runoff are discussed. The pattern suggested is: ground ice - pore solutions - active layer runoff - surface runoff - surface water.

METHODS

Tested was massive ground ice that is usually exposed by slumps, segregated ice lenses that are melting after the active layer detachments, and pore solutions from the newly formed active layer out of

the landslide and at the slip surface. For the ground ice, element and ionic concentration was measured in melted water and is presented in milligrams per liter of water. For pore solutions, ionic concentration in water extraction taken from dries soil samples was determined and shown in grams per 100 grams of soil (or in %). Concentration of elements was not determined in pore solutions due to technical problems.

Conventional methods briefly described in (Leibman 1996) were used to determine the chemical composition of pore water (ice) and ground ice.
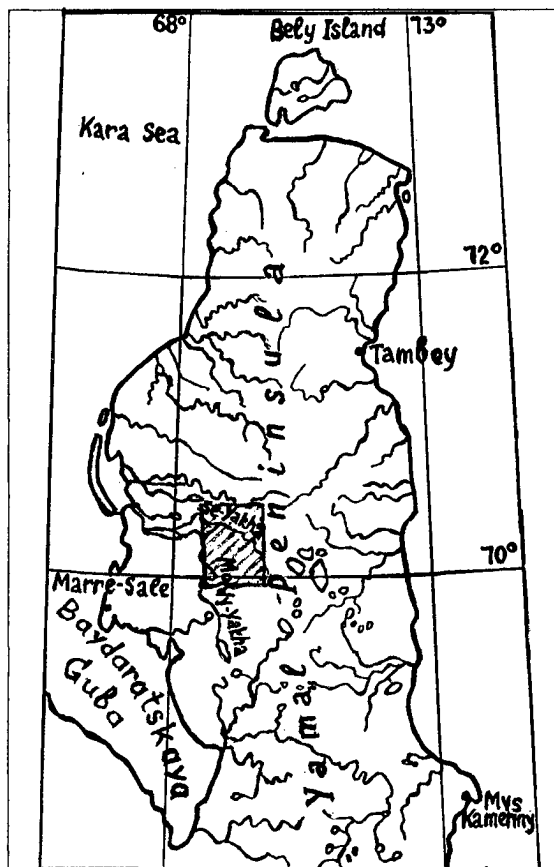
Figure 1. Study area and sampling locations

RESULTS AND DISCUSSION

Ionic distribution in different types of ground ice, and within the active layer and upper permafrost

We have subdivided and considered two types of slope processes, of those affecting chemical elements migration in the active layer and on the surface.

The first type: slumps slipping along the surface of massive near-surface ground-ice sheets. Several peculiar features are important in this discussion. The period between peaks of activation coveres several years (Leibman and others 1997). About 20-30% of the slopes in the study area to the north of Se-Yakha river (Fig. 1) are disturbed by these slumps. Slumps expose massive ground ice, subjecting it to thaw. This ice contains such elements as Fe, Mn, Al, Si, Cu, Co, P, Cd . Total ions concentration is up to 176 mg/L (Table 1). Melting massive ice adds these elements into the surface runoff and finally into the drainage network.

The second type involves landslides that remove fresh active-layer deposits and expose saline perennially frozen clay with segregated ice lenses. The period between peaks of activation lasts for, probably, hundreds of years (Leibman and others 1997). Segregated ice lenses contain up to 226 mg/L of water-soluble salts and up to 193 mg/L of iron, which is very high for ice. (Table 1). The specific composition of runoff is formed also as a result of ground water filtration through the newly formed active layer exposed by active layer detachments on slopes. It was pointed out by Trofimov and Galliulin (1989), that concentration in the samples of active-layer water in the discharge zone was up to 32 g/L, with the average out of 14 samples of about 12,7 g/L, Na and Cl prevailing in their tests).

Ionic migration within the active layer was investigated in this study as well. Three bore-holes were cored on a landslide slope: borehole #1 on the undisturbed slope out of the slide, #2 within the zone of post-slide accumulation (dampish site), and #3 within the zone of active erosion (drained and eroding site) (Fig. 2). Total concentration and ion composition of samples taken layer by layer was determined; in bore-hole #1 - starting with 70 cm depth, that correlates with 0.0 cm depth of bore-holes #2 and #3 (Fig. 2). The 70 cm depth in the bore-hole #1 is set equal to zero on Figures 3-10.

Analysis of the ion composition in the three cores showed changes in ionic distribution in the active layer and upper permafrost during the 5 annual cycles of freeze-thaw: since 1989 when the permafrost table was exposed and subjected to seasonal freeze-thaw to 1993 when it was sampled. In the undisturbed site (Fig. 3, bore-hole #1) the total amount of soluble salts (determined as dry residue after evaporation of solution in mg/L) increases with depth. In the shearing surface the total content of salts in the newly formed active layer exceeds that in the active layer of the undisturbed site and on the whole decreases with depth (Fig. 3, boreholes #2, 3).

121

Salt concentration in the uppermost permafrost below the depth of 90 cm is the same in both undisturbed and exposd areas and is about 1%. This may indicate the similar salt distribution on both out of slide and landslide-affected slopes before the sliding took place.

Total salt content in the active layer under the shearing surface depends on the drainage. At the dampish site, two horizons of accumulation of the water-soluble salts are subdivided. The upper, near-surface one is probably formed due to the washing into it of the active-layer water, seeping from the landslide scarp. The lower horizon of accumulation at the depths of 40 cm is due to the squeezing of the salts under the seasonal freezing of water-saturated active layer (Fig. 3, borehole #2). Increased ions concentration in this layer in winter may be found even in the normally fresh deposits (Anisimova 1981).

At the drained site, there is one distinct horizon of accumulation and two horizons of washing out (Fig. 3, borehole #3). Salt concentration in the horizon of accumulation is about 1.5% at a depth of 20-30 cm and may result from evaporation and moving of salts through capillaries towards the surface. From the uppermost, 5-10 cm deep, horizon salts are washed out by rain and melted water. The lowermost horizon at the active layer base looses salts by the lateral filtration of the active-layer water through the zone of post-cryogenic cracks, inheriting the cryogenic structure of the frozen (in winter) active layer. Here the rate of filtration may be very high (Leibman and others 1993). At the same time, high concentration below the active-layer base at the drained site may be due to migration of salts towards the freezing front and fixing of the salts in the permafrost zone (Chistotinov 1973).

The most mobile Cl ion is the first to be washed out of the active layer, and its content in the active-layer deposits compared with the uppermost permafrost, is greatly reduced. At the same time, some of the Cl ions are drawn up to the drained surface by evaporation and redistributed by the surface runoff to the dampish sites (Fig. 4).

Table 1. Elements and ions content in various types of ground ice in Central Yamal

Type of ground ice	Concentration range for elements and ions, mg/L; maximum and minimum out of:		
	8 samples	5 samples	3 samples
	Vitreous massive	Muddy massive	Segregated
Elements			
Ca	0.22-2.49	0.74-14.4	0.9-40.6
Mg	0.26-6.49	1.34-83.4	0.33
Fe	1.18-23.7	11.8-383.0	0.20-193.0
Mn	<0.1-1.13	0.08-5.08	0.11-1.60
Al	0.52-23.6	5.70-365.0	0.85-13.8
Si	2.16-49.6	15.5-197.0	5.92-6.06
K	<0.05-3.0	1.2-52.5	1.0-30.0
Na	2.0-19.0	2.8-26.5.	3.0-36.5
Cu	<0.01-0.04	0.04-0.28	<0.01-0.1
Cd	<0.01	0.02-0.14	<0.01-0.08
Co	0.01	0.01-0.11	0.04-0.21
P	<0.10-0.58	0.52-2.88	0.10-5.57
Sr	0.01-0.04	0.04-0.28	0.20-0.96
Cations and anions			
HCO_3^-	12.2-25.6	45.2-104.0	0.0
SO_4^{2-}	3.3-31.3	13.2-23.9	125.0
Cl^-	4.9-53.4	12.8-17.0	29.8
Ca_2^+	0.8-6.0	5.6-30.1	44.9
Mg_2^+	0.5-4.9	4.9-9.1	11.4
K^++Na^+	6.4-29.0	5.1-21.2	6.2
Dry residue (evaporated out of 1 liter of water)	26-116	80-176	226
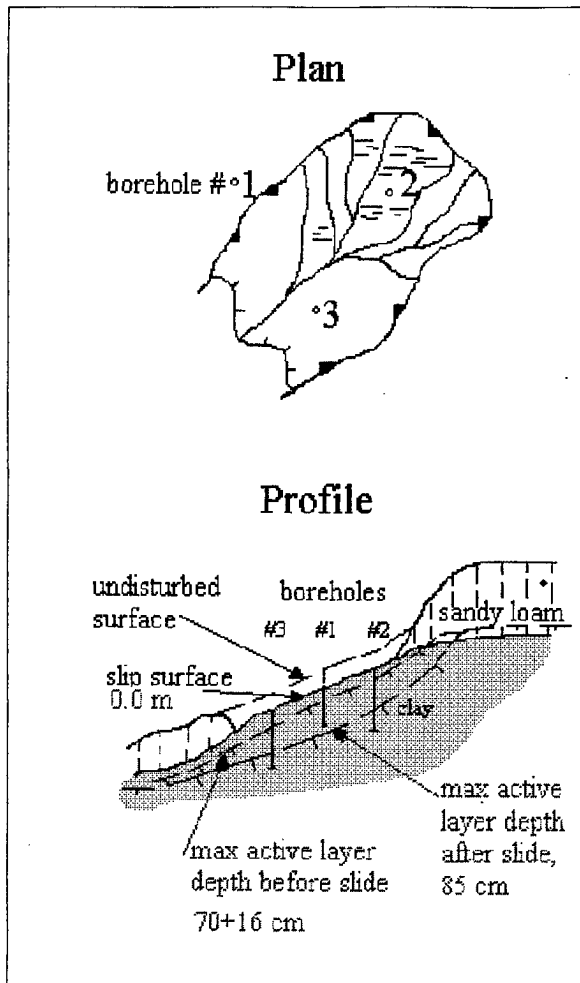
Figure 2. Borehole location in plan and profile: borehole #1, not in slide; bore-hole #2, concave, dampish site; borehole #3, convex, drained site.

SO₄ ion content in the active layer of the shearing surface (Fig. 5) is higher than at the undisturbed site: having been brought into the thaw zone, former permafrost was subjected to the temperature above zero which activated the biochemical and exchange processes, supplying the pore solution with Na_2SO_4. At the dampish site the SO_4 ion concentration process is active only near the active-layer base.

HCO_3 ion in the active layer of the shearing surface is more highly concentrated than that at the undisturbed site (Fig. 6). Ions concentrate mainly at the depths of 10-30 cm and decrease downward.

The distribution of cations after 5 annual cycles of freeze-thaw is as follows (Figs. 7-10):
(a) K-ion accumulates in the upper portion of the profile at the drained site, being drawn up to the drained surface by evaporation. The dampish site shows the same trend, but to a less degree (Fig. 7).
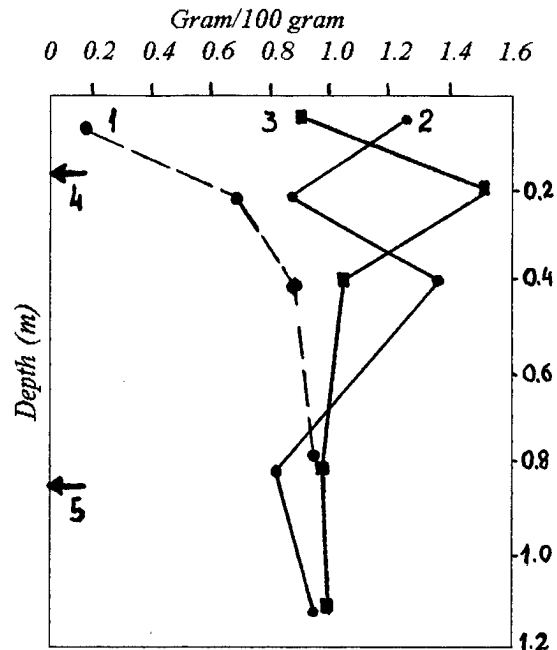
Figure 3. Distribution of dry residue in the profile: 1,2,3, bore-hole numbers; 4, maximum active layer depth before detachment (86-70=16 cm), 5, maximum active layer depth after detachment.
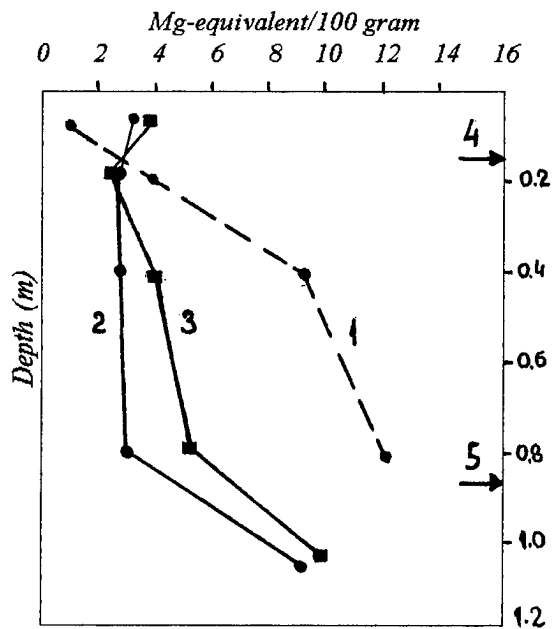
Figure 4. Distribution of Cl ion in the profile, 1-5 as on fig. 3.

(b) Na ion concentration decreases by a factor of 2 at the active layer bottom at the dampish site, compared with the undisturbed site, and is slightly lower at the drained site due to ion's mobility and active washing

123
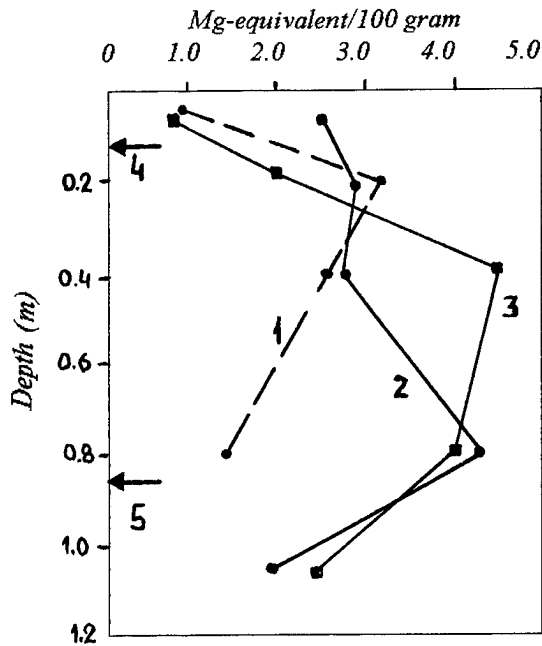
Figure 5. Distribution of SO₄ ion in the profile: 1-5 as on fig. 3.
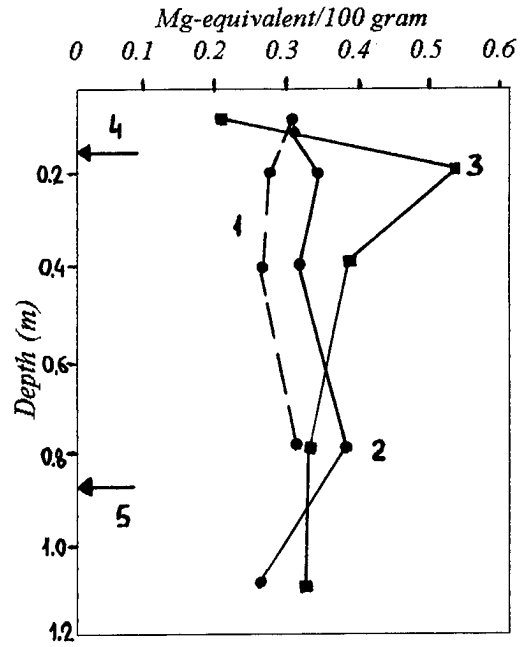
Figure 7. Distribution of K ion in the profile: 1-5 as on fig. 3.
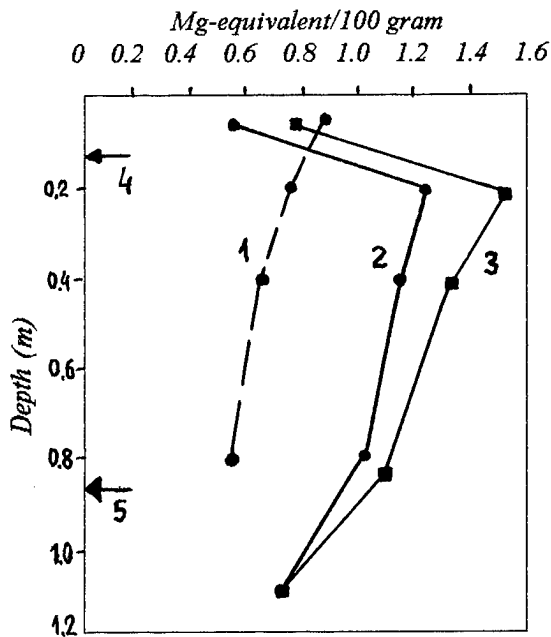
Figure 6. Distribution of HCO₃ ion in the profile: 1-5 as on fig. 3.

out through the post-cryogenic cracks in the active layer (Leibman and others 1993). Near the surface where post-cryogenic structure is not distinguished, the difference between Na concentration at the three sites decreases. And at the surface, Na concentration

at the undisturbed site is the lowest, as it was washed over a much longer period of time (Fig. 8).

(c) Redistribution of Ca ion into two zones of accumulation, with higher concentration at the active-layer base, is characteristic of the dampish site with the pattern similar to that for K ion but with a higher amplitude of concentration change. This may show the difference in Ca and K ions mobility in relation to suction towards both the surface and the freezing front. At the same time, the drained site is characterized by the reduction of Ca ion concentration downwards by suction. Higher total Ca ion at the dampish site may also be attributed to the more active biological processes (Fig. 9).

(d) Mg ion distribution is close to that of Ca ion but is characterized by only one zone of accumulation at the dampish site: near the surface. Still, it is much higher at the active-layer base, compared with the drained and undisturbed sites (Fig. 10).

Runoff composition

Distribution of ions described in the previous section influences the chemical composition of the surface water. Testing of the Se-Yakha river water, both chemical composition and suspended solids on Yamal Peninsula (Concern PROMECOLOGIA) from 1988 to 1991 showed the peak of concentration in

124
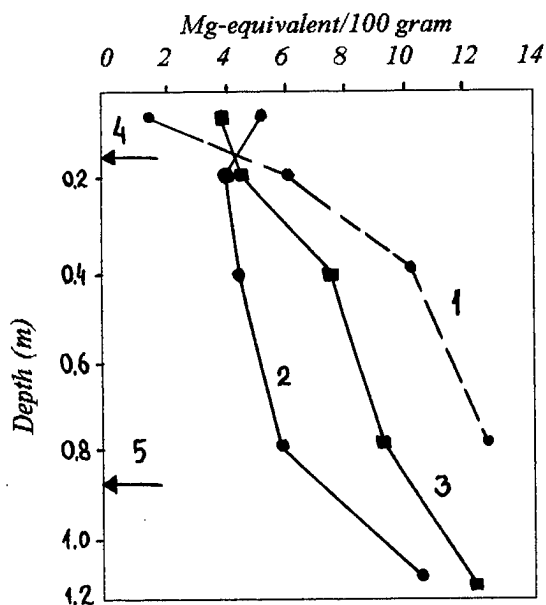
Figure 8. Distribution of Na ion in the profile: 1-5 as on fig. 3.
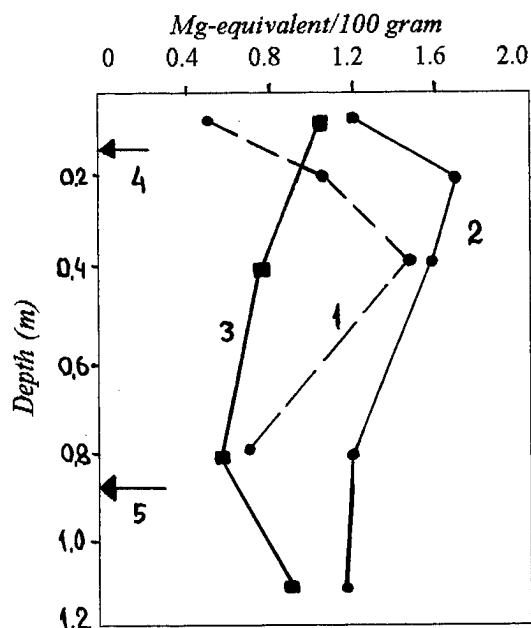
Figure 9. Distribution of Ca ion in the profile: 1-5 as on fig. 3.

1990. This abrupt rise is, most likely, due to landslide activity in mid-August, 1989 (Leibman 1995).

Maximum values of total water ions concentration were noted in 1990 and were 210 mg/L (Fig. 11). At the same time suspended solids concentration was maximum, due to erosion of the exposed landslide scars and landslide masses that

moved into the ravines and streams. As the 1989 sampling was undertaken before the landslide period, the peak was noted only the next year. Concentration of water-soluble salts in 1990 was
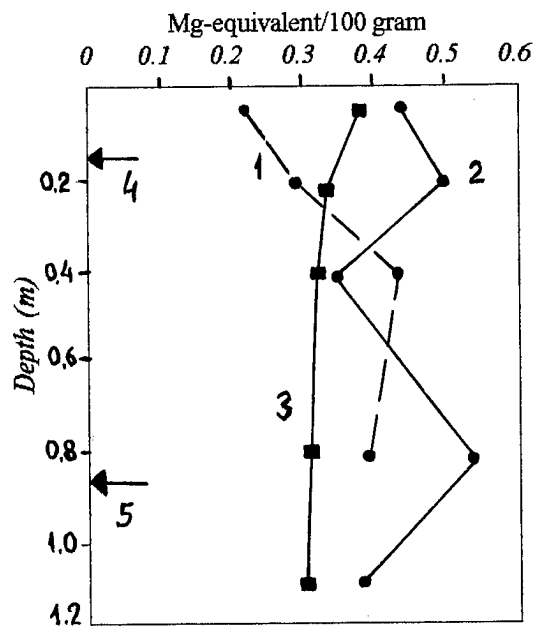
Figure 10. Distribution of Mg ion in the profile: 1-5 as on fig. 3.

almost 5 times higher, compared with 1989 before the landslide period (Fig. 11). In 1991 the total ions concentration of the river water decreased but still was higher than that before the landslide period (tests of 1988-1989, Fig. 11).

The ion composition changed as follows: the peak ions concentration of 1990 coincides with the maximum concentration of the HCO_3 ion and (Na+K) ions, whereas concentrations of Cl and SO_4 ions in 1991 were higher than in 198901990 (Fig. 11). This may be explained by the washing out of the deeper horizons: the next year the uppermost permafrost (the most saline portion of the profile) was involved in the seasonal thaw, and started to be washed out.

Though there was no testing of the micro-elements or heavy metals in the river water, we can assume that there is the influence of the melted massive ice, with its specific chemical composition, on the river run-off. It is known (Leibman and others 1997), that slumps occur more regularly than active-layer detachment slides, so the difference in the chemical composition of runoff due to the massive ground ice melting from year to year should be less expressed. Still, the chemical composition of the river

water accounting for the elements shown in Table 1 should be different, compared with rivers that have no input from slumpy slopes.

CONCLUSIONS

1. Bringing to the surface the active layer base and the uppermost layers of permafrost by the natural climatic activation of slope processes, and by excavations and constructioi'n of embankments from the active layer deposits, is an essential factor in the distribution of water-soluble salts and micro-elements throughout the Western Yamal.
2. Hydrochemical condition of the active layer is controlled, along with the composition of air precipitation and ground pore solutions, by the repetitiveness of periods of the landslide activity.
3. The surface run-off carries water-soluble salts and suspended solids from the exposed active-layer base in the watersheds to deposit them in the flood plain soils and water basins temporally changing the "background" concentrations.
4. The next year after the period of profound landslide activity shows high peaks of concen[the surface water.
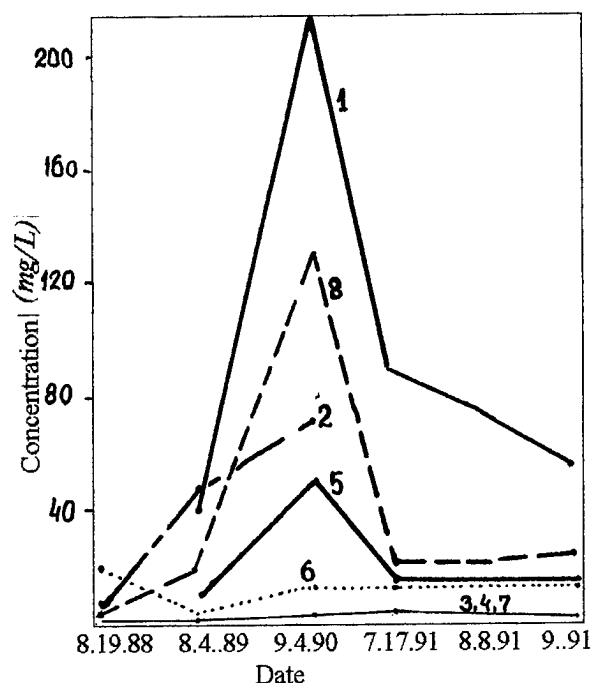
Figure 11. Concentration of ions and suspended solids in Se-Yakha River water, 1988-1991. 1, ions sum; 2, suspended solids. 3, Ca, 4, Mg, 5, Na+K, 6, Cl, 7, SO₄, 8, HCO₃.

REFERENCES

1. Anisimova, N.P. 1981. Cryohydrochemical peculiarities of the frozen zone. (In Russian.) Nauka Publisher, Novosibirsk.
2. Chistotinov, L.V. 1973. Moisture migration in freezing nonsaturated ground. (In Russian.) Nauka Publisher, Moscow.
3. Leibman, M.O. 1995. Cryogenic landslides on the Yamal Peninsula, Russia: Preliminary observations. Permafrost and Periglacial Processes 6: 259-264. John Wiley and Sons Ltd., London.
4. Leibman, M.O. 1996. Results of chemical testing for various types of water and ice, Yamal Peninsula, Russia. Permafrost and Periglacial Processes 7: 287-296. John Wiley and Sons Ltd., London.
5. Leibman, M.O., F.M. Rivkin, I.D. Streletskaya. 1993. Chemical and physical features of the active layer as related to the landslides on Yamal Peninsula. p. 257-262. *In* Joint Russian-American Seminar on Gryopedology and Global Change. Post-Seminar proc. November 15-16, 1993, Pushchino.
6. Leibman, M.O., I.D. Streletskaya, M.A. Konyakhin. 1997. Assessment of the surface dynamics of the Bovanenkovo gas field (Central Yamal) in 1949-1990. (In Russian.) Geomorphology 2:00-00. Moscow (in press)
7. Trofimov, A.V., V.M. Galliulin. 1989. Formation of the Central Yamal water chemical composition in relation to the water supply of gas production plants. (In Russian.) p.35-39. *In* Rational nature usage under the development of oil-condensate deposits of West Siberia. Trans. of scientific information. Tyumengastechnology press, Tyumen.

126

Solute Movement in the
Active Layer, Taymyr, Siberia

J. BOIKE[1], W.K.P. VAN LOON[2], P.P. OVERDUIN[3], AND H.W. HUBBERTEN [1]

ABSTRACT

Time domain reflectometry (TDR) has been used extensively for determining the dielectric constant and water content of soils, and relationships for measuring soil water conductivity are being developed. The technique is particularly well-suited to use in the Arctic, where in situ and potentially remote methods are important. The objective of this study is to evaluate TDR as a field technique for bulk electrical conductivity σ_b and soil water electrical conductivity σ_w in arctic soils. Calibration measurements of σ_b were carried out at a field site in Siberia (74° 32'14''N; 98° 35'52''E). TDR-determined σ_w using the model of van Loon et al. (1991) is compared to electrical conductivity σ_w of solution obtained with suction cups. Best results are obtained when using a probe specific calculated soil electrical conductivity σ_s, rather than one value for this soil type. This is thought to be a reflection of soil coarseness and heterogeneity. Data of σ_w obtained for this field site are reported for one field site in Siberia from spring to fall 1995. Infiltration into the frozen soil in spring and exclusion of solutes during fall freeze-back were observed using TDR.

Key words: Siberia, active layer, time domain reflectometry, bulk electrical conductivity, solute exclusion

INTRODUCTION

Understanding the processes of solute and water migration in frozen ground and during phase changes (thawing and freezing) has become a major challenge and resulted in the development of new techniques. Adequate in situ methods for determining soil water electrical conductivity (σ_w) for arctic field applications are still being developed. One method for measuring the temporal evolution of solute concentrations at specific depths is the use of suction cups. Its major disadvantages are the unknown, but potentially large measuring volume and failure in frozen ground.

Time domain reflectometry (TDR) has become widely used for in situ determination of soil volumetric water content (θ) and bulk electrical conductivity (σ_b). Whereas the determination of θ has been widely applied (Patterson and Smith 1980; Stein and Kane 1983; Roth et al. 1990), the use of TDR determined σ_b for the calculation of σ_w in frozen and unfrozen ground is still under discussion. Although a number of theoretical and empirical methods have been proposed (Mualem and Friedman 1991; Rhoades et al. 1989), no simple relationship between σ_w and σ_b is applicable to all soils. In addition, arctic field soils are often very coarsely structured (regolithic) and can exhibit a heterogeneous texture. They have a high mineral or high organic matter content and are subjected to a seasonal thawing and freezing cycle possibly damaging or deforming instruments. Moreover, controlled laboratory experiments and field data often appear to be inconsistent. For example, Heimovaara et al. (1995) report that the same soil studied in the field under natural conditions and in laboratory experiments through the addition of salt gave different relationships between σ_w and σ_b. To parameterize this relationship in a way useful for field use, it thus seems necessary to collect data for calibration via in situ instruments in the field.

Dynamics of solutes during freezing and thawing from a field site in northern Sweden (north of Uppsala) were reported by Lundin and Johnsson (1994). They applied the quasi theoretical model for frozen soils by van Loon et al. (1991) to calculate solute concentrations in frozen soils from TDR determined σ_b. Our objective is to evaluate the use of TDR as a method for in situ field measurements of σ_b using the model of van Loon et al. (1991) within the context of results from an arctic soil type in Siberia.

BULK SOIL ELECTRICAL CONDUCTIVITY

The amplitude of the TDR signal at very long times can be used to determine σ_b (Heimovaara et al. 1995), which is a compound of σ_w and soil

[1] Alfred-Wegener Institute for Polar and Marine Research, Telegrafenberg A 43, 14473 Potsdam, Germany
[2] Department of Agricultural Engineering and Physics, AGROTECHNION, University of Wageningen, Bomenweg 4, 6703 HD Wageningen, The Netherlands
[3] Department of Geography, York University, 4700 Keele Street, North York, Ontario, M3J 1P3, Canada

surface electrical conductivity σ_S. For calculation of σ_b, calibration of triple-wire probes and the TDR system were carried out with a range of solutions with known electrical conductivities following the method of Heimovaara et al. (1995). The value of σ_b was corrected for the temperature dependence of the water viscosity v (van Loon et al. 1991):

$$\sigma_b[T] = \sigma_b[25]v[T] \approx$$
$$\sigma_b[25][0.588 + 0.0193\,T + 0.00014T^2] \quad [1]$$

where T is temperature in [°C].

Van Loon et al. (1991) developed the following theoretical model for σ_b between unfrozen water content θ_u, saturated water content θ_{sat}, electrical conductivity of the liquid phase σ_w and soil surface conductivity σ_s:

$$\sigma_b = \sigma_s(1 + 3\theta) + \frac{(2 - \theta)\theta^2}{(2 - \theta_{sat})\theta_{sat}}\sigma_w \quad [2]$$

The coefficients σ_w and σ_s are determined through multiregression analysis and were shown to be highly significant for the frozen soil-water system studied in the laboratory columns.

STUDY SITE AND METHODS

This paper reports results from field work carried out in 1994 and 1995 in the Levinson-Lessing catchment, Taymyr Peninsula, Siberia, the northernmost continental area of the circumpolar Arctic (74°26.3'N, 98°46.4'E). This study uses data collected from a single site ('2x') which is located midway up on a calcareous, south west-facing slope with low inclination (7°). It is classified as loamy skeletal carbonatic calcareous Pergelic Cryorthent. Soil grain size characteristics of one bulk sample are given in Table 1.
Solifluction lobes and soil stripes indicate active cryogenic processes. Vegetation covers less than 5 % and is dominated by patches of *Dryas octopetala* and *Salix spec.*

During the summer of 1994, soil pits were excavated to the depth where frozen ground was encountered. At each site, triple wire TDR probes, PT 100 temperature probes, wells, piezometers and suction cups (5 cm long, pore size 2 μm; Gravquick) were installed. The TDR probes used in this study consist of three parallel steel rods (0.5 cm diam., 25 cm long, 3 cm spaced apart), connected to a 50 Ω coaxial cable and held in place by an epoxy resin (Heimovaara 1993). TDR waveforms were recorded in the field using a Tektronix 1502 B cable tester, a portable laptop and the program of Heimovaara and de Water (1993). Volumetric water content θ in unfrozen soils was calculated from the dielectric constant ε using the composite approach of Roth et al. (1990) and in frozen soils using the formula of Smith and Tice (1988). Although Spans and Baker (1995) found that their independent calibration of TDR in frozen soils deviated from the formula of Smith and Tice (1988) we used the latter formula since no calibration for this soil was undertaken.

RESULTS AND DISCUSSION

Relationship between σ_b and σ_w at site '2x'

The σ_b is a function of σ_s and σ_w, therefore reflecting the heterogeneity of the soil matrix (differences in θ, σ_s and soil geometry). This relationship is not easily defined, as demonstrated in Figure 1 where TDR measured values of σ_b are
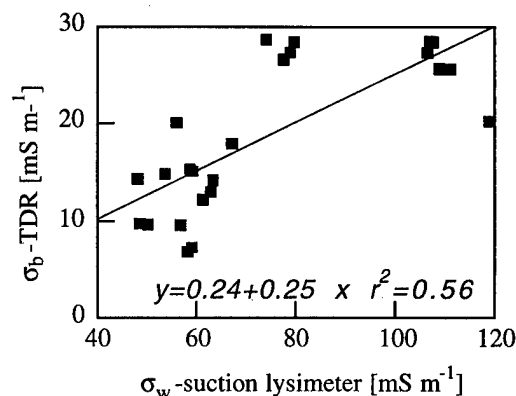
Figure 1. Comparison of σ_b calculated from TDR measurements with σ_w from suction lysimeters.

Table 1. Soil characteristics of site '2x'.

Bulk density [kg m⁻³]	Porosity [m³ m⁻³]	Saturated hydraulic conductivity [cm s⁻¹]	Grain size [% weight]			
			>2 mm	Sand	Silt	Clay
1.69·10³	0.34-0.42	7.9·10⁻⁶ (at 73 cm depth)	44	36.2	17.8	2
		3.0·10⁻⁴ (at 37 cm depth)				

Table 2. Values of σ_S estimated for model [2] for site '2x'. Parameter obtained by simultaneously fitting all data obtained from this site are marked "all sites" in the first column. The number of data points in each set is n.

probe depth [cm]	1 σ_S determined by multiregression analysis			2 σ_S calculated using equation [2] and suction lysimeter data as σ_w	
	σ_S [$\mu S\ cm^{-1}$]	r^2	n	average σ_S [$\mu S\ cm^{-1}$]	n
11	51 (51)	0.4 (0.65)	40 (34)*	n.a.	n.a.
23	26	0.72	39	-24	7
34	34	0.74	42	-28	6
47	-1	0.92	39	-21	4
52	-14	0.84	38	-55	2
65	22	0.96	43	-58	4
78	13	0.99	43	n.a.	n.a.
all sites	23 (22)	0.61 (0.61)	284 (278)*	-33	23

* when 6 outliners are taken out

compared to values of σ_w from suction cup solutions. The nonlinearity of these two parameters was also demonstrated by Dasberg and Dalton (1985).

As a next step, we investigated the importance of σ_S for defining σ_b. Values of σ_S were determined in two different ways: 1) through multiregression analysis following the model of van Loon et al. (1991) and 2) using the soil suction lysimeter data as σ_w in [2] and calculating σ_S as the unknown variable. These calculations were undertaken for each probe and for the entire site to account for heterogeneity of the soil. As can be seen in Table 2, the σ_S determined by multiregression analysis is generally small, but positive, with two exceptions. This suggests that the model is consistent within itself. However, the σ_S determined using the suction lysimeter data as σ_w yields negative σ_S values. Negative σ_S values were also calculated by van Loon et al. (1990) when data of Hayhoe and Balchin (1988) were analyzed the same way. They interpreted these negative σ_S as a result of limited water contents. A generally low σ_S for site '2x' is to be expected based on the observed soil coarseness (Table 1).

The relationship between σ_w from suction lysimeters and TDR-calculated σ_w is shown in Figure 2. Figure 2a shows this comparison for TDR-calculated σ_w omitting σ_S in [2]. When this term is omitted, the TDR-determined σ_w are generally too low compared to the suction lysimeter σ_w, although there is a relatively good linear correlation ($r^2 = 0.78$; Fig. 2a). This suggests that a basis for refining the relationship is including the contribution of σ_S. Figures 2b and 2c show the relationship when σ_S is

considered. In Figure 2b, probe specific σ_S values determined through 1) multiregression analysis and 2) calculated on the basis of suction lysimeter data σ_w (Table 2) are used in [2] and graphed against the suction lysimeter σ_w data. The same comparison is undertaken using one site specific σ_S value from the multiregression analysis ($\sigma_S = 23\ \mu S\ cm^{-1}$) and one average calculated value ($\sigma_S = -33\ \mu S\ cm^{-1}$) in Figure 2c. Using probe and site specific σ_S determined through multiregression analysis, the model consistently underestimates σ_w by about 50 %. The best fit between TDR determined σ_w and suction lysimeter σ_w is obtained when using the probe specific calculated σ_S values (Fig. 2b). However, these negative values may rather represent a fitting parameter for model [2] than a physical quantity since σ_S values should be ≥ 0. These results demonstrate that the multiregression approach of van Loon et al. (1991) is only a good method for calculating relative σ_w for this site. For the absolute determination of σ_w for this field soil, probe specific calibration in addition to suction lysimeter data are required.

Seasonal dynamics of σ_w

Figure 3 shows the seasonal dynamics of σ_w in frozen and unfrozen ground in the profile '2x' from 14 June to 15 October, 1995. The σ_w values are calculated using [2] and probe specific, calculated σ_S values for depths 23 to 65 cm. For depths 11 and 78 cm, the site calculated average value of $\sigma_S = -33\ \mu S\ cm^{-1}$ is used since no probe specific value is available. Although this approximation might not give an accurate absolute value of σ_w at these depths, relative statements are justified.

129
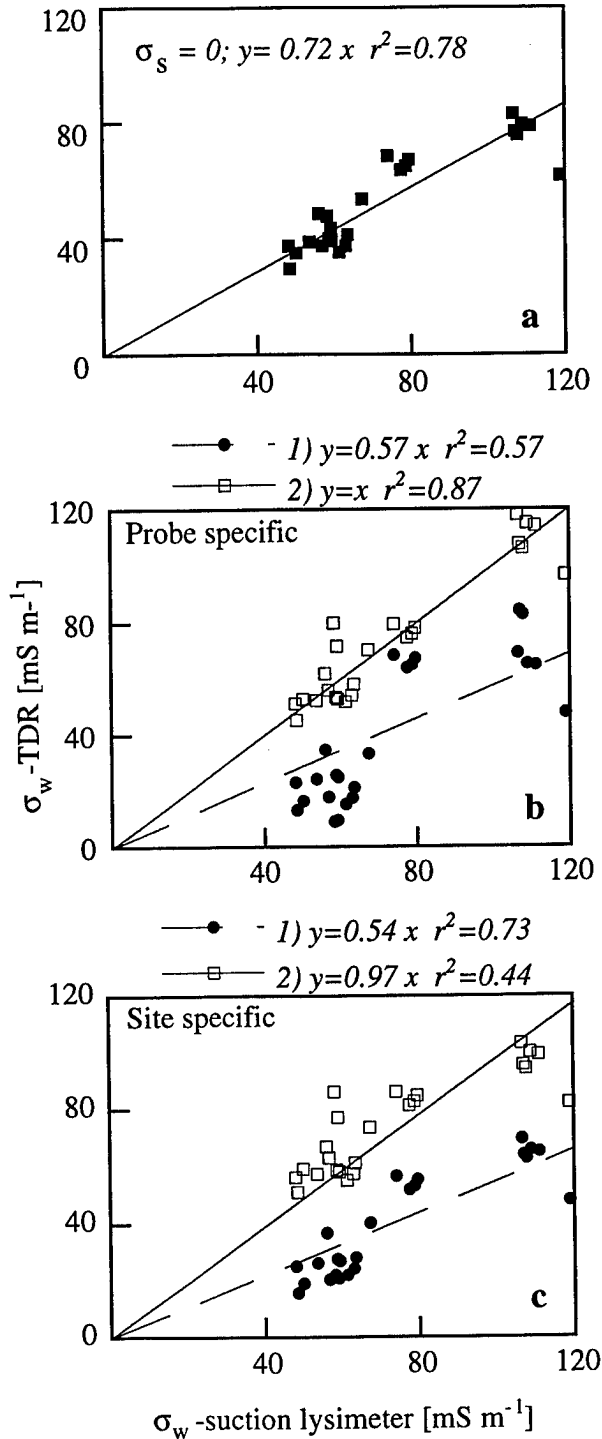
Figure 2. TDR determined σ_W using equation [2] compared with σ_W from suction lysimeters. a) σ_S = 0; b) σ_S determined probe specifically through 1) multiregression analysis and 2) calculated using suction lysimeter σ_W and c) σ_S determined site specifically through 1) multi regression analysis and 2) calculated using suction lysimeter σ_W.

Overall, the σ_W values during the summer in the unfrozen ground are relatively stable, ranging around 100 mS m⁻¹, whereas in the frozen ground they are about 4 to 15 times higher. In the lower, unfrozen ground (65 and 78 cm), σ_W values are higher compared to the upper depths. A possible explanation for this could be the dissolution of a concentrated solute layer at the previous years' thawed-frozen interface observed in permafrost-affected soils.

Infiltration into frozen ground

Data for σ_W are not available for the snowmelt that started on 5 June, which could give indication of snowmelt water infiltration into the frozen ground. However, in soil depths below 52 cm, an increase in σ_W is observed in the frozen ground before thawing. This could indicate the infiltration of suprapermafrost groundwater into the frozen ground. An increase of σ_W in frozen ground during snowmelt was observed using TDR by Lundin and Johnsson (1994), which they interpreted as infiltration of snowmelt water.

Freeze-back

The active layer is saturated up to about 8 cm below the surface before freeze-back starts (Boike et al. 1997). In the frozen ground, σ_W range between 200 to 600 mS m⁻¹ with the exception of highest values of up to 1500 mS m⁻¹ at 11 cm depth. With the exception of 1500 mS m⁻¹, these values lie in the range reported by Lundin and Johnsson (1994).

In September, when air temperatures decrease and fall below 0 °C, soil temperatures decrease quite uniformly at all depths and the phase change, characterized by the zero curtain effect, is initiated. During the first part of the phase change in September, soil temperatures are just below 0°C and σ_W increases slowly (Fig. 3). Starting in October, air temperatures fall sharply down to -15 °, soil temperatures decrease and σ_W increases rapidly. This increase of σ_W during the period of phase changes can be explained by exclusion of solutes from the ice during freezing which has been reported by Hallet (1978). Differences in σ_W within the profile are related to the initial water content of the soil. At depths of 11, 34 and 65 cm, freezing proceeds somewhat faster and σ_W are higher relative to other depths due to faster decreasing water contents (Boike et al. 1997) (Fig. 3). This preferential freezing within the profile apparently depends on the heterogeneity of the soil and the resulting differences in water content. These results support the observation by Panday and Corapcioglu (1991) that the exclusion of solutes within a freezing soil system is determined by

130
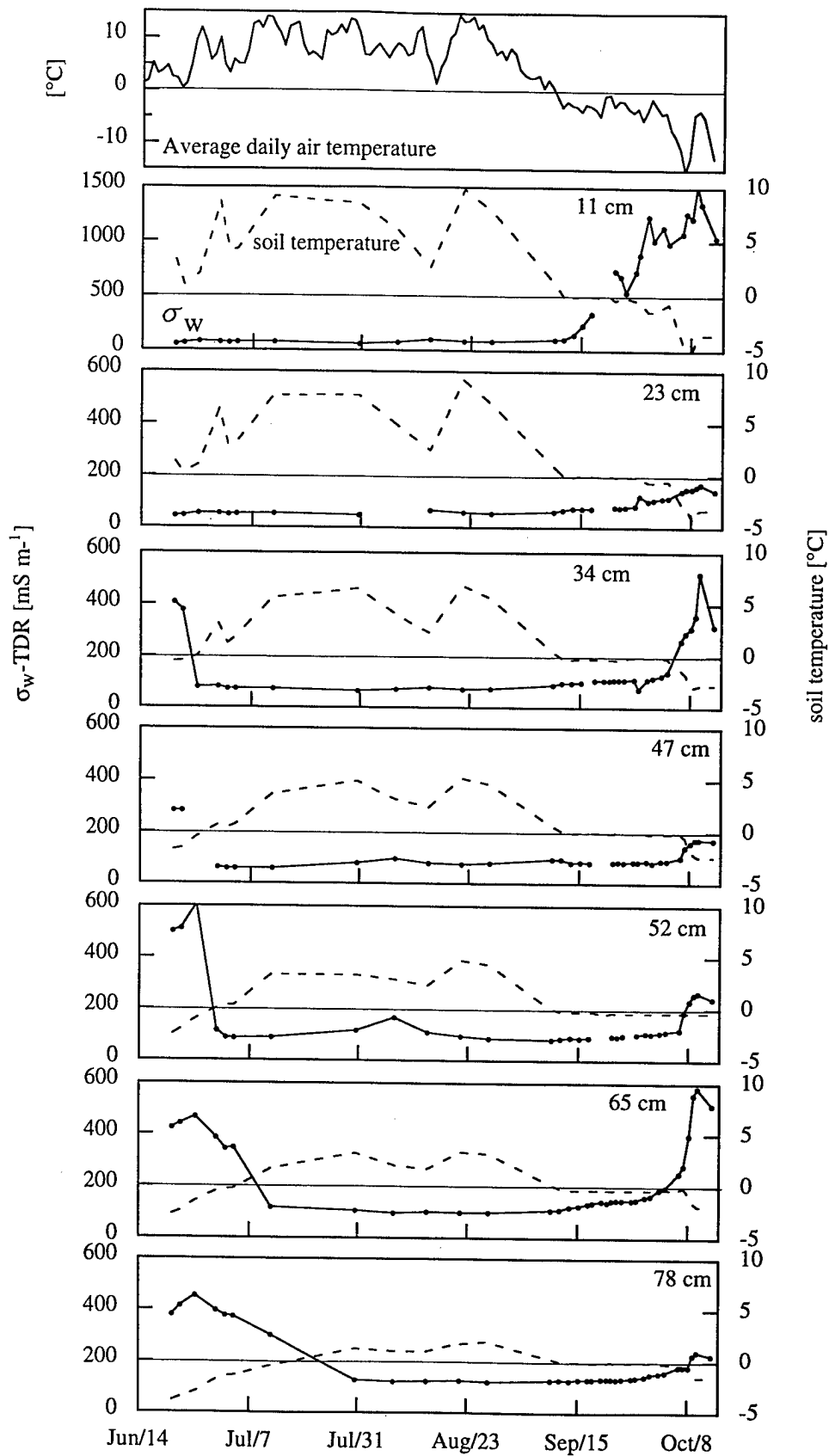
Figure 3. Seasonal dynamics of σ_w at site '2x' from 14 June to 15 October 1995. Probe specific calculated σ_s are used to calcuate σ_w for depths 23, 34, 47, 52, and 65 cm. For depths 11 and 78 cm, the average site specific calculated σ_s value is used.

a complex interplay between hydraulic and thermal properties.

CONCLUSIONS

Generally, TDR is a promising in situ technique to calculate (σ_w from σ_b for arctic field soils. Optimal results are achieved when the model of van Loon et al. (1991) is used with a probe specific calibrated σ_s through the use of suction lysimeter data. Further improvements could be made by incorporating a soil characteristics term that is related to the coarseness and tortuosity of the soil.

TDR measurements have been used to study the seasonal dynamics of σ_w in frozen and unfrozen ground. Strong temperature dependence of σ_w in the frozen ground was observed in the range of 50–100 mS m^{-1}, but variations in σ_w as a result of phase change were much greater, in the range of 200–500 mS m^{-1}. The magnitude of conductivity changes associated with phase changes, i.e., of solute exclusion, depends on the freezing rate and therefore the initial water content of the soil.

REFERENCES

Boike, J., K. Roth and P.P. Overduin. 1997. Thermal and hydrological dynamics of the active layer at a continuous permafrost site (Taymyr Peninsula, Siberia). Submitted to Water Resources Research.

Dasberg, S. and F.N. Dalton. 1985. Time domain reflectometry field measurements of soil water content and electrical conductivity. Soil Sci. Soc. Am. J. 54: 293–297.

Hallet, B. 1978. Solute redistribution in freezing ground, 86–91. In Permafrost. Proc. ,Vol. 1, Third Int. Conference. National Research Council of Canada, Ottawa, Canada.

Hayhoe, H.N. and D. Balchin. 1988. Time domain reflectometry and electrical conductance measurements during seasonal frost. Cold Regions Science and Technology 15: 195–200.

Heimovaara, T.J. 1993. Design of triple-wire time domain reflectometry probes in practice and theory. Soil Sci. Soc. Am. J. 57: 1410–1417.

Heimovaara, T.J. and E. de Water. 1993. A computer controlled TDR system for measuring water content and bulk electrical conductivity. Report # 41, Laboratory of Physical Geography and Soil Science, University of Amsterdam.

Heimovaara, T.J., A.C. Focke, W. Bouten and J. M. Verstraaten. 1995. Assessing temporal variations in the soil water composition with time domain reflectometry. Soil Sci. Soc. Am. J. 59: 689–698.

Lundin, L. C. and H. Johnsson. 1994. Ion dynamics of a freezing soil monitored in situ by time domain reflectometry. Water Resources Research 30 (12): 3471–3478.

Mualem, Y. and S.P. Friedman. 1991. Theoretical prediction of electrical conductivity in saturated and unsaturated soil. Water Resources Research 27(10): 2771–2777.

Patterson, D.E. and M.W. Smith. 1980. The use of time domain reflectometry for the measurement of unfrozen water content in frozen soils. Cold Regions Science and Technology 3: 205–210.

Panday, S.P. and M.Y. Corapcioglu. 1991. Solute rejection in freezing soils. Water Resources Research 27(1): 99–108.

Rhoades, J.D., N.A. Monteghi, P.J. Shouse and W.J. Alves. 1989. Soil electrical conductivity, water content and surface conductivity on bulk electrical conductivity. Soil Sci. Soc. Am. J. 53: 433–439

Roth, K., R. Schulin, H. Flühler and W. Attinger. 1990. Calibration of time domain reflectometry for water content measurement using a composite dielectric approach. Water Resources Research 26(10): 2267–2273.

Smith, M.W. and A.R. Tice. 1988. Measurement of the unfrozen water content of soils: A comparison of NMR and TDR methods, 473–477. In K. Senneset (ed.) Permafrost. Proc., Vol. 1, Fifth Int. Conference, 2–5 August 1988, Trondheim, Norway.

Spaans, E.J.A. and J.M. Baker. 1995. Examining the use of time domain reflectometry for measuring liquid water content in frozen soil. Water Resources Research 31(12): 2917–2925.

Stein, J. and D. Kane. 1983. Monitoring the unfrozen water content of soil and snow using time domain reflectometry. Water Resources Research 19(6): 1573–1584.

van Loon, W.K.P., P.H. Perfect, P.H. Groenevelt and B.D. Kay. 1990. Application of time domain reflectometry to measure solute re distribution during soil freezing. In Proceedings Int. Frozen Soil Symp., CRREL Report 90–1, Hanover, N.H., USA: 186–194.

van Loon, W.K.P., P.H. Perfect, P.H. Groenevelt and B.D. Kay. 1991. Application of dispersion theory to time domain reflectometry in soils. Transp. Porous Media 6: 391–406.

The Effect of Pore Solution Concentration and Composition Upon the Electric and Elastic Properties of Frozen Saline Soils

O.P. CHERVINSKAYA[1], Y.D. ZYKOV[2], AND A.D. FROLOV[3]

ABSTRACT

Electric and elastic properties of frozen sandy-clayey soils saturated with solutions of various composition and concentration have been determined. Significant differences between these properties in saline and nonsaline soils are interpreted. First estimates are given of the critical concentration of pore solutions, which makes it possible to separate objectively the frozen from the unfrozen saline soils for the sand-clay series.

Key words: permafrost, salinity, elasticity, resistivity, permittivity.

INTRODUCTION

Frozen saline sandy-argillaous grounds occur frequently in the cryolithozone, and in particular, everywhere along coastal areas of Arctic seas. Their pore solutions are characterized by a chloride composition with a prevalence of Na^+ and Mg^{2+} ions (Dubikov and Ivanova 1990). This salinity type is called marine to distinguish it from continental salinity that has a predominance of magnesium and calcium carbonates, and sulphates.

The physical properties of frozen saline soils are of high scientific and practical significance. They are required for the design of field geophysical studies and interpretation of their results, systematic monitoring and for the development of non-destructive techniques to measure the kinetics of changes in the phase composition and state of soils.

The electric and elastic properties of a frozen medium have proven to be most sensitive to changes in its phase composition and state (Frolov 1976, Zykov and Chervinskaja 1989). Therefore our laboratory studies were focused mainly on these properties. The main results are discussed in this paper.

BACKGROUND

The principal peculiarity distinguishing frozen grounds from the thawed ones is their specific Spatial Crystalline-coagulant Cryogenic Structure (SCCS) (Frolov 1976). Another distinctive feature of frozen grounds is the simultaneous presence of ice and liquid phases in diverse energy states. As a result there exists an extended temperature interval over which phase changes occur. The unfrozen liquid phase content is dependent on adsorbtional capability, microirregularities in relief, and heterogeneity of active surfaces of the soil's solid-matrix grains. There are possibly, two principal cases of forming SCCS, hence all properties of frozen soils. First, when the appearance and evolution of SCCS is predominantly influenced by a mineral matrix, as in the case of frozen fresh soils and well-known cryogenic processes. Second, when the formation and peculiarities of SCCS are determined by the initial concentration and ionic composition of pore solution, e.g.,frozen saline soils. Evidently, a boundary soil state should be determined by a definite critical initial concentration of pore solution C_{cr}, making it possible to distinguish saline and nonsaline frozen soils. Nonetheless, until now no adequate unified criterion has been established for determining C_{cr}.

At a fixed temperature of frozen saline soil, the liquid phase content has been found to increase almost linearly with increasing pore solution concentration. This behavior is close to the situation typical for solutions. Relevant experiments (Ershov 1995)

133

also indicate that the liquid phase depends on the ionic composition of pore solution. For saline soils saturated with solutions of sodium salts, the unfrozen liquid phase content decreases irregularly in the following series $NaCl-NaNO_3-Na_2SO_4-Na_2CO_3$. For the last two, this decrease is only 10-15%, whereas the NaCl predominance in pore solution leads to a two-hold and even greater increase of the unfrozen liquid phase content in comparison with carbonate and sulphate composition. A noticeable shift, proportional to the initial concentration, of freezing temperature below 0°C is observed for frozen saline soils. The width of the temperature range and the rates of phase transformations also undergo substantial changes, which are especially strong in sandy soils.

There are also the changes in the solid matrices of SCCS for saline soils. The mean ice crystal size decreases. A considerable portion of pore solution salts pass into saline ice. The mineral matrix may also changes associated with coagulation of clay and dispersion of sand particles (Frolov 1995).

As a whole, a frozen saline soil is a composite material with SCCS containing a larger number of weakening elements (boundary intergrain zones with a high content of liquid phase, doped pore ice, etc.), which causes the soil plasticity to increase. When the temperature of such soil decreases, accompaned by the freezing of brine and precipitation of salt crystal hydrates, there appear some consolidating intergrain zones, which eventually become prevalent, and the mediums rigidity and fragility increase.

SAMPLING AND EXPERIMENTAL PROCEDURE

Due to the complexity of frozen soils any field study aimed at establishing basic regularities is practically impossible. Therefore, we have carried out the laboratory studies of electric and elastic properties on samples. The main characteristics of these soils are presented in Table 1.

Table 1. Properties of soils used in labaratory experiments.

Soils	Granulometric content (%) Diametr (mm)			Plasticity number I_P (%)	Dry soil density (g/cm^3)
	> 0.05	0.05-0.005	< 0.005		
Quartz sand	99.9	0.1	-	-	2.66
Sand	94.7	4.5	0.8	-	2.71
Sandy-loam	75.9	14.4	9.7	3.2	2.71
Loam 1	51.0	28.4	20.6	7.9	2.72
Loam 2	12.0	74.9	13.1	11.2	2.69
Clay	15.4	41.8	42.8	17.8	2.70
Kaolin	1.0	26.0	73.0	21.0	2.65

Before sample preparation the soils were washed in distilled water, with subsequent drying at 105°C. The dry soils were mixed with equal amounts of salt solutions of defined concentration and composition. The prepared soil pastes were then packed into cylindrical conteainers and compacted to a specified volume. To form a massive cryotexture, samples were frozen at -30°C under a slight load (~ 0.5 kg/cm^2). The initial moisture of samples ranged of 10-15 to 30-50 % (by weight) and covered the interval from incomplete to total filling (and even slight oversaturation) of pores.

Basically we have studied the frozen soil models with a marine-type salinity, i.e., the samples were saturated with NaCl solutions. To estimate the deviations in properties of soils with continental and mixed salinity types, some experiments used solutions of other salts, and with the salt mixtures in various proportions. After the end of every measurement series, each sample was checked for the changes in its major components.

Dielectric permittivity ε_{eff}, electrical resistivity ρ, and ultrasonic propagation velocities V_P, and V_S or V_R were determined with standard techniques (Frolov 1976, Ershov 1985) at fixed temperatures, increasing from about -25° to -1°C. Elastic moduli were calculated from measured velocities and soil densities using the formulas of continuous medium

elasticity theory. Before measurements, samples remained at each temperature for many tens of hours to achieve a quasi-equilibrium state.

RESULTS AND DISCUSSION

Critical concentration of pore solution

The differences in physical properties frozen saline soil SCCS may help establish objective criteria for determining C_{cr}. The quantity of such experiments carried out to date is obviously insufficient. Nonetheless, the available data allow some useful generalizations.

Our studies of dielectric properties (Frolov and Fedyukin 1983, Frolov et al. 1993) established that for the quartz sand samples saturated with sodium and potassium chloride solutions over a wide concentration range, Ccr (5 x 10^{-3} mole/L (0.3 g/L (Fig.

1a). This value proves to be virtually coincident with Ccr distinguishing saline and practically fresh ice. At an initial concentration $C_i < C_{cr}$, the frozen sand and ice display properties close to those of their fresh analogs, whereas at $C_i > C_{cr}$, there appear substantial differences between dielectric properties of saline and praktically fresh cryogenic formations.

Other indirect investigations of the strength and formation of cryotextures (Panchenko and Aksyonov 1990, Khimenkov and Minaev 1990 and others) suggest as a first approximation that C_{cr} (for chloride composition of pore solutions) increases linearly with increases in clay fraction (Fig. 1b) and reaches ~ 0.5 mole/L for heavy clays.

The lowest C_{cr} values ($\sim 5.10^{-3}$ mole/L) characteristic of quartz sands and ice are associated with changes in properties of solutions (structure, viscosity, etc.) due to the interaction of ions. High C_{cr} values for clayey soils are connected with ion-exchange properties of their mineral surfaces. In these soils, a considerable portion of ions interact with active surfaces of the mineral matrix, and the solution concentration affects little the kinetics of soil freezing and SCCS formation.

Elastic and electric properties

Marine salinity type

The investigation of the velocities of elastic wave propagation velocities and the dynamic moduli of elasticity confirms, on the whole, the above-mentioned common peculiarities of frozen saline soils and allows their quantitative characterization. Saline sands were found to exhibit the strongest changes in velocities V_P and V_S (and accordingly, in SCCS) at various initial concentrations of pore solutions $C_i > C_{cr}$. For example, the experiments show that at -5°C in frozen NaCl saline sand, as C_i is increased 40 times (from 0.7 to 29 g/L), V_P decreases nearly 3 times (from 3900 to 1400 m/s). In clays, such a V_P decrease is less than two times.

The variation of Poisson's ratio v proved to be most characteristic (Fig. 2). In sandy and clayey soils the variation $v = f(C_i)$ correlates well with the C_{cr} values. For the frozen sand, at $C_i > C_{cr}$ (~ 0.5 g/L) v shows a rather sharp 1.75-fold increase from 0.2 to 0.33-0.35, followed by a gradual rise to a level of 0.37-0.39 (at $C_i = 1$ mole/L), which is nearly coincident with that of the thawed material. For the frozen light clay, such an increase of v to the level characteristic of the thawed material (0.44-0.45) starts at C ~ 10 g/L (see Fig. 1b). Over the C_i interval from 0 to 10 g/L, for the clay studied, $v = 0.34$-0.35 and proves
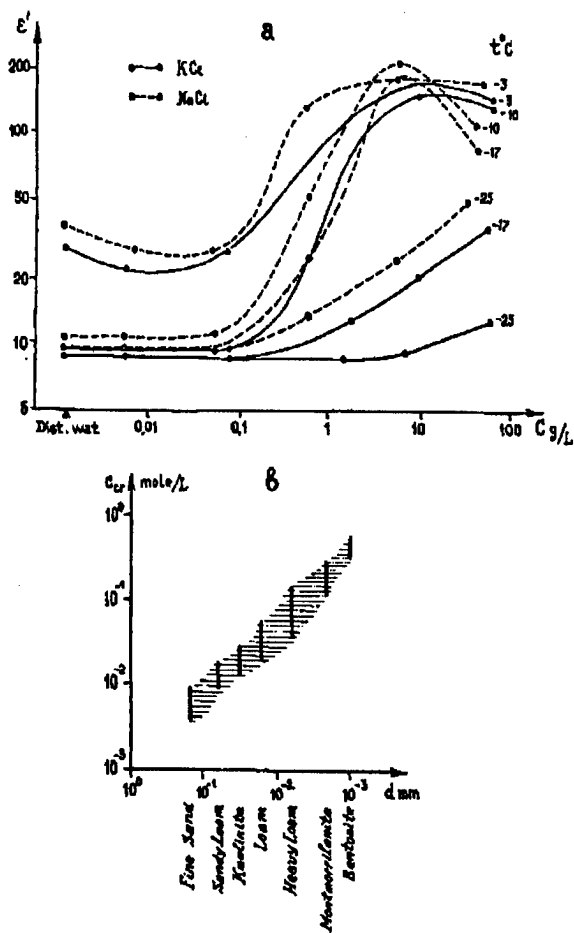
Figure 1. Critical initial concentration of pore solution for: (a) quartz sand (from DP measurements); (b) various sandy-clayey soils (from generalizations).

135
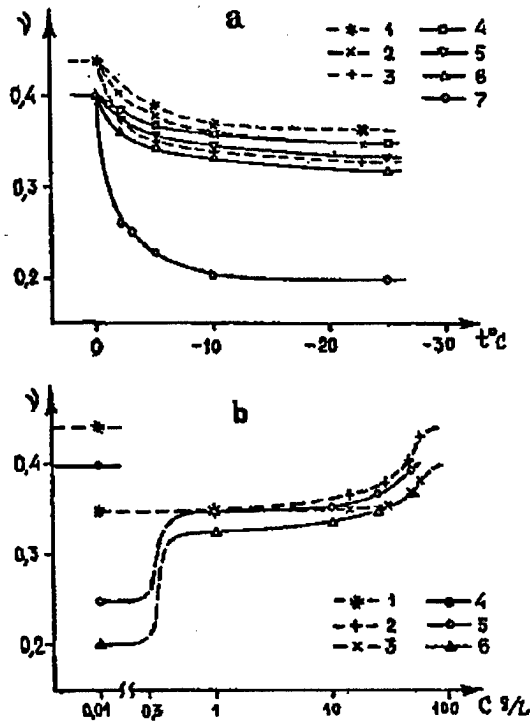
Figure 2. (a) Poisson's ratio of frozen saline soils vs. temperature. Plots 1-3: clay with initial pore solution concentration C_i= 45,30, and 0-10 g/L; plots 4-7: sand with C_i=30,10,2,0 g/L. (b) Poisson ratio vs. initial pore concentration. Plots 1-3: clay at t>0, t=-5, t=-10°C; plots 4-6: sand at the same temperatures, respectively.

to be independent of concentration. Therefore, at these C_i values the frozen clay may be considered freshwater saturated.

A similar pattern is also characteristic of other dynamic elastic moduli (Fig 3). The strongest changes in Young's modulus E and shear modulus G occur in the frozen saline sand. The clayey soils are characterized by a gradual decrease of E and G values.

The electric properties of frozen soils are mainly determined by the content and conductivity of the unfrozen liquid phase, as well as by the heterogeneity of the soils. The latter most strongly influences the effective dielectric permittivity ε'_{eff} at frequencies below 50 kHz, due to the effect of macrodipolar polarization (Frolov 1976, Frolov and Fedyukin 1983). Therefore, the temperature dependence of ε'_{eff} for frozen saline quartz sand saturated with sodium and potassium chloride solutions (Fig. 4) is similar to that of frozen clayey soils. Thus, according to the temperature spectra of ε'_{eff}, the most intensive changes in

SCCS of rather strongly saline sands (C_i = 1 to 5 x 10^{-1} mole/L) take place in two stages: near the temperature of the beginning of soil freezing and near the eutectic temperature t_{eu} for a given composition of pore solution. This is related to dramatic changes in the degree of unfrozen liquid phase discreteness during pore ice formation (first stage) and precipitation of salt crystal hydrates at the second stage. These states are characterized by ε'_{eff} maxima (Fig. 4). Between these states, abnormally high values of ε'_{eff} are preserved, which are due to the macrodipolar polarization effect in discrete domains of unfrozen pore solution, which persist up to t_{eu}.

In the case of relatively low salinity ($C_i \sim 10^{-2}$ mole/L), there is only the first maximum. However, the temperature spectra of ε'_{eff} for frozen saline sand display substantial differences from those of frozen fresh sand. At high pore solution concentrations (C_i > 1 mole/L), phase transformation increases smoothly from the temperature of freezing onset (which is considerably lower than 0°C) to t_{eu}; t_{eu}, the decrease of ε'_{eff} in sufficiently saline sand (C_i > 10^{-1} mole/L) is similar to that occurring in i.e., the first maximum is virtually absent. It is noteworthy that at temperatures below fresh sand at temperatures after the onset of freezing (Fig.4). This analogy suggests that variation of the liquid phase content and the decrease in the size of its discrete accumulations occur similarly in both these states of frozen sand. Since the temperature, at which the liquid phase totally freezes in fresh sand is estimated at -25 to -30°C (Frolov 1976), it may be expected that the analogous state will be achieved in saline sand at temperatures 25-30°C below t_{eu} of the saturating pore solution. The existence of such a situation is confirmed by the ε'_{eff} (t) dependence for the frozen sand saturated with KCl solution with $t_{eu} \sim$ -11°C (Fig. 4). At temperatures below -12°C the left segment of curve 2 is analogous to the ε'_{eff} (t) curve for fresh sand at t < -2°C. Further studies are necessary to check and explain this fact in view of the substantial deviation of the of solution freezing process in a porous medium from the theory of free solutions.

The electrical resistivity ρ of both saline and fresh sandy-clayey soils was found to increase upon freezing and during subsequent temperature decrease. However, its value decreases sharply at higher salinity levels ($C_i \gg C_{cr}$). Upon freezing of fresh-water-saturated sand, ρ increases 10^4-10^5 times; at C_i = 10^{-1} mole/L this increase is 10 - to 100-fold; increases only by a factor of 2 at C_i = 1 mole/L. Thus, as C_i increase above C_{cr}, (of the frozen sandy soils approaches that of the frozen claey soils. It follows that

136
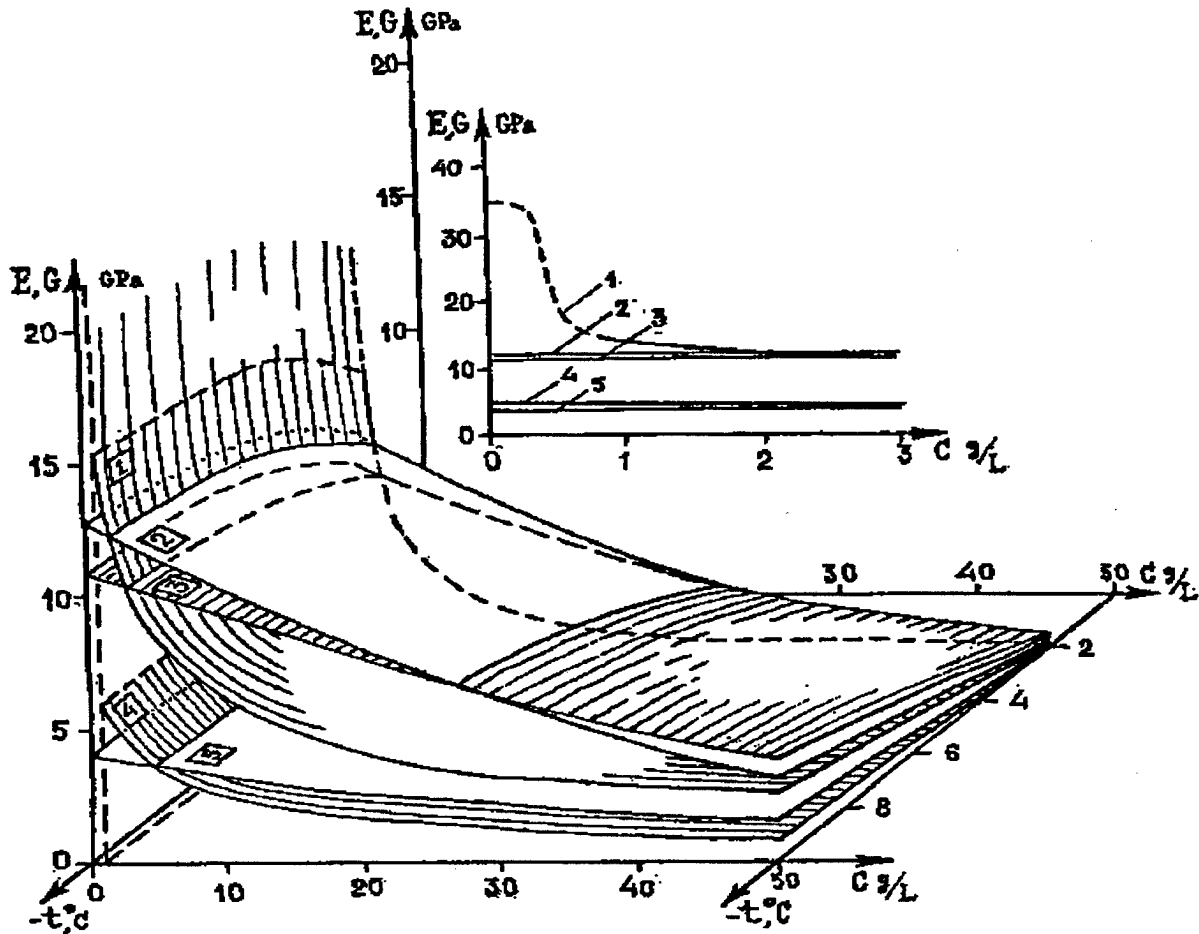
Figure 3. Dynamic elastic moduli E (1,2,3) and G (4,5) vs. temperature and initial pore solution concentration. Sand: plot 1,4; loam: plot 2; clay: plot 3,5.

at certain value of C_i the resistivity ρ becomes virtually independent of the lithological composition of frozen sandy-clayey soils (Zykov et al.1990). In the studied samples of silty sand, sandy loam, loam, and kaolin saturated with NaCl solutions, this state is reached at $C'_i \sim (0.4$-$0.6) \times 10^{-1}$ mole/L (Fig. 5a). At initial concentrations of saturating solutions exceeding C'_i, ρ decreased identically for all soils mentioned above. This means that the SCCS, which determines the section and tortuosity of current routes, forms similarly in these frozen soils because ρ is determined solely by the concentration-dependent resistivity of pore solution. This is also confirmed to a considerable extent by the dependencies of the and Young's modulus presented in fig.5b. At the indicated initial pore solution concentration C'_i, both elastic modulus E and G have similar values in soils of different lithological composition. However, at $C_i < C'_i$, the elastic moduli of frozen saline sand

prove to have lower values. Possibly, this is associated with the lower rigidity of frozen saline sand SCCS due to the presence of larger polycrystalline formations of saline pore ice than occur clayey soils.

Continental and mixed salinity types

To estimate the differences in the formation and magnitudes of the elastic and electric properties of frozen soils continental and mixed salinity types, a limited number of experiments were carried out on loam samples saturated with solutions of chlorides and with a group of carbonates and sulfates taken in different proportions. Both ρ and V_P were measured in the range from positive temperatures to -20°C. The ratios of the two salt groups in the saturating solutions were set discretely: 0/1, 0.25/0.75, 0.5/0.5, 0.75/0.25 and 1/0.

Let us consider first the extreme cases (Fig 6). The similarity of the ρ and V_P variations upon tran-

137
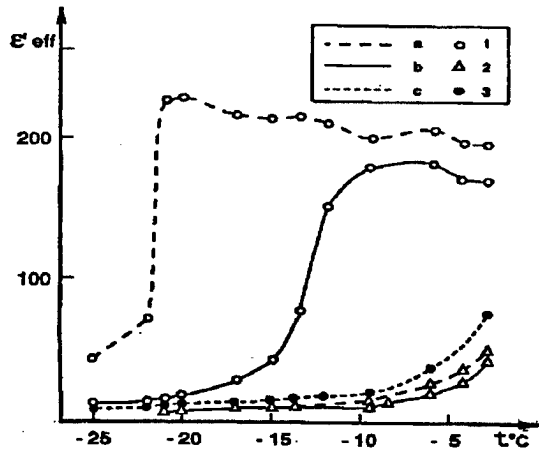
Figure 4. Temperature dependencies of ε'_{eff} for frozen sand saturated with distilled water and solutions of NaCl and KCl. Plot a: NaCl; b: KCl; c: distilled water; 1,2,3: $C_i = 10^{-1}, 10^{-3}$, and 0 mole/L, respectively. Frequency 10KHz.

Figure 6. Effect of pore solution composition on ρ and V_P of frozen loam (a),(b): vs. temperature. Plot 1: $NaHCO_3$; 2: Na_2SO_4; 3: $MgCl_2$; 4: NaCl; 5: sea water salt; 6: fresh water. (c),(d): vs. Na_2SO_4 content (in parts of unit) in the mixed composition $(NaCl + Na_2SO_4)$ saturating solution; pore solution concentration = 30 g/L.

sition to the frozen state and with subsequent temperature decrease is seen to universal in frozen soil with any pore solution composition. However, the composition of the saturating solution strongly influence the freezing temperature and the intensity of the changes seen in ρ and V_P. The latter circumstance divides the dependencies obtained into two groups: (1) chloride salinity (marine type) and (2) carbonate-sulfate salinity (continental type), which display both common features and definite distinctions. The second group has substantially higher values of ρ and V_P, with also have greater temperature gradients of variation (intensity of phase transformations) from down to -5°C. This interval may be defined as the first stage of saline soil freezing. During this stage an ice matrix of soil SCCS forms totel pore liquid de-

Figure 5. Initial pore solution concentration's influence on the correlation of ρ and E magnitudes with soil lithology (plasticity number J_P). Curve index: concentration (g/L), temperature -5°C.

crease, discreteness of pore liquid increase, and the concentration of the unfrozen pore solution increase. In the second stage of freezing, in the temperature range from -5° to -20°C, (ρ and V_P in soil with carbonate-sulfate salinity are virtually analogous to those for fresh-water-saturation soil.

Second, the elastic wave velocity in the thawed soil is virtually the same for fresh and saline soils at any composition of saturating solution, whereas the elasticity (as well as rigidity) is determined basically by the quantity of liquid phase and ice in the intergrain zones. The differences in resistivities obtained in thawed soil are related to the ionic composition of the pore solution. Resistivity is lower for chloride saturating solutions.

Third, comparison of the initial concentrations of pore solutions with those of water extracts taken at the end of the measurements showed that carbonate-sulfate concentration decrease considerably. Apparently, part of the dissolved salts form poorly soluble complexes by interacting with mineral grains. This indicates the complexity of physics-chemical proc-

138

esses occurring in saline soils in during their freeze-thaw cycles, and this fact should be taken into account. In the case of saturation with chloride solutions the above-mentioned concentration decrease was not observed, and the temperature dependencies of ρ and V_P (Fig. 6a,curves 3-5) were virtually independent of the cation type in the dissolved salts.

Let us consider now the results of experiments on loam saturated with mixtures of NaCl and Na_2SO_4 taken in different proportions (Fig. 6 c, d). These salts were chosen because the major effect is exerted by their anions: Cl^-, SO_4^-, HCO_3^-. Replacement of HCO_3^- by SO_4^- in solution had no substantial effect on the ρ and V_P dependencies. The figure clearly demonstrates that the increase of sodium sulfate content in the saturating solution induces a proportional increase in both ρ and V_P. This increase becomes sufficiently evident at the sulfate content exceeds 20%.

Thus, according to the values of parameters determining electric and elastic properties, the marine type of salinity includes soils with a predominance of chlorides in pore solutions and with sulfate and carbonats content no more than 20-30%. The continental type of salinity is characterized by pore solution with chloride content up to 15-20% (the left part of the graph in Fig. 6c). Mixed pore solutions, containing from 60 to 20% chlorides, characterize the mixed salinity type of which display properties intermediate between those of marine and continental salinity types.

CONCLUSION

Our experiments and respective generalizations provide the first basic objective landmarks for development of an integral concept aimed at comprehensive interpretation of the specificities of formation and evolution of SCCS and physical properties of frozen soils with different salinity types. This aim may be achieved through further studies covering the other mineral matrixes and concentrations of saturating solutions. The study of electric and elastic properties of saline soils appears to be good approach in such investigations.

Our experimental studies also show the possibility of modeling the formation of SCCS and physical properties of virtually any frozen sandy-clayey soil with the help of frozen sands saturated with solutions of different concentration and ionic compositions.

REFERENCES

Dubikov G.I., N.V.Ivanova. 1990. Saline frozen soils and its abundance in the USSR territory. p. 3-9. *In* S.S.Vialov (ed.) Coll. Saline Frozen Soils as the Foundations of Constructions. Nauka Press, Moscow.

Ershov E.D. (ed.).1985. Laboratory methods to study frozen soils. Mosc. Univ. Press.

Ershov E.D.(ed.).1995. Principles of geocryology, Part 1, Physico-chemical bas of geocriology. Mosc. Univ. Press.

Frolov A.D..1976. Electric and elastic properties of frozen earth materials. Nedra Press. Moscow.

Frolov A.D., I.V.Fedyukin. 1983. On the polarization of frozen soils in the alternative electromagnetic fields. p. 90-95. Izvestia VUZov, Geologia i Razvedka, N6, Moscow.

Frolov A.D. list other authors. 1993. Specificity of phase transformations in the cryogenic saline sandy soils. p. 262-271. *In* Proc. Joint Russian-American Seminar on Cryopedology and Global Change, Pushchino, Russia,

Khimenkov A.N.,A.N.Minaev. 1990. Salinity influence on frozen soil cryostructure formation. p. 55-62. *In* S.S.Vialov (ed.) Coll. Saline frozen soils as the fundamentation of constructions. Nauka Press, Moscow. p. 55-62.

Panchenko V.I., V.I.Aksionov. 1990. Phisico-chemical approaches for frozen soils classification by salinity. p. 70-73. Ibid.

Zykov Yu.D. List other authors. 1990. Electric and acoustic properties of saline frozen soils. p. 128-135. Ibid.

Zykov Yu.D., O.P.Chervinskay. 1989. Acoustical properties of icy soils and ice. Nauka Press, Moskow.

Modeling Equations for Two-Dimensional Coupled Heat, Fluid and Solute Transport in Variably-Saturated, Variably-Frozen Soils

J.L. NIEBER[1], M.J. FRIEDEL[2], AND B.S. SHARRATT[3]

ABSTRACT

The governing equations for the time-dependent and multidimensional coupled flow of water and air, and transport of heat and aqueous phase solutes are presented. The boundary conditions appropriate for the application of the governing equations to a realistic field problem are illustrated. Numerical solution procedures, including the temporal and spatial discretization methods, nonlinear iterative methods and matrix equation solution methods, are discussed.

Key words: Heat transport, moisture flow, air flow, solute transport, freezing soils

INTRODUCTION

The redistribution of dissolved chemicals (solutes) in heterogeneous, variably-saturated soil (unsaturated zone) during natural ground freezing is of practical interest to engineers and water resource managers seeking to minimize contamination of ground water supplies during winter (Baker and Osterkamp 1988, Wilson and Vinson 1983, Kay and Groenevelt 1983, Seyfried et al. 1990). Understanding solute redistribution is also important in artificially induced freezing where concentration and/or containment of hazardous compounds may be conducted for remediation (Ayorinde and Perry 1990, Iskandar and Jenkins 1985). Both naturally and artificially induced freezing influence the simultaneous transport of heat, water, and solutes in the unsaturated zone (Williams and Smith 1989, Seyfried et al. 1990).

Solute exclusion occurs due to the inability of ice crystals to incorporate alien molecules (Panday and Corapcioglu 1991). Exclusion causes solute to move from freezing to an adjacent unfrozen solution, resulting in elevated pore water concentrations that migrate ahead of the freezing front. Because concentrated solutions migrate with the freezing front, they have the potential to accumulate chemicals near the maximum extent of frost penetration (Beke and Palmer 1989). The accumulated chemicals may then pose a risk to ground water supplies, since the maximum extent of frost penetration can easily extend below the soil horizons where the major part of microbiological action and soil adsorption activity exists.

Water movement in the unsaturated zone has received much investigation; however, most experimental and numerical analyses have assumed isothermal conditions (Freeze 1971, Nieber et al. 1994). With the exception of a few laboratory studies, it wasn't until the mid-1950s that the first mathematical model was presented which included nonisothermal conditions (Philip and de Vries 1957, de Vries 1958). In this model, the simultaneous transport of water and heat are based on the principles of porous media hydraulics. In particular, the liquid and vapor phases were expressed as functions of soil water content, mean soil temperature, and soil air content. In using this model, some investigators have noted a disparity between the predicted and observed values of soil water movement. One cause of these disparities was attributed to the inaccuracy of the soil-water transport coefficients (e.g., diffusivities). Recognizing that the transport phenomenon is also affected by an osmotic potential gradients (due to solute concentration gradients), an expanded set of governing equations was developed (Nassar and Horton 1989, Nassar and Horton 1992).

Since coupled transport processes are important in cold climate regions, several unsaturated zone models have been developed, including those reported by Harlan (1973), Jame and Norum (1973), Pikul and Allmaras (1984), Benoit et al. (1988) and Flerchinger and Saxton (1989). Of these, the model by Flerchinger and Saxton is the most rigorous, as it accounts for coupled transfer of water, heat and solute while also considering a climate-driven boundary condition at the soil surface. All of these models consider the coupled transfer processes to be vertical and one-dimensional in the soil profile.

[1] Department of Biosystems and Agricultural Engineering, University of Minnesota, St. Paul, Minnesota 55108, USA
[2] NAWQA, U.S. Geological Survey, Urbana, Illinois 61801, USA
[3] USDA, Agricultural Research Service, North Central Soil Conservation Research Laboratory, Morris, Minnesota 56267, USA

In the present paper we describe the formulation for a model for multidimensional coupled water and air flow, and heat and aqueous phase solute transport. There exist many applications where such a model is needed. A very simple example is the case where one wishes to examine heat and mass transport processes in a soil cultivated with ridges. It is obvious that the processes for a such a system will be two-dimensional at least, if not three-dimensional. For the purpose of illustration, the boundary conditions for this type of problem are presented in this paper. Other potential applications of the model include the analysis of coupled transport processes near a cryogenically isolated waste site and the freezing of soil beneath foundations, with consideration for the possible uplifting of the foundation by frost heaving.

MATHEMATICAL MODEL

The governing equations and the proposed form of the parameter relationships for a numerical solution model are presented in this section. The numerical solution formulation is presented later. The governing equations are based on a porous media hydraulics approach to the analysis of coupled heat and mass transport processes (Philip and de Vries 1957). An alternative approach to this one is the irreversible thermodynamics approach presented by Taylor and Cary (1964). The equations presented here are essentially the same as those presented by Nassar and Horton (1989, 1992) with the exception that the ice phase terms are added, and equations for air flow are considered. Definitions of terms in equations are given in the Appendix.

Mass and energy balance equations

Mass and energy balance equations are used to express the state of the system under consideration. The conservation of mass equation for water, considering the three phases of liquid water, ice and water vapor, is given by

$$\rho_l \frac{\partial \theta_l}{\partial t} + \rho_i \frac{\partial \theta_i}{\partial t} + \rho_l \frac{\partial \theta_v}{\partial t} = -\rho_l \nabla \cdot \overline{q}_l - \rho_i \nabla \cdot \overline{q}_i - \rho_l \nabla \cdot \overline{q}_v \qquad (1)$$

The conservation of mass equation for the air phase in the porous medium is given by

$$\frac{\partial (\rho_a \theta_a)}{\partial t} = \nabla \cdot (\rho_a \overline{q}_a) \qquad (2)$$

The volumetric flux terms, the $\overline{q}_j\text{'s}$, can be quantified by choosing an appropriate constitutive law for each

phase. For the liquid water and air phases this is given by Darcy's law, while for the water vapor this is given by Fick's law of diffusion along with a possible mass flux due to the convective movement of the air. A constitutive law for the ice phase can be given by viscoelastic theory.

For liquid water flow the Darcy flux is given by the combined effects of water content gradient, temperature gradient and solute gradient. For air flow the Darcy flux is given by the combined effects of air pressure gradient and air density gradient. These fluxes are expressed as

$$\overline{q}_l = K_l \nabla h_l - D_{l_T} \nabla T - D_{l_c} \nabla c - K_l \vec{k} \qquad (3)$$

$$\overline{q}_a = -K_a \nabla h_a - \frac{K_a}{\rho_l g} \frac{\partial \rho_a}{\partial z} \vec{k} \qquad (4)$$

The flux of water vapor is given by

$$\overline{q}_v = (-D_{v\theta} C_l \nabla h_l - D_{vT} \nabla T - D_{v_c} \nabla c - \rho_l \theta_v \overline{q}_a) / \rho_l \qquad (5)$$

In the preceding formulation, the porous medium is assumed to be rigid.

Although the flow of the ice phase could be described by viscoelastic theory, in the present analysis we assume that the ice phase flux is given by $\overline{q}_i = 0$.

The conservation of mass equation for the sorbing solute is given by

$$\frac{\partial \theta_{lc}}{\partial t} + \frac{\partial \rho_b K_b c}{\partial t} = -\nabla \cdot \left(\frac{J}{\rho_l} \right) \qquad (6)$$

In eq. (6) it is assumed that all of the solute is rejected into the liquid phase during freezing. This phenomenon has been observed in both laboratory and field studies. The general explanation is that ice crystals cannot easily incorporate alien molecules, but grow only by association. While solute retardation by sorption is included in the present analysis, the effects of precipitation/dissolution are not.

The expression for the solute flux is given by the sum of the terms for molecular diffusion, convection, hydrodynamic dispersion, and salt sieving. This flux is related to the temperature gradient, moisture gradient, solute concentration gradient, and the liquid water convection. The solute flux is defined as

$$\overline{J} = -D_{sh} \nabla c - D_{mT} \nabla T + D_{siev} \nabla \theta_l + V \theta_l c \qquad (7)$$

The conservation of energy equation for the soil system can be expressed as

141

$$A_1 \frac{\partial T}{\partial t} + A_2 \frac{\partial \theta_l}{\partial t} + A_3 \frac{\partial \theta_i}{\partial t} + A_4 \frac{\partial c}{\partial t} =$$
$$\nabla.(\lambda \nabla T) - L_v \rho_l \nabla.q_v - C_l(T - T_o)\rho_l \nabla.q_l$$
$$- (C_p q_v + C_l q_l).\nabla T \qquad (8)$$

The substitutions of eqs. (3) and (5) into eq. (1), eq. (4) into eq. (2), eq. (7) into eq. (6), and eqs. (3) and (5) into eq. (8) lead to a set of four coupled nonlinear second-order, partial differential equations. These equations provide the basis for solving for the five field variables, water pressure (or liquid water content), air pressure, ice content, temperature and solute concentration (h_l, h_a, θ_i, T, C). Alternatively we could solve for these variables using the equations in their primitive (first order or prior to substitution) forms. Regardless of the form of the equations solved, the equation set involves a complex combination of liquid water, water vapor, temperature and solute dependent conductivities, diffusivities, and gradients. Before discussing the method for solving for field variables, we need to present several parameter equations needed to compute saturation, conductivity, and capacitance.

Phase equilibria and capillary pressures

The temperature at which liquid water changes phase to ice depends on the hydraulic pressure of the water, the osmotic pressure due to solutes in the liquid water, and the pressure of the ice phase. This temperature is the phase equilibria temperature and can be derived from the Clapeyron equation (Miller 1980, Williams and Smith 1989). The equilibrium equation for pure water in equilibrium with ice is given by

$$h_l = \frac{L_f}{273} Tg + h_i \frac{\rho_l}{\rho_i} \qquad (9)$$

When solutes are present they produce a double layer effect in the form of the osmotic potential, and for this, eq. (9) is extended to account for the solute presence with

$$h_l = \frac{L_f}{273} Tg + h_i \frac{\rho_l}{\rho_i} + \Pi \qquad (10)$$

In eq. (9) the h_l is the water pressure head for pure water, while in eq. (10) the h_l is the water pressure head for the water containing solutes. The pressure heads h_l, h_i and Π are all expressed in equivalent depths of water.

Within a porous medium, the volumetric contents of various phases are usually expressed in terms of the capillary pressures between phases that have interfaces

with one another. In a system containing liquid water, ice and air, the water and ice and the air and ice will form interfaces. Thus there are two definable capillary pressures, given by

$$h_{il} = h_i - h_l$$

$$h_{ai} = h_a - h_i$$

These capillary pressures will be referenced in the next sections for definitions of phase saturations.

Liquid water content and capillary pressure relations

The relationship between the air-water capillary pressure and water saturation is described using the following three-parameter power relationship (van Genuchten 1980):

$$S_{l_e} = \frac{S_l - S_r}{1 - S_r} = \left(\frac{1}{\left(1 + [\alpha h_{al}]^n\right)} \right)^m \quad h_{al} > 0 \qquad (11)$$

$$S_{l_e} = 0 \qquad h_{al} \le 0 \qquad (12)$$

This relationship was developed to describe effective saturation in unfrozen soil conditions containing air and water. It has also been applied to other pairs of fluid phases, such as water and oil or air and oil (Parker et al. 1987) and has been extended to three phase systems containing water, air and a nonaqueous phase liquid.

The relationship given by eqs. (11) and (12) can be extended to the case of a three-phase system in unsaturated frozen soils. The three-phases present for this case are water, ice and air. Borrowing from the three-phase equations of Parker et al. (1987), we obtain for the three-phase system,

$$S_{l_e} = \frac{S_l - S_r}{1 - S_r} = \left(\frac{1}{\left(1 + [\alpha_{il} h_{il}]^n\right)} \right)^m , h_{il} > 0$$

$$S_{l_e} = 1.0 \qquad h_{il} \le 0$$

$$S_{t_e} = \frac{(S_l + S_i) - S_r}{1 - S_r} = \left(\frac{1}{\left(1 + [\alpha_{ai} h_{ai}]^n\right)} \right)^m , h_{ai} > 0$$

$$S_{t_e} = 1.0 \qquad h_{ai} \le 0$$
$$S_a = 1 - S_t = 1 - S_l - S_i$$

The parameters α_{il} and α_{ai} are related to the surface tension of the paired phases. The surface tensions between ice-water, air-ice and air-water are related by Antonov's rule (Miller 1980),

$$\sigma_{ai} = \sigma_{al} + \sigma_{il}$$

These surface tensions are related to the temperature, and such a relation is approximated by

$$\sigma_{jk}(T) = \sigma_{jk_o} e^{(T-T_o)}$$

Hydraulic conductivity and liquid water content relations

The hydraulic conductivity of the porous medium to liquid water in a porous medium containing air and water can be represented by the relation given by van Genuchten (1980),

$$K_l(S_{l_e}) = K_{ls}S_{l_e}{}^{0.5}[1-(1-S_{l_e}\frac{1}{m})^m]^2 \quad (13)$$

It is noted in this relation that the parameter m is uniquely related to the parameter n, that is $m = 1 - \frac{1}{n}$. Other forms of the unsaturated hydraulic conductivity can be derived for the more general case where m is independent of n.

Parker et al. (1987) have assumed that the relation given by eq. (13) applies to the water phase in a three-phase system where the water is the wetting phase. For the case where water, ice and air are present it will be assumed that the unsaturated hydraulic conductivity for the liquid water phase is given by eq. (13). The hydraulic conductivity of the air phase, the least wetting of the three phases, is given by

$$K_l(S_{a_e}) = K_{a_s}S_{a_e}{}^{0.5}[1-S_{t_e}\frac{1}{m}]^{2m}$$

Darcy's law does not apply to flow of water in the ice phase. Instead, the flow of the ice would be governed by viscoelastic laws rather than by Stokes' law, the basis for the Darcy flux law. Thus a different constitutive relation is needed in the governing flow equations if one wants to consider $\bar{q}_i$.

Boundary conditions

The types of boundary conditions appropriate to apply the governing equations to practical field problems are described using an example of freezing in an agricultural field situation where two-dimensional effects are significant. The solution domain of interest is illustrated in Figure 1. It involves an agricultural field with ridge tillage cultivation. Of interest is the two-dimensional

distribution of freezing and the resulting two-dimensional redistribution of solutes initially present in the soil profile. Since the ridges are equally spaced we can reduce the region considered to the smaller region contained within the dotted line.

The boundary conditions include: (1) two vertical boundaries across which periodic boundary conditions are imposed; (2) the bottom horizontal boundary along which the mass and heat energy fluxes and/or state variables can be confidently specified if the boundary is sufficiently far from the soil surface; and (3) the soil surface boundary, at which the atmospheric conditions play an important role in determining the mass flux and the energy flux across the soil surface. An example of a periodic boundary condition would be to specify that the flux passing across the left boundary equal in magnitude (and opposite in sign) to the flux passing across the right boundary.
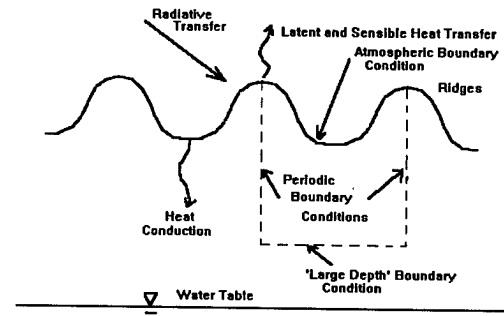
Figure 1. Profile view of the soil surface and deeper soil profile in a field cultivated with ridges. Energy fluxes are indicated.

The boundary condition at the upper boundary is represented by an energy balance equation, which includes shortwave and longwave radiation terms, and terms associated with the fluxes of latent and sensible heat across the boundary. It is the sensible heat flux and latent heat flux terms, plus the outward going longwave radiation term (function of surface temperature), which couple directly to the governing equations operating in the porous media within the solution domain. The energy balance equation is written as

$$\sum_{j=s,ld,lu} R_j - H_L - H_s = 0$$

Overview of simplifying assumptions

Mathematical solutions of coupled heat and mass transport in soils are typically constructed using a number of simplifying assumptions. In the present mathematical formulation we have made the following

143

assumptions: (1) the porous medium is rigid, that is, it does not deform by way of stresses imposed by outside or interior forces; (2) Darcy's law applies to the flux of liquid water and air, while Fick's law applies to the flux of water vapor by diffusion and Fourier's law applies to the conduction of heat; (3) the ice is immobile in the pores; (4) the ice pressure is zero; and (5) the buoyancy effect due to solute concentration gradients in the dissolved phase are negligible. These assumptions are also commonly used in most models for isothermal, as well as nonisothermal heat and mass transport in porous media. The third assumption is implicit in all models of soil freezing. The assumption of zero ice pressure is common among most models for freezing soils. Due to this assumption it is not possible to model the process of frost heaving, because that process requires that ice pressures be above zero for ice formation to overcome the overburden pressures of the overlying soil and thereby allow the formation of ice lenses. To consider the ice pressure to be nonzero would require a set of equations describing the mechanical equilibrium of the porous skeleton and the ice. Such equation could come from linear elastic theory, nonlinear elastic theory, or viscoelastic theory.

NUMERICAL SOLUTION FORMULATION

The governing partial differential equations and the boundary conditions form a set of highly nonlinear equations. At present it is impossible to derive analytical solutions for these equations, so numerical solution methods are necessary. In the following we will discuss the issues of discretizations in the temporal and spatial domains, iterative matrix solution methods, and methods for solving the nonlinear algebraic equations.

The four governing partial differential equations for the variables h_l, h_a, θ_i, T and c can be written as

$$\sum_{\Omega \in h_l, h_a, T, c, \theta_i} \left[X \frac{\partial \Omega}{\partial t} - \nabla \cdot (R \nabla \Omega) \right] + \sum_{\Lambda \in T, c; \Gamma \in l, v} \left[\nabla \cdot (\overline{q} \Gamma \Lambda) \right] = 0$$

The shorthand notation used to represent the four equations is intended to simplify the description of the numerical solution. Not all variables appear in every equation. Although there are five dependent variables listed here, only four appear in the equations as unknowns at any given location in the solution domain. At locations where the porous medium is not frozen, the variable θ_i is not included in the equations, while at locations where the porous medium is frozen the pressure variable h_l is known from the temperature T and the variable θ_i becomes an unknown in the equations.

The most common numerical methods available to solve the governing equations include the finite element method and the finite difference method. While the finite difference method is somewhat simpler to implement for regular geometries, the finite element maintains a distinct advantage for irregular geometrical regions. For many practical applications, like the one described in Figure 1, the finite element method affords greater flexibility.

The discretization of the governing equations with the finite element or finite difference method leads to a coupled set of nonlinear algebraic equations. These nonlinear equations have to be solved by sequential iterative methods like the Picard or Newton methods. The Picard method is the simpler of the two methods, but leads to much slower rates of convergence.

For multidimensional problems the discretized equations can lead to very large matrix storage requirements if direct matrix inversion methods are used. Iterative matrix solution methods can be employed to reduce the memory requirements and also to speed the rate of matrix inversion. For symmetric matrices having low condition number, methods such as the successive over-relaxation procedure, can yield satisfactory rates of matrix inversion, but for the type of matrices encountered in the present problem, the matrices are nonsymmetric and can have relatively high condition number. For this case iterative methods such as the bi-conjugate gradient method (Saad 1996) or the GMRES method (Saad 1996) are needed to attain convergence of the matrix inversion.

One final point to make here is that some of the governing equations are of the convective-dispersive or convective-diffusive type, and therefore contain convective terms, which could for some sets of physical parameters cause the solutions of the equations by conventional method to be oscillatory. These oscillatory problems usually arise for instances where the convective transport is large compared to the diffusive or dispersive transport. For the conditions considered in freezing processes, the convective component will probably not be so dominant, and therefore oscillatory behavior is not expected. However, if convective dominating conditions occur, improved solutions can be obtained by special treatment of the convective term with upstream weighting techniques, or with operator splitting methods.

REFERENCES

Ayorinde, O.A., and L.B. Perry. 1990. Fate and transport of contaminants in frozen soils. *In:* K.R. Cooley (ed.), Frozen soil impacts on agricultural, range, and forest lands, Cold Reg. Res. Eng. Lab., Special Report 90-1, p. 202-211.

Baker, G.C., and T.E. Osterkamp. 1988. Salt redistribution during laboratory freezing of saline sand columns. *In*: R.H. Jones and J.T. Holden, (eds), Proceedings, Fifth International Symposium on Ground Freezing, Balkema, Rotterdam, p. 29-33.

Beke, G.J., and C.J. Palmer, 1989. Subsurface occurrences of mrabilite in a mollisol of southern Alberta, Canada. A case study. Soil Sci. Soc.Am. J., 53:1611-1614.

Benoit, G.R., R.A. Young, M.J. Lindstrom, 1988. Freezing induced field soil water changes during five winters in west central Minnesota. Trans. ASAE, 31:1108-1114.

de Vries, D.A., 1958. Simultaneous Transfer of Heat and Moisture in Porous Media. Trans.Am. Geophys. Union, 39:909-915.

Flerchinger, G.N., and K.E. Saxton, 1989. Simultaneous heat and water model of a freezing snow-residue-soil system, 1. Theory and development. Trans. ASAE, 32: 573-578.

Freeze, R. A. 1971. Three-dimensional transient saturated-unsaturated flow in a groundwater basin. Water Resour. Res., 7:347-366.

Harlan, R.L. 1973. Analysis of coupled heat-fluid transport in partially frozen soil, Water Resour. Res., 9:1314-1323.

Iskandar, I.K., and T.F. Jenkins. 1985. Potential use of artificial ground freezing for contaminant immobilization, In: Proceedings of the International Conference on New Frontiers for Hazardous Waste Management, Pittsburgh, PA, September, 15-18, 1985, p. 128-137.

Jame, Y.W., and D.I. Norum. 1973. Heat and mass transfer in freezing unsaturated porous medium, Water Resour.. Res., 9:1314-1323.

Kay, B.D., and P.H. Groenevelt. 1983. The redistribution of solutes in freezing soil: exclusion of solutes in permafrost. *In:* Fourth International Conference, p. 584-588, National Academy of Sciences, Washington, D.C.

Miller, R.E. 1980. Freezing phenomena in soils. In: (D. Hillel, ed.), Applications of Soil Physics, Academic Press, p. 254-299.

Nassar, I.N., and R. Horton. 1989. Water transport in unsaturated nonisothermal salty soil: II. Theoretical developments. Soil Sci. Soc.Am. J., 53:1330-1337.

Nassar, I.N., and R. Horton. 1992. Simultaneous transfer of heat, water, and solute in porous media: I. Theoretical development. Soil Sci. Soc.Am.J., 56:1350-1356.

Nieber, J.L., M.J. Friedel, and H.M. Muir, 1994. VARSAT2D: Finite-Element Analysis of Variably Saturated Two-Dimensional Flow. BuMines IC 9373, 30 pp.

Panday, S., and M.Y. Corapcioglu., 1991. Solute rejection in freezing soils. Water Resour. Res., 21:99-108.

Parker, J.C., R.J. Lenhard and T. Kuppusamy, 1987. A parametric model for constitutive properties governing multiphase flow in porous media, Water Resour. Res., 23:618-624.

Philip, J.R., and D.A. de Vries. 1957. Moisture movement in porous materials under temperature gradients. Trans. Am. Geophys. Union, 38:222-232.

Pikul, J.L., and R.R. Allmaras. 1984. A field comparison of null-aligned and mechanistic soil heat flux. Soil Sci. Soc. Am. Proc., 48:1207-1214.

Saad, Y. 1996. Iterative Methods for Sparse Linear Systems, PWS Publ., 447 pp.

Seyfried, M.S., B.P. Wilcox, and K.R. Cooley. 1990. *In:* K.R. Cooley (ed.), Frozen soil impacts on agricultural, range, and forest lands, Cold Reg. Res. Eng. Lab., Special Report 90-1, p. 125-134.

Taylor, S.A., and J.W. Cary. 1964. Linear equations for the simultaneous flux of matter and energy in a continuous soil system. Soil Sci. Soc. Am. Proc., 28:167-172.

Van Genuchten, Th.M. 1980. A closed form equation for predicting the hydraulic conductivity of unsaturated soils. Soil. Sci. Soc. Am. J., 44:892-898.

Williams, P.J., and M.W. Smith. 1989. The frozen earth, fundamentals of geocryology, Cambridge University Press, Cambridge, MA, 306 pp.

Wilson, R.C., and T.S. Vinson. 1983. Solute redistribution and freezing rates in a coarse-grained soil with saline pore water, Transp. Res. Rep.,83-15, Oreg. State Univ., Corvallis.

ACKNOWLEDGMENT

APPENDIX

Definitions of terms used in the body of the text are presented here.

j index for water phase: l (liquid), i (ice), v (vapor)

θ_j volumetric water contents in phase j

$\bar{q}_j$ the volumetric flux of water phase j

ρ_j the density of water phase j

θ_a volumetric air content

ρ_a density of the air phase

$\bar{q}_a$ volumetric flux for the air phase

h_l liquid water pressure head moisture capacitance

D_{lT} thermal liquid diffusivity

D_{vT} thermal vapor diffusivity

$D_{v\theta}$ isothermal vapor diffusivity

D_{l_c} solute liquid diffusivity

D_{v_c} solute vapor diffusivity

$K_l(\theta_l)$ hydraulic conductivity for water

$K_a(\theta_a)$ hydraulic conductivity for air

T temperature

$\bar{k}$ the unit vector in the vertical direction

t time

c molal solute concentration

$\bar{J}$ molal solute flux

K_d sorption distribution coefficient

ρ_d dry bulk density of the porous medium

D_{Sh} combined diffusion-dispersion coefficient

D_{m_T} diffusion coefficient in soil solution due to temperature gradient

D_{siev} solute diffusion coefficient due to salt sieving

V average pore velocity of the liquid water

$$A_1 = C_s + \frac{\theta_a f_r}{\rho_l}\frac{\partial \rho_{v_o}}{\partial T}$$

$$A_2 = C_l \rho_l (T - T_o) + \frac{\theta_a \rho_{v_o} f_r g M}{\rho_l R T}\frac{\partial h_l}{\partial \theta_l} - \frac{\rho_{v_o} f_r}{\rho_l}$$

$$A_3 = L_f \rho_i + C_i \rho_i (T - T_o) - \frac{\rho_{v_o} f_r}{\rho_l}$$

$$A_4 = \frac{\theta_a \rho_{v_o} f_r M v \delta}{\rho_l}$$

ρ_{v_o} water vapor density at reference temperature, T_o

g gravity acceleration constant

h_i ice pressure head

Π osmotic pressure head

h_{il} ice-water capillary pressure

h_{ai} air-ice capillary pressure

h_a air pressure head

h_{al} air-water capillary pressure head

S_{l_e} effective saturation for the liquid water phase;

S_l, S_i, and S_a saturations for the water, ice and air phase respectively

S_t total saturation of the two most wetting phases, water and ice

S_{t_e} effective total saturation

α_{il}, α_{ai} capillarity parameters related to the ice-water surface tension and the air-ice surface tension, respectively

n, m empirical parameters related to the pore size distribution of the porous medium

$\sigma_{jk_o}, \sigma_{jk}(T)$ values of σ for the fluid pair (jk) at the reference temperature T_o and at the temperature T

K_{l_s}, $K_l(S_{l_e})$ saturated hydraulic conductivity and the unsaturated hydraulic conductivity of the porous medium to liquid water

K_{a_s}, $K_a(S_{a_e})$ saturated hydraulic conductivity and the unsaturated hydraulic conductivity of the porous medium to air

X symbol for generalized transport coefficient

Θ symbol for generalized capacitance coefficient

Ω, Λ symbols for generalized dependent variables

R_s, R_{ld}, R_{lu} solar radiation (shortwave), sky radiation (longwave) and outgoing radiation (longwave), respectively

H_L, H_s latent heat exchange and sensible heat exchange

Movement of Water and Ions in Frozen Clay by Electroosmosis

M. MIZOGUCHI[1], T. ITO[1], AND K. MATSUKAWA[2]

ABSTRACT

Soil decontamination is of great concern in regard to environmental problems. Although numerous attempts are being made to clean up contaminated soils with the use of in-situ and non-in-situ techniques, none of these is a panacea because of the complexity of soils and the presence of multiple contaminants. As one of in-situ cleanup methods, the combination of artificial ground freezing and electroosmosis techniques might be useful to decontaminate polluted soils. In the present study, movement of water and sodium ions has been measured in frozen clay at subzero temperatures under an electrical gradient (3 V/cm) for 24 hours. Then the experimental results have been simulated by a simple model based on a convective diffusion equation.

Key words: Electroosmosis, soil decontamination, artificial ground freezing, electric field, environmental restoration.

INTRODUCTION

Restoration of contaminated soils is becoming an important and serious problem related to industrial wastes in Japan. Application of electric fields in soils has recently been produced an in-situ means of environmental restoration. Although several methods (Probstein and Hicks, 1993, Acar and Alshawabkeh, 1993) are proposed to clean up contaminated soils by a direct-current electric field for developmental steps, the methods must be understood based on fundamental phenomena.

The principal mechanisms by which contaminant transport takes place under an electric field are electromigration, electroosmosis, and electrophoresis. In clayey soil that adsorbs most of contaminants, electroosmosis is the dominant mechanism. In electroosmosis liquid containing ions moves relative to a stationary charged surface of the soil particle. Even in frozen soil the liquid in a thin double layer can move by electroosmosis (Hoeksta and Chamberlain, 1964). When soil water freezes to ice, most ions are expelled from the ice phase and remain in the water phase. The exchangeable cations

surrounding the soil particle are crowded in the film of unfrozen water on the surface. In this unfrozen film the conditions for electroosmosis are satisfied. This characteristic of the freezing process suggests a potential of an effective soil decontamination method by the combination of freezing and electroosmosis.

The objective of the study is to understand the fundamental transport phenomena in frozen soil under an electric field. In the present study, movement of water and ions has been measured in frozen clay at subzero temperatures under an electric field in order to clarify the mechanism of electroosmosis in frozen clay. Then a simple model considering both unfrozen water content and ion concentration has been proposed to predict the movement of water and ions in frozen clay under an electric field.

EXPERIMENT

The experimental apparatus is shown in Figure 1. The experiments were conducted in a rectangular sample cell (35 mm x 80 mm x 2.9 mm) which was sealed by two plates and a 3-mm thick rubber sheet. The sample cell was small for a practical field scale, but it was adequate to understand the fundamental phenomena of electroosmosis in frozen clay. Platinum electrodes were used at each end to allow flow through the cell. Effluent was collected in a reservoir under each end.
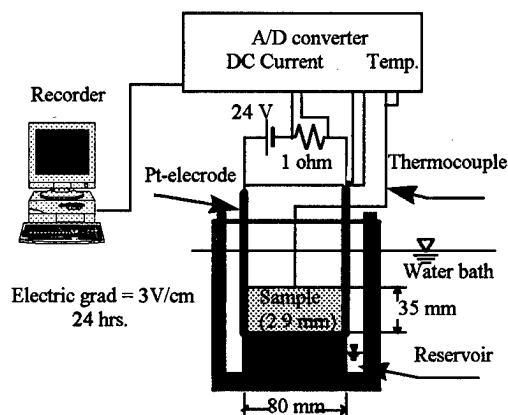
Figure 1. Experimental apparatus.

[1] Mie University, 1515 Kamihama, Tsu 514, Japan
[2] Chiyoda Corporation, Tsurumi-ku, Yokohama 230, Japan

Table 1. Experimental conditions

Initial water content (%)	300	500	500	500	700
Initial NaCl content (meq/100 g clay)	0	0	20	50	0
Temperature (°C)	-3, -2, -1, -0.5, +1	for each			

Saturated clay samples were prepared from dry powder bentonite clay, Kunimine Koukakougyou, Kunigel-V1. The dry powder was mixed with an aqueous solution of known concentration of NaCl to a liquid fraction of approximately 300%, 500% and 700 % by weight. Table 1 shows the experimental conditions. The homogenized mixture was put into the cell, removing trapped air. After being frozen rapidly in a coolant at -32 °C for 1 hour, the cell was immersed in a water bath for 24 hours to keep a desired temperature. Then a direct-current electrical potential gradient of 3 V/cm was applied across the sample cell. Freezing a sample rapidly at low temperatures has the advantage that little water movement occurs during freezing. In addition, the freezing pretreatment has also the advantage that little shrinkage of clay and little loose contact with the electrodes occur by electroosmosis comparing nonfrozen clay.

After each experiment, the clay plug was removed from the cell and sliced into eight pieces for water content and chemical analysis of the pore liquid. For the measurement of pH, 5 g of distilled water was mixed with 0.1 g of dry powder of the sliced piece and the pH of the solution was measured. For the measurement of Na^+, another 0.1 g of dry powder of the sliced piece was diluted with a 0.5 M $(NH_4)_2SO_4$, and the Na^+ concentration of the solution was analyzed using an ion chromatography.

RESULT AND DISCUSSION

Figure 2 shows moisture distribution in frozen clay at -1 °C after 24 hours under the electric field of 3 V/cm. The moisture is shown as net mass to compare dependence of initial water content. Moisture moved from the anode toward the cathode and decreased in the vicinity of the cathode. The lower the initial water content was, the more the moisture moved. The dependence of moisture movement on initial water content may be attributed to the amount of unfrozen water content, or ice content, in frozen clay. Since the sample of lower initial water content contains more clay particles, it should contain more total mass of unfrozen water adsorbed around a clay particle at -1 °C.
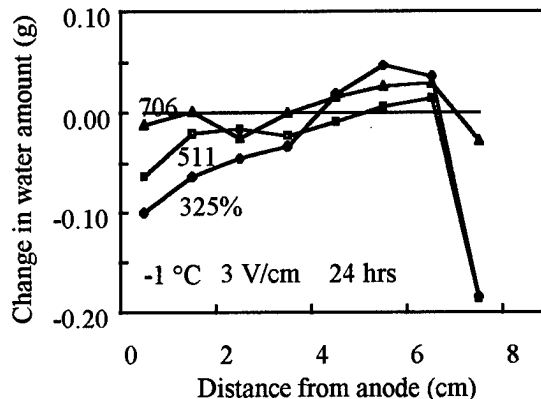
Figure 2. Moisture distribution in frozen clay at -1 °C after 24 hours under an electric field.
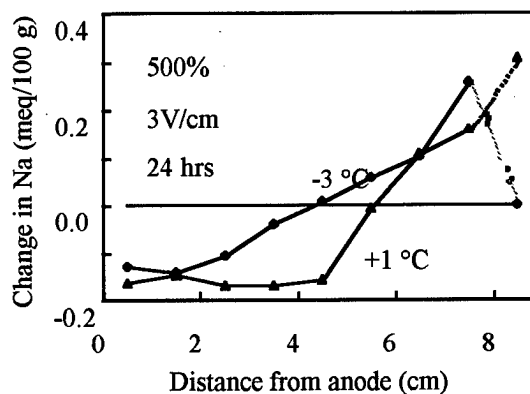
Figure 3. Na-ion distribution for frozen and nonfrozen clays after 24 hours under an electric field.

Figure 3 shows sodium distribution for frozen and nonfrozen clays with 500 % initial water content after 24 hours under the electric field of 3 V/cm. Sodium decreased in the region of the anode and increased in the region of the cathode. It should be noted that sodium can move even in frozen clay. This result indicates that the concentrated unfrozen water can move in the frozen clay by electroosmosis. While the sodium distribution was linear for frozen clay, sodium was swept at a constant concentration in the 5-cm region from the anode for nonfrozen clay. The difference of distribution between the frozen and the nonfrozen clays is attributed to flow rate of water in the sample which is affected by ice.

Figure 4 shows pH distribution for frozen and nonfrozen clays with 500 % initial water content after 24 hours under the electric field of 3 V/cm. pH also decreased in the region of the anode and increased in the region of the cathode as well as the sodium distribution. This indicates that Na^+ is exchanged by H^+ to keep electrical neutrality during

148

removal of cations by an electric field. Comparing the frozen and nonfrozen samples, pH of the frozen sample was higher than that of the nonfrozen sample. This result indicates that an acid front, which causes cation exchange and removal of sodium, advances faster in the nonfrozen sample than the frozen sample.
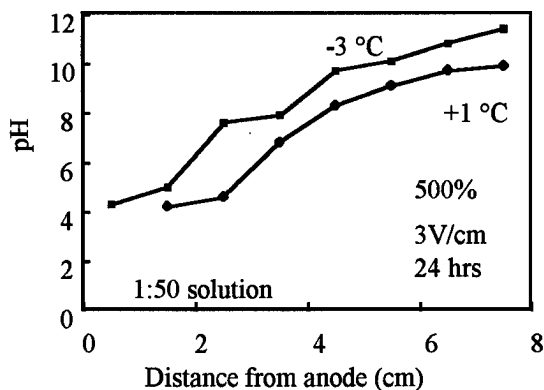
Figure 4. pH distribution for frozen and nonfrozen clays after 24 hours under an electric field.
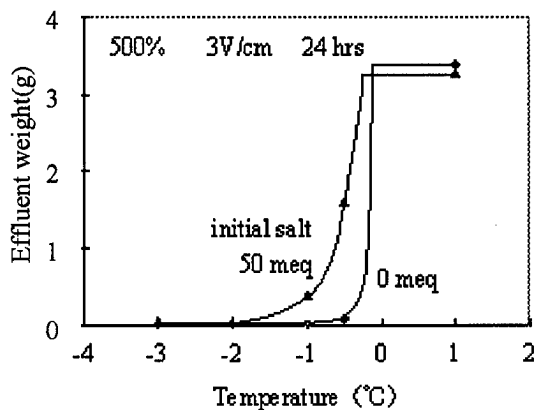
Figure 5. Effluent weight vs. temperature after 24 hours under an electric field.
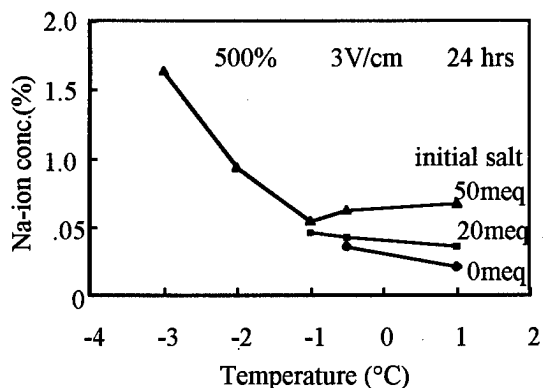
Figure 6. Na-ion concentration in effluent.

Figure 5 shows effluent weight vs. temperature for samples containing sodium chloride with 500 % initial water content after 24 hours under the electric field of 3 V/cm. Plots are experimental and lines are presumed from unfrozen water content obtained by Mizoguchi and Nishizawa (1993). Little water was moved in the frozen sample compared to the nonfrozen sample. This result indicates that freezing is a disadvantage in dewatering from the sample. However, as the sample contains salt, dewatering appeared dependent on both temperature and salt concentration even in the frozen sample. Moreover, sodium concentration was higher in the effluent from the frozen sample than the nonfrozen sample, and increased with decreasing temperature as shown in Figure 6. The high concentration in effluent at low temperature may be attributed by the mechanism of freezing and electroosmosis, in which most ions are expelled from the ice phase and concentrated into the residual unfrozen liquid when soil water freezes, and the concentrated unfrozen liquid is moved by electroosmosis.

In the application of electric methods to decontaminate soils, the cost to move the pore fluid is proportional to the electroosmotic flux, independent of the contaminant concentration (Probstein and Hicks, 1993). However, freezing has the advantage in both concentrating ions and reducing the fluid movement. In addition, although spacial variation in permeability can nullify the decontamination process if electroosmotic flow in the fine soils induces a pressure gradient that causes a return flow through the coarser region (Probstein and Hicks,1993), freezing can keep the thin double layer for the electoosmotic flow according to the temperature. Thus, the combination of freezing and electroosmosis has a great potential to decontaminate polluted soils.

NUMERICAL ANALYSIS

The convective liquid velocity from electroosmosis is proportional to the zeta potential ζ of the surface and to the applied electric field strength E. For a thin double layer in comparison to the pore size, this velocity is given by the Helmholz-Smoluchwski relation (Probstein and Hicks, 1993):

$$u_{eo} = \varepsilon \zeta E / \mu \tag{1}$$

where ε is the permittivity of the solution and μ is its viscosity. From the definition of electric field strength,

149

$$E = -\frac{d\phi}{dx} \qquad (2)$$

where ϕ is the electric potential. In electromigration the ion velocity is proportional to the electric field strength and the ionic charge number z (Probstein and Hicks, 1993):

$$u_{em} = vzFE \qquad (3)$$

where v is the ion mobility and F is Faraday's constant. Diffusion can also play an important role in the transport of ions and water in the soil. The diffusion velocity is given by

$$u_{df} = -D\frac{dC}{dx} \qquad (4)$$

where C is the concentration of water or ions, and D the diffusivity.

Because of interaction between water and ions, hydration, we cannot distinguish strictly electroosmosis from electromigration in a soil under an electric field; water molecules will be dragged simultaneously when the ions move by electromigration and excessive ions will be transported together with the water molecules moved by electroosmosis. Therefore, we define here the mass velocity of water or ions by an electric field to be simply proportional to electric field strength without distinction between electroosmosis and electromigration;

$$u_{ef} = kEC \qquad (5)$$

where k is an empirical constant, electrical mass flow factor, determined for a specific soil system.

Considering mass balance based on eqs. (4) and (5), a convective diffusion equation is obtained:

$$\frac{\partial C}{\partial t} = \frac{\partial}{\partial x}\left(D\frac{\partial C}{\partial x}\right) - \frac{\partial}{\partial x}\left(kC\frac{\partial \phi}{\partial x}\right) \qquad (6)$$

Applying a low-order finite differential method to eq (6) yields the following equation:

$$C_{i,j+1} = C_{i,j} + rD(C_{i+1,j} - 2C_{i,j} + C_{i-1,j})$$
$$+ rk\{C_{i-1,j}(\phi_{i,j} - \phi_{i-1,j}) + C_{i,j}(\phi_{i+1,j} - \phi_{i,j})\}$$
$$(i = 2 \text{ to } 7) \qquad (7)$$

$$r = \frac{\Delta t}{\Delta x^2} \qquad (8)$$

where $C_{i,j}$ represents the mass content of water or ions, molar per unit volume of frozen clay, in the i-th element at the j-th time. This equation is applicable to the elements without the electrodes. Note that we discuss eight elements here corresponding to the experiment and that k and D are constants. Applying a series resistance model for the frozen clay, an electric potential at each element, ϕ_i, can be determined by the Ohm's law:

$$\phi_i = \phi_0\left(1 - \frac{\sum_{n=1}^{i} R_n - \frac{R_i}{2}}{\sum_{n=1}^{8} R_n}\right) \qquad (9)$$

where ϕ_0 is the electric potential at the anodes. Assuming that each resistance is proportional to the element length, Δx, and inversely proportional to the cation concentration of unfrozen water, CN_i, at each element,

$$R_i = \beta\frac{\Delta x}{CN_i} \qquad (10)$$

where β is a constant. Substituting eq. (10) to (9) gives the relation between ϕ_i and CN_i:

$$\phi_i = \phi_0\left(1 - \frac{\sum_{n=1}^{i} \frac{1}{CN_n} - \frac{1}{2CN_i}}{\sum_{n=1}^{8} \frac{1}{CN_n}}\right) \qquad (11)$$

It should be noted that an electric potential is a function of the cation concentration of unfrozen water at each element.

At the electrodes, water is consumed by electrolysis:

$$2H_2O \rightarrow 4H^+ + O_2(g) + 4e^- \quad \text{at anode} \qquad (12)$$

$$2H_2O + 2e^- \rightarrow 2OH^- + H_2(g) \quad \text{at cathode} \qquad (13)$$
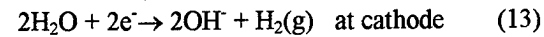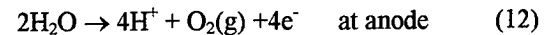
Therefore, the boundary conditions for water movement are given by

150

$$CW_{1, j+1} = CW_{1, j} + rD(CW_{2, j} - CW_{1, j})$$
$$+ rkCW_{1, j}(\phi_{2, j} - \phi_{1, j}) - I\frac{\Delta t}{2F\Delta V}$$

<div align="right">at anode   (14)</div>

$$CW_{8, j+1} = CW_{8, j} + rD(CW_{7, j} - CW_{8, j})$$
$$+ rkCW_{7, j}(\phi_{7, j} - \phi_{8, j}) - I\frac{\Delta t}{F\Delta V}$$

<div align="right">at cathode   (15)</div>

where ΔV is the volume of an element, I the direct current, and $I=\phi_0/\Sigma R_n$. Since there is no consumption, on the other hand, the boundary conditions for sodium movement are given by

$$CN_{1, j+1} = CN_{1, j} + rD(CN_{2, j} - CN_{1, j})$$
$$+ rkCN_{1, j}(\phi_{2, j} - \phi_{1, j})$$

<div align="right">at anode   (16)</div>

$$CN_{8, j+1} = CN_{8, j} + rD(CN_{7, j} - CN_{8, j})$$
$$+ rkCN_{7, j}(\phi_{7, j} - \phi_{8, j})$$

<div align="right">at cathode   (17)</div>

Table 2. Model parameters used in numerical analysis for water and ions movement in frozen clay by electroosmosis

Sample length	$L = 8$ (cm)
Applied voltage	$\phi_0 = 24$ (V)
Element length	$\Delta x = 1$ (cm)
Time step	$\Delta t = 600$ (sec)
Element volume	$\Delta V = 1.02$ (cm^3)
Electrical mass flow factor	$k=3\times10^{-6}$ (cm^{2}V^{-1}sec^{-1})
Diffusivity for water	$DW=1\times10^{-5}$ (cm^{2}V^{-1}sec^{-1})
Diffusivity for Na ion	$DN=1\times10^{-6}$ (cm^{2}V^{-1}sec^{-1})

The parameters used in the model are listed in Table 2. The calculation can be made easily to get some graphs setting some parameters on a worksheet. Figure 7 shows comparison of model and experiment for moisture distribution under the electric field of 3 V/cm for 24 hours. Excellent agreement is observed between the model and experiment: decrease at the anode and increase at the cathode, and easy movement at lower water content. Despite

considering water consumption of water by electrolysis at the electrodes, the model did not simulate the rapid decrease in moisture at the cathode observed in the experiment. This difference between the model and experiment indicates that there are other mechanisms than electrolysis for the decrease in moisture at the cathode.
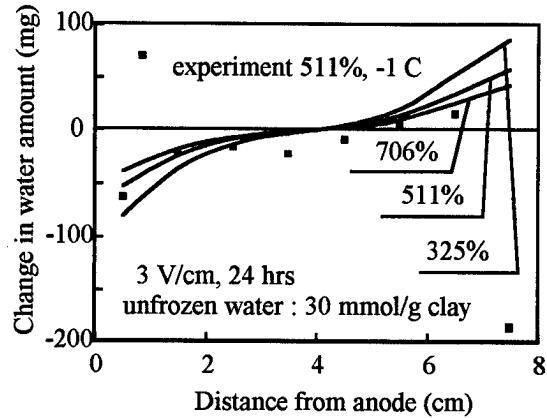
Figure 7. Comparison of model and experiment for moisture distribution under an electric field.
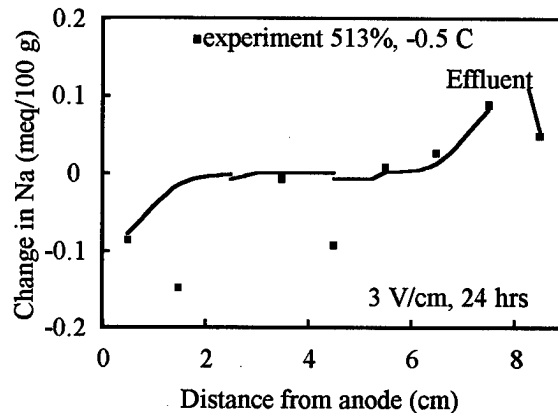
Figure 8. Comparison of model and experiment for Na ion distribution under an electric field.

Figure 8 shows a comparison of model and experiment for Na distribution under the electric field of 3 V/cm for 24 hours. The model simulated well the Na movement in the frozen clay at -0.5 °C due to an electric field. The present model may be useful for predicting the distributions of moisture and cation in frozen clay under an electric field, despite the simplifying assumptions including convective flow and diffusion. Given an appropriate boundary condition at the cathode, information on effluent,

such as effluent amount and concentration, will be obtained by the model. In addition, pH distribution in soil and concentration in effluent may be predicted by an advanced model considering the acid front and cation exchange.

CONCLUSION

To understand the fundamental phenomena in frozen soil under an electric field, movement of water and ions has been measured in frozen clay at subzero temperatures. It was found from the experiment that as the water content was low, and as the initial salt and the temperature content were high, water in the frozen clay was easy to move by an electric field. In addition, as the temperature was low, an insignificant amount of unfrozen water was removed with high cation concentration. These results suggest that soil freezing process has a potential for an effective removal of contaminants from polluted soil as a method for pretreatment before electroosmosis. A numerical analysis also indicates that a simple model of coupled electrolysis, diffusion and convection flow is applicable to predict the transport phenomena in frozen soil under an electric field. Although more studies are needed on full scale applications, such as soil type, contact with the electrodes, freezing method and applicable species of ions, the combination of freezing and electroosmosis techniques will have great promise for an effective means of decontaminating waste sites.

REFERENCES

Acar, Y. B. and A N. Alshawabkeh. 1993. Principles of electrokinetic remediation. Environ. Sci. Technol. 27:2638-2647.

Acar, Y. B., A N. Alshawabkeh and R. J. Gale. 1993. Fundamentals of extracting species from soils by electrokinetics. Waste management. 13: 141-151.

Hoekstra, P. and E. Chamberlain. 1964. Electroosmosis in Frozen Soil. Nature. 203:1406.

Mizoguchi, M and J. Nishizawa. 1993. Measurement of unfrozen water content in saline frozen clay by NMR method. Proceedings of Japanese Society of Irrigation, Drainage and reclamation Engineering. 40-41. (In Japanese)

Mizoguchi, M and K. Matsukawa. 1996. Concentration methods for contaminates in soil. Japanese Patent. H8-243536.

Probstein, R. F. and R. E. Hicks. 1993. Removal of contaminants from soils by electric fields. Science. 260:498-503.

Soil Electrical Properties Modified by Freezing

G.C. McINTOSH[1] AND B.S. SHARRATT[2]

ABSTRACT

Freezing modifies various electrical properties of soils. The electrical modifications, changes in the conductivity (resistance) and dielectric constant and the generation of a small potential difference across the frozen/unfrozen interface, can be used to determine the location of the freezing front through automated techniques. We conducted a laboratory experiment to investigate the change in the resistance as the soil freezes and to use this change to monitor the location of the freezing front. We found that the slope of the resistance vs. time curve changed distinctly at the depth of the 0°C isotherm, and the change accurately indicated the depth of frost.

Key words : Electrical resistance, soil freezing.

INTRODUCTION

Determining the depth of frost is useful in many modeling programs describing water and heat flow in soils. This information is also necessary for estimating burial depths of water lines and in ecosystem management, as snow melt runoff can impact soil degradation and nutrient availability.

A standard technique for determining the frost depth in soils is through the use of the frost tube. The frost tube is a plastic tube filled with water and dye or with a sand, water and dye solution. The tube is inserted vertically into a plastic pipe that is buried in the soil. As the water in the tube freezes, the dye is expelled from the ice and a line of demarcation indicates the depth of frost. The frost tube requires human intervention to determine and record the frost depth.

As soils freeze, there are changes in various electrical properties, including the dielectric constant, the electrical potential difference, and the electrical resistance. These changes can be used to automatically monitor the depth of frost. The change in the dielectric constant can be ascertained by

153

monitoring the change in capacitance (Brach et al. 1985) or in the wave propogation velocity (Baker et al. 1982) to determine the frost depth. Yarkin (1986) indicated that a measurable potential difference is generated across the freeze front that might be used to determine the depth of frost. Outcalt et al. (1989) and Outcalt and Hinkel (1996a; 1996b) have used measurements of the electrical potential to determine the soil-water solute concentration and how it changes in freezing soil. The electrical resistance of a soil also changes as the soil freezes. Hayhoe and Balchin (1986) used electrical current passed through steel rods at different depths in a soil to determine the depth of frost. Atkins (1989) developed an electrical resistance probe to monitor the frost depth under a paved surface.

The objective of this study was to continue the investigation of the electrical resistance changes of freezing soils, to compare various techniques for determining the frost depth in soils, and to develop an automated probe to determine the depth of frost in soils.

THEORY

Electrical conductivity
The electrical conductivity, σ (Ω^{-1} m^{-1}), of a material is related to the density, charge, and mobility of charge carriers by the equation (Blakemore 1974):

$$\sigma = nq^2 \frac{\tau}{m} \qquad (1)$$

where n is the density of charge carriers (m^{-3}), q is the electrical charge (C), τ is the mean time between collisions (s), and m is the mass of the charge carrier (kg). The mean time between collisions, τ, depends on the motion of the charge carriers. For example, as the soil becomes colder or as water changes from the liquid to the solid, the mobility of the charge carriers is greatly constrained. Therefore, τ decreases as does the conductivity of a soil.

The conductivity of partially frozen soil can be partitioned as follows (Hoekstra 1965):

$$\sigma = \sigma_P + \sigma_I + \sigma_F \qquad (2)$$

where σ is the total conductivity, σ_P is the conductivity of the soil particles, σ_I is the conductivity of the ice, and σ_F is the conductivity of a film of unfrozen water and solutes that coats the soil particles. This film is responsible for the bulk of the conductivity of frozen soils (Hoekstra 1965).

Electrical resistance
The resistance, R (Ω), depends on σ and the geometry of the sample measured according to:

$$R = \frac{l}{\sigma A} \qquad (3)$$

where l (m) is the length of the sample or the distance through which the charge carriers move and A (m^2) is the cross-sectional area through which the charge carriers move.

Resistance measurements

For many materials, including soils, an electrical bridge circuit can be used to determine resistance. This technique requires applying a voltage to a series combination of the sample of unknown resistance R_s and a known, fixed resistor R_F. The total voltage V applied can be compared with the voltage drop measured across the unknown resistance V_s to measure R_s. The equation describing this relationship is

$$\frac{V_s}{V} = \frac{R_s}{R_s + R_F}. \qquad (4)$$

Solving for R_s

$$R_s = R_F \frac{V_s/V}{1-(V_s/V)}. \qquad (5)$$

EXPERIMENT

An experiment was carried out to ascertain how the electrical resistance of an agricultural soil changes upon freezing and thawing. Although Atkins (1989) and Hayhoe and Balchin (1986) measured changes in electrical resistance of soil undergoing freezing, there is a lack of comparisons of different techniques for detecting the frost depth in soils.

Method

A resistance probe, based on the design of Atkins (1989), was used to measure soil electrical resistance. The 1-m-long resistance probe was made from a 1-in. (2.5-cm) PVC pipe. One strand of 20-gauge wire was wrapped around half of the circumference of the

pipe at 1-cm increments. The depth of measurement was from 1.0 to 33.0 cm. Resistances were measured between nearest pairs of wires using a data logger (Campbell Scientific, Inc. CR-10). The 32 resistance measurements were multiplexed to the data logger. An AC bridge circuit was used to make the measurements to avoid the electrical polarization of the water molecules. Such polarization would affect the repeatability of the resistance measurements. The circuit used in our study is illustrated in Figure 1.
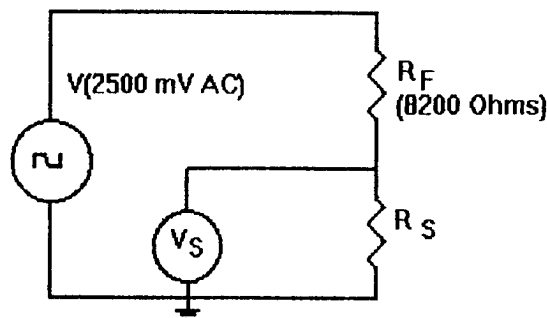
Figure 1. Schematic of the AC bridge circuit used to determine R_s.

A thermocouple probe was used to measure soil temperatures. The 1-m-long probe was constructed from 1-in. (2.5-cm) PVC with copper-constantan thermocouple connections protruding through the sidewall of the pipe and cemented to the pipe at 1.0-cm intervals to a depth of 30.0 cm. The thermocouples were multiplexed to a data logger. A frost tube was constructed for determining the depth of soil frost. The 1-m-long tube was constructed of 1/2-in. (1.3-cm) Tygon tubing filled with a water-fluorescent dye solution. A thread was suspended down the center of the tube to stabilize the
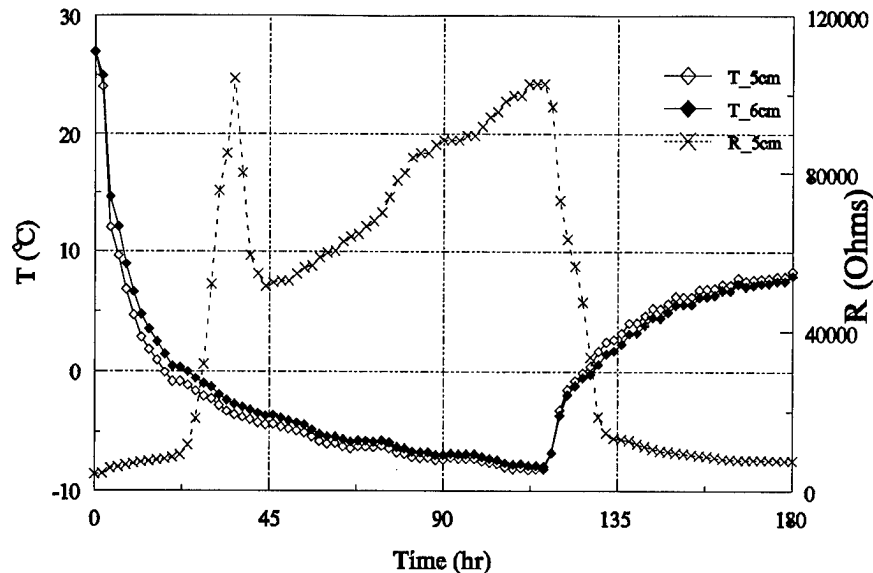
Figure 2. Soil temperature at a depth of 5- and 6-cm and the resistance between 5- and 6-cm as a function of time.

column of ice. This water-filled tube was inserted into a 1/2-in. (1.3-cm) PVC pipe.

The resistance probe, thermocouple probe, and frost tube were placed in the center of a 0.3-m-diam., 1.0-m-long PVC pipe. Soil (Barnes loam) with a water content of 25% by volume was packed into the pipe at a density of 1.2 Mg m^{-3}. Soil was tamped around the probes and tube to ensure good thermal contact.

The experiment was carried out in a controlled temperature freezer set to maintain a temperature of -10±1°C. The soil was allowed to freeze throughout the 0.3-m measurement depth after which the freezer temperature was set to +10±1°C. The soil column froze to a depth of 30 cm in approximately four days, whereas the column thawed in about three days.

Soil resistance and temperature sensors were monitored at 60-s intervals. Data were averaged over 5-minute intervals. The frost tube was monitored periodically throughout the experiment.

RESULTS

Typical data of the variation in resistance and temperature as the soil column froze and thawed are illustrated in Figure 2. These data are from the 5- to 6-cm depth. Since the resistance probe measures the resistance between two depths in the soil, the temperatures at both depths are included in the figures. The distinct changes in the slope of the resistance vs. time curve indicate the change in state of the soil water from liquid to solid and vice versa. These distinct changes occur as the
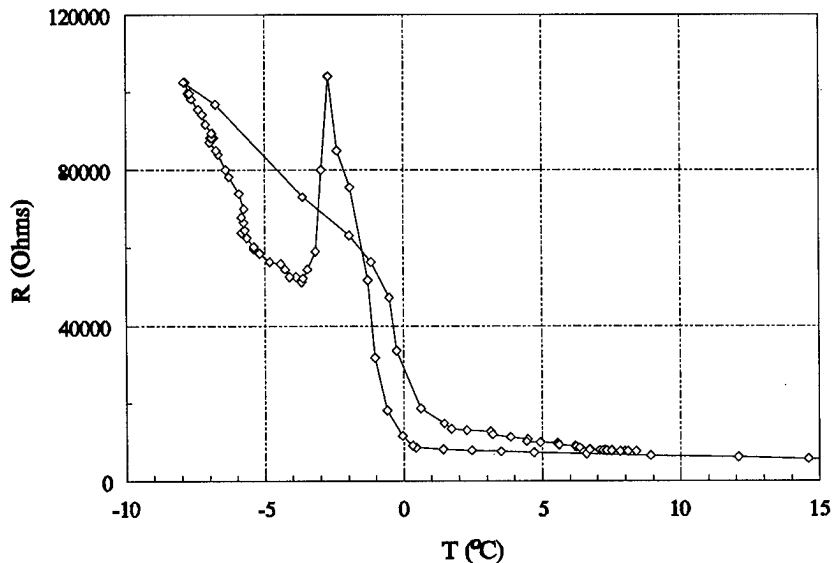
Figure 3. The resistance between 5- and 6-cm as a function of the temperature at 6-cm.

temperature, monitored by the thermocouple probe, crosses the 0°C isotherm.

The distinct changes in the slope of the resistance curves indicate the change in the mobility of the charge carriers as described in equation 1. As the water in the bulk of the soil freezes, the current paths are restricted between soil particles by the less conductive ice. However, a film of higher conductivity liquid water remains around the soil particles at temperatures below 0°C. The resistance changes from one dominated by the mobility of charge carriers in bulk water to one dominated by the decreased mobility of charge carriers along the surfaces of the soil particles, and the measured resistance increases. This process is reversed as the soil thaws.

Another change in the slope

of the resistance vs. time curve occurs as the soil cools from approximately -2 to -4°C (Fig. 2). This change appears to be associated with the change in state of the soil water and is being investigated. Inaccuracies in the measurement system may result as the resistance of the soil increases, where, as V_S approaches V, the circuit is less accurate. Therefore, small changes in V_S result in very large changes in the calculated R_S (see equation 5). This increased inaccuracy may contribute to the observed slope change. Increasing the value of R_F should improve the response of the system at low temperatures as the ratio of V_S to V would be smaller and measured more accurately.

Figure 3 displays the resistance of the 5- to 6-cm depth vs. the temperature, T (°C), at 6-cm. Again changes in the slope of the curve

157
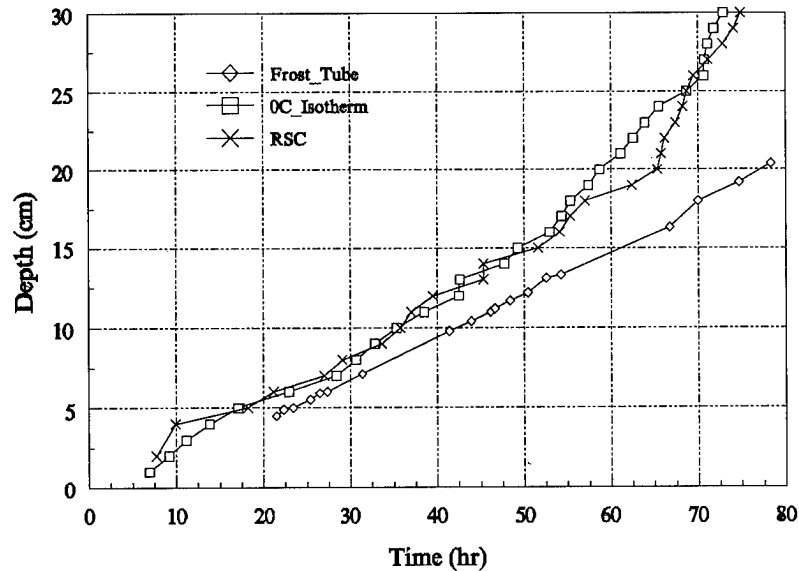
Figure 4. The depth of the RSC, the 0°C isotherm, and the ice depth in the frost tube as a function of time.

indicate the change in the number and/or mobility of the charge carriers. This curve also shows the unexpected reduction in the resistance as the soil cools from -3°C to -4°C at this depth. At temperatures below -4°C the resistance increases as the film of liquid water surrounding soil particles thins, and the water becomes more viscous. The resistance is generally larger during the thawing of the soil than during the freezing of the soil. This increase in resistance may be due to a reduction in the number and mobility of available charge carriers as a result of the freeze/thaw cycle. Soil water is purified through the freezing process (Outcalt et al. 1989) and moisture is lost from the soil during the frozen period (Outcalt and Hinkel 1996a).

Figure 4 compares the data from the resistance probe, thermocouple, and frost tube as the soil froze. The depth at which a change occurred in the slope of the resistance probe data is plotted against time. The thermocouple data indicate the location of the 0°C isotherm with time. The frost tube data indicate the position of the ice depth in the tube vs. time. The 0°C isotherm and the change in the slope of the soil resistance generally follow each other quite well. The frost tube ice depth lagged behind the resistance and temperature measurements. This lag may be due the freezing point depression of the frost tube solution as the ice depth in the tube followed the -1°C isotherm.

CONCLUSIONS

The resistance probe used in

this experiment can be used to locate and monitor the motion of the frost depth in soil automatically. Specific samples and depths vary in the value of the resistance, but the change in slope of the resistance vs. time curve is similar at all depths. Further development is needed to improve the methodology and produce a general algorithm to extract the location of the frost depth from the shape of the resistance vs. time curve.

REFERENCES

Atkins, R.T. 1989. Determination of frost penetration by soil resistivity measurements. Symposium on State of the Art of Pavement Response Monitoring Systems for Roads and Airfields. 87-100.

Baker, T.H.W., J.L. Davis, H.N. Hayhoe, and G.C. Topp. 1982. Locating the frozen-unfrozen interface in soils using time domain reflectometry. Can. Geotech. J. 19:511-517.

Blakemore, J.S. 1974. Solid state physics, 2nd ed. Saunders Co., Philadelphia

Brach, E.J., A.R. Mack, H.N. Hayhoe, and B. Scobie. 1985.

Ag. and For. Meteor. 34:173-181.

Hayhoe, H.N. and D. Balchin. 1986. Electrical determination for soil frost. Can. Agri. Eng. 28:77-80.

Hoekstra, P. 1965. Conductance of frozen bentonite suspensions. Soil Sci. Soc. Proc. 29:519-522.

Outcalt, S.I., D.H. Gray, and W.S. Benninghoff. 1989. Soil temperature and electric potential during diurnal and seasonal freeze-thaw. Cold Regions Science and Technology. 16:37-43.

Outcalt, S.I., and K.M. Hinkel. 1996a. Thermally driven sorption, desorption, and moisture migration in the active layer in central Alaska. Phys. Geog. 17:77-90.

Outcalt, S.I., and K.M. Hinkel. 1996b. The response of near-surface permafrost to seasonal regime transitions in tundra terrain. Arc. and Alp. Res. 28:274-283.

Yarkin, I.G. 1986. USA Cold Regions Research and Engineering Laboratory, CRREL Special Report 86-12.

Tillage, Management and Erosion

Tillage Induced Air Permeability
Modified by Soil Freezing

B.S. SHARRATT[1] AND D. HUGGINS[2]

ABSTRACT

Air permeability is intrinsically related to soil structure and is influenced in part by soil water content and porosity. This study determined the extent to which freezing and thawing affects the structure of a loam by measuring changes in air permeability. Soil cores were extracted from tillage plots (moldboard plow, ridge, and none) following corn harvest in the fall of 1993 in Minnesota. Side-wall flow between the soil and plastic pipe was minimized by pouring a band of rubberized asphalt between the pipe and soil. The cores were saturated and allowed to drain, after which an air permeameter was connected to the pipe for measuring air flow through the soil core before freezing and after one, five, and 10 freeze-thaw cycles. Prior to freezing, air permeability was greatest for moldboard plow (0.04 mm^2) compared to ridge tillage and no tillage (0.02 mm^2). One freeze-thaw cycle resulted in an increase in permeability for all tillage treatments, which appeared to persist after 10 freeze-thaw cycles. Enhanced permeability of the tillage treatments suggests that freezing and thawing can create fracture planes and pathways in soils for more rapid movement of air and water.

Key words: Porosity, soil structure, soil stability.

INTRODUCTION

Soil structure comprises the arrangement of soil particles, soil aggregates, and the accompanying pore space. This arrangement influences the transmission of soil water and air, both of which are important for the growth and productivity of plants. Structure also governs mechanical impedance and thus the mobility of soil fauna as well as the stability of soils. Despite the importance of soil structure in engineering applications and crop production systems, our understanding is incomplete concerning environmental factors which cause change in soil structure.

Forces exerted by freezing and thawing can cause changes in soil structure. Indeed, fracture planes and sorting of soil particles can develop owing to repeated freezing and thawing (van Vliet-Lanoe and Coutard, 1984). Degradation of structure is also evident in northern climate regions where exposed aggregates near the soil surface erode during the winter from repeated freezing and thawing or freeze-drying (Staricka and Benoit, 1995).

Soil structure has been assessed qualitatively based upon the visual arrangements of soil particles and aggregates in a soil profile. Fish and Koppi (1994) observed, however, that changes in soil structure can be quantified by assessing the intrinsic permeability of soil to air. Larin (1963) used air permeability as an index for measuring changes in soil structure caused by freezing and thawing. Larin (1963) noted that air permeability was inversely related to water content of a frozen soil. In addition, the porous structure created by fall tillage resulted in a greater permeability compared with no tillage prior to spring snowmelt in the USSR.

Soil structure modified by tillage in the fall is subject to change during the winter in the northern United States. Indeed, the occurrence of sub-freezing temperatures in this region affects the integrity of the soil matrix as a result of forces

exerted by pore ice. The purpose of this study was to ascertain whether repeated freezing and thawing affects the structural stability of soils subject to different tillage practices in the North Central United States.

METHODS

Air permeability was determined on soil core samples taken from tillage plots located near Lamberton, Minnesota (44°15'N, 95°20'W). Samples were collected after corn harvest and tillage operations in the fall of 1993. Tillage plots included no tillage (no disturbance to the soil other than from the planting operation), ridge tillage, and conventional tillage. Ridge tillage consisted of row cultivating after crop emergence (June) whereas conventional tillage consisted of fall moldboard plow, spring disk before planting, and row cultivation after crop emergence. Plots were established on a Normania loam (fine-loamy, mixed mesic Aquic Haplustolls) in 1986 and cropped in alternate years to corn and soybeans. Soil characteristics of the three tillage treatments are presented in Table 1.

Soil cores

Soil core samples were taken by tamping plastic pipe, 0.3 m diameter, by hand 0.30 m into the soil. The inside of the pipe was coated with PAM to facilitate ease of inserting the pipe into the soil. The pipe was excavated and transported to a laboratory for assessing air permeability. The bottom of the soil core was trimmed to achieve a planar surface. To minimize preferential flow along the sidewall of the pipe, soil adjacent to the sidewall on the top and bottom of the soil core was excavated to a depth of 0.05 m. The resultant gap between the soil and pipe was filled with rubberized asphalt. Cheese cloth was secured to the bottom of the soil core, after which the core was placed upright on a rigid metal screen. The soil core-screen assembly was inserted into a tray of de-aerated water for 48 h to facilitate saturating the core in a constant temperature room (20°C). The soil core was then allowed to drain for 24 h prior to obtaining the weight of the core.

Air permeability

The core-screen assembly was placed on a support to ensure air exchange beneath the assembly, after which an air permeameter was secured to the top of the pipe. A constant flow of saturated air was maintained into the hood of the permeameter at a rate of 71.2 mm³ h⁻¹. Air pressure was measured inside the hood of the permeameter after the air flow stabilized, usually within 60 s. Concurrent measurements included ambient air temperature and pressure.

Air permeability was assessed prior to soil freezing and after one, five, and 10 freeze-thaw cycles. After measuring air permeability of the soil core, the core was insulated on all sides except at the top. A 0.2-m layer of fiberglass insulation was wrapped around the pipe to facilitate a one-dimensional freeze and thaw. The insulated core was placed inside a freezer, maintained at -20°C, for 48 h. The core was then removed from the freezer to the constant temperature room and allowed to thaw for 48 h prior to measuring air permeability. The duration of the freezing and thawing cycle was sufficient to achieve temperatures below or above 0°C throughout the soil core. The top of the core was covered with plastic for the duration of the experiment, except during the measurement of air permeability, to prevent soil evaporation.

Air permeability was calculated using the steady-state convective air flow equation:

$$Q = -K_a A(\Delta P)$$

where Q is volumetric air flux (mm³ s⁻¹), K_a is the conductivity of the soil to air (mm s⁻¹), A is the cross sectional area of the soil core (m⁻²), and P is the gradient in soil air pressure (mm mm⁻¹). Air permeability is related to the apparent air conductivity by the equation:

$$K_a = (0.001k_a\rho g)\mu^{-1}$$

where k_a is permeability (mm²), ρ is air density (g mm⁻³), g is the gravitational acceleration (mm s⁻²), and μ is the air dynamic viscosity (g mm⁻¹ s⁻¹). Air density and viscosity were determined at the measured ambient air temperatures and pressures.

RESULTS AND DISCUSSION

Air permeability was determined on soil cores that were nearly saturated at a volumetric water content of 0.45 and water potential of 0.03 MPa (Table 1). Although soil water content affects changes in structure that arise as soils freeze, no attempt was made to include water content as a variable in this study. Structural changes, however, would be magnified in this study because changes

162

Table 1. Soil physical properties of moldboard plow, ridge-tillage, and no-tillage treatments.[*]

Tillage treatment	Bulk density (kg m⁻³)	Particle size distribution			Matric potential (kPa)	Volumetric water content
		sand	silt (%)	clay		
No	1.39	44	30	26	- 0.4	0.27
Ridge	1.40	47	29	24	-0.3	0.27
Conventional	1.43	49	27	24	-0.4	0.33

[*] data for 0-0.3 m depth, except matric potential and particle size determined for 0-0.15 m depth.

are more pronounced as wet compared to dry soils freeze and thaw (Pawluk, 1988).

Prior to freezing the soil core samples, the air permeability of the moldboard plow treatment was greater than the ridge-tillage and no-tillage treatments. Air permeability was 0.040 mm² for moldboard plow, 0.031 mm² for no tillage, and 0.022 mm² for ridge tillage. The greater apparent permeability of the moldboard plow may be caused by the fracture planes resulting from the fall tillage operation. Larin (1963) noted that the air permeability of a clay loam was greater when subject to the moldboard plow compared with no cultivation. Larin's findings, however, were assessed while the soil was frozen and several months after fall tillage in the USSR.

Permeability of all tillage treatments increased after one freeze-thaw cycle (Fig. 1). An increase in permeability of 160% was measured for the moldboard plow whereas permeability increased by 45% for no tillage and 35% for ridge tillage. This suggests that pore size or continuity increased and/or that tortuosity of flow paths decreased after freezing and thawing. The large change in permeability of the moldboard plow may result from the furrow slice fracturing with freezing and thawing. Fracturing of the furrow slice may result from either desiccation or ice segregation, both of which create more cleavage planes through which air flows. Enhancement of permeability of soils caused by freezing was also observed by Chamberlain and Gow (1979). They observed that the permeability of fine-grained soils increased after freezing and thawing due to the development of shrinkage cracks during freezing.

As freezing and thawing intensified (more cycles), permeability declined for the no-tillage and moldboard plow treatments (Fig. 1). Air permeability decreased by 30 and 20% for no tillage and moldboard plow, respectively, between the first and fifth freeze-thaw cycles. The soil matrix of

these tillage treatments possibly consolidated following the first freeze-thaw cycle. The decrease in permeability of no tillage and the moldboard plow suggests an instability of flow paths with further freezing and thawing. In contrast to no tillage and moldboard plow, permeability of ridge tillage increased by 85% between the first and fifth freeze-thaw cycle.

No change in permeability was noted for the moldboard plow treatment between the fifth and tenth freeze-thaw cycle. Permeability of no tillage, however, increased by 20% whereas permeability of ridge tillage decreased by 35%.
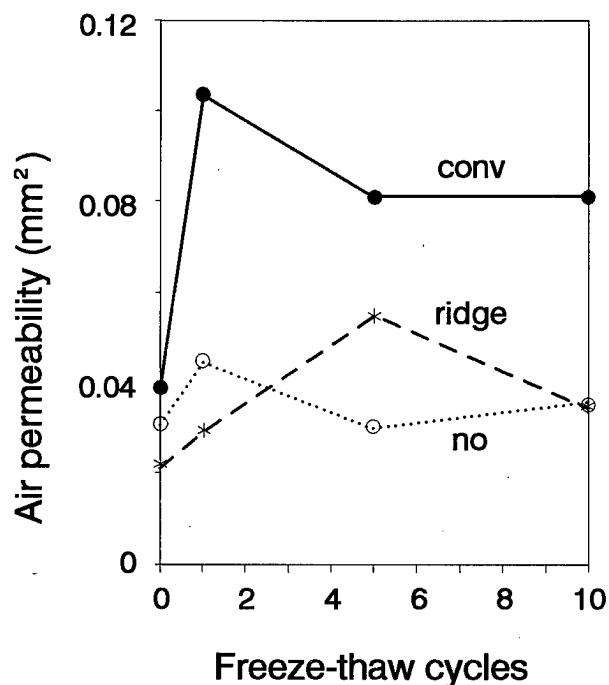
Figure 1. Air permeability of a loam subject to conventional (conv), ridge, and no tillage and as a function of cyclic freezing and thawing.

163

Soil freezing and thawing increased air permeability of the three tillage treatments. In addition, permeability after 10 freeze-thaw cycles appeared to be enhanced by more intensive tillage. For example, permeability of moldboard plow (the most intensive tillage treatment) increased by 107%, from 0.040 to 0.082 mm^2. The least intensive tillage treatment, no tillage, resulted in a 16% increase in permeability from 0.031 to 0.036 mm^2. Ridge tillage, a minimum tillage practice with one cultivation, resulted in a 61% increase in permeability from 0.022 to 0.035 mm^2. The increase in permeability suggests a redistribution of soil pores with respect to their size (Domzhal and Us'yarov, 1994) and/or a decrease in tortuosity of flow paths in soils subject to freezing and thawing. Flow paths characteristic of the no-tillage treatment were less affected by freezing and thawing compared to ridge tillage and moldboard plow.

PERSPECTIVES

Soil freezing and thawing can aid in the development of soil structure. This study suggests that freezing and thawing cause changes in soil pore size and distribution, continuity, and/or tortuosity, all of which influence soil structure. Permeability of soil to air was greater after each freeze-thaw cycle compared to that prior to the initiation of the experiment. Thus, freezing and thawing influence flow path characteristics which enhance permeability. Changes in air permeability of dry soils resulting from freezing and thawing may not be as great as those observed in this study.

Therefore, fall soil moisture prior to the onset of soil freezing may determine the extent to which changes in soil structure and permeability occur overwinter in the North Central United States.

REFERENCES

Chamberlain, E.J. and A.J. Gow. 1979. Effect of freezing and thawing on the permeability and structure of soils. Eng. Geol. 13:73-92.

Domzhal, K. and O.G. Us'yarov. 1994. Formation of inhomogeneity in pore spaces in heavy swelling soils upon freezing-thawing. Colloid J. 56:287-292.

Fish, A.N. and A.J. Koppi. 1994. The use of a simple field air permeameter as a rapid indicator of functional soil pore space. Geoderma 63:255-264.

Larin, P.A. 1963. Air permeability of frozen soils as a function of autumn plowing and moisture. Soviet Soil Sci. p. 158-163.

Pawluk, S. 1988. Freeze-thaw effects on granular structure reorganization for soil materials of varying texture and moisture content. Can. J. Soil Sci. 68:485-494.

Staricka, J.A. and G.R. Benoit. 1995. Freeze-drying effects on wet and dry soil aggregate stability. Soil Sci. Soc. Am. J. 59:218-223.

van Vliet-Lanoe, B. and J. Coutard. 1984. Structures caused by repeated freezing and thawing in various loamy sediments: A comparison of active, fossil and experimental data. Earth Surface Processes and Landforms 9:553-565.

Aggregate Stability Response to Freeze-Thaw Cycles

G.A. LEHRSCH[1]

ABSTRACT

Research has suggested that 1 to 3 freeze-thaw cycles (FTCs) may increase the stability of soil aggregates, when field-moist aggregates are wet sieved. The objectives of this laboratory experiment were to quantify aggregate stability of relatively wet aggregates from the Ap horizons of four soils when subjected to either 0, 1, 2, or 4 FTCs and, secondly, to identify a threshold number of FTCs for each soil below which aggregate stability increases. Moist soil was packed into 28-mm-diam., 50-mm-tall brass cylinders by tapping to a dry bulk density of $1.15\ Mg\ m^{-3}$, sealed in polyethylene bags, then slowly frozen convectively at $-5°C$ for 48 h, then thawed at $+6°C$ for 48 h for each FTC. The first 1 to 2 FTCs in general increased aggregate stability, but additional FTCs had little effect. For 3 of 4 soils, 2 to 3 FTCs appeared to increase aggregate stability to a plateau or threshold. FTCs increased aggregate stability, when averaged across the four soils, more in the 0- to 15-mm depth increment than in the 15- to 30-mm increment.

Key words: Freezing, thawing, soil physical properties, wet sieving, soil depth

INTRODUCTION

Aggregate stability is an important soil property because soil susceptibility to water and wind erosion increases, in part, as aggregate stability decreases (Lehrsch 1995, Luk 1979). Soils with relatively unstable aggregates can seal readily with rain or irrigation and, upon drying, form crusts easily. Sealing reduces infiltration and increases runoff whereas crusting hinders seedling emergence (Lehrsch 1995). Both processes impair crop production.

Wet aggregate stability is a dynamic property. Both management factors and climatic processes cause stability to vary temporally (Lehrsch 1995). Management factors include tillage, irrigation, and crop residue management. Climatic processes include precipitation (wetting), evaporation (drying), freezing, and thawing. In temperate regions, freezing and thawing cause stability to vary greatly (Bullock et al. 1988, Lehrsch et al. 1991, Mostaghimi et al. 1988, Staricka and Benoit 1995). In many areas subject to freezing, wind and water erosion can occur in the spring before vegetation covers clean-tilled fields. If surface soil aggregates were to enter the winter relatively stable, though they would be weakened somewhat by winter freezing (Lehrsch and Jolley 1992), they could nonetheless better resist breakdown and movement from these erosive forces in the spring.

Wet aggregate stability can also increase under some conditions. For example, soil drying during periods of low rainfall or in soil near and below enlarging ice lenses (Czurda et al. 1995) can precipitate cementing or bonding agents like $CaCO_3$, silica, gypsum or iron oxides at contact points between primary particles or smaller aggregates. This precipitation often enables aggregates to withstand subsequent disruption by water (Kemper et al. 1987, Lehrsch et al. 1991, Perfect et al. 1990). Drying both gathers and arranges clay domains at contacts between sand and silt particles, increasing aggregate stability (Lehrsch 1995, Rowell and Dillon 1972).

Aggregate stability can be decreased by freeze-drying aggregates on or near the soil surface (Staricka and Benoit 1995) and, in general, by freeze-thaw cycles. Ice lenses that form and enlarge during freezing

---

likely cause potential fracture planes to develop in nearby aggregates (Lehrsch et al. 1991). Failure along these planes of weakness is likely responsible for the reduced stability and weakened structure of relatively wet, mineral soils that undergo many FTCs (Benoit 1973, Hinman and Bisal 1968, Mostaghimi et al. 1988). Results from some studies (Bisal and Nielsen 1964, Lehrsch et al. 1991) have suggested, however, that there may be a relatively small number of FTCs, up to about four, during which stability may increase. Unfortunately, where not protected by residue, vegetative cover, or snow, aggregates in the uppermost 30 mm of many south-central Idaho soil profiles may freeze and thaw 30 to 40 times from fall to spring (J.L. Wright 1996, personal communication). Through these seasons, aggregates at the soil surface may freeze and thaw at cycles ranging from diurnal to weekly, or longer (Hershfield 1974).

Management practices may be modified to control, somewhat, the FTCs that surface aggregates are subjected to. Wheat (*Triticum aestivum* L.) stubble, rather than being plowed after harvest, may be left standing to mulch the surface and reduce the number of subsequent freeze-thaw events (Pikul and Allmaras 1985). Standing stubble would also trap snow to insulate the soil and, in dryland cropping regions, lead to increased water storage in the profile. Crop residue from minimum tillage production systems, or organic materials from manure applications, on the soil surface may also lessen the number of FTCs that surface aggregates experience.

This laboratory study was both a follow-up to and extension of two earlier studies (Lehrsch et al. 1991 and 1993). In this study, the freezing chamber was held at $-5\,°C$ (Lehrsch et al. 1992, Rowell and Dillon 1972) to slowly freeze the soil, thereby permitting water redistribution as the soil froze. To better measure treatments effects on stability, aggregates from shallow (15-mm) layers were analyzed, as recommended by Cary (1992). In this study, all soil samples when frozen contained water at the same matric potential, -33 kPa. In earlier studies, due in part to logistical constraints, we were unable to adequately study changes that occurred in the stability of relatively wet aggregates subjected to 1, 2, and 4 FTCs. Recent findings (Lehrsch et al. 1991) suggest, however, that we need to better understand how moist aggregates respond to just a few FTCs. Thus, this experiment was designed to i) quantify the aggregate stability response of relatively wet, field-moist aggregates from four continental U.S. soils, two differing primarily in clay content and two in organic C, to up to 4 FTCs and ii) identify a threshold number of FTCs for each soil below which aggregate stability increased.

MATERIALS AND METHODS

The study was conducted as a three-factor experiment with a factorial arrangement of two factors, soils and freeze-thaw cycles, laid out in a randomized complete block design. The third factor was sampling depth, either 0-15 or 15-30 mm. It was modeled as a subplot treatment (or repeated measure) for each combination of the first two factors. Each treatment was replicated six times. Ap horizons of four soils were studied: a Barnes loam (*Udic Haploboroll*) from Morris, Minnesota, a Sharpsburg silty clay (*Typic Argiudoll*) from Lincoln, Nebraska, a Palouse silt loam (*Pachic Ultic Haploxeroll*) from Pullman, Washington, and a Portneuf silt loam (*Durixerollic Calciorthid*) from Kimberly, Idaho. Some index properties of the four soils are given in Table 1. The Barnes, Palouse, and Portneuf soil samples were taken from fallowed fields in the spring of 1988. After the Barnes and Palouse samples were air mailed to Kimberly, samples of all three soils were stored, field-moist, in air tight containers at $+6\,°C$ until used. The Sharpsburg sample was taken in May of 1996 from a field planted to winter wheat, shipped to Kimberly, and stored as were the other soils until used.

All soils were field-moist (initial water contents ranged from 0.12 to 0.14 kg kg^{-1}, Table 1) and sieved through a 4-mm sieve prior to packing. Just before the <4-mm fraction of each soil was packed, its water content was slowly raised by vapor-wetting until its soil water was at a matric potential of -33 kPa (according to water contents given by Elliot et al. 1989). Water contents at that potential ranged from 0.22 to 0.27 kg kg^{-1} (Table 1).

The sample handling and preparation procedures were nearly identical to those reported in Lehrsch et al. (1991). In brief, tapping was used to pack moistened soil, to a dry bulk density of 1.15 Mg m^{-3}, into brass cylinders 50 mm tall with inside diameters of 28 mm. Each packed cylinder was then sealed in a Ziploc[1], polyethylene bag to inhibit water loss and prevent later freeze-drying, and placed into a cavity in a polystyrene foam tray. The foam, at least 70 mm beneath and 20 mm beside each cylinder, served as insulation so that freezing occurred primarily downward from the surface. The packed samples were then subjected to either 0, 1, 2, or 4 FTCs. The 0-cycle samples were not frozen. The packed soil for the other cycles was then slowly frozen, convectively and without access to additional water, at $-5\,°C$ (plus or minus 1 °C) for 48 h,

---

[1]Mention of trade names is for the reader's benefit and does not imply endorsement of the products by the USDA.

Table 1. Soil properties.

Soil type	Sand	Silt	Clay	COLE[†] (cm cm⁻¹)	Base sat. (%)	Exch. Ca	CEC	Org. C (g kg⁻¹)	Initial agg. stab.[‡] (%)	Field-moist	When packed[§]
	(g kg⁻¹)					(cmol kg⁻¹)				(kg kg⁻¹)	
Barnes loam	490	340	170	0.030	100	-	19.5	16.0	35	0.14	0.22
Sharpsburg silty clay	30	560	410	0.086	94	19.4	29.4	13.3	85	0.12	0.27
Palouse silt loam	100	700	200	0.026	82	12.7	19.6	13.2	87	0.13	0.26
Portneuf silt loam	220	660	120	0.012	100	-	12.6	9.9	46	0.14	0.25

[†]Coefficient of linear extensibility.
[‡]Measured on the stored soil about 90 days before the experiment was performed.
[§]Equal to the water content at a matric potential of -33 kPa.

then thawed at +6°C (plus or minus 1°C) for 48 h for each freeze-thaw cycle. A data logger and thermocouple within each freezing chamber recorded ambient air temperatures. After the appropriate samples had been frozen for the last time and had thawed for 48 h, they were brought to room temperature by resting on a lab bench for 2 h. Each sample was then removed from its cylinder and sectioned to obtain samples from 0-15 and 15-30 mm. The samples from each layer were not air-dried but immediately sieved gently, by hand, to obtain moist, 1- to 4-mm aggregates. Four g of these were then vapor-wetted to 0.30 kg kg⁻¹ within 30 min using a non-heating vaporizer (Humidifier No. 240, Hankscraft[1], Reedsburg, Wisconsin). Immediately thereafter, the aggregates were sieved in distilled water for three min to measure aggregate stability (Kemper and Rosenau 1986, as modified by Lehrsch et al. 1991). The principal modification was that field-moist 1- to 4-mm aggregates, rather than air-dry 1- to 2-mm aggregates, were vapor-wetted before sieving. Analyses of variance were performed using SAS (SAS Institute Inc. 1989)[1]. A broad inference analysis was conducted to broaden the scope of applicability. In such an analysis, the variation between replications was included as part of the error term used to determine whether soils, FTCs, or their interaction significantly affected aggregate stability. In the analysis of variance, probabilities ≤ 0.105 were considered statistically significant.

RESULTS AND DISCUSSION

Analysis of variance

A Bartlett's test indicated that not all treatment variances were statistically equal. Upon examination, the variances for Palouse, cycle 0, depths 0-15 and 15-30 mm averaged 163 while the variances of the remaining 30 treatment combinations averaged 44. Since no transformation was found to equalize such disparate variances, a weighted analysis of variance (AOV) was performed, using as weights the reciprocals of these two average variances. When compared to the results from a non-weighted AOV, the results from the weighted AOV differed little. The residuals from fitting the statistical model using a weighted analysis exhibited a mean of 0 and were normally distributed (Shapiro-Wilk W= 0.984, P= 0.634). The weighted AOV revealed that aggregate stability was affected by a pair of two-way interactions: one between soils and FTCs (P= 0.001) and the other between sampling depths and FTCs (P= 0.104).

Interaction between soils and freeze-thaw cycles

FTC effects upon aggregate stability were soil-dependent. Increasing FTCs tended to increase each soil's aggregate stability, when averaged across both sampling depths (Fig. 1). The stability increase, from 0 to 1 FTC, was significant for Barnes (P<0.001) and
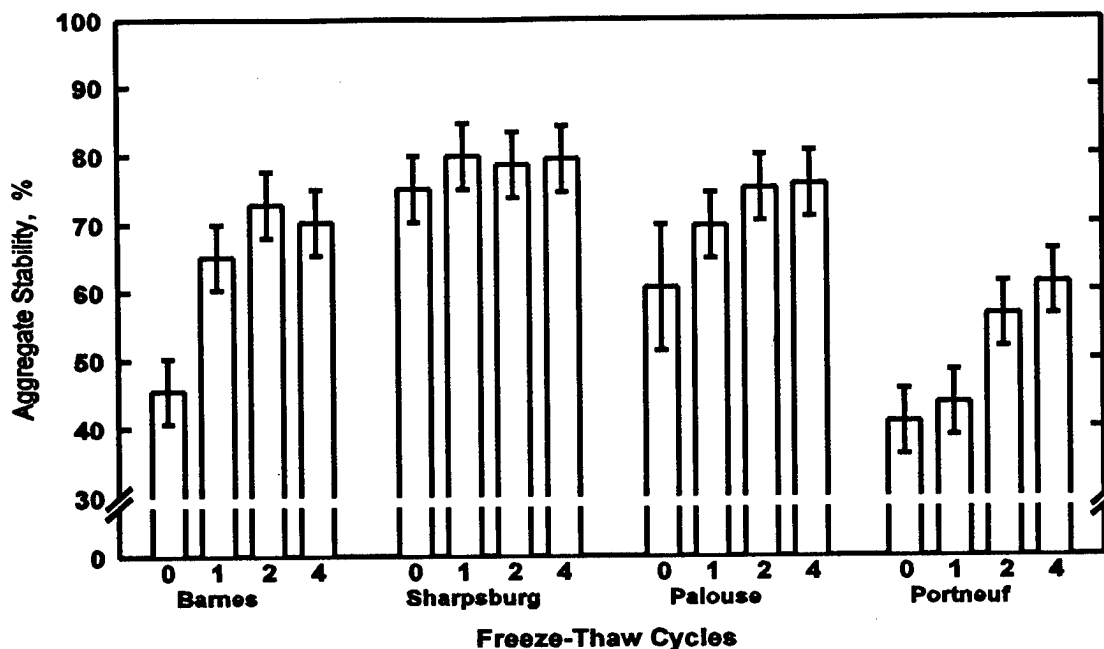
Figure 1. Aggregate stability of each soil measured at each freeze-thaw cycle, averaged across sampling depths. Each mean (n = 12) is shown with its 95% confidence limits.

Palouse (P= 0.085). Perfect et al. (1990) also reported wet aggregate stability to increase after just one FTC. From 1 to 2 FTCs, the increase was significant for Barnes (P= 0.028) and Portneuf (P<0.001). No other adjacent FTC means within each soil differed at a probability of less than 0.100. The Sharpsburg soil, with 410 g clay kg^{-1}, was the only soil that did not show a significant response from any one FTC level to an adjacent one. Its aggregate stability stabilized at about 79%, however, from 1 to 4 FTCs.

This increase in stability of field-moist aggregates with particularly the first 1 or 2 FTCs (Fig. 1) was considered by Lehrsch et al. (1991) to be a normal or common response. Lehrsch et al. (1993) described a process that could cause these increases. In brief, ice formation in inter-aggregate pores or ice lens enlargement could bring nearby soil particles into contact. Slightly soluble, inorganic bonding agents would then move or, to minimize their potential energy, diffuse to those contact points (Kemper et al. 1987). Once there, the bonding agents would precipitate, thereby increasing the aggregate's stability, as the soil dried due to freezing-induced soil water redistribution (Czurda et al. 1995, Kemper et al. 1987, Perfect et al. 1990). Since this precipitation was likely irreversible (Kemper et al. 1987), these bonding agents did not re-enter the soil solution during subsequent thawing periods. As FTCs accrued, more of the bonding agents that had remained in solution in the unfrozen water

films surrounding soil particles during previous freezing episodes likely precipitated from the soil solution, further strengthening the aggregates. This precipitation mechanism may explain the increase in aggregate stability with the first few FTCs. Freezing and ice formation have been reported (Bisal and Nielsen 1964, Czurda et al. 1995, Perfect et al. 1990, Rowell and Dillon 1972) to improve aggregation and increase aggregate stability. In the frozen samples in my experiment, neither ice lenses nor frost heaving were observed. Some ice crystals were seen, however, on the soil surfaces. Initial tests revealed that, within the packed cylinders, freezing caused little detectable vertical water redistribution.

Aggregate stability differed little, for most soils, from 2 to 4 FTCs (Fig. 1). Portneuf stability changed (increased) the most, from 56.6 to 61.3%, though significant only at P= 0.175. These minimal changes that occurred after 2 FTCs support the view that either a threshold or possibly a plateau was reached after just two to four FTCs. Only the Barnes decreased in stability from 2 to 4 FTCs (though again significant only at P= 0.453). Mostaghimi et al. (1988), who wet sieved air-dried aggregates, found Barnes' aggregate stability to decrease sharply from 3 to 6 FTCs.

The data in Fig. 1 suggest that the aggregate stability of the Barnes and Palouse soils reached a plateau, or possibly a threshold, from 2 to 4 FTCs. To statistically test this tentative finding, a trend analysis

168

was performed (Table 2). It confirmed that the Barnes' and Palouse's aggregate stability responded in a curvilinear (that is, quadratic) manner to increasing FTCs.

Table 2. Trend analysis of freeze-thaw cycle effects on aggregate stability.

Trend	Significance			
	Barnes	Sharpsburg	Palouse	Portneuf
Linear	**†	NS	**	**
Quad-ratic	**	NS	*	NS

† *, ** Significant at the 0.05 and 0.01 probability levels, respectively.

The responses, fitted to data averaged across both depths, were:

$$AS_{Bar} = 46.0+21.8(FTC)-3.9(FTC)^2 \quad (R^2= 0.79) \quad [1]$$

and

$$AS_{Pal} = 60.6+10.8(FTC)-1.8(FTC)^2 \quad (R^2= 0.42) \quad [2]$$

where AS was aggregate stability, expressed as a percentage, and FTC was the number of freeze-thaw cycles experienced. Equations [1] and [2] indicate that each soil's aggregate stability would be greatest just before or at 3 FTCs. The Portneuf was the only soil of the four we studied whose aggregate stability responded linearly (i.e., linear trend significant but quadratic not) to FTCs. Its response was:

$$AS_{Por} = 41.0+5.5(FTC) \qquad (R^2= 0.70) \qquad [3]$$

Numerous findings in this experiment were similar to those reported by Lehrsch et al. (1991, 1993). The stability of field-moist aggregates of Barnes loam increased with the first 2 or 3 FTCs. After Sharpsburg aggregates were frozen and thawed at least once, their stability was about 80% and did not significantly change thereafter with accruing FTCs. Palouse aggregates, when frozen at water contents ranging from 0.26 to 0.30 kg kg^{-1}, exhibited a monotonic increase in stability through 4 or 5 FTCs. The stability of the Portneuf changed little from 0 to 1 FTC. In this experiment, however, its stability from 1 to 2 FTCs increased from 43.6 to 56.6% (significant at $P<0.001$). I have no explanation, other than that given above, for this highly significant 13 percentage-point increase.

Interaction between sampling depths and freeze-thaw cycles

FTC effects upon aggregate stability, averaged across four soils, differed from one depth to the other (Fig. 2). A trend analysis performed on the data shown in Fig. 2 confirmed ($P<0.001$) that, at each depth, aggregate stability responded curvilinearly to freeze-thaw cycles. The fitted responses were:

$$AS_{0-15} = 56.9+13.2(FTC)-2.2(FTC)^2 \quad (R^2= 0.87) \quad [4]$$

and

$$AS_{15-30} = 53.9+9.1(FTC)-1.4(FTC)^2 \quad (R^2= 0.64) \quad [5]$$

Eqns. [4] and [5] also indicate that, at each depth, aggregate stability would be greatest at 3 or just more than 3 FTCs.
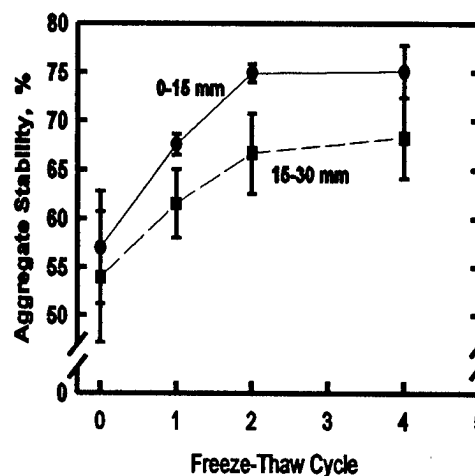
Figure 2. Freeze-thaw cycle effects on aggregate stability, averaged across four soils, measured at each sampling depth. Each mean (n = 6) is shown with its 95% confidence limits.

At each level of FTC, aggregate stability at 0-15 mm exceeded that at 15-30 mm (Fig. 2). The data also reveal that these differences increased with each cycle through 2 FTCs. For all soils averaged across all FTCs, aggregate stability at 0-15 mm, 68.6%, was nearly 10% greater (significant at $P<0.001$) than at 15-30 mm, 62.6%.

The data in Fig. 2 also reveal that, with each FTC up to two, aggregate stability increased more near the surface than below it. Aggregates near the surface experienced less overburden pressure or, in other

words, were less constrained from moving about. Unconstrained aggregates are more stable than constrained aggregates after freezing (Bullock et al. 1988, Lehrsch et al. 1991). These differences in stability with depth at each FTC were, however, relatively small, generally less than seven percentage points. Fall plowing or rototilling to reduce surface bulk density to maximize any aggregate stability increase with FTCs is not recommended.

Aggregate stability at each depth increased most with the first FTC (Fig. 2). In both the 0-15 and 15-30 mm layers, the increase in aggregate stability per unit increase in FTC decreased with increasing FTCs. This finding supports the view that slightly soluble bonding agents were being removed from the soil solution by being precipitated at intra-aggregate contact points (Kemper et al. 1987, Lehrsch et al. 1991). Most would likely have been precipitated with the first FTC. Thereafter, only those bonding agents that had remained in solution during previous freezes could have been precipitated (Lehrsch et al. 1991). Thus, progressively less strengthening of aggregates would have occurred as FTCs accrued. The data shown in Fig. 2 support this precipitation hypothesis.

Regardless of depth, aggregate stability of field-moist aggregates increased with the first two FTCs (Fig. 2). Eqns. [1], [2], [4], and [5] predict aggregate stability to be greatest near 3 FTCs. These findings suggest that, if possible, land managers should allow soils to freeze two or three times in the fall to increase their stability and, thus, resistance to wind and water erosion. Alternatively, managers could minimize the FTCs that surface soil experiences by, for example, establishing winter cover crops or adopting minimum tillage production systems to increase crop residues on the soil surface. Any practice that would better insulate the soil should help stabilize surface aggregates. Data in Fig. 2 also show that aggregate stability changed little from 2 to 4 FTCs, regardless of depth. With more FTCs, aggregate stability would likely decrease (Benoit 1973, Mostaghimi et al. 1988).

Organic C and clay effects on aggregate stability

In a related study conducted earlier (Lehrsch et al. 1991), soils that differed in organic C and those that differed in clay content responded differently to freezing and thawing. When slowly frozen, as in this experiment, relatively wet aggregates from those same soils may not have responded in the same manner. The two soils differing in organic C and the two differing in clay content were thus compared. Because the soil by cycle interaction (Fig. 1), was significant ($P<0.001$), comparisons were made at each level of FTC. The Palouse, with 33% more organic C than the Portneuf

(Table 1), was significantly more stable than the Portneuf at each level of FTC. In contrast, the stability of the Sharpsburg, with more than twice the clay of the Barnes (Table 1), was significantly more stable than the Barnes only at FTC levels of 0 and 1. Higher clay contents, possibly related to clay aggregate formation (Rowell and Dillon 1972) or clay bridging between sand and silt particles (Kemper et al. 1987), appear to some way strengthen aggregates after FTCs of 0 and 1 but not after 2 or more. During the first FTC, dispersed clay may move about (Rowell and Dillon 1972) and lodge in low potential energy resting places within aggregates, imparting little additional stability to those aggregates with subsequent FTCs.

Additional studies could be conducted to identify the physical and/or chemical constituents that may be i) moving into or out of each soil layer (Perfect et al. 1990), and ii) causing the aggregate stability changes observed in this study, as well as others (Lehrsch et al. 1991, 1993). Any additional studies should focus on only one or two soils (e.g., Palouse and Portneuf) and add a sodium silicate and/or 2 g kg^{-1} CaSO$_4$ treatment (Lehrsch et al. 1993). Larger cylinders should be used so that a larger sample will be retrieved from each shallow depth increment. In this larger sample, investigators should measure aggregate stability and water dispersible clay (Pojasok and Kay 1990) and analyze a number of chemical constituents, including soluble Ca, soluble silica, organic C, and polysaccharides. If a suitable extraction and analysis procedure can be developed, soluble organic carbon should also be measured on selected treatments, particularly to compare soils with quite different (high and low) organic C contents. Experimenters should consider using the model ICE-1 (El-Kadi and Cary 1990) to estimate water flow and water redistribution during freezing to assist in interpreting their findings.

CONCLUSIONS

The stability of wet-sieved, field-moist aggregates of Barnes, Palouse, and Portneuf soils increased with 1 and/or 2 FTCs. From 2 to 4 FTCs, little additional change occurred. The stability of Sharpsburg silty clay aggregates was not significantly affected by FTCs. For all soils but the Portneuf, 2 to 3 FTCs appeared to increase stability to a plateau or threshold. FTCs increased aggregate stability more at 0-15 than 15-30 mm. Averaged across soils at each depth, stability increased more with the first than the second FTC.

170

REFERENCES

Benoit, G. R. 1973. Effect of freeze-thaw cycles on aggregate stability and hydraulic conductivity of three soil aggregate sizes. Soil Sci. Soc. Am. Proc. 37:3-5.

Bisal, F., and K. F. Nielsen. 1964. Soil aggregates do not necessarily break down over-winter. Soil Sci. 98:345-346.

Bullock, M. S., W. D. Kemper, and S. D. Nelson. 1988. Soil cohesion as affected by freezing, water content, time and tillage. Soil Sci. Soc. Am. J. 52:770-776.

Cary, J. W. 1992. Comments on "Freezing effects on aggregate stability affected by texture, mineralogy, and organic matter." Soil Sci. Soc. Am. J. 56:1659.

Czurda, K. A., S. Ludwig, and R. Schababerle. 1995. Fabric changes in plastic clays by freezing and thawing. p. 71-91. *In* K. H. Hartge and B. A. Stewart (eds.) Soil structure: Its development and function. CRC Press, Inc., Boca Raton, FL.

El-Kadi, A. I., and J. W. Cary. 1990. Modelling the coupled flow of heat, water, and solute in freezing soils, including heave. Software for Eng. Workstations 6:48–51.

Elliot, W. J., A. M. Liebenow, J. M. Laflen, and K. D. Kohl. 1989. A compendium of soil erodibility data from WEPP cropland soil field erodibility experiments 1987 and 1988. NSERL Report No. 3. USDA-ARS National Soil Erosion Research Lab., W. Lafayette, Indiana.

Hershfield, D.M. 1974. The frequency of freeze-thaw cycles. J. Applied Meteorol. 13:348-354.

Hinman, W.C., and F. Bisal. 1968. Alterations of soil structure upon freezing and thawing and subsequent drying. Can. J. Soil Sci. 48:193-197.

Kemper, W.D., and R.C. Rosenau. 1986. Aggregate stability and size distribution. p. 425-442. *In* A. Klute (ed.) Methods of Soil Analysis, Part 1. 2nd ed. ASA, Madison, Wisconsin.

Kemper, W. D., R. C. Rosenau, and A. R. Dexter. 1987. Cohesion development in disrupted soils as affected by clay and organic matter content and temperature. Soil Sci. Soc. Am. J. 51:860-867.

Lehrsch, G. A. 1995. Soil - Temporal variation in aggregate stability. p. 311-313. *In* S. P. Parker (ed.) 1996 McGraw-Hill Yearbook of Science & Technology. McGraw-Hill, Inc., New York.

Lehrsch, G. A., and P. M. Jolley. 1992. Temporal changes in wet aggregate stability. Trans. ASAE 35:493-498.

Lehrsch, G. A., R. E. Sojka, D. L. Carter, and P. M. Jolley. 1991. Freezing effects on aggregate stability affected by texture, mineralogy, and organic matter. Soil Sci. Soc. Am. J. 55:1401-1406.

Lehrsch, G. A., R. E. Sojka, D. L. Carter, and P. M. Jolley. 1992. Reply to "Comments on 'Freezing effects on aggregate stability affected by texture, mineralogy, and organic matter.'" Soil Sci. Soc. Am. J. 56:1659.

Lehrsch, G. A., R. E. Sojka, and P. M. Jolley. 1993. Freezing effects on aggregate stability of soils amended with lime and gypsum. p. 115-127. *In* J. W. A. Poesen and M. A. Nearing (eds.) Soil surface sealing and crusting. Catena Verlag, Cremlingen-Destedt, Germany.

Luk, S. H. 1979. Effect of soil properties on erosion by wash and splash. Earth Surf. Proc. 4:241-255.

Mostaghimi, S., R. A. Young, A. R. Wilts, and A. L. Kenimer. 1988. Effects of frost action on soil aggregate stability. Trans. ASAE 31:435-439.

Perfect, E., W. K. P. van Loon, B. D. Kay, and P. H. Groenevelt. 1990. Influence of ice segregation and solutes on soil structural stability. Can. J. Soil Sci. 70:571-581.

Pikul, J. L., Jr., and R. R. Allmaras. 1985. Hydraulic potential in unfrozen soil in response to diurnal freezing and thawing of the soil surface. Trans. ASAE 28:164-168.

Pojasok, T., and B. D. Kay. 1990. Assessment of a combination of wet sieving and turbidimetry to characterize the structural stability of moist aggregates. Can. J. Soil Sci. 70:33-42.

Rowell, D. L., and P. J. Dillon. 1972. Migration and aggregation of Na and Ca clays by the freezing of dispersed and flocculated suspensions. J. Soil Sci. 23:442-447.

SAS Institute Inc. 1989. SAS/STAT user's guide, ver. 6. 4th ed. SAS Institute, Inc., Cary, NC.

Staricka, J. A., and G. R. Benoit. 1995. Freeze-drying effects on wet and dry soil aggregate stability. Soil Sci. Soc. Am. J. 59:218-223.

Overwinter Changes in Aggregate Size Distribution
of a Loam in West Central Minnesota

M.J. LINDSTROM[1] AND B.S. SHARRATT[1]

ABSTRACT

Changes in surface structure and stability during winter in northerly climatic regions can result in a highly erodible soil surface. Soil aggregates can fracture by the combination of freezing and thawing and freeze drying, making the resultant soil fragments more susceptible to wind erosion. A study was conducted over the winters of 1989–90 and 1990–91 near Morris, Minnesota, on a Barnes-Aastad loam association to determine changes in aggregate size, as affected by tillage and crop rotations. Aggregate size distribution was determined by dry sieving in the fall after tillage and again in the spring before tillage. Overwinter processes influenced aggregate size, with the magnitude and direction of change influenced by soil water during the winter season. In the first year of this study, when the soil was moist prior to the first fall freeze but dried by sublimation during the winter, aggregates degraded to size fractions susceptible to wind erosion. In the second winter when snow melt recharged surface soil water, aggregate size increased from fall to spring on treatments with surface residue.

Key words: Aggregate size, freeze-drying, wind erosion.

INTRODUCTION

Soil structural properties at the surface and near-surface commonly change during the winter in response to climate-soil interactions. In the northern Corn Belt of the United States, harvested fields are often moldboard plowed in the fall. A rough, cloddy surface commonly results from this practice, but overwinter processes generally ameliorate the soil surface into a friable condition suitable for seedbed preparation in the spring. Farmers who utilize the moldboard plow benefit from soil clod and aggregate breakdown during winter and are in effect using winter processes as a tillage tool. The winter processes responsible for the changes in soil structure have been attributed to such factors as wetting, drying, freezing, and thawing.

The changes that occur over winter in soil structure and stability can result in a highly erodible soil condition. The soil erodibility factor (K) used in the Revised Universal Soil Loss Equation (RUSLE) has been adjusted to account for seasonal change such as freezing and thawing, soil water content, and soil consolidation (Renard et al. 1991). Soil aggregates may breakdown over the winter, leaving the soil susceptible to wind erosion. However, aggregates may also consolidate into larger aggregates or collapse into a massive structure. Chepil (1954) and Bisal and Ferguson (1968) reported an increase in the erodible fraction (soil aggregates < 0.84 mm in size) due to winter processes, whereas Bisal and Nielson (1964) state that no general conclusion can be made on the effect of freezing and thawing on soil aggregate size in the field. Anderson and Wenhardt (1966) found that a clay loam was less susceptible to wind erosion in the spring than the previous fall, indicating over winter aggregation decreased the proportion of erodible fraction in the soil. The largest decrease in erodible soil aggregates during the winter occurred in tillage treatments with surface residue.

Chepil (1954) showed that soil cloddiness was reduced from fall to spring if the soil was occasionally moist during winter. He also noted little change in cloddiness during the winter when the soil was dry. Similar findings have been reported by Unger (1991). The breakdown of coarse aggregates during the winter was attributed to expansion of ice crystals

within the aggregates. Bisal and Nielson (1964) reported that freezing wet clods and aggregates decrease aggregate size, but that water content and method of drying will, however, determine erodibility after drying. They found that when frozen soil is allowed to thaw before drying, water in the soil will result in a consolidating effect on the fractured soil aggregates. However, the soil was more erodible when water was removed (freeze-dried) when frozen. Both Chepil (1954) and Bisal and Ferguson (1968) found that fine-textured soils were most susceptible to aggregate breakdown. Similar changes in aggregate size during winter have been reported by Unger (1991) and Layton et al. (1993).

Changes in soil structure caused by freezing and thawing are not as apparent for dry soils. In contrast, aggregation may occur as wet, frozen soils thaw during the spring. Wet soils also have the highest potential to breakdown into smaller structural units . As pore water expands during freezing, the increase in ice pressure disrupts structural bonds (Miller, 1980). In northern regions where soils freeze during winter, ice within the soil matrix near the soil surface can be removed by sublimation. Soil particles are then detached from larger aggregates and subject to movement by wind. Staricka and Benoit (1995) found that freeze-drying caused a decrease in structural stability with increasing soil water contents.

This study was initiated to examine temporal changes in soil structural properties as affected by tillage and crop rotation for use in the development of the Soils Submodel of the Wind Erosion Prediction System (WEPS) (Hagen, 1991). This paper will present data on changes in aggregate size distribution in a Barnes-Aastad soil association during two winters in west central Minnesota as influenced by tillage and cropping.

MATERIALS AND METHODS

Plots were established in the spring of 1988 on a Barnes (fine-loamy, mixed, Udic Haploborolls)-Aastad (fine-loamy, mixed, Pachic Udic Haploborolls) association near Morris, Minnesota. Three replicates of plots were randomly split with crop rotation as the main plot and tillage as the subplots.

Tillage treatments consisted of fall moldboard plow, spring disk (MP); fall chisel plow, spring disk (CP); and a ridge till system (RT) where ridges were formed during the early growing season (June). The next season's crop was planted on the ridge with neither fall nor spring tillage. Crop rotations included

continuous corn (*Zea mays* L.) (CC), corn-soybean (*Glycine max* L.) (CSB) with both crops present each year, and continuous fallow (CF). Corn stalks were chopped after harvest on all tillage treatments and all plots were cultivated twice during the growing season for weed control. Fall tillage was performed after harvest in mid-October. Spring tillage was performed just prior to planting. Planting occurred in late-April to mid-May.

Approximately 5 kg of soil from the surface 5 cm were collected from each subplot within two days after fall tillage in 1989 and 1990. Additional soil samples were again taken in mid-April prior to spring tillage and planting. These samples were air dried and aggregate size distribution was determined by dry sieving with a rotary sieve. Sieve sizes were 0.5, 1.0, 2.0, 3.0, 5.0, 9.0, 12.0, and >12 mm. Geometric mean weight diameter (GMD) of each sample was determined using the method of Kemper and Chepil (1965).

RESULTS AND DISCUSSION

Precipitation was near normal for the 1989 crop year and below normal for 1990. Snowfall was above normal for both the winters of 1989–90 and 1990–91. Surface soil water recharge occurred during the fall of 1989 from above normal rainfall in September. Little recharge occurred in the fall of 1990. Snow cover in the fields was primarily intermittent during the winter of 1989–90 because of redistribution by wind, providing little opportunity for soil water recharge during the thaw period. A warmer-than-normal period started in late January of 1991 and continued through June. This warming trend coincided with greater than normal snowfall in February and March, providing an opportunity to recharge the soil water reservoir in late winter.

Aggregate GMD for fall and spring sampling by crop rotation and tillage treatments are shown in Table 1 for the two years of the study. Analysis of variance for these same treatments are shown in Table 2. Differences in GMD between tillage systems was observed during the fall sampling both years with the RT tillage treatment having a smaller GMD than the MP or CP treatments. No differences were observed with the rotation treatments or with the rotation by tillage interaction. Significant differences between tillage systems were again observed both years in the spring sampling with the MP tillage treatment have a smaller GMD than the CP or RT treatments. No differences was observed with the

Table 1. Geometric mean diameters (GMD) of soil aggregates as influenced by crop rotation and tillage after fall tillage and prior to spring tillage over two winter seasons.

	Fall 1989			Fall 1990		
Crop	Tillage			Tillage		
Rotation	MP	CP	RT	MP	CP	RT
	------------- GMD (mm) ----------------					
CSB	20.6	21.8	4.0	9.8	8.8	2.7
SBC	24.2	6.9	2.4	10.4	6.3	2.3
CC	13.4	4.6	3.6	8.0	9.6	3.0
CF	16.8	5.0	1.7	11.3	3.5	2.2
	Spring 1990			Spring 1991		
CSB	0.7	0.9	1.3	1.3	4.1	7.8
SBC	0.6	1.4	1.4	1.6	3.6	8.8
CC	0.8	1.5	1.2	1.7	8.0	10.6
CF	1.1	1.0	1.1	2.7	1.9	2.2

Table 2. Analysis of variance for geometric mean diameters (GMD) of soil aggregates after fall tillage and prior to spring tillage over two winter seasons.

	Fall 1989	Fall 1990
	P	P
Tillage (T)	0.07	0.01
Rotation (R)	NS	NS
TXR	NS	NS
	Spring 1990	Spring 1991
Tillage (T)	0.03	0.02
Rotation (R)	NS	NS
TXR	NS	0.02

rotation treatments either year. A rotation by tillage interaction was observed in the spring of 1991, but not in 1990.

In the spring of 1990, GMD values were decreased in size over the winter season for both the rotation and tillage treatments. The winter of 1989–90 was cold with only intermittent snow cover, which was rapidly removed by the wind. The soil surface was moist going into the winter season. However, freeze-drying of the surface layer may have resulted due to a lack of snow cover and persistent winds (Staricka and Benoit, 1995). Aggregate GMD was larger in the spring of 1991, particularly with tillage (CP and RT) and crop rotations (CSB, SBC, and CC) treatment that left surface residue. This is most evident in the RT treatment where aggregate GMD increased overwinter for all crop rotation treatments with the exception of the CF rotation treatment. During the winter of 1990–91, snow cover was maintained throughout most of the winter on treatments which supported surface residue which protected the surface aggregates from freeze-drying. In mid-March, 30 cm of snowfall with a high snow water equivalent which replenished the surface soil

water during thaw providing an opportunity for aggregates to reform. The lower GMD values observed with the MP tillage rotation treatments, where residue cover was minimal, as compared to the RT and CT tillage treatments with cropping during the spring of 1991 indicates the potential for surface residues to stabilize surface aggregates against winter breakdown. However, data from 1989–90 show how surface aggregate size can decrease during winter. This decrease occurred despite the presence of surface residues (CP and RT tillage treatments). Moist soils at the onset of soil freezing, but dried by sublimation, and lack of surface soil water later in the winter season are judged to be the cause of this decrease in aggregate size. Considerable soil movement by wind was experienced in the spring of 1990 and was a direct effect of overwinter processes reducing soil aggregate size.

Aggregate break down during the winter of 1989–90 for the MP tillage treatment combining all rotations is shown in Figure 1. The GMD's measured in the spring of 1990 show essentially all values approaching one. We suggest that a GMD approaching a value of one would be susceptible to wind erosion. In the spring of 1991 the GMD's for the MP
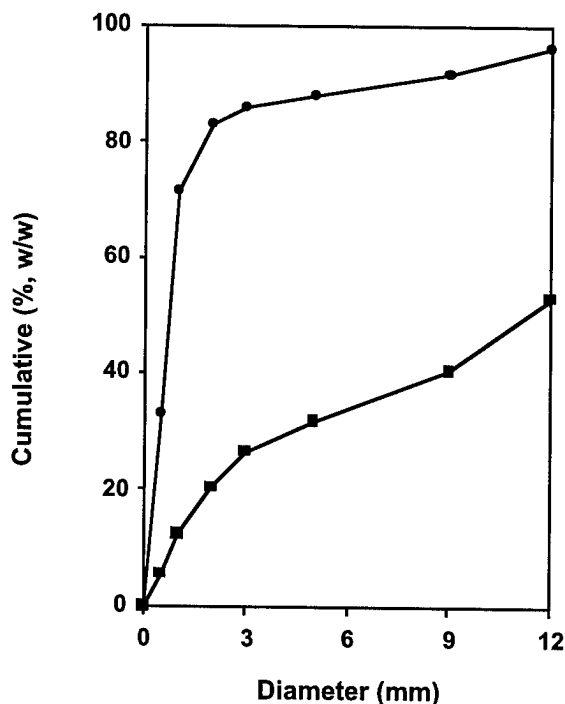
tillage treatment and the CF rotation treatment are considerably reduced compared to the other treatments and are approaching GMD values of one that may become vulnerable to wind erosion. The CP and RT tillage treatments that were cropped had GMD values much greater than one, therefore would appear to have little susceptibility to wind erosion.

CONCLUSIONS

Overwinter processes can influence aggregate size distributions the following spring. Experience has shown farmers in the northern Corn Belt that rough, cloddy fields resulting from fall tillage operations will generally breakdown during the winter season into a friable soil surface suitable for seedbed preparation in the spring. Maximum breakdown of soil aggregates occurs when the soil freezes at a high water content and subsequently dried by sublimation. Cold winter temperatures in combination with high wind speeds aid the sublimation process. This process of aggregate breakdown has the potential to result in a soil surface susceptible to wind erosion. In a situation where the surface soil water content is recharged late in the winter season when thawing conditions are present, disrupted soil particles may reform into larger aggregates. Surface residues can have a stabilizing effect on aggregate sizes by maintaining a snow cover over the soil surface which protects the surface from wind and provides an opportunity for soil water recharge. However, in winters with little snow cover aggregate breakdown can still occur even with surface residue.

Figure 1. Cumulative aggregate size distribution for the moldboard plow (MP) tillage treatment across all crop rotations (n=12) in the fall of 1989 and spring of 1990.

REFERENCES

Anderson, C.H., and A. Wenhardt. 1966. Soil Erodibility, fall and spring. Can. J. Soil Sci. 46: 255–259.

Bisal, F., and W.S. Ferguson. 1968. Monthly and yearly changes in aggregate size of surface soils. Can. J. Soil Sci. 48: 150–164.

Bisal, F., and K.F. Nielson. 1964. Soil aggregates do not necessarily break down over winter. Soil Sci. 98: 345–346.

Chepil, W.S. 1954. Seasonal fluctuations in soil structure and erodibility of soil by wind. Soil Sci. Soc. Am. Proc. 18: 13–16.

Hagen, L.J. 1991. A wind erosion prediction system to meet users needs. J. Soil Water Conserv. 46: 106–111.

Kemper, W.D., and W.S. Chepil. 1965. Size distribution of aggregates. *In*: C.A. Black, et. al. (eds.) Methods of Soil Analysis, Agronomy No. 9, American Society of Agronomy, Madison, WI, USA. pp. 499–510.

Layton, J.B., E.L. Skidmore, and C.A. Thompson. 1993. Winter-associated changes in dry-soil aggregation as influenced by management. Soil Sci. Soc. Am. J. 57:1568–1572.

Miller, R.D. 1980. Freezing phenomena in soils. p. 254-299. *In*: D. Hillel. Applications of Soil Physics. Academic Press, New York.

Renard, K.G., G.R. Foster, G.A. Weesies, and J.P. Porter. 1991. RUSLE: Revised Universal Soil Erosion Equation. J. Soil Water Conserv. 46: 30–33.

Staricka, J.A. and G.R. Benoit. 1995. Freeze-drying effects on wet and dry soil aggregate stability. Soil Sci. Soc. Am. J. 59: 218–223.

Unger, P.W. 1991. Overwinter changes in physical properties of no-tillage soil. Soil Sci. Soc. Am. J. 55: 778–782.

176

The Effect of Freezing Cycles on Water Stability of Soil Aggregates

D.F. DAGESSE[1], P.H. GROENEVELT[1], AND B.D. KAY[1]

ABSTRACT

The role of freezing and thawing processes in controlling soil aggregate stability is addressed. Fast freezing of soil aggregates at high water contents results in a reduction in wet aggregate stability, and an increase in the generation of dispersible clay. Incubation at temperatures above freezing, following a frozen period, reduces the effects of freezing. Greater deterioration was noted as a result of the treatments involving two temperature cycles as compared to just one. Soil pH appears to play a role in determining the stability of soil aggregates during freezing conditions, although the effects are confounded with those of the organic matter content of the soil.

Key words: Freeze-thaw, pH, soil aggregates, water stability.

INTRODUCTION

The literature contains references that credit the freezing process with either soil structural degradation (e.g., Willis 1955, Birecki and Gastol 1968) or structural rehabilitation (e.g., Fippin 1910, Hubbell and Staten 1951). Some studies suggest that both improvement and degradation are possible, depending on specific over-winter conditions (Bisal and Nielsen 1967, Bryan 1971, Layton et al. 1993, Larney et al. 1994), including the time of testing (Alderfer 1946), and the initial soil conditions (Rost and Rowles 1940). Therefore, the change in soil structural stability resulting from the freeze-thaw process remains a topic of considerable debate in the literature. The objective of this study was to test the following hypotheses:

1. Fast freezing at high water contents leads to a decrease in the structural stability of soil aggregates.
2. Freezing following a period of incubation is more destructive than freezing followed by incubation, or by no incubation period.
3. The number of cycles of freeze-thaw, or thaw-freeze, is a factor in the extent of the reduction structural stability.
4. Soil pH is a determining factor in the level of structural stability.

MATERIALS AND METHODS

The experimental material was from a liming experiment on a Brookston clay soil (Typic Haplaquept) (Johnston and Brimner 1988). This material represents a soil with consistent physical properties with the exception of pH, as a result of the application of various levels of lime. The experimental units are field samples with pH values of 5.1, 5.6, 6.0, and 6.4, collected from the location of the liming trials.

Natural soil aggregates from the four field samples, each of different pH, were obtained within a single field from 5.4- by 6.0-m plots of the original liming experiment. Soil aggregates in the 1- to 2-mm size fraction were sieved from the bulked field samples.

To test the hypotheses, six different treatments involving combinations of freezing at -15°C and incubation or thawing at +15°C were used. The details of each treatment are outlined in Table 1.

Aggregates from each of the four field samples were brought to a gravimetric moisture content of 30% by misting with distilled water. Three replicates from each of the four samples were sealed in foil containers to prevent moisture loss, and placed in environmental chamber set at either of the two temperatures for the required time periods.

Measures of wet aggregate stability and dispersible clay following each treatment and subsequent thawing, if applicable, were obtained via the method of Pojasok and Kay (1990).

RESULTS

Structural stability was adversely affected by the freezing process. Analysis of variance revealed that the temperature treatments were highly significant ($P<0.01$). Wet aggregate stability and dispersible clay values for the samples incubated at +15°C for the entire two-week period were significantly different from the corresponding values for the samples which experienced freezing (Fig. 1).

The samples that underwent the different freezing treatments experienced much lower wet aggregate stability values than the samples that

---

Table 1. Treatment methodology.

Treatment Type	Treatment Duration (days)													
	1	2	3	4	5	6	7	8	9	10	11	12	13	14
T	Unfrozen													
T/F	Unfrozen							Frozen						
T/F-½	Unfrozen				Frozen			Unfrozen				Frozen		
F/T-½	Frozen				Unfrozen			Frozen				Unfrozen		
F/T	Frozen							Unfrozen						
F	Frozen													

Notes: F = Frozen @ -15°C   T = Thawed (unfrozen) @ +15°C

were never frozen. Differences between freezing treatments were not statistically significant ($P>0.1$). The same general pattern was observed between the dispersible clay values, with two exceptions. First, there was no significant difference between the dispersible clay values for the T/F (thaw/freeze) and T/F-½ (two thaw/freeze cycles) treatments ($P=0.03$). Secondly, an anomalously high dispersible clay value occurred with the F/T-½ (two freeze/thaw cycles) treatment.

The ordering of the magnitude of deterioration of the treatments for wet aggregate stability was as follows: F > T/F-½ > T/F > F/T-½ > F/T > T. This differed somewhat in the case of dispersible clay, where the order was: F/T-½ > T/F-½ > T/F > F/T > F > T.

To assess the influence of the varying pH levels on structural stability during the freezing process, the effects of the varying pH levels were compared based on whether the sample had experienced freezing of any kind, or whether it had remained unfrozen for the two-week study period. The wet aggregate stability-pH relationship was found to be curvilinear for both the frozen and unfrozen treatments, with maximum stabilities occurring at a pH of approximately 5.8. The

dispersible clay data also assumed a curvilinear form, although maximums occurred at the highest pH level (pH 6.4). In both cases, the frozen samples exhibited lower wet aggregate stabilities and higher dispersible clay values than did the unfrozen samples (Fig. 2).

DISCUSSION

Samples frozen for the entire two-week period and thawed only at the end of the experiment, immediately before stability measurement, experienced the greatest deterioration. Conversely, samples that experienced a period of thaw before stability testing (T, T/F, T/F-½) had greater stabilities. Also, the length of time in which the samples were incubated at +15°C seems to have played a role, as those that experienced 3½ days at the thawing temperature after freezing (F/T-½) had lower stabilities than those thawed for the full 7 days (F/T). This suggests that the thawing period allows for some of the lost stability to be regained through a recementation or age hardening process (e.g., Dexter et al. 1988). Conversely, samples that were incubated at +15°C first and then frozen consistently exhibited lower stabilities than those

178
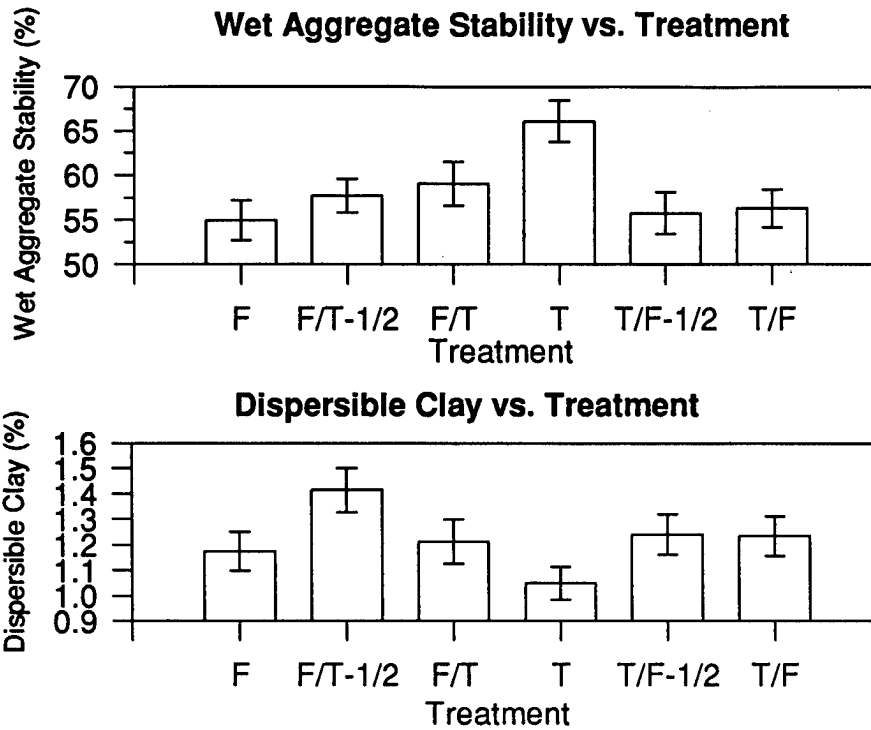
Figure 1. Wet aggregate stability and dispersible clay vs. treatment
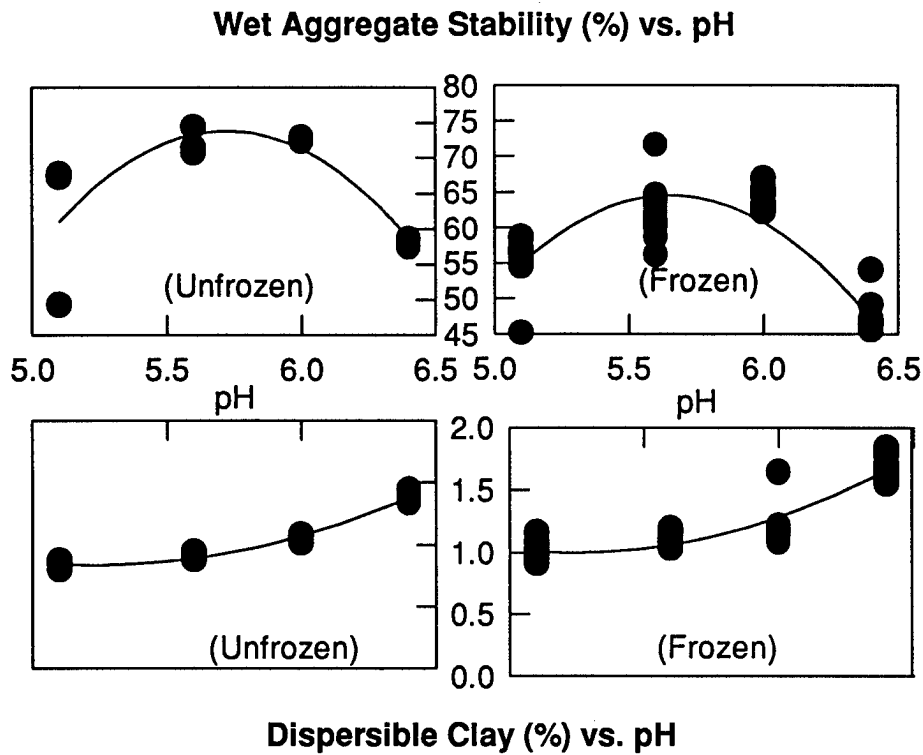
Figure 2. Wet aggregate stability and dispersible clay - pH relationships.

that were frozen first and had a follow-up period of incubation at +15°C. Therefore, there is no apparent benefit to an unfrozen incubation period prior to freezing, as any age-hardening effects were negated by the freezing process.

The destructive effects of freezing may have a cumulative effect with an increased number of freeze-thaw cycles, as suggested in previous studies (e.g., Fippin 1910, Efimov et al. 1981). Both treatments involving two freeze-thaw cycles (T/F-½ and F/T-½) were more destructive than their counterparts involving only one cycle (T/F and F/T). An anomaly to this pattern exists in the data for the samples that were frozen for the entire two-week period, which exhibited the greatest breakdown. The absence of any rehabilitative incubation period at temperatures above freezing before stability determination may be responsible.

Dispersible clay measurements revealed patterns similar to those from the wet aggregate stability data. The samples that experienced freezing temperatures generated more dispersible clay than the continuously unfrozen samples. Also, more dispersible clay resulted from a greater number of temperature cycles. There did not, however, appear to be as much as a reduction in dispersible clay generation if a thaw period followed freezing, as was the case with wet aggregate stability. The highest value of dispersible clay, generated by the F/T-½ treatment, suggests that any recementation process may not be capable of reattaching clay prised from the surface during ice formation. Conversely, age hardening during the pre-freezing incubation at +15°C during the T/F-½ treatment may have been responsible for the lower dispersible clay generation during subsequent freezing.

The apparent role of pH was to increase wet aggregate stability to a maximum value, followed by a decrease. While the increased concentration of Ca^{+2} ions, resulting from the liming operation, would be thought to increase the stability of the clay (e.g., Locat et al. 1990), the decrease at the highest pH levels was somewhat puzzling. It was found, however, that the organic matter content of the samples was positively correlated with the pH, reaching a maximum value at the same intermediate pH. As organic matter is accepted as an effective cementing agent (e.g., Tisdall and Oades 1982), any direct effects of pH are possibly overshadowed by the effects of the different organic matter contents.

The effects of pH on the dispersible clay measurements were quite different from those for wet aggregate stability. The positive relationship between pH and dispersible clay suggests that

increased concentrations of Ca^{+2} favoured the liberation of clay from the aggregate surfaces. Increased cementation within the individual aggregates may have occurred at the expense of the binding of clay to the surface of the aggregates.

While freezing had the general effect of lowering the level of wet aggregate stability, the curvilinear pH effect remained unaffected. This was reflected in the analysis of variance where the pH and treatment interaction was not significant. This was not so with the dispersible clay data, however, where the analysis of variance displayed a highly significant pH and treatment interaction ($P<0.01$). This is in spite of a similar pattern as was the case for wet aggregate stability, in a general increase in the extent of deterioration for those samples that underwent freezing conditions.

CONCLUSIONS

This research set out to address four hypotheses regarding the role of the freeze-thaw process in controlling the structural stability of a clay soil, and to investigate the role of soil pH in this process.

1. Fast freezing of soil aggregates at high water contents results in a reduction in wet aggregate stability, and an increase in the generation of dispersible clay.

2. Freezing following a nonfrozen period is more destructive than when freezing is followed by a nonfrozen period. A post-freezing period of thawing allows for some of the lost stability to be regained through age hardening or recementation within the soil aggregates.

3. The number of temperature cycles seems to play a role in determining the extent of structural deterioration from the freezing process. For both wet aggregate stability and dispersible clay, greater deterioration was noted as a result of the treatments involving two temperature cycles as compared to just one during the two-week study period.

4. pH appears to play a role in determining the stability of soil aggregates during freezing conditions. The exact mechanism remains unclear, however, as the effects of pH are confounded with those of the organic matter content of the soil.

REFERENCES

Alderfer, R.B. 1946. Seasonal variability in the

aggregation of Hagerstown silt loam. Soil Sci. 62: 151-169.

Birecki, M. and J. Gastol. 1968. To the problem of influence of soil freezing and thawing upon soil physical and chemical properties and plant yield. Roczniki nauk Rolniczych. 94-A-3: 363-379.

Bisal, F. and K.F. Nielsen. 1967. Effect of frost action on the size of soil aggregates. Soil Sci. 104: 268-272..

Bryan, R.B. 1971. The influence of frost action on soil-aggregate stability. Inst. Brit. Geog. Trans. 54: 71-88

Dexter, A.R., R. Horn and W.D. Kemper. 1988. Two mechanisms for age-hardening of soil. J. Soil Sci. 39: 163-175.

Efimov, S.S., N.N. Kozhevnikov, A.S. Kurilko, M. Nikitana and A.V. Stepanov. 1981. Influence of cyclic freezing-thawing on heat and mass transfer characteristics of clay soil. Eng. Geol. 18: 147-152.

Fippin, E.O. 1910. Some causes of soil granulation. Proc. Amer. Soc. Agron. 2: 106-121.

Hubbell, D.S. and G. Staten. 1951. Studies on soil structure. USDA Soil Conservation Service, Tech. Bull. #363.

Johnston, R.W., and J.H. Brimner. 1988. Limestone on acid clay soil: Effects on yield and on soil and plant nutrient content. Highlights of Agricultural Research in Ontario. 11: 11-14.

Larney, F.J., C.W. Lindwall, and M.S. Bullock. 1994. Fallow management and overwinter effects on wind erodibility in Southern Alberta. Soil Sci. Soc. Amer. J. 58: 1788-1794.

Layton, J.B., E.L. Skidmore, and C.A. Thompson. 1993. Winter-associated changes in-dry-soil aggregates as influenced by management. Soil Sci. Soc. Amer. J. 57: 1568-1572.

Locat, J., M.-A. Berube, and M. Choquette. 1990. Laboratory investigation on the lime stabilization of sensitive clays: Shear strength development. Can. Geotech. J. 27: 294-304.

Pojasok, T. and B.D. Kay. 1990. Assessment of a combination of wet sieving and turbidimetry to characterize soil structural stability of moist aggregates. Can. J. Soil Sci. 70: 33-42.

Rost, C.O. and C.A. Rowles. 1940. A study of factors affecting the stability of soil aggregates. Soil Sci. Soc. Amer. Proc. 5: 421-433.

Tisdall, J.M. and J.M. Oades. 1982. Organic matter and water stable aggregates in soils. J. Soil Sci. 33: 141-163.

Willis, W.O. 1955. Freezing and thawing, and wetting and drying in soils treated with organic chemicals. Soil Sci. Soc. Amer. Proc. 19: 263-267.

Amelioration of Soil Compaction
by Freezing and Thawing

B.S. SHARRATT[1], W. VOORHEES[1], AND G. McINTOSH[2]

ABSTRACT

Large tractors and implements driven over wet soils can cause compaction, a concern for the long-term productivity of fine-textured soils. Swedish experiments suggest that subsoil compaction can persist over 11 years despite annual freezing below the depth of compaction. There is also evidence that, in proximity to the soil surface, a decline in soil density and penetration resistance occurs overwinter in the northern United States in response to natural forces such as freezing and thawing. A paucity of information exists, however, on the persistence of compaction beyond a decade. Wagon wheel ruts are evident along some pioneer trails that traversed the continental United States in the late 1800's, suggesting that compaction can persist for over a century. One such trail, the Wadsworth Trail that traversed western Minnesota from 1864 to 1871, was the focus of this investigation where we examined soil physical properties across a portion of the trail. Physical properties assessed were soil water content, thermal conductivity, penetration resistance, water infiltration, and air permeability. Soil density appeared to be greater within the area occupied by the wheel ruts, compared to that outside the wheel track, as suggested by the higher penetration resistance and lower water and air infiltration. Indeed, complete amelioration of physical properties that characterize compacted soils was not evident after at least 85 years. This information suggests that for a sustainable and productive ecosystem, compaction of soils should be minimized by either using confined wheel traffic patterns or curtailing traffic on wet soils.

INTRODUCTION

The advent of large tractors and implements bolstered the efficiency of farming operations during the twentieth century. Fewer transverses across fields during planting and harvesting are required today as compared with yesteryear, owing to wider implements and the greater horsepower of the tractor. This improved efficiency in field operations, however, may not always be beneficial to long-term soil productivity. For instance, soil compaction resulting from usage of large machinery is a growing concern in many parts of the world (Hakansson et al. 1987).

Compaction causes physical changes to soils which may be both beneficial or detrimental to ecological processes of the soil system. Compaction generally results in a rearrangement of soil particles into dense aggregates. The loss of pore space, particularly macropores in fine-textured soils, can reduce rates of water infiltration or cause a lack of aeration for plants. Soils of the northern U.S. Corn Belt are particularly vulnerable to compaction. These soils are generally fine-textured and are often wet at the time of fall harvest and spring planting. Indeed, runoff in this sub-humid region is greatest during April (near planting) and again peaks in the fall during October (time of harvest). Runoff in fall and spring in the northern Corn Belt is promoted by both the low evaporative rates and high soil water content during these seasons (Baker et al. 1979).

The natural forces associated with drying and wetting as well as freezing and thawing can affect

---

soil structure. These changes may be most apparent in soils composed in part by montmorillonite, the lattice of which shrinks and swells upon drying and wetting or freezing and thawing. Structural changes caused by freezing and thawing have been observed by Pawluk (1988) and Van Vliet-Lanoe et al. (1984). Indeed, after 100 freeze/thaw cycles, they noted granic fabric development in an otherwise structureless loam and clay loam. Van Vliet-Lanoe et al. (1984) also reported that, under favorable thermal and water regimes, soil structure can develop after 18 to 25 freeze/thaw cycles.

The northern Corn Belt is a region characterized by subfreezing temperatures and soils that shrink and swell. In central Minnesota, air temperatures below 0°C occur from November through March, and the depth of soil freezing can exceed 1 m. In addition, this area undergoes about 80 freeze-thaw cycles per year (Hershfield 1974), which is sufficient to cause structural changes in soils.

This paper reviews our current state of knowledge concerning the effect of freezing and thawing on soil compaction. We also present some experimental evidence that soil compaction may persist for more than 100 years.

AMELIORATING COMPACTION BY FREEZING AND THAWING: A REVIEW

There is little information about the long-term persistence of physical properties that characterize compacted soils. Studies that have assessed temporal changes in density of compacted soils were conducted over a decade or less. Nevertheless, there is a preponderance of evidence to suggest that amelioration of compaction is a process requiring many years, if not decades. The following information sources describe temporal variations in soil structure or density following compaction. These sources represent experiments conducted over time periods that range from 11 years (first citation) to one winter (last citation).

Etana and Hakansson (1994)

Soil properties were assessed 11 years after compacting soils at nine locations in Sweden. The soils ranged from 6 to 85% clay and were subject to wheel traffic by vehicles having an axle weight of 10 Mg. Soils were near field capacity at the time of compaction and were subject to conventional tillage (moldboard plow to a depth of 0.25 m) during the fall of subsequent years. Despite annual freezing to a depth of greater than 0.4 m, little change was noted in soil density below the depth of tillage.

Blake et al. (1976)

Soil physical properties were assessed nine years after compacting a clay loam with a load of 0.75 MPa in southwestern Minnesota. The soil was wet (-0.03 MPa water potential) when compacted and normally froze to 0.9 m each winter. Experimental treatments consisted of cropping systems (corn vs. alfalfa) and fall soil water content (irrigated vs. nonirrigated). Conventional tillage with a moldboard plow was used for corn. These authors found that compaction persisted below the depth of tillage, despite variations in cropping systems as well as soil water content prior to freezing.

Hakansson et al. (1987)

An international series of 26 experiments was undertaken over eight years to assess the response of crops to subsoil compaction in regions with soil freezing. All experiments included tillage treatments to alleviate compaction near the soil surface. Some conclusions drawn from this study included: 1) vehicular axle loads of 10 Mg may impair soil productivity for decades or even permanently, 2) subsoil compaction was persistent despite an annual freeze and thaw below the depth of compaction, and 3) effects of axle loads on soil productivity vary with soil type, soil wetness at time of compaction, and climate.

Schjonning and Rasmussen (1994)

Six years after applying a load of 0.22 MPa to a wet, coarse-sandy soil in Denmark, subsoil compaction was evident to 0.60 m. Compaction persisted despite an annual tillage operation to a depth of about 0.2 m and a winter climate typified by subfreezing temperatures during 9 months of the study period.

Voorhees et al. (1978)

Field experiments were conducted over two winters in southwestern Minnesota where soils typically freeze to 0.9 m. An unsaturated silty clay loam was compacted with a vehicular load of 0.5 MPa. Conventional tillage on the compacted plots consisted of a fall moldboard plow and spring disk in both years. Bulk density and penetration resistance were assessed in the wheel row and between wheel tracks in the spring prior to disking. Natural forces affecting the soil matrix during the winter, as well as fall tillage, resulted in no surface compaction. Subsoil compaction, however, was evident below the depth of tillage to 0.45 m. The authors concluded that freezing and thawing during winter did not ameliorate subsoil compaction.

Kay et al. (1985)

Field studies were conducted over two winters in Ontario to assess overwinter changes in soil density. A silt loam and clay loam were subject to conventional (fall moldboard plow) and no tillage. The soils froze to a depth of greater than 0.6 m. The authors found that near-surface bulk density decreased by 40% from fall to winter, and then increased by nearly 40% from winter to spring. No apparent change in soil density was therefore observed in either tillage treatment as a consequence of freezing and thawing. Failure of these soils to attain a low bulk density after spring thaw was attributed to the instability of the soil matrix during thaw consolidation.

Krumbach and White (1964)

Changes in the bulk density of a loam during one winter were measured on a non-vegetative and alfalfa plot in Michigan. The soil was compacted to a density of 1.6 Mg m^{-3} prior to freezing in the fall. The authors found that the density of the frozen soil was generally lower than prior to soil freezing. Changes in soil density that occurred with freezing were inversely related to changes in soil water content. Nevertheless, the surface and subsurface density were the same after spring thaw as compared to before freezing in the fall.

Voorhees (1983)

Overwinter changes in bulk density and penetration resistance were observed on a silty clay loam in southwestern Minnesota. The soil was compacted in the fall prior to soil freezing by conventional field operations with tractors weighing less than 7.3 Mg. Soil compaction was partially ameliorated to a depth of about 0.1 m. In treatments with no fall tillage, bulk density in the surface 75 mm decreased by 7% while penetration resistance decreased by nearly one-half. However, subsurface compaction persisted throughout the study period.

SOIL COMPACTION AFTER 100 YEARS: A REALITY?

There is little experimental evidence that soil compaction is ameliorated by annual freezing and thawing. Indeed, subsoil compaction may persist for more than a decade. Visual evidence of pioneer trails in the mid-continental United States suggests that soil compaction can persist for more than a century. These trails, particularly the Oregon Trail and Mormon Trail, were well traveled from the 1840's to the 1870's. Approximately 350,000

people emigrated over the Oregon Trail from Missouri to the Pacific Coast during the period 1841 to 1866 (Schlissel 1982). In addition, about 85,000 members of the Church of Jesus Christ of Latter Day Saints emigrated along the Mormon Trail from Iowa to Utah from 1847 to 1869 (Encyclopedia Americana 1986). Wagon wheel ruts are yet visible along portions of these pioneer trails. Ruts along the Oregon Trail are apparent at South Pass, Wyoming, where vegetation has not obscured the wheel tracks (Fig. 1). These and other pioneer trails traversed portions of the United States with extreme climate conditions that include extended periods of subfreezing temperatures.

Another pioneer trail well traveled during the 1860's in the northern United States was the Wadsworth Trail. This trail was developed in 1864 to carry military supplies from St. Cloud, Minnesota, to Fort Wadsworth, Dakota Territory (now Fort Sisseton, South Dakota). Following the Sioux conflict in Minnesota in 1862, the United States government proposed the construction of Fort Wadsworth to thwart conflicts between Native Americans and settlers in the Dakota Territory. Military supplies were carried to St. Cloud via the Mississippi River, and by overland trail from St. Cloud to Fort Wadsworth. Gagers Station was established along the Wadsworth Trail in about 1866 and was the most important stop along the trail from 1866 to 1871 (Hall 1938). However, Gagers Station was short lived due to the extension of the railroad into western Minnesota in 1871. In that year, a community arose along the railroad 8 km south of Gagers Station (currently Morris, Minnesota). Military cargo was thereafter shipped
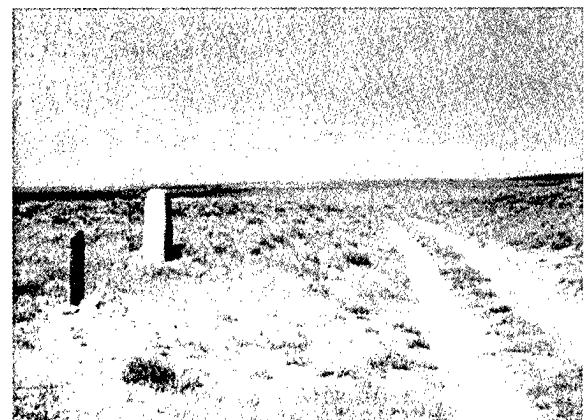
Figure 1. Wagon wheel ruts along the Oregon Trail in Wyoming.

184

by railroad to Morris and by overland trail from Morris to Fort Wadsworth. Gagers Station was sold in 1872.

Gagers Station served as a haven for military personnel, pioneer settlers, and miners. Little evidence of the Wadsworth Trail exists today, owing to the development of the lands in this region for agriculture. However, wagon wheel ruts are apparent 1 km southeast of Gagers Station. These ruts were largely created by oxen and horses pulling wagons that could carry 3.5 Mg in military cargo (Hall 1938). We are uncertain of the year when the trail near Gagers Station was last utilized as a road. The trail 1 km southeast of Gagers Station traversed across land owned by the proprietor's neighbor, suggesting that this portion of the trail was no longer utilized when an issue arose concerning land ownership. The Stevens County map of 1910 indicates the existence of a 2.5-km private road leading eastward from Gagers Station to a county road. This county road was built in a north-south direction in 1882. Then, in 1888, another county road, located 0.8 km east of Gagers Station, was built to aid travel between Morris and destinations northward. Therefore, the private road was most likely established prior to 1888. Nevertheless, the trail south of Gagers Station ceased to exist by at least 1910.

Experimental protocol

Wagon wheel ruts along the Wadsworth Trail are only apparent for a distance of 40 m near Gagers Station. The ruts are located along the crest of a glacial till ridge about 8 km north of Morris, Minnesota (45°39'N, 96°54'W). In accordance with historical preservation, the ruts were examined using non-destructive soil sampling techniques to assess whether soil compaction and structural modifications are apparent after traffic ceased along the trail more than 85 years ago. After the trail was abandoned, the land was in pasture and has been idle since 1963. The trail has been overgrown with Kentucky bluegrass and native grasses such as big bluestem and switchgrass. Bur oak are also prevalent across the glacial ridge.

Three transects were examined along the trail. Elevation changes along these transects are illustrated in Figure 2. Wheel ruts 0.3 m wide are bisected by higher terrain between ruts. The width of the trail was about 2 m. At 11 equidistant sites along each 6-m long transect, vegetation from a 0.35-m area was cleared to expose the soil surface. Within these cleared areas, the following soil properties were assessed: penetration resistance, air
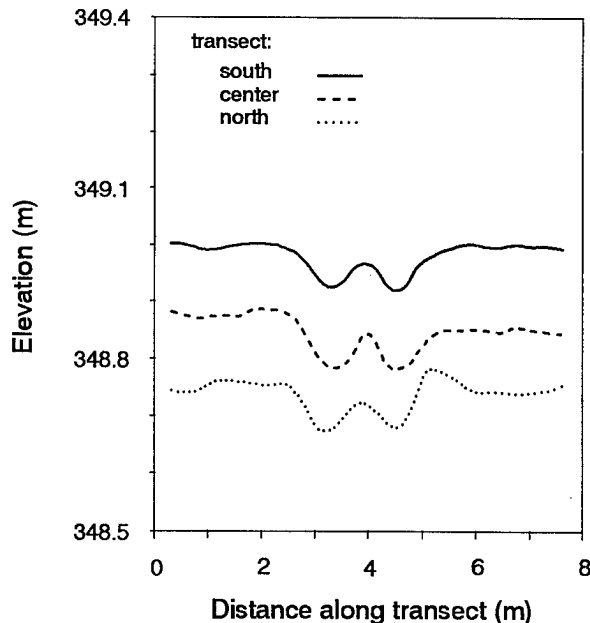
Figure 2. Elevation (above MSL) across three transects of the Wadsworth Trail.

permeability, water infiltration, soil water content, and thermal conductivity. Measurements were performed 17-19 September 1996.

Penetration resistance was measured using a 30° cone with a 19-mm base. The maximum resistance was determined at 50-mm depth increments to 0.3 m. Air permeability was assessed with an air permeameter. Air from the permeameter was constrained to flow into the soil using a 125-mm-diameter plastic pipe, which was driven into the soil at the center of the cleared area to a depth of 0.1 m. A constant flow rate of saturated air was established after which the chamber pressure and temperature were recorded. Concurrent measurements were made of atmospheric pressure. Soil water content was assessed at the outer edge of the cleared area by time domain reflectometry. Probes 0.3 m in length were inserted vertically into the soil. Thermal conductivity was measured by inserting a 125-mm-long probe vertically into the soil and monitoring the temperature rise and heat pulse of the probe with a data logger. The double-ring infiltrometer was used to assess infiltration over a time of 0.75 h. Preliminary measurements indicated that near steady-state infiltration was achieved at this time. The infiltrometer consisted of a 0.3-m-diameter plastic pipe centered over the 125-mm pipe. Water was maintained at the same height in the inner and outer rings. The rate of fall in the height of the water table in the inner ring was used to determine infiltration rates.

Cleared areas were covered for 24 h following water infiltration to minimize evaporation. Measurements were then repeated of penetration resistance, air permeability, soil water content, and thermal conductivity.

RESULTS

The climate prior to the commencement of this study was typified by below-normal rainfall. Rainfall during July and August 1996 was 55% below the 30-year average of 89 mm in July and 76 mm in August. The dry summer extended into September when only 16 mm of rain was received on 10 September. This deficit in precipitation resulted in dry soil on 17 September when soil water content in the upper 0.3 m of the profile was about 0.13 $m^3 m^{-3}$.

Soil physical properties were assessed along three transects of the trail near Gagers Station. Although some differences were evident in physical properties across each transect, results are presented for one transect owing to the similarity in spatial variations across the transects. No differences were found in volumetric soil water content at the initiation of this study or 24 h after ponded infiltration (Table 1).

Thermal conductivity of dry soil on 17 September varied from 0.4 to 1.6 $W\ m^{-1}\ C^{-1}$ across the transect. Conductivity at all locations on the transect increased by 0.3 to 2.0 $W\ m^{-1}\ C^{-1}$ following ponded infiltration. The conductivity on both sampling dates was generally greater in proximity to the wheel rut. Thermal conductivity increases with soil density, but is also influenced by other physical factors such as soil water content.

Table 1. Soil properties at equidistant sites along a 6-m transect of the Wadsworth Trail.

Date	Distance[1]	Water content	Thermal conductivity	Penetration resistance at 5-10 cm	10-15 cm	Water infiltration	Air permeability
	(m)	($m^3\ m^{-3}$)	($W\ m^{-1}\ °C^{-1}$)	(MPa)		(mm min^{-1})	(mm^2)
17 Sep	0	0.11	0.7	1.26	1.21	17. 5	>1.2
	0.61	0.12	0.8	1.56	1.51	11.8	>1.2
	1.22	0.14	0.8	1.35	1.31	10.5	>1.2
	1.83	0.13	0.6	1.34	1.70	4.8	>1.2
	2.44	0.13	1.1	1.46	1.92	12.5	>1.2
	3.05	0.12	1.6	1.55	1.85	16.0	>1.2
	3.66	0.13	0.6	1.33	1.90	5.8	>1.2
	4.37	0.13	0.6	1.22	1.41	6.8	>1.2
	4.88	0.12	0.8	1.16	1.26	14.0	>1.2
	5.49	0.10	0.4	1.26	1.50	22.3	>1.2
	6.10	0.11	0.8	1.16	1.25	16.2	>1.2
19 Sep	0	0.34	1.0	0.45	0.37		0.21
	0.61	0.31	1.1	0.45	0.45		0.20
	1.22	0.31	1.8	0.44	0.43		1.14
	1.83	0.32	2.6	0.55	0.48		0.09
	2.44	0.32	2.9	0.88	0.55		0.17
	3.05	0.30	2.1	0.77	0.56		0.46
	3.66	0.32	1.2	0.77	0.42		0.14
	4.37	0.31	2.2	0.38	0.38		0.24
	4.88	0.30	2.1	0.63	0.56		0.21
	5.49	0.29	1.2	0.32	0.36		0.37
	6.10	0.30	1.4	0.43	0.41		0.20

[1] East and west wheel ruts at 2.44 and 3.66 m, respectively, and the shoulders of the trail at 1.83 and 4.37 m.

Penetration resistance over the depth interval of 5 to 15 cm are reported in Table 1. These depths (5-10 and 10-15 cm) represent those most susceptible to compaction from wheel traffic as well as those which are little affected by surface biomass (crown and roots of plants). Resistance decreased by about 75% after the dry soil was subject to ponded infiltration. Averaging the results from both depth intervals, penetration resistance was greatest within or between wheel ruts (distance of 2.44 to 3.66 m along the transect) compared to other locations along the transect. For example, on 17 September, resistances within or between the wheel ruts were 1.6 MPa or higher while resistances at other locations on the transect were 1.2 to 1.5 MPa. Likewise, on 19 September, penetration resistance was 0.6 MPa or higher within or between the ruts and less than 0.6 MPa at the other locations.

Water infiltration and air permeability perhaps best define differences in soil structure across the trail. Near steady-state infiltration was lowest in proximity to the wheel ruts compared to other locations on the transect (Table 1). For example, infiltration on the shoulder of the east rut (distance of 1.83 m along the transect) or in the west wheel rut and shoulder (distance of 3.66 and 4.37 m along the transect, respectively) was 50% lower as compared to other locations. Cumulative infiltration over 0.75 h substantiate the differences in steady-state infiltration. Air permeability could not be assessed on 17 September due to the porous structure of the dry soil. Permeabilities at all locations along the transect exceeded 1.2 mm². Loam and clay loam soils of this region shrink and swell upon drying and wetting; thus the presence of large macropores allowed for rapid air exchange between the pressure chamber and soil atmosphere. At the time of this study, earthworm casts were also prevalent at the soil surface. This also suggests that preferential flow channels created by earthworms may have allowed for rapid air exchange through the soil. Permeabilities on 19 September confirm the results obtained from water infiltration. Permeabilities in the wheel ruts or on the shoulder of the trail were 20 to 50% smaller compared with other locations along the transect.

Some physical properties in proximity of the wheel ruts are yet atypical of properties outside the trail despite traffic along the trail near Gagers Station ceasing more than 85 years ago. Penetration resistance, water infiltration, and air permeability appeared to be altered either on the shoulder or in the wheel ruts compared to locations at both ends of the transect. Physical properties on the shoulder of the trail were likely affected by wagon wheel or animal traffic.

PERSPECTIVES

There is evidence from both previous studies and this field study that soil compaction can persist for a decade or century. Although the results of this study confirm differences in physical properties of a wheel track vs. non-tracked areas, no attempt was made to assess plant responses to these differences in physical properties. Nevertheless, conventional practices used today in farming operations may affect soil physical properties that could persist for a century. Therefore, to preserve the integrity of our soils for future generations, management practices must be implemented to confine wheel traffic on agricultural soils as well as to limit traffic on wet soils.

ACKNOWLEDGMENT

REFERENCES

Baker, D. G. , W. W. Nelson, and E. L. Kuehnast. 1979. Climate of Minnesota. Part XII. The hydrologic cycle and soil water. Minnesota Agric. Exp. Stn. Tech. Bull. 322.

Blake, G. R. , W. W. Nelson, and R. R. Allmaras. 1976. Persistence of subsoil compaction in a Mollisol. Soil Sci. Soc. Am. J. 40:943-948.

Encyclopedia Americana. 1986. Grolier Incorporated, Danbury, CT.

Etana, A. and I. Hakansson. 1994. Swedish experiments on the persistence of subsoil compaction caused by vehicles with high axle load. Soil Tillage Res. 29:167-172.

Hakansson, I. , W. B. Voorhees, P. Elonen, G. S. Raghavan, B. Lowery, A. L. Van Wijk, K. Rasmussen, and H. Riley. 1987. Effect of high axle-load traffic on subsoil compaction and crop yield in humid regions with annual freezing. Soil Tillage Res. 10:259-268.

Hall, G. C. 1938. The Wadsworth Trail. Grace Cynthia Hall, Morris, MN.

Hershfield, D. M. 1974. The frequency of freeze-thaw cycles. J. Applied Meteorol. 13:348-354.

187

Kay, B. D. , C. D. Grant, and P. H. Groenevelt. 1985. Significance of ground freezing on soil bulk density under zero tillage. Soil Sci. Soc. Am. J. 49:973-978.

Krumbach, A. W. Jr. and D. P. White. 1964. Moisture, pore space, and bulk density changes in frozen soil. Soil Sci. Soc. Am. Proc. 28:422-425.

Pawluk, S. 1988. Freeze-thaw effects on granular structure reorganization for soil materials of varying texture and moisture content. Can. J. Soil Sci. 68:485-494.

Schjonning, P. and K. J. Rasmussen. 1994. Danish experiments on subsoil compaction by vehicles with high axle load. Soil Tillage Res. 29:215-227.

Schlissel, L. 1982. Women's diaries of the westward journey. Schocken Books, New York.

Van Vliet-Lanoe, B. , J. Coutard, and A. Pissart. 1984. Structure caused by repeated freezing and thawing in various loamy sediments: A comparison of active, fossil and experimental data. Earth Surface Processes Landforms 9:553-565.

Voorhees, W. B. , C. G. Senst, and W. W. Nelson. 1978. Compaction and soil structure modification by wheel traffic in the Northern Corn Belt. Soil Sci. Soc. Am. J. 42:344-349.

Voorhees, W. B. 1983. Relative effectiveness of tillage and natural forces in alleviating wheel-induced soil compaction. Soil Sci. Soc. Am. J. 47:129-133.

Freeze-Thaw Effects on the Hydrologic Characteristics of Rutted and Compacted Soils

L.W. GATTO[1]

ABSTRACT

U.S. Army training exercises compact and often rut soils, which can increase hillslope runoff and concentrate surface flows, and enhance soil erosion. My objectives are to determine the effects of freeze–thaw (FT) on vehicular ruts, which concentrate flows and often erode to gullies. A noncohesive silt was rutted with a pickup truck, then frozen and thawed three times. Frost heave, rut geometry, soil compression, shear strength, and infiltration were measured. Results show that 1) ruts start to freeze later and thaw slower than uncompacted soil; 2) once ruts start to freeze, they freeze faster than unrutted soil; 3) the ruts heave an average of 0.2 to 3.2 mm more than unrutted soil; 4) the infiltration in ruts increases by 62%, unconfined compression strength decreases by 16% and shear strength by 14%, and rut hydraulic radius decreases an average of 9% after three FT cycles. These results suggest that the volume of water flowing in these ruts would be lower, the rut soils would be weaker (more erodible) and the rut flow velocity would be lower after the FT cycles. Future experiments will investigate rut and rill responses in different soils at variable FT rates.

Key words: Vehicular ruts, freeze–thaw, infiltration, soil strength, erosion potential.

INTRODUCTION

Soil erosion by water occurs naturally on hillslopes and is a function of the erodibility (detachability) of soil particles and the energy of surface runoff to detach and transport sediment (erosivity) (Table 1). Soil erodibility is a function of interparticle friction, bond-

Table 1. Factors that determine the severity of water erosion (Lal and Elliot 1994).

I. Climatic Erosivity
1. Rainfall erosivity
   - a measure of the ability of rain to detach sediment particles and surpass the infiltration capacity of soil so that overland flow begins
   - also called the energy-intensity (EI) parameter, a function of rainfall volume, raindrop impact and peak intensity
2. Runoff erosivity
   - a measure of the ability of flowing water to detach and transport sediment particles
   - a function of runoff volume and peak flow

II. Soil Erodibility
   - a measure of the susceptibility of sediment particles to being detached and transported by flowing water
   - a function of soil texture, structure and permeability, organic matter content, chemical constituents and clay mineralogy

III. Topography
   - hillslope length, steepness and shape influence overland flow velocities and turbulence which partially determines the likelihood of rill formation

IV. Land Use
   - disturbance to a soil surface influences the effectiveness of raindrop impacts in moving soil particles, soil infiltration rates and overland flow velocities and turbulence

[1] U.S. Army Cold Regions Research and Engineering Laboratory, 72 Lyme Road, Hanover, New Hampshire 03755-1290, USA

ing and interlocking, and erosivity is a function of run-off volume and velocity. Water can flow over soil in broad, shallow sheets or concentrated in rill or gully channels. Concentrated flow is faster and more turbulent than sheet flow and are more erosive.

Morgan (1977) determined that 40 times more sediment was transported in rills than overland out of rills on a 11° slope. Mutchler and Young (1975) determined that more than 80% of eroded hillslope sediment is transported in rills. In addition, Meyer et al. (1975) found a threefold increase in soil loss following rill development on a hillslope. Rill erosion is clearly geomorphically significant (Slattery and Bryan 1992).

Soil crusts and vegetation generally increase soil resistance to flowing water. Vegetation reduces flow velocity as well. Off-road vehicular changes soil hydrologic characteristics by destroying soil crusts, damaging vegetation, loosening surface soils, altering soil structure, weakening soil aggregates, changing soil surface configuration and compacting soils. These changes increase the likelihood of soil erosion by water.

Vehicles can also rut a soil surface, which increases erosion potential. Voorhees et al. (1979) reported that wheeled-vehicles ruts can act as channels to concentrate surface runoff. Foltz (1993) determined that 200–400% more erosion occurs on rutted vs. unrutted roads. Thus, vehicular ruts are hydraulically similar to rills, especially when oriented downslope.

The U.S. Army is concerned about soil erosion on military training lands. Managers of these lands must be equipped with state-of-the-art, land-management techniques for minimizing and repairing vegetation damage and reclaiming eroded lands.

BACKGROUND

Fourteen U.S. Army and National Guard installations are located in the northern U.S. where frozen soil can dramatically increase runoff rates and volumes during rain events and snowmelt. In addition, the strength of frost-susceptible soils is often at an annual low in the spring (Fig. 1) because of excess soil water after thaw. This excess water enhances soil creep and failure, and soil erodibility by raindrops and surface flows. And yet, past research has not addressed how seasonal soil freeze–thaw (FT) cycling influences vehicular ruts, natural rills, soil compaction and erodibility.

Kok and McCool (1990) report that the effects of soil FT is one of the least understood aspects of the soil erosion mechanics, even though FT processes have been investigated for years. Gerits et al. (1990) and Kirkby (1980) state that such dynamic processes are the most important experimental topics in the soil erosion arena. Consequently, incorporating the effects of FT on soil compaction and strength, runoff and erosion into soil erosion models remains a high priority (Papendick and Saxton 1990) and impedes improvements in soil erosion prediction capability (Nearing et al. 1994).

The objective of the experiments reported herein was to begin to fill this important gap in the knowledge of soil erosion mechanics. I observed and measured the effects of soil FT cycling on the surface soil strength and infiltration in vehicular ruts. My hypotheses were that the geometry of vehicular ruts in frost-susceptible soils changes due to FT-induced soil creep and that FT changes soil strength and infiltration in ruts. Such changes would affect the volume and velocity of water flow in ruts.
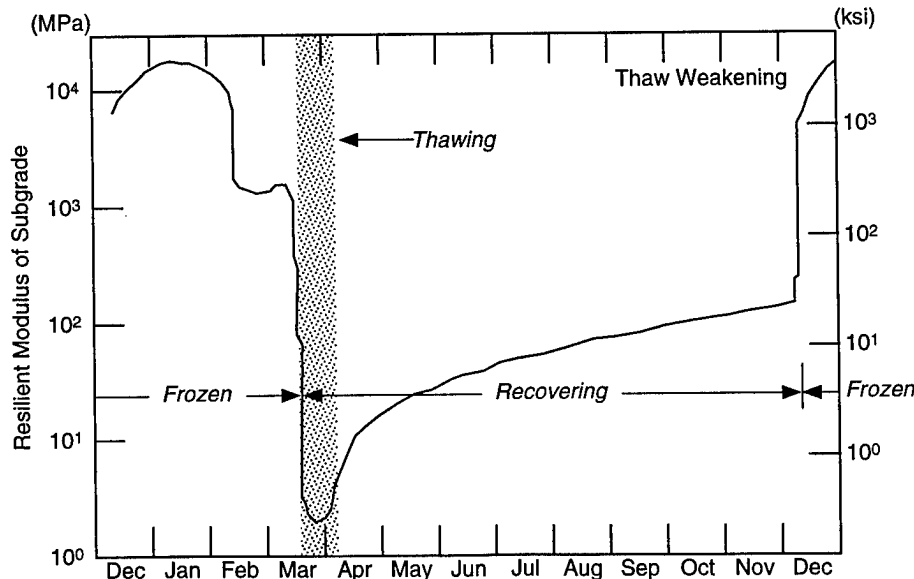
Figure 1. Temporal changes in the resilient modulus (i.e., soil strength) of a low plasticity silt (Johnson et al. 1978).

190

EXPERIMENTAL SETUP AND METHODS

Four, 1.2-m (w) × 2.4-m (l) × 0.6-m (d) soil bins were (Fig. 2) constructed of two layers of pressure-treated, 1.9-cm-thick plywood with exterior reinforcement. Bins were insulated with 5.1-cm polystyrene boards. Each bin was set horizontal and was a closed system without a source of water. The soil used was a low-plasticity (liquid limit = 28%, plastic index = 1), inorganic, clayey silt (locally called Hanover silt). The soil was placed in the bins with a backhoe and leveled with a rake. After the addition of 20.3 cm of soil to the bin, I tamped it to a thickness of about 15.2 cm. The surface was roughened with a rake before additional soil was added to reduce the development of boundaries within the soil. Three layers were prepared in each bin this way. Table 2 lists characteristics of the surface of the topsoil layer.

Soil-resistivity gages (RG) consisting of a PVC

rod with 18 copper rings and 10 thermocouples (Fig. 3) were mounted to the bottom of each bin, one under the rut location, the other out of the rut, before soil was placed in the bins. The RGs measure the change in soil electrical resistance as the soil water between ring pairs freezes and thaws. The resistance increases
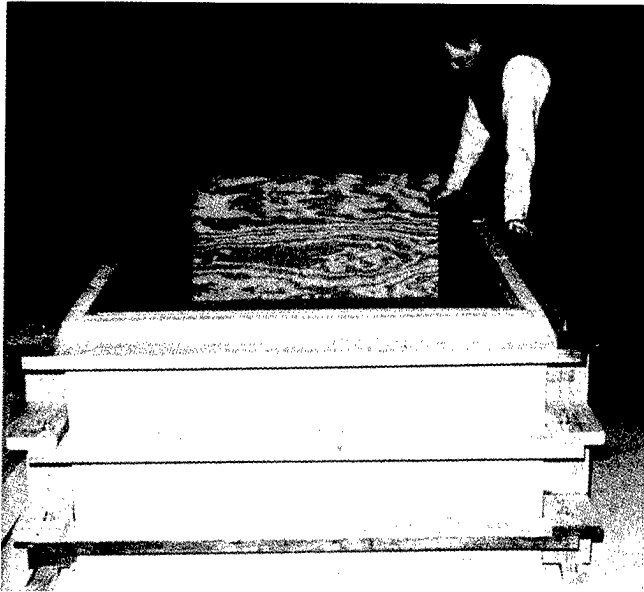
Figure 2. Soil bin construction.
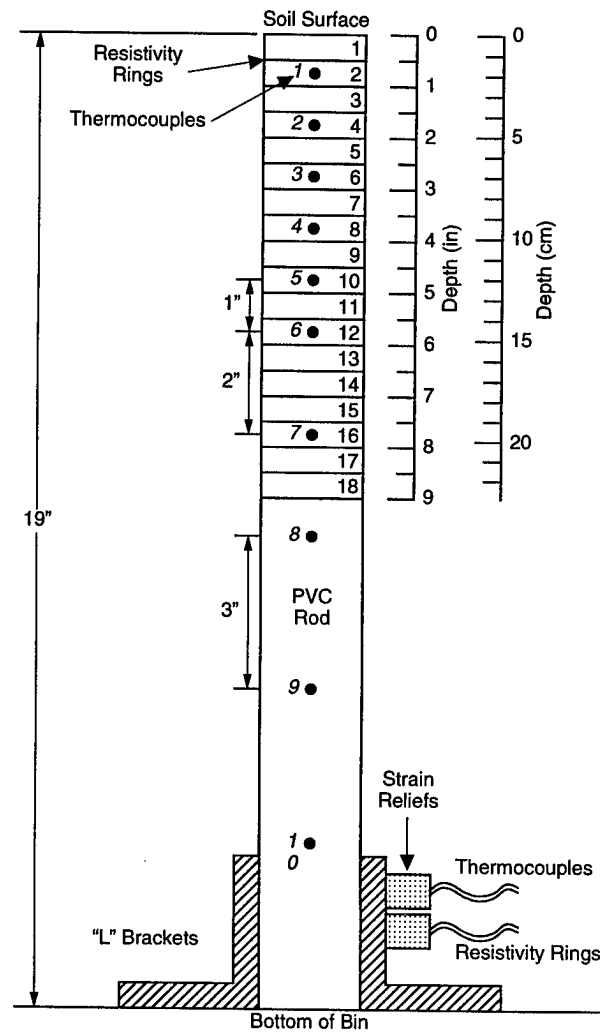
Figure 3. Resistivity gage configured following Atkins' (1979, 1990) specifications.

Table 2. Characteristics of the surface of the top soil layer in each bin before rutting and FT cycles.

Bin	γ lb/ft³	(Mg/m³)	γd lb/ft³	(Mg/m³)	e	n	w (%)	q (%)	S (%)
B1	103.8	1.66	88.5	1.42	0.90	0.47	17.3	24.5	52
B2	99.4	1.59	85.6	1.37	0.97	0.49	16.1	22.1	45
B3	102.7	1.65	90.6	1.45	0.86	0.46	15.5	22.5	49
B4	94.4	1.51	81.1	1.30	1.08	0.52	16.4	21.3	41

γ = moist unit weight   w = gravimetric water content
γd = dry unit weight   q = volumetric water content
e = void ratio   s = saturation
n = porosity

191
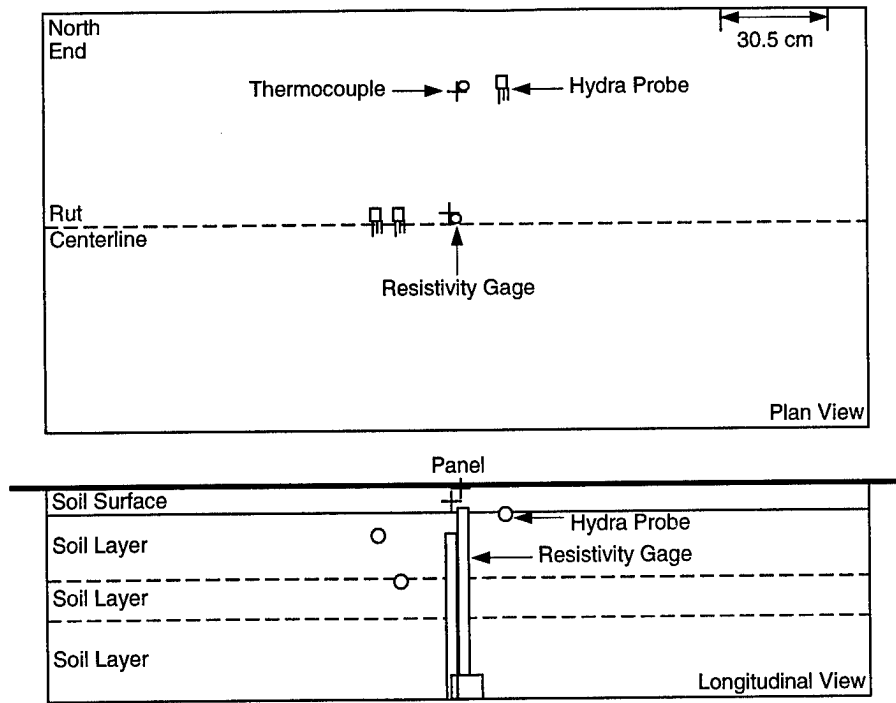
Figure 4. Instrument setup for all bins.

dramatically during freezing and decreases during thaw. This marked change in resistance is a more reliable indication of the phase of soil water than soil temperature alone (Atkins 1979) and the combined soil temperatures and resistances serve as a check on soil frost depth.

Hydra probes (Vitel, Inc. 1994) were positioned in the soil (Fig. 4) before the ruts were made. The probes measure the soil complex dielectric which consists of a capacitive and a conductive electrical response. As a soil gets wetter, the capacitive response increases and with appropriate calibration the dielectric measurement is directly related to volumetric soil water content. The probes monitor soil water redistribution during freeze–thaw cycles.

An empty pickup truck was driven on the soil many times in forward and reverse directions to produce

measurable ruts. Freezing panels were placed on the top of the bins about 12.7 cm above the soil surface during the freeze and were removed to expose the bin soil to the ambient building air during thaw. The soil was frozen and thawed three times in this fashion. Thermocouples measured the temperature of the freezing panels, the air 3.8 cm above the soil, the air 70 cm above the soil during thaws, and the soil surface in and out of the ruts. Temperatures, soil resistivities and soil water contents were recorded every three hours.

Compacted soil has higher compressive and shear strengths than that of soil uncompacted, so I measured strength changes to determine the effect of FT on the compacted rut soil. I measured strength and infiltration of the surface soil only because as Shainberg et al. (1994) pointed out soil detachment by rill or over-
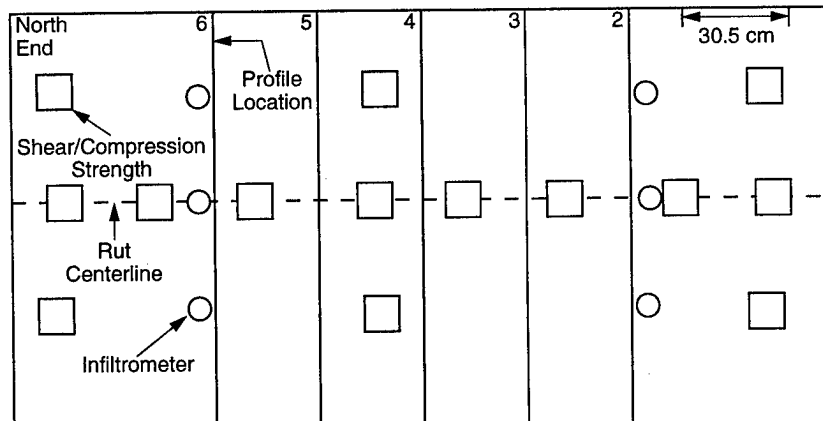
Figure 5. Strength and infiltration time measurement sites (plan view).

192

land flows depends on soil particle binding forces at the soil/water interface. Compressive strength was measured with a pocket penetrometer (Soil test CL-700A) and shear strength with a Torvane shear device (Soil test CL-600A). Changes in compaction result in infiltration changes as well. I measured the infiltration time needed for 1.3 cm of water to drain into the soil from a 5.1-cm-ID plastic tube inserted into the soil. Measurement sites are shown in Figure 5.

I measured the vertical distances between a datum (aluminum bar) and the soil surface before and after each freeze and thaw to determine frost heave and rut geometry. Distances were measured at least every 5 cm along the bar except where closer measurements were necessary to adequately define the rut cross-sectional area (A) and perimeter (P). Rut geometry was profiled at five locations per bin (Fig. 5). Estimated error for all measurements was <1mm.

RESULTS AND DISCUSSION

Thermal/water regime

The first freeze (F1) lasted 19.1 days, F2 was 9 days and F3, 8.8 days. The freeze panel temperature at the beginning of F1 was held at –6°C for about 4.9 days, was lowered to –12°C for 3.3 days and was lowered again to –17°C for 2.8 days. The panels were then raised to –1°C and maintained at that temperature for 8.1 days. Panel temperature during F2 and F3 was –6°C. Frost penetration during F1 was 5.1 cm/day under the ruts and 3.5 cm/day outside the ruts (Table 3). Frost penetration in the ruts during F1 was faster possibly because the compacted soil had less air-filled voids and more particle-to-particle contacts per unit volume than the uncompacted soil and better heat transfer to the cold air (Farouki 1981). Penetration

rates in and out of the ruts were similar (Table 3) after the compacted soil was loosened after FT1, during F2, 2.5 cm/day in and 2.9 cm/day out, during F3, 1.7 and 2.0 in and out, respectively.

The soil froze to about 39 cm in the ruts and 43 cm out of the ruts during F1, to 16 cm in and 22 cm out during F2 and 10 cm in and 14 cm out during F3. The soil surface in the ruts took about twice as long to start freezing than the surface out of the ruts, which may explain why the frost depth in was less than that out of the ruts. The ambient air temperature during the first thaw (T1) was 5 to 12°C, 13–19°C during T2, 21–25°C during T3.

The changes in soil water distribution at the three Hydra probe depths are similar during all FT cycles. Water at the out-of-rut depth of 1.3 to 3.6 cm starts freezing earliest, but freezes slowest possibly because more water is present to freeze having been drawn here from the soil below. The amount of soil water in this near surface zone outside the rut after FT1 is 10% higher than before F1 and 13% higher after FT2. Soil water content in the rut at 5 to 7.4 cm depth was 6% higher after FT1 and 3 to 7.5% higher after FT2, and that in the rut at 16.5 to 18.8 cm was 2% lower after FT3 to 4% higher after FT1. The water in the unrutted soil drains more rapidly than that in the ruts during thaw.

Soil compaction and infiltration

Soil compaction changes soil pore geometry (Gupta et al. 1989) reduces the interconnectedness of larger pores (Hillel 1980), increases soil bulk density, which reduces infiltration (Akram and Kemper 1979) and increases soil penetration resistance (Voorhees et al. 1986). Lower infiltration results in increased surface runoff volumes (Eckert et al. 1979, Mathier and

Table 3. Frost penetration rates and depths.

	Penetration rate (cm/day)						Frost depth (cm)					
	F1		F2		F3		F1*		F2		F3	
	IR	OR	IR	OR	IR	OR	IR	OR	IR	OR	IR	OR
	5.3		3.0		1.5		37		13.4		9.5	
		3.6		2.8		2.0		42		21*		13.4
	3.6		2.0		1.8		40		17.2		12.1	
		3.0		2.8		2.0		43		22*		14.6
	4.1		2.5		1.8		38		15.9		8.3	
		4.1		2.8		2.0		42		21*		10.9
	7.4		2.5		1.8		39		18.4		10.9	
		3.3		3.0		2.0		44		23*		15.9
Avg=	**5.1**	**3.5**	**2.5**	**2.9**	**1.7**	**2.0**	**39**	**43**	**16.2**	**21.8**	**10.2**	**13.7**

IR = in rut; OR = out of rut.

* Estimated depth of 0°C isotherm given here because frost was deeper than the deepest ring pair.

193
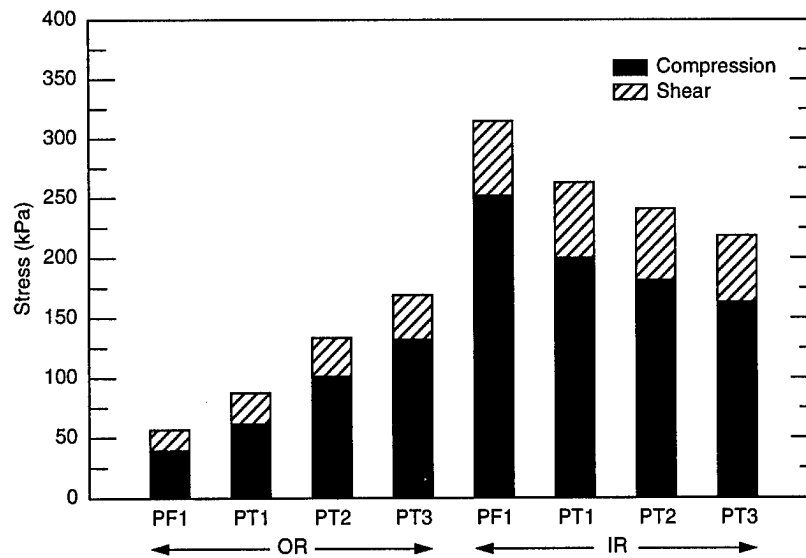
Figure 6. Soil strength after three FT cycles; PF = prefreeze; PT = post thaw.
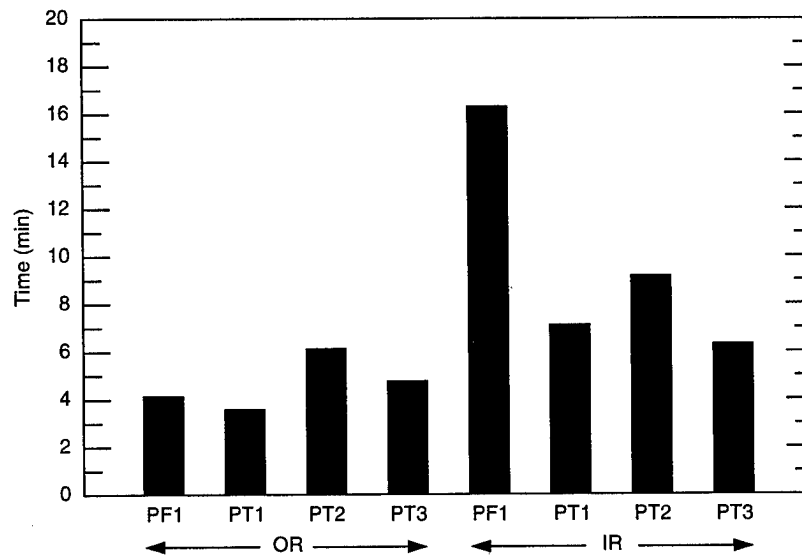
Figure 7. Infiltration times after three FT cycles.

Roy 1993) and longer runoff periods (Hinckley et al. 1983). Compacted soils, however, can be loosened by shrinking and swelling, root growth and freeze–thaw so that infiltration can be enhanced (Canarache 1991, Thurow et al. 1993). Chamberlain and Gow (1979) found that FT increased vertical permeability in four fine-grained soils. The ice formed in the pores of compacted soil during freezing can push soil grains apart and reduce soil density. The degree of this soil expansion depends on volumetric soil water content as freezing begins, soil porosity and texture, rate of frost penetration and the number of FT cycles (Webb et al. 1983).

The out-of-rut soil gained strength with each FT cycle due to FT-induced consolidation, while the compacted rut soil was weakened. Before F1 the rut soil was six times stronger in compression and 50% stronger in shear than that out of the rut and weakened with

each FT cycle (Fig. 6). Compressive strength was reduced by 22% after FT1 and an additional 13% after the subsequent 2 FT cycles. Voorhees et al. (1978, 1983, 1986) concluded that FT was more effective when the soil was wetter at freezeup and that the combined effects of FT, and wetting and drying reduced soil penetration resistance by 20–50%. Shear strength was reduced by 1%, virtually unchanged after three FT cycles.

The infiltration time in the IR soil decreased by 62% after the three FT cycles (Fig. 7) and increased slightly in the OR soil probably due to the consolidation. Akram and Kemper (1979) reported that soil compaction was reduced and soil infiltration increased after one FT cycle in a loamy sand, two cycles in one sandy loam and three cycles in another sandy loam, and was still increasing in a clay loam after four cycles.These results suggest that the reduc-

194
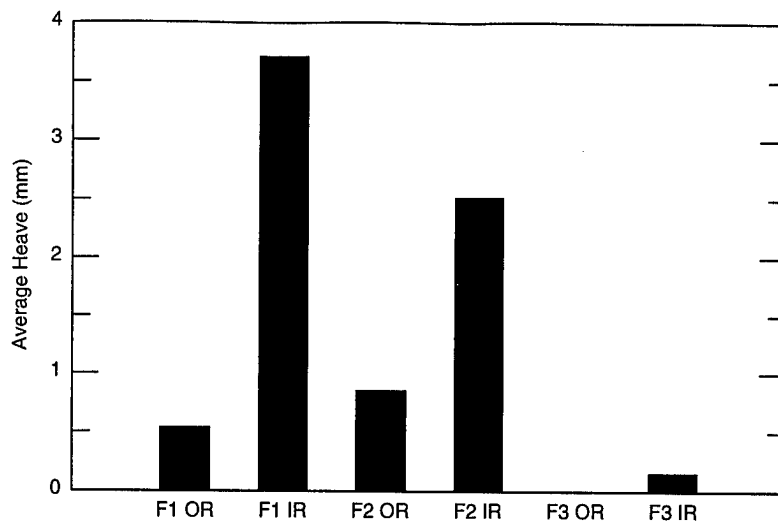
Figure 8. Average frost heave based on 80 measurements per freeze.

tion in compaction and IR infiltration time could lead to less runoff volume and reduced flow erosivity but more erodible (weaker) soil in these ruts.

Frost heave

The amount of frost heave that occurs during freezing is a measure of the amount of ice formed, which is partially a function of the volume to water drawn to the freezing zone from the subsoil (Miller 1980). Heave was measured at four IR points and four OR along each of the five profiles per bin. The bottom of the ruts heaved an average of 3.2 mm more than the soil outside during F1 (Fig. 8). This could have resulted from the differences in thermal conductivities within and outside of the ruts. In addition, the compacted rut soil had less void volume and thus may heave more with less void to accommodate the volume expansion during freeze.

Hydraulic geometry

Frost-induced soil creep along rill sideslopes can obliterate rill channels over one winter (Carson and Kirkby 1972, Schumm 1956). I am unaware of such studies of vehicular ruts until this experiment, which showed that rut shape changes due to FT processes as well. The ruts got shallower and wider at the top along the rut crest (Fig. 9) due to rut sideslope soil creep, slides and flows during thaw.
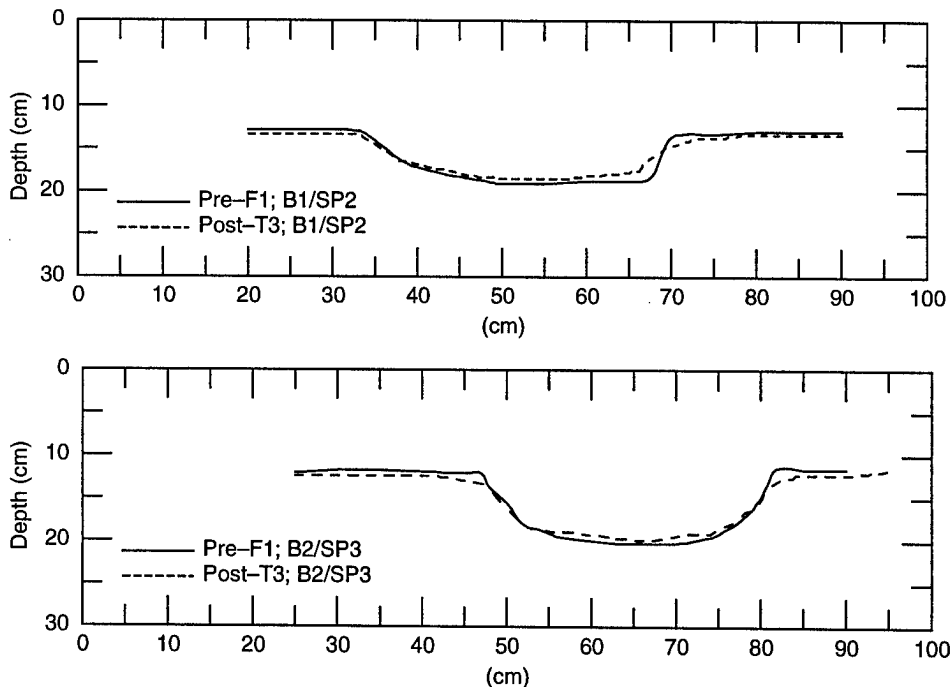
Figure 9. Typical rut cross sections before F1 and after T3.

195
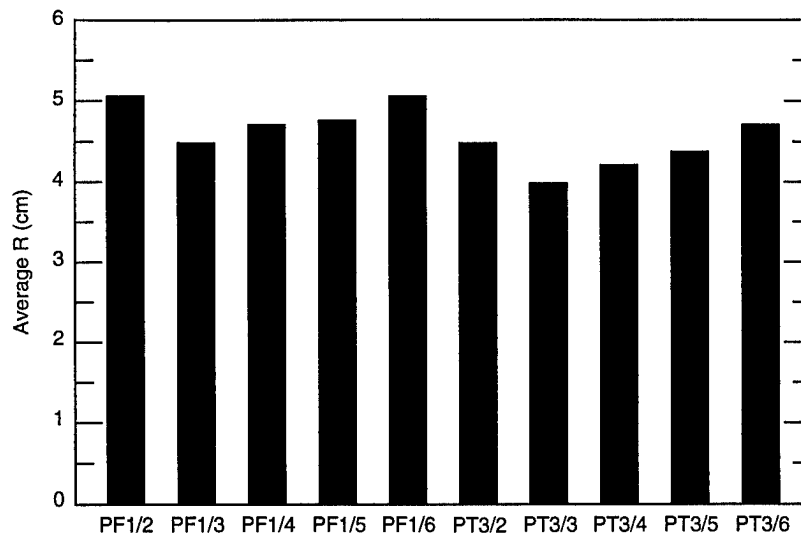
Figure 10. Change in the hydraulic radius of ruts (assuming a bank-full flow) after three FT cycles; last number in the sequence, e.g., PF1/2, is the profile location in the bins.

Open-channnel flows in rivers, rills and ruts are hydraulically similar in that they are usually significantly deeper than the height of the coarsest roughness elements within their respective channels (Thornes 1980, Hairsine and Rose 1992). The velocity of such flows is a function of channel characteristics, i.e., channel roughness (C) and hydraulic radius (R), and slope (S) and can be approximated by the Chezy equation, $V = C\sqrt{RS}$, among others. Thus, channel geometry and changes in it are important in determining rill or rut flow erosivity.

The hydraulic radius, R (A/P), of the ruts in this experiment decreased an average of 9% (Fig. 10) with the cross-sectional changes that were measured after the three FT cycles. The effect of this decrease would be that flows in the ruts after the FT cycles would be shallower and broader than before the FT and more like overland, sheet flow with lower velocity and erosivity than before FT.

However, in the field rut cross-sectional shape and thus flow velocity is determined by a variety of sediment infilling processes and sediment removal by intermittent flows. However, these results suggest that FT-induced soil creep can be an important infilling process, and its importance depends on the amount of excess pore water at thaw that saturates the surface soils, making them susceptible to the mass failures.

CONCLUSIONS

The results reported herein are from only three FT cycles in only one soil type and are thus preliminary. But these initial findings show that soil FT cycling changes the hydraulic geometry of vehicular ruts and the compaction, infiltration and strength of the soil within the ruts, which suggests that FT could have a

significant effect on hillslope soil erodibility and rut flow erosivity. Future experiments will investigate the effects of FT on ruts and compaction in different soils at various soil water contents exposed to different FT rates and the heat loss along rut crests during soil freezing. That loss may be enhanced because two soil surfaces, rut sidewalls and the soil just outside the rut crest, are present for heat conduction to the air. This enhanced loss may cause more water to migrate to this zone, resulting in a larger volume of ice at thaw. Our results will ultimately be used to modify the winter processes, hydrology, soils and hydraulics of overland flow components of the Water Erosion Prediction Project soil erosion model for application on Army training lands.

ACKNOWLEDGMENTS

REFERENCES

Akram, M., and W.D. Kemper. 1979. Infiltration of soils as affected by the pressure and water content at the time of compaction. Soil Sci. Soc. Am. J. 43: 1080–1086.

Atkins, R.T. 1979. Determination of frost penetration by soil resistivity measurements. USA Cold Regions Research and Engineering Laboratory, Special Report 79–22.

Atkins, R.T. 1990. Frost resistivity gages: Assembly and installation techniques. USA Cold Regions

Research and Engineering Laboratory, Technical Note (unpublished). October.

Canarache, A. 1991. Factors and indices regarding excessive compactness of agricultural soils. Soil and Tillage Research 19: 145–164.

Carson, M.A., and M.J. Kirkby. 1972. Hillslope form and process. Cambridge University Press, Cambridge, Great Britain, p. 191–193.

Chamberlain, E.J., and A.J. Gow. 1979. Effect of freezing and thawing on the permeability and structure of soils. Engineering Geology 13: 73–92.

Eckert, R.E., M.K. Wood, W.H. Blackburn and F.F. Peterson. 1979. Impacts of off-road vehicles on infiltration and sediment production of two desert soils. Journal of Range Management 32(5): 394–397.

Farouki, O.T. 1981. Thermal properties of soils. USA Cold Regions Research and Engineering Laboratory, Monograph 81-1.

Foltz, R.B. 1993. Sediment processes in wheel ruts on unsurfaced forest roads. PhD Dissertation, University of Idaho, Moscow, ID.

Gerits, J.J.P., J.L.M.P. de Lima and T.M.W. van den Broek. 1990. Overland flow and erosion. Chapter 6, In M.G. Anderson and T.P. Burt (ed.), Process studies in hillslope hydrology, John Wiley and Sons, New York, p. 173–214.

Gupta, S.C., P.P. Sharma and S.A. DeFranchi. 1989. Compaction effects on soil structure. Advances in Agronomy 42: 311–338.

Hairsine, P.B., and C.W. Rose. 1992. Modeling water erosion due to overland flow using physical principles, 2. Rill flow. Water Resources Research 28(1): 245–250.

Hillel, D. 1980. Fundamentals of soil physics. Academic Press, New York.

Hinckley, B.S., R.M. Iverson and B. Hallet. 1983. Accelerated water erosion in off-road vehicle use areas. Chapter 5, In R.H. Webb and H.G. Wilshire (ed.), Environmental effects of off-road vehicle impacts and management in arid regions, Springer-Verlag, New York, p. 81–96.

Johnson, T.C., D.M. Cole and E.J. Chamberlain. 1978. Influence of freezing and thawing on the resilient properties of a silt soil beneath an asphalt concrete pavement. USA Cold Regions Research and Engineering Laboratory, CRREL Report 78-23.

Kirkby, M.J. 1980. Modelling water erosion processes. Chapter 6, In M.J. Kirkby and R.P.C. Morgan (ed.), Soil erosion, Wiley and Sons, New York, p. 183–216.

Kok, H., and D.K. McCool. 1990. Freeze thaw effects on soil strength. USA Cold Regions Research and Engineering Laboratory, Special Report 90-1, p. 70–76.

Lal, R. and W. Elliot. 1994. Erodibility and erosivity.

Chapter 8, In R. Lal (ed.), Soil erosion research methods.St. Lucie Press, Delray Beach, FL, and Soil and Water Conservation Society, Ankeny, IA, p. 181–208.

Mathier, L., and A.G. Roy. 1993. Temporal and spatial variations of runoff and rainwash erosion on an agricultural field. Hydrological Processes 7: 1–18.

Meyer, L.D., G.R. Foster and M.J.M. Romkens. 1975. Source of soil eroded by water from upland slopes. Agricultural Research Service Report S-40, p. 177–189.

Miller, R.D. 1980. Freezing phenomena in soils. Chapter 11 In D. Hillel (ed.), Applications of soil physics, Academic Press, New York, p. 254–299.

Morgan, R.P.C. 1977. Soil erosion in the United Kingdom: Field studies in the Silsoe area, 1973–1975. National College of Agricultural Engineering Occasional Paper, 4.

Mutchler, C., and R. Young. 1975. Soil detachment by raindrops. Agricultural Research Service Report S-40, p. 113–117.

Nearing, M.A., L.J. Lane and V.L. Lopes. 1994. Modeling soil erosion. Chapter 6 In R. Lal (ed.), Soil erosion research methods, St. Lucie Press, Delray Beach, FL, and Soil and Water Conservation Society, Ankeny, IA, p. 127–156.

Papendick, R.I., and K.E. Saxton. 1990. Frozen soil impacts: research needs. USA Cold Regions Research and Engineering Laboratory, Special Report 90-1, p. 220–223.

Schumm, S.A. 1956. Evolution of drainage systems and slopes on badlands at Perth Amboy, NJ. Geological Society of America Bulletin 67: 597–646.

Shainberg, I., J.M. Laflen, J.M.Bradford and L.D. Norton. 1994. Hydraulic flow and water quality characteristics in rill erosion. Soil Sci. Soc. Am. J. 58: 1007–1012.

Slattery, M.C., and R.B. Bryan. 1992. Hydraulic conditions for rill incision under simulated rainfall: A laboratory experiment. Earth Surface Processes and Landforms 17: 127–146.

Thornes, J.B. 1980. Erosional processes of running water and their spatial and temporal controls: A theoretical viewpoint. Chapter 5, In M.J. Kirkby and R.P.C. Morgan (ed.), Soil erosion, Wiley and Sons, New York, p. 129–182.

Thurow, T.L., S.D. Warren and D.H. Carlson. 1993. Tracked vehicle traffic effects on the hydrologic characteristics of central Texas rangeland. Transactions ASAE 36(6): 1645–1650.

Vitel, Inc. 1994. Hydra soil moisture probe user's manual (version 1.2). Chantilly, VA 22021.

Voorhees, W.B. 1983. Relative effectiveness of tillage and natural forces in alleviating wheel-induced soil compaction. Soil Science Society of America J. 47: 129–133.

Voorhees, W.B., C.G. Senst and W.W. Nelson. 1978. Compaction and soil structure modification by wheel traffic in the northern corn belt. Soil Sci. Soc. Am. J. 42: 344–349.

Voorhees, W.B., R.A. Young and L. Lyles. 1979. Wheel traffic considerations in erosion research. Trans. ASAE 22: 786–790.

Voorhees, W.B., W.W. Nelson and G.W. Randall. 1986. Extent and persistence of subsoil compaction caused by heavy axle loads. Soil Sci. Soc. Am. Jour. 50: 428–433.

Webb, R.H., H.G. Wilshire, M.A. Henry. 1983. Natural recovery of soils and vegetation following human disturbance. Chapter 14, *In* R.H. Webb and H.G. Wilshire (ed.), Environmental effects of off-road vehicle impacts and management in arid regions, Springer-Verlag, New York, p. 279–302.

Spatial Variability of Frost Depth
in a Depressional Catchment

E.S. BROOKS[1], J.L. NIEBER[2], AND B.N. WILSON[2]

ABSTRACT

The spatial variability of frost depth was measured within a catchment in south-central Minnesota during the winter of 1994-95. The spatial distribution of site-specific factors including residue biomass, soil bulk density, and total water content was measured within the catchment, and the spatial distribution of topographic indices were calculated for the catchment using the TAPES-G model. These topographic indices and site specific factors were correlated with measured frost depth and date of complete soil thaw. Regression equations were derived to predict maximum frost depth and date of complete thaw. Results point out the effectiveness of topographic indices to quantify the spatial distribution of frost depth.

Key words: Frost depth, spatial variability, topographic indices

INTRODUCTION

Runoff and erosion in agricultural lands are highly affected by freezing soils. In regions that experience seasonally frozen soils, it is essential to consider frozen soil hydrology when developing large, long-term hydrologic watershed models. To develop these models it is desirable to consider the spatial variability of frost depth. The key to understanding and predicting the occurrence and depth of freezing in soils is understanding which factors will significantly alter the formation of a frozen layer in the soil. These factors have been thoroughly investigated in a number of studies. The formation of a frozen soil layer is affected by moisture content, bulk density, residue cover, compaction, land use, albedo, type of tillage, snow cover, soil type, slope-aspect, and depth to the water table (Dingman 1976, Flerchinger and Saxton 1989). The variability of many of these factors can be related to the topographic variability within a landscape (Moore et al. 1993).

In the present study, site specific properties and topographic indices have been measured in a small catchment and correlated to observed frost depth. These same parameters were then used in a stepwise linear regression for prediction of frost depth variability within the landscape. The purpose of these analyses was to determine those factors which adequately describe the spatial variability of frost depth in the catchment. These analyses provided a better understanding of the main factors governing soil freezing and support the use of topographic indices to describe the large-scale spatial variability of frost depth.

SITE DESCRIPTION

The research site is located in Faribault County in south-central Minnesota. The site is best described as a depression where ground water recharge is focused in a central low-lying area due to surface runoff and shallow lateral subsurface flow. The total area of the site is approximately 5.7 ha. A plan view of the site is presented in Figure 1. Corn and soybeans are grown on 4 ha of the catchment, mainly on the flat and east-facing slopes; 0.3 ha consists of a flat lowland wet area with perennial grasses, and the remaining 1.4 ha is wooded with a variety of deciduous trees. A wide range of slope aspects are represented in the catchment with slopes ranging from 6 to 35% on hillslopes around the depression. Volumetric water content in the catchment ranges from 15% to 50% in the predominantly loam soil. The water table depth fluctuates seasonally within 1 m in the depression area

[1] Department of Agricultural and Biological Engineering, Riley-Robb Hall, Cornell University, Ithaca, New York 14853, USA
[2] Department of Biosystems and Agricultural Engineering, University of Minnesota, 1390 Eckles Avenue, St. Paul, Minnesota 55108, USA
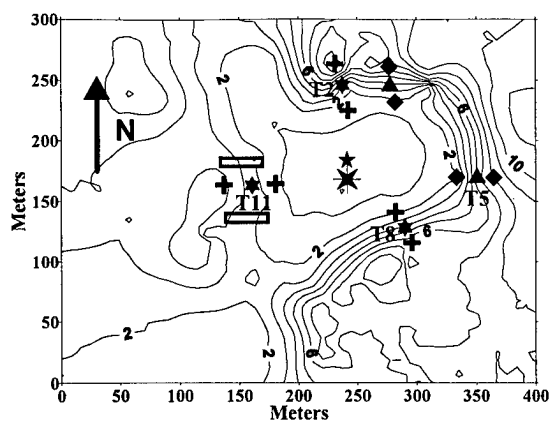
▲ N-C Probe, TDR   **◆** N-C Probe   **✳** Weather Station   **★** FT, TDR
✚ FT, N-C Probe   **✳** FT, N-C Probe,TDR   **◇** N-C Probe ▭ Runoff Plots

Figure 1. Illustration of catchment topography and layout of instrumentation at the research site. Elevations are in meters above the depression. FT, frost tube; N-C, neutron - capacitance; TDR, Time Domain Reflectometry. T2 - Tube 2, T5 - Tube 5, T8 - Tube 8, T11 - Tube 11.

while remaining deeper than 3 m on the surrounding slopes. The soil is classified as Clarion and Estherville series, with higher fractions of sand in places on the upper slopes and more silt and clay in the depression area. The bulk density ranges from around 1.4 g/cm^3 in the cropped areas to 0.9 g/cm^3 in the north-facing forest area. Vegetation is thickest on south-facing slopes with wild raspberry brush and shrubs, while the residue layer is thickest in the lowland depression area due to perennial wetland grasses. Significant snow drifting occurs in a northwest to southeast direction with main drifts gathering on the upper sections of south-facing slopes, in the depression area, and on the toe-slope sections of the north-facing slopes. There was no cultivation done to the cropped section of the field before the winter of 1994-95, which resulted in high residue in the field due to corn stubble and post-harvest corn stalks. Average yearly rainfall for the region is 74 cm. The average temperature for the period April 1994 to April 1995 was 7.6 °C.

SITE INSTRUMENTATION

The data collection for the research site included automated hourly measurements and weekly manually read instrumentation. A weather station located in the depression area recorded hourly air temperature, solar radiation, net radiation, wind speed, relative humidity, and soil temperature at 15 and 46 cm. Rainfall and pan evaporation were also recorded at the weather station. The water table depth was measured using 12 piezometers. Continuous depth to water table

measurements were made in the depression while weekly measurements were made at locations around the depression. The layout of instrumentation at the site is illustrated in Figure 1 (piezometers not shown).

Soil moisture measurements were taken weekly at five transects, 3 locations per transect, at specific locations throughout the site. Transects were installed along the down slope gradient at locations representing the four major slope aspects in both the wooded and cropped areas. At each location in the transect, access tubes were installed to a depth of 2 m to allow for weekly total water content readings by a neutron probe and liquid water content measurements with a capacitance probe at 15-cm increments. Liquid water content was also measured weekly using TDR (time domain reflectometry) at midslope locations in each transect at depths of 20, 40, 60, and 80 cm. The measurements from these three instruments quantified total water content, liquid water content, and ice content at each location.

The primary means for characterizing the spatial variability of frost depth was through soil temperature and frost tube measurements. Hourly soil temperature data was measured in the depression area, as described earlier, and at the midslope location on the north-facing wooded slope. Readings were made using thermocouples at 10, 20, 40, 60, 80, and 120 cm. Weekly soil temperature measurements were also recorded manually using thermocouples at midslope locations next to the TDR instrumentation in each transect at depths of 20, 40, 60, and 80 cm. Frost tubes, filled with blasting sand and fluorescein dye (Rickard and Brown 1972), were used to indicate frost depth. These were installed next to the moisture content instrumentation at 12 locations throughout the site.

Weekly snow depth measurements were made using a fixed grid of graduated snow sticks. Snow density was also measured by weighing 5-cm diam. cores. The site was partitioned into zones having similar snow depths. Measurements were made to adequately represent the variability within these zones.

Surface runoff was also measured at the site using collection trenches and tipping bucket flow gages on both the north- and south-facing wooded slopes. Two (0.0041-ha) runoff plots recording both surface runoff and subsurface lateral flow were also installed on the east-facing field slope. The runoff data are not the focus of this report and therefore will not be discussed further.

TOPOGRAPHIC MODEL

The TAPES-G model (Topographic Analysis Programs for the Environmental Sciences) developed by Moore (1992) is a grid based model, which relies on a DEM (digital elevation model) to determine the topographic characteristics within a given landscape. The driving algorithm is a second-order, central-difference scheme centered on the interior node of a moving 3 x 3 square-grid network. The slope, aspect, specific catchment area, flow path length, profile curvature, and plan curvature are primary attributes calculated by the model. Secondary attributes are calculated by combining these primary attributes into indices that can be used to indicate the spatial variability of a wide range of hydrologic processes.

The wetness index, used in this analysis, is a topographic index based on the specific catchment area and land slope commonly used to indicate the spatial variability of soil water content (Moore and Hutchinson 1991). The solar incidence angle, the angle between a direct solar beam and the normal to a hillslope, is a topographic index derived from the slope and aspect and used to quantify the spatial variability of direct solar radiation (Lee 1978).

These topographic attributes were calculated for the catchment using a 5-m grid spacing DEM which was developed from a detailed survey of the site. Table 1 summarizes the main topographic attributes considered in the analysis for five of the measurement locations. The potentially significant site-specific parameters considered in the analysis included the residue biomass, soil bulk density, snow depth, and average total water content. Using the topographic and site-specific parameters, correlation and stepwise multiple linear regression analyses were performed to determine the factors most significantly influencing the spatial variability of frost depth and date of complete thaw. Data for all 12 of the frost depth measurement locations were used in the analyses.

Table 1 Topographic attributes used in the correlation and regression analysis.

Location	Slope	Aspect	Specific catchment area	Wetness index	Plan curvature	Profile curvature	Solar incidence angle[#]
	(%)	(degrees)	$(m^2 -m^{-1})$		(m^{-1})	(m^{-1})	(degrees)
Tube 2	22.3	208.9	22.3	4.5	7.89	1.68	40.6
Tube 5	7.9	264.3	84.2	6.4	3.39	0.04	50.9
Tube 8	21.4	341.5	15.1	3.7	-1.35	0.09	62.8
Tube 11	6.6	70.8	21.0	5.2	3.80	0.00	52.6
Depression	0.0	*****	150.0	10.0	0.00	0.00	51.3

[#]Solar incidence angle taken from 1 March.

RESULTS

Representative observations
In this section we discuss observations of snow depth, soil temperature and frost depth at the depression site. The purpose of this discussion is to provide the reader with a sense of the sensitivity of the measured variables to location within the catchment.

Snow depth
Snow depth distribution within the catchment for the 1994-95 winter is illustrated in Figure 2. The spatial variability of snow depth is large, with the largest difference in snow depth being between the locations on the south-facing wooded slope and the depressional area. The large spatial variability is attributed to the significant blowing and drifting of snow in the catchment. At the site the prevailing wind direction in the winter months is primarily from the northwest. Due to the open end on the northwest boundary of the

catchment, significant quantities of snow were blown into the catchment and drifted on the west-facing and north-facing slopes and in the depression.

It is rather surprising that the snow depths were large on the east-facing slope, considering that this area is cultivated and completely open to the prevailing wind. The relatively large snow depths on this slope were probably due to the fact that corn stubble on the surface promoted snow accumulation on that slope.

The depressional area had the largest amount of snow depth during the entire winter period. This area has a dense cover of grass, and it is this cover that accounts for the capture of snow blown into the catchment from surrounding areas.

Aspect, of course, has a significant influence on the depth of snow since it determines the amount of incident solar radiation at the site. The date for the large thaw of snow occurred around 22 February. The snow melted completely at all of the locations, except

201

on the north-facing slope. On the north-facing slope the snow cover remained through 10 March. A large snowfall on 5 March brought snow depths back to over 10 cm at all locations, but within a few days the snow had thawed at all locations.

Soil temperature

Soil temperatures were manually measured on all slopes of the catchment, but at midslope on the north-facing slope the temperatures were measured continuously near tube 8 by an electronic data logger. Measurement depths included 10, 20, 40, 60, 80 and 120 cm.

Soil temperatures at tube 8 are illustrated in Figure 3 for four depths, along with the mean daily air temperature. As expected, the temperatures fluctuated much more at the shallower depths in response to fluctuating surface temperatures, while temperature variations were dampened at the larger depths. Temperatures dropped below zero (Celsius) at some point in the winter for all of the depths except for the 80-cm depth (and 120-cm depth which is not shown).

Figure 3. Soil temperature measured at tube 8, on the north-facing wooded slope, through the winter of 1994-95, at depths of 10, 20 40 60 and 80 cm. Average daily air temperature in the depression is also plotted.
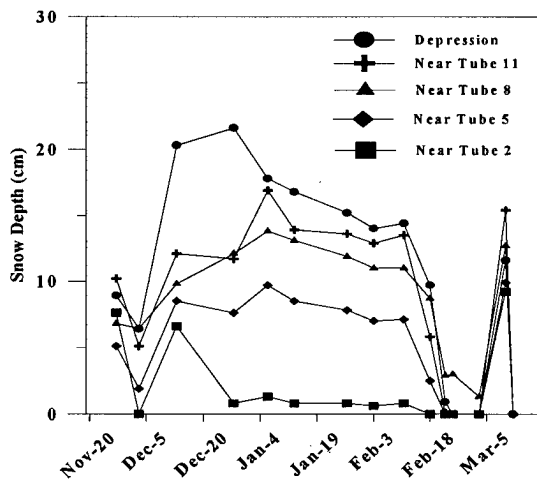
Figure 2. Snow depth measured at specific locations in the catchment during the winter of 1994-95.

Frost depth

Frost depths were recorded using frost tubes, and could also be inferred from soil temperatures and ice content measurements. In this section we refer to the data collected from frost tubes. The spatial and temporal variation in frost depth at various locations in the catchment are illustrated in Figure 4.

It is expected that a large snow depth would delay and impede frost penetration into the soil profile. However, such a correlation is not apparent when comparing the snow depth distributions in Figure 2 with the frost depth distributions. This is because there are other factors that also assist in controlling the

Figure 4. Frost depth measured at specific locations in the catchment during the winter of 1994-95.

migration of the frost front into the soil. These factors will be examined in the correlation analysis to follow.

Correlation analysis

The significance of each of the selected factors was first considered using the Pearson correlation coefficient. Correlations were performed between the frost depth on measurement days F_d, the maximum frost depth, the date of complete thaw, and the various topographic and site specific parameters.

Table 2 summarizes these correlations for all variables except for F_d. The factors most highly correlated to maximum frost depth were the total water content, residue biomass, bulk density, and the specific catchment area. The lone factor most highly correlated to date of complete thaw was solar incident angle.

The correlations for F_d manifested a strong temporal pattern. Those attributes that were well correlated to F_d while the soil was freezing were found to become insignificant while the soil was thawing. The factors most highly correlated to F_d during soil freezing were the same ones most highly correlated to maximum frost depth. The factor most highly correlated to F_d during soil thawing was solar incidence angle.

Snow depth was found to have minimal correlation with the frost depth. However, the spatial variability in snow depth had a high correlation to the date of complete thaw. This is interesting because it indicates the insulation of the shallow snow pack was not enough to affect how deep the soil froze; however, it suggests that the snow did significantly insulate the soil while the soil was thawing.

The solar incidence angle was also directly related to the snow depth. Like the snow depth, the solar incidence angle was not correlated to the frost depth while the soil was freezing, but became the most significant factor when the soil was thawing. This indicates that the spatial variability of incident solar radiation governed the spatial variability of the thawing process.

Another key observation is that the maximum frost depth was only moderately correlated with the date of complete thaw. The correlation suggests that deep freezing soils take longer to thaw yet the moderate correlation points to the fact that other factors are important.

The correlations shown in Table 2 indicate that several of the factors are highly correlated to each other. For instance, the total water content was highly correlated with specific catchment area and the wetness index. In addition, the residue biomass, slope and bulk density have a moderate correlation to the spatial distribution of water content in the catchment. These correlations are in agreement with the findings of Moore et al. (1993).

Table 2 Correlation between maximum frost depth and date of complete thaw to measured site specific properties and topographic attributes.

	Max. frost depth	Day of complete thaw	Snow depth*	Residue biomass	Bulk density	Total water content**	Solar incidence angle	Specific catchment area
Max. frost depth	1	0.441	0.273	-0.526	0.500	-0.462	0.187	-0.560
Day of complete thaw		1	0.637	0.289	-0.209	0.191	0.819	-0.065
Snow depth*			1	0.259	-0.045	0.505	0.815	0.361
Residue biomass				1	-0.851	0.782	0.279	0.714
Bulk density					1	-0.515	-0.231	-0.434
Total water content**						1	0.293	0.900
Solar incidence angle							1	0.130
Specific catchment area								1

* Measured on February 11
** 1994-95 winter mean for top 40 cm depth

Stepwise multiple linear regression analysis

Because several key parameters describing the spatial variability of frost depth were well correlated yet interdependent, a stepwise multiple linear regression analysis was conducted to determine which factors could be used to predict the spatial variability of frost depth and date of complete thaw. In the regression procedure a factor was included in the regression model, if it significantly improved the model predictions at the specified confidence level (95% unless otherwise noted).

Table 3 shows the results of the models used to predict the spatial variability of the maximum frost depth in the catchment. The specific catchment area was the most significant parameter for the regression, yielding an r^2 of 0.314 with a standard error of 14.0 cm. Snow depth was the next most significant parameter to be added into the regression, and this improved the r^2 to 0.574 and the standard error to 11.7 cm. The use of the snow depth variable in the regression is suspicious because the regression coefficient for the variable is positive, resulting in the model predicting a deeper maximum frost depth with a deeper snow depth.

Table 3 Stepwise linear regression results for maximum frost depth.

Model #	Attributes	Coefficient	Std. error	Student's T	P	r^2	Std. error (cm)
1.	constant	69.582	5.252	13.2	0.000	0.314	14.0
	specific catchment area	-0.212	0.099	-2.1	0.058		
2.	constant	60.710	5.775	10.5	0.000	0.574	11.7
	specific catchment area	-0.286	0.009	-3.3	0.010		
	snow depth	1.454	0.620	2.3	0.044		
3.	constant	98.507	27.379	3.6	0.007	0.659	11.1
	specific catchment area	-0.324	0.088	-3.7	0.006		
	snow depth	2.694	1.059	2.5	0.035		
	solar incidence angle	-53.119	37.699	-1.4	0.197		

Table 4 Stepwise linear regression results for date of complete thaw.

Model #	Attributes	Coefficient	Std. Error	Student's T	P	R^2	Std. Err (days)
1.	constant	47.788	8.966	5.3	0.000	0.671	5.4
	solar incidence angle	45.812	10.143	4.5	0.001		
2.	constant	44.727	6.064	7.4	0.000	0.867	3.6
	solar incidence angle	49.086	6.853	6.9	0.000		
	profile curvature	-3.084	0.846	-3.7	0.005		
3.	constant	36.195	6.669	5.4	0.001	0.913	3.1
	solar incidence angle	54.996	6.555	8.4	0.000		
	profile curvature	-3.013	0.728	-4.1	0.003		
	slope	0.225	0.110	2.1	0.075		

The third and last variable added (added at a significance level of 80%) to the regression was the solar incidence angle. This improved the standard error to 11.1 cm. The regression coefficient for the solar incidence angle variable has the correct sign, so it is reasonable to keep this variable in the regression. Since snow depth and solar incidence angle were found to be highly correlated in Table 2, it would probably be wise to eliminate snow depth from the regression model and develop a model based on specific catchment area and solar incidence angle alone.

It is interesting that among the parameters listed in the correlation analysis the specific catchment area by itself describes the variability of maximum frost depth with a standard error of only 14.0 cm. Addition of other variables does not improve the error significantly. This demonstrates that the effect of the several key significant factors on the spatial variability of frost depth can be best described by the spatial pattern of the specific catchment area alone.

The results of the regression analysis for predicting the date of complete thaw is represented in Table 4. At the 95% significance level both the solar incidence angle and the profile curvature predicted the date of complete thaw with a standard error of 3.6 days and a coefficient of determination of 0.867. The slope, added to the model at a significance level of 92%, improved the standard error to 3.1 days. As indicated in the correlation analysis, the solar incidence angle clearly was the most important factor when considering the timing of the thaw. Like the prediction of the maximum frost depth, snow depth was not added to the model even though it was highly correlated to the day of complete thaw due to the fact that it was highly correlated to the solar incidence angle. The profile curvature, positive on the concave toe-slope portion of a slope and negative on the convex upper portion of the slope, was added to the model even though it was not one of the most significant correlation attributes. This points to the fact that the concave toe slope portion of a slope tended to

be wetter, froze less deep, and thawed quicker than the upper portions of the slope.

DISCUSSION AND CONCLUSIONS

The results from this analysis demonstrate that on a small scale the spatial variability of frost depth is dependent upon several factors. However, in terms of large scale hydrologic modeling, topographic indices can be used to indicate this spatial variability.

Out of all the key factors considered in the analysis, it is significant that the two parameters used in predicting the spatial variability of the maximum frost depth and the date of thaw were both topographic attributes. For the catchment, both the specific catchment area and the solar incidence angle were the most significant topographic attributes. The catchment area best dictated the spatial variability of the frost depth when the soil was freezing and the solar incidence angle most significantly influenced the thawing of the soil.

Although snow depth would be considered an important variable in this analysis, it did not add to the prediction model. These correlations were determined on a given catchment over a single winter period. It would be unrealistic to assume that snow depth will be insignificant in general. Measurements for other winter periods will be necessary to further examine the significance of snow depth in this catchment.
To further consider the effect specific factors have on soil freezing, two models, the SHAW model (Flerchinger and Saxton 1989) and the modified Stefan equation (Walter 1995), have been compared to the measured frost depth throughout the site. Correlating the output of these local soil freezing models with location specific catchment factors for various winter conditions should provide a more complete model of soil freezing variability in landscapes.

REFERENCES

Dingman, S.L. 1975. Hydrologic effects of frozen ground. Cold Regions Research and Engineering Laboratory. Special Report 218. U.S. Army Corps of Engineers. Hanover, New Hampshire.

Flerchinger, G.N., and K.E. Saxton. 1989. Simultaneous heat and water model of a freezing snow-residue-soil system, I. Theory and development. Trans. ASAE, 32:565-571.

Lee, R. 1978. Forest Microclimatology. Columbia University Press, New York, 276 pp.

Moore, I.D. 1992. Terrain analysis programs for the environmental sciences: TAPES. Agricultural Systems and Information Technology. 4(2):37-39.

Moore, I.D., and M.F. Hutchinson. 1991. Spatial extension of hydrologic process modeling. In: Chall. Sustain. Dev. Nat. Conf. Publ., Institute of Engineers, Australia, 3:803-808.

Moore, I.D., T.W. Norton and J.E. Williams. 1993. Modeling environmental heterogeneity in forested landscapes. Jour. Hydrol., 150:717-747.

Rickard, W., and J. Brown. 1972. The performance of a frost-tube for the determination of soil freezing and thawing depths. Soil Sci. 113(2):149-154.

Walter, M.T. 1995. Winter-time hydrologic modeling over a three-dimensional landscape. Doctoral thesis. Dept. of Biological Systems Engineering. Washington State University. Pullman, WA. 97 pp.

ACKNOWLEDGMENT

Crop and Soil Management to
Increase Water Infiltration into Frozen Soil

J.L. PIKUL, JR.[1] AND J.K. AASE[1]

ABSTRACT

Crop and soil management to trap snow and reduce spring-runoff have potential to increase soil water storage. A randomized field-design using ripped and non-ripped soil was used to test whether tillage improved water infiltration into frozen soil. Studies were conducted on annually grown spring wheat (*Triticum aestivum* L.) near Culbertson, Montana. Soil was a Dooley sandy loam (fine-loamy, mixed Typic Argiboroll). Ripping was with a single shank at regular intervals on the contour. Soil water was measured using neutron attenuation and volumetric determinations. Final infiltration rate on frozen soil averaged 17 mm h^{-1} and 2 mm h^{-1} on ripped and non-ripped treatments, respectively. In spring, average water content of the top 1.2 m of soil, to a distance 1.5 m downslope from the rip, was 32 mm greater on ripped treatments compared to non-ripped treatments at comparable slope positions. There were no differences in wheat yield between treatments. Infiltration measurements show that soil ripping has potential to decrease water runoff.

Key Words: soil ripping, ponded infiltration, preferential flow, spring wheat, soil water storage

INTRODUCTION

Soil freezing and thawing affect large agricultural areas, as well as range and forest land. Within the United States, Formanek et al. (1990) estimated that nearly 1.2 million km^2 of crop land, 1.3 million km^2 of forest land and 1.8 million km^2 of grazing land are impacted by freezing and thawing. From an agricultural perspective, defining interactions of freeze-thaw on movement of water and chemicals is of high importance.

Water infiltration into frozen soil is primarily determined by soil water content at the time of freezing (Kane, 1980). The freezing process also induces water flux from unfrozen soil to the freezing front. Typical patterns of water redistribution near the surface during diurnal freezing and thawing cycles have been shown by Pikul et al. (1989). An increasingly tortuous water flow path develops as pore space fills with ice. In the inland Pacific Northwest, which has a winter precipitation pattern, soils often freeze at a high water content resulting in a nearly impermeable condition. Air-filled macropores provide important preferential water flow paths through frozen soil and increase water infiltration (Gray et al., 1990; Zuzel and Pikul, 1987).

The importance of freeze-thaw on agricultural lands as related to runoff and erosion hazards is recognized and considerable research has been conducted to identify problems and possible solutions. However, implementing solutions at the field scale can be difficult. Typically, soil erosion control efforts have been through tillage and residue management systems that maintain adequate surface roughness and suitable amounts of crop residue on the surface. Allmaras et al. (1979) have shown that erosion control in eastern Oregon often requires combinations of tillage, residue management, contouring, or terracing. Growers must plan on having sufficient residue cover following fall planting. The Natural Resources Conservation Service (NRCS) determines percentage surface cover to meet acceptable soil loss tolerances, but even the best management practices may fail to reduce water

runoff and erosion when the soil is frozen or partially frozen (Saxton et al., 1981).

On rangelands, various mechanical treatments such as ripping, pitting and contour furrowing have been used to create surface storage and increase water infiltration opportunity. For example, in eastern Montana contour furrowing of sloping land with low infiltration capacity improved precipitation-use efficiency (Wight and Siddoway, 1972). Where snowfall is significant, contour furrowing of range land increased snow water accumulation by 60% and soil water recharge by 161% compared to natural range (Neff and Wight, 1977).

On cropland, the objectives of tillage are to incorporate residues or amendments, control weeds and prepare the soil for seeding. Tillage to specifically prepare fields for spring runoff is generally not a consideration. Experiments designed to test the effect of tillage on overwinter soil water storage are often executed using whole-field tillage implements such as disk or chisel plows. Interpretation of the effectiveness of tillage on water infiltration is difficult because whole-field tillage destroys vertical crop residue essential for snow trapping and increases evaporative soil water loss. On the Canadian prairies, where snowfall accounts for approximately 30% of the annual precipitation, Maulé and Chanasyk (1990) reported that snowmelt recharge, measured from fall to post-melt in the spring, was 36% greater in fields that were chiseled in the fall compared to fields that were not chiseled. Contrary to the findings of Maulé and Chanasyk (1990), earlier literature reviews (Lal and Steppuhn, 1980) reported that on the Canadian prairies, tillage did not increase overwinter soil water storage.

Management practices that combine the use of stubble management for snow catch and contour-ripping for water infiltration have potential to reduce runoff and increase soil water storage. In southern Saskatchewan, Canada, Gray et al. (1990) reported greater spring wheat yields on plots that had been managed for snow catch and water infiltration than on undisturbed stubble check plots. In the inland Pacific Northwest where freezing and thawing account for a significant portion of soil erosion problems, Saxton et al. (1981) used slot-mulching, also termed vertical mulching (Spain and McCune, 1956), to reduce water runoff from frozen soil. Saxton et al. (1981) found that water runoff was 10 times greater on no-till check plots as compared to slot mulch plots. Pikul et al. (1992) have shown that soil ripping can intercept and infiltrate meltwater through frozen soil and that spacing of soil rips can

be estimated from historic precipitation patterns and permeability of unfrozen subsoil.

Methods that increase snowmelt infiltration when the soil is frozen need to be considered as part of the management plan in regions where soil water limits plant growth and where soil erosion may be a problem. Our hypothesis is that tillage-induced macroporosity provides important preferential water flow paths through slowly permeable frozen soil. Our objective was to investigate soil ripping as a tillage practice to improve water infiltration into frozen soil.

MATERIALS AND METHODS

Field experiments were conducted during 4 winters near Culbertson, Montana on a Dooley sandy loam with about a 5% slope. Spring wheat was grown annually since 1991. Each fall, except 1991, a single 50-mm-wide parabolic sub-soiling shank was used to rip the soil 0.30 m deep on 6-m contour intervals. In 1991, a 50-mm-wide straight shank chisel was used to create a rip when the soil was frozen 0.1 m deep. This subsoiling tillage was used on rip plots. There was no subsoiling on plots called no rip.

Statistical design was completely randomized with three replications of rip and no rip treatments. Plots were 79 m long and 23 m wide with the long axis parallel to the slope. Statistical comparisons were made using least significant differences (LSD) at $P = 0.05$ with the no rip treatment as a control.

Prior to seeding spring wheat, both rip and no rip treatments received 34 kg N ha^{-1} broadcast as ammonium nitrate. Seedbeds for spring wheat were prepared with 0.45-m wide medium-crown sweeps. Treatments were seeded on the contour to spring wheat at about 2.1 million viable seeds ha^{-1} using a double disk drill with 0.2-m row spacing. In all years, except 1993, wheat was harvested using a conventional combine header. Stubble height was about 0.20 m. Stubble remained intact over winter. In 1993, wheat was harvested with a stripper header (Wilkins, et al., 1996) which left stubble almost 0.6 m tall. Wheat yield was measured on each plot at six slope positions by taking 18-m by 1.46-m swaths on the contour.

Infiltration frames were 1.16 m long by 0.61 m wide by 0.3 m deep and were installed on each replication of each treatment prior to soil freezing in 1992, 1993, and 1994. Inside edges of the infiltration frames were sealed with bentonite clay to prevent water leakage along the metal-soil interface. For the rip treatment, infiltration frames were centered over

the rip with the long axis of the infiltration frame oriented parallel to the rip. Soil outside the frame and adjacent to the rip was removed, backfilled and packed to eliminate lateral flow of water from inside the frame to the rip. On no rip treatments, frames were oriented with the long axis parallel to the wheat rows. Constant-head infiltration tests were made in January 1993 when the soil was frozen to a depth that exceeded 1 m; in February 1994 when the soil was frozen 0.3 m deep; and in January 1995 when the soil was frozen about 0.6 m deep. Ponded infiltration imitates runoff events where water accumulates in the rip or in the furrow. Average depth of ponded water was 100 mm on no rip treatments. Water temperature for infiltration tests was close to 0° C. An estimate of surface storage was made by rapidly filling the rip or furrow with water.

Soil water content was measured using neutron attenuation. Three neutron access tubes were located at the upper, middle, and lower slope positions for a total of nine tubes per replication and 27 tubes per treatment. Soil water was measured to a depth of 1.83 m at 0.3-m increments just prior to soil freeze-up and at soil thaw. At the time of infiltration tests soil water of the surface 50 mm was determined gravimetrically outside the frame.

At spring thaw, soil water was measured at 0.3 m increments to a depth of 1.2 m along a 3-m transect perpendicular to the rip and at similar slope positions on no rip plots. Cores were taken at 0.3 m intervals along the transect. Gravimetric water measurements were converted to volumetric measurements using an average soil bulk density of 1.58 Mg m^{-3}.

Soil temperature was measured at 0.3 m on rip and no rip treatments using three thermocouples wired in parallel to spatially average temperature. For temperatures (T) below freezing, freezing degree days were calculated as $(T_{max} + T_{min})/2$.

RESULTS AND DISCUSSION

Culbertson, Montana is located in an area of low Chinook frequency (Caprio et al., 1981). Typically, there is one freeze cycle where the soil can freeze as early as the first part of November and remain frozen through March.

Cumulative freezing degree days (FDD) were used to characterize the weather for the test years (Fig. 1). The winter of 1993 had the lowest air temperatures but had the least frozen soil and cumulative soil FDD at 0.3 m (Table 1). During the 1993-1994 winter, tall stubble trapped 69 mm of snow water equivalent (Table 1). Compared to the other two winters (Table 1), additional snow depth during 1993-1994 provided thermal insulation and reduced the depth of frozen soil. Cumulative air FDD for the winter seasons indicate that winters of
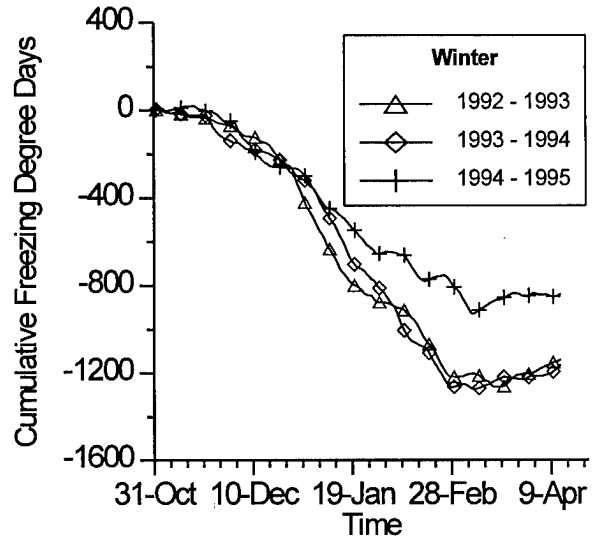
Figure 1. Cumulative air freezing degree days at the infiltration test site.

1992 and 1993 were similar in that each of these years accumulated about -1270 °C FDD days by the end of February (Fig. 1).

Table 1. Cumulative freezing degree days (FDD) and selected soil characteristics on the day of the infiltration tests.

Winter	Day of infiltration test	Snow water equivalent (mm)	Cumulative air FDD (from 1 Nov)	Cumulative soil FDD at 0.3 m (from onset of freezing at 0.3 m)		Depth of frozen soil (m)		Soil temperature at 0.3 m (C)	
				Rip	No Rip	Rip	No Rip	Rip	No Rip
1992-1993	Jan 20-21	28	-799	-158	-150	1.0	1.0	-3.7	-3.2
1993-1994	Feb 16-17	69	-1077	-48	-27	0.3	0.3	-0.9	-0.7
1994-1995	Jan 31- Feb 1	27	-654	-95	-93	0.7	0.6	-1.1	-1.3

Table 2. Selected soil and water infiltration characteristics for infiltration tests on frozen soil.

| Infiltration Test | Soil water content ($m^3 m^{-3}$) on first day of infiltration tests ---------------- soil depth ---------------- | | | Surface storage | Temperature of water used for test | Infiltration final rate | Cumulative infiltration[‡] |
	0-5mm	0-0.3 m	0.3-0.6 m	mm	°C	mm hr^{-1}	mm
20 Jan 1993							
Rip		0.18	0.16	49*	0	12*	98*
No rip	0.30	0.18	0.12	11	0.3	1	17
LSD(0.05)		ns[†]	ns	4		6	17
21 Jan 1993							
Rip				9*	0	3	14*
No rip				0	0	1	2
LSD(0.05)				3		ns	8
16 Feb 1994							
Rip		0.20	0.16	56*	2.5	9*	99*
No rip	0.24	0.18	0.18	5	3.0	1	14
LSD(0.05)				8		3	8
17 Feb 1994							
Rip				11*	2.2	2	15*
No rip				0	1.2	1	1
LSD(0.05)				1		ns	7
31 Jan 1995							
Rip		0.16*	0.14	49*	3.5	30	134*
No rip	0.53	0.13	0.10	6	3.5	5	24
LSD(0.05)		0.027	ns	19		ns	74
1 Feb 1995							
Rip				17*	4.2	14	33*
No rip				2	3.7	4	5
LSD(0.05)				9		ns	25

† Significant at the 0.05 probability level (*) or not significant (ns)
‡ Cumulative values for 2 h test on day 1 and 1 h test on day 2

Water infiltration was measured on two consecutive days in each of the three winters. On the first day of the tests there were significant differences in water infiltration rate (WIR) and cumulative water infiltration (CWI) between treatments (Table 2). Three-year average CWI following 2 h was 110 mm on rip treatments and 18 mm on no rip treatments. Surface storage accounted for 51 mm of the CWI on the rip treatments and 7 mm on the no rip treatments. On the second day of the tests, surface storage was 12 mm on the rip treatments and 1 mm on the no rip treatment. Final infiltration rates on the second day of the tests were not significantly different between treatments. On the rip treatment, final WIR on the second day was significantly less than final WIR on the first day of tests. We suspect that water froze in the soil pores following the first test and plugged pores that were previously air-filled. Infiltration rates on the first day of the tests in 1993 and 1994 are shown in Figure 2.
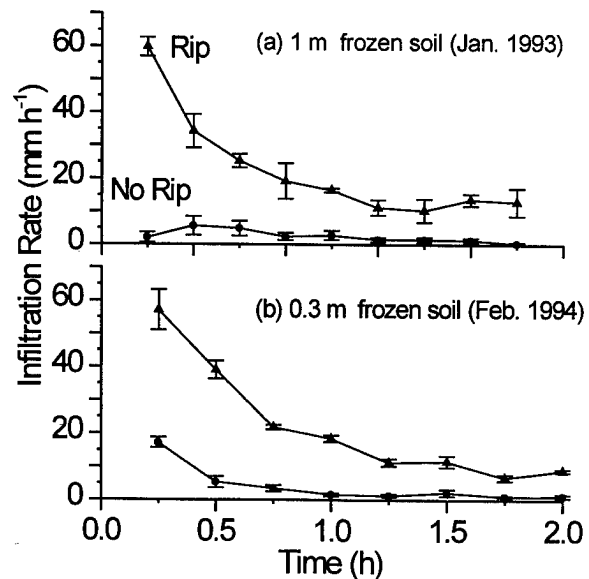
Figure 2. Water infiltration into frozen soil on the first day of infiltration tests in 1993 and 1994. Error bars show one standard deviation.

Table 3. Water storage efficiency, water use by wheat, and wheat yield on rip and no rip treatments

	Winter 1991	Summer 1992	Winter 1992	Summer 1993	Winter 1993	Summer 1994	Winter 1994	Summer 1995[‡]
Water storage efficiency				— % —				
Rip	0.60		0.46		0.29		0.76	
No rip	0.67		0.49		0.37		0.66	
LSD(0.05)	ns[†]		ns		ns		ns	
Precipitation (mm)	50		60		64		97	
Water use				— mm —				
Rip		331		301		338		
No rip		341		290		348		
LSD(0.05)		ns		ns		ns		
Precipitation (mm)		344		318		243		
Wheat yield				— kg ha^{-1} —				
Rip		2577		2157		2958		292
No rip		2463		2182		2880		249
LSD(0.05)		ns		ns		ns		ns

† Significant at the 0.05 probability level (*) or not significant (ns)   ‡ Crop hail damaged in 1995

At the field scale, our tests failed to show any significant differences in water storage efficiency, water use by wheat, or wheat yield between treatments (Table 3). Water storage efficiency is the ratio of soil water storage to precipitation. Soil water storage was determined using a grid of 54 neutron access tubes. Individual tubes were several meters distant from the rips and consequently soil water measurements at the tube locations did not indicate water changes in close proximity of the rip.

Gravimetric soil water measurements in positions close to the rips provided evidence that spring runoff was channeled into the rip. Within a 3-m transect centered over the rip there were significant differences in soil water content between treatments (Table 4). In 1994, there was over 69 mm of snow

Table 4. Soil water to a depth of 1.22 m measured in a 3-m transect over the rip and at a comparable slope position on no rip treatments.

Treatment	Soil water (mm)
6 April 1994	
Rip	291*
No rip	251
LSD(0.05)	30
12 April 1995	
Rip	261*
No rip	236
LSD (0.05)	15

water equivalent (Table 1) at the start of a thaw on 27 February. By 14 March all the snow was melted. During this rapid thaw, visual observations confirmed runoff on the no rip plots and water accumulation in the ripping troughs. Soil temperature measurements at the time of melt indirectly suggest that warm water from the surface had infiltrated to the 0.3 m depth on the rip treatment (Fig. 3). Soil temperature at 0.3 m had registered
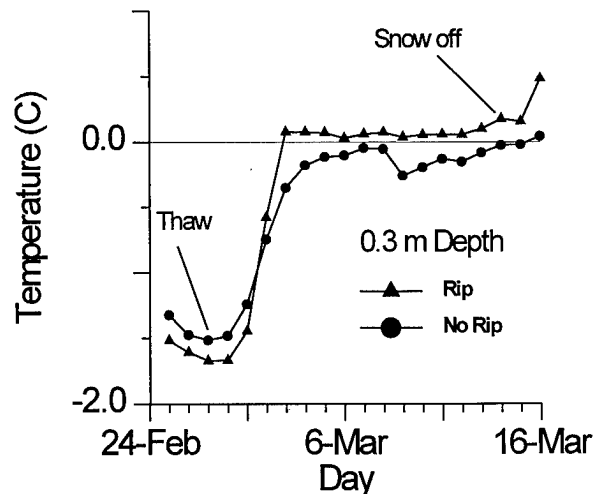
Figure 3. Soil temperature at 0.3 m during spring thaw in 1994. Temperature sensors at 0.3 m are at the depth of tillage on the rip treatment.

consistently lower on the rip treatment than on the no rip treatment until the thawing began.

Infiltration rates into frozen soil have been shown to be closely linked to soil water content at the time of freezing. Annual wheat cropping provides ideal opportunities to efficiently use precipitation and reduce soil erosion. Previously, we have shown that no-tillage annual spring wheat production was the most efficient crop and soil management from the standpoint of crop yield and water use efficiency (Aase and Pikul, 1995). In an experiment adjacent to this study (data not shown), soil water content in the top 0.6 m of the soil profile at freeze-up on plots following spring wheat harvest was 70% of that following fallow.

From an infiltration stand point it is desirable to annual crop because soil on annual cropped fields freezes at a lower water content than fallow fields. Although we did not directly compare infiltration into frozen soil on fields that were fallowed versus fields that were cropped, we speculate that because of soil water content differences, infiltration will be greater on annually cropped soils than on fallowed soils.

Soil ripping and annual cropping provide soil and crop management to minimize water runoff. Surface crusts and tillage pans are disrupted by ripping and preferential flow paths in the ripping trough serve to bypass the tortuous pathways near the surface and contribute to increased water infiltration. Because there were no differences in wheat yield between treatments, the application of contour ripping seems best suited to situations where runoff and soil erosion are problems. Practices that protect soil from erosion also stabilize yield and maintain soil productivity.

REFERENCES

Aase, J.K. and J.L. Pikul Jr. 1995. Crop and soil response to long-term tillage practices in the Northern Great Plains. Agron. J. 87:652-656.

Allmaras, R.R., S.C. Gupta, J.L. Pikul,Jr., and C.E. Johnson. 1979. Tillage and plant residue management for water erosion control on agricultural land in eastern Oregon. *In* Effects of Tillage and Crop Residue Removal on Erosion, Runoff, and Plant Nutrients. Soil Cons. Soc. Am. Spec. Pub. No. 25. Ankeny, Iowa.

Caprio, J.M., G.K. Grunwald, and R.D. Snyder. 1981. Snow barrier potential for harvesting moisture in transects across Chinook areas in Montana. Montana Agricultural Experiment Station Research Report No. 174.

Formanek, G.E., G.B. Muckel, and W.R. Evans. 1990. Conservation applications impacted by soil freeze-thaw. p 108-112. *In* K.R. Cooley (ed.) Frozen soil impacts on agricultural, range, and forest lands. Proc. International Symposium. Spokane, WA. 21-22 Mar. 1990. CRREL Special Report 90-1. US Army Corps of Engineers, Cold Regions Research and Engineering Laboratory, Hanover, NH.

Gray, D.M., R.J. Granger, and W. Nicholaichuk. 1990. Snowmelt infiltration into completely-frozen subsoiled soils. p.161-170. *In* K.R. Cooley (ed.) Frozen soil impacts on agricultural, range, and forest lands. Proc. International Symposium. Spokane, WA. 21-22 Mar. 1990. CRREL Special Report 90-1. US Army Corps of Engineers, Cold Regions Research and Engineering Laboratory, Hanover, NH.

Kane D.L. 1980. Snowmelt infiltration into seasonally frozen soils. Cold Regions Sci. and Tech. 3:153-161.

Lal, R., and H. Steppuhn. 1980. Minimizing fall tillage on the Canadian Prairies-A review. Can. Agric. Eng. 22:101-106.

Maulé, C.P., and D.S. Chanasyk. 1990. The effects of tillage upon snow cover and spring soil water. Can. Agric. Eng. 32:25-31.

Neff, E.L., and J.R. Wight. 1977. Overwinter soil water recharge and herbage production as influenced by contour furrowing on eastern Montana rangelands. J. Range Management. 30:193-195.

Pikul, J.L. Jr., L. Boersma, and R.W. Rickman. 1989. Temperature and water profiles during diurnal soil freezing and thawing: Field measurements and simulation. Soil Sci. Soc. Am. J. 53:3-10.

Pikul, J.L. Jr., J.F. Zuzel, and D.E. Wilkins. 1992. Infiltration into frozen soil as affected by ripping. Trans. ASAE. 35:83-90.

Saxton, K.E., D.K. McCool, and R.I. Papendick. 1981. Slot mulch for runoff and erosion control. J Soil and Water Cons. 36:44-47.

Spain, J.M., and D.L. McCune. 1956. Something new in subsoiling. Agron. J. 48:192-193.

Wight, J.R., and F.H. Siddoway. 1972. Improving precipitation-use efficiency on rangeland by surface modification. J. Soil and Water Conservation. 27:170-174.

Wilkins, D.E., C.L. Douglas, Jr., and J.L. Pikul, Jr. 1996. Header loss for Shelbourne Reynolds stripper-header harvesting wheat. Applied Engineering in Agriculture. ASAE. 12(2): 159-162.

Zuzel, J.F., and J.L. Pikul, Jr. 1987. Infiltration into a seasonally frozen agricultural soil. J. Soil Water Cons. 42:447-450.

Freezing and Colloid Aggregation

R.R. BLANK[1]

ABSTRACT

Soils of a montane meadow in the northern Sierra Nevada range contain high amounts of sand-sized particles. X-ray diffraction, elemental analysis, micromorphology, chemical treatment, and freezing experiments were used to deduce the petrogenesis of these particles. The particles are yellowish-red, platy to tabular, and composed of accreted crystalline domains. Based on optical properties, they appear to have weathered from biotite; however, the lithology of the surrounding rock types refutes this suspicion. In soil thin sections, they occur in root channels and voids as oriented masses with visible accretionary laminae. Particles similar in form and optical properties to the soil minerals were synthesized by repeated freezing and thawing of high iron kaolinite extracted from the soils. Synthesis of the data supports the conclusion that these soil particles formed via accretionary freeze-thaw-aided growth from colloids. The large proportion of the freeze aggregates in the sand-sized fraction of these soils suggests they are important for physical stability and infiltration. Argillans in soils subjected to frequent freeze-thaw cycles may be formed by freeze accretion of colloids and not illuviation.

Key Words: Argillans, kaolinite, montane meadow.

INTRODUCTION

Pathways that lead to soil particles adhering together to form large aggregates include binding by roots and fungal mycelia, gluing by polysaccharides, and compaction in the gut tracts of some soil invertebrates. For aeration, root elongation, and permeability, aggregation is critical in enhancing the health and productivity of the soil.

Freezing can also increase the aggregation of soil (Fippin 1910, Perfect et al. 1990, Lehrsch et al. 1991). One aspect of this aggregation concerns soil clays (Ahlrichs and White 1962, Lincoln and Tettenhorst 1971, Rowell and Dillon 1972, Saunders et al. 1986). The freeze-aided aggregation of clay appears nonpermanent and can be reversed by agitation (Lincoln and Tettenhorst 1971).

Freezing of halloysite, extracted from northern Idaho forested loessial soils, can form aggregates that are stable and appear crystalline; i.e., under the petrographic microscope they appear as uniform optical domains (Blank and Fosberg 1991). The optical properties of these freeze aggregates are similar to those of vermiculite, a potential weathering product of biotite. In the Idaho study, particles were extracted from the soil similar in optical properties to the laboratory-produced aggregates. Because the soils developed in biotite-containing loess and schist, the suspected freeze agglomerates could have weathered from the biotite.

Most recently, the soil genesis and morphology of a montane meadow in the northern Sierra Nevada range was studied (Blank et al. 1995). These soils contained an abundance of particles in the sand-sized fraction that appeared similar to the laboratory-produced freeze aggregates in the Idaho study. Moreover, most particles could not be a weathering product of biotite, as the parent materials of the Sierra-Nevada study site are not plentiful in biotite. The purpose of this paper is to report on the petrogenesis of these particles.

MATERIALS AND METHODS

Site characteristics

The study area is in the northern Sierra Nevada range along the upper reach of Grizzly Creek, a tributary of the Feather River (120° 37 W 39° 59 N). The surrounding uplands are forested by lodgepole pine [*Pinus contorta* ssp. *murrayana* (Grev. & Balf.) Critchf.], white fir [*Abies concolor* (Gordon & Glend.) Lindley], and Jeffrey pine [*Pinus jeffreyi* Grev. & Balf.]. The dominant vegetation on the meadow consists of Kentucky bluegrass [*Poa pratensis* L.], baltic rush [*Juncus balticus* Willd.], Nebraska sedge [*Carex nebrascensis* Dewey] and tufted-hairgrass [*Deschampsia caespitosa* (L.) Beauv.]. The elevation is 1800 meters and precipitation averages approximately 90 cm per year, 85 % of which is in the form of snow. The soil temperature regime is frigid bordering on cryic. The meadow developed in Quaternary lacustrine deposits; surrounding bedrock geology is mapped as Miocene, Oligocene, and Pliocene pyroclastics with minor Miocene andesite, Mesozoic granodiorite and Paleozoic marine limestone and dolomite (Burnett and Jennings 1962).

The soils

The soils of this montane meadow have recorded climatic and vegetation changes in the latter half of the Holocene (Blank et al. 1995). Three soils were characterized in detail: stream edge, mid-floodplain, and forest-edge. The soils are grossly similar in morphology, although there is a gradient of decreasing wetness from stream edge to forest edge and the forest edge pedon has coarser-textured upper horizons. Pedons are classified as Typic Humaquepts. Pedons have highly decomposed surface O horizons, dark colored A and B horizons with high clay content, and tephra-rich 2C horizons which overlie paleosol high clay 3Btgb horizons (Tables 1 and 2). The clay mineralogy is disjunct; horizons above the paleosol B are dominated by kaolinite, horizons below are dominated by smectite (Blank et al. 1995).

Laboratory

Suspected freeze aggregates in soil were isolated from all horizons of the three pedons by first removing organic carbon with repeated hydrogen peroxide treatment, followed by dispersion in hexametaphosphate. Centrifugation was used to remove the clay-sized fraction and sieving was used to separate the silt-sized fraction from the sand-sized fraction. All subsequent characterization of suspected freeze aggregates was done on the sand-sized fraction. Quantification of suspected freeze aggregates from each

soil horizon was gaged by the line count method (Brewer 1976). To isolate suspected freeze aggregates, decanting after shaking with water was used. The specific gravity of the suspected freeze aggregates was less than other minerals. Isolated material, combined from several soil horizons was characterized by optical microscopy, total elemental analyses, x-ray fluorescence, and x-ray diffraction. In addition, particles were treated with 30% hydrogen peroxide and hot citrate-dithionite, washed with deionized water, dried and then microscopically examined.

Table 1. Description of pedon collected from mid-floodplain position.

Horizon	Depth (cm)	Matrix color moist	Primary structure
Oa	0-10	10YR 2/1	1&2, m & c, gr
A	10-20	10YR 2/1	1, c, sbk
AB	20-28	2.5Y 2/0	1&2, m, pr
Bt	28-46	2.5Y 2/0	3, f & m, pr
2C	46-58	10YR 5/2	2, m & c, pr
3Btgb	58-81	2.5Y 2/0	3, m, pr
3Cg	81-107+	5Y 5/2	massive

Table 2. Selected chemical and physical properties of the mid-floodplain soil.

Horizon	pH	Organic carbon	Particle size sand	silt	clay
			----------------- g kg^{-1} ----------------		
Oa	5.00	155	117	637	246
A	5.29	56	162	289	549
AB	5.39	30	144	308	547
Bt	5.58	18	105	449	446
2C	5.96	9	168	554	279
3Btgb	5.69	11	91	520	389
3Cg	5.83	10	105	557	338

Colloids for laboratory freezing experiments were obtained via centrifugation of aqueous extracts of soil above the paleosol B horizon. Centrifugal force and time were adjusted so that colloids less than 1 micron in size remained in suspension. The process was repeated on other samples until several liters of solution were obtained. Splits (approximately 25 mL) of this mother liquor were placed in 50-mL polypropylene tubes for two treatments: 1) one-week

freeze, one-week thaw in closed containers so that samples remained wet (wet treatment); 2) one-week freeze, then after thawing, clear liquid poured off so that any freeze aggregates that formed were air dried (wet-dry treatment). Before the wet-dry treatment was re-frozen, approximately 25 mL of deionized water was added. Replicates of these freeze-thaw cycles were examined after 1, 2, 4, 8, and 12 months. Freeze aggregates that formed in the experiments were characterized by optical microscopy, x-ray diffraction, and total elemental analysis. As with suspected freeze aggregates, we studied the influence of hydrogen peroxide and hot citrate-dithionite treatment on the aggregates.

RESULTS

Characterization of suspected freeze agglomerates from soil

Suspected freeze aggregates were plentiful in most horizons of the soils studied, but especially in the forest edge pedon (Table 3). Color of the particles ranged from yellowish red to reddish brown. The morphology of the particles were mostly in platy to subhedral units (Fig. 1). The suspected freeze-aggregates have a distinctive microgranular texture with many dark inclusions. In some particles, minute pieces of diatom tests occurred. In reflected light, the particles have a golden metallic luster. Particle refractive index was variable with the highest about 1.644 and the lowest about 1.590. Most sand-sized particles consist of several optically uniform regions welded together. Acute bisectrix interference figures of large optically uniform areas are biaxial negative with a 2V of less than 15 degrees.

Although suspected freeze aggregates, isolated by decanting, appeared to be pure by visual examination, x-ray diffraction indicates multiple minerals present (data not shown).

Table 3. Percentage of suspected freeze aggregates (FA) in the very fine sand fraction.

Stream edge pedon		_Forest edge pedon_	
Horizon	FA	Horizon	FA
A	10	A	18
AB	10	AB	30
Bw	22	Bt1	37
2C	22	Bt2	47
3Btgb	1	2Btb	62
3Cg	13		

The suspected freeze aggregates have an elemental content similar to biotite (Table 4). As compared to < 2 μm material taken from the soil, suspected freeze aggregates are lower in Si and Al and much higher in Fe and Ti.
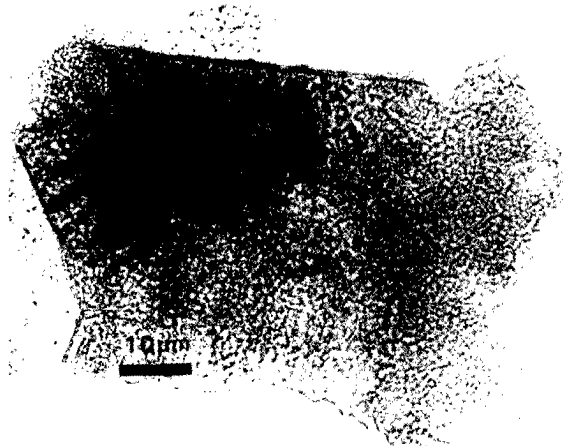
Figure 1. Photomicrograph of suspected freeze aggregate extracted from the soil.

Table 4. Elemental content (% by weight) of colloid material from the A, Bt, and 2Btg horizons as compared to freeze aggregates (FA) and biotite.

Element	A	Bt	2Btg	FA	Biotite
Si	25.08	24.40	23.66	20.2	18.29
Al	16.86	16.01	15.17	10.8	8.35
Fe	5.75	5.52	9.18	15.5	14.19
K	1.16	1.86	2.89	2.9	7.71
Mg	1.84	3.72	1.34	4.2	8.15
Ca	0.18	0.15	dl	0.8	0.14
Ti	0.44	0.38	0.44	1.2	1.40

Biotite values taken from Table 1.24 in Newman and Brown (1987).

Micromorphology

Thin sections of the O horizons of the soils were prepared from both the stream edge and mid-floodplain soils. These thin sections show that particles, optically identical to those extracted from the soils, occupy voids and root channels. Suspected freeze agglomerates in thin section often display accretionary laminae (Fig. 2). In crossed-polarized light, this particle showed over 10 distinct optically uniform domains. Another characteristic of suspected freeze aggregates in thin section is the layering in

optical orientation on the periphery of channels and pores (Fig. 3). In crossed-polarized conditions, these features are identical in appearance to illuvial argillans. It is highly unlikely such features represent illuvial argillans because the thin section covers only the top 5 cm of the soil.
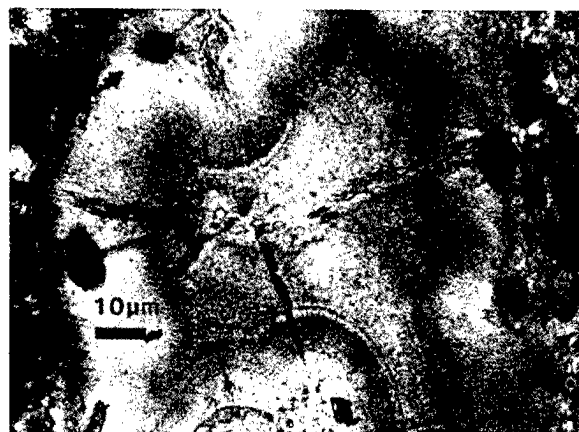
Figure 2. Thin section photomicrograph (plane-polarized light) of suspected freeze aggregate showing accretionary laminae.
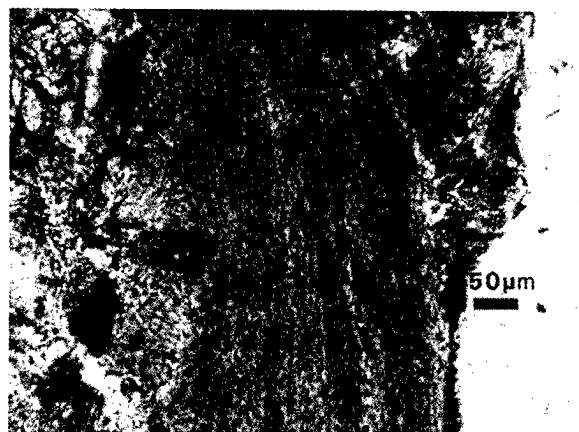
Figure 3. Thin section photomicrograph (crossed-polarized light) showing suspected freeze agglomerate appearing as an argillan.

Laboratory synthesis of freeze aggregates

The initial starting colloidal mixture was dominantly kaolinite (Fig. 4). The elemental content of colloids differed among horizons (Table 4), but for this experiment, colloids from all horizons above the paleosol were combined. After one week of freeze-thaw cycles, the colloids had aggregated together into a yellowish brown paste-like material that dispersed readily with agitation. With two months of freeze-thaw cycles, the aggregates that formed were over 200 μm in diameter and still dispersed with intense agitation. Aggregates in the wet-dry treatment, however, resisted dispersion to a greater extent than the wet treatment. At 2 months there were some distinct birefringent domains usually on particle edges.

After four months of freeze-thaw cycles, for both wet and wet-dry treatments, colloids had aggregated into stable units that resisted dispersion with intense agitation. Birefringent domains were large, some encompassing the entire sand-size aggregates. Dark striations and splotches occurred in most aggregates. The faces of individual aggregates are increasingly euhedral. By eight months of freeze-thaw cycles the aggregates were very stable and most varied from 20 to 1000 microns in diameter. Many aggregates consisted of one birefringent domain. Common forms included platy, subrounded equant, and lath-like (Fig. 4).

There was considerable change in x-ray diffraction characteristics with increasing freeze-thaw cycles (Fig. 5). After 1 month, as compared with the wet treatment, the wet-dry treatment had very subdued 001 and 002 lattice reflections and increased reflection of the 020 lattice spacing. By 2 months, treatment differences were minimal. As compared to the initial colloid treatment, prominent changes included: decreases in 001 and 002 lattice reflections; large increases in 020, 201, and 130 lattice reflections. These changes are consistent with the formation of halloysite.
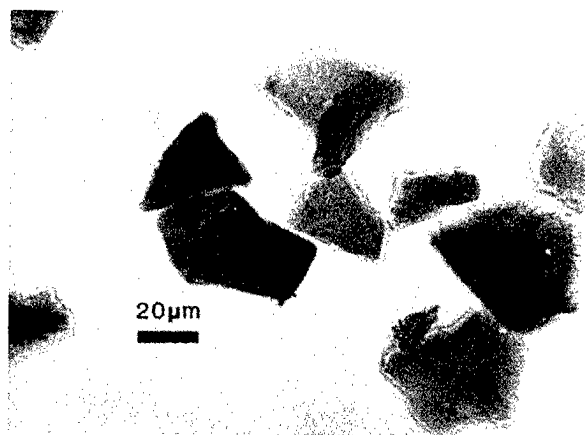
Figure 4. Photomicrograph of laboratory synthesized freeze aggregate (plane polarized light) after 8 months of freeze-thaw cycles.

215

When treated with hot citrate-dithionite or 30% hydrogen peroxide, laboratory-produced freeze aggregates, which were mostly dark brown, turned a golden brown more like aggregates in soil. One must be aware that the suspected freeze aggregates in soil were initially treated with hydrogen peroxide; thus, their natural coloration may have been darker. Synthetic aggregates were preferentially attacked by citrate-dithionite in lighter colored regions that showed no birefringence; there was a kinetic hindrance to citrate-dithionite in those regions where lattice orientation produced an optical indicatrix. The birefringent regions remaining were usually in lath-like units.
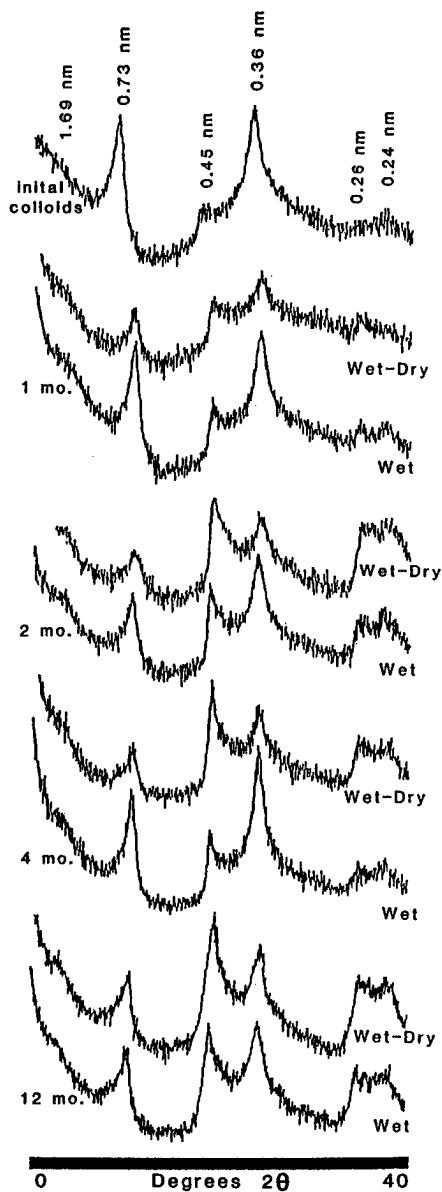
Figure 5. X-ray diffractograms of synthetic freeze aggregates after various lengths of freeze-thaw cycles.

Synthetic aggregates, washed after citrate-dithionite treatment, dried unusually: the non-birefringent particles readily aggregated together into large plate-like units. Peroxide treatment attacked particle edges, but when this material dried, there was no welding of particles as occurred with citrate-dithionite. Suspected freeze aggregates from soil, treated with citrate-dithionite, turned a yellowish green. Like synthetic aggregates, they readily aggregated together when dried. When suspected freeze aggregates were treated with hydrogen peroxide, the coloration was not altered appreciably, but clear and light colored regions were preferentially attacked. Like synthetic aggregates, peroxide-treated natural aggregates did not weld together when dried.

DISCUSSION

Suspected freeze aggregates, isolated from montane meadow soils, are formed via the freeze-aided accretion of colloidal kaolinite. Three lines of evidence support this conclusion. First, there is a strong similarity between laboratory-produced freeze aggregates and suspected freeze aggregates from soil. In addition, suspected freeze aggregates could not have weathered from precursor micaceous minerals because the soil parent material or surrounding rock type are simply not plentiful in biotite or muscovite. Finally, the presence of suspected freeze aggregation in microsites such as pores and root channels, along with features of accretionary growth, is compelling evidence for freeze aggregation for the following reason.

When soil freezes in nature, particles migrate ahead of the freezing front (Corte 1962). If the migrating particles include colloids conducive to freeze-aggregate formation, extrapolation of our laboratory and micromorphology results would predict that capture and concentration of the colloid by the freezing front should lead to the formation of larger and stable freeze-aggregates.

Experiments by Saunders et al. (1986) provide a potential explanation of this phenomenon. They concluded that slow freezing forces clay particles to "zone-refine" at the growth interference faces of ice crystals; the surfaces are "ice-cleaned" or removed of surface contaminants that could inhibit particle bonding. Clay surfaces can then form bonds or "cold weld." Using Saunders et al. (1986) model, we hypothesize, that as a consequence of freezing aqueous suspension, kaolinite is surface cleansed of contaminants that could inhibit particle bonding.

216

Once cleansed, the kaolinite crystals are forced together by the growing ice lattice in some mosaic.

The high Fe content of freeze aggregates and the attack of the aggregates by citrate-dithionite, suggests that an Fe-oxyhydroxy compound may be a welding agent. The fact that freeze-produced agglomerates have distinct habits suggests that the agglomeration process is not random; random accretion would likely produce spherical agglomerates. It would be unlikely that the growing ice lattice could mold agglomerates into platy and lath-like habits. Clearly then, kaolinite crystals accrete to thermodynamically favored positions.

Freeze-aggregation may be important for select precursor colloids. Freezing of aqueous suspension of several types of smectite does not produce aggregates capable of remaining intact upon intense agitation (Lincoln and Tettenhorst 1971, Rowell and Dillon 1972, Saunders et al. 1986).

CONCLUSIONS AND IMPLICATIONS

The freeze-aided aggregation of colloidal kaolinite, in montane meadow soils of the northern Sierra Nevada range, results in the formation of silt-and sand-sized stable particles. Formation of freeze-produced aggregates could occur widely in temperate climates, given the correct precursor colloidal mineralogy, which at this time appears to be high Fe halloysite or kaolinite. Over time, the formation of such aggregates could influence the physical and chemical properties of soil within the region of freezing soil temperatures. It would certainly affect the particle size distribution of the soil by changing clay to silt-and sand-sized material.

Trapping of the migrating colloids would likely occur at discontinuities in the soil where the freezing front would overtake these particles. This would occur in invertebrate channels, unoccupied root channels, and soil structural voids. Under these conditions, freeze-produced agglomerates resemble illuvial argillans. Some illuvial argillans, presently interpreted to be emplaced via colloids in percolating water (Buol and Hole 1961), actually formed via freeze aggregation.

ACKNOWLEDGMENTS

REFERENCES

Ahlrichs, J.L. and J.L. White. 1962. Freezing and lyophilizing alters the structure of bentonite gels. Sci. 136:1116-1118.

Blank, R.R. and M.A. Fosberg. 1991. Effects of freezing on colloidal halloysite: Implications for temperate soils. Clays Clay Min. 39:642-650.

Blank, R.R., T.J. Svejcar, and G.M. Riegel. 1995. Soil genesis and morphology of a montane meadow in the northern Sierra Nevada range. Soil Sci. 160:136-152.

Brewer, R. 1976. Fabric and mineral analysis of soils. Robert E. Kreiger Co., Huntington, New York.

Buol, S.W. and F.D. Hole. 1961. Clay skin genesis in Wisconsin soils. Soil Sci. Soc. Amer. Proc. 24:377-379.

Burnett, J.L. and C.W. Jennings. 1962. Geologic map of California - Chico sheet. California Division of Mines and Geology, Sacramento, CA.

Corte, A.E. 1962. Vertical migration of particles in front of a moving freezing plane. J. Geophys. Res. 67:1085-1090.

Fippin, E.O. 1910. Some causes of soil granulation. Proc. Amer. Soc. Agron. 2:106-121.

Lehrsch, G.A., R.E. Sojka, D.L. Carter, and P.M. Jolly. 1991. Freezing effects on aggregate stability affected by texture, mineralogy, and organic matter. Soil Sci. Soc Amer. J. 55:1401-1406.

Lincoln, J. and R. Tettenhorst. 1971. Freeze-dried and thawed clay. Clays Clay Min. 19:103-107.

Newman, A.C.D. and G. Brown. 1987. The chemical constitution of clays: in Chemistry of Clays and Clay Minerals, Miner. Soc. Mono. No. 6, A.C.D. Newman, ed., Longman Sci. & Technical, Essex, England, 1-128.

Perfect, E., W.K.P. Van Loon, B.D. Kay, and P.H. Groenevelt. 1990. Influence of ice segregation and solutes on soil structural stability. Can. J. Soil Sci. 70:571-581.

Rowell, D.L. and P.J. Dillon. 1972. Migration and aggregation of Na and Ca clays by the freezing of dispersed and flocculated suspension. J. Soil. Sci. 23:442-447.

Saunders, R.S., F.P. Fanale,T.J. Parker, J.B. Stephens, and S. Sutton. 1986. Properties of filamentary sublimation residues from dispersions of clay in ice. Icarus 66: 94-104.

Impact of Freezing and Thawing on the
Stability of Casts Produced by Earthworms

E.C. BERRY[1], A.A. SWALLA[1], D. JORDAN[2], AND J.K. RADKE[1]

ABSTRACT

Aggregates within earthworm casts are usually more water stable than aggregates found in the bulk surface soil. Research has demonstrated that aggregate stability within earthworm casts varies among species of earthworms, soil texture, age of casts, and food sources. The objectives of this study were to examine the effects of freezing and thawing on the stability of intact (undisturbed) *Lumbricus terrestris* (L.) casts in different soils, under different soil moisture contents, and various freezing regimes compared to those in the bulk surface soil. Casts produced by *L. terrestris* were more water stable than the bulk surface soil. Stability was reduced when casts and bulk surface soil were frozen and then air dried. Air drying also reduced the stability of both the earthworm casts and the bulk surface soil. These studies are continuing and will aid in understanding the effects of earthworms and their casting activities on soil structure in soils that freeze.

Key words: *Lumbricus terrestris*, casts, cast stability, freeze-thaw cycles, soil structure

INTRODUCTION

Soil structure is defined as the arrangement of particles and associated pores in soils. Aggregate formation involves the physical forces of shrinking and swelling in soils created by changes in soil water status, freezing and thawing cycles, tillage, or by the movement of larger soil animals (Oades 1993). Stabilization is primarily due to inorganic materials such as oxides of aluminum and iron, distribution of root systems, or action or activities of micro- and mesofauna (Oades 1993). It is accepted that earthworms modify soil structure by burrowing, burying above ground litter, ingesting mineral soil and mixing it with partially digested plant debris and ejecting this mixture on the soil surface or within the soil matrix, and mixing of soil horizons (Lavelle 1988, Berry 1994). Burrowing is generally associated with earthworms searching for food, reproduction activities, escaping unfavorable environmental conditions, and their colonization of new areas. During these processes, earthworm casts (a mixture of feces and soil) are deposited either on the surface of the soil or within burrows in the soil matrix (Lavelle 1988). Location of the casting activity is usually species dependent (Edwards and Bohlen 1996). Horizontal burrowing species, such as *Aporrectodea trapezoides* (Dugés), deposit their casts below the soil surface and vertical burrowing species, such as *Lumbricus terrestris* (L.), most often deposit their casts at the surface. Casts have been observed to weigh 45 to 200 g, to be 5-10 cm high and 8 cm wide (Lee 1985). To form these casts, earthworms may ingest 1.5 to 2600 Mg ha^{-1} of organic residue and soil (Watanabe and Ruaysoongnern 1984).

The stability of casts are a function of the organic matter that earthworms consume and the microbial activity within the casts after excretion to the soil (Shipitalo and Protz 1988, Shipitalo and Protz 1989). Casts that are deposited on the soil surface have different shapes, sizes, structure and composition. These characteristics may determine their function in soil structure. Globular casts are made of round or flat units and are fairly resistant to erosion, whereas granular casts are made of accumulation of small fine-textured pellets that are susceptible to erosion (Lee 1985, Mulongoy and Bedonet 1989).

Earthworm casts deposited on the surface of the soil are usually more water stable than aggregates in the bulk soil. Research has demonstrated that aggregate stability varies among earthworm species, soil texture, age of casts, and food sources. Mechanisms by which earthworms produce and stabilize soil aggregates are complex and poorly understood. Several theories (as cited by Tomlin et al. 1995) have been proposed for increased stability of earthworm casts. These include (1) stabilization by secretions within the earthworm (Dawson 1947), (2) stabilization by plant debris within the casts (Dawson 1947, Parle 1963, Lee and Foster 1991), (3) stabilization by fungal hyphae (Parle 1963, Marinissen and Dexter 1990, Lee and Foster 1991), (4)

stabilization by bacterial gums (Swaby 1950), or (5) stabilization by wetting and drying cycles with or without organic bonding (Shipitalo and Protz 1988, Shipitalo and Protz 1989). Additionally, West et al. (1991) demonstrated that increased aggregate stability of earthworm casts and tunnel walls result from grain bridging of organic-enriched materials. In Midwestern soils where freezing and thawing frequently occur, stability of casts are affected by these processes.

EXPERIMENTAL PROCEDURE

Our objective was to examine the effect of freezing and thawing on the stability of casts produced by *L. terrestris* in 3 soil types. Soil types and collection locations consisted of a Monona (Fine-silty, mixed, mesic Typic Hapludolls) silty loam collected from Treynor, Iowa, Webster (Fine-loamy, mixed, mesic Typic Haplaquolls) clay loam collected from Ankeny, IA, and Putnam (Fine, montmorillonitic, mesic Mollic Albaquals) silt loam collected from near Novelty, Missouri. Test containers (plastic 28 x 40 x 15 cm) were prepared from each soil type. All containers were maintained at 29.5% soil moisture (wet weight). Ten adult *L. terrestris* from colonies reared at the National Soil Tilth Laboratory for 2 generations were introduced to each container. Earthworms in the test containers were fed on partially decomposed horse manure (Berry and Karlen 1993). Casts were collected from each container 7 d later. Casts were placed in petri dishes, sealed with parafilm and held at 4°C until time of analysis. Treatments consisted of (1) wet sieved intact casts, (2) casts that were air dried and then frozen for 48 hrs at -20°C, (3) frozen wet at -20°C and then air dried, (4) air dried for 48 hrs, (5) wet sieved bulk soil, (6) bulk soil that was air dried and then frozen for 48 hrs at -20°C, (7) frozen for 48 hrs at -20°C and air dried, and (8) air dried bulk soil for 48 hrs. Aggregate stability was determined by using a modification of Yoder's (1936) procedure. Treatments were wet sieved at 200 rpm, 1.3 cm stroke, for 5 min. Size classes were determined by collecting the samples on sieves of 4.0, 2.0, 1.0, 0.5, and 0.25 mm. Samples were air dried for 24 hrs at 70°C. Samples were weighed and 50 ml of 5000 ppm hexametaphosphate was added to each sample. To disperse the clay, samples were gently agitated during the next 24 hr period and sieved through a 53.0-µm sieve. The samples were dried

again for 24 hrs at 70°C. The samples were weighed and placed into crucibles to burn off the organic matter (450 °C) for 24 hrs. Samples were again weighed to determine sand weight.

RESULTS AND DISCUSSION

Data presented are preliminary and experiments are ongoing. Therefore statistical analyses are not presented. A summary of the soil characteristics for the 3 soils is presented in Table 1.

Table 1. Summary table showing percentages of sand, silt, and clay of test soil

	Monona silt loam	Putnam silt loam	Webster clay loam
Sand	5.6	5.7	30.7
Silt	67.5	76.2	38.6
Clay	26.4	18.1	30.9

These soils were selected because fine-grained soils are more frost susceptible than are soils with a higher percentage of sand (Czurda et al. 1995). Usually higher percentages of clay are found in Webster soils than in either Monona or Putnam soils, therefore the Webster soils should be more susceptible to freezing and thawing.

Comparison of water-stable aggregates in casts produced by *L. terrestris* and aggregates in the bulk surface soil summed across all treatments are shown in Figure 1. Casts formed by *L. terrestris* from the Putnam soils were less stable than casts in the Webster and Monona soils. Aggregates in the earthworm casts in the Webster soils were slightly more stable than those in the Monona soils. However, in the bulk surface soil samples, the Monona soils had fewer water-stable aggregates than either the Putnam or Webster soils.

Differences in aggregate stability among the sample treatments are shown in Figure 2. Earthworm casts and bulk surface soil samples that were first frozen and then air dried had fewer water-stable aggregates than did samples that were air dried and then frozen. This is not surprising because samples that were frozen and then air dried were first subjected to the forces from freezing and then to forces generated with rewetting.
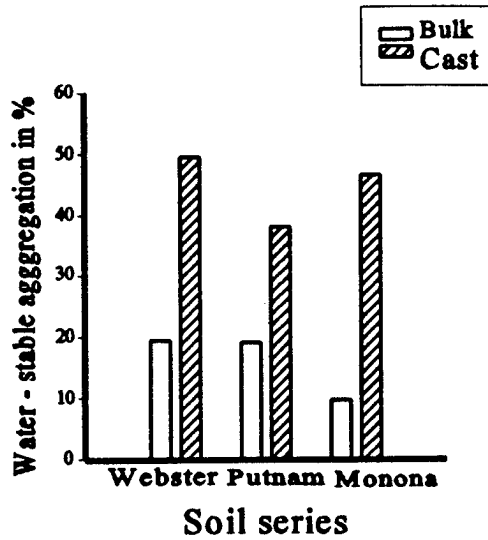
Figure 1. Percentage water-stable aggregates for each soil series (summed over treatments).
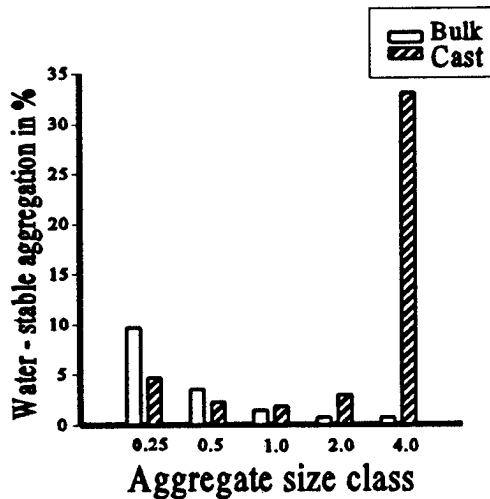
Figure 2. Percentage water-stable aggregates for each treatment (summed over soils).

Soil samples that have not been subjected to drying are usually more stable than those that have been dried and rewetted (Reid and Goss 1981, Kemper and Rosenau 1986, Beare and Bruce 1993). Across all soil types and treatments, the percentage of water stable aggregates found in the earthworm casts were higher than the percentages found in the bulk surface soils (Table 2).

Table 2. Percentage stable aggregates in earthworm casts and bulk surface soil (adjusted for sand).

Sample treatment	Earthworm casts	Bulk soil
Webster		
Wet	70.30	37.19
Air-dried frozen	57.17	21.78
Frozen-air dried	42.63	16.32
Dry	48.65	19.80
Putnam		
Wet	72.38	46.37
Air dried-frozen	41.33	17.73
Frozen-air dried	30.14	14.45
Dry	42.41	24.91
Monona		
Wet	75.92	52.82
Air dried-frozen	46.16	9.69
Frozen-air dried	50.45	6.79
Dry	42.71	12.23

L. terrestris casts had higher percentages of sand than the bulk surface soil samples regardless of soil type (Table 3).
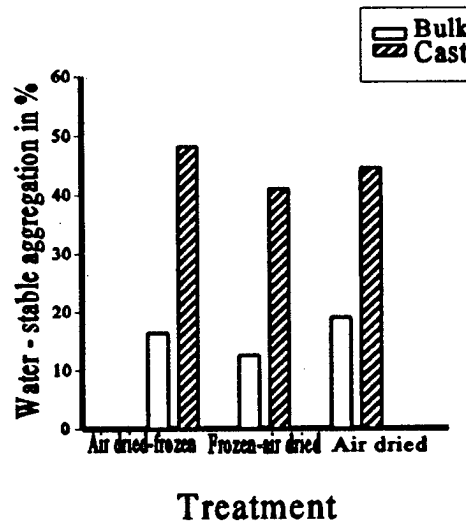
Figure 3. Percentage water-stable aggregates in total soil by class size (mm).

220

Table 3. Percentage residue in stable portion of earthworm casts and bulk surface soil.

Sample treatment	Earthworm casts	Bulk soil
Webster		
Wet	3.72	0.27
Air dried-frozen	4.33	0.19
Frozen air-dried	4.25	0.21
Dry	3.29	0.33
Putnam		
Wet	3.98	1.24
Air dried-frozen	4.28	1.24
Frozen-air dried	4.03	1.06
Dry	4.77	1.31
Monona		
Wet	4.26	0.94
Air dried-frozen	3.90	0.53
Frozen-air dried	3.43	0.51
Dry	4.53	0.29

Differences in the amounts of sand retained on the sieves between the casts and bulk surface soil may be due to: (1) sand granules were physically protected by the casts whereas sand granules within the bulk surface soil were allowed to pass through the sieves, or (2) earthworms were selective in the size of particles that deposited in their casts.

Percentage residue remaining in the stable portion of the soil samples are presented in Table 4. These data are similar to those presented for sand. In all soils and treatments, higher amounts of residue were found within the earthworm casts compared to the bulk surface soil. *L. terrestris* collect and feed on residue found on the surface of the soil. Portions of this material is retained within the casts (Berry 1994) and therefore yield higher amounts of residue in the casts.

Comparisons of the stability of earthworm casts and bulk surface soil across all soil types according to class size are presented in Figure 3 and within each soil type in Table 5. Higher percentages of water-stable aggregates in the earthworm casts were retained on the larger sieves compared to the small sieves. However,

Table 4. Stability of earthworm casts and bulk surface soil.

Percent of total soil in size class[1]

Sample treatment	Earthworm casts					Bulk surface soil		
	0.25	0.50	1.00	2.00	4.00	0.25	0.50	1.00
Webster								
Wet	0.40	0.59	0.70	0.41	68.21	9.00	8.44	6.41
Air dried-frozen	4.57	2.14	1.24	2.46	46.74	12.04	5.17	1.93
Frozen-air dried	4.49	1.46	0.71	1.54	34.43	11.40	3.26	0.75
Dry	4.04	1.82	0.95	1.61	40.22	9.38	3.76	1.56
Putnam								
Wet	1.37	1.54	1.87	2.62	64.95	8.73	9.57	6.89
Air dried-frozen	5.03	2.42	1.74	3.06	29.04	10.64	4.70	1.85
Frozen-air dried	5.73	3.26	2.34	3.53	15.27	8.66	3.77	1.47
Dry	6.01	3.73	1.79	3.60	27.26	13.29	6.71	3.33
Monona								
Wet	0.52	0.48	0.52	1.46	72.90	6.31	5.29	4.85
Air dried-frozen	4.65	2.18	1.55	4.24	33.51	7.09	1.43	0.74
Frozen-air dried	4.28	1.51	4.14	4.02	36.50	5.28	0.73	0.44
Dry	2.91	1.28	1.39	2.34	34.76	9.07	2.05	0.61

[1]Sieves in mm

within the bulk surface soil, higher percentages of stable aggregates were retained on the smaller sieves than on the larger sieves. Regardless of soil series, water stable aggregates were generally greater on large sieves, thereby supporting our contention about the composition of earthworm casts.

SUMMARY AND CONCLUSIONS

Aggregate stability in earthworm casts may be affected by soil types (series), freezing and thawing cycles, wetting and rewetting cycles, and by particle size distribution. Particle size distribution may be dependent on soil type and specific earthworm activities in a given soil ecosystem. In our study, the percentage of sand found in the casts and bulk soil may have been due to the activity of the *L. terrestris* or due to physical protection of sand granules. Residue also has a role in the formation of water-stable aggregates in casts. Across all soils, percentage residue was higher in earthworm casts than in the bulk soils.

Table 5. Stability of earthworm casts and bulk surface soil.

| | Percent of total soil in size class[1] | | | | | | | | | |
| | Earthworm casts | | | | | Bulk surface soil | | | | |
Sample treatment	0.25	0.50	1.00	2.00	4.00	0.25	0.50	1.00	2.00	4.00
					Webster					
Wet	0.40	0.59	0.70	0.41	68.21	9.00	8.44	6.41	5.76	7.57
Air dried-frozen	4.57	2.14	1.24	2.46	46.74	12.04	5.17	1.93	1.20	1.45
Frozen-air dried	4.49	1.46	0.71	1.54	34.43	11.40	3.26	0.75	0.60	0.31
Dry	4.04	1.82	0.95	1.61	40.22	9.38	3.76	1.56	1.86	3.22
					Putnam					
Wet	1.37	1.54	1.87	2.62	64.95	8.73	9.57	6.89	4.46	16.69
Air dried-frozen	5.03	2.42	1.74	3.06	29.04	10.64	4.70	1.85	0.52	0.00
Frozen-air dried	5.73	3.26	2.34	3.53	15.27	8.66	3.77	1.47	0.51	0.04
Dry	6.01	3.73	1.79	3.60	27.26	13.29	6.71	3.33	0.92	0.64
					Monona					
Wet	0.52	0.48	0.52	1.46	72.90	6.31	5.29	4.85	7.72	28.65
Air dried-frozen	4.65	2.18	1.55	4.24	33.51	7.09	1.43	0.74	0.20	0.22
Frozen-air dried	4.28	1.51	4.14	4.02	36.50	5.28	0.73	0.44	0.15	0.17
Dry	2.91	1.28	1.39	2.34	34.76	9.07	2.05	0.61	0.31	0.25

[1]Sieves in mm

REFERENCES

Beare, M.H. and R.R. Bruce. 1993. A comparison of methods for measuring water-stable aggregate: Implications for determining environmental effects on soil structure. Geoderma 56:87-104.

Berry, E.C. 1994. Earthworms and other Fauna in the Soil. p. 61-90. *In* J.L. Hatfield and B.A. Stewart (ed.) Soil Biology: Effects on Soil Quality. Lewis Publishers, New York, NY.

Berry, E.C. and D.L. Karlen. 1993. Comparison of alternative farming systems. II. Earthworm population density and species diversity. J. Alternative Agric. 8:21-26.

Czurda, K.A., S. Ludwig, and R. Schababerle. 1995. Fabric Changes in Plastic Clays by Freezing and Thawing. *In* K.H. Hartge and B.A. Stewart (ed.) Soil Structure: Its Development and Function. Lewis Publishers, New York, NY.

Dawson, R.C. 1947. Earthworm microbiology and the formation of water-stable aggregates. Soil Sci. Soc. Am. Proc. 12:512-516.

Edwards, C.A. and P.J. Bohlen. 1996. Biology and Ecology of Earthworms. Chapman & Hall, New

York, NY.

Kemper, W.D. and R.C. Rosenau. 1986. Aggregate stability and size distribution. *In* A. Klute (ed.) Methods of soil analysis. Part 1. 2nd ed. Agronomy. 9:425-442.

Lavelle, P. 1988. Earthworm activities and the soil system. Biol. Fertil. Soils 1988:237-251.

Lee, K.E. 1985. Earthworms: Their ecology and relationships with soils and land use. Academic Press, New York, NY.

Lee, K.E. and R.C. Foster. 1991. Soil fauna and soil structure. Aust. J. Soil Res. 29:745-775.

Marinissen, J.C.Y. and A.R. Dexter. 1990. Mechanisms of stabilization of earthworm casts and artificial casts. Biol. Fertil. Soils 9:163-167.

Mulongoy, K. and A. Bedoret. 1989. Properties of worm casts and surface soils under various plant covers in the humid tropics. Soil Biol. Biochem. 21:197-203.

Oades, J.M. 1993. The role of biology in the formation, stabilization and degradation of soil structure. Geoderma. 56:377-400.

Parle, J.N. 1963. A microbiological study of earthworm casts. J. Gen. Micro. 31:13-22.

Reid, J.B. and M.J. Goss. 1981. Effect of living roots of different plant species on the aggregate stability of two arable soils. J. Soil Sci. 32:521-541.

Shipitalo, M.J. and R. Protz. 1988. Factors influencing the dispersibility of clay in worm casts. Soil Sci. Soc. Am. J. 52:764-769.

Shipitalo, M.J. and R. Protz. 1989. Chemistry and micromorphology of aggregation in earthworm casts. Geoderma 45:357-374.

Swaby, R.J. 1950. The influence of earthworms on soil Aggregation. J. Soil Sci. 1:195-197.

Tomlin, A.D., M.J. Shipitalo, W.M. Edwards, and R. Protz. 1995. Earthworms and their influence on soil structure. p. 159-183. *In* P.F. Hendrick (ed.) Earthworm Ecology and Biogeography in North America. Lewis Publishers, New York, NY.

Watanabe, H. and S. Ruaysoongnern. 1984. Casts production by the Megascolecid earthworm *Pheretima* sp. in northeastern Thailand. Pedobiologia 26:37-44.

West, L.T., P.F. Hendrix and R.R. Bruce. 1991. Micromorphic observation of soil alteration by earthworms. Agriculture, Ecosystems and Environment. 34:363-370.

Yoder, R.E. 1936. A direct method of aggregate analysis of soils and a study of the physical nature of erosion losses. J. Am. Soc. Agron. 28:337-351.

Spatial Variability of
Frozen Soil Runoff at Different Scales

M.S. SEYFRIED[1], G.N. FLERCHINGER[1], AND M.D. MURDOCK[1]

ABSTRACT

Soil freezing can cause dramatic reductions in infiltration rates, which have been associated with major flooding and erosion events in northern latitudes. In this paper we analyzed field runoff data collected at scales ranging from 1-m^2 to 13 ha with the intent of identifying practical scales for modeling frozen soil runoff. We found that: (i) there is extremely high spatial variability of runoff at the 1 m^2 scale which is probably due to the highly variable snow distribution affected by vegetation, (ii) this variability is effectively "averaged out" at the scale of 30-m^2 plots, and (iii) an increase in scale introduces a new source of variability, topography, which must be accounted for. It may be that at larger scales topographic effects are also "averaged out."

Key words: Frozen soil, surface runoff, spatial variability, scale.

INTRODUCTION

Soil freezing can result in dramatic reductions in infiltration rates (Kane 1980, Trimble et al. 1958). As a consequence, flooding and erosion from frozen soils are important processes in much of the northern USA, Canada, Northern Europe and Asia (Garstka 1945, Bates and Bilello 1966, Dunne and Black 1971, Johnsson and Lundin 1991, Hayhoe et al. 1992, Seyfried and Flerchinger 1994, and Vasilyev 1994). In the interior Pacific Northwest (USA), most of the major flooding and erosion events are associated with rain and snowmelt on frozen soil (Johnson and the McArthur 1973). Despite the acknowledged impact of soil freezing on infiltration and runoff for a significant portion of the world, our understanding of these processes is poor relative to analogous processes in unfrozen systems. It is not surprising that frozen soil runoff is generally a weakness in hydrological models for areas of seasonally frozen soil (Leavesley 1989, Wilcox et al. 1991).

Hydrologic models of frozen soil runoff can be useful for estimating or predicting early season runoff from snowmelt-dominated basins, estimating flooding hazard from rain on frozen soil events, and/or erosion. We are particularly interested in process-oriented models because they are potentially useful at locations where calibration is not possible and under environmental conditions (e.g., those resulting from management changes) that are not within the calibration data set. This requires that knowledge of the processes involved, which is usually obtained from controlled experiments performed under homogeneous conditions, be represented under field conditions, which are spatially heterogeneous.

The magnitude and nature of spatial variability may change considerably with the modeling scale (Seyfried and Wilcox 1995). For example, soil-water content may be known to vary distance from a tree stem due to the foliage. This may be regarded as deterministic and represented on a map, when modeling at a meter scale. If, however, the modeling scale is multiple kilometers, it may be possible, in fact necessary, to describe that variability in a stochastic manner as the patterns of soil-water content are repeated numerous times within the model resolution scale. In another words, the "tree source" of spatial variability may be effectively "averaged out" at the larger scale. The choice of modeling scale depends not only on the application scale, but also on the nature of spatial variability and availability of critical model parameter data.

In this paper we present data illustrating how runoff from frozen soil varies in space and with scale in a rangeland watershed. The event described took place in March of 1993. The runoff variability is related to measurable landscape features. Implications for modeling are discussed.

MATERIALS AND METHODS

Site Description

All work was conducted in the Reynolds Creek experimental watershed, which is located in southwest Idaho. Previous work at the watershed has shown that the soil infiltration capacity is high, 5.5 to 8.5 x10^{-6} m/s, relative to almost all typical precipitation rates because most of the precipitation

---

[1]USDA, Agricultural Research Service, Northwest Watershed Research Center, 800 Park Blvd., Boise, Idaho 83712, USA

comes from large frontal systems characterized by low rainfall intensities or snow (Hanson 1982). Exceptions are the occasional thunderstorm and frozen soil runoff events. The latter are of particular interest because they can result in widespread, even regional flooding. We have established that most of the flooding and erosion events at Reynolds Creek are related to frozen soil conditions (Johnson and McArthur 1973, Seyfried et al. 1990). The historical data were sufficient to identify frozen soil as a source of runoff but was not sufficient to provide information concerning the spatial variability of critical parameters affecting frozen soil runoff at different scales.

Although conditions conducive to frozen soil runoff events can occur anywhere in Reynolds Creek, we have found that most events occur between the 1400-1800 m elevations where there is sparse vegetative cover and shallow but fairly persistent snow cover (Seyfried et al. 1990). In areas with deep snow and more vegetation the snow insulates the soil and absorbs winter or early spring rains. In areas with less persistent snow cover the soil thaws more quickly and has less snowmelt contribution to events. These conditions are well represented by the Lower Sheep Creek subwatershed in Reynolds Creek.

Lower Sheep Creek is a small, 13-ha watershed within Reynolds Creek with a mean annual precipitation of 379 mm, about half of which is snow. Strong winds are common throughout the winter months which result in the redistribution of snow into protected areas. On average, there is very little runoff (8.3 mm) from Lower Sheep Creek. We found that there were 16 "significant" runoff events during a 13-year period of record and that about 86% of the total runoff came from frozen soil events (Seyfried et al. 1990).

The dominant soils are classified as a fine-loamy, montmorillonititc, frigid Typic Argixeroll. Some general features of the soil profile are a pronounced silt loam "cap" in the upper 20 to 25 cm, which is underlain by a distinctive argillic horizon (40% clay). In the 60 to 90 cm depths there is a zone of $CaCO_3$ accumulation. Rock content increases with depth to a maximum at around 65 cm depth where it is more that 50% by weight.

The vegetation through the watershed is primarily low sagebrush (*Artemesia arbuscula*) which is about 40 cm tall and, along with grass and forbs, covers about 40% of the ground surface. The remainder is either bare ground or rock. The density of cover is highly uniform within the watershed.

Data Collection

Watershed transect

We monitored soil-water content, soil temperature, and snow depth at 10 locations, approximately 40 m apart, across the watershed (Fig. 1). Soil water content from 0-45 cm depth was measured by time domain reflectometry (TDR) when there was little or no snow cover. Soil temperature and resistance at 5 cm were measured with fiberglass resistance sensors at each visit. Soil liquid water content can be inferred, qualitatively, from the sensor resistance (Seyfried and Murdock 1993), which can also be used to determine if the soil is frozen. Snow depth was measured at each site when present.
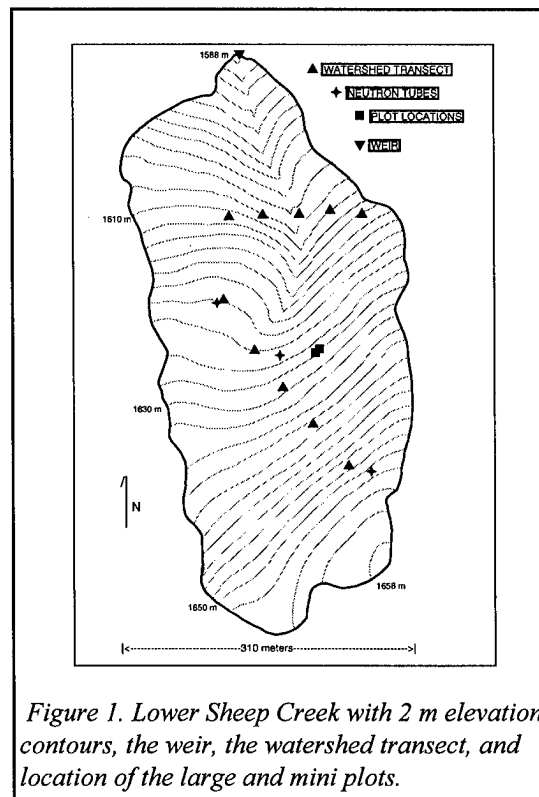
Figure 1. Lower Sheep Creek with 2 m elevation contours, the weir, the watershed transect, and location of the large and mini plots.

Surface Runoff

Runoff was monitored at three scales: the 1-m^2 scale, represented by four "mini" plots, the 30-m^2 scale, represented by two "large" plots, and the entire 13-ha subwatershed monitored at a weir at the topographic low of the watershed. The mini plots, labeled M1 through M4, were roughly oblong and varied in surface area from 0.7 to 1.3 m^2. Two mini plots, M1 and M3, encompassed unvegetated shrub interspace areas and the other two mini plots, M2 and M4, encompassed shrubs.

Runoff was collected at the topographic low of each plot and piped to an enclosed, vertical PVC pipe in a 1.3 m deep trench. The height of water in the pipe was monitored with a float recorder connected to a data logger. The large plots were duplicate, adjacent, 10.7 by 3 m runoff plots enclosed with sheet metal borders and separated by 3 m as described by Simonton and Renard (1982). Slopes for the two plots were 15%. Surface runoff was collected in a buried 1325-L stock tank. The height of water was monitored continuously with a float recorder connected to a data logger. In both cases a methanol-water mixture was added to the tank bottoms to prevent float freezing. Flow through the weir was calculated from the height of water behind the weir as measured with a float recorder. Runoff volumes are reported per unit area.

Snow depth

In addition to the watershed transect, snow depth was monitored within the two large plots at 11 locations separated by 1-m along the length of each adjacent plot. One reading was also taken in the center of each of the four mini plots. Snow density was estimated from large can samples collected in the vicinity of the plots so that snow water content could be estimated.

Surface cover

Vegetation canopy and surface cover were measured in late Spring with a vertical point frame (Abrahams et al. 1988) at 10 equally spaced cross sections in the plots. There were 60 points per cross section, resulting in a total of 600 measured points per plot. The average shrub coverage for the two plots was 33%, with no significant (α=0.05) difference between them. This sparsely vegetated area is of particular interest because it is most conducive to frozen soil runoff (Seyfried et al. 1990).

RESULTS AND DISCUSSION

Lower Sheep Creek Runoff

Runoff from the mini plots varied by a factor of 3 in the space of a few meters. Although there was a small amount of surface runoff recorded from M1 earlier in the year, almost all the runoff was recorded between day of year (DOY) 68 and 80 when there was a combination of relatively warm temperatures and rainfall (Fig. 2).

The total runoff for the four mini plots (62 mm for M1, 63 mm for M2, 95 mm for M3 and 30 mm for M4) was highly variable. All runoff occurred on days

73, 74, 75, and 76. Since there was only 37.08 mm of precipitation during this period, most of the runoff was due to snowmelt. In addition, the temporal pattern of runoff was quite variable among the four plots (Fig. 3), which indicates that the relative rankings of the runoff from the different plots would likely vary with different climatic conditions. There was no consistent relationship with cover type.

In contrast to the mini plots, the runoff from the two large plots was practically identical, both in terms of the total amount (39 mm for the north plot and 39 mm for the south plot) and the timing (Fig. 4). This runoff all occurred on days 73 and 74, which
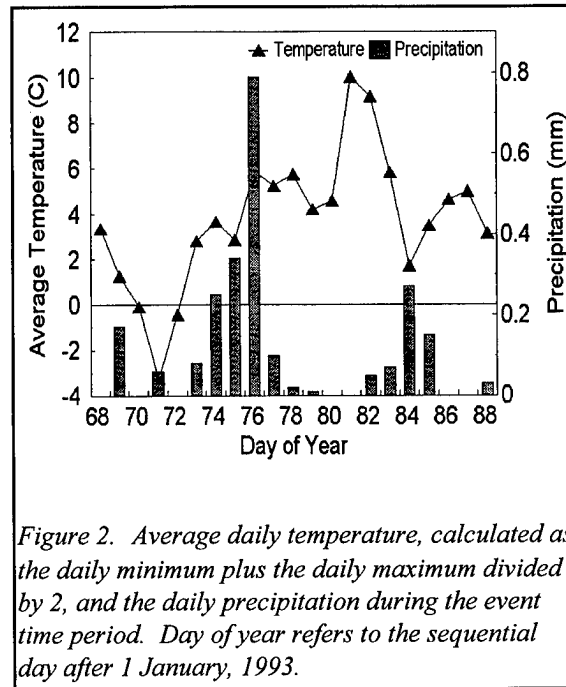
Figure 2. Average daily temperature, calculated as the daily minimum plus the daily maximum divided by 2, and the daily precipitation during the event time period. Day of year refers to the sequential day after 1 January, 1993.
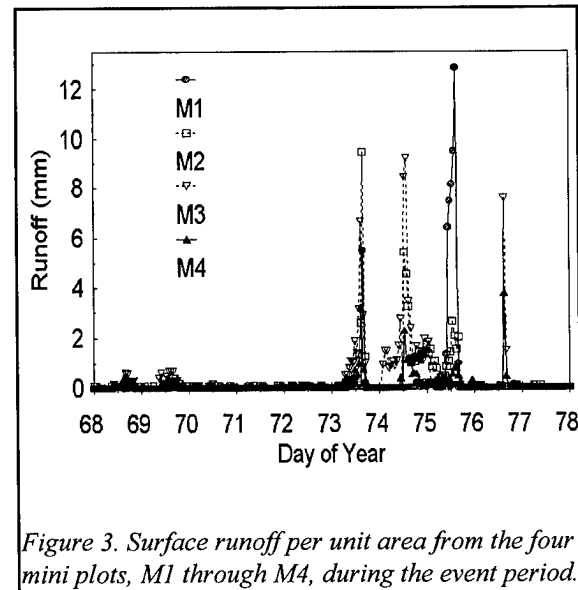
Figure 3. Surface runoff per unit area from the four mini plots, M1 through M4, during the event period.

226
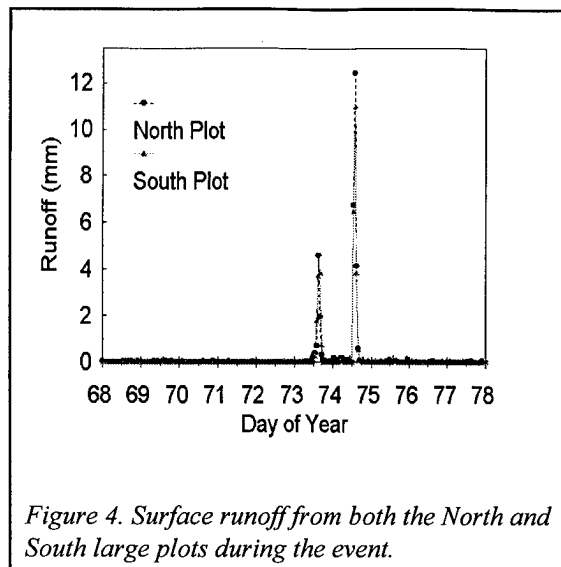
Figure 4. Surface runoff from both the North and South large plots during the event.
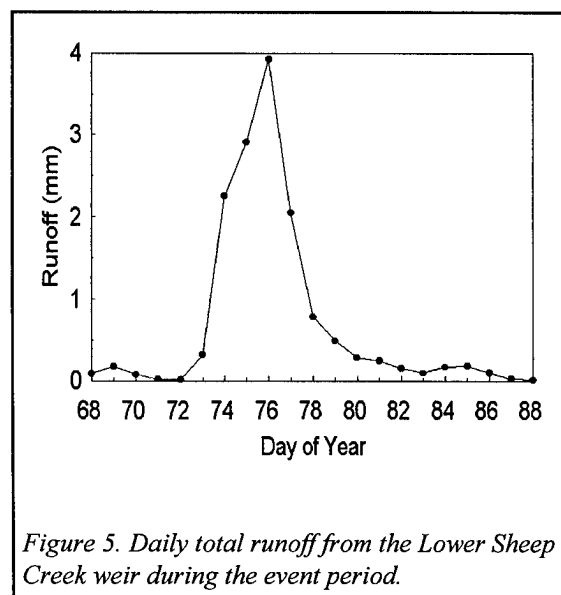
Figure 5. Daily total runoff from the Lower Sheep Creek weir during the event period.

had only 8.4 mm of precipitation. This uniformity in total runoff has been noted on other events. It implies that whatever the sources of variability of runoff are at the 1-m² scale, they are sufficiently replicated within a 3- by 10-m plot so as to be effectively "averaged out."

The weir runoff presented a total runoff of 15 mm with a different temporal distribution (Fig. 5). The broader, smoother temporal pattern is to be expected from a larger drainage area because there is a broader distribution of travel times. The much lower total runoff and the long, slow decline in flow for the watershed, indicate that additional factors affect the flow rate. Apparently an additional source of

variability has been added as the result of the larger scale of consideration.

Sources of Variability

High spatial variability of runoff generation within a watershed has been observed in a wide variety of watersheds (Amerman and McGuiness 1967) and has been attributed to differences in depth to water table (Troendle 1985) and variability of snow water input (Flerchinger et al. 1992). The Lower Sheep Creek subwatershed is small enough that we assume that precipitation was spatially homogeneous. The runoff patterns, however, were highly heterogeneous. Since it is not practical to intensively monitor runoff across watersheds at small scales, we would like to know if there are more easily measured landscape features that can be related to runoff, especially if the spatial variability of those features changes with scale in the same way that the spatial variability of runoff changes with scale. These features may either be the sources, or linked to the sources, of the spatial variability of runoff and be used as surrogate for them.

In this study we examined three related features, the soil water content, snow depth and soil temperature. We found that neither soil-water content nor soil temperature varied as the runoff, but both were in fact, quite independent of it. Snow depth, however, did seem to be closely related. Snow depth is important for two reasons: it provides an amount of water input, and it insulates the soil to maintain freezing conditions.

Snow Depth

The data collected from the mini plots shows the general trend of snow accumulation during the winter and ablation at the time of the event seen at all scales (Fig. 6). As with surface runoff, there is very high spatial variability of snow depth within a few meter area. Meter-scale variability was also very high in the large plots (Fig. 7). Despite this high spatial variability, the average snow depth between the two large plots agreed closely, as was observed for other years. There was no significant difference in snow depth ($\alpha = 0.05$) between the large plots for any of the sampling dates. These results are consistent with the observation that variations in snow depth are the result of the interactions between shrubs and the wind. We have noted that the vegetation on the two plots is practically identical. If the shrub or interspace area is considered to be about 0.7 m², then there were over 40 "replications" of the "shrub effect" within each plot.

227
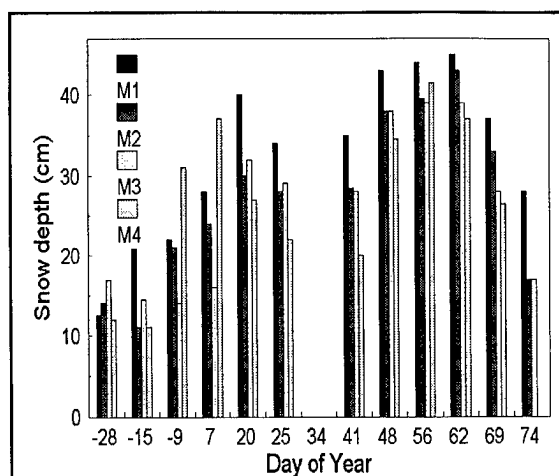
Figure 6. Snow depth of the four mini plots. Negative Day of Year refers to the number of days prior to 1 January, 1993.
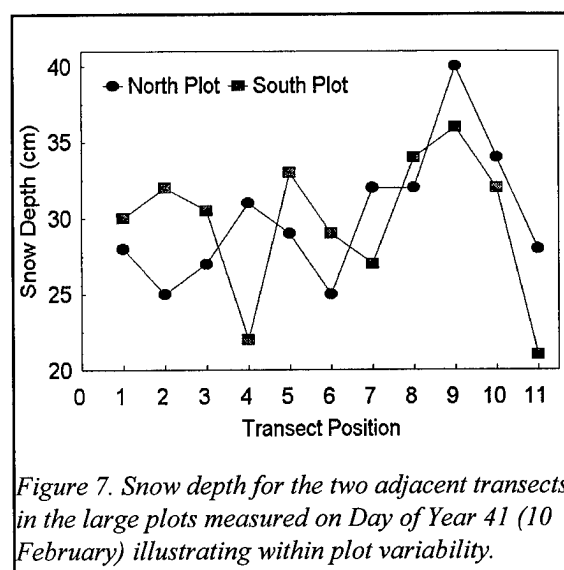
Figure 7. Snow depth for the two adjacent transects in the large plots measured on Day of Year 41 (10 February) illustrating within plot variability.

Figure 8. Average snow depth for the North and South plots compared with the watershed transect (WT) over the season. Negative Day of Year refers to the number of days prior to 1 January, 1993.

The average snow depths for the watershed transect, while following the same trends, were significantly lower than the large plots ($\alpha = 0.05$) for DOY 20 through 69 (Fig. 8). This is consistent with the greater runoff recorded at the plots. In addition, the watershed transect snow depth variability was greater than for the large plots except after the first snows. The standard deviation for the watershed transect was about 7 as compared with that of about 4 for the large plots (similar sample size). The early snows generally result in a uniform distribution of snow throughout the watershed, but as the season progresses, snow is redistributed by wind action and tends to accumulate in topographic lows at the expense of the ridges. This process of topographically controlled snow redistribution by the wind takes place in addition to the vegetation controls described previously. In other words, the vegetation effects are nested within the topographic effects. Additional snow measurements indicate that the watershed transect did not represent the full range of conditions within the watershed. In particular, the accumulation of snow in the channel, where snow depths were much greater.

The lower runoff at the weir is probably due to the lower average snow depth across the watershed than in the plots. The highly variable snow depth may be responsible for the very different temporal pattern of runoff. For example, the relatively deep channel areas may contribute snowmelt for some time after the majority of the watershed is devoid of snow cover.

Modeling Implications

One approach to process modeling at the watershed scale is to use point models, which usually describe the processes of heat and water transport in the soil profile in one dimension. For practical purposes of describing soil and vegetation parameters, these models may be considered to be roughly 1-m^2 scale models although homogeneity over larger areas is sometimes assumed. To represent a larger area, the point-scale models are run repeatedly in a grid pattern over the area of interest.

We have shown that runoff at the 1-m^2 scale is highly variable as the result of interactions between

228

the vegetation (shrubs) and wind-blown snow. Interactions include deposition of snow to the lee side of shrubs, different density of snow within the shrub canopy, and differential melting rates due to shading and heat absorption by the relatively low albedo shrubs. Modeling snowmelt runoff a the 1-m² scale therefore requires, in addition to soil and weather parameters, either (i) intensive spatial and temporal information concerning snow depth within each meter, or (ii) a model capable of calculating shrub-snow interactions. Considering the enormous efforts required to obtain the necessary inputs, especially where the snow cover is intermittent, and the lack of models capable of simulating shrub-snow interactions, this approach seems impractical at best if larger areas are of interest.

In contrast to the mini plots, the runoff from the two large plots was essentially identical. This is consistent with results from 1990 and 1995, the only other years on record we measured significant amounts of runoff. The spatial variability of point measurements, such as snow depth, generally increases with scale, but if the scale increase is within a given population it may remain constant (Wilding and Drees, 1983). In this case the primary causes of spatial variability, wind interactions with vegetation, remain constant as the scale is increased to 30-m² plots. Since we are interested in surface runoff, which integrates the effects of all points within the contributing area, aggregating many 1 m² plots into fewer, larger plots, results in a large reduction in variability.

This means that there is a precisely defined amount of runoff which can, in principle, be modeled. In the terminology of Seyfried and Wilcox (1995), the deterministic length scale of the shrub source of runoff variability is on the order of 10 m. There is no need to explicitly describe the position of shrubs and runoff at this scale may be represented as a stochastic combination of point inputs, by a probability distribution function for example, or a simple average which modifies parameters to account for the "shrub effect."

Extension to the larger watershed introduced an additional source of spatial variability, topography. We found distinct differences both in the amount and timing of runoff measured at the weir compared with that on the large plots. Topographic effects, like shrub effects, change the amount of runoff and may overwhelm the shrub effects, which we consider to be nested within the larger-scale, topographic effects. Therefore, it is important that topographic effects be considered as the spatial scale of interest increases.

The topographic features responsible for the additional snow distribution are fairly subtle and completely invisible at the scale of commonly available digital elevation data (e.g., 30 m). This is true of much more pronounced topographic features at Reynolds Creek which have been extensively described (Flerchinger et al. 1992, Stephenson and Freeze 1974). Therefore, explicit modeling at the small watershed scale requires detailed, generally unavailable topographic information as well as algorithms for redistribution of snow by wind. This kind of information, shown in Figure 2, is rarely available, and so this approach has relatively little applicability. If the area of interest is that particular watershed, then predictions can be made from calibrated models. If larger areas are of interest, it may be that the effects of small topographic features are "averaged out" as was the case for shrub effects if larger scales are considered.

REFERENCES

Abrahams, A. D., A. J. Parsons, and S. Luk. 1988. Hydrologic and sediment responses to simulated rainfall on desert hillslopes in southern Arizona. Catena 15: 103-17.

Amerman, C.R., and J. L. McGuinness. 1967. Plot and small watershed runoff: Its relation to larger areas. Trans. ASAE 10: 464-66.

Bates, E. A., and M. A. Bilello. 1966. Defining the cold regions of the northern hemisphere. USA Cold Regions Research and Engineering Lab. , Hanover, NH, Tech Report 178.

Dunne, T., and R. D. Black. 1971. Runoff processes during snowmelt. Water Resources Research 7: 1160-1172.

Flerchinger, G. N., K. R. Cooley, and D. R. Ralston. 1992. Groundwater response to snowmelt in a mountainous watershed. J. of Hydrol. 133: 293-311.

Garstka, W. U. 1945. Hydrology of small watersheds under winter conditions of snow cover and frozen soil. Trans. Amer. Geophys. Union 25: 838-71.

Hanson, C. L. 1982. Distribution and stochastic generation of annual and monthly precipitation on a mountainous watershed in southwest Idaho. Water Resour. Bull. 18: 875-83.

Hayhoe, H. N., R. G. Pelletier, and S. Moggridge. 1992. Analysis of freeze-thaw cycles and rainfall on frozen soil at seven Canadian location. Canadian Agri. Eng. 34: 135-42.

Johnson, C. W., and R. P. McArthur. 1973. Winter storm and flood analysis, Northwest interior. *In*:

Proceedings of the Hydraulic Division Specialty Conference, ASCE, Bozeman, MT, 359-69.

Johnsson, H., and L. Lundin. 1991. Surface runoff and soil water percolation as affected by snow and soil frost. J. of Hydrol. 122: 141-59.

Kane, D. L. 1980. Snowmelt infiltration into seasonally frozen soils. Cold Regions Science and Technology 3: 153-61.

Leavesley, G. H. 1989. Problems of snowmelt runoff modelling for a variety of physiographic and climatic conditions. Hydrological Sci. 34: 617-34.

Seyfried, M. S. 1993. Field calibration and monitoring of soil-water content with fiberglass electrical resistance sensors. Soil Sci. Soc. Am. J. 57: 1432-36.

Seyfried, M. S., and G. N. Flerchinger. 1994. Influence of frozen soil on rangeland erosion. Soil Sci. Soc. Am. Special Pub #38: 67-82.

Seyfried, M. S., and B. P. Wilcox. 1995. Scale and the nature of spatial variability: field examples having implications for hydrologic modeling. Water Resour. Res. 31 1: 173-84.

Seyfried, M. S., B. P. Wilcox, and K. R. Cooley. 1990. Environmental conditions and processes associated with runoff from frozen soil at Reynolds Creek Watershed. In: (K.R. Cooley, Ed.) Frozen Soil Impacts on Agricultural, Range, and Forest Lands, 125-34.

Simonton, J. R., and K. G. Renard. 1982. Seasonal change in infiltration and erosion from USLE. Proceedings of Hydrology and Water Resources of Arizona and the Southwest, University of Arizona: American Water Resources Association.

Stephenson, G. R., and R. A. Freeze. 1974. Mathematical simulation of subsurface flow contributions to snowmelt runoff. Water Resour. Res. 10: 284-94.

Trimble, G. R., R. S. Saryz, and R. S. Pierce. 1958. How type of frost affects infiltration. Journal of Soil and Water Conservation 13: 81-82.

Troendle, C. A. 1985. Variable source are models. p. 347- 404. In T. P. Burt (ed.), Hydrological forecasting. John Wiley, New York.

Vasilyev, A. 1994. Modelling wash-off and leaching of pollutants by spring-time flow. J. of Hydrol. 159: 215-22.

Wilcox, B. P., M. S. Seyfried, K. R. Cooley, and C. L. Hanson. 1991. Runoff characteristics of sagebrush rangelands: Modeling implications. J. of Soil and Water Cons. 46: 153-58.

Wilding, L.P., and L.R. Drees. 1983. Spatial variability and pedology. P. 83-116. In L. P. Wilding et al., (ed.) Pedogenesis and soil taxonomy. I Concepts and interactions. Elsevier, Amsterdam, The Netherlands.

Erosion Impacts of the Soil-Thawing Process

J. FROESE[1] AND R.M. CRUSE[2]

ABSTRACT

Over 50% of annual soil loss in many regions of the world occurs during the relatively brief period of soil thawing. Current literature does not discuss the mechanisms causing these high loss rates. The objectives of this paper are to 1) propose soil hydraulic and mechanical processes and conditions which occur on a soil interrill surface during rainfall; 2) suggest impacts of a subsurface frozen layer on these processes and conditions; and 3) identify frozen-layer effects on soil detachment from raindrop impact. A frozen layer beneath the surface restricts infiltration, causing water to accumulate above the impermeable layer. It is hypothesized that restricted infiltration, high matric potential, and low soil shear-strength stop surface seal formation, greatly increase detachment from impacting rainfall, and greatly increase soil erodibility. Research indicates that as matric potential nears 0 Pa, soil detachment from raindrop impact is four times greater than can be explained by shear-strength estimates in the detachment zone. These high matric potentials add considerably to the erosion potential of soils with thawed surfaces and frozen subsurface layers.

Key words: Detachment, erosion, matric potential, shear-strength, frozen layer

INTRODUCTION

Soil is most erodible when thawing. The most critical period seems to be when the surface (1 to 3 centimeters) is thawed and a subsurface frozen layer remains. Kirby and Mehuys (1987) determined that over 50% of annual soil loss in many regions of the world occurs during this relatively brief thaw period. Shear-strength (the internal resistance to externally applied forces before soil failure occurs) controls soil erodibility and when it is exceeded a shear plane develops and soil particles slide over each other initiating the erosion process. Shear-strength is calculated by Coulomb's equation (1776):

$$\tau = C + \tan \phi \, (\sigma_n) \qquad [1]$$

where τ = shear-strength along the plane of failure (g cm^{-2})
   C = apparent cohesion (g cm^{-2})
   ϕ = angle of internal friction
   σ_n = applied load normal to the shear plane (g cm^{-2}).

The applied load normal to the shear plane is the sum of the external (compression and mass of soil) and internal (matric-potential forces) loads. That is,

$$\sigma_n = (s + M_s/A) - \Psi_m(X) \qquad [2]$$

where s = mechanically added load (g cm^{-2})
   M_s = mass of soil above shear plane (g)
   A = cross sectional area of the shear plane (cm^2)
   Ψ_m = soil-water, matric potential normal to the shear plane (Pa).
   X = f(degree of soil saturation; 1 at saturation, 0 at desiccation)

The term X is necessary because pore water under tension (internal load) influences strength similarly to the application of an external load, and as soil desaturates the effectiveness of pore water under

---

[1] Department of Natural Resource Sciences and Landscape Architecture, 1112 H.J. Patterson Hall, University of Maryland, College Park, Maryland 20742, USA
[2] Department of Agronomy, 3212 Agronomy Hall, Iowa State University, Ames, Iowa 50011, USA

tension to induce an internal load is lowered. Since pore size distribution and pore shapes vary between soils, pore water shape or configuration varies, and the relationship between X and percent saturation also varies (Yong and Warkentin, 1966).

On the soil interrill surface (where there can be little ponded or flowing water), applied load is zero leaving strength controlled by cohesion and Ψ_m. Conditions which promote a Ψ_m of zero throughout the detachment zone and which reduce cohesion lead to low τ values and high soil-erosion potential. The objectives of this paper are to 1) propose soil hydraulic and mechanical processes and conditions that occur on a soil interrill surface during rainfall; 2) suggest impacts of a subsurface frozen layer on these processes; and 3) identify frozen-layer effects on soil detachment from raindrop impact.

MECHANICAL AND HYDRAULIC PROCESSES AND CONDITIONS DURING RAINFALL

Figure 1 outlines the proposed status of the Ψ_m gradient from the surface to the 0.5 cm depth, surface τ, infiltration, soil bulk density, and detachment for stages of interrill seal development during rainfall. At the start of the first stage without a frozen layer, the soil is dry throughout the top 0.5 cm and so the Ψ_m gradient is low. Consequently, τ is relatively high and detachment is low (equations 1 and 2). No seal is present, therefore the bulk density is relatively low, infiltration is relatively high, and a large Ψ_m gradient quickly develops between the surface and subsurface layer. As time progresses during the rainstorm (stage II), surface Ψ_m increases resulting in a decrease in τ. In this weakened condition, detachment of soil particles on the soil surface accelerates, seal formation is initiated and bulk density increases. As the wetting front passes the 0.5 cm depth, Ψ_m at this depth increases and the Ψ_m gradient in this surface layer decreases. During stage III, Ψ_m has reached its peak (0 Pa) throughout the 0 to 0.5 cm layer, the potential gradient nears unity, and τ is consequently at its nadir. In this condition, detachment peaks (Cruse and Francis 1984) and the seal bulk density continues to increase, thereby decreasing infiltration. Stage IV is characterized by the impact of the developed seal on hydraulic and τ characteristics. This high bulk density layer serves to increase τ (Bradford et al. 1987), thereby diminishing soil detachment. The development of this high bulk density seal during a rainfall event explains Poesen's (1981) observation that once the soil is near field capacity or wetter,

strength or cohesion will stop decreasing and actually increase. A decrease in soil detachment is associated with this increased strength. Infiltration reaches its nadir and the potential gradient remains near unity. At stage V, water flow through the high bulk density layer is restricted. The hydraulic conductivity of this layer has been reduced by seal development while that of the subseal layer has not been altered. Matric potential at the base of the seal begins to decline as water is drawn from the bottom of the seal down into the soil profile faster than it is transmitted through the top of the seal. This establishes a Ψ_m gradient between the seal surface and the seal base (Edwards and Larson 1969). With this change in Ψ_m, τ further increases and detachment is reduced. Bulk density remains high and infiltration increases sightly due to the Ψ_m gradient. The final stage is characterized by the stabilization of the Ψ_m gradient and, consequently, the other factors.
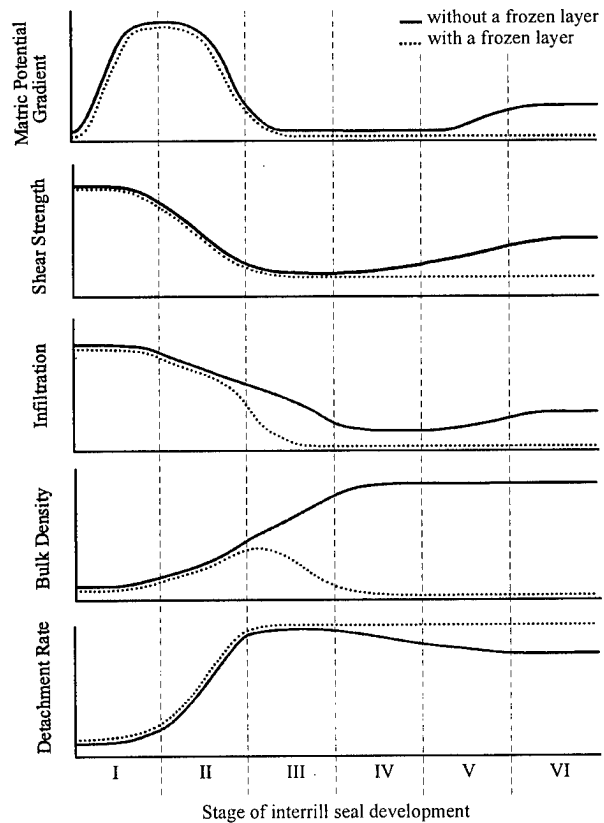
Figure 1. Soil characteristics in the detachment zone (surface 0.5 cm) during rainfall without and with a frozen layer

With the presence of a subsurface frozen layer, such as one may find during spring-thaw conditions, the attributes of the soil surface during a rainstorm change markedly. The initial two stages

are similar to conditions without the subsurface frozen layer. However, by stage III, the presence of an ice lens halts infiltration, causing water to runoff. Under these conditions, a seal is restricted from developing. Shear-strength is at its lowest, and soil detachment remains at its peak. The system stabilizes (stage IV) under these highly erosive conditions.

MATERIALS AND METHODS

Soil cores were constructed using Nicollet (glacial till) (mixed mesic Aquic Hapludoll) and Galva (loess) (mixed mesic Typic Hapludoll) A-horizon material. Three soil states were examined: never frozen, frozen and thawed, and thawed surface with an impermeable layer one cm beneath the surface. Matric forces were applied to the core base with a tension table. Shear-strength cores were equilibrated at -225, -520 and -1010 Pa. Detachment cores were equilibrated at 0, -65, -560 and -1045 Pa. Shear-strength was measured via a drained, unconfined compression test. Modified aluminum cupcake tins (a hole slightly larger than the diameter of the core was cut into the base of the cupcake tin and the top edge of the tin was curved inward) captured the particles detached from single water-drop impact. The shear-strength portion of the experiment employed a completely randomized factorial design with three replications, while the detachment portion employed a completely randomized split plot factorial design with three replications.

RESULTS AND DISCUSSION

The freeze/thaw process did not significantly affect the linear relationship between τ and Ψ_m between -225 and -1010 Pa (Fig. 2). At an applied Ψ_m of 0 Pa, the impermeable subsurface layer in the partially thawed soils resulted in soil detachment four times greater than that occurring in the thawed soils which did not have an impermeable subsurface layer (Fig. 3).

As Ψ_m approached 0 Pa, detachment increased dramatically with small matric potential increases (Fig. 4). The surface Ψ_m and τ of partially thawed cores were estimated indirectly. That is, given the experimentally derived relationship between detachment and Ψ_m, as well as the relationship between Ψ_m and τ, detachment values of partially thawed cores were used to determine both
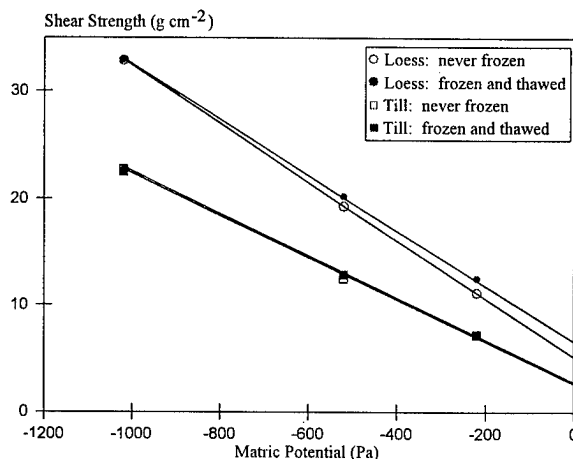
Figure 2. Effect of matric potential on shear-strength
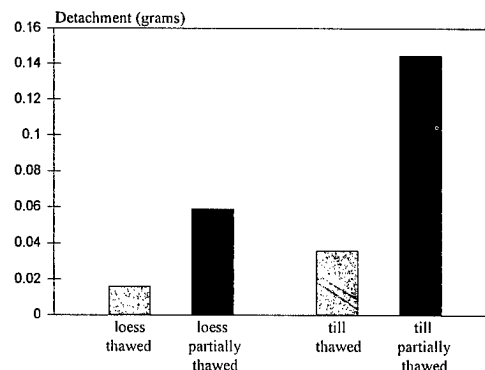
Figure 3. Soil detachment at 0 Pa applied matric potential
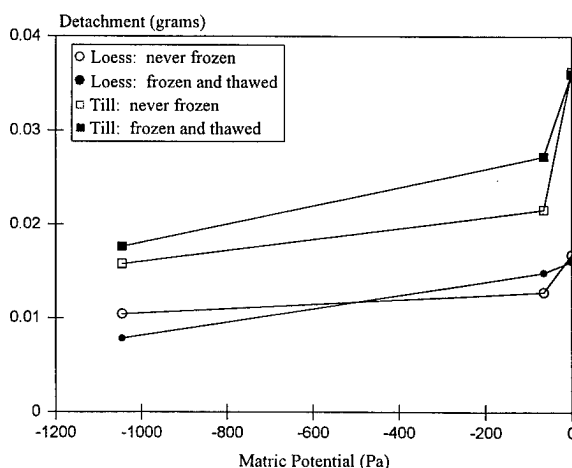
Figure 4. Effect of matric potential on detachment

233

their surface Ψ_m and τ. These derived Ψ_m and τ values for partially thawed soil were unrealistic. This suggests that the detachment process was affected by the impermeable layer and high Ψ_m through some factor other than, or in addition to, matric potential-caused τ modifications.

CONCLUSIONS

Soil hydraulic and strength properties are dynamic near the soil surface during rainfall. A frozen, impermeable, subsurface layer changes the surface dynamics substantially. An impermeable subsurface layer may limit surface seal development since infiltration and downward water movement is restricted and the resulting runoff will transport detached particles from the detachment area. In the absence of a surface seal a Ψ_m gradient near the surface fails to develop. Water which accumulates above the impermeable layer may drive the Ψ_m to 0 Pa throughout the detachment zone. Matric potential effects on τ and detachment are thus eliminated. Shear-strength becomes a function solely of cohesion. As a result, detachment rates are high and seem to be considerably higher at a Ψ_m of 0 Pa than expected based on soil τ values.

REFERENCES

Bradford, J.M., J.E. Ferris, and P.A. Remley. 1987. Interrill soil erosion processes: I. Effect of surface sealing on infiltration, runoff and soil splash detachment. Soil Sci. Soc. Am. J. 51:1566-1571.

Coulomb, C.A. 1776. Essai sur une application des r'egles des maximis et minimis a quelques problemes de statique relatifs a l'architecture. Mem. Acad. Roy, pres. divers Savants. 7, Paris, p. 38.

Cruse, R.M. and P.B. Francis. 1984. Shallow-layer soil water potential changes due to waterdrop impact. Soil Sci. Am. J. 48:498-500.

Edwards, W.M. and W.E. Larson. 1969. Infiltration of water into soils as influenced by surface seal development. Trans. ASAE. 12:463-470.

Kirby, P.C. and G.R. Mehuys. 1987. The seasonal variation of soil erosion by water in southwestern Quebec. Can. J. Soil Sci. 67:55-63

Poesen, J. 1981. Rainwash experiments on the erodibility of loose sediments. Earth Surface Processes and Landforms. 6:285-307.

Yong, R.N. and B.P Warkentin. 1966. Cohesive Soil Strength. P. 281-349. Macmillan Company, New York.

Surface Cover Effects on Soil Loss from Temporally Frozen Cropland in the Pacific Northwest

D.K. McCOOL[1], K.E. SAXTON[1], AND J.D. WILLIAMS[2]

ABSTRACT

Erosion on cropland in the Northwestern Wheat and Range Region (NWRR) of the Pacific Northwest is caused in large part by runoff from low intensity rains and snowmelt when the soil is thawing. Under these conditions, crop management elements such as crop residue have different effects on runoff and erosion than they do under nonfrozen conditions with high-intensity rainstorms. The primary differences are that under NWRR conditions, the erosion is caused by flowing water rather than raindrop impact and that the soil is weakened because of dispersion and high moisture content. An eight-year study at the Palouse Conservation Field Station near Pullman, Washington, provided data to isolate the effect of surface cover on erosion and to fit a relationship for use in the Revised Universal Soil Loss Equation. The relationship indicates a greater relative effect of surface cover when compared to high-intensity summer rainstorm conditions.

KEYWORDS: water erosion, freeze/thaw, cropland, surface cover, Pacific Northwest

INTRODUCTION

Surface cover is an important element in controlling erosion on cropland. Of all factors in erosion control during critical and vulnerable periods in a crop rotation (usually seedbed before crop cover develops), surface cover is without doubt the most important. This is as true in the Northwestern Wheat and Range Region (NWRR) as it is elsewhere. However, the unique causes and processes of erosion in the NWRR merit special attention. Runoff from low intensity rain and snowmelt on thawing saturated silt loam soil is a major part of the erosion process, occurring at any time during the winter, and frequently resulting in highly visible rill erosion. For these winter erosion events, interrill erosion is a low portion of the total soil loss. One cannot assume that crop management components such as surface cover, incorporated residue, canopy cover, surface roughness and antecedent soil moisture have the same effect in the NWRR as in areas of the USA subjected to higher intensity summer precipitation when soil particles are not dispersed by frost action. Thus, for more accurate erosion prediction, there is need to evaluate the effect of these crop management components, and particularly surface cover, on soil loss in the NWRR.

This manuscript reports results of an eight-year runoff plot study at the Palouse Conservation Field Station (PCFS) near Pullman, Washington and analysis of the data to isolate and develop a relationship for the effect of surface cover on soil erosion. The relationship is in a form compatible with the Revised Universal Soil Loss Equation (RUSLE) (Renard et al. 1997).

---

[1]USDA, Agricultural Research Service, Biological Systems Engineering Department, Washington State University, Pullman, Washington 99164-6120, USA

[2] USDA, Agricultural Research Service, Columbia Plateau Conservation Research Center, P.O. Box 370, Pendleton, Oregon 97801, USA

BACKGROUND

Methodology to isolate the effect of the various crop management components that influence soil erosion has evolved over a period of time. In initial versions of the Universal Soil Loss Equation (USLE) (Wischmeier and Smith 1965), rough categories of surface residue were used to determine soil loss ratio (*SLR*) values (ratio of treatment soil loss to that from continuous, tilled fallow) at various crop stage periods. Wischmeier (1973) proposed a subfactor approach to calculating *SLR* values, wherein *SLR* was a product of subfactors for residue mulch, incorporated residue, detachability, surface roughness and other components. McCool et al. (1976) used this approach in a paper describing an adaptation of the USLE to nonirrigated cropland of the NWRR. By 1987, sufficient runoff plot data had been collected in the NWRR to indicate that surface residue was more important under winter runoff erosion conditions there than in regions which have higher intensity summer storms. Early results indicated that 1,100 kg/ha of surface residue reduced soil loss to as little as 8% of the soil loss experienced when there was no surface residue (McCool et al. 1987). In the RUSLE model, different relationships were given for the effect of surface residue on interrill, mixed rill and interrill, and rill erosion. Surface residue was indicated as being more effective for preventing rill erosion than interrill erosion (Yoder et al. 1997).

EXPERIMENTAL SETUP

The runoff plots of the study were located at the Palouse Conservation Field Station (PCFS) about 3 km northwest of Pullman. Data reported in this paper was collected from the fall of 1978 through the spring of 1986. Thirty-year average annual precipitation at the site is 540 mm; about 250 mm of this falls during the primary erosion season, December through March. Soil at the site is a Palouse silt loam (fine silty, mixed Mesic-Pachic, Ultic, Haploxeroll).

Bordered runoff plots were placed on a south-facing hillslope with slope of 15 to 26%. Runoff was collected at the lower end of each plot and flowed by gravity into a large tank. The contents of the tank were agitated using a pump, and an aliquot was collected from a splitting tee when the tank was emptied by the pump; the aliquot was then stirred and samples were collected for determining sediment concentration. The plots were 3.66 m wide and ranged from 12.0 to 45.9 m in length. At least one plot of each treatment was 22.1 m long.

Each plot area was assigned one of the following six crop management treatments: continuous bare fallow, tilled (*CBF-T*), winter wheat (*Triticum aestivum L.*) following summer fallow, tilled (*WW/SF-T*), winter wheat following spring wheat (*Triticum aestivum L.*), tilled (*WW/SW-T*), winter wheat following winter wheat, direct-stubble or no-till seeded (*WW/WW-NT*), winter wheat following spring peas (*Pisum sativum L.*) with one plot tilled and seeded and another direct-stubble seeded (*WW/P*), and small grain stubble rough tilled with a chisel or moldboard plow (*RTS*). Each treatment was applied to two or three plots.

The absence or presence of tillage for the *WW/P* treatment had little effect on runoff or soil loss, so these plots were treated as replicates. Similar surface cover and roughness were observed for chiseled stubble and for moldboard plowing with the furrow slice turned upslope, so these data were treated as *RTS* replicates for the purpose of this analysis.

DATA COLLECTION

Runoff volume was determined from a volume/depth relationship for each collection tank. In general, runoff measurements and sediment samples were taken daily, at which time the tanks were emptied. This routine was followed even if an event lasted for more than one day; total runoff for extended events consisted of the sum of several days' measurements. Daily or event soil loss was calculated by multiplying runoff volume by sediment concentration. The event total soil loss was divided by plot area to give soil loss per unit area. These values were totalled for each winter erosion season to give annual winter soil loss per unit area for each plot. The annual totals for all plots with a given treatment were averaged to

give an annual treatment value. These annual treatment values were then averaged across the years of the study to give the treatment average in Table 1.

Surface cover was estimated by comparison with photos showing known quantities of residue mass per unit area or percentage residue cover. Canopy cover was also determined by comparison with photos showing known percentage cover. Because of the narrow alleys between treatments and the use of contour seeding, it was necessary to seed all winter wheat plots at the same time. Thus, there was no early seeding into summer fallow and no associated early growth. The plots all had low amounts of canopy cover. For canopy cover values see Table 1.

In the early stages of the project, surface roughness was estimated by counting or estimating surface clods of a given size in a square meter. Later in the project, matching with photos showing specific random roughness (standard deviation about the mean elevation) values was used to rank the random roughness on the plots. Random roughness values, a mean of fall and spring observations, are given in Table 1.

Initially, ridge height was determined by use of a ruler and straight edge. Later, ridge heights were determined using a 1.83-m wide profile meter that was set up across and up and down the plot to document plot conditions in the fall, and again in the spring. See Table 1 for ridge height values.

Incorporated residue was estimated as residue production minus surface cover after seeding or tillage and estimated decomposition. The average residue production was 7170 kg/ha for the winter and spring wheat and 3740 kg/ha for the spring peas. The incorporated residue was estimated to be uniformly distributed throughout the tillage depth, which ranged from 50 to 200 mm, depending on treatment. Incorporated residue values are given in Table 1.

DATA ANALYSIS

The soil loss ratio (SLR) is the loss from a given treatment relative to soil loss from an area in continuously tilled fallow. The SLR can range from slightly greater than zero to 1.0, and is assumed to be the product of a number of subfactors including prior land use (PLU), canopy cover (CC), surface cover (SC), surface roughness (SR) and antecedent soil moisture (SM). The SLR for a given treatment was calculated as the average treatment soil loss divided by the soil loss from the CBF-T plot. The SLR values for the treatments are given in Table 2. All treatment subfactor values except SC were calculated based on the estimated or measured conditions on the plots and commonly accepted relationships for the subfactors (Yoder et al. 1997). The surface cover subfactor (SC) was then calculated as

Table 1. Surface and near-surface conditions of treatments on runoff plots at the Palouse Conservation Field Station, 1978-1986 average.

Treatment	Average Winter Soil Loss (t/ha)	Surface Residue Cover (%)	Canopy Cover (%)	Surface Roughness, Random Roughness (mm)	Contour Ridge Height (mm)	Estimated Incorporated Residue	
						Roots B_{ur} [kg/(ha mm)]	Crop Residue B_{us} [kg/(ha mm)]
CBF-T	159	0	0	6.4	0	0	0
WW/SF-T	17.0	11.8	10	12.7	25	1.1	13.2
WW/SW-T	1.32	42.5	5	25.4	51	4.4	55.6
WW/WW-NT	0.103	96.5	5	6.4	25	3.3	14.7
WW/P	1.82	58.0	5	12.7	25	1.9	54.9
RTS	0.36	52.5	0	50.8	76	3.3	28.9

$$SC = SLR / \left(PLU \cdot CC \cdot SR \cdot SM \right). \quad (1)$$

The prior land use subfactor (PLU) is based on surface consolidation and incorporated biomass

$$PLU = C_f \cdot C_b \cdot exp - [(c_{ur} \cdot B_{ur}) +$$
$$(c_{us} \cdot B_{us} / C_f^{c_{uf}})] \quad (2)$$

where PLU = prior land use subfactor

C_f = surface soil consolidation subfactor

C_b = effectiveness of subsurface residue in consolidation

B_{ur} = mass density of live and dead roots in upper 25 mm of soil [kg/(ha mm)]

B_{us} = mass density of incorporated surface residue in upper 25 mm of soil [kg/(ha mm]

c_{uf} = factor for impact of soil consolidation on effectiveness of incorporated residue

c_{ur} and c_{us} = calibration coefficients.

For the treatments in this study, the value of C_f was 1 for all plots but the no till treatment. That treatment was applied to a new plot area each year; the C_f value at one year after last tillage was estimated at 0.9. Values of C_b, c_{uf}, c_{ur} and c_{us} were 0.951, 0.5, 0.0902 ha mm/kg, and 0.0188 ha mm/kg, respectively. These values, which are given in Chapter 5 of Agriculture Handbook 703 (Yoder et al. 1997), were calibrated using information from Van Liew and Saxton (1983), and are considered to represent the effect of incorporated biomass under NWRR conditions. Estimated values of B_{ur} and B_{us} are given in Table 1 and calculated values of PLU are given in Table 2.

The canopy cover subfactor (CC) is based on percentage cover and effective height of the crop canopy:

$$CC = 1 - F_c \, exp(-0.33H) \quad (3)$$

where CC = canopy-cover subfactor

F_c = fraction of land surface covered by canopy

H = fall distance of water drops that strike canopy, m.

The value of H was less than 0.1m for these treatments and it was set to 0.0 in the calculated values of CC that appear in Table 2.

The surface roughness subfactor (SR), in simplified form for NWRR conditions, is

Table 2. Soil loss, crop management subfactors and support practice factors for treatments on runoff plots at the Palouse Conservation Field Station, 1978-1986 average.

Treatment	Aver. Winter Soil Loss (t/ha)	SLR	Surface Residue Cover (%)	PLU	CC	SR	SM	PC	SC
CBF-T	159	1.0	0	1.0	1.0	1.0	1.0	1.0	1.0
WW/SF-T	17.0	.107	11.8	.70	.90	0.90	1.0	0.50	.38
WW/SW-T	1.32	.0083	42.5	.24	.95	0.76	0.5	0.30	.32
WW/WW-NT	0.103	.00065	96.5	.53	.95	1.0	0.5	0.50	.0052
WW/P	1.82	.0114	58.0	.30	.95	0.90	0.67	0.50	.133
RTS	0.36	.0023	52.5	.43	1.0	0.55	0.5	0.15	.130

$$SR = \exp[-0.026(R_u - 6.1)] \qquad (4)$$

where SR = surface roughness subfactor

R_u = random roughness at a given time, mm.

The value of R_u is based on the initial tillage roughness modified by a decay function due to the smoothing effect of rain.

$$R_u = 6.1 + \left[D_r\left(R_i - 6.1\right)\right] \qquad (5)$$

where D_r = roughness decay coefficient

R_i = initial roughness after tillage, mm.

D_r is then defined as

$$D_r = \exp\left[\frac{1}{2}(-0.0055\,P_t) + \frac{1}{2}(-0.00070\,EI_t)\right] \qquad (6)$$

where P_t = precipitation since a tillage operation, mm

EI_t = rainfall energy - intensity factor since a tillage operation, MJ mm/(ha h).

Calculated values of SR for the main winter erosion period are given in Table 2.

The soil moisture subfactor (SM) accounts for the influence on infiltration and permeability of antecedent moisture in the soil profile. A more complete explanation is given by Yoder et al. (1997). Values of SM for the treatments are given in Table 2.

All treatments but the CBF-T plots were seeded or tilled on contour. A supporting practice subfactor (PC) for contouring must be applied to all other treatments to make conditions comparable to the CBF-T treatment. Thus, the PC factor should be added to equation (1).

$$SC = SLR\,/\,(PLU\cdot CC\cdot SR\cdot SM\cdot PC) \qquad (7)$$

where PC = contour support practice factor.

PC values calculated with the RUSLE program using ridge height values in Table 1 are given in Table 2.

The product of the PLU, CC, SR, SM and PC values was divided into the SLR to obtain a value of SC for each treatment (Table 2). The SC values are plotted versus percent residue cover in Figure 1. An exponential relationship has been found to fit most data sets of SC and percentage cover. The relationship

$$SC = \exp(-bM) \qquad (8)$$

where SC = surface cover factor, dimensionless

b = fitted coefficient

M = percentage surface cover

was used to fit the data. The value of b was 0.046 and the coefficient of determination was 0.87.

RESULTS AND DISCUSSION

The results of this analysis indicate surface residue to have a greater effect on soil erosion under conditions of runoff from low intensity rainfall and snowmelt on thaw-weakened soils typical of the NWRR as compared to higher intensity summer storms that are the primary cause of soil erosion in other areas of the USA. In the RUSLE, the value of the coefficient b for conditions with primarily interrill erosion is about 0.025, and for conditions with a mix of rill and interrill erosion is about 0.035. The value of the coefficient b in this analysis, 0.046, differs slightly from that given for rill erosion, 0.050, in RUSLE. At a surface residue cover of 50% (about 1,100 kg/ha of small grain residue), the percentage of expected erosion as compared to no surface residue is about 30% for interrill, 17% for mixed rill and interrill and 10% for NWRR conditions. The relatively greater benefits of residue under NWRR winter conditions may be due in some part to the low intensity rainfall and snowmelt where interrill erosion is low, and where runoff is reduced in both volume and rate as compared to high intensity storms. There is less tendency for short residue pieces to be lifted and floated from the soil surface as compared to areas with higher intensity rainfall. The loss of residue protection can be seen in the spring under the more intense rainstorms of that period, when

239
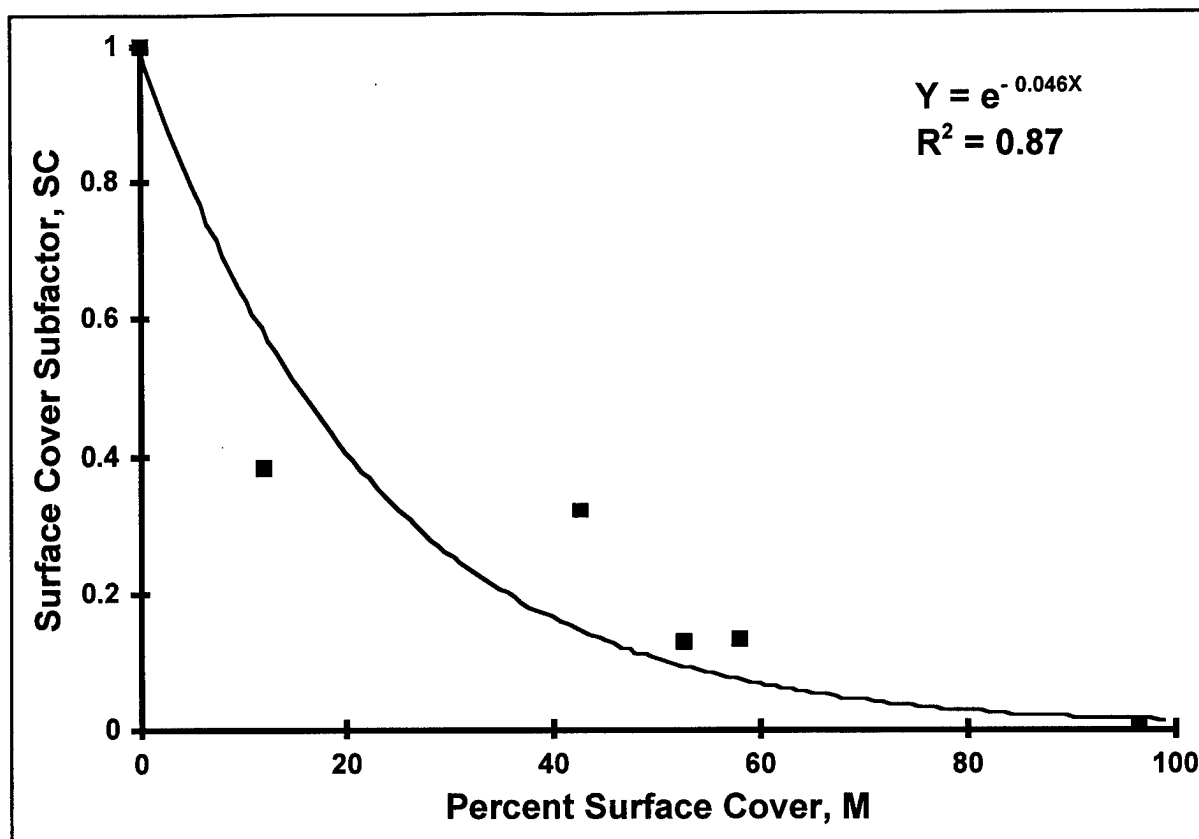
Figure 1.   *Effect of percentage surface cover, M on surface cover subfactor, SC.*

short pieces of surface residue are sometimes floated into waterways and culvert entrances. Because erosion in the NWRR is dominated by recurring winter events, proper crop management in the fall prior to the winter erosion season is very important in erosion control. Similarly, ability to quantify crop management components, and to develop relationships that describe their effect on soil erosion, are essential to improved erosion prediction in the NWRR.

SUMMARY

A range of crop management treatments was installed on runoff plots at the Palouse Conservation Field Station near Pullman, Washington. Data from the plots was used to develop a relationship for the effect of surface cover on soil erosion where erosion is caused in large part by runoff from low-intensity rain and snowmelt on soils that may be in a thawing, saturated condition with impeded infiltration. The relationship is

similar to that developed from data on highly disturbed soils that are susceptible to rilling. The relationship indicates greater relative benefits from a given amount of surface cover as compared to conditions where higher intensity rainstorms on less dispersed soils dominate the erosion process.

REFERENCES

McCool, D. K., J. F. Zuzel, J. D. Istok, G. E. Formanek, M. Molnau, K. E. Saxton, and L. F. Elliott. 1987. Erosion processes and prediction for the Pacific Northwest. *In* L. F. Elliott (ed.) Proc., STEEP-Soil Conservation Concepts and Accomplishments. May 20-21, 1986, Spokane, WA. p. 187-204.

McCool, D. K., M. Molnau, R. I. Papendick, and F. L. Brooks, Jr. 1976. Erosion research in the dryland grain region of the Pacific Northwest: Recent developments and needs. *In* Soil Erosion: Prediction and Control, Soil Conservation Soc. Amer. Ankeny, IA. p. 50-59.

Renard, K. G., G. R. Foster, G. A. Weesies, D. K. McCool, and D. C. Yoder. 1997. Predicting Soil Erosion by Water: A Guide to Conservation Planning with the Revised Universal Soil Loss Equation (RUSLE). USDA-ARS Agriculture Handbook 703. (In Press).

Van Liew, M. W., and K. E. Saxton. 1983. Slope steepness and incorporated residue effects on rill erosion. Transactions of ASAE 26(6):1738-1743.

Wischmeier, W. H. 1973. Conservation Tillage to Control Water Erosion. *In* Proceedings of the National Conservation Tillage Conference. Mar. 28-30, 1973. Des Moines, IA. p. 133-141.

Wischmeier, W. H., and D. D. Smith. 1965. Predicting rainfall-erosion losses from cropland east of the Rocky Mountains: Guide for selection of practices for soil and water conservation. USDA-ARS Agriculture Handbook 282.

Yoder, D. C., J. P. Porter, J. M. Laflen, J. R. Simanton, K. G. Renard, D. K. McCool, and G. R. Foster. 1997. Chap. 5. Cover-Management factor (C). *In* Predicting Soil Erosion by Water--A Guide to Conservation Planning with the Revised Universal Soil Loss Equation (RUSLE). USDA-ARS Agriculture Handbook 703. (In Press).

Cool-Period Soil Erosion Due to
Rilling in Prince Edward Island, Canada

G. RICHTER[1], L. EDWARDS[2], R.-G. SCHMIDT[1], B. BERNSDORF[1], AND J. BURNEY[3]

ABSTRACT

Sloping fields in Prince Edward Island (P.E.I.) show severe cool-period erosion damage following potatoes due to rilling and sediment deposition. The cool period is characterized by much snow accumulation and frequent snowmelts. To examine accurately the extent of soil movement over affected fields, a system of actual field measurements of rills and sediment deposition zones was devised and applied in early spring to a number of field sites in potato rotation with cereal grain or forages (for hay) as intervening crops. Cool-period erosion from untilled grain/forage land averaged 0.1 t/ha compared to 8 t/ha from tilled grain/forage fields. After potato cropping, overall soil loss increased to 20.3 t/ha with tillage and 19.8 t/ha without tillage. Between 33% and 80% of the sediment stayed in the fields; however, sediment deposition affected only small areas of these fields, <1%-3%.

Key words: Snowmelt erosion, rill erosion, sediment deposition, agricultural fields.

INTRODUCTION

Sloping fields under row-crop cultivation in Prince Edward Island (P.E.I.) are subject to hydraulic erosion. The soil is predisposed to this process because of (1) the prevailing humid temperate climate which produces an average cool-period precipitation of more than 500 mm mostly as snow, (2) slopes that exceed 10% in the upper reaches of many fields, (3) the predominant narrowness of the fields, and (4) the intensiveness of potato cultivation. More than 50% of the annual soil erosion occurs during the cool period (between late fall and early spring)(Burney and Edwards 1995) which is characterized by about 40 freeze-thaw cycles (Edwards 1991) and frequent snowmelts. More than 60% of the cool-period precipitation is in the form of snow.

Potatoes occupy more than 25% of the area in field crops in P.E.I., and are rotated with cereal grains or forage crops in two- or three-year sequences. Fields, following cultivation, show severe rilling and associated sediment deposition at their downslope ends and in contiguous ditches and streams by the end of spring especially after snowmelt.

More than 90% of cool-period erosion in P.E.I. is due to rilling. Thus, recent studies on local soils have addressed the problem of rill erosion, simulating cool-period conditions and prevailing soil management systems (Frame et al. 1992, Burney and Edwards 1993, Burney and Edwards 1996, Leyte et al. 1996). There is, however, insufficient natural rill development for a specific rill erosion study under most laboratory or small plot conditions. Some attempts have been made to adjust the Universal Soil Loss Equation (USLE) (Wischmeier and Smith 1978) and other models for cool-period situations in the American Northwest (Zuzel et al. 1982, McCool et al. 1982), the Pacific Region of Canada (van Vliet et al. 1993, Hayhoe et al. 1993) and the Atlantic Region of Canada (Edwards and Burney 1991, Chow et al. 1990, Hayhoe et al. 1995), but these have yet to deal in specific detail with cool-period rill erosion. However, whether we are dealing with empirical equations, process-based models or simple computations, the generation of actual field-measured values for the required parameters of crop and field practices is urgently needed to replace estimated values. In the present study, therefore, field measurements of rill dimensions and sediment deposits were made in early spring to estimate cool-period erosion damage.

METHODOLOGY

General

Field procedure principally involved (1) mapping in the fall to define the geomorphological features, the inclination and the natural flow directions of runoff and (2) mapping and measurement of erosion forms after snowmelt in the spring to determine

---

[1] University of Trier, Physical Geography Department, 54286 Trier, Germany
[2] Agriculture and Agri-Food Canada, Research Centre, P.O. Box 1210 Charlottetown, Prince Edward Island, C1A 7M8, Canada
[3] Technical University of Nova Scotia, Agricultural Engineering Department, P.O. Box 1000, Halifax, Novia Scotia, B3J 2X4, Canada

erosion processes, erosion damage and sediment deposition.

The study was conducted from fall 1993 to spring 1996 on 20 field sites totalling more than 200 ha on 14 farms. The sites were potato fields under rotation with potato-cereal grain-forages or potato-cereal grain. Grain overwintered as stubble in 3-yr rotations, but could be fall tilled in 2-yr rotations. Forages were herbicide killed and/or fall-tilled, or left intact until spring. Soil type ranged from fine sandy loams to sandy loams that were mostly moderately to well drained (MacDougall et al. 1981). Slopes averaged 5 to 7% with a few inclined up to 14% in the upper reaches. Slope lengths were between 250 and 950 m. Field geomorphology showed one or more of the following features: plain surfaces, undulating surfaces, arching lines, and channeled lines, which are strongly determinative of erosion flow.

Pre-winter cropping management and soil management factors were examined, including crop rotational stage and tillage status.

Geomorphological mapping in the fall

The mapping method adopted in this study was based on a progression of field procedures assembled by Bernsdorf et al. (1995) for the specific purpose of measuring soil loss or sediment deposition under cool-period conditions such as exist in P.E.I.

Orthophotos at a scale of 1:2,500 were used as base maps. Field mapping was facilitated by using *differential global positioning system* (DGPS) methods and *geographic information systems* (GIS) software. Maps were constructed to show field outlines and provide basic geomorphological information up to the micromorphological level (drainage lines, water divides, plowing direction). The base maps also showed inclination along the dominant slope and in the direction of ploughing - mostly coincidental in this study. The use of an inclinometer at 20-m intervals on most slopes afforded reliable estimates of slope averages.

Erosion mapping in spring

Reconnaissance was done on a field-by-field basis to select the measurement procedure appropriate with the erosion damage. Measurement had to be confined to the period between the last ground frost and first spring tillage.

Two mapping methods were applied, separately or in combination, to the study sites (based upon the complexity of the terrain) and comprised a transect method and a single-form mapping method. The transect method was used mostly in field situations where erosion forms (rills, gullies, sediment deposition zones) were (1) too numerous for individual mapping, (2) similar in size, or (3) easily grouped by depth and width.

Transects were run as straight lines (transect lines) to intersect, at 90°, the principal runoff direction (runoff line) which could coincide with slope direction, ploughing lines or remnant furrows. The diversity of the erosion forms determined the distances between transects (40-50 m). Thus, a large variation in depth or width of the erosion forms in any one field meant smaller intervals between transects.

The single form mapping method was adopted where the focus was on a particular erosion form (e.g., with special or peculiar geographic or geomorphic characteristics) and was carried out in either of two ways, viz. *regular* or *irregular interval measurements*. Regular interval measurements were applied where the erosion form went through progressive change in depth or width from the beginning to the end. The cross-sectional measurements, taken at regular intervals along the length of the erosion form, were averaged and multiplied by the length to give total soil loss (volume) from that erosion form. Most of the erosion forms, however, showed sufficient variability along their lengths to warrant *irregular interval measurements*. This involved dividing a given erosion form into segments of uniformity (or near uniformity), which inevitably produced segments of varying lengths. A representative cross-sectional measurement was taken for each segment and multiplied by its length to compute soil loss (volume). This value was then tallied for all segments along the entire length of the particular erosion form. This latter circumstance resulted in a greater total of segments than *regular interval measurements*, thus lending itself to detailed mapping of the affected erosion forms and repeat studies of the same positions. Mapping of the large rills in this study was DGPS-aided. Sediment deposition was measured by depth and area of the deposition zone.

Data organization and computation

Field measurements were recorded, transect-by-transect, as numbers and classes (by width and depth) of the smaller rills. Data were organized into maps to include field perimeter, geomorphic features, large rills, gullies and deposition areas (in m^2). Rills were summed over all transects by cross-section (in m^2 or cm^2) and length to compute soil loss volume expressed in cubic meters (converted to tonnes) for each site. Areas of deposition were similarly calculated. The results were stratified by crop cover and tillage status for 20 sites over four cool periods. Simple comparisons of erosion and deposition amounts were also done for these periods. Results for cereal grains and forages will be combined for discussion.

243

RESULTS AND DISCUSSION

Erosion damage

The amount of soil loss seen in this study seemed to be influenced greatly by the state in which the land overwintered, and was thus determined mainly by the immediately preceding crop and tillage status. Table 1 shows great contrasts in soil erosion between potato land and cereal (overwintering as stubble) or forage land. Because of their gramineous nature, the cereal and most of the forages have been seen to provide, generally, good ground cover and soil stability. This observation was particularly striking for untilled fields where erosion was practically nil, averaging 0.1 t/ha from stubble or sod. In contrast, with tillage, erosion on cereal or forage land averaged 8.1 t/ha. Tilled potato land produced >2.5 times the erosion as did tilled cereal or forage land, but showed only slight average increases over erosion on untilled potato land. The foregoing thus shows the vulnerability of potato land whether it be tilled or untilled.

The high degree of erosion damage seen after potatoes was undoubtedly associated with the characteristically high-intensity cultivation and heavy-traffic harvesting that leave the soil poorly aggregated (Edwards 1988) and with little organic matter compared to that under cereal grain or forages (Edwards et al. 1994). Moreover, the soil structure is further damaged by soil freeze/thaw which averages about 40 cycles annually in P.E.I. (Edwards 1991)

Sediment deposition

The interplay of erosion and deposition is seen in Table 2. Deposition was noticeable at most of the sites, but the total area occupied by sediment deposits in a given field averaged 1.6% of the area of the field, and ranged between <1% and 4.3%. The terrain generally favored a convergence of rills and limited deposition to downslope corners, fence lines and a few depressions. Despite the elevated levels of erosion observed in many of the fields in this study, up to two-thirds of the eroded soil could be found accumulated in the originating fields. This could, however, be as low as one-third of total eroded soil - the remainder being washed into ditches or streams. In extreme cases of this study, sediment importation

Table I. Cool-period (post-harvest) assessment of soil erosion from feld sites in potato rotations in Prince Edward Island, Canada (1993–1996).

Cool period	After cereal grains or forages (for hay)					
	Untilled field			Tilled field		
	Number of sites	Total area (ha)	Average soil loss (t/ha)	Number of sites	Total area (ha)	Average soil loss (t/ha)
1992/93	1	6.5	0.1	4	22.9	10.4
1993/94	5	39.2	0.0	3	23.0	7.0
1994/95	5	29.1	0.0	7	49.2	10.8
1995/96	9	56.2	0.3	4	30.1	2.8
Σ/–x	20	131.0	0.1	18	125.2	8.1

	After potatoes					
	Untilled field			Tilled field*		
	Number of sites	Total area (ha)	Average soil loss (t/ha)	Number of sites	Total area (ha)	Average soil loss (t/ha)
1992/93	5	37.5	26.5	0		
1993/94	1	3.0	58.8	1	9.4	6.6
1994/95	3	12.9	9.2	1	6.5	32.5
1995/96	5	40.8	14.1	1	5.6	29.1
Σ/–x	14	94.2	19.8	3	21.5	20.3

*A site that was plowed along the slope after potatoes and showed an extreme soil loss of 108 t/ha during the study period is not tabulated.

Table 2. Cool-period erosion and sediment deposition on eleven field sites after potato cropping in Prince Edward Island, Canada (1993–1996).

1 Site number	2 Year (spring)	3 Total area of field (ha)	4 Area of sediment deposition (ha)	5 4 as % of 3 (5)	6 Erosion (t)	7 Sediment deposition (t)	8 7 as % of 6 (%)
1	1993	12.7	0.1	0.7	53	49	83
	1996		0.1	0.8	75	53	71
2	1994	9.4	0.2	1.8	62	204*	330
	1996		0.3	3.3	136	252*	186
3	1993	6.0	0.042	0.7	77	26	34
	1995		0.2	2.5	65	137*	209
5	1995	6.5	0.1	1.2	211	86	41
6.2	1996	6.0	0.2	2.8	147	108	74
6.3	1993	7.3	0.3	4.3	369	118	32
	1996		0.1	2.1	95	122*	128
10.1	1994	3.0	0.009	0.3	59	5	9
10.2	1993	5.6	0.028	0.5	200	68	34
	1996		0.1	0.9	163	30	19
12	1996	4.3	0.030	0.7	133	23	17
13	1995	14.5	0.3	2.3	1559	621	40
15	1996	20.1	0.1	0.5	328	114	35
			0.080	0.4			
		—	—	1.6	—	—	83.8**

Mean

* In part, imported by runoff from neighbouring fields

** Adjusted to 40.6% discounting sites with sediment importation

from neighboring fields was observed (sites 2, 3 and 6.3 - Table 2), particularly where compacted snow or ice in upslope border ditches facilitated cross-border flow.

There is little doubt of the quantitative importance of sediment deposition in assessing soil loss from a field. It is, however, of little practical value under the circumstances encountered in this study because deposition occurred in parts of the field that were at a disadvantage for farming. Moreover, these were typical areas of accretion consisting mostly of poorly aggregated (mostly particulate) soil material that was poorly drained and of doubtful productivity. This condition results from a process that leaves mainly the

sand fraction on the field while the silt, clay and organic matter fractions are washed off site.

CONCLUSION

The most influential factor in cool-period soil erosion under the circumstances of this study is cropping practice. The most striking example was erosion damage estimated in excess of 100 t/ha from a bare (plowed) potato field, compared to only a trace from an adjacent forage field that was only lightly tilled. These fields were of similar dimensions, orientation and slope, and were measured on the same day by identical personnel.

Although snow is the predominant form of winter precipitation, rain is common but is mostly gentle and may have little or no direct effect on soil loss where accumulated snow serves as a blanket. Winter runoff occurs, therefore, firstly on snow and is clear. When the snowmelt (meltwater) finally comes into direct contact with the ground, the soil surface develops a thin soupy layer, still on a firmly frozen base, and forms incipient rills whose development may be interrupted by refreezing, or may continually progress to deep rills or gullies.

Cool-period anti-erosion measures range from earth works such as terrace or berm construction, to agronomic methods such as winter cover crops. All have had some measure of success. However, under the unpredictable winter conditions which may locally include heavy snowfalls, strong winds, winter rains, freeze/thaw cycling and snowmelts, any cool-period conservation measure could be in jeopardy in a bad year.

REFERENCES

Bernsdorf, B., G. Richter, and R.-G. Schmidt. 1995. Die Kartierung der Schneeschmelz-Erosion - Problem und Möglichkeiten der Felderhebung. Forschungsstelle Bodenerosion - Universität Trier (Germany) Heft 14, 80 pp.

Burney, J.R. and L.M. Edwards. 1993. Size distribution of sediment in rill runoff in response to variations in ground cover, freezing, slope and compaction of a fine sandy loam. J. Agric. Engng. Res. 56: 99-109.

Burney, J.R. and L.M. Edwards. 1995. Sediment monitoring in a Bedeque Bay watershed. - P. 21-40 in R.D. Elliot and P. Chan, ed. Ecological Monitoring and Research in Atlantic Canada: A focus on Agricultural Impacts in Prince Edward Island. Workshop Proceedings, 22-24 February, 1995. Environment Canada, Dartmouth, Nova Scotia.

Burney, J.R. and L.M. Edwards. 1996. Modelling cool season soil water erosion on a fine sandy loam soil in Prince Edward Island. Can. Agric. Eng. 38(3): 149-156.

Chow, T.L., J. -L. Daigle, I. Ghanem, and H.

Cormier. 1990. Effects of potato cropping on water run-off and soil erosion. Can. J. Soil Sci. 30: 137-148.

Edwards, L.M. 1988. The effects of slope position and cropping sequence on soil physical properties in Prince Edward Island. Can. J. Soil Sci. 68: 763-774.

Edwards, L.M. 1991. The effect of alternate freezing and thawing on aggregate stability and aggregate size distribution of some Prince Edward Island soils. Journal of Soil Science 42: 193-204.

Edwards, L.M. and J.R. Burney 1991. Sediment concentration of interrill runoff under varying soil, ground cover, soil compaction and freezing regimes. J. Environ. Qual. 20: 403-407.

Edwards, L.M., D. Angers, and B. Sanderson. 1994. Changes in soil structure and organic matter under potato rotations. Agri-Info. Factsheet: 94-23. Agdex: 515: 2pp.

Frame, P.A., J.R. Burney, and L.M. Edwards. 1992. Laboratory measurement of freeze/thaw, compaction, residue, and slope effects on rill erosion. Canadian Agricultural Engineering. 34: 143-149.

Hayhoe, H.N., R.G. Peltier, and L.J.P. van Vliet. 1993. Estimation of snowmelt runoff in the Peace River region using a soil moisture budget. Can. J. Soil Sci 73: 489-501.

Hayhoe, H.N., R.G. Peltier, and D.R. Coote. 1995. Estimating snowmelt erosion indices for Canada. J. Soil and Water Cons. 50: 174-179.

Leyte, J.C., L.M. Edwards, and J.R. Burney. 1996. Laboratory measurement and modelling the effects of mulching and furrowing on post-harvest soil water erosion on potato land. Can. Agr. Eng. (In Press).

MacDougall, J.L., C. Veer, and F. Wilson. 1981. Soils of Prince Edward Island. LRRI Contribution No. 141, Agriculture & Agri-Food Canada, Research Branch, Ottawa.

McCool, D.K., D.H. Wischmeier, and L.C. Johnson. 1982. Adapting the Universal Soil Loss Equation to the Pacific Northwest. Transactions of the ASAE 25: 928-934.

van Vliet, L.J.P., R. Kline, and J.W. Hall. 1993. Effects of three tillage treatments on seasonal runoff and soil loss in the Peace River Region. Can. J. Soil Sci. 73: 469-480.

Wischmeier W.H. and D.D. Smith. 1978. Predicting rainfall erosion losses: A guide to conservation planning. Agriculture Handbook No. 537. USDA, Washington, DC.

Zuzel, J.F., R.R. Allmaras, and R. Greenwalt. 1982. Runoff and soil erosion on frozen soils in Northeastern Oregon. J. Soil & Water Cons. 37: 351-354.

Heave and Groundwater

Differential Frost Heave in Seasonally Frozen Soils

A.C. FOWLER[1] AND C.G. NOON[1]

ABSTRACT

The formation of some forms of patterned ground, notably earth hummocks and stone circles, is associated with seasonal freezing and a spatial instability in the resulting frost heave. We analyse the Miller model of frost heave for such spatial instability, by incorporating three-dimensionsal heat and mass transfer, and allowing the frozen soil to deform as a viscous medium. We find that the heaving process is generally (but not always) stable, but that if account is taken of a surface snow cover, then the insulating thermal properties of the snow predict that instability will occur if a dimensionless parameter $\mathcal{N} > 0.02$. The parameter $\mathcal{N}$ is given by $\mathcal{N} = \eta_f v_s/(\rho_f g d^2)$, where η_f is the frozen soil viscosity, v_s is the surface heave rate, ρ_f is the frozen soil density, g is gravity, and d is the depth of the freezing front. This implies that the propensity for differential frost heave depends on the soil heaving characteristics, as well as the rate of frost penetration.

Key words: patterned ground, differential frost heave

INTRODUCTION

In tundra regions subject to a cold climate, many types of regular geometric formations are observed. These formations are referred to as patterned ground, and differential frost heave is thought to be a possible mechanism for their formation. Some forms of isolated patterned ground (e.g. pingos and palsas) can be directly attributed to frost heave. For the more interesting earth hummocks and stone circles (see, for example, Williams and Smith 1989), differential frost heave has been suggested as an organising mechanism (Van Vliet-Lanoë 1991), although other mechanisms have been suggested, for example thermal convection (Krantz et al. 1988) or the 'cryostatic pressure' theory (Van Vliet-Lanoë 1991). In this paper we summarise recent work by Noon (1996) which demonstrates that the Miller model of secondary frost heave, when suitably modified to allow for three-dimensional (differential) frost heave, has an instability mechanism in it which predicts that in certain conditions, differential frost heave will spontaneously occur in the seasonal freezing of soils, and thus lead to the formation of patterned ground.

THE MILLER MODEL

Miller (1972, 1978) developed a model for secondary frost heave which allowed for the existence of a partially frozen fringe between the frozen soil near the surface and the unfrozen soil beneath. In particular, it includes a mechanism for distinct lens formation within the frozen fringe. While it is perhaps the most conceptually complete model available, it is hampered by the fact that its mathematical formulation (O'Neill and Miller 1982, 1985) is dauntingly complex. However, Piper et al. (1988) showed how certain (accurate) approximations allowed the model to be simplified, and more recently Fowler and Krantz (1994) extended this earlier analysis, and showed that the one-dimensional Miller model could be reduced to a single pair of first order

[1] Mathematical Institute, Oxford University, 24–29 St. Giles', Oxford OX1 3LB, England

ordinary differential equations for the positions of the ground surface and the freezing front, from which all other quantities, such as lens thickness and spacing, can be derived. The nature of this simplification is summarised in the following section.

THE FOWLER-KRANTZ-NOON REDUCTION

Fowler and Noon (1993) and Fowler and Krantz (1994) use four approximations to simplify the Miller model. In turn, these are the assumptions that (i) gravitational effects are small; this is more of a convenience than a necessity, but is accurate except on a regional scale, and certainly in the present case; (ii) the advection of sensible and latent heat is small, and in particular, heat conduction is essentially in equilibrium; (iii) the frozen fringe is thin (relative to the depth of frost penetration): this is an accurate approximation, due to the fact that the generalised Clapeyron equation allows only a small temperature jump across the fringe (relative to a typical seasonal variation). The final approximation which enables a dramatic reduction in the model complexity is based on (iv) the strong dependence of soil permeability on the pore water fraction in the frozen fringe. As a result, the pore water pressure only varies within a boundary layer which lies inside the frozen fringe, and the governing differential equations can be solved in the fringe.

The consequence of the fringe being thin is that its location is effectively specified as a surface $z = z_f(x, y, t)$, where z is a coordinate normal to the (original) ground surface, and x, y are horizontal. Equally the ground surface is given by a surface $z = z_s(x, y, t)$. It is convenient to express these and other variables in dimensionless form, and to this end we choose a length scale d appropriate to our situation: for example, a typical depth of the active layer. Equally, the temperature scale ΔT represents a typical seasonal freezing temperature (degrees below zero Celsius). In terms of these, we define a (thermal) velocity scale

$$U = \frac{k_f \Delta T}{\rho_w L d},\qquad(1)$$

where k_f is the thermal conductivity of the frozen ground, ρ_w is the density of water, and L its latent heat. For values $k_f \sim 2$ W m^{-1} K^{-1}, $\Delta T \sim 20$ K, $\rho_w \sim 10^3$ kg m^{-3}, $L \sim 3.3 \times 10^5$ J

kg^{-1}, $d \sim 5$ m, we have $U \sim 2.4 \times 10^{-8}$ m s^{-1}. From these we have the time scale

$$t_f = \frac{d}{U} \sim 2 \times 10^8 \text{ s};\qquad(2)$$

note that this is longer than the seasonal time scale 3×10^7 s.

If temperatures, distances, lengths and velocities are scaled with the values above, then Noon (1996) showed, following Fowler and Krantz (1994), that the normal velocity of the frozen fringe, denoted V_f, and the normal ice flux at the lowest ice lens within the fringe, denoted V_i, are related by

$$\begin{aligned} V_f(\phi - W_m) &= V_i + G_f - G_l, \\ V_i &= \alpha[(W_l - W_m)V_f + G_l], \end{aligned}\qquad(3)$$

where the dimensionless heat fluxes are given by

$$\begin{aligned} G_f &= -(k_u/k_f)\frac{\partial T}{\partial n} \text{ at the freezing front,} \\ G_l &= -\frac{\partial T}{\partial n} \text{ at the lowest ice lens,} \end{aligned}\qquad(4)$$

k_u is the thermal conductivity of unfrozen soil, and in the present case we can take the small geothermal heat flux G_f as zero. In the equations (3), ϕ is the unfrozen soil porosity, W_m (which could be zero) is the soil's minimum obtainable water content on freezing, W_l is the pore water volume fraction at the lowest ice lens in the fringe, and α is a dimensionless heaving parameter which depends both on W_l and on the soil characteristics.

W_l itself depends on the dimensionless effective pressure in the unfrozen soil, and it is only insofar as this is taken as independent of z_f that gravity is neglected.

Miller model in one dimension

If we denote the normal velocity of z_s as V_s, then in one spatial dimension (upwards), Miller's rigid ice assumption specified the heave rate by prescribing

$$V_s = V_i.\qquad(5)$$

Since, for steady conduction, we can write $G_l \propto (z_s - z_f)^{-1}$, we see that (3) forms a pair of ordinary differential equations for z_s and z_l; solutions have been given by Fowler and Noon (1993).

EXTENSIONS TO THREE DIMENSIONS

The equations (3) apply as much in three dimensions as in one, but we can no longer

assume $V_i = V_s$. Instead, V_s must be related to V_i by consideration of the rheology of the frozen soil. In addition, where the rigid ice assumption allows one to take V_i as spatially uniform in one dimension, this is not possible in three dimensions, and we have replaced Miller's assumption of rigidity with the physically based thermal regelation model (based on work by Römkens and Miller (1973) and Gilpin (1979)) which allows the ice flux $\mathbf{u}_i$ *within the fringe* to be proportional to $-\nabla T$. In particular, the normal component of $\mathbf{u}_i$, u_{in}, at the lowest lens is not necessarily equal to V_i. The theory behind the equations (3) is still valid, but the definition of α is different.

We assume that the frozen soil deforms as a viscous medium. The creep behaviour of frozen soil is considerably more complicated (Sayles 1988, Fish 1994), and the assumption of viscous deformation is taken here as a first simple approach. In three dimensions, we have to solve for the temperature T and frozen soil velocity $\mathbf{u}$ in the region $z_f < z < z_s$, where $(3)_1$ determines the location of z_f, and $(3)_2$ gives the normal flux there. We thus have to solve

$$\nabla^2 T = 0 \quad \text{in} \quad z_f < z < z_s, \qquad (6)$$

with prescribed temperature on z_s and $T = 0$ on z_f. To examine possible instabilities we first pose the condition

$$T = -1 \quad \text{on} \quad z = z_s, \qquad (7)$$

i.e., an isothermal surface.

The equations describing slow flow (including gravity) are Stokes's equations, and can be written in the dimensionless form (using $\eta_f k_f \Delta T / \rho_w L d^2$ as the pressure scale, where η_f is the frozen soil viscosity)

$$\nabla p = \nabla^2 \mathbf{u} - \Pi \mathbf{k},$$

$$\nabla . \mathbf{u} = 0, \qquad (8)$$

and the gravity parameter is

$$\Pi = \frac{g L d^3}{\eta_f k_f \Delta T}, \qquad (9)$$

with typical value, if $\eta_f = 10^{14}$ Pa s (Sayles 1988), of $\Pi \approx 1$.

We apply boundary conditions of no normal or tangential stress at z_s, together with a kinematic condition there, which determines z_s. At z_f, the normal velocity is equal to the normal ice flux V_i

given by $(3)_2$, z_f is determined by $(3)_1$, and we finally suppose that the unfrozen soil is undeformable, so that a no slip condition is applied. Other choices are clearly possible.

STABILITY ANALYSIS

The basic solution is that of one-dimensional heave. We analyse its stability by linearising the domain boundaries and the variables about their basic states, thus obtaining a linear set of equations and boundary conditions. The basic solution is time dependent, as $z_s - z_f$ increases with time as the freezing front penetrates downwards. We adopt a quasi-static approach (Robinson 1976) in which it is assumed that instabilities occur much faster than frost penetration, so that solutions of the perturbation equations proportional to $e^{\sigma t}$ can be sought. We restrict attention to two spatial dimensions x, z; solutions are then proportional to $\exp(\sigma t + ikx)$, where σ is the growth rate and k is the wavenumber, and in the usual way we derive a dispersion relation in the form $\sigma = \sigma(k)$ from the analysis.

In keeping with the two time derivatives ($\partial z_s / \partial t$ and $\partial z_f / \partial t$) which occur in the problem, we find that there are two modes, and these can in fact be characterised as being due to the gravitational relaxation of z_s (we call this the gravity mode), and the relaxation of z_f in the presence of heave: this is called the thermal mode.

In figure 1 we show typical examples of the dependence of σ on k for the gravity mode and the thermal mode. The formulae describing these functions are excessively complicated and the details of the analysis will appear elsewhere. Typically, the growth rates are negative, indicating stability. However, it is possible to obtain unstable modes, as indicated in figure 2. We see that instability can occur through a degeneracy in the solutions of the dispersion relation $a(k)\sigma^2 + b(k)\sigma + c(k) = 0$, when a goes through zero. The infinite growth rate at finite wavelength is reminiscent of a resonance phenomenon, and while it is unusual, is by no means unknown; see Murray (1989, chapter 17.4) for examples in biology. The formulae are so complicated that it is difficult to be dogmatic, but essentially this instability is predicted to occur for large enough values of α, corresponding to higher permeabilities and thus coarser soils. If this instability does occur, it seems likely to be

rather violent (due to the infinite growth rate!).
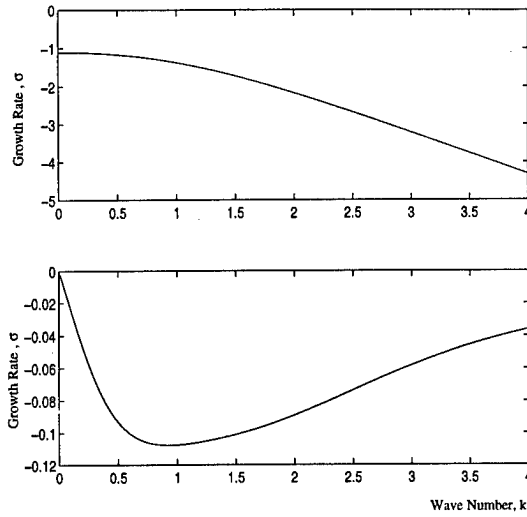
Figure 1: *A typical example of the dependence of thermal mode σ (upper) and gravity mode σ (lower) versus k for $\alpha = 0.1$, $\Pi = 1$. Note the difference in scale. Essentially $\sigma \sim \Pi$ for the gravity mode, while $\sigma \sim \alpha$ for the thermal mode.*
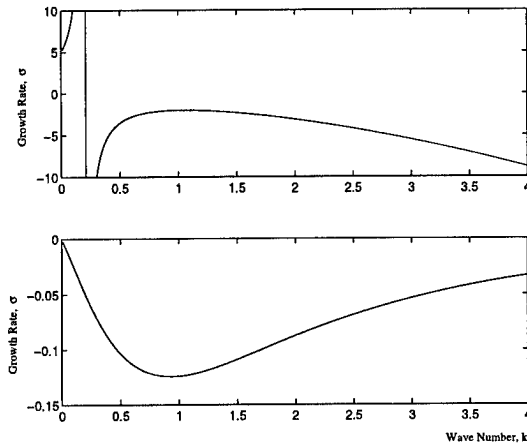
Figure 2: *The thermal mode has become violently unstable for wavenumber $k < k_c \approx 0.2$. This would suggest rapid formation of patterned ground, presumably at a wavelength close to $2\pi/k_c$ (in this example). The parameters are still $\alpha = 0.1$, $\Pi = 1$, but another parameter C in the dispersion relation has been changed from 1 to 1.2; this can be effected by changing γ, for example.*

THE EFFECT OF SNOW COVER

One of the mechanisms commonly cited as a reason for the growth of hummocks is the variability in snow covering overlying the hummocks (Williams and Smith 1989). During the winter months troughs of hummocks fill with snow and hence the snow covering is greater in the troughs than on the crests. Because snow acts as an insulator, the crests are subject to greater cooling and thus more heave, which allows for a further possible instability mechanism.

To study this, we consider a layer of snow of (dimensionless) thickness h overlying an initially flat ground surface. We suppose that the snow surface remains flat during the evolution of z_s, and we replace the condition $T = -1$ at $z = 0$ (the undisturbed ground surface) by solving $\nabla^2 T = 0$ in $z_s < z < h$, with $T = -1$ at $z = h$, T continuous at $z = z_s$, and

$$\delta \left. \frac{\partial T}{\partial n} \right|_{z_s+} = \left. \frac{\partial T}{\partial n} \right|_{z_s-}, \qquad (10)$$

where $\delta = k_s/k_f$ is the ratio of the thermal conductivities of snow and frozen soil.

As before, we derive a quadratic dispersion relation for $\sigma(k)$. For simplicity, we neglect the effects of the perturbation in load on the heave parameter α. (In the absence of snow cover, the same assumption always gives stability, so that the instability (in the thermal mode) mentioned in section 5 for high α relies on its variation with load.) Figure 3 shows a typical plot of the gravity and thermal modes. For these unstable modes, the freezing front and surface perturbations are out of phase, as observed (Tarnocai and Zoltai 1978), Williams and Smith 1989, Van Vliet-Lanoë 1991).

If we assume that instability arises via an exchange of stability (i.e. $\sigma = 0$), then one can calculate analytically the critical condition for instability to occur. The relevant bifurcation parameter is $\mathcal{N}$, defined by

$$\mathcal{N} = \frac{(\phi - W_l)\alpha}{\Pi\{\phi - W_m - \alpha(W_l - W_m)\}}, \qquad (11)$$

or more simply, $\mathcal{N} = V_i/\Pi$. Since in one dimension, V_i is the heave rate, we can write $\mathcal{N}$ as the dimensionless group

$$\mathcal{N} = \frac{\eta_f v_s}{\rho_f g d_f^2}, \qquad (12)$$

250

where v_s is the dimensional heave rate, ρ_f is the frozen soil density, and in this analysis the length scale $d \ (= d_f)$ has been specifically taken to be the (slowly evolving) depth of the frozen front.

We then find that instability occurs at wavenumber k if

$$\mathcal{N} > \frac{(\sinh 2k - 2k)}{4k^3(1-\delta)}(\tanh k \tanh kh + \delta), \quad (13)$$

and this defines a positive increasing critical value of $\mathcal{N}$ as a fraction of k. The minimum value occurs at $k = 0$, and defines a critical value of $\mathcal{N}$,

$$\mathcal{N}_c = \frac{\delta}{3(1-\delta)}. \quad (14)$$

With typical values $k_s = 0.1$ W m^{-1} K^{-1}, $k_f = 2$ W m^{-1} K^{-1}, we have $\delta \approx 0.05$, thus $\mathcal{N}_c \approx 0.02$. We conclude that differential frost heave is predicted by the Miller model provided the parameter $\mathcal{N}$ given by (11) is greater than this critical value.
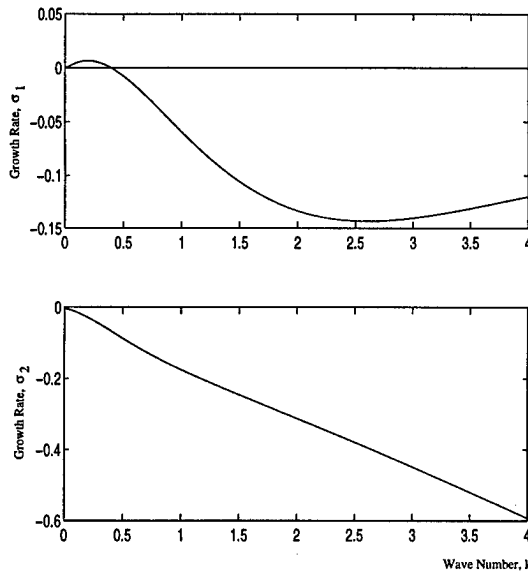
Figure 3: *Growth modes in the presence of snow cover. We take* $\alpha = 0.1$, $\Pi = 1$, $\delta = 0.05$, $h = 1$. *The upper (gravity) mode indicates long wavelength instability for* $k \lesssim 0.5$.

DISCUSSION

The Miller model can be extended to describe three-dimensional frost heave, but the rigid ice assumption must be replaced. Gilpin's model of thermal regulation provides a useful alternative. It can then be systematically reduced to give two messy but explicit expressions for the ice flux to the fringe, and the frost penetration rate.

Together with Laplace's equation for the temperature, the frozen soil rheology must be prescribed. We have chosen to model the frozen soil as a viscous medium overlying a rigid substratum, though this choice is easily modified. We have then found two possible instability mechanisms. In the first, instability relies on the variation of α with load (excess load suppresses heave), and is only practical for relatively high values of α, corresponding, for example, to silts or sands. This mechanism could then serve as an explanation for stone circles. Alternatively, while this mechanism is not viable for finer soils, the effect of snow cover can cause instability by enhancing heave at the crests. Here we find instability if the frost depth d_f is less than a critical value,

$$d_f < \left[\frac{\eta_f v_s}{\rho_f g \mathcal{N}_c}\right]^{1/2}. \quad (15)$$

For a silt with $v_s = 10^{-9}$ m s^{-1}, this gives $d_f < 14$ m, and suggests that this mechanism of instability is feasible, although it must also be pointed out that in order for the effect to be viable in practice over a seasonal time scale, the growth rates need to be higher than indicated in figure 3, and this is likely to provide a more severe constraint on d_f. Also, v_s decreases as d_f increases, and of course the whole analysis has been based on a quasi-static approach. Further investigations will warrant a full two or three-dimensional numerical simulation.

REFERENCES

Fish, A.M. 1994 Creep and strength of frozen soil under triaxial compression. *CRREL Special Report* 94–32. CRREL, Hanover, New Hampshire.

Fowler, A.C. and Noon, C.G. 1993 A simplified numerical solution of the Miller model of secondary frost heave. *Cold Reg. Sci. Tech.* **21**(4), 327-336.

Fowler, A.C. and Krantz, W.B. 1994 A generalized secondary frost heave model. *SIAM J. Appl. Math.* **54**(6), 1650-1675.

Gilpin, R.R. 1979 A model of the 'liquid like' layer between ice and a substrate with applications to wire regelation and particle migration. *J. Colloid Interface Sci.* **68**, 235-251.

Krantz, W.B., Gleason, K.J. and Caine, N. 1988 Patterned ground. *Scientific American*, 44-50.

Miller, R.D. 1972 Freezing and heaving of saturated and unsaturated soils. *Highway Res. Rec.* **393**, 1-11.

Miller, R.D. 1978 Frost heaving in non-colloidal soils. In *Proc. Third. Int. Conf. Permafrost*, pp. 708-713.

Murray, J.D. 1989 Mathematical biology. Springer-Verlag, Berlin.

Noon, C.G. 1996 Secondary frost heave in freezing soils. D. Phil. thesis, Oxford University.

O'Neill, K. and Miller, R.D. 1982 Numerical solutions for a rigid ice model of secondary frost heave. Technical report, CRREL Rep. 82-13.

O'Neill, K. and Miller, R.D. 1985 Exploration of a rigid ice model of frost heave. *Water Resour. Res.* **21**(3), 281-296.

Piper, D., Holden, J.T. and Jones, R.H. 1988 A mathematical model of frost heave in granular materials. In *Proc. Fifth Int. Conf. Permafrost*, pp. 370-376.

Robinson, J.L. 1976 Theoretical analysis of convective instability of a growing horizontal thermal boundary layer. *The Physics of Fluids* **19**(6), 778-791.

Romkens, M.J.M. and Miller, R.D. 1973 Migration of mineral particles in ice with a temperature gradient. *J. Colloid Interface Sci.* **42**, 103-111.

Sayles, F.H. 1988 State of the art: Mechanical properties of frozen soil. In *Fifth Int. Symp. Ground Freezing*, pp. 143-159.

Tarnocai, C. and Zoltai, S.C. 1978 Earth hummocks of the Canadian Arctic and Subarctic. *Arctic and Alpine Research* **10**(3), 581-594.

Van Vliet-Lanoë, B. 1991 Differential frost heave, load casting and convection: Converging mechanisms; a discussion of the origin of cryoturbations. *Permafrost and Periglacial Processes* **2**, 123-139.

Williams, P.J. and Smith, M.W. 1989 *The Frozen Earth. Fundamentals of Geocryology.* Cambridge University Press.

Thirty-Five Years of Measuring Frost Depths in Wisconsin Soils

A.E. PETERSON[1]

ABSTRACT

The measurement of depth of Wisconsin's frozen soils is possible due to a unique frost depth survey made possible by the cooperation of cemetery caretakers and funeral directors in Wisconsin who collect the data while digging graves. Their observations about frost penetration, snow cover, soil moisture content, and related factors are useful in monitoring the conditions of hay and pasture, as well as fall planted small grains. Knowledge of frost depth also permits more accurate predictions of the spring runoff from snowmelt and beginning of spring field work. Contractors, commercial industries, insurance companies, utilities with underground facilities such as water and gas lines, and winter sports facilities also have need for this information. The collection of this data is a joint project between the College of Agricultural and Life Sciences of the University of Wisconsin, the University of Wisconsin Extension, the Wisconsin Agricultural Statistics Service and the National Weather Service.

Key words: Frost depth, cemeteries, funeral directors, biweekly report.

INTRODUCTION

Regardless of the freezing mechanism, frost depth measurements are very difficult Early frost depth measurements were made using a King soil tube and hammer (Atkinson and Bay 1940). Cores were removed from the tube and examined for ice crystals. The depth to which these crystals occurred was recorded as frost depth. The tube would also "give" as it passed from the frozen to the unfrozen soil. The method was laborious and time-consuming and often resulted in broken tubes and hammers. The use of gypsum blocks and a Wheatstone bridge (Bouyoucos and Mick 1948) permitted measurement of the sharp increase in resistance when the soil froze. Although accurate, neither method seemed feasible for providing frost depth on a statewide basis. Since previous frost depth collecting methods were so laborious and the visual method so accurate, it was decided to solicit the cooperation of funeral directors and cemetery officials throughout Wisconsin (Peterson et al. 1963). Development of a mailing list was difficult but was accomplished through information supplied by the Wisconsin State Board of Health, which licenses all Wisconsin funeral directors and embalmers and by the Cooperative Extension Agent in each county. Cemetery officials were selected where services were held regularly, and funeral directors were selected when they served a number of cemeteries in areas where services are infrequent (rural areas). County extension agents also provided names within their county. Locations were picked to give a good cross section of the various soil types in Wisconsin as well as geographical distribution in a county (Fig. 1). Practically all locations are still reporting in 1997. The prevailing westerly winds preclude any appreciable lake effect except in the very northern counties.

Previous studies indicated that frost penetration is considerably deeper with bare soil than under sod cover (Bay et al. 1952). Since soil in cemeteries is usually covered with turf, state-wide comparisons are made under similar conditions, whereas others may be working in protected areas one week and bare soil the next week. Therefore, frost depths reported in this

---

[1] Department of Soil Science, University of Wisconsin, 1525 Observatory Drive, Madison, Wisconsin 53706, USA
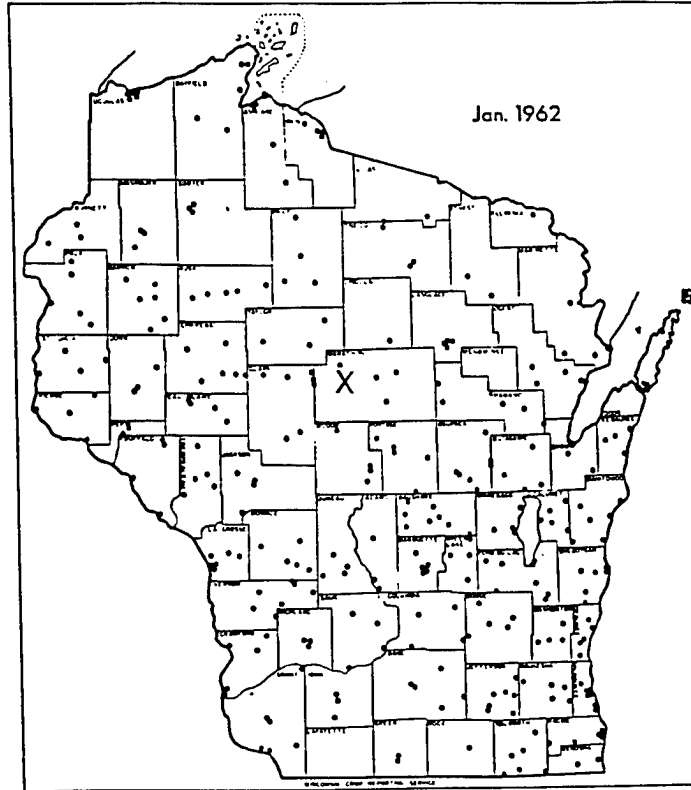
Figure 1. Location of Wisconsin frost reporters.
X = *Crossing of 45th latitude and 90 longitude.*

survey are considered minimum since they were made under sod cover. Snow depth must also be considered since the thermal conductivity of moist soil is four to ten times greater than for snow (Storey 1955) depending upon several factors including the age and compactness of the snow. Wisconsin is the only known state to conduct such a survey even though Minnesota and Michigan were encouraged to develop such a survey in the 1970s.

PROCEDURE

The Snow and Frost Depth report is published biweekly from 1 November to 1 April by the Wisconsin Agricultural Statistics Service during the months when their weekly *Crop Weather Reports* is not published. The reporting procedure for one period is as follows: Early in the week, the questionnaires (Fig. 2) are mailed with the request that they mail them back by Saturday. The following Monday the replies are tabulated by the Wisconsin Agricultural Statistics Service; representatives of the National Weather Service, the University of Wisconsin College of Agricultural Life Sciences and University Extension discuss the information and prepare a release for that Monday afternoon. No correction for area is made for the counties; thus it might not represent a true state average. However, this system has been used since the survey started, so the comparison between years is still valid. A state map (including counties) indicating both frost and snow depth is provided (Fig. 3). The average frost depth for each county is recorded on the state map and contours for the average depth are estimated across the state. Graphs indicating the present and long-term averages for both frost and snow depths are also included (Fig. 4). Maps similar to Figure 3 are now reproduced on the back of the one page release along with selected "Comments from Reporters" and the mailing information. Copies of the release are sent to the observers, newspapers, radio, television, and wire services.

Observers are asked to report not only the frost and snow depth but also the type of soil, the direction of the slope and other weather comments. Thus, observers are able to keep in the habit of returning a report even though they had no grave openings in the reporting period. Slope of the terrain has an important effect on the amount of solar energy received locally and, therefore, the length of time the snow will remain on the ground. Wind directions during heavy snowfall usually change slowly from northeast to northwest, and much of the drifting is experienced during the cold

254

1. Name of Cemetery---------------County where located--------

2. What is the present depth of frost penetration?-------------..............inches

3. What is the present depth of snow cover?---------------..............inches

4. What is the soil type of the cemetery?...Sandy-------Silt------Clay----

5. Does this cemetery site slope?-----------Yes...........No..........

      North.............South.............East........West............

6. Other Weather Comments (such as temperature, snow drift, winds, etc.)

Reported by------------------------------------Date----------

Street Address
or Route No.---------------------------------Post Office------

Figure 2. Cemetery caretakers and funeral directors questionnaire.

SNOW DEPTH
January 10, 1997

Meters
< .025
.025-.152
.178-.305
.330-.609
.635-.914
.939-1.22

FROST DEPTH
January 10, 1997

Meters
< .025
.025-.152
.178-.305
.330-.609
.635-.914
.939-1.22
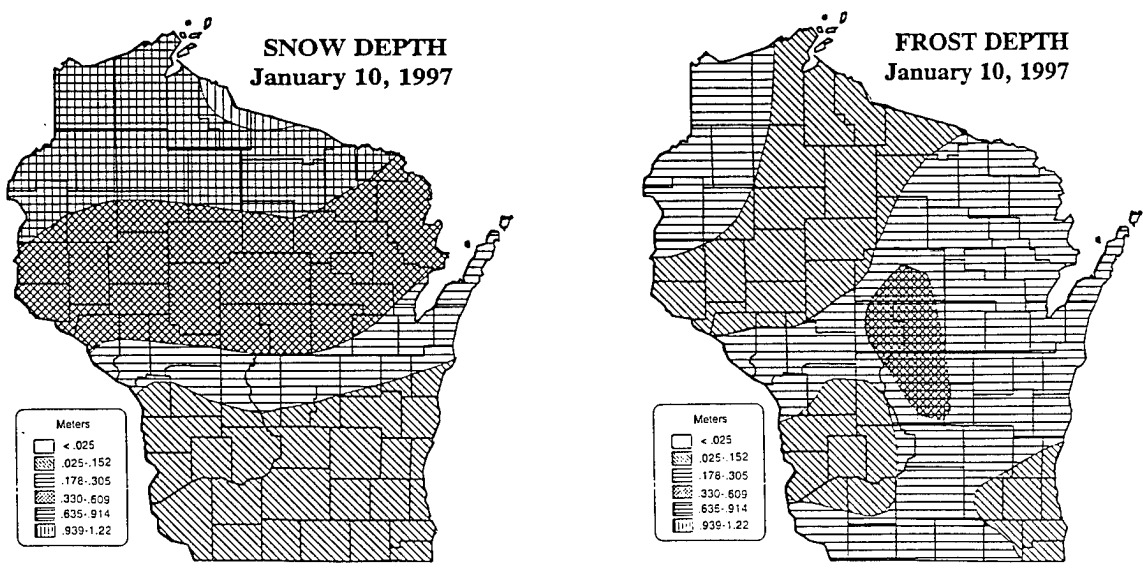
Figure 3. Wisconsin frost and snow depth maps.

northwesterly winds at the end of the storm. Thus, the snow cover will be deepest on the side of the hill where snowdrifts accumulate with northwesterly winds.

The survey started in 1961, with returns being mailed to the University Extension in Madison. Publication officials initially felt the information was too gruesome and refused to release it to the public. However, the Department of Soil Science tabulated the results and prepared the state maps that were copied overnight to glossy prints and the prints were delivered to the Associated Press and United Press International wire services for distribution. The interest shown by both the daily and weekly papers to publish the maps indicated a substantial interest in this type of information. The Wisconsin Crop Reporting Service was also very interested in predicting when farmers

would be able to commence field work, and this information permitted increased accuracy for such predictions. They also indicated an interest in distributing the release through their network and thus developed the procedure that has been in use for 35 years. In 1960-1961 two pilot reports were made, and in 1961-1962, after clearance from USDA Division of Standards, reports were made twice a month from December into April.

An editorial shortly after the survey began stated that "Giving credit where credit is due is the policy of this paper. Today we commend the funeral directors and cemetery caretakers. We've been a little tough on morticians in the past, so we welcome this opportunity to pass on some posies (or should we say daisies?). At any rate, the Wisconsin Crop Reporting

Wisconsin, Late March 1987–1996
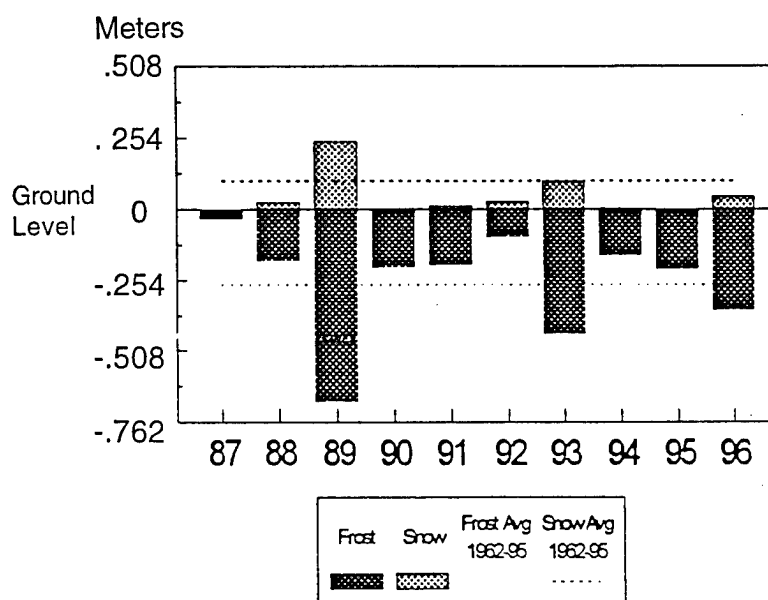
Figure 4. Average frost and snow depths.

Service bulletin, announcing that, as of December 6, the state was relatively free of frost and had a limited snow cover add this comment: This report is based on a survey made with the help of funeral directors and cemetery caretakers throughout the state. Information from these people is especially valuable because of their experience and accuracy in observing frost penetration and snow depth. Also, since all cemeteries are covered with sod, uniform comparisons can be made on a state-wide basis! Nice going fellows. There's nothing grave about that report."

RESULTS AND DISCUSSION

The response from funeral directors and cemetery officials has been most gratifying. Between 60 to 70% of the questionnaires have usually been returned by the Monday deadline. Another 10% usually arrive too late for the release, but are used to calculate the final weekly depths. Quotes from the observers are also very useful, especially as they refer to soil moisture conditions down to a depth of 1.6 m. Attempts to quantify the soil moisture content at the various depths have not been successful, but "overnight water standing in the bottom of the grave" tells us that the soil is likely to be saturated. If no graves have been opened during the last 2-week period, reporters are asked to at least provide the snow depth. Also this keeps them in the habit of reporting something every 2 weeks.

The frost depths by reporting periods for the 35 years is given in Table 1, while the snow depth for the same

period is given in Table 2. The inverse relationship between snow and frost depth is obvious, unless the snow cover arrives well after the cold weather and the soil is already frozen to a considerable depth. Wisconsin has nine Agricultural Reporting Districts (Fig. 5) and the average frost and snow depth from 1961-1996, by the reporting districts, is given in Table 3. These tables update the information provided in two bulletins from the Wisconsin Agricultural Reporting Service entitled Wisconsin Snow and Frost 1961 to 1977 and Wisconsin Snow and Frost 1978 to 1988. Long-term trends are difficult to establish, but the more years of data available, the more reliable are the comparisons. The National Weather Service (NOAA) uses a 30-year average in many weather-related matters.

Each biweekly report contains "Comments from Reporters" and are selected to especially report on soil conditions and activities, i.e. earthworm movement, honeycomb frost, ice layer on surface of soil, etc. Note the observer's prediction of things to come!!! They are arranged from north to south so that readers can see the pattern across the state.

The excessive snow accumulation in the Upper Mississippi Valley region in the winter of 1969 caused the Flood Forecast Center in Minneapolis to predict serious spring flooding. Numerous Wisconsin localities even started sandbagging and diking their vulnerable areas. The Weather Bureau (according to an Associated Press dispatch) warned Chippewa Falls "that runoff from a heavy north-country layer of snow might produce the region's worst flood in history." However,

Table 1. Wisconsin Frost Depth measurements 1961-1996

FROST DEPTHS 1961-96 average (meters)

Year	early DEC	mid DEC	late DEC	mid JAN	late JAN	mid FEB	late FEB	mid MAR	late MAR
1961-62	.043	.081	-	.165	.203	.307	.328	.290	.206
1962-63	.008	.221	-	.330	.513	.724	.813	.876	.729
1963-64	.064	.163	-	.320	.391	.389	.439	.432	.315
1964-65	.135	.257	-	.386	.610	.775	.823	.927	.813
1965-66	.051	.043	.084	.208	.358	.447	.561	.511	.183
1966-67	.061	.191	.269	.305	.318	.323	.406	.455	.323
1967-68	.091	.102	.267	.541	.658	.663	.892	1.011	.874
1968-69	.010	.081	.180	.183	.132	.175	.193	.165	.104
1969-70	.074	.091	.102	.117	.145	.173	.211	.206	.094
1970-71	.023	.028	.130	.211	.246	.274	.236	.229	.175
1971-72	.023	.038	.104	.168	13.9	.523	.635	.721	.569
1972-73	.051	.130	.117	.244	.257	.262	.318	.208	.048
1973-74	.023	.104	.137	.310	.300	.320	.320	.104	.107
1974-75	.053	.104	.114	.262	.424	.518	.503	.478	.284
1975-76	.028	.135	.246	.386	.429	.447	.254	.175	.056
1976-77	.173	.231	.343	.538	.757	.871	.765	.411	.066
1977-78	.051	.048	.094	.152	.241	.323	.406	.414	.231
1978-79	.043	.076	.127	.163	.175	.191	.196	.117	.033
1979-80	.018	.102	.168	.292	.411	.622	.747	.864	.749
1980-81	.043	.193	.368	.617	.711	.859	.605	.401	.213
1981-82	.013	.130	.226	.269	.348	.414	.338	.295	.127
1982-83	M	.142	.163	.229	.295	.358	.229	.066	.030
1983-84	.041	.076	.102	.099	.155	.0981	.071	.183	.142
1984-85	.018	.051	.145	.234	.391	.589	.577	.493	.323
1985-86	.048	.074	.086	.102	.135	.127	M	.117	.033
1986-87	.058	.107	.091	.089	.254	.305	.320	.173	.036
1987-88	.015	.033	058	.264	.305	.384	.490	.366	.175
1988-89	.015	.178	.277	.467	.556	.579	.729	.754	.693
1989-90	.079	.307	.617	.688	.655	.643	.599	.523	.208
1990-91	.008	.038	.175	.269	.315	.315	.345	.348	.201
1991-92	.020	.028	.124	.089	.244	.302	.356	.196	.102
1992-93	.008	.046	.114	.234	.348	.378	.422	.472	.450
1993-94	.030	.013	.224	.356	.485	.569	.480	.394	.168
1994-95	.015	.056	.053	.272	.320	.399	.513	.564	.216
1995-96	.094	.173	.234	.305	.376	.478	.505	.495	.353
1961-96 Average	.046	.111	.179	.282	.366	.432	.460	.412	.269

M = Missing figure

Table 2   Wisconsin Snow Depth measurements 1961-1996

SNOW DEPTHS 1961-96 Average (meters)

Year	early DEC	mid DEC	late DEC	mids JAN	late JAN	mid FEB	late FEB	mid MAR	late MAR
1961-62	.066	.269	-	.312	.328	.307	.480	.615	.394
1962-63	.003	.043	-	.097	.203	.196	.211	.262	.193
1963-64	.048	.124	-	.114	.089	.178	.127	.135	.089
1964-65	.066	.104	-	.137	.127	.249	.236	.147	.236
1965-66	.147	.112	.099	.201	.244	.124	.079	.023	.157
1966-67	.003	.066	.206	.333	.323	.363	.465	.343	.269
1967-68	.043	.048	.064	.112	.089	.094	.104	.066	.003
1968-69	.033	.030	.297	.554	.478	.480	.389	.274	.142
1969-70	.003	.178	.333	.340	.343	.307	.211	.132	.064
1970-71	.025	.140	.206	.419	.505	.612	.546	.391	.318
1971-72	.145	.064	.208	.163	.231	.272	.335	.409	.173
1972-73	.013	.231	.198	.211	.104	.122	.127	.051	.003
1973-74	.061	.137	.160	.168	.147	.259	.236	.025	.064
1974-75	.015	.132	.132	.112	.198	.290	.343	.401	.231
1975-76	.069	.046	.097	.213	.340	.246	.157	.173	.053
1976-77	.051	.079	.104	.198	.254	.198	.074	.064	.008
1977-78	.180	.165	.152	.218	.302	.361	.323	.282	.069
1978-79	.112	.157	.224	.340	.665	.665	.696	.485	.145
1979-80	.015	.018	.015	.117	.097	.168	.112	.124	.036
1980-81	.064	.028	.086	.097	.043	.221	.033	.013	.003
1981-82	.046	.056	.185	.378	.582	.521	.310	.279	.089
1982-83	M	.023	.071	.124	.152	.333	.132	.066	.091
1983-84	.163	.361	.295	.310	.290	.119	.030	.053	.025
1984-85	.008	.038	.079	.130	.185	.244	.251	.185	.025
1985-86	.394	.371	.391	.353	.328	.333	M	.287	.069
1986-87	.038	.053	.051	.053	.094	.051	.023	.010	0
1987-88	.018	.173	.180	.218	.356	.267	.173	.046	.023
1988-89	.061	.046	.104	.124	.094	.137	.157	.297	.241
1989-90	.025	.058	.107	.081	.155	.109	.147	.076	0
1990-91	.015	.091	.152	.241	.246	.119	.109	.079	.013
1991-92	.104	.084	.099	.074	.079	.071	.104	.038	.028
1992-93	.015	.099	.061	.071	.218	.122	.112	.150	.099
1993-94	.069	.013	.058	.206	.282	.381	.221	.038	.003
1994-95	.043	.107	.020	.074	.132	.084	.048	.193	0
1995-96	.175	.165	.160	.218	.457	.356	.224	.196	.051
1961-96 Average	.069	.111	.148	.203	.250	.256	.215	.183	.097

M = Missing figure

258
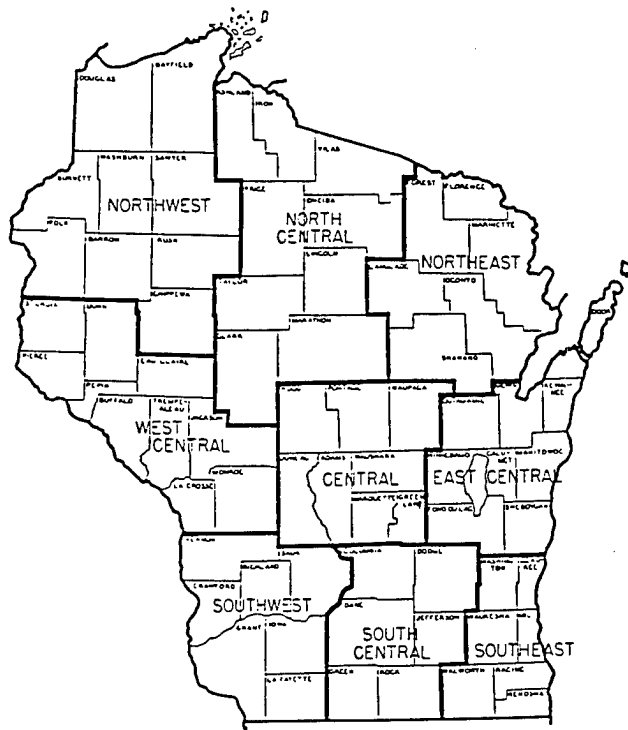
Figure 5. Agricultural Statistics Districts.

Table 3   Average Wisconsin Frost and Snow Depths by Districts 1961-1996

FROST DEPTHS 1961-96 Average (meters)

Div.	early DEC	mid DEC	late DEC	mid JAN	late JAN	mid FEB	late FEB	mid MAR	late MAR
NW	.058	.142	.206	.318	.411	.480	.541	.503	.409
NC	.051	.109	.165	.246	.315	.394	.445	.417	.318
NE	.071	.150	.213	.318	.386	.457	.511	.478	.338
WC	.046	.122	.201	.318	.439	.488	.551	.472	.267
C	.051	.132	.221	.356	.467	.544	.617	.541	.356
EC	.036	.099	.165	.269	.345	.411	.447	.406	.269
SW	.033	.086	.140	.246	.330	.391	.414	.345	.183
SC	.028	.084	.145	.249	.335	.394	.414	.340	.188
SE	.023	.079	.135	.226	.277	.328	.310	.262	.135
State	.044	.111	.177	.283	.367	.432	.472	.418	.274

SNOW DEPTHS 1961-96 Average (meters)

Div.	early DEC	mid DEC	late DEC	mid JAN	late JAN	mid FEB	late FEB	mid MAR	late MAR
NW	.102	.157	.216	.287	.353	.361	.335	.307	.198
NC	.102	.147	.208	.284	.328	.351	.315	.295	.191
NE	.076	.137	.188	.272	.307	.310	.290	.264	.150
WC	.079	.109	.163	.213	.254	.274	.234	.193	.094
C	.064	.099	.147	.206	.244	.262	.208	.193	.091
EC	.043	.084	.122	.170	.211	.216	.175	.155	.066
SW	.048	.089	.117	.157	.175	.185	.132	.104	.030
SC	.041	.081	.107	.142	.165	.168	.122	.089	.028
SE	.025	.064	.079	.124	.152	.163	.107	.066	.025
State	.064	.107	.150	.206	.244	.254	.213	.185	.097

259
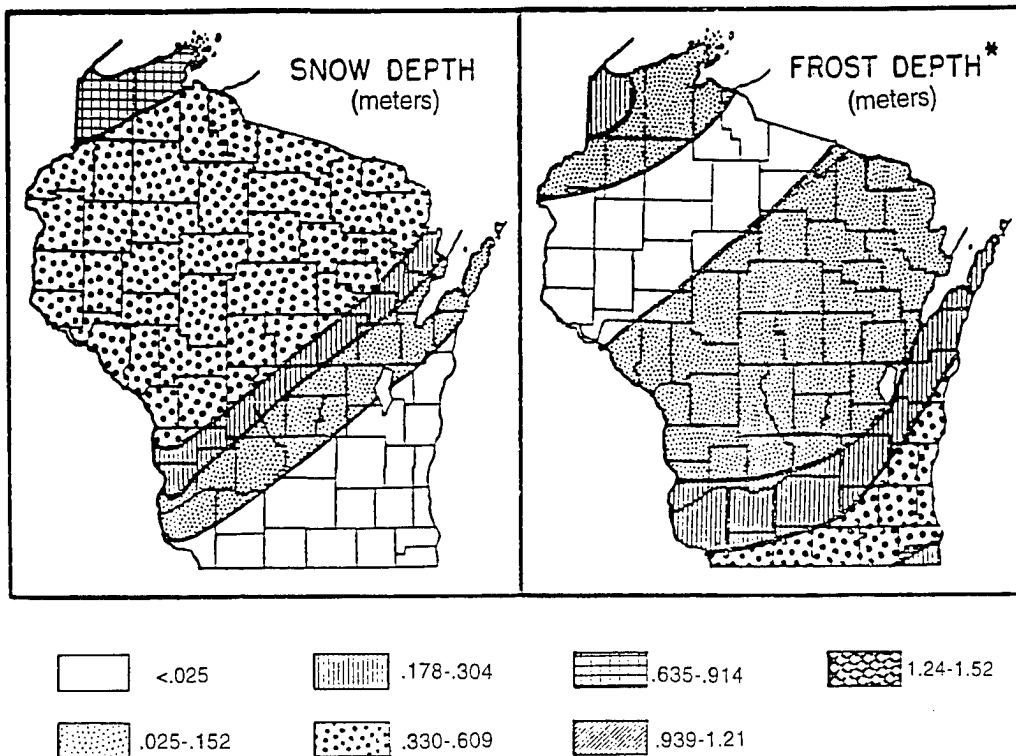
Figure 6. Snow and frost depths that did not produce the predicted spring floods.

there was very little frost in Wisconsin due to the early snow cover and the March 1969 report (Fig. 6) clearly summarized what was already known about the season. Thus, our news release stating that chances of flooding should be minimal, due to the lack of frozen soil, attracted considerable attention. When flooding did not develop, considerable controversy was generated as to whom should pay for the unused flood protection, dikes, etc. From then on, frost depth has been considered in the early spring flood forecasts for the Upper Mississippi Valley area.

SUMMARY

The winter activities m Wisconsin continue to increase and the knowledge of the frozen soil is important to many. The long-term historic value increases with each additional year of data. In spite of changes in personnel at all three of the cooperating institutions, the survey will continue, largely because it "fits" so well.in the Wisconsin Agricultural Statistics schedule. Their normal Crop Weather Reports cover from 1 April to 30 October. Thus the 1 December to 1 April Frost Survey period provides continuity for year-round weather and crops reports.

REFERENCES

Atkinson, H.B. and C.E. Bay. 1940. Some factors affecting frost penetration. Trans. Amer. Geophys. Union, 3:935–947.

Bay, C.E., G.W. Wunnecke, and O.E. Hays. 1952. Frost penetration into soils as influenced by depth of snow, vegetative cover, and air temperatures. Trans. Am. Geophys. Union 33: 542–546.

Bouyoucos, G.J. and A.H. Mick. 1948. A fabric absorption unit for continuous measurement of soil moisture in the field. Soil Science 66: 217–232.

Peterson, A.E., M.W. Burley and C.D. Caparoon. 1963. Frost depth survey: A new approach in Wisconsin. Weatherwise 3:11–16.

Storey, H.C. 1955. Frozen soil and spring and winter floods, p. 179–184 In USDA Yearbook of Agriculture. Washington, D.C.

Soil Moisture Dynamics in
Areas of Discontinuous Permafrost

L.D. HINZMAN[1], E.K. LILLY[1], D.L. KANE[1], AND R.A. JOHNSON[1]

ABSTRACT

Concern regarding contaminant migration on Fort Wainwright, Alaska, prompted an effort to develop an understanding of local hydrologic processes. Hydrology in discontinuous permafrost is extremely complicated and many obstacles were encountered in attempts to model transport plumes. In this area, the presence of ancient sloughs, discontinuous permafrost, low hydraulic gradients and the rise and fall of the Chena River that flowed adjacent to the area studied make this system very complex. The process of infiltration of surface water to the groundwater represents a major unknown, not just in regard to magnitude, but also in terms of spatial distribution of recharge. An understanding of the temporal dynamics of groundwater recharge was obtained through measurements of precipitation input (rainfall and snowmelt) and the response of soil moisture and groundwater levels. The results of this study indicate that summer precipitation amounts just meet evaporative demands and do not allow for significant groundwater recharge.

Keywords: soil moisture, TDR, groundwater recharge, permafrost, water balance

INTRODUCTION

The flux of water vertically across the soil surface is an important variable that is both generally unknown in Interior Alaska and spatially variable depending upon local conditions. Soil moisture dynamics represent an important parameter affecting processes such as evapotranspiration, recharge and the surface thermal regime. As a component of our groundwater investigation, we attempted to quantify the rates of rainfall recharge in a zone of discontinuous permafrost. We based this analysis upon measurements of precipitation, snowmelt and evaporation, soil moisture changes, changes of groundwater table and vertical hydraulic gradients.

The necessity of obtaining continuous meteorologic data for use in assessing dynamic soil moisture processes is clear. Knowledge of surface moisture flux is equally important in quantifying our groundwater resources. To this end, we must be able to describe the time series processes of rainfall and snowmelt infiltration. In order to accomplish these tasks, we must be able to describe the abstractions due to evaporation and soil moisture storage.

BACKGROUND

The thermal condition of the near surface soils has a major impact upon soil moisture dynamics in several aspects (Kane et al., 1978). The most important factor is not simply if the soil is frozen or thawed and to what depth, but the moisture content of the frozen soil (Luthin and Guymon 1974). Kane and Stein (1983 a,b,c) demonstrated that in Interior Alaska, the majority of groundwater recharge occurs during spring snowmelt, while the soils are still frozen. The rate of infiltration into frozen ground was primarily controlled by the antecedent moisture content during the preceding autumn. Given an unlimited source of water, infiltration occurs at a rate approximately equal to the saturated hydraulic conductivity (after an initial brief period of high infiltration caused by pore pressure gradients due to drier soils in advance of the wetting front). The infiltration into a dry frozen soil was approximately half of that of the same soil when thawed, basically because of changes in water viscosity at lower

temperatures. Infiltration into ice-rich frozen soil was almost 50 times less than that of the same soil in a frozen dry condition.

By controlling the rate of infiltration, the moisture content of frozen soil can also affect the amount of surface runoff. An investigation of the effects of autumn rains upon subsequent spring snowmelt runoff clearly displayed the importance of soil moisture in controlling infiltration to groundwater during snowpack ablation (Sand and Kane 1986). The snowmelt runoff was greatest during years with high snowpack if the autumn rains were heavy. Snowmelt runoff was diminished during years where the preceding autumn rains were light, all other factors being equal. In spite of lower infiltration rates into frozen ground, most groundwater recharge appears during the spring melt event (Gieck and Kane 1986). The relatively low summer precipitation rates in Interior Alaska is such that summer potential evapotranspiration usually meets or exceeds available precipitation (Braley 1980). Groundwater recharge can occur during

heavy sustained rain events that occasionally occur in late July or August. The subsurface temperatures also affect the rate of water movement through changes in viscosity. Viscosity of water increases as temperature decreases; thus, at lower temperatures, infiltration is reduced. In the Fairbanks area, this reduction is about a factor of two between summer and spring. The process of infiltration of surface water to groundwater represents a major question, not just in regard to magnitude, but also in terms of spatial distribution of recharge.

Methods

The study area was within the bounds of the Ft. Wainwright Army post, located just outside Fairbanks, Alaska (Fig. 1). The area of intensive measurements included the south slope of Birch Hill and a portion of the valley floor. Instruments were installed at three sites (Fig. 1). The primary meteorologic station (Met 1) was located at the break in the slope between Birch Hill and the valley floor. A second site (Met 2), measuring soil temperatures
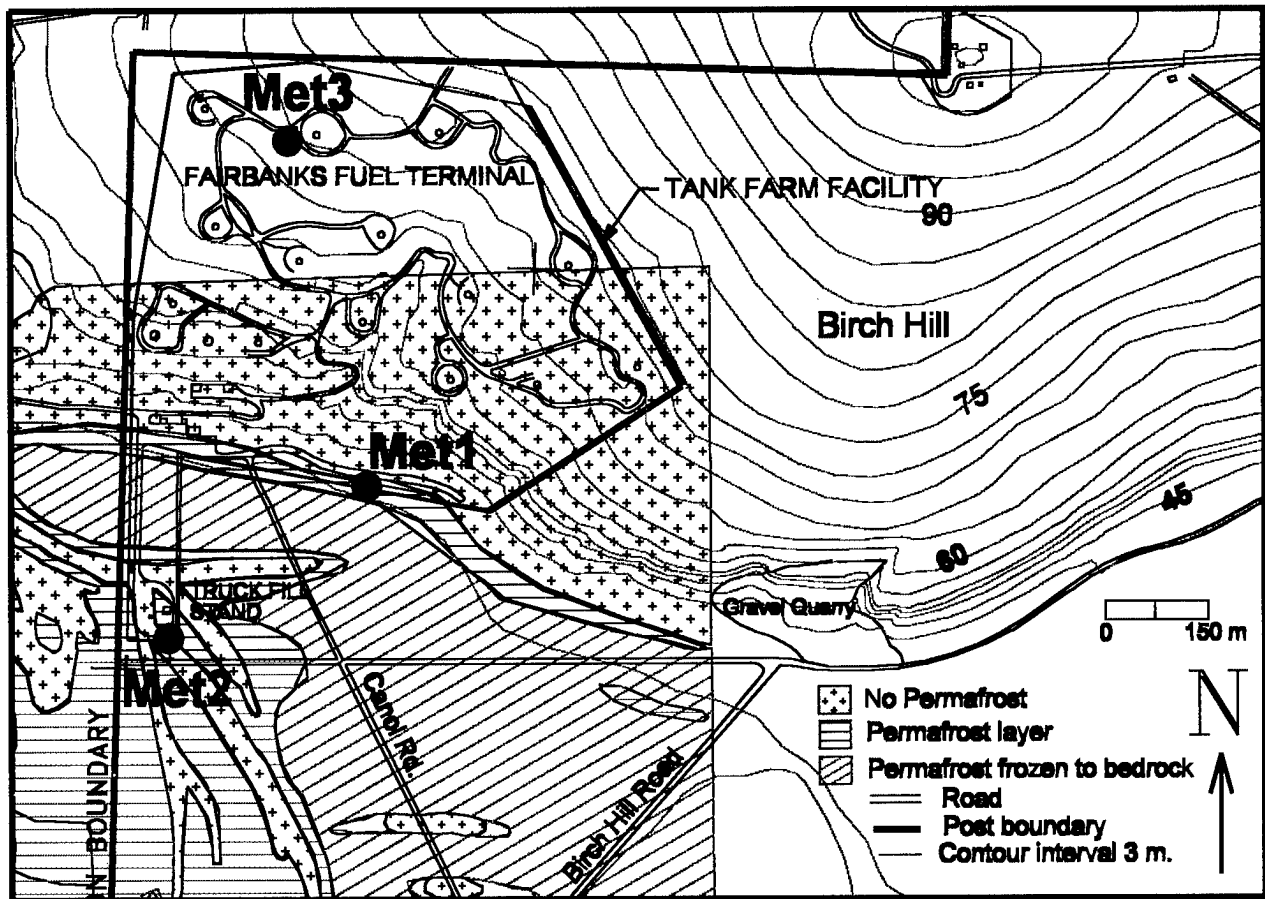
Figure 1. Map of study site indicating position of meteorologic stations and permafrost distribution as determined by Lawson et al. (1994).

and moisture, was located near the Truck Fill Stand (TFS). The third site (Met 3), which measured air temperature, relative humidity, precipitation, soil temperature and soil moisture, was added near the top of Birch Hill. The vegetation of Birch Hill is dominated with tall birch and some interspersed aspen. The undisturbed portions of the valley floor are covered with a thick mat of mosses and lichens and have a high density of black spruce with some birch. The south slope of Birch Hill is apparently permafrost free, while the valley floor is underlain by discontinuous permafrost. Permafrost is absent under roads or other major disturbances and under significant natural drainages or ponds. The thickness of the active layer above the permafrost varies substantially from about 50 cm in low wet areas with thick organic mats to more than a meter in better-drained areas.

Fairbanks is in a zone of discontinuous permafrost; meaning that permafrost generally exists in low lying areas and on the north-facing hillslopes. Hillsides with southern exposures, areas near significantly large ponds or drainages, are usually permafrost free. It is frequently difficult to judge the presence or absence of permafrost based upon currently existing conditions, as formation and/or ablation may require hundreds or even thousands of years under natural conditions. Construction of roads or other clearing of land rapidly accelerates permafrost degradation. The area selected for this study is highly variable in permafrost distribution.

Although most of the valley floor at the base of Birch Hill is dominated by permafrost, there exist large channels that are permafrost free (Fig. 1). These channels were formed under once active sloughs of the Chena River. Although these sloughs were abandoned hundreds of years ago as the Chena River meandered across the valley, the thermal relict of their presence remains. Permafrost is also absent under several roads constructed since 1940.

Meteorologic station

The ground surface represents a boundary condition in regional and site specific hydrologic models for which water flux must be specified. The hydrologic processes that must be quantified are rainfall precipitation, evaporation, snowmelt, runoff and infiltration. The thermal processes include evaporation/condensation, snowmelt and those which affect ground freezing and thawing. Evaporation and snowmelt are hydrologic processes that are most easily quantified through energy balance analyses. To ensure our capability to quantify these processes, meteorologic data were collected at three stations in the study area. Instruments included are displayed in Fig. 2.

The data were recorded on a Campbell Scientific CR10 data logger. Climatic parameters (air temperature, relative humidity, radiative components, and wind speed) were measured every two minutes, averaged and recorded hourly. Wind speed and direction, measured every two minutes,
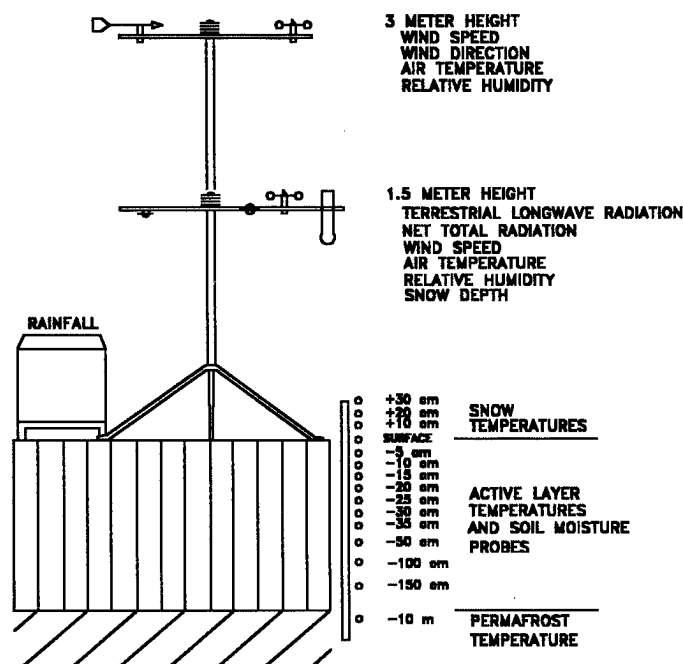
Figure 2. Schematic of primary meteorologic station located as indicated on Figure 1 as Met1.

were used to record the average hourly wind vector and standard deviation of direction and magnitude. Precipitation and wind run were continuously totalized and recorded each hour. Unfrozen soil moisture was measured using a Tektronix time domain reflectometer (TDR) and recorded every six hours. Soil temperatures were measured every two minutes, averaged and recorded hourly.

RESULTS

The data indicate that at the primary meteorologic station, the summer of 1994 was slightly cooler and drier than the 30-year average collected by the National Weather Service while the summer of 1995 was slightly warmer and wetter than the 30-year average. Neither year was particularly anomalous for Fairbanks summers. The snow water content was measured at many locations prior to initiation of spring snowmelt and daily during melt. In 1994 and 1995, the snow was quite uniformly distributed across the study area. The initial snowpack water content averages for spring 1994 and 1995 were 7.7 cm and 13.3 cm, respectively. In April 1994, the Fairbanks Field Office of the Natural Resources Conservation Service reported a snow water equivalent of 9.9 cm. The April 1995 value was 13.2 cm. These both compare to a 30-year average of 9.9 cm (NRCS, 1994, 1995). These data indicate that the snowpack of 1994 was close to the long-term average snowpack, while 1995 was significantly higher than average. The early winter snowpack (prior to March) in 1995-96 was abnormally low but by the end of March, was about average (9.7 cm) (NRCS, 1996). Although this did impact subsurface thermal processes, it did not directly impact soil moisture dynamics until the spring of 1996, as only rarely does Fairbanks experience significant midwinter melt events. A snow survey of snowpack depth and water content was collected at 10 points daily during snowmelt.

Soil moisture data were collected using an automated time domain reflectometer and recorded on a logging system manufactured by Campbell Scientific, Inc. The Campbell conversion algorithm which calculates soil moisture based upon measurements of soil dielectric constant, is not accurate when the soil is frozen (Boike, pers. comm.); however, it appears to function quite well during thawed conditions. The near-surface soil moisture (top 60 cm) was monitored to enable calculation of changes in stored soil moisture from day to day. As was expected, the surface organic layer was most sensitive to small rain events and surface drying, displaying the greatest variation in moisture content (Fig. 3 a and b). Rapid changes in soil moisture were damped out with depth. It is possible to determine changes in stored soil moisture from day to day by assuming soil moisture measurements were representative of a depth of soil above and below each probe. The sum of these moisture values multiplied by the associated depth of soil yields a depth of water in the soil profile. The change in soil moisture is simply the difference from one day to the next. A comparison of the soil moisture changes shows an expected dependence upon precipitation events (Fig. 4 a and b).

Using these data it is possible to calculate a water balance of the soil profile for a selected area:

$$\delta S = P - E - I \qquad (1)$$

where δS = change in soil moisture, depth of water
          in cm
       P = precipitation input, cm
       E = loss to evapotranspiration or gain from
          condensation, cm
       I = loss from soil profile by percolation to
          lower depths, cm.

It is possible to calculate evapotranspiration using several methods (Kane et al. 1990). Evapotranspiration was estimated following the method of Priestley and Taylor (1972) which relates potential evaporation to net surface energy flux. Net surface energy flux is calculated using a simplified surface energy balance, and relates actual evapotranspiration to potential evaporation by an empirical parameter α:

$$Q_e = \alpha\, s/(s+h)\, (Q_{net} - Q_c) \qquad (2)$$

where Q_e = Energy available for evaporation (W/m^2)
       α = the ratio of actual evapotranspiration to
          potential evaporation
       s = the slope of the specific humidity and
          temperature curve (°C^{-1})
       h = psychrometric constant in terms of specific
          humidity (°C^{-1})
       Q_{net} = net radiation (W/m^2)
       Q_c = energy conducted into the ground (W/m^2)

α was taken as 1.13 as described in (Rouse, 1976). Rouse and Stewart (1972) and Stewart and Rouse (1976) found, in a subarctic setting, that they could describe ($s/s+h$) as a linear function of screen air temperature.

$$s/(s+h) = 0.406 + 0.011(T_a) \qquad (3)$$

where T_a is the screen air temperature (°C).

264
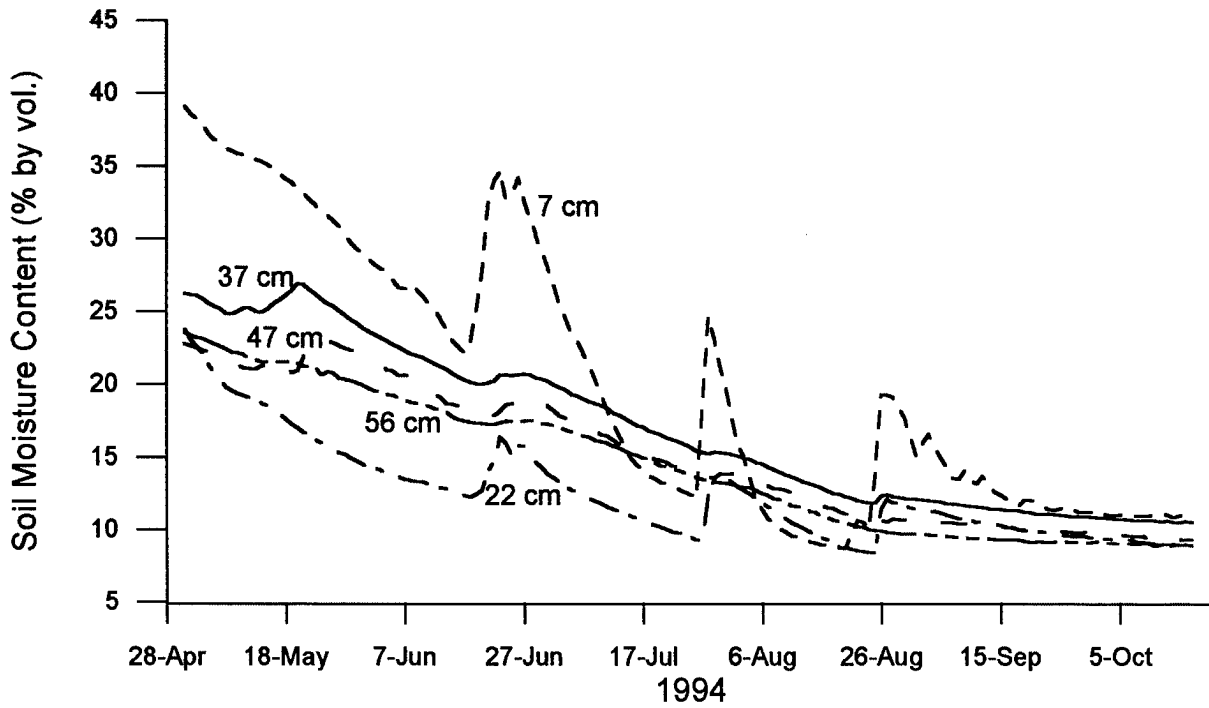
Figure 3a. Daily average moisture content at various depths as measured by automated time domain reflectometer in 1994 at the base of Birch Hill.
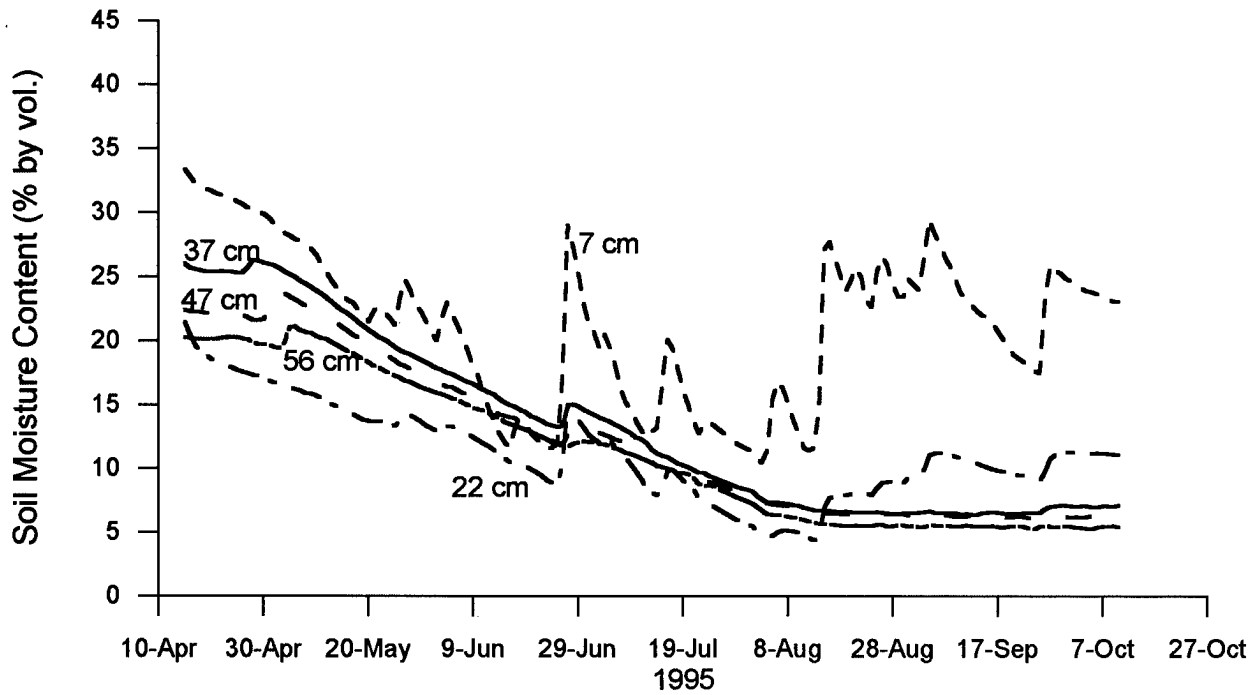
Figure 3b. Daily average moisture content at various depths as measured by automated time domain reflectometer in 1995 at the base of Birch Hill.

Q_{net} was measured 1.5 m above ground surface at the meteorological station using a Q6 Net Radiometer by Radiation and Energy Balance Systems. Q_c was calculated using measured soil temperatures at 7 and 22 cm depths, along with an estimated value of the thermal conductivity of the soils. Thermal conductivity of soils was estimated as 0.4 W/m°K based on values reported by Hinzman et al. (1991).

With measurements of soil moisture change and calculated estimates of evapotranspiration, one may calculate losses from the surface soil profile to percolation into groundwater (Fig. 4 a and b). In these calculations, negative values of percolation indicate moisture wicked back into surface soil layer to satisfy evaporative demands. These calculations assume no lateral movement of water in the soil profile. Although, there is probably saturated subsurface flow from Birch Hill to the valley floor, this water apparently enters the valley soil system in lower depths (Bolton and Lilly, in prep.) and does not affect these one-dimensional analyses.
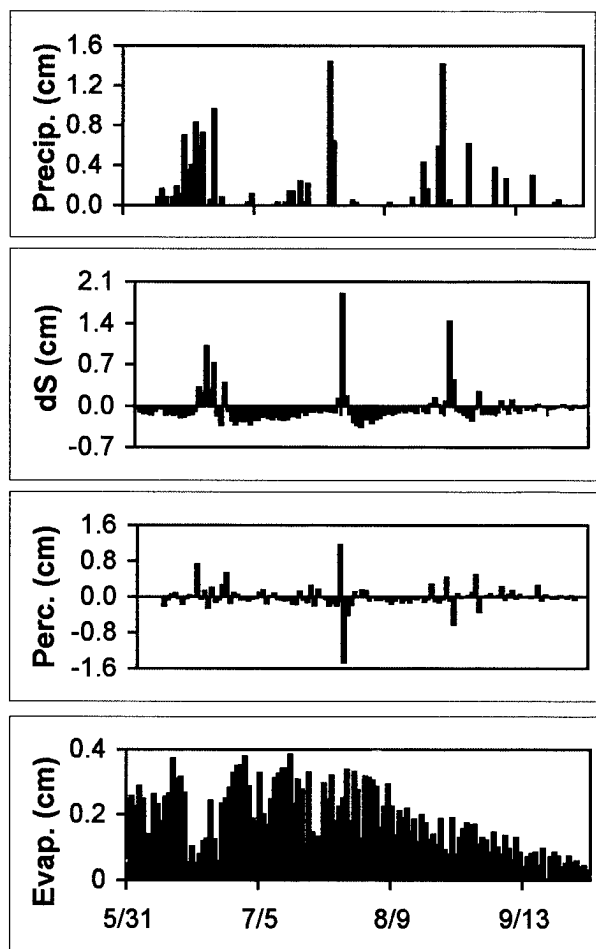
Figure 4a. Daily precipitation, changes in soil moisture, percolation from surface soil layer, and calculated evapotranspiration in 1994.
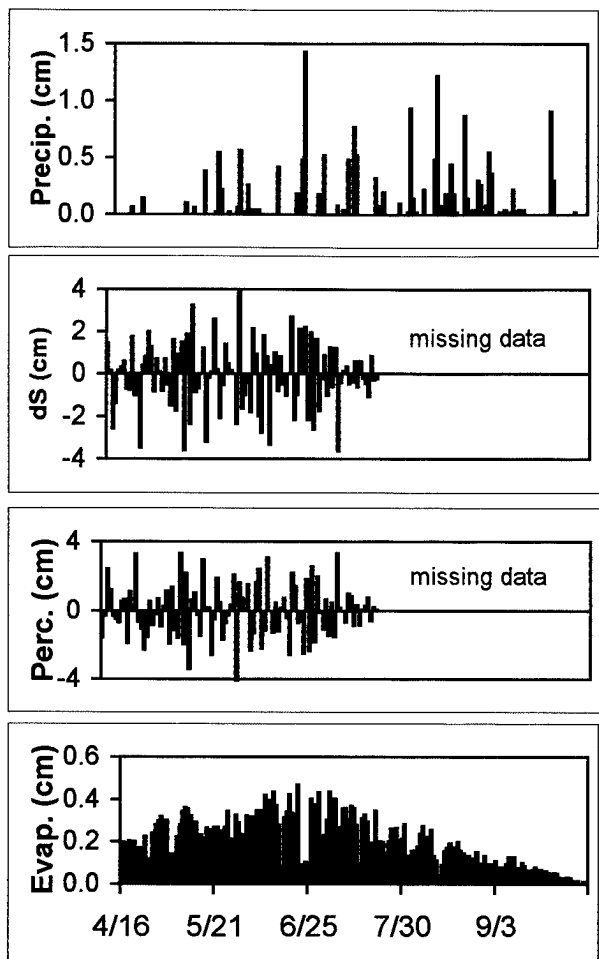
Figure 4b. Daily precipitation, changes in soil moisture, percolation from surface soil layer, and calculated evapotranspiration in 1995.

CONCLUSIONS

Water balance calculations on the surface soil layer indicate that the sum total percolation was quite close to zero during the summer months after spring melt; this is consistent with other studies. In both years, our soil moisture measurements are only valid after snowmelt was completed. Although this does not provide an estimate of the total annual groundwater recharge, it does provide confirmation that the summer precipitation essentially just meets evaporative demand and does not yield a significant contribution to groundwater resupply. Since there is relatively little groundwater recharge during the summer, contaminant transport processes (moving contaminants from the vadose zone into the saturated zone) will probably only be influenced by snowmelt in the spring or heavy precipitation events during late summer.

266

REFERENCES

Boike, J. 1995. Personal Communication. Alfred Wegener Institute, Potsdam, Germany.

Bolton, W.R. and M.R. Lilly. In prep. Geohydrology in alluvial and bedrock aquifers in the Columbia Creek basin area, Fairbanks, Alaska. U.S.G.S. Water Resources Investigation Report.

Braley, W.A. 1980. Estimates of evapotranspiration from barley and rapeseed in interior Alaska. M.S. Thesis, Univ. of Alaska, Fairbanks, 116 pp.

Gieck, R.E. and D.L. Kane. 1986. Hydrology of two subarctic watersheds. *In D.L. Kane (ed.)* Proc. Cold Regions Hydrology Symposium. Am. Water Resources Association. pp. 283-291.

Hinzman, L.D., D.L. Kane, C.S. Benson, and K.R. Everett. 1991. Hydrologic and thermal properties of the active layer in the Alaskan Arctic. Cold Regions Science and Technology, 19(2):95-110.

Kane, D.L., R.E. Gieck, and L.D. Hinzman. 1990. Evapotranspiration from a small Alaskan Arctic watershed. Nordic Hydrology, 21(4/5):253-272.

Kane, D.L., J.D. Fox, R.D. Seifert, G.S. Taylor. 1978. Snowmelt infiltration and movement into frozen soils. Third International Conference on Permafrost. National Research Council of Canada. pp. 200-206.

Kane, D.L. and J. Stein. 1983a. Physics of snowmelt infiltration into seasonally frozen soils. Proc. Advances in Infiltration, American Society of Agricultural Engineers. pp. 178-187

Kane, D.L. and J. Stein. 1983b. Water movement into seasonally frozen soils. Water Resources Research, 19:1547-1557.

Kane, D.L. and J. Stein. 1983c. Field evidence of groundwater recharge in interior Alaska. Proc.

Fourth International Conference on Permafrost. National Academy Press, pp. 572-577.

Lawson, D.E., S.A. Arcone, J.C. Strasser, A. Delaney, C. Williams and D. Albert. 1994. Geologic and geophysical analyses of permafrost and groundwater conditions, Ft. Wainwright, Alaska. 1993 Progress Report. Prepared for 6th ID, Ft. Richardson, AK, and Corps of Engineers, Alaska District, Anchorage, AK, 28 pp.

Luthin, J.N. and G.L. Guymon. 1974. Soil moisture - vegetation - temperature relationships in central Alaska. Journal of Hydrology, 23:233-246.

Natural Resources Conservation Service. 1994. Alaska Basin Outlook Report April 1, 1994. 29 pp.

Natural Resources Conservation Service. 1995. Alaska Basin Outlook Report April 1, 1995. 30 pp.

Natural Resources Conservation Service. 1996. Alaska Basin Outlook Report April 1, 1996. 31 pp.

Priestley, C.H.B., and R.J. Taylor. 1972. On the assessment of surface heat flux and evaporation using large scale parameters. Monthly Weather Review, 100(2):81-92.

Rouse, W.R. 1976. Microclimatic changes accompanying burning in subarctic lichen woodland. Arctic Alpine Research, 8:357-376.

Rouse, W.R, and R.B. Stewart. 1972. A simple model for determining evaporation from high latitude upland sites. Journal of Applied Meteorology, 11:1063-1070.

Sand, K. and D.L. Kane, 1986. Effects of seasonally frozen ground on snowmelt modeling. *In D.L. Kane (ed.)* Proc. Cold Regions Hydrology Symposium. Am. Water Resources Association. pp. 321-327.

Stewart, R.B., and W.R. Rouse. 1976. Simple models for calculating evaporation from dry and wet tundra surfaces. Arctic and Alpine Research, 8(3):263-274.

Borehole Electrometry for
Monitoring the Active Layer Dynamics

S.A. BOIKOV[1], A.M. SNEGIREV[1], AND A.D. FROLOV[2]

ABSTRACT

To select most effective electrometric borehole techniques for monitoring the active layer and perennial thawing of frozen grounds, field and concomitant laboratory studies were conducted at the geophysical test site in the area of projected water reservoir on the Vilui river in West Yakutia. Stationary installations were devised to test the efficiency of micrologging techniques for measuring apparent electrical resistivity, spontaneous and electrode potentials, and electrode resistance using various measurement modes. This yielded interesting practical results and methodological findings with regard to non-conventional ways of study the active layer dynamics and of the phase interface position spatial and temporal variability.

Key words: Seasonal thawing and freezing , frozen grounds, temperature, resistivity, electrode potentials and resistance.

INTRODUCTION

Borehole thermometry is traditionally regarded as a major technique for studying the dynamics of seasonally thaw and frozen layers (STL and SFL, respectively). This method remains predominant in general monitoring of the cryolithozone and yields fairly reliable data on the position of the thawing front indicated from a commonly distinct transition through 0^0C. However, in the course of freezing, a "zero curtain" may form in a considerable portion of STL when a temperature of 0^0C remains invariable at different depths during a few months. Under such conditions, temperature measurements virtually fail to provide adequate information on the frozen or thawed ground state and the depth of freezing front (Boikov and Snegirev, 1995). Furthermore, the thermometric method proves to be inapplicable to monitor the position of thawing front in saline grounds when their temperature of freezing (or thawing) are not known beforehand.

Various surface- and borehole-based electrometric techniques are currently used to study the depth of seasonal thawing and freezing. The accuracy of land-surface techniques is not high, especially in the case of seasonal freezing measurements. Electrometry in boreholes is more accurate, though it also sometimes fails to provide unequivocal information on the position of the seasonal thaw-freeze front. nevertheless ,electrical parameters of frozen soils , including saline ones , are the most sensitive to phase changes . Therefore ,we have concentrated , our studies just on the elaboration of electrometrical borehole techniques free from thermometry limitations.

Besides tests of various types of borehole installations based on the apparent resistivity (AR) method and others, our studies included development and perfection of less traditional techniques, such as measurement of electrical potentials and resistance between pairs of solid (metal) electrodes. Results of similar studies may be found in a few earlier reports (Parameswaran and Mackay, 1983; Parameswaran and Johnson, 1985). We conducted the studies as perennial observations in the field and laboratory conditions. Some results obtained during several years are presented and discussed in this paper.

[1] Vilui Permafrost Research Station (VPRS) of Melnikov Permafrost Institute, Russian Academy of Sciences, Chernyshevsky, Republic Sakha (Yakutia), Russia
[2] United Scientific Council on Earth Cryology, Russian Academy of Sciences, Fersman Street 13, Moscow, 117312, Russia

SITE AND COMPOSITION OF FIELD WORKS

A hydroelectric power station which is under construction on the Vilui river is situated in the zone of continuous permafrost. Through taliks are developed exclusively under the river bed. The lower cryolithozone horizon is composed by highly mineralized rocks with lenses of highly saline underground waters (solutions) at negative temperatures (cryopegs).

After filling the reservoir with water, the constituent rocks of its bottom and waterside borders will be subjected to an intensive warming impact of water mass that will be conducive to a partial degradation of permafrost, formation of a thawing pan under the water body and activation of other concomitant processes.

The major purpose of comprehensive geophysical studies which are underway at a VPRS base set up in the area of forthcoming flooding is to investigate the temporal and spatial variability of parameters of geocryological section of the waterside border zone under the impact of water reservoir. An important task of geophysical studies consists in the development of methodology and adequate techniques for monitoring the active layer dynamics.

To study the dynamics of seasonal freezing and thawing, several experimental observation sites were set up the VPRS base and equipped to allow a broad range of measurements. These sites are located on terraces I and II above the Vilui flood plain in which the alluvial sediments are represented mostly by fine sands with interlayers of sandy loams and loams. The minimal volume of work to be done at each site includes the following operations: periodic direct measurements of STL thickness with a probe, measurement of STL and SFL thickness with a Danilin "frozen-ground-meter", less frequently by drilling the control boreholes and using a probe with an opening anchor. Geophysical studies in boreholes included regular (at 30- to 3-5-day intervals) measurements of temperature and electrical parameters of soils (ρ_a, R_e, ΔU_e). In some boreholes the moisture of soils was measured recurrently with a neutron meter and less frequently with a γ-densitometer.

DISCUSSION OF RESULTS

Application of various electrometric techniques to study the active layer dynamics provided results which are briefly discussed below.

Determination of Apparent Resistivity (ρ_a)

The application of AR method to study the dynamics of STL and SFL thickness suffers certain restrictions. In particular , relatively small thickness of these layers requires special "microinstallations". Thorough investigation of thin active layer dynamics imposes more rigorous requirements to the depth determination of electrical sensor location in the course measurements and to the quality of electrode grounding. Some problems of this kind are removed by placing into boreholes stationary electrical "plaits" (garlands of electrodes) filled up with ground - buried installations. Examples of systematic ρ_a measurements and some conclusions regarding their informativeness were reported in our earlier paper (Boikov and Snegirev, 1995).

The use of "microinstallations" for ρ_a measurements does not remove a considerable effect of the ground-air interface. The character of ρ_a variation proves to be dependent of the installation type. For deeper parts of the seasonally thawing layer there where obtained practically undistorted ρ_a curves . The relationship between the phase interface position and particular points on the ρ_a variation curve was not always evident. Frequently, the transition from the thawed to frozen state occurs without a sufficiently sharp change of electrical resistivity and masks by the effects of lithology changes, soil moisture gradient etc.. At some fixed depths, the changes in ρ_a magnitude over of annual cycle of measurements are a gradual character (Fig. 1a) without the sharp variations correspond to
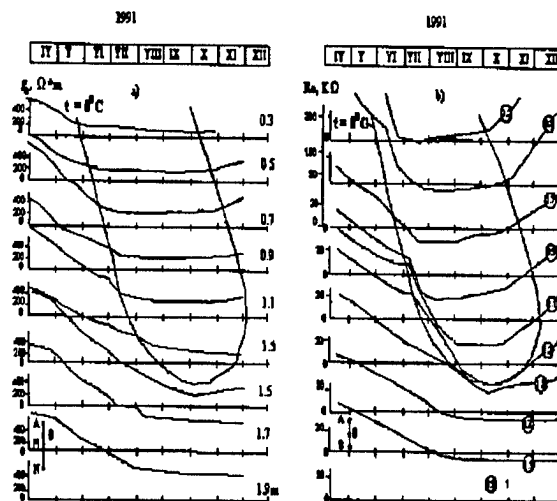
Figure 1. Variation of ρ_a (a) and R_e (b) vs. time and depth during the thawing-freezing cycle. 1.-depth of the installation center.

phase transitions. This was also confirmed by the results of special laboratory measurements during continuous freeze-thaw cycles of samples.

So, in this situation, the only criterion of the thawed state of grounds may be the level of minimal ra values which varies in different lithological horizons and is not known in advance, especially in studies of a progressive thawing.

On the whole, the multipoint character of AR devices (availability of several electrodes) and the commensurability of the interelectrode distance with the thickness of STL and SFL prove to be serious disadvantages of the AR method. In this respect preference should be given to the two-electrode installations. This and some other reasons imply that better prospects for detailed studying the active layer dynamics may are for the techniques based on the use of a single mobile electrode. For instance, the measurements of spontaneous potentials, of electrode potentials and resistance current logging etc.. Some results of such measurements are presented below.

Electrode Resistance (R$_e$)

The practice of permafrost studies gives some examples of frozen ground electrical resistance measurements directly between pairs of electrodes regularly spaced on special probes called "electric-frozen-ground-meters". Measurement of R$_e$ between pairs of electrodes seems to be technically simple and widely accessible for wide use. Special techniques of measurements (observance of equal polarity during current passage, short current pulses, use of stationary reference electrodes etc.) provides for high accuracy and reliable comparability of the results derived from measurements at different time and allows their use to characterize the active layer dynamics.

In contrast to p$_a$, the magnitude of R$_e$ is dependent not only on the electrical resistivity and geometry of the medium but proves also to be largely sensitive to the level of transitive resistance in the electrode-grounding system. Such resistances may display substantial differences in frozen and thawed grounds.

According to long-time observations, the values of R$_e$ during thawing or freezing of grounds vary within a wider range than those of p$_a$. Furthermore, the screening effects of the surface on the R$_e$ magnitude are much weaker, whereas the depth of seasonal thawing displays better correlation with changes in R$_e$. The character of seasonal thawing and freezing of soils is better reflected in the graphs

of R$_e$ temporal variations (Fig. 1b) than in those of p$_a$ (Fig. 1a).

Results of laboratory measurements performed on samples of various soils (including saline ones) are also indicate on a higher sensitivity of the parameter R$_e$ to phase transitions (Fig. 2). In this case,
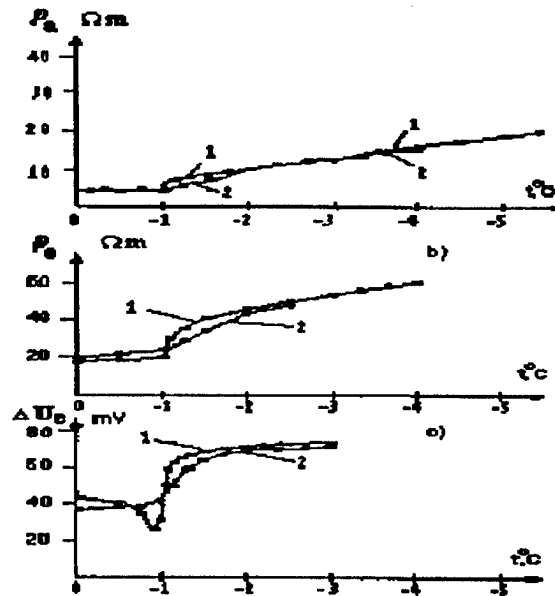
Figure 2. Temperature dependencies of apparent resistivity (p$_a$), electrode resistance (R$_e$) and electrode potentials (ΔU$_e$) during freezing (1) and thawing (2) of saline ground.

compared to the curves of p$_a$ dependence on temperature (Fig. 2a), those of p$_e$ (normalized resistances of the face electrodes R$_e$ relative to the sample length and area) near the point of phase transitions (-1°C) are better differentiated for both freezing and thawing samples and reveal more distinctly the point of phase transitions.

Field measurements of R$_e$ may be performed not only in series for neighboring pairs of electrodes but also between each electrode of an electric plait and the stationary reference electrode. The purpose of reference electrode is usually served by the lower larger (to reduce transitive resistances) electrode of the electrical plait. Such way of measurement ensures maximal removal of screening effects and, that is the most important, offers the possibility of unequivocal comparison of measured R$_e$ values with temperature in the same point. Figure 3a shows an example of different measurement modes and demonstrates that measurements reference to the lower electrode provide a sufficiently distinct

delineation of the phase interface position, despite a varying level of R_e , especially within the STL limits.
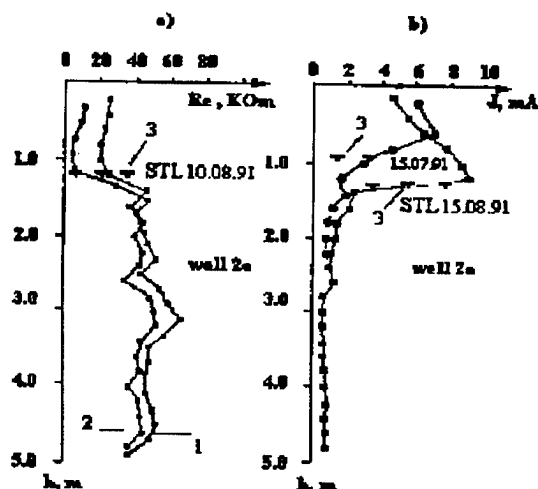
Figure 3. The character of changes R_e and I magnitudes with depth during of active layer thawing.
1. Measurement of R_e between pairs of electrodes.
2. Measurement of R_e relatively a stationary reference electrode.
3. Position of the STL sole at the moment of measurement.

Electrical Current (I)

Our experiments on the measurement of electric current (I) yielded definitive positive results, though it has not yet been included in the program of systematic observations. The curves of current (I) variation as a function of depth are essentially a mirror reflection of R_e curves which is globally confirmed by respective measurements, although the use of different technical means for measuring R_e and I brings in differences of the curve shapes (Fig. 3a,b).

The preference given by us to R_e measurements is also explained by the fact that R_e is a parameter which, similarly to ρ_a, reflects more objectively the state of medium. Statistical processing of the results of ρ_a and R_e measurements revealed a close correlation of these parameters with temperature and between themselves. An example shown in Fig. 4 demonstrates that different (linear and logarithmic) approximations of ρ_a, R_e and t values measured during annual observation cycle provided high values of correlation coefficient r^2 amounting to 0.77, 0.86 and 0.88 for $\rho_a = f(t)$, $R_e = f(t)$ and $\rho_a = f(R_e)$, respectively.
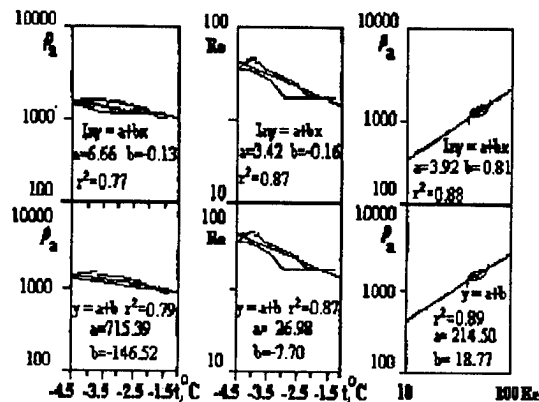
Figure 4. Regressive dependencies between temperature (t), apparent resistivity (ρ_a) and electrode resistance (R_e), depth 4.3 m; observation period: 13.05.92 to 12.04.93.

Spontaneous (ΔU_S) and Electrode Potentials (ΔU_e).

Interesting data on the changes of spontaneous potentials (SP) at the STL sole ranged up to a few tens millivolts were obtained in the cryolithozone conditions for estimating the possibility of differentiation of frozen and thawed grounds in geocryological sections (Melnikov, 1979).

Despite the apparently bright prospects of SP method, its use in systematic borehole observations does not seem be realistic, because its application is based on the use of nonpolarizable electrodes with liquid electrolyte which not suitable for long-time measurements. Continuous use of electrolytes in boreholes may be conducive to a substantial "pollution" of the soils under study, change its basic electrical parameters and even perturb certain natural processes. From the technical viewpoint, it seems impossible to establish an entire network of annually functioning nonpolarizable electrodes with stable parameters.

In our studies the SP method was used for the test measurements some results of which are shown in Fig. 5a. These results were obtained are with a nonpolarizable copper electrode moving along a borehole and the measurements were realized relatively an analogous reference electrode placed at depth of about 25 m. Curve 1 (Fig. 5a) represents measurements at the moment of maximal thawing depth , which was equal to 1.8 m, whereas curve 2 reflects the state of total STL freezing. In both curves the STL sole is characterized by relatively

271
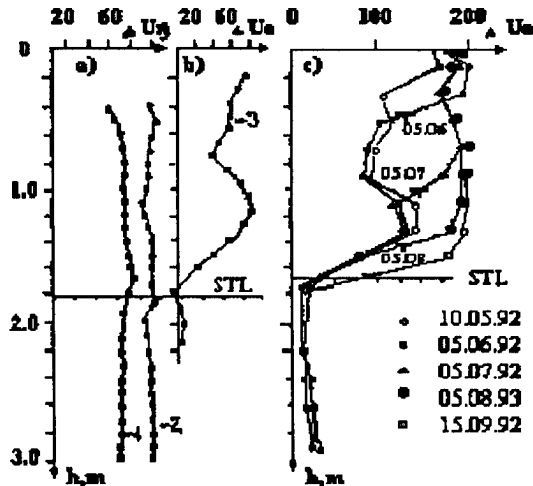
Figure 5. Comparison of spontaneous (a) and electrode (b, c) potentials in the sole of the seasonally thawed layer.

small changes in ΔU_s. At the same time, along curve 3 (Fig. 5b) the STL boundary remains clear-fixed even at the time of its total freezing.

Measurements of electrode potential differences (ΔU_e) between solid metal electrodes installed in ground filled boreholes have also proved to be effective (Fig. 5c). In most electrical garlands there were lead electrodes, but we also tested copper, brass and steel ones. At initial stages of our studies, each garland carried its own lower larger (to reduce contact resistance) reference electrode. Subsequently, measurements were performed relatively two reference electrodes - a nonpolarizable copper electrode and a metal lead one placed under stationary temperature conditions in the sole of the layer of annual temperature oscillations (depth of about 25 m).

In the measurements of electric potential differences generated by pairs of metal electrodes, of crucial importance are the distinction in grounding conditions of them. There were soil dispersiveness and mineral composition, ionic composition and concentration of soil saturating solutions and, basically, the frozen or thawed state of the - contacting medium.

The graphs representing measurements of (lead) electrode potentials in Fig. 5c illustrate a highly informative character of this method in studies of the dynamics of seasonal thawing and the possibility of determination of the STL thickness at the moment of its total freezing.

Figure 6a shows examples of changes in potentials of lead electrodes during the yearly period

of systematic observations. Let us try to formulate the basic regularities of these curves changes as a function of time.

The results presented in Fig. 6a reflect measurements of electrode potentials relatively a reference electrode placed in the frozen portion of geologic section. When the time goes from the winter to spring and to summer seasons a progressive decrease in ΔU_e values is observed in conformity with the increasing temperature of
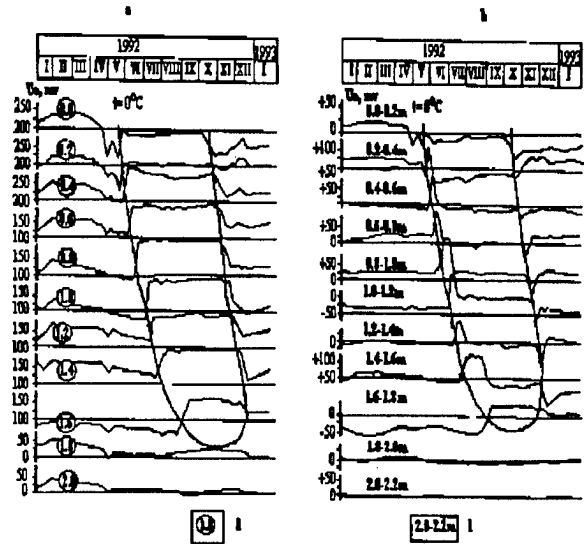
Figure 6. The character of electrode potential variation as a function of depth and time during an annual observation cycle.

grounds. Subsequent thawing of ground near the electrode induces a dramatic rise of ΔU_e values with an amplitude of their increment ranging from 50 to 100 mV. These values remain high with slight variations throughout the entire period of thawed ground state until the onset of ground freezing. When the ground is freezing near the electrode, the values of ΔU_n drop sharply, though the amplitude of their decrease is somewhat lower than in the case of thawing. Subsequent cooling of the frozen ground induces its structural -phase transformations which in turn are conducive to a gradual or stepwise growth of ΔU_e to its winter maximum. Below STL, the ΔU_e curves display only very slight oscillations.

Thus, analysis of changes in electrode potentials with time at different depth makes it possible:
- to delineate unequivocally the portion of geological section affected by phase transitions and to determine the maximal STL thickness;
- to fix clearly the times of ground thawing and freezing at the depth of electrode situation;

- to note the total coincidence of the results of electrometric and temperature measurements, when the latter may be unequivocally interpreted;

- to state that the electrometric measurements of ΔU_e data are more informative than the thermometric ones for the period of "zero curtain";

- to see that the error in establishing the phase interface position in the section is determined by the distance between sensors and does not exceed ±0.5 of this magnitude.

In the case when there are industrial interferences, considerable variations of natural electric field, instability of reference electrodes and other effects, it is advisable to represent the measurement results as the potential differences between next electrode pairs (Fig. 6b). Owing to the similarity of conditions into which each pair of electrodes is placed (composition, moisture, temperature etc.) the differences in the magnitude of electrode potentials at the same phase state of ground are minimal and stable in time. The maximal potential differences in a next electrode pair arise when the phase interface passes between them, i.e. one electrode proves to be in the thawed ground portion and the other in the frozen one. Than the seasonal thawing induces formation of a positive ΔU_e anomaly, whereas the downward and upward freezings generates negative and positive anomalies, respectively.

Figure 7 shows a low sensitivity of ΔU_e values to
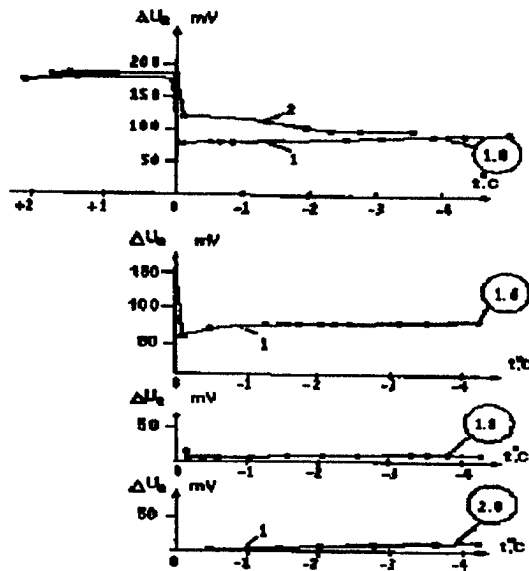
Figure 7. Temperature dependence of electrode potentials during freezing (1) and thawing (2). Numerals at respective curves indicate the depth of measurements.

temperature changes both in frozen and in thawed ground state and the crucial role of the ground phase state changes near the electrodes. In these circumstances the jump of ΔU_e occurs within a very narrow temperature range, basically within the limits of 0.1 to 0.2^0C that in principle allows the use of this method irrespective of temperature measurements. An analogous sharp character of ΔU_e changes in points of phase transitions was also established in laboratory studies of saline ground samples (Fig. 2c). This is indicative of a good perspective for the use of the electrode potential method possibly jointly with thermometry in studies of phase transitions in saline grounds too, because concomitant measurements of ΔU_e and t^0 allow the determination of both phase transformations and temperatures of phase transitions.

CONCLUSION

Most of the electrometric techniques discussed above are a highly effective for measurements of the STL thickness, whereas the transient positions of the STL boundaries are determined less reliably. This circumstance may be explained by the fact that the STL sole is the most contrasting electrical boundary that is also associated with the specifics of the composition of STL constituent soils under their long-term processing in freezing-thawing cycles, formation of ice-rich layers at the interface between STL and the underlying frozen grounds etc. This contrast may also be preserved to some extent under winter conditions during STL freezing that affects differently the results derived by different electrometric techniques. Under freezing conditions the STL sole is most reliably determined through measurements of electrode potentials.

Summarizing the results of our studies, we should note that, when taken separately, none of the discussed geophysical methods is universal in relation to such a complex and dynamic system as the active layer. Nonetheless, the method of electrode potentials and the thermometry may be regarded as priority techniques in such studies.

REFERENCES

Boikov, S.A. and A.M. Snegirev. 1995. Assessment of the informativeness of different electrometric techniques in studies of the dynamics of seasonal freezing and thawing. p. 166-185. *In* A.D.Frolov

(ed). Geofizicheskie issledovaniya kriolitozony (Geophysical Studies of the Geocryolithozone) no. 1, Moscow.

Melnikov, V.P. 1978. Seasonal variability of natural electric field during freezing and thawing of the active layer. Deposited at VINITI at no. 3305-78, Moscow.

Parameswaran, V.R. and J.R. Mackay. 1983. Field measurements of electrical freezing potentials in permafrost areas. p. 962-967. *In* Permafrost Proceedings. Fourth Int. Conf., Alaska, National Acad. Press, Washington, USA.

Parameswaran, V.R. and G.H. Johnson. 1985. Electrical potentials developed during thawing of frozen ground. p. 9-15. *In* Proceedings of Fourth Int. Symp. on Ground Freezing, Sapporo, Japan.

Snow

Some Features of Mechanical Property Changes During Snow Densification

A.D. FROLOV[1] AND V.N. GOLUBEV[2]

ABSTRACT

On the basis of experimental data analysis on elastic moduli of snow and of theoretical simulation, there were obtained and grounded the critical densities of ≈ 130, ≈ 330 and ≈ 550 kg/m^3. These densities limit the transitive states of dry coherent snow that arose during densification. Each transitive state is characterized by its own dominant mechanism of medium structural reorganization and completed by definite degree of new ordering, i.e. by increase of coordination number of snow grain packing. The regularities of snow mechanical properties changes are different for each transitive state and it is impossible to describe them by one universal function with the same error for the whole snow density range.

Key words: critical densities, snow elastic moduli, microstructure, coordination number.

INTRODUCTION

During snow densification and diagenesis the structural transformations cause significant changes in their elastic, strength and other properties. Practically between all physical properties of dry coherent snow and it structure there are correlations (Arons and Colbeck 1995). The mechanical properties have been chosen as an illustrative example cause their high sensitivity to structural changes of snow medium. So, the moduli of elasticity increase by several orders from downy snow to massive ice. Snow densification involves complete reorganization of medium structure, occurrence of the new spatial ordering in arrangement of the grains and formation between them of more and more rigid bonds. It is unlikely possible to imagine these transformations as monotonous process.

Two critical densities of ice formations, ≈ 550 kg/m^3 and ≈ 820 kg/m^3, are well know. The first characterizes a limiting state of a dense dry coherent snow or its transition to firn, and the second - a transition of firn in porous ice with closed pores. Thus, these two critical densities limit a transitive state from snow to ice with one dominant mechanism of densification and formation of new structural order. In the density interval ≈ 820-917 kg/m^3 the dominant mechanism that is responsible for transformation of porous ice to the massive one should be other. However, whether the similar transitive states of snow at the density < 550 kg/m^3 are available and also limited by some critical densities (narrow intervals of densities) remains unclear. The purpose of this study is to reveal critical densities for snow and to compare them with the theoretical estimations of structural transformations, achieved on the basis of regular grain packing model. The data on critical densities will be useful for a comprehension of the correct way to determine the snow physical property change regularities. These knowleges are necessary for solve the problems of snow cover dynamics and of it impact on freezing and thawing of active layer. The main results obtained are discussed in this paper.

BACKGROUND

Basis of our hypothesis is that the structural changes of dry snow during densification should

occur by means of diverse dominant mechanisms of ordering in the different density intervals of medium. Hence, the whole range of density from powder snow to massive ice should be subdivided into a number of subranges which are characterised by different prevailing mechanisms of structure transformation. Borders of these transitive states should be the critical densities (narrow density intervals), at which the formation of certain order of structure ends, a transition to the next stage begins, with other prevailing mechanism of densification, finishing by a new more perfect structure ordering. Such transitions of snow-ice medium from one state to another are possible to consider as structural analogy of phase transitions of the second type. At the critical densities a degree of medium spatial ordering (structural entropy) and rigidity of structure apparently reach some boundary values. Respectively there is the modification of the dominant mechanism of structure formatting and of the mechanical property changes.

As the moduli of elasticity and strength characteristics of a snow medium are structurally sensitive parameters, they were chosen for the analysis and theoretical modelling. It is best to estimate the dynamic characteristics of elasticity without destruction of the medium by use the seismic-acoustic techniques. Many researchers have studied the acoustic properties of snow-ice formations in various density intervals (see reviews Mellor 1977, Voitkovsky 1977). Usually, the authors aspired to present the laws of property changes as a continuous (linear or nonlinear) function of snow density and extended them to a wide density range. The elastic properties of snow with small densities ($<$300 kg/m^3) are much less studied, compared to dense snow. Traditionally the experimental data on investigated parameters of snow physical properties are presented as a function of density (ρ) or porosity (P) of medium (for instance Kohnen 1972, Mellor 1977, Voitkovsky 1977). Frolov and Fedyukin (1996a) established that the better comparative parameter, allowing more precisely to allocate the boundary states of structural transformations is porosity factor K_p , equal to the ratio of pore volume V_e (emptiness)to volume of solid part of medium V_c :

$$K_p = V_e / V_c = P / (1-P) = (\rho_i / \rho_s) - 1$$

where: ρ_i = 917 kg/m^3 - density of massive ice. The K_p magnitude for ice formations changes from 0 (massive ice) up to 20-30 (powder snow ρ_s $<$30-50 kg/m^3). According to the theory of globular grain media a factor K_p is connected closer to the medium structure as compared with a density. Further

analysis considers elastic, strength and structural characteristics changes of a snow medium as the functions of K_p.

TECHNIQUE

As a basis for the analysis we have chosen the data on propagation velocities of longitudinal V_p and shear V_s elastic waves obtained by seismic method in Greenland and Antarctica by Kohnen (1972) (from 300-350 kg/m^3 up to ice density) and our data for snow from 30-50 kg/m^3 up to 500 kg/m^3 resulting from seismic and acoustic studies in Kolsky Peninsula. In result has been obtained over the averaged data on velocity values for the whole density range from dry powder up to massive ice (Frolov and Fedyukin 1996a). We did not consider the velocity dependence of ice formations on moisture content and temperature. All dynamic moduli were calculated by use the formulas of the theory of elasticity of continuous medium. Certainly, for very friable snow the absorption factor of elastic oscillations grows by the order, and instantaneous cohesion of snowfalls according to measurements up to 10^{-3} - 10^{-4} kg/cm^2. Such medium already requires a nonelastic model, therefore the obtained values of dynamic moduli of elasticity in the field of small density are less reliable. But to search the snow for critical densities and to establish the common laws the elastic approximation is quite acceptable. The comparison of our generalizations with other published data (Mellor 1977, Voitkovsky 1977 and others) has not revealed contradictions. The statistical analysis shows that the changes of acoustic and elastic parameters cannot be described by one smooth function with an identical error in the whole density range, including a polynomial of reasonable order (up to fifth). This confirmed our hypothesis and expediency of critical densities search.

For the analysis of structural transformations and theoretical estimation of changes connected with the mechanical properties, the model of regular packing of grains in the form of spheres and polyhedrons of the certain forms, having among themselves rigid bonds were accepted. In the first approximation, assuming identical size of the grains and their regular distribution in the volume of medium, the model allows estimate of mechanical properties of snow-ice formations. These estimations based on certain parameters of structure and appropriate properties of massive ice (Golubev 1981). The basic parameters of structure are: a) coordination number i, determined by amount of the nearest grains directly bounded with a central grain, b) parameters of medium friability (K_s

=L/D) and of rigidity (b_s =d/D), where D - average size of the grains, L - average distance center to center of the contacting grains, and d - the average linear size of the contact area. The process of snow densification is examined as a regular change in the grain packing, accompanying with respective alteration of the magnitudes: i, K_s and b_s . Surely, there are various correlations between the structural parameters for snow of a certain density. The analysis of the possible variants of the various form grain contacts allows to establish the most probable ratios of parameters K_s and b_s and to estimate coordination number i of structure for snow of various densities, using expression describing the of snow density as a function of these parameters (Golubev 1981). In this paper there are also the analytical expressions allowing estimation of the module of elasticity E_s, Poisson's ratio v_s and tensile strength σ_s of snow through it parameters of structure and appropriate properties of ice:

$$E_s, V_s, \sigma_s = E_i, V_i, \sigma_i \cdot F_{1,2,3}\left(i, K_s, b_s\right)$$,

where the index "i" means the appropriate properties of massive ice. Calculations using these equations allow us to establish the probable ranges of E_s, v_s and σ_s changes at various densities of snow.

RESULTS AND DISCUSSION

Representation of the acoustic and elastic characteristics of snow-ice formations as a functions of K_p and analysis of their first and second derivatives have revealed (Frolov and Fedyukin 1996 a,b) a series of critical densities including two known earlier: r = 130-160 kg/m^3 , r = 330-360 kg/m^3 , r = 530-570 kg/m^3 , r = 820-840 kg/m^3 ,and r = 700-720 kg/m^3 ,which is allocated much less precisely. Figure 1 shows the appropriate dependences for Poisson's ratio and Young modulus normalized by their values for massive ice (E_i = 10 GPa, v_i =0,34). Dependence for the shear module is the same, as for E_s at G_i = 3,7 GPa. The values of critical densities obtained using the functions of various parameters differed a little in the above mentioned limits - narrow intervals of their meanings. This series of critical densities divides all variety of dry coherent snow-ice formations on the set of transitive states. There has appeared possible universal approximation of law of the mechanical properties change by smooth functions, as:

$$lg Y = b_i \cdot lg K_p + b_2$$
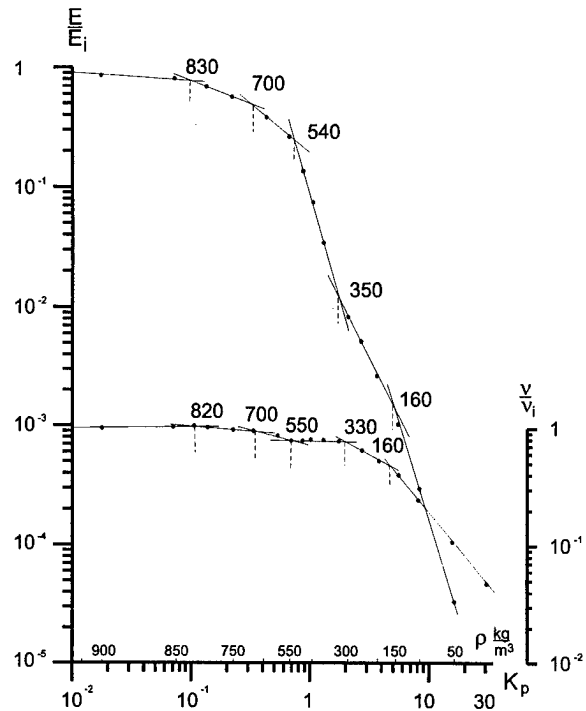
Fig.1. Average experimental data on elastic Young's modulus E and Poisson's ratio v of snow-ice formations v.s. porosity factor K_p ; E_i and v_i - values for massive ice.

where Y - average magnitudes of the longitudinal V_p and shear V_s of elastic waves propagation velocities, or corresponding them acoustic resistivities Z_p and Z_s or various moduli to elasticity (E, G, K, λ). Calculation of the coefficient b_1 and b_2 of these equations has allowed to establish quantitative distinctions in medium properties changes for the different transitive states. For real snow there were obtained three transitive density subranges: $\approx$ 30-150 kg/m^3 , 150-350 kg/m^3 and 350-550 kg/m^3 . The first corresponds to downy friable snow practically without space regular structure, the second - to friable granular snow in the course of structuring and the third - to well structured dense snow, the properties of which are the most investigated.

These data are compared to the results of numerical simulations, carried out the basis of regular grain packing model. At the first stage it was necessary to estimate the most probable magnitudes of the structural parameters at various densities of medium. Figure 2 shows probable intervals of these parameter values as a function of porosity factor K_p .

The intervals are established from analysis of the possible contact variants of spheres, cubes and rhombododecahedrons. Use of porosity factor is more

277
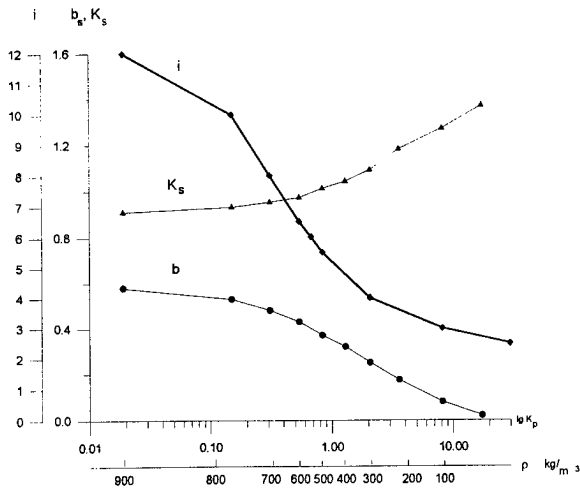
Fig.2. *Structural parameters (i, K_s and b_s) of snow-ice formations vs. porosity factor K_p.*

convenient for the analysis of physical properties and structural peculiarities of snow.

Presented curves allocate several snow density subranges in limits of which the laws of structural parameters changes are modified, which is especially displayed at the second derivatives analysis. The changes of law of coordination number i increase during snow densification are obtained near by following values: $\approx$ 130, 330, 550, and 830 kg/m^3 and for parameter of rigidity b_s at the densities about 100 and 730 kg/m^3. Decrease of structure friability parameter K_s becomes less intensive at the density about 550 kg/m^3. Table 1 presents the most probable

Table 1. Probable correlations between snow density and structural parameters

Coordination number	K_s	b_s	Density ρ_s kg/m^3
3	1.1 - 1.3	0.1 - 0.3	130 ± 40
4	1.0 - 1.3	0.2 - 0.4	320 ± 40
6	0.9 - 0.5	0.3 - 0.5	550 ± 40
8	0.9 - 0.95	0.4 - 0.6	690 ± 40
10	0.9	0.4 - 0.6	810 ± 30
12	0.9	0.5 - 0.6	890 ± 30

correlations between the magnitudes of structural parameters and density of snow. The correlations were obtained on the basis of analysis of the regular packing grains of the certain geometrical forms and confirmed by special studies of natural snow . The values of coordination number i correspond to friable hexagonal pacing (i = 3), tetrahedral (i = 4), cubic (i =6), octahedral (i = 8) and to various kinds of the dense hexagonal grain packing (i = 10-12)

Critical narrow density intervals (Table 1) characterizing the formation of a new snow medium order hence a modification of structural parameters changes appeared in a good conformity with above-mentioned critical densities determined from acoustic and elastic characteristics.

Then, we estimated, theoretically, the intervals of Poisson's ratio v_s , Young's modulus E_s and tensile strength σ_s values depending on the changes of structural parameters during snow densification. Figure 3 demonstrates the results as a function of snow porosity factor K_p . Changes in the dependence
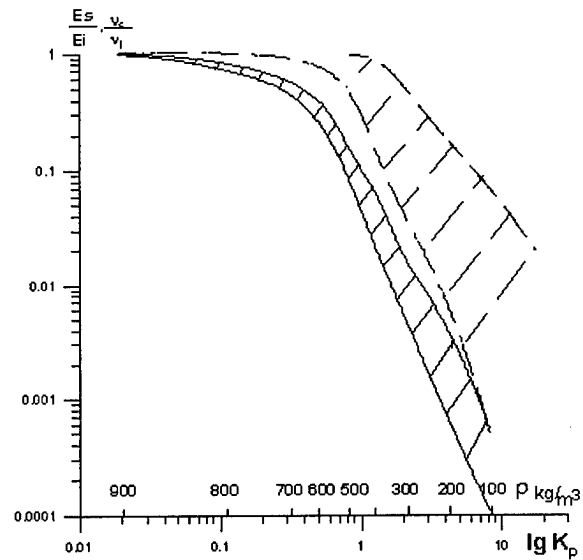
Fig.3. *Results of theoretical estimation of modulus E (solid lines) and Poisson's ratio v (dashed lines) of snow-ice formations (probable magnitudes).*

character of the elastic modulus E_s are tied to the values of density 300-350 kg/m^3 and 700-800 kg/m^3, and the second derivative of E_s changes the sign close to 550 kg/m^3 . It corresponds to average values of the structure coordination numbers i, which equal 4, 6 and 8-10, i.e. transition from friable to more dense packing. Practically in the same intervals are marked the changes of snow tensile strength (Golubev 1982). The appreciable changes of dependence character of Poisson's ratio obtained at 150-250 kg/m^3 and 550 kg/m^3 , i.e. when the coordination number i is equal 3 and 6. The snow tensile strength σ calculated with use of structural parameters values (indicated in Table 1) and of the elastic modulus for massive ice is in good correlation with results of experimental research and is equal for three snow critical densities, $4 \cdot 10^2$ Pa, $6 \cdot 10^3$ Pa and $1,2 \cdot 10^5$ Pa respectively.

278

CONCLUSION

The good correlation of experimental and analytical estimations of E_s, v_s and σ_s allows us to consider the offered model of regular grain packing as sufficiently adequate to real dry snow for estimation of its mechanical and other properties. Allocated critical densities, limiting the transitive state intervals during snow densification is necessary to take into account the analysis and description of the densification mechanisms and changes of mechanical properties of snow. The approximations described in this paper are quite applicable for forecast estimations of the acoustic characteristics, elastic moduli and tensile strength of dry coherent snow using its density values. The described approach are also available for the similar estimations of thermal and other properties of snow with different densities. All these properties are important for solution the problems of snow cover dynamics and it influence on soil seasonal freezing and thawing.

REFERENCES

Arons E.M. and S.C.Colbeck 1995. Geometry of heat and mass transfer in dry snow: a review of theory and experiment. p.463-493. v.33, N4. AGU., USA.

Frolov A.D. and I.V.Fedyukin. 1996a. Acoustic characteristics of snow-ice formations in the density range from 30 To 917 kg/m^3. p. 181-184.. *In* V.S.Yamtshikov, (ed.) Problems of Geoacoustics: techniques and tools. Proceedings of V-th Session of Russian Acoustic Society. Moscow.

Frolov A.D. and I.V.Fedyukin. 1996b. On the regularities of elastic properties changes in the snow-ice formations from 30 To 917 kg/m^3. p.72-73. Intern. Symp. on Phys. and Chem. of Ice, Hanover, New Hampshire, Abstracts. USA.

Golubev V.N. 1981. The dependence of elastic properties of snow from structure. p.65-72. Data of glaciological studies, N44. Moscow.

Golubev V.N. 1982. The influence of snow structure on its mechanical properties. p.109-113. Data of glaciological studies, N45. Moscow.

Kohnen H. 1972. On the relation between seismic velocities and density in firn and ice. p.925-935. Zeitschrift für Geoph. Band 38, Würzburg, Germany.

Mellor M. 1977. Engineering properties of snow. p.15-66. Journ. of Glaciology, v.19, IGS, Cambridge, England.

Voitkovsky K.F. 1977. Mechanical properties of snow. 126 p. Nauka, Moscow.

Ablation of Shallow Seasonal Snowcovers

K. SHOOK[1] AND D.M. GRAY[1]

ABSTRACT

Shallow snowcovers of open environments disintegrate into a mosaic of patches of snow and bare ground when they ablate. This disintegration affects the geometry and area of snowcover, which control the contributing areas of melt, runoff, infiltration and soil water recharge, and the energetics of the melt process. This paper discusses: (a) the effects of snow patchiness on areal albedo and the small-scale advection of sensible energy and (b) the synthesis of a patchy snowcover by applying melt fluxes to the frequency and spatial distributions of the snow water equivalent.

Key words: snow, melt, ablation, patchy snowcover, albedo

INTRODUCTION

Snowmelt involves the change of phase from ice to liquid water, and therefore the energy equation is the physical framework for calculating snowmelt. When the equation is applied to a control volume of snow, the fluxes of energy penetrating the snow surface and retained by the volume may be expressed as changes in internal energy. The volume has as its lower boundary the snow-ground interface and as its upper boundary the snow-air interface.

The energy equation requires that the amount of energy used for the phase change plus the sum of the fluxes transferred to the volume by radiation, convection, conduction, and advection must equal the change in internal energy. That is, in the vertical direction

$$Q_m + Q_n + Q_h + Q_e + Q_g + Q_a - \frac{\Delta U}{\Delta t} = 0, \quad (1)$$

where Q_m = energy available for snowmelt
Q_n = net radiation
Q_h = turbulent flux of sensible heat exchanged at the surface due to a difference in temperature between the surface and overlying air
Q_e = turbulent flux of latent energy exchanged at the surface due to vapor movement as a result of a difference in vapor pressure between the surface and overlying air
Q_g = ground heat flux due to conduction
Q_a = energy due to vertical advection such as heat added by falling rain and
$\Delta U/\Delta t$ = rate of change of internal (stored) energy in the volume of snow per unit surface area per unit time.

In applying eq. 1, the fluxes of energy directed towards the control volume are taken as positive; those directed away from the volume are negative. Daily melt, M (mm), is calculated from Q_m (W/m^2) by the expression:

$$M = 0.270 Q_m. \quad (2)$$

Shallow snowcovers of open environments disintegrate, forming mosaics of patches of snow and

---

bare ground, as they melt. This disintegration complicates the application the energy equation because of the changes that occur in the geometry and area of snowcover; therefore in the contributing areas of melt (and runoff and soil water recharge) and in the energetics of melt. The last are brought about mainly by alterations to the albedo, temperature and roughness of the ground surface, which affect primarily the flux of net shortwave radiation and the small-scale turbulent transfers of sensible energy from snow-free to snow-covered areas. Proper modelling of snowmelt of a patchy snowcover requires that the effects of these variations be considered in the simulation.

This paper discusses the interactions of snow patchiness with areal albedo and the advection of sensible heat from snow-free patches to adjacent patches of snow. It is demonstrated that the areal depletion in snowcover can be synthesized by applying melt fluxes to the spatial distribution of the snowcover water equivalent. The relative contributions of melt by net radiation, large-scale and small-scale advection at various stages during the ablation of a shallow snowcover are demonstrated.

INFLUENCE OF PATCHES ON AREAL ALBEDO AND SMALL-SCALE ADVECTION

Areal Albedo

The depletion in snow-covered area that accompanies the melt of a shallow seasonal snowcover decreases the areal albedo. This decrease is due to (a) the increase in area of bare ground with low albedo and the corresponding decrease in the area of snow with high albedo, and (b) changes in structure and composition of the snow (becoming thinner, wetter, dirtier, etc.). For ablating, shallow seasonal snowcovers of the Canadian prairies, the association between areal albedo and snow-covered area is approximately linear over large ranges in area (Shook 1993). The data in Figure 1 exemplify this trend. The upper limit of albedo is established primarily by the average albedo of the snow surface following the start of melt, the lower limit is set by the average albedo of the snow-free ground surface.

A linear association between areal albedo and snow-covered area provides a simple model for simulating changes in albedo in snowmelt simulations. The relationship implies that the snow albedo does not vary greatly during ablation and that the major factor controlling the decay in areal albedo is the fraction of bare ground. It is assumed that the

areal albedo of a partially-ablated, shallow snowcover, A, is the sum of the individual reflections of solar radiation by the snow and soil patches. Therefore, a simple expression for A as a function of the albedo of snow, A_{sn}, the albedo of the snow-free ground, A_g, and the fraction of snow-covered area, f_{sn} is:

$$A = A_{sn} f_{sn} + A_g (1 - f_{sn}).$$ (3)
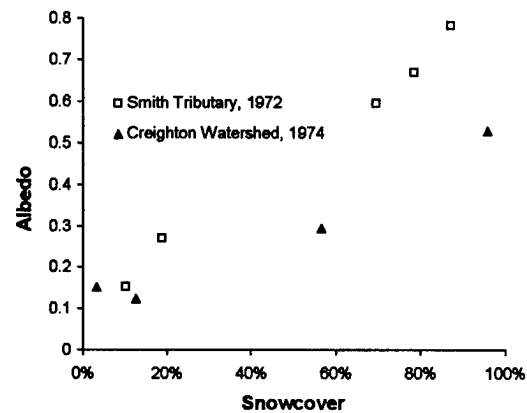
Figure 1. Relation between areal albedo and area of snowcover monitored on two small watersheds in southwestern Saskatchewan during snow ablation in 1972 and 1974.

Fitting a linear regression to the data for the Smith Tributary in Figure 1 gives an intercept of 0.096 and a slope of 0.75 with a correlation coefficient, $r^2 = 0.99$. The corresponding values for the albedos of ground and snow by eq. 3 are $A_g = 0.096$ and $A_{sn} = 0.85$, respectively. A similar analysis applied to the measurements for the Creighton Watershed gave the corresponding statistics: intercept = 0.095, slope = 0.42, $r^2 = 0.95$, $A_g = 0.095$ and $A_{sn} = 0.52$. The lower albedo for snow on the Creighton Watershed is due to a shallow, dirty snowcover and underlying vegetation protruding through the snow. The results of these analyses confirm that changes in the reflectance of snow during ablation are small and have very little effect on the areal albedo of a patchy snowcover.

Before concluding the discussion of areal albedo, it is pertinent to mention that field experience has demonstrated that in flat, open environments there is often a high correlation between areal and point estimates of albedo (O'Neill 1972; Shook 1995). Areal albedo estimates are determined from airborne sensors, point values are calculated from measurements of reflected shortwave radiation made by inverted hemispherical radiometers. The similarity of the point and areal

281

measurements can be explained by the fractal properties of snow. "Point" measurements of reflected shortwave radiation are averages over a small area. As snow is fractal, i.e., self-similar in its spatial distribution, bare ground will be found throughout the area of a partially ablated snowcover that is included within the field-of-view of an inverted hemispherical radiometer. The increasing presence of bare ground explains the large decline in measured albedo without requiring a corresponding decrease in albedo of the snow surface. Likely, point estimates can be used to establish reasonable approximations of the association between areal albedo and snow-covered area.

Small-scale advection and the transfer of sensible energy

When a snowcover becomes patchy, the horizontal transfer of energy due to the movement of air from patches of bare ground to adjacent patches of snow becomes increasingly important to melt. Usually, the melting of small patches of snow is dominated by turbulent energy fluxes until they disappear, whereas melting of large snow fields is dominated by radiation fluxes early in the season and by turbulent fluxes late in the season as they decrease in area.

For patchy snow covers, standard methods for calculating the turbulent transfers of sensible and latent heat must be applied with caution since they assume a vertical, one-dimensional flux and therefore cannot be used near the edge of a patch. A more accurate approach is to calculate the sensible and latent transfers by two- or three-dimensional models that consider the development of the boundary layer beginning at the leading edge of snow.

Figure 2 plots measurements of air temperature monitored at heights of 2 cm and 40 cm over a patchy snowcover. These data show the air temperature at 2 cm responding more rapidly to the presence of patches of snow or bare ground than the temperature at 40 cm. Over ground, the temperature at each height stabilizes and becomes reasonably constant at fetch distances between 2 and 5 m. The rapid stabilization in temperature with fetch suggests that (a) most of the sensible heat transfer occurs along the leading edge of snow, and (b) a field-averaged measurement of the surface temperature of soil patches is likely to be a fairly good approximation of the surface temperature upwind of a snow patch.
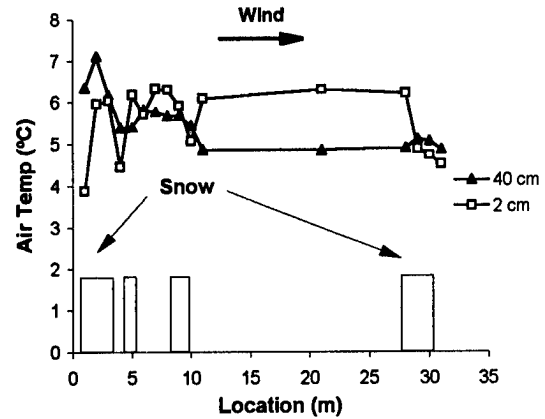
Figure 2. One-minute average air temperature at 2 and 40 cm over a patchy snow cover monitored at Trail Valley, NWT, 28 May, 1993.

An approximation of melting of a patchy snowcover due to small-scale advection is described by Weisman (1977). This model assumes that (a) the snowcover is ripe (saturated with meltwater) and isothermal at 0 °C and (b) outside the snow-patch boundary layer the airflow is unaffected by the snow; i.e., the atmospheric wind, humidity and temperature profiles are similar to those immediately upwind of the snowpack. Weisman's approximate solution relates the dimensionless melt energy at a point ($\hat{M}'$) as a function of the dimensionless fetch ($\hat{x}$) downwind of the leading edge:

$$\hat{M}' = a\hat{x}^{-b} \tag{4}$$

where a, b = parameters whose magnitudes depend on atmospheric stability (values tabulated by Weisman 1977)

$\hat{x}$ = dimensionless distance downwind = x/z_0, where z_0 is the roughness height (m).

Conversion of the dimensionless melt, $\hat{M}'$, of eq. 4 to a dimensional melt energy, M', is accomplished by multiplying $\hat{M}'$ by the energy flux at the leading edge of the snowpack:

$$M' = \hat{M}'\left[\rho\, u_{*a}\, c_p\left(T_s - T_a^0\right) + \rho\, u_{*a}\, h_v\left(q_s - q_a^0\right)\right] \tag{5}$$

where: ρ = density of air (kg/m^3)

c_p = specific heat of air (J/kg °C)

h_v = latent heat of vaporization of water (J/kg)

T_s = temperature of snow surface (°C)

282

T_a^0 = temperature of soil upwind of the patch (°C)

q_s = specific humidity of air at snow surface (dimensionless), and

q_a^0 = specific humidity of air at soil surface (dimensionless).

An example of the variation in the small-scale turbulent flux with fetch distance determined by Weisman's approximation is shown in Figure 3. This curve was constructed using field measurements made on 11 March, 1996, over a patch of snow located in a flat field of summerfallow near Saskatoon, SK. The data show the flux decreasing from 188 W/m² at 0.1 m from the leading edge of snow to 141 W/m² at 1 m, 106 W/m² at 10 m and to less than 80 W/m² for fetches greater than of 100 m.
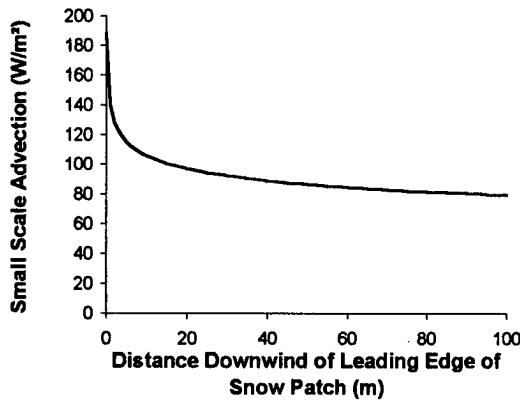
Figure 3. Variation in small-scale advective flux with fetch distance over a single snow patch, estimated by Weisman's approximation. Hydrometeorological data monitored on a patchy snowcover on a field of summerfallow near Saskatoon, SK, on 11 March, 1996.

Figure 4 compares estimates of melt by small-scale (Weisman) and large-scale (associated with the movement of large, warm air masses) advective fluxes during the ablation of a shallow snowcover on a flat field of fallow near Saskatoon, SK, in 1994. Both advective fluxes were estimated from field measurements The data show that the contribution to melt by small-scale advection reaches a maximum rate at the end of ablation when the area of snowcover is small and the daily net radiation and maximum air temperature are high (see Figure 5). Under common meteorological conditions, small-scale advection increases with decreasing snow-covered area due to (a) the increase in fetches of bare ground and the decrease in size of patches of snow and (b) the increase in ratio of edge-length

(perimeter) to area of the patches). During the late stages of ablation (22-31 Mar), the energy supplied by small-scale advection to melt trends with the variation in daily maximum temperature.
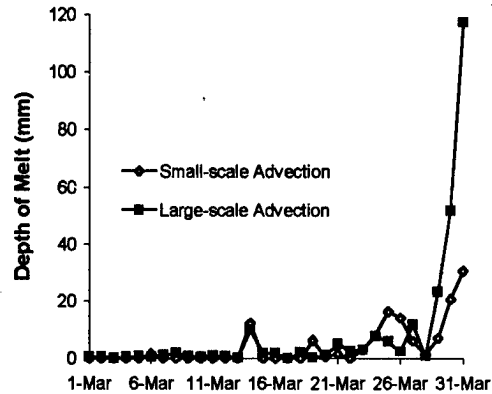
Figure 4. Estimated small-scale (Weisman) and large-scale advective fluxes during ablation of a shallow snowcover from a flat field of summerfallow near Saskatoon, SK, in 1994. Melt is expressed as the daily volume of meltwater produced per unit area of snowcover (mm).
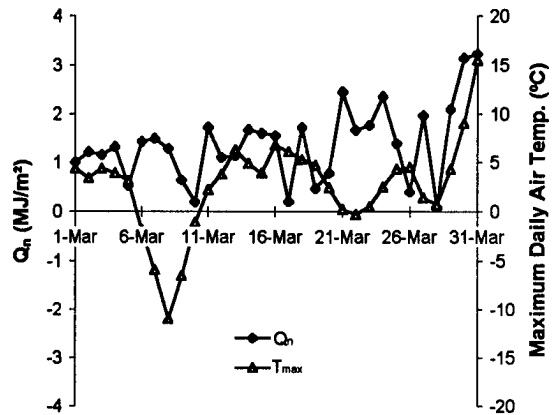
Figure 5. Daily net radiation and maximum air temperature during ablation of seasonal snowcover — Saskatoon, SK, 1994.

GEOMETRY OF PATCHY SNOW COVERS

To include the effects of the patchiness of a snowcover on the contributing areas of melt, infiltration, soil water recharge and runoff and on the radiative and convective energy transfers at the ground surface, a measure of the geometrical character of the snow field must be incorporated in snowmelt simulations. Shook (1993, 1995) and Shook et al. (1993a, b) show that the fractal character of the spatial distribution of the water

283

equivalent controls the geometries of a patchy snowcover. Figure 6 plots normalized values of the perimeters and areas for snow patches that were: (a) generated by applying melt fluxes to the spatial distribution of the water equivalent (synthetic) and (b) determined by image analyses of aerial photographs of ablated snowcovers on a flat field of fallow near Saskatoon, SK, and on the Smith Tributary, a 1.9-km² watershed in grass, fallow and wheat stubble on variable terrain in southwestern Saskatchewan (51° 19' N, 108° 25' W). The data represent the case of about 50% snowcover. Note that the displacements of the curves in horizontal and vertical directions are due to differences in the scales of the measurements and simulations. The data show perimeter length increasing exponentially with perimeter area. Each curve has roughly the same slope
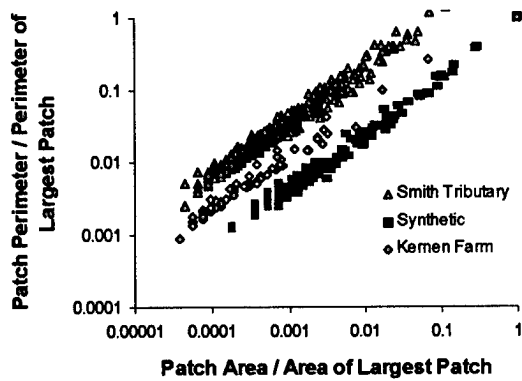
Figure 6. Normalized perimeter-area relationships from synthetic frequency distribution of water equivalent, Kernen Farm fallow field and Smith Tributary with 50% snowcover.
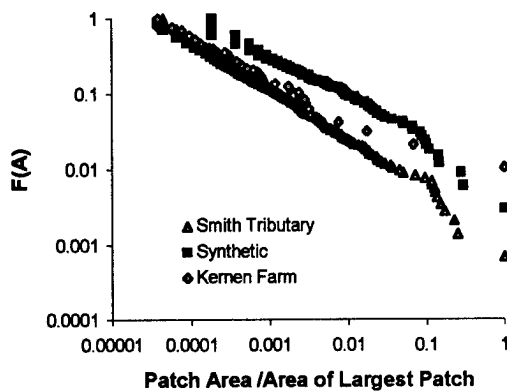
Figure 7. Normalized area-frequency relationships for snow patches from synthetic frequency distribution of water equivalent, fallow field and Smith Tributary — 50% snowcover.

Figure 7 plots the normalized frequency distributions of the snow patches for the three snowcovers. They show that the size distributions of small patches generally follow a power law (Korcak's law - Shook 1995) whereas the larger patches depart from the trend. The hyperbolic size distribution of the patches implies that a major part of the total snow-covered area is contained in a few patches. Generally, the 200 largest patches account for over 90% of the total snow-covered area (Shook 1993).

Lognormal frequency distribution of snow water equivalent

For shallow snowcovers of open environments, the frequency distribution of the snow water equivalent (*SWE*) can be approximated by the two-parameter lognormal probability density function. The distribution can be expressed in linear form as:

$$SWE = \overline{SWE}(1 + KCV), or \qquad (6)$$

$$SWE = \overline{SWE} + Ks, \qquad (7)$$

where: SWE = natural value of the snow water equivalent having an exceedance probability equal to that of the frequency factor, K (Chow 1954)

$\overline{SWE}$ = arithmetic mean of the natural values

CV = coefficient of variation of the natural values

s = standard deviation of the natural values.
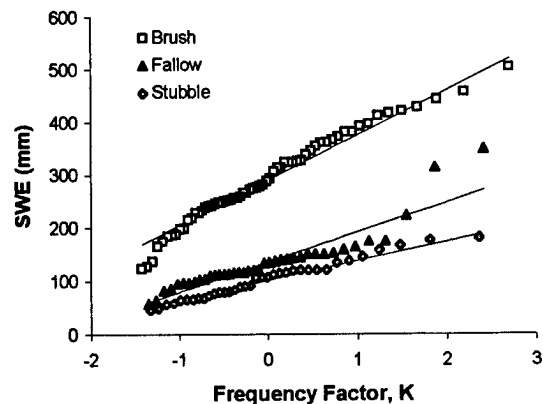
Figure 8. Lognormal distribution fitted to point measurements of snow water equivalent taken on open landscapes in brush, fallow and wheat stubble — Smith Tributary, SK, 1972.

Figure 8 plots point measurements of water equivalent and fitted lognormal distributions for (a) a relatively-flat

284

field in wheat stubble, (b) an undulating field of fallow and (c) a relatively-flat low area with scattered brush. The respective coefficients of determination, r^2, between the measured and fitted SWE-values for the landscapes are 0.92, 0.98 and 0.99, respectively.

Variation in coefficient of variation of snow water equivalent with landscape class

At moderate (field) scales within relatively homogeneous climatic regions of the Canadian prairies, the spatial distribution of the water equivalent of a snowcover is strongly influenced by vegetation and topography. McKay (1970) and Steppuhn and Dyck (1974) found that stratifying a watershed according to terrain and vegetative variables, then sampling snowcovers of the same landscape class, reduced the coefficient of variation of the water equivalent, CV. Shook (1995) lists representative CV-values for various landscapes within a prairie environment. They range from $CV \cong 0.30$ for stubble on various landscapes to $CV \cong 0.60$ for fallow on the crest of hills, knolls and ridges and for scattered brush in the lee of abrupt, sharp slopes. The effects of variations in CV on the depletion in snow-covered area are shown in Figure 9. These simulations were produced by applying a constant melt flux to snowcovers with a mean water equivalent of 130 mm and CV-values of 0.3, 0.35, 0.4 and 0.5 (Shook et al. 1993). The results demonstrate that the smaller the value of CV, the more rapid the depletion of snow-covered area. This is expected because the peakedness of the frequency distribution of SWE increases with decreasing CV. Therefore, the smaller the coefficient of variation, the larger the number of SWE - values clustered close to the mean.
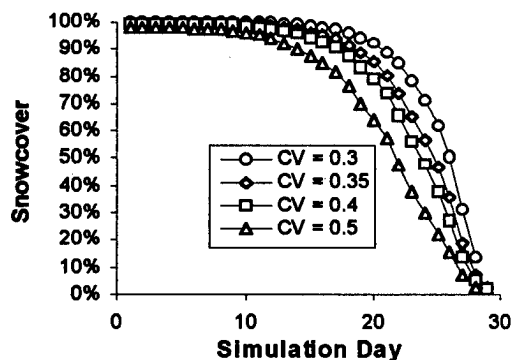
Figure 9. Snowcover depletion curves derived by applying a constant melt rate to snowcovers with a mean water equivalent of 130 mm and coefficients of variation of water equivalent, CV, equal to 0.3, 0.35, 0.4 and 0.5.

Relative contributions of snow melt energy fluxes

The ablation of snow from Smith Tributary in 1972 was simulated to illustrate the relative contributions of the different sources of energy to melting of a patchy snow. In the simulation, net radiation was measured and the large-and small-scale advective fluxes were estimated from field measurements using the temperature-index approach and the Weisman approximation (eq. 4), respectively. The program PSAS (Prairie Snow Ablation Simulation) developed by Shook (1995) was used for the simulation. PSAS applies the energy fluxes to the frequency distribution of the snow water equivalent to determine the areal depletion in snow cover. Figure 10 shows close agreement between the simulated and measured curves of snow-cover depletion.
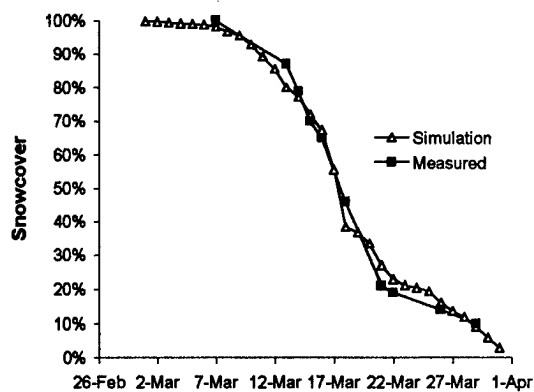
Figure 10. Simulated and measured depletion in snow-covered area from the Smith Tributary, Bad Lake, SK, in 1972.

Figure 11 plots the cumulative fraction of the total melt energy furnished by the various sources to the simulation The data show that energy supplied by large-scale advection, which was due to the persistence of large, warm air mass(es) over the region, dominated the melt process. Large-scale advection produced roughly 72% of the melt, radiation about 23% and small-scale advection about 5%. The relatively small contribution of the small-scale advective flux is due to two related factors. First, when the snowcover is largely continuous (i.e., > 50%), the fetches available for transfer of heat to the air are short, resulting in there being little energy available for small-scale advection. Second, when the snowcover is largely ablated (i.e., < 50%) the smaller snow-covered area reduces the ability of large, small-scale advective fluxes to melt appreciable quantities of snow.
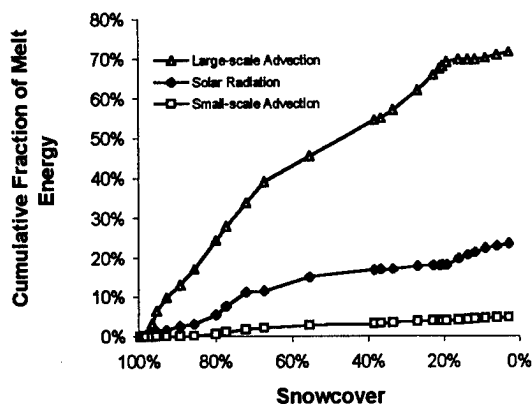
Figure 11. Cumulative fraction of net melt energy supplied by net radiation, large-scale advection and small-scale advection - Smith Tributary, Bad Lake, SK, 1972.

SUMMARY AND CONCLUSIONS

The relationship between areal albedo and snow-covered area of an ablating shallow snowcover is approximately linear. This association implies that the fraction of bare ground controls the areal albedo and the albedo of snow remains reasonably stable throughout depletion. It provides a simple means of adjusting the net radiative flux at the ground surface in snowmelt simulations.

The small-scale advective flux of sensible energy from patches of bare ground to adjacent patches of snow decreases rapidly with increasing fetch from the leading edge of snow. To include the effects of small-scale advection on melt in snowmelt simulations it is necessary to reproduce the geometries of the patches. The results of image analyses of aerial photographs of partially-ablated snowcovers demonstrate that (a) the area-frequency and perimeter-area relationships of patches of soil and snow can be described by fractal geometry and (b) the cause of the fractal patch structure is the spatial distribution of the water equivalent. These findings are used to simulate the areal depletion in snow-covered area of a natural snowcover by applying melt fluxes to the spatial and frequency distributions of the water equivalent.

Simulations of the ablation of a prairie snowcover are presented for a year in which heat supplied by large-scale advection is the primary

source of energy for melt. For the event, small-scale advection to the snowpack energy budget accounted for only about 5% of the total melt energy.

LITERATURE CITED

Chow, V.T. 1954. The log-probability law and its engineering applications, Proc. Am. Soc. Civil Engrs., 80(536): 1-25.

McKay, G.A. 1970. Precipitation. In D.M. Gray (ed) Handbook on the principles of hydrology, Secretariat Can Nat. Comm. Int. Hydrol. Decade, Nat. Res. Council Can., Ottawa, ON.

O'Neill, A.D.J. 1972. The energetics of shallow prairie snowpacks. Ph.D. Thesis, Univ. Sask., Saskatoon, SK, 1-197.

Shook, K. 1993. Fractal geometry of snowpacks during ablation. M.Sc. Thesis, Univ. Sask., Saskatoon, SK, 1-178.

Shook, K. 1995. Simulation of the ablation of prairie snowcovers. Ph.D. Thesis. Univ. Sask., Saskatoon, SK, 1-189.

Shook, K., D.M. Gray and J.W. Pomeroy. 1993. Temporal variation in snowcover area during melt in prairie and alpine environments, Nordic Hydrol. 24, 183-198.

Shook, K., D.M. Gray and J.W. Pomeroy 1994 Geometry of patchy snowcovers. Proc. 1993 Annual Meet. Eastern Snow Conf. June 8-10, 1993, Quebec City, QUE., 89-96.

Steppuhn, H. and G.E. Dyck. 1974. Estimating true basin snowcover. Advanced Concepts and Tech. in the Study of Snow and Ice Resour., Nat. Acad. Sci., Washington, DC, 314-328.

Woo, M.K. and P. Marsh 1977. Determination of snow storage for small eastern high Arctic basins. Proc. 1977 Annual Meet. Eastern Snow Conf., Feb. 3-4, 1977, Belleville, ON, 147-162.

Weisman, R.W., 1977. Snowmelt. A two-dimensional turbulent diffusion model. Water Resour. Res. 13(2):337-342.

Estimating Snowmelt Infiltration into Medium and Fine-Textured Frozen Soils

L. ZHAO[1] AND D.M. GRAY[1]

ABSTRACT

This paper uses a numerical simulation to study the effects of diurnal cycling in surface temperature on infiltration into a frozen soil. Cumulative infiltration for two cases of cycling of temperature are compared with estimates predicted by a parametric correlation. The correlation is based on infiltration into a frozen soil with a constant, continuous supply of water at the surface during quasi steady state flow. It requires information on surface saturation, initial soil saturation, initial soil temperature, saturated hydraulic conductivity and infiltration opportunity time. The comparisons demonstrate that the amounts of infiltration under cycling of temperature usually are less than those predicted by the correlation. However, the differences are relatively small (usually < 10%). Comparisons of seasonal snowmelt infiltration by a modified correlation that accounts for the effects of cycling show reasonable agreement with field estimates determined from measurements of soil water changes.

Key words: Infiltration, frozen soil, numerical analysis, diurnal cycling.

INTRODUCTION

In northern regions, melting of the seasonal snowcover is one of the most important events of the water year. Water from melting snow supplies reservoirs, lakes and rivers and recharges soil moisture and groundwater storage. Partitioning of the snow water resource to runoff and soil water largely depends on the infiltrability of the underlying frozen ground at the time of snowmelt. Infiltration of meltwater into frozen soil is a complicated process as it involves coupled heat and mass flow with phase changes. The process is affected by the thermal and hydrophysical properties of the soil, the soil temperature and moisture regimes, and the quantity and the rate of release of meltwater from the snowcover.

Gray *et al.* (1985) reported the results of a comprehensive field study of snowmelt infiltration into medium and fine-textured, completely frozen soils of the Canadian Prairies. They grouped these soils according to their infiltrability for snowmelt as:

Unlimited: soils containing large, surface-connected, air-filled macropores (e.g., cracks) that are capable of infiltrating most or all meltwater.

Limited: infiltration depends primarily on the snowcover water equivalent and the water/ice content of the 0-300 mm soil layer at the time of melt. The relationship between snowmelt infiltration, *INF*, snowcover water equivalent, *SWE*, and the premelt moisture content of the 0-300 mm soil layer, S_i, is:

$$INF = 5(1 - S_i)SWE^{0.584}, \qquad (1)$$

in which *INF* and *SWE* are in mm and S_i is the degree of pore saturation, mm^3/mm^3.

287

Restricted: infiltration is impeded by ice lens on the soil surface or at shallow depth. The amount of snow water that infiltrates is small and most of the meltwater goes to direct runoff and evaporation.

Equation 1 is useful for determining seasonal amounts of soil water recharge and runoff. Conversely, it is limited for forecasting and predicting the temporal variation of a hydrological variable because it lacks a time parameter.

Recently, rigorous, physically-based, numerical studies of infiltration into frozen soils have been undertaken by Tao and Gray (1994), Zhao et al. (1996) and Zhao and Gray (1996). The results from the simulations show that the infiltration process can be described by two flow regimes: a transient regime and a quasi steady state regime. The transient regime, which occurs immediately after the application of water at the soil surface, is of relatively-short duration. It is followed by the quasi steady state regime. Zhao and Gray (1996) found that the variation in cumulative infiltration, INF, with time, t, into a frozen, silty-clay soil during quasi steady state flow can be approximated as:

$$INF = 1.25 \; S_o^{4.4}\left(1 - S_i\right)^{1.9}\left(k_s t\right)^{0.5}\left(\frac{273.15 - T_i}{273.15}\right)^{-0.35}, \quad (2)$$

in which S_o = surface saturation, S_i = initial soil moisture content, $k_s t$ = the product of hydraulic conductivity, k_s, and time, t, and T_i = initial soil temperature. INF is in cm, when k_s is in cm/h, t is in hour, and T_i in Kelvin. The expression assumes a completely frozen soil of "Limited Class" having a constant supply of water at the soil surface.

In nature, snow ablation is seldom continuous, usually being interrupted by the diurnal cycling of solar radiation and the movement of cold air masses. This paper uses a numerical simulation of one-dimensional, coupled heat and mass flow with phase changes in a homogeneous, frozen soil to study the effects of daily freeze-thaw cycles on infiltration. A modified form of Equation 2 that accounts for the effects of cycling of temperature on infiltration is developed.

FORMULATIONS AND SIMULATIONS

The numerical simulations used to describe infiltration and heat flow are based on the simultaneous solution of energy, continuity and momentum equations of one-dimensional, transient, heat and mass flow in an unsaturated, homogeneous soil. Complete details of the formulations and numerical procedures used by the model are described by Zhao et al. (1996) and Zhao and Gray (1996). Only those expressions required for proper interpretation of the results and discussions presented in subsequent parts of the paper are described herein. They are:

Liquid phase momentum equation:

$$V_l = k_l\left(\frac{\partial p_c}{\partial Z} + 1\right). \quad (3)$$

Volumetric constraint:

$$\theta_l + \theta_i + \theta_g = \phi. \quad (4)$$

Freezing point depression equation (Cary & Mayland 1972, Flerchinger and Saxton 1989):

$$\theta_l = \phi\left[\frac{h_{il}\left(T - 273.15\right)/T + CRT}{g\psi_o}\right]^{-\frac{1}{\lambda}}. \quad (5)$$

Liquid permeability and capillary pressure (Brooks and Corey 1966)

$$k_l = \alpha k_s S_e^{3 + 2/\lambda}, \quad (6)$$

and

$$p_c = \psi_o S_e^{-\frac{1}{\lambda}}, \quad (7)$$

in which an impedance factor,

$$\alpha = 10 e^{-E\theta_i}, \quad (8)$$

is used to account for the reduction in permeability due to the presence of ice.

Effective saturation

$$S_e = \frac{\theta_l - \theta_r}{\phi - \theta_i - \theta_r}. \quad (9)$$

Note that the ice is treated as part of the solid phase.

Saturation

$$S = \frac{\theta_l + \theta_i}{\phi}. \qquad (10)$$

In equations 3-10

$C =$ solute concentration, mol/kg
$E =$ a calibrated impedance parameter
$g =$ gravity, m/s^2
$h =$ enthalpy change, J/kg
$k_s =$ saturated hydraulic conductivity, cm/s
$k_l =$ unsaturated hydraulic conductivity, cm/s
$p_c =$ hydraulic head, m
$R =$ universal gas constant
$S =$ saturation
$S_e =$ effective saturation
$T =$ temperature, K
$V_l =$ liquid velocity, cm/s
$Z =$ length, m
$\alpha =$ impedance factor
$\phi =$ porosity
$\lambda =$ pore-size distribution index
$\mu =$ viscosity, N·s/m^2
$\theta =$ phase volume fraction
$\rho =$ density, kg/m^3
$\psi =$ air entry potential, m

Subscripts

$o =$ surface,
$a =$ air,
$g =$ gas,
$i =$ ice,
$l =$ liquid,

The simulations assume specified initial and boundary conditions. Initially, the temperature, T, and total moisture content (liquid water plus ice), S, are assumed constant throughout the soil matrix at $T_i = -4$ °C and $S_i = 0.4$, respectively. After $t > 0$, the boundary conditions at the soil surface are specified for each case.

Table 1. Soil properties.

K (m^2) (k_s, cm/h)	7.44×10^{-14} (0.15)
λ	0.18
ψ_n (m)	0.7033
ϕ	0.49
θ_r	0
C (mol/kg)	0
T_i (K)	269
E	7

Table 1 lists the parameters and their values used in the numerical calculations. The soil physical properties (moisture-tension and hydraulic conductivity) were derived from laboratory and field data for a silty clay loam collected near Saskatoon, Saskatchewan (Miller 1994) and the empirical relationships reported by Rawls et al. (1982).

RESULTS AND DISCUSSIONS

The movement of water in medium and fine-textured frozen soils is controlled by the relative liquid permeability, k_l, and the capillary pressure gradient, $\partial p_c/\partial z$, which are functions of the liquid water content, θ_l. In turn, θ_l, is determined from the soil temperature T (see Equation 5). These relationships couple the heat and mass transfer processes. They are complex and nonlinear, which inhibit the derivation of analytical solutions that describe the effects of a single component on infiltration.
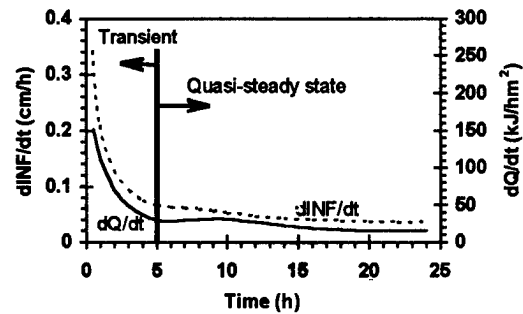
Figure 1. Variations in dINF/dt and dQ/dt with time at: $S_i = 0.40$, $S_o = 0.75$, $T_i = -4$ °C, and $k_s = 0.15$ cm/h.

Figure 1 presents the results of a simulation with a constant supply of water and constant temperature at the soil surface ($S_o = 0.75$, $T_o = 0$ °C). The data show the infiltration rate, dINF/dt (the liquid velocity), and the heat transfer rate, dQ/dt, at the soil surface decreasing with time, at first rapidly and then slowly. The trends show the infiltration process comprising two flow regimes: a transient regime and a quasi-steady state regime (Zhao et al. 1996). The transient regime follows immediately the application of water at the soil surface. Usually, its duration is relatively short (a few hours), depending on the permeability, surface condition, initial water content and initial temperature of the soil. During the transient regime the infiltration rate and the heat transfer rate decrease rapidly. The quasi steady state

289

regime occurs where the changes in the infiltration rate and the heat transfer rate with time are relatively small.

The effects of melt-freeze cycles on infiltration were studied using controlled boundary conditions.

Case 1

The surface water saturation is set at $S_o = 0.75$ for the duration of the simulation and the surface temperature, T_o, cycles over a 24-h period (see Figure 2). At the start of the simulation T_o is at the initial soil temperature, i.e., $T_o|_{t=0} = T_i = -4$ °C. During the first 12 h, T_o increases at a linear rate to 0 °C at $t = 1$ h., where it remains for the following eleven hours. In the second 12-h period T_o decreases at a linear rate to -1 °C at the end of the first hour, then remains constant at -1 °C for eleven hours. The temperature begins to increase again at 24 hours and starts the second cycle.
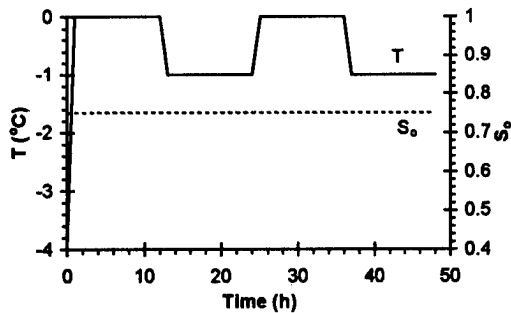
Figure 2. The prescribed variations of surface temperature and moisture conditions with time for Case 1.
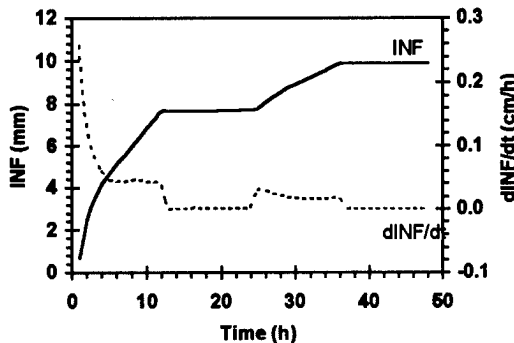
Figure 3. Variations in cumulative infiltration and infiltration rate with time at $S_i = 0.40$, $T_i = -4$ °C, and $k_s = 0.15$ cm/h for Case 1.

Variations in cumulative infiltration, *INF*, and the infiltration rate, *dINF/dt*, with time due to the cycling of surface temperature described in Figure 2 are plotted in Figure 3. Over the interval, 0 - 12 h, the infiltration-rate is a maximum when the surface temperature reaches 0 °C, then decreases rapidly to a reasonably-constant value. About 8 mm of water infiltrates into the frozen soil. During the freezing period (12 - 24 h), *dINF/dt* quickly decreases to zero after the surface temperature drops to below 0 °C. In the third 12-h period (24 h - 36 h) the infiltration rate increases to a maximum and then decreases, at first rapidly, then slowly. Infiltration for this period is about 2 mm. The melting period is followed by the second freezing cycle.
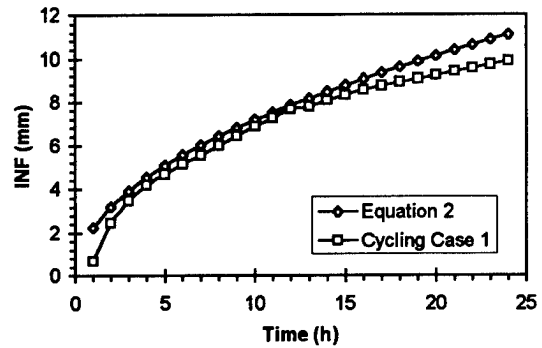
Figure 4. Comparison of cumulative infiltration results obtained with cycling simulation case 1 and Equation 2.

The infiltration opportunity time, the total time that the liquid water is available at the surface for infiltration, throughout the two cycles in temperature is 24 h. Figure 4 plots cumulative infiltration when the surface temperature is cycled according to the pattern given in Figure 2 and the amount predicted by Equation 2, which assumes a constant supply of water at the surface (i.e., $T_o = 0$ C and infiltration is continuous) as a function of opportunity time. The curves show that the amounts of infiltration by Equation 2 are always larger than the corresponding amounts when the surface water supply is interrupted. The differences are 70% (1.6 mm) after 1 h, 3% (0.2 mm) after 12 h and 11% (1.2 mm) after 24 h. Equation 2 estimates cumulative infiltration assuming only quasi steady state flow whereas the simulation includes infiltration during transient flow. This difference causes the discrepancies between the two curves to be relatively-large during the early initial period of infiltration ($t < 1$ h). At $t = 12$ h, quasi steady state is reached for the cycling case and

the differences among infiltration amounts for the two conditions are small. In the second infiltration cycle, the soil temperature near the surface is lower than under continuous infiltration. The lower temperature results in a higher ice content, which decreases the infiltration rate. The difference in cumulative infiltration amounts by the simulation and Equation 2 increases from 3% at $t = 12$ h to 11% at $t = 24$ h.

Case 2

The cycling in surface temperature is the same as in Case 1 except it takes 2 h following the start of a melt cycle for the surface temperature to increase from - 4 °C to 0 °C and 2 h to decrease from 0 °C to -1 °C at the end of each melting period. Initially, the surface moisture condition is at $S_o = 0.4$ and increases to $S_o = 0.75$ at 2 h, where it remains for the rest of simulation. The surface conditions as functions of time are plotted in Figure 5.
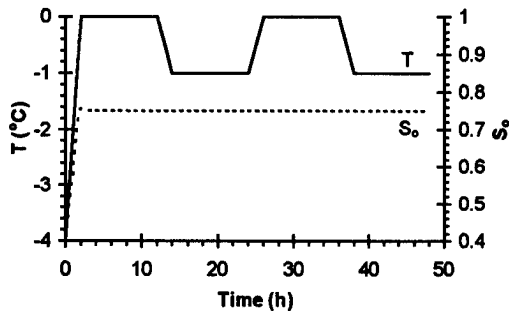
Figure 5. The prescribed variations of surface temperature and moisture conditions with time for Case 2.
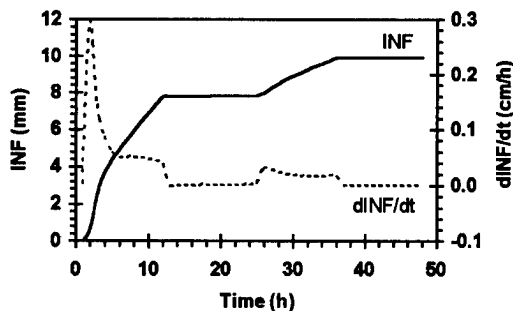
Figure 6. Variations in cumulative infiltration and infiltration rate with time at $S_i = 0.40$, $T_i = -4$ °C, and $k_s = 0.15$ cm/h for Case 2.

Figure 6 plots the variations in simulated infiltration and infiltration rate with time over two cycles of surface moisture and temperature. The data show the infiltration rate increasing to a maximum at $t = 2$ hours, then decreasing. The shape of the remainder of the curve is similar to that found for Case 1 (see Figure 3). The amounts of infiltration at the end of the first and second infiltration periods for this case are the same as those for Case 1.

The variation in cumulative infiltration with time obtained from the simulation is compared with the corresponding curve calculated by Equation 2 in Figure 7. At $t = 1$ hour, simulated infiltration is zero, whereas the amount estimated by Equation 2 is 2 mm. The difference between the two decreases with increasing time over the first melting cycle. At $t = 12$ h, the difference is zero. During the second melting cycle, the difference increases due to the effects of the lower temperature and higher ice content in the upper layer of the soil on the simulated infiltration rate. The difference in infiltration is 2 mm or 11% at $t = 24$ h.
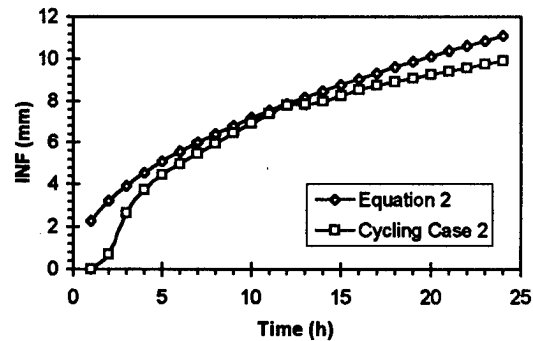
Figure 7. Comparison of cumulative infiltration results obtained with cycling simulation Case 2 and Equation 2.

The examples above suggest that the effects of diurnal cycling of surface temperature on cumulative infiltration are relatively-small. Therefore, lacking additional comparisons and a full understanding of the interactions between terms of Equation 2, it is suggested that for estimates of infiltration for interrupted melt events an average factor equal to 0.92 be applied to the expression. That is:

$$INF = 1.15 \ S_o^{4.4}(1 - S_i)^{1.9}(k_s t_{tot})^{0.5}\left(\frac{273.15 - T_i}{273.15}\right)^{-0.35}.$$

$$\text{(11)}$$

Comparison with field data

To calibrate and to verify the trend described by Equation 11, comparative tests were conducted that related infiltration by the expression with field estimates of seasonal snowmelt infiltration. The field data consisted of 63 sets of measurements made at various locations in the Province of Saskatchewan, Canada, between 1978 and 1991 in uncracked, completely-frozen soils of Limited Class. Each set of observations included: (a) snow water equivalent prior to appreciable melt, (b) measurements of snow depth and profiles of total soil moisture (water + ice) and soil temperature before, during (infrequent) and after snow ablation, and (c) soil textural composition. Infiltration was derived from soil moisture changes. The textural information was used to estimate soil permeability by the empirical associations reported by Rawls and Brakensiek (1985). More details of the experimental facility and procedures can be found in Granger et al. (1984).

Unfortunately, two parameters required by the correlation (Equation 11), the surface saturation S_o, and the infiltration opportunity time, t_{tot}, were not available in the field data. Therefore, the comparative tests are not stringent and rigorous. It is assumed that surface saturation is constant throughout ablation at $S_o = 0.90$. The infiltration opportunity time was estimated by setting Equation 11 equal to the formulation for seasonal infiltration of Equation 1 reported by Gray et al. (1985). That is,

$$11S_o^{4.4}(1-S_i)^{1.9}(k_s t_{tot})^{0.5}\left(\frac{273.15-T_i}{273.15}\right)^{-0.35}$$
$$= 0.1 \times 5(1-S_i)SWE^{0.584} \qquad (12)$$

The field data were grouped according to the snow water equivalent into class intervals representing 10 mm of water. For each interval, average values for initial water saturation, S_i, initial soil temperature T_i, snow water equivalent, SWE, and saturated hydraulic conductivity, k_s, were calculated. These average values in Equation 12 gave:

$$t_{tot} = 0.65SWE - 5. \qquad (13)$$

Using the infiltration opportunity time calculated by Equation 13, INF was recalculated by Equation 11 using the specific values of S_i, T_i, SWE, and k_s, for each site. Calculated and measured infiltration values are plotted in Figure 8. The standard

deviation of the difference among values is 11 mm. The agreement in the data suggests that Equation 11 gives reasonable practical estimates of snowmelt infiltration into frozen ground when the infiltration opportunity time is known. Additional verification and validation tests of Equation 11 by field measurement is needed.
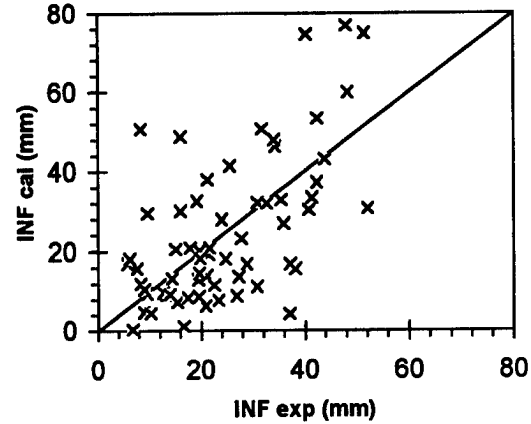
Figure 8. Comparison of correlation 11 with field data.

CONCLUSIONS

Water infiltration into frozen soils can be described by two flow regimes: a transient regime followed by a quasi steady state regime. Transient flow occurs immediately after water is applied at the surface. During this regime the infiltration rate and the surface heat transfer rate experience large and rapid decreases. In the quasi steady state regime, the infiltration rate and heat transfer rate decrease slowly.

Infiltration into a frozen soil is reduced by the diurnal cycling of surface temperature because of the increases in ice content within the surface soil layers that accompany nocturnal freezing. For a specific opportunity time the change (decrease) due to cycling, relative to the amount of infiltration that would occur under conditions when the temperature and moisture supply at the soil surface are constant, is small. Reasonable estimates of infiltration under conditions of diurnal cycling of temperature can be made by applying a correction factor to a parametric equation for quasi-steady state flow that relates cumulative infiltration to surface saturation, initial soil saturation, initial soil temperature, saturated hydraulic conductivity and infiltration opportunity time.

REFERENCES

Brooks, R.H. and A.T. Corey, 1966. Properties of porous media affecting fluid flow, *J. Irrig. Drain. Div. Amer. Soc. Civil Eng.*, **92**, 61-88.

Cary, J.W. and H.F. Mayland, 1972. Salt and water movement in unsaturated frozen soil, *Soil Sci. Soc. Am. Proc.*, **36**: 549-555.

Flerchinger, G.N. and K.E. Saxton, 1989. Simultaneous heat and water model of a freezing snow-residue-soil system I: theory and development, *Transactions of the ASAE*, **32**: 565-571.

Gray, D.M., P.G. Landine and R.J. Granger, 1985. Simulating infiltration into frozen prairie soils in streamflow models, *Can. J. Earth Sci.*, **22**, 464-474.

Miller, D.K. 1994. Soil heat flux during spring thaw, M. Sc. thesis, University of Saskatchewan, Canada.

Rawls, W.J., D.L. Brakensiek, and K.E. Saxton, 1982. Estimation of soil water properties, *Transactions of the ASAE*, **25**, 1316-1330.

Rawls, W.J. and D. L. Brakensiek, 1985. Prediction of soil water properties for hydrologic modeling, In *Watershed management in the eighties*, E.B. Bruce and T. J. Ward eds. Am. Soc. Civil Eng., New York, NY, 293-299.

Tao, Y.-X and D.M. Gray, 1994. Prediction of snowmelt infiltration into frozen soils, *Numerical Heat Transfer*, Part A, **26**, 643-665.

Zhao, Litong, D. M. Gray, and D. H. Male, 1996. Numerical analysis of simultaneous heat and water transfer during infiltration into frozen ground, *Journal of Hydrology*, (submitted).

Zhao, Litong and D. M. Gray, 1996. Parametric expressions for estimating infiltration into frozen soils, *Hydrological Processes*, (submitted).

II. CHEMISTRY
Carbon

Effect of Fire on Temperature, Moisture, and CO₂ Emissions from Soils Near Tok, Alaska

An Initial Assessment

K.P. O'NEILL[1], E.S. KASISCHKE[2], D.D. RICHTER[1], AND V. KRASOVIC[3]

ABSTRACT

The soils of the boreal forest are a significant active sink for terrestrial carbon. Short growing seasons, low temperatures, and moist soils limit decomposition of organic matter, resulting in thick accumulations of carbon-rich material on the forest floor. Wildfire is a primary control on forest succession patterns and carbon cycling in the boreal forest. Increased temperature, melting permafrost, and a more available food and nutrient supply greatly enhance microbial decomposition rates after fire, allowing for significant CO₂ efflux from recently burned soils despite the absence of living roots. Under a global warming scenario, fire activity in this region is expected to increase, releasing stored CO₂ to the atmosphere and potentially changing a region which is now a primary sink for terrestrial carbon into an equally significant source. This paper discusses initial results from a study to monitor changes in soil thermal and moisture conditions after wildfire and the effect that these changes have on CO₂ emissions from the soil.

Key words: CO₂ , soil respiration, fire, boreal forest, temperature

INTRODUCTION

Although the boreal forest biome covers less than 10% of the earth's terrestrial surface, this region contains more than 714 Pg (1 Pg = 10^{15} g) of carbon, or 37% of the global total (Olson et al. 1983; Schlesinger 1984; Apps et al. 1993). In the forested portions of this biome, the vast majority of this carbon is stored in moss and partially decomposed organic material on the forest floor (Apps et al. 1993; Kurz et al. 1992; Kurz and Apps 1993; Kolchugina and Vinson 1993). More significantly, boreal soils are still active sinks for terrestrial carbon; short growing seasons, low temperatures, and moist soils limit decomposition of organic matter, resulting in thick accumulations of carbon-rich material on the forest floor (Harden et al. 1992; Botch et al. 1995; Billings,1987). Any disturbance which alters these high rates of carbon sequestration has the potential to significantly perturb the global carbon cycle.

Wildfire is a primary control on carbon storage in the boreal forest. Between 5 and 10 million hectares of boreal forest burn every year, primarily in fires > 2000 hectares in size. (Stocks 1991; Kasisichke et al.1993; Alaska Fire Service 1994). Ecosystem response to these fires occurs over many time scales, from the immediate release of greenhouse gases volatilized during combustion of organic material to the long-term alteration of the soil carbon budget. A doubling of atmospheric CO₂ and the consequent changes in global climate could increase fire activity in the boreal forest by up to 40%, releasing vast quantities of stored carbon to the atmosphere and potentially changing a region which is now a primary sink for terrestrial carbon into an equally significant source (Wotton and Flannigan 1993; Flannigan and Van Wagner 1991).

Numerous models suggest that microbial activity and decomposition rates in boreal soils are directly related to soil moisture and temperature (Funk et al. 1994; Billings 1987; Whalen 1991). Both of these factors change after fire. Decreases in soil albedo and loss of insulating moss layers raise sub-surface temperatures and encourage microbial decomposition of stored carbon otherwise unaffected by fire (Dyrness

[1] Nicholas School of the Environment, Duke University, Durham, North Carolina 27706, USA
[2] Center for Earth Sciences, Environmental Research Institute of Michigan, Ann Arbor, Michigan 48113-4001, USA
[3] Department of Applied Science, College of William and Mary, Williamsburg, Virginia 23187, USA

et al. 1986; Viereck 1983; Schlentner and Van Cleve 1984). Mobilization of soil nutrients by permafrost meltwater, ash deposition, and increased decomposition may enhance net primary production (MacLean et al. 1983; Viereck et al., 1983). Lowered evapotranspiration and melting permafrost may also transform anaerobic soils into aerobic soils, further increasing microbial activity and emissions of CO_2 (Funk et al. 1994; Matthews and Fung 1987; Fung et al. 1991). The net effect of these processes is unknown.

This paper discusses initial results from a study to monitor changes in soil thermal and moisture conditions after wildfires and the effect that these changes have on CO_2 emissions from the soil. The study is divided into two distinct phases. In the first. we focus upon three different vegetation types within a single fire scar to determine if post-fire soil respiration significantly differs as a function of vegetation or soil drainage. In the second, we evaluate the long-term impact of wildfire on soil carbon flux in black spruce forest soils by examining a sequence of seven fire scars ranging in age from 1 month to 140 years.

SITE DESCRIPTION

More than 40,000 hectares of forest near Tok, Alaska (63°18'N latitude, 142°45'W longitude) burned in a series of wildfires during July and August of 1991. The fire stopped abruptly at the edge of town due to a shift in wind direction (Ray Kramer, personal communication); thus, much of the boundary between burned and unburned forest is not related to any difference in soil or vegetation characteristics.

This site provides a special opportunity to examine burned and unburned control sites across a range of soil and vegetation conditions. Study sites are all located on the floodplain of the Tanana River on nearly level terrain with an average elevation of 500 m. Forest vegetation is strongly associated with soil drainage class; on well drained alluvial soils, initial colonization is by quaking aspen (Populous tremuloides Michx.) followed by white spruce (Picea glauca [Moench] Voss). Poorly drained, clay-rich soils are dominated by black spruce (Picea mariana [Mill.] B.S.P). Paired burned and unburned plots were established within the three major soil-vegetation complexes found at Tok: 1) black spruce on silty clay 2) white spruce on gravelly silt 3) aspen on clayey silt.

To evaluate the long term impact of wildfire on black spruce soils, we identified an age-sequence of fire scars; stand ages were .08 (1 month), 2, 6, 9, 80, and 140 years. The fire sequence extends along the Alaska Highway from Tetlin Junction to Delta Junction, a distance of approximately 220 km. The time since last fire was determined by historical record for recent burns and by tree ring analysis for more mature stands. Sites were located on soils of similar texture (clayey silt with inter-bedded gravel), drainage, and slope position. All fire scars examined had a burn boundary which was caused by a non-natural feature (e.g. a road or fire break). For this reason, we were able to identify comparable controls for each of our burned sites.

METHODS

Measurements were conducted from July 1 to August 10, 1996. Burned and unburned plots were

Table 1: Summary of soil respiration, temperature, and moisture measurements by site. Standard deviations shown in parentheses. Temperature measurements were collected 5-cm below the top of the O-Horizon.

Site	Treatment	Respiration (g CO2 m^-2 hr-1)	Temperature (Degrees C)	% Moisture (Oven-Dry Basis)	n
1996	Burned	0.307 (0.141)	13.5 (3.1)	206.2 (87.6)	28
	Unburned	0.886 (0.535)	14.93 (4.0)	262.8 (54.7)	53
1994	Burned	0.391 (0.216)	13.8 (3.2)	66.09 (39.8)	63
	Unburned	1.107 (0.514)	19.26 (4.1)	194.2 (144.8)	35
1990	Burned	0.845 (0.276)	15.2 (3.2)	107 (32.2)	121
1987	Burned	1.131 (0.435)	12.0 (1.9)	MD	10
80 year	Unburned	0.995 (0.468)	9.2 (2.8)	403.1 (142.1)	106
140 year	Unburned	1.67 (0.684)	18.3 (2.8)	121.2 (151.9)	10
White Spruce	Burned	0.726 (0.236)	11.7 (2.3)	80.11 (27.1)	36
	Unburned	1.23 (0.345)	10.8 (2.8)	154.3 (45.4)	61
Aspen	Burned	0.566 (0.329)	MD	48.54 (44.5)	20
	Unburned	0.942 (0.372)	11.1 (2.3)	MD	20

296
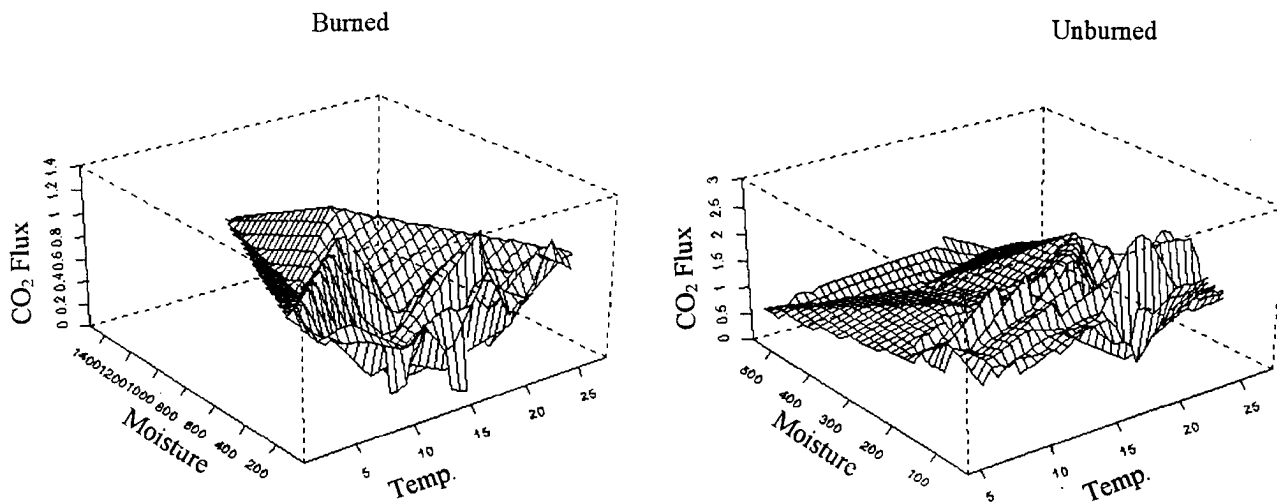
Burned

Unburned

Fig. 1. CO_2 flux (g CO_2 m^{-2} hr^{-1}) as a function of soil temperature (°C) and moisture for burned and unburned sites. Figure was created using the interpolation and perspective subroutines in S-Plus.

established on a 50-by 30-m grid located within each site; grid points were 10 m apart. The number of grid points varied between 12 and 15. Each plot was visited at least twice during the study period; on each visit, grid points were sampled between 4 and 6 times over an 8-hour period.

CO_2 emissions were measured both at the surface of the organic mat and at three horizon boundaries within the organic profile (living and dead moss, fibric, and humic) with a portable infrared gas analyzer. In this method, a 1170 cm^3 opaque chamber is placed on the forest floor, covering an area of 78.5 cm^2. The rate of increase of CO_2 concentration within the chamber is then measured over a maximum 2-minute period to provide both concentration (ppm) and flux. The instrument records measurements as g CO_2 m^{-2} hr^{-1}; measurement stops when the change in carbon concentration becomes non-linear (Parkinson 1981; Thierron and Laudelout 1996). Living moss and vegetation were not removed prior to measurement in order to limit site disturbance and the subsequent potential for increased decomposition. At the 80-yr black spruce site, CO_2 emissions were measured from the surface as well as within the fibric, humic, and mineral soil. Temperature was simultaneously measured at the surface of the forest floor and at depths of 5, 10, and 20 cm within the organic soil. At the conclusion of the sample collection, 10-to 20-cm cores of organic material were collected from each measuring point for determination of volumetric moisture.

Microbial respiration model

CO_2 flux from the soil represents the net result of microbial decomposition, root and moss respiration, and photosynthetic uptake by surface mosses. Each of these components is impacted differently by fire and, thus, the proportion of soil respiration contributed by each component may be expected to change as a soil recovers from fire disturbance. As an initial attempt to resolve the relative contributions from these components, we employed a model for microbial respiration proposed by Bunnell and Tait (1977) and later modified by Schlentner and Van Cleve (1984):

(1) $BRESP = (M/(a_1 + M)) * (a_2/(a_2 + M)) * a_3 *$
$((1/(a_6 + a_4^{(t-10/10)}) + a_5)$

where BRESP is the respiration rate in g CO_2 evolved m^{-2} $hour^{-1}$, T is the soil temperature in °C, M is the soil moisture as a % of dry weight, a_1 is the % water content (dry weight basis) at which microbial activity is at half its optimal value, a_2 is % water content (dry wt basis) at which gas exchange is limited to half its optimal value, a_3 is the respiration rate that would occur at 10°C if neither moisture nor O_2 is limiting, a_4 is the Q^{10} coefficient, a_5 is the lower limit of CO_2 evolution, and a_6 is (1/ upper limit of respiration - a_5).

To approximate the portion of measured soil respiration that was produced by microbial decomposition in black spruce stands, we used Eq. 1 to estimate CO_2 flux using gravimetric moisture

297

contents and 20 cm temperatures measured at burned and unburned sites, and parameters a_1 through a_6 were collected from the literature. In cases where parameters for black spruce ecosystems were not available, estimates were made from published data so as to maximize the contribution by microbial activity. Root and moss respiration were then estimated as the total measured flux minus the modeled microbial respiration.

RESULTS

A summary of moisture, temperature, and soil respiration data from all sites is shown in Table 1. Although temperature measurements were made at three depths within the soil profile, we are reporting only those temperature measurements collected at the 5-cm depth. As organic material becomes more decomposed, its bulk density increases and hydraulic conductivity decreases. For this reason, organic horizons have different heat capacities depending on the degree of decomposition. Since the thicknesses of organic horizons vary widely between sites, simply measuring temperature at an arbitrary depth from the surface does not ensure that these measurements are comparable. The 5-cm depth was least affected by any temperature effects caused by horizonation. Moisture contents show a high degree of variation; coefficients of variation range from 21 to 125%. This can be explained in two ways: 1) plots were specifically located to sample a range of moisture conditions and 2) samples collected on different dates were averaged together. Despite this, unburned sites still showed significantly higher moisture contents than burned sites. Figure 1 shows the relationship between moisture, temperature, and CO_2 emissions for all burned and unburned sites.

Aspen, White Spruce, and Black Spruce

Within the Tok fire scar, unburned sites were significantly wetter and colder than burned sites regardless of soil texture or drainage class, and showed significantly higher rates of CO_2 emission. In mature, unburned, stands, 5-cm temperatures were higher in aspen and white spruce than in black spruce. This relationship changed in burned stands, with black spruce having higher temperatures. This is most likely an artifact of the sampling method; due to differences in burn severity between sites, post-fire 5-cm temperatures were taken from colder mineral soil in aspen stands and from warm, upper organic horizons in black spruce stands. Unburned black spruce soils had moisture contents more than two times greater than those found in white spruce. Although the magnitude of these values changes, these relationships remained the same for burned profiles.

In unburned soils, CO_2 emissions were highest for the white spruce sites; no significant difference was found between aspen and black spruce soils. However, in burned sites, black spruce soils had the greatest emissions, followed by white spruce and aspen. Fires in aspen stands tend to burn to mineral soil whereas the greater moisture content and thicker organic mat found in black spruce sites tends to limit combustion to the upper, dry, portions of the profile. Therefore, burned aspen stands tend to have less material available for microbial decomposition than burned black spruce stands. Additionally, aspen and white spruce trees tend to root in mineral soil while black spruce root intensively within the organic profile. This could allow for more rapid transfer of root respired CO_2 to the surface in black spruce soils.
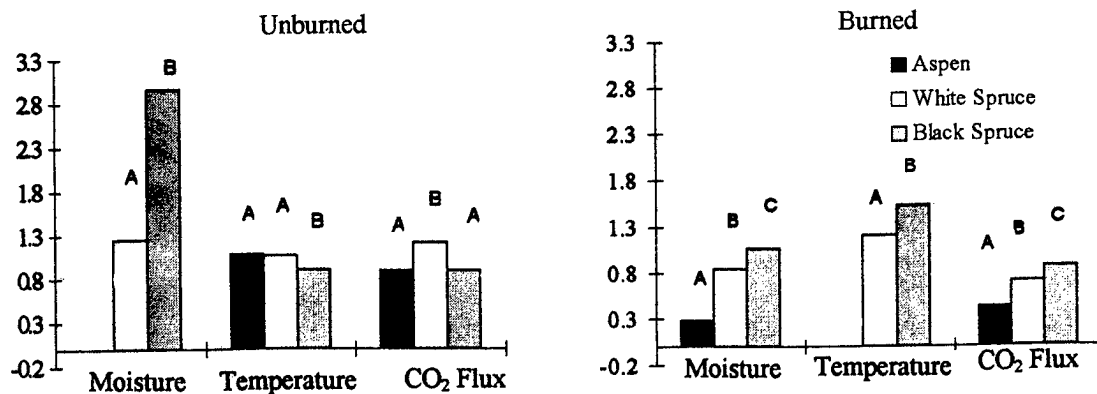
Fig. 2. Temperature, moisture, and CO_2 emissions from three different soil systems. Temperature is reported in °C/10 (to aid in visual scaling), moisture as gravimetric oven-dry %, and CO_2 flux in g CO_2 m^{-2} hr^{-1}. Bars labeled with different letters are significantly different at the alpha=0.5 level.

298
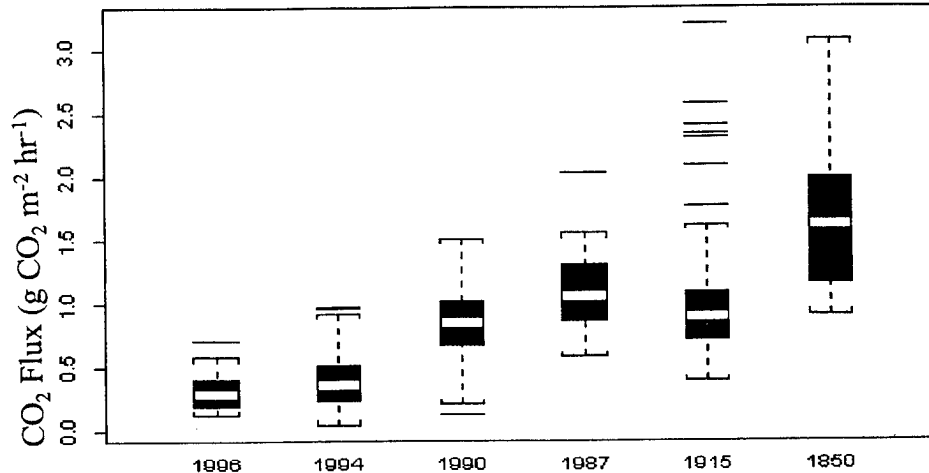
Fig. 3. Soil respiration as a function of time since last fire. The length of the box represents the IQR; the box is divided at the median. Whiskers represent the largest observation within 1.5 times the IQR. All observations beyond these limits are plotted separately.

Burn Chronosequence

The winter of 1995-96 experienced an unusually low snowfall. The lack of an insulating snow layer for much of the winter caused the soils to freeze more deeply than normal (Richter and Kasischke, unpublished data). As a result, soils at the unburned control sites (2, 6, 9, 80, and 140 year old stands) were still frozen up to the base of the organic profile until late July. In contrast, permafrost was absent from the upper 1.5 meters of burned profiles. The one exception to this was the 1996 burn. Depth to permafrost was measured in both burned and unburned stands 1 month after the fire; no significant difference was observed. Depth to permafrost was measured again six weeks later (2.5 months after the burn). At that time, depth to permafrost had increased an average of 15 cm in the burned site.

At all points along the chronosequence, CO_2 fluxes from the soil surface were higher from unburned soils than in burned soils. This corresponds to the greater moss and root biomass contained at these unburned sites. In general, CO_2 flux increased with time since the last fire (Fig. 3). The strength of this relationship is undoubtedly weakened by inter-site differences in productivity as well as variations in burn severity. In an attempt to correct for potential inter-site variability, we divided emissions from each burned soil by its unburned control. In the first month following fire, emissions were reduced to 30% of pre-burn levels and recovered to 50% after 9 years. During this same period of time, moss and understory vegetation began to re-grow; thus, it is likely that increases in root biomass and moss respiration account for part of this increase.

CO_2 flux is not constant throughout the organic soil profile. Fig. 4 shows mean fluxes from 15 grid points measured at genetic horizon boundaries within the organic soil profile. Emissions measured at the surface are significantly lower than those measured below the photosynthetic part of the moss. An analysis of variance showed significant differences between fluxes from different horizons with the exception of the fibric and humic horizons. Since the field differentiation of these two horizons is difficult and somewhat subjective, it is not surprising that there is some overlap between these categories. Emissions increased with depth, with surface emissions on average 40% of those found in the deeper humic and fibric layers.

BRESP model

Figure 5 shows model predictions for microbial respiration as a function of time since fire. Emissions observed immediately after the fire could be adequately explained by microbial activity alone. As time since fire increases, the proportion of the CO_2 flux that comes from root mass increases, until after 80 years, less than 20% of emissions come from microbial respiration. The model is most sensitive to changes in whichever site parameter (moisture or temperature) is most limiting at time of measurement (Schlentner and Van Cleve 1984; Bunnell and Tait 1974).

DISCUSSION

Emissions of CO_2 from the forest floor represent the net result of CO_2 release during the respiration of soil microbes, roots, and moss and the photosynthetic

299
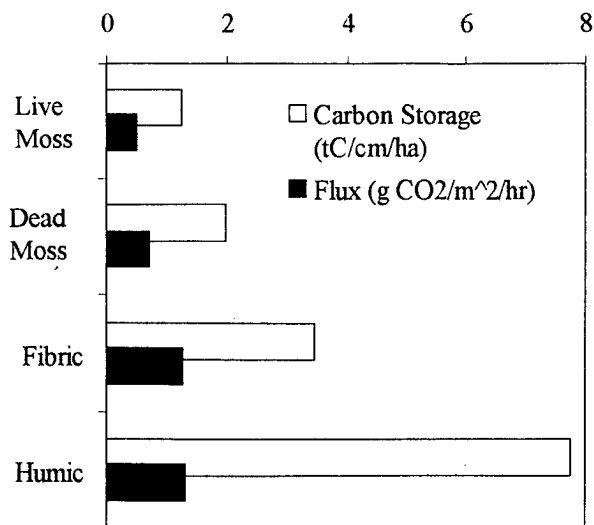
Fig. 4. Carbon storage and flux from genetic organic horizons within an 80-year old black spruce stand.

uptake of CO_2 by mosses. In an unburned soil, emissions are dominated by root and moss activity. After fire, moss uptake and root respiration are removed from the respiration equation and CO_2 emission is dominated by microbial decomposition. In addition, these post-fire respiration rates are greatly enhanced due to increased temperature, more available food sources, and more favorable moisture conditions. This can be most clearly seen in the 1996 burn in which soil respiration rates are nearly 60% of those seen in the unburned control, despite the absence of living roots or moss (Table 1). Since the permafrost had not yet melted nor the subsoil temperature changed significantly at the time of these measurements (1 month after the fire), much of this response must be due to more available nutrients and food sources for soil microbes in the form of labile carbon. The burned to unburned emission ratio drops to 26% after two years (1994 burn); at this time, most of the labile carbon pool has been consumed, nutrients are less available, and microbial activity is slowing down. However, roots and moss are still absent and do not contribute to soil emissions. As root and moss biomass recover and soil temperature and moisture re-equilibrate to pre-fire levels, soil respiration rates rise, eventually attaining pre-fire levels. Because of the irregular temporal spacing of the fire chronosequence, we are not yet able to determine at what time this equilibrium is re-attained.

An analysis of nearly 600 CO_2 measurements taken over a six week period at both burned and unburned sites suggest that CO_2 emissions tend to increase with increasing temperature for those moisture contents which are neither too low nor saturating (Fig 1a and 1b). Although this supports results found by Schlentner and Van Cleve (1984),

the relationship between moisture, temperature, and soil respiration is not strongly expressed in these sites. One explanation is that moss, roots, and soil microbes respond differently to temperature and moisture fluctuations. While an increase in temperature tends to increase microbial metabolism and respiration rates, it also increases moisture stress in mosses. In response to increased evapotranspiration, mosses close their stomates, reducing photosynthetic activity and decreasing uptake of CO_2. Additionally, both photosynthesis and respiration in mosses are highly dependent on extremely localized atmospheric conditions. For example, an increase in temperature may not cause a reduction in photosynthetic activity if the relative humidity immediately surrounding the moss is high. As a result, moss dynamics may either amplify or negate emissions from the decomposing organic horizons. The relative contribution of moss uptake is difficult to estimate. The chamber used to measure surface CO_2 flux was opaque and the sampling time, although short, was not standard for all measurements; thus, photosynthetic uptake may have been reduced during measurement, but this reduction was not consistent between samples.

CO_2 efflux is not constant throughout the organic soil profile (Fig 4). Surface fluxes are significantly lower than fluxes from lower depths. This increase with depth could have several causes: 1) greater decomposition and lower gas diffusivity with depth accumulate large amounts of CO_2 within lower horizons even though absolute production rates are lower, 2) roots are not evenly distributed throughout the soil, resulting in different rates of CO_2 production, and 3) respiration from non-photosynthetic parts of mosses add to CO_2 production
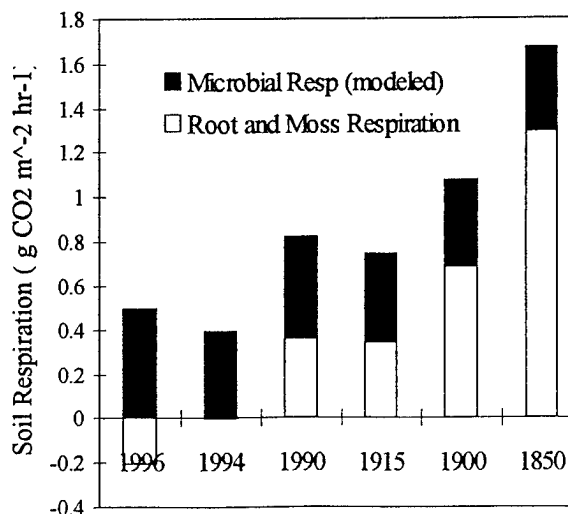
Fig. 5. Changes in components of soil respiration over time since fire. Values represent site means.

300

at depth. Surface emissions are lower than those found deeper in the profile because they represent the net effect of soil respiration and photosynthetic uptake.

Results from the BRESP model suggest that CO_2 flux from soils of mature black spruce stands is dominated by root respiration. Immediately following a fire (1996 burn) the model predicts higher CO_2 flux from microbial respiration alone than was actually measured in the field; in other words, more than 100% of post-fire soil respiration can be explained by microbial respiration. The model continues to predict a relatively high microbial respiration until 1990, when this number drops to 56% of the total soil CO_2 flux. Although this decrease can be partially explained by the re-growth of understory trees, associated root systems, and mosses, differences in burn severity between sites may also contribute to this shift. In mature (80 to 140 year), unburned, black spruce stands, the model suggests that 64-77% of total soil respiration comes from root respiration. By this time, canopy trees have re-grown, root systems have been re-established, and mosses carpet the forest floor. Due to the constraints of our chronosequence, we were unable to model results from burned stands greater than six years old; thus, at this time, it is difficult to determine at what point CO_2 production becomes dominated by root respiration. It should be emphasized that this model was not verified for our field sites and no laboratory measurements were made to assess the validity of model parameters obtained from the literature. In addition, these parameter values are likely to vary spatially, vertically within the soil profile, and as a function of time. Use of a single parameter value for all locations and times undoubtedly introduces significant error into the model. Nonetheless, the results from this approach offer encouraging agreement to field observations of root re-growth and measurements of soil respiration.

Although this data set provides some interesting insights into fire and soil dynamics, several key points must be kept in mind: 1) the data presented were collected from a single season and may not adequately represent time-averaged values, 2) slight variations between sites may mask or account for significant portions of changes observed over time, and 3) sites were sampled on different dates under different ambient conditions with no means of quantifying these differences. The winter of 1995-96 experienced an unusually low snowfall which resulted in atypical soil moisture and temperature conditions during the study period. However, soil moisture measurements have been collected at the Tok aspen, white spruce, and black spruce sites since 1991 and preliminary soil temperature measurements and depths to permafrost were collected in August of

1995. Although the magnitudes of these variables have changed, the general relationships between temperature and moisture in these three vegetation types remained the same. Thus, it seems reasonable to expect that patterns of CO_2 emission between the soils of these three vegetation types has also remained similar. Every effort was made to ensure the comparability of sites along the chronosequence; chemical analysis of soils should help reveal any differences in site fertility or drainage.

CONCLUSIONS

Wildfire has the capacity to alter the long term processes of carbon uptake, storage, and respiration by increasing soil temperature, melting permafrost, and changing soil moisture conditions. As a result of these changes, microbial decomposition rates were greatly enhanced immediately following fire, allowing for significant CO_2 efflux from recently burned soils despite the absence of living roots. As black spruce forests recover from burning, the proportion of soil respiration coming from microbial activity decreases, until, in mature black spruce stands, emissions are dominated by root respiration.

The effect of fire on soil respiration appears to vary as a function of soil drainage and texture. Well drained aspen and white spruce stands tend to have thinner organic horizons which burn to mineral soil. The thicker organic horizons found in black spruce sites tend to hold more moisture and limit combustion to the upper parts of the organic profile. As a result, these black spruce sites often have greater amounts of carbon available for microbial decomposition after fire, and, as a consequence, higher post-fire CO_2 fluxes.

REFERENCES

Alaska Fire Service. 1994. Fire statistics and season summary. Bureau of Land Management, U.S. Department of Interior, Fairbanks, AK.

Apps, M.J., W.A. Kurz, R.J. Luxmoore, L.O. Nilsson, R.A. Sedjo, R. Schmidt, L.G. Simpson, and T.S. Vinson. 1993. Boreal forests and tundra. Water Air Soil Pollut. 70:39-53.

Billings, W.D. 1987. Carbon balance of Alaskan tundra and taiga ecosystems: Past, present, and future. Quat. Sci. Review. 6:165-177.

Botch, M.S., K.I. Kobak, T.S. Vinson, and T.P. Kolchugina. 1995. Carbon pools and accumulation in peatlands of the former Soviet Union. Glob. Biogeochem. Cycles 9(1):37-46.

Bunnell, F.L., D.E.N. Tait, P.W. Flanagan, and K. Van Cleve. 1977. Microbial respiration and substrate weight loss - I. A general model of the influences of abiotic variables. Soil Biol. Biochem. 9:33-40.

Dyrness, C.T., L.A. Viereck, K. Van Cleve. 1986. Fire in taiga communities of interior Alaska. Pages 74-86 in K. Van Cleve, F.S. Chapin III, P.W. Flannigan, L.A. Viereck, and C.T. Dyrness, (ed.). Ecological Series vol. 57: Forest ecosystems in the Alaskan taiga. Springer-Verlag, New York, USA.

Flannigan, M.D. and C.E. Van Wagner. 1991. Climate change and wildfire in Canada. Can.J. For. Res. 21:61-72.

Fung, I., J. John, J. Lerner, E. Matthews, M. Prather, L.P. Steele, and P.J. Fraser. 1991. Three-dimensional model synthesis of the global methane cycle. J. Geophys. Res. 96:13,033-13,065.

Funk, D.W., E.R. Pullman, K.M. Peterson, P.M. Crill., and W.D. Billings. 1994. Influence of water table of carbon dioxide, carbon monoxide, and methane fluxes from taiga bog microcosms. Glob. Biogeochem. Cycles. 8(3):271-278.

Harden, J.W., E.T. Sundquist., R.F. Stallard, R.K. Mark. 1992. Dynamics of soil carbon during deglaciation of the Laurentide ice sheet. Science. 258:1921-1924.

Harden, J.W., K.P. O'Neill, S.E. Trumbore, H. Veldhuis and B.J. Stocks. in review. Moss and soil contributions to the annual net carbon flux in a maturing boreal forest (OBS-NSA).

Kasischke, E.S., N.H.F. French, L.L. Borgeau-Chavez, and N.L. Christensen. 1995. Estimating release of carbon from 1990 and 1991 forest fires in Alaska. J. Geophys. Res. 100(D2):2941-2951.

Kasischke, E.S., N.L. Christensen, and B.J. Stocks. in press. Fire, global warming, and the carbon balance of boreal forests. Ecol. Applications.

Kasischke, E.S., L.L. Borgeau-Chavez, and N.H.F. French. in review. Patterns of biomass burning during wildfires in a spruce-forest complex in interior Alaska.

Kasischke, E.S., N.H.F. French, P. Harrell, N.L. Christensen, Jr., S.L. Ustin, and D. Barry. 1993. Monitoring of wildfires in boreal forests using large area AVHRR NDVI composite data. Remote Sens. of the Env. 44:61-71.

Kolchugina, T.P. and T.S. Vinson. 1993. Framework to quantify the natural terrestrial carbon cycle of the former Soviet Union. Pages 259-276 in T.S. Vinson and T.P. Kolchugina, editors. Carbon cycling in boreal forests and sub-arctic ecosystems, USEPA Conference Proceedings, September, 1991.

Kurz, W.A., M..J. Apps, T.M. Webb, and P.J. McNamee.1992. The carbon budget of the Canadian forest sector: phase I. Forestry Canada, Vancouver, British Columbia, Canada. Information Report NOR-X-26.

Kurz, W.A. and M.J. Apps. 1993. Contribution of northern forests to the global carbon cycle: Canada as a case study. Water Air Soil Pollut. 70:163-176.

Matthews, E. and I. Fung. 1987. Methane emissions from natural wetlands: Global distribution, area, and environmental characteristics of sources. Glob. Biogeochem. Cycles. 1:61-86.

Olson , J.S., J.A. Watts, and L.J. Allison. 1983. Carbon in live vegetation of major world ecosystems. ORNL-5862. Oak Ridge National Laboratory, Oak Ridge, Tennessee.

Parkinson, K.J. 1981. An improved method for measuring soil respiration in the field. J. Appl. Ecol. 18:221-228.

Schlentner, R.E. and K. Van Cleve. 1984. Relationships between CO_2 evolution from soil, substrate temperature, and substrate moisture in four mature forest types in interior Alaska. Can. J. For. Res. 15:97-106.

Schlesinger, W.H. 1984. Soil organic matter: a source of atmospheric CO_2. P. 111-127 in The role of terrestrial vegetation in the global carbon cycle, G.M. Woodwell, editor. Wiley, New York.

Stocks, B.J. 1991. The extent and impact of forest fires in northern circumpolar countries. P. 197-202 in Global biomass burning: atmospheric, climatic, and biospheric implications, J.S, Levine, editor. The MIT Press, Cambridge, Mass.

Thierron, V. and H. Laudelout. 1996. Contribution of root respiration to total CO_2 efflux from the soil of a deciduous forest. Can. J. For. Res. 26:1142 - 1148.

Viereck, L.A., C.T. Dyrness, K. Van Cleve, and M.J. Foote. 1983. Vegetation, soils, and forest productivity in selected forest types in interior Alaska. Can. J. For. Res. 13:703-720.

Whalen, S.C., W.S. Reeburgh, and K.S. Kizer. 1991. Methane consumption and emission by taiga. Glob. Biogeochem. Cycles. 5:261-273.

Wotton, B.M., and M.D. Flannigan. 1993. Length of fire season in a changing climate. The Forestry Chronicle. in press.

Early Winter CH_4 and CO_2 Emissions from Alpine Grassland Soils at Qingshuihe, Qinghai-Tibet Plateau[1]

JIN HUIJUN[2], CHENG GUODONG[2], AND LIN QING[2]

ABSTRACT

In early winter, the CH_4 flux varied from -32 to 48 $\mu g\ m^{-2}h^{-1}$, with an average of 1.8 $\mu g\ m^{-2}h^{-1}$ from the grassland surface, whereas the CO_2 flux ranged from -124.7 to 313.8 mg $m^{-2}h^{-1}$, with an average of 0.3 mg $m^{-2}h^{-1}$. At depths of 30, 50 and 80 cm in Qingshuihe in November, the fluxes of methane varied from -19 to 6.7 $\mu g\ m^{-2}h^{-1}$ and the CO_2 flux changed from -55.4 to 26.7 mg $m^{-2}h^{-1}$. At 120 cm, the CH_4 flux varied from -14.2 to 36.0 $\mu g\ m^{-2}h^{-1}$, averaging 2.0$\mu g\ m^{-2}h^{-1}$; the CO_2 absorption rates ranged from -237.2 to 96.2 mg $m^{-2}h^{-1}$, averaging -25.8 mg $m^{-2}h^{-1}$. At 200 cm in permafrost, methane was sequestered at rates from -18.5 to 32.9 $\mu g\ m^{-2}h^{-1}$, with an average of -2.1 $\mu g\ m^{-2}h^{-1}$; CO_2 was trapped at rates from -6.6 to 9.7 mg $m^{-2}h^{-1}$, with an average of -1.3 mg $m^{-2}h^{-1}$.

Key words: CO_2 and CH_4, emission and sequestration, alpine grassland and permafrost.

INTRODUCTION

The globe's largest area covered by high altitudinal permafrost, the Qinghai-Tibet Plateau, accounts for 85% of the world's high altitudinal permafrost. A large amount of carbon has been deposited and sequestered in the formation of permafrost resulting from the strong uplifting of the Qinghai-Tibet Plateau during the Quaternary. The high thermal sensitivity and the temperatures of the plateau permafrost suggest that a substantial amount of methane might be released into the atmosphere when rising ground temperatures and the subsequent general retreating and thinning of the permafrost occur as the results of climatic warming. However, how the predicted dramatic changes of heat and moisture conditions in the active layer and shallow permafrost in the plateau permafrost regions will affect the emission and release mechanisms of the trapped CH_4 and organic materials is still poorly known. We tried to study the emissions, absorption and sequestration of CH_4 in the active layer and shallow permafrost through the observation of the emission rates on the undisturbed soils at different depths with a closed static chamber technique in Qingshuihe in November 1995.

THE STUDY REGION

Sampling site B (35°26'N, 93°35'E; elevation 4500m) is on the moist grassland dominated by *Stipa purpurea* on the first terrace of the Qingshuihe River in the continuous permafrost zone of the Qinghai-Tibet Plateau. The soils are lacustrine sediments at site B. Sampling site C was set up on the water surface of the Qingshuihe River. The river bed is rich in dark silt. The sediments are unfrozen within 100 cm beneath the water. The sampling sites D, E, F, G, H and I are in the soil at depths of 30, 50, 80, 120, 140, and 200 cm in the vicinity of site B. During the observation period, the weather was sunny and the ground surface was free of snow.

SAMPLING METHODS

The closed static chamber (polycarbonate, 65 × 65 × 90 cm) technique was applied in the measurements of methane flux from the dry grassland surface at site B and from the water surface at site C. The chamber at site B was inserted about 7 cm into the soil; the chamber at the site C was inserted 5 cm into the river bed, where the water was quiet and 20 cm in depth. A water exclusion method was applied in the sampling. A syringe of 250 mL in capacity was used as the pump to suck gas samples from the static chambers through the infusion system

the overtopping soils. The gas sampling started on 5 November 1995 and continued 2-4 times a day until 24 November 1995. During the sampling, air and ground temperatures were recorded.

RESULTS AND DISCUSSIONS

Emission rates of CH_4 from the grassland surface at Qingshuihe

At Site B, the CH_4 emission rates varied from -16.1 to 23.9 $\mu g\ m^{-2}h^{-1}$, with an average of 1.82 $\mu g\ m^{-2}h^{-1}$ (Table 1). The emission rates display diurnal variations: the rates are generally high at noon, afternoon and evening, which may

Table 1: CH_4 emission rates in Qingshuihe

Site	CH_4 concentrations ($\mu g\ g^{-1}$)			CH_4 emission rate ($\mu g\ m^{-2}h^{-1}$)		
	Minimum	Mean	Maximum	Minimum	Mean	Maximum
B (0.0)	0.828	0.949	1.103	-16.1	1.82	23.9
D (0.3)	0.772	0.904	1.103	-5.2	0.09	5.8
E (0.5)	0.772	0.922	1.324	-13.8	-0.37	9.2
F (0.8)	0.882	1.041	1.103	-19.0	-1.74	6.7
G(1.2)	0.828	0.981	1.214	-14.2	2.04	36.0
H(1.4)	0.828	1.108	1.159	-69.0	-2.15	25.2
I (2.0)	1.103	1.183	1.269	-18.5	-2.12	32.9
C (River)	0.772	0.949	1.214	-21.0	1.56	37.1

connecting the chamber and saturated saline water. The gas samples were stored in glass bottles of 250 mL capacity, and a rubber seal was tightly placed on the mouth of the bottle under the saline water. The residual water in the sample bottles was about 30~50 mL. The bottles were sealed with wax and they were kept upturned until the analyses on the mass chromatograph (Finnigen MAT-271) in the State Key Laboratory of Gas Geochemistry and Biogeochemistry, Lanzhou Institute of Geology, in December of 1995. The precision of the MAT-271 is 0.1 pp mV (0.05 $\mu g\ g^{-1}$) for CH_4 and 1 pp mV (1.5 $\mu g\ g^{-1}$) for CO_2.

The gas samples from the soil at different depths were collected using the revised static chambers made of vertically parallel steel tubes with diameters of 160-165 mm and lengths of 30, 50, 80, 120, 140 and 200 cm, in accordance with the sampling depth in the soils. A gas valve was placed on the top of each tube. The tubes were set in the soil layers at different depths. These soil layers were exposed by careful clearing of

result from the daily freeze-thaw cycles and the strong photochemical reactions during the day on the plateau.

The average emission rates of methane from the grassland surface in Qingshuihe in November are quite low compared with the annual average emission and absorption rates observed in similar soils in temperate grasslands, tundra and deserts. The annual average CH_4 consumption rates in semiarid temperate grasslands vary from 33~114 $\mu g\ m^{-2}h^{-1}$ (Mosier et al. 1991, Tate and Striegl 1993), which is similar to the values in the Nevada desert (Striegl et al. 1992). The annual average CH_4 emission rates are 22.3±24 $\mu g\ m^{-2}h^{-1}$ in various soils in Germany (Koschorreck and Conrad 1993).

The emission rates of CO_2 from the moist and clayey alpine grassland surface vary from -124.7 to 313.2 mg $m^{-2}\ h^{-1}$, with an average of 0.3 mg $m^{-2}\ h^{-1}$ (Table 2).

305

Table 2. CO₂ emission rates in Qingshuihe compared with other regions.

Site	emission rates (mg m⁻² h⁻¹)			sampling data
	Minimum	Mean	Maximum	Observation period
B(surface)	-124.7	0.3	313.2	95.11.05-14
D(30cm)	-55.4	-2.9	26.7	95.11.05-14
E(50cm)	-26.4	-1.2	14.4	95.11.05-09
F(80cm)	-6.6	-1.3	9.7	95.11.05-09
G(120cm)	-237.2	-25.8	96.2	95.11.05-09
H(140cm)	-300.3	-41.3	48.1	95.11.05-09
I(200cm)	-69.8	-6.2	102.7	5.11.05-09
C(River)	-81.7	-3.2	32.2	95.11.05-14

September-April CO₂ emission rates in high latitude tundra

Month	Emission rates(mg m⁻² h⁻¹)	Study region	Year	References
September	12.2	Alaska	1965	Kelley et al., 1968
Oct.-Dec.	24.4-27.5	Alaska	1965	Kelley et al., 1968
December	39.7	NE Siberia	1989	Zimov et al., 1993
Jan.-Feb.	6.1-7.6	Alaska	1966	Kelley et al., 1968
January	19.9	NE Siberia	1990	Zimov et al., 1993
February	10.7	NE Siberia	1990	Zimov et al., 1993
Mar.-Apr.	3.1-4.6	Alaska	1966	Kelley et al., 1968

Emission rates of CH₄ from the water surface of the Qingshuihe River

The observations during 5-14 November 1995 indicates that emission rates of CH₄ from the river bottom of the Qingshuihe River varied from -21.0 to 37.1 μg m⁻²h⁻¹, with an average of 1.56 μg m⁻²h⁻¹. Diurnal variations of CH₄ emission rates also are noticeable: the emission rates in the afternoon and evening are higher than at night and in the early morning.

MEASUREMENTS AT SITES D, E, F, G, H AND I

CH₄ flux rate variations

From the vertical variations of CH₄ emission rates at different depths (Table 1), the mean CH₄ flux rates are positive at the ground surface and at 30 and 120 cm in the subsurface; are negative at 50, 80, 140 and 200 cm.

Ground water level may influence the CH₄ flux in Qingshuihe. The positive flux rate in the active layer is observed at the depth of 120 cm, which is located in the waterlogged, anaerobic environment between the water table (110 cm) and the permafrost table (140 cm), favoring methanogenesis.

The results at Qingshuihe suggest that the CH₄ flux rates are weakly correlated with soil moisture and temperature.

CO₂ flux rate variations

CO₂ is absorbed or trapped at depths of 30, 50, 80, 120, 140 and 200 cm (Table 2), with the two largest mean uptake rates of 25.8 mg m⁻²h⁻¹ at 120 cm and -41.3 mg m⁻²h⁻¹, which are an order of magnitude higher than those at other depths.

CONCLUSIONS

1. The emission rates of CH₄ from the water surface in the Qingshuihe River, Qinghai-Tibet Plateau are much smaller than those

306

observed in the high latitudes. The measurements from the water bottom of lakes and rivers between 50°-70°N indicate that the mean emission rates of CH_4 range from 150 to 3,200 $\mu g\ m^{-2}h^{-1}$, which are two orders higher than that (1.56 $\mu g\ m^{-2}h^{-1}$) observed in the Qingshuihe River. The observed values of CH_4 emission rates at high latitudes vary from 83 $\mu g\ m^{-2}h^{-1}$ to 10,800 $\mu g\ m^{-2}h^{-1}$ (Whalen and Reeburgh 1990, Moore and Knowles 1990, Ritter et al. 1991), which are also much higher than that in the Qingshuihe River. The CH_4 emission rates in the Qingshuihe River also display diurnal variations, which might be attributed to photochemistry under the strong plateau solar radiation. The oxidation of CH_4 to CO_2 by photochemical reactions stimulated by the strong radiation and high temperatures during the 8:00 to 20:00 period may be responsible for the low CO_2 emission rates in the afternoon and evening and the high emissions during the night and in the morning.

2. The observed results may suggest that the alpine grassland is emitting methane at a flux rate about 1 to 2 $\mu g\ m^{-2}h^{-1}$ during early winter. The CO_2 flux from the moist and clayey alpine grassland surface at Qingshuihe range from -124.7 to 313.2 mg $m^{-2}h^{-1}$, with an average of 0.30 mg $m^{-2}h^{-1}$. It seems that the mean CO_2 flux from alpine grassland surfaces during October and November in the Cumaer Highland of the Northern Qinghai-Tibet Plateau is between 0 and 1 mg $m^{-2}h^{-1}$, which is quite low compared with that reported in Northeastern Siberia (Zimov et al. 1993) and Alaska (Kelley et al. 1968).

3. The soils at 120 cm in the active layer tend to release methane at an average rate of 2.0 $\mu g\ m^{-2}h^{-1}$; the other layers tend to absorb and sequester methane. These values are about 2 $\mu g\ m^{-2}h^{-1}$. The flux rates of CO_2 are negative in the active layer, implying the sequestration of CO_2 by freezing and by frozen soils. The average CO_2 uptake rates (-41.3~-25.8 mg $m^{-2}h^{-1}$) in the vicinity of the water table (120cm) and the permafrost table is an order of magnitude higher than that of other layers (-1.2 to 6.2 mg $m^{-2}h^{-1}$).

REFERENCES

Kelley, J. J., D. F. Weaver and B. P. Smith. 1968. The variation of carbon dioxide under the snow in Arctic. Ecology 49(2), 358-361.

Koschorreck, M., and R. Conrad. 1993. Oxidation of atmospheric methane in soils: Measurements in the field, in soil cores and in soil samples. Global Biogeochemical Cycles 7(1), 109-121.

Moore, T. R., and R. Knowles. 1990. Methane emissions from fen, bog, and swampy peatlands in Quebec. Biogeochemistry 11, 45-61.

Mosier, A., D. Schmel, D. Valentine, K. Bronson, and W. Parton. 1991. Methane and nitrous oxide fluxes in native, fertilized and cultivated grasslands. Nature 350, 330-332.

Ritter, J. A., C. Watson, J. Barrick, G. Sachse, J. Collins, G. Gregory, B. Anderson, and M. Woerner. 1991. Airborne boundary-layer measurements of heat, moisture, CH_4, CO_2 and O_3 fluxes over Canadian boreal forest and northern wetland regions. EOS 72, 34.

Striegl, R. G., T. A. McConnaughey, D. C. Thorstenson, E. P. Weeks, and J. C. Woodward. 1992. Consumption of atmospheric methane by desert soils. Nature 357, 145-147.

Tate, C. M., and R. G. Striegl. 1993. Methane consumption and carbon dioxide emission in tallgrass prairie: effects of biomass burning and conversion to agriculture. Global Biogeochemical Cycles 7(4),735-748.

Whalen, S. C., and W. S. Reeburgh. 1990. Consumption of atmospheric methane by tundra soils. Nature 346, 160-162.

Zimov, S. A. , I. P. Zemiletov, S. P. Daviodov, Yu. V. Voropaev, S.F. Prosyannikov, C. S. Wong, and Y.-H. Chan. 1993. Wintertime CO_2 emissions from soils of Northeastern Siberia. Arctic 46, 197-204.

Additional Methane Emission from Thawing Cryosols Yamal Peninsula, Russia

F.M. RIVKIN[1]

ABSTRACT

The additional methane emission that may occur due to climate warming depends on the content of methane in cryosols and the increasing thickness of the seasonally thawed layer. The content of the methane varies from 0.01 to 12 mL/kg in the upper horizons of the cryosols. One can predict that the surface of the permafrost will be decreased by 0.1-0.5 m as a result of the climate warming on the Yamal Peninsula. The surface of the permafrost will decrease by 0.03-0.8 m by different technogenic transformations of the natural landscapes and 0.2-0.5 m by climate warming. We estimate that the potential supplementary emission may range up to 1000 m^3/km^2 as a result by the increasing of the depth of the seasonal thaw by 0.1 m.

Key words: Additional methane emission, syncryogenic sediments, epicryogenic sediments, thermokarst depressions, sub-river-bed taliks.

INTRODUCTION

Recent studies, conducted in different regions (both outside and within the boundaries of the gas fields) (Gilichinsky et al. 1993, Rivkina et al.1992, 1995, Rivkin 1996b, Yakushev and Istomin 1990) have demonstrated that perennially frozen ground contains a tremendous pool of radiationally active gases, methane included. The methane level in frozen ground exhibits substantial variations, depending on their genesis, and freezing conditions, and may be regarded as a specific paleomarker (Gilichinsky et al. 1993, Rivkina et al. 1992, 1995, Rivkin 1996). Some frozen grounds (epicryogenic formation) have been found to contain methane, whereas others (syncryogenic) proved to be methane-free or contain it in minor quantities.

It is known that the expected climate warming at northern latitudes will result in a higher mean-annual temperature of soils and an increased depth of their seasonal thawing. Irrespective of their technogenic or natural origin, the deeper thawing or the degradation of frozen ground will create preconditions for the additional emission to the atmosphere of methane and carbon dioxide cryoconserved in frozen ground in situ. Furthermore, the deeper seasonal thawing (primarily in hydromorphic areas) will promote the methane production during the summer period and thus contribute to its higher emission.

The most realistic climatic scenario resulting from the greenhouse effect will be an increase of the mean annual temperature by 1-2°C. According to different estimates, the rise of the mean annual air temperature in Yamal by 1-2°C will increase the depth of seasonal thawing of ground by 20-50 cm.

Recent technogenic perturbations of the land surface are conducive to consequences that are to a considerable extent analogous to those expected from climate warming. Disturbances in the natural cover of tundra provoke a 0.03 to 0.8 m increase in the depth of seasonal thawing of soils. Under favorable conditions the methane enclosed in this layer may also be released to the atmosphere.

Evidently, the consequences of the technogenic impact on frozen ground (specifically, the increased depth of seasonal thawing) have much in common with the predicted effects of global climate warming. Therefore, the technogenic effects on frozen ground may be regarded as an actual natural model of climate warming, including the estimation of additional methane emission.

The experience gained in exploiting gas fields shows that the extraction and transport of gas by pipe-lines are unavoidably accompanied by its losses resulting from breakdowns, technological emissions, microleakages, etc.(Rivkin 1995,1996a). From this view point, the elucidation of the regional regularities of methane level in frozen ground and mapping of respective areas are, in our opinion, an important component of the monitoring of natural conditions in gas and oil fields. This makes it possible to differentiate the contributions of technogenic losses of methane during gas extraction and its spontaneous emission from natural landscapes to the total methane level in the atmosphere above gas fields.

---

[1] Industrial Research Institute for Engineering of Construction, Laboratory of Geocryologi, 18, Okruzhnoi pr., Moscow, 105058, Russia, PNIIIS

RESEARCH AREA AND METHODS

Our studies were carried out at three sites of the Bovanenkovo gas deposit in the Yamal Peninsula (Fig. 1). The northern sites are situated in the Nguri-Yakha River Valley in its middle and upper reaches. The upper part of the site profile is represented by a complex of polygenetic sediments of the Upper Pleistocene ($mIII^{3-4}$) and Holocene age and composed of sands, sandy loams and clays. The tops of terraces are formed of sandy loams. Silty sands lie below and reach the surface only in the marginal parts of watersheds at control marks below 18.0 m. Remaider of the second terrace with absolute marks of surface of terrace than 18 m above sea level are composed of sands. Sands are lined with saline loams ($mIII^{2-3}$, third marine terrace) with reticular cryotextures characteristic of epigenetic rocks. Loams are often associated with thick ice sheets. The southern (second, Fig. 1) site is located on the surface of the third marine terrace ($mIII^{2-3}$) and formed mostly by silty sands and sandy loams.
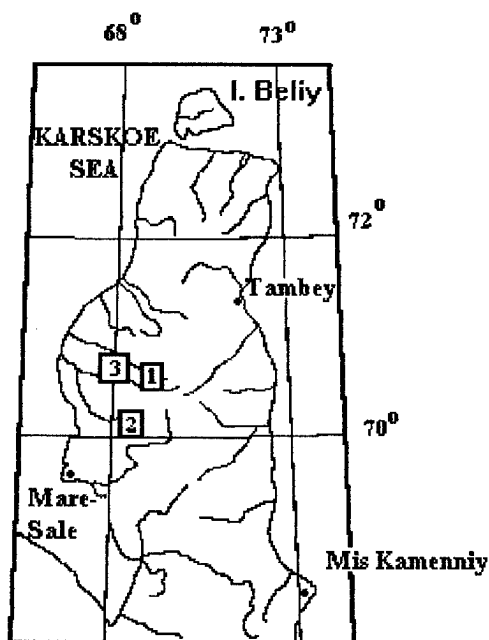
Figure 1. Research area: Yamal Peninsula. Sites of the research: 1 and 2(1994), 3(1995).

Samples for analysis (130 samples of frozen cores) were taken from 19 boreholes up to 10 m deep. The core temperature was from -2 to -7°C. Gas was sampled from frozen cores during their thawing in airtight flasks. Gas samples were preserved in vials with saline seals. During sampling of frozen ground from boreholes were conducted, parallel measurements of methane emission to the atmosphere were performed by the nontransparent chamber technique at semi-stationary and mobile observation posts. Methane levels were determined with the help of a stationary chromatograph with a flame-ionization detector.

RESULTS

The basic results of our studies are presented in Table 1. Methane distribution in the upper horizons of frozen ground is extremely irregular. In a number of boreholes methane was absent throughout their depth; in others it was present in ground at all depths. There were also boreholes where no methane was detected in the upper part of the section, whereas it was present in the embedding frozen grounds (Fig. 2 and 3). The methane level in frozen ground varies from 0 to 22.45 mL/kg. The average methane content in the test area of Middle Pleistocenec marine terraces was 0.5-0.6 mL/kg, whereas the average methane level in marshy lake troughs and thermokarst depressions was 6.0-6.5 mL/kg. In the upper part of the profile, the content of methane in a 1-m-thick layer beneath the zone of seasonal thawing varies within a smaller range: from 0.0 to 13.3 ml/kg. On terraces and in marshy depressions its mean level is 0.4-0.5 ml/kg and 2.6-2.8 mL/kg, respectively. Virtually no methane has been revealed in alluvial sediments.

The mean daily fluxes of methane from the surface of natural landscapes are not large and vary from 0 to 2-3 mL/(m^2.h) on dry surfaces of watershed sites reaching 130 mL/(m^2.h) in the hydromorphous areas of lake depressions. Relatively small methane fluxes from natural landscapes contrasted with abnormally high methane emissions (up to 1200 mL/(m^2.h) in the hydromorphous areas of stream and river valleys.

DISCUSSION

In the cryogenetic respect, the Upper Pleistocene ($mIII^{2-3}$, $mIII^{3-4}$) sediments are characterized by a two-layer structure. Their upper 5- to 10-m-thick part is defined as syncryogenic, whereas the lower portion is regarded as epicryogenic. The cryogenetic two-layer character of the geologic profile in this region was confirmed by the results of numerous studies based on cryolithological analysis of basal profiles (Geokrilogiya SSSR 1989).

The studies conducted outside the boundaries of gas-bearing provinces revealed fairly stable relationships between the methane content in frozen grounds and their genesis (Gilichinsky et al. 1993, Rivkina et al. 1992, 1995). These regularities suggest that in the area under study one should also expect the

309

presence of methane in the epicryogenic frozen grounds and its absence in the syncryogenic ones. The ubiquitous presence of methane in the profiles described earlier as cryogenetically two-layer ones is indicative of either the regional specifics of the methane distribution in frozen ground or the cryogenetic homogeneity of the profile within the limits of the test area.

Outside the boundaries of the gas deposit (Fig. 2, B), methane was present in samples taken at marks of 32 m and below. At the terrace top (absolute mark of 32 m) no methane was detected down to a depth of 5 m. Apparently, this is became the upper (syncryogenic) part of the profile of frozen ground has partially degraded on the surface of the third marine terrace, as a result of land upheaval in the Late Pleistocene. At high terrace marks the syncryogenic

methane-free frozen ground has been preserved and lie near the surface. At marks below 32 m the syncryogenic frozen ground have degraded, and the surface is occupied by the epicryogenic methane-bearing frozen grounds. Possibly, the absolute mark of 32 m should be regarded as the regional boundary between the epicryogenic and syncryogenic profile portions. Thus, the methane-bearing rocks are localized at the periphery of terraces, whereas in their central parts, the syncryogenic rocks lie on the surface.

Within the gas field boundaries (Fig. 1, sites 1 and 3) all boreholes are situated on different geomorphological levels but at marks below 32 m (Fig. 2 and 3). Methane was revealed in nearly all wells, except those exposing recent and Pleistocenec alluvial sediments (Table 1). As all the boreholes at

Table 1. Methane distribution in near-surface permanently frozen sediments of gas deposit Bovanenkovo (Yamal Peninsula).

Suite	*Sediments*	CH_4 mL/kg *		
		sections		
		1(1994)	*2(1994)*	*3(1995)*
mQ$_{III}^{2-3}$, late	sand	-	0.0-2.4 0.8(7)	-
Pleistocene	sandy-loam	-	0.0-1.13 0.51(2)	-
marine	loam	-	-	0.06-0.63 0.33(3)
sediments	ice**	-	-	0.05-0.09 0.07(4)
mQ$_{III}^{3-4}$, late	sand	0.0-1.28 0.41(13)	-	0.01-3.39 0.28(21)
Pleistocene marine	sandy-loam	0.0-13.24 2.34(16)	-	0.09-0.42 0.25(4)
sediments	ice***	-	-	0.24-0.43 0.34(2)
aQ$_{III}^{3-4}$, late	sand	0.0(1)	-	-
Pleistocene alluvial sediments	ice**	0.0(1)	-	-
lQ$_{IV}$, Holocene	sand	-	-	0.13-4.5 1.44(47)
lacustrine	sandy-loam	-	-	0.02-5.53 3.63(5)
sediments	loam	-	-	22.45(1)
	peat	1.48(1)	-	2.11(1)

* In numerator: the minimal and maximal values; in denominator: the average value and (in the brackets) the number of investigated probes.
** Sheet ice.
*** Wedge ice

310
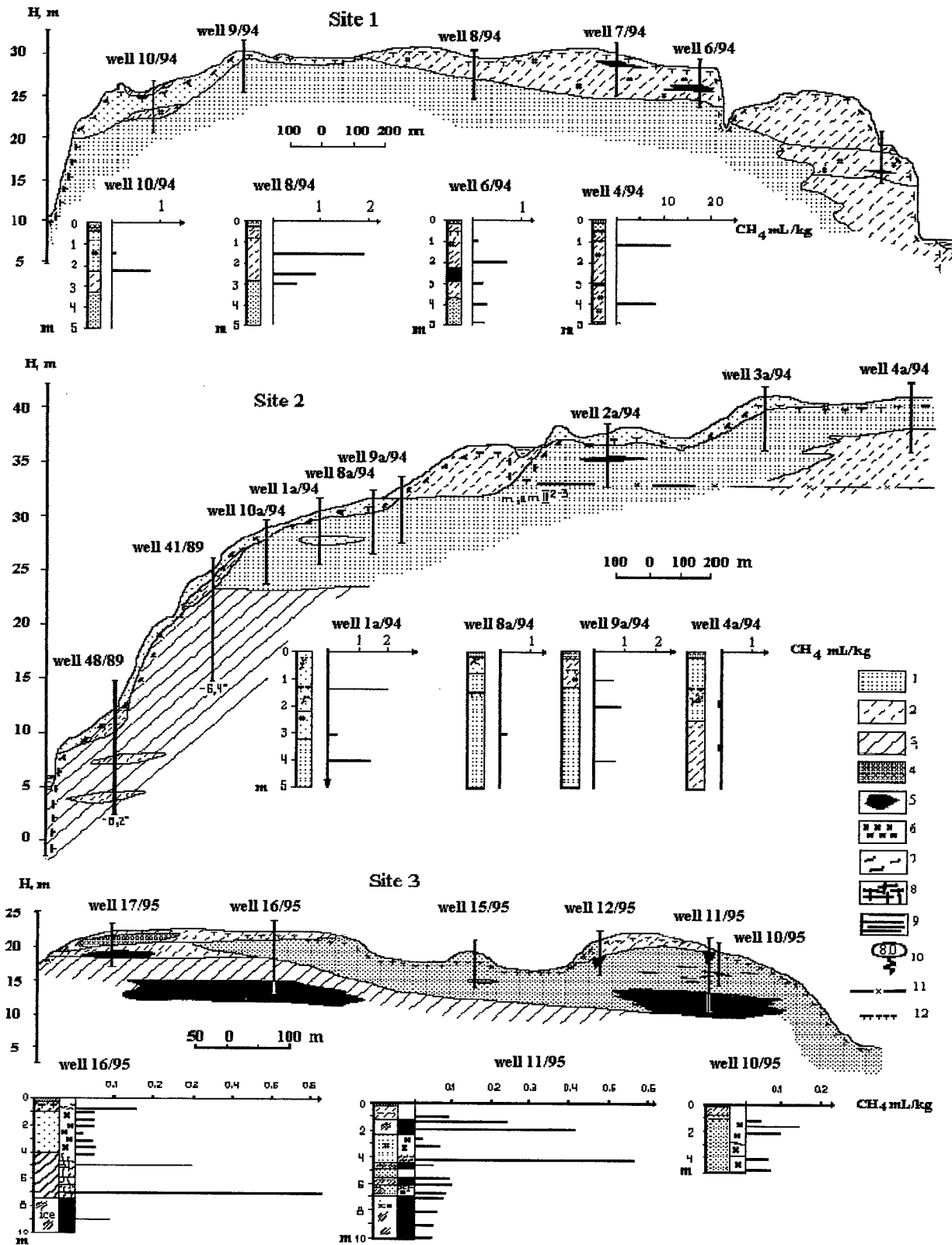
Figure 2. Distribution of methane in near-surface permanently frozen sediments (sites of the research at Figure 1): 1) sand; 2) sandy-loam; 3) loam; 4) peat; 5) ice; 6) massive cryogenic structure; 7) ice stakes cryogenic structure; 8) reticulate cryogenic structure; 9) layered cryogenic structure; 10) daily fluxes of methane, mL/(m² . h);11) proposed border of syncryogenic and epicryogenic frozen ground; 12) permafrost table.

311
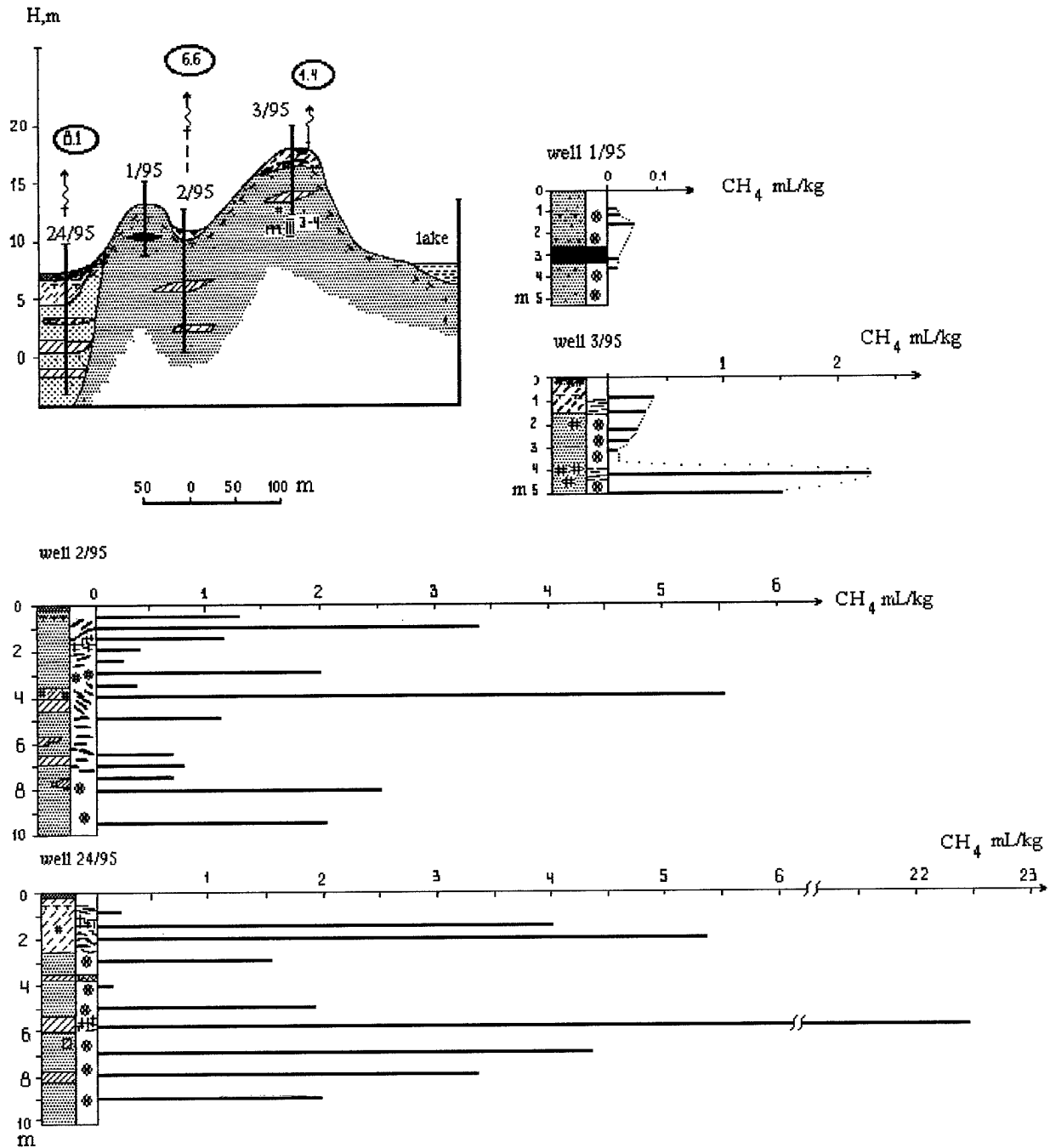
Figure 3. The distribution of methane in near-surface frozen sediments on the thermokarst lake depression (khasyrey) and marine terrace: North part gas deposit Bovanenkovo (legend in Fig. 2).

sites 1 and 3 are situated below the mark of 32 m, one cannot rule out that here, too, bacame the syncryogenic methane-free portion of the frozen ground profile was destroyed as a result of land upheaval. Possibly, it was preserved in the areas of terraces with higher absolute marks.

It is noteworthy that the thick solid layer of frozenground covering the gas deposit seems to be

impermeable for methane. This is confirmed by the comparison of the results of measurements of the methane concentration in frozen ground, methane emission from the surface, studies of the phase composition of methane in frozen ground, and their permeability to gases (Gilichinsky et al. 1993, Rivkina et al.1995, Rivkin 1996). However, there are data pointing to an increased methane flux in the zones of

most recent tectonic disturbances. Apparently, a higher methane flux in the study area is also associated with the existence of taliks under river beds and lakes. Our single observation pointed to the existence of an abnormally high methane flux in river valleys from the sub-river-bed taliks.

Analysis of the methane content in frozen ground shows that its highest levels are associated with thermokarst depressions: valleys of the thermokarst lakes (khasyrey) and thermokarst troughs of the runoff from terrace slopes; such an increased methane content appears to be of a secondary character. The methane conservation in the Upper Pleistocenec sediments occurred here at the end of Late Pleistocene as a result of land uplifting and epigenetic freezing of ground. The methane concentration in this ground reflects the biogeochemical situation at the moment of freezing. The Holocene warming resulted in a wide development of thermokarst processes in the area under study and was conducive to the formation of numerous lakes and sublake taliks. The anaerobic conditions favorable for methane production and accumulation were predominant in such areas (Gilichinsky et al. 1993, Rivkina et al. 1995). Subsequent epigenetic freezing of taberal sediments and sublake taliks led to methane conservation. Thus, the thermokarst modification of the relief in the Holocene resulted in the methane saturation of frozen graunds, which form nowadays marshy lake craters and other thermokarst depressions. The methane content in the constituent frozen graunds of such areas is one- to two orders of magnitude higher than that on marine terraces.

On marine terraces, where the frozen grounds did not virtually thaw in the Holocene, the mean methane content in the 1-m-thick layer below the zone of seasonally thawed grounds is no more than 0.4-0.5 mL/kg. In lake depressions the methane level varies within the range from 0 to 3.5 mL/kg with an average of 2.6-2.8 mL/kg.

A definite correlation was observed between the methane level in frozen graunds and their dispersion (Rivkin 1996b). A trend toward the increase in the methane content with a higher degree of dispersion was revealed in the following sequence: sand, loamy sand, loam. This is, however, manifested only within the limits of the same genetic type of sediments. For instance, the methane content in Holocenic lake sands is lower than in lake sandy loams, though it is one order of magnitude higher than in sediments of the Upper Pleistocene.

CONCLUSION

Thus, the area under study was found to include several natural landscapes differing by methane content in the upper part of their profiles. However, the data reported to date are insufficient for a substantiated delineation of landscapes on the basis of this parameter.

Methane is absent in the most recent and Pleistocene syncryogenic alluvial sediments as well as in the upper (syncryogenic) portion of the profile of marine terraces at absolute marks higher than 32 m above sea level. Methane is contained in epicryogenic marine sediments forming high terraces at absolute marks below 32 m, marshy lake depressions, thermokarst ravines on the slopes of marine terraces.

For the time being, analysis of the results obtained has allowed the differentiation of the territory of one of the three studied sites (site 3) with regard to the methane content in the 1-m-thick layer under the upper limit of frozen grounds, and this layer will be the first to thaw in case of warming or technogenic impact. Three levels with substantially different methane contents in the frozen graund may be distinguished (Tabl. 2):
- Contemporary floodplains and alluvial terraces (< 0.01 mL/kg);
- Marine terraces (up to 0.5 mL/kg);
- Thermokarst lake depressions (khasyrey) (up to 3 mL/kg).

It is noteworthy that the surface layer of this site is formed mostly by sands in which the methane content is low, even in lake depressions. In the lake depressions formed by sandy loams, the mean methane level reaches 12 mL/kg. Such a zoning allows a quantitative estimation of the additional methane flux, which will potentially be released to the atmosphere during the degradation of perennially frozen grounds.

At the site under study, a 10-cm lowering of the upper limit of frozen ground may potentially be the cause of additional methane emission (without account for the changes in the methane release due to the increased thickness and the hydromorphic character of the seasonally thawed layer):
- On marine terraces the additional methane emission may achieve 150 m^3/km^2;
- On khasyreys formed by sands - up to 300 m^3/km^2;
- On khasyreys formed by clays - up to 1300 m^3/km^2.

The area of the Bovanenkovo deposit is about 2000 km^2. According to rough estimates, the marshy lake depressions account for 10-15% of the total area or 200-300 km^2. This means that upon a 10-cm-deep degradation of frozen grounds, the additional methane emission may be substantial, even from the surface of marshy landscapes alone. On the other hand, the increase in the depth of seasonal thawing on

drained sandy terraces will not be conducive to any considerable modification of the methane release.

Table. 2 Diagram of the CH₄ level in upper thick part of frozen ground.

Level	*Suite and cryogenetic type*	*Section*	*Sediments*	*CH₄, mLl/kg*
I. Marine terraces	mQ_{III}^{2-3}, mQ_{III}^{3-4} late Pleistocene marine sediments. Cryogenic type: Upper: thick part is syncryogenic, Lower portion is epicryogenic	nonerosional dry surfaces	sand	0.01-0.1
			sandy-loam, loam	0.1-0.5
		bogginess depressions (ravines) on the slopes of terraces	sand	0.5-1.5
			loam	?
II. Alluvial terraces	mQ_{III}^{3-4}, late Pleistocene and Holocene alluvial sediments	dry plain surfaces	sand, sandy-loam	0
III. Lake depressions	lQ_{IV}, Holocene lacustrine	bogginess plain surfaces	Upper portion: thick sandy-loam, in the Lower portion : sand	1.5-2.5
			loam	12

REFERENCES

Geocryology of the USSR, West Siberia 1989. Moscow: Nedra, 356 p. (in Russian).

Gilichinsky, D.A., E.M.Rivkina and V.A.Samarkin 1993. The microbiological and biogeochemical research in permafrost: paleoecological implication. *In* Proceedings of the 6th Int. Conf. on Permafrost. Beijing, 1993, v. 3, pp. 869-874.

Rivkin, F.M. 1995. Technogenic taliks along main gas pipe-lines as sources of greenhouse gases. *In* Evolutionary and Geocryological Processes in Arctic Regions and the Problem of Global Environmental and Climatic Changes in the Cryolithozone. Scientific Board on Earth's Geocryology, Russian Academy of Sciences. Abstracts of Annual Assembly. Pushchino, 1995, p. 90 (in Russian).

Rivkin, F.M. 1996a. Some results of the studies of the methane emission along gas pipe-lines (northern part of West Siberia). *In* Scientific Board on Earth's Geocryology, Russian Academy of Sciences. Abstracts of Annual Assembly.

Pushchino, 1996, pp. 156-157. (in Russian).

Rivkin, F.M. 1996b. Methane in frozen grounds and certain aspects of its emission (Bovanenkovo gas-condensate deposit, Yamal peninsula). *In* Proceedings of the First Conf. of Russian Geocryologists. Moscow, 1996, v. 2, pp. 273-278 (in Russian).

Rivkina, E.M., V.A. Samarkin and D.A. Gilichinsky 1992. Methane in perennially frozen grounds of the Kolyma-Indigirka lowland. *Dokl. RAN*, v. 323, No. 3, pp. 559-562 (in Russian).

Rivkina, E.M., D.A.Gilichinsky, S. McKay, V.E. Ostroumov, V.A.Samarkin, C. Cniba, N.V. Ostroumova 1995. Methane in permafrost grounds: distribution, aggregation state, paleoreconstruction and prognosis. *In* Evolutionary and Geocryological Processes in Arctic Regions and the Problem of Global Environmental and Climatic Changes in the Cryolithozone. Scientific Board on Earth's Geocryology, Russian Academy of Sciences. Abstracts of Annual Assembly. Pushchino, 1995, p. 90 (in Russian).

Nitrogen

Soil and Plant N Dynamics of
Annual Barley in Interior Alaska

V.L. COCHRAN[1]

ABSTRACT

Interior Alaska's long days promote rapid plant growth and N uptake, while low soil temperatures limit the supply of N. This paper presents the results of several studies, and relates the availability of various N sources to barley N uptake. Potential grain yields are about 3000 kg ha^{-1} yr^{-1} requiring 100 kg N ha^{-1}. The soil contains 10 kg NO$_3$-N ha^{-1} at spring planting; another 30 kg N will mineralize from the soil organic matter by crop maturity. The crop must get 60 kg N ha^{-1} from external sources. Green manure will supply 30 kg N ha^{-1} to the barley crop. Therefore, 30 kg N ha^{-1} must be applied as fertilizer following a green manure crop. Continued use of green manure in rotation with barley is expected to increase the rate of soil N mineralization, but it will take several years to meet the demands of a barley crop.

Key words: Nitrogen mineralization, denitrification, nitrification, green manure, nitrous oxide.

INTRODUCTION

Large-scale farming in interior Alaska began with the clearing of 40,000 ha of native forest near Delta Junction, Alaska (64° N latitude) in 1978 (Lewis and Thomas 1982). These newly cleared soils contained large amounts of semi-decomposed forest litter with a C:N ratio of 18:1 (Cochran et al., 1989). Laboratory incubations indicated that, at room temperature and water content at or above field capacity, these soils would mineralize considerable N (Sparrow et al.,1988). However, field conditions are seldom at ideal temperature and water content. Crops are often planted as soon as the soil thaws sufficiently for tillage and planting operations to start in early May. Soils are still cold and often rainfall is low and the soil dries to the depth of tillage during much of the growing season. Mineralization of N from soil organic matter depends on favorable conditions

for microbial activity. Both low temperatures and low water content are detrimental to these processes. Much of the plant growth and N uptake occurs during a time when there is little mineralization of N.

The short growing season with long days and mild temperatures of interior Alaska promotes rapid growth and nutrient uptake during the spring and summer months which do not always coincide with the ability of the soil to supply them. This paper summarizes the results of field studies on soil N mineralization, soil N immobilization and mineralization by barley straw, gaseous N losses, and N mineralization from green manured legumes with emphasis on relating this to available soil N and to N uptake requirements of a barley crop.
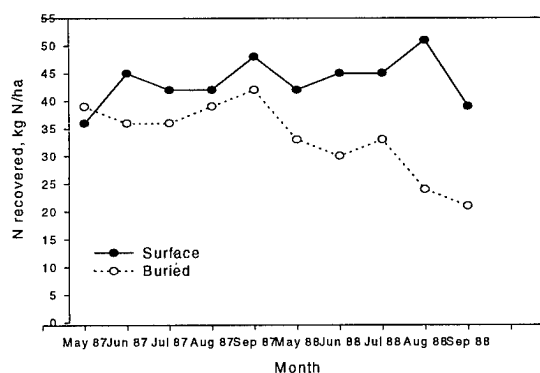
FIG. 1. *Total N recovered from barley straw in litter bags either buried 7.5 cm deep or placed on soil surface and removed at monthly intervals during the summers of 1986 and 1987.*

RESULTS

N immobilization and mineralization by straw

A study by Cochran (1991) used recovery of total N from barley straw placed in litter bags to determine that both surface and buried barley straw immobilized about 10 kg N

ha[-1] of soil N during the first year of decomposition. During the second year, buried straw mineralized 15 kg N ha^{-1} for a net gain of 5 kg N ha^{-1} over the two year period. Surface residues continued to immobilize N through most of the second season with a maximum of 15 kg N ha^{-1}, for a net difference between placements of 20 kg N ha^{-1} (Fig. 1). This is consistent with the generally accepted need for extra N fertilizer for several years after shifting from conventional tillage to no-tillage grain production in northern climates.

Soil N mineralization

The rate and timing of the mineralization of organic N to the nitrate and ammonium forms that are available to plants depends on the physical conditions of the soil such as soil water content, temperature, and the amount and availability of C in soil organic matter. The rate of solute diffusion to sites of microbial activity increases with increasing water content (Papendick and Campbell 1981); whereas, gaseous diffusion decreases with increasing water content. Linn and Doran (1984) found that aerobic microbial activity was greatest near 60% water- filled pore space. At lower water contents, either water stress or slower diffusion of nutrients to the active site slowed aerobic microbial activity. At higher water contents, oxygen diffusion was limiting and activities shifted toward anaerobic conditions. Biological activity usually follows a Q_{10} of about 2. This generally holds for microbial organisms adapted to cool soil as well. Thus, microbial activity in subarctic soils with adequate water increases as the soils warm.

Cochran et al. (1988) used undisturbed soil cores in polyethylene bags placed back in the core holes in plots planted to barley to determine that the time of N mineralization varied between years, but the seasonal total was about 40 kg N ha^{-1} (Fig. 2). There was no difference between till and no-tillage, This agrees with the above litter bag study that found no significant difference between tillage practices the first year. The spring of 1986 was cooler than normal while the following year the spring was warmer than normal, yet the total amount of N mineralized was the same indicating that annual N mineralization was constant even though there were climatic differences. At no time was there a negative response indicating that gross mineralization always exceeded gross immobilization. Water content in the

polyethylene bags was near field capacity thoughout the study; thus, differences in time of N mineralization between years were likely due to difference in soil temperature.
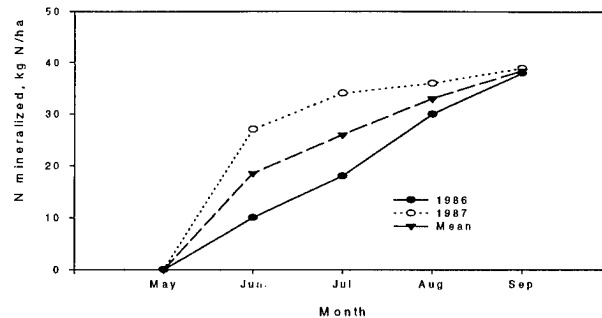
FIG 2. *Increase in mineral N recovered from undisturbed soil cores placed at original soil depth in closed polyethylene bags at planting and removed during the summers of 1986 and 1987.*

Gaseous N losses

Gaseous N losses can be significant via denitrification pathways when nitrate and available carbon are present in the absence of adequate oxygen (Broadbent and Clark 1965). These soils contain substantial levels of decomposable organic material (Cochran et al. 1989, Sparrow et al. 1988); however, these soils do not have layers impermeable to water and excess water soon drains once the soil thaws in the spring. After planting, the soils are seldom above field capacity.

Emissions of N_2O were measured by a modification to the vented static chamber method described by Hutchinson and Mosier (1981). Chamber bases (18 X 36 cm) were inserted into the soil immediately after planting and centered over the fertilizer band, such that the area inside the chamber base extended one-half the distance to the fertilizer band on either side. Changes in gas concentration was determined by covering the base with a fitted top, removing an air sample with an airtight syringe at 15-min. intervals for 30 min. and analyzing the gas on a gas chomatograph equipped with [63]Ni electron capture detector. Calculated gas flux was based on changes in concentration during the sampling period using the procedures of Hutchinson and Mosier (1981) Emissions of N_2O never exceeded 5 g N ha^{-1} day^{-1} in the control plots or more than 11 g N ha^{-1} day^{-1} for plots fertilized

with 90 kg N ha^{-1} as urea during the summer (Fig. 3). Emissions of N_2O from the fertilized plots corresponded to the time of oxidation of the urea fertilizer and was attributed to nitrification and not denitrification (Blackmer and Bremner 1978, Cochran et al.1981). Total N loss as N_2O from the fertilized plots was less than 1 kg N ha^{-1} indicating that gaseous N losses were minimal during the growing season and after urea was applied.

this time, there was a loss of both N and total dry matter. Loss of both N and dry matter were parallel indicating that the loss was likely from leaf drop and not from volatile N loss as found by Hooker et al. (1980) during winter wheat senescence in a hot dry climate. These conditions seldom occur in interior Alaska and are not likely the cause of N loss.
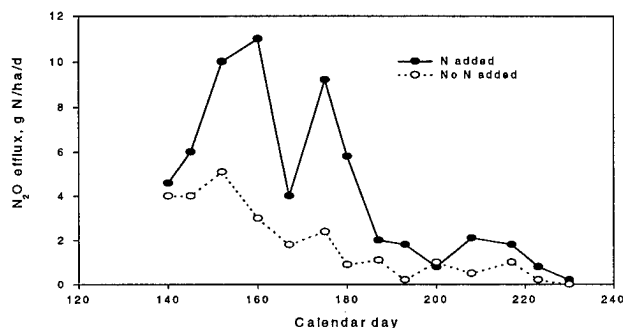
FIG. 3. *Nitrous oxide emission from soil during 1993, that received 90 kg N ha^{1} as urea banded 7 cm deep compared to a zero N control.*
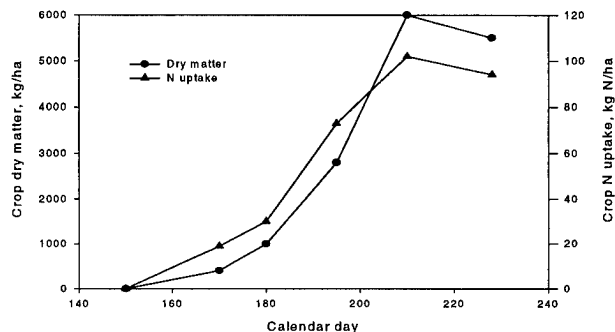
FIG. 4. *Dry matter production and N uptake of well fertilized barley in 1993.*

No measurements of N_2O emissions were made during the spring thaw at this site. At this time, the soils are often subject to excess water that could promote denitrification. Studies made at Fairbanks during spring thaw found negligible increases in N_2O emissions until urea was applied (Cochran et al. 1995). The soils are near freezing at this time, so microbial activity is reduced which, in turn, would reduce the likelihood of having appreciable denitrification.

Plant N uptake and dry matter production
Relatively large amounts of N fertilizer are required to obtain maximum yields of barley. To determine when and how much N is required, barley was grown with the recommended rate of N fertilizer (90 kg N ha^{-1}). Plant samples from 2 m row were obtained at biweekly intervals from mid-tillering until physiological maturity in July. Samples were air dried, weighed for total dry matter, ground, and analyzed for total N using dry combustion and mass-spectrometry. The results showed that about 80% of plant growth and total N uptake occurred during a 30 day period prior to peaking at day 210 (Fig. 4). After

Available N vs. plant requirements
Maximizing small grain plant growth and grain yield require minimizing the stresses on the plant from germination to maturity (Klepper et al. 1982). Early stress caused by lack of water, mineral nutrition, or extreme temperatures will reduce the number of tillers and the number of fertile florets on the head, reducing plant growth and yield. Figure 5 shows the relationship of plant N requirements to available soil N. Available soil N is mineral N at seeding plus that mineralized between seeding and crop maturity. The crop needs exceeded the soils ability to supply adequate N (critical point) within 30 days after planting. The crop requires 100 kg N ha^{-1},and the soil supplies 40 kg Nha^{-1} leaving a deficit of 60 kg N ha $^{-1}$ (Fig. 5). Without additional N from external sources, the plant growth and grain yields would be permanently suppressed (Klepper et al. 1982). Thus, external sources supplying 60 kg N ha^{-1} to the plant are required to assure normal yields. Green manure of a previous crop is one option for supplying additional N. Sparrow et al.(1995) found that green manured legumes will supply about 30 kg N ha^{-1} to the succeeding crop. Nitrogen mineralization rates developed by

317
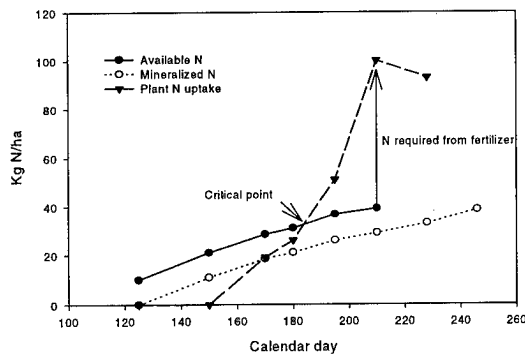
FIG. 5. *Comparison of available N with barley uptake needs during a typical growing season.*

FIG. 6. *Comparison of available N sources, including green manure (G.M.), with barley uptake needs during a typical growing season.*

Koenig and Cochran (1994) were used to calculate the rate that this N would be mineralized and available to a growing barley crop. Green manure delays reaching the point at which time N becomes critical (critical point) by less than 3 weeks (Fig. 6). Thus, 30 kg N ha^{-1} must come from timely application of mineral fertilizer to meet the crop needs. About 25% of the N in green manure is available the first year (Koenig and Cochran 1994). The remaining N in the green manure will be released over a period of years. The continued use of green manure should increase the N mineralization potential of the soil, but it may take many years to reach levels adequate to meet all of the crop needs.

Historically, plant uptake of fertilizer N by small grains has been less than 70%; therefore, N in excess of that required by the plant must be applied. Long term fertilizer plots near Delta Junction have shown that for recropped barley , and applications of 90 kg N ha^{-1} is required for maximum yields unless the season is unusually dry (Knight, Associate Professor of Agronomy, University of Alaska Fairbanks, personal communication 1994).

It should be noted that the soil continued to mineralize N after crop uptake ceased. This N is subject to leaching and/or denitrification during spring thaw when snowmelt often exceeds the water holding capacity of the soil. Continued use of green manure or other sources of organic N are expected to increase the ability of the soil to mineralize N. This will increase the amount of N mineralized after crop maturity. This N will be

subject to leaching or denitrification losses. If not lost, it will be available for succeeding crops, further reducing the need for fertilizer N.

CONCLUSIONS

Information from several studies were combined to show the N dynamics of barley grown in interior Alaska. These studies showed that while barley straw immobilizes mineral N, it does not exceed the soil's ability to mineralize N through microbial decomposition of soil organic matter. The rate at which N mineralizes is much slower than that required by a growing barley crop, and external sources of N are needed to meet crop needs. About 25% of green manure is available the first year, which falls far short of meeting that required by the crop. Since 75% of the N in green manure is not mineralized the first year, there should be an increase in the N mineralization potential of the soil. The continued use of green manure should eventually raise N mineralization to levels where little or no mineral N is required. However, there are no long term studies to verify this.

Measurement of N_2O emissions indicated that during the growing season there is little gaseous N loss; however, these measurements were made on well-drained soils. No measurements were made during spring thaw when soils were near saturation for a short time, and denitrification of soil nitrate carried over from the previous season may have occurred.

318

LITERATURE CITED

Blackmer, A.M., and J. M. Bremner. 1978. Nitrous oxide emissions from soils during nitrification of fertilizer nitrogen. Science 199:245-246.

Broadbent, F.E., and Francis E. Clark. 1965. Denitrification. *In* W.V. Bartholomew and Francis E Clark (ed.) Soil nitrogen. Agronomy 10:343-359. Am. Soc. Agron. Madison. WI.

Cochran, V.L. 1991. Decomposition of barley straw in a subarctic soil in the field. Biol. Fertil. Soil 10:227-232.

Cochran, V.L., E.B. Sparrow, and S.D. Sparrow. 1988. Effects of clearing, tillage, and crop residue management on N and P mineralization in subarctic soils. P 412-413. *In* Challenges in dryland farming: A global, perspective. Proc. Int. Conf. On Dryland Farming. Amarillo - Bushland, TX Aug. 15-19. Texas Agric. Exp. Stn.

Cochran, V.L., L.F. Elliott, and C.E. Lewis. 1989. Soil microbial biomass and enzyme activity in subarctic agricultural and forest soils. Biol. Fertil. Soil 7:283-288.

Cochran, V.L., L.F. Elliott, and R.I. Papendick. 1981. Nitrous oxide emissions from a fallow field fertilized with anhydrous ammonia. Soil Sci. Soc. Am. J. 45:302-310.

Cochran, V.L., S.F. Schlentner, and A.R. Mosier. 1995. CH$_4$ and N$_2$O flux in subarctic agricultural soils. *In* R. Lal, J. Kimble, E Levine, and B.A. Stewart (ed.). Soil management and greenhouse efects. Adv. Soil Sci. CRC Press. oca Raton, FL.

Hooker, M.L., D.H. Sander, G.A. Peterson, and L.A. Daigger. 1980. Gaseous N losses from winter wheat. Agron. J. 72:789-792.

Hutchinson, G.L. and A.R. Mosier. 1981. Improved soil cover methods for field measurement of nitrous oxide fluxes. Soil Sci. Soc. Am. J. 45:311-316.

Klepper. B., R.W. Rickman, and C.M. Peterson. 1982. Quantitative characterization of vegetative development of small grains. Agron. J. 75:789-792.

Koenig, R.T. and V.L. Cochran. 1994. Decomposition and nitrogen mineralization from legume and non-legume crop residues in a subarctic agricultural soil. Biol. Fertil. Soil 17:269-275.

Lewis, C.E., and W.G. Thomas. 1982. Expanding subarctic agriculture: Social, political, and economic aspects in Alaska. Interdispl. Sci. Rev. 7:178-187.

Linn, C.M., and J.W. Doran. 1984. Aerobic and anaerobic microbial populations in no-till and plowed soils. Soil Sci. Soc. Am. J. 48:794-799.

Mosier, A.R. and L. Mack. 1980. Gas chromatographic system for precise, rapid analysis of nitrous oxide. Soil Sci. Soc. Am. J. 44:1121-1123.

Papendick, R.I., And G.S. Campbell. 1981. Theory and measurement of water potential. P 1-22. *In* J.F. Parr, W.R. Gardner, and L.F. Elliott (ed.). Water potential relations in microbiology. Spec. Publ. No. 9 Soil Science Society America, Madison, WI. 1981.

Sparrow, S.D., V.L. Cochran, and E.B. Sparrow. 1995. Residual effects of harvested and green manured legumes on a subsequent barley crop in a subarctic environment. Can. J. Plant Sci. 75:453-456.

Sparrow, S.D., and V.L. Cochran. 1988. Carbon and nitrogen mineralization in subarctic agricultural and forest soils. Biol. Fertil. Soil 6:33-38.

Effects of Past Fertilizer Treatments on the Fate of Newly Added Fertilizer Nitrogen Applied to Cereal Crops in Siberia

P.A. BARSUKOV[1]

ABSTRACT

A long-term field experiment at Narim Experimental Station in the taiga zone of West Siberia has three soil treatments: no fertilizer, mineral fertilizer only and mineral plus organic fertilizers. These treatments served as prior fertilization backgrounds for the microplot experiment in which newly added ^{15}N-labelled fertilizers were used. The results show that long-term application of mineral fertilizers with manure has a strong positive effect on the fate of newly added fertilizer nitrogen. The increased plant uptake of added fertilizer nitrogen is accompanied by the increase of fertilizer efficiency and cereal crops yield. The decrease of nitrogen losses by such previous fertilization is also beneficial to the environment.

Key words: Gaseous losses, immobilization, nitrogen fertilizer, plant uptake, Siberian soils

INTRODUCTION

The economic and environmental implications of fertilizer use call for a complete understanding of their long-term effects. It is known that repeated fertilizer application over many years brings changes in the physical, chemical and biological properties of soils (Mercik and Nemeth 1985; Asmus et al. 1987; Sharma et al. 1988; Jenkinson 1989; Martensson and Witter, 1990). Through changes in soil properties, different previous fertilizer practices could have different effects on the fate and efficiency of newly added fertilizers. If fertilization negatively affects soil properties, it leads to less favourable conditions for plant growth and devel-opment, decreasing crop yields and fertilizer efficiency. In such a case additional expenditures are needed to op-timise soil properties and/or to apply the increased doses of fertilizers to maintain a similar level of productivity. The optimal fertilization system should be highly effec-tive during the application and in the long run should not decrease the soil fertility, or the efficiency of newly applied fertilizers, or increase fertilizer losses, with its negative effects on the environment.

The study of these problems requires careful distinc-tion between the effects of past and newly added fertil-izer inputs. Microplot field experiments using soils from long-term experiments can achieve this, provided the previous and newly added inputs can be distinguished, for example, by the use of ^{15}N-labelled fertilizer. How-ever, there were only few published experiments of this type, in the European part of Russia and Italy. Pok-rovskaya (1983), Shevtsova (1988) and Ciardi et al. (1988) used data from any long-term experiments and considered nitrogen as the main nutrient limiting crop yield.

Approximately 30 million hectares of arable land in Siberia has unusual bioclimatic conditions which influ-ence nitrogen transformation processes in the soil, in-cluding transformation of fertilizer nitrogen. Results from 102 field experiments using ^{15}N-labelled fertilizers with spring cereals in the territory of the former USSR showed that fertilizer nitrogen uptake by these crops accounts for a mean of 24% of total nitrogen applied in Siberia and 39% in the European part of past USSR. The amounts of fertilizer nitrogen left in the soil (A_p horizon) at harvest in these two regions are 51% and 33%, respectively; fertilizer nitrogen losses are 25% and 28%, respectively (Gamzikov et al. 1985). In Siberia the influence of previous mineral fertilization on plant up-

take of nitrogen from newly added fertilizers was studied only in pot experiments (Gamzikov et al. 1985). The data can not be adequately extrapolated for the region, with ever increasing fertilizer applications.

In this paper we estimate, using ^{15}N balance data, the effects of the previous fertilizer treatments on the fate of newly-added fertilizer nitrogen used for cereal production in the taiga zone of W. Siberia.

MATERIALS AND METHODS

Experiments were done on a podzolic loamy sand soil at Narim Experimental Station, situated in the southern part of the W. Siberian taiga. The experimental site has the following average climatic characteristics: average annual temperature, -4.1°C; annual precipitation, 475 mm; maximum depth of snow cover, 54 cm; maximum depth of frozen soil layer, 1.1 m; frost-free period, 111 days (Kukharskaya et al. 1975).

The fate of ^{15}N-labelled fertilizer nitrogen was studied in a field microplot experiment lasting from 1983 to 1990 and situated approximately 200 m from a 35-year-old field experiment. The plot size was 1 m², and the treatments were replicated six times. The plots were isolated laterally by polyethylene film to a depth of 20 cm, equivalent to the A_p horizon. A_p horizon soil for the microplot experiment was removed from the A_p horizon of plots of the long-term experiment which had received the following treatments: (1) no fertilizer; (2) mineral fertilizers only (240 kg/ha each of N, P_2O_5 and K_2O over each 7-year crop rotation period); (3) the same amount of mineral fertilizers plus 40 Mg/ha of half-rotted manure per crop rotation period.

These long-term treatments served as prior fertilization backgrounds for the microplot experiment and are designated by the symbols F_0, NPK and NPK+M, respectively. After 35 years the soils of the long-term experiment had the properties given in Table 1.

The crop rotation and fertilizer treatments for the seven years of the microplot experiment were akin to those of the long-term experiment except that the F_0 soil was treated with mineral fertilizers in the microplot experiment. The following crop rotation was used in both experiments: pea and oats mixture, barley, clover, winter rye, spring wheat, pea and oats mixture, oats. Similar total amounts of mineral fertilizers were applied for 7 years in plots F_0 and NPK: 300 kg/ha of N and 240 kg/ha of P_2O_5 and K_2O each. In plots NPK+M the rotation application of fertilizers amounted to 40 Mg/ha of farm-yard manure and 240 kg/ha of each of P_2O_5, K_2O and N. From these amounts of fertilizers 60 kg/ha of each of N, P_2O_5 and K_2O were applied in spring to all

Table 1. Selected properties of soil taken from the 35-year experiment and used for the microplot experiment.

Property	F_0	NPK	NPK+M
pH_{KCl}	4.4 b	4.2 a	4.8 c
Exchangeable Al (mg/kg)	49 b	63 c	7 a
Base saturation (%)	60 b	55 a	75 c
Organic C (%)	0.70 a	0.76 b	0.88 c
Total N (%)	0.087 a	0.091 b	0.105 c
Potentially available organic N (mg/kg)	26 a	27 a	35 b
NH_4^+ - N fixed by clay (mg/kg)	37 a	36 a	39 a
Exchangeable NH_4^+ - N (mg/kg)	9.7 a	7.4 a	7.5 a
NO_3^- - N (mg/kg)	2.2 b	1.8 a	5.3 c
Available P (mg P_2O_5/kg)	0.26 a	0.41 a	0.95 b
Available K (mg K_2O/kg)	12.4 a	16.7 b	19.1 c

Values within rows not sharing the same letter are significantly different (P<0.05).

the plots when they were cropped to barley, wheat and oats. Winter rye received only nitrogen fertilizer (60 kg/ha) at the end of the summer, at rye tillering. The first crop in rotation, pea and oats mixture, received 60 kg/ha of mineral nitrogen in plots F_0 and NPK and 40 Mg/ha of manure in plot NPK+M. Other crops in rotation did not received nitrogen fertilizer at all. This paper discusses the fate of the nitrogen applied to the microplots cropped to barley, wheat and oats, i.e. in the microplots that were similarly fertilized.

Fertilizers were applied in the form of urea (to barley and oats), ammonium sulphate (to wheat), triple superphosphate, and potassium chloride. The ^{15}N content of urea and ammonium sulphate was 30-38 atom %. The soil from the long-term experiment was not previously given ^{15}N-labelled fertilizer.

All cultivation procedures were done by hand. Through the growing season the microplots were hand weeded. Harvesting was done when the grain was waxy ripe. Soil samples were taken from the 0-20 cm layer (A_p horizon) from 15-25 points on every plot after harvesting of each crop. Plant samples were digested in a mixture of sulphuric and perchloric acid (Ginzburg et al. 1963). Soil samples were digested using the reducer-catalyst (Kudeyarov 1972). Total N in the digest was determined by the Kjeldahl method described by Bremner and Mulvaney (1982). Potentially available

Table 2. Amounts and percentages of newly added fertilizer nitrogen taken up by cereal crops grown on soils given different previous fertilizer treatments.

Crop	F_0		NPK		NPK+M	
	g/m^2	%	g/m^2	%	g/m^2	%
Barley	1.81 a	30.2 a	1.76 a	29.3 a	2.37 b	39.5 b
Wheat	2.00 a	33.3 a	2.05 a	34.2 a	2.28 b	38.0 b
Oats	2.07 a	34.5 a	2.12 a	35.3 a	2.33 b	38.8 b

Values within rows not sharing the same letter are significantly different (P<0.05).

organic N in soil was measured by the method of Gianello and Bremner (1988). Soil microbial biomass nitrogen was measured using the chloroform fumigation-incubation method (Jenkinson and Powlson 1976) in fresh soil samples. Nonexchangeable ammonium was determined by the Silva and Bremner method as described by Keeney and Nelson (1982). Other analyses were performed by the methods of Sokolov (1975). Extractants for available phosphorus and potassium determinations were 0.06 M K_2SO_4 and 0.01 M $CaCl_2$, respectively. All analyses for nitrogen were made in triplicate, the others were replicated. Nitrogen isotope composition was determined with an MX-1304 mass spectrometer. The results of soil and plant analyses are quoted on air-dry weight basis (15% moisture for crops).

RESULTS AND DISCUSSION

Uptake by plants of the newly added fertilizer nitrogen

Despite differences in weather conditions during the growing periods and the biological properties of the crops, barley, wheat and oats grown on the microplots took up similar amounts of fertilizer nitrogen (Table 2). The recovery of newly added nitrogen by these crops was the same on soil previously treated with mineral fertilizers and on soil that had previously received no fertilizer, but the utilization of newly added nitrogen on soil previously treated with mineral and organic fertilizers was 4-10% greater. Differences in crop yields according to previous fertilizer treatments show a similar pattern (Table 3). Yields on soil previously treated with mineral and organic fertilizers were 9-34% greater than on soils given other previous treatments. It therefore seems that the soil previously treated with both mineral and organic fertilizer was more favourable for growth and yield of cereals. High content of P, extractable by salt solution of low concentration, and of potentially available organic nitrogen at the beginning and at the end of the experiment (see Tables 1 and 4), as well as

after harvesting other crops during the experiment, provide evidence that this soil contains more plant-available phosphorus and nitrogen. Moreover, plant

Table 3. Grain yields (g/m^2) after application of 60 kg/ha each of N, P_2O_5 and K_2O to soil with different long-term previous fertilizer treatments.

Crop	F_0	NPK	NPK+M
Barley	325 a	335 a	418 b
Wheat	299 a	306 a	402 b
Oats	317 a	306 a	345 b

Values within rows not sharing the same letter are significantly different (P<0.05).

uptake of nitrogen, phosphorus and potassium during the rotation was higher in microplots NPK+M. In addi-

Table 4. Selected properties of soil taken at the end of the microplot experiment (after oats harvesting).

Property	F_0	NPK	NPK+M
pH_{KCl}	4.2 b	4.1 a	4.6 c
Exchangeable Al (mg/kg)	55 b	72 c	10 a
Microbial biomass[*] (mg/kg)	396 a	389 a	499 b
Microbial biomass N[*] (mg/kg)	63 a	62 a	80 b
Potentially available organic N (mg/kg)	25.0 a	22.6 a	32.2 b
NH_4^+ - N fixed by clay (mg/kg)	36 a	35 a	38 b
Exchangeable NH_4^+ - N (mg/kg)	4.4 a	5.0 a	7.6 b
NO_3^- - N (mg/kg)	1.2 a	1.1 a	1.7 a
Available P (mg P_2O_5/kg)	0.70 a	0.87 b	1.36 c
Available K (mg K_2O/kg)	13.9 b	14.2 b	10.9 a

Values within rows not sharing the same letter are significantly different (P<0.05).

[*] data made by N.B. Naumova (Institute of Soil Science and Agrochemistry, Novosibirsk, Russia)

Table 5. Amounts and percentages of nitrogen from newly added fertilizers immobilized in soils (A_p horizon) with different previous fertilizer treatments.

Crop	F_0		NPK		NPK+M	
	g/m^2	%	g/m^2	%	g/m^2	%
Barley	3.05 b	50.8 b	2.72 a	45.3 a	3.27 b	54.5 b
Wheat	2.67 b	44.5 b	2.37 a	39.5 a	2.93 c	48.8 c
Oats	2.55 b	42.5 b	2.24 a	37.3 a	2.71 b	45.2 b

Values within rows not sharing the same letter are significantly different (P<0.05).

tion to the greater amounts of available major mineral nutrients, this soil is also less acid and has much (7-9 times) less exchangeable aluminium (Table 1). Aluminium can inhibit nitrate uptake by plants (Keltjens and Van Ulden, 1987). This is probably important for these soils which show rapid nitrification of ammonium, including ammonium derived from fertilizer despite their low pH values (Barsukov, unpublished work).

Our results agree with those of the others who have found that previous applications of organic and mineral fertilizer increase the crop uptake of newly added fertilizer nitrogen by 2.5-15.5% of the amount applied, compared with soils previously unfertilized. Previous treatments with only mineral fertilizers also increase crop utilization of fresh fertilizer nitrogen, compare previously unfertilized soils, but mainly on medium- and heavy-loam soils (Asarova, 1976; Pokrovskaya, 1983; Gamzikov et al., 1985; Ciardi et al., 1988; Shevtsova, 1988).

Residual nitrogen of newly added fertilizers

Immobilization of fertilizer nitrogen in soil results mainly from nitrogen assimilation by microorganisms, and fixing of ammonium was probably negligible. This is indicated by the small values of fixed ammonium (Table 1).

The amount of newly added fertilizer nitrogen retained by the soil was greatest where the previous treatment had been organic manure plus mineral fertilizers (Table 5). This was because the soil treated with organic manure had a larger microbial biomass as a result of greater abundance of easily available carbon as a source of energy (Schnurer et al. 1985; McGill et al. 1986), and there was more nitrogen immobilized in the larger biomass. For example, the soil microbial biomass after harvesting oats is given in the Table 4. Although the microbial biomass was similar in soil previously unfertilized and soil treated with mineral fertilizers only, the amount of newly added fertilizer nitrogen immobilized was 5-6% greater in the previously unfertilized soil. This was probably because of the greater turnover rate of microbial biomass nitrogen in the previously unfertil-

ized soil. Naumova and Barsukov (1991) studied soil microbial C and N in the same plots of long-term experiment that were used as previous fertilization backgrounds in our microplot experiment. By relating the sum of statistically significant increments in seasonal dynamics changes in microbial biomass to the seasonal average microbial biomass, the turnover time of microbial C was estimated to be 4.6 months in the F_0 plots, and 8.1-9.0 months in the NPK and NPK+M plots. The same estimates for biomass N were 5.0 and 10.1-11.6 months, respectively. The turnover rate, and the immobilization rate as its constituent, should influence the amount of immobilized nitrogen, particularly in case of ammonium fertilizer or urea are applied, as in our experiment. This is because, of the two mineral forms (NH_4^+ and NO_3^-) of nitrogen assimilated by soil microorganisms, NH_4^+ predominates (Wickramasinghe et al. 1985; Recous et al. 1990).

In field and laboratory experiments, Ciardi et al. (1988) also found greater amounts of newly added nitrogen remaining in soil previously unfertilized, compared to soil previously given mineral (N and P) fertilizers. In pot experiments with loamy soil, the amount of immobilized fertilizer nitrogen in soil with prior fertilization background F_0 was 3.5% higher, compared to NPK background, and 2.2% higher, compared to soil with NPK+M background. However, in other experiments (the pot experiment of Gamzikov et al. (1985) with sandy soil, and in the microplot experiment of Pokrovskaya (1983) with heavy clay loam) no effects of previous treatments on residual amounts of newly-added fertilizers were found.

Losses of nitrogen from newly added fertilizer

Among available papers reporting on the losses of newly added nitrogen associated with prior fertilizer treatments, only two (Asarova 1976; Pokrovskaya 1983) are known to us, and they are contradictory.

Losses of nitrogen from soils which do not suffer erosion can occur by gaseous diffusion of N_2 or N_2O to the atmosphere or by leaching of nitrate to deeper soil horizons. Earlier investigations (Gamzikov et al. 1985;

323

Table 6. Amounts and percentages of nitrogen from newly added fertilizers not accounted for in the A_p-horizon - plant system of soils with different previous fertilizer treatments.

Crop	F_0		NPK		NPK+M	
	g/m^2	%	g/m^2	%	g/m^2	%
Barley	1.14 b	19.0 b	1.52 c	25.4 c	0.36 a	6.0 a
Wheat	1.33 b	22.2 b	1.58 c	26.3 c	0.79 a	13.2 a
Oats	1.38 b	23.0 b	1.64 b	27.4 b	0.96 a	16.0 a

Values within rows not sharing the same letter are significantly different (P<0.05).

Barsukov 1990) established that if fertilizer is applied at optimum rates and times in the West Siberia taiga, no significant leaching of fertilizer nitrogen occurs beyond the root zone.

After harvesting the last crop in the rotation (oats), the distribution of ^{15}N-labelled fertilizer nitrogen was studied in the 0-100-cm layer of our microplots. Below 40 cm essentially no fertilizer nitrogen was found, and in the 20-40-cm layer the residual fertilizer nitrogen was only 4-6% of that applied. Moreover, ^{15}N-labelled nitrogen was not found in mineral forms below 20 cm depth. Nitrogen fertilizers can hardly be leached below 100 cm in significant amounts if precipitation would exceed evaporation during period after application of the fertilizers when nitrogen is still in mobile forms. Only about 3% of the total fertilizer-derived N retained by soil is still remained in mineral form by tillering of cereals in West Siberian Podzoluvisol (Gamzikov et al., 1985). Significant precipitation at this time (the 3rd decade of May to the 1st decade of July) is not typical in West Siberian taiga zone (Kukharskaya et al., 1975) and it was not observed during the years when our microplot experiment was carried out. However, some insignificant quantities of fertilizer nitrogen that was remineralized during autumn, could be leached in spring with the melting of snow. Thus, the greater part (about 85%) of the fertilizer nitrogen which cannot be accounted for in the A_p-horizon-plant system was probably lost in gaseous forms. Similar results have been obtained over a wide range of soil and climatic conditions (Gamzikov et al. 1985; Powlson 1988). In our experiment the most likely process leading to gaseous nitrogen losses is denitrification. The pH of the soils was too low for significant losses by ammonia volatilization (Smirnov 1982), but denitrification can occur in acidic soils (Smirnov 1982; Zumft et al. 1988).

The amounts of newly added fertilizer nitrogen not accounted for were largest for the soil previously treated with mineral fertilizers only (Table 6). For soil previously unfertilized the losses of newly added nitrogen were 4.0-6.4% less than this, possibly because of more intense microbial immobilization of nitrogen. Moreo-

ver, greater nitrogen losses through chemical reactions involving NO_2^- could have occurred in the more acid soil previously treated with mineral fertilizers (Smirnov 1982; Haynes and Sherlock 1986). The small (6-16%) losses of fertilizer nitrogen from soil previously treated with both organic and mineral fertilizers reflect the greater uptake by the plants and soil microorganisms.

CONCLUSION

The data allow us to conclude that long-term application of mineral fertilizers, even in small amounts (34 kg/ha/year each of N, P_2O_5 and K_2O) to acid soils with light granulometric composition and little buffering capacity causes changes in soil properties. These changes result in the increased losses of newly added fertilizer nitrogen, compared to previously unfertilized soil, although they do not affect the use of fertilizer nitrogen by cereal crops. It may be assumed that under prolonged time and/or increased dosage of fertilizer use, the negative effects of mineral fertilization will accumulate. The latter will decrease of plant uptake of newly applied fertilizers, fertilizer efficiency and crop yields. In such a situation, additional practices are needed to improve the efficiency of nitrogenous fertilizers and crop production, e.g. the application of lime to optimize soil acidity and decrease the content of mobile aluminium in the soil (Myskow et al. 1989), or the use of crops and cultivars adapted to acid soil (Klimashevskiy 1991).

The uptake and efficiency of newly added mineral fertilizer nitrogen, and crop yields, are improved when long-term fertilization includes both mineral fertilizers and organic manure. It should be emphasized that even small amounts of manure (40 Mg/ha) applied once every 7 years are enough to increase the abovementioned parameters and to decrease losses of newly added fertilizer nitrogen. It is known that loss of nitrogen in the form of nitrates and nitrites through leaching to ground waters, and in the form of nitrogen and dinitrogen oxides through denitrification, have a negative effect on the environment contributing to the degrada-

tion of the ozone screen and to the global "greenhouse" effect (Bouwman 1986).

The strong positive effect, which the application of mineral fertilizers together with organic manure has on the fate of newly added fertilizer nitrogen allows us to recommend such fertilization practice for wide use in the West Siberian taiga.

ACKNOWLEDGEMENTS

We thank the Administration of the Narim Experimental Station for making the long-term field experiment available for our studies.

REFERENCES

Asarova, N. X. 1976. Structure of nitrogen fund and fate of mineral fertilizer nitrogen depending on prior fertilization in long-term experiments. (in Russian.) Doklady Timiryazevskoi Sel'shohozyaistvennoi Academii 218:110-117.

Asmus, F., G. Kittelmann, and H. Gorlitz. 1987. Einflublangjahriger organischer Duengung auf physikalische Eigenschaften einer Tieflehm-Fahlerde. (in German.) Archiv fuer Acker- und Pflanzenbau und Bodenkunde 31:41-46.

Barsukov, P. A. 1990. Practical and ecological aspects of long-term fertilization (in the southern taiga zone of West Siberia). (in Russian.) Izvestiya Sibirskogo Otdeleniya Academii Nauk SSSR. Seriya Biologicheskih Nauk 3:109-115.

Bouwman, A. F. 1989. Exchange of greenhouse gases between terrestrial ecosystems and the atmosphere *In* A. F. Bouwman (ed.) Soils and the greenhouse effect. John Wiley and Sons, England.

Bremner, J. M., and C. S. Mulvaney. 1982. Nitrogen - total. *In* A. L. Page et al. (ed.) Methods of soil analysis. Agronomy 9:595-624. Am. Soc. of Agron., Inc., Madison, Wis.

Ciardi, C., P. Nannipieri, G. Toderi, and G. Giordani. 1988. The effect of past fertilization history on plant uptake and microbial immobilization of urea-N applied to a two-course rotation. p. 110-124. *In* D. S. Jenkinson and K. A. Smith (ed.) Nitrogen efficiency in agricultural soils. Elsevier Applied Science, London.

Gamzikov, G. P., G. I. Kostric, and V. N. Emeliyanova. 1985. Fate and transformation of fertilizer nitrogen. (in Russian.) Nauka, Novosibirsk.

Gianello, C., and J. M. Bremner. 1988. A rapid steam distillation method of assessing potentially available organic nitrogen in soil. Communications in Soil Science and Plant Analysis 19:1551-1568.

Ginzburg, K. E. , G. M. Scheglova, and E. V. Vulfius. 1963. Accelerated method of soil and plant digestion. (in Russian.) Soviet Soil Science 5:89-96.

Haynes, R. J., and R. R. Sheplock. 1986. Gaseous losses of nitrogen. p. 242-302. *In* Mineral nitrogen in the plant-soil system. Academic Press, London.

Jenkinson, D. S. 1989. The long-term effects of nitrogen fertilization. Nouvelles de la science et des technologies 7:21-214.

Jenkinson, D. S., and D. S. Powlson. 1976. The effects of biocidal treatments on metabolism in soil. 5. A method for measuring soil biomass. Soil biology and biochemistry 8:209-213.

Keeney, D. R., and D. W. Nelson. 1982. Nitrogen - inorganic forms. *In* A. L. Page et al. (ed.) Methods of soil analysis. Agronomy 9:643-698. Am. Soc. of Agron., Inc., Madison, Wis.

Keltjens, W. G., and P. S. R. van Ulden. 1987. Effects of Al on nitrogen (NH_4^+ and NO_3^-) uptake, nitrate reductase activity and proton release in two sorghum cultivars differing in Al tolerance. Plant and Soil 104:227-234.

Klimashevskiy, E. L. 1991. Genetic aspects of plant mineral nutrition. (in Russian.) Agropromizdat, Moscow.

Kudeyarov, V. N. 1972. The method of total nitrogen determination in soil and plant. (in Russian.) Agrokhimiya 11:125-127.

Kukharskaya, V. L., T. L. Petkun, E. L. Tihonova, I. M. Toschakova, and M. I. Chernikova. 1975. Agroclimatic resources of the territory. (in Russian.) p. 9-73. *In* Agroclimatic resources of the Tomsk region, Gidrometeoizdat, Leningrad.

Martensson, A. M., and E. Witter. 1990. Influence of various soil amendments on nitrogen-fixing soil microorganisms in a long-term field experiment with special reference to sewage sludge. Soil Biology and Biochemistry 22:977-982.

McGill, W. B., K. B. Cannon, J. A. Robertson, and F. D. Cook. 1986. Dynamics of soil microbial biomass and water soluble organic C in Breton L after 50 years of cropping to two rotations. Canadian Journal of Soil Science 66:1-19.

Mercik, S., and K. Nemeth. 1985. Effects of 60 years N, P, K and Ca fertilization on EUF-nutrient fractions in the soil and on yields of rye and potato crops. Plant and Soil 83:151-159.

Myskow, W, T. Lasota, S. Martyniuk and S. Zieba. 1989. Effect of quality and quantity of soil organic matter on the efficiency and transformation of fertil-

izer nitrogen: investigations with the use of ^{15}N. Zentralblatt fuer Mikrobiologie 144:509-515.

Naumova, N. B., and P. A. Barsukov. 1991. Influence of long-term fertilization on microbial biomass content and dynamics in turf-podzolic soil. (in Russian.) Siberian Biological Journal 3:59-67.

Pokrovskaya, M. D. 1983. Plant uptake and transformations of fertilizer nitrogen in turf-podzolic soil having different past fertilization history. (in Russian.) PhD Thesis, Moscow Agricultural Academy.

Powlson, D. S. 1988. Measuring and minimising losses of fertilizer nitrogen in arable agriculture. p. 231-245 *In* D. S. Jenkinson, and K. A. Smith (ed.) Nitrogen efficiency in agricultural soils. Elsevier Applied Science, London.

Recous, S., B. Mary, and G. Faurie. 1990. Microbial immobilization of ammonium and nitrate in cultivated soils. Soil Biology and Biochemistry 22:913-922.

Schnurer, J., M. Clarholm, and T. Rosswall. 1985. Microbial biomass and activity in an agricultural soil with different organic matter contents. Soil Biology and Biochemistry 17:611-618.

Sharma N., L. L. Srivastava, B. Mishra, and N. C. Srivastava. 1988. Changes in some physiochemical properties of an acid red soil as affected by long-term use of fertilizers and amendments. Journal of the Indian Society of Soil Science 36:688-692.

Shevtsova, L. K. 1988. Humus and nitrogen status of main soil kinds under conditions of long-term fertilization. (in Russian.) ScD Thesis, Moscow State University.

Smirnov, P. M. 1982. Questions of nitrogen agrochemistry (in experiments with ^{15}N). (in Russian.) Moscow Agricultural Academy Press, Moscow.

Sokolov, A. V. (ed.) 1975. Agrochemical methods of soil test. (in Russian.) Nauka, Moscow.

Wickramasinghe, K. N., G. A. Rodgers, and D. S. Jenkinson. 1985. Transformations of nitrogen fertilizers in soil. Soil Biology and Biochemistry 17:625-630.

Zumft, W. G., A. Viebrock, and H. Korner. 1988. Biochemical and physiological aspects of denitrification. p. 245-279. *In* J. A. Cole and S. J. Ferguson (ed.) The nitrogen and sulphur cycles. Cambridge University Press.

The Effect of Freezing on Soil Moisture and Nutrient Distribution at Levinson-Lessing Lake, Taymyr Peninsula, Siberia

P.P. OVERDUIN[1] AND K.L. YOUNG[1]

ABSTRACT

This paper reports on a study undertaken in the 1995 fall season at Levinson-Lessing Lake (74°30'N, 98°30'E) on the Taymyr Peninsula, Siberia, examining soil water solute concentrations and distribution in the active layer and upper frozen ground during freeze-back. Cores of both the active layer and frozen ground were harvested, sectioned and their soil waters extracted for solute concentration analyses when the active layer was frozen to depths of 0.04 – 0.15 m. Moisture profiles show an enrichment of total moisture above the frozen front. Solute concentration and distribution change dramatically during freeze-back, although no systematic effect on solute movement was observed. Increases in Mn_{aq}, Fe_{aq}, SO_4^{2-} and NO_3^- at different depths are observed as freezing progresses. Changes in oxidation potential seem to determine concentration profiles during freeze-back.

Key words: Active layer, nutrients, freezing, solute exclusion, Siberia

INTRODUCTION

The active layer of permafrost regions undergoes a yearly freeze-thaw cycle, redistributing soil moisture and dissolved materials vertically within a soil profile (Kay and Groenevelt 1983). Each fall, as a result of falling net radiation and air temperature, the ground temperature at the surface drops, reaches the freezing temperature of the soil water, and remains there until the soil water is frozen. Freezing thus initially occurs from above, and the progress of the freezing front downward through the active layer creates large local temperature gradients at the phase change boundary. The frost table at the base of the active layer can also rise to meet the descending freezing front, which occurs more commonly in cold permafrost. While it is clear that steep ionic concentration and moisture gradients exist across the freezing fringe, their effects are not well understood (Lunardini 1981).

Change of soil water solute profiles during freezing is potentially affected by four processes: (1) solute exclusion from freezing soil, (2) soil water flow (as a result of hydraulic or osmotic gradient or convection), (3) diffusion, and (4) microbial reduction.

Although solute exclusion, the process whereby solvent molecules preferentially bond during freezing, has been theorized at the freezing front in soils (Hallet 1978), tested under laboratory conditions (Ershov et al. 1992), and modelled (Panday and Corapcioglu 1991) there is little work concerning its impact under field conditions. Qiu et al. (1988) found that ion migration did occur in freezing soils in a laboratory study. In solution and moist sand, migration occurred towards the unfrozen region; however, in clay and silt columns, solutes tended to migrate towards the freezing zone. Kay and Groenevelt (1983) and Hallet (1978) observed increasing solute concentrations in the unfrozen parts of their soil cores from field studies. Panday and Corapcioglu (1991) found that their iterative solution to the mass balance and conservation of energy equations yielded solute concentration profiles matching laboratory studies. In addition, the upward movement of vapour during the dry winter and the migration of water to the active layer/frozen ground interface in the summer and fall could result in a net seasonal accumulation of highly concentrated soil waters in the lower layers of the active layer. Increased solute concentrations at depth in the active layer have been indirectly observed by a number of researchers, usually as an increase in the total dissolved solids in soil water flushing out of the active layer in late summer, when it reaches its greatest depth. These increases were attributed to evaporative concentration effects, the exposure to thawing of deeper and less weathered active layer soil matrices and/or to solute exclusion (e.g. Schiff et al. 1991). These processes would contribute to an

[1] Department of Geography, York University, 4700 Keele Street, North York, Ontario, M3J 1P3, Canada

increase in deep active layer solute concentrations. The saturation of this layer of soil for most of the year, and the movement of moisture to the active layer/frozen ground interface (and potential ice segregation) suggest that there are greater amounts of moisture present for most of the year at the base of the active layer. This translates into a greater potential release of solutes, particularly if the active layer depth increases beyond this region in any thaw season.

OBJECTIVE

This study concentrates on solute concentrations in the soil solution, and the changes that occur in their distribution as the freezing front descends. The objective of this study is to measure the vertical distribution of moisture and soil water solutes at a field site in the active layer during freeze-back. The results will be used to comment on the importance of solute exclusion in determining solute redistribution as a result of freezing.

METHOD

Three sampling sites were chosen at Lake Levinson-Lessing (74°30'N, 98°30'E), Taymyr Peninsula, Siberia, which is one of the study sites of an international co-operative research effort led by the Alfred Wegener Institute for Polar and Marine Research, Potsdam, Germany, and by the Arctic and Antarctic Research Institute, St. Petersburg, Russia. This lake basin has been part of a larger research project investigating recent processes and the palaeoenvironment of the Taymyr Peninsula, the results of which this study attempts to complement by providing a link between soil water chemistry and seasonality in groundwater chemistry. Results from only one of the three sampling sites are reported here.

An automatic weather station recorded hourly averages of air temperature, relative humidity (both at 1-m height), net radiation, wind speed and direction (both at 2-m height) and precipitation. Time domain reflectometry (TDR) was used to measure in situ soil moisture with probes installed in the 1994 season at the end of summer (see Topp 1980). The probes used were triple-wire probes, 243 mm long, with 5 mm diameter wires, separated by 30 mm. The estimated error of the volumetric water content is 0.03 [cm^3 cm^{-3}] (Boike et al. 1997). Triple-wire TDR probes were installed horizontally at depths of 0.10, 0.13, 0.28 and 0.31 m. Soil temperature was measured adjacent to each TDR probe using a PT100

thermistor (± 0.1 °C). Details of the field techniques are outlined in Siegert and Bolshiyanov (1995). An attempt was made to measure the soil oxidation potential using the method of Pfisterer and Gribbohm (1989). Five platinum electrodes were inserted to 25.5-cm depth in the soil 8 to 9 cm from a salt bridge at the same depth, and the potential between each electrode and the salt bridge was measured. Unfortunately, the effects of freezing on the salt bridge rendered measurement impossible during most of freeze-back.

Water samples from the unfrozen active layer were collected using suction cups (50 x 20 mm, 0.2 μm from Gravquick, Denmark) installed in 1994 at one shallow and one deep location (0.15 and 0.30 m) in a total active layer depth of 0.45 m. The suction cups were surrounded with a soil slurry on installation to ensure contact with the surrounding soil matrix. Further water samples were recovered from wells and piezometers located at the TDR measurement site. pH and electrical conductivity of collected water samples were measured in the field within four hours of sampling. Additional sample volumes were frozen immediately after sampling and transported back to the institute in Potsdam, Germany, for ion concentration analysis.

Soil push cores were collected from the thin frozen layer at the top of the active layer and of the unfrozen active layer, down to the top of the permafrost. Further coring into the permafrost was performed using a Russian Dryshba motor and a 0.3-m slotted coring bit. Later in the season, as the frozen layer thickened, the cores were drilled using either the auger or a 1.5-m long stainless steel tube. The cores were sliced, packed individually and frozen immediately after coring and remained frozen at -20 °C until soil water extraction took place. Selected cores were sectioned and dried for gravimetric determination of water content.

Immediately after a quick thawing, soil samples from the soil cores were centrifuged at 1000 and 3000 rpm for 10 minutes each to remove soil water, following the method outlined in Carter (1993). The solution thus collected was filtered immediately into two bottles (cleaned with ultrapure HNO_3, triple rinsed with double deionized water and rinsed with the sample) and prepared for analysis. Anion analysis occurred within two days of centrifugation, during which period the samples were held at 4 °C. The cation analysis moiety of the sample was acidified to pH 2 or less and cooled until analysis. Anion concentrations were measured using a Dionex ion chromatograph (Dionex-100) and cation concentrations were measured in triplicate using

inductively coupled plasma spectrometry (Perkin Elmer Optima 3000). Ions were chosen for analysis based on ease of measurability with low sample volumes; ions thought to be conservative (F^-, Cl^-, Br^-, Ca^{2+}, Mg^{2+}, Na^+, K^+, Si_{aq}), reduction-oxidation species (SO_4^{2-}, Fe_{aq}, Mn_{aq}, Al_{aq}) and biochemically important species (NO_2^-, NO_3^-, PO_4^{3-}, TDP) were chosen.

RESULTS

Features of the study site and its soil are presented in Table 1. The soil is a loosely structured

Table 1. Site characteristics for core sampling site, Levinson Lessing Lake, Siberia.

Site data:	Value:
Site elevation	54 m a.s.l.
Slope	1.5 °
Aspect	SSE
Soil bulk density [g/cm^3]	0.80 (n=48)
Porosity	0.53 (n=45)
d_{75}	0.06 mm (n=4)
d_{25}	0.36 mm (n=4)
Botanical zone [a]	Tundra
Dominant vegetation (> 10%)	*Dryas sp., Carex sp.*
Bryophyte cover	98 % (n=5)
Mean July temperature	+ 12.3 °C
Annual precipitation	283 mm
Frost free period	50 d
Permafrost thickness [a]	500-700 m
Soil type [b]	regosolic cryosol (pergelic cryaquept)

a: Atlas Arctici 1985; b: Pfeiffer et al. 1996.

Pergelic Cryaquept (regosolic cryosol) (Pfeiffer et al. 1996). It is probably the weathering product of the upslope bedrock outcrop of greywacke. The active layer is predominantly mineral, with a thin organic layer comprising the upper few centimeters of the profile. Plant cover is continuous tundra vegetation. Fall microclimatic data is presented in Figure 1. The general trend of cooling follows the decrease in net radiation (Q^*). The ground temperature responds and the "zero curtain" effect (Harris et al. 1988) is easily observed at 0.15-m depth. About 14 % of the soil volume is occupied by unfrozen water at both of the upper TDR probes.

Water samples collected from a lysimeter at a depth of 0.15 m had pH values of 7.2 - 7.8; the conductivity, however, began to increase immediately after the onset of freezing and increased
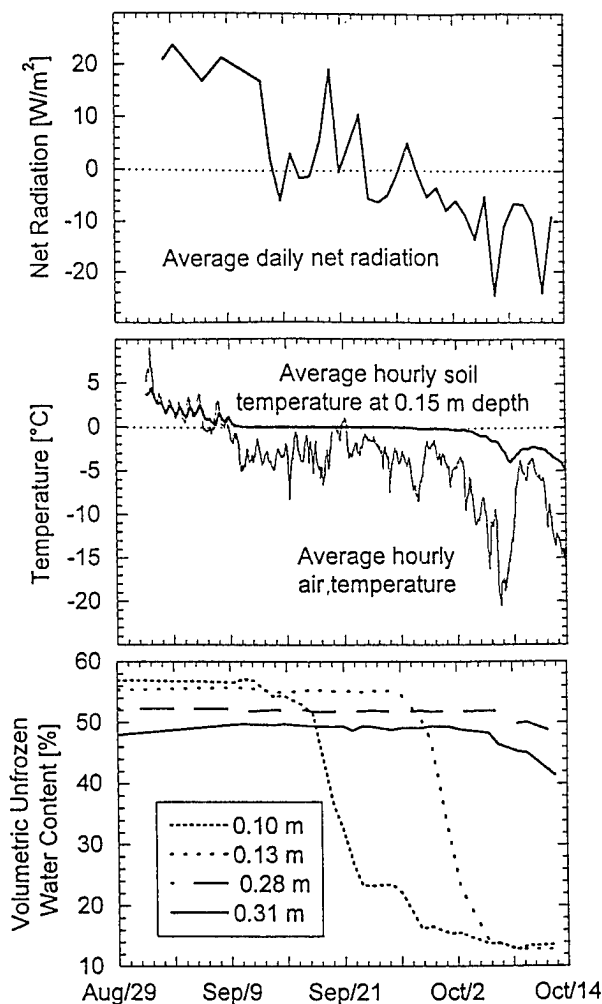
Figure 1. Microclimate and soil moisture during freeze-back at Levinson-Lessing Lake, Taymyr Peninsula, Siberia, in 1995. The top graph shows average hourly air and ground temperatures, the latter at a depth of 0.15 m.

throughout the sampling period (Figure 2). This increase was largely due to an almost doubling of [Ca^{2+}], [Mn^{2+}] and a tripling of the concentrations of silica species, all of which occurred concomitant to twofold decreases in SO_4^{2-} concentrations over the same period.

The results of a single core harvested on 24 September and used for gravimetric moisture determination is presented in Figure 3. The thick dashed lines indicate the position of the descending freezing front, and of the frost table below. The depths between are still unfrozen. There is a steep increase in total moisture content with depth from the surface down to the freezing front. The soil at the
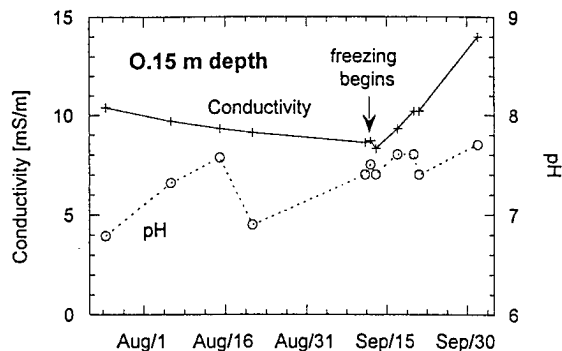
Figure 2. Variations in pH and conductivity over the end of summer and fall for samples collected with a suction cup at 0.15-m depth. The onset of ground freezing is indicated.

surface has completely frozen, with an unfrozen water content of less than 0.20. There is a marked decrease in total moisture content corresponding to the frost front, with a sharp increase 0.05 m deeper. From this point downward the water content decreases to a minimum of 0.30 immediately above

through this depth by 3 October, and only a small peak in the SO_4^{2-} concentration remains. [Mn_{aq}] peaks somewhat later, increasing from detection limits (0.01 ppm) to almost 1.5 ppm (Fig. 4). It continues to increase, first above the frost table, and by 3 October has increased at and above the freezing front, suggesting release into the soil solution after freezing has occurred. The concentration increase occurs both above and below the frozen front, similar to the moisture content distribution. Of the elements presented, [Fe_{aq}] has the most dramatic range of concentrations, increasing to almost 35 ppm (Fig. 4), with the bulk of the increase occurring between the freezing front and the frost table.

DISCUSSION

Due to the destructive nature of sampling, the graphs do not represent the development of a profile, but rather a sampled profile within a 1-m radius of a point designated as the sampling site. Small local variations in the topography are reflected neither in the freezing front position nor in the frost table

Table 2. Results of paired comparisons of means using a student's t-test. Means (d) and standard deviations (σ) of the differences between compared cores, t-values (t) and the degrees of freedom (df) are given for each test. The significance level is p=0.05 for all tests.

Core:	September 13, 1995				September 24, 1995				October 3, 1995			
Species:	x	σ	t	df	x	σ	t	df	x	σ	t	df
Cl^-	0.24	2.12	1.38	4	0.32	2.49	0.40	9	1.50	3.14	1.58	10
SO_4^{2-}	1.66	2.06	2.12	4	0.62	4.76	0.41	9	3.45	13.1	0.86	10
NO_3^-	0.78	2.56	-0.60	4	1.97	3.36	-1.86	9	1.01	1.60	1.73	10
Mn_{aq}	0.12	0.13	-0.25	4	0.00	0.13	0.42	9	0.26	0.70	0.63	10
Fe_{aq}	0.89	1.45	1.80	4	0.60	4.57	-0.09	9	2.27	9.38	1.31	10

the frost table.

Figure 4 presents ion profiles for cores harvested on three dates. Freezing had already begun by 13 September and was not yet complete by 3 October, and the position of the freezing front is indicated on each graph by a thick dashed line. Figure 4 shows the development of a spike of NO_3^- from 0.21 to 0.24 m depth. The general increase in both Cl^- and SO_4^{2-} in the top portion of the profile is the result of enrichment via evaporation and sublimation (Fig. 4), which become very important heat flow pathways during freezing (Boike et al. 1997). The chloride ion shows almost no change in concentration over the sampling period and neither ion profile is much affected by the descent of the freezing front. The latter ion has increased just below the frozen fringe by 24 September. The freezing front has passed

position, but will affect the thicknesses of the frozen and thawed portions of the profile between cores. It is thus more appropriate to compare profiles relative to the positions of the frost boundaries, than to the depth from the ground's surface. At each sampling event a minimum of two cores were harvested to allow comparison. Time considerations and difficulties associated with drilling in coarse materials prevented us from harvesting enough cores for a larger sample size. The profiles from each group of cores all show peaks at similar depths that vary only in absolute concentration, not in relative peak height, and a student's t-test provided no evidence to suggest that the cores were significantly different for all ionic profiles presented here (Tbl. 2).

The very low unfrozen water contents at the surface of the ground increase with depth and temp-

September 24

Total volumetric water content
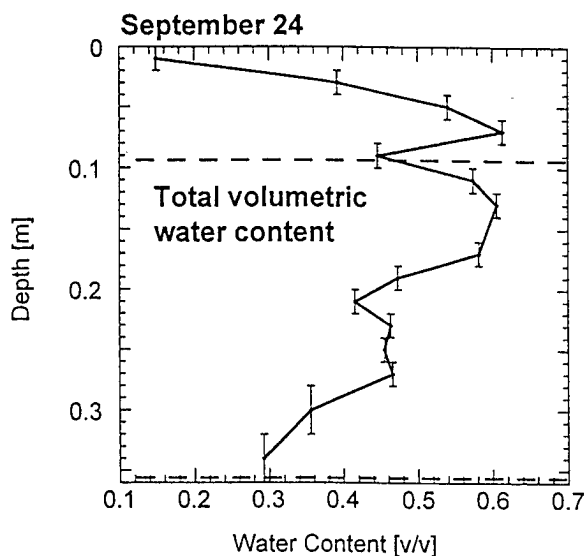
Figure 3. A total volumetric water content profile for 24 September. Dashed lines indicate the position of the frost table (lower) and the freezing front (upper).

erature to the freezing front. Sublimation is an important sink for released latent heat in the fall, and contributes to decreased volumetric water contents at the surface. The marked decrease in water content at the freezing front itself relative to depths just above and below it suggests a migration of water through the frozen fringe towards the region of phase change.

Solute concentrations change with the freezing of the active layer. Kay and Groenevelt (1983) observed the development of a NO_3^- peak positioned directly subjacent to the freezing front, unlike the one evident in Fig. 4, which appears 120 mm below the freezing front. This was attributed to the cumulative effect of solute exclusion over a number of repeated freeze-thaw cycles, and perhaps to the accumulation of solutes through convective transport of soil water to the freezing front as a consequence of ice lens formation. They analyzed their cores for NO_3^- only, performing a simple soil water extraction. The profiles analyzed here become difficult to explain using solute exclusion and convection, both transport processes. Concentrations of both NO_3^- and Cl^- on 13 September, for example, are very low. NO_3^- increases dramatically between 0.21- and 0.24-m depth by 3 October, an increase that cannot be accounted for by a decrease at some other depth. And whereas NO_3^- increases, Cl^-, with similar mobility, shows no effect at all. Bulk soil solute concentrations show the same patterns. Kay and Groenevelt (1983) go on to clarify the role of solute exclusion in a laboratory study, analyzing partially frozen sand cores for Cl^- content.

Their findings are similar to ours: although solute exclusion may be occurring, there is no evidence at the scale of core sectioning used in this study (20 to 40 mm sections) for redistributive effects.

In their soil column studies, Stähli and Stadler (1996) froze columns of sand and loam from both ends and monitored the bulk electrical conductivity and water content using TDR. They observed dramatic increases in salt concentration (calculated from bulk electrical conductivity) midway down the core relative to its ends. They concluded that, after an initial increase in solute concentration due to exclusion, a combination of convective solute transport to the freezing front and diffusive transport away from it resulted in their observed solute increases. The development of Fe_{aq} and NO_3^- peaks in the unfrozen ground fit this pattern, but are probably not the result of diffusion or convection but of changes in oxidation potential. Again, there are no concomitant decreases elsewhere in the profile to provide solute material for redistribution. The peaks develop during the period in which the sulfate peak disappears, and the Mn_{aq} peak develops, both at the position of the freezing front on 3 October (0.10 to 0.20 m). The Mn_{aq} peak shows higher concentrations immediately above and below the frost front.

The process of solute exclusion does not suffice to explain the observed profiles of solute distribution, especially for ions that are important in reduction-oxidation equilibria. There is no evidence for a concentration of solutes at depth in the active layer as a result of ice formation. The increasingly reductive character of the thawed region does, however, favour the release of reduced species such as Mn^{2+} and Fe^{2+} into the soil solution. Where groundwater effluxes (into a lake littoral zone, or a sampling trench), this would cause an increase in solute concentration, as observed by Lewkowicz and French (1982) and by Overduin (1993), or as indicated by the increase in soil water conductivity observed in this study. Further work includes analysis of additional ions, calculation of soil water conductivity from TDR waveforms, and thermodynamic modelling of the soil solutions.

CONCLUSIONS

Freeze-back results in an enrichment of soil moisture immediately above and below the freezing front. The effect of moisture migration into frozen soil redistributes soil moisture, primarily upwards. On the basis of soil water solute concentration profiles, freezing does not result in observable macroscale solute redistribution. The increasingly reducing
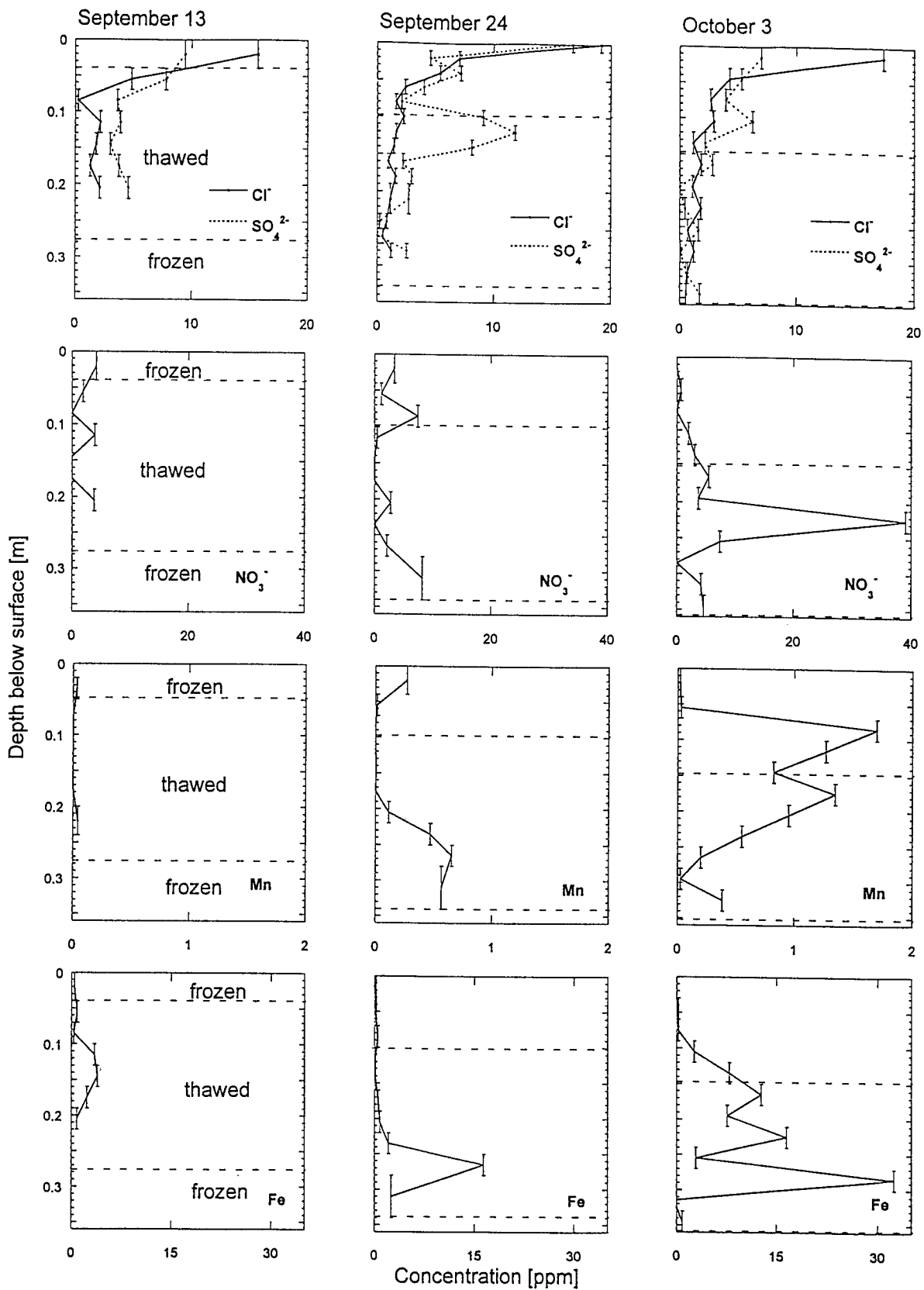
Figure 4. Soil water nitrate, chloride (solid line) and sulfate (dashed line), manganese and iron concentration profiles for three cores collected on 13, 24 September and 3 October. Dashed lines indicate the positions of the frost table (lower) and the freezing front (upper).

nature of the soil, as it is separated from atmospheric influence by a frozen layer, results in the release of reduced species at depth. An increase of NO_3^- under these conditions suggests a high spatial variability of oxidation potential vertically in the soil column.

REFERENCES

Bliss, L.C., G.H.R. Henry, J. Svoboda and D.I. Bliss. 1994. Patterns of plant distribution within two polar desert landscapes. Arctic and Alpine Research, 26(1):46-55.

Boike, J., K. Roth and P.P. Overduin. 1997. Thermal and hydrological dynamics of the active layer at a continuous permafrost site (Taymyr Peninsula, Siberia). Submitted to Water Resources Research.

Carter, M.R. (ed.) 1993. Soil sampling and methods of analysis. CRC Press Inc., Florida.

Cragin, J.H. 1995. Exclusion of sodium chloride from ice during freezing. Eastern Snow Conference. In Proceedings of the 1995 Annual Meeting, Toronto, Canada, 259-262.

Ershov, E.D., Yu.P. Lebedenko, E.M. Chuvilin and N.S. Naumova. 1992. Mass transfer in freezing saline soils. In Proceedings, 1st Int'l Conference on Cryopedology, November 10-14, Pushchino, Russia.

Hallet, B. 1978. Solute redistribution in freezing ground. In Permafrost: Third Int'l Conference, 1:86-91.

Harris, S.A., H.M. French, J.A. Heginbottom, G.H. Johnston, B. Ladanyi, D.C. Sego and R.O. Everdingen. 1988. Glossary of permafrost and related ground-ice terms. Technical Memorandum 142, NRCC, Ottawa, Canada.

Kay, B.D. and P.H. Groenevelt. 1983. The redistribution of solutes in freezing soil: Exclusion of solutes. In Permafrost: 4th Int'l Conference, Nat'l Academy of Sciences, Washington, D.C.

Lewkowicz, A.G. and H.M. French. 1983. The hydrology of small runoff plots in an area of continuous permafrost, Banks Island, N.W.T.Proceedings of the Fourth Canadian Permafrost Conference, Calgary, Alberta. Ottawa, N.R.C.C.

Lunardini, V.J. 1981. Heat transfer in cold climates. Van Nostrand Reinhold Company, New York.

MacKay, R. 1982. Downward water movement into frozen ground, western arctic coast, Canada. Canadian Journal of Earth Science. 20:120-134.

Overduin, P.P. 1993. Thermodynamic equilibria modelling of groundwater contributions into an acidic High Arctic lake. unpublished B.Sc.

Thesis, Wilfrid Laurier Univ., Waterloo, Canada.

Panday, S. and M.Y. Corapcioglu. 1991. Solute rejection in freezing soils. Water Resources Research 27(1):99-108.

Pecher, K., 1994. Hydrochemical analysis of spatial and temporal variations of solute composition in surface and subsurface waters of a high arctic catchment. Catena, 21:305-327.

Pfeiffer, E.-M., A. Gundelwein, T. Nöthen, H. Becker and G. Guggenberger. 1996. Characterization of the organic matter in permafrost soils and sediments of the Taymyr Peninsula, Siberia and Severnaya Zemlya, Arctic Region, p. 46-63. In Reports on Polar Research 211, Alfred Wegener Inst. for Polar and Marine Research, Bremerhaven, Germany.

Pfisterer, U. and S. Gribbohm. 1989. Zur Herstellung von Platinelektroden für Redoxmessungen. Z. Pflanzenernährung Bodenkunde, 152:455-456.

Qiu, G., W. Sheng, H.Cuilan and K. Zheng. 1988. Direction of ion migration during cooling and freezing processes. In Proceedings of the 5th Int'l Conference on Permafrost, Trondheim, Norway, 442-447.

Schiff, S.L., M.C.English, M. Ecclestone, R. Elgood, M. Hinton and L. Pezzuto. 1991. Constraints on the origin of acidity in Colour Lake, Axel Heiberg Island. NHRI Science Report No. 2, National Hydrology Research Institute, Saskatoon.

Siegert, C. and D. Bolshiyanov. 1995. The Russian-German Cooperation: The Expedition Taymyr 1994. In Reports on Polar Research 175, Alfred Wegener Inst. for Polar and Marine research, Bremerhaven, Germany.

Smith, M.W. and A.R. Tice. 1988. Measurement of the unfrozen water content of soils: a comparison of NMR and TDR methods. In Proceedings of the 5th Int'l Conference on Permafrost, Trondheim, Norway, 1:473-477.

Stähli, M. and D.C. Stadler. 1996. Water and solute dynamics in freezing soil columns, p. 31-48. In Water and solute dynamics in frozen forest soils, measurements and modeling, (D. C. Stadler), unpublished PhD Thesis. ETH No. 11574, Zürich, Switzerland.

Topp, G.C., J.L.Davis and A.P. Annan. 1980. Electromagnetic determination of soil water content: measurements in coaxial transmission lines. Water Resources Research. 16(3):574-582.

van Loon, W.K.P., 1991. Heat and mass transfer in frozen porous media. unpublished Ph.D. Thesis, Agricultural Univ., Wageningen, the Netherlands.

Effects of Freezing and Thawing on N_2O Production in Soil Under Different Agricultural Practices

D. PRÉVOST[1], E. van BOCHOVE[1], AND F. PELLETIER[1]

ABSTRACT

Freezing and thawing cycles have been shown to induce soil physical and biological changes such as disruption of structure (aggregate stability) and stimulation of denitrification. The latter is a major process involved in production of nitrous oxide (N_2O), a greenhouse gas. The increase in denitrification following freezing may be attributed to the diffusion of newly available organic substrates from disrupted aggregates to denitrifying micro-organisms. However, agricultural practices influence the aggregate stability (resistance to physical disruption), the macro-porosity and the organic matter content of soil. The objective of this study was to evaluate the effect of freezing and thawing cycle on N_2O production in a Kamouraska clay soil submitted to different crop rotations and tillage practices. Experiments were conducted in soil slurries to favor substrate diffusion and in undisturbed soil cores to simulate field conditions. In slurries, a freezing and thawing cycle increased denitrification rates by 32% and soils from no-tillage with a 2-yr barley-red clover rotation (NT-R) exhibited higher denitrification rates (92%) than those from conventional-till moldboard plowing with continuous barley (CT-C). In soil cores taken in November, N_2O production was also increased after thawing and related to agricultural practices. Relationships involved between denitrification, soil structure and C release from organic matter are discussed with respect to the contribution of agriculture to N_2O emissions during cold season.

Key words: nitrous oxide, freezing/thawing, agricultural practices

INTRODUCTION

The high levels of N_2O emitted during spring represent a significant proportion of the annual emission of this greenhouse gas in temperate regions (Bremner *et al.* 1980). These fluxes may be indicative of denitrification events associated with freezing and thawing. Freezing and thawing cycles induce physical disruption of the soil structure, and diffusion of soluble carbon, which promotes biological activities such as denitrification. In fertilized soils, denitrification is often related to organic C, which provides energy to denitrifiers. However, agricultural practices influence the content and the storage of soil C and the aggregate stability (resistance to physical disruption). No-till management has been reported to improve aggregate stability and increase C and N content (Angers and Carter 1996). In this study we hypothesize that the effects of freezing and thawing on N_2O production will be influenced by agricultural practices.

[1] Research Center, Agriculture and Agri-Food Canada, 2560 Hochelaga Blvd., Sainte-Foy, Québec G1V 2J3, Canada

The objectives were to determine the magnitude of the effect of freezing and thawing cycle on N_2O production in soils from different agricultural practices. Experiments were performed in soil slurries to determine denitrification activities in conditions that remove substrate diffusion constraints, and in dynamic soil cores to evaluate N_2O in conditions where diffusion is function of the undisturbed soil structure.

MATERIAL AND METHODS

Cultivated plots were located at the Agriculture Canada and Agri-Food Experimental Farm at La Pocatière, Québec, on a Kamouraska clay soil. The plots were arranged in a split-plot design with four replicates with crop sequence treatment as the main plot and tillage practice as the subplot treatment. Two contrasted cropping-tillage combinations treatments were selected 1) no-tillage with a 2-yr barley-red clover rotation (NT-R) and 2) conventional-till moldboard plowing with continuous barley (CT-C). Soil samples were collected in the 0-5 cm depth in October 1995 and soil cores were collected at 0-5 cm depth in October (after growing season) and in November 1995 (after plowing).

Sieved soil samples (6mm) and cores were frozen at -12 °C for 20-24 hours. Unfrozen controls were kept at 4 °C. After thawing, denitrifying enzyme activity (DEA) (Martin et al. 1988) in slurries (sieved soils) was determined in the presence NO_3^-, 10% C_2H_2 (acetylene) and N_2 (anaerobic conditions) under mild agitation. Soil cores were successively incubated under aerobic (ambient air) and anaerobic ($N_2+C_2H_2$) conditions, with a gas recirculation system. Gas samples were collected periodically and injected into a gas chromatography (GC) to quantify N_2O and CO_2.

RESULTS AND DISCUSSION

Effects of freezing/thawing cycle and agriculture practice on DEA

Both freezing/thawing cycle and agricultural practices had a significant effect on DEA (Fig. 1). Denitrification rates were higher in

frozen/thawed than in unfrozen treatments. Since N was not limiting and aggregates were not broken under experimental conditions for DEA, the burst of denitrification after freezing may be attributed to the release of organic C-substrates previously sequestred in aggregates that are disrupted by freezing or from microbial biomass and microfauna that are killed by the freezing process (Soulides and Allison 1961, Bullock et al. 1988). The increases in denitrification following freezing were similar for both agricultural practices (32%). Soils from NT-R exhibited higher denitrification rates (92%) than those from CT-C. These higher denitrification rates in soils from NT-R may be due to the higher mineralizable organic C content found in soils from this practice (results not shown). This is in agreement with other studies showing that soil conservation management systems (e.g. reduced tillage, rotation) result in higher aggregate stability and stock of organic matter compared with conventional systems.
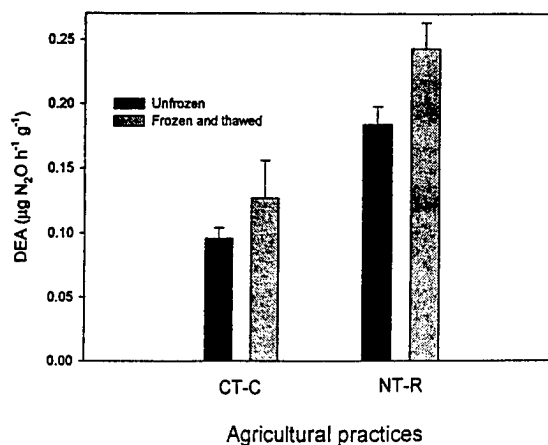
Figure 1. Effect of thawing and agriculture practices on DEA in soil slurries; CT-C : conventional-till continuous culture, NT-R : no-tillage-rotation; agricultural practices and freeze treatments indicate significant differences (P<0.0005 and P<0.05); interaction between treatments is no significative.

Effects of freezing /thawing cycle on N_2O and CO_2 emissions in soil cores.

Measurements of N_2O made under aerobic (ambient air) conditions represented the net emission of N_2O evolved from soils whereas measurements in anaerobic conditions and in the presence of acetylene represented the potential of N_2O production by denitrification. Agricultural practices and freezing/thawing cycle showed a significant effect on N_2O emission from soil sampled in November but not from that sampled in October (Table 1, Fig. 2).
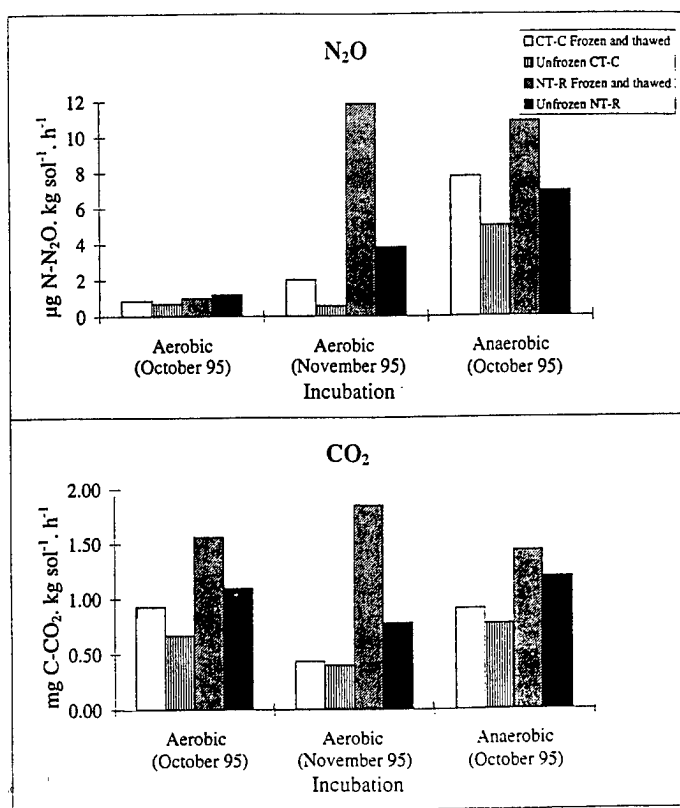
Figure 2. Effect of freezing/thawing cycle and agricultural practices on N_2O and CO_2 emissions in undisturbed soil cores under aerobic (ambient air) and anaerobic (N_2 + 10% C_2H_2) incubations.

In soil from November 1995, emissions were significantly higher in NT-R than in CT-C soils and in frozen/thawed than in unfrozen soils, indicating probably that environmental factors for denitrification (eg. water content that regulates oxygen availability) were more likely present in

the late autumn where the weather was wet. Furthermore, N_2O production in soil cores from October incubated in conditions that favor denitrification (anaerobic) was influenced by agricultural practices and freezing. It is known that, in agricultural soils, oxygen is the dominant factor limiting denitrification, and when anaerobic zones are present, C availablility would limit denitrification (Firestone and Davidson 1989). As it was observed in slurries, undisturbed soils from NT-R practice exhibited higher N_2O emission than those from CT-C when soil factors were not limiting for denitrification (ca 500% in November). Soil cores collected in October and incubated under anaerobic conditions showed also the tendancy (results not significant) to produce more N_2O production in NT-R than in CT-C soils (ca 138%) (Fig. 2). In November, nitrous oxide emission was also increased similarly in both agricultural practices (ca 220%) after a freezing/thawing cycle. This is in agreement with other studies showing that the thawing of a frozen soil can cause temporal increase in N_2O production by denitrification (Christensen and Tiedje 1990).

Emissions of CO_2 from soil cores were significantly affected by agricultural practices and by freezing/thawing cycle, except for the aerobic incubation in October. In general, CO_2 emissions, which are mainly due to microbial respiration, followed the same tendancy than N_2O emissions (Fig. 2). They were higher in NT-R than in CT-C soils probably reflecting the higher mineralizable C (not shown) that can support denitrification. There was also a burst of CO_2 emission following freezing, which supports the increase in microbial activity, such as dentrification.

In summary, soils from no-tillage-rotation practice (NT-R) showed higher capacities to denitrify than those from conventional-till-continuous culture (CT-C). These soil properties were reflected in the levels of N_2O emitted from undisturbed soils when conditions for denitrification were not limiting. This study also showed that freezing/thawing cycle increase denitrification activity which may result in higher net N_2O emissions from soils.

Table 1. Non-parametric analysis of N_2O and CO_2 emissions versus freezing/thawing cycle and agricultural practices from data obtained from undisturbed soil cores.

Incubation	Agricultural practices (CT-C vs NT-R)		Freezing/Thawing effect (Frozen vs unfrozen)	
	N_2O	CO_2	N_2O	CO_2
Aerobic (october 95)	NS	§	NS	NS
Aerobic (november 95)	§	§	§	§
Anaerobic (october 95)	NS	§	NS	§

REFERENCES

Angers, D.A. and M.R. Carter. 1996. Aggregation and organic matter storage in cool, humid agricultural soils. p. 193-211. *In* Carter, M.R. and B.A. Stewart (eds.) Advances in Soil Science. Structure and organic matter storage in agricultural soils.

Bremner, J.M., S.G. Robbins, and A.M. Blackmer. 1980. Seasonal variability in emission of nitrous oxide from soil. Geophys. Res. Lett. 7:641-644.

Bullock, M.S., W.D. Kemper, and S.D. Nelson. 1988. Soil cohesion as affected by freezing, water content, time and tillage. Soil Sci. Soc. Am. J. 52:770-776.

Christensen, S., and J.M. Tiedje. 1990. Brief and vigorous N_2O production by soil at spring thaw. J. Soil Sci. 4:1-4.

Firestone, M.K., and E.A. Davidson. 1989. Microbiological basis of NO and N_2O production and consumption in soils. p 7-21. *In* M. O. Andreae and D.S. Chimel (eds) Exchange of Trace Gases between Terrestrial Ecosystems and the atmosphere. John Wiley, New York.

Martin, K., L.L. Parsons, R.E. Murray, and M.S. Smith. 1988. Dynamics of soil denitrifier populations: relationships between enzyme activity, most-probable-number counts, and actual N gas loss. Appl. Environ. Microbiol. 54:2711-2716.

Soulides, D.A., and F.E. Allison. 1961. Effects of dying and freezing soil on carbon dioxide production, available mineral nutrients, aggregation and bacterial population. Soil Sci. 91:291-298.

The Effect of Permafrost on Dissolved Organic Carbon Exports from Two Subarctic Streams

R. MacLEAN[1], J.G. IRONS III[1], M.W. OSWOOD[1], AND W.H. McDOWELL[2]

ABSTRACT

We collected soil, stream and groundwater samples from two watersheds in interior Alaska near Fairbanks. Each watershed is drained by a second order stream. Both basins are about 500 ha in area but one has considerably more permafrost soils (50% by area) than the other (3%). The permafrost-dominated watershed had a more flashy hydrology, lower stream ionic conductivity and exported almost three times the dissolved organic carbon (DOC) than the permafrost-free stream (9.78 vs 3.79 kg ha^{-1} yr^{-1}). In the permafrost-dominated watershed, runoff is restricted to the upper carbon rich soil horizons where it is enriched with DOC.

Key words: permafrost, dissolved organic carbon

INTRODUCTION

Permafrost is discontinuously distributed in the Alaskan interior, occurring mainly as a function of aspect and forest dynamics (Viereck et al. 1986). Shady north-facing slopes and valley bottoms often have permafrost whereas permafrost is usually absent on sunny south-facing slopes and hill crests. Forest type is closely correlated with permafrost distribution in the Yukon-Tanana Uplands with colder permafrost-prone soils dominated by black spruce (*Picea mariana*) and warmer permafrost-free soils typically supporting mixed hardwood/white spruce (*Picea glauca*) forest.

Permafrost has a profound effect on the hydrology of subarctic streams (Carlson 1974, Dingman 1973), and has been found to regulate their inorganic chemistry (Ray 1988). Stream basins dominated by permafrost are more prone to rapid increases in flow than those with less permafrost because frozen soils and ice lenses have lower permeability than warmer soils (Slaughter and Kane 1979).

In this paper we describe how the distribution of permafrost in two second-order subarctic watersheds influences the concentrations and exports of dissolved organic carbon (DOC). DOC is an important facet of the quality of stream water. It influences microbial productivity (Meyer 1990, Wotton 1988), water color and the mobility of trace metals (Kullberg et al. 1993). DOC exports are also an important part of watershed carbon budget estimates (McDowell and Likens 1988, Dosskey and Bertsch 1994, Grieve 1994, Lydersen and Henricksen 1994).

MATERIALS AND METHODS

Study site

The two study basins (C2 and C3) are located in the Caribou-Poker Creeks Research Watershed 50 km northeast of Fairbanks, Alaska (Fig. 1). Both are of similar area and elevation (table 1). C3 is a colder shaded basin (53% permafrost rich soil types) and C2 is a warmer basin with limited permafrost (3% pemafrost rich soil types). Vegetation in the two basins is closely correlated with permafrost and aspect. Warmer slopes support birch (*Betula papyrifera*), aspen (*Populus tremuloides*) and white spruce. Colder slopes support black spruce which becomes more sparsely distributed and stunted with increasing permafrost.

[1] University of Alaska Fairbanks, Department of Biology and Wildlife, Irving I Building, Alaska 99775, USA

[2] University of New Hampshire Durham, Department of Natural Resources, James Hall, Durham, New Hampshire 03824, USA
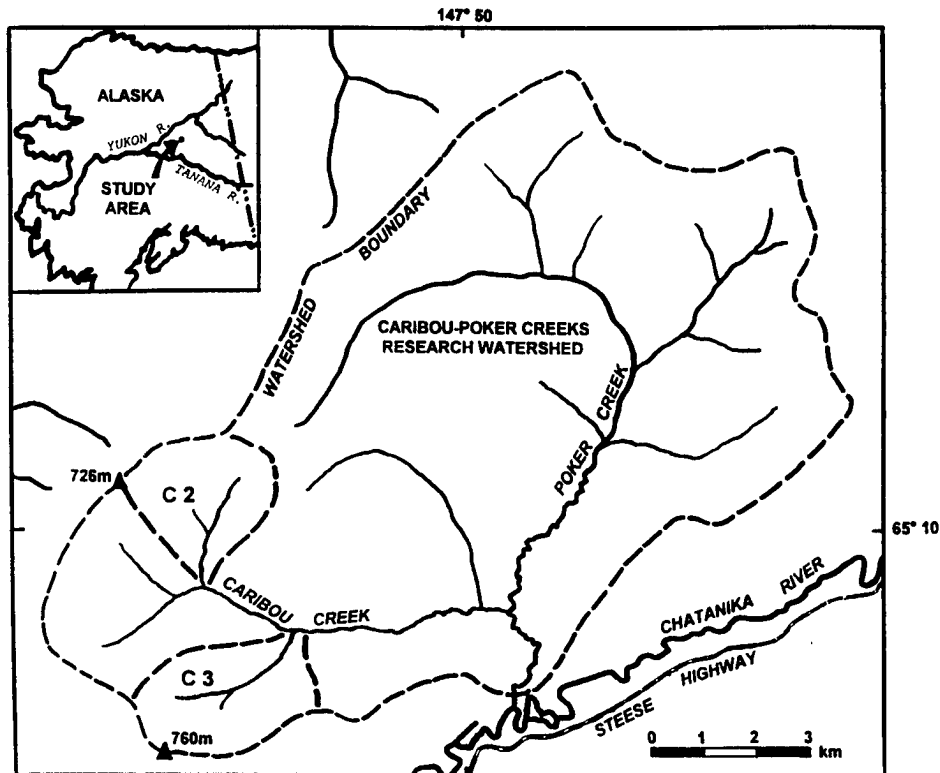
Figure 1. Location of Caribou-Poker Creeks Research Watershed and study basins C2 and C3

Table 1. Physical characteristics of study basins.

Basin	Area (ha)	Elevation range (m)	Total stream length (m)	Area underlain by permafrost rich soil (%)	Annual degree-days above 0°C
C2	520	323-738	2200	3	713
C3 (colder)	570	224-770	2600	53	353

Olnes and Gilmore silt loams (Typic cryothents). Soils on cold faces with more extensive permafrost are Ester silt loams (Histic lithic cryaquepts, Rieger et al. 1972).

Valley bottoms are usually treeless and shrubby. Permafrost can be found underneath most of the valley bottoms and the water table is often visible as ponding in depressions between low shrubby hummocks. The vegetation in these lowlands is dominated by dwarf birch (*Betula glandulosa.*), blueberry (*Vaccinium* spp.), willow (*Salix* spp.) and alder (*Alnus tenuifolia*). The soils are described as Karshner silt loams (Pergelic cryaquepts, Rieger et al. 1972)

Data collection

Stream discharge was recorded using Parshall flumes near the mouth of each basin.

A single set of streamwater samples was collected in November 1994 and again in January 1995. Regular biweekly samples were collected from before snow-melt (21 March 1995) until after streams froze over (17 October 1995). Additional stream samples were collected every two days during high flows following snow melt or heavy rain.

We conceptualize the hydrology of the two streams as being driven by four runoff pathways

339
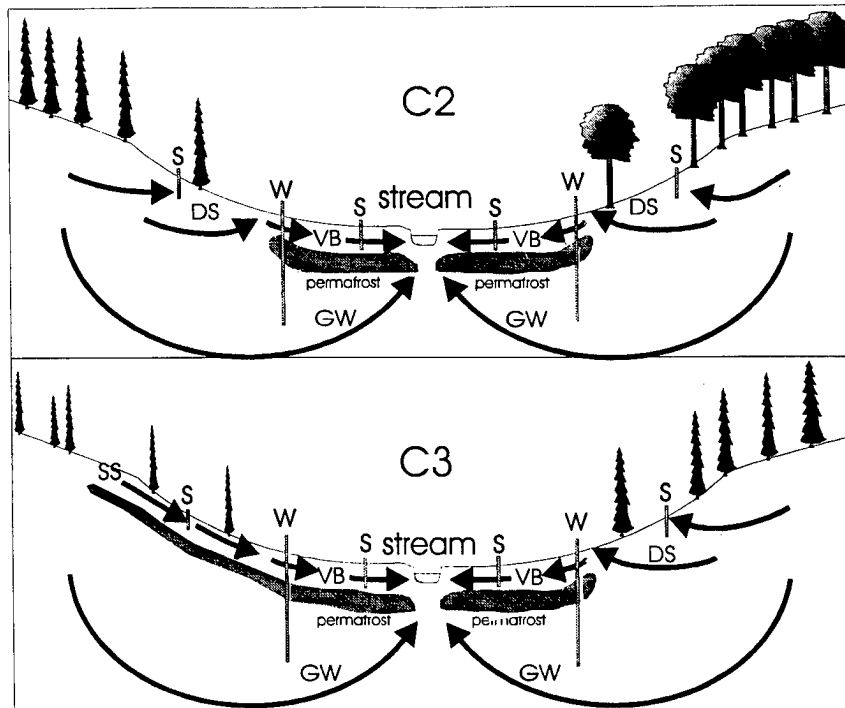
Figure 2. Hypothetical flow pathways in low permafrost (C2) and high permafrost (C3) basins. SS is shallow soil flow (O and A horizons), DS is deep soil flow (B and C horizons), VB is displaced valley bottom water and GW is groundwater. W and S are wells and soil water samplers respectively.

(Fig. 2.). Shallow soil flow (SS) occurs where permafrost is present and runoff travels through the upper organic soil horizons. Deep soil flow (DS) occurs where permafrost is absent and where runoff occurs through mineral soil horizons. Ground-water (GW) is defined for our purposes as water that infiltrates deeper than 1 m. Valley bottom water (VB) is a mixture of ground-water, shallow and deep subsurface water and direct precipitation which collects on top of the permafrost in the valley bottoms adjacent to the stream.

Soil and ground water samples were collected from soil water suction samplers at 0.3 to 0.5 m depth and wells at > 2 m depth on 9 dates between 11 July and 4 September. Suction samplers were positioned in transects to intercept the flow paths described above (Fig 2.). Four replicate transects were installed in each watershed (not including wells). Three wells were installed in each watershed and a variable number of suction samplers were installed at the sources of springs.

Chemical Analyses

Conductivity measurements were made in the laboratory using a 6V Hach conductivity/TDS meter. DOC measurements were made using high temperature catalytic oxidation with infra red detection of CO_2 (Shimadzu 500; Cauwet 1994).

RESULTS AND DISCUSSION

Hydrology

Stream discharge in C3 during 1995 was flashy in comparison to C2 (Fig. 3a, 3b.). This is typical of these two streams (Ford 1973, Ray 1988) and typical of differences between permafrost-free and permafrost-dominated watersheds in general (Haugen *et al.* 1982). Baseflow (the flow occurring between hydrograph peaks) is fed mainly by groundwater in both streams. Permafrost-free areas are not thought to generate overland flow or shallow subsurface flows (Haugen *et al.* 1982) but are thought to be the contributing zones for deep subsurface and groundwater flows. In C3, baseflow is lower than baseflow in C2 because permafrost reduces infiltration to groundwater.
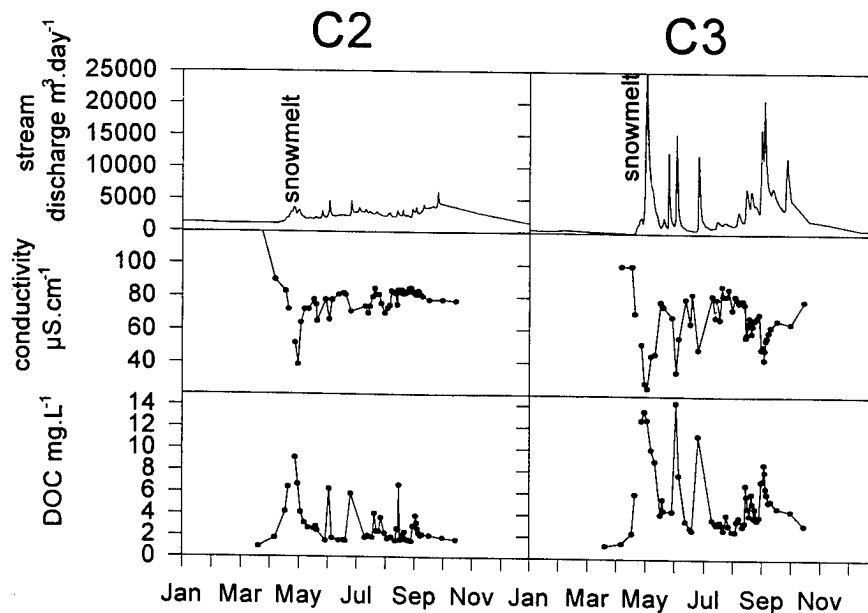
Figure 3. Stream discharge, conductivity and dissolved organic carbon (DOC) *concentrations for C2 and C3 during 1995*

Dingman (1971) studied runoff characteristics in nearby Glenn Creek and suggested that hydrograph peaks in permafrost-dominated basins like C3 consisted of water from two main sources: overland flow from saturated soils in valley bottoms and delayed flow through the moss and soil organic layers on the valley floor and hillsides underlain by permafrost. Both these pathways conform to the variable source area model (Beven and Wood 1983) and expand and shrink depending on antecedent moisture levels (Ray 1988).

Hydrograph peaks in C2 are much more damped following rainfall or snowmelt than those in C3. The water in these peaks probably originates from saturated areas in valley bottoms as in C3. The sluggish response seen in C2 is apparently because valley bottom water is not displaced as rapidly following rain. This rainwater and snowmelt infiltrates deeper and moves more slowly in C2 than it does in C3.

Chemistry

The ionic chemistry of C2 and C3 measured in 1995 and earlier (Hilgert and Slaughter 1983, 1984, Ray 1988) supports the hydrologic model described above. Rainstorms dilute stream water in C3 to a far greater extent than they do in C2 as measured by

conductivity (Fig. 3c, 3d). The longer rainwater is in contact with soil and bedrock, the more ionizable substance it will dissolve. The higher conductivity of stream water in C2 is consistent with the longer residence time and deeper flow paths of its contributing soil and groundwater. The lower conductivity of stream water in C3 is consistent with shorter residence times and shallower flow paths.

Soil water samples taken at 0.3 to 0.5 m from mixed forest, spruce forest and spruce forest with permafrost (Fig. 4a) have low conductivity ($<20\mu$S cm^{-1}) whereas samples taken from groundwater have high conductivity ($>90\mu$S cm^{-1}). Hillside spring water in C3 has a higher conductivity than well water implying a much deeper origin. Samples from valley bottom soils and from the stream are a mixture of water from these sources and should be intermediate in their conductivity. In C2 well water and valley bottom water have similar conductivity suggesting that the valley bottom water is dominantly of groundwater origin. In C3 valley bottom water has lower conductivity than well water. This suggests that there is a larger proportion of dilute water of shallow origin present.

As flow rates increase in the streams, DOC concentrations rise while conductivity decreases (Fig 3e, 3f). Conductivity is negatively correlated with

341
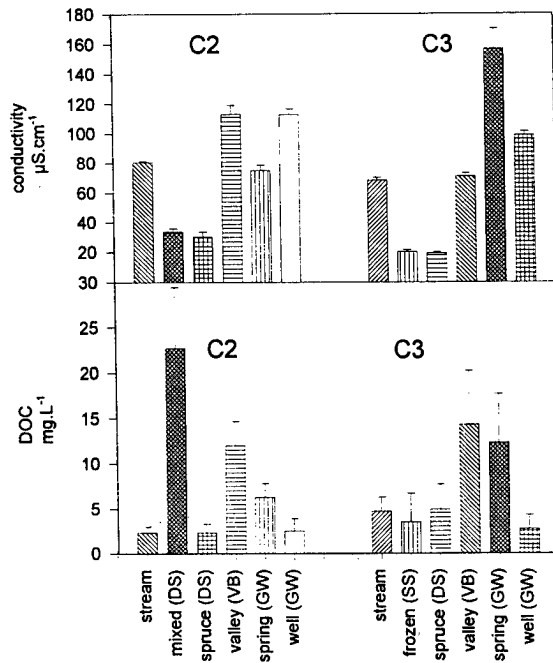
Figure 4. Conductivity and dissolved organic carbon (DOC) *concentrations in stream, soil and groundwater.* Mixed (DS) *is deep soil water from mixed forest,* spruce (DS) *is deep soil water from spruce forest,* frozen (SS) *is shallow soil water from spruce forest over permafrost.* Valley (VB) *is valley bottom water and* spring (GW) *and* well (GW) *is groundwater from either springs or wells. Error bars show standard error.*
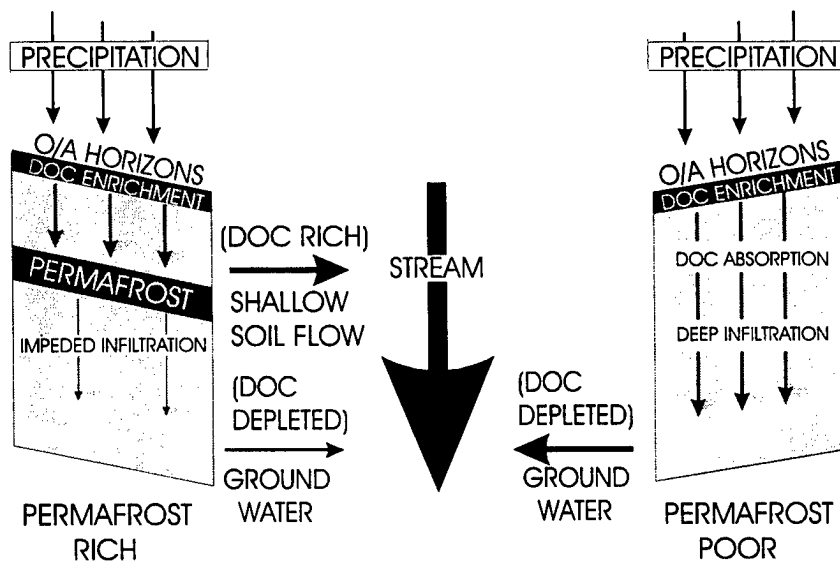
Figure 5. A model of differences in the hydrology and DOC exports of permafrost rich and permafrost poor soils.

DOC concentrations in stream, soil and groundwater. DOC levels are highest in shallow soil water samples and lowest in groundwater (Fig. 4b) while the reverse is true for conductivity. DOC tends to be entrained in the organic horizons but absorbed by mineral soil (McDowell and Wood 1984, Qualls and Haines 1991). DOC can also be (Ford and Naiman 1989). Interestingly, the highest DOC concentrations were found in the mineral horizons 0.5 m beneath mixed hardwood forest floor in C2. We would expect higher concentrations in samples from the wet organic soils over permafrost and under spruce in C3. Mixed hardwood soil is warmer, drier and subject to greater evapotranspiration demand from trees. This may concentrate DOC.

By integration of stream concentration data (Fig. 3e, 3f) and interpolating over the 4 winter months, for which we have little data, we estimate that C3 exported almost three times the amount of DOC that C2 did in 1995 (9.8 vs 3.8 kg ha^{-1} yr^{-1}). This difference in exports appears to be caused by the shallower flow paths in C3 relative to C2 rather than by any difference in DOC concentrations in surface soil.

CONCLUSIONS

The extensive distribution of permafrost in C3 maintains a high water table throughout the basin. Additional water introduced through rainfall or snowmelt lifts the water table into the organic horizons and enables the entrainment of DOC and reduces the chances of absorption by mineral soils or microbial immobilization (Fig 5.). Permafrost in C2 is restricted to valley bottoms. This allows deeper and slower infiltration of water in C2 and may facilitate adsorption or immobilization of DOC thus reducing concentrations in the stream. The discontinuous distribution of permafrost throughout the subarctic appears to be an important determinant of DOC concentrations in the streams of this region.

REFERENCES

Beven, K. and E.F. Wood. 1983. Catchment geomorphology and the dynamics of runoff contributing areas. J.Hydrol. 65:139-158.

Carlson, R.F. 1974. Permafrost hydrology: An Alaskan's experience. p. 51-57. *In* R. Demers (ed.) Permafrost hydrology. Environment Canada, Ottawa.

Cauwet, G.1994. HTCO method for dissolved organic carbon analysis in seawater: influence of catalyst in blank estimation. Mar. Chem. 47:55-64.

Dingman, S.L. 1971. Hydrology of the Glenn Creek watershed, Tanana River basin, central Alaska. U.S. Army CRREL Report 297, Hanover, New Hampshire

Dingman, S.L. 1973. The water balance in arctic and subarctic regions. U.S. Army CRREL Special Report 187. Hanover, New Hampshire.

Dosskey, M.G. and P.M. Bertsch. 1994. Forest sources and pathways of organic matter transport to a blackwater stream: a hydrologic approach. Biogeochem. 24:1-19.

Fiebig, D.M. and M.A. Lock. 1991. Immobilization of dissolved organic material from groundwater discharging through the stream bed. Freshwater Biol. 26:45-55

Ford, T.R. 1973. Precipitation-runoff characteristics of the Caribou Creek Research Watershed near Fairbanks, Alaska. Unpubl. M.S. thesis. University of Alaska Fairbanks.

Ford, T.E. and R.J. Naiman. 1989. Groundwater-surface water relationships in boreal forest watersheds: dissolved organic carbon and inorganic nutrient dyamics. Can. J. Fish. Aquat. Sci. 46:41-49

Grieve, I.C. 1994. Dissolved organic carbon dynamics in two streams draining forested catchments at Loch Ard, Scotland. Hydrol. Proc. 8:457-464.

Haugen, R.K., C.W. Slaughter, K.E. Howe, S.L. Dingman. 1982. Hydrology and climatology of the Caribou-Poker Creeks Research Watershed, Alaska. U.S. Army CRREL Report 32-26, Hanover, New Hampshire.

Hilgert, T.W., C.W. Slaughter. 1983. Water quality and streamflow in the Caribou-Poker Creeks Research Watershed, central Alaska, 1978. USDA Forest Service publication PNW-RN-405.

Hilgert, T.W., C.W. Slaughter. 1984. Water quality and streamflow in the Caribou-Poker Creeks Research Watershed, central Alaska, 1979. USDA Forest Service publication PNW-RN-463.

Kullberg, A., K.H. Bishop, H. Anders, M. Tunsson and R.C. Petersen Jr. 1993. The ecological significance of dissolved organic carbon in acidified waters. Ambio 22:331-337.

Lydersen, E. and A. Henriksen. 1994. Total organic carbon in streamwater from four long term monitored catchments in Norway. Environ. Int. 20:713-729.

McDowell, W.H. and T. Wood. 1984.
Podzolization: soil processes control dissolved
organic carbon concentrations in stream water.
Soil Sci. 137:23-31.

McDowell, W.H. and G.E. Likens. 1988. Origin,
composition and flux of dissolved organic carbon
in the Hubbard Brook valley. Ecol. Monog.
58:177-195.

Meyer, J.L. 1990. Production and utilization of
dissolved organic carbon in riverine ecosystems.
p. 281-299. *In* E.M. Perdue and E.T. Gjessing
(ed.) Organic acids in aquatic ecosystems. John
Wiley and Sons, New York..

Qualls, R.G. and B.C. Haines. 1991. Geochemistry
of dissolved organic nutrients in water percolating
through a forest ecosystem. Soil Sci. Soc. Am. J.
55:1112-1123.

Ray, S.R. 1988. Physical and chemical
characteristics of headwater streams at Caribou
Poker Creeks Research Watershed, Fairbanks.
Alaska. unpubl. M.S. thesis. University of Alaska
Fairbanks.

Rieger, S., C.E. Furbush, D.B. Schoephorster, H.
Summerfield Jr. and L.C. Geiger. 1972. Soils of
the Caribou-Poker Creeks Research Watershed.
U.S.Army Cold Regions Research and
Engineering Lab., Hanover, New Hampshire.

Slaughter, C.W. and D.L. Kane. 1979. Hydrologic
role of shallow organic soils in cold climates.
Canadian Hydrology Symposium '79, Cold
Climate Hydrology Proceedings. p. 380-389.

Vervier, P. and Naiman, R.J. 1989. Spatial and
temporal fluctuations of dissolved organic carbon
in subsurface flow of the Stillaguamish River.
Arch. Hydrobiol. 123:401-412.

Viereck, L.A., K. Van Cleve and C.T. Dyrness.
1986. Forest ecosystem distribution in the taiga
environment. p. 22-43. *In* K. Van Cleve, F.S.
Chapin III, P.W. Flanagan, L.A. Viereck, C.T.
Dyrness (ed.) Forest ecosystems in the Alaskan
taiga. Springer Verlag, New York.

Wooton, R.S. 1988. Dissolved organic material and
trophic dynamics. Biosci. 38:172-178.

Phosphorus

The Influence of Fertilization on Phosphorus Status
of Seasonally Frozen Arable Siberian Soils

R.P. MAKARIKOVA[1] AND P.A. BARSUKOV[1]

ABSTRACT

Phosphorus status in the arable horizon (0-20 cm depth) of the most typical Siberian soils, Podzoluvisol, Greyzem and Chernozem under long-term fertilization was studied. Application of any phosphorus containing fertilizers resulted in increase in content of total P and of inorganic P bound with Ca, Al, Fe cations. The content of organic P was not changed under low P fertilizer doses (12-15 kg P/ha·year), and was increased in other fertilized soil, independent of fertilizer form (organic or mineral or combined), as compared to unfertilized soil. Significant correlation between P availability indices and Ca-, Al- and Fe-associated P was absent.

Key words: Phosphorus, fertilization, arable soil, Siberia.

INTRODUCTION

In general, most Siberian soils are characterised by high total P content which is attributed mostly to high P level in loess blown from Altay-Sayan mountain system and Kazachstan hills, and relatively low rate of P mobilization under cold climatic conditions (Shumilova 1963; Ginzburg 1981). Siberian soils are usually frozen for more than 5 months in a year. In spring, soils start to thaw slowly, and sometimes the lowest parts of the root layer in East Siberia may stay frozen until August. After application, fertilizer phosphorus is rapidly transformed into poorly solved forms and insoluble P accumulates in the soil.

Phosphorus taken up by plants does not often correspond to total P content. The P availability indices developed in the European part of Russia, where climatic conditions are quite different from these in Siberia, do not provide reliable estimates (Averkina 1986; Berhin et al. 1989). One reason may be that under low temperatures plants are more likely to be affected by lack of P supply (Black 1968).

The aim of the work was to study changes in P fractions under long-term fertilization, and to determine how well P availability indices correlate with soil P fractions. There are only few publications devoted to the influence of fertilization on phosphorus status of Siberian soils (Kuznetzova 1983; Berhin et al. 1984), and only Chernozem was mainly under consideration.

MATERIALS AND METHODS

Soils

Three soils, differing in physical and chemical properties, cultivation history and climatic conditions were used: loamy sand Podzoluvisol, heavy-textured loam Greyzem, and medium-textured loam Chernozem (FAO classification). The ploughed (0-20 cm depth) layer was sampled after spring cereal crops were harvested. Subsamples (4-5) were taken at random from one experimental plot and mixed together. One mixed sample was taken from each of three field replications of long-term experiments.

Podzoluvisol was sampled from the following plots of the 37-year experiment in the West Siberian taiga: (1) no fertilizer, (2) mineral fertilizers at 34.3, 15.0, 28.5 kg/ha·year of N, P and K, respectively, (3) the same rate of mineral fertilizers plus 5.7 Mg/ha·year of livestock manure. The plots were cropped for grain and grass in a 7-year rotation.

Greyzem was sampled from the following plots of the 20-years long experiment in East Siberian forest-steppe: (1) no fertilizer, (2) mineral fertilizers at 60, 25 and 52 kg/ha·year of N, P and K, respectively, (3) mineral fertilizers at 30, 12.5 and 26 kg/ha·year of N, P and K, respectively, plus 6 Mg/ha·year of livestock manure, (4) 12 Mg/ha·year of manure. The plots were cropped for grain and silage corn in a 7-year rotation.

Chernozem was sampled from the plots of the 13-year experiment in West Siberian forest steppe: (1) no fertilizer, (2) mineral fertilizers at 22.5, 12.0, and 22.8 kg/ha·year of N, P, and K, respectively, (3) mineral fertilizers under the same rate plus 6 Mg/ha·year of livestock manure, (4) mineral fertilizers at 45, 24, and 45.6 kg/ha·year of N, P, and K, respectively, and (5) mineral fertilizers at 67.5, 36, and 68.4 kg/ha·year of N, P, and K, respectively, for 10 years of grain, grass, corn and beet crops rotation.

Fertilizers were applied as urea, ammonium nitrate, triple superphosphate, and potassium chloride in all experiments.

Soil chemical properties are shown in Table 1. Indices of P availability indicated high P supply in all soils. Climatic conditions for soil sites are different. The climate as a whole gets warmer and dryer from north (Podzoluvisol) to south (Chernozem) (Table 1). But Greyzem is more cold among other soils.

Tukey-test was used for the statistic analysis of differences in fertilizer treatments. The relations between P fractions and P fertilizer doses were investigated with regression analysis by Student-criterion.

Analyses

Fresh soil samples were sieved through 2-mm mesh sieve and thereafter were air-dried. Total P content was determined by the vanadium molybdate method after digesting soils with a mixture of sulphuric and perchloric acids (Olsen and Sommers 1982). Fractionation of inorganic P was carried out according to Chang and Jackson (1957) with modification (Negovelov and Pestova 1978). Organic P content was calculated as the difference between total and inorganic P. Available P was extracted by different methods using the following extractants: 0.2 N HCl, 0.5 N CH₃COOH, 0.006 N HCl, and 1% (NH₄)₂CO₃ (Sokolov 1975). The P content in the extracts was measured according to the procedure of Murphy and Riley (1962).

Total C content was quantified by wet combustion. Soil pH was measured in a 1:2.5 soil/water slurry, using a glass electrode (Sokolov 1975). All analyses were carried out in triplicate. All results are expressed on a per kg of dry soil basis.

Table 1. Properties of soils at the beginning of long-term experiments, and climatic conditions at the soil sites.

Characteristic	Podzolu-visol	Greyzem	Chernozem
Properties			
Clay, %	12.5	25.5	25.1
Silt, %	7.5	19.9	20.9
Sand, %	80.0	54.6	54.0
pH$_{H2O}$	5.1	6.5	6.8
Total C, g/kg	9	30	35
Total P, mg/kg	534	1262	1025
P availability index*	85	197	82
Climatic condition			
Average annual temperature, °C	- 4.1	-1.4	+0.1
Precipitation for a year, mm	450-500	350-450	250-400
Maximum snow cover deep, cm	50-60	30-40	20-40
Maximum depth of frozen soil layer, cm	110-120	180-200	140-160
Frost-free period, days	100-121	90-110	100-140

* 0.2 N HCl was used as extractant for Podzoluvisol and Greyzem, and 0.5 N CH₃COOH for Chernozem.

RESULTS

On the whole the studied soils, arranged according to content of total P, of organic P and of sum of inorganic P fractions, were: Podzoluvisol < Chernozem < Greyzem (Tables 1 and 2). The content of organic P was 37-46% of total P in Podzoluvisol and 50-59% in other soils (Table 2). The sum of Ca, Al and Fe-bound P was 20-24% of total P in Podzoluvisol, 12-14% in Greyzem, and 5-9% in Chernozem. Among these three fractions, inorganic P was mainly bound to Fe. Occluded P fraction was on the average of 36% of total P in Podzoluvisol, of 31% in Greyzem, of 39% in Chernozem. This immobile form accounted for 56-65% of the inorganic P content in Podzoluvisol, 67-75% - in Greyzem, and 80-88% in Chernozem. Indices of P availability, determined by methods commonly used in Russia, indicated high P supply in all soils.

Long-term cultivation of soils resulted in significant changes in soil phosphorus status (Table 2). In unferti-

Table 2. The influence of fertilizers on P status in Siberian soils (arable horizon), mg P/kg.

Plot of long-term experiment*	Average rate of P per year	Total P	Organic P	Inorganic P				P availability indices**	
				Ca-P	Al-P	Fe-P	Occluded P	1st	2nd
Podzoluvisol									
F_0	0	414 a	174 a	12 a	12 a	59 a	157 a	78 a	4.8 a
$(NPK)_1$	15	480 a	179 ab	17 b	24 b	73 b	187 b	89 b	6.2 b
$(NPK)_1 + M$	24	501 a	229 b	18 b	26 b	70 b	158 a	87 b	5.4 ab
Greyzem									
F_0	0	1172 a	594 a	28 a	27 a	90 a	433 a	97 a	3.5 a
$(NPK)_2$	25	1404 b	785 b	38 b	44 b	113 b	424 a	100 a	5.7 b
$(NPK)_1 + M$	22	1413 b	806 bc	40 b	39 b	105 a	423 a	101 a	5.3 ab
$(M)_2$	20	1427 b	846 c	38 b	38 b	113 b	392 a	88 a	5.5 b
Chernozem									
F_0	0	959 a	523 a	11 a	13 a	31 a	381 a	93 a	2.1 a
$(NPK)_1$	12	1046 a	527 a	13 a	17 b	31 a	458 b	96 a	4.9 b
$(NPK)_2$	24	1210 c	687 c	22 b	26 c	42 b	433 ab	112 b	8.7 c
$(NPK)_3$	36	1188 bc	630 bc	29 c	33 d	49 c	447 b	138 c	10.5 d
$(NPK)_1 + M$	22	1079 ab	604 b	19 b	18 b	40 b	398 a	106 ab	5.5 b

Notes. Values within parts of columns corresponding different soils not sharing the same letter are significantly different (P<0.05).

* F_0 means no fertilizer. $(NPK)_1$ means 34.3 kg N/ha, 15 kg P/ha, and 28.5 kg K/ha for Podzoluvisol; 30 kg N/ha, 12.5 kg P/ha, and 26 kg K/ha for Greyzem; 22.5 kg N/ha, 12 kg P/ha, and 22.8 kg K/ha for Chernozem. $(NPK)_2$ and $(NPK)_3$ is the same rate as $(NPK)_1$ but multiplied by 2 and 3, respectively. M means 5.7 Mg/ha of manure for Podzoluvisol, and 6 Mg/ha for Greyzem and Chernozem. $(M)_2$ is the same rate as M but multiplied by 2.

** 1st means using the extractant 0.2 N HCl for Podzoluvisol and Greyzem, and 0.5 N CH_3COOH for Chernozem. 2nd means extractant 0.006 N HCl for Podzoluvisol and Greyzem, and 1% $(NH_4)_2CO_3$ for Chernozem.

lized plots the content of total P decreased in all 3 soils at an estimated rate of 3.2, 4.5, and 5.1 mg P/kg·year in Podzoluvisol, Greyzem, and Chernozem, respectively. As compared to unfertilized plots, in soil receiving fertilizers total P content was 9-26% increased due to the corresponding increase in both organic and inorganic forms of P.

Although transformation of fertilizer derived P into soil depended on soil type and fertilization practice, some similar patterns can be stated. The content of organic phosphorus was not changed under low P fertilizer doses (12-15 kg P/ha·year), and was 20-32% (on the average 28%) increased in other mineral fertilizer treatments and was 15-42% (on the average 31%) increased in other organic or combined organic and mineral fertilizers treatment, as compared to unfertilized soil. Organic fertilizers affected directly on an increase in soil organic P, but mineral fertilizer resulted in it, probably due to uptake and conversion by micro-organisms and plants.

The content of inorganic P bound with Ca, Al, Fe cations, which play a most important role in providing P for plant growth, was significantly increased in all 3 soils and all fertilization practices. There are only some unclear exceptions to this rule: Fe-P in Greyzem under treatment $(NPK)_1+M$, and Ca-P and Fe-P in Chernozem under treatment $(NPK)_1$. In Chernozem, where three increasing doses of P fertilizer were used, the content of these Ca-, Al- and Fe-associated P fractions varied in proportion with P rate. The sum of these three inorganic fractions in soils of mineral fertilizer treatments in rates 12, 24 and 36 kg P/ha·year was increased on 0.5, 2.7, and 4.3 mg P/ha per year on the average, as compared to unfertilized soil, respectively.

The effect of fertilizer application on occluded forms (i.e. immobile and, therefore, unavailable for plant uptake) was less pronounced than other P fractions. The accumulation of occluded P on 19% and 14-20% was only under mineral fertilizer treatments in Podzoluvisol and Chernozem, as compared to unfertilized soil, respectively.

The P availability indices determined by less-strong extractants, 0.006 N HCl and 1% $(NH_4)_2CO_3$, as compared to those determined by 0.2 N HCl and 0.5 N CH_3COOH extractants, better corresponded to fertilizer P dose applied in experiments ($R^2=0.597$ in comparison

with R^2=0.437). Significant correlation between P availability indices and inorganic P forms bound with Ca, Al and Fe cations was absent.

REFERENCES

Averkina, S. S. 1986. Mobile phosphate determination in soils of Novosibirsk district. *In* Soil fertility and plant mineral nutrition. (in Russian.) SO VASCH-NIL Pub., Novosibirsk.

Berhin, U. I., E. G. Chagina, and E.D. Yanzen. 1984. The fractions of mineral phosphorus in some soils of West Siberian sourt. (in Russian.) Agrochimija 9:21-27.

Berhin, U. I., E. G. Chagina, and E. D. Yanzen. 1989. The index of phosphorus availability for cereal crops in West Siberia. (in Russian.) Agrochimija 6:112-116.

Black, C. A. 1968. Soil-plant relationships. John Wiley and Sons, Inc., New York.

Chang, S. C., and M. L. Jackson. 1957. Fractionation of soil phosphorus. Soil Sci. 84:133-144.

Ginzburg, K. E. 1981. Phosphorus of main soil types of the USSR. (in Russian.) Nauka, Moscow.

Kuznetsova, L. Z. 1983. The influence of fertilizers on phosphorus status of Chernozem leached. (in Russian.) p. 106-109. *In* Phosphorus in Siberian soils. SO VASCHNIL Pub., Novosibirsk.

Murphy, J., and J. P. Riley. 1962. A modified single solution method for determination of phosphate in natural waters. Anal. Chim. Acta 27: 31-36.

Negovelov, S. F., and N. G. Pestova. 1978. The analysis of soil mineral phosphorus by fractionation method. (in Russian.) Pochvovedenie 3:140-146.

Olsen, S. R., and L. E. Sommers. 1982. Phosphorus. *In* A.L. Page et al. (ed.) Methods of Soil Analysis, Part 1. Agronomy 9:403-430. Am. Soc. of Agron., Inc., Madison, Wis.

Schumilova, E. V. 1963. Mesozoic and Cainozoic depositions of West Siberian lowland. (in Russian.) SO AN SSSR Pub., Novosibirsk.

Sokolov, A. V. (ed.). 1975. Agrochemical methods of soil studies. (in Russian.) Nauka, Moscow.

Physical Chemistry

Physical Chemistry of Geochemical Solutions at Subzero Temperatures

G.M. MARION[1] AND S.A. GRANT[1]

ABSTRACT

Theoretical developments, specifically the Pitzer equations and thermoporometry, coupled with improved experimental data on the thermophysical properties of supercooled solutions indicate that quantitative estimates are possible for the thermophysical properties of aqueous electrolyte solutions in frozen porous media. The Pitzer equations are statements of a solution's excess Gibbs energy. When fully parameterized, the Pitzer equations allow the calculation of activity coefficients, osmotic coefficients, enthalpies, entropies, Gibbs energies, heat capacities, and molal volumes of highly concentrated aqueous electrolyte solutions to temperatures below −50°C. While developed to calculate capillary pressures for pure pore liquids, the theoretical development that yielded thermoporometry can be extended directly to pore solutions composed of complex electrolyte solutions, by which freezing behavior of chemically realistic natural soils can be calculated.

Application of the FREZCHEM model to an arctic permafrost soil demonstrated that significant amounts of water may remain liquid in saline soils as the result of salt exclusion from ice during the freezing process and the formation of brine pockets. These simulations also demonstrated that freezing should cause the precipitation of gypsum and hydrohalite in these soils. The model calculated the amount of liquid water, the activity of water, and solute concentrations at the mean annual temperature (−13°C) for this arctic site and demonstrated that environmental conditions are marginally suitable for microbial activity in frozen soils under these extreme conditions. Frozen soils have the potential to serve as a refugium for life. Extending the results of thermoporometry to electrolyte solutions, the effect of different initial NaCl solutions and soil freezing curves on capillary pressure could be calculated well.

Key words: Pitzer equations, thermoporometry, frozen ground, mineral solubility, capillary pressure.

INTRODUCTION

While some air bubbles may be trapped in water-saturated frozen ground, it is generally thought that the thermodynamic relations between ice and liquid trapped in the ground's pore space determine to a large extent the frozen ground behavior. Since the ice phase is rigid and impermeable, the compositions of the frozen-ground pore-solutions have pronounced effects on the physical, mechanical and chemical behavior of frozen ground. A quantitative description of these effects has been elusive persuading most researchers to assume expediently, but perhaps wrongly, that the thermo−physical properties of frozen-ground pore solutions were identical to those of pure liquid water. Recent theoretical and experimental developments suggest that vastly improved quantitative estimates are possible for the thermophysical properties of aqueous electrolyte solutions in frozen porous media. Two theoretical developments have been responsible: the Pitzer equations and thermoporometry.

The Pitzer equations have been widely used to estimate solute and solvent activities in concentrated brines (>10 molal) over a wide temperature range (−54°C to 250°C) (Harvie and Weare 1980, Møller 1988, Plummer et al. 1988, Raju and Atkinson 1990, Spencer et al. 1990, Pitzer 1991,1995, Marion and Grant 1994, Marion 1997, Marion and Farren, in submission). When fully parameterized, the Pitzer equations allow the calculation of mean-ionic and single-

ion activity coefficients, osmotic coefficients, enthalpies, entropies, Gibbs energies, heat capacities, and molal volumes of highly concentrated aqueous electrolyte solutions to temperatures below $-50°C$.

The thermodynamic treatment justifying thermoporometric measurements can be modified for complex pore-solution compositions allowing accurate estimation of capillary pressures of geochemical solutions in frozen ground.

In this paper, we will examine the Pitzer equations and thermoporometric concepts, followed by a review of several geochemical models incorporating these concepts, and finally discuss two applications of these principles to elucidate the physical chemistry of solutions at subzero temperatures.

PITZER EQUATIONS

The Pitzer equations have proven to be a reliable mathematical framework by which the thermophysical properties of mixed aqueous electrolyte solutions can be calculated accurately over wide ranges of temperature, pressure and composition. The Pitzer equations are statements of a solution's excess Gibbs energy, which, with standard thermodynamic relations, allow the calculation of most thermophysical solution properties such as solution and solvent partial molar Gibbs energies, enthalpies and entropies, as well as heat capacities and volumes. To illustrate the utility and flexibility of the Pitzer equations, consider the osmotic coefficient and single-ion activity coefficients of a mixed electrolyte solution, the estimation of which are of fundamental importance in any geochemical model (Plummer et al. 1988, Spencer et al. 1990, Marion and Grant 1994).

The osmotic coefficient ($\phi_{H_2O(l)}$) and single-ion activity coefficients for a cation "M" (γ_M) and an anion "X" (γ_X) are given by

$$\left(\phi_{H_2O(l)} - 1\right) = \frac{1}{RT}\frac{1}{\Sigma_i m_i}\left(\frac{\partial G_m^E}{\partial \omega_{H_2O(l)}}\right)_{T,p,n_i}$$

$$= \frac{2}{\Sigma_i m_i}\left(-\frac{A_\phi I_m^{3/2}}{1+bI_m^{1/2}}\sum_c\sum_a m_c m_a\left(B_{ca}^\phi + ZC_{ca}\right)\right.$$

$$+\sum_{c<c'}\sum m_c m_{c'}\left(\Phi_{cc'}^\phi + \sum_a m_a\Psi_{cc'a}\right)$$

$$\left.+\sum_{a<a'}\sum m_a m_{a'}\left(\Phi_{aa'}^\phi + \sum_c m_c\Psi_{caa'}\right)\right), \quad (1)$$

$$\ln\gamma_M = \frac{1}{RT}\left(\frac{\partial G_m^E}{\partial n_M}\right)_{T,p,\omega_{H_2O(l)},n_{i,i\neq M}}$$

$$= z_m^2 F + \sum_a m_a\left(2B_{Ma} + ZC_{Ma}\right)$$

$$+\sum_c m_c\left(2\Phi_{Mc}^\phi\right) + \sum_a m_a\Psi_{Mca}$$

$$+\sum_{a<a'}\sum m_a m_{a'}\left(\Phi_{aa'}^\phi\right) + z_M\sum_c\sum_a m_c m_a C_{ca} \quad (2)$$

$$\ln\gamma_X = \frac{1}{RT}\left(\frac{\partial G_m^E}{\partial n_X}\right)_{T,p,\omega_{H_2O(l)},n_{i,i\neq X}}$$

$$= z_X^2 F + \sum_c m_c\left(2B_{cX} + ZC_{cX}\right)$$

$$+\sum_a m_a\left(2\Phi_{Xa}^\phi + \sum_c m_c\Psi_{cXa}\right)$$

$$+\sum_{c<c'}\sum m_c m_{c'}\left(\Phi_{cc'X}^\phi\right) + |z_X|\sum_c\sum_a m_c m_a C_{ca} \quad (3)$$

where
- G_m^E = the excess Gibbs energy of the solution (J kg^{-1})
- R = the gas constant (J K^{-1} mol^{-1})
- T = temperature (K)
- p = pressure (Pa)
- m_i = molality of ion "i" (mol kg^{-1})
- n_i = amount of ion "i" (mol)
- $\omega_{H_2O(l)}$ = mass of solvent (kg)
- A^ϕ = the Debye-Huckel parameter (kg$^{1/2}$ mol$^{-1/2}$)
- b = a constant which is equal to 1.2 kg$^{1/2}$ mol$^{-1/2}$
- a, a' = indices for anions
- c, c' = indices for cations
- z_i = the charge number of the i-th ion.

Z is a variable equal to $\Sigma_i m_i|z_i|$ and I_m is the molality-based ionic strength defined by:

$$I_m = \frac{1}{2}\Sigma m_i z_i^2. \quad (4)$$

Four ion-interation terms, or their derivatives, are used in eq. 1–3: The virial coefficients for ionic interaction C_{ij} (kg^2 mol^{-2}) and Ψ_{ijk} (kg^2 mol^{-2}) are generally taken to be constants, whereas B_{ij} and Φ_{ij} are calculated by

$$B_{ij} = \beta_{ij}^{(0)} + \frac{2\beta_{ij}^{(1)}}{\alpha_1^2 I_m}\left[1 - \left(1 + \alpha_1\sqrt{I_m}\right)\exp\left(-\alpha_1\sqrt{I_m}\right)\right]$$

$$+ \frac{2\beta_{ij}^{(2)}}{\alpha_2^2 I_m}\left[1 - \left(1 + \alpha_2\sqrt{I_m}\right)\exp\left(-\alpha_2\sqrt{I_m}\right)\right], \quad (5)$$

and

$$\Phi_{ij} = \theta_{ij} + E_{\theta_{ij}}(I_m) \qquad (6)$$

where α_1 and α_2 are constants assigned values of 1.4 $kg^{1/2}\, mol^{-1/2}$ and, 12 $kg^{1/2}\, mol^{-1/2}$, respectively, for 2-2 electrolytes and $\alpha_1 = 2.0$ for other electrolytes. $\beta_{ij}^{(0)}$, $\beta_{ij}^{(1)}$, $\beta_{ij}^{(2)}$, and θ_{ij} (all $kg\, mol^{-1}$) are experimentally fitted constants. $E_{\theta_{ij}}(I_m)$ ($kg\, mol^{-1}$) is a complex function of ionic strength that can be calculated numerically.

The ion-strength derivatives of both B_{ij} and Φ_{ij} can be defined as

$$\Phi'_{ij} = \frac{\partial \Phi_{ij}}{\partial I_m} \qquad (7)$$

and

$$B'_{ij} = \frac{\partial B_{ij}}{\partial I_m}, \qquad (8)$$

which in turn allow the definition of

$$\Phi_{ij}^{\phi} = \Phi_{ij} + I_m \Phi'_{ij} \qquad (9)$$

and

$$B_{ij}^{\phi} = B_{ij} + I_m B'_{ij} \qquad (10)$$

In addition to which, the following relation

$$C_{ca}^{\phi} = 2C_{ca}\sqrt{z_c |z_a|} \qquad (11)$$

is noted. F is a complex function of A^{Φ}, I_m, and the salt-interaction coefficients:

$$F = f^{\gamma} + \sum_c \sum_a m_c m_a B'_{ca} + \sum_{c<c'} \sum m_c m_{c'} \Phi'_{cc'}$$
$$+ \sum_{a<a'} \sum m_a m_{a'} \Phi'_{aa'} \qquad (12)$$

with

$$f^{\gamma} = -A_{\phi}\left(\frac{I_m^{1/2}}{1+bI_m^{1/2}} + \frac{2}{b}\ln\left(1+bI_m^{1/2}\right)\right). \qquad (13)$$

(Plummer et al. 1988, and Pitzer 1991, 1995).

Although algebraically complex, in practice calculation of osmotic or activity coefficients from the Pitzer model requires only the parameters $\beta_{ij}^{(0)}$, $\beta_{ij}^{(1)}$, $\beta_{ij}^{(2)}$, C_{ij}^{ϕ}, Φ_{ij}, θ_{ij} and ψ_{ijk} for the appropriate solution phase ions at the appropriate temperature. Sources of these parameters include Harvie et al. (1984), Møller (1988), Plummer et al. (1988), and Pitzer (1991, 1995). For specific applications at cold temperatures, see the papers by Spencer et al. (1990), Marion and Grant (1994), and Marion and Farren (in submission).

THERMOPOROMETRY

The physical and mechanical properties of frozen ground are determined to a large extent by the amount of unfrozen liquid remaining in the pore space of the solid matrix. The liquid-water content of frozen ground is generally thought to be a capillary-pressure saturation relation, similar to the soil-water retention curve in unsaturated unfrozen soils. While the capillary-pressures of frozen soils saturated by pure water can be estimated easily, the inclusion of electrolyte effects is more challenging.

Capillary pressure (Pa), p_c, in frozen porous media can be defined as:

$$p_c = p^l - p^s \qquad (14)$$

where p^l and p^s are the pressures in the aqueous solution (or pure water) phase and solid phase, respectively.

If one assumes, reasonably, that capillary pressure arises from the work required to distort the ice–liquid interface as the volume of liquid changes in the porous matrix, the following relation is derived:

$$dp_c = d\left(\gamma^{ls}\left(\frac{dA_{s,m}^{ls}}{dV_m^l}\right)\right) \qquad (15)$$

where γ^{ls} is the liquid–ice interfacial tension (N m^{-1}), and $A_{s,m}^{ls}$ is the liquid–ice molar interfacial area (m^2 mol^{-1}) and V_m^l molar volume of the liquid (m^3 mol^{-1}) (Brun 1977).

Therefore, the capillary pressure of liquid water in a frozen porous medium at temperature T can be calculated by:

$$\int_0^{pc} dp_c \equiv p_c = \int_{T_0}^{T} \frac{S_{m,H_2O}^{*l} - S_{m,H_2O}^{*s}}{V_{m,H_2O}^{*l}} dT \qquad (16)$$

where T_0 (K) = the freezing point of bulk liquid phase
S_{m,H_2O}^{*l} = the molar entropy of the liquid (J K^{-1} mol^{-1})
S_{m,H_2O}^{*s} = the molar entropy of the ice (J K^{-1} mol^{-1})
V_{m,H_2O}^{*l}(K) = the molar volume of the liquid (m^3 mol^{-1}).

To evaluate the right-hand side of eq. 16, the following properties must be measured or estimated for all temperatures of interest:
1. The freezing point of the liquid phase in bulk.
2. Entropy of the liquid phase, which can be calculated from the entropy of water at a reference point and

the constant pressure heat capacity of water from the reference point to T:

$$\Delta_{T_1}^{T_2} S_m^* = \int_{T_1}^{T_2} \frac{C_p^*}{T} dT \qquad (17)$$

The heat capacities (C_p, J mol^{-1}) of normal and supercooled water at 0.1 MPa are known precisely to approximately $-35°C$ (Speedy 1987).

3. Entropy of the ice phase.

4. Molar volume of the liquid phase. The molar volume of supercooled water has been measured to approximately $-32°C$ (Hare and Sorensen 1987).

Similarly, the ice–solution capillary pressure for a pore solution of a aqueous NaCl solution can be calculated as a function of temperature with (Grant et al. 1997):

$$p_c = \int_{T_0}^{T} \frac{S_m^l - x_{H_2O}^l S_{m,H_2O}^{*s} + x_{NaCl}^l \frac{d\mu_{NaCl}^l}{dt}}{V_m^l} dT \qquad (18)$$

where $x_{H_2O}^l$ and x_{NaCl}^l are the mole fractions of water and NaCl in the solution; S_m^l, the molar entropy of the solution (J K^{-1}mol^{-1}) and μ_{NaCl}^l chemical potential of NaCl in solution. To calculate ice–solution capillary pressure, the quantities in the integrand must be calculated. These quantities are:

1. Mole fractions of the solute and solvent,
2. Melting point of the solution,
3. Molar entropy of ice,
4. Molar entropy of the liquid solution,
5. Molar volume of the liquid solution,
6. Temperature derivative of the solute chemical potential.

Equation 18 can be evaluated with reasonable accuracy because the necessary thermophysical properties of NaCl solutions, their constant-pressure heat capacities and densities, have been measured reasonably well. Sodium chloride is one of the very few salts for which there have been any solution heat-capacity and density measurements at subzero temperatures. Researchers at the Cold Regions Research and Engineering Laboratory (CRREL) have begun a program to measure these solution properties for electrolytes of geochemical importance, which will allow the evaluation of formulae similar to eq. 18 for complex electrolyte solutions.

GEOCHEMICAL MODELS

A number of geochemical models have been published in recent years that incorporate the Pitzer equations, enabling the models to simulate geochemical processes in concentrated brines. The PHRQPITZ model is a variation of the PHREEQE model that incorporates the Pitzer equations (Plummer et al. 1988). This general purpose chemical equilibrium model includes 37 minerals and is parameterized for the temperature range: 0 to 60°C. The Spencer-Møller-Weare (SMW) model is parameterized for the temperature range $-54°$ to 25°C and includes 15 Cl and SO$_4$ salts of Na, K, Ca, and Mg (Spencer et al. 1990). This was the first model capable of describing concentrated brines at subzero temperatures. Unfortunately a working version of the SMW model was never published by the authors. The FREZCHEM model is essentially a working version of the SMW model and includes the same salts and temperature range (Marion and Grant 1994). More recently, Mironenko et al. (in press) developed a Gibbs energy minimization algorithm for the FREZCHEM model (FREZCHEM2) that is more efficient than the original algorithm for solving sets of nonlinear equations. Gypsum solubility and Pitzer parameters for Ca-SO$_4$ interactions at subzero temperatures have recently been estimated (Marion and Farren in submission) for incorporation into the FREZCHEM model. In a following application, the current FREZCHEM model with gypsum solubility will demonstrate the utility of this model for examining geochemical processes at subzero temperatures.

APPLICATIONS

Geochemistry of a frozen arctic soil

While the majority of water in frozen ground is ice, liquid water has been measured in frozen soil even at very cold temperatures. Liquid water persists in frozen soil due to colligative (i.e., freezing-point depression) and interfacial processes. As soils freeze, solutes are excluded from the ice phase and concentrate into brine pockets, which lowers the freezing point of the residual liquid brine. Estimating the liquid water content of frozen soils is critical for many applications such as contaminant transport, soil strength, frost heaving, and geochemistry (Marion 1995). The FREZCHEM model estimates the liquid water due to brine concentration and ignores interfacial effects. Thermoporometry, as discussed in the following section, can, in principle, combine physical and chemical processes and shows promise as a means of integrating interfacial and bulk-chemical processes. In this section on geochemistry, we will demonstrate the utility of the FREZCHEM model for estimating the liquid water contents and the concentrations of soluble ions at subzero temperatures due to brine formation and discuss the implications of soil freezing as a process for the precipitation of soil minerals and the implications for frozen soil as a refugium for life.
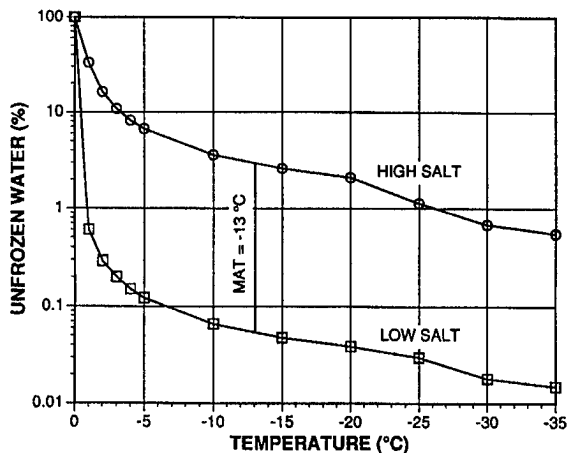
Figure 1. The FREZCHEM model estimates of unfrozen water in two soil horizons (Table 1) as affected by temperature.

Figure 2. The FREZCHEM model estimates of chemical concentrations in the unfrozen brine (high salt case, Table 1) as affected by temperature.

Data for the FREZCHEM simulations were taken from Gilichinsky (1993) and are from an arctic permafrost soil from the Kolyma Lowland, Russia. They were selected to represent "low salt" and "high salt" soil horizons (Table 1). The calculated ionic strengths of these two solutions are 100-fold different, despite being from the same soil profile. This difference in initial salt concentration plays a major role in model estimates of liquid water as a function of temperature (Fig. 1). At a temperature of –1°C, less than 1% of the water remains liquid in the low salt horizon due to brine concentration, while 33% remains liquid in the high salt horizon. At the mean annual temperature for this Kolyma Lowland site (–13°C), 0.055% and 3.0% of the soil water remains liquid in the low and high salt horizons, respectively (Fig. 1).

The concentration of cations and anions rise during the freezing process as salts are concentrated in the liquid brine (Fig. 2). For example, the ionic strength for the high salt horizon begins at 0.1624 mol kg^{-1} and rises to 8.53 mol kg^{-1} at –35°C; at –5°C the calculated ionic strength is 1.86 mol kg^{-1}. This rapid concentra-

Figure 3. The FREZCHEM model estimates of the distribution of total (A) calcium and (B) sodium (high salt case, Table 1) as affected by temperature.

tion of salts during the freezing process is the reason why the Pitzer equations are necessary for describing these highly saline solutions.

When these solutions freeze, minerals will precipitate whenever their solubility product is exceeded. During the simulations used for the high salt case (Fig. 1 and 2), both gypsum ($CaSO_4 \cdot 2H_2O$) and hydrohalite ($NaCl \cdot 2H_2O$) precipitate (Fig. 3). Gypsum is slightly

Table 1. Soluble cation and anion concentrations in a low salt (–50 m) and a high salt (–10 m) horizon of an arctic permafrost soil (calculated from data in Gilichinsky 1993).

Element	Low salt (moles/kg)	High salt (moles/kg)
Na + K	0.00121	0.0720
Ca	0.00029	0.0124
Mg	0.00036	0.0136
Cl	0.00179	0.0992
SO$_4$	0.00036	0.0124
Ionic strength	0.00163	0.1624

353

undersaturated at 0°C but is precipitating gypsum by −1°C, largely due to freeze concentration of all solutes, including Ca and SO_4. By −5°C , 77.2% of the original Ca precipitates as gypsum. Hydrohalite, on the other hand, only begins precipitating at −23.1°C; by − 30°C, 84.2% of the original Na precipitates as hydrohalite. Freeze concentration of solutes and precipitation of salts control the solution phase chemical composition. The decrease in Ca, SO_4 and Na concentrations at low temperatures (Fig. 2) occurs where precipitation of salts becomes more important than freeze concentration. In addition to gypsum and hydrohalite, a small amount of mirabilite ($Na_2SO_4 \cdot 10\ H_2O$ also precipitates, primarily between −15° and −30°C; this precipitation is what causes the Ca and SO_4 concentrations, initially the same (Table 1), to separate over that temperature range (Fig. 2). However, all of the mirabilite eventually redissolves by −35°C for the high salt case with the associated Na precipitating as hydrohalite and the associated SO_4 precipitating as gypsum. In the low salt case (data not presented), a small amount of mirabilite remains at −35°C. Because Na and K concentrations were lumped together in the primary data source (Gilichinsky 1993), we treated "Na + K" as if it were entirely Na in our simulations. Had we explicitly recognized K, then KCl would begin to precipitate at a temperature dependent on its absolute concentration. For example, assuming that K is 10% of "Na + K," then the first appearance of KCl is at −29.3°C and −27.1°C for the low and high salt cases, respectively. The last salt to precipitate from these soil solutions is $MgCl_2 \cdot 12\ H_2O$, which begins precipitating at −36.0°C, which is the eutectic temperature for these specific soil solutions (both high salt and low salt cases). Therefore brine (a solution phase) cannot exist at or below a temperature of −36.0°C in these soils from the Kolyma Lowland; at or below −36.0°C, only the solid phases: ice, $NaCl \cdot 2\ H_2O$, KCl, $CaSO_4 \cdot 2\ H_2O$, $Na_2SO_4 \cdot 10$ H_2O, and $MgCl_2 \cdot 12\ H_2O$ can exist in thermodynamic equilibria. The mean January temperature for the Kolyma Lowland is −35°C (Gilichinsky 1993), which suggests that at least the surface horizons during the winter may approach the eutectic, and one should find gypsum and hydrohalite precipitating in the winter as the result of freeze concentration of salts.

The presence of liquid water, the activity of water (a measure of salinity), and temperature are particularly important factors controlling microbial activity and as a consequence the possibility of soils serving as a refugium for life in frozen environments. Dormant cells have survived being subjected to temperatures approaching absolute zero (−273°C) and water activities approaching 0.0 (Mazur 1980, Kushner 1981). The ranges for growth of microorganisms are more narrow. There are no confirmed cases of microbial growth be-

low −12°C or at water activities below 0.6 (Mazur 1980, Kushner 1981). Most bacteria require water activities above 0.9, while most fungi require water activities above 0.85. The lowest water activity for which microbial growth has been demonstrated was for the fungus *Xeromyces bisporus*, which can survive at water activities as low as 0.61 (Mazur 1980).

Viable microorganisms have been extracted from permafrost layers that were formed 3–4 million years ago and have remained frozen without substantial degradation since that time (Gilichinsky 1993). These are, in fact, the Kolyma Lowland soils that we are using in our simulations (Table 1, Fig. 3). Have these microorganisms remained in the dormant state all this time or is it possible that these microorganisms might grow under frozen conditions? The mean annual temperature at the Kolyma Lowland site (−13°C, Fig. 1) is just below the lower limit for microbial activity (−12°C), so presumably temperature is probably not prohibitive for growth within this frozen permafrost soil, at least at some times of the year. The water content in brine pockets at the mean annual temperature is 3.0% for the high salt case (Fig. 1), so liquid water, which is essential for microbial growth, would also be available. And finally, the calculated water activity at −13°C is 0.882, which is within the range reported for microbial activity. This solution at −13°C has an ionic strength of 3.98 mol kg^{-1}, which demonstrates that microbial activity is compatible with highly saline environments. Temperature, liquid water, and the activity of water are marginally suitable for microbial activity in these frozen Kolyma Lowland soils. Along the same vein, Zimov et al. (1996) have measured significant CO_2 effluxes from forest tundra during the winter at a site along the Kolyma River, Russia. They attributed these fluxes to winter respiration, suggesting that significant biological activity occurs in frozen environments, as we hypothesized might be the case based on the FREZCHEM simulations.

Thermoporometry

Equation 18 was tested by measuring the liquid–water contents of kaolinite pastes that we equilibrated with NaCl solutions with molalities of 0.1, 0.01, and 0.001 mol kg^{-1} (Grant et al. 1997). The pastes were cooled to −60°C and the liquid-water contents were measured by pulsed NMR. Figure 4 presents a plot of the relationship between equilibrating temperatures and liquid-water contents. Capillary pressures were estimate with eq. 18 via an implementation of the Pitzer equations for NaCl (Archer 1992). NaCl is one of the few electrolytes for which apparent molar heat capacity data are available at subzero temperatures (Thurmond and Brass 1980).

Figure 5 presents the relationship of calculated capillary pressures and liquid water contents, which indi-
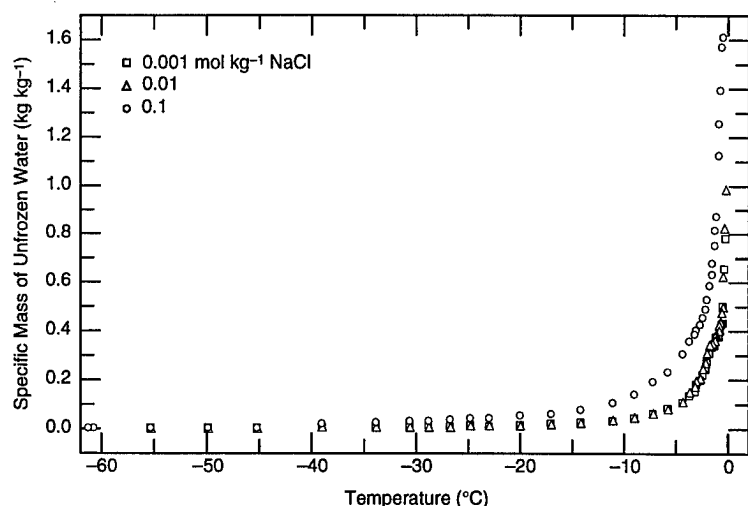
Figure 4. Unfrozen water contents, as measured by pulsed NMR, of freezing kaolinite pastes cooled from 0°C to –55.3°C. The equilibrating solutions of the pastes were initially 0.1 mol kg^{-1} (O), 0.01 mol kg^{-1} (Δ) and 0.001 mol kg^{-1} (□) NaCl.
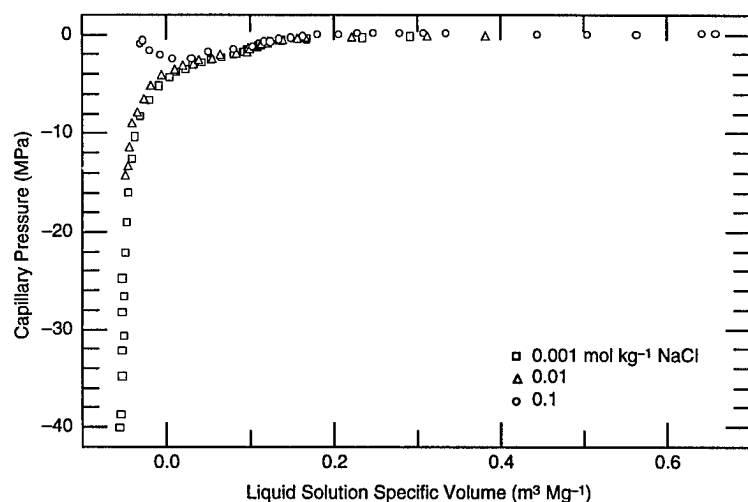
Figure 5. Relationships between unfrozen-solution specific volumes and ice-solution capillary pressures for kaolinite pastes cooled from 0° to –55.3°C. The equilibrating solutions of the pastes were initially 0.1 mol kg^{-1} (O), 0.01, mol kg^{-1} (Δ) and 0.001 mol kg^{-1}, (□) NaCl.

cate that this relationship is constant for all initial equilibrating solution molalities and equilibrating temperatures. In this way, the effect of electrolytes on the liquid water contents of frozen ground can be calculated explicitly.

CONCLUDING REMARKS

Whether one is interested in the geochemistry of mineral solubility in frozen soils or demonstrating the feasibility of microbial growth in a frozen terrestrial

environment or on a frozen planet such as Mars (Carr 1996), simulating soil chemical properties under frozen conditions clearly requires a model parameterized for high solute concentrations and extreme cold (Fig. 2) such as the FREZCHEM model. These models hold promise as a major new tool for the exploration of biogeochemical processes in frozen media (Spencer et al. 1990, Marion and Grant 1994, Marion 1997, Marion and Farren, in submission). Though the results with NaCl-saturated kaolinite are encouraging, the application of thermoporometry to frozen soils cannot be implemented until:

1. Sufficient heat capacity and density data are collected for supercooled electrolyte solutions at subzero temperatures so that the Pitzer model can be used to estimate precisely geochemical solution entropies and volume.

2. The interaction of ionic solutes with layered silicates can be incorporated.

REFERENCES

Archer, D.G. 1992. Thermodynamic properties of the NaCl + H$_2$O system. 2. Thermodynamic properties of NaCl(aq), NaCl·H$_2$O (cr), and phase equilibria, J. Phys. Chem. Ref. Data, 793–829.

Brun, M., A. Lallemand, J.-F. Quinson and C. Eyraud. 1977. A new method for the simultaneous determination of the size and shape of pores: The thermoporometry, Thermochim. Acta, 21, 59–88.

Carr, M.H. 1996. Water on Mars. Oxford University Press, New York.

Gilichinsky, D.A. 1993. Viable microorganisms in permafrost: The spectrum of possible applications to new investigations in science for cold regions. p. 211–221. In: V.J. Lunardini and S.L. Bowen (eds.). *Fourth International Symposium on Thermal Engineering and Science for Cold Regions*. CRREL Special Report 93–22. USA Cold Regions Research and Engineering Labratory, Hanover, New Hampshire.

Grant, S.A., G.E. Boitnott and A.R. Tice. 1997. Effect of dissolved NaCl on freezing curves of kaolinite, montmorillonite and sand pastes. CRREL Special Report, USA Cold Regions Research and Engineering Labratory, Hanover, New Hampshire.

D.E. Hare and C.M. Sorensen. 1987. The density of supercooled water: II, Bulk samples cooled to the homogeneous nucleation limit, J. Chem. Phys. 87, 4840–4845.

355

Harvie, C.E., N. Møller, and J.H. Weare. 1984. The prediction of mineral solubilities in natural waters: The Na-K-Mg-Ca-H-Cl-SO$_4$OH-HCO$_3$-CO$_3$- H$_2$O system to high ionic strengths at 25°C. Geochim. Cosmochim. Acta, 48:723–751.

Harvie, C.E. and J.H. Weare. 1980. The prediction of mineral solubilities in natural waters: The Na-K-Mg-Ca-Cl- SO$_4$-H$_2$O system from zero to high concentration at 25°C. Geochim. Cosmochim. Acta, 44:981–997.

Kushner, D. 1981. Extreme environments: Are there any limits to life? p. 241–248. *In* C. Ponnamperuma (ed.) Comets and the Origin of Life. Reidel Publ. Comp., Dordrecht, Holland.

Marion, G.M. 1995. Freeze–thaw processes and soil chemistry. CRREL Special Report 95–12. USA Cold Regions Research and Engineering Laboratory, Hanover, New Hampshire.

Marion, G.M. 1997. A theoretical evaluation of mineral stability in Don Juan Pond, Antarctica. Antarctic Science (in press).

Marion, G.M. and R.E. Farren. in submission. Gypsum solubility at subzero temperatures. Soil Sci. Soc. Am. J.

Marion, G.M. and S.A. Grant. 1994. FREZCHEM: A chemical- thermodynamic model for aqueous solutions at subzero temperatures. CRREL Special Report 94-18. USA Cold Regions Research and Engineering Labratory, Hanover, New Hampshire.

Mazur, P. 1980. Limits to life at low temperatures and at reduced water contents and water activities. *In* Origins of Life, 10:137–159.

Mironenko, M.V., S.A. Grant, and G.M. Marion. in press. FREZCHEM2: A chemical-thermodynamic model for aqueous solutions at subzero temperatures. CRREL Special Report. USA Cold Regions Research and Engineering Labratory, Hanover, New Hampshire.

Mironenko, M.V., S.A. Grant, and G.M. Marion. in submission. Calculation of electrolyte-solution densities at subzero temperatures. Solution Chemistry.

Møller, N. 1988. The prediction of mineral solubilities in natural waters: A chemical equilibrium model for the Na-Ca-Cl- SO$_4$-H$_2$O system, to high temperature and concentration. Geochim. Cosmochim. Acta, 52:821–837.

Pitzer, K.S. 1991. Ion interaction approach: Theory and data correlation. p. 75–153. *In* K.S. Pitzer (ed.). Activity coefficients in electrolyte solutions (2nd Ed.). CRC Press, Boca Raton, Florida.

Pitzer, K.S. 1995. Thermodynamics (3rd Ed.). McGraw-Hill, Inc., New York.

Plummer, L.N., D.L. Parkhurst, G.W. Fleming, and S.A. Dunkle. 1988. A computer program incorporating Pitzer's equations for calculation of geochemical reactions in brines. U.S. Geol. Surv. Water-Resources Investigations Report 88-4153. Reston, Virginia.

Raju, K.U.G. and G. Atkinson. 1990. The thermodynamics of "scale" mineral solubilities. 3. Calcium sulfate in aqueous NaCl. J. Chem. Eng. Data, 35:361–367.

Speedy, R.J. 1987. Thermodynamic properties of supercooled water at 1 atm. J. Phys. Chem., 91, 3354–3358.

Spencer, R.J., N. Møller, and J.H. Weare. 1990. The prediction of mineral solubilities in natural waters: A chemical equilibrium model for the Na-K-Ca-Mg-Cl-SO$_4$-H$_2$O system at temperatures below 25°C. Geochim. Cosmochim. Acta. 54: 575–590.

Thurmond, V.L., and G.W. Brass. 1988. Activity and osmotic coefficients of NaCl in concentrated solutions from 0° to –40°C, J. Chem. Eng. Data, 33, 411–414.

Zimov, S.A., S.P. Davidov, Y.V. Voropaev, S.F. Prosiannikov, I.P. Semiletov, M.C. Chapin, and F.S. Chapin. 1996. Siberian CO$_2$ efflux in winter as a CO$_2$ source and cause of seasonality in atmospheric CO$_2$, Climatic Change. 33:111–120.

Physicochemical Factors Affecting Soil Acidity
In Seasonally Frozen Soils

N.F. BONDARENKO[1], Yu.V. GURIKOV[1], AND E.M. SAVELIEVA[1]

ABSTRACT

A unified molecular model of nonequilibrium phase transition of water (crystallization of an ice from water electrolyte solution) has been developed. This model was applied to homogeneous electrolyte solutions and model soil systems. We showed that phase transition of water in water systems produces a set of interdependent physicochemical phenomena: electrical crystallization potentials (ECP) between liquid and solid phases, fusion of foreign anions (Cl⁻) in growing ice, change of hydrogen index (acidifying) of the frozen part (after thawing) and increase of cation movement. Our theoretical predictions were confirmed by experiment with homogeneous water electrolyte solutions and disturbed samples of soil.

Key words: Water-ice phase transition, electric crystallization potential, hydrogen index, soil acidity, freezing-thawing.

Climatic and anthropogenic factors can exert an adverse effect on the fertility of the seasonally frozen soils in northern regions. To decrease their influence it is necessary to create optimal agricultural management strategies using our scientific knowledge of mechanisms of physicochemical processes in an open ecosystems. The phase transition of water has a pronounced effect on nonequilibrium processes of energy-and mass exchange and effects on the temperature-moisture regime of the upper horizons of the soil profile.

The most important properties of frozen soils are:

1. The presence of a moving boundary between liquid (soil moisture) and solid (ice) phases.

2. Cyclic repetition of the seasonal processes of freezing-thawing results in accumulation of some residual changes in northern soils, for example an increase in soil acidity.

It is well known that high ECP arise between liquid and solid phases under nonequilibrium crystallization of ice from dilute water electrolyte solutions (Workman and Reynolds 1950).

We developed a special molecular model of the nonequilibrium phase transition of water which connects ECP phenomena and interface charge separation with structure polarization of ice growing under nonequilibrium conditions from electrolyte solution (Gurikov et al. 1975). Our model uses the concept of orientation D, L-defects (Onsager and Dupui 1962).

We have shown that structure polarization of a growing ice is caused by polarization of a set of orientation defects in consequence of displacement of positively charged D-defects (two protons on the intermolecular hydrogen bond in ice structure) on a freshly prepared interphase boundary.

Structure polarization of surface zone of ice results in ion charge separation in liquid phase and thereby creates the conditions for selective capture of foreign anions (e.g., Cl⁻) by solid phase under nonequilibrium crystallization of ice from electrolyte solution.

To exclude the possibility of simultaneous capture of the anion and counterion (cation), it is necessary that mean distance between members of the anion-cation pair would exceed the characteristic size of the interphase zone.

This condition limits concentration interval $c < c_0$, where $c_0 = 10^{-12}/X^2$ and c is expressed as mole/m^3. ECP and attendant phenomena can be observed in this interval only. If the thickness of the interphase zone X is 10 nm, then $c_0 = 1$ mole/m^3. For higher concentrations the charge separation effect should disappear. By virtue of the fact that soil moisture is a dilute salt solution with an electrolyte concentration in the above interval, we can expect that selective infusion of ions into the ice phase and attendant phenomena (ECP) can also occur in the freezing process of the soils.

We made special measurements of capture coefficients of anion Cl⁻ and appropriate cations in water electrolyte solutions using X-ray radiometric method (Savelieva 1986). Indeed capture coefficients of Cl⁻ was found to be more than the same for cations K^+, Na^+, Ca^{+2} (Table 1) in the above concentration interval. Analogous results were obtained in experiments with the model soils (Table 2).

We applied above-mentioned model of the non-equilibrium crystallization of ice from water electrolyte solution to description of physicochemical processes in the frozen model soil. Taking into account that the rate of accumulation of excess negative charges in the ice phase is determined by competition between processes of appearance and annihilation (recombination) of the orientational defects, we obtained the formula for ECP as a function of concentration of electrolyte solution (Gurikov et al. 1975):

$$E = (4F/e_{ef})\, c\, k(c)\, X^2 \qquad (1)$$

Table 1. Capture coefficients* of Cl⁻ anion and K⁺ and Ca⁺² cations under nonequilibrium crystallization of water solutions of KCl and CaCl₂.

Electrolyte	c	K⁻	K⁺	K
	10^{-5}	0.61	0.21	0.40
KCl	10^{-4}	0.50	0.18	0.32
	10^{-3}	0.41	0.17	0.24
	10^{-2}	0.16	0.13	0.03
	10^{-5}	0.67	0.17	0.50
CaCl2	10^{-4}	0.60	0.16	0.44
	10^{-3}	0.50	0.14	0.36
	10^{-2}	0.22	0.12	0.10

* Capture coefficients K⁻, K⁺ are determined as ration of anion and cation concentrations in the solid phase to that in the initial solution; K = K⁺− K⁻.

Table 2. Capture coefficients of Cl⁻ anion and Na⁺ cation under freezing of model soil samples* according to its moisture (W).

Electrolyte	W (%)	K⁻	K⁺	K	E (v)
	10	0.190	0.180	0.010	1.8
NaCl	20	0.215	0.200	0.015	2.8
	30	0.280	0.260	0.020	4.0
	40	0.580	0.550	0.030	6.0

* Quartz sand moistened by solution of NaCl with concentration 10^{-1} mole/m³.

where F is the Faraday number, e_{ef} is the effective dielectric permeability in the interphase zone, $k(c)$ is the difference of the capture coefficients of anions and corresponding cations as function of concentration and X is the characteristic length (thickness) of the interphase zone. Equation 1 allows receipt of a quantitative estimate of ECP and at least the correct qualitative description of the concentration dependence of ECP.

By applying the approach based on thermodynamics of nonequilibrium processes, we set a linear relationship between the difference of the capture coefficients for anions and corresponding cations and the change of pH under nonequilibrium crystallization

$$k(c) = A\, \Delta(\text{pH}) \qquad (2)$$

where $\Delta(\text{pH})$ is the difference of pH values in phases of solution and ice and A is a constant coefficient, depending on pH value in the solution before freezing.

Selective infusion of ions into the ice phase leads to a set of important physicochemical consequences:

1. Electric polarization of ice–water solution interface and rise of ECP.

2. Redistribution of H⁺ and OH⁻ between the liquid and solid phases, and a corresponding change of hydrogen index to acid (in ice phase) and alkaline (in solution phase) sides.

An increase of proton content in the solid phase provides compensation of the excess negative charge within solid phase and an increase in OH⁻ content in the liquid phase compensation for excess positive charge in solution phase.

Our theoretical conclusions were confirmed by the model experiments with homogeneous water electrolyte solutions and disturbed samples of soil.

We have found that frozen parts of samples have an acid reaction (after thawing).It should be noted that measured values of ECP and changes of pH in model soil systems are significantly below the same, in the case of electrolyte solutions (Table 2 and 3. It can be explained by that a part of water in dispersed systems is in bound state and doesn't take in phase reactions.

Based on eq. 1 and 2 we can make some conclusions about physicochemical changes in the disturbed soil samples after freezing (Savelieva 1986). Our essential results are:

1. Seasonally freezing-thawing model soils are attended with a drop of pH. This may explain the phenomenon of pH-shock (Israel 1983), consisting

in sharp decrease of pH (acidifying) of the lake waters during spring thawing of snow on water reservoir territories. We suppose that acidifying of melted snow (thawing waters) can initiate a chain of physicochemical processes involving an increase of actual acidity of soils. Centuries-old influence may produce changes of potential soil acidity that apparently explains observed global acidifying of soils in the northern regions.

We showed that the degree of acidifying of the freezing soil samples depends on the initial values of its pH and moisture content (before freezing). It was shown that actual soil acidity across a ridge in an agricultural field changes after freezing the top of the ridge becomes more acid than its bottom (Bondarenko et al. 1980).

2. Another important consequence of nonequilibrium freezing consists of spring acidifying effects on the soil equilibriums (e.g., carbonate–calcium equilibrium, ion–exchange equilibrium between soil absorbing complex and soil moisture content) that must result in an increase of ion soil movement in frozen soils. Thus we have shown (Bondarenko et al. 1989) that concentration of Ca^{+2} after freezing increases 1.5 times in the frozen part of the brown forest soil (the samples were taken from horizon A, depth 0.2 m) (Table 3).

This result is easily explained by displacement of the carbonate-calcium equilibrium under influence of excess of H^+ ion in accordance with the equation (Orlov 1985):

$$(Ca^{+2}) = Const\ (H^+)^2/P$$

where (Ca^{+2}), and (H^+) are concentrations of corresponding ions in soil solution, P is partial pressure of CO in soil air.

Table 3. Change of pH under freezing of samples* of the brown forest soil of Sakhalin Island (freezing goes from the top).

	pH		Water soluble CA $mg/m^3 \times 10^3$	
W (%)	top	bottom	top	bottom
30	4.82	5.70	5.7	4.3
50	4.81	4.95	5.6	4.0
80	4.79	5.00	7.0	3.6

* Quartz sand moistened by solution of NaCl with concentration 10^{-1} mole/m^3.

3. Changes of electrophysical states of soils are produced by the influence of nonequilibrium freezing effects on the distribution of migratory currents of ions and moisture in frozen soils. It is believed that interface ECP between the liquid and solid phases may cause the electroosmotic current of moisture to move to the freezing front. As we have showed experimentally, maximum flow of water in the frozen test soil samples corresponds to the greatest change of pH (Bondarenko et al. 1979), which corresponds to maximal values of ECP according to our model.

Our results confirm the results of the latest work (Benedictova 1992). Benedictova observed the increase of intensity of migratory currents of ions and moisture content in the more acid soil solutions.

On the whole our approach, based on a unified physicochemical model of nonequilibrium phase transition of water in water systems, forms a theoretical foundation for understanding the peculiarities of northern soils consisting of increases of ion movement and preferential accumulation of foreign anions (Ostroumov and Makeev 1955) and acidifying of frozen parts of rocks and soils.

REFERENCES

Benedictova, N.A. 1992. Physicochemical processes in frozen rocks under its interaction with salt. Moscow State University. (In Russian).

Bondarenko, N.F., I.B. Uskov, Yu.V. Gurikov, E.M. Savelieva, and L.V. Kozyreva. 1980. A possibility of soil acidity adjusting on fields. *In* Proc. Acad. of Agriculture, 9: 37–39. (In Russian).

Bondarenko, N.F., Yu.V. Gurikov, E.M. Savelieva, and O.V. Skobeleva. 1989. Connection between ion movement and electric phenomena in frozen systems. p. 52–56. *In* Physics and physicochemistry of root layer of soil. Agrophysical Research Institute Publ., Leningrad (St. Petersburg). (In Russian).

Gurikov, Yu.V., E.M. Savelieva and N.F. Bondarenko. 1975. A possible explanation of occurrence of potential difference between electrolyte solution and growing ice crystal. Russ. J. of Phys. Chem., 49(6):1447–1449. (In Russian).

Israel, Yu.A., I.M .Nazarov, A.Ya. Presman. 1989. Acid Rains. 2nd Edition. Hydrometeoizdat, Leningrad (St. Petersburg). (In Russian).

Onsager, L., and M. Dupuis. 1962. Electric properties of ice. p.317–340. *In* Thermodynamics of Irreversible Processes. IL, Moscow. (In Russian).

Orlov, D.S. 1985. Chemistry of soils. Moscow State University Publ., Moscow. (In Russian).

Ostroumov, V.V., and O.V. Makeev. 1985. Temperature field of soils. Regularities of development. Moscow State University Publ., Moscow. (In Russian).

Savelieva, E.M. 1986. Influence of phase transition water–ice on hydrometeorological processes in system atmosphere–soil. Ph.D. dissertation, Agrophysical Research Institute, Leningrad (St. Petersburg).

Workman, E., and S. Reynolds. 1950. Electrical phenomena occurring during freezing of dilute aqueous solutions and their possible relationship to thunderstorm electricity. Phys. Rev., 78: 254–255.

Ground Freezing for Containment of Hazardous Waste
Engineering Aspects

I.K. ISKANDAR[1] AND F.H. SAYLES[1]

ABSTRACT

The use of frozen soils has been proposed as an alternative method to contain hazardous waste. This technology has recently been advanced and adopted for application, and several demonstration projects are proposed. This paper describes engineering aspects of artificial soil freezing for containment of hazardous waste, geological conditions, environmental issues, advantages and limitations, performance monitoring and research needs.

INTRODUCTION AND DESCRIPTION OF THE TECHNOLOGY

Ground freezing can be used to control the spread of hazardous waste. This promising method is environmentally friendly and offers a safe alternative to other methods for waste retention in many cases. The method can be used in conjunction with other waste containing systems since frozen soil adheres well to many other materials. However, to use artificial ground freezing for hazardous waste retention, the site must be suitable with regard to geology, groundwater conditions and chemicals present at the site. Iskandar (1986) provides a comprehensive literature review covering the effect of ground freezing on uncontrolled hazardous waste sites and points out some of the advantages of ground freezing as an alternative to other methods of hazardous waste retention such as slurry walls, grouting, etc.

The purpose of this paper is to summarize recent information and experience in the application of ground freezing for containment of hazardous waste.

DESCRIPTION OF THE GROUND FREEZING METHOD

Essentially, the ground freezing systems consist of freezing pipes evenly spaced in the ground along the perimeter of the volume that is to be isolated. Inside each freezing pipe is a concentric "feed-pipe," which supplies a chilled fluid as a coolant. The coolant flows inside the feed-pipe, up the annulus formed by the two pipes and then back to the refrigeration plant. The cold exterior pipe freezes the adjacent soil, forming a frozen soil column the length of the freezing pipe. The diameter of the frozen soil column increases with time at a rate depending upon the freezing pipe temperature, specific soil type, moisture conditions and thermal conditions at a given site. A series of freezing pipes properly spaced and aligned can form a continuous frozen barrier when the diameters of the frozen soil columns merge (Fig. 1). The thickness of the frozen soil barrier can be
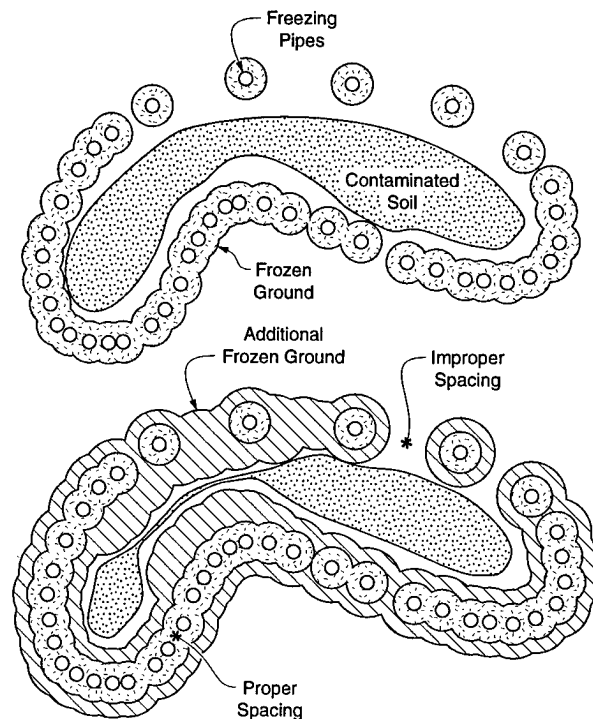
Figure 1. Properly spaced and aligned freezing pipes form a continuous frozen barrier when the diameters of the frozen soil columns merge.

[1]U.S. Army Cold Regions Research and Engineering Laboratory, 72 Lyme Road, Hanover, New Hampshire 03755-1290, USA

increased by continuing the circulation of cold brine in the single row of freezing pipes, by lowering the freezing pipe temperature or by installing additional rows.

Ground freezing for subsurface construction is common in engineering practice today. The first recorded application of artificial ground freezing was on a mine-shaft project near Swansea, Wales, in 1862, although the process had been proposed in France a few years earlier (Schmidt 1895). In 1883, F. H. Poetsch (Kohler 1883) in Germany patented the method which, with improvements, is still in use.

A new development began in France in 1962 with the injection of liquid nitrogen at a temperature of $-183°C$ directly into the freezing pipes (Ritter 1962). The nitrogen was allowed to expand and exhaust to the atmosphere still at very low temperatures. At present, virtually all artificial ground freezing for construction purposes is accomplished either by circulating coolant from a refrigeration plant or by liquid nitrogen injection. In the Arctic and Subarctic, advantage can be taken of the cold environment where thermal siphons are useful in maintaining ground frozen for many years in discontinuous permafrost areas; for example, the supports for the Alaskan oil pipeline use this system. The frozen soil method offers two concepts for retaining waste. One concept is to freeze the entire waste area into a solid block of frozen soil, thus freezing the waste in situ. For small areas where the contaminated soil does not include storage vessels that would rupture from frost action during freezing, this concept may be simpler to install. A second concept, of course, is to create a frozen soil barrier to confine the unfrozen waste within prescribed soil boundaries. This latter concept is the subject of this paper.

GENERAL REQUIREMENTS FOR A SUBSURFACE WASTE CONTAINMENT SYSTEM

A system for retaining contaminated waste under subsurface conditions must possess the following capabilities:

1. Be impervious to the waste materials that are to be contained, as well as materials surrounding the outside of the container including ground and surface waters.
2. Be versatile enough to permit the complete enclosure of contaminated volumes having different shapes and sizes. This requirement includes providing a seal above and beneath the contained volume.

3. Be capable of installation in a variety of geological conditions.
4. Not contribute to the degradation of the surrounding environment during the waste retention period or after the contaminant and retaining system are removed.
5. Be evaluated for integrity and leakage by means of an accurate monitoring system.
6. The retaining system must have sufficient strength and rigidity to resist pressures from the surrounding soil and groundwater if the contaminated soil is to be removed for processing.
7. Upon decommissioning, the removal of the retaining system would leave the site in the same natural state as the surrounding area.

To evaluate the suitability of frozen ground barriers for containment of hazardous waste, a comparison of frozen soil barriers against these requirements will be discussed.

APPLICABILITY OF GROUND FREEZING TO CONTAINMENT OF CONTAMINATED WASTE

The applicability of ground freezing for use in containment of contaminants may be evaluated by comparisons with the preceding list of general requirements for a subsurface containment system. It is useful to compare in detail the ground freezing system with each of these general requirements in turn.

Imperviousness

Seepage through frozen soil consists essentially of two processes: hydraulic conductivity which can be described by Darcy's law; and diffusion of water and chemical solutions migrating through the interconnected unfrozen water films surrounding each of the soil particles.

Hydraulic conductivity

Hydraulic conductivity in frozen soils is similar to that in unfrozen soils: that is, the movement of the fluid through pores of the soil and ice matrix. For saturated flow Darcy's law for hydraulic conductivity is written

$$q = kiA$$

where q = rate of flow (L^3/s)
$\quad\quad\ k$ = coefficient of permeability (L/s)
$\quad\quad\ i$ = gradient
$\quad\quad\ A$ = area.

362

Andersland et al. (1995), using a falling head permeameter, tested a frozen gravelly sand at –10°C with ice saturation ranging from 0% to over 90% using decane, an immiscible liquid, as a permeating liquid. For this nearly saturated gravelly sand, they found Darcy's coefficient of permeability (k) to be less than 10^{-5} cm/s; i. e., the permeability was smaller than their measuring system could measure. They also found that for soils with ice saturation less than 72% were permeable to decane; however, when slurries of bentonite (7.5 and 10% by weight) were added to gravelly sand to produce 84% saturation or greater, the frozen soil was impervious to decane.

Dash et al. (1995) conducted permeability tests using 2.5-cm (1-in.) diameter tubes to form vertical columns of soil in which the middle zone of the soil column was cooled to a temperature below freezing. Water was injected into the chilled zone to create a frozen soil barrier across the diameter of the tube. A solution of either chromate (4 g/L) or trichloroethylene (TCE) (6 g/L) was used as a permeate in falling head hydraulic conductive tests. Both gravelly sand and clayey silt soils were tested using this procedure. The results of these tests indicated that for temperatures in the range of –10°C to –26°C the coefficient of permeability (k) was less than 4×10^{-10} cm/s. The same soils in the unfrozen state had coefficients of permeability of 4.45×10^{-2} cm/s and 7.6×10^{-4} cm/s respectively. The duration of each of these tests was less than 5 days.

Diffusion

Water and chemicals can migrate through frozen soil by diffusion in both the ice matrix and the unfrozen interconnected water films surrounding each soil particle. Two methods of estimating the importance of diffusion through a frozen silt barrier will be discussed. First consider Fick's first law:

$$J = -D\, dc/dx \tag{1}$$

where J = mass flux [mole/liter^2 (M/L^2)-t]
  D = diffusion coefficient
  c = concentration of the solution (M/L^2)
  x = the direction of the diffusion (L)

To illustrate the application of this equation and to gain some sense of the quantities involved, consider the case where a sodium chloride (NaCl) solution with a molarity of 2 (2M) is to be retained within a frozen clay barrier where the temperature midway between the freezing pipes is about –3°C. Murrmann et al. (1968) measured D to be about 4×10^{-7} cm^2/s for a bentonite paste at –3.1°C. For this

illustration this value for (D) will be used. For a unit area of barrier surface and a barrier thickness of 3 m, the value of (J) can be estimated from eq. 1.

Inside the barrier,

$$c = 2 \times (58.4428/1000) = 0.116 \text{ g/cm}^3$$

Outside the barrier, say, $c = 0$

Then:

$$J = dQ/dt = - (4 \times 10^{-7}) \, ((0 - 0.116)/300)$$
$$= 1.55 \times 10^{-10} \text{ g/cm}^2\text{–s}$$

After 100 years, diffusion per square centimeter where the barrier temperature is –3.0°C is estimated to be:

$$Q = 1.55 \times 10^{-10} \times 3600 \times 24 \times 365$$
$$= 0.005 \text{ g/cm}^2$$

This value is extremely small considering that probably less than 3% of the barrier would have a temperature near –3°C. Also, it should be noted that it is assumed that J is a steady-state flux for the entire 100 years.

Dash (1995) suggested that the following equation might be used to assess the migration of chemical solutions through a frozen soil barrier:

$$C/C_0 = \text{erfc}(x/2\sqrt{Dt}) \tag{2}$$

where C = concentration of the solution at a given point (M/L^3)
  C_0 = concentration of a solution at the source (M/L^3)
  x = distance from the source to a given point (L)
  D = diffusion coefficient of the frozen soil (L^2/t)
  t = time.

Using the same conditions given in the previous illustration for Fick's first law for a time period of 1 year:

$$C/C_0 = \text{erfc}(300/2) \times (4 \times 10^{-7} \times 3.1536 \times 10^7)^{1/2}$$

$$C/C_0 = \text{erfc}(133.5)$$

The value for erfc(133.5) is less than 1.5×10^{-12}
  For a period of 100 years:

$$C/C_0 = \text{erfc}(4.2) = 1.5 \times 10^{-8}$$

Then for a 2M solution of NaCl as the source: $C_0 = 0.116$ g/cm^3. The concentration of the leakage after 100 years becomes:

$$C = (1.5 \times 10^{-8}) (0.116) = 1.74 \times 10^{-9} \text{g/cm}^3.$$

Both of the preceding examples indicate that NaCl migration is quite small even after a 100-year period. Both methods assume that the apparent self-diffusion coefficient (D) is constant. Murrmann et al. (1968) measured apparent self-diffusion coefficients in a bentonite paste at different temperatures and reported that the coefficients decreased with the decrease in frozen soil temperature.

To assess the effect of temperature, Nakano et al. (1986) proposed the equation:

$$D(u) = D_0 (u-u_c)^b \qquad (3)$$

where D_0 and b = positive numbers.
u_c = initial moisture content of the "dry soil" into which moisture migrates from a soil having greater moisture content.

Using experimental data, the constants in eq 3 were evaluated for Morin clay at −1°C.
Then :

$$D(u) = 1.21(u-3.8 \times 10^{-3})^{0.272}$$

where $D(u)$ is in units of cm^2/days.

This equation represents the data for this clay reasonably well. It should be noted that since (u) decreases with decreasing temperature, that $D(u)$ also decreases with temperature, thus making eq. 3 consistent with the findings of Murrmann et al. (1968).

Equations 1 and 2 can be used to estimate the time for a specific chemical solution to migrate through a given frozen soil barrier thickness. Conversely, if the design life (t) of the barrier can be established, then the required minimum thickness of a frozen barrier could be estimated for protection against migration by using these same equations.

By analogy with heat transfer, a simple equation for estimating the depth of penetration of a weak solution into a frozen soil barrier is:

$$\text{Depth of penetration } Z = 2 \sqrt{Dt} \qquad (4)$$

where D = diffusion coefficient (L^2/t).

For a frozen clay barrier with a design life of 100 years,

$$Z = 2 \ (4 \times 10^{-7}(100) \ 3.1536 \times 10^7)^{1/2} = 71 \text{ cm}.$$

Of course, eq. 4 also can be used to estimate the time for a chemical solution to migrate through a barrier of known thickness.

These methods for assessing the relative importance of migration of chemicals by diffusion require reliable values for the coefficient of diffusion, as well as clear practical criteria for an acceptable level of diffusion through a given frozen soil barrier.

Chemical erosion

The erosion of a frozen soil barrier by the chemicals that are being retained by the barrier can adversely affect the performance of the barrier and in an extreme case destroy it if remedial action is not taken. The variables that could affect the rate and extent of erosion of a frozen soil barrier include the solubility of the retained chemical in water, the total amount of the chemical present, the temperature of the barrier, the degree of ice saturation of the soil, and the type of soil forming the barrier. Chemicals that are water soluble can depress the freezing point of water below the temperature of the retaining barrier and thus melt the ice matrix from within the frozen soil. For the erosion to occur, the concentration of the chemical solution must be high enough to reduce the freezing point of the ice. It also must be of sufficient quantity as to not be diluted by the ice melt and then freeze after dilution. Using two-dimensional laboratory models where miniature freezing pipes were placed and frozen into gravelly sand, Andersland et al. (1995) demonstrated that when the freezing point of a contaminate is lower than the temperature of the frozen soil barrier, erosion will progress until the contaminate encounters a zone within the barrier with a temperature lower than the freezing point of the contaminate. At this location erosion will cease.

Andersland et al. (1995) proposed a classification of frozen soil erosion potential for common water soluble or miscible chemical compounds. They define the "erosion potential" of a chemical as the ability of a saturated aqueous solution of the chemical to erode a frozen soil barrier by melting the ice matrix. The classification of a chemical solution as to its erosion potential is related to the freezing point temperature range of the saturated solution.

Geometrically adaptable to contaminated waste sites

An important feature of frozen ground barriers is that they can be installed in a variety of geometric shapes to accommodate specific site conditions. The
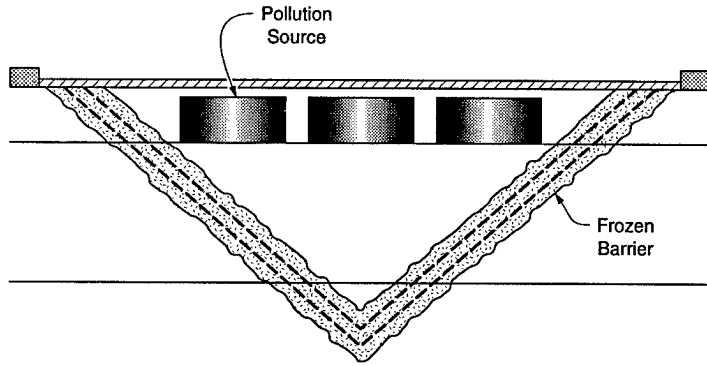
Figure 2. A V-shaped frozen barrier.

barrier can be frozen into any configuration in which the freezing pipes can be placed, including vertical pipes evenly spaced along the perimeter of the waste area to intercept a horizontal impervious geological strata or zone, inclined pipes to intercept an impervious barrier such as another line of freeze pipes to form a V-shaped type enclosure (Fig. 2), or by arranging the pipes to form a U-shaped trough, which can be accomplished by navigational (i.e., directional) drilling (Fig. 3).
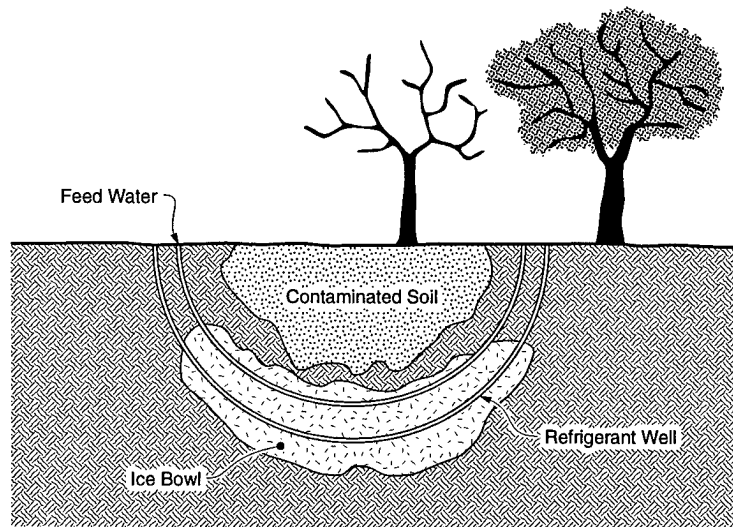
Figure 3. A U-shaped frozen barrier formed by navigational drilling.

Vertical frozen soil barriers can extend to depths of a 30 m or more. However, the depth is usually only limited by the capability of maintaining the proper freezing pipe spacing and lateral alignments throughout their lengths. The V-shaped container has the advantage of providing a self-contained bottom, making it suitable for enclosing long relatively narrow contaminate waste volumes such as waste buried in trenches where no impervious strata exists within an economical depth. Also, a U-shaped frozen bar-

rier configuration can be used to form complete enclosure, including a bottom as well as sides. At the present time pipe installations having horizontal distances of up to about 1.5 km can be placed using a navigational drilling system. This capability, although expensive, provides the option of enclosing a waste area of large horizontal extent.

The thickness of a frozen soil barrier can be adjusted to meet the requirements of the site conditions. The thicker the barrier the less permeable it would be and the greater resistance to chemical erosion should be expected. A typical single row of freezing pipes spaced at about 1.5 m can freeze a barrier with an effective thickness of about 1.3 m in about 45 days (Sanger and Sayles 1979). Multiple rows of freezing pipes can be used to form a thicker barrier during the same period.

To prevent surface water from entering the enclosed area, ground freezing panels can be placed over the ground surface within the frozen barrier perimeter. However, it may be more economical to cover the surface with an impervious membrane under 60 or 90 cm of soil for protection against traffic.

Geological conditions

Frozen soil barriers can be installed in all types of soils where sufficient water is available to fill the pores of the soil with ice when the soil is frozen, that is, above 90% saturation. This water requirement often means that a high groundwater table be present at the site. Fine-grained soils such as clays and silts often have sufficient water available, retained in their pores, to form an adequate barrier even though they lie above the water table. Even if these soils are only partially saturated, when the freezing pipes are chilled below freezing temperatures, the water from the surrounding soil will migrate toward the freezing front and often make up enough of the ice deficit to establish an adequate containment barrier. To determine whether sufficient water is available to create a barrier, the natural water content of the soil at the site must be measured if it cannot be estimated with sufficient accuracy. At sites where there is insufficient groundwater to form an ice saturated barrier, it is quite difficult to add enough water and distribute it throughout these relatively impervious fine grain soils to create an impervious

barrier. In such a case another type of containment system may be necessary to consider.

Sites where the soils consist of highly pervious sands and gravel and the water table is above the top of the contaminated area, ground freezing is an excellent choice for a frozen soil barrier. However, if boulders are present, some difficulty in placing the freezing pipes may be experienced. At those highly pervious sites where groundwater is below the required depth of the barrier, the addition of water to fill the soil voids with ice would be difficult. The water must be distributed uniformly near the freezing pipes at a rate close to the freezing rate of the soil; otherwise the water will drain away before it freezes. If freezing rate is too fast, the water can freeze prematurely and block the soil pores against the passage of water to the freezing front. Using results of laboratory tests, Dash et al. (1995) suggest that water be added in discrete amounts at time intervals spaced to allow the water to freeze with minimum loss in drainage. Andersland et al. (1995) created laboratory scale frozen gravelly sand barriers by injecting a bentonite slurry into the soil. They suggest that this method is feasible for the formation of a frozen soil barrier where the use of natural bentonite is environmentally acceptable. Since both suggestions are preliminary, further testing and development are necessary before they can be used in the field.

Structural adequacy

During the period of time that the frozen soil barrier is serving as an enclosure for contaminated waste, its structural strength and rigidity is of minor concern compared to its permeability. However, when it is time to remove and process the enclosed contaminated soil, the frozen barrier would serve not only as an impervious barrier but also as a structural retaining wall that would permit excavation of the contaminated soil from behind it. In addition, where the "U" or "V" enclosure configurations are employed, the bottom of the enclosure would resist earth and groundwater pressure against disrupting the bottom of the enclosure. In the event that large deformations of any portion of the barrier are observed, or a structural failure appears to be a possibility, both the rigidity and the strength of the barrier can be increased by either lowering its temperature or increasing the thickness of the enclosure walls. The thickness of the barrier walls can be increased by lowering the circulating coolant temperature thus fostering the growth in the frozen wall thickness. The thickness can also be increased by installing and activating additional rows of freezing pipes. Where a

local structural failure or seepage through the frozen wall requires remedial measures, then additional freezing pipes can be installed at these problem areas. During excavation of the waste within the enclosure, the excavated area would be unobstructed since no bracing would be required to support the frozen soil barrier wall. This arrangement permits easy access for excavation and hauling equipment or for equipment to be used in the decontamination process.

Environmental issues

The construction, operations and decommissioning processes of a frozen soil containment enclosure are all environmentally friendly. Except for the freezing pipes, any heating pipes and piping for instrumentation only in situ natural soil materials are mobilized to form a frozen barrier. Part of the decommissioning process would be the removal of these pipes from the ground. A frozen ground barrier clearly does not alter the quality or quantity of the existing groundwater, although direction of groundwater flow would be diverted locally around the enclosure.

At some sites where the freezing pipes cannot be installed by driving, it may necessary to drill holes for the placement of these pipes. The drill cuttings from the holes may require processing or special disposal if they are contaminated by the waste that is to be confined. There is a certain amount of noise connected with the installation of the freezing pipes and the above-ground cooling system, but the construction period would last for only a few days depending upon the size of the enclosure being developed. During the operation of the cooling system, the sounds from the refrigeration plant can be reduced by mufflers and sound insulation at site locations where it is considered necessary.

ADVANTAGES AND LIMITATIONS

Like all barriers or containment systems, the frozen ground method has both advantages and limitations. For guidance in selecting frozen soil barriers and for use in comparison with other enclosure systems, these advantages and limitations are summarized here.

Advantages

The advantages of frozen soil barriers for the confinement of hazardous waste include:

1. Frozen soil barriers can be installed in all types

of soils where sufficient water is available to fill the pores of the soil.

2. The thickness of the barrier can be controlled by either adjusting the temperature of the coolant or by installing additional rows of freezing pipes.

3. Openings in the barrier can be closed by adding freezing pipes to the areas in question.

4. Frozen soil barriers can be used with other cleanup technologies such as metal chelation, solidification and bioremediation.

5. Frozen soil barriers can be used to concentrate liquid waste.

6. The slow freezing process has potential for soil decontamination.

7. Except for the freezing pipes and piping for instrumentation, only in-situ natural materials are mobilized to form the frozen barrier. Therefore, this technology may be acceptable to the general public and government regulators.

8. Minor cracks in the barrier are self-healing by virtue of the presence of groundwater that can freeze within the crack to seal it.

9. The extent of the barrier can be controlled by adjusting the coolant temperature and by installing heating pipes where it is necessary to protect facilities that are located adjacent to or within the barrier confines.

10. The frozen barrier can serve as a structural retaining wall for later excavation and processing of contaminated soil.

11. A frozen soil barrier can be repaired when damaged mechanically or thermally by replacing earth that may have been removed or installing additional freezing pipes in the damaged area.

Limitations

The limitations of this technology reflect the fact that one barrier system is not necessarily the best for all sites. However, ground freezing is a viable system for many site conditions with the following limitations:

1. Sufficient ground water must be available to saturate the soil with ice when it is frozen.

2. Groundwater velocity must be less than about 1 m/day or the freezing soil columns may not merge to form a continuous barrier.

3. The mechanical refrigeration systems require continuous inspection and maintenance.

4. High frost heave pressures can develop in adjacent facilities if precautions are not taken. Such facilities can be protected by the installation of heating pipes.

5. When the barrier is thawed during decommissioning, adjacent facilities may settle if precautions are not taken to prevent frost heaving when the freezing pipes are installed.

6. Frozen barriers are not effective for all contaminant types and high concentrations.

7. Expensive directional drilling may be required to seal beneath contaminated soil.

8. Reliable sensors are needed to detect barrier leakage; it may be difficult to determine if the bottom is truly sealed.

9. Organic interference with frozen soils requires further investigation.

CASE STUDY

A demonstration of ground freezing technology was conducted at Oak Ridge, Tennessee, during 1994 in a clayey silt and sand fill (SEG1995). The configuration consisted of a double row of perimeter freezing pipes which formed a V-shaped enclosure designed to retain simulated hazardous waste (Fig.2). The outside and inside plan dimensions at the ground surface were 17 × 17 m and 10 × 10 m, respectively, producing a barrier thickness of about 3.5 m. The freezing pipes were installed at an angle of 45° and the frozen barrier extended to a maximum depth of 8.5 m below the ground surface. Heating pipes were located inside the contained unfrozen soil in a row parallel to the freezing pipes. A tank was located near the center of the enclosed unfrozen soil. This tank was used to release water and water-based tracers into the enclosed soil to test the permeability of the barrier. The barrier and the adjacent area contained sensors for recording temperatures, soil conductivity, hydrostatic pressures, and movements of the tracers. In addition, a number of observation wells were installed. The demonstration showed that a frozen soil barrier can be created which is impervious to water and the water-based tracers that were used.

Lessons learned are that the test period was too short (about 4 months) and the types of tracers employed should be more aggressive, i.e., immiscible solutions or solutions similar to the contaminants that are to be encountered when this technology is applied in the field. Many aqueous tracer solutions freeze when they contact frozen soil.

MONITORING

1. At a given site, alignment surveys establish the freezing pipe locations at the ground surface.

The location of the subsurface portion of the freezing pipes is determined by passing a slope inclinometer down each pipe. The extent of the frozen soil is evaluated using temperature, conductivity sensors and probes where possible.

2. At the present time, defects in a frozen barrier are detected by analyses of continuously recorded temperature, conductivity, piezometer and observation well readings taken at critical locations within the barrier and adjacent areas.

3. Quality control of the barrier can be assessed in a general way by observing the inlet and outlet temperatures of the liquid coolant near the refrigeration plant along with the observations listed in the preceding item (2).

ECONOMIC FACTORS/ COST ANALYSIS

The cost of installing a frozen soil barrier depends to a large extent upon the soil type, moisture conditions and thermal conditions of a specific site. In addition, the construction costs are related to time restraints for completion of the barrier which in turn are dependent upon freezing pipe spacing, coolant temperature, energy and equipment configuration.

The general relationship between initial installation costs and the spacing of freezing pipes is shown in Figure 4 (Sullivan et al. 1984). This figure also shows the components of the total cost curve which includes costs for drilling for the freezing pipes, fuel for the refrigeration system and refrigeration equipment rental. To facilitate the design of a frozen ground barrier, Sullivan et al. (1990) developed a computer spreadsheet analyses program that optimizes the design and costs of a frozen barrier. This program utilizes the physical and thermal properties of soil as well as the economic factors including the details of the installation and operation costs of the entire freezing system.

It is of interest to estimate the cost of a frozen ground barrier The following estimate of cost is for a V- shaped configuration of the freezing pipes extending 13.7 m deep into the ground where the width of the "V" at the ground surface is about 10.7 m. The frozen surface area of the perimeter of a frozen soil barrier having a single line of freezing pipes is estimated to be 1500 m². For comparisons of cost with other systems this estimate is computed on a square meter basis.

Capital costs include: drilling; purchase of the freezing piping, rental of a 100-ton refrigeration plant for 50 days for the initial ground freezing, pur-
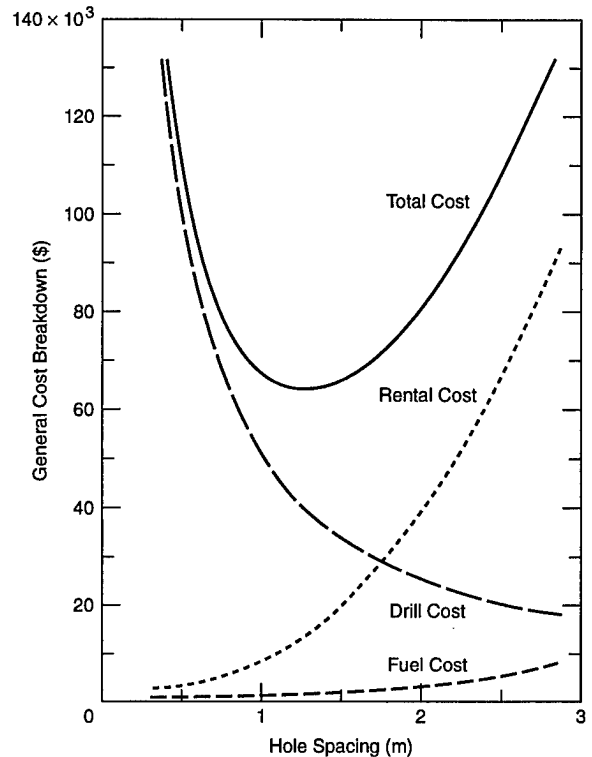
Figure 4. Cost factors for frozen ground barriers.

chase of a 25-ton refrigeration plant to maintain the ground frozen for an extended period of time, equipment and labor to install the freezing system and operate it until the specified barrier thickness is formed, and the electricity cost for the first 100 days. For this case the initial capital cost per square foot is estimated at $60.50.

Operation and maintenance costs include electricity after the first 100 days; refrigeration maintenance, and maintenance of headers and freezing system. The cost of operations and maintenance per square foot per year is estimated to be = $1.95.

The cost of contractor initial mobilization is estimated to be $10,000

The cost of decommissioning the facility is estimated to be $200,000

It should be noted that these costs are somewhat higher than those presented by Iskandar (1986) due primarily to inflation.

SUMMARY AND CONCLUSIONS

1. This technology is well established and available in the construction industry as noted in the introduction and there exists reliable companies willing and capable of installing frozen ground barriers.

2. Since the installation of frozen ground barriers disturb existing ground minimally and only existing in situ materials are utilized, it seems reasonable to expect that this technology is generally environmentally acceptable to both the general public and government regulators.
3. The testing of frozen soil barriers of large scale models or field tests should have a duration time of at least one year.
4. If tracers are used to evaluate the permeability of a frozen soil barrier, the tracer should be immiscible with water.
5. The chemical erosion of the ice within the frozen soil needs to be assessed in greater detail for chemicals that are likely to be contained by frozen soil barriers.
6. Hydraulic conductivity for saturated frozen gravelly sand and clayey silt at temperatures lower than $-10°C$ are less than 10^{-5} cm/s.
7. The migration of water and chemical solutions through frozen soil appears to be extremely small but additional studies are required to confirm the published information.

DEVELOPMENT GAPS
AND RESEARCH NEEDS

1. If this technology is to be used in dry soil such as gravelly sand, an effective field method for injecting water into the soil near the freezing pipes while freezing is in progress must be developed and tested in large scale laboratory tests or a field demonstration before applying this method to a contaminated site.
2. Sensitive instrumentation is needed for monitoring and detecting leaks within and through the frozen barrier.
3. An acceptable performance level for the barrier must be defined. For example, how much leakage is acceptable for the different chemical waste concentrations?
4. The rate of diffusion of contaminants through the unfrozen water films in frozen silt and clay soil needs to be determined experimentally

REFERENCES

Andersland, O. B., and S. H. Davies, and D. C. Wiggert.1995. Performance and formation of frozen containment barriers in dry soil. Rust Geotech Inc.

Dash, J.G., H. Fu, and R. Leger.1995. Bench scale testing of Hanford and Oak Ridge soils. Final report of the Low Temperature Physics Laboratory of the University of Washington. Appendix A of the Scientific Ecology Group, Inc. Final Report: Demonstration of Ground Freezing Technology at SEG Facilities in Oak Ridge, TN

Dash, J. G. 1995. Ice technology for hazardous waste management. Department of Physics, University of Washington, Seattle.

Iskandar, I.K. 1986. Effect of freezing on the level of contaminants in uncontrolled hazardous waste sites. Part 1: Literature review. U. S. Army Cold Regions Research and Engineering Laboratory Special Report 86-19 p. 36

Kohler, G. 1883. Berg-und Huttenmannische Zeitung, No. 38, XII Jahrg.,Sept. 21.

Murrmann, R.P., P. Hoekstra, and C. Bialhowski. 1968. Self-diffusion of sodium ions in frozen Wyoming bentonite-water paste. Soil Sci. Am, Proc. 32:501–506.

Ritter, C.L. 1962. Recent developments in liquefaction and transportation of natural gas. Chem. Eng. Progr., 48, No.11.

Sanger, F.J. and F.H. Sayles. 1979. Thermal and rheological computations for artificially frozen ground construction. *In* Ground Freezing (H. Jessberger, Ed.). New York: Elsevier Publishing Company

Schmidt, M.F. 1895. L'emploi de la congelation pour l'execution de travaux dans les terrain aquiferes (Use of freezing for work in waterbearing ground).

SEG Scientific Ecology Group, Inc. 1995 Final report: Demonstration of ground freezing technology at SEG Facilities in Oak Ridge, TN.

Sullivan, J.M., Jr., D.R. Lynch, and I.K. Iskandar. 1984. The economics of ground freezing for management of uncontrolled hazardous waste sites. *In* Proceedings, 5th National Conference on Management of Uncontrolled Hazardous Waste Sites, 7–9 November, Washington, D.C.

Sullivan, J.M., Jr., K.E. Duprey, and I.K. Iskandar. 1990. Economics of ground freezing as a means of hazardous waste containment: A spreadsheet analysis program. Special Report (in preparation) USA Cold Regions Research and Engineering Laboratory, Hanover, NH.

The Effects of Freezing and Organic Matter Transformation On Soil Physical Status

E.V.BALASHOV[1]

ABSTRACT

Changes in the water retention properties and swelling and shrinkage of samples of a dernopodzolic sandy loam soil were studied after 17 weeks of freezing at $-10°C$ and after 13- or 27-week microbial removal of soil organic matter at $65°C$, respectively. Total carbon content declined from 21.8 to 20.7, 19.4 and 18.3 g kg^{-1}, respectively, after three soil treatments. These soil treatments contributed to soil sample shrinkage. There were no significant differences in the relationships between bulk density and water content in the untreated and treated soil samples at initial bulk density of 1.08–1.10 Mg m^{-3} during first cycle of shrinkage. If initial values of bulk density of soil samples rose from 1.10 to 1.30 Mg m^{-3}, a greater increase in the differences between these relationships was observed, especially for the frozen and 27-week incubated soil samples which had bulk densities greater than 1.45 and 1.60 Mg m^{-3} after the third cycle of the shrinkage process.

Key words: Soil freezing, microbial removal of organic matter, bulk density, swelling and shrinkage of soil.

INTRODUCTION

Soil organic matter is known to play an important role in the control of physical, chemical and biological status of soils that are in continuous use. Native and agricultural dernopodzolic soils show a distinct profile distribution of humus and its constituents (Birjukova and Orlov 1993). Freezing and thawing affect the mobility and transformation of humic constitutents (humic and fulvic acids, humins) of organic matter in the seasonally frozen dernopodzolic soils (Pereverzjev 1987).

Compared with total organic carbon content, few data have been reported on the importance of changes in the content of soil humic substances for different parameters of soil physical status (Savage et al. 1969, Rosell et al. 1989). However, many agricultural practices are designed to change the composition of humic substances, which contain a great amount of weakly available nutrients.

There are two conventional laboratory techniques for quick removal of organic matter from soil samples to simulate humus degradation. These techniques use chemical solutions or high temperatures to mineralize all total organic carbon by wet or dry combustion (Nelson and Sommers 1982, Inbar et al. 1989). Unfortunately, use of these methods causes essential changes in the properties of the mineral solid phase of soils (Benito and Diaz-Fierros 1992). This does not allow us to exactly determine the contribution of organic matter to possible changes in a soil's physical and chemical properties.

Recent studies showed the advantages of hot water and thermophilic microflora for quick removal of mineralizable organic matter from soil samples without damaging the soil's mineral solid phase (Schulz 1990, Balashov et al. 1994). The objective of the present studies was to evaluate the effects of long-term freezing and microbial action on organic matter content, water retention, and swelling and shrinkage of a dernopodzolic sandy loam soil.

MATERIALS AND METHODS

Chemical and physical properties of soil

Disturbed field moist samples of dernopodzolic sandy loam soil were taken at the depth of 20 cm on

---

a plot after growing cereals. The air-dried soil samples were moistened to 60% of complete saturation and stored in plastic bags at $-10°C$ for 17 weeks or incubated in glass vessels (500 cm^3) at 65°C for 13 or 27 weeks. Small open containers with 20% KOH solutions were placed into the glass vessels to absorb the CO_2 released by mineralization of organic matter by thermophilic microorganisms. Before and after transformation of organic matter by freezing or thermophilic microflora the total carbon content was determined by wet combustion according to Tjurin's procedure (Kaurichev 1986).

Water retention of soil samples passed through a 2-mm sieve was determined by a pressure-plate apparatus at 25°C temperature and -5 to -300 kPa pressure. Measurements of swelling and shrinkage during three repeated cycles of saturation and drying were carried out using a Vasiljev's device (Vadjunina and Korchagina 1986). This device consists of a round metal plate with 1-mm holes, a 25-cm^3 retaining ring, a rigid metal support with set screws, and an vertical deformation meter (± 0.01-mm sensitivity) with a 10-mm unit circle. The retaining ring is placed on the round metal plate. Then disturbed air-dried soil sample, passed through a 2-mm sieve, is placed into the retaining ring. The vertical deformation meter is fastened by screws above retaining ring with soil sample covered by a round plastic plate. This plastic plate is a support for a moving vertical rod of the vertical deformation meter. Water is added to cover the round metal plate, but not cover the ring. The soil sample is moistened by capillarity until maximum saturation is observed. The swelling (or shrinkage) is recorded as a height (in mm) of the saturated soil sample. A total weight of the whole device is recorded to calculate the saturation water content of the soil sample studied. During the drying cycle, the total weight of the whole device and the readings of the vertical deformation meter are recorded at regular time intervals until constant weight of soil sample is obtained. Then the final linear dimensions (height and diameter) of the air-dried soil sample are recorded. The same soil sample is used later to determine the swelling and shrinkage during two next cycles of the saturation and drying. The soil water content is determined gravimetrically after oven drying at 105°C. The swelling and shrinkage deformations are reported as a percentage of soil sample volume changed during three cycles of saturation and drying. Three initial values of bulk density (1.08–1.10; 1.20; 1.30–1.32 Mg m^{-3}) were chosen for studies of the swelling and shrinkage processes.

RESULTS AND DISCUSSION

Carbon Mineralization

The 17-week freezing treatment and 13- or 27-week microbial incubation treatments of the soil samples decreased the total carbon content from 21.8 to 20.7, 19.4 and 18.3 g kg^{-1}, respectively. Our earlier data showed that similar mineralization of organic matter by thermophilic microflora caused a decrease in total carbon content of brown humic acids by 5% in a light-textured dernopodzolic soil (Balashov et al. 1994).

Water Retention Properties

Water retention curves relating water potential and volumetric water content of dernopodzolic sandy loam soil at a bulk density of 1.40 Mg m^{-3} are presented in Fig.1. There were more or less pronounced differences in water retention of soil samples after their freezing or incubation. At water potentials of -10 to -100 kPa, the greatest decrease in water retention was observed with decreasing total carbon content. Compared with the energetically active organic matter, the light-textured parent material derived from quartz and micaceous minerals played a minor role in the water retention of the soil samples after microbial incubation. At water potentials of less than -100 kPa, there were no distinct differences in water retention of this soil after the treatments studied.
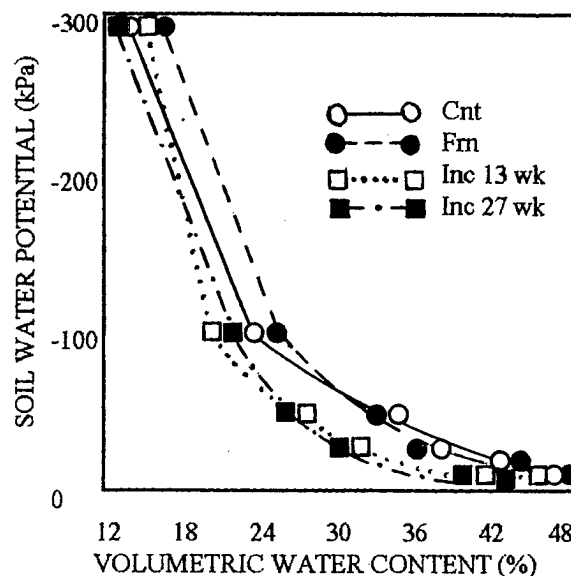
Figure 1. Water retention curves of the control (Cnt), frozen (Frn) and 13- and 27-week incubated (Inc) samples of dernopodzolic soil at bulk density of 1.40 Mg m^{-3}.

Table 1. Maximum deformation of dernopodzolic sandy loam soil after saturation and drying at different total carbon content and initial bulk density.

Treatment	Total Carbon Content	Initial Dry Bulk Density	Swelling (+) and shrinkage (-) at						Saturation Water Content	
			saturation			drying				
			during cycles of							
			1	2	3	1	2	3	1	3
	g kg⁻¹	Mg m⁻³	%						%	
Control	21.8	1.08	-0.7	+1.8	+0.9	-6.1	-0.4	-2.8	59	52
		1.20	+2.3	+3.2	+2.8	-5.6	-4.0	-2.7		
		1.32	+2.5	+1.6	+1.0	-4.4	-2.6	-1.2	44	35
Freezing of 17 weeks	20.7	1.10	-0.4	+0.4	+0.9	-5.1	-2.9	-2.3	48	46
		1.30	+1.5	+2.2	+1.4	-4.3	-3.8	-2.6	45	38
Incubation of 13 weeks	19.4	1.08	+0.5	+1.2	+0.6	-4.6	-2.2	-1.5	52	42
		1.20	+1.0	-0.7	-0.6	-4.5	-2.1	-1.2		
		1.30	+2.4	-0.6	+1.1	-4.0	-2.7	-2.2	43	38
Incubation of 27 weeks	18.3	1.10	+0.1	-0.2	-0.4	-5.6	-1.4	-0.7	49	34
		1.20	+0.6	-0.2	-0.4	-1.3	-1.4	-2.0		
		1.30	+0.4	-1.2	-0.7	-4.7	-2.4	-2.0	43	40

Swelling and Shrinkage

Swelling is defined by hydration of soil particles as a result of interface interactions between water and solid phase of soil. The degree of swelling depends on properties of the organic and mineral components of soil solid phase, initial organic matter and soil water contents, and the bulk density of the soil. Usually, at a given organic matter content, the swelling of air-dried soil, increases with increasing bulk density.

Measurements of total soil deformation, determined from swelling and shrinking of the dernopodzolic sandy loam soil, are presented in Table 1. At relatively low initial bulk density of 1.08–1.10 Mg m⁻³, the decrease in total carbon content caused by freezing or incubation did not cause significant differences in swelling or shrinkage during three cycles of saturation and drying to an air-dried state.

At the highest initial bulk density of 1.30–1.32 Mg m⁻³, swelling of soil samples declined with decreasing total carbon content in incubated samples, especially those incubated for 27 weeks.

In the incubated samples of dernopodzolic sandy loam soil, the predetermined increase in initial bulk density did not contribute to swelling because of microbial removal of organic matter.

Mineralizable organic matter, such as soluble humic substances, was more involved in the interface interactions between water and the solid phase of soil, compared to the energetically inert sand par-

ent material. In almost all cases, the repeated cycles of saturation and drying caused a decrease in swelling and shrinkage, and volumetric water content at complete saturation (Table 1).

Changes of bulk density with volumetric water content of soil samples with initial bulk densities of 1.08–1.10 and 1.30–1.32 Mg m⁻³ are presented in Fig. 2 and 3, respectively.

In soils with initial bulk density of 1.08–1.10 Mg m⁻³, there were no significant changes in bulk density and water content relationships for the untreated soil samples during the first and third cycles of drying (Fig. 2). During the first cycle of shrinkage, differences between these parameters also were not significant in the treated soil samples, compared with the untreated soil samples. Final values of bulk density of the soil samples were equal to 1.24–1.25 Mg m⁻³. However, during the third cycle of shrinkage, removal of mineralizable organic matter as a result of freezing or 27-week incubation led to an increase in soil bulk density. The values were equal 1.20, 1.33,1.32 Mg m⁻³ for the control, frozen and 27-week incubated soil samples.

In samples with initial bulk density of 1.30–1.32 Mg m⁻³, more marked changes in bulk density with water content in the untreated and treated soil samples were observed (Fig. 3). At this initial bulk density, compared with that of 1.08–1.10 Mg m⁻³, the combined effects of organic matter transformation and the third cycle of shrinkage resulted the higher
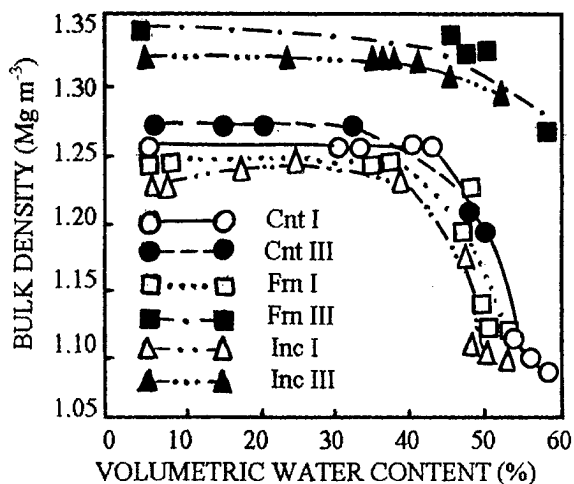
Figure 2. Changes in bulk density with water content of the control (Cnt), frozen (Frn) and 27-week incubated (Inc) samples of dernopodzolic soil during the first (I) and third (III) cycles of shrinkage at initial bulk density of 1.08–1.10 Mg m⁻³.

Figure 3. Changes in bulk density with water content of the control (Cnt), frozen (Frn) and 27-week incubated (Inc) samples of dernopodzolic soil during the first (I) and third (III) cycles of shrinkage at initial bulk density of 1.30–1.32 Mg m⁻³.

bulk densities. Such final bulk densities as 1.41 (control); 1.46 (freezing) and 1.63 (27-week incubation) Mg m⁻³ showed a clear trend of more compaction with decreasing organic matter content.

It is known that the force producing shrinkage is surface tension at the air-water-soil solid interfaces. In the beginning of process, shrinkage occurs in proportion of the volume of water removed. Then a point is reached at which interactions between particles arise. Further shrinkage is defined by the degree of compression and re-orientation of particles as a result of the increased surface tension at the solid phase-water interfaces.

In the frozen and incubated samples of dernopodzolic sandy loam soil, the transformation of organic matter seems to reduce the repulsive interactions between particles which, during drying-induced compression, could result in closer packing than that of particles with organic matter at their surfaces.

At a soil bulk density of more 1.40 Mg m⁻³, unfavorable conditions for root growth are usually observed in light-textured soils.

CONCLUSIONS

This study demonstrated that soil physical and hydrophysical properties depended on the content of mineralizable organic matter, which was affected by long-term freezing and activity of microrganisms.

Explanation of changes in soil bulk density with moisture content should be based on a consideration of the origin and content of organic matter as well as initial degree of soil compaction.

REFERENCES

Balashov, E.V., S.S. Islamov, and V.S. Zuyev. 1994. Influence of microbiological transformation of carbon-containing compounds on humus and physical status of soils. p. 140–141. In Proc. Int. Conf. on Agricultural Engineering, Milano, 29 Aug.–1 Sept., 1994. Milano, Italy.

Benito, F., and F. Diaz-Fierros. 1992. Estudio de las sustantias estabilizantes de la agregasion en suelos ricos en materia organica. II. Metodos sustractivos de analisis. (in Spanish.) Agrochimica 36:340–348.

Birjukova, O.N., and D.S. Orlov. 1993. Reserves of organic matter and types of humus in soils and peats of the North of European region of Russia. (in Russian.) Pochvovedenie 10:39–51.

Inbar, Y., Y. Chen, and Y. Hadar. 1989. Nuclear magnetic resonance and infrared spectroscopy of composed organic matter. Soil. Sci. Soc. Am. Proc. 53:1695–1701.

Kaurichev, I.S. (ed.). 1986. Soil science practice. (in Russian.) Kolos Publ., Moscow, Russia.

Nelson, D.W., and L.E. Sommers. 1982. Total car-

bon, organic carbon, organic matter. *In* A.L. Page et al. (ed.) Methods of soil analysis. Part 2. 2nd ed. Agronomy 9:539–579.

Pereverzjev, V.N. 1987. Biochemistry of humus and nitrogen of soils of Kolsky Peninsula. (in Russian.) Gydrometeoizdat Publ., Leningrad. USSR.

Rosell, R.A., A.E. Andriulo, M. Schnitzer, M.B. Crespo, and A.M. Miglierina. 1989. Humic acid properties of an Argiudoll soil under two tillage systems. Science of the Total Environment 81 and 82:391–400.

Savage, S.M., J.P. Martin, and L. Letey. 1969. Con-tribution of humic acids and a polysaccharide to water-repellency in sand and soils. Soil Sci. Soc. Am. Proc. 33:149–151.

Schulz, E. 1990. Die heisswasserextrahierbare C-Fraktion als Kenngrosse zur Einschaetzung des Versorgunszustandes der Boeden mit organischer Substanzen. (in German.) Tagunsber. Akad. Landwirtschaftwiss. DDR 295:265–275.

Vadjunina, A.F., and Z.A. Korchagina. 1986. Methods of investigations of soil physical properties. (in Russian.) Agropromizdat Publ., Moscow, Russia.

Organic Matter

Characterization of the Organic Matter in Subarctic and Arctic Tundra Soils in North Siberia

A. GUNDELWEIN[1] AND E.-M. PFEIFFER[1]

ABSTRACT

Isotope compositions ($\delta^{13}C$) of total organic carbon (TOC) and four different density fractions of TOC are determined at two different sites in northern Siberia (Labaz Lake Region/Taimyr Peninsula with a subarctic climate and Bolshevik Ostrov/Severnaya Zemlya Archipel with an arctic climate). Most of the organic carbon is stored in the light fractions, which represent the weakly decomposed organic matter with a density < 1.6 g/cm³ and humified fine material and micro aggregates with a density of 1.6-2.0 g/cm³. All fractions are showing an enrichment of ^{13}C in comparison to the plant material, which are the main C sources. The light fraction has smaller $\delta^{13}C$-values than the heavy fraction, the humified organic-mineral complexes with a density 2.0-2.4 g/cm³. The strongest enrichment of the heavy carbon isotope ^{13}C is observed in a depth of 5-20 cm below the surface, where temperature and water conditions are favorable to methanogenesis.
The data present the weak decomposition of soil organic matter (SOM) under arctic and subarctic conditions.

Key words: SOM, cryosols, density fractionation, C-isotopes, $\delta^{13}C$-value

INTRODUCTION

More than 20 % of the earth's land surface is covered by permafrost soils (Washburn 1979) and roughly 14% of the world carbon pool are thought to be stored in these permafrost soils (Post 1982).

Therefore these soils could be an important potential source of carbon and greenhouse gases like carbon dioxide and methane. Knowledge about carbon dynamics in permafrost soils is an important prerequisite for estimation of future development of climate change and global warming.

The objective of this study is to characterize recent decomposition processes on soil carbon on patterned ground under different climatic conditions, by using carbon fractionation of the soil organic matter (SOM) and stable isotope investigations. Some decomposition processes are leading to an enrichment or depletion of ^{13}C. So $\delta^{13}C$-values of total organic carbon (TOC) and different carbon fractions of SOM will help to understand the role of different carbon fractions for the carbon decay under permafrost conditions.

STUDY AREA

The study areas are located in the northern part of Middle Siberia at Taimyr Peninsula and Severnaya Zemlya (Northern Land). Investigations were carried out in this region at two sites with different climatic conditions: at Lake Labaz with its typical subarctic tundra and on Severnaya Zemlya representing the arctic desert (Fig.1). More details are given in Pfeiffer et al 1996.

Lake Labaz (72°N, 100°E) is the most southern investigation point. It represents the typical treeless subarctic tundra with a continental climate regime (mean July air temperature: 12°C, mean annual

air temperature: -13°C, mean annual precipitation: 235mm) and continuous permafrost (thickness of permafrost > 400 m). The landscape is moderately hilly with lake depressions. More than 90 % of the soils of Lake Labaz area are water-affected, gleyic loamy-clayey soils with a thickness of the active layer near 0.5 m (Pergelic Cryaquepts). Often an accumulation horizon of organic materials and reduced oxides above the permafrost table could be observed.

Site 3 (Table 1. Site 10 from Severnaya Zemlya is described in Table 2.) is a typical soil of Lake Labaz region. Solifluction is wide-spread and predominant patterned ground structures are nonsorted low- and high-centred polygons ("Taimyr-Polygons") and nonsorted circles (earth hummocks), typical vegetation are small shrubs like *Salix* and *Betula*, *Carex*, mosses and lichens.

Table 1. Characterization of site 3, Lake Labaz.

Location:	Northern shore of Lake Labaz, near small thermokarst Lake.
Soil classification:	Loamy, nonacid, Pergelic Cryaquept.
Vegetation:	Humid type of subarctic treeless tussock tundra with *Betula, Eriophorum,Carex,* mosses,lichens.
Parent material:	Loamy cryoturbated sediments.
Patterned ground:	Nonsorted circles.
Permafrost :	> 50 cm.

Profile 3a (apex)

Depth (cm)	Horizon	Description
0 - 05	A	Humic, loamy sand, greyish-yellowish brown (10YR4/2), many roots, massive-platy, <1vol% rock fragments.
05 - 08	Cg1	Weak silty clay, grey (5Y4/1), platy-massive, 1 vol% rock fragments, medium roots.
08 - 44	Cg2	Weak silty clay, brown (10YR4/4), 1 vol% rock fragments, medium roots, platy-massive, reduced iron.
44 - 50	Cg3	Weak silty clay, grey (5Y3,5/1), 1vol% rock fragments, medium roots, platy-massive, reduced iron.
> 50	Cgf	Weak silty clay, 1 vol% rock fragments, no roots, ice lenses, permafrost boundary.

Profile 3b (trough)

0 - 17	Oe	Brownish black (5YR2.5/1), moderate decomposed peat.
17 - 27	Acg	Weak silty clay, brownish black (2.5Y5/3), moderatly rooted, massive structure, <1vol% rock fragments.
> 27	Oef	Moderate decomposed frozen peat, < 1 vol% rock fragments, permafrost boundary.

Table 2. Characterization of site 10, Severnaya Zemlya.

Location:	Severnaya Zemlya, Bolshevik Island, Lake Trovdoja (max. depth 7 m).
Soil classification:	Clayey-skeletal, mixed, nonacid, Pergelic Cryaquept.
Vegetation:	*Papaver polare,Carex arctisiberia*, mosses, lichens.
Parent material:	Alluvial sands/gravels with a fine earth texture of clayey silt.
Patterned ground:	Nonsorted circles.
Permafrost:	> 47 cm depth.
Hydrology:	Very wet, slope near lake.

Profile 10a (apex)

Depth (cm)	Horizon	Description
0 - 01	Ai	Loamy silt with 10% fine gravels, olive brown (2,5Y4/3), massive structure.
01 - 22	AC	Silty sand with 25% medium gravels, light olive brown (2.5Y5/3), single grain structure.
22 - 38	C1	Medium sand with 50% medium gravels, greyish brown (2.5Y5/2).
38 - 47	C2	Medium sand with 75% coarse gravels, light brownish grey (2,5Y6/2).
> 47	Cf	Permafrost boundary.

Profile 10b (trough)

0 - 04	A	Clayey silt (tU) with 25% medium gravels and 5% stones, dark olive brown (2.5Y3/3), massive structure.
04 - 20	AC	Loamy silt (lU) with 25% coarse gravels and 10% stones, light olive brown (2.5Y5/3).

The *Severnaya Zemlya Archipelago* is located between Kara Sea and Laptev Sea and represents the arctic desert region. The northern investigation area is located on Bolshevik Island near Lake Trovdoja (79°N, 101°E). Severnaya Zemlya is characterized by a marine arctic climate (the mean July temperature is 3°C and the mean annual air temperature is -13°C. The mean summer precipitation does not exceed 60 mm (Mikhaylov 1960)). The soils are rather virgin arctic desert soils, weakly differentiated cryosols, including wet and organic-rich soils. Site 10 (Table 2) is a typical soil profile of the Severnaya Zemlya region. Patterned ground structures are weakly sorted and nonsorted circles, polygons and nets; typical vegetation are mosses and lichens.

METHODS

Methods of soil mapping and site description are described in Pfeiffer *et al.* (1996).
Total organic carbon (TOC) is determined using a C-H-N-analyzer (Heraeus Company), dissolved organic carbon (DOC) is determined using a DOC-analyzer (Ströhlein Company).

SOM is fractionated by density (Beudert 1988). Four fractions with different densities are separated by mixing up soil with a solution of water and sodium-polytungstenate ([$Na_6H_2W_{12}O_{40}$] x H_2O) of defined density, followed by centrifugation and filtration.

The separated fractions are:
→ not or weakly decomposed organic matter with a density of < 1.6 g/cm³,
→ fine, decomposed organic material and micro-aggregates with a density of 1.6-2.0g/cm³,
→ complexes of organic matter and mineral soil with a density of 2.0-2.4 g/cm³ and
→ mineral soil with a density of > 2.4g/cm³.

δ^{13}C-samples from plants, SOM and the different fractions are prepared by converting TOC to CO_2 in a special vacuum combustion line and measuring δ^{13}C with a ratio isotope mass spectrometer MAT 250 (Finnigan Company), using a CO_2-lab-standard calibrated against *Pee De Belemnitella americana*, Cretaceous formation (PDB). Standard deviation is 0.1-0.4 ‰. The δ^{13}C-value is defined as

$$\delta^{13}C = \frac{(^{13}C/^{12}C)_{sample} - (^{13}C/^{12}C)_{PDB}}{(^{13}C/^{12}C)_{PDB}} * 1000 \text{ [‰ PDB]}$$

RESULTS

The soil formed in the patterned ground of Lake Labaz is a Cryosol of the typical hummock tundra with moderate gleying, developed in cryoturbated loamy sediments (nonacid Pergelic Cryaquept with pH (CaCl₂) about 5.2). The TOC is about 2 % and 0.2 % total nitrogen. In the trough part of the patterned ground, thick organic material is accumulated (Pergelic Cryofibrist).
The presented site from Lake Labaz shows a distinct difference in the carbon accumulation in the

apex (site 3a) and trough (site 3b) part of the patterned ground. The carbon content is significantly higher in the trough, where about 35% organic carbon is accumulated in the O-horizons than in the apex with 2-5 %. In mineral horizons with similar C-contents the composition of TOC is nearly the same, as well in different depths as in trough and apex parts of the patterned ground: C contents of the single fractions are rising from the heavy to the light fractions, light fractions have much higher C-contents than heavy fractions (table 3).

Table 3. Nitrogen and carbon contents of SOM and different density fractions [w/w %].

Site 3a horizon	Depth [cm]	Bulk soil TOC [%]	Bulk soil N-t [%]	Density < 1.6 g/cm³ C [%]	Density 1.6-2.0 g/cm³ C [%]	Density 2.0-2.4 g/cm³ C [%]	Density >2,4g/cm³ C [%]
A	0 - 5	4.8	0.3	27.7	8.7	1.3	0.1
Cg2	8 -30	2.1	0.2	31.7	10.1	1.5	0.1
	30 - 44	2.4	0,2	35.5	13.5	1.6	0.1
Cg3	44 - 50	4.0	0.3	27.9	13.9	1.2	0.2
Site 3b							
Oe	0 - 17	33.6	1.7	13.4	20.7	10.0	0.6
ACg	17 - 27	3.8	0.3	34.2	11.9	1.3	0.1

The quantity of fractions are rising from light weight to heavy fractions. So every single fraction contents about 1/3 of TOC in every depth. The only exception can be seen in the upper part of the C2-horizon of site 3a, where the light fraction only contents about 20% of TOC (Fig.2).

In the surface horizons with higher C-contents (A horizon of site 3a, Oe horizon of site 3b) the quantity of the light fraction is much higher than in the deeper horizons, so this fraction contents more than 50% of TOC in the surface layers.

At Lake Labaz site the δ^{13}C-analysis of TOC shows a slight discrimination of the heavier ^{13}C-carbon in the SOM (mean δ^{13}C: -25.8 ‰) of about 3‰ in com-parison to the carbon source of the plants (mean δ^{13}C: -29.1 ‰. compare Fig. 3a,b). The heavy carbon isotope ^{13}C is especially enriched in a depth of 5-20 cm below ground. The heavy fractions are enriched in ^{13}C.

No difference was found between apex and trough of the patterned ground, neither concerning TOC nor concerning single fractions of SOM.

The nonsorted circle site 10 from Severnaya Zemlya represents a weakly developed Cryosol (clayey-skeletal, mixed, nonacid Pergelic Cryaquept). It has organic carbon contents of about 1.25% in the apex area (site 10a) and 6.96% in the trough (site 10b, compare Fig.4). The δ^{13}C of the mosses and lichens have an average value of about -23.50 ‰ and of the vascular plants *Carex* and *Papaver* of about -27.2 ‰. The δ^{13}C-carbon in the SOM range about -24.54 ‰.

DISCUSSION

The slight enrichment of ^{13}C in the soil of Lake Labaz could be considered as a result of the restricted carbon turnover and decomposition of organic matter under subarctic conditions. δ^{13}C-values of SOM correspond to δ^{13}C-values of SOM of other tussock tundra soils of Alaska with δ^{13}C of about -25.7 ‰ (Ping *et al.* 1996).

The high quantity of the weakly decomposed, light fraction in the surface layers of trough and apex parts can be explained as result of the permanent input of fresh and undecomposed plant material. The litter input for site 3 at Lake Labaz is about 30-50 g/m²*year (Gundelwein *et al.* 1997). In the deeper horizons the SOM is mixed by cryoturbation. Microbial activity and decay of SOM are low. Soil temperatures at site 3 in summer is nearly 15°C in the upper layer, 5°C in 10 cm depth and nearly 0°C in 30 cm depth (Sommerkorn 1995). The lower decomposition rate in deeper horizons will be caused by lower soil temperatures (Swift *et al.* 1979). These results correspond with studies of the degree of humification of SOM in arctic environments. Grishina and Todorova (1970) found high portions of fulvic acids in different soils of the Taimyr Peninsula as an expression of low decomposition activity in these arctic soils.

δ^{13}C-values of SOM-fractions often increases with the degree of humification, caused by an enrichment of the heavier ^{13}C during decomposition (Fig. 3a,b). It is well known that ^{13}C content of SOM increases during aerobic (Balesdent and Mariotti 1996) and especially during anaerobic decomposition processes, which are dominated by methanogenesis (while ^{13}C contents of methane are depleated in comparison to the origin SOM (Agren *et al.* 1996, Quay *et al.* 1988, Sugimoto and Wada 1993)). For those processes the δ^{13}C-value of SOM is a useful parameter to characterize the anaerobic carbon turnover (Pfeiffer 1994). The wet soils of polygon tundra show high methane emission rates of about 120 mg CH_4*m^{-2}*d^{-1} (Sommerkorn *et al.* 1997, Samarkin *et al.* 1997). Methanogenesis takes place in a depth of 5-20 cm, where the water- and temperature regime is favored for CH_4 producing microbes. This is expressed in an enrichment of ^{13}C of TOC and a smaller quantity of the light fraction in this depth. An enrichment of ^{13}C in carbon fractions of water-saturated horizons as a result of methanogenesis was also obeserved in SOM studies in Alaska (Ping *et al.* 1996). A weak enrichment of ^{13}C near permafrost boundary could be interpreted as a relict horizon in which methanogenesis took place in the past or an accumulation of leached, water soluble products of recent methanogenesis.

The SOM accumulation at the arctic site of Severnaya Zemlya (site 10) is dominated in the initial Ai-horizon by mosses and lichens. These plants are more enriched in ^{13}C (mean -23.5‰) than the vascular plants (*Carex, Papaver:* mean -27.2‰) of this site.

The organic matter of the AC-horizon has ^{13}C-values of about -24.8 ‰, which can be considered as dominated by the roots of the vascular plants and represents a mixture of mosses/lichens and vascular plant carbon.

The very weak shift to a heavier ^{13}C-values of SOM on the top of the permafrost layer can be explained by leachate of soluble organic compounds, mostly of the mosses and lichens. The main soluble C-compounds under arctic conditions are fulvic acids (Mikhaylov 1960, Chugunova 1979), which are closer in ^{13}C-value to the plant carbon source (Nissenbaum and Schallinger 1974).

So the very weak ^{13}C-discrimination at Severnaya Zemlya islikely the result of C input of different plant material with different ^{13}C enrichments and as the effect of leached soluble organic compounds of the lichens and mosses rather than as a result of C decomposition processes at this arctic site.

Stable carbon isotope values as well as density C fractions are useful parameters to determine the decomposition processes in permafrost-affected soils in arctic and subarctic environments. More investigations of TOC and single fractions of TOC, accompanying stable isotope measurements, are necessary to explain the C turnover in permafrost soils.

[14]C dating of the different fractions would be valuable to calculate the residence time of SOM and their fractions.

ACKNOWLEDGEMENTS

REFERENCES

Agren, G.I., E. Bosatta and J. Balesdent. 1996. Isotope discrimination during decomposition of organic matter: a theoretical analysis. Soil Sci. Soc. Am. J. 60:1121-1126.

Balesdent, J. and A. Mariotti. 1996. Measurement of soil organic matter turnover using ^{13}C natural abundance. p. 83-111. In: T.W. Boutton and S.Yamasaki (ed.) Mass spectrometry of soils. Marcel Dekker, New York.

Beudert, G. 1988. Morphologische, naßchemische und 13C-NMR-spektroskopische Kennzeichnung der organischen Substanz von Waldhumusprofilen nach Dichtefraktionierung. Bayreuther Bodenkundliche Berichte 9. Lehrstuhl Bodenkunde, Bayreuth (in German).

Chugunova, M.V. 1979. Some chemical properties of soils of Mys Chelyuskin. The arctic tundra and polar deserts of Taymyr.: 74-77. Leningrad (in Russian).

Grishina, L.A. and N.I. Todorova. 1970. Composition of soil organic matter of tundra soils on Taimyr Peninsula. Vetsnik MGU, Ser.6 (3):80-85 (in Russian).

Gundelwein, A., H. Becker and E.-M. Pfeiffer. 1997. Production and decomposition of organic matter in a subarctic tundra at Taimyr Peninsula/Northern Siberia. Pedobiologia (in press).

Mikhaylov, S. 1960. Some features of the sod arctic soils on Bolshevik Island. Soviet Soil Science: 649-652 (in English).

Nissenbaum, A. and K.M. Schallinger. 1974. The distribution of stable carbon isotopes (^{13}C/^{12}C) in fractions of soil organic matter. Geoderma 11:137-145.

Pfeiffer,E.-M. 1994. Methane fluxes in natural wetlands (marsh and moor) in northern Germany. Current Topics in Wetland Biogeochemistry, Vol. 1:36-47.

Pfeiffer, E.-M, A. Gundelwein, T. Nöthen, H. Becker and G. Guggenberger. 1996. Characterization of the organic matter in permafrost soils and sediments of theTaymyr Peninsula/Siberia and Severnaya Zemlya/Arctic Region. p.46-83. In H.-W. Hubberten (ed.) Russian-German cooperation: The expedition Taymyr 1995 and the expedition Kolyma 1995 of the ISSP Pushchino group. Polar Research 211. Alfred-Wegener-Institut, Bremerhaven.

Ping, C.L, G.J. Michaelson, A. Cherkinsky and R.L. Malcolm. 1996. Characterization of soil organic matter by stable isotopes and radiocarbon ages of selected soils in Arctic Alaska. Proceedings of the 8th Meeting of the International humic SubstancesSociety, September 9-14, Wroclaw, Poland (in press).

Post, W.M., W.R. Emanuel; P. J. Zinke and A.G. Stangenberger. 1982. Soil carbon pools and world life zones. Nature 298:156-159.

Quay, P.D., S.L. King, J.M. Lansdown and D.O. Wilbur. 1988. Isotopic composition of methane released from wetlands: Implications for the increase in atmospheric methane. Global Biogeochem. Cycles 2:385-397.

Samarkin,V.A., A. Gundelwein and E.-M. Pfeiffer. 1997. Studies of methane production and emission in relation to the microrelief of a polygonal tundra in Northern Siberia. Polarforschung (in press).

Sommerkorn, M. 1995. Microbial communities and carbon turnover in the Tundra.p.41-52. In C. Siegert and D. Bolshiyanov (ed.) Russian-German cooperation: The expedition Taymyr 1994. Polar Research 175. Alfred-Wegener-Institut, Bremerhaven.

Sommerkorn, M., A. Gundelwein, E.-M. Pfeiffer and M. Bölter. 1997. Carbon dioxide and methane fluxes from an arctic tundra in North Siberia. Polarforschung (in press).

Sugimoto,A. and E. Wada. 1993. Carbon isotopic composition of bacterial methane in a soil incubation experiment: Contributions of acetate and CO_2/H_2. Geochimica et Cosmochimica Acta 57:4015-4027.

Swift, M.J., O.W. Heal and J.M. Anderson. 1979. Decomposition in terrestrial ecosystems. In P.J. Anderson, P. Greig-Smith and F.A. Pitelka (ed.) Studies in ecology. Vol.5. Blackwell Scientific Publ. London.

Washburn,A.L. 1979. Permafrost features as evidence of climatic change. Science Review 15:327-402.

Humus Formation in Forest Frozen Soils
in the Barkal Region

B.M. KLENOV[1]

ABSTRACT

High accumulation of organic matter and calcium salts of humic asids in humus horizons of the soils of the Baikal area is related to calcareous nature of bedrocks and weak removal of plant decomposition and humification products. The humate-fulvate type of humus is a consequence of low-intensity weathering of parent rock. On the whole, the nature of humic asids of frozen soils of the Baikal Region is regionally specific, but their structural principles are characteristic of soil humic acids in general.

Key words: Humus composition, humus horizon, humic asids, fulvic asids, frozen soils, elementary composition, decomposition.

INTRODUCTION

The organic matter of the soils of the Baikal area, its northern part especially, has been studied insufficiently; there are only data concerning total organic matter content. As for fundamental investigations of humus , the data are rare. Because humus composition and and its nature can elucidate more clearly soil genesis and fertility, it is very important in the regions, especially with respect to agriculture.

The present paper deals with the data that show some specific features of humus and humic acids in the soils of the northern part of the Baikal Area. The material under investigation has been sampled in the northern part of Irkutsk Region and Buryat Republic.

BACKGROUND

Soil cover of the territory under question is primarily represented by sod-calcareous soils. The soils are most commonly sod-calcareopus leached and typical calcareous heavily textured. These soils are formed on various reliefs under the canopy of dark-coniferous and small-leaved forests and more rarely under meadow and steppe herbs. Parent materials are sandy loamy and loamy alluvium and eluvio-deluvium forming from calcareous shist rocks of different colors.

Typical and leached sod-calcareous soils vary to a small extent. The specific feature of typical soils implies that carbonates occur in the surface (up to 20% of calcium carbonate). As for the leached soils, the calcareous material is concentrated in the illuvio-calcareous horizon, presumably within the limits of the second half-meter layer. Sod-calcareous soils are characterized by high base saturation, i.e., from 20 to 50 meq per 100 g soil. The reaction of typical soils is weakly alkaline in the upper profile and obviously alkaline in the lower profile. As for the leached soils , it is close to neutral in the upper profile and weakly alkaline in the remaining part of the soil profile.

The thickness of the humus horizon in sod-calcareous soils ranges from 20 to 30 cm, more rarely to 45 cm; its color is most commonly dark-grey or dark-grey with reddish hue. The structure in virgin variants is crumby-granular or small-nutty, that in the ploughed variants is large-blocky or blocky. According to present classification (Orlov and Grishina 1981), these soils are high in humus (6-10%) and medium in humus (4-6 %).

Humus formation has been going on here under the influence of a strongly continental climate. Mean annual air temperature is -4^0 C, mean annual precipitation is within 400 mm, which mostly falls in the second half of the growing season. The duration of the growing season is 90-110 days. The sum of positive temperatures (higher than $+10$ C^0) is only equal to 1300-1600 ^{0}C during the growing season. Thanks to low winter temperatures and shallow snow covers, the soils freeze to 2 m or more; then they thaw slowly. On the whole, the area under study is situated within the limits of the southern border of spreading of permafrost. Against this background of severe hydrothermal conditions, the area is notable for poor floristic composition of herbaceous species, which is the main source of humus. Continuous areas of light-coniferous taiga with herb-green moss and herb-clusterberry associations are prevalent here. Deforested areas with meadow herbs are small. Short periods of active soil formation and poor plant litter lead to slow rates of humus formation; under such conditions, humus accumulation should not take place. However soils are rich in humus. Because of prolonged periods of seasonal frost and occurence of permafrost, the removal of plant decomposition and humification products from the soil profile is restricted. Moreover, due to high reaction capacity, decomposition products can be fixed by soil minerals, where calcium is of crucial importance.

METHODS AND MATERIALS

Humus content was determined by generally accepted wet combustion method, nitrogen by Kjeldahl method. Humus composition was determined by Tyurin' s method as modified by Ponomareva and Plotnikova (1980). According to this technique, the substances are extracted as follows: bitumen, humic acids (HA), fulvic acids (FA) and insoluble in reagents residue. Among HA and FA fractions, combined with Ca and combined with hydrooxides of sesquioxides forms are estimated. This paper only deals with total sum of these acids.Elementary composition analysis has been carried out for prevalent HA alkaline-extracted after soil decalcification with dilute sulphuric acid in the course of investigation of humus composition. Elementary composition of HA was assessed by gas-chromatographic method by means of apparatus CHN-1 (Czechoslovakia), light absorption has been investigated by apparatus UV-Vis Specord (Germany).

RESULTS AND DISCUSSION

As shown in Table 1, the highest humus content is characteristic of virgin soils developed under meadow associations (profile 86); the least humus content is under forest canopy (profile 156). Arable soils vary in humus content depending on the degree of their utilization. On the whole, the humus content is closely related to conditions of humus formation, i.e., to restricted removal of humus substances from soil profile in this case, as well as to soil physico-chemical properties and soil texture. In particular, more heavily-textured soils and soils rich in exchangeable cations stand out because they have the highest humus content.

All the soils under question have a very low nitrogen supply, which depends on humus content and type of vegetation. The C:N ratio is as a rule, 13-18, which conceivably might be due to low participation of leguminous plants in the formation of soil organic matter. This fact may reflect on the nature of humic acids per se. Specifically, the C:N ratio of humic acids (HA) in the studied soils varies within the same limits (Table 2).

Bitumen in the soils under consideration are found in small quantities (4-8%) and are characteristic of automorphic soil types.

The greater part of humus is represented by HA and FA. According to the generally accepted classification (Orlov and Grishina 1981), the humus is a humate-fulvate type because HA is prevalent; $C_{HA}:C_{FA}$ ratio ranges generally within the limits 1.0-0.5. One should note that most of the HA and FA (at about 60-80%) is extracted from the soil only after decalcification.

As for content of insoluble residue (humin), its distribution within the limits of the soil profile and among soils shows no regularity and seems to be dependent on the content of substances of humin and non-humin nature (lignified semidecomposed plant debris) as it was shown elsewhere (Klenov 1981).

As shown in the soils under investigation, FA are dominant in the humus composition. One might expect under such conditions as neutral or weakly alkaline reactions and calcareous parent materials the prevalence of HA as for example in chernozems and rendzinas. In boreal forests of the Baikal Region it does not take place probably because of the percolating water regime, when formed HA are split into FA. Moreover, calcareous parent material is noted here for the availability of highly dispersed clayey particles of silicate group minerals and less

Table 1. Humus content and composition of sod-calcareous soils.

Horizon, depth, cm	Humus, %	C:N	Bitumen	HA	FA	Residue	$C_{HA}{:}C_{FA}$
			Humus composition, per cent of total organic carbon				
Profile 86. Sod-calcareous leached soil. Grassy-gramineous meadow							
Asod 0-10	13.51	18	5.1	25.2	45.4	24.3	0.5
A1 10-20	5.60	18	3.2	31.8	45.6	19.4	0.7
A1 25-35	4.22	14	5.3	34.9	33.8	26.0	1.0
Profile 156. Sod-calcareous leached soil. Pine grassy-small shrubby forest							
A1 5-10	4.49	16	4.6	20.1	33.9	41.4	0.6
Profile 160. Sod-calcareous leached soil. Lea							
Aplow 0-10	2.01	13	5.7	24.3	37.4	32.6	0.6
"	2.05	13	7.6	31.2	39.4	21.5	0.8
Profile 51. Sod-calcareous leached soil. Ploughland, oat							
Aplow 0-20	6.98	13	2.3	36.1	42.0	19.6	0.8
"	6.06	14	7.6	28.0	34.1	30.3	0.8
Profile 149. Sod-calcareous typical soil. Ploughland, barley							
Aplow 0-20	1.79	14	1.4	30.4	42.5	25.7	0.7

Table 2. Elementary composition and optical properties of humic acids.

Horizon, depth, cm	C	H	N	O	C:H*	C:N*	$D_4{:}D_6$ HA	$D_4{:}D_6$ FA
Profile 86								
Asod 0-10	44.70	4.97	3.89	46.44	0.75	13.40	3.1	4.3
A1 10-20	43.40	4.32	2.70	49.58	0.84	18.75	3.3	4.3
A1 25-35	47.45	4.13	3.01	45.41	0.96	13.40	3.2	4.0
Profile 156								
A1 5-10	53.29	6.33	4.58	35.80	0.70	13.57	3.0	4.0
Profile 160								
Aplow 0-10	46.06	4.86	3.58	45.49	0.79	15.01	3.0	4.7
" 10-20	52.05	5.97	5.03	36.95	0.73	12.07	3.5	4.5
Profile 51								
Aplow 0-20	48.27	4.60	3.50	43.63	0.88	16.08	3.1	4.0
A1 20-25	49.21	4.41	3.70	42.68	0.93	15.51	3.5	4.5
Profile 149								
Aplow 0-20	48.46	5.30	4.04	42.20	0.77	13.99	3.3	4.0

* atomic ratio

soluble dolomite , which is resistant to weathering, compared to calcite (Koposov 1979). Clayey admixtures reduce the solubility of $CaCO_3$; therefore HA and FA which are formed here in large quantities are not neutralized to a degree as in chernozems or rendzinas (Kononova 1963, Jacquin et al 1980).

While studying the nature of HA, the characteristics such as elementary compositin and optical properties may be of much current interest. Literature data indicate that elementary composition of HA and FA depends on factors that have not yet been clarified completely. As for HA , their elementary composition varies within the limits: C 50-60%, H 3-6%, N 1.7-5% and O 31-39%. In the soils under investigation these limits are mainly wider for C and O and narrower for H and N. The atomic ratios of C:H are 0.7-1.0. These are more typical of FA, which are known to be less carbonized and less aromatic as compared to FA. The low degree of condensation of the aromatic nucleus is supported by $D_4:D_6$, i.e., by ratios of optical density indices and wavelengths of 465 and 665 millimicrons respectively. By optical properties, HA resembles most commonly FA. It should be noted that the data of Table 2 concern HA and FA as extracted from decalcified soil samples. Directly extractable (without preliminary decalcification) forms of HA have C:H atomic ratios of 0.5-0.7 or H:C ratios (recently accepted in the literature) that are much higher than 1, which is evidence of the predomonance of aliphatic structure in molecules of these compounds.

CONCLUSIONS

The indices of humus status in soils of the northern part of the Baikal Region are in compliance with its bioclimatic features: a short-term period of biological activity , seasonal and permanent frost and sufficient moisture constitute significant hinderances to removal of products of organic matter decomposition and lead to accumulation of humus, which is , however, of a very simple nature, i.e., its condensation is low. The low content of nitrogen in organic matter is due in our opinion to the low number of leguminous species in the vegetation. Our data show that under prolonged agriculture , the main humus characteristics, such as $C_{HA}:C_{FA}$ ratio, are left practically unchanged, which bears witness to conservation of general trends in soil-forming processes.

REFERENCES

Jacquin F., C.Haidouti, J.C.Muller. 1980. Dynamique de la materiel organique
en sols carbonates cultives. Bull. Assn. Trans Etude Sol 1:27-36.
Klenov B.M. 1981. Humus of soils of Western Siberia. "Nauka" Publ. House,
Moscow. 144 p. (In Russian).
Kononova M.M. 1963. Soil organic matter. USSR Ac. Sc. Publ. House,
Moscow. 314 p. (In Russian).
Koposov G.F. 1979. Sod-calcareous soils of the Baikal Area. In book: Soils of
BAM Area. "Nauka" Publ. House: 60-68. (In Russian).
Orlov D.S, L.A.Grishina. 1981. Handbook in humus biochemistry. Moscow
Univ. Publ. House. 270 p. (In Russian).
Ponomareva V.V., T.A.Plotnikova.1980 Humus and soil formation. "Nauka" Publ. House, Leningrad. 222 p. (In Russian

Exchangeable Cations and Composition of Organic Matter in Soils as Affected by Acidification and Freezing

T. POLUBESOVA[1] AND L. SHIRSHOVA[2]

ABSTRACT

The combined effect of acidification and freezing on chemical properties of seasonally frozen soils of Russia (Cryaquept, Cryaquent, Ferrod, Orthod and Argiboroll) has been studied in laboratory experiments. Soil acidity was artificially decreased and subsamples were stored at $-12°C$ and at $+9°C$. Soil organic matter was fractionated using ion-exchange resins and content of exchangeable Ca^{2+}, Mg^{2+}, Na^+, K^+, H^+ and Al^{3+} were measured. Freezing has a strong impact on the exchangeable cation content. Combined acidification and freezing led to significant changes in the content of all exchangeable cations. Fraction composition of the humic substances of acidified and frozen samples in most cases is similar to that of the untreated samples. We think the variations in the surface properties under acidification and freezing are a result of modification of the surfaces of soil particles caused by changes in their microstructure.

Key words: Freezing, acidification, exchangeable cation content, pH, fraction composition of soil organic matter.

INTRODUCTION

Both acidification and cyclic freezing and thawing are common in northern soils. Acidification alter soil pH, content of exchangeable cations and composition of soil organic matter (James and Riha 1989, Lindsay and Walthall 1989, Ulrich et al. 1980, Zhang et al. 1991).

Soil acidification had been examined in detail in studies in which soil samples were treated with synthetic solutions. Strong acid treatments with solutions having pH between 2 and 3 caused a decrease in exchangeable calcium and magnesium and an increase in concentrations of these cations in soil solution (Clayton et al. 1991, Li et al. 1988, Susser and Schwertmann 1991, Vance and David 1989). An increase in exchangeable aluminum content has also been reported (Lilieholm and Feagely 1988, Natscher and Schwertmann 1991, Rampazzo and Blum 1992).

Strong acidification results in leaching of fulvic acids, an increase in soil organic matter solubility, and higher stability of humic acids because of coagulation of colloids in solutions (Chertov and Menshikova 1983). Shirshova (1991) observed high aggregation of humic acids at pH between 4 and 5. Acidification caused changes in the ratio of the hydrophyllic and hydrophobic components of dissolved organic compounds (Vance and David 1989).

Data on the effects of freezing and thawing on the ratios of exchangeable cations and on soil pH are scarce. It has been found that long-term freezing causes a decrease exchangeable Ca^{2+} in an Argiboroll and an increase in exchangeable Ca^{2+} and Mg^{2+} in a Haplustoll (Polubesova et al. 1994). Freezing-thawing cycles in Spodosol decreased soil pH (Savel'eva 1984).

To our knowledge, the combined effect of acidification and freezing on soil chemical properties has not been studied for soils. Such an effect has been observed in studies of minerals. Dispersion of quartz due to cyclic freezing and thawing enhanced by preliminary acidification of the pore solution (Konishchev and Rogov 1992). An increase in solubility was found for minerals subject to the combined action of acidification and cyclic freezing-thawing (Martynenko et al. 1992).

The objectives of this work were a) to assess effects of acidification and long-term freezing on the contents of exchangeable cations and on the composition of soil organic matter, and b) to test the

hypothesis that the combined action of acidification and long-term freezing may modify the effects of each of those factors.

MATERIALS AND METHODS

Soil samples were collected from the upper horizons of soils that had experienced seasonal freeze-thaw cycles. The list of soils included a Cryaquept (Khallerchin Tundra), a Cryaquent (Kolyma Lowland), a Ferrod (Kolsky Peninsula), Orthods from arable land and from the pine forest (Leningrad region), and an Argiboroll from arable land (Vladimir region), all in Russia.

Soil samples were air dried, sieved and fractions 1 mm and smaller were used. Selected data on soil properties are summarized in Table 1. Particle size distribution was determined using the hydrometer method applied to samples subject to sodium pyrophosphate dispersion (Gee and Bauder 1986). Organic carbon content was determined by the dichromate oxidation technique (Nelson and Sommers 1982). Content of noncrystalline aluminum and iron forms were determined by oxalate extraction (McKeague and Day 1966).

To acidify a soil, 2.5 L of 0.001M HCl were added to 0.5 kg of the soil. The suspension was mixed by an electric stirrer for 0.5 hour and then allowed to settle for 20 min. pH was measured in the supernatant. One or two such treatments (depending on the soil) caused pH to decrease by 1 ± 0.1.

To assess an effect of acidification on soil properties, 0.25kg of soil, acidified as explained above, was placed in plastic bag and stored at of $+9°C$ for 2 months. To assess the effect of long-term freezing on soil properties, distilled water was added to air-dried soil samples in the ratio of 1:4, and samples were kept at $-12°C$ in a refrigerator for 2 months. To assess the combined effect of acidification and freezing on soil properties, 0.25 kg of soil, acidified as explained above, was placed in a plastic bag and stored in the refrigerator at $-12°C$ for 2 months.

Soil moisture content was calculated from the weight loss of air-dried soil after oven drying for 24 h at 105°C. Soil pH was measured in 1:2.5 soil-water and in soil-1M KCl suspensions with an ion-selective electrode. Content of exchangeable Ca^{2+}, Mg^{2+}, Na^+, and K^+ were determined in 10 sequential extractions with 1M CH_3COONH_4 at 1:4 soil-solution ratio. Content of Ca^{2+} and Mg^{2+} in extracts were determined by complexometric titration with EDTA disodium salt. Content of Na^+ and K^+ were determined using flame photometry. To determine the sum of the exchangeable H^+ and Al^{3+}, 250 mL of 1M KCl solution were added to 100-g soil samples. After 1 h of shaking, the suspensions were filtered through paper filters and 50 mL portions of filtrates were boiled for 5 minutes, then titrated with 0.02 M NaOH solution. The sum of the exchangeable H^+ and Al^{3+} content was estimated from the titration. Exchangeable H^+ content was determined by titration of a duplicate 50-mL portion of filtrate, in which Al was complexed by the addition of the 3mL of 3.5 % NaF.

The humic substance were obtained by sequential extractions (Shirshova and Khomutova 1992) as follows: (1) isolation of HS-1 fraction by resin with sulphogroups in Na^+ form in distilled water, (2) extraction of the HS-2 fraction by carboxylic resin in distilled water, and (3) extraction of the HS-3 fraction with 0.1M NaOH.The amount of humic substances in each fraction was determined from the carbon content by dichromate oxidation (Nelson and Sommers 1982).

All measurements were done in triplicate. Statistical significance of the difference between two means was tested using a t-test with a 0.05 significance level.

Table 1. Selected physical and chemical properties of the soil studied.

Soil	Horizon and depth, cm	Particle	composition %	C_{org} %	Fe_2O_3 %	Al_2O_3 %
		<0.01 mm	<0.001 mm			
Cryaquept	Ae, 0-2	88.88	3.52	14.50	1.087	0.945
Cryaquept	Bh, 7-10	95.24	1.96	1.19	1.430	0.867
Cryaquept	Bo, 15-35	94.52	4.08	0.62	1.888	0.862
Cryaquent	AB, 0-20	74.48	6.48	1.70	2.288	1.040
Ferrod	Boh, 7-15	95.92	1.44	0.34	1.201	1.134
Orthod (arable)	Ap, 0-10	85.84	2.52	2.25	0.515	0.567
Orthod (forest)	A1, 10-20	87.24	2.16	2.32	0.505	0.520
Argiboroll	B, 27-35	65.68	17.36	0.62	0.744	0.662

RESULTS
Untreated soils.

Untreated soils differ among samples in exchangeable cation concentration, pH and composition of organic matter as shown in Fig.1 and Table 2. The fraction HS-3, extracted with 0.1M NaOH, was the main fraction in Cryaquent and in Orthod soils. In the Argiboroll, the dominant component of the organic matter was the HS-2, and most of the organic matter was extracted with resins in fractions HS-1 and HS-2 (Table 2).
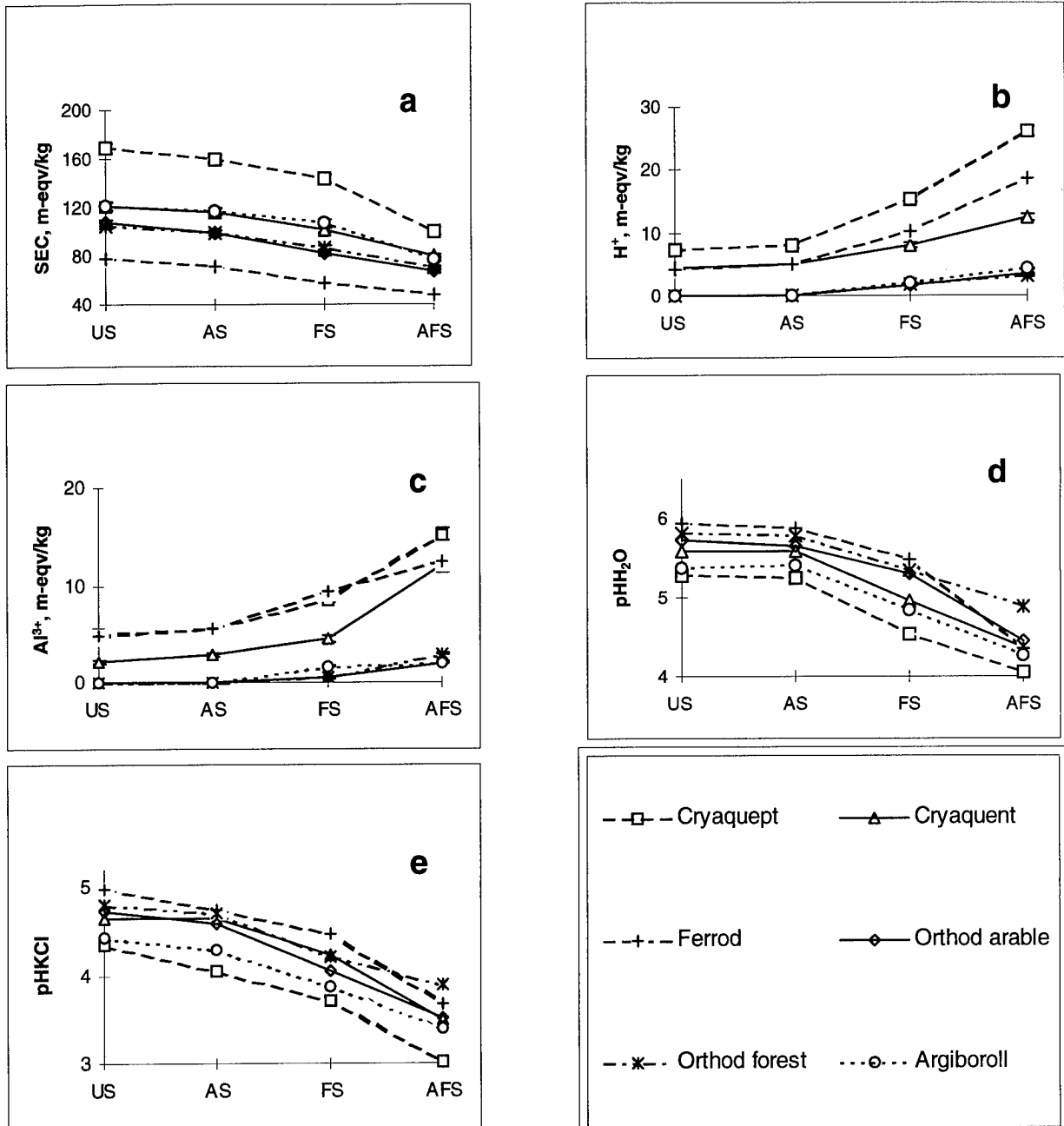
Fig 1. Effects of acidification, freezing, and their combined impact on: (a) - the sum of exchangeable Ca^{2+}, Mg^{2+}, Na^+, K^+ (SEC), (b) - exchangeable H^+ content, (c) - exchangeable Al^{3+} content, (d) - pHH_2O and (e) - pHKCl.

US - untreated, AS - acidified samples, FS - frozen samples, AFS - acidified and frozen samples.

Table 2. Effects of acidification, freezing , and their combined impact on the fraction composition of the soil humic substances.

Sample	Organic carbon content in HS fractions: (kg/kg×10⁻²)			
	HS-1	HS-2	HS-3	Sum of the fractions
	Cryaquent			
US	0.12±0.0036	0.21±0.0063	0.32±0.0096	0.65±0.0120
AS	0.08±0.0024*	0.26±0.0078*	0.28±0.0084*	0.62±0.0117
FS	0.13±0.0039	0.24±0.0072*	0.30±0.0090	0.67±0.0122
AFS	0.11±0.0033	0.25±0.0075*	0.28±0.0084*	0.64±0.0177
	Orthod (forest), 10-20 cm			
US	0.09±0.0027	0.26±0.0078	0.38±0.0114	0.73±0.0140
AS	0.06±0.0018*	0.26±0.0078	0.38±0.0114	0.69±0.0139
FS	0.08±0.0024*	0.27±0.0081	0.40±0.0120	0.75±0.0167
AFS	0.06±0.0018*	0.27±0.0081	0.39±0.0117	0.72±0.0143
	Argiboroll, 27-35 cm			
US	0.16±0.0048	0.56±0.0168	0.11±0.0033	0.83±0.0178
AS	0.18±0.0054*	0.60±0.0180	0.10±0.0033	0.88±0.0264
FS	0.14±0.0042*	0.51±0.0153	0.08±0.0024*	0.73±0.0219*
AFS	0.16±0.0048	0.57±0.0171	0.10±0.0033	0.83±0.0181

US - untreated samples; AC - acidified samples; FS - frozen samples; AFS - acidified and frozen samples.
* statistically significant changes

Acidification.

The acidification followed by storing soils at +9°C did not have a significant effect on the amounts of exchangeable cations. Statistically significant changes were found only for Na^+ in two upper horizons of the Cryaquept and the Ferrod. The exchangeable Ca^{2+} content decreased 2-5%, and the exchangeable Mg^{2+} content decreased 5-13% in almost all soils studied, with the exception of the samples from upper horizon of the Cryaquept. In the latter, changes in the exchangeable Mg^{2+} content were not observed. The exchangeable K^+ content did not change after acidification, but the exchangeable Na^+ content decreased 7-22%.(Fig.1a)

The exchangeable H^+ and Al^{3+} content and their sum $S(H^+ + Al^{3+})$ increased 19-27% in the Cryaquept, Cryaquent, and Ferrod soils(Fig 1b and c). A statistically significant increase of exchangeable H^+ and of the sum of the exchangeable H^+ and Al^{3+} was found for the Bh and Bo horizons of the Cryaquept and the Ferrod. Acidification did not cause significant changes of exchangeable H+ and Al $^{3+}$ in the Orthod soils. In the Argiboroll, significant increase were obtained for the sum of H^+ and Al^{3+}.

pH(H_2O) of the all acidified soils kept at +9°C did not differ from the pH values of the untreated samples, but the value of pH(KCl) decreased by 0.1-0.3 units (Fig.1 c and d). All changes in pH(KCl) are statistically significant.

The fractionation of acidified soils gave different results for the tundra soils and the forest soils (Table 2). In the Argiboroll, the carbon content in the HS-1 and HS-2 fractions increased 13% and 7%, respectively. The total content of extractable carbon increased 6% in this soil. The opposite effects were observed in the samples of the Cryaquent and the Orthod soil, in which the carbon content of the HS-1 fraction decreased 33%. Carbon content of the HS-3 fraction decreased 13% in Cryaquent samples.

Freezing.

Freezing had a strong impact on the exchangeable cation content (Fig.1 a,b,c). Content of exchangeable Ca^{2+}, Mg^{2+}, and Na^+ decreased 12-30%, 3-21%, and 10-28%, respectively. The exchangeable K^+ content did not change. A drastic increase in exchangeable H^+ and Al^{3+} contents was observed in the Cryaquept, Cryaquent, and Ferrod, in which exchangeable H^+

and Al^{3+} content increase 1.7-2.8 times. The sum of exchangeable H^+ and Al^{3+} increased 2.9-4 times in Orthod and Argiboroll soils.

The direction of changes in the exchangeable H^+ and Al^{3+} was consistent with the soil acidification induced by freezing. $pH(H_2O)$ in the frozen soils decreased by 0.4-0.75 units, and the $pH(KCl)$ decreased by 0.51-0.67 pH units (Fig.1 b,c,d,e)

The carbon in the organic matter fractions was susceptible to freezing. We observed significant 11% and 13% decreases in HS-1 fraction content of the Orthod and the Argiboroll, respectively. The content of the HS-3 fraction was reduced 27% in the Argiboroll.

Joint effect of acidification and freezing.
Acidification with freezing led to large changes in the amounts of all exchangeable cations.(Fig.1 a,b,c). Concentrations of Ca^{2+}, Mg^{2+}, Na^+ decreased 31-42%, 22-44%, and 53-58%, respectively. Concentrations of exchangeable H^+ and Al^{3+} rose in Cryaquept, Cryaquent, and Ferrod 2.9-5.4, 2.5-5.5 and 3.3-7.9 times, respectively. The content of exchangeable H^+ grew to 3.1-3.5 mmolc kg^{-1} in the Orthod and to 4.3 mmolc kg^{-1} in the Argiboroll. The content of exchangeable Al^{3+} increased to 2.0-2.9 mmolc kg^{-1} in Orthods and to 2.0 mmolc kg^{-1} in the Argiboroll.

Two months' freezing of the acidified soils caused a reduction of soil $pH(H_2O)$ by 0.9-1.6 pH units, and the reduction of $pH(KCl)$ by 0.9-1.3 pH units (Fig.1 d,e).

Carbon content of the organic matter fractions was similar to those of the untreated samples (Table 2). A significant decrease was found only in the HS-1 fraction of the Orthod soil (33%), and in the HS-3 fraction of Cryaquent (13%). A significant 19% increase was observed for the HS-2 fraction of Cryaquent.

A significant correlation was found between the sum of exchangeable hydrogen and aluminum $S(H^+ + Al^{3+})$ and $pH(H_2O)$ over all soil samples. The regression equation was $S(H^+ + Al^{3+}) = 11.0378 - 1.9114\ pH(H_2O)$, with $r^2 = 0.84$.

DISCUSSION

The results indicated that freezing and acidification affected the content of exchangeable cations and the pH in the same way in the all soils studied. The magnitude of this effect varied between soils.

The soils that were acidified to reduce soil pH by 1 and stored at +9°C for 2 months restored their original values of pH. The pH range immediately after acidification was 4.2-5.0, and was within the range of the buffer region corresponding to ion exchange reactions and dissolution of soil minerals (Kauppi et al. 1986). Hence, we hypothesized that $pH(H_2O)$ regained initial values due to proton consumption during ion exchange and dissolution of the soil minerals. At the same time, the protons were easily released from the surfaces of the soil particles in presence of 1M KCl, i.e., the bonds between protons and surfaces weakened. The decrease in exchangeable Ca^{2+}, Mg^{2+} and Na^+ was insignificant. These results differ from the results of other authors (Li et al. 1988). The difference is probably a result of the different experimental conditions. Li and coworkers (1988) showed a significant reduction in the exchangeable Ca^{2+} and Mg^{2+} content after treatment of soils with sulphuric acid. This treatment possibly led to a substantial destruction of soil minerals and to changes in the surface properties of the soil particles. In our experiments, the acidification was done once and then the samples were kept for a long time above 0° C. Under these conditions, ion exchange reactions and dissolution of minerals could occur and microorganisms were active. Since products of the reactions were not leached, conditions were favorable for the restoration of the initial exchangeable cation content and pH.

The maximum values of the exchangeable H^+ and Al^{3+} in the initial untreated samples, as well as in the treated frozen and acidified samples were found in the soils with higher amounts of the amorphous hydroxides of aluminum. This can be seen from the comparison of data in Table1 and Fig.1. The trends of increasing exchangeable H^+ and Al^{3+} are consistent with the decrease of the $pH(KCl)$ in the Cryaquent and the Ferrod soils.

The long-term freezing resulted in the significant decreases in $pH(H_2O)$ and $pH(KCl)$ and in large changes in the exchangeable cation content. The cause of these changes could be a modification of the particle surfaces and a formation of new solid-liquid interfaces in the soil due to alterations of the microaggregate structure of the soil particles, as was observed in the structure of the clay minerals (Anderson and Hoekstra 1965, Konishchev 1981).

The reduction in exchangeable Ca^{2+}, Mg^{2+}, and Na^+ contents after long-term freezing is in agreement with data obtained in previous experiments with the Argiboroll (Polubesova et al. 1994). Cyclic seasonal changes in exchangeable Ca^{2+} content were found in a seasonally frozen Argiboroll (Ponizovsky and Polubesova 1991). The content of exchangeable Ca^{2+} decreased over the winter and increased over the summer.

The increase in exchangeable H^+ and Al^{3+} during freezing could be caused by particle surface

modification. Sites containing exchangeable H^+ and Al^{3+} might become more accessible for exchange than sites containing exchangeable Ca^{2+}, Mg^{2+} and Na^+. Hence, it is possible that freezing leads to an increase in the surface variable charge related to functional groups of iron and aluminum hydroxides, and of kaolinite and organic matter (Sposito 1989, 1992).

The direction of changes in organic matter fraction after freezing was opposite to that after acidification. Soils could be subdivided in two groups according to their response to freezing and acidification: the Cryaquent and the Orthod would form one group and Argiboroll would represent another one. The decrease in recovery of humic substances during long-term freezing is consistent with that observed in Udic Argiboroll (Polubesova et al. 1994). This implies that the freezing may have a similar effect on all soils of the same type.

The effect of acidification and freezing together on exchangeable cation content and on soil pH is synergistic. The decrease in exchangeable Ca^{2+}, Mg^{2+}, Na^+ content and the increase in exchangeable H^+ and Al^{3+} is much larger with acidification and freezing together than when the acidification and freezing acted separately. The combined effect led to the decrease of soil pH by 1-1.5 pH units. Samples that were acidified and then frozen maintained a low pH after long-term freezing. Initial values of pH were restored in acidified samples kept at temperatures above 0°C. We conjectured that freezing had reduced the buffer capacity of soils because the ion exchange and mineral dissolution occur to a limited extent at temperatures below 0°C. Consequently, freezing was favorable for keeping soil acidified. A related hypothesis was that freezing modified soil particle surfaces in the acidified sample, as well as in the untreated one and lead to the formation of new interfaces between the solid and liquid phases. Content of exchangeable Ca^{2+}, Mg^{2+}, and Na^+ decreased during freezing following acidification, possibly because of the lower accessibility of the surface sites responsible for their exchange. Conversely, the content of exchangeable H^+ and Al^{3+} could increase below 0°C because of the better accessibility of the surface sites. The exchangeable K^+ content remained unchanged in all treatments. This could be because the K^+ mainly occupied sites in the lattice of clay minerals.

CONCLUSIONS

Our experiments show that chemical compositions of seasonally frozen soils may vary seasonaly. These results suggest also that certain requirements have to be imposed on storing samples of seasonally frozen soils for chemical analysis. Freezing can modify the effects of natural or antropogenic soil acidification. Variations in soil surface properties due to acidification and freezing may be caused by changes in microsctructure. All these hypotheses represent interesting fields to explore.

REFERENCES

Anderson, D.J., and P. Hoekstra. 1965. Migration of interlamellar water during freezing and thawing of Wyoming bentonite. Soil Sci. Soc. Am. Proc. 29:498-504.

Chertov, O.G., and G.P. .Menshikova. 1983. The changes of the Gray Forest soils under the impact of acid rains. Izvestiya Akademii Nauk SSSR. N6:906-914.

Clayton, J.L., D.A. Kennedy, and T. Nagel. 1991. Soil response to acid deposition, Wind River Mountains, Wyoming. 2. Column leaching studies. Soil Sci. Soc. Am. J. 55:1433-1439.

Gee, G.W., and J.W. Bauder. 1986. Particle-size analysis. p. 383-411. In Methods of soil analysis. Part 1. Physical and mineralogical methods. Amer Soc. of Agronomy Inc., Soil Sci. Soc. of America Inc., Madison, Wisconsin.

James, B.R., and S.J. Riha. 1989. Aluminum leaching by mineral acids in forest soils. 1. Nitric-sulfuric acid differences. Soil Sci. Soc. Am. J. 53:259-264.

Kauppi, P., J. Kamari, M. Posch, and E. Matzner. 1986. Acidification of forest soil: model development and application for analyzing impacts of acidic deposition in Europe. Ecological modelling. 33:231-253.

Konishchev, V.N. 1981. Formation of the rocks composition in the cryolithosphera. Nauka Publ., Novosibirsk.

Konishchev, V.N., and V.V. Rogov. 1992. Cryotransformation of the mineral components of soils in different physico-chemical conditions. p. 114-118. In Proceedings of the 1st International Conference on Cryopedology. Pushchino, Russia, November 10-14, 1992. ONTI NCBI Publ., Pushchino.

Li, C.S., J.C. Bockheim , J.E. Leide , and D.A. Wentz. 1988. Potential for buffering of acidic precipitation by mineral weathering in a forested Entisol. Soil Sci. Soc. Am. J. 52:1148-1154.

Lilieholm, B.C., and S.E. Feagely. 1988. Effect of simulated acid rain on soil and leachate acidification of a Lexington silt loam. Soil Sci. 146:44-50.

Lindsay, W.L., and P.M. Walthall. 1989. The solubility of aluminum in soils. p.221-239. In G. Sposito (ed.) The environmental chemistry of aluminum. CRC Press, Boca Raton, Florida.

389

Martynenko, I.A., O.P. Leporsky, S.N. Sedov , V.V. Rogov, and S.A. Shoba. 1992. The study of the cryoweathering of the soil minerals in relation to the formation of the podzolic soils. p. 122 -127. *In* Proceedings of the 1st International Conference on Cryopedology. Pushchino, Russia, November 10-14, 1992. ONTI NCBI Publ., Pushchino.

McKeague, J.A., and J.H.Day. 1966. Dithionite- and oxalate extractable Fe and Al as aids in differentiating various classes of soils. Can. J. Soil Sci. 46:13-22.

Natscher, L., and U. Schwertmann. 1991. Proton buffering in organic horizons of acid forest soils. Geoderma 48, N1-2:93-106.

Nelson, D.W., and L.E. Sommers. 1982. Total carbon, organic carbon and organic matter. p. 539-579. *In* Methods of soil analysis. Part 2. Chemical and microbiological properties. Am. Soc. of Agronomy Inc., Soil Sci. Soc. Am. Inc., Madison, Wisconsin.

Polubesova, T., L.T. Shirshova , M. Lefevfre, and V.A. Romanenkov. 1994. Effect of freezing-thawing on soil and clay surface properties. Pochvovedenie N7:72-78.

Ponizovsky, A.A., and T. Polubesova. 1991. Seasonal variations of the composition of soil solutions and of the surface properties of soil particles in an arable gray forest soil. Soviet Soil Science. 23:35-45.

Rampazzo, N., and W.E.H. Blum. 1992. Changes in chemistry and mineralogy of forest soils by acid rain. Water, Air and Soil Poll. 61:209-220.

Savel'eva, E.M. 1984. The effect of the freezing-thawing on moisture and acid conditions in the agricultural field. Nauchno-technicheskiy bulleten po agronomicheskoi fizike. N58:45.

Shirshova, L.T. 1991. Polidispersity of the humus substances. Nauka Publ., Moscow.

Shirshova, L.T., and T.E. Khomutova. 1994. The response of humic substances to soil acidification and freezing. Environment International. 20:405-410.

Sokolova, T.A. 1993. The chemical fundamentals of the amelioration of acid soils. Moscow State Univ. Publ. Moscow.

Sposito G. 1989. Surface reactions in natural aqueous colloidal systems. Chimia 43:169-176.

Sposito G. 1992. Characterization of particle surface charge. p. 291-314. *In* Buffle, J. and H.P. Leeuwen (ed.) Environmental particles. Lewis Publ., Boca Raton, Florida.

Susser, P., and U. Schwertmann. 1991. Proton buffering in mineral horizons of some acid forest soils. Geoderma N1-2:63-76.

Ulrich, B., R. Mayer , and P.K. Khanna. 1980. Chemical changes due to acid precipitation in loess-derived soil in Central Europe. Soil Sci. 130:193-199.

Vance, G.F., and M.B. David. 1989. Effect of acid treatment on dissolved organic carbon retention by a spodic horizon. Soil Sci. Soc. Am. J. 53:1242-1247.

Zhang, F.S., X.N. Zhang, and T.R. Yu. 1991. Reactions of hydrogen ions with variable charge soils. 1. Mechanisms of reactions. Soil Sci. 151:436-443.

Optimization of Crop Nutrition on Podzolic Soils of the European Northeast

G.YA. ELKINA[1]

ABSTRACT

The study, conducted on seasonally-frozen podzolic soils in the middle taiga subzone, showed positive effect of liming upon humus status of the soils. Following 11 t ha^{-1} of a dolomitic meal application along with organic fertilizers (manure, peat from 100 to 400 t ha^{-1}), humus content in the soils increased from 16.3 to 19.0-24.4 g kg^{-1}, and the humic acid carbon : fulvic acid carbon ratio increased from 0.70 to 0.85-1.31. Application of 4 to 11 t ha^{-1} of a dolomitic meal caused decrease in all forms of the soil acidity; pH (in KCl) values rose from 4.0 to 4.9 (at 4 t ha^{-1}) and to 5.9 (at 11 t ha^{-1}). A ten-year study of changes in the soil acidity and base saturation showed a long-term effect of liming upon the parameters. Inorganic fertilizers were applied following the optimum nutrition method providing for both macro- and micronutrient application. Potato yield increased by 3.6 t ha^{-1} (with 19.8 t ha^{-1} in a control site), and annual grasses showed 22.0 t ha^{-1} increase (with 7.4 t ha^{-1} in a control).

Key words: Liming. fertilization, humus, soil acidity, crop capacity.

INTRODUCTION

Podzolic seasonally frozen soils of the middle taiga subzone in their natural condition have scarcely favorable properties for crop growth. They are characterized by high acidity, low humus content, and fulvic acid predominance in humus composition. Besides, a poor nutrient supply is typical. The amelioration process of these soils is rather prolonged. Raising the humus content, lowering acidity, and providing crops with necessary nutrients are the most important ways of soil fertility optimization.

The effect of lime and organic and inorganic fertilizers on soil properties and crop capacity was studied in the middle taiga subzone at 6-7 km distance from the city of Syktyvkar.

MATERIALS AND METHODS

Field experiments were carried out on a seasonally- frozen loamy podzolic soil with the following agrochemical properties: humus content of 16.3 g kg^{-1}, pH (KCl) of 4.0, sum of exchangable cations of 2.6 cmol kg^{-1} soil, hydrolytic acidity of 6.2 cmol kg^{-1} soil, available phosphorus content of 103 and potassium of 92 mg kg^{-1}, hydrolyzable nitrogen of 27 mg kg^{-1}.

Humus status of the soils was studied in the field experiment providing heavy application of organic fertilizers and dolomitic meal (11 t ha^{-1}). Manure at rates of 100, 200, and 400 t ha^{-1}, peat mold at 200 t ha^{-1}, and a peat-manure mixture containing 200 t ha^{-1} of each component were applied prior to potato planting over two successive years. Humus content (after Turin) and fractional composition of humus (after Ponomareva and Plotnikova) were determined in samples taken after harvesting in the second year. Description of these and other methods are given in "Methods for Agrochemical Research" (1975).

RESULTS AND DISCUSSION

Humus status

Before the trial began, the soil contained as low as 16.3 g kg^{-1} humus, and the humus type was fulvic-humic. Organic fertilizer application and liming improved considerably this soil humus status. Manure application increased humus content to 19.0-24.4 g kg^{-1} proportionately with application rate. The effect of both manure and dolomitic meal application was highest on soils which had high acidity and low base saturation. The most pronounced changes in humus content followed the application of pure peat and a peat-manure mixture. Humus content increased to 32.3 g kg^{-1} and 36.8 g kg^{-1} respectively, and this higher increase was attributed to a more stable organic matter composition in peat compared to manure. Organic fertilizers changed the humus composition due to increased portion of humic acids.

[1] Institute of Biology, Komi Science Center, Ural Branch, Russian Academy of Sciences, 28 Communisticheskaia, Syktyvkar 167610 Russia

The ratio of C (humic acids)/C (fulvic acids) increased from 0.70 to 0.85-1.31. The most significant changes took place where 400 t ha⁻¹ of manure, peat, or peat/manure mixture were added. Among humic acid fractions, that bound with calcium demonstrated the highest increase, from 1.0 to 35.0-88.0 g kg⁻¹. Before the experiment, the soil practically lacked this fraction.

Due to the organic fertilizers an increase in nutrient supply has been achieved. The addition of 100 t ha⁻¹ of manure increased the available phosphorus content by 63 mg kg⁻¹ soil and a 400 t ha⁻¹ rate increased it by 214 mg kg⁻¹, i.e., every 100 t of manure caused an increase of 30 mg kg⁻¹. Available potassium content increased proportionately with the manure rates, by 24-163 mg kg⁻¹. The nitrogen supply also increased. Over the growing period, nitrate nitrogen content varied from 44 to 184 mg kg⁻¹ soil in the plots fertilized with manure. At the same time in the control plots it varied from 21 to 73 mg kg⁻¹.

The ameliorating effect of the organic fertilizers was manifested in crop capacity. Potato yield increased 1.5 to 2.5 times (Fig. 1) due to manure application in the favorable- weather year of
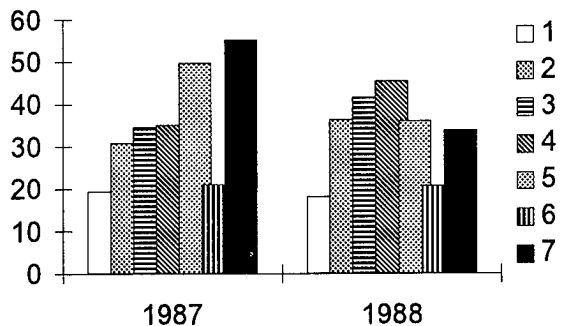
Figure 1.Effect of organic fertilizers upon potato yield. 1, control; 2,3, 100 t ha⁻¹ of manure; 4, 200 t ha⁻¹ of manure; 5, 400 t ha⁻¹ of manure; 6, 200 t ha⁻¹ of peat; 7, 200 t ha⁻¹ of manure and 200 t ha⁻¹ of peat; 1,3,4,5,6,7, 11 t ha⁻¹ of dolomitic meal..

1987. Also, the addition of a peat-manure was efficient. Peat application was ineffective because of its low nutrient content.

Liming and soil acidity

Calcium and magnesium involvement into soil formation following the addition of dolomitic meal changed significantly the absorbing capacity of the podzolic soils. Base saturation increased from 29.0-30.9% to 50.1% under a 4 t ha⁻¹ rate and to 76.8% under a 11 t ha⁻¹ rate (Table 1). Hydrogen replacement in the soil absorbing complex caused a decrease in all forms of acidity. The pH (KCl) changed from 4.0 to 4.9-5.9. The amount of change depended on a liming rate. In

the process, every subsequent step in the acidity lowering was achieved by additional lime application. Change in soil pH by 0.1 unit was provided with 0.42 t ha⁻¹ of dolomitic meal at the application of 4 t ha⁻¹ and with 0.55 t ha⁻¹ at the application of 11 t ha⁻¹. The soil reaction (pH) change per unit of lime material was higher at the smaller lime rates.

A 9-year study on changes in soil acidity and base saturation showed that the maximum pH value had been reached in the fourth year of 11 t ha⁻¹ of dolomitic meal application and in the first and second years of a 4 t ha⁻¹ rate (Fig.2). In subsequent years, soil acidification took place, the
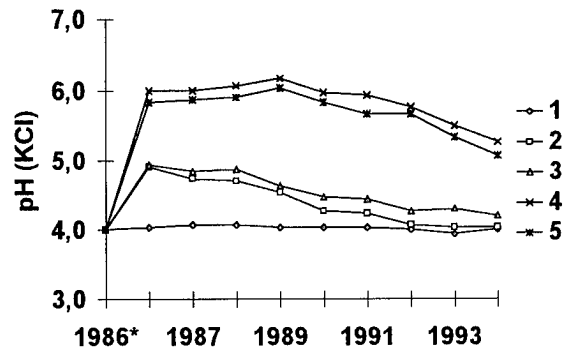
Figure 2. Acidity dynamics in the experiment with liming and inorganic fertilizers application.
1, control; 2, 4 t ha⁻¹ of dolomitic meal; 3, 4 t ha⁻¹ of dolomitic meal and an inorganic fertilizers; 4, 11 t ha⁻¹ of dolomitic meal; 5, 11 t ha⁻¹ of dolomitic meal and an inorganic fertilizers.
* 1986, before the trial began.

strongest one having been observed in the case of inorganic fertilizer application. Along with active acidity, other forms of acidity underwent changes (Table 1). Hydrolytic acidity showed minimum values after liming, but increased significantly by the end of the observation period, especially under inorganic fertilizer application. Also, in time, soil base saturation decreased due to calcium and magnesium leaching and crop removal. Exchangable acidity demonstrated the most pronounced changes. Heavy liming caused a decrease in exchangable aluminium content down to values close to 0, and such a content, which is harmless to crops, persisted until the end of the observation period.

The most pronounced effect of liming upon crop capacity followed the dolomitic meal application at a rate of 11 t ha⁻¹; the potato yield exceeded that in a control site by 7.5 t ha⁻¹ (Fig. 1). In the experiment with annual grasses, green material yield gains of 8.4 t ha⁻¹ (at a rate of 4

Table 1. Effect of liming upon physical-chemical parameters of the Podzolic soil .

		Versions of the experiment			
Year	Control	Dolomitic meal (4 t ha $^{-1}$)	Dolomitic meal (4 t ha $^{-1}$) and inorganic fertilizers	Dolomitic meal (11 t ha $^{-1}$)	Dolomitic meal (11 t ha $^{-1}$) and inorganic fertilizers
Hydrolytic acidity, cmol kg $^{-1}$					
1986*	6.15	6.28	6.17	6.25	6.29
1986**	6.03	4.61	4.69	2.15	2.20
1994	6.19	5.43	5.91	3.03	3.45
Exchangable hydrogen, cmol kg $^{-1}$					
1986*	0.03	0.03	0.03	0.03	0.03
1986**	0.03	0.03	0.02	0.01	0.01
1994	0.03	0.02	0.03	0.01	0.01
Exchangable aluminium cmol kg $^{-1}$					
1986*	1.14	1.12	1.10	1.07	1.05
1986**	1.15	0.11	0.10	0.02	0.02
1994	1.12	0.35	0.72	0.03	0.04
Exchangable acidity cmol kg $^{-1}$					
1986*	1.17	1.15	1.13	1.10	1.08
1986**	1.18	0.14	0,12	0.03	0.03
1994	1.15	0.37	0.75	0.04	0.05
Exchangable calcium cmol kg $^{-1}$					
1986 *	1.80	1.76	1.79	1.91	1.81
1986**	1.86	2.84	2.61	4.41	4.17
1994	1.69	2.35	2.12	4.72	4.47
Exchangable magnesium cmol kg $^{-1}$					
1986*	0.86	0.80	0.79	0.89	0.91
1986**	0.79	1.79	1.66	2.69	2.61
1994	0.80	1.64	1.04	3.15	2.98
Soil base saturation % .					
1986*	30.2	29.0	29.5	30.9	30.2
1986**	30.6	50.1	47.7	76.8	75.5
1994	28.7	42.3	37.8	72.2	68.3

* 1986, before the trial establishment.
** 1986, after the trial establishment.

t ha^{-1}) and 13.4 t ha $^{-1}$ (at a rate of 11 t ha^{-1}) have been obtained due to liming. Although a clover was grown within seven years after liming, the effect of dolomitic meal was strong the whole time, especially at the lime rate of 11 t ha^{-1}.

Optimization of nutrition

Previous studies of the effect of inorganic fertilizers on crop growth and yield (Zabolotskaya et al. 1978; Zabolotskaya 1985) showed that these fertilizers have high efficiency on podzolic soils. The strongest effect was achieved by nitrogen addition; phosphorus took second place. Potassium addition was efficient only if the crops were

well provided with nitrogen and phosphorus. Crop nutritive requirement was highest in spring and early summer when soils were not yet warmed thoroughly.

As different approaches to calculation of fertilizer requirement are in use, we undertook a study of the diagnostic capabilities of each approach. The following approaches were tested: a balance method, average rates currently recommended by the State Agrochemical Service, and a method of optimum nutrition.

To calculate fertilizer rates based on the balance method, we used the data on nutrient removal from soils and fertilizers, and coefficients of fertilizer recovery, published by Zabolotskaya

et al. (1978) for podzolic soils of the European northeast. The balance method stipulated liming at a rate of 4 t ha⁻¹.

The nitrogen, phosphorus, and potassium rates recommended by the Agrochemical Service are as follows: 120 kg ha⁻¹ of a primary nutrient for potatoes, 60 kg ha⁻¹ for annual grasses, and 45 kg ha⁻¹ for clover, provided 4 t ha⁻¹ lime is added in each case.

The third approach stipulated a complex nutrition optimization by 13 chemical elements

based on the method developed by Rinkis (Rinkis et al. 1989). An optimum nutrient intensity (determined in 1 m HCl) is supposed to be achieved following the method. Taking into account the study soil properties, some corrections have been made for the possibility of nutrient fixation by the soil. Another modification was the use of a dolomitic meal whose rate (11 t ha⁻¹) had been calculated for the optimumisation of calcium and magnesium nutrition. The amounts of nutrients added during 9 years of the complex optimization
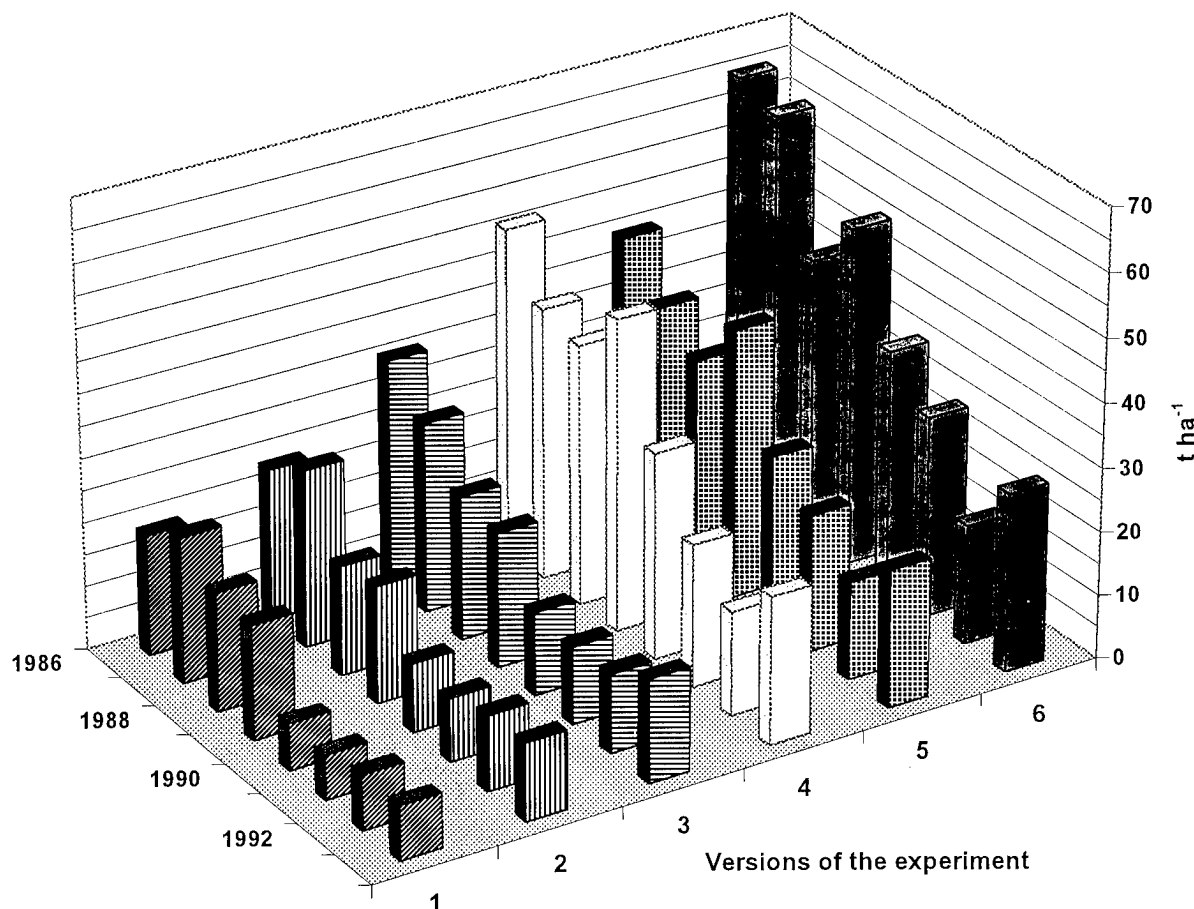
Figure 3. Effect of liming and inorganic fertilizers on crop yield.
1, control; 2, 4 t ha⁻¹ of dolomitic meal; 3, 11 t ha⁻¹ of dolomitic meal; 4, inorganic fertilizers at the rates calculated by the balance method; 5, fertilizers at the rates recommended by the State Agrochemical Service; 6, fertilizers at the rates calculated by the complex optimization method.
1986-1989, potatoes; 1990-1992 annuaal grass; 1993, clover.

experiment total: nitrogen, 959 kg ha⁻¹; phosphorus, 714; potassium, 1199; calcium 2600; magnesium, 600; copper, 17.3; zinc, 31.1; cobalt, 0.74; molybdenum, 1.38; and boron, 9.1 kg ha⁻¹ of a primary nutrient. The amounts added after the balance method total 1097 kg ha⁻¹ of nitrogen,

756 kg ha⁻¹ of phosphorus, and 1157 kg ha⁻¹ of potassium.

The highest crop capacity (Fig. 3) has been achieved using the complex optimization method. Average potato yield was 56.3 t ha⁻¹ with 19.8 t ha⁻¹ in a control site, annual grasses yield (green

material) was 29.4 and 7.4 t ha $^{-1}$ correspondingly. Significant yield gains were also obtained using the balance method of rate calculation. Yield gains of 26.2 t ha^{-1} for potatoes and 16.1 t ha $^{-1}$ for green material were achieved. A study of the yield quality showed that nitrate content did not exceed the maximum permissible concentration in all versions of the experiment.

CONCLUSION

The results presented demonstrate high efficiency of inorganic fertilizers, especially when applied with lime, macro-, and micronutrients. The study revealed a positive action of organic fertilizers, lime, and inorganic fertilizers on soil productivity and soil ecological status. Basic methods for podzolic soil amelioration in the European northeast are shown.

REFERENCES

Metody agrohimicheskogo issledovaniya (Methods for agrochemical research). (In Russian.) 1975. Kolos publ. Moscow.

Rinkis G.Ya., H.K.Ramane, G.V.Paegle, and T.A.Kunitsckaya.1989. Systema optimizatsii i metody diagnostici mineralnogo pitaniya rastenii (The system of optimization and methods of diagnostic of crop nutrition). (In Russian.) Zinatne publ. Riga.

Zabolotskaya, T.G. 1985. Biologicheskiy krugovorot elementov v agrotsenozah i ih produktivnost (Biological cycling of nutrients and agrocenosis productivity). (In Russian.) Leningrad.

Zabolotskaya, T.G., I.I.Yudintseva, and A.V.Kononenko. 1978. Severnyu podzol i udobreniye (Northern Podzol and Fertilizer). (In Russian.) Syktyvkar publ. Syktyvkar.

Nitrogen Cycle in the Taiga Zone
of the Republic of Komi

V.A. BEZNOSIKOV[1]

ABSTRACT

The results of investigations of nitrogen cycle in arable loamy podsolic soils are presented. The magnitudes of in- soil migrations, gaseous losses, immobilizations-mineralizations. A quantitative estimation of the correlation of soil nitrogen and fertilizers in the plant nitrogen fund was carried out. A new approach to rationing fertilizers for planned harvest is substantiated.

Key words: Migration, mineralization-immobilization, gaseous losses.

INTRODUCTION

The urgency of investigations on the problems of the nitrogen cycle is determined by the need for rational soil use and regional natural conditions.

Further industrial development and use of nitrogen fertilizers create some extra problems: energetic, economic and ecologic, caused by high power-consumption of industrial fertilizer synthesis, high solubity of ammonium and nitrate salts, and fairly low efficiency of fertilizers. Moreover, applying growing quantities of nitrogen-containing compounds into soil is the most gross interference into biological rotation (Starchenkov 1983).

The aim of the work was to substantiate methods of effective use and conservation of the soil nitrogen fund, safe methods of estimating plants needs for optimal "artificial" nitrogen, ecologically clean farming practices for podsolic soils, nitrogen transformation and movement in soil-fertilizer-plant system.

MATERIALS AND METHODS

The investigations were conducted in 1984-1990 at the Vylgort scientific-experimental biological station of the Komi Scientific Centre,

Ural Department, RAS, on typical podsolic arable soils with different stages of cultivation. A physico-chemical soil description of sample plots was published by Beznosikov et al. (1991). The soils are silty loams with a sharp difference in silt content between horizons A_2 and B.

For comparative description of a podsolic soil's nitrogen fund in a taiga zone (Komi Republic, Perm region), soil samples were taken from profile cuts made during root observations, and also from vertical cuts on sample plots (Beznosikov 1983).

The study of the nitrogen cycle in arable podsolic soils was conducted on 1 m^2 microplots placed on level watersheds, and 3° slopes (microcatena) of south-eastern exposure. Eight plots of each type were under investigation. Placing of sloped plots was at four heights. Distance between the plots was 5 m. Tagged ^{15}N nitrogen silt (calcium nitrate - Nc, ammonium nitrate - Na, sodium nitrate -Ns) with concentration of 20-40 atomic % at the dose 12 g N m^{-2} was applied annually on two plots at each height, beginning from the lower plots to avoid their pollution by nitrogen fertilizers with surface flow.

For studying lateral migration and balance of applied nitrogen in range together with the main plots at distances of 20, 50, 70, 100, 140, 200, 280, 300, 400 cm from the place the fertilisers were applied, extra plots on the slope were added. One part of the plots was fallow, another was planted (*Avena sativa* L., *lolium multiflorum* Lam. Var. *Vester Voldicum.* Wittm.). The control of overground biomass, of reap-root residues was performed on the main and extra plots, and plant and soil samples were taken for determining total and marked nitrogen. In 1988 an extra version of autumn sodium nitrate application was added. Soil was sampled in autumn, winter and spring to a depth of 100 cm at intervals of 10 cm.

On sample plots four plastic lysimeters of Ye.I.Shilova's construction were installed (Shilova 1955) at both 20 and 50 cm depth. A relative quantity of intrasoil (vertical) discharge was

---

[1] Institute of Biology, Komi Science Centre, Ural Department, Russian Academy of Sciences, 167610 GSP, Syktyvkar, St. Kommunisticheskaya 28, Russia

estimated. Using on the volume of lysimeter's water.

The investigation of the composition of the soil nitrogen pool was performed by the method of acid hydrolysis (Shkonde et al., 1964).

A quantitative estimation of the indicators of soil nitrogen cycle was performed with an isotope indication method. The following assumptions are the basis of this method (Freed et al., 1952): soil nutrient is used in proportion with marked elements of applied silt; the degree of soil nitrogen absorption by plants and microorganisms, and loss sizes are expressed in the same relative values as for applied marked nitrogen.

COMPOSITION OF THE NITROGEN POOL

Carbon accumulation in the form of humus depends upon organic nitrogen participating in humus formation, and the amount of nitrogen accumulation determines humus accumulation (Tyurin 1965). The interconnection of these indicators of potential fertility confirms the unity of natural factors in humus and nitrogen accumulation. The peculiarities of soil forming conditions in the middle taiga subzone are as follows: short duration of biologically active period; lack of warmth and moisture surplus slow down the decomposition and synthesis of organic matter, and cause nitrogen deficiency in podsolic soils.

The composition of the nitrogen pool of loamy podsolic soils at different cultivation stages is shown in Table 1. The accumulation of organic matter and nitrogen under the forest is slower than in cultivated areas. This is due to redominant development of biological processes in upper horizons.

Table 1. Composition of nitrogen fund of typical laomy podsolic soils.

Horizon	Sampling depth, cm	Nitrogen, mg kg^{-1}					C: N
		Gene-ral	Mineral	Eeasy to hydrolyse	Difficult to hydrolyse	Non-hydrolyscd	
INTENSIVELY CULTIVATED SOIL, 1-88							
A$_p$	0-25	1300	17.7 (1.4)	156.8 (12.1)	284.9 (20.4)	860.6 (66.1)	9.9
A$_2$B$_1$	30-40	450	21.5 (4.8)	71.9 (16.0)	151.8 (33.7)	204.8 (45.5)	7.6
B$_1$	53-63	339	21.7 (6.4)	59.9 (17.7)	89.6 (26.4)	167.6 (49.5)	5.6
CULTIVATED SOIL, 2-88							
A$_p$	0-18	693	8.0 (2.5)	44.9 (6.5)	209.4 (30.2)	421.2 (60.8)	9.7
A$_2$B$_1$	30-40	339	15.3 (4.5)	37.2 (11.0)	129.6 (38.2)	156.9 (46.3)	7.3
B$_1$	55-65	239	5.0 (2.1)	34.2 (14.3)	91.8 (38.4)	107.0 (45.2)	5.4
NEWLY CULTIVATED SOIL, 5-88							
A$_p$	0-15	817	21.9 (2.7)	47.6 (5.8)	276.2 (33.8)	470.9 (57.7)	9.2
A$_2$B$_1$	25-35	347	7.5 (2.2)	32.5 (9.4)	147.3 (42.4)	159.2 (46.0)	7.5
B$_1$	57-67	323	0 (0)	58.8 (18.2)	124.9 (38.6)	139.3 (43.2)	5.3
FOREST SOIL, 6-89							
A$_2$	3-10	368	3.1 (0.8)	58.2 (15.8)	48.2 (13.1)	258.5 (70.3)	8.5
A$_2$B$_1$	15-20	258	4.7 (1.8)	44.4 (17.2)	64.1 (24.8)	144.8 (56.2)	7.3
B$_1$	50-60	240	2.7 (1.1)	24.1 (10.0)	52.1 (21.7)	161.1 (67.2)	5.0

Note: In parentheses: % from total nitrogen.

The enrichment of podsolic soil humus with nitrogen (C:N) is slow and it does not depend upon the stage of cultivation. Podsolic soil cultivation weakly affects the intensity of nitrogen accumulating processes. This is due to significant annual nitrogen removal from soil with harvest, and low doses of organic fertilizers.

Most of the nitrogen in podsolic soils is in organic form (97-99%) and only a small part is in mineral form. As compared to the other studied soils of the taiga zone, the podsolic soils of the Republic of Komi have lowest nitrogen content. They are more subjected to hydrolysis and less resistant to the impact of natural and anthropogenic factors

as compared to sod-podzolic and grey forest soils of the Perm region (Table 2). First of all, this is connected with low base saturation and low humus content in podzolic soils, as well as humus "aggressiveness".

MIGRATION AND LOSSES OF FERTILIZER NITROGEN

Migration of fertilizer nitrogen in loamy podzolic soils is connected with the features of intrasoil water runoff: during spring snow melt and summer strong rains, the upper layers become saturated, and this temporarily water-saturated horizon restrains moisture movement down the profile. In soils formed on loamy materials, the horizontal runoff dominates the vertical, and on level surfaces its influence does not decrease, as the influence of microrelief increases.

A five-year, year-round measurement of lysimeter waters in our experiments indicated that precipitation infiltration deeper than 0-50 cm was not significant. During autumn it constituted 8,3%, and during spring 2,5% of annual precipition. During the same periods, infiltration from the arable layer (0-20 cm) was 31,0% and 35,0%. Mean annual moisture infiltration deeper than the arable layer was 23,0%, and from the subarable layer it was 4,5%.

The study of descending migrations in loamy podsolic soils in summer period indicated, that under plants most of the marked fertilizer nitrogen accumulated in upper (0-40 cm) soil, mostly in the A_p. Maximum leaching of fertilizer nitrogen in the profile was seen in fallow. Fertilizer nitrogen in fallow migrated deeper than the arable layer, up to 60 cm depth, with a quantity of 4,3-8,8 kg h^{-1}, and it was not found lower.

Small descending migration of fertilizer nitrogen is caused by some peculiarities of podzolic soils: presence of illuvial horizon with maximum accumulation of iron and aluminium oxides, that have isoelectric points 8,1 and 7,1 respectively. Such isoelectric oxide parameters in an acid medium (pH_{KCl} in B_1 horizon =3,63) cause the formation of positively charged sorption centres, which leads to adsorption of nitrate ions of B_1 at the rate of 2,5 mg N kg^{-1} of soil. The absorption of nitrates by soil is significantly higher in B_1 than in A_p. This is confirmed by quantitative correlation between absorbed and mobile ions (Ap 2,17/5,36 against B_1 5,0/6,25). The illuvial horizon is of hard consistence, low porosity, high silt content and low infiltration (less than 0,02 m/day). Low removal of nitrate ions occurs due to a "salt sifting" phenomenon (Nai et al. 1980), as loamy soils with narrow pores act as semi-permeable membranes

and are more pervious to water than to salt. The illuvial horizon is an absorption barrier and stops the migration of nitrate nitrogen.

Soil freezing in autumn and winter leads to fertilizer nitrogen concentration on the borderline of the frozen layer (thermocapillary removal). On the one hand, a frozen layer becomes a nitrogen accumulator (Fig. 1), and on the other, a water-holder in spring, when "upper waters" with dissolved nitrogen transfers laterally. A small intrasoil vertical runoff in spring confirms this.
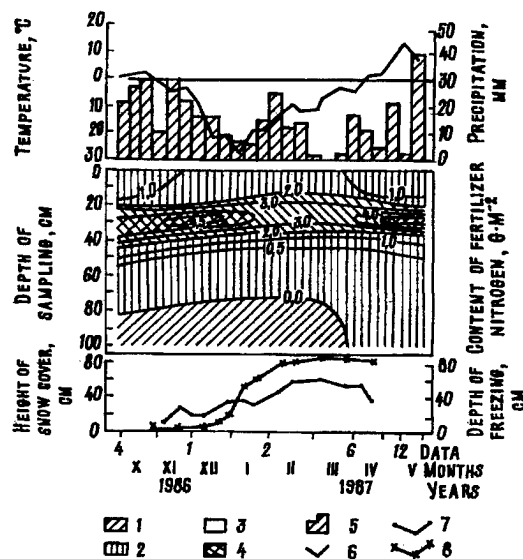
Figure 1. Isoscheme of distribution of ^{15}N fertilizers in the soil profile during autumn-winter period. Conventional signs: 1- no nitrogen; presence of nitrogen: 2 - 5-10, 3 - 10-30, 4 - > 30 mg/100g of soil; 5 - preipitation; 6 - air temperature; 7 - depth of soil freezing; 8 - height of snow cover.

Even annual precipitation within the norm (1984) only slightly affected horizontal moisture redistribution on the slope. Moisture quantity on different slope plots and on different dates varied not more than by 2-3%. Nitrogen transport in upper part of the slope was not significant, fertilizer nitrogen in soil under plants was found at a distance of 50 cm, and in fallow at a distance 100 cm from the place it was applied.

Intense precipitation (1985) leads to saturation of arable layer and moisture and nitrogen redistribution on the hard, weakly pervious illuvial horizon of the slope. Fertilizer nitrogen under plants was found at a distance of 200 cm from the place of application: in fallow, it was 400 cm (Fig. 2, 3. Table 3). It is possible

398

Soil	Nitrogen, mg kg⁻¹			
	Mineral	Easy to hydrolyse	Difficult to hydrolyse	Non-hydrolysed
Podzolic cultivated	8,0 (1,2)	38,2 (5,7)	174,3 (26,0)	449,5 (67,1)
Intensively cultivated	13,5 (1,4)	90,4 (9,3)	181,6 (18,6)	689,5 (70,7)
Sod-podzolic	27,9 (1,3)	161,3 (7,3)	312,6 (14,2)	1698,2 (77,2)
Grey forest	37,0 (1,3)	169,0 (5,7)	492,6 (16,6)	2276,4 (76,4)

In parentheses: % from general nitrogen
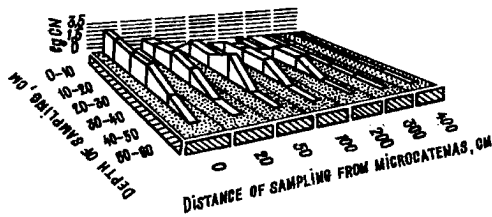
Figure 2. Intrasoil migration of ^{15}N *fertilizers under plants, 1985.*
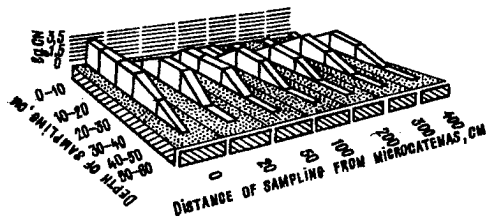
Figure 3. Intrasoil migration of ^{15}N *fertilizers in fallow, 1985.*

that nitrogen was leached at greater distances from the place of application (nitrogen was not determined outside the distance of 400 cm).

Most of the moisture on loamy soils moves sideways off the soil, leading to lateral removal of 17% of the applied nitrogen. Moisture and nitrogen redistribution on the slope of "open" type (outlet into draining hollows: transeluvial processes) partly excludes nitrogen from the biological cycle in agrocenosis and leads to possible environment pollution. Nitrogen leaching with surface runoff on catenas of the "closed" type (outlet into saucer-like lowering: eluvial-accumulative processes) causes nitrogen heterogeneity in geochemical agrolandscapes. Downward migration of fertilizer nitrogen in loamy soils reaches the root layer and does not prevent plants from obtaining nitrogen.

Caseous losses are the main component of non-productive losses of fertilizer nitrogen. On average, during three years on podzolic

loamy soils it was 14,1-21,8% under plants and 38,0-43,0% in fallow. Nitrogen losses from nitrate salt were higher than from ammonium by 5-6%. Gaseous losses of soil nitrogen varied from 45 in cultivated to 85 kg h⁻¹ in intensively cultivated soils.

THE PROCESSES OF MINERALIZATION-IMMOBILIZATION

The processes of mineralization-immobilization of nitrogen compounds are the basis of the nitrogen cycle in soils. In our studies, we used the technique of isotope indication. We conducted a quantitative evaluation of these processes in loamy podsolic soils, and on the basis of our data (on the correlation of soil nitrogen of different cultivation levels and of fertilizer nitrogen in plants) we validated the optimization of nitrogen fertilizers for the planned harvest.

The experimental data indicated that in these soils the compounds of the nitrogen cycle swing from mineralization-immobilization processes to mineralization processes. This process depressed pools and caused nitrogen deficit in arable podzolic soils. Total nitrogen mineralization on the background of complete (N, P_2O_5, K_2O) mineral fertilizer in arable horizon of intensively cultivated soil is higher (99 mg N kg⁻¹), than in the cultivated one (52 mg N kg⁻¹). In flow rate of mineralized nitrogen, net-mineralization cotstitutes the biggest part. Nitrogen flow from soil, as the content of general mineralized nitrogen, decreases from 75 mg N kg⁻¹ in intensively cultivated to 37 in cultivated soil. In the structure of mineralized soil nitrogen, the nitrogen accessible for plants is 32% in cultivated and 44% in intensively cultivated soils. The accumulation of nitrogen accessible for plants did not completely characterise nitrogen mineralization capability of podzolic soils of different

cultivation rates, as part of nitrogen was exposed to re-immobilization (16-25 mg N kg^{-1}), and part of it was lost due to denitrification (18-34 mg N kg^{-1}). During the vegetative period, 43-60% of soil nitrogen losses have been compensated, including 36-50% compensated by soil nitrogen immobilization, and 7-10% compansated by fertilizers nitrogen.

The kinds of organic substrates applied to the soil, and freezing and thawing of soil affect the processes of nitrogen mineralization-immobilization in podsolic soils.

Applcation of carbon that is easily absorbed by soil biota (glucose) increases the intensity of the soil nitrogen mineralization process and non-productive losses. The use of organic fertilizers, characterized by high content of unhydrolised components (peat-excrement, peat-lignin compost, lignin), increases nitrogen immobilization and leads to retardation of mineralization processes and preservation of the soil nitrogen.

Experimental data on nitrogen mobilization capability of podzolic soils, obtained by the isotope method, allowed us to determine the impact of soil nitrogen and fertilizers on plant nutrition. The results on nitrogen removal by biomass of *lolium multiflorum* Lam. Var. *Vester Voldicum.* Wittm. *and Avena sativa* L. indicate, that during formation of vegetation the soil nitrogen plays the main role. Mineralized nitrogen by plants from podzolic soils constitutes 48-51% on cultivated soils and

69-78% on intensively cultivated ones. High soil nitrogen consumption by plants is connected with high lability of nitrogen compounds and low resistance of the nitrogen pools of podsolic soils. Recently, the fact that nitrogen fertilizers increase nitrogen mineralization was completely proved (Kudeyarov 1989).

During our studies it was established that extra nitrogen use by plants (due to fertilizer application) is determined by the rate of their cultivation. Nitrogen fertilisers promote the release of soil nitrogen in cultivated soils from 9 to 13, on intensively cultivated soils, from 9 to 30 kg h^{-1}. The amount of extra-nitrogen increases with increase of fertilizer rate. Due to extra ingress of nitrogen into plants, 14-22% of harvest was formed on cultivated soils, and 20-30% on intensively cultivated soils. So, in nitrogen variety of plants one-third is the proportion of extra-nitrogen.

Balance calculations on applying different forms of nitrogen fertilizers (ammonium and nitrate) showed that about 29% from the total fertilizers quantity was used for the formation of harvest biomass (Table 3). The results of laboratory experiments showed that soil freezing and thawing and applying nitrogen fertilizers to soil lead to mobility increase of soil nitrogen and its accumulation in soil. Probably, this is explained by enhancement of mineralization and destruction of organic matter under the

Table 3. Balance of fertilizer nitrogen in soil laver 0-100 cm, percent of introduced (average for 1984-1986 years).

Index	Under plants			In fallow		
	Place of fertiliser application	On micro-catena	Total	Place of application fertiliser	On micro-catena	Total
Used by aboveground	28,4	2,4	30,8	-	-	-
oats mass	28,2	2,8	31,0	-	-	-
Left in soil and in reap-	38,6	16,5	55,1	46,2	15,8	62,0
root	37,6	10,7	48,3	42,5	14,5	57,0
in that, lower than	2,6	-	2,6	3,1	-	3,1
40 cm	4,7	-	4,7	5,1	-	5,1
Total found	67,0	18,9	85,9	46,2	15,8	62,0
	65,8	13,5	71,3	42,5	14,5	57,0
Losses	-	-	14,1	-	-	38,0
	-	-	20,8	-	-	43,0

Note. The upper lines are the figures of version PK+Na$_{120}$; the lower lines, PK+Nc$_{120}$ (Ns$_{120}$).

400

impact of freezing and thawing and calcium nitrate presence. Feezing impact on mineralization of nitrogen is explained by aggregate destruction and exposure of new surfaces for micro-organism activity (Black 1968). It is also possible, that during freezing the breakage of microbial tissues occurs, where nitrogen is the basic element, and subseguent melting leads to organic matter decomposition with nitrogen release. The process has both biotic and abiotic character.

CONCLUSION

The study of features of the nitrogen cycle of arable lands of loamy soils by use of an isotope tracer method allowed us to evaluate ecological peculiarities of nitrogen behaviour in the soil-plant-environment system, and to determine the direction of the processes of nitrogen transformation and the effect of nitrogen fertilizers on soil.

Nitrogen compounds of podzolic soils have higher mobility and lower resistance to factors of environment that of sod-podzolic and grey forest soils do. In podzolic soils the compounds of the nitrogen cycle (mineralization-immobilization) are removed by mineralization processes. Mineralized soil nitrogen plays the main role in the formation of nitrogen plant pool.

During evaluation of the migration processes of fertilizer nitrogen it was determined that nitrogen excavated from root-habitat plant layers was not significant in the annual cycle and it does not render a significant impact on fertilizer nitrogen balance. Weak downward nitrogen migration is connected with the genesis of loamy podzolic soils: seasonal presence of water-impermable frozen layer, formation of illuvial horizon weakly-permeable to water; characterized by strong expansion with water absorption, low porosiby, high nitrate sorption capability. The illuvial horizon is a nitrogen accumulator that prevents downward nitrogen migration and non-productive losses.

Analysis of year-round lysimeter water showed insignificant precipitation infiltration out of the arable and subarable layers. Maximum autumn precipitation did not lead to significant increase of the quantity of lysimetrical waters. Most of moisture on loamy podsolic soils moves sideways off the soil and leads to lateral outwash of nitrogen. Moisture and nitrogen redistribution on the slope of an "open" type (transeluvial processes) partly excludes nitrogen from the biological cycle in the agrocenosic and leads to danger of environmental pollution. Nitrogen outwash by surface flow on the slope of "a closed" type (eluvial-accumulative processes) creates nitrogen heterogeneity in the geochemical agrolandscape.

Freezing of soil during autumn and winter promotes nitrogen movement with rising water flow to the freezing front and its concentration in the frozen layer. This process is connected with convective movement of moisture and dissolved nitrogen, caused by temperature gradient (thermo-capillary removal).

Cryogenic dehydration and soil thawing lead to destruction of organic - nitrogen - containing matter and accumulation of mineral nitrogen in soil. The process has both biotic, and abiotic character.

Balance calculations showed that in podzolic soils the coefficients of nitrogen fertilizer use by plants are 28-35%. An important component of fertilizer use and the soil nitrogen cycle is gaseous losses caused by denitrification.

Nitrogen fertilizers on podzolic soils with low productivity under biological rotation are a strong biogeochemical factor. On the one hand, this is caused by the fact that nitrogen in these soils is low and its deficit, together with inadequate and unstable heat provision, depresses the productivity of the northern agroecosystem; on the other, an excess of nitrogen fertilizers leads to increased mineralization of the natural stocks of organic nitrogenous compounds, to soil destruction, and weakening of self-restoring mechanisms of the soil.

Climatic conditions and the topography of the middle taiga subzone of the Republic of Komi determine the features of the nitrogen cycle in arable podzolic soils: insignificant nitrogen outwash from arable layer, high gaseous losses, especially in fallow, and low coefficients of fertilizer nitrogen use by plants. Comparatively high lateral outwash at the surface is an important component of the nitrogen cycle on slope agricultural systems.

REFERENCES

Beznosikov, V.A. 1983. Effects of nitrogen fertilizers on main soils of Pre-Urals. In Russian. Agrochemistry 3:3-8.

Beznosikov, V.A., I.A. Lavrova, G.M. Turkina. 1991. Fertilizer nitrogen balance on sloped loamy podsolic soils of the middle taiga subzone of Komi ASSR. In Russian. Agrochemistry 5: 3-9.

Black, C.A. 1968. Soil-plant relationship. New York.

Dospekhov, G.A. 1985. Technique of field experience. In Russian. Moscow: Agropromizdat.

Freed, M., L.Dean. 1952. A concept concerning the measurements of available soil nutrients. Science Soil Vol.73. 4:263-271.

Gamzikov, G.P. 1981. Nitrogen in agriculture of Western Siberia. In Russian. Moscow: Nauka.

Kudeyarov, V.N. 1989. Nitrogen cycle in soil fertilizers efficiency. In Russian. Moscow: Nauka.

Nai, P.Kh., P.B.Tinzher. 1980. Solution movement and soil-plant system. In Russian. Moscow: Kolos.

Shkode., I.M.Koroleva. 1964. On essence and mobility of soil nitrogen. In Russian. Agrochemistry.10:17-36.

Shilova, Y.I. 1995. Methods of receiving soil solution in nature conditions. In Russian. Soil Science. 3:15-21.

Starchenkov, Ye.P. 1983. Regulation of mineral nutrition of plants. In Moldova. Kishinew.

Response of Soil Organic Matter to Change
of Air Temperature in Forest Ecosystems

E.F. VEDROVA[1]

ABSTRACT

Observations were made in the 80-year pine forests of the Middle Siberia (54°N, 92°E). A high humus loamy soil substratum (C-humus = 6.59, C- biomass = 3.53%) is more sensitive to changing of humus formation conditions than a loamy sand one with low humus content (C humus =1.90, C biomass = 6.10%). Simulation of the full destruction of the litter and grass cover caused the loss of 18% humus supply in the loamy during 11 years of the experiment. The increase of the average daily air temperature of July by 2.4°C, July's temperature from 8 to 20 o'clock by 3.1–3.4°C and August's temperature by 1.2–2.5°C caused the intensive humus mineralization in the loamy sand and the loss of 48–51% of its primary supply.

Key words: Soil organic matter, mineralization, humification.

INTRODUCTION

The general model of organic matter transformation of terrestrial ecosystems can be elaborated based on clear understanding of the plant residues and soil humus decomposition processes. This becomes true when the forecasted response both of individual structural components and of ecosystem on air temperature increase is needed in connection with the expected global climate warming.

To determine rate of the decomposition of organic matter in forest soils, how quickly its primary supply is reestablished at the disturbance of its natural structure and configuration of accumulative part of forest soil profile finally, how the change of hydrothermic regime influences on the rate and directionality of transformation processes of soil organic matter the

method of field experiment was used (Vedrova 1980, Gadgiev and Dergacheva 1995, Ivanov and Alexandrovsky 1984, Rode 1971, Bonan and Van Cleve 1992).

MATERIALS AND METHODS

Observations were made in the 80-year pine (*Pinus sylvestris*) forests of the Krasnoyarsk forest-steppe (54°N,92°E). The sedge-bracken pine forest (Site I) is growing on the dark grey forest soil and the grass-cowberry pine forest (Site II) is growing on soddy-pine soil (Vedrova 1980, Pleshikov et al. 1976). The grass was cut, the litter was gathered and weighed in experimental plots (6×0.75 m). Then 20-cm of the surface soil was removed from these plots. The polyethylene film was fixed at the side walls of the trench. After thorough mixing samples of litter and soil were taken for chemical analysis and moisture determination. Then the trench was filled with homogenized weighed soil material: one loamy (Ah horizon dark grey soil) and one loamy sand (Ah horizon soddy-pine soil). According to granulometric composition, the loamy contains 30% physical clay (< 0.01 mm), 38% fine sand (0.25–0.05 mm) and 18% middle sand (1–0.25 mm). Carbon (C) humus level makes 6.59% here. In the loamy sand physical clay makes 18%, fine sand 33% and middle sand 38%. C-humus concentration is 1.90%. The soil laid and thickened by covering with a capron net with 0.5-cm cells where the weighed litter was distributed. To determine the rate of plant residue decomposition and humus supply changes in the soil material in the plots of this variant ("a"), the mass of annual litter-fall and grasses was taken into account. Litter storage was periodically determined, plant and soil samples were taken for analysis.

In one of the variants of the experiment ("g") the

---

[1]Institute of Forest, Russian Academy of Science, Siberian Branch, Academgorodok, Krasnoyarsk 660036, Russia

litter was not put in the plots. The surface of plots in this variant was cleaned from litterfall and grass vegetation during the experiment.

Each soil material was put back in the place of its taking away and also it was moved to another site (from the Site I to the Site II one and vice versa).

The experiment lasted for 11 years. The carbon content of plant samples was determined according to Anstett's method modified by Ponomareva and Nikolaeva (*In* V.V. Ponomareva and T.A. Plotnicova 1975). Carbon content of soil organic matter was determined using Tyurin's method (Arinushkina 1970) before and after treatment of soil samples by heavy liquor (Vedrova and Tchagina 1977). It allowed the organic matter to be divided into two fractions: (1) not connected with the mineral part of soil (underground "biomass") and (2) humus adsorbed by clayey minerals.

RESULTS AND DISCUSSION

The grass-cowberry and sedge-bracken pine forests are 6 km apart and have developed in similar climatic conditions. Mean annual precipitation is 402 mm. Average temperatures are $19.6°C$ in July and $-21.2°C$ in January. Average daily July temperature in the site II is $2.4°C$ higher than in the site I one. At the same time maximum air temperature in the site II is $10-12°C$ in July and $5-10°C$ in August higher than the site I. During the day, differences in temperature saves for $10-12$ hours (from 8 to $18-20$ o'clock). During the night, as a rule, the air in the site I cools more slowly, staying warmer by $2-3°C$. Amplitudes of daily temperature fluctuation in site II make $20-25°C$ in July and $15-20°C$ in August. Daily temperature differences in the site I very seldom exceeds $10°C$

The loamy soil in experiment had similar temperatures in both sites but the loamy sand in undisturbed site II was warmer by $1.0-1.5°C$. The light granulometric composition of loamy sand, low moisture capacity promote the flow of meltwater and of summer–autumn precipitation to the deep layers. The rapid warming up in site II is followed by drying up both of the soil and the litter. During growing season the moisture content of 5-cm layer loamy sand is often close to the wilting point (5.2%) The litter and the upper layer of loamy in both sites during the summer remained more moist than those of loamy sand. The increased moisture of the loamy (29–50%) in comparison with loamy sand (9–32%) is also observed in the variant ("g"), where litter is absent.

In the variant "a" with loamy sand the carbon supply in plant residues, being decomposed during the first 4 years, were similar in both sites (Table 1). Their decomposing occurred intensively, but with the different specific rate: under undisturbed conditions the carbon loss for mineralization and humification was 115 mg C $g^{-1}C$ yr^{-1}, at changed site it was 166 mg C $g^{-1}C$ yr^{-1}. The difference is caused by slow decomposing of underground biomass in Site II (116 against 176 mg C $g^{-1}C$ yr^{-1}). Different specific rate of decomposition of plant residues caused carbon loss of 46% in Site II and 66.5% in Site I during the first 4 years. There was noticeable increase of C-humus concentration up to 2.7–2.9% (against 1.9%) in Site II and up to 2.8–4.3% in Site I which was unexpected. At the same time 9% of the total decomposed material was humificated in Site II. In Site I humification accounted for 15% of the loss. The specific rate of humification was 10.4 mg C g^{-1} C yr^{-1} in the first case, and 25.6 mg C g^{-1} C yr^{-1} in the second one.

During the following 7 years, decomposition rate of plant residues in the loamy sand decreased by 1.5 and 2.5 times, in Site II and Site I, accordingly. This period is characterized by mineralization of newly formed humus. Mineralization rate is similar in both sites: 31.5 and 32.6 mg C g^{-1} C yr^{-1}. The loss of 22% humus under the grass-cowberry pine forest conditions correlates with its store for the previous 4 years (+29%). As a result, humus supply in loamy sand in the conditions undisturbed for soddy-pine soils reverted for 11 years to its primary state (Table 1). When replaced to Site I the loamy sand accumulated 126 g C m^{-2}, which account for 26% of primary supply The average decomposition rate of litter during 11 years on the loamy sand surface is equal in both sites (61–64 mg C g^{-1} C yr^{-1}), but the underground biomass decomposed more rapidly in Site I (68 against 58 mg C g^{-1} C yr^{-1}).

In the variant without litter on the experimental plot surface the soil humus and biomass took part in decomposition processes. The intensive biomass decomposing occurs in the first 4 years (Table 2). Its losses make 55 and 72% of the primary supply in Site II and Site I, accordingly. Decomposition rate of the underground biomass in Site II was 136 mg C g^{-1} C yr^{-1} (versus 116 mg C in the "a" variant) In Site I the underground plant residues in the loamy sand decomposed at similar rate in both variants. Biomass decomposition is followed by accumulation of the newly formed humus. Humification rate in the Site II is 40 mg C g^{-1} C yr^{-1} and exceed that rate in variant with litter ("a"). Under the canopy of the sedge-bracken pine forest (Site I) humification rate

Table 1. Carbon balance. Loamy sand. Variant "a."

Parameters	Undisturbed site (Site II)			Disturbed (Site I)		
	At begining	For 11 years	At final	At begining	For 11 years	At final
Carbon supply, $g.m^{-2}$:						
litter	859		925	800		905
underground biomass	1574		838	1573		463
Total	2433		1763	2373		1368
Carbon in litterfall		2193			1975	
in roots		738			242	
Total		2931			2217	
Decomposition (total):		5364			4590	
litter + litterfall		3052			2775	
underground biomass		2312			1815	
Carbon loss (total) :		3601			3222	
litter + litterfall		2127			1870	
underground biomass		1474			1352	
Rate decomposition ($g\ C.\ m^{-2}.yr^{-1}$):		327			293	
litter + litterfall		193			170	
underground biomass		134			123	
Specific rate of decomposition ($mg\ C.g\ C^{-1}.yr^{-1}$):		61			64	
litter + litterfall		63			61	
underground biomass		58			68	
Soil humus store (0 - 3 cm), $g.m^{-2}$	489		491	489		615
C - humus accumulation (or losses), %		0.4			26.0	

Table 2. Decomposition of underground biomass and humus in loamy sand. Variant "g."

Parameters	Carbon supply, g C m^{-2}			
	Undisturbed site		Disturbed site	
	Humus	Biomass	Humus	Biomass
Begining of experiment	595.0	1879.9	525.9	1661.7
in 4 yr	896.6	854.8	691.4	469.1
in 6 yr	656.4	1296.1	654.3	1185.2
in 11 yr	606.2	1608.9	701.5	997.5
Loss (accumulation) :				
in 4 yr	+301.6	-1025.1	+165.5	-1192.6
the next 2 yr	-240.2	+441.3	-37.1	+716.1
the next 5 yr	-50.2	+312.8	+47.2	-187.7
total 11 yr	+11.2	-271.0	+175.6	-664.2
% to primary supply	2		33	

supply increased 33% (Table 2) in comparison with the primary one. The newly formed humus was adsorbed by fine (0.005–0.001 mm) and middle (0.01–0.005 mm) dust fractions of loamy sand. In the primary substratum these dust fractions contained 6 and 2% of carbon. In 11 years carbon concentration increased to 10 and 17–22% in fine and middle dust, accordingly.

Transformation of plant residue on the surface and 10-cm layer of the loamy left in undisturbed site (Site I) is characterized by regularities which were described above for variants with loamy sand without site change (Table 3): (1) sharp increase of decomposition intensity (g C m^{-2} yr^{-1}) and specific rate (mg C g C^{-1} yr^{-1}) during the first 4 years of the experiment; (2) decrease of these parameters by 2–3 times in the following years; (3) re-establishment of the humus primary supply in the soil material of the "a" variant during 11 years.

In the variant "g" of the loamy the remaining biomass was nearly totally decomposed (97%) during the first 4 years. Humus accumulation was not significant (Table 4). In the following years the synthesis of newly formed humus through transformation of moss residue in loamy did not compensate humus decomposition. As the result, the loamy

of plant residue is similar in both variants (25.9–25.6 mg C g^{-1} C yr^{-1}).

Beginning from second year on the experimental plots of the variant "g" green mosses appeared that were removed for 4 years thoroughly. Four years later the moss removal became impracticable because of physical disturbance of plot surface. Fresh moss residue which increased the supply of organic carbon in the soil substratum was simultaneously a catalyst of mineralization of organic matters including "unripe" humus (Carlyle 1993). As a result, in 11 years, humus supply in the loamy sand in Site II returned to the primary level. In Site I fresh organic residue in the loamy sand did not alter the controlling process of humus accumulation. The humus

405

Table 3. Carbon balance. Loamy. Variant "a."

Parameters	Undisturbed site (Site I)			Disturbed site (Site II)		
	At begining	For 11 years	At final	At begining	For 11 years	At final
Carbon supply (g.m^{-2}) :						
litter	646		1071	649		884
underground biomass	2195		1722	2203		1656
Total	2841		2793	2852		2540
Carbon in : litterfall		2544			2296	
roots		2131			2739	
Total		4675			5035	
Decomposition (total):		7516			7887	
litter + litterfall		3190			2945	
underground biomass		4326			4942	
Carbon loss (total) :		4723			5347	
litter + litterfall		2119			2061	
underground biomass		2604			3286	
Rate decomposition (g C . m^{-2}.yr^{-2}) ;		430			486	
litter + litterfall		193			187	
underground biomass		237			299	
Specific rate of decomposition (mg C .g C-1 .yr-1) :		57			62	
litter + litterfall		60			64	
underground biomass		55			60	
Soil humus store (0-10 cm), g C .m^{-2}	4096		3984	4108		2152
C-humus accumulation (or losses) :		-112			-1956	
% to primary C-humus store		37.8			55.4	

Table 4. Decomposition of underground biomass and humus in loamy. Variant "g."

Parameters	Carbon supply, g C . m^{-2}			
	Undisturbed site		Disturbed site	
	Humus	Biomass	Humus	Biomass
Begining of the experiment	4095.8	2194.7	4090.7	2192.0
in 4 yr	4210.6	74.7	3112.0	378.7
in 6 yr	3976.0	787.6	2954.7	1626.7
in 11 yr	370.7	1433.8	1997.3	1704.0
Loss (accumulation) :				
in 4 yr	+114.8	-2120.0	-978.7	-1813.3
the next 2 yr	-234.6	+712.9	-157.3	+1248.0
the next 5 yr	-605.3	+646.2	-957.4	+77.3
total in 11 yr	-725.1	-760.9	-2093.4	-488.0
% to primary supply	17.7		51.2	

(Vedrova 1996). It can be assumed that air temperature increase during the first decade will slightly change the stand productivity on high humus dark grey soils as well as the rate of residue decomposing, but will increase humus mineralization. Then the overall mineralization of plant residue and soil humus (the layer 0–10 cm) will 20.8 t C ha^{-1} yr^{-1} and the ecosystem of the sedge-bracken pine forest will transform to carbon source.

has lost 18% humus to the end of the experiment.

Replacing of the loamy to Site II increased the humus mineralization. During 11 years the loamy in the variant "a" has lost 48 and in the "g" variant 51% of primary humus supply. Specific rate of humus decomposition in these variants makes 43.3 and 46.5 mg C g^{-1} C yr^{-1}. Humus mineralization was followed by decrease of saturation of clay particles (< 0.001 mm) by carbon.

Under current climatic conditions, the 80-year pine forests, where the experiment was carried out, act as carbon sink: annual accumulation in the phytomass exceeds the return to the atmosphere

CONCLUSION

Forest litter destruction, stirring of humus-accumulative horizon of soils without changing hydrotermic parameters resulted in active decomposition of plant residues during the first 4 years of the experiment. During the following seven years, loamy and loamy sand under undisturbed conditions reestablished their primary humus supply.

Full removal of the litter and grass cover did not change the humus supply in the loamy sand in 11 years. This occurred due to organic carbon reserve increase through the dying off tissues of green

mosses, growing on the substratum surface and due to their further transformation. The high humus loamy soil is more sensitive to removing of the main humus formers. Absence of litter and grasses with root system was not compensated by mosses. As a result, the loamy soil has lost 18% of humus supply during the experiment.

The increase of the average daily air temperature in July by 2.4°C, of July temperature from 8 to 20 o'clock by 3.1–3.4°C and of August temperature by 1.2–2.5°C caused the intensified humus mineralization in the loamy and the loss of 48–51% of its primary supply.

The humus horizon of the soddy-pine loamy sand soil after replacing in the site, where temperature and moisture regime are more equal in comparison with natural conditions of forming of this soil type, accumulated the newly formed humus. Humus supply increased 26–33% in 11 years.

REFERENCES

Arinushkina, E.V. 1970. Methods of soil chemical analyses. MGU, Moskow, Russia.

Bonan, G.B., and K. Van Cleve. 1992. Soil temperature, nitrogen, mineralization, and carbon source-sink relationship in boreal forests. Can. J. Res. 22: 629–639.

Carlyle, J.C. 1993. Organic carbon in forested sandy soils: properties, processes, and the impact of forest management N.Z.J. Forest. Sci., V, 23., N.3: 390–402.

Gadgiev, I.M., and M.I. Dergacheva. 1995. Experimental research of soil evolution Pochvovedenie, 3: 277–289.

Ivanov, I.V., and A.L. Alexandrovsky. 1984. Methods for studying of soil evolution and age Puschino, Russia.

Ponomareva, V.V., and T.A Plotnicova. 1975. Determination of carbon and nitrogen content in peaty soils by Anstett's method in modification of Ponomareva and Nikolaeva. p. 79–83. In V.V. Ponomareva and T.A. Plotnikova (ed.) Methods for determination of soil humus content and composition. Leningrad, Russia.

Pleshikov, F.I., E.P. Popova and E.F. Vedrova. 1976. Soils. p. 37–79. In N.V. Orlovsky (ed.) Soil factors of the pine forests productivity. Nauka, Novosibirsk, Russia

Vedrova, E.F 1980. Influence of pine stands on soil Nauka, Novosibirsk, Russia.

Vedrova, E.F., and E.G. Tchagina. 1977. Removing rootlets and other plant residues from soil with heavy liquids, Pochvovedenie, 2: 147–148.

Vedrova, E.F. 1996. Carbon balance in pine forests of Krasnoyarsk forest-steppe. Lesovedenie, 5: 51–59.

Contaminants

The Use of Frozen-ground Barriers for Containment and In-situ Remediation of Heavy-metal Contaminated Soil

G.E. BOITNOTT[1], I.K. ISKANDAR[1], S.A. GRANT[1]

ABSTRACT

Barriers formed from artificially frozen ground have been proposed for isolating heavy-metal contaminated soils. In this bench-top study, we examined the effectiveness of a frozen-ground barrier in containing heavy-metal-laden liquid generated during soil remediation. A soil, artificially contaminated with Cd, Cu, Ni, and Zn, was placed above a frozen water-saturated uncontaminated soil layer. The temperature of the frozen layer was maintained at –3°C. The contaminated soil was flushed with a 0.1 M EDTA solution. Over 90% of the Cu and Zn and over 80% of the Cd and Ni were recovered from the unfrozen layer. Most of the remaining metals were found in a narrow zone of soil at the boundary between the frozen and unfrozen layers, while smaller amounts appear to have migrated into the barrier, apparently by diffusion in liquid-water films. The experiments demonstrated that the frozen-soil barrier prevented the migration of most of the metal–EDTA complexes, even at only –3°C. While the mechanism for the movement of small amounts of metals into this layer remains unclear, we suspect cooling below –3°C would improve the barrier's performance.

Key words: Frozen barriers, heavy metals, soil remediation, permafrost, containment.

INTRODUCTION

When metals, many of which exist naturally in soil, are present in elevated concentrations, they are considered contaminants and can be harmful to human health. It is therefore necessary to identify, isolate, and remediate metal-contaminated soils. Heavy-metal contaminated soil can either be remediated in-situ or the soil can be removed for ex-situ remediation (Ellis et al. 1986, Bricka et al. 1993, Iskandar and Adriano 1996, personal communication). In-situ soil remediation is usually simpler and cheaper.

Metals can be extracted from contaminated soils by pumping a complexing agent through the soil. An aqueous extracting solution of ethylenediaminetetraacetic acid (EDTA) has been shown to be an effective chelator of many heavy metals in a wide variety of soil types (Norvell 1984; Mobley 1988; Peters and Shem 1995), and is often chosen as an appropriate carrier liquid.

Frozen-ground barriers have been proposed to isolate heavy-metal contaminated soil during remediation (Iskandar and Jenkins 1985, Iskandar 1986, Andersland et al. 1996). Barriers formed by artificially freezing the ground around a volume of soil contaminated with heavy metals can prevent groundwater seepage into and out of this area, and thus isolate the soil during cleanup. Before frozen ground can be routinely used for soil remediation, its effectiveness as a barrier to the complexing liquid and complexed metals must be evaluated. In the following experiment we analyzed the performance of a frozen barrier during remediation of a metal-contaminated soil with EDTA.

MATERIALS AND METHODS

A laboratory experiment was set up to simulate the in-situ removal of heavy metals from a contaminated soil. An uncontaminated sandy silt (Windsor silt loam, Lebanon Landfill sand) was collected locally. The soil was passed through a 420-μm sieve and air dried (initial water content of 1% w/w) before being used as the primary soil in this experiment. Single-element stock solutions, containing 5000 mg/L of Cd, Cu, Ni, and Zn were prepared from $CdSO_4$, $CuSO_4$, $NiCl_2$, and $ZnSO_4$, respectively. From these stock solutions, a mixed-metal solution was made that contained 222 mg Cd/L (1.97 mM), 1340 mg Cu/L (21.08 mM), 778 mg Ni/L (13.25 mM), and 2513 mg Zn/L (38.44 mM).

The mixed-metal solution was used to saturate three individual subsamples of the dried soil (18% w/w moisture content). These metal-spiked subsamples are

---

Table 1. The concentrations of heavy metals in the soil used in this study compared to the averaged concentrations found in worldwide "natural" soils.

Metal	Worldwide soils* ($\mu g/g$)	Uncontaminated soil ($\mu g/g$)	Contaminated soil ($\mu g/g$)
Cd	0.06–1.1	0.45	43.5
Cu	6–80	15.3	209.6
Ni	4–55	16.5	147.0
Zn	17–125	21.1	429.3

* (McBride 1994)

referred to as the "contaminated soil." The contaminated soil contained acid-extractable metal concentrations of 43.5 µg Cd/g, 210 µg Cu/g, 147 µg Ni/g, and 429 µg Zn/g (all concentrations are expressed on a dry-weight basis)–concentrations considered to be well above the natural range of these elements found in most soils (Table 1). A fourth subsample of soil (the control) was wetted with double-deionized water (intended moisture content of 18%, actual 17% w/w). A larger amount of the sieved and dried soil (the "uncontaminated soil") was saturated with double-deionized water (intended moisture content of 18%, actual 19% w/w). Each container of wetted soil was sealed and refrigerated for two weeks while the soil and solution equilibrated.

The apparatus (Fig. 1) consisted of four sealed cylindrical chambers with insulated cooling coils, and two recirculating constant-temperature baths. Each chamber was 15.2 cm high by 7.6 cm in diameter, had inlet and outlet ports through the top endcap, and a porous polypropylene plate and drainage port on the bottom endcap. A copper coil, connected to a recirculating constant-temperature bath set to –3°C, was fitted around the bottom half of the chamber and was used to maintain the frozen layer. A second coil, connected to a 10°C constant-temperature bath, was placed above the first coil.

The equilibrated uncontaminated soil was compacted into the bottom half of each chamber to a wet bulk density of 1.9 g/cm³. The copper coils were placed around the chambers and were then insulated. The soil was cooled and its temperature held constant at –3 ± 0.1°C for 31 days, at which point it was observed to be completely frozen. Once the soil was frozen (the frozen layer), a POREX porous polypropylene filter connected to outlet tubing was placed on top of the frozen soil in each chamber. The upper halves (the unfrozen layer) of three of the chambers were each then filled with 565 g of contaminated soil, while the fourth was filled with 600 g of the control soil. The second circumferential coil, placed at the base of the unfrozen layer cooled this zone to 10°C. The chambers were then sealed and allowed to equilibrate for 18 days.

Each day, following the 18-day equilibration period, filtered leachate was removed from approximately 7 cm below the unfrozen soil surface with a hand-operated vacuum pump attached to the exit tubing. Leachate was removed until flow stopped. From reservoirs above the chambers, an extracting solution dripped through the inlet port onto the upper surface of the unfrozen layer. Flow rates varied from 0.1 to 1 mL/min. Flow was stopped when the soil column no longer accepted liquid. In this manner, contaminated solution was removed and fresh, uncontaminated solution was added daily, with a 12- to 24-hour hold period between removals. This procedure was designed to simulate a worst-case scenario, in which the leachate was allowed to stand above the frozen soil, thus providing time for any interactions with it.

The first liquid introduced into the chambers was double-deionized water, which began the extraction of the easily soluble metals. After a few water washings (less than 0.5 pore volumes), a 0.1 M Na–EDTA (the disodium salt of EDTA) solution was introduced into the chambers for subsequent washings. After the contaminated soils and the control were washed in this manner 21 times, the leachate from the contaminated soils did not exhibit the characteristic blue-green color of Cu-Ni-complexed EDTA. At this time, double-deionized water was again introduced to flush out the remaining EDTA solution. Due to the lack of leachate flow, it became necessary to stop rinsing with water and continue rinsing with 0.01M CaCl₂ (Mobley 1988).

Figure 1. Apparatus designed to test the effectiveness of a frozen soil layer as a barrier during in-situ removal of heavy metals from a contaminated soil. A hand pump was connected to the outlet tubing and was used to remove leachate from the chambers. Each chamber was fitted with an insulated coil connected to a recirculating constant-temperature bath.

410

After the final leachate removal, the chambers were dismantled. The soil columns were horizontally sectioned at 1-cm intervals using a Teflon spatula. Although the uncontaminated soil was sampled with the coils still functioning, it was no longer frozen. Each soil section was placed in a polypropylene container, sealed, and stored at −10°C until analysis.

ANALYTICAL METHODS

The concentrations of Cd, Cu, Ni, and Zn in the collected leachates were measured using a Perkin-Elmer 5100 PC flame-atomic absorption spectrophotometer. Samples were diluted as necessary, and background matrices were matched in the analytical blank and standards.

At the start of the experiment, we measured the gravimetric moisture content of the frozen-layer uncontaminated soils and the unfrozen-layer contaminated and control soils. Moisture contents were also measured for each 1-cm soil section removed when the chambers were dismantled.

Acid-digestable metals were removed from a representative subsample of each of the collected soil samples using a closed-vessel, microwave, acid-digestion procedure. The soils were well mixed before 5-g divisions were oven dried (110°C) for a minimum of 12 hours. The procedure of Kingston and Jassie (1988) was followed for calibration of the microwave oven. A slightly modified version of the digestion and sample preparation method of Hewitt and Reynolds (1990) was used. A 0.5-g division of oven-dry sample was mixed with 10 mL of concentrated nitric acid in a Teflon vessel. The capped vessel was heated for 140 s at 603 W followed by 10 min at 494 W. After digestion, the solutions were diluted with double-deionized water and allowed to settle before analysis. Three NIST Standard Reference Soils (2704 Buffalo River sediment, 2709 San Joaquin soil, and 2711 Montana soil) were also digested in this manner to evaluate the efficiency of the digestion procedure. The analyses of these standard materials showed recoveries of 103% for Cd, 100% for Cu, 94% for Ni, and 90% for Zn. Concentrations of Cd, Cu, Ni, and Zn in the digested soils were measured using flame-atomic absorption spectroscopy.

RESULTS AND DISCUSSION

Leachate samples

Analyses of the leachate showed that EDTA solution equal to 5 to 6 pore volumes removed most of the metals in the unfrozen layer within 30 days (Fig. 2).
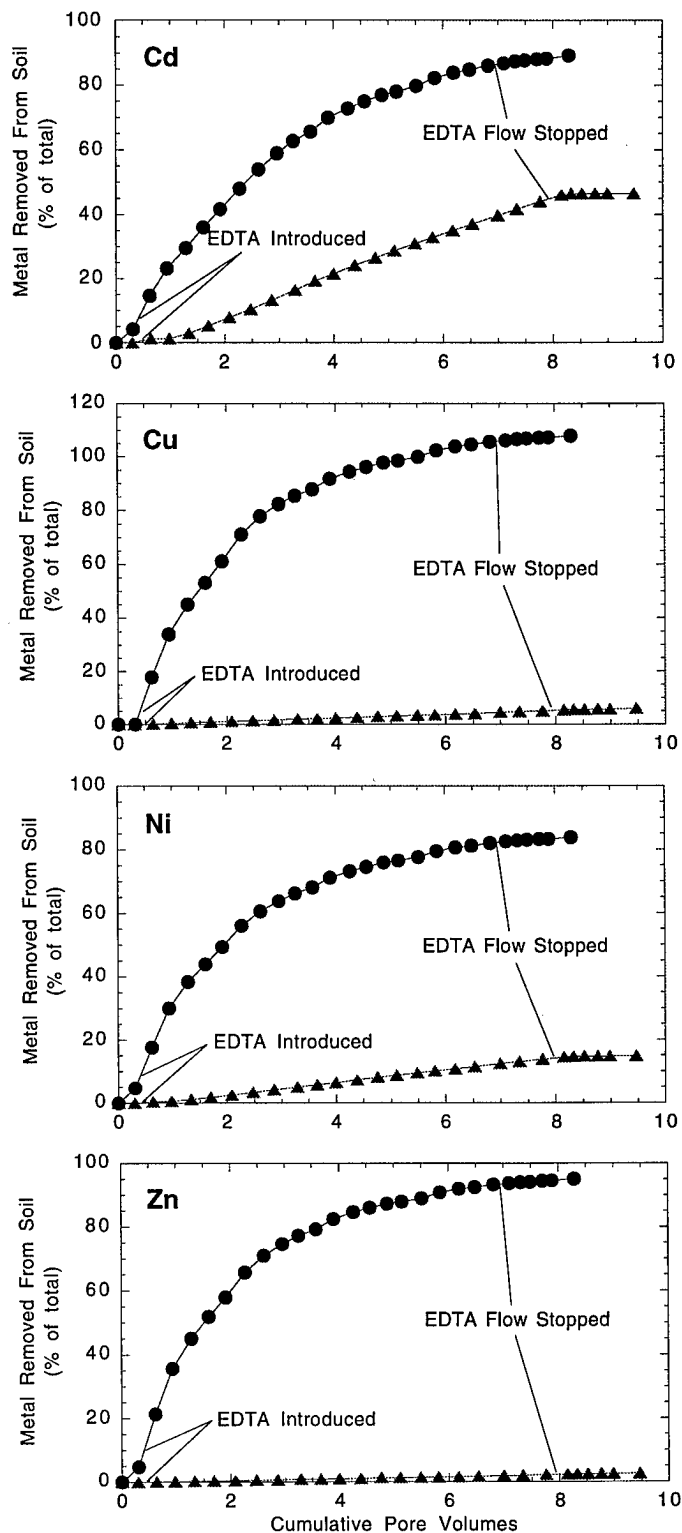
Figure 2. Metal in leachate removed from the unfrozen layer. The curves show the adequacy of EDTA in extracting Cd, Cu, Ni, and Zn from this soil. Percentages are based on the total acid digestable concentration (natural + spike) of each metal initially present in the contaminated soil (unfrozen layer). The contaminated soil data are averages of the three replicate chambers. ▲ control; ● contaminated soil.

411

Table 2. The cumulative amounts and percentage of total Cd, Cu, Ni, and Zn measured in leachate removed from the contaminated soil and the control.

Cumulative pore volume (mL)	Cd Removed from unfrozen layer (mg)	(%)	Cu Removed from unfrozen layer (mg)	(%)	Ni Removed from unfrozen layer (mg)	(%)	Zn Removed from unfrozen layer (mg)	(%)
				Contaminated Soil *				
0.3 ± 0.0	0.9 ± 0.1	4.2	0.0 ± 0.0	0.0	3.3 ± 0.3	4.7	9.9 ± 0.9	4.8
0.6 ± 0.0	3.1 ± 0.2	14.6	17.6 ± 3.1	17.8	12.4 ± 1.5	17.6	43.9 ± 5.1	21.3
0.9 ± 0.0	4.8 ± 0.4	23.1	33.6 ± 5.2	33.9	21.1 ± 3.0	30.0	73.3 ± 8.7	35.6
1.3 ± 0.1	6.1 ± 0.5	29.4	44.7 ± 6.6	45.1	27.0 ± 3.8	38.3	92.5 ± 10.8	45.0
1.6 ± 0.1	7.5 ± 0.8	35.8	52.7 ± 7.2	53.1	30.9 ± 3.9	43.9	106.6 ± 10.9	51.8
1.9 ± 0.1	8.6 ± 1.0	41.5	60.7 ± 7.8	61.2	34.7 ± 3.9	49.3	118.9 ± 11.1	57.8
2.3 ± 0.2	10.0 ± 1.0	48.0	70.7 ± 7.7	71.1	39.5 ± 3.4	56.0	135.0 ± 10.5	65.6
2.6 ± 0.2	11.2 ± 1.0	53.9	77.4 ± 7.3	77.9	42.7 ± 3.1	60.6	145.8 ± 9.5	70.8
3.0 ± 0.2	12.3 ± 1.0	59.0	81.9 ± 7.1	82.3	45.0 ± 2.9	63.8	153.4 ± 8.7	74.5
3.3 ± 0.3	13.1 ± 0.9	62.8	85.0 ± 6.8	85.4	46.6 ± 2.8	66.2	158.7 ± 8.3	77.1
3.6 ± 0.3	13.7 ± 0.8	65.6	87.4 ± 6.0	87.7	48.0 ± 2.3	68.0	162.8 ± 6.8	79.1
3.9 ± 0.3	14.6 ± 0.8	69.8	91.3 ± 5.7	91.7	50.1 ± 2.1	71.1	169.7 ± 6.3	82.4
4.3 ± 0.3	15.2 ± 0.7	72.7	94.1 ± 5.1	94.4	51.6 ± 1.8	73.2	174.2 ± 5.1	84.6
4.6 ± 0.3	15.6 ± 0.7	74.9	95.8 ± 5.2	96.1	52.6 ± 1.8	74.6	177.0 ± 5.0	86.0
4.9 ± 0.3	16.0 ± 0.6	76.8	97.4 ± 4.8	97.7	53.5 ± 1.5	75.8	179.6 ± 4.3	87.2
5.2 ± 0.3	16.2 ± 0.6	77.9	98.2 ± 4.6	98.5	54.0 ± 1.4	76.5	181.0 ± 3.9	87.9
5.5 ± 0.3	16.6 ± 0.5	79.7	99.6 ± 4.5	99.9	54.7 ± 1.3	77.6	183.1 ± 3.6	88.9
5.8 ± 0.4	17.1 ± 0.4	82.2	102.0 ± 4.0	102.3	56.0 ± 1.1	79.4	186.9 ± 2.8	90.8
6.2 ± 0.3	17.5 ± 0.3	83.9	103.5 ± 3.6	103.8	56.8 ± 1.0	80.6	189.3 ± 2.5	91.9
6.5 ± 0.3	17.7 ± 0.3	84.8	104.3 ± 3.6	104.5	57.2 ± 0.9	81.1	190.5 ± 2.3	92.5
6.8 ± 0.3	17.9 ± 0.3	86.0	105.3 ± 3.3	105.5	57.8 ± 0.8	82.0	192.1 ± 2.0	93.3
7.1 ± 0.3	18.1 ± 0.2	86.8	105.9 ± 3.2	106.1	58.2 ± 0.8	82.5	193.0 ± 1.9	93.7
7.3 ± 0.3	18.2 ± 0.3	87.4	106.3 ± 3.3	106.5	58.4 ± 0.8	82.8	193.6 ± 2.0	94.0
7.5 ± 0.4	18.3 ± 0.2	87.7	106.5 ± 3.2	106.7	58.5 ± 0.8	83.0	194.0 ± 1.9	94.2
7.7 ± 0.4	18.4 ± 0.2	88.1	106.8 ± 3.2	107.0	58.7 ± 0.7	83.2	194.4 ± 1.8	94.4
7.9 ± 0.4	18.4 ± 0.2	88.3	106.9 ± 3.2	107.1	58.7 ± 0.7	83.3	194.6 ± 1.7	94.5
8.3 ± 0.4	18.6 ± 0.2	89.2	107.6 ± 3.2	107.8	59.1 ± 0.7	83.8	195.8 ± 1.7	95.1
				Control				
0.3	0.0	0.0	0.0	0.0	0.0	0.0	0.0	0.0
0.6	0.0	1.3	0.0	0.2	0.0	0.4	0.0	0.1
1.0	0.0	1.3	0.0	0.4	0.0	0.6	0.0	0.2
1.3	0.0	3.0	0.0	0.6	0.0	1.2	0.0	0.3
1.7	0.0	5.3	0.0	0.9	0.2	1.8	0.0	0.3
2.1	0.0	7.9	0.0	1.1	0.2	2.6	0.0	0.5
2.5	0.0	10.4	0.1	1.4	0.3	3.4	0.0	0.6
2.9	0.0	13.2	0.1	1.7	0.4	4.2	0.0	0.7
3.3	0.0	16.4	0.2	2.0	0.4	5.0	0.0	0.8
3.7	0.0	19.2	0.2	2.2	0.5	5.8	0.0	0.9
4.0	0.0	21.5	0.2	2.4	0.6	6.5	0.1	1.0
4.4	0.0	24.1	0.2	2.6	0.6	7.3	0.1	1.1
4.8	0.0	26.4	0.2	2.9	0.7	8.1	0.1	1.2
5.1	0.0	28.6	0.3	3.2	0.8	8.8	0.1	1.3
5.5	0.0	30.8	0.3	3.4	0.8	9.5	0.2	1.4
5.8	0.0	32.7	0.3	3.6	0.9	10.1	0.2	1.5
6.2	0.0	34.9	0.3	3.8	0.9	10.8	0.2	1.6
6.5	0.0	36.9	0.3	4.1	1.0	11.5	0.2	1.7
7.0	0.0	39.6	0.4	4.5	1.1	12.4	0.2	1.9
7.3	0.0	41.6	0.4	4.8	1.1	13.0	0.2	2.0
7.8	0.1	44.0	0.4	5.1	1.2	13.8	0.2	2.2
8.1	0.1	46.1	0.4	5.4	1.2	14.4	0.3	2.4
8.3	0.1	46.5	0.4	5.6	1.3	14.6	0.3	2.4
8.5	0.1	46.5	0.4	5.6	1.3	14.7	0.3	2.5
8.8	0.1	46.5	0.5	5.7	1.3	14.7	0.3	2.5
9.0	0.1	46.5	0.5	5.7	1.3	14.7	0.3	2.5
9.5	0.1	46.5	0.5	5.9	1.3	14.9	0.3	2.6

* Average of 3 test chambers

412

Little additional metal was recovered after 7 to 8 pore volumes, so EDTA flow was stopped. Essentially all of the Cu was removed from the contaminated soil, whereas only 84% of the Ni was Na–EDTA extractable (Table 2). Recoveries of Cd and Zn were somewhat better than Ni, with removal of 89% Cd and 95% Zn. Other studies using EDTA as the extracting solution have also shown poorer recovery of Ni than other heavy metals (Ellis et al. 1986, Mobley 1988).

Small amounts of liquid (less than 2 mL) periodically accumulated in the drainage tubing below the frozen layer in the control chamber and in one of the contaminated-soil chambers. The liquid that drained from the control contained metal concentrations similar to the background levels measured in the leachate from this chamber. The liquid that was recovered from the drainage tubing below the contaminated chamber, however, was the same blue/green color as the leachate

and had high metal concentrations (38 mg Cd/L, 313 mg Cu/L, 165 mg Ni/L, and Zn not measured).

Soil samples

Although a relatively small percentage of the initial metal present in the soil remained after washing with Na–EDTA, what percentag did remain clearly showed the effectiveness of the frozen layer as a barrier to metal–EDTA complexes. A peak in the concentration of each of the metals was observed at the boundary between the frozen and unfrozen layers (Fig. 3). The high concentrations of metals observed at the base of the unfrozen layer might reflect the leachate removal method's inability to completely pump fluid from this section. This does not, however, fully explain the observed peaks. The four metals (particularly Ni) continued to exhibit significantly elevated concentrations 2 cm into the frozen layer. It is likely that this interval
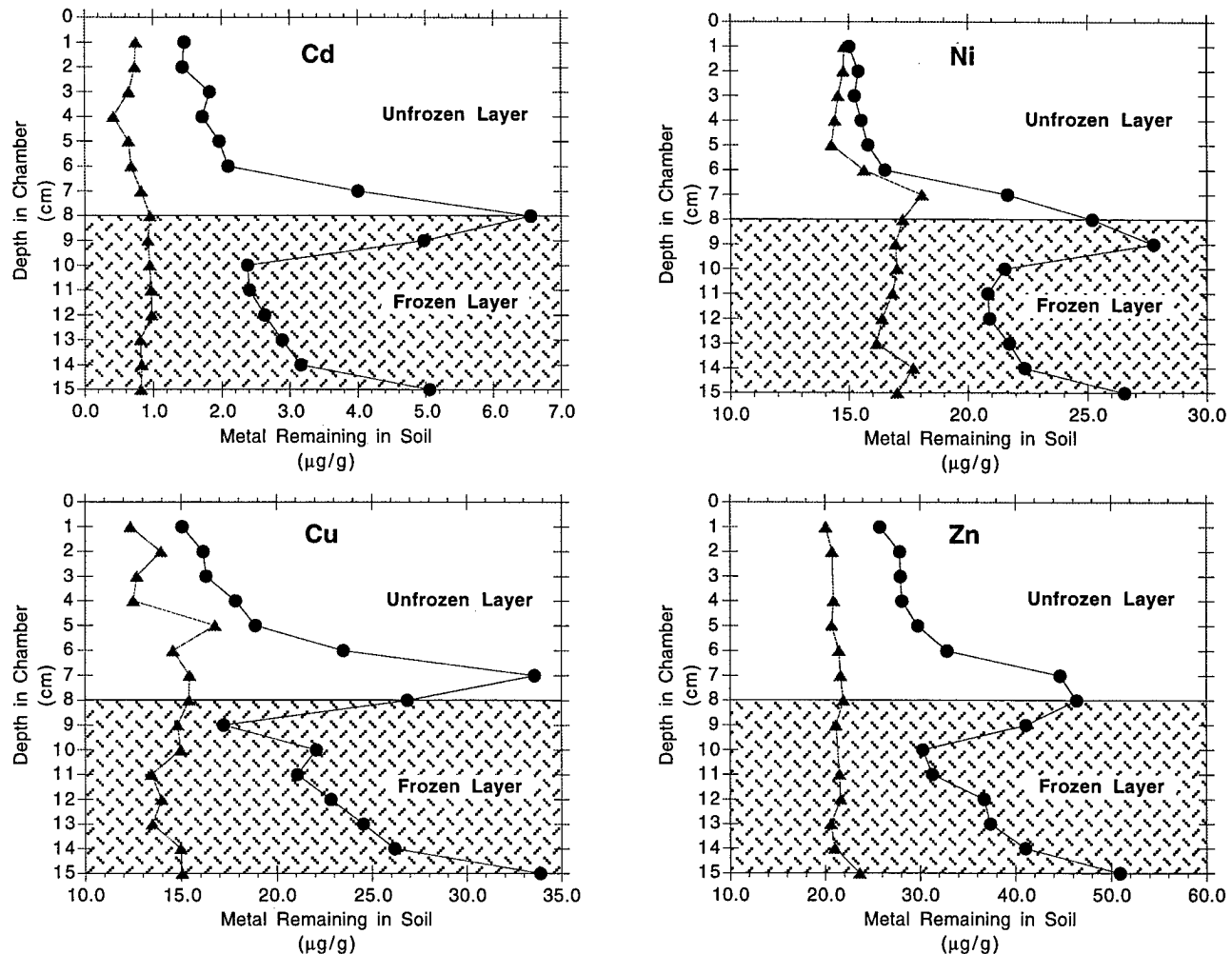
Figure 3. Metals extracted from soil sections after soil washing. Profiles show a peak in metal concentration at the boundary between the unfrozen and frozen layers. A second rise in concentration is observed at the base of the frozen layer, while throughout the frozen layer, Cd, Cu, Ni, and Zn levels remain slightly elevated. ▲ control chamber; ● contaminated chambers.

Table 3. Cd, Cu, Ni, and Zn measured in soil sections after soil remediation.

Depth in chamber (cm)	Cd remaining in soil		Cu remaining in soil		Ni remaining in soil		Zn remaining in soil	
	Control chamber ($\mu g/g$)	Contaminated chambers ($\mu g/g$)	Control chamber ($\mu g/g$)	Contaminated chambers ($\mu g/g$)	Control chamber ($\mu g/g$)	Contaminated chambers ($\mu g/g$)	Control chamber ($\mu g/g$)	Contaminated chambers ($\mu g/g$)
0–1	0.75	1.46 ± 0.42	12.4	15.1 ± 1.5	14.8	15.0 ± 0.3	20.1	25.8 ± 0.9
1–2	0.73	1.43 ± 0.48	13.9	16.2 ± 0.6	14.8	15.4 ± 0.7	20.8	27.9 ± 1.1
2–3	0.65	1.82 ± 0.43	12.7	16.3 ± 0.4	14.5	15.2 ± 0.6	27.8 *	27.9 ± 0.5
3–4	0.42	.1.72 ± 0.37	12.5	17.9 ± 1.6	14.4	15.5 ± 0.9	20.9	28.1 ± 0.6
4–5	0.64	1.96 ± 0.23	16.8	18.9 ± 0.9	14.3	15.8 ± 0.5	20.7	29.8 ± 1.6
5–6	0.68	2.10 ± 0.25	14.6	23.5 ± 1.3	15.6	16.5 ± 0.7	21.5	32.8 ± 0.4
6–7	0.82	4.00 ± 0.37	15.4	33.6 ± 1.8	18.1	21.7 ± 0.5	21.6	44.7 ± 2.0
7–8	0.95	6.55 ± 1.07	15.4	26.9 ± 3.4	17.3	25.2 ± 0.7	21.9	46.4 ± 2.9
8–9	0.92	4.97 ± 0.90	14.8	17.2 ± 0.9	17.0	27.8 ± 1.2	21.2	41.1 ± 1.8
9–10	0.95	2.38 ± 0.33	15.0	22.1 ± 4.1	17.0	21.5 ± 0.2	45.6 *	30.3 ± 0.6
10–11	0.97	2.40 ± 0.18	13.4	21.1 ± 1.9	16.8	20.8 ± 0.8	21.5	31.3 ± 3.2
11–12	0.98	2.63 ± 0.30	14.0	22.8 ± 3.3	16.4	20.9 ± 1.0	21.6	36.7 ± 9.6
12–13	0.81	2.88 ± 0.66	13.5	24.5 ± 2.8	16.2	21.7 ± 1.9	20.6	37.4 ± 8.8
13–14	0.83	3.16 ± 0.98	15.0	26.2 ± 5.3	17.7	22.4 ± 2.5	21.0	41.1 ± 12.7
14–15	0.82	5.06 ± 0.62	15.0	33.9 ± 4.9	17.0	26.5 ± 2.7	23.6	50.9 ± 7.7

(The left side of the table is labeled "Unfrozen layer" for rows 0–1 through 8–9, and "Frozen layer" for rows 9–10 through 14–15.)

* Sample contaminated during analysis

was at times unfrozen, a consequence of its contact with the overlying warmer soil and added solution.

Throughout the originally uncontaminated frozen layer, metal concentrations were higher than in the overlying cleaned soil and the control, although they were generally lower than the peak concentrations measured in the boundary layers. A second increase in concentration was observed in the bottom section of the frozen layer. At no depth in the frozen layer was the metal concentration as low as concentrations found in the control (Table 3). Apparently, there was some migration (although a small amount compared to the original contaminants) of heavy-metals into and through the frozen layer from the overlying contaminated soil. Inasmuch as fluid was observed in the drain tubing of two of the chambers, the metals were most likely complexed with EDTA in the leachate, and possibly moved along pathways of unfrozen water in the frozen soil. Alternatively, the higher-than-background metal concentrations may be an effect of free-ion migration through the frozen soil.

The removal of leachate by mechanical pumping had an expected desaturating effect on the contaminated soil (Fig. 4). Additionally, the moisture profile in the frozen layer appeared to be altered during the remediation of the overlying soil. Moisture content, measured in soil layers after the experiment was completed, gradually increased with increasing depth into the frozen layer. The starting soil was uniformly saturated. Most of the moisture trend can be accounted for by the redistribution of water initially present within the frozen layer.
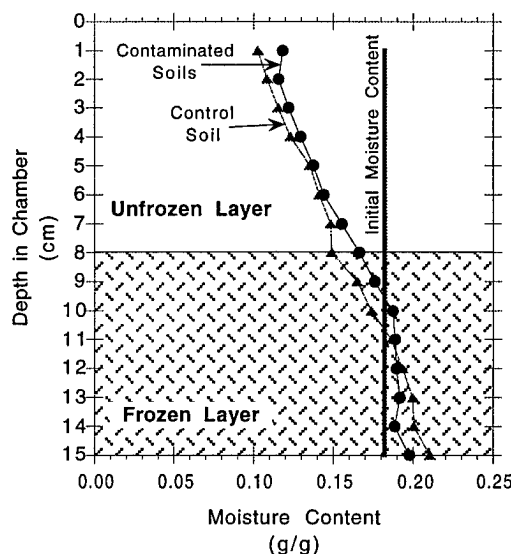
Figure 4. Moisture content variation in soil sections after soil washing. Soil was initially saturated to approximately 18%. The unfrozen layer was left undersaturated after the final removal of leachate. The moisture profile observed in the frozen layer suggests liquid movement within this section.

CONCLUSIONS

We have reaffirmed that soil washing with EDTA is a useful tool for the in-situ remediation of soils contaminated with heavy metals. Additionally, we have shown that metal–EDTA complexes did not substan-

414

Table 4. Mass balances of Cd, Cu, Ni, and Zn in soil from the test chambers before and after soil remediation.

	Cd		Cu		Ni		Zn	
	Control chamber (mg)	Contaminated chambers (mg)	Control chamber (mg)	Contaminated chambers (mg)	Control chamber (mg)	Contaminated chambers (mg)	Control chamber (mg)	Contaminated chambers (mg)
"Natural" metal present in uncontaminated soil	0.3	0.3	8.4	8.4	9.1	9.1	11.6	11.6
"Natural" + added metal present in contaminated soil	0.2	20.9	8.0	100.6	8.6	70.6	10.9	206.0
Metal recovered in leachate	0.1	18.6	0.5	107.6	1.3	59.1	0.3	195.8
Metal extracted from uncontaminated soil	0.5	1.8	7.7	12.8	9.0	12.3	11.6	20.6
Metal extracted from contaminated soil	0.2	1.1	7.6	10.4	8.2	8.4	11.8	16.3
Metal initially present in soil from entire chamber	0.5	21.1	16.4	109.0	17.7	79.6	22.5	217.6
Total metal recovered from soil in entire chamber	0.8	21.6	15.7	130.7	18.5	79.8	23.6	232.6
Increase (decrease) of metal in frozen layer	0.2	1.6	(0.8)	4.4	(0.1)	3.2	0.0	9.0
Metal recovery from entire chamber (%)	163	102	96	120	105	100	105	107

tially penetrate the frozen barrier. Within experimental and analytical error, the mass of metal initially present in the soil closely matches what is removed in the leachate during the cleanup attempt and subsequently in the digested soils (Table 4). We are confident that the majority of the contaminants were chelated by the EDTA, and that they were removed in the leachate. The EDTA solution can be added to the soil by a simple gravity-fed mechanism, and mechanical pumping can efficiently remove most of the chelated liquid.

The data suggest that there was some seepage of leachate into and through the frozen layer. The layer may have been, at times, incompletely frozen. The leachate might have melted pathways through the frozen soil, causing the barrier to corrode. At –3°C there is likely some unfrozen water present in the frozen soil that could provide pathways for leachate flow. We believe that artificially frozen ground can be an effective method of containing metal-contaminated soils and liquids during soil remediation, but that the temperature of the barrier should be maintained colder than –3°C.

REFERENCES

Andersland, O.B., D.C. Wiggert, and S.H. Davies. 1996. Frozen soil subsurface barriers: formation and ice erosion. J. Contam. Hydrol. 23:133–147.

Bricka, R.M., C.W. Williford, and L.W. Jones. Environmental Laboratory, Waterways Experiment Station. 1993. Technology assessment of currently available and developmental techniques for heavy metals-contaminated soils treatment. USACE Rep. IRRP-93-4. U.S. Army Corps of Engineers, Washington, DC.

Ellis, W.D., T.R. Fogg, and A.N. Tafuri. 1986. Treatment of soils contaminated with heavy metals. p. 201–207. In Land disposal, remedial action, incineration, and treatment of hazardous waste. Proc. of the Twelfth Annual Research Symposium, Cincinnati, Ohio. 21–23 April. 1986.

Hewitt, A.D., and C.M. Reynolds. 1990. Dissolution of metals from soils and sediments with a microwave-nitric acid digestion technique. Atomic Spectroscopy 11(5):187–192.

Iskandar, I.K., and T.F. Jenkins. 1985. Potential use of artificial ground freezing for contaminant immobilization. p. 128–137. In Proc. International Conference on New Frontiers for Hazardous Waste Manage-ment, Pittsburgh, PA. 15–18 Sept. 1985.

Iskandar, I.K. 1986. Effect of freezing on the level of contaminants in uncontrolled hazardous waste sites, Part 1: Literature review. USA Cold Regions Research and Engineering Laboratory, Special Rep. 86-19. Hanover, NH.

Kingston, H.M., and L.B. Jassie. 1988. Monitoring and predicting parameters in microwave dissolution. p. 93–154. In H.M. Kingston and L.B.

Jassie (ed.) Introduction to microwave sample preparation. Theory and practice. American Chemical Society, Washington, DC.

McBride, M.B. 1994. Environmental chemistry of soils. Oxford University Press, New York.

Mobley, K. 1988. Potential use of chelating agents for decontamination of soils. M. Engineering thesis. Dartmouth College, Hanover, NH.

Norvell, W.A. 1984. Comparison of chelating agents as extractants for metals in diverse soil materials. Soil Sci. Soc. Am. J. 48:1285–1292.

Peters, R.W., and L. Shem. 1995. Treatment of soils contaminated with heavy metals. p. 255–274. *In* H.E. Allen, C.P. Huang, G.W. Bailey, and A.R. Bowers (ed.) Metal speciation and contamination of soil. Lewis Publishers, Boca Raton.

Peatlands in the Discontinuous Permafrost Zone
Along the Norman Wells Pipeline, Canada

M.M. BURGESS[1] AND C. TARNOCAI[2]

ABSTRACT

The 869 km Norman Wells oil pipeline, in operation since 1985, runs from Norman Wells, N.W.T. south through the Mackenzie Valley and Alberta plateau to Zama, Alberta. Peatlands occur in small pockets in the northern portion of the pipeline route covering 10-40% of the terrain, while in the south they cover over 60% of the terrain, mainly in the form of peat plateaus (which are perennially frozen) and fens (unfrozen). Observations from research sites established to document the impact of the pipeline on permafrost and terrain conditions, allowed an assessment of environmental changes in peatlands resulting from pipeline construction and operation, and from natural changes. Little change occurred in the fen type of peatlands. However, disturbance to the bog type has been greater, including scraping, exposure and erosion of the peat surface, very slow recovery of vegetation, pronounced thermal degradation (up to 6 m) and surface settlement (up to 2.0 m in the pipeline trench area).

Key words: Peatlands, pipeline, permafrost, peat plateaus, environmental impact.

INTRODUCTION

The 869 km Norman Wells oil pipeline runs from Norman Wells, N.W.T. south through the Mackenzie Valley and Alberta Plateau to Zama, Alberta (Fig. 1). The route provides a transect through the discontinuous permafrost zone, beginning in widespread permafrost in the north (underlying 60-80% of the terrain) and ending in sporadic permafrost
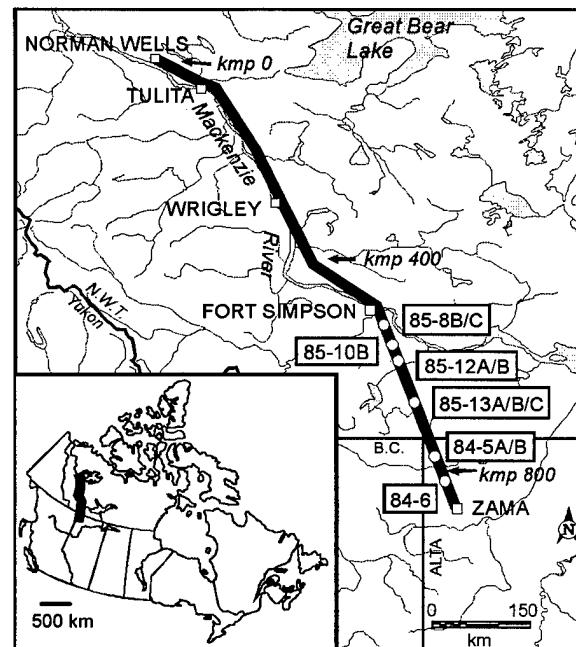
Figure 1. Pipeline route and peatland sites.

in the south (20-30%). The 328 mm (12-in) small diameter pipeline, in operation since 1985, is buried in unconsolidated Quaternary deposits: lacustrine and moraine terrain units are dominant in the north, and organic and moraine terrain in the south (Kay et al. 1983). Peatlands cover up to 75% of the terrain in the south, mainly in the form of peat plateaus (which are perennially frozen) and fens (unfrozen).

In collaboration with the pipeline company Interprovincial Pipe Line (IPL), research sites were established in the mid-1980s along the pipeline route to document and understand the impact of the pipeline

[1] Geological Survey of Canada, Natural Resources Canada, Ottawa, Ontario K1A 0E8, Canada
[2] Research Branch, Agriculture and Agri-Food Canada, Ottawa, Ontario K1A 0C6, Canada

Table 1. Location and description of peatland study sites along the Norman Wells pipeline.

Site	Kmp	Latitude	Longitude	Elev. (m)	Landform	Peat Thickness (m)		Initial Permafrost Base (m) **		Initial Active Layer (cm)		1995 Active Layer (cm)	
						ON	OFF	ON	OFF	ON	OFF	ON	OFF
85-8B	558.2	61°36'09"	121°05'27"	190	palsa bog	2.1-2.7	2.4	1.2-3.4	4.6	<100	100-200***	<200 to uf	200-300
85-8C	558.3	61°36'00"	121°05'18"	190	palsa bog	0.5-1.6	1.2	3.4-3.7	3.2	50-150	<100	thawed	na
85-10B	588.7	61°21'15"	120°51'53"	244	peat plateau	2.4-2.6	2.3	1.8-2.6	2.3	sf or <100	50-100	thawed	100-150
85-12A	608.6	61°11'33"	120°42'24"	298	fen	0.15-1.2	1.2	sf	sf	sf	sf	sf	sf
85-12B	608.7	61°11'29"	120°42'21"	300	peat plateau (2 m high)	2.9-3.2	4.8	6.7-7.0	4.5-6.1	50-100	50-100	up to 450	100-150
85-13A	682.2	60°34'06"	120°17'20"	634	peat plateau	1.5	na	6.1	na	<100	na	thawed	na
85-13B	682.4	60°34'00"	120°17'16"	634	peat plateau	1-1.2	na	5.2-6.1	na	100-150	na	thawed	na
85-13C	682.6	60°33'53"	120°17'14"	634	fen	4.9	na	sf	na	sf	na	sf	na
84-5A	783	59°45'30"	119°30'59"	552	peat plateau	3.2-3.7	3.8	14.7	14	<100-200	<100	200-300	200-300
84-5B	783.3	59°45'25"	119°30'47"	552	peat plateau	6.6-7.0	6.9	10.7	11.3	<50-200	<100	200-350	100-200
84-6	819.4	59°27'42"	119°14'48"	574	collapse scar	5.2	na	sf	na	sf	na	sf	na
84-6	819.5	59°27'41"	119°14'46"	575	peat plateau	4.6-5.5	5.6	8.5-9.8	8.3	50-100	<100	200->550	100-200

Notes: sf = seasonal frost, i.e. no permafrost; na = not applicable or not available; ON = on right-of-way; OFF = off right-of-way; ** = based on borehole log and/or temperature data; *** = shallow pond at ground surface about 3 m in diameter. Active layers are relative to initial sensor depths which were relative to ground surface elevation at time of installation, i.e. depths have not been corrected for heave or subsidence of the ground surface.

project on permafrost and terrain conditions, and to compare observed behaviour with predicted response (MacInnes et al. 1990). Several of the instrumented study sites are located in peatlands south of Fort Simpson (Fig. 1 and Table 1).

At each site, a series of boreholes were drilled, cased with PVC tubing, backfilled with silicone and instrumented with temperature cables to depths of up to 20 m, both on and off the right-of-way (ROW). The exception was site 85-13 where only one hole was drilled on-ROW at each of A, B and C. Shorter cables have sensors spaced every 50 to 100 cm; deeper cables, every 1 m for the top few metres. At several sites, air temperature sensors were later installed off-ROW, as well as shallow soil temperature probes (8 sensors to 1.5 m): one on-ROW and one off-ROW. Measurements have been obtained either manually or via data loggers over the last 12 years at each site. Level surveys have been periodically undertaken to determine changes in topography and surface settlement.

This paper focuses on an assessment of the environmental changes in peatlands resulting from pipeline construction and operation, and from natural changes. A description of the peatland types, a discussion of pipeline design, construction and operation, and a review of climate conditions are first presented.

PEATLANDS ALONG THE PIPELINE

Peatlands, which are formed by the accumulation of plant materials, are organic wetlands that have 40 cm or more peat. The Norman Wells pipeline is located in

the High Boreal and Subarctic Peatland Regions (National Wetlands Working Group 1988). The occurrence of peatlands along the pipeline route has been determined from an examination of the ditch log database (a digital record of conditions in the trench at the time of construction (Geo-Engineering 1992) for terrain with 40 cm or more peat, and from IPL's terrain mapping of the corridor at a scale of 1:20,000. Peatlands are common in all of the pipeline areas. They occur as small pockets that cover about 12-38% of the terrain in the northern portion of the pipeline route. In the south, they are the dominant surficial deposits, covering over 60% of the terrain south of the Mackenzie River crossing.

Peatland types

The boreal and subarctic regions are dominated by bogs and fens (National Wetlands Working Group 1988; Vitt et al. 1994).

Bogs:

Bogs are peat-covered wetlands in which the vegetation shows the effects of a high water table and a general lack of nutrients. The bog surface is often raised, but if it is flat or level with the surrounding wetlands, it is virtually isolated from mineralized soil waters. Hence the surface waters of bogs are strongly acid and the upper peat layers are extremely deficient in nutrients. The dominant peat materials are undecomposed sphagnum and moderately decomposed woody moss peat underlain, at times, by moderately to well decomposed sedge peat. Besides sphagnum mosses, heath shrubs are also common. Trees may be absent; if present, they form open-canopy forests of low, stunted trees. The common bog
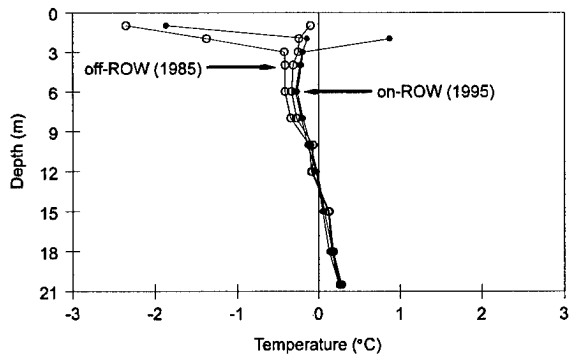
Figure 2. Ground temperature envelopes (minimum and maximum recorded during the year) at the off-ROW cable(open circle)in 1985 and at the deep on-ROW cable in 1995, site 84-5B(solid circle).

types of peat landforms occurring along the pipeline are peat plateau bogs, palsa bogs, and collapse scar bogs. With the exception of collapse scar bogs, these bog types are associated with permafrost in the pipeline area. Detailed descriptions of bogs are given by Glooschenko et al. (1993); Zoltai and Tarnocai (1975); Zoltai et al (1988a); Zoltai et al. (1988b).

Seven of the study sites on the pipeline are located in peat plateaus. Five of the sites have >3 m of peat; and up to 7 m of peat occurs at site 84-5B. Permafrost extended into the underlying mineral soil at 6 of the sites, and varied in thickness from 1.8 to 14.7 m. The greatest thicknesses were observed at the southernmost sites (84-5A/5B and 84-6) on the higher elevations of the Alberta Plateau. Permafrost temperatures are a few tenths of a degree below 0°C and temperature gradients are often low or near isothermal (Fig. 2). Ice contents within the peat were between 5% and 30% at sites 84-5A, 84-5B and 85-10B; while at sites 85-12B and 84-6 ice contents were often >40% and up to 80%. Two sites are located in palsa bogs (85-8B and 85-8C). A collapse scar bog occurs at the north end of site 84-6.

Fens:

Fens are peatlands that are also characterized by a high water table. They have a very slow internal drainage by seepage down very low-gradient slopes. The dominant peat materials are shallow to deep, well- to moderately-decomposed sedge or woody sedge peat. Depending on the water quality and quantity available, fens may or may not be vegetated with trees or shrubs. The common fen types occurring along the pipeline are northern ribbed fens and horizontal fens. Unlike bogs, fens are generally free of permafrost except for ribbed fens, which can contain some permafrost under the slightly elevated ribs. Detailed descriptions of fens are given by the National Wetlands Working Group (1988) and Zoltai and

Tarnocai (1975).

PIPELINE CONSTRUCTION AND OPERATION

The Norman Wells pipeline involves many unique design and mitigative features adopted to minimize disturbance to thaw sensitive permafrost terrain and to ensure pipe integrity. Detailed discussions of the design and construction features can be found in Nixon et al. (1984) and MacInnes et al. (1989). A summary of aspects relevant to peatlands follows.

Construction

Pre-construction activities for overland segments, excluding slopes and water crossings, involved ROW clearing up to 25 m in width during the winter prior to construction. South of kmp (kilometrepost) 400, about 25% of the route was located in previous clearings; thus much of the peatlands along the pipeline were newly cleared for construction.

Construction occurred over two winters, using a seasonal snow road of packed or cleared snow. The ditchline and the travel side of ROW were graded as required to provide a stable working platform. On peat plateaus this often involved a considerable amount of blading and scraping of the peat surface. A trench about 1 m wide by 1-1.2 m deep was excavated using Arctic and conventional ditchers, or a ripper/dozer in bouldery terrain. Excavated material was placed on the spoil side of the ROW. Native spoil was placed into and mounded over the trench (or select backfill when native material was ice rich). In peatlands, native spoil was often blocky frozen peat (blocks up to 50 cm) that could not easily be compacted. All the peatland study sites are on newly cleared ROW and had native spoil backfill.

Figure 3. Peat plateau site 84-5B, in the spring after construction (28/04/84). Travel side is on the right.

419

Revegetation efforts, undertaken to reduce erosion, focused on seeding and fertilizing mineral soils only, defined as soils where ditching exposed mineral soils. Peatlands with >1-1.2 m of peat were therefore not included in this revegetation program. Post construction activities on the ROW in peatlands have generally occurred in winter and have been limited.

Thermal design and pipe operating temperatures

The oil is chilled at Norman Wells and enters the line at temperatures approximating that of the surrounding permafrost (until 1993 chilling was kept to a constant temperature year round). The pipe was not expected to contribute significantly to permafrost thaw; rather, greater thermal disturbance was predicted to arise from ROW clearance. The level of soil and thermal disturbance in the trench was greater than that of the rest of ROW, and mean annual pipe temperatures are thus generally warmer than conditions at a similar depth on ROW (Burgess and Riseborough 1990). Oil temperatures increase by 1.5-3°C in passing through pump station compressors at kmp 336 and 585, and this increase requires more than 20 km to decay.

Mean annual pipe temperatures (MAPT) increased with distance from Norman Wells, reaching values > 0°C by kmp 80 and remaining above 0°C for the rest of the route. As well, MAPT increased with time as the overall ROW warmed in response to clearing and construction disturbance and to increased throughput (Burgess 1992). For southern segments of the route, i.e. where most peatlands occur, MAPTs have been >2°C since the second year of operation, and have locally reached values of >6°C. Since start-up, pipe temperatures have generally never dropped below 0°C in the winter months at the southern peatland sites.

In 1993, a seasonal cycle was introduced to the chilling in Norman Wells. This operational change has had the greatest influence on the first 100 km of the route (Nixon and MacInnes 1996) and has therefore not had an affect on most of the peatlands.

CLIMATE

The pipeline corridor experiences a cold continental climate with a wide annual temperature range (45°C) and relatively low levels of precipitation. Mean annual air temperature is -6.4°C at Norman Wells, -4.2°C at Fort Simpson and -2.0°C at High Level Alberta (Environment Canada 1982). South of Fort Simpson the pipeline rises in elevation onto the Alberta Plateau and there is a reversal of the latitudinal temperature trend. Mean annual precipitation is in the range 320-390 mm, with about 40-50% in the form of snow (Environment Canada 1982). Local variability in temperature and precipitation are superimposed, largely due to topographic differences.

The summer of 1994 was the warmest on record in the Valley and precipitation levels were very low. As a result a major forest fire burned across the pipeline right-of-way from kmp 140 to 200 during July and August 1994. A warm summer followed in 1995. Dry and warm conditions in early summer lead to fires in the Tulita and Norman Wells region in June 1995, crossing the pipeline ROW from kmp 42 to 95.

Climate change

The pipeline corridor is located within the Mackenzie District Climate Region, the district which has seen the greatest increase in annual average air temperature in Canada in the last century (1.7°C) (Environment Canada 1995). Increase for 1961-1990 in this district has been on the order of 0.4 to 0.6C° per decade on average. By contrast, the pattern of total precipitation change since 1948 in the Mackenzie District, shows only a slight increasing trend. However the pattern in snow cover, a parameter more critical to ground thermal regime (Goodrich 1982), shows a decreasing trend (Stuart et al. 1991).

Peatlands and climate sensitivity/variability

Stuart et al. (1991) concluded that the combined effect of air temperature increase and snow depth decrease over the last 50-100 years in the Mackenzie Valley was to produce a net warming of the ground surface. This conclusion is corroborated by the observations of the distribution of bog landforms in western continental Canada (south of 60° latitude) by Vitt et al. (1994) and Halsey et al. (1995) who have noted permafrost degradation in bogs in response to climate warming since the Little Ice Age. Their analyses revealed that where mean annual air temperatures are currently between 0.5 and -3.5°C, permafrost in peatlands is in disequilibrium with climate (i.e. much of it is relict), and that there is a lag in its response to climate warming due to the insulating effect of sphagnum. Thus under future or continued warming, large amounts of permafrost may persist for some time in disequilibrium.

Although permafrost is defined as earth material perenially below 0°C, it can exist where mean annual ground surface temperatures are greater than 0°C. This is possible due to the thermal offset phenomena within the active layer (Goodrich 1978). The ratio between thawed and frozen conductivities is low for organic soils, explaining why permafrost at the southern margins is largely confined to peatlands.

Permafrost can thus also persist in equilibrium or aggrade where ground surface temperatures are slightly above 0°C.

ENVIRONMENTAL CHANGES

Pipeline related

The results presented below draw on data and observations at the study sites as well as general observations along the remainder of the ROW.

Revegetation

Fens generally showed very little effects of the disturbance, and, if some of the root layer was removed, it quickly regenerated. Bogs were more greatly affected. This was especially true for peat plateaus because of their elevated, and hence drier, surface conditions, and of the severe blading and absence of a seeding program. Revegetation by native species on bogs, was slow or, in areas that were severely scraped, almost non-existent for the first 6-8 years (Fig. 4) due to the destruction of the root system. These severely scraped peat plateaus are now sparsely vegetated (Fig. 5) or unvegetated. When exposed the peat surfaces were severely eroded by wind erosion and as a result of oxidation.

Figure 4. Site 84-6, in August 1989. Vertical cuts from ditching are visible in the left wall of the ditch. Note: tension cracks and subsidence adjacent to ditch. Collapse scar bog visible in the background.

Subsidence of peat materials on the ROW

Very little or no subsidence has occurred on ROW areas in fens. These peatlands are not associated with permafrost, so subsidence only occurs if their hydrology is altered. This generally did not happen on the ROW, except, perhaps, along the pipe trench. On peatlands affected by permafrost (peat plateaus and palsas), however, the ROW area subsided significantly compared to the adjacent off-ROW areas.

Figure 5. Photo of site 84-5B, in September 1996.

This subsidence was even greater along the trench.

The native backfill in peat plateaus generally subsided in the first few summers following construction, often revealing the very distinct sidewall cuts made by the ditcher (Fig. 4). The warm pipeline operating temperatures led to additional thaw and settlement around the pipe. As the thaw bulb grew, tension cracks appeared parallel to the trench and the adjacent walls began to collapse into the trench. On peat plateaus it is not uncommon for a 3 m or more wide strip along the pipe trench to have collapsed, creating a wide trench that is between 0.5 and 2-m deep (Fig. 6). This situation is also illustrated in Figure 7 for sites 84-5B and 85-12B (note: ground surface elevations are based on level surveys across the ROW using a local datum and have an estimated accuracy of 20 cm). At site 85-12B, located near the edge of a 2 m high peat plateau, collapse of >1.5 m has been accelerated by thermal and hydrological erosion along the subsided ditchline at the edge of the peat plateau. Subsidence at 12B has also been greater than at 5B due to the higher ice content of the peat at the former site. Note also in Figure 7 that the pipe has settled from 1985 to 1995, by as much as 1 m.
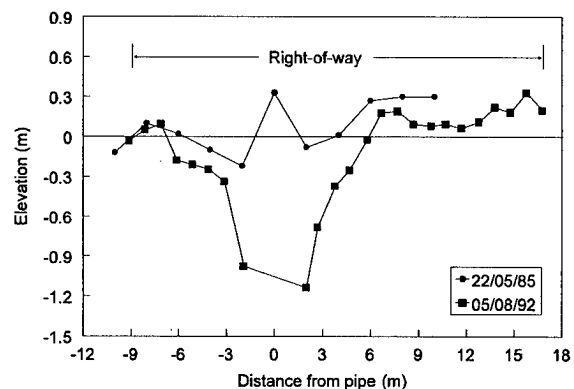

Figure 6. Level surveys on a transect at site 85-12B.

421

Ground Thermal Changes

In peat plateau and palsa bogs, thaw depths on ROW have steadily increased, and permafrost has often completely degraded (see for example 1995 active layers for palsa sites 85-8B, 85-8C and for peat plateau site 85-10B and 85-13A/B in Table 1). Figure 3 includes a plot of the 1995 annual envelopes at the on-ROW deep borehole at 84-5B. When compared to the envelopes for the off-ROW borehole in 1985, the increase in active layer and near surface ground temperatures on the ROW is apparent.

The zone of permafrost that has thawed since pipeline operation began is shown with dark shading on the cross-sections of Figure 7, and is based on position of the 0°C isotherm in 1985 and 1995. At site 5B where peat thickness is around 7 m and permafrost thickness was initially about 11 m, thaw had reached depths of 2.5 - 3 m on ROW by 1995. At site 12B, where peat thickness ranges from 3-5 m and permafrost was initially 7 m thick, 1995 thaw depths reached up to 4.5 m on the ROW. The greater thermal changes at 12B versus 5B are likely due to the former's proximity to the collapsing edge of the peat plateau, to the much greater disturbance by blading at the collapse scar/peat plateau interface, as well as its warmer pipe temperatures (influence of the pump station 25 km north of 12B).

Ground temperatures on peatlands have not stabilized in response to the pipeline construction and operation, as can be deduced from the continued increase in thaw depths and the near-isothermal permafrost temperature gradients in the 1995 temperature envelope on-ROW in Figure 3.

Changes in thaw depths off-ROW are also given in Table 1 and plotted in Figure 7. Thermal effects from the ROW clearing extend into the off-ROW. Soil probes have shown very little change in thaw depths and no surface settlement at these off-ROW sites in the southern peat plateaus. By contrast the temperature cables (data used for cross-sections) showed a slight increase in thaw depth and a greater depth of thaw than the soil probe, with <50 cm settlement. This difference may be due to the negligible level of disturbance at the soil probe versus the borehole. Surface disturbance around boreholes instrumented with temperature cables was greater than at soil probes, the former being drilled with a truck-mounted rig, the latter with a small hand-held auger. Near surface sensors (to 2-m depth) on the temperature cables reflect this local disturbance, especially off-ROW in the "natural terrain". By contrast, on-ROW the major ground surface disturbance around boreholes arises from clearing and construction. The deeper sensors off-ROW integrate
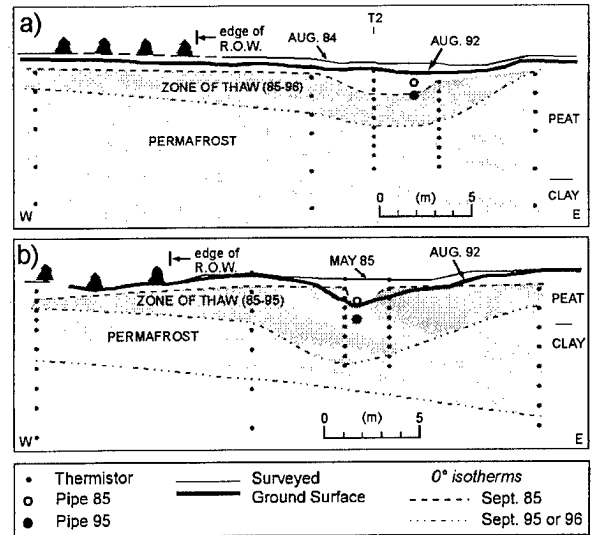
Figure 7. Cross sections of sites 84-5B (a) and 85-12B (b), showing elevation of ground surface at or near time of site establishment as well as at the time of the most recent level survey. Dark shaded areas represent permafrost that has thawed since 1985.

temperatures over a wider area (10s of metres) and thus are less sensitive to the disturbance in the immediate vicinity (1 to 2-m radius) of the borehole.

In unfrozen peatlands, such as site 85-12A, where vegetation was cleared for construction, ground temperatures have also increased up to a few degrees on the ROW. Ground temperature increases have also occurred in both frozen and unfrozen mineral terrain (Burgess 1992). The rate of increase in temperature for permafrost terrain is in large part a function of the initial ground thermal regime and the soil moisture content (Burgess and Riseborough 1990). The closer the initial permafrost temperature to 0°C and the higher the ice content, the greater will be the lag in thermal response due to latent heat effects.

Erosion

Subsidence along the ditchline has lead to the accumulation of water in the trench following snowmelt or precipitation events on elevated peat plateaus. In fens, because of the presence of a very high water table, the subsided ditch is also frequently filled with water. On gently sloping terrain (where no drainage control structures were put in place), water flow has occasionally lead to erosion along the ditchline and deposition of backfill on the ROW.

Since the ROW on peatlands was not revegetated after construction, considerable wind erosion occurred and organic matter was lost because of degradation, especially on peat plateaus. The dark-coloured surface peat warms up very quickly during the summer, with the upper centimetres reaching the air temperature, or

higher. The surface peat thus dries and becomes susceptible to wind erosion. These exposed peat surfaces are also subjected to breakdown of peat materials by oxidization, and possibly also by UV radiation. These processes result in slow erosion of peat materials. Where ROW surfaces were vegetated and their wetness maintained, as in all of the fen areas along the pipeline, this erosion did not occur.

Natural

The 1994 and 1995 forest fires affected more and larger areas than all the fires in the previous decade (1996 pers. comm.Paul Rivard, GNWT fire office), including areas along the pipeline. The 1994 fire along the pipeline occurred in mid-summer, when the thaw layer was deep and the organic material was dry. As a result, in places the peat material burned to the mineral soil, even in areas where the peat was about 40 cm thick. On the other hand, the fire affecting the pipeline in 1995 occurred in early summer, when the active layer was shallow, only the near surface peat had thawed and the peat material was relatively moist. As a result, only the surface burnt and, therefore, relatively less organic material was lost than in 1994.

Natural flooding has occurred from Manner's Creek, which runs through the area where sites 85-8B and 8C are located. This area consists of a large palsa, peat plateau and fen complex. The high water levels, especially those after floods in the summer of 1988 triggered thermal erosion in the form of subsidence and collapsing on the frozen peatlands.

All perennially frozen peatlands go through a natural cycle of early (when permafrost development begins), mature (stable), and overmature stages. During this latter stage, thermal degradation results in melting of ground ice, causing the peatland surfaces to collapse. Such natural collapse was evident on ROW at site 84-5B, and is illustrated on Figure 7 by the deep initial active layer near T2. This process is more or less in equilibrium with the climate, but the rate of collapse will increase, if climate warming occurs.

The near 0°C temperatures and near isothermal temperature gradient observed off-ROW at site 5B, for example, suggest a recent warming of the ground surface and illustrate the disequilibrium in the frozen peatland response to climate warming. Temperatures rise to near 0°C, remaining there until phase change occurs; once melted, temperatures increase further.

SUMMARY

1. Peatlands are dominant along the southern portion of the Norman Wells pipeline, covering more than 60% of the terrain south of Fort Simpson. The main peatland types are peat plateaus which are frozen and fens which are unfrozen. Twelve study sites were established to examine peatland response to the pipeline project. Observed peat thickness in the peat plateaus reached values of up to 7.0 m, while permafrost in peat plateaus on the Alberta Plateau reached thicknesses of 14.7 m.

2. Several pipeline construction and operation activities have lead to changes in peatlands, largely to peat plateaus. The main activities are clearing of the ROW vegetation, blading of the ROW surface, trenching, backfilling and warm pipe operating temperatures (mean annual >0°C).

3. Revegetation of peat plateaus was slow due to the destruction of the root system during blading and to the exclusion of peatlands from the ROW fertilizing and seeding programs. Very little revegetation by native species occurred in the first 6-8 years after construction. Fens revegetated quickly since they suffered less impact from blading and had a higher water table.

4. Wind erosion occurred on dried surface peat exposed on bladed peat plateaus. The exposed peat surfaces were also subjected to breakdown of peat by oxidization, and possibly by UV radiation.

5. Thaw depths have increased in peat plateaus and palsas along the pipeline, and in several cases, permafrost that was initially up to 6 m thick has degraded completely on the ROW. Thaw depths are greater in the vicinity of the trench, due to ditching/backfill disturbance, to subsidence and collapse, and to the warm pipe temperatures. Thaw depths off-ROW have also slightly increased (although the amount may be biased due to disturbance related to installation of the deep temperature cables).

6. Surface subsidence on peat plateaus has been significant on-ROW, and concentrated in a 3-m or more wide strip along the pipe ditch. Thaw settlement and collapse has created a wide trench, 0.5 to 2 m deep, and frequently flanked by tension cracks. Subsidence on fens has been minimal and is generally confined to the original trench backfill.

7. Ground temperatures on peatlands have not stabilized in response to the pipeline construction and operation. In fact initial ground temperature profiles indicated that locally permafrost was not in equilibrium with the current climate.

8. Thaw depths and thaw settlement on peat plateaus continue to increase after 10 years.

9. Flooding, forest fires and natural cyclical collapse also contributed to peatland changes along the pipeline and to the degradation of peat plateaus.

REFERENCES

Burgess, M.M. 1992. Analysis of the pipe and ditch thermal regime, Norman Wells Pipeline. Proc. 11th Int. Conf.. Offshore Mechanics and Arctic Eng., Calgary, Book No. H0744B, Volume V, Part A, p. 575-584.

Burgess, M.M. and D.W. Riseborough. 1990. Observations on the thermal response of discontinuous permafrost terrain to development and climate change - An 800 km transect along the Norman Wells pipeline. Proc. Fifth Can. Permafrost Conf., Collection Nordicana No. 54, Laval University, p. 291-297.

Environment Canada. 1982. Canadian Climatic Normals 1951-1980. Vol 2, Temperature and Vol 3 Precipitation. Atmospheric Environment Service, Canadian Climate Program Publication.

Environment Canada. 1995. The State of Canada's Climate: Monitoring Variability and Change; Environment Canada State of the Environment Report No. 95-1.

Geo-Engineering (M.S.T.) Ltd. 1992. Ditchwall database for the Norman Wells to Zama oil pipeline. Volume II: Revisions for UTM coordinates. Geological Survey of Canada, Open File 2539, 234 pp + diskette.

Glooschenko, W.A., C. Tarnocai, S.C. Zoltai and S. Glooschenko. 1993. Wetlands of Canada and Greenland. p. 21-42. *In:* Proc. 1st Int. Conf. Cryopedology. Nov. 10-12, 1992, Pushchino, Russia. Russian Academy of Sciences.

Goodrich, L.E. 1978. Some results of a numerical study of ground thermal regimes. Proc. Third Int. Conf. Permafrost, Vol.1, Ottawa, National Research Council, p. 29-34.

Goodrich, L.E. 1982. The influence of snow cover on the ground thermal regime. Can. Geotech. J., 19(4):421-432.

Halsey, L.A., D.H. Vitt and S.C. Zoltai. 1995. Disequilibrium response of permafrost in boreal continental western Canada to climate change; Climate Change, 30:57-73.

Kay, A.E., A.M. Allison., W.J. Botha and W.J. Scott. 1983. Continuous geophysical investigation for mapping permafrost distribution, Mackenzie Valley, N.W.T., Canada. Proc. Fourth Int. Permafrost Conf. Fairbanks Alaska, 17-22 July, 1983. National Academy Press. p. 578-583.

MacInnes, K.L., M.M. Burgess, D.G. Harry and T.H.W. Baker. 1989. Permafrost and Terrain Research and Monitoring: Norman Wells Pipeline, Vol. I. Environmental and Engineering Considerations. Envir. Studies Rep. No. 64. Dept Indian and Northern Affairs Canada.

MacInnes, K.L., M.M. Burgess, D.G. Harry and T.H.W. Baker. 1990. Permafrost and Terrain Research and Monitoring: Norman Wells Pipeline, Vol. II. Research and Monitoring Results: 1983-1988. Envir. Studies Rep. No. 64. Dept Indian and Northern Affairs Canada.

National Wetlands Working Group (ed.). 1988. Wetlands of Canada. Ecological Land Classification Series No. 24. Sustainable Development Branch, Environment Canada. Polyscience Publishers, Montreal, Canada.

Nixon, J.F. and K.L. MacInnes. 1996. Application of pipe temperature simulator for Norman Wells oil pipeline. Can. Geotech. J., 33 (1):140-149.

Nixon, J.F., J. Stuchly, and A.R. Pick. 1984. Design of Norman Wells pipeline for frost heave and thaw settlement. Proc. 3rd Int. Offshore Mech. & Arctic Eng.Symp. New Orleans, Feb. 1984.

Stuart, R.A., D.A. Etkin and A.S. Judge. 1991. Recent observations of air temperature and snow depth in the Mackenzie Valley area and their implications on the stability of permafrost layers. Atmospheric Environment Service, Canadian Climate Centre Rep. 91-2.

Vitt, D.H., L.A. Halsey and S.C. Zoltai. 1994. The bog landforms of continental western Canada in relation to climate and permafrost patterns. Arctic and Alpine Research, 26(1):1-13.

Zoltai, S.C. and C. Tarnocai. 1975. Perennially frozen peatlands in the western arctic and subarctic of Canada. Can. J. Earth Sciences, 12:28-43.

Zoltai, S.C., C. Tarnocai, G.F. Mils. and H.Veldhuis. 1988a. Wetlands of subarctic Canada. p. 55-96. *In:* National Wetlands Working Group (ed.) Wetlands of Canada. Ecological Land Classification Series No.24. Sustainable Development Branch, Environment Canada. Polyscience Publishers, Montreal, Canada.

Zoltai, S.C., S. Taylor, J.K. Jeglum, G.F. Mills and J.D. Johnson. 1988b. Wetlands of Boreal Canada. p. 97-154. *In:* National Wetlands Working Group (ed.) Wetlands of Canada. Ecological Land Classification Series No.24. Sustainable Development Branch, Environment Canada. Polyscience Publishers, Montreal, Canada.

Peculiarities of Distribution of Technogenic Hydrocarbons Through the Vertical Profile of Peat and Tundra Gley Soils of Forest-Tundra Landscapes in Western Siberia, Polluted as a Result of Oil-Gas Condensate Extraction

A.P. SADOV[1]

ABSTRACT

Distribution features of technogenic hydrocarbons are investigated in vertical profiles of peat and tundra-gley soils in the forest tundra of western Siberia, polluted from the outflow of oil and gas condensate extraction products. It was concluded that the vertical profile of pollutants in the soils depends on the type of technogenic stream, the oil bearing capacity of the substrate and the amount of time after pollution.

Key words : Tundra forest soils, oil and gas condensates, pollution, technogenic hydrocarbons, Western Siberia.

INTRODUCTION

One of the largest ecological problems, especially for landscapes of northern Russia, is the pollution of the environment with oil and petroleum (Glasovskaya & Pikovski 1985).

The area where hydrocarbon raw materials are extracted expands, basically at the expense of the ecologically most unstable areas of northern Russia. This indicates the importance for an impact assessment of these pollutants on the natural environment in this region. For northwestern Siberia, it is especially important to study the effects of oil and gas condensate raw production on the landscape.

The behavior of oil and oil products in the soils of Western Siberia is investigated only on a local scale. Existing work considers only podzolic, peat-podzolic, peat-bog and floodplain soils of the middle taiga zone (Kakhatkina et al. 1982, Slavnina et al.

1984, Gornikova & Seredina 1985; Slavnina et al. 1989, Golovenko & Nikiforov 1991).

Processes of migration, accumulation and breakdown of oil and oil products in the soils of the northern landscapes of western Siberia are almost not studied. Only some experimental work about the behavior and transformation of oil in tundra-gley soils of Western Siberia was completed (Glasovskaya & Pikovski 1985, Pikovski 1993). In other soil types of northern landscapes these features are not studied. Not clear is the behavior of technogenic hydrocarbons (TGH) in peat-gley and peat-bog soils, which cover an extensive area in the region.

Features of migration and accumulation of oil and oil products in the mentioned soil types are characterized based on a study of the tundra-forest soils of the Nadim-Purovksi River divide (Urengoy oil and gas condensate area).

Regional features of tundra-forest landscapes of this region are high humidity, active gley formation, bog processes and peat accumulation. Widespread are permafrost and frost processes. The listed factors determine specific soil profile features and the spatial structure of the soil cover, as well as the behavior and fate of hydrocarbons in the soil.

METHODS

The research was executed on the territory of the Urengoy oil and gas condensate deposit, total surface area about 6000 km^2. In the study area the vertical distribution of TGH in polluted tundra-gley and peat soils was investigated. In total 51 profiles were included, of which 12 were polluted with oil, 10 with condensate, 4 with sewage water and 5 with boring solution. The actual time of pollution was determined based on official GAZPROM documents.

[1] Moscow State University, Faculty of Geography, Department of Landscape Geochemistry and Soil Geography, Voroby'e Gory, 119899 Moscow, Russia

In order to investigate only vertical migration of TGH in the soil profile, and to exclude horizontal migration of pollutants, all investigated profiles were located in the direct neighborhood of an outflow point. On all sites profile pits were dug up to permafrost or groundwater depth.

For all identified genetic horizons soil samples were collected. To prevent contamination samples were packed in closed plastic bags.

From all samples hydrocarbons were determined using a luminescence - bituminological method. The luminescence of TGH can be observed visually with solute concentrations exceeding 10^{-6} gr/ml. The solution fluid used is hexane. For the determination of the amount of TGH in the soil standard solutions with known densities and cappilarity are prepared from a solution with known TGH concentration. The density of standard solutions as well as sample extract is determined with a fluorimeter, while the cappilarity is determined with the use of chromatographic paper. The concentration of TGH in the soil is determined according to

$$Q_J = \left(\frac{(V \cdot C_J)}{p} \right) \cdot K_p \qquad (1)$$

$$Q_H = \frac{(V \cdot C_H)}{p} \qquad (2)$$

where
$Q_{J,H}$ = amount of TGH in 1 gram soil
V = volume of extraction solution (ml)
p = weight of soil (gr)
K_p = dilution factor
$C_{J,H}$ = graphical TGH concentration.

The subscript J refers to the density measurements and the subscript H to the cappilarity measurements (Florovskaya 1957). The TGH content in the soil is obtained by averaging the results of formula 1 and 2.

A basis for comparison, appropriate non-polluted areas were selected within the limits of the study area. To excluded any significant type of pollution, the areas were selected at maximum distances from technogenic objects, being at least 1 km, and without indications of pollution. Sites were selected such that external (vegetation, topography) and internal features (soil profile) were identical to the features of polluted sites. In total 11 sites were selected. Five sites were characterized by a tundra-gley soil profile, and six by a peat soil profile. Profile description, sampling and analysis were identical to the techniques used for polluted sites.

DISCUSSION

Distribution of hydrocarbons in non-polluted soils

The investigation showed that the concentrations and overall distribution of TGH in a specific soil type were almost identical for all sites. Selected representative profiles for different soil types are presented in Table 1. Background values for the TGH content in non-polluted soils of the Urengoy area vary, depending on the original soil type. Minimum contents of TGH - less than 0.05 g/kg - are found in mineral layers of tundra-gley soil. Maximum TGH contents are characteristic for peat layers, occurring in pure peat soils and peat horizons of tundra-gley soils. As a rule maximum values do not exceed 0.45 g/kg soil.

The vertical distribution of hydrocarbons depends on the sorption characteristics of individual soil horizons. Independent of natural conditions, regional geochemical fields with increased TGH content in soils are formed around hydrocarbon raw material production areas (Pikovski 1981, Solntseva 1988, Pikovski 1993). This is caused by a general pollution of soil and landscape from all sources of technogenic (TG) activities, as well as increased natural upward diffusion of hydrocarbons due to soil cracking catalyzed by drilling activities.

Table 1. Content of hydrocarbons in typical non-polluted forest tundra soils.

Soil type, observation point	Horizon index	Depth (cm)	Hydrocarbons (g/kg soil)
Tundra peat-	T1	4-12	0.13
gley,	T2	12-26	< 0.05
5m-91	Bhgf	26-31	< 0.05
	Glf	38-45	< 0.05
Peat on old	T1	0-20	0.45
peat,	T2	20-40	0.35
91-1	T3	40-60	0.35

Hydrocarbon content in polluted soils

The superficial infiltration of TG streams containing oil and oil products into soils results in an increased TGH content of 1 to 4 orders of magnitude (Table 2).

Even after one-time TG pollution, the content of pollutants may increase up to several hundred g/kg. The highest pollution occurs with flows of crude oil or commodity oil (> 450 g/kg, Table 2).The flow of

Table 2. Maximum hydrocarbon content in polluted soils, depending on the type of pollution.

Type of TG flow, pollution frequency	Soil type, observation point	Horizon index	Depth (cm)	TGH g/kg soil
Crude oil, one-time	Tundra peat-gley, Tr-58	T1	0-5	462.0
		T3	12-35	3.75
		BH	35-53	0.46
		GH	53-85	0.67
Condensate one-time	Bog-peat, Ur-KP	Oh	0-5	3.20
		T1	5-10	21.50
		T2	10-20	81.70
		T3	20-35	1.30
Sewage with TGH, one-time	Tundra peat-gley, 5m-10	T1	0-5	17.80
		T2	5-21	0.90
		Bg	21-48	1.10
		G	80-90	0.20
Sewage with TGH, multiple	Tundra peat-gley, 5m-118	O	0-4	625.0
		T1	4-25	75.0
		T2	25-36	75.0
		G	45-60	0.75

other pollutants into the soil (condensates, sewage water with oil products, boring water, etc.) does not lead to such high pollution levels (not exceeding 80 g/kg). This difference is caused by the concentration of hydrocarbons in TG streams, as well as by their individual composition.

In case of multiple TG streams, the volume of pollutants in the soil strongly increases. The research showed that with a regular flow of sewage water with oil products and oil waste the concentration of TGH in the soil increases up to 625.0 g/kg (Table 2; point 5m-118).

Independent of the type of pollution, the highest concentration of TGH occurs in organic horizons of tundra gley and peat soils. Also for one type of TG stream, the amount of hydrocarbons that is bound by peat horizons is higher than in dry-peat or sod horizons. This is caused by differences in sorption surface area, as well as an unequal effective capacity of different substrates and capillary binding forces (Guseva & Solntseva 1996).

In mineral soil horizons, the highest concentrations of oil products are observed in light-textured (sandy) horizons, which have a higher porosity and thus retain hydrocarbons in amounts of several tens of grams. This was also observed by other researchers (Pikovski 1993). In heavy-textured (loamy) substrates of tundra-gley soils, the concentration of pollutants does not exceed several

g/kg, due to their low effective porosity and low permeability for large hydrocarbon molecules. From the presented data it is clear that the concentration of TGH in soils depends on the type of pollutant, the intensity of pollution (continuous, regular or once) and characteristics of the receiving soils (moisture content at the moment of pollution, specific surface area, pore volume etc.). These relations were also experimentally confirmed by determining the oil bearing capacity of soils (Bratsev 1988, Guseva & Solntseva 1996).

Thus, different types of soils are characterized by different factors, responsible for processes of migration and accumulation of oil and oil products. Depending on the vertical soil profile, features of the vertical distribution of TGH are determined.

Vertical distribution of techogenic hydrocarbons

The surface infiltration of any type of TG flow into the soil results in a variety of distribution profiles for TGH.

The maximum amount of pollutants can be found in the upper horizons of a soil profile (Table 3, Tr-57). This type of distribution is typical for permeable and uniform substrates (peat and sand), in which vertical migration prevails. This was also confirmed experimentally (Guseva 1995, Solntseva et al. 1996). With low amounts of hydrocarbons in TG flows the pollutants almost completely are bound in the upper part of the soil, dependent on the oil bearing capacity of this horizon.

It is possible that in the soil more than one pollution maximum occurs (Table 3, 27-3, GK-50). In this case, a concentration of pollutants occurs at greater depths in addition to the topsoil. Thus the maximum concentration of oil products may occur in the middle or even lower part of the soil profile. This, as a rule, occurs after a certain period of time following pollution, presuming that the pollution is not repeated (Table 3, X-33). The amount of TGH in the lower part of the soil profile may exceed the concentration in the topsoil 1.7 to 13 times, depending on the oil bearing capacity. Secondary internal distribution of pollutants occurs when properties of the substrate change (density, moisture content, composition): a) above denser peat layers, often due to a change in botanical composition (Table 3, 27-3); b) above permafrost, especially with large amounts of ice (Table 3, X-33); and c) above mineral horizons with heavy texture, especially gleyic (Table 3, N-47). Changes in internal distribution with changes in substrate, due to changes in speed and mechanism of vertical migration, are also observed in other natural conditions (Kalachnikova et al. 1985, Slavnina et al.

1989), and was experimentally described by modeling field situations and soil columns (Lippok 1966, Solntseva et al. 1996).

Table 3. Variations of hydrocarbons distribution in profiles of polluted soils.

Soil type, observation point	Pollutant, time after accident	Horizen index	Depth (cm)	TGH, (g/kg soil)
Peat, Tr-57	Oil, 3 months	T1	0-12	97.4
		T2	12-36	20.7
		T3	36-50	18.6
		T4	> 50	10.0
Peat, 27-3	Boring solutions, 1 year	Oh	0-6	8.4
		T1	6-15	2.2
		T2	15-40	6.3
		T3	40-50	4.0
		Tm	> 50	< 0.01
Tundra peat-gley, GK-50	Conden-sate, 1 month	Oh	0-8	65.5
		T	8-31	15.0
		G	31-45	0.5
Peat, X-33	Oil, 1 year	T1	0-7	10.0
		T3	18-40	17.4
		Tm	> 40	< 0.01
Tundra peat-gley, N-47	Oil, 1 year	T	0-9	96.4
		Bhg	9-16	73.3
		G1	16-27	1.3

The data of Table 3 indicate that with respect to TGH, soil horizons act as concentrators, accumulating pollutants (geochemical barrier-accumulators) and as "screens", hampering the vertical migration and forcing the pollutants to move in a horizontal direction (geochemical barrier-screen).

Active concentrating horizons are organic and fine-textured soil horizons. The accumulative possibilities of different substrates are not equal. High capacity barrier accumulators (peat) as well as horizons with lower capacities (sod and fine-textured mineral layers) are distinguished. Pollutants that exceed the oil bearing capacity of the substrate (at a certain moisture content) flow vertically into deeper horizons or laterally following the relief characteristics, where their concentration may decrease by only one order of magnitude (Table 3, N-47).

The unequal oil bearing capacity or oil permeability causes differences in the internal distribution of oil products up to 2-4 orders of magnitude (Table 2).

Repeated or continuous flows of pollutants into landscapes, often where TG compounds are burned or in cases of accidental outflow of sewage water with oil products onto the same area, lead to increased concentrations of pollutants in the soil profile. Thus, in a peat horizon of a tundra peat-gley soil, the amount of TGH increased 2.5 times in 4 years (the period between observations) on average with 4 g/kg each year (Table 4). With a continuing flow of polluted compounds into the soil even in heavy textured horizons, pollutants will accumulate (including gley horizons). High initial moisture content of soils causes an insignificant accumulation of pollutants, even in light-textured horizons. Regular observation showed that repeated outflow of sewage water with oil products increased the amount of pollutants in the gley horizon on average 2.5 times, although the average level of their absolute accumulation stays very low, not more than 1 g/kg soil, indicating an increase of 0.165 g/kg each year. This is ten times less than in peat horizons of the same soil type (Table 4).

Table 4. Changes in hydrocarbon content of tundra gley soils, following repeated pollution with sewage water containing oil products.

Horizen index	Depth (cm)	Hydrocarbons (g/kg soil)	
		Observations 1991	Observations 1995
O	0-7	8.00	20.00
G1	7-24	0.35	1.00
Cg	40-66	0.35	1.00

CONCLUSIONS

Investigations of TGH distribution features in tundra-forest soils of Western Siberia, polluted with hydrocarbon raw material, showed that:

1. The accumulation and redistribution of pollutants in profiles of tundra-gley and peat soils is governed by identical processes.

2. In the soil types studied, the maximum concentration of TGH after pollution is observed in organic horizons. The concentration of pollutants depends mainly on the oil bearing capacity of the horizon, which is determined by the type of organic material, moisture content, density etc.

3. In mineral horizons of tundra-gley soils the concentration of TGH is significantly lower. Under equal conditions, the concentration of pollutants in sand and loam horizons compared with peat horizons is 1 to 3 orders of magnitude lower.

4. With time, in both soil types studied a gradual migration of the main amount of TGH into deeper organic horizons of the profile is observed.

5. In tundra-gley and peat soils, for TGH two main groups of soil-geochemical barriers were distinguished: barrier-concentrator and barrier-screen. The first group concerns organic soil horizons (peat and coarse-humus), the second - heavy textured mineral soil horizons (including gley) as well as frozen horizons. Repeated observations on polluted soils showed that both barriers do not act as complete barriers; with large amounts of pollutants the barrier will "break" and TGH will occur in deeper horizons.

REFERENCES

Bratsev, A.P. 1988. Absorption of oil and oil products in peat soils. p. 29-35. *In* Impact of mineral prospecting on Bolshezemelskaya tundra environment. Rep. 90. Komi Science Center, Syktyvkar, Russia (in Russian).

Florovskaya, B.N. 1957. Luminescence-bituminological method in geology. Nedra Publishers, Moscow, Russia (in Russian).

Glasovskaya, M.A., and Yu.I. Pikovski. 1985. Complex experimental study of the factors supporting self-purification and rehabilitation of soil polluted by oil in different natural zones. p. 185-191. *In* T.I. Bobovnikova and S.G. Malakhov (ed.) Migration of polluting substances in soils and adjacent environments. 3rd All-Union Symposium, Obninsk, Russia, Sept. 1981. Gidrometeoizdat, Leningrad, Russia (in Russian).

Golovenko, V.V., and A.S. Nikiforov. 1991. Landscape-morphological features of soils of Middle Priobye polluted by oil. p. 119-123. *In* Results and directions of scientific research in the area of oil extraction on the deposits of Western Siberia. Tyumen, Russia (in Russian).

Gornikova, S.V., and V.P. Seredina. 1985. Influence of oil on the physical-chemical soil properties of the oil-gas regions of the Tomski North. Tomsk University, Tomsk, Russia (in Russian).

Guseva, O.A., and N.P. Solntseva. 1996. Modeling of oil bearing and oil yielding capacities of tundra landscape soils in European Russia. p. 417-420. *In* Proc. 4th International Symposium on the Geochemistry of the Earth Surface, England.

Kalashnikova, I.G., T.A. Maslivets, A.A. Oborin, and Yu.I. Pikovski. 1985. Transformation of oil in podzolic soils of Middle Priobye. p. 74-80. *In* T.I. Bobovnikova and S.G. Malakhov (ed.) Migration of polluting substances in soils and adjacent environments. 4th All-Union Symposium, Obninsk, June 1983. Gidrometeoizdat, Leningrad, Russia (In Russian).

Kakhatkina, M.I., V.P. Seredina, and L.A. Izerskaya. 1982. Change of soil properties under influence of pollution by oil. p. 66-67. *In* Problems of environmental protection in regions with intensively developed industry. Kemerovo, Russia (in Russian).

Lippok, W. 1966. Modelversuche uber das Verhalten von Heizol EL in porosen Medim. Deutsche wasserkundliche Mitteilungen, 10-5:145-157.

Pikovski, Yu.I. 1981. Geochemical features of technogenic flows in regions of oil extraction. p. 134-149. *In* M.A. Glasovskaya (ed.) Technogenic flows of substances and conditions of natural ecosystems. Nauka Publishers, Moscow, Russia (in Russian).

Pikovski, Yu.I. 1993. Natural and technogenic flows of hydrocarbons in the environment. Moscow State University Publishers, Moscow, Russia (in Russian).

Slavnina, T.S., M.I. Kakhatkina, V.P. Seredina, and L.A. Izerskaya. 1984. Influence of pollution by oil and oil products on soil properties. p. 141-144. *In* Melioration of lands of Siberia. Krasnoyarsk, Russia (in Russian).

Slavnina, T.S., M.I. Kakhatkina, V.P. Seredina, and L.A. Izerskaya. 1989. Pollution by oil and oil products. p. 186-207. *In* Bases of use and protection of soils of Western Siberia. Science, Novosibirsk, Russia (in Russian).

Solntseva, N.P., O.A. Guseva, and S.V. Goryachkin. 1996. Modeling migration processes of oil and oil products in soils in European Russia. Vestnik Moscow State University, Pedology 2:10-17 (in Russian).

Solntseva, N.P. 1988. General features of soil transformation in the regions of oil extractions (forms, processes, models). p. 23-42. *In* M.A. Glasovskaya (ed.) Rehabilitation of oil-polluted soil ecosystems. Nauka Publishers, Moscow, Russia (in Russian).

Predicting Diauxy During
Bioremediation in Organic Soil

D.M. WHITE[1] AND H. LUONG[1]

ABSTRACT

Bioremediation is effected by the nature and con-
centration of natural organic matter (NOM) in soil.
While soil conditions (e.g., pH, temperature, moisture
content) can be engineered to encourage microbial
degradation of a contaminant, subsurface organisms
may prefer the soil NOM to the contaminant (i.e.,
diauxic growth). The purpose of this paper is to
present, in concept, a method by which pyrolysis-gas
chromatography/mass spectrometry (GC/MS) could
be used to predict diauxic growth in contaminated
organic soil. Specific compounds in NOM were
selected to represent six biochemical classes: lignin,
lipids, primary polysaccharides, secondary polysac-
charides, protein and amino sugars. The concentration
of each compound was quantified by pyrolysis-GC/
MS in six organic soils from Alaska. Using the rela-
tive percentage of biochemicals in each sample, the
soils were ranked according to their propensity to
exhibit diauxic growth during bioremediation.

Keywords: tundra, bioremediation, pyrolysis, soil

INTRODUCTION

Many soils in Alaska contain a high concentra-
tion of natural organic matter (NOM). Due to oil
development and use in Alaska, soils have been con-
taminated with a variety of petroleum products. Natu-
rally occurring microorganisms will degrade
petroleum in soil given sufficient time and favorable
environmental conditions. In soils containing a high
concentration of NOM, however, the petroleum may
not be the preferred microbial substrate until easily
degradable NOM has been consumed (diauxic

growth). As a result, bioremediation may or may not
be successful in the anticipated time frame.

The method proposed herein was developed to
predict diauxic growth during bioremediation based
on the biochemical character of NOM in soil. The rel-
ative percentage of a suite of indicator compounds
was quantified by pyrolysis-gas chromatography/
mass spectrometry (GC/MS) in six organic soils from
Alaska. The indicator compounds were selected to
represent six biochemical classes of nonhumic matter:
lignin, lipids, primary polysaccharides, secondary
polysaccharides, proteins and amino sugars. Based on
accepted theories in soil microbiology, the soils were
ranked according to their relative propensity to
exhibit diauxic growth during bioremediation.

BACKGROUND

Natural organic matter

Natural organic matter consists of compounds
derived from plant and animal remains, microbial
decomposition and synthesis, and chemical polymer-
ization (humic substances). The breakdown and trans-
formation of NOM, referred to as the process of
humus formation, is characterized by three distinct
phases: a) rapid decomposition of some of the chemi-
cal constituents by microorganisms, b) synthesis of
new substances by microorganisms, and c) formation
of resistant complexes by various processes of con-
densation and polymerization (Waksman 1952).
Although NOM is commonly classified as only humic
acid, fulvic acid and humin, nonhumic molecules
(unaltered biochemical compounds) are abundant in
organic soils (Stevenson 1994). Nonhumic molecules
can be biochemically classified as primary and sec-
ondary polysaccharides, amino sugars, proteins, lip-

---

[1] Water Research Center, 248 Duckering, University of Alaska Fairbanks, Fairbanks, Alaska 99775, USA

ids, and lignin. The decomposition of nonhumic molecules in soil is a function of both substrate concentration (e.g., pseudo-first-order kinetics) and microbial substrate preference (e.g., based on the energy value of specific compounds). It is generally accepted that in an aerobic soil environment, compounds are degraded in the following order: sugars and starches, proteins, cellulose, lipids and lignin (Waksman 1952). A petroleum spill in organic soil could be considered an instantaneous input of lipids to the soil's NOM. The concentration may or may not be appreciable compared to the bulk concentration of organic matter. For example, the petroleum from a spill of 10,000 mg/kg dry soil constitutes only 1% of the soil mass whereas the NOM may constitute 80% of the soil mass. The specific degradation rate for petroleum, therefore, will depend on the concentration of petroleum compared to NOM and the relative percentage of different biochemicals in NOM (e.g., lipids, lignin, etc.). For petroleum spills where the input of "lipids" is small compared to the concentration of biodegradable NOM, petroleum degradation may be delayed by microbial diauxy, or two phase growth. Organisms exhibit diauxy in multisubstrate systems if one substrate is appreciably more biodegradable than another. Diauxy in bioremediation has long been known to exist. Since diauxy is only problematic in organic soils, however, research on the problem has received little attention (NRC 1995). The effect of humic molecules on diauxy in soil was not considered since the humic fraction of NOM is generally considered far more recalcitrant than the nonhumic fraction (i.e., including petroleum) (Stevenson 1994).

Pyrolysis-GC/MS

During pyrolysis, a sample is rapidly heated in a vacuum or stream of inert gas (e.g., helium). The two most common techniques are Curie point pyrolysis and controlled temperature programming pyrolysis. In the latter (used in this research), a sample is placed in a quartz tube (2.5 cm long with a 2 mm ID), wrapped in a coiled platinum filament and heated at a controlled rate. When the sample heats, volatile molecules in the sample evaporate and nonvolatile molecules crack into volatile fragments. All compounds are collected, separated, and identified by a GC/MS.

A chromatogram of pyrolyzed organic matter is commonly called a fingerprint (Stevenson 1994). Fingerprinting organic matter enables scientists to gain insight into complex organic mixtures (Bracewell et al. 1989). The complex array of pyrolyzed molecular fragments, however, has kept pyrolysis from becoming a widely used quantitative technique (Bruchet et

al. 1990, Bracewell et al. 1976). One particularly complicating factor is that any one pyrolysis product may be derived from more than one parent molecule. Pyrroles, for instance, are pyrolysis products of both porphyrins and a variety of proteinaceous compounds (e.g., proline, hydroxyproline, glutamine) (Bracewell et al. 1989, Irwin 1979). Pyridines are pyrolysis products of both proteins and nucleic acids, and hydrocarbons are produced by both proteins and lipids (Irwin 1979). Although the interpretation of the origin of many pyrolytic fragments can be extremely complex, the origin of certain molecules is easily determined (Bracewell et al. 1989). For the research described herein, only those molecules with easily identifiable origins were included in analyses.

MATERIALS AND METHODS

Soil collection

All studies reported on herein were conducted with organic soil collected from various locations in Alaska (see Table 1). The soils ranged in organic con-

Table 1. Identification of samples.

Sample ID	NOM (%)	Sample location
U1	21	Umiat
U2	60	Umiat
CF2	54	Mile 12, Old Denali Highway, AK
CF5	13	Seward Peninsula (near Nome)
TL	38	Arctic Coast (near Teshekpuk Lake)
PM	51	Lazy Mountain, (near Palmer)

tent from 10 to 60% by weight, based on ashing at 550 °C (ASTM 1987). The soils were air dried and ground with a mortar and pestle to disaggregate the soil without breaking stones. The soils were then sieved through a no. 60 sieve (0.25 mm sieve opening) to isolate and recover soil fines. Only the material passing the no. 60 sieve was used for pyrolysis to ensure homogeneity in minute samples.

Pyrolysis-GC/MS

Soil samples ranging in mass between 2 and 35 mg were quantified using a Sartorious Microbalance and packed into quartz tubes. This mass range was

431

used since previous research demonstrated that samples with a mass of less than 2 mg did not give a quantifiable signature and samples with a mass greater than 35 mg did not fit entirely within the quartz tube (White 1995). Samples were held in quartz tubes by a plug of quartz wool at each end.

Pyrolysis was conducted with a CDS Model 1000 pyrolyzer and a Model 1500 GC interface. The interface temperature was set at 235 °C with a pyrolysis heating time of 0.1 seconds, a final temperature of 700 °C, and hold time of 9.9 seconds. The pyrolysis reactor was mounted on an HP 5890 Series II gas chromatograph, with a Supelco SPB 35 (35% Ph Me silicon) column, 60 m x 0.25 m x 0.25 μm. The GC temperature program was 45 °C for 5 minutes, 2 °C / min to 240 °C and hold for 25 min. The GC was plumbed directly to an HP 5971A Series Mass Selective Detector on electron impact (EI) mode. The MS scanned mass units 45 to 650. All mass spectra were compared to the NBS54K spectral library. Helium served as a carrier gas at a flow rate of 0.5 cm³/ minute. Each sample was injected with a split ratio of 1:50. A standard curve was prepared by pyrolyzing known masses of poly-alpha-methylstyrene which has been shown to give quantitative yields (Wampler 1996). The standard curve was fit with a straight line passing through zero and having an "r^2" value of 0.99.

Soil samples (packed in a quartz tube) were injected with 5 μL of a poly-alpha-methylstyrene internal standard (8g/L in methylene chloride). Following pyrolysis, a suite of peaks were identified and quantified according to peak height above baseline. The peaks were chosen as representatives of the biochemical classes: primary polysaccharides, secondary polysaccharides, amino sugars, proteins, lipids and lignin (see Table 2). The response for each compound selected was normalized using the internal standard. The compounds were then sorted according to biochemical class and reported in relative percentages for each soil. Since the same compounds were selected from each soil, any two soils could be directly compared based on a set of five assumptions:

1. Primary polysaccharides are the most rapidly degraded organic compounds in soil and would provide an excellent alternative substrate for microorganisms during bioremediation.
2. Proteins are easily degraded and may serve as alternative substrates for microorganisms during bioremediation.
3. Amino sugars and secondary polysaccharides also may serve as alternative substrates for microorganisms during bioremediation. More

importantly, however, secondary polysaccharides and amino sugars are indicative of a high concentration of microorganisms and a history of microbial decomposition. The presence of secondary polysaccharides and amino sugars in soil represents the recent decay of easily degradable organic matter. Soils with relatively high percentages of secondary polysaccharides and amino sugars would not likely contain an appreciable concentration of alternative substrates for diauxy during bioremediation.
4. Lipids are somewhat recalcitrant and would be poor alternative substrates during bioremediation. A high concentration of lipids relative to primary polysaccharides would indicate a history of microbial decomposition.
5. Lignin is also somewhat recalcitrant and would be a poor alternative substrate during bioremediation. Some soils may contain disproportionate amounts of lignin due to variations in plant cover.

Table 2. Post pyrolysis molecules selected for analysis.

Biochemical class	Molecular ion, m/z	Post pyrolysis molecular fragment(s)
Primary polysaccharide	126, 128	Hexose, anhydro-monomer
Secondary polysaccharide	96, 110	Furfural and dimethyfuran
Amino sugar	135	Acetamide and methylacetamide
Lipid	267	n-C_{19}
Lignin	108, 150, 164	p-Hydroxyphenol compounds

RESULTS

According to the first assumption, the soils with the greatest potential for diauxic growth are those with the highest relative concentration of primary polysaccharides. As shown in Table 3, the relative percentage of primary polysaccharides in each sample was used as an indicator of the propensity for each soil to exhibit diauxic growth. Given the additional information in assumptions 2-5, a qualitative characterization of the relative decomposition in each sample was used to support this ranking.

432

Table 3. Comparison of the percentage of primary polysaccharides in each sample.

Soil sample	NOM (%)	Primary polysac-charides (%)	Relative propensity to exhibit diauxic growth
PM	51	30%	1
TL	38	28%	2
CF2	54	26%	3
UM2	60	20%	4
UM1	21	14%	5
CF5	13	0%	6

Samples with little potential for diauxy

The biochemicals quantified in soils CF5 and UM1 are shown in Fig. 1 as a percentage of the respective total. No primary polysaccharides or proteins were detected in sample CF5. In addition, a large percentage of lignin and lipids, the most recalcitrant of the soil biochemicals, were detected. Compared to the other soils tested, therefore, CF5 underwent extensive decomposition (i.e., based on assumptions 1,2,4 and 5). Since secondary polysaccharides are microbial breakdown products of primary polysaccharides, and are considered to be appreciably more recalcitrant than their respective parent molecules, the presence of secondary polysaccharides is consistent with the theory that CF5 contained decomposed organic matter (assumption 3) (Bracewell et al. 1989). This observation is also consistent with the fact that compared to the other soils, CF5 had the lowest concentration of NOM. Soils with active decomposition generally contain low concentrations of NOM. Sample CF5 has a relatively low propensity to exhibit diauxy as compared to the other soils investigated.

Sample UM1 had a relatively small percentage of biochemicals associated with primary polysaccharides and a relatively large percentage of biochemicals associated with lipids and secondary polysaccharides. According to assumptions 1,3 and 4, UM1 is a soil with a history of decomposition. Since UM1 was taken from a tundra meadow, the low concentration of lignin is not surprising. The large percentage of biochemicals from secondary polysaccharides and lipids and small percentage of primary polysaccharides are indicative of medium to highly decomposed NOM. Based on the apparent history of decomposition in soil UM1, little potential for diauxy would be expected.

CF5

UM1
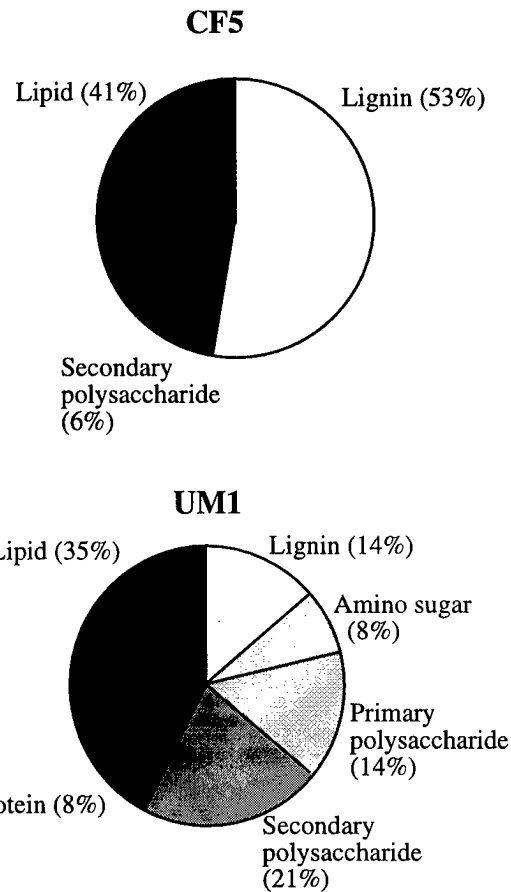
Figure 1. Relative percentage of biochemicals in samples CF5 and UM1

Samples with a medium propensity for diauxy

Analyses of samples UM2 and CF2 are illustrated in Fig. 2. Sample UM2 had a larger percentage of amino sugars and secondary polysaccharides than any of the other soils tested. According to the first three assumptions, the NOM in UM2 underwent a moderate amount of microbial decomposition.

In sample CF2, the percentage of biochemicals corresponding to lignin, amino sugars, and secondary polysaccharides suggests a history of active microbial decomposition. The large percentage of primary polysaccharides and low percentage of lipids, however, suggest that biodegradable organic matter is still present. Because the results from both samples UM2 and CF2 point toward a history of decomposition, but also contain biodegradable organic matter, both soils were considered intermediate candidates for diauxy.
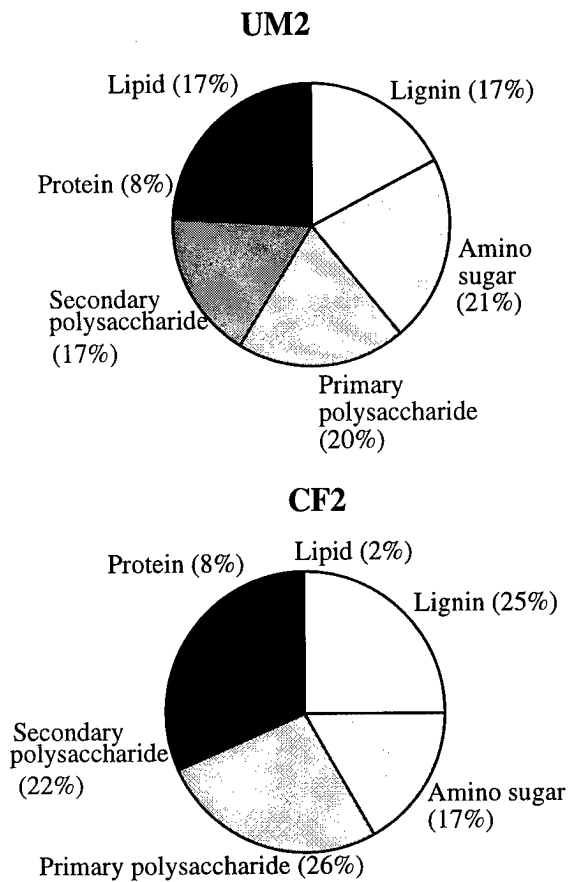
433

UM2

Lipid (17%)　Lignin (17%)

Protein (8%)

Amino sugar (21%)

Secondary polysaccharide (17%)

Primary polysaccharide (20%)

CF2

Protein (8%)　Lipid (2%)

Lignin (25%)

Secondary polysaccharide (22%)

Amino sugar (17%)

Primary polysaccharide (26%)

Figure 2. Relative percentage of biochemicals in samples UM2 and CF2.

Samples a high propensity for diauxy

In sample TL (see Fig. 3), a relatively large percentage of primary polysaccharides were observed, along with a small percentage of amino sugars and secondary polysaccharides. According to the first and third assumptions, this soil contains poorly degraded organic matter and has a high propensity for diauxy.

Sample PM contained a large percentage of both primary polysaccharides and lignin along with a small percentage of lipids (see Fig. 3). This is indicative of NOM which contains more easily degradable organic matter than any of the other soils. Sample PM, therefore, has a high propensity for diauxy.

DISCUSSION

The objective of the proposed analysis was to predict the effectiveness of bioremediation in organic soils based on the potential for diauxic growth on NOM. The method developed facilitates a comparison of the potential for diauxy between all soils tested. As

shown in Table 3 and supported by additional information from Fig. 1-3, soil samples were ranked according to their propensity to exhibit diauxic growth during bioremediation. It is important that this

TL

Lignin (16%)

Lipid (29%)

Amino sugar (5%)

Protein (10%)

Primary polysaccharide (28%)

Secondary polysaccharide (12%)

PM

Protein (6%)　Lipid (2%)

Secondary polysaccharide (17%)

Lignin (34%)

Primary polysaccharide (30%)

Amino sugar (11%)
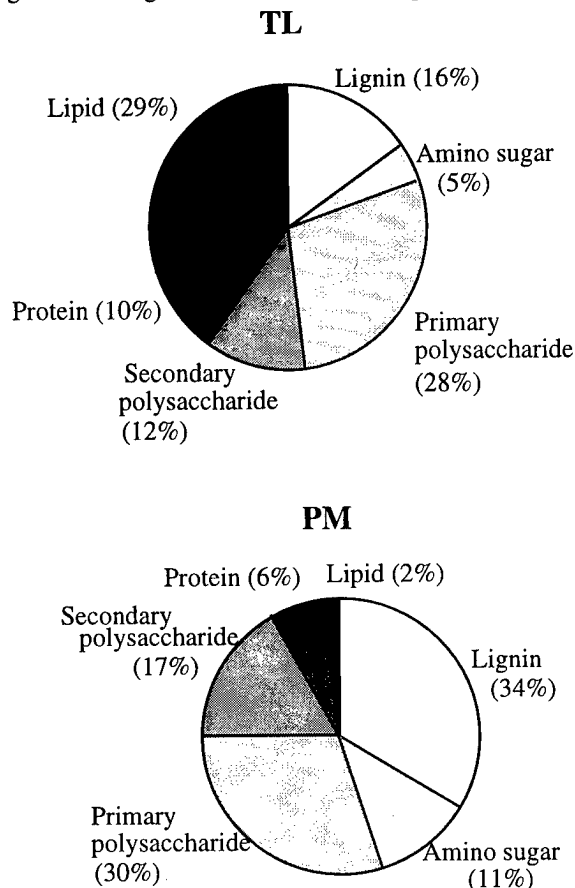
Figure 3. Relative percentage of biochemicals in samples TL and PM.

type of analysis be conducted since it cannot be assumed that all soils with a high concentration of NOM will necessarily exhibit diauxic growth. To illustrate this point, the correlation coefficient between the concentration of soil biochemicals and percent NOM was calculated (see Table 4). The absence of correlation between the percent NOM and relative percentage of soil biochemicals suggests it would be incorrect to assume that soil with a high concentration of NOM has a high potential for diauxic growth.

In order to be successful, the method proposed needed to identify a suite of compounds from which the relative propensity for diauxic growth could be predicted. Although an exhaustive study would be needed to quantify all soil biopolymers, the premise of this study was that only a few compounds from each class are needed to make useful characterizations. As long as the same compounds are chosen to

represent each class of biochemicals in test soils, a comparison is simply based on the relative concentration of these compounds and soil microbiology.

Table 4. Correlation between the concentration of NOM and each biochemical class.

Biochemical classification	Correlation coefficient
Lignin	0.21
Amino sugar	0.30
Primary polysaccharide	0.15
Secondary polysaccharide	0.03
Protein	0.14
Lipid	0.19

Method Limitations

The best way to conduct a soil characterization analysis is to include all compounds in each class of soil biochemical. There are wet chemical methods for this and other isolation and quantification techniques available (e.g., HPLC). All have limitations, however, and insofar as the simplicity of sample preparation is concerned, pyrolysis-GC/MS is the most practical technique for characterizing soil NOM.

The real limitation to pyrolysis-GC/MS lies in the interpretation of the origin of certain pyrolyzed molecular fragments. The more compounds that are included, the less dependable the interpretation of the data becomes (i.e., as compounds will be included that have multiple parent molecules). The key to the success of this method is to select the appropriate suite of compounds.

CONCLUSIONS

Predicting success in bioremediation of Alaska's contaminated organic soil requires a sophisticated analysis of the soil organic matter. The basic premises of the method were demonstrated:
- A suite of molecules was selected to represent the six major fractions of nonhumic soil biochemicals.
- The relative percentage of each biochemical was compared between soils to evaluate relative degrees of decomposition.

- The relative percentage of the most easily degraded compounds was compared to predict the propensity for diauxy and the success of bioremediation.

REFERENCES

ASTM. 1987. Standard test methods for moisture, ash, and organic matter of peat and other organic soils. p. 384-386. *In* Annual Book of ASTM Standard Methods. ASTM, Philadelphia, PA.

Bracewell, J. M., G.W. Robertson, and K.R. Tate, K.R. 1976. Pyrolysis-gas chromatography studies on a climosequence of soils in tussock grasslands, New Zealand. Geoderma 15: 209-215.

Bracewell, J. M., K. Haider, S. Larter, and H.-R. Schulten. 1989. Thermal degradation relevant to structural studies of humic substances. 181-222. *In* M. H. B. Hayes, P. MacCarthy, R. L. Malcolm and R. S. Swift (eds.) Humic Substances II. John Wiley and Sons Ltd. NY.

Bruchet, A., C. Rousseau, and J. Mallevaile. 1990. Pyrolysis-GC/MS for investigating high molecular weight THM precursors and other refractory organics. J. A. W. W. A. September: 66-74.

Irwin, W. J. 1979. Analytical pyrolysis - An overview. J. Anal. and Appl. Pyrol. 1: 89-122.

NRC. 1993. In Situ Bioremediation. National Academy Press. Washington DC.

Stevenson, F. J. 1994. Humus Chemistry. John Wiley and Sons, NY.

Wampler, T. 1996. Personal communication.

Waksman, S.A. 1952. Soil Microbiology, John Wiley and Sons, NY.

White, D.M. 1996. Unpublished research.

ACKNOWLEDGMENTS

Investigation of an Abandoned
Diesel Storage Cavity in Permafrost

E.J.A. SPAANS[1], J.M. BAKER[2], I.K. ISKANDAR[3], B. KOENEN[3], AND C. PIDGEON[3]

ABSTRACT

In 1974 an experiment was conducted to test the feasibility of storing diesel fuel in an unlined cavity created in permafrost. A test cavity was excavated, and at the conclusion of the experiment the diesel was not removed, but sawdust was added to adsorb the diesel, and the shaft leading from the cavity to the surface was backfilled with gravel. In 1994, diesel fuel was observed on the soil surface in the vicinity of the shaft. The entire gravel shaft was contaminated with diesel; the soil outside the shaft exhibited much lower levels of contamination. A video camera lowered into the cavity showed massive ice on all cavity walls. We tentatively conclude that during the years 1975-1994 water entered the gravel shaft, migrated downward to the cavity, and displaced the diesel fuel which moved upward through the shaft. The permafrost cavity failed to provide an environmentally sound enclosure for the diesel.

Key words: Permafrost, diesel, contamination.

INTRODUCTION

Frozen soil, if it is air-free or nearly so, has historically been considered essentially impermeable to fluid flow. On this basis, engineers in both the United States and the former Soviet Union proposed that fuels could be stored in unlined cavities within permanently frozen soil (permafrost). Such cavities could be build in an expeditious manner and serve as fuel storage-facilities during military activity to protect fuel from remote detection and attack (Swinzow 1974). The feasibility of such an installation was tested in a field experiment in 1971-1972 at the Experimental Field Station of the Cold Regions Research and Engineering Laboratory's (CRREL) Alaska Division near Fairbanks. The experiment was described by Swinzow (1974); relevant details are provided later in this report. Briefly, a cavity was melted in the permafrost with hot water, the slurry was pumped out, and it was replaced with diesel fuel. Temperatures in and around the cavity were monitored, and the quality of the fuel was periodically checked. At the conclusion of the experiment, the cavity was filled with sawdust to adsorb the fuel and the shaft was filled with gravel (Swinzow 1974).

Faran (1993) mistakenly reported that the diesel had been removed from the cavity before the sawdust was added. Thus there was a surprise when a site investigation by consultants in 1994 revealed the presence of diesel fuel close to the surface in one of the access pipes leading to the cavity. Remediation was ordered, but it was decided that it would be conducted in a manner that would allow investigation of the circumstances that caused the movement of the fuel. The three objectives of this project were to cleanup the contaminated site without compromising the permafrost's integrity, to investigate why diesel appeared on the surface, and to determine whether diesel had moved into the soil surrounding the installation.

INSTALLATION (after Swinzow 1974)

The experiment was conducted in marginal, discontinuous permafrost, on the assumption that structural design and construction methods that perform well in warm regions would also work in colder permafrost at higher latitudes. Permafrost at the experimental site reaches a depth of about 45 m, and the active layer varies from 0.6 to 4 m depending on the vegetation. In March 1971, a hole (1.22-m diam., 6.7 m deep) was drilled in the ground and observations of the exposed profile indicated that the permafrost started at a depth of 3.3 m. At the time, only the upper 2.3 m of the active layer was frozen, with unfrozen soil present between 2.3- and 3.3-m depth. The entire profile consisted of fine, organic rich, ice-saturated (60% by volume) silt.

Subsequently, 757 L of 80°C water was poured into the hole to melt a cavity in the permafrost. The silty mud was pumped out, leaving an irregularly shaped cavity with a diameter of about 1.8 m. The cavity was ventilated to allow the walls to refreeze before they were briefly sprayed with cold water to form a fine ice glaze to prevent dust formation in the cavity. Pipes were installed from the surface to the cavity to allow filling or emptying of the cavity. In order to preserve the permafrost surrounding the cavity, a heat exchanger was installed through which
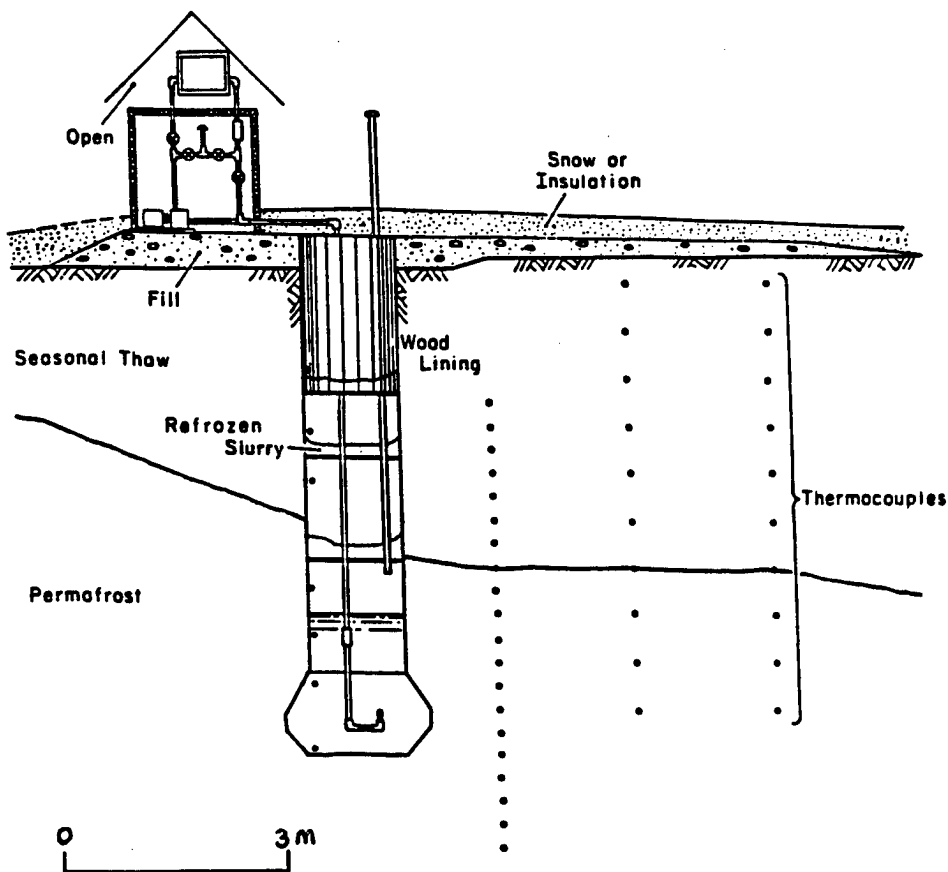
Figure 1. Cross-sectional view of the installation showing the temperature measuring points, the method of sealing, and surface detail (not to scale). Only return flow pipe is shown (from Swinzow 1974).

the fuel could be circulated and chilled during periods when the outside air was sufficiently cold.

The top of the permafrost in the area was not level, due to vegetation variations. One concern was that water released from the active layer during thaw might flow along the permafrost boundary and into the cavity. Hence, three wooden platforms were installed in the shaft; one immediately below the permafrost, and two above it. To seal the platforms, a 0.3 m layer of silt slurry was applied on top of each platform and allowed to freeze. The mouth of the shaft was lined with wood to prevent possible slump in the summer. The area around the shaft was covered with fiberglass insulation to prevent any detrimental thaw. Thermocouples were installed to monitor temperature in and around the cavity. Figure 1 (from Swinzow 1974) shows the installation. Upon completion of the construction of this fuel storage facility, the cavity was filled with 3785 L of diesel fuel. Temperatures were continuously observed while fuel was circulated once the following Spring.

In September 1974, the need arose to dismantle the installation. The wooden platforms were penetrated with an auger (0.76 m diam.) until access

to the cavity was established. Visual observations showed that there had been no influx of water from the top of the permafrost, there were no signs of disturbance in the permafrost or seepage of petroleum, and a sample of the fuel from the cavity showed no sign of deterioration. Several cubic yards of sawdust were poured into the cavity to adsorb the fuel and the shaft was filled with gravel. This information was found in a footnote to the Swinzow (1974) report, and it evidently had escaped the notice of Faran (1993) who reported in a history of research at Farmers' Loop that the diesel had been pumped out at the conclusion of the experiment. The site evidently was undisturbed for the ensuing 20 years, until Dames and Moore representatives discovered diesel fuel in one of the access pipes of the tank.

From April through September 1995, CRREL representatives periodically bailed fluid from the access pipes, recovering a total of 95 L. In September 1995, a full scale recovery was initiated yielding about 1800 L on day one, and an additional 380 L until the middle of October. A total of approximately 2271 L of fluid was recovered in 1995; the chemical composition of these fluids is

unknown. The fluid's appearance and the presence of a distinct sheen on the fluid's surface persuaded the investigators to process the fluid (as water contaminated with fuel) through Ft. Wainwright's activated carbon system. The sample taken from one of the access pipes by consultants was analyzed and reported as relatively undegraded arctic diesel. Analysis of a groundwater sample from an adjacent monitoring well showed low levels of volatile fuel components present (0.8 mg/L benzene, 1 mg/L toluene, 0.7 mg/L ethylbenzene, and 2.0 mg/L xylene). Samples taken from the other two nearby wells showed no contamination.

EXCAVATION

Excavation and concurrent investigation of the contaminated site started on 21 June 1996, when a hollow auger was drilled through the gravel into the cavity. The auger tip was extracted approximately 0.7 m from the lowest point in the cavity then secured in place with a drilling plate. The gravel was actually an unsorted mixture of gravel, sand, and silt. Excess gravel was found mounded around the shaft, which was probably done when the shaft was filled, but there was a bowl-shaped depression of about 0.8 m in the center. Fiberglass insulation from the original installation was visible about 0.5 m below the top of the mound, and that level was assumed to be the level of the original soil surface. All subsequent depths are referenced to this surface. The level of the fluid inside the auger was 3.6 m below the surface. We were unable to pump fluids out of the auger due to what was later determined to be a blockage in the pump filter. Excavation started and was interrupted when a depth of 2 m was \ reached to allow examination of the profile. Soil was sampled into 250 mL jars by locally scraping about 4 cm off the profile with a knife, then inserting the jar into the soil. Care was taken not to touch the soil with hands, and the knife was cleaned with methanol both before and once during the scraping to avoid contamination. Head space in the jars was minimal. The profile was sampled at 1.02 and 0.41 m below and 0.20 m above the original surface. At these depths, one sample was taken from within the shaft and one from 0.15 to 0.20 m outside of the shaft (south). The samples outside the shaft were taken from the undisturbed soil except for the sample 0.20 m above the surface, which was taken from the gravel mound. Figure 2 shows the frost line as observed from the pit face. It shows the enhanced thawing of the gravel shaft. This was probably due to

the lower heat capacity of the gravel relative to the ice-rich soil.

When a depth of 2.8 m was reached, excavation resumed but from a different angle due to operational difficulties with the backhoe. Soil samples were taken at 2.24 and 1.63 m below the surface, inside and outside the shaft. Samples outside the shaft were taken from the soil, this time from the north and west side of the shaft. Distance to the shaft was difficult to determine since the excavation had obscured the exact position of the shaft, but it was estimated to be < 1 m. Large pieces of wood and fiberglass insulation were encountered at several depths in the shaft.
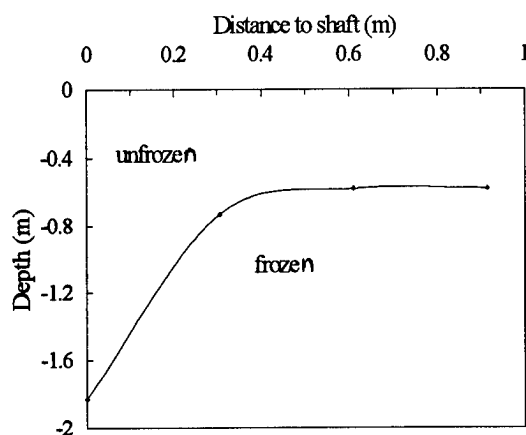
Figure 2. Unfrozen and frozen soil as observed from the pit face. It demonstrates the influence of the shaft to the temperature profile in the soil.

At this point the pump had been repaired, so the cavity was pumped out and all fluids collected in 55-gall. drums. Approximately 1170 L of fluid were recovered. Added to the 2271 L already collected, this brought the total amount of fluids recovered from the cavity to 3441 L. Samples were taken from all drums with a bailer and stored in 40-mL VOC vials, again with negligible head space. Another set of soil samples was taken at depths of 2.84 and 2.24 m, after which the excavation was terminated because the backhoe could not reach any deeper. Large ice chunks were encountered in the shaft at 2.8-m depth. Six ring samples were taken from the surrounding soil with 10-cm diam. thin-wall PVC conduit cut to about 9-cm length, to measure ice content and porosity.

At two points during the excavation, after the fluid had been pumped out, a video camera was lowered through the hollow center of the auger to

observe the cavity. The camera is intended for tank inspection (model BTC-TK, Bartz Technology Company, Santa Barbara, CA) and can fit inside a 10-cm hole. It is mounted on extension poles and can be swiveled by means of a lever at the end of the extension poles. The camera was connected to a monitor to allow real-time inspection of the cavity. Large ice formations were visible on the bottom and side walls of the cavity and there was no evidence that the wall had melted at any point. Neither gravel nor sawdust was found in the cavity. A tape of the footage is appended to this report. The camera, which had autofocus and zoom capabilities, was a valuable tool for inspection of the cavity.

At this point the excavation had been open for two days and the walls were beginning to slump. The auger was removed, and a split-spoon sampler mounted on a drilling rig was first rinsed with methanol and then lowered into the hole left by the auger at an angle of about 10°. One sample of the bottom of the cavity was taken, placed in a plastic sleeve, sprayed with dry ice, put in a cooler, and stored in the permafrost tunnel. The sample had gravel at the top, then ice (0.35 m), and then frozen, relatively undegraded, sawdust (0.25 m). The sample did not extend to the bottom of the sawdust layer. The gravel on top of the core had evidently fallen in the cavity when the auger was removed. This was the conclusion of the field investigation. CRREL representatives finished the excavation and removed the contaminated soil (which was temporarily stored on a high density polypropylene liner on site) to a lined cell near the back gate on the site. The cell dimensions are approximately 10 by 13 m, with roughly 0.6 m of soil throughout the cell. An estimated amount of 100 m³ of a sandy to silty gravel was placed in and around the excavation site.

METHODS OF SAMPLE ANALYSIS

Soil and liquid samples were analyzed at CRREL in Hanover. The Dionex Accelerated Solvent Extractor (ASE 200 model) was used. After large pebbles were removed, 10 g of field moist samples were mixed with equal amounts of anhydrous sodium sulfate and placed in separate 22-mL extraction vessels. The samples were then extracted for 10 minutes at elevated temperature and pressure in the Dionex extraction apparatus using 1:1 hexane:acetone as solvent. The extracts were collected in a 40-mL vial and concentrated down to 1 to 3 mL. Total petroleum hydrocarbon

determinations by gas chromatography were performed on 1.0 μL injections of the concentrated extracts. (Total peak areas of samples calculated against response factor of total peak area of 5000 ppm no. 2 diesel standard from Restek Corp.). Recovery (Richter et al. 1995) of diesel was 101% with 2.4% RSD ($n=3$). Extraction method and instrument met the requirements of U.S. EPA SW-846 Method 3545 for accelerated solvent extraction of semi-volatiles.

Moisture content on the ring samples was determined gravimetrically, and particle size distribution was determined on two ring samples with the hydrometer method (Gee and Bauder 1986).

RESULTS SAMPLE ANALYSIS

Results of the petroleum analysis of the soil samples are graphically represented in Figure 3. Except for one sample at 2.24-m depth, all petroleum contents within the shaft are two to three orders of magnitude higher than in the undisturbed soil. The results demonstrate that the shaft was contaminated with diesel over the entire length, and that diesel has migrated into the soil. Petroleum contents in the mound may be lower due to evaporation of petroleum from the surface. Why the soil at 2.24 m contained such a high amount of diesel is unclear. Bulk densities of the six ring samples were 1.37, 1.28, 1.33, 1.32, 1.36, and 1.44 Mg/m³, with an average value of 1.35 Mg/m³. Volumetric moisture contents for the same samples were 0.45, 0.52, 0.47, 0.51, 0.43, and 0.48, respectively, with an average value of 0.48. With an estimated particle density of 2.6 Mg/m³, this indicates that the soil was fully saturated. It can thus be assumed that under frozen conditions, this indeed is an ice-rich soil, although the ice contents would be lower than the value of 0.6 as reported by Swinzow (1974). Particle size analysis of the soil revealed 6% clay, 69% silt, and 25% sand, which would classify the material as a silt loam.

Analysis on volatile organic carbons (VOC) was performed on the liquid samples taken from the 55-gall. drums. Data are presented in Table 1. Total petroleum accounted for only 0.5% of the sample. It is, however, difficult to interpret these results; when sampling a volume that contains two immiscible fluids the sample composition depends on such factors as the depth of sampling and the rate at which the bailer was lowered.
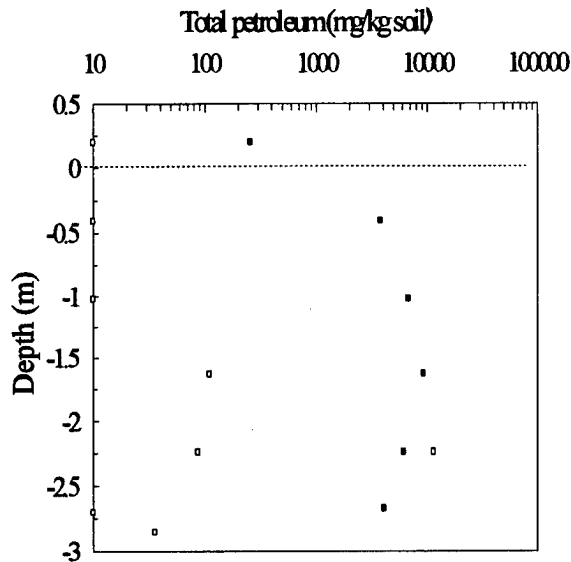
Figure 3. Logarithmic graph of petroleum content vs. depth for samples from within (closed symbols) and from outside (open symbols) the shaft. The four samples with nondetectable petroleum contents were assigned a value of 10 mg/kg, which is the detection limit of the method, to allow for a logarithmic scale.

Table 1. VOC analysis on six samples taken from the fluids pumped out of the cavity.

Benzene (ppb)	Toluene (ppb)	Ethylbenzene & Xylenes (ppb)	Total petroleum (ppm)
291	478	155	3053
355	645	213	3722
278	491	224	5273
299	652	224	4081
364	680	227	5014
288	540	273	5842

DIESEL-WATER INTERACTIONS

Since liquid water, ice, and diesel were simultaneously present in the cavity, we decided to investigate the interaction between the diesel and water more closely. Diesel and water are immiscible, but we wanted to verify experimentally whether the freezing point of water is depressed either by water

soluble compounds in the diesel or by the presence of diesel by itself.

Arctic diesel is a mixture of kerosene and diesel, but the mixing ratio of these compounds is not unique. Hence we tested two factors, the kerosene / diesel no. 2 mixing ratio (100:0, 90:10, 50:50, 0:100) and the ratio of water to diesel (10:90, 50:50, 90:10), yielding a total of 12 samples. The volume of each sample was 80 mL. The different mixtures of diesel were poured into 100 mL beakers, after which the water was added by squirting it onto the wall of the beaker to minimize mixing with the diesel. One thermocouple was fitted inside every beaker, close to the bottom. One beaker with only pure water was also prepared. The beakers were then placed inside a growth chamber and equilibrated at 1°C. The temperature in the growth chamber was then set to ramp from 1 to -10°C over a 11-hr period. The temperature in the beaker dropped, but as soon as nucleation occurred in the water phase the temperature would rise rapidly and remain at the freezing point of the water until all the water had frozen. Then the temperature dropped to ambient temperature in the growth chamber. Nucleation in the pure water occurred at -0.6°C, and in the water/diesel mixtures typically at -5°C. The experiment was repeated after thawing the samples and thoroughly mixing each one of them. The measured freezing point of the pure water was -0.06°C, and for the water/diesel mixtures it ranged from -0.19 to -0.06°C, with a value typically around -0.11°C. These measurements should be seen as preliminary, since the cold diesel above the water is a sink for heat and may have slightly affected the temperature measurement in the water phase. This was particularly evident in the beakers with only 10% water where the thermocouples were partly exposed to the diesel. From these data, however, there was no clear correlation between freezing point and either kerosene / diesel no. 2 mixing ratio, or with the water / diesel mixing ratio. No differences were detected between the first and the second run, indicating that the additional mixing did not affect the freezing point. Freezing point in the samples from the tank were measured in a similar fashion, except that the measurements were taken in 40-mL vials. They yielded -0.12, -0.11, -0.15, -0.13, and -0.11°C for sample no. 7282, 6998, 8015, 8090, and 8120, respectively.

DISCUSSION

This cavity was a unique case of long-term storage of fuel in permafrost. Unfortunately, the

440

system is not sufficiently described to permit a quantitative analysis of the results. There are too many uncertainties about initial and boundary conditions of the system; the thickness of the ice film on the walls of the cavity, the shape of the cavity, the effect of insulation present on the soil surface and in the shaft on the energy balance of the cavity, drainage and infiltration in the gravel, snow catch in the depression on top of the shaft, etc. Transport processes in frozen soil are highly sensitive to temperature, particularly close to the freezing point. Hence small errors in a simulated temperature distribution in the system resulting from the uncertainties mentioned could lead to substantial errors with respect to phase partitioning and diesel movement in the cavity-shaft system. It is, however, worthwhile to at least speculate why diesel was present at the surface.

We hypothesize that water had entered the cavity through the gravel shaft, sank because its density is higher than that of diesel, and froze at the bottom. Ice formation in the cavity would cause displacement of the diesel into the shaft. Video images and the core sample taken from the bottom of the cavity indicated the presence of large amounts of ice in the cavity.

The amount of heat added to the permafrost when hot water was poured into the hole was at the most 247 MJ (0.757 m^3 x 972 kg m^{-3} x 4.19 kJ kg^{-1} °C^{-1} x 80°C). Assuming a porosity of 0.48 in the permafrost, and neglecting the heat capacity of the soil, this could melt a cavity of at most 1.68 m^3 (247 MJ / 333 kJ kg^{-1} / 917 kg m^{-3} / 0.48). A total of 3785 L of diesel was poured into the cavity, and with 1680 L stored in the cavity, 2105 L must have been stored in the shaft. The diameter of the shaft was 1.22 m, leaving the top of the diesel at 4.9 m below the surface.

The sawdust and gravel introduced into the cavity at the conclusion of the experiment inevitably elevated the level of the diesel in the shaft, but by how much is uncertain. In the laboratory we found that adding sawdust to diesel only slightly increases the volume, and that the sawdust, after it adsorbs diesel, is denser than the diesel. That agrees with the observation that sawdust was present at the bottom of the cavity underneath the ice. Gravel appeared only in the shaft, but not in the cavity. The drilling crew that drilled the auger through the shaft noticed that gravel was present down to the top of the cavity, but none of it was seen inside the cavity. Moreover, the fluids pumped out of the cavity were clear and free of soil particles. Why the gravel did not enter the cavity is curious. At any rate, if one assumes a

porosity of 0.4 in the gravel, the added gravel would have displaced the diesel and brought its level to 2.2 m from the surface. Since the conclusion of Swinzow's experiment in 1974, Fairbanks has received approximately 6 m of precipitation which would be ample water to displace diesel in the shaft to the surface.

We should bear in mind that the description of the process where infiltrated water freezes at the bottom of the cavity is rather abstract. The entire walls of the cavity were covered with irregularly shaped ice structures, and large chunks of ice (air pockets as well) were encountered in the shaft.

We have not been able to close the mass balance on the diesel. No analysis was done on the 2271 L of fluid recovered in 1995, so its composition is unknown. Analysis of the 1170 L of fluid pumped during excavation in 1996 showed that it contained only a small amount of diesel. A portion of the diesel is adsorbed to the soil and gravel, but evidently much of it must have been lost by evaporation from the shaft, a hypothesis supported by the concentration gradient in the surface 1.5 m shown in Figure 3.

The water in the cavity coexisted with the ice on the walls of the cavity. We tentatively conclude that its solute concentration was sufficient to depress its freezing point below the temperature of the surrounding frozen soil and ice.

CONCLUSIONS

It is not possible to make a definitive statement, on the basis of this study, about the mobility of diesel fuel confined in an unlined permafrost cavity. The videotape showed ice on all visible walls with no evidence that there had ever been any thawing at the depth of the cavity. However, logistical difficulties prevented thorough sampling of the soil bordering the cavity on the sides and bottom.

Serious mistakes, made when the initial experiment was concluded in 1974, were the likely cause of the diesel contamination found at the soil surface. Drilling through the caps in the shaft and backfilling the shaft with gravel created a pathway for water migration into the cavity. This also disrupted the thermal regime in the vicinity of the cavity, so that the active layer extended deeper in the soil immediately surrounding the shaft. We conclude that water from melting snow and rainfall moved downward through the gravel. The sawdust that had been added did not bind the diesel sufficiently to prevent its displacement by the denser water, so the fuel moved upward through the gravel-filled shaft.

The presence of small, but measurable concentrations of diesel in the soil outside the shaft is interesting, but inconclusive. As mentioned above, it appears that the thermal properties of the gravel-filled shaft may have caused the surrounding soil to thaw much deeper than elsewhere (Fig. 2), bringing the displaced diesel into contact with unfrozen soil. Since there were no soil temperature measurements made during the past twenty years, this remains conjecture.

LITERATURE

Farran, K. 1993. Farmer's Loop research area site history. US Army Cold Regions Research and Engineering Laboratory Technical Memorandum.

Gee, G.W. and J.W. Bauder. 1986. Particle-size analysis. In A. Klute (ed.) Methods of soil analysis. Part 1. 2nd ed. Agron. Monogr. 9, ASA, Madison, WI. p.383-409.

Richter, B.E., J.L. Ezzel, W.D. Felix, D.W. Later, K.A. Roberts. 1995. An accelerated solvent extraction system for the rapid preparation of environmental organic compounds in soil. Am Lab 27(4):24-8.

Swinzow. 1974. Experimental protected military POL installation. US Army Cold Regions Research and Engineering Laboratory Technical Report 254, 12 pp.

Soil Organic Matter of Spodic Horizons in Soils of Coastal Continental Antarctica and Germany

L. BEYER[1], H. KNICKER[2], H.-P. BLUME[1], M. BÖLTER[3], AND D. SCHNEIDER[1]

ABSTRACT

In Antarctica ornithogenic soils from penguin guano play an important role in nutrient cycles in the ecosystem. However, little is known about their pedogenesis. The soil organic matter (SOM) of relic ornithogenic soils in coastal continental Antarctica, which showed morphological features like a Podzol, was compared to spodic horizons in Germany. Our goal was to unravel the little knowledge of organic matter of ornithogenic soils by means of wet-chemistry and nuclear magnetic resonance spectroscopy (NMR). In contrast to the German soils the SOM of the Antarctic soils was characterized by a high percentage of amino derivatives from proteins, polysaccharides, urates and chitin, resulting in a mean C-to-N ratio of 10. The high content of carboxyl carbon units probably derived from amino and other organic acids. The pattern of the ^{15}N-NMR spectra of the penguin guano suggested the presence of uric acid. Concerning the podzolization process our data suggested the migration of organic acids, not-humified carbohydrates and N-containing moieties, from the topsoil into the spodic horizons of the ornithogenic soils. In the SOM of Podzols formed under temperate climate conditions N-compounds, and non-humified carbohydrates were of minor importance within the SOM translocation processes.

Keywords: Antarctica, ornithogenic soils, podzolization, penguin guano, soil organic matter

INTRODUCTION

In Antarctica ornithogenic soils from penguin guano play an important role in nutrient cycles. In the pedogenesis of relic ornithogenic soils three processes have been described: (I) Myrcha and Tatur (1991) suggest the formation of oxalic acids in the top few centimeters and simultaneous concentration of recalcitrant soil compounds, such as chitin, urates and phosphate minerals. (II) Campbell and Claridge (1987) note, that the mechanism of iron removal induces a pale soil colour. (III) Tatur (1989) and Tatur and Keck (1990) remark about the maritime Antarctica, the leaching of iron and organic P fractions and an accumulation at the subsoil. Consequently Tatur (1989) describes a profile with a dark brownish horizon (7-20 cm) under a pale gray one (2-5 cm). These features are typical for Podzols in the temperate regions with respect of the formation of AE and Bh horizons (FAO 1989, 1994, Soil Survey Staff 1994). Applying this knowledge, Blume and Bölter (1993) describe for the first time Podzols in coastal continental Antarctica (Wilkes Land). These soils are characterized by a pale colored "AE" horizon (10YR5/2) and a spodic "Bh" horizon (5YR3/1.5). In the present paper the organic matter of the suggested spodic horizons will be compared to spodic horizons under temperate climate conditions in order to get more information about the SOM genesis in Antarctic soils described by Blume and Bölter (1993). SOM has been been investigated by means of wet chemistry (Beyer et al. 1993) and carbon-13 nuclear magnetic resonance spectroscopy (Fründ and Lüdemann 1989).

MATERIALS AND METHODS

Site

The relic ornithogenic soils are located in the coastal continental Antarctica (66°18'S, 110°32'E). The mean annual temperature is -9.3°C. The annual precipitation (176 mm) is mostly snow. Soil classification was carried out according World Reference Base for Soil Resources (FAO 1994). The Podzols in Germany are located on pleistocene sands in the Northwest German Lower Plaine (Blume 1986). The mean annual temperature is 8.3°C. The annual precipitation is about 800 mm. Soil classification was carried out according to the FAO system (FAO 1989). A short comparative description of the sites and the investigated soil horizons is given in Table 1 und Figure 1.

---

[1] Institute of Plant Nutrition and Soil Science, University of Kiel, Olshausenstraße 40, D-24098 Kiel, Germany
[2] Institute of Biophysics and Physical Biochemistry, University of Regensburg, D-93040 Regensburg, Germany
[3] Institute of Polar Ecology, University of Kiel, Wischhofstraße 1-3, Gebäude 12, D-24148 Kiel, Germany

Table 1. Vegetation and B horizons from Podzols in Germany and coastal continental Antarctica.

horizon	pH CaCl$_2$	TOC	N$_t$	C/N	depth cm	reference
		– mg g^{-1} –				

Germany

Haplic Podsol under *Picea abies* & *Pinus silvestris*

Bh	3.2	16.3	0.5	35	49-59	Blume et al.
Bsh	3.6	9.2	0.4	26	59-74	(1993)

Haplic Podzol under *Picea abies* Vac.

Bsh	4.0	80.0	3.3	24	8-14	Beyer (1995)

Haplic Podzol under *Calluna vulgaris* & *Vaccinium myrtillus*

Bsh1	4.2	16.3	0.5	35	44-75	Lamp and Siem
Bsh2	4.3	10.7	0.3	38	75-120	(1993)

Stagno-gleyic Podzol under *Larix decidua* & *Fagus sylvatica*

Bsh	3.8	16.2	0.8	22	10-20	Beyer (1995)

Antarctica

Lepti-gelic Podzol with scattered lichen vegetation

Bh	4.3	44.7	4.3	11	5-10	Blume and Bölter
Bs	4.6	29.2	3.1	9	10-15	(1993)

Gelic Podzol with scattered lichen vegetation

Bh	4.3	40.7	3.7	11	8-11	unpublished
Bs	4.4	29.2	3.2	9	11-18	

TOC: total organic carbon
N$_t$: total nitrogen

Chemical analysis

The general determinations were carried out according to Schlichting et al. (1995). Soil organic matter fractionation was carried out according to Beyer et al. (1993).

Cross-polarization magic angle spinning carbon-13 and nitrogen-15 nuclear magnetic resonance spectroscopy (CPMAS ^{13}C and ^{15}N-NMR)

The CPMAS ^{13}C-NMR-spectra were taken at 2.3 Tesla (25.2 MHz) with a Bruker MSL 100 equipped with a commercial 7 mm CPMAS probe at a rotation frequency of 4 kHz according to Fründ and Lüdemann (1989). The CPMAS ^{15}N-NMR-spectrum was obtained on a Bruker MSL 300 spectrometer at a frequency of 30.4 MHz. The CPMAS spectrum was obtained in a probe of similar design as used for the ^{13}C NMR studies at a rotation frequency of 4.5 kHz according to Knicker and Lüdemann (1995) and Knicker et al. (1995).

RESULTS AND INTERPRETATION

The soil samples of Antarctica had a considerable higher content of total nitrogen (N$_t$) and much more narrow C/N ratio (Fig.1). This fact is not astonishing, because the C-to-N ratio in penguin guano and current ornithogenic soils ranges between 1 and 5 (Collins et al. 1975, Tedrow 1977). The high N$_t$ level probably reflected the high amount of α-NH$_2$-N, which caused the very high mean percentage of 46% from total nitrogen (Fig.1). This was much higher as known from soil horizons under temperate climate conditions (mean 25% of N$_t$) (Fig.1: N$_t$). Hence the protein level in the ornithogenic soils was more than four times higher in the Antarctic soils compared to the reference soils in Germany (Fig.2). In addition compared to the German soils, the Antarctic soil horizons showed significantly higher amounts of proteins, hemicellulose and cellulose. Also the lipid fraction was slightly higher in latter than in the German soils (Fig.2).
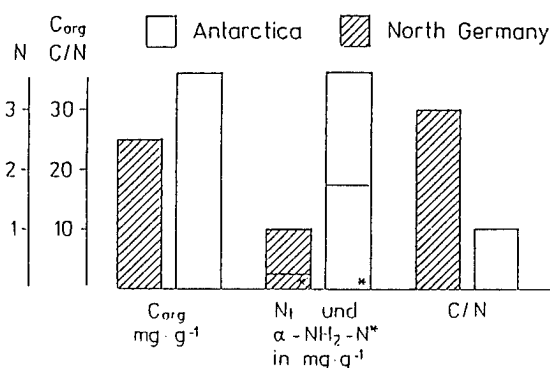
Figure 1. Mean carbon and nitrogen concentration in B soil horizons in Podzols of Germany and Antarctica.

Podzolization in temperate regions is characterized by transfer of fulvic acids into the subsoil (Beyer 1995). In relation to other humic fractions this dominance of fulvic acids can be observed in the German spodic horizons, but was not found in the Antarctic samples (Fig.2). In addition, the data suggest that non-humified material was translocated into the spodic horizons (Fig.2). According to recent literature the carbohydrates in the Antarctic soils are deriving from metabolic processes of mosses, lichens and algae at the soil surface and leaching into the topsoil (Bölter 1993 and references cited therein). These "leftovers" are only partly used by soil bacteria, whereas the remainder is obviously translocated into the subsoil.

In all NMR investigations significant signal intensity was found in the chemical shift region of carboxylic (160-220 ppm) and alkylic (0-45 ppm) carbon (Fig.3). This confirms previous studies (Beyer 1995, Skjemstad et al. 1992, Sorge et al. 1994). According to these authors this is explained with an enrichment of paraffinic structures. Beside such paraffinic structures, proteinaceous material and fatty acids give signals in these chemical shift regions. Evidence for the selective enrichment of such structures during pedogenesis was recently found by Fründ et al. (1994). For soils in the temperate climate regions, the
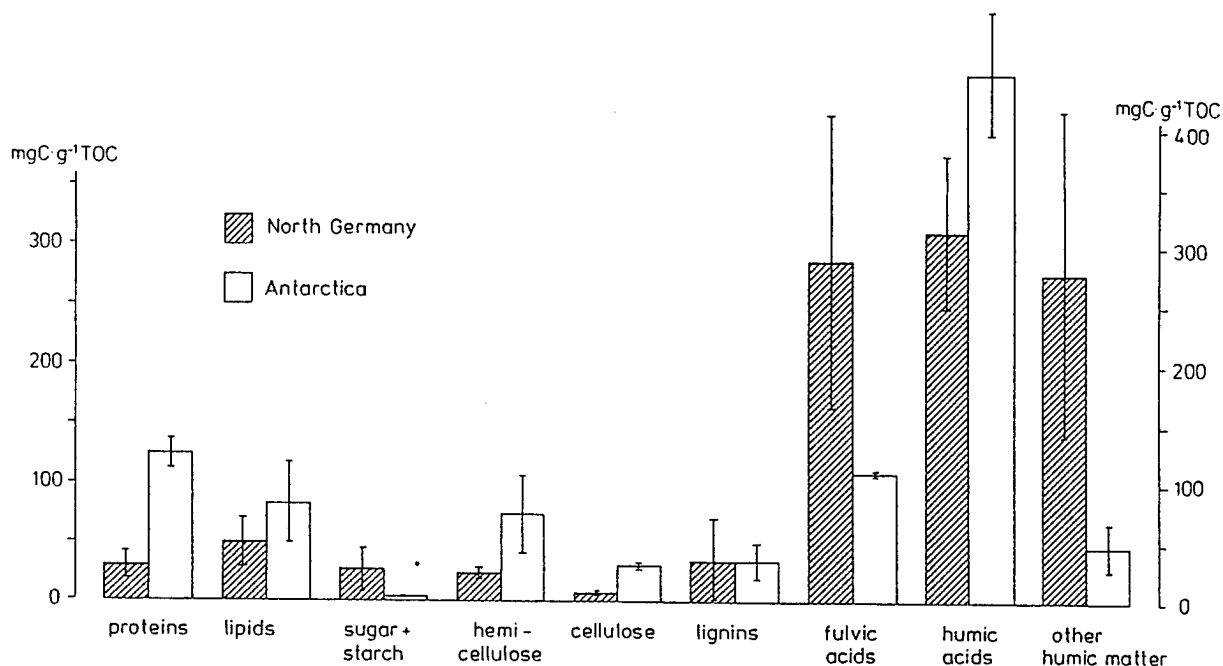
Figure 2. *Mean composition of litter and humic compounds in spodic horizons in Podzols of Germany and Antarctica.*
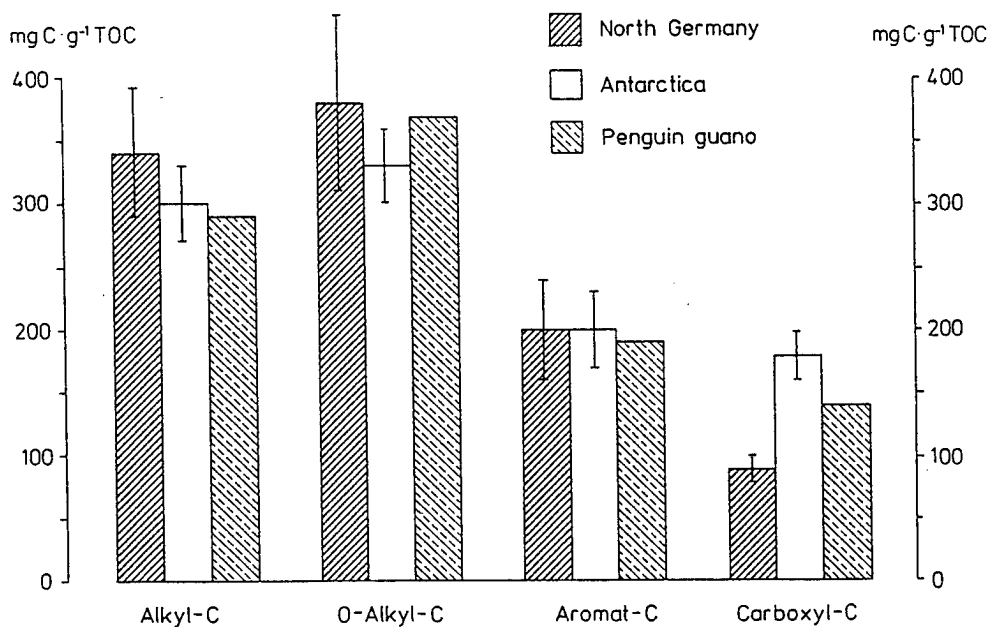
Figure 3. *Mean composition of CPMAS ^{13}C-NMR carbon units of total soil organic matter in spodic horizons in Podzols of Germany and Antarctica and this of penguin guano.*

signal intensity in the chemical shift region between 60 and 110 ppm is most likely assigned to cellulotic and hemicellulotic material of terrestrial plant precursors (Kögel-Knabner 1993), which are of major importance in the fulvic acid fraction. This fraction was to be found in the

German soil samples according to the wet chemical analysis (Fig.2). The signal intensity in the chemical shift region of aromatic carbons (110-160 ppm) in the spectra of the German soils originates most likely from lignins and lignin derivatives (Kögel-Knabner 1993). This may be derived from

445

leaching and migration of these compounds from the organic layer, the AE and E horizon and/or are selective preservation in the Bh and Bhs horizons (Beyer 1995). A particulary high amount of carboxyl carbon was determined for the ornithogenic soils (Figure 3), which confirms previous results obtained by Wilson et al. (1986), documenting a carboxyl content of 16 ± 2% in humic matter extracts of ornithogenic soils. According to them, this peak may arise from oxalate and derivatives. In addition Myrcha and Tatur (1991) proposed that these organic moieties are the main acid components in the soil solution.
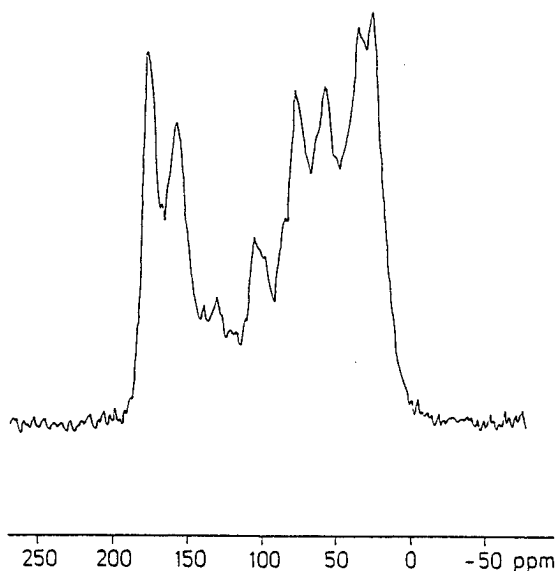
amide-functional groups, most probably in peptide bonds (Knicker et al. 1994). Other pronounced signals can be observed in the chemical shift region from -200 to -240 ppm. This region embrace the signals of pyrrolic, indolic
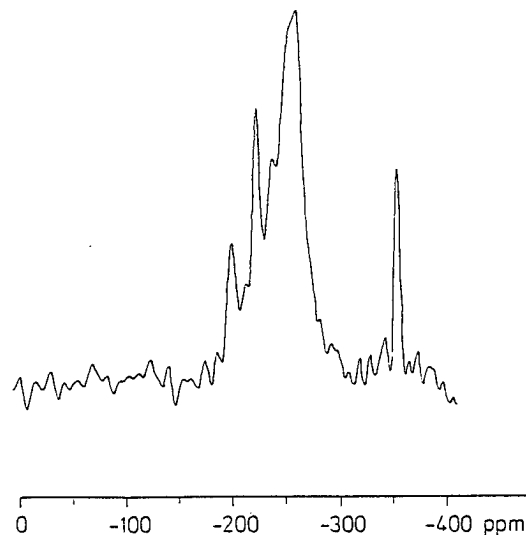

Figure 5. *CPMAS 15N-NMR spectrum of penguin guano.*

Figure 4. *CPMAS 13C-NMR spectrum of penguin guano.*

Both Antarctic Podzols are located on abandoned penguin rookeries (Blume and Bölter 1993). The main part of the organic matter derived from the guano of these animals. Therefore NMR signals originating from proteins, urea and uric acid (2,6,8-trioxypurine), their salts and degradation products could be expected (Myrcha and Tatur, 1991). In the 13C-NMR spectrum of the penguin guano (Fig.4) the peak at 25 ppm derives from terminal CH_3 groups (Breitmaier and Voelter 1990). The appearance of this peak together with the carboxyl signal (170 ppm) suggest the presence of amino acids (Kalinowski et al. 1984, Breitmaier and Voelter 1990, Wilson 1987). Beyond this α-NH_2-C (45-60 ppm) and carbonyl could be derived from the urea derivatives (Breitmaier and Voelter 1990). Furthermore Myrcha and Tatur (1991) emphasized the significance of chitin (from the exoskeleton of krill: *Euphausia superba*) in the penguin guano. Likewise chitin contains α-NH_2-C and carbonyl-C. In summary the narrow C-to-N ratio derived from amino moieties. This conclusion was confirmed by the expression of the 15N-NMR spectrum (Fig.5). The spectra shows intense signal at -358 ppm and -275 ppm, which can be assigned to ammonia and

and imidazolic-N but also the signals of nitrogen in chitin and uric acid structures (Berger et al. 1992, Martin et al. 1981). Considering the fact, that uric acid (2,6,8-trioxypurine) is a major component of guano, the signals in this region originate most likely from uric acid. The high N_t content, the narrow C/N ratios (Fig.1) and the high protein content (Fig.2) in the Antarctic soils suggested that, in the ornithogenic soils, peptides may be major contributors to the signal intensity in the chemical shift range of carboxylic and alkylic carbon. This is not surprising given the precursors of the ornithogenic soils and the pattern of the NMR spectra of the penguin guano as shown in Figure 4 and 5.

While the signal intensity in the chemical shift region of aromatic carbon (110-160 ppm) in the 13C NMR experiments the German soil horizons (Fig.3) were most likely assigned to lignin and lignin derivatives (see above), the intensity in the aromatic region of the Antarctic soil horizons cannot be explained with such compounds due to their absence at this ite. At the surface of the ornithogenic soils a vegetation cover is completely missing (Smith 1990, Blume and Bölter 1993) and there is no source of lignin (Wilson et al. 1986). The signals of the aromatic structures may be derived from heterocyclic moieties, which probably are found in the penguin guano (Fig.4). This was also seen in the 15N NMR spectra of the penguin guano (Fig.5). Such compounds could derive from uric acid (Kalinowski et al. 1984, Wilson 1987, Breitmaier and Voelter 1990, Berger et

al. 1992), which is indicated in the ^{15}N spectrum of the penguin guano. Also in its ^{13}C spectrum signals can be assigned to uric acid (2,6,8-trioxypurine) and its derivatives. They are well visible at 97, 136, and 153 ppm (Fig.4) and can be suggested as peaks or shoulders in the Antarctic soil spectra (not shown). The very high amount of O-alkylic-C in the ornithigenic soils of Antarctica (Fig.3) is certainly not derived from hemicellulose and cellulose as known from the German Podzols (Fig.2). The penguin diet consists mainly of marine crustaceans (krill), which are rich in proteins and chitin (Croxall and Lishman, 1987). The building blocks of chitin are amino sugars. These moieties are also considered to belong to the 45-110 ppm region (Breitmaier and Voelter 1990).

CONCLUSIONS

In Antarctica, ornithogenic soils from penguin guano are characterized by a high carbon and nitrogen content and a C-to-N ratio between 2 and 10. Blume and Bölter (1993) were the first to classify these soils as Gelic Podzols. Their "spodic" horizons are characterized by a high percentage of amino derivatives from proteins, polysaccharides, urates and chitin, as a result of the penguin diet and the guano dropping. Therefore the SOM composition is completely different to the Podzol-SOM known from Germany. The N-containing components are responsible for the low C-to-N ratio between 9 and 11 in contrast to the spodic horizons in Germany with a ratio of 22-38. In addition the ^{13}C-NMR shows a high carboxyl content, probably deriving from oxalate derivates and the ^{15}N-NMR spectra indicates the appearance of uric acid derivates. The data suggest the migration of organic acids and carbohydrates from the topsoil into the spodic horizons of the ornithogenic. The decrease of the C-to-N in the deeper horizons indicates two possibilities of pedogenesis. First, N-containing moieties move downwards together with the carbohydrate and acid components. The second possibility may be the bleaching of the top few centimeters during migration and simultaneous volatilization of the N-compounds. More significant details concerning this matter are expected as results of further investigations of complete profiles and soil from non-ornithogenic parent material.

ACKNOWLEDGMENTS

REFERENCES

Beyer, L. 1995. Soil organic matter of spodic horizons in Podzols of the Northwest German Lower Plaine. Sci.Total Environ.181: 167-180.

Beyer, L., C.Wachendorf, and C.Köbbemann. 1993. A simple wet chemical extraction procedure to characterize soil organic matter (SOM): 1. Application and recovery rate. Commun.Soil Sci.Plant.Anal.24 (13&14): 1645-1663.

Berger, S., S.Braun, and H.-O.Kalinowski. 1992. 15N-NMR-Spektroskopie. Thieme, Stuttgart, Germany.

Blume, H.-P. 1986. Soils and Landscapes in Schleswig-Holstein. Mitt.Dtsch. Bodenkundl.Ges.51: 1-131.

Blume, H.-P., and M.Bölter. 1993. Soils of Casey Station (Wilkes Land, Antarctica). p.96-103. Proceedings 1st International Conference of Cryopedology. Russian Academy of Sciences, Pushchino.

Blume, H.-P., W.Aey, J.Fortmann, and O.Fränzle. 1993. Soils of sediment basin of Lübeck and the Hanse City Lübeck (German). Mitt.Dtsch.Bodenkundl.Ges. 71: 181-205.

Bölter, M. 1993. Effects of carbohydrates and leucine on growth of bacteria from Antarctic soils (Casey Station, Wilkes Land). Polar Biol.13: 297-306

Breitmaier, E., and W.Voelter. 1990. Carbon-13 NMR spectroscopy. VCH, Weinhein, Germany.

Campbell, I.B., and G.G.C.Claridge. 1987. Antarctica: Soils, Weathering Processes and Environment. Elsevier, Amsterdam.

Collins, N.J., J.H.Baker, and P.J.Tilbrook. 1975. Signy Island, maritime Antarctic. Ecol.Bull.20: 345-374.

Croxall, J.P., and G.S.Lishman. 1987. The food and feeding ecology of penguins. p.101-133. In J.P.Croxall (ed.) Seabirds, feeding ecology and role in marine ecosystems. University Press, Cambridge.

FAO. 1989. Soil map of the world. Tech.Pap.20, ISRIC, Wageningen.

FAO. 1994. World reference base for soil resource. Draft. Wageningen, Rome.

Fründ, R., and H.-D.Lüdemann. 1989. The quantitative analysis of solution- and CPMAS 13C NMR spectra of humic material. Sci.Total.Environ.81/82: 157-168.

Fründ, R., G.Guggenberger, K.Haider, H.Knicker, I.Kögel-Knabner, H.-D.Lüdemann, J.Luster, W.Zech, and M.Spiteller. 1994. Recent advances in the spectroscopic characterization of soil humic substances and their ecological relevance. Z.Pflanzenernähr.Bodenk.157: 175-186.

Kalinowski, H.-O., S.Berger, and S.Braun. 1984. 13C-NMR-Spektroskopie. Thieme, Stuttgart, Germany.

Knicker, H.; R.Fründ, and H.-D.Lüdemann. 1994. N-15-NMR studies of humic substances in solution. p.501-506. In N.Senesi, and T.M.Miano (ed.) Humic substances in the

global environment and implications on human health. Elsevier, Amsterdam.

Knicker, H., and H.-D.Lüdemann. 1995. N-15 and C-13 CPMAS and solution NMR studies of N-15 enriched plant material during 600 days of microbial degradation. Org.Geochem.23: 329-341.

Knicker, H., G.Almendros, F.J.González-Vila, H.-D.Lüdemann, and F.Martin. 1995. 13C and 15N NMR analysis of some fungal melanins in comparison with soil organic matter. Org.Geochem.23: 1023-1028.

Kögel-Knabner, I. 1993. Biodegradation and humification processes in forest soils. p.101-135. In J.M. Bollag, and G.Stotzky (ed.) Soil Biochemistry. Vol.8, Marcel Dekker, New York.

Lamp, J., and K.Siem. 1993. Soils of the Holstian Geest. Mitt.Dtsch.Bodenkundl.Ges.71: 79-98.

Martin, G.J., M.L.Martin, and J.P.Gouesnard. 1981. 15N NMR spectroscopy. Springer, Berlin

Myrcha, A., and A.Tatur. 1991. Ecological role of the current and abandoned rookeries in the land environment of the maritime Antarctic. Pol.Polar Res.12: 3-24.

Skjemstad, J.O., A.G.Waters, J.V.Hanna and J.M.Oades. 1992. Genesis of podzols on coastal dunes in Southern Queensland. IV.Nature of the organic fraction as seen by 13C

nuclear magnetic resonance spectroscopy. Aust.J.Soil Res.30: 667-681.

Smith, R.J.L. 1990. Plant community dynamics in Wilkes Land, Antarctica. Proc.NIPR Symp.Pol.Biol.3: 229-244.

Sorge, C., M.Schnitzer, P.Leinweber and H.-R.Schulten. 1994. Molecular-chemical characterization of organic matter in whole soils and particle-size fractions of a Spodosol by pyrolysis field ionization mass spectrometry. Soil Sci.158: 189-203

Schlichting, E., H.-P.Blume, and K.Stahr. 1995. Bodenkundliches Praktikum. Blackwell, Berlin, Germany. 2.Edition.

Soil Survey Staff. 1994. Keys to Soil Taxonomy. USDA - Soil Conservation Service. 6.Edition.

Tatur, A. 1989. Ornithigenic soils of the maritime Antarctica. Pol.Polar Res. 10: 481-532.

Tatur, A., and A.Keck. 1990. Phosphates in ornithogenic soils of the maritime Antarctic. Proc.NIPR Symp.Pol. Biol.3: 133-150.

Tedrow, J.C.F. 1977. Soils of Antarctica. p.518-554. In J.C.F.Tedrow (ed.) Soils of the polar landscapes. Rutgers University Press, New Brunswick.

Wilson, M.A. 1987. NMR techniques and application in geochemistry and soil chemistry. Pergamon Press, Oxford.

Wilson, M.A., K.M.Goh; P.J.Collin, and L.G.Greenfield. 1986. Origins of humus variation. Org.Geochem.9: 225-231.

Distribution of Oil and Oil Products in Soils of Tundra Landscapes Within the European Territory of Russia (ETR)

N.P. SOLNTSEVA[1] AND O.A. GUSEVA[1]

ABSTRACT

Development of the oil industry in Russia centers around the oil fields of Arctic and Subarctic regions. Ecological problems of northern regions result mainly from the extreme vulnerability of tundra and forest–tundra landscapes under both mechanical and geochemical impacts. Among the most severe problems, the pollution of soil with oil and oil products is emphasized.

To assess the state of oil-polluted soils, the levels of possible accumulation of bituminous substances (BS) were studied, as well as the processes of BS migration and the internal/external factors influencing these processes. The values of oil-bearing capacity and oil permeability were determined that governed the rate of pollutants accumulation and their distribution within the vertical profile of soil.

Key words: Pollution, soil oil, migration, geochemical barriers.

OBJECTS AND METHODS OF STUDY

The BS behavior in soils was studied by the example of the Bolshezemelskaya Tundra of the ETR (to the west of Pechora low reaches), which is a gently sloping hilly lowland with average absolute elevations of 100 to 150 m. The annual precipitation is about 500 to 590 mm, the average annual temperature ranges from –4° to –6°C. The area is characterized by a short cold summer and prolonged winter. The leading landscape-forming factors are the cryogenesis with its accompanying processes, gley formation, swamping and peat accumulation.

Among the objects of study there were the main types of tundra soils, namely tundra peaty-gley soils (Gelic Distric Gleysols), tundra eluvial-gleyed podzolized soils (Cryic Stagnic Podzoluvisols), iron-humus-illuvial podzols (Gelic Carbic Podzols), peaty soils (Gelic Histosols), and peatbogs (Gelic Histosols).

The BS behavior in soils were studied by the following methods.

Experimental

Field investigation

The oil was in amounts of 501 L/m^2. Radial distribution of pollutants was studied 7 days after this procedure.

Laboratory investigation

The oil-bearing capacity of soils was assessed in the laboratory. The soil samples with undisturbed structure were saturated with oil under different moisture conditions. Oil yield was estimated by washing oil-saturated samples with water and a subsequent solution of oil with hexane. The resulting extract was dried out, after which the amount of oil products was measured by weighing.

Empirical

The BS distribution in soils polluted during the spills of oil and oil products was studied at different periods after the accidents. The BS amount in soils was determined by the luminescent–bituminological methods using a hexane extract.

RESULTS AND DISCUSSION

Oil pollution results in the deep transformation of all components of natural ecosystems. The irreversible changes of soil morphology and its physical and chemical properties are quite possible, thus modifying both soil profiles and the soil cover over vast territories (Solntseva 1988, Pikovsky 1993).

The BS behavior in soil is rather complicated and

---

[1]Moscow State University, Moscow, Russia

poorly understood. There are just a few field and laboratory experimental studies available (Bartz et al. 1969, Lippok 1966, Bratsev 1988, Glazovskaya and Pikovsky 1981, etc.), which are inadequate to determine with a fair degree of reliability the general features of BS behavior in peaty and waterlogged soils. Thus it has become necessary to study the actual BS distribution in the soil mass and to perform further field and laboratory experiments.

Field modeling of oil products migration in the soils of tundra landscapes has revealed a case dependence of seepage rate and distribution of BS within the soil profile on composition and physical and chemical properties of the substratum. Injection of such oil products as diesel oil, into light-textured tundra soils, namely iron-humus-illuvial podzols, with relatively uniform mineral substratum results in the emergence of regularly shaped isometric infiltration contours (Fig. 1a). The BS migration is determined mainly by capillary and gravitation processes. In less permeable mineral substrata the shape of infiltration bodies is dictated by the location of "unstable" tones, i.e., fractures, wedges, large capillary etc. (Fig. 1b). In this case migration is governed by capillary and diffusion processes, the gravitation ones being of less importance.

The highest shape diversity is characteristic of infiltration contours in soils with thick peat horizons. It is due to variable composition and density of peat, the degree of its decomposition, the depth of groundwater table, the presence or absence of permafrost. High water content in peat and near-surface occurrence of permafrost or above-permafrost waters cause the lateral "extension" of the infiltration contour within the soil profile.

Deep permafrost and relatively loose organogenic layer with low moisture content are associated with "downfall" seeping of pollutants resulting in the quasic-isometric shape of the infiltration contour.

Experimental studies of BS radial distribution and the results of empirical observations (Fig. 2) prove the dissimilar distribution of pollutants in different soil types which is the result of specific relationships between the gravitation capillary and the diffusion processes, on the one hand, and the occurrence of the intrasoil barriers, on the other. The levels of pollutant accumulation in genetic horizons of soils are also different in accordance with their oil-bearing capacity and permeability.

During the first year after bituminous pollution of soil surface the bulk of pollutants is localized in the upper horizons. The highest BS concentrations (up to 550 g per 1 kg of dried matter) are found in peat horizons (Fig. 2a). The results of experiments show that under quasi-natural moisture content (50 to 85% of maximum field capacity) the oil-bearing capacity of peat could be even higher, i.e., up to 715 g of oil per 1 kg of soil. The decrease in moisture content of peat down to 25 to 50% results in the increase of their oil-bearing capacity up to 1500 g/kg.

The degree of BS accumulation depends both on the oil-bearing capacity of recipient substrata and the amount and composition of pollutants. Under the same profile of pollutant distribution with their maximum concentrations in upper horizons and the sharp decrease in lower ones, the BS amount in oil polluted soils (Fig. 2a) is an order higher than in the same soils polluted with gas condensate (Fig. 2b).

The profile of BS distribution in iron humus-illuvial podzols is more complicated. During the first

1—infiltration contours; 2—input point
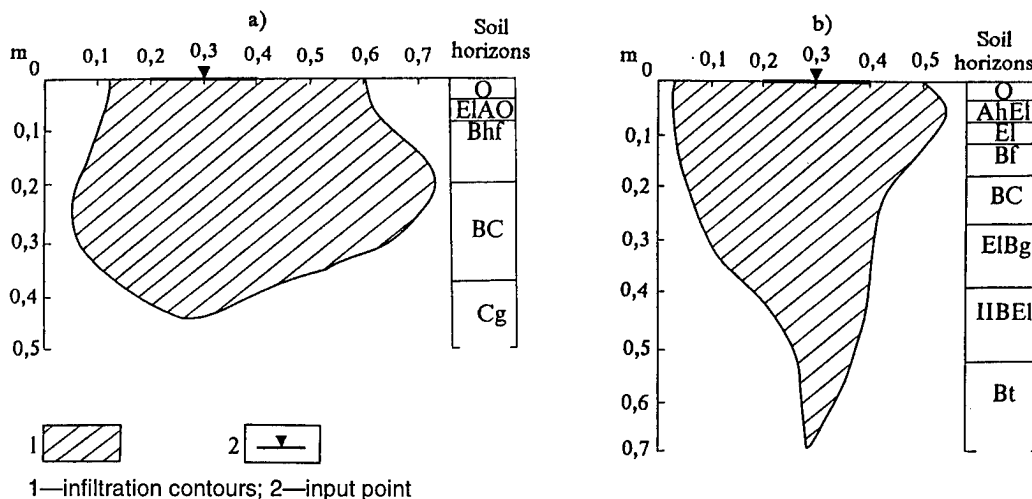
a. Tundra eluvial-gleyed podzolized soils.   b. Podzols iron-humus-illuvial.

Figure 1. Shapes of infiltration bodies in tundra soils (diesel oil, 7 days after input).

450

year after oil spill (Fig. 2e) there are already two peaks of pollutants accumulation; within the organo-genic horizons on the organic absolution barrier (hor.Ap) and within the illuvial horizon on less capacious mineral absorption barrier (hor.Bh). The capacity of the upper barrier is twice that of the lower one—130 and 60 g/kg, respectively. The same localization of BS in podzols is described in several publications (Solntseva and Pikovsky 1980, Pikovsky 1993).

Oil concentration in sand horizons of polluted tundra soils amounts to 65 g/kg; during laboratory experiments it was up to 100 g/kg, even under the maximum moisture saturation. Despite the greater surface of solid phase, the loamy substrata retain less oil than sandy ones (up to 10 to 20 g/kg). This proves different for the oil-bearing capacity of soil substrata with different texture, porosity and fracturing. These distinctions govern the uneven concentration of pollutants along the vertical profile of soils, as well as the subsequent transformation of BS pattern. Experimental studies (Bartz et al. 1969) and direct dynamic observations on the behavior of oil products on polluted soils (Solntseva 1995) have shown that the shape of original infiltration bodies formed immediately after the input of pollutants into soil is modified with time. The structure of infiltration bodies becomes much more complicated because of their dimensions and the degree of contrast in BS accumulation within different parts of the polluted oil mass.

The study of polluted soils of the Bolshezemelskaya Tundra proves the redistribution of BS with time—their concentrations decrease within the upper peaty horizons as they increase in the lower ones. The BS concentrations in the lower part of soil profile could become 3 to 4 times higher than in the upper horizons. This redistribution, as well as the contrasts in BS accumulation in different horizons, depend both on the type of soils and the time span since their pollution. The BS concentrations in soil mass could be rather even (Fig. 2c). This is typical of high-polluted soils with uniform substrata not long after the accident (within 1 to 3 years). The most common secondary profile of BS is characterized by intrasoil accumulations (Fig. 2d) with 5 to 6 times more pollutants than the upper soil horizons. One of the mechanisms of the downward transfer of maximum pollutant concentrations is partial washing of oil components by atmospheric precipitation. Redistribution of light oil fractions goes on much faster than of viscous and heavy ones. Different oil-bearing capacity and oil penetrability of particular soil horizons result in sharp changes of BS downward migration

rate. Under certain dimensions of capillaries and pores, the BS molecules couldn't penetrate them. Such substrata become radial barriers. It was found that the main barriers to vertical movement of pollutants within the tundra soils are frozen grounds, heavy loams and clays, especially gleyic ones. The occurrence of impermeable, "true" radial barriers hinders the vertical movement of pollutants (Fig. 2c is for permafrost ground barrier, Fig. 2d is for gleyic barrier). The BS concentrations in such substrata slightly exceed the background values for a particular territory even if the concentration of pollutants in upper horizons is very high. For example, the concentration of BS in gleyic horizons is 0.5 to 2.0 g/kg, while in upper organogenic horizons it exceeds 500 k/kg (Fig. 2c). Groundwater is also a kind of radial barrier, because it diverts vertical movement of hydrocarbons into soil-ground flow. In such cases the high groundwater table, as well as the near-surface permafrost, support the rapid lateral spreading of pollutants resulting in lower residual accumulation of BS in soils.

Even in the absence of distinct radial barriers, the highest oil concentrations could be found in the middle part of the vertical soil profile (Fig. 2f, g). Secondary accumulation of pollutants in peaty horizons within the middle part of soil profile is due to the higher oil-bearing capacity of these horizons, as compared with litter and underlying peat layers. It has been found experimentally that oil is carried in soils both by absorption processes and by its penetration into pores and planes (Guseva and Solntseva 1996). Due to their low density the layers of litter abound in large pores and channels with weak capillary forces potential). That's why some voids are free of pollutants. As the density of peat grows, voids become less numerous while the diameter of capillaries decreases. Under the optimum combination of capillary and absorption processes, the oil-bearing capacity of peat reaches its maximum values. Further increases in peat density reduce the effective space of larger and capillary pores, thus reducing the oil-bearing capacity of soils. All this produces the complex radial distribution of BS even in rather uniform substrata.

Thus, the total amount of oil within the soil mass is also a function of the soil horizon system, as well as of the oil-bearing capacity and permeability of particular soil horizons. In reality, soils with lower oil-bearing capacity but free of radial barriers could carry more oil as compared to less developed ones with higher bearing capacity. For example, deep podzols with profile down to 80–100 cm and free of impermeable barriers could carry even more oil than

a. Tundra peaty-gley soils (1 yr after oil spill).

b. tundra peaty-gley soils (0.5 yr after gas condensate spill).

c. Peaty frozen soil (3 yr after oil spill).

d. Peaty-gleysols (1 yr after gas condensate spill).

e. Podzols iron-humus-illuvial (1 yr after oil spill).

f. Peatbogs (5 yr after oil spill).

1 ▨▨ Radial barriers:
2 ▥▥ 1. Organic absorption
2. Local mineral absorbtion
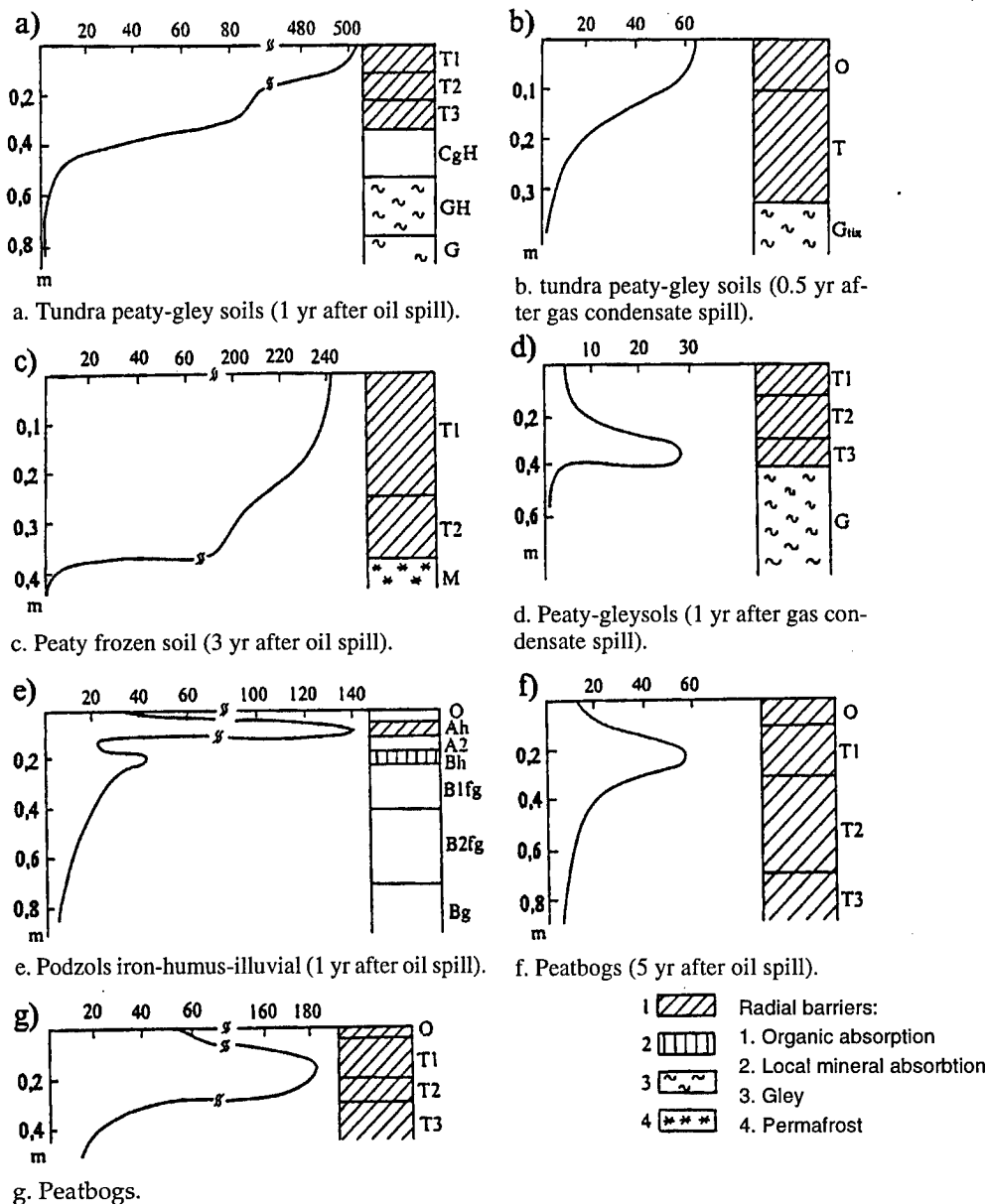3 ∿∿ 3. Gley
4 ✱✱✱ 4. Permafrost

g. Peatbogs.

Figure 2. Bituminous substances radial distribution (g/kg) in tundra soils.

peaty soils with high groundwater table or near-surface permafrost, i.e., with "true" barriers within the profile.

CONCLUSIONS

Distribution of oil and oil products within the vertical profile of tundra soils is of a complex nature, influenced by both natural and technogenic factors. The main natural factors include the genetic properties of soils, presence/absence of intrusion mechanical and physical and chemical barriers within soil profile, composition and water-physical properties of substrata, which determine the possible oil-bearing capacity and oil penetrability of soil material. The composition and volume of technogenic flows control the amount of pollutants injected in soils. The BS redistribution is greatly dependent upon the elapsed time from the spills. The post-technogenic redistribution of BS in the vertical profile of soils is highly dynamic, thus increasing the intrasoil contrasts in pollutants concentrations and supporting the formation of secondary accumulations in the soil. The BS migration and accumulation in soils are governed by the gravitation and capillary processes, as

well as by diffusion, which are active in all directions. Total amount of oil and oil products retained in the soil depends both on the properties of substratum and the depth of soil penetrable to pollutants.

The complex nature of northern soils results in a wide variety of possible levels of pollutant accumulation in different soil areas. Spatial contrasts of BS concentrations in soils are determined by different oil bearing capacities and profile depths, on the one hand, and by the area of their localization, on the other. Therefore it isn't possible to evaluate the potential risk of soil pollution with oil and oil products until the maximum volumes of pollutants, that could be carried by different soils, are taken into account.

REFERENCES

1. Bartz, J. et al. 1969. Ol und Bezinversickerungs-versuche in der Oerrheinebene Gas und Wasserfach, 110(22): 592–595.
2. Bratsev, A.P. 1988. Absorption of oil and oil products by peat soils. Impact of mineral prospecting of the Bolshezemelskaya Tundra environment. Syktyvkar, p. 29–36 (In Russian).
3. Eisenhut, E. 1969. Gesteinsabhangigkeit bei Auswirkung von Olunfallen. Gesundheitsingenieur, 90(2): 49–51.
4. Guseva, O.A., and N.P. Solntseva. 1966. Modelling of Oil Bearing and Oil Yielding Capacities of Tundra Landscape Soils at the European Part of Russia (EPR). International Sympo-

sium on the Geochemisty of the Earth's Surface, Yorkshire, England, p. 417–420.
5. Glazovskaya, M.A., and Yi.I. Pikovsky. 1981. Complex experimental studies of factors supporting self-purification and rehabilitation of oil-polluted soils in different natural zones. Migration of pollutants in soils and adjacent environments. Proc. III All-Union Workshop, Obninsk. L.: Gidrometeoizdat, p. 185–191 (In Russian).
6. Lippok ,W. 1966. Modelverscuhe uber das Verhalten von Heozul El in porosen Medium. Koblenz, deutsche gewasserkundliche Mittejlungen,10(3): 145–157.
7. Pikovsky, Yu.I. 1993. Natural and technogenic flows of hydrocarbons in the environment. M.: Izd-vo Mosk. un-ta, 205 p. (In Russian).
8. Solntseva, N.P. 1982. Impact of technogenic flows on forest soils morphology in the areas of oilfields. Extraction of mineral deposits and geochemistry of natural ecosystems. M.: Nauka, p. 29–70 (In Russian).
9. Solntseva, N.P. 1988. General features of soil transformation in the areas of oil extraction (forms, processes, models). Rehabilitation of all-polluted soil ecosystems. M.: Nauka, p. 23–42 (In Russian).
10. Solntseva, N.P. 1995. Impact of oil extraction on soils of the Bolshezemelskaya Tundra. Environmental problems associated with the development of oil and gas resources in Far North. Part 2. M.: VNIIGAZ, p. 15–54 (In Russian).

III. ECOLOGY
Pedology

Some Properties of Seasonally Frozen Soils of Northeastern Europe

G.V. RUSANOVA[1]

ABSTRACT

Spodosols of the forest zone of the Pechora and Vychegda Basins and Inseptisols of the Barents Sea coastal tundra were studied. Properties (macro- and micromorphology), and physical chemical characteristics of this soils are presented. Analyses have demonstrated that the main pedogenic processes in taiga soils are descending illuvial migration of Al-Fe humus compounds, and in tundra soils, cryogenic aggregation and cryoturbation, and weakening of migrational processes.

Key words: Sandy soils, macro- and micromorphology, physical-chemical properties, taiga and tundra soils, toposequences.

INTRODUCTION

Seasonally freezing soils commonly occur in the Northern Hemisphere and clearly demonstrate the features of cyclic processes of freezing and thawing.

Mechanisms of soil formation and rearrangement of the microfabric in soils on sandy deposits are studied in detail in Western Europe (De Coninck 1983), Canada (Page and Guillet 1991, Fox and Protz 1981, Tarnocai and Smith 1993), in Eastern Europe (Targulian 1971, Gerasimova et al. 1992). Conformities of these processes and mechanisms are studied at a lesser extent in catenary and longitudal soil sequences in the Russian European Northeast. This study attempts to remedy this deficiency.

MATERIALS AND METHODS

Studied objects are soils of toposequences of the middle and northern taiga, and also a subzone of typical tundra. These soils were described by Rusanova (1987) and classified according to the Russian Soil Classification. The group of taiga soils includes Spodosols and Aquods (U.S. Soil Taxonomy), or Iron Podzols and Iron Humus Podzols, Peaty Podzolic Gleysolic soils (Russian Soil Classification), and in tundra—Inseptisols (Distric Cambisols) or Podburs (in the Russian Classification).

The amorphous iron (Fe_o) and alumina (Al_o) were extracted by oxalic acid NH_4 oxalate buffer method, and the free iron (Fe_d) was extracted by citrate-bicarbonate-dithionite with an atomic absorption spectrophotometer. Bases (Ca, Mg) were extracted by NH_4OAc (pH 7.0). Total carbon was determined by oxidation. The pH (H_2O and KCl) values were determined using a 1:1 soil: solution ratio. Thin sections of 4·5 cm and 30 μm thick were prepared (Mochalova 1956).

RESULTS AND DISCUSSION

The soil microfabric is the most informative for diagnostics of pedogenesis. The fine dispersed mass is mainly concentrated in intergrain spaces as a heterogenic coatings (with embedded silt particles), on skeleton grains in taiga soils, and in the form of coatings and cryogenic-coagulated aggregates in tundra soils. The composition of grain coatings in the illuvial horizon reflects the main soil-forming processes in taiga: illuviation of Al-Fe-humus compounds and also downward movement of clay and silt particles (Table 1). Above-mentioned fabric types are common to the freezing-thawing and permafrost-affected soils. Predominance of cryogenic processes is reflected in tundra soils.

The eluvial-illuvial type of plasma distribution is observed in the taiga soil profile. The accumulative-illuvial type takes place in the profile of tundra soils.

---

[1] Institute of Biology, Komi Science Centre, Ural Division, Syktyvkar, Russia

Table 1. Characteristics of coatings of soils.

Subzone	Soils*	Horizon	Coatings
Middle taiga	Iron Podzol	A2	Absence of coatings
		Bf	Ochreous-brown (ferrugineous) Thin and rare brown (clay)
	Iron Humus Podzol	A2	Absence of coatings
		Bh	Brown (ferrugineous-humus) and light brown (clay) with silty particles, thick
		Bf	Brown (humus-ferrugineous) with silty particles and clay
	Peaty-Podzolic Gleysolic	A2g	Absence of coatings
		Bh	Dark brown (humus), thick with cracks
		Bf	Thick brown (ferrugineous), orange in reflected light, thick
Northern taiga	Iron Podzol	A2	Brown-like (clay) and yellow-brown (ferrugineous), thin
		Bh	Brown (ferrugineous-humus), broken,with silty particles rare clay
		Bf	Reddish-brown (humusferrugineous), with cracks, silty particles
	Iron Humus Podzol	A2	Light brown (clay), thin
		Bh	Dark brown, ferrugineous-humus, thick with cracks
		Bf	Dark brown (humus-ferrugi-neous), broken, rare clay
Subarctic tundra	Podbur	A0A1	Clots of humus plasma, silty particles around organic aggregates
		Bh	Brown (ferrugineous-humus) coatings, brown clots around skeleton grains
		S	Brown (ferrugineous-humus) coatings on grains

* Russian Soil Classification

With the increase of climatic and topo-lithogenic humidity in the taiga zone, the character of illuvial coatings is changed: thickening and color intensification reflect quantitative and qualitative changes of Al-Fe humus compounds migration (Table 2).

Soils formed in homogeneous sandy deposits belong to the group of Iron Podzols. In case of weak lithological heterogenity of deposits they are under increasing gleying and Fe-humus compounds cementation. In the sand underlain by clay deposits, gleying is dominant. At the most early stages of soil formation, the process of ortsand (cemented layer, iron humus ortstein) initiation took place. Currently, in ortsand layers, it is possible to observe accumulation of crystallized Fe oxides in comparison with the horizon. Ortsand formation takes 5–6 thousand years (Moore 1976). The mechanism of formation is different: illuvial and hydrogenic accumulation on the background of lithological heterogenity of deposits, or superposition of illuviation on lithological layer.

Micromorphological evidence indicates that the composition of ortsand cementation corresponds to the following: clay dominates in automorphic well drained soils (Iron Podzols). In the poorly drained soils (Peaty Podzolic Gleysolic) cementation was with a relatively high percentage of Fe, Al hydroxides. A similar content of crystallized Fe oxides in ortsand of gleysolic and automorphic podzols is found. Let us assume simultaneity of the formation of this layer and the stage of automorphic development of gleysolic soils during the early pedogenesis stages.

Formation of the whitish tongues in podzol profile is supposedly different (Dobrovolsky et al. 1981, Zaidelman 1974) In some cases it is possible to speak about the relation between tongue formation with depression of microrelief, or localization of water movement or ice wedge development at early stages of soil formation in the other case. Edges of tongues are similar to Bf horizon. The mechanism of their genesis is eluvial-illuvial differentiation of Fe, Al with humus.

The organic-accumulative horizon of the Distric Cambisols was characterized by a aggregated struc-

Table 2. Chemical characteristics.

Zone	Soil	Horizon	Depth (cm)	Humus (%)	(%) Fe(o)	Al(o)	Fe(d)	pH H₂O	KCl	meq/100g Ca	Mg
Middle taiga	Iron 1 Podzol	A2	7–12	1.70	0.20	0.20	0.33	4.3	3.3	0.07	0.01
		Bf	12–17	1.91	0.75	0.44	0.85	5.7	4.8	0.87	0.76
	Iron Humus–	A2g	20–24	0.73	0.19	0.22	0.35	5.3	4.0	0.08	0.01
	Podzol	Bhf	24–25	3.69	0.74	0.44	0.90	5.1	4.3	0.18	0.03
	Peaty– Podzolic	A2g	14–24	0.77	0.11	0.32	0.12	4.5	3.4	0.01	0.01
	— Gleysolic	Bh	24–30	4.20	0.44	0.87	0.51	4.4	3.6	—	—
Northern taiga	Iron Podzol	A2	5–20	0.21	0.12	0.14	0.20	4.8	3.7	0.5	0.1
		Bf	28–38	0.42	0.85	0.62	1.09	4.9	4.4	—	—
	Iron Humus	A2	4–14	0.20	0.22	0.39	0.24	5.3	4.0	0.2	0.1
	Podzol	Bh	22–23	2.68	0.78	1.62	0.86	4.7	4.0	—	—
Tundra	Podbur	AOA1	0–4	5.69	0.65	0.34	—	4.9	3.9	1.6	1.0
		Bh	4–10	1.59	0.57	0.44	—	5.2	4.1	0.8	0.6
	Shallow	AOA1	0–7	4.85	0.49	0.39	—	5.0	4.3	0.5	0.3
	Podbur	Bh	7–15	1.73	0.51	0.40	—	—	—	—	—

ture: rounded organic aggregates with silty coatings, cluster-like clots of humus-Fe plasma in the interiors and on skeleton grains. Humus-Fe coatings are on some grains. The main processes in the horizon are cryogenic and transformation of organic matter.

The Bh horizon is characterized by Fe-humus films on grains and coagulated aggregates on pore walls and grain edges. Microzones above the ortsand layer indicate gleying.

Ortsand (S) is present with evidence of cryoturbation and illuviation of humic and humic-Fe compounds in the form of coagulated aggregates and coatings. The main soil- forming processes are cryogenic mass aggregation, Al-Fe-humus migration, cryoturbation, accumulation and transformation of organic matter.

The evidence for frost action and gleying on the soil fabric is more noticeable in a case of shallow active layer (frost table close to soil surface, 30 cm).

CONCLUSION

The main illuvial Al-Fe-humus migration process that determines the genetic essence of Spodosols is accompanied by acid pH, fulvic humus, and base insaturation. Microfabric investigations showed that a fine dispersed mass is concentrated in a form of heterogenic coatings on the skeleton grains in Bf horizon. The eluvial-illuvial type of plasma distribution demonstrates the main Al-Fe-humus migration process in taiga soils. Changes in character of grain coatings take place to the north (subzone of the northern taiga) and toposequence downwards: thickening, color intensification reflecting qualitative and quantitative changes in the Al-Fe-humus migration process, and increase of gleying. In tundra soils a fine dispersed mass is concentrated as coatings and coagulated aggregates among skeleton grains. The accumulative-illuvial character of plasma distribution in profile reflects dominance of cryogenic processes and weakening of Al-Fe-humus migration in tundra soils.

REFERENCES

De Coninck, F., and D. Righi. 1983. Podzolization and sodic horizon. Soil micromorphology. 2: 389–407.

Dobrovolsky, G.V., Nikitin, E. D., and T.V. 1981. Afanasieva. Taiga soil formation within continental conditions. Nauka, M.

Gerasimova, M.I., Gubin, S.V., and S.A. Shoba. 1992. Soil micromorphology in nature zones of the USSR Nauka, Pushchino.

Fox, C.A., and R. Protz. 1981. Definition of fabric distributions to characterize the rearrangement of soil particles in the turbic cryosols. Can. J. Soil Sci. 61: 29–34.

Mochalova, E.F. 1956. Soil thin section preparation. Pochvovedenie. 10: 40–46.

Moore, J.R. 1976. Sesquioxide cemented soil horizons in the Northern Quebec: their distribution, properties and genesis. Can. J. Soil Sci. 56(4): 333–344.

Page, F., and B. Guillet. 1991. Formation of loose and cemented B horizons in podzolic soils: Evaluation of biological actions from micromorphological features. C/N values and C^{14} datings. Can. J. Soil Sci. 71: 485-494.

Rusanova, G. 1987. Micromorphology of taiga soils. Nauka. L.

Tarnocai, C., and C.A.S. Smith.1993. The formation and properties of soils in the permafrost regions of Canada. p. 21–42. *In* Proc. 1st Intern. Conf. on Cryopedology. Pushchino.

Targulian, V.O. 1971. Soil formation and weathering in cold humid regions. Nauka. M.

Zaidelman, F.R. 1974. Podzolic-gleying formation. Nauka. M.

Humus Composition and Transformation in a
Pergelic Terric Cryohemist of Coastal Continental Antarctica

L. BEYER[1], H.-P. BLUME[1], C. SORGE[2], H.-R. SCHULTEN[2], AND H. ERLENKEUSER[3]

ABSTRACT

Organic matter of an Antarctic peat soil was studied with special emphasis on soil formation processes. An integrated approach, including wet-chemical analyses, cross-polarization magic angle spinning carbon-13 nuclear magnetic resonance spectroscopy (CP/MAS ^{13}C-NMR), and pyrolysis-field ionization mass spectrometry (Py-FIMS), was applied to characterize the soil organic matter (SOM) composition at different depths. Dead moss was the fresh organic matter. Aliphat-C units dominate in the SOM. Alkyl compounds consist of lipids, fatty acids and sterols. The aromatic structures identified by CP/MAS ^{13}C-NMR and by Py-FIMS demonstrate that lignin input is not necessary for the formation of aromatic humic structures. Within the humification process, carbohydrates are less mineralized in Antarctica than under temperate climate conditions and these moieties also dominate in the SOM of deeper horizons. The extremely cold climate conditions of Antarctica retard the transformation of fresh organic residues. Nevertheless, alkyl carbon units are incorporated into the complex humic matter and enriched due to a selective preservation.

Keywords: Antarctica, peat soil, soil organic matter genesis, CPMAS ^{13}C NMR spectroscopy, pyrolysis

INTRODUCTION

In the maritime Antarctic climate region, peat formation due to the accumulation of organic matter is well documented (Campbell and Claridge 1987). Histosols are mainly formed by debris of mosses and algae (O'Brien et al. 1979, Smith 1979) and are widespread (Campbell and Claridge 1987). According to Bockheim and Ugolini (1990) in the coastal continental Antarctica this soil formation process is not evident. However, Blume et al. (1997) described different kind of Gelic Histosols (Cryofibrists and Cryohemists), which are associated with Leptosols, Regosols and Podzols (Blume and Bölter 1993). Usually, analyses of organic matter in Antarctic soils are confined only to the loss on ignition and the determination of organic C and N (Campbell and Claridge 1987). Only Wilson et al. (1986) and Wilson (1990) have investigated Antarctic mosses and soil humic acids by CP/MAS ^{13}C-NMR spectroscopy. Thus, the knowledge of humus composition and transformation processes as well as its formation under the extreme Antarctic climate conditions is scarce. Therefore, in the present paper, the soil organic matter (SOM) of a peat soil (pergelic Terric Cryohemist) presented by Blume and Bölter (1993) near Casey Station (Wilkes Land) was investigated. An integrated approach using the classical wet-chemical humus analyses, CP/MAS ^{13}C-NMR spectroscopy and direct pyrolysis-field ionization mass spectrometry was used to characterize SOM composition and transformations.

MATERIALS AND METHODS

Site

The soil is located south of the Australian Casey Station, Wilkes Land (66°18'S, 110°32'E) in the coastal continental Antarctica. The mean annual temperature is -9.3°C. The annual precipitation (176 mm) is mostly snow.

Soil

The top horizon (LH) of the pergelic Terric Cryohemist consists of dead mosses (Ceratodon purpurea), which are colonized by lichens (Usnea antarctica). In the deeper horizons (H1-H3) the mosses are more humified and colored brownish-black (Table 1). According to the carbon-14 measurements the H1 layer has an estimated age of 850 year before present and the H2 layer of 1420 years before present.

Field measurements

The soil was classified according to the Soil Survey Staff 1994). The amount of humification was estimated by squeezing the moist soil sample between the fingers (Schlichting et al. 1995): humification level (HL) 1 indicates no humification and HL 10 complete humification. Electrical conductivity was measured in the 1:2.5 water extract. The pH values were determined in the 1:2.5 extract using 10 mM $CaCl_2$ (Schlichting et al. 1995).

Table 1. Site description of the pergelic Terric Cryohemist.

Ho.	Depth cm	HL	Munsell Colour	Moisture[a] status	pH $CaCl_2$	$EC_{2.5}$[b] mS	Gravel mg g^{-1}
LH	0-3	1-2	ND	Dry	4.8	0.72	0
H1	-8	3-5	5YR2.5/1.5	Dry	3.9	0.61	31
H2	-16	8-9	5YR2.5/1.5	Moist	3.8	0.20	85
H3	-28	8-9	5YR2.5/1.5	Moist	3.8	0.13	210

Ho. soil horizon, HL humification level
ND not determined
[a] in the field during sampling in January
[b] electrical conductivity (1:2.5) water extract

Carbon-14 measurements

The carbon-14 dating was performed on the total organic fraction after removal of carbonates by HCl (2%, 40°C, 2h), the stable carbon isotope ratios were determined by mass spectrometry and carbon-14 ages were normalized to $\delta^{13}C = 25$ mg g^{-1}).

Chemical analyses

Total organic carbon was measured by dry combustion in a Coulomat 702 (Ströhlein Instruments). Soil organic matter was estimated by loss on ignition at 600°C in a common furnace (Heraeus Instruments). The extraction of total nitrogen was carried out according to the Kjeldahl method (Jones 1991). The SOM fractionation was carried out according to Beyer et al. (1993, 1996a). Nitrate-N and Ammonium-N were extracted with 20 mM $CaCl_2$ according to Schlichting et al. (1995) and measured by flow injection analysis (Jones 1991) using a Tecator flow injection analyzer (Perstorp Analytical).

Cross polarization magic angle spinning carbon-13 nuclear magnetic resonance spectroscopy (CP/MAS ^{13}C-NMR)

The CP/MAS ^{13}C-NMR spectra and SOM subunits were obtained at 2.3 tesla (25.2 MHz) in a Bruker MSL 100 spectrometer equipped with a commercial 7mm CPMAS probe at a rotation frequency of 4 kHz according to Fründ and Lüdemann (1989).

Pyrolysis-field ionization mass spectrometry (Py-FIMS)

The Py-FIMS mass spectra were recorded using a double-focusing Finnigan MAT 731 mass spectrometer according to Schulten (1987, 1993).

RESULTS AND DISCUSSION

Selected soil properties at various depths are presented in Table 1 and 2. The humification level increases with soil depth (Table 1), which suggests a considerable change of the humificaton degree from the LH to the H2 horizon. Total organic carbon (TOC) and losses on ignition as a criterion for SOM content decreased with increasing profile depth (Table 2). However, TOC was increasingly enriched in the organic matter of deeper horizons (TOC/SOM). This was in agreement with the increase of humification.

Table 2. Properties of the pergelic Terric Cryohemist.

Hor.	TOC mg g^{-1}	N_t mg g^{-1}	C/N	SOM	TOC SOM	N_t SOM	α-NH_2 -N mg g^{-1}	NO_3^- -N ng g^{-1}	NH_4^+ -N	N_{org} mg g^{-1}
LH	287	15	19	553	.52	28	8.7	5	79	6.7
H1	195	22	9	378	.53	58	8.0	105	67	13.9
H2	188	21	9	318	.59	65	5.9	31	28	14.7
H3	159	13	12	259	.61	c51	5.0	7	32	8.0

Hor. horizon, TOC total organic carbon, N_t total nitrogen
SOM Soil organic matter
N_{org}: N_t - (α-NH_2-N + NO_3^--N + NH_4^+-N)

Between 3 and 16 cm, the total nitrogen (N_t) concentrations were higher as in the top and lowest horizons. This was due to the higher proportions of organic, non-α-NH_2-N (N_{org}). The α-NH_2-N concentrations continuously decreased with increasing soil depth. Again a strong nitrogen enrichment in the second and third soil horizon (H1 and H2) was found (N_t/SOM). In the whole soil profile, soluble, inorganic NO_3^--N and NH_4^+-N fractions were of minor importance. However, there was a considerable nitrate peak in the second soil horizon (H1). The highest nitrogen supply in the third soil horizon (H2) as well as its humification level and the carbon and nitrogen enrichment suggest a remarkable change of the humus compositions especially from the 850-year-old soil horizon (H1) to the 1420-year-old soil horizon (H2). This hypothesis must be proven with the data of the SOM investigations.

Figure 1 shows the distribution of the investigated litter compounds in the peat soil. As expected from the increasing humification level visible in the field (Table 1) a clear decrease from the first (LH) to the second soil horizon (H1) of the polysaccharides was detectable. However, surprisingly the change from the second (H1) to

the third soil horizon (H2) was much less. A similar pattern was found with the data of the classical alkaline-extraction procedure (Fig.2). In the first soil horizon
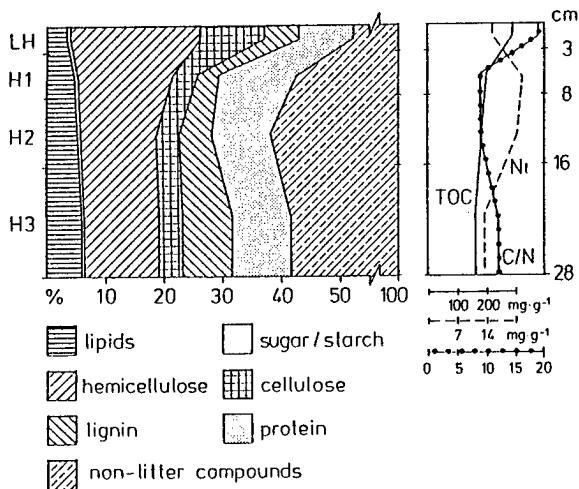

Figure 1. Litter compounds in the soil organic matter of different soil horizons (LH, H1, H2, H3) in a pergelic Terric Cryohemist from mosses in the coastal continental Antarctica (cm legend see Fig.2 and 3).
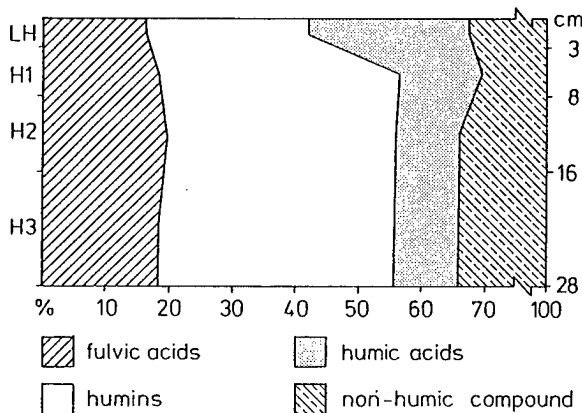

Figure 2. Humic compounds in the soil organic matter of a pergelic Terric Cryohemist from mosses in the coastal continental Antarctica (legend see Fig.1).

(LH) probably the large humin fraction contains little modified organic litter components (e.g., Kögel-Knabner 1993a), whereas in the H1 the humin fraction partly has been oxidized into humic acids (e.g., Hatcher and Spiker 1988). These chemical changes are typical within the humification process (Kögel-Knaber 1993b). The increase of the proteins as well as the slight, but significant increase of the lipids was probably induced by the increasing microbial soil colonization in deeper soil horizons (Beyer et al. 1993). According to the common SOM fractionation, no seperation between the living and dead organic matter is possi-

ble (Beyer et al. 1996b). However, again no differences were detectable between the second (H1) and third soil horizon (H2), despite the differences in the humification level (HL) (Table 1).
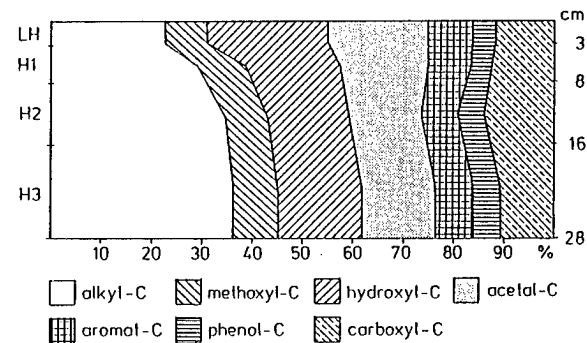

Figure 3. CP/MAS 13C-NMR subunits in the soil organic matter of a pergelic Terric Cryohemist from mosses (legend see Fig.1).

In Figure 3 the integrated areas below the CP/MAS 13C-NMR spectra are shown. In all soil horizons, methoxyl-C, aromat-C and phenol-C moieties were of lesser importance compared to acetal, hydroxyl and alkyl carbon structures. Carboxyl-C and alkyl-C compounds increased especially from the 850-year-old (H1) to the 1420-year-old soil horizon (H2). The NMR spectroscopy was the first method used in this paper that significantly indicated a chemical modification within the visible humification differences of these two horizons. The increase of alkyl-C with the peat depth has been described for Histosols in the temperate climate (Wachendorf et al. 1996). The decrease of the O-alkyl-C (glucose units) suggests the decomposition of carbohydrates from moss debris from the LH to the H layers and the enrichment or formation of carboxyl- and alkyl-C during the soil formation the pergelic Terric Cryohemist. Of special interest was the detection of aromatic-C, although mosses as plant precursors for the SOM do not contain lignins (Hurst and Burges 1967).

According to the Py-FIMS measurements, in the temperature range from 100°C to 350°C between 43% and 56% of the pyrolysis-induced total ion intensity could be assigned to seven significant biomarkers of SOM: carbohydrates, amino acids and peptides, N-containing pyrolysis products, alkyl-aromatics and lipids supplemented by free n-C16 to n-C34 fatty acids and steroles (Fig.4 and 5). Carbohydrates and lipids dominated the molecular-chemical composition of SOM in all soil horizons. Proportions of carbohydrates and alkylaromatics changed only insignificantly with profile depth. The proportion of amino acid and peptides signals on the total ion intensity soil slightly increased with profile depth (Fig.4). This was in agreement with the wet chemical protein data (Fig.1) and the rising NMR peaks at
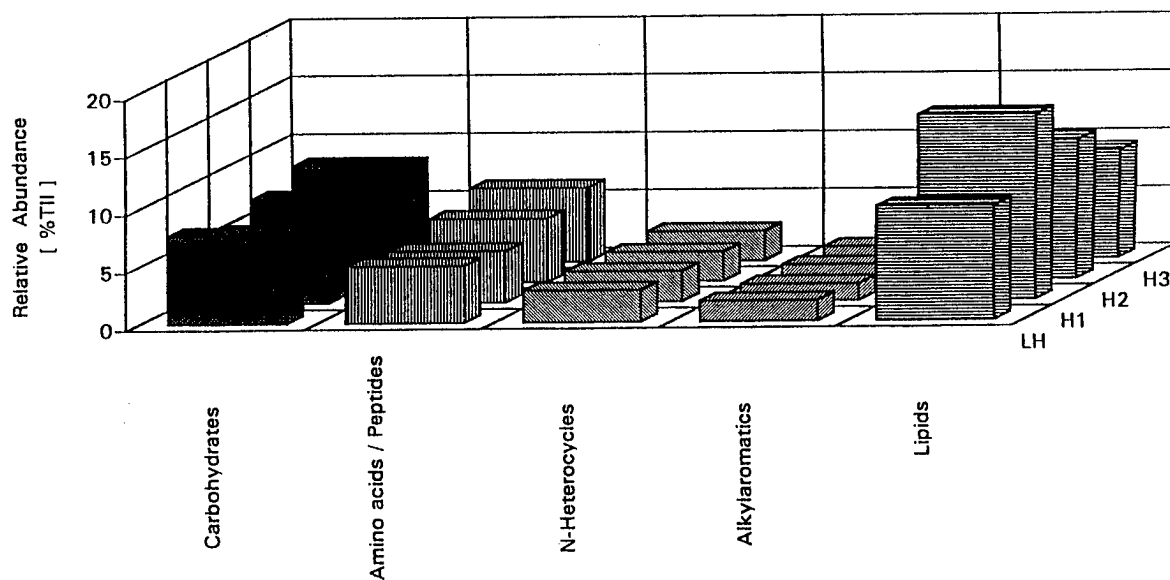
461

Figure 4. Summed relative abundances (percentage of Total ion intensity: TII) of typical biomarkers of soil organic matter after Py-FIMS of different soil horizons of a pergelic Terric Cryohemist in coastal continental Antarctica.
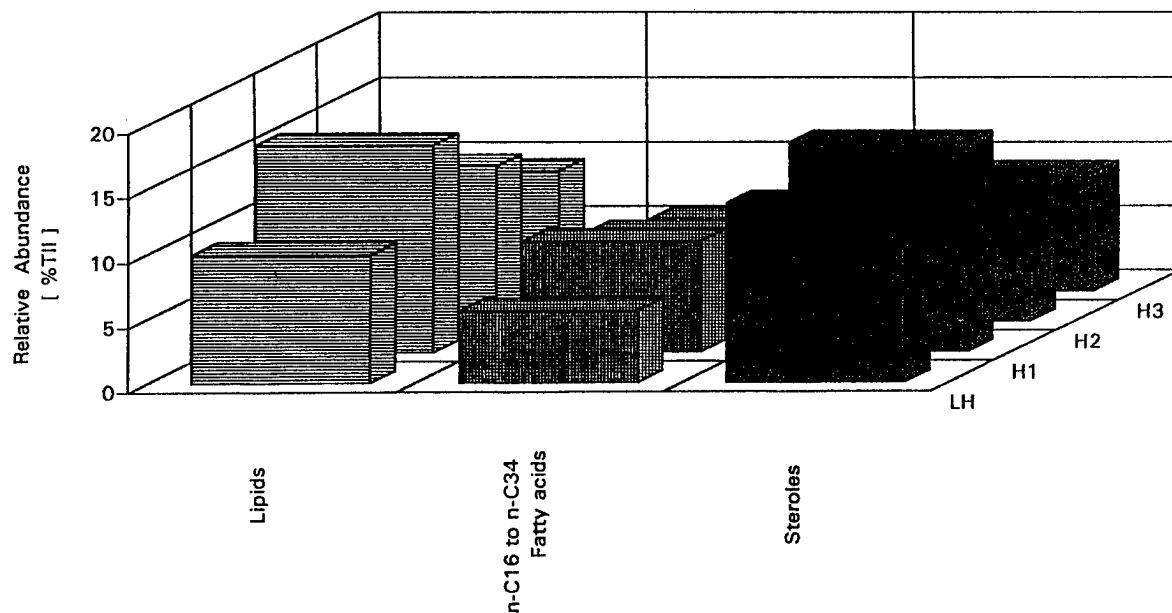

Figure 5. Summed relative abundances (percentage of Total ion intensity: TII) of lipid-derived biomarkers of soil organic matter after Py-FIMS of different soil horizons of a pergelic Terric Cryohemist in coastal continental Antarctica.

20-30 ppm (not shown). Py-FIMS data suggest that these SOM compounds are not much incorporated in the humified matter, because of its volatilization below 350°C (Beyer et al. 1996b).

The lipids and the other lipid-derived biomarkers increased in second (H1) to the third horizons (H2) compared to the LH layer (Fig.5). This was again in agreement with the wet-chemical data (Fig.1 and 2) and the NMR data (Fig.3).

However, in contrast to alkyl carbon units observed with NMR, lipids, fatty acids and steroles decreased continously from the second to the fourth layer (Fig.5). Probably the alkyl carbon units were enriched due to a selective preservation within the change from the LH to the H1 layer, because of the removal from carbohydrates. On one hand these moieties could may be mineralized. This could be deduced from the wet chemical and NMR data (Fig.1 and 3).

462

On the other hand the carbohydrates could be incorporated into the more thermostable moieties (volatilization above 350°C) as the considerable appearance of the humic acid fraction suggest (Fig.2). This fraction contains up to 30% little modified carbohydrates (Novak and Bertsch 1991). During the humification process from the second (H1) to the third (H2) (and probably also to the fourth (H3)) layer the alkyl carbon units become more thermostable and the used Py-FIMS procedure only detects the free parts of total alkyl carbon, which has been detected with the NMR. The increase of thermostabilization within the humication process is well known (Beyer et al. 1996b and references cited therein). From this point of view, the Py-FIMS confirms the optical differentiation of the H1 and the H2 layer (Table 1).

CONCLUSIONS

Dead moss material is the fresh organic matter of soil formation in the pergelic Terric Cryohemist. According to the CP/MAS carbon-13 NMR data, aliphatic-C units (acetal, hydroxyl, alkyl) dominate in the SOM. Only scarce humification was visible in the first soil layer (LH). Therefore, the high amount of carboxyl groups are probably derived from fatty acids and proteins (Wilson 1987). Tentative assignments by Py-FIMS indicate that the alkyl compounds consist of lipids, fatty acids and sterols. The aromatic compounds are not lignin-originated, because the typical signals in Py-FIMS were missing. Py-FIMS data suggest that alkyl-aromatics were present in the necrotic mosses. Under temperate conditions these compounds are typical structural building blocks of humic substances (Schnitzer and Schulten 1992).

The data suggest, that carbohydrates were mineralized and/or incorporated into the more stable humic matter within the humification process. The degradation of the nitrogen-free polysaccharides in the soil profile is confirmed by the drastic change in the C-to-N ratio from the first to the second layer. The most striking feature of the CP/MAS ^{13}C-NMR data is the very considerable increase of alkyl-C. The alkyl carbon units were enriched due to a selective preservation within the change from the first to the second layer. During the further humification the alkyl carbon units become more stable and are not detectable as free moieties, because of the incorporation in the complex humic matter. The chemical degradation of the organic matter is not as intensive as that in soils under temperate climate regimes (Kögel-Knabner 1992, 1993b). The governing influence are the extremely cold conditions, which strongly retard the transformation of fresh organic residues (Wilson 1990). Therefore, in this Antarctic peat soil, carbohydrates dominate in the composition of the SOM in the deeper horizons. They are associated with the recalcitrant alkylic compounds. Schnitzer et al. (1990) observed similar effects

in the organic layer of Canadian subarctic soils.

Mosses as plant precursors of the organic matter in peat soils do not contain lignin (Hurst and Burges 1967). Thus, the aromatic structures identified by CP/MAS ^{13}C-NMR and by Py-FIMS demonstrate that lignin input is not necessary for the formation of aromatic humic structures. The source of these compounds might be aromatic amino acids (Breitmaier and Voelters 1989). On the other hand the synthesis of these compounds is also possible from ketonic and carboxylic structures (Ziechmann 1980). The occurrence of aromatic constituents in SOM of an Antarctic Histosol is in line with results of Wilson et al. (1986), who determined aromatics in humic acid fractions from soils.

ACKNOWLEDGMENTS

REFERENCES

Beyer, L., Wachendorf, C., and C. Köbbemann. 1993. A simple wet chemical extraction procedure to characterize soil organic matter. 1. Application and recovery rate. Comm. Soil Sci.Plant Anal.24: 1645-1663.

Beyer, L., Köbbemann, C., and B. Vogt. 1996a. A simple wet chemical extraction procedure to characterize soil organic matter. 2.Reproducibility and verification. Comm. Soil Sci.Plant Anal.29: 2229-2241.

Beyer, L., Deslis, K., Wachendorf C., and B.Vogt. 1996b. Estimation of soil organic matter composition according to a simple thermo-analytical approach. Comm.Soil Sci. Plant Anal. (submitted).

Blume,H.-P., and M.Bölter. 1993. Soils of Casey Station (Wilkes Land, Antarctica). Proc. 1st Int.Conf.Cryopedology 1992. Russ. Academy of Sciences, Pushchino. p.96-103.

Blume, H.-P., Beyer, L., Bölter, M., Erlenkeuser, H., Kalk, E., Kneesch, S., Pfisterer, U., and D.Schneider. 1997. Pedogenic zonation in soils of the southern circum-polar region. Advances in GeoEcology (in press).

Bockheim, J.G., and F.C.Ugolini. 1990. A review of pedogenic zonation in well-drained soils of the southern circumpolar region. Quat.Res. 34, 47-66.

Breitmaier, E., and W. Voelter. 1990. Carbon-13 NMR Spectroscopy. 3rd ed. Chemie, Weinheim.

Campbell, I. B., and G.G.C. Claridge. 1987. Soils, Weathering Processes and Environment. 1st ed. Elsevier,

463

Amsterdam.

Fründ, R., and H.-D. Lüdemann. 1989. The quantitative analysis of solution-and CPMAS 13C-NMR spectra of humic materials. Sci.Total Environm. 81/82, 157-168.

Hatcher, P.G., and E.C. Spiker. 1988. Selective degradation of plant biomolecules. p. 59-74. In F.H. Frimmel and R.F. Christman (eds.) Humic Substances an their role in environment. 1st ed. Wiley, New York.

Hurst, H.M., and Burges. 1967. Lignin and humic acids. In A.D.McLaren and G.H.Peterson (ed.) Soil Biochemistry, Vol.1. 1st ed. Marcel Dekker, New York.

Jones, J.B. 1991. Kjeldahl Method for Nitrogen Determination. 1st ed. Micro-Macro Publishing, Athens.

Kögel-Knabner, I. 1992. Forest soil organic matter: Structure and formation. Bayreuther Bodenkundliche Berichte 14: 1-102.

Kögel-Knabner, I. 1993a. Structure and degradation processes of organic matter (German). Mitt.Dtsch.Bodenkundl.Ges 69: 251-254.

Kögel-Knabner, I. 1993b. Biodegradation and humification processes in forest soils. p. 101-135. In J. M. Bollag and G. Stotzky (ed.) Soil Biochemistry, Vol.8. 1st ed. Marcel Dekker, New York.

Novak, J.M., and P.M. Bertsch. 1991. The influence of topography on nature of humic substances in soil organic matter at a site in the Atlantic Coastal Plain of South Carolina. Biogeochemistry 15: 111-126.

O'Brien, R. M. G., Romans, J. C. C., and L. Robertson. 1979. Three profiles from Elephant Island, South Shetland Islands. British Antarctica Survey Bulletin 47: 1-12.

Schlichting, E., Blume, H.-P., and K. Stahr (1995): Bodenkundliches Praktikum. 2nd ed. Blackwell, Berlin.

Schnitzer, M., and H.-R. Schulten. 1992. The analysis of soil organic matter by pyrolysis-field ionization mass spectrometry. Soil Sci.Soc.Am.J.54: 98-105.

Schnitzer, M., Tarnocai, C., Schuppli, P., and H.-R. Schulten. 1990. Nature of the organic matter in Tertiary Paleosols in the Canadian Arctic. Soil Science: 149, 257-267.

Schulten, H.-R. 1987. Pyrolysis and soft ionization mass spectrometry of aquatic/terrestrial humic substances and soils. J.Anal.Appl.Pyrolysis 12, 149-186.

Schulten, H.-R. 1993. Analytical pyrolysis of humic substances and soils: Geochemical, agricultural and ecological consequences. J.Anal.Appl. Pyrolysis 25: 97-122.

Smith, R. J. L. 1979. Peat-forming vegetation in the Antarctic. p. 38-67. In E. Kivunen et al. (ed.) Classification of Peat and Peatlands. 1st ed. Int. Peat Society, Helsinki.

Soil Survey Staff. 1994. Keys to Soil Taxonomy. USDA-SCS, Washington.

Wachendorf, C., Beyer L., and H.-P.Blume. 1996. Structures and functions of peat ecoystems with different use in Northern Germany. IV.Chemical composition of litter and peat of Histosols. Abstracts 10th Peat Congress, Vol.1: 196.

Wilson, M. A., 1987. N.M.R. Techniques and Applications in Geochemistry and Soil Chemistry. 1st ed. Pergamon Press, Oxford.

Wilson, M. A. 1990. Application of nuclear magnetic resonance spectroscopy to whole soil. p. 221-260. In P. MacCarthy et al. (ed.) Humic Substances in Soil and Crop Sciences. 1st ed. ASA-CSSA-SSSA, Madison.

Wilson, M. A., Goh, K. M., Collin, P. J., and L.G. Greenfield. 1986. Origins of humus variations. Org.Geochem.9: 225-231.

Ziechmann. W. 1980. Huminstoffe. 1st ed. Chemie, Weinheim.

Temperature Regime of Gley-Podzolic Soils of the European Northeast (Komi Republic)

I.V. ZABOEVA[1]

ABSTRACT

Gley-podzolic soils of true-mossy forests of the northern taiga subzone, according to the temperature regime, are classified as cold soils with long seasonal freezing. In winter, the temperature at the soil surface is -2°C, the depth of freezing averages 0.6 m; during the extreme years (one year in ten), up to 1.2 m. In the lower part of the frozen layer the temperature is no lower than -1°C. Under the frozen part the temperature is mostly constant, about +1°C. The soil thaws by 10-15 May, warming up slowly, reaching only +5°C at 1 m depth by the end of July. The temperature regime in the frost litter (A_o horizon) differes greatly from that of mineral soil horizons. Optimum temperatures (15°C and higher) begin during the second decade of June, and they persist 10-15 days. Warming of B_f and B horizons takes place much later and is very short. Small heat resources prevent the roots of arboreal plants from penetrating into the soil. Their main mass is located in the litter.

Key words: Gley-podzolic soils, cold soils with prolonged seasonal freesing, heat resources.

INTRODUCTION

The Komi Republic belongs to the three climatic regions: arctic, Atlantic-arctic, Atlantic-continental. The part of the Republic north of the Polar Circle belongs to the arctic region; the central area (up to 63°N), to the Atlantic-arctic region; and the rest, to the Atlantic-continental.

Mean annual temperature in the south is +1°C and decreases to the north to -6°C. Annual precipitation in the same direction decreases from 625 to 450 mm. The majority of precipitation occurs during the frost-free season. In the annual cycle, the period with stable low temperatures below -2°C increases northwards fron 140 days up to 210 days. The active vegetative period with the mean temperature above 10°C lasts about 110 days in the southern part of the KR. To the north, the number of such days decreases to 45 days. The sum of positive temperatures decreases from 1600 to 600 degrees. Latitudinal subzones are distinguished according to bioclimatic and soil characteristics. The clearest zonality is shown in automorphic soils developed in loamy soil-forming material. Tundra frozen soils are developed in the far north and north east of the Rebublic. They cover 4232000 ha, 10.3% of the Republic area. Severe climate and woodless tundra determine the character of tundra soil formation and coarse cryogenic rocesses of frost heave and freezing out.

Frost mound peatlands and boggy tundra soils are widespread in watersheds. Large tundra territories comprise natural grazing basins for reindeer herding. Forest tundra is situated in the south (up to 66°30'N), with the typical combination of tundra and gley-podzolic humic-illuvial soils, and with wide distribution of relict frost mound peatlands.

The main part of the Komi Republic is located in taiga zone where podzolic soils predominate. Their total are is 9500000 ha. We distinguish three subzonal soil subtypes: gley-podzolic in the northern taiga (its southern border is 63°N); typical podzolic in the middle taiga (up to 60°N); sod-podzolic in the southern taiga.

RESULTS AND DISCUSSION

Gley-podzolic soils are well developed under true-mossy spruce forests of levees. A subtype peculiarity of these soils involves accumulation of mobile humus substances of illuvial (transit) nature in the upper horizons, products of cley destruction and organic-mineral complexes migrate with the escending flow of soil solutions. Poor naturel fertility and deficiency of heat predetermine the poor biological productivity of these soils. But because of the normal water regime they are used as arable lands. The arable land area in gley-podzolic soils in the northern taiga subzone is 23700 ha. Typical podzolic soils of the middle taiga can be found in drained levees with true-mossy spruce

---

forests. Acid hydrolisis of mineral material can be regarded as a profile-forming process that destroys primary and secondary minerals and removes the destruction products.

Podzolic horizon A_2, with evidence of seasonal gley, is expressed under thin peatified litter ($A0$). It lacks silt, sesquioxides, and has low exchange capacity. in the lower horizons (A_2B and B), an eluvial process takes place in combination with a slightly expressed illuvial accumulation of organic-iron new formations. The soils belong to seasonally frozen moderate cold soil group, according to the temperature regime. The moisture regime is pereolative. natural fertility is poor. Humus content is low (in A_2 is 15 g kg⁻¹). Humus is of predominantly fulvic composition, not valuable from the agricultural point of view; soils are structureless and have high acidity. These soils form the main agricultural land fund. About 45000 ha of plowed lands are located on these soils. In the very south of the KR there is a gradual transition of sod-podzolic soils of the south taiga subzone, covering an insignificant part of the territory of the Republic. Sod-podzolic soils are formed under *Oxalis acetosella* true-mossy spruce forests with herb admixture in the cover. Sod formation is connected with the vegetation change and more favourable climatic conditions in the southern taiga subzone. Sod formation takes place in the same soil profiles in which podzilization develops. It leads to a dark-grey sod horizon (A_1, 5-10 cm) formation, of granular structure, located underneath a raw humus litter ($A0$). A light podzolic A_2 horizon is situated under the sod horizon, and father below a brown B horizon is formed. Up to 5% of the humus (derived from roots) is accumulated in the A_1. Such soil has higher natural fertility in comparison with typical podzolic soils. The arable land percentage in the south taiga is considerable: 16000 ha of arable land are on sod-podzolic soils.

Table 1 shows that the land fund of the KR is very important for forestry: 100000 ha are arable land, which is 0.2% of the total area of the KR.

The natural fertility of podzolic soils used for agriculture is not significant. But due to the sufficient moisture content, podzolic soils are rather responsive to fertilizers. Investigations showed that to get a potato yield of 30-40 t ha⁻¹ or clover yield of 8-9 t ha⁻¹ of dry mass, there is a need in the taiga zone to use optimum rates of inorganic fertilizers with a background of organic fertilizer application and liming; solar radiation, moisture regime and heat are sufficient. A rich yield of crops (potato, cabbage, some root crops, grasses) depends most of all on soil conditions. Under virgin taiga conditions, the podzolic process plays the leading role in soil formation, along with pereolative moisture regime. But despite this, soil fertility is restored because biological accumulation of nutrients prevails over removal.

North taiga gley-podzolic soils ($A0$-A_{2hg}-B_f-BC-C profiles) belong to the group of cold soils with long seasonal freezing, according to temperature regime. They are frozen for 7-7.5 months. During this period the surface mean temperature is -2°C. Freezing depth varies from 0.6 m up to 1.2 m from year to year. In the lowest part of the frozen layer, temperature does not decrease below -1°C. Soil thawing starts at 10-15 of May. Rate of the 5°C temperature penetration into the soil is about 1 meter for 1.5 month. Such slow warming is caused by the insulating litter ($A0$) 5-7 cm thick. The temperature regime of the AO differs greatly from that of mineral horizons. Onset of optimal temperatures (15°C and higher) in the litter is observed in the second part of June. In the podzolic horizon, temperature achieves that level at the end of June and remains the same for 10-15 days. Warming up of the B_f and B_1 horizons takes place with a long delay and is very short. The root layer, at 0.2 m, is warmed up to 7-9 degrees on average. In the BC and C horizons (1-1.5 m depth), the temperature reaches 5° in the middle of August. During the first decade of September we notice heat loss. At this depth temperature is rather constant: during 11 months at 2-4°C.

Table 1. Distribution of land fund and agricultural lands of the Komi Republic according to biochemical zones and subzones.

Natural zones, subzones	Mean annual air (°C)	Number of days in year with t >10°C	Air degree days >10°C	Mean annual precipitation (mm)	Land fund (10^3 ha)	Percentage of the Republic area	Arable land (10^3ha)
Tundra	-6.3	48	574	448	1099	2.6	3
Forest Tundra	-4.8	59	752	400	2484	6.0	5
Far North Taiga	-2.3	71	929	480	7228	17.4	8
Northern Taiga	-1.4	85	1199	525	15082	36.3	20
Middle Taiga	+0.3	100	1454	550	10016	24.0	40
Southern Taiga	+1.0	110	1582	615	186	0.5	24

Poor heat resources prevent the roots of arboreal plants from penetrating the soil. The main root mass, up to 90%, is concentrated in the upper layer (5-7 cm), in the AO horizon. They form a dense net. In the northern taiga, the period of active root growth lasts one month. Complete termination of root growth takes place in the beginning of September. Deficiency of heat resources reduces the time of phytomass active accumulation to 30-40 days. This period is not stable; nearly every year we observe low temperature during it. It causes a decrease in annual growth, and in some years a temporary stop of growth processes (Bobkova, K.S. 1987, p. 155). There are no indicators of cryoturbation in gley-podzolic soils. The active soil formation process lasts for 2.5-3 months (in the interval of mean daily temperatures of 5° or more). This condition causes low the biological productivity of gley-podzolic soils. Comparison of the temperature regime of arable gley-podzolic soil with that of a virgin one demonstrates strong arboreal vegetation influence, especially that of moss litter on the thermal properties of soil. Mean annual temperature at 20 cm in forest soil is considerably lower than that in arable land. The sum of active temperatures in this layer in June-August is two times lower in the forest than in arable land: 400°C, compared to 930°C. But a temperature of 9°C on the soil surface occurs later in autumn in the forest than in the arable land

As a rule, forest soil under snow is in the thawed state.

Thicker snow cover and protection from winds limit soil freezing to 40-60 cm, and enhance soil thawing from both its bottom and top. In spring, the whole reserve of winter precipitation enters the forest. K.S. Bobkova's investigations showed adaptation of conifer species to the northern sever conditions. The growth process in spruce root takes place at lower soil temperatures in the northern taiga subzone. With a 3-4°C temperature in the root layer, satisfactory aeration and water provision, physioligical processes are very intensive in roots and on short notice. The temperature regime is considerably better in arable gley-podzolic soil. In the 0-20 cm layer during the vegetative growth period the temperature is 4-5 degrees higher than under the forest. For two months the temperature remains in the range from 10-15 in the root layer of arable soil. The sum of positive temperatures in the layer allow cultivation of forage crops for green mass. Under northern taiga conditions the period of active soil formation is decreasing in general. Lack of heat in the northern areas leads to some weakening of the podzol forming process.

CONCLUSIONS

According to the temperature regime, gley-podzolic soils of the Komi Republic belong to the moderately cold type and take the northernmost position within this type. Their root layer is 20 cm thick and it does not warm up to the biologically active temperatures.

REFERENCES

Bobkova, K.S. 1987. Biological productivity of conifer forestsin the European North east.- Nauka, Leningrad.

Ecosystems

The Ecology of Long-Term Seasonally Frozen Soils of the Taiga in Siberia

V.N. GORBACHEV[1] AND R.M. BABINTSEVA[2]

ABSTRACT

Specific solodic long-term seasonally frozen soils of the taiga are a complex natural formation which has in its profile both modern and relict attributes. The soils develop on red color aeolian residue of which the sodium cation is a major constituent. They are distinguished by a sharp profile differentiation according to eluvium-illuvial type, weak acid reaction of the upper profile and alkaline reaction of the lower profile, sodium ion is periodically present in the absorbing complex, the illuvial horizon is characterized by a prismatic structure, carbonates lie shallow (60-70 cm. Formation of these soils is connected with the peculiarities of the past and present bioclimatic situation in which forest processes play the leading part. Soil development is a polygenetic process.

Key words: Ecology, seasonally frozen soils, frost processes, solodization, polygenetics.

INTRODUCTION

The territory of Siberia is very heterogeneous according to geological, geomorphological and bioclimatic conditions. However it is characteristic for most of the taiga zone soils to have long-term seasonal frost in the profile. Influence of the frost on soil formation is dissimilar under different ecological conditions.

For most of the territory adjacent to the Yenisey River (Siberia) soil, formation during the Pleistocene and the whole of the Holocene occurred under taiga conditions on mother rocks (parent material) devoid of carbonate. During this period, the climate became less continental, there was an increase of precipitation, and frost disappeared at some periods of the Pleistocene. These conditions favored the succession from pine and larch to dark-coniferous species such as spruce, fir, and Siberian pine (Krasheninnikov 1951).

Grichuk (1955) singles out eight stages of the vegetation cover development in connection with the climate change. Periodic changes of bioclimatic conditions influenced direction of soil formation within certain geomorphological regions. The change of soil formation direction was facilitated, at some parts and at certain periods, by the development of denudation processes. In particular, in the Yenisey River territory, podzolic soils can often be found in which there is a discrepancy between the depths of podzolic and illuvial horizons. The latter can reach up to 3-4 m. It is connected with the damage of the upper part of podzolic soils by denudation processes, and the illuvial horizons being very deep proves that the podzol formation process was long.

Recurrence of soil formation at former periods can be judged by the relict attributes which are present in the modern southern taiga soils - residual humus horizons, frost cryoturbations, etc.

Most taiga soils have a deep podzolic horizon due to their development under the conditions of a long-term influence from acid products of organic residue decomposition and leaching water. The modern bioclimatic situation of the Yenisey River territory in Siberia (relatively favorable correlation of warmth and moisture and dominance of dark coniferous taiga) enhances the intensive development of podzolic processes and, conse-

[1] Krasnoyarsk State Agricultural University, P.O. Box 8750, Akademgorodok, Krasnoyarsk, 660036, Russia

[2] Institute of Forest, Siberian Branch of Russian Academy of Sciences, P.O. Box 8750, Akademgorodok, Krasnoyarsk, 660036, Russia

quently, podzolic soils are becoming widespread (Gorbachev 1967, Gorbachev and Popova 1992).

In most of the taiga in the Yenisey River territory of Siberia, soil formation occurred mainly on rocks devoid of carbonate. But in the Angara River territory, this process occurred under conditions of high calcareousness of mother rocks that contain significant concentrations of sodium. The presence of sodium and gypsum intercalations in the deposits of the red color formation point to the former salinity of mother rocks (Gorbachev 1980). Considering that the modern morphostructure of the Siberian Plateau was formed in the Pleistocene (Adamenko 1971), the soil formation process can be assumed to be very long historically, tens and hundreds of thousands of years. Being close to the glacial zones, the soils were under their cold influence for the whole of the Pleistocene. Frost appeared in the palaeosoils during the period of Samarovsk Glaciation (170.000-250.000 BC). Frost retreated at the interglacial periods when the climate became warmer, which is indicated by frost cryoturbations in the red color deposits.

Using the existing literature data of spore-pollen and carpological analyses, it can be inferred that soil formation was polygenetic before the Holocene. Existence of various landscapes (from polar tundras and tundra steppes to forb and meadow steppes) during the period from Samarovsk Glaciation to the beginning of the Holocene is indicative of a wide range of soil formation types: tundra, taiga, forest-steppe and steppe.

Early in the Holocene there was a predominance of taiga, forest steppe and steppe landscapes in the territory of the modern southern taiga near the Angara River. Large territories were occupied with open areas where xerophyte steppe vegetation species were present, which are characteristic of solonetzic soils (Reverdatto 1960). Changeability of the bioclimatic situation influenced the formation of the whole range of the southern taiga soils - taiga solodic red-brown, grey solodic, turf-carbonate, pseudo-podzolic and others. However most of the modern soils found in the Angara River territory bear traces of the former xerothermic stage - high carbonate content, alkalinity, residual humus horizons, and frost cracks filled with foreign matter (Gorbachev and others 1982)

TAIGA SOLODIC RED-BROWN SOILS

We will now look at the ecological peculiarities of long-term seasonally frozen soils using the ex-

ample of taiga solodic red-brown soils. These soils develop under plains and steep slopes of different exposures mainly under pine forests on deposits of the residual red-color and red-color-variegated crust of weathering. They are characterized by the red color of the profile (the deeper the soil layer, the more intense the color is); the presence of forest litter and humus horizon enriched to a large extent with charcoal; by a distinct eluvium-illuvial soil profile in which the A2 horizon stands out; the A2 horizon is brown with a red shade and SiO_2 spots and has platy-cloddy or platy-nuciform structure and clear distinction of peds sides (the lower side is brown containing fine gravel and charcoal, the upper is of mat color; by the illuvial horizon B being isolated, having a coarse nuciform or prismatic structure, with clay, brown-red or red color, and peds covered with a thick clay cutan; by the postcryogene slaty structure of the lower profile; the presence of small intercalations of sandstones, argillites and siltstones at different depths; by the presence of calcium carbonates at depths of 60-70 cm.

The taiga solodic red-brown soils are distinguished by a small content of fulvate type humus and exchangeable bases and hydrogen, by the presence of exchangeable sodium at some periods, by a weak acid reaction of the upper profile and alkaline reaction of the lower profile (Table 1).

The chemical composition reflects a clear differentiation of the soil profile according to eluvium-illuvial type. Relatively high magnesium content in the illuvial horizons indicates that magnesium together with Fe, Al, and SiO_2 forms rather stable secondary materials. Predominance of total and exchangeable magnesium over calcium in the eluvium and illuvial horizons indicates that destruction of the soil minerals has not yet reached the limit characteristic of podzolic processes, as magnesium is a constituent of the most highly dispersive secondary minerals. This explains the formation of the coarse-nuciform and prismatic structure of the illuvial horizon and the high density characteristic of solonetzic soils.

The taiga solodic red-brown soils are characterized by a small number of microorganisms with a sharp predominance of bacterial groups (Gorbachev and others 1982). The unfavorable temperature regime of the soils limits the development of sporulating bacteria forms and actinomycetes. Therefore the process of organic matter decomposition is incomplete and takes place only in the upper part of the soil profile.

The mesofauna of the soils is represented by invertebrates with a predominance of insects. In

470

Table 1. Chemical properties of taiga solodic red-brown long-term seasonally frozen soil.

Depth (cm)	Humus (%)	Water pH	Exchange cations, equivalent to milliequivalents (meq) per 100 g of soil		
			Ca^{2+}	Mg^{2+}	Na^+
0-5	—	5.10	15.0	7.1	0.0
5-12	1.54	5.25	7.6	7.6	1.67
13-20	0.66	5.00	5.7	6.2	2.14
40-50	0.52	6.63	13.8	9.3	0.6
70-80	0.40	8.17	12.4	8.2	0.0
110-120	0.21	8.45	10.1	5.6	0.5
140-150	0.12	8.56	8.8	7.5	1.8

case of large invertebrates, predators prevail over saprophages. The number of earthworms is not high. As a whole, the quantitative and qualitative composition of mesofauna and microflora can be explained by the severe cold conditions of the soils.

The listed attributes and properties of the soils point to the development of a variety of soil processes in the past and present. First of all, it should be noted that profile differentiation according to eluvium-illuvial type occurred, mainly, in the former moister soil formation stages, probably in the optimal stage of Holocene. At present, the taiga solodic red-brown soils are in a relative balance with the environment bioclimatic situation (little precipitation, deep freezing of soils and their late thawing , predominance of evaporation in the spring and summer). Frost cracks filled with foreign matter and high calcareousness of the lower profile are relict attributes. However it would be more properly to consider the carbonate horizon as a relict-modern formation. Many of the soil properties are variable and very dynamic in time, such as humidity, temperature, pH, oxidative-reductive potential, moving oxides, and biological activity. Variability of the soil properties is connected with a different degree of development in time of the soil processes - humus accumulation,

alkaline and acid hydrolysis, lessivage, gleyification, and frost processes. The latter play the leading part in soil formation. Deep freezing and late thawing result in the soils being moist for a long time. In this case overfrost vadose is formed which is preserved in the soil profile till the beginning of August in some years. The result is the development of the eluvium-gley process. At dry periods of time mineralized solutions from the lower layers are periodically drawn to the soil surface due to predominance of evaporation over precipitation. It leads to alkalinization of the soil profile. Production of sodium in soil solutions is connected with its release as a result of breakdown of low red-color deposits. The study of the dynamics of the soil solution composition reveals that sodium content varies greatly during the vegetation period (Table 2).

In doing so, the highest sodium content is found in the soil solution of the mother rock, and at the end of July and August in the upper horizons as well. Thus, the described soils are distinguished by a whole range of specific properties. Along with the named peculiarities , attention should be paid to the presence of moving SiO_2 in the soils. It points to the fact that solodization occurs in them (Gedroits 1926).

Table 2. Sodium content in the soil solution of taiga solodic red-brown long-term seasonally frozen soil.

Depth (cm)	Beginning of July	End of July	Middle of August
	(% from the sum of exchangeable cations)		
5-12	6	43	50
13-20	10	4	78
40-50	1	34	20
70-80	28	9	10
140-150	44	34	72

CONCLUSIONS

To complete the characterization of the taiga solodic red-brown long-term seasonally frozen soils, the following should be noted. The described soils are distinguished by a relative old age. Their profile differentiated according to the eluvium-illuvial type , mainly, at the former soil formation stages during the optimal moist stage of the Holocene. The modern bioclimatic situation is favorable for the development of variable water regimes in the soils, which leads to periodic alkalinization of the profile during dry periods followed by solodization during moist periods. The fact that lessivage and gleyification develop at different times is connected to a large extent with this cycling of water processes. Soil formation is a polygenetic process. Forest logging (Babintseva et al. 1984) and forest fires (Gorbachev and Popova 1992, 1996) also cause great changes in the ecology of long-term seasonally frozen soils of Siberia

REFERENCES

Adamenko, O.M. 1971. The main stage of neotectonic motions and of intensive development of hydronet. Eopleistocene. p. 186-202 . *In* Plateaus and Lowlands of Eastern Siberia. Nauka Publishing House, Moscow.

Babintseva ,R.M., V.N.Gorbachev, N.D.Sorokin. 1984. Ecological aspects of reforestation under modern forest logging. Forestry Journal, no. 5, p. 19-25. Nauka, Moscow.

Gedroits, K.K. 1926. Solodization of soils . Leningrad.

Gorbachev, V.N. 1967. The soils of the territory down the Angara river and of the Yenisey river mountain-ridge., Nauka Publishing House, Moscow.

Gorbachev, V.N. 1980. Loose cover deposits in the middle of the territory adjacent to the Angara river, their composition, genesis and soil formation. p. 21-39. *In* Genesis and geography of forest soils. Nauka Publishing House, Moscow.

Gorbachev V.N. 1982. Geography of forest soils in the Angara river territory. p. 88-110, Nauka Publishing House, Moscow.

Gorbachev, V.N., V.K. Dmitrienko, E.P. Popova, N.D. Sorokin. 1982. Soil ecological study in forest bio-geocenoses. Nauka, Novosibirsk.

Gorbachev, V.N., and E.P. Popova 1992. Soil cover of the southern taiga in Central Siberia., Nauka Publishing House, Novosibirsk.

Gorbachev, V.N., and E.P.Popova . 1996. Fires and Soil Formation. p. 331-336. *In* Fire in Ecosystems of Boreal Eurasia. Kluwez Academic Publishers, Dozdzecht/ Boston/ London.

Grichuk, M.P. 1955. To the history of vegetation in the Angara river watershed. p. 335-338. *In* USSR Academy of Sciences Reports . Vol. 102. no. 2.

Krasheninnikov, I.M. 1951. The main ways of development of the Southern Ural vegetation in connection with palaeogeography of Northern Eurasia in Pleistocene and Holocene. p. 170-217. *In* I.M.Krasheninnikov Geographic research. Geography Literature Publishing House, Moscow.

Reverdatto, V.V. 1960. Glacial and steppe relics in the flora of Central Siberia in connection with the history of flora. p. 111-131. *In* Scientific readings in memory of M.G.Popov. Novosibirsk.

Impacts of Tracked Vehicles on Properties of Tundra Soils

N.P. BUCHKINA[1]

ABSTRACT

The use of tracked vehicles in connection with development of new gas- and oilfields resulted in greater loads on the tundra soil of the Yamal Peninsula in Russia. Studies of the morphological, physical, and chemical properties of the native and vehicle-disturbed soils were carried out to evaluate the susceptibility of tundra soil to different mechanical impacts. Disturbance of native microrelief and formation of ruts resulted in greater water flow into the disturbed plots. The vehicle-induced mixing of the upper, organogenic, and lower, mineral, horizons caused the formation of new organomineral horizons which are not characteristic to the native tundra soils. These changes in conditions of soil formation affected the above-mentioned soil properties. Differences in properties of the native and disturbed soils were influenced by initial bulk density, number of passages, degree of gleying, depth of organogenic horizons, type of soil, and its location on a relief.

Key words: Tundra soils, tracked vehicles, physical and chemical properties.

INTRODUCTION

In the present time, tracked vehicles are widely used in the tundra zone of Russia for transportation. Their use has increased in connection with the development of new gas- and oilfields in the tundra zone of the Yamal Peninsula. There is a number of papers in which the effects of tracked vehicles on properties of tundra soils are being evaluated.

In these studies the changes in soil properties were determined immediately after the passes of tracked vehicles (Vasilyevskaya et al., 1986). However, the problems of tundra soils' stability under the mechanical impacts of vehicles, as well as problems of self-recovery of disturbed tundra soils, were not solved. Few data are reported on the long-term recovery of tundra soil properties affected by the mechanical impacts of the tracked vehicles. Such data will allow to evaluate the importance of the temporal changes in key soil properties and regimes during the soil recovery processes.

The objective of the present studies was to study what happened in tne morphological, physical and chemical properties of tundra soils after 5 years of recovery period.

MATERIALS AND METHODS

The territory of our research was a central part of the Yamal Peninsula in the subzone of northern hypoarctic tundra. The peaty-gley cryozems on slopes (profiles DL-2-93 and SD-2-93) and flat sites (profiles DL-1-93 and SD-1-93), and the alluvial peaty-gley soils on a floodplain near a lake (profile DL-3-93) were studied before and 5 years after 4 and 100 passes of tracked vehicles.

The soil samples were taken from the surface (0-10 cm) and underlying (10-20) horizons before (profiles DL-1-93, DL-2-93, DL-3-93, SD-1-93, SD-2-93) and five years after 4 passes (profiles DL-1n-93, DL-2n-93, DL-3n-93) and 100 passes (profiles SD-1n-93, SD-2n-93) of tracked vehicles. Design characteristics of the tracked vehicle used are: total weight - 8200 kg; width of rut - 2600 mm; width of

[1] Agrophysical Research Institute, 14, Grazhdansky Prospect, St. Petersburg, 195220 Russia

track - 580 mm; average ground contact pressure - 24.0 kPa; mean speed off road (random travel) - 10-14 km per hour. At the moment, random travel of tracked vehicles over the tundra is allowed only during the winter period. In summer, only roads should be used for any transportation. The vehicle-disturbed areas must not exceed a width of 10 m. Four passes of the vehicle applied within a short time frame. One hundred passes of the vehicle were applied within a one month.

All soil samples were taken in August, 1994. Only one profile was dug on each of above-mentioned plots. The microstructural properties of soils were determined with thin sections in two replications. The total carbon content and losses on ignition (*) were determined by conventional wet and dry combustion methods (Kaurichev, 1986). The measurements of water vapor adsorption isotherms for the soil samples studied were carried out using a vacuum chamber method at 25°C. Based on the

adsorption isotherms obtained, specific surface areas were calculated using the BET model (Zuyev, 1987). The water retention curves of soil samples passed through a 2-mm sieve were measured by a pressure-plate apparatus in the range of water potentials of -5 to -100 kPa at 25°C. Hydrolitic acidity of soil samples was determined by Kappen's procedure with extraction of H^+ and Al^{3+} by 1 N CH_3COONa solution. Available potassium (K) and phosphorus (P) contents were measured by Kirsanov's procedures, using 0.02 N HCl for extraction. Total nitrogen content (N) of soil was determined by Anstet's method. Base saturation (V) and exchangeable calcium (Ca) and magnesium (Mg) contents were measured by conventional procedures. All the above-mentioned properties of soils were determined in three replications for each soil sample. Average values of measured parameters were used to interpret the results.

Table 1. Values of pH, total carbon content (C), total nitrogen content (N), C/N ratio, hydrolitic acidity (HA), content of exchangeable Ca and Mg, degree of saturation by bases (V), content of available P and K in tundra soils before and 5 years after impacts of tracked vehicles

Site Profile no	Depth	pH (KCl)	C	N	C/N	HA	Exchangeable Ca	Mg	V	Available P	K
	cm		g kg⁻¹			mq 100 g⁻¹	g kg⁻¹		%	mg kg⁻¹	
Flat;											
DL-1-93	0-5	4.6	473.0*	10.9	20	29.9	4.5	1.2	52	140	323
DL-1-93	9-19	4.5	9.0	0.9	13	2.3	0.5	0.3	68	19	59
DL-1n-93	0-8	4,1	16.0	1.3	21	3.2	0.4	0.2	50	5	54
DL-1n-93	9-19	4.6	15.0	2.3	16	25	0.8	0.2	70	12	71
Slope											
DL-2-93	0-6	4.5	400.0*	9.1	16	262	4.3	1.1	53	80	426
DL-2-93	6-14	4.5	7.0	0.5	6	17	0.7	0.3	76	34	42
DL-2n-93	0-6	4.4	37.0	3.5	12	79	1.2	0.3	51	13	136
DL-2n-93	7-15	4.1	9.0	0.6	9	32	0.7	0.2	63	16	76
Floodplain											
DL-3-93	0-10	4.1	4.0	0.6	8	19	0.3	0.1	54	16	39
DL-3-93	15-25	3.4	6.0	0.3	4	50	0.3	0.1	33	12	27
DL-3n-93	0-10	3.8	11.0	0.6	9	40	0.2	0.1	24	10	25
DL-3n-93	15-25	3.5	4.0	0.4	5	28	0.2	0.1	38	12	33
Flat											
SD-1-93	0-6	4.2	87.0*	5.4	17	229	2.5	0.7	44	125	289
SD-1-93	10-20	4.6	6.0	0.4	5	15	0.7	0.2	78	15	1
SD-1n-93	0-10	3.8	20.0	0.8	10	70	0.4	0.2	32	29	55
SD-1n-93	10-20	4.0	8.0	0.5	6	28	0.6	0.2	62	31	75
Slope											
SD-2-93	0-10	4.6	62.0*	3.4	21	122	2.7	0.7	64	58	443
SD-2-93	10-20	4.7	12.0	0.8	10	17	0.9	0.2	79	45	146
SD-2n-93	0-10	4.5	2.3	2.1	14	43	1.0	0.3	62	7	110
SD-2n-93	10-20	4.3	2.0	3.6	15	36	0.8	0.2	63	29	125

RESULTS AND DISCUSSION

The vehicle-induced mixing of the upper (organogenic) and lower (mineral) horizons formed new organomineral horizons in soils on the disturbed plots. Chemical and physical properties of these organomineral horizons differs considerably from those of undisturbed organogenic horizons (Tables 1, 2).

Table 2. Physical properties of undisturbed soils and disturbed soils after 5 years of recovery period.

Site; Profile no.	Horizon	Passages no.	Depth	S	Water content at water potentials (kPa)	
					-5 to -30	-30 to -100
			cm	$m^2 g^{-1}$	%	
Flat;	V, AT					
DL-1-93	Bh, Bg	0	0-5	181	23.5	12.5
DL-1-93	AT, Ba	0	9-19	38	8.3	12.8
DL-1n-93	G	4	0-8	39	13.3	12.7
DL-1n-93		4	9-19	64	11.5	14.8
Slope;						
DL-2-93	OV, AT	0	0-6	272	18.2	18.6
DL-2-93	Bg	0	6-14	30	14.2	19.2
DL-2n-93	AT	4	0-6	68	23.2	12.1
DL-2n-93	G	4	7-15	36	15.8	7.5
Floodplain;						
DL-3-93	V, T, AB	0	0-10	22	24.6	10.5
DL-3-93	G	0	15-25	14	20.0	14.3
DL-3n-93	TA, Bfe	4	0-10	37	21.1	6.2
DL-3n-93	G	4	15-25	8	19.3	10.8
Flat;						
SD-1-93	OV, AT	0	0-6	111	22.4	10.5
SD-1-93	G	0	10-20	31	5.0	19.5
SD-1n-93	AT	100	0-10	58	6.6	23.2
SD-1n-93	G	100	10-20	36	1.6	25.1
Slope;						
SD-2-93	O, AT	0	0-10	76	18.3	13.4
SD-2-93	Bg	0	10-20	44	1.8	21.1
SD-2n-93	TA, Bg	100	0-10	51	9.4	27.2
SD-2n-93	G	100	10-20	73	16.4	21.6

S - specific surface area of soil

Changes in composition of soil solid phase in the new horizons and acceleration of plant residue decomposition decreased total carbon and nitrogen, exchangeable bases and easily available phosphorus and potassium in the surface horizons of the disturbed soils. The organomineral horizons also have lower pH, hydrolytic acidity, specific surface area and water-holding capacity. Mineral horizons of the disturbed soils at the depth of 20 cm also indicated differences in chemical and physical properties. Contents of total carbon and nitrogen, easily available P and acidity increased after the vehicle disturbance of mineral horizons. Specific surface area and water retention also were higher in the disturbed mineral horizons than in the undisturbed horizons. Content of total carbon showed a weak positive correlation with acidity (R^2 = 0,21-0,27) and a strong positive correlation with a content of total nitrogen (R^2 = 0,97-0,99) in the mineral horizons of disturbed soils. The C/N ratio also was greater in the mineral horizons of disturbed soils. The increase in total carbon in the mineral horizons of disturbed soils probably is related to their mechanical mixing or input of weakly decomposed plant residues from the upper organomineral horizons. The quicker decomposition of plant residues in the disturbed tundra soils contributed to formation of nitrogen-containing organic substances (Buchkina and Zvereva,1996). A strong positive correlation of organic matter content with water retention of the disturbed soils (R^2 = 0,83-

475

0,98), compared to a poor correlation between these parameters of the undisturbed soils ($R^2 = 0,02-0,46$) indicated a hydrophilic nature of the organic compounds formed (Buchkina et al., 1996). These organic compounds in soil solution moved downward the soil profile. Then the organic compounds participated in leaching and redistribution of nutrients. An increase in the content of easily available K in the mineral horizons of disturbed soils may be caused by (1) partial transformation of weakly soluble compounds into easily soluble ones by an increase in soil acidity, or (2) the decrease in grain sizes of K-containing minerals, caused by low temperatures, as was observed in our micromorphological investigations (Buchkina 1996). The above-mentioned changes in chemical and physical properties were clearly observed in the peaty-gley cryozems on the flat sites.The soils from such plots are characterized by shallow organogenic horizons. Tracks of vehicles mixed up these horizons with underlying mineral material, forming organomineral horizons. Thicker organogenic horizons prevented mixing of the organogenic and mineral horizons by a few vehicle passes. However, a high number of passages of tracked vehicles caused complete disturbance of organogenic horizons. Of the soils studied, the peaty-gley soils on a floodplain near a lake demonstrated the least change in their morphological properties. A gley process was very clearly observed in these soils and hence, the input of additional water into vehicle ruts had little effect on the processes in these soils. Besides, the soils of floodplains were almost structureless and had high initial bulk density.

CONCLUSIONS

Impacts of tracked vehicles on tundra soils resulted in formation of new organomineral horizons

which were not evident in the undisturbed soils. The degree of changes in properties of tundra soils was defined by the number of vehicle passages, initial depth of organic horizons, degree of gleying and initial bulk density.

REFERENCES

Buchkina, N.P., and T.S. Zvereva. 1996. Transport-induced changes in tundra soils micromorphology. p. 94. *In* Soil Micromorphology. Proc. 10th Int. Working Meeting on Soil Micromorphology, Moscow, July 8-12 1996. Moscow State University Publ., Moscow, Russia.

Buchkina, N.P., V.S. Zuyev, and E.V. Balashov. 1996. Degradation of tundra soils as influenced by tracked vehicles. p. 50-51. *In* Towards Sustainable Landuse. Proc. 9th Conference of the ISCO, Bonn, August 25-30 1996. German Federal Ministry for the Environment, Nature Conservation and Nuclear Safety Publ., Bonn, Germany.

Buchkina, N.P. 1996. Soils of typic tundra of the Yamal Peninsula and their stability to the mechanical impacts. (in Russian.) Essay of Ph.D. diss. Agrophysical Research Institute. St. Petersburg, Russia.

Kaurichev, I.S. (ed.). 1986. Soil science practice. (in Russian.) Kolos Publ., Moscow, Russia.

Vasilyevskaya, V.D., V.V. Ivanov, and L.G. Bogatyrev. 1986. Soils of Western Siberia North. (in Russian.) Moscow State University Publ., Moscow.

Zuyev, V.S. 1987. Technique of measurement and calculation of parameters of the BET equation according to water vapor adsorption. (in Russian.) Bulletin on Agronomical Physics 64:54-58.

Nature Restoration Strategy in the Far North

I.B. ARCHEGOVA[1]

ABSTRACT

Rich reserves of mineral resources in the Far North induce explorers to develop rational approaches to resource extraction that take into account the specific natural conditions and ecosystem structure. The proposed approach consolidates both resource extraction and restoration of destroyed ecosystems into a single system. An original outline has been developed stipulating a two-stage process of nature restoration. All measures proposed are aimed at the conservation of natural balance in a northern region subjected to industrial activity.

Key words: Nature use, nature restoration, biological restoration, the North.

INTRODUCTION

The main reserves of energy and other mineral resources of European Russia are located in the north of the Komi Republic. An intensive prospecting and extraction of these resources along with oil and gas pipeline construction took place during the past decades. The natural environment was subjected to technogenic (anthropogenic) disturbance, which created ecological problems. It should be emphasized that official information still does not allow us to assess the real scale of the technogenic disturbance. In particular, no disturbed land inventory, ecological monitoring, or mapping is carried out. Although variable in climate, northern Russia reveals considerable commonality in ecosystem structure conditioned by climate severity and permafrost at shallow depths. First of all, there is a thin and autonomous living tier including a plant community, a substratum biocomplex, and the soil layer of biogenic accumula-

tion (fertile layer). The latter holds the root system of the plant community and a substratum biocomplex transforming plant residues (biological cycle of organic matter). The fertile layer is mainly organic, which emphasizes its linkage with living ecosystem components. The thin living tier isolates from heat the mineral strata located within the zone of present freezing and thawing. Indirectly, the living tier affects the mineral strata's relationship with the permafrost. Such a tight spatial interrelation of the main components of living systems, along with the autonomy of these systems that are self-sustaining in the severe conditions, results in the well-known vulnerability of the ecosystems. An ecosystem is rapidly destroyed under heavy technogenic influence. Destruction of the biogenic cumulative layer causes more contrasting temperature fluctuations within the zone of seasonal freezing and disrupts the balance with permafrost. This results in a rapid erosion progress, whose velocity exceeds that of the self-restoration process. Thus, the effect of a technogenic factor is aggravated. Given this background, it is necessary to intensify the restoration process. The objective of this paper is to present a model for nature restoration in the Far North.

THE NATURE RESTORATION MODEL

A long-term study in the European Northeast of Russia allowed us to develop the concept of an active approach to disturbed land restoration, to develop an optimal technology, and to make the meaning of some terms more precise. The poor development of agriculture in the territory (separate centers only), the distinctive quality of traditional methods of management based on biological resources, and the indigenous population's way of

[1]Institute of Biology, Komi Science Center, Ural Branch, Russian Academy of Sciences; 28 Kommunisticheskaya str., Syktyvkar 167610 Russia

life and its dependence on the natural environment were taken into account. The land restoration measures traditionally used in the middle latitudes, as well as the whole restoration concept providing for recurrent land use mainly in agriculture, cannot be automatically applied to the Far North. Reestablishment of natural ecosystems, conservation of biological diversity, and biosphere balance in a region become the main purposes of nature restoration in the North. As a result, a traditional Russian term "recultivatsia" (recultivation) does not reflect this concept. This broadened concept of land restoration is better reflected by the term "prirodovosstanovlenie" (nature restoration) that we proposed elsewhere by analogy with the "prirodopolzovanie" (nature use, nature management). It is, however, expedient to keep the term "recultivatsia" to designate restoration of agricultural lands for recurrent use.

Nature restoration in the proposed meaning refers not only to applied concerns, but also to a basic ecological problem dealing with restoration of zonal ecosystems. Introduction of the term "nature restoration" into practice indicates an ideological change in the interaction between nature and society. Consumer ideology is replaced by a creative idealogy. A system of nature restoration can only be developed on the basis of a general conception of nature use covering all forms of natural resource exploitation (Kurazhlovsky 1969, Reimers 1990). In spite of a broad interpretation of the term "nature use," it was easily introduced into practice. Rational nature use provides for both economic exploitation of natural resources and their efficient restoration with due regard for the interests of a constantly developing economy (Reimers 1990, p. 405). Nature use, as we

see it, is not only resource use, but the whole system of interaction between human society and the natural environment in the process of labor activities. Both society and environment alter in the course of this interaction.

The general outline of rational nature use is presented in Figure 1. Social and economic problems are beyond the scope of this paper. Transformation of natural ecosystems can be purposeful. It is such in the case of an agricultural activity, which results in "replaced" ecosystem formation artificially supported by a special system of measures. But mineral resource exploitation, as well as other kinds of multi-aspect technogenic activity, results in an unregulated effect upon natural ecosystems up to their complete destruction. The post-technogenic sites increase in area, which leads to disruption of ecological balance in the region. Consequences are especially grave in the regions with stressful life-support conditions. The absence of developed agriculture in a northern region supports a temporary illusion of "impunity" from environmental damage. The illusion persists until a certain critical environmental condition is reached that forces scientists and bodies of power to nature restoration activity. At that time, a post-technogenic wasteland becomes a subject of nature restoration activity directed to zonal ecosystem construction over again, i.e., creation of a "secondary zonal" ecosystem. Restoration of initial biological diversity and, finally, conservation of biosphere balance in the region are achieved at that time. Activities directed to nature protection are also included in our outline of rational nature use. Protected ecosystems not only serve as a standard of zonal ecosystems, but also as a source of material for successful nature res-
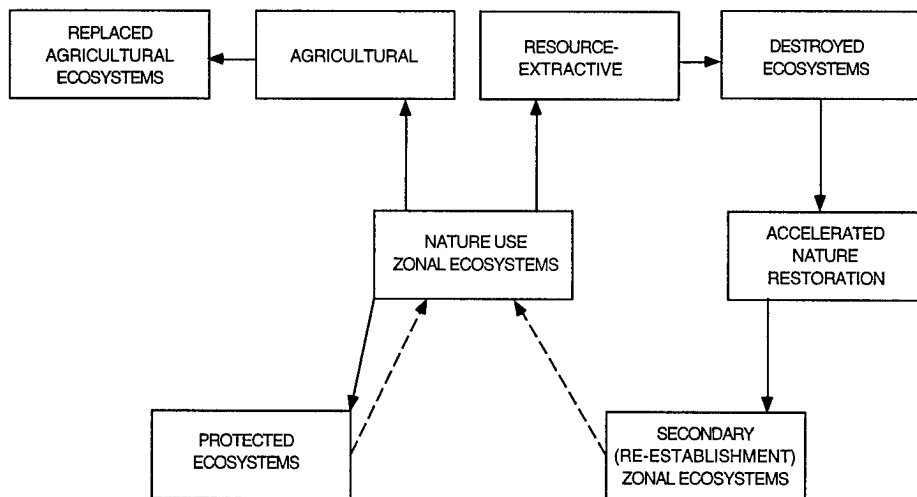

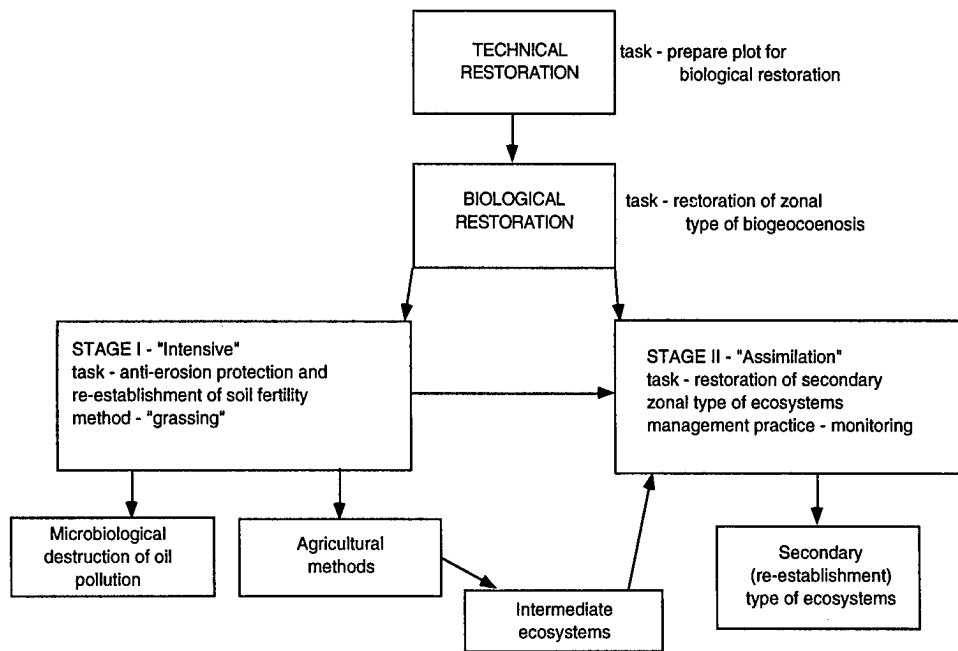*Figure 1. The scheme of rational system of nature use.*

Figure 2. The scheme of accelerated nature restoration.

toration. This way, rational nature use implies an indissoluble process of nature use–nature restoration and nature protection. Practical implementation of the proposed approach should rest on ecological norms and economic calculations that need to be worked out.

The outline of nature restoration is shown in Figure 2. Biological restoration is subdivided into two stages. It is conditioned by the slowness of the self-restoration of a zonal plant community in automorphic landscape positions in the North. The "intensive" stage accelerates restoration of the fertile layer of biological accumulation with a mixture of agrotechnical practices. Success is indicated by the formation of a productive plant community. Native species of perennial herbs that possess a high sod-forming capacity adapted to the severe climate are best for this purpose. Herb seeding in conjunction with organo-inorganic fertilizer application ensures formation of an "intermediate" ecosystem in 3 to 5 years. The ecosystem includes a productive herb community preventing erosion and a corresponding soddy soil. At the second stage, this "intermediate" ecosystem is transformed into a secondary zonal ecosystem. The process duration is 10 to 15 years (Archegova 1992, Archegova et al. 1995). The introduction of the first stage accelerates initiation of a self-restoration succession. At the "intensive" stage of nature restoration, practices providing for pollutant (e.g., oil) elimination can be applied, or the production and application of nontraditional fertilizers

that optimize the technology of restoration can be undertaken. This way, the nature restoration process is a regulated one, at least, at its first stage.

We tested and proposed for use a number of perennial species adapted to the northern conditions. A new fertilizing-seeding material was proposed that allows seeding and application of an organo-inorganic fertilizer in one operation. The technology of manufacture of a biologically activated fertilizing-seeding material in a granulated state (BAG) has been developed (Skupchenko 1993). First, a compost is prepared using waste products like lignin, sawdust, or poultry manure reworked by a biotechnological method. Then inorganic fertilizers, microbiological compounds, and herb seeds are added. Following mixing, the material is granulated. The application of the BAG decreases the amount of organic fertilizer and combines two agricultural operations–sowing and fertilization. This is important for improving the recultivation process.

CONCLUSION

In this paper, I presented a concept for disturbed ecosystem restoration in the Far North. The essence of this concept is the unity of two processes–nature use and nature restoration. The latter means secondary zonal ecosystem restoration. The original scheme of nature restoration in the Far North has been developed and recommended as a two-stage process.

REFERENCES

Archegova, I.B. (ed.). 1992. Biologicheskaia rekulti-
vatsia na Severe (Biological recultivation in
the North). Syktyvkar Publ. (In Russian).

Archegova I.B., S.V.Degteva, T.V.Evdokimova,
E.G.Kuznetsova. 1995. Kontseptsia prirodovo-
sstanovlenia narushennyh ekosystem Severa
(The restoration conception for disturbed eco-
systems in the North). *In* Proc. Republ. Conf.,
Economic Strategy of the Komi Republic en-
tering to the XXI century,. Syktyvkar. p. 140–
143. (In Russian).

Kurazhkovsky Yu.N. 1969. Ocherki pripodopolzo-
vaniya (Essays on nature use). Misl Publ. Mos-
cow. (In Russian).

Reimers N.F. 1990. Prirodopoltsovanie (Nature use).
Mysl Publ. Moscow.

Skupchenko K.V. 1993. Ispolzovanie othodov proiz-
vodstva dlya izgotovleniya biologicheski
aktivnyh organicheskih kompakt-udobrenii
(Use of industrial wastes for manufacture of
biologically active organic compact fertiliz-
ers): The Yamal-Tsentr gas pipeline. Sykty-
vkar Publ. (In Russian).

Biology

Bacterial Biomass and Properties of
Arctic Desert Soils
(Archipelago Severnaya Zemlya, Northern Siberia)

M. BÖLTER[1] AND E.-M. PFEIFFER[2]

ABSTRACT

During August 1995 sites at Severnaya Zemlya (northern Siberia) were examined for soil microbiological investigations in relation to environmental properties. The environment at Severnaya Zemlya is a polar desert with patchy distributions of higher plants, mosses and lichens. The most denuded area was at Komsomolsk Island, north of the Akademik Nauk Glacier. Soils were decribed as pergelic cryaquepts, pergelic cryortents, and lithic cryortents with weak A- and O- horizonts. Relationships between plants and microbes show the establishment of microbial biocoenoses, mainly in the root systems of different vascular plants. Such microenvironments may provide model systems for studies of degradation and accumulation processes in polar deserts. The results of this study will be discussed in relation to soil properties and soil organic matter contents, with emphasis on size classes of bacterial communities.

Key words: Arctic desert soils, soil microbiology, bacteria, permafrost, Severnaya Zemlya

INTRODUCTION

Although the northernmost areas are generally regarded as hostile and extreme, they sustain sparse but distinct plant and animal communities as well as related microbial populations which support short food chains in soils. Life in this region is limited by short growing seasons, water defiency, and shortage of nutrients. Most of these systems can be described as autochthonous, and they are restricted to small delimitated areas, so-called oases (Bornkamm 1987, Freedman et al. 1994). Close interactions between individual organisms, substrates and environmental constraints are needed to survive.

The archipelago of Severnaya Zemlya belongs to the northernmost regions of the Eurasian continent; it is located in the region of the Soviet polar deserts. It has a continental climate, with unique florogenetic elements (Alexandrova 1988). There are several botanical studies of these areas available (summarized by Alexandrova 1988), but no detailed studies of soil microbiology.

The aim of this study is to survey of microbial communities in relation to different soils and plants with respect to organic matter contents, soil structure and microenvironments. This study is part of joint program dealing with the environmental development of central Siberia in the Holocen. (cf. Siegert and Bolshiyanov 1995, Bolshiyanov and Hubberten 1996).

MATERIAL AND METHODS

Sampling was carried out during an expedition to Severnaya Zemlya (78-81°N, 92-104°E) between August 8 and 12, 1995 (cf. Figure 1).

Site description

The landscape is strongly influenced by erosion processes. The northern island (Komsomolsk Island) is situated in the northern belt of the arctic polar deserts. The temperature of the warmest month does not exceed 1°C. Nearly 70% of the surface is covered by ice, mainly by the Akademic Nauk Glacier. Areas free of ice are on plains at altitudes of 100-200 m, they are formed by bedrocks and marine quaternary sediments (Alexandrova 1988). Vegetation is extremely impoverished and showed only few higher plants (4 species) besides some mosses and lichens at places visited (Kanda 1996). The southern islands (October Revolution Island and Bolshevik Island) belong to the southern belt of the arctic polar desert. They are less glaciated and the July temperature ranges between 1.3 and 1.6°C in coastal areas (Alexandrova 1988). Vegetation is better developed and a great variety of higher plants was monitored (Kanda 1996). Soil development is very restricted and

---

[1] Institut für Polarökologie, Christian-Albrechts-Universität zu Kiel, Wischlofstr. 1-3, D-24148 Kiel, Germany
[2] Institut für Bodenkunde, Universität Hamburg, Allendeplatz 2, D-20246 Hamburg, Germany

only virgin and weakly differentiated soils have been described (Alexandrova 1988). Calcareous and non-calcareous soils as well as hydromorphic gley soils with slight humus accumulations and weak weathering horizons are predominant; all soils have a pergelic soil temperature regime (Pfeiffer et al. 1996). Only soils underneath plants show an accumulation of brown humic material. Differences in soils along the slopes are due to individual soil moisture regimes, particle size classes and plant cover. Mineral soils and soils in polygon centers are less developed. Calcerous and non-calcerous soils as well as hydromorphic gley soils with slight humus accumulations and weak weathering horizons are predominant. All soils have a pergelic soil temperature regime (Pfeiffer et al. 1996).
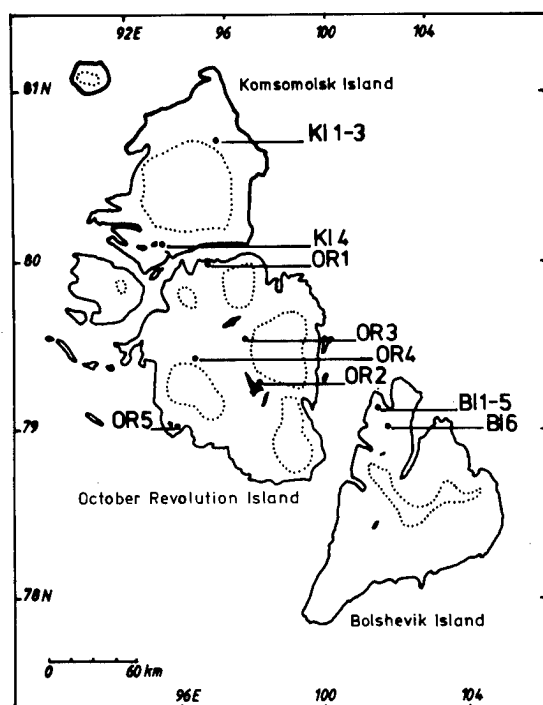
Figure 1. Sampling sites at Severnaya Zemlya. Dotted lines indicate glaciated areas.

Sampling and analyses

Sampling was carried out with respect to different soil cover (barren soils, custs and cushions) and plants (Table 1). Generally, surface layers (0-2 cm) and layers underneath cushions (2-4 cm) were analysed for microbes, samples for further analyses on organic matter and soil descriptions were obtained from pits, which were dug to depths of permafrost or bedrock. All samples for microbiological analyses were taken in 100 ml plastic containers and stored at ambient temperature during the expedition (< 0° C), and later

in a freezer until analysis in order to prevent changes of the microbial community due to temperature and storage effects. Water and organic matter content (LOI, loss on ignition) were analyzed according to standard procedures (drying at 105° C and ignition at 550° C, respectively). Soil colours were determined according to Munsell Soil Colour Charts (1994), soil morphology is decribed according to the German soil survey manual (AG Bodenkunde 1994). Bacterial counts (TBC) and biomass (TBM) estimations were performed by epifluorescence microscopy and image analysis (Bölter et al. 1993) using measures of length (l) and diameter (d). Biovolumes were calculated by use of these parameters and geometrical formulas of spheres, cylinders or ellipsoids. Biomass (μg C) was calculated using the assumption that bacteria contain 80% water and that 50% of the dry matter is represented by carbon (Schlegel 1992).

RESULTS

Soils

Surface layers generally have a high stone content (desert pavement). Most soils show high water content due to infiltration of melt water into the surface layers. The impermeable permafrost layers thus leads to muddy and partly water-logged soils. An accumulation of organic material in O/A- horizons is the predominant process where mosses and lichens perform cushions. Distinct developed A- horizons with slight acuumulations of humic material was found mainly on old moraines and vegetated sites with higher gedres of plant cover. The thickness of the active layer at the sampling sites ranged between 0.35 m in fine textured soils and more than 0.85 cm in coarse textured soils (Pfeiffer et al. 1996). Soil classifications are available for sites BI1, OR1, and OR5 (Pergelic Cryaquept), for BI6, OR2, and OR4 (Pergelic Cryotent), for BI5 and KI4 (Lithic Cryortent), and for KI1 (Pergelic Cryopsamment).

Soil organic matter

A- horizons have C_{org}-contents between 0.5 and 11.5%, O- horizons between 21 and 44%, mineral horizons about 0.1%; total organic nitrogen of A-horizons show an average of 0.2% N (range: 0.01 - 0.7%) (Pfeiffer et al. 1996). The highest values of organic matter (> 20% LOI) were found only in cushions of plants, i.e., mosses or higher plants (samples BI3.1, BI4.1, BI5.1, OR2.1) or where lichens covered the soils to a higher extent (samples OR5.1, KI4.1). All other soils show values below 10% LOI or much lower, e.g., at denuded areas of Komsomolsk Island.

Table 1. Description of samples taken at Severnaya Zemlya in 1995. Munsell colours and actual water contents (% H₂O) are given in paranthesis. BI: Bolshevik Island; OR: October Revolution Island; KI: Komsomolsk Island (compare Fig. 1).

Site	Date	Sample	Depth (cm)	Description
BI1*	Aug. 9			Flat area, waterlogged, mosses, cover < 5%, patterned ground
		BI 1.1	0-2	Wet loamy sand, stones > 50%, (2.5Y 4/3; 25.1%)
BI2*	Aug. 9			Dry loamy sand, patterned ground with small polygones, mosses and fruticose and crustose lichens, cover 10-20%
		BI 2.1	0-2	Loamy sand, stones 30%, few lichens and shoots of mosses (2.5Y 5/3; 12.2%)
		BI 2.2	2-4	Loamy sand, some roots, (2.5Y 4/3; 14.4%)
BI3*	Aug. 9			Wet area with moss cushions, plant cover 70%.
		BI 3.1	0-1	Sample from surface soil with moss cushion and ongrowing lichens, (7.5YR 2/0; 54.3%)
		BI 3.2	1-3	Loamy sand (2.5Y 4/4; 30.0%)
BI4*	Aug. 9	BI 4.1	5	Sample from peaty matter underneath a cushion of *Novosieversia glacialis*, (10YR 2/2; 55.5%)
BI5*	Aug. 9			Soil covered with crusts of lichens and moss cushions between large rocks.
		BI 5.1	0-1	Crust of wet moss and lichens (7.5Y 2/0; 38.0%)
		BI 5.2	1-3	Loamy sand (5Y 3/1)
BI6	Aug. 12			Block field at Mushketova Glacier, small polygones, no plant growth, crustose lichens only on rocks [79°10'N, 102°09'E]
		BI 6.1	0-2	Loamy sand from polygon center (5Y 4/2; 9.6%)
		BI 6.2	2-4	Loamy sand (5Y 4/2; 9.3%)
OR1	Aug. 10			Flat plain on fjell, wet surface, plant cover < 10% [80°05'59"N, 95°45'23"E]
		OR1.1	0-2	Wet loamy sand, no organic debris (7.5YR 4/4; 17.7%)
OR2	Aug. 10			Fjell area near cliff with bird colony (*Rissa tridactyla*), soils with vascular plants, mosses and lichens [70°22'45"N, 97°44'22"E]
		OR 2.1	0-2	Wet soil crust with moss and lichens, (7.5YR 3/3; 48.0%)
		OR 2.2	2-4	Loamy sand, stones > 50%, (7.5YR 3/4; 25.6%)
OR3	Aug. 11			Fjell area covered with stones ("desert pavement"), wet [77°36'30"N, 97°11'18"E]
		OR 3.1	0-1	Sandy loam, stones < 5%, (7.5YR 4/3; 14.9%)
		OR 3.2	1-3	Sandy loam, stones < 5%, (7.5YR 4/2; 12.9%)
OR4	Aug. 11			Fjell area with polygon nets, plant cover < 10% [79°32'14"N, 95°44'16"E]
		OR 4.1	0-1	Soil crust with lichens, (5YR 3/4; 22.5%)
		OR 4.2	1-4	Loamy sand, stones 10%, (5YR 3/4; 13.8%)
OR5	Aug. 11			Fjell area, slope 5%, vascular plants and mosses < 10% [79°06'10"N, 91°12'04"E]
		OR 5.1	0-2	Loamy sand, wet, no plant debris (5YR 3/3; 46.9%)
		OR 5.2	0-2	Sample from soil with plant roots (*Saxifraga oppositifolia*), (5YR 3/2; 3.5%)

* sites BI 1-5 are located around a lake near Prima Station (pos. 70° 16' 44"N, 101° 37' 24"E)

Table 1. (continued)

Site	Date	Sample	Depth	Description
KI1*	Aug. 10			Plain area, deglaciated, 10 m off glacier front, no plants
		KI 1.1	0-1	Sand (2.5Y 5/3; 9.2%)
		KI 1.2	2-5	Sand, vesicular structure, (2.5Y 5/4; 6.7%)
		KI 1.3	5-10	Sand, vesicular structure, (2.5Y 5/4, 8.8%)
KI2*	Aug. 10			Small depression in glacier foreland, some moss shoots
		KI 2.1	0-2	Sand, (2.5Y 4/3; 18.9%)
KI3*	Aug. 10			Outcrop of morain material (~25 m²), 100 m up glacier
		KI 3.1	0-2	Sand, (2.5Y 5/2, 14.7%)
KI4	Aug. 10			Glacier foreland, 50 m off glacier front, vascular plants and lichens close to abandoned nest of *Branta bernicla*. [80°10'48"N, 94°07'05"E]
		KI 4.1	0-2	Sand with organic crust of lichens, stones 20%, wet, (2.5Y 2/0; 38.4%)
		KI 4.2	2-5	Sand, roots, stones 50%, (7.5YR 3/4; 21.0%)

*Sites KI 1-3 were close to Akademik Nauk Glacier at pos. 80°50'13"N, 96°19'08"E

Microbes

Algae or cyanobacteria were found only seldom during the microscopical inspections. Only few diatoms were seen in samples from Komsomolsk Island (KI1, KI2). Bacterial counts vary mostly between 0.1 and $1.0 \cdot 10^9$ cells per gram dry soil, bacterial biomass ranges between 0.5 and 5 µg C per gram dry soil. Direct relationships to bacterial counts or biomass cannot be established, albeit samples BI4.1 and OR2.1 show highest figures in these samples. The relationship between bacterial counts and biomass is linear, hence, there is also no direct relationship between LOI and MCV. Only samples BI3.1, BI4.1 and BI5.1 also have high values of MCV, but samples OR3.1, OR5.1 and KI4.1 do not show elevated mean cell volumes.

No bacteria were found in size classes where $l > 2.25$ µm, and only 4 samples showed bacteria with $l > 2.0$ µm (BI4.1, BI5.2, BI6.2, OR3.1); they represented always less than 1.1% of the total community. Even between 1.5 and 2 µm length the highest portion was 4.6% in sample BI4.1. Hence, a strong shift to the small forms takes place in these soils, and cocci ($d < 0.5$ µm) and rods ($l < 1.0$ µm) dominate the size spectra by 46 and 39% in mean, respectively. Two examples of such size class distributions are presented in Figure 2: sample BI4.1

size class [µm]	0,25	0,50	0,75	1,00	1,25	1,50	1,75	2,00	2,25
% per group	8,44	30,38	23,63	13,08	14,35	4,64	2,53	2,11	0,84
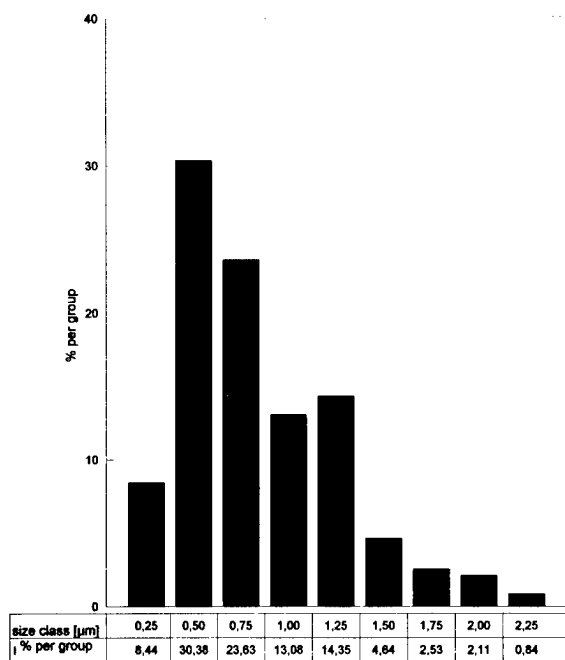
Figure 2a. Histogram of length distribution of bacteria from sample BI4.1 (n= 237).

size class [µm]	0,25	0,50	0,75	1,00	1,25	1,50
% per group	16,27	38,10	29,37	10,71	5,16	0,40
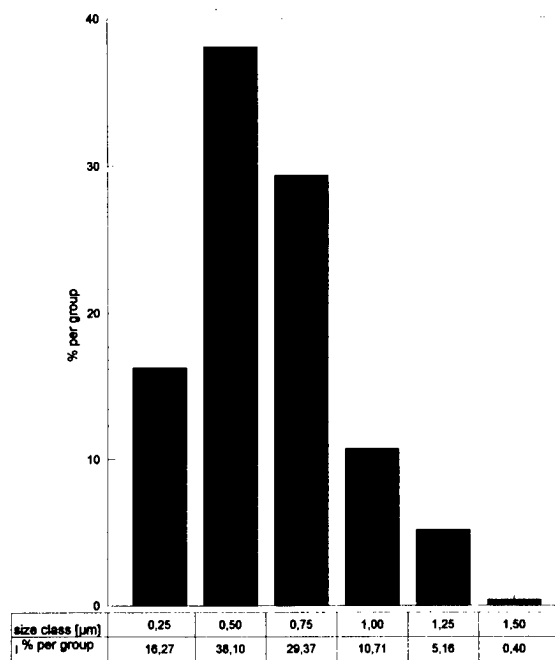
Figure 2b. Histogram of length distribution of bacteria from sample KI1.2 (n=252)

484

with highest amount of organics and sample KI1.2 at the low scale of organic matter content.

DISCUSSION

Arctic tundras and cold deserts are the dominant landscapes of polar environments. Due to the harsh climatic harsh conditions, the majority of the living biomass and organic material is located the soil. Bunnell (1981) stated that life in tundras mainly occurs below the surface; this also seems applicable to polar deserts, which have only plant aggregations rather than a continuous plant cover (Alexandrova 1988). The data for bacterial biomass, however, suggest that life in polar deserts is restricted to surface layers. The patterns also show a strong decrease of bacterial biomass with increasing depth even at few centimeters below surface (Table 2). Only in root systems (samples BI4.1, OR3.1-3.2) show elevated values of bacterial biomass.

Aspects of changing microbial communities in tundra environments have also been stressed by Parinkina (1989) who describes an increasing oligotrophy with depth. This effect is mirrored also by generally descreasing mean cell volumes with depth (Table 2). Parinkina (1974) showed data of sites in a polar desert region (Daksatas Plateau) where total bacterial counts obtained by epifluorescence microscopy were between 1.3 and $6.9 \cdot 10^9$ g^{-1} dry weight; the highest counts were observed in soil samples underneath moss cushions. This agrees with the data described for the sample from site BI4.1, which was taken in a cushion of *Novosieversia glacialis*. But only few reports are available about polar soils and they are mostly based on viable counts (*e.g.*, Jordan *et al.* 1978, Holding 1981).

Although only a few samples were analysed during this study, relevant differences in the bacterial communities of tundra-like environments and polar desert biotopes became evident from comparisons between size distributions of samples from tundra sites (Taymyr Peninsula) and those from polar desert environments (Severnaya Zemlya). It could be shown that tundra sites tend to favour larger forms, especially rod shaped bacteria (Bölter 1996). Small bacteria, mainly cocci, but also small rods in higher numbers are representative in samples from polar desert soils, except those from root systems of plants or directly related to moss cushions. A study of bacterial communities by cultivation from Spitsbergen soils showed about 33% cocci (Janowiec *et al.* 1993).

Parinkina (1989) concluded that composition and other characterististic of microfloras depend on

climatic and environmental conditions. Any such patterns, however, need verification by parameters of microbial activity and related organic nutrients; their estimation by LOI as performed here can only be regarded as a rough indication. Nevertheless, some trends of relationships between LOI and parameters of the bacterial community became visible. Detailed studies especially at low levels of organic matter (< 10% LOI) are necessary.

The dominant controlling factor for the bacterial community structure is the abundance and quality of available organic matter, which in turn is controlled by soil features and climate. Further, these soils are impoverished in inorganic nutrients, which prevents

Table 2. Data of organic matter (loss on ignition, LOI) and parameters of the bacterial community (total bacterial count, TBC; total bacterial biomass, TBM; mean bacterial cell volume, MCV) at Severnaya Zemlya Islands. All data, except MCV, are related per gram dry weight. BI: Bolshevik Island, OR: October Revolution Island, KI: Komsomolsk Island.

Sample	LOI (%)	TBC ($n \cdot 10^9$)	TBM (μg C)	MCV (μm^3)
BI 1.1	5.4	0.65	3.53	0.054
BI 2.1	5.8	0.70	4.15	0.059
BI 2.2	4.9	0.29	1.92	0.065
BI 3.1	30.3	0.34	2.31	0.067
BI 3.2	7.9	0.05	0.27	0.048
BI 4.1	91.2	3.23	23.76	0.074
BI 5.1	50.1	0.37	2.70	0.074
BI 5.2	8.6	0.08	0.54	0.064
BI 6.1	6.7	0.11	0.76	0.070
BI 6.2	7.3	0.10	0.63	0.064
OR 1.1	6.9	0.59	2.56	0.044
OR 2.1	24.7	1.05	5.21	0.050
OR 2.2	8.2	0.28	1.11	0.047
OR 3.1	6.4	0.24	1.57	0.066
OR 3.2	6.0	0.41	1.66	0.041
OR 4.1	7.4	0.28	1.27	0.046
OR 4.2	6.3	0.11	0.56	0.050
OR 5.1	13.1	0.65	3.83	0.059
OR 5.2	5.6	0.58	2.62	0.046
KI 1.1	3.9	0.06	0.27	0.048
KI 1.2	3.5	0.04	0.18	0.044
KI 1.3	3.4	0.02	0.08	0.052
KI 2.1	3.3	0.06	0.36	0.064
KI 3.1	4.9	0.01	0.09	0.068
KI 4.1	14.4	0.28	1.39	0.050
KI 4.2	7.0	0.18	0.77	0.042

the decomposition of high molecular weight organic matter (Alexandrova 1988, Pfeiffer *et al.* 1996) and thus may lead to conditions of starvation and prevents the new production of biomass.

Striking differences in direct counts and counts of viable bacteria also show evidences of oligotrophic characteristics of these environments. Parinkina (1974) concluded that tundra biotopes with high levels of organic matter may contain higher numbers of dead or inactive cells compared to soils with low organic matter content.

On the other hand, my results may be a hint that there is a basic population of small (oligotrophic?) bacteria which serves as a minimal community and which is present in any environment. This basic community may change by growth and division of cells already present or by germination of spores or dorming states of resting cells. It can be regarded as an additional description of soils from marginal environments in relation to the plant community studies of Svoboda & Henry (1987).

Although some general aspects of microbial communities can be elucidated from those studies, it has to be taken into account that small-scale patterns often override such trends. Studies on microscales often show wider ranges of individual parameters, not only of the environmental, but also of microbiological properties (*e.g.*, Bölter 1992, 1995, Elliott & Svoboda 1994). Besides this, short-term shifts in temperature and nutrient availabilty must be taken into account when such studies are performed, as these effects may cause shifts in community structure.

Thus, figures as presented here can be only regarded as snapshots of a changing environment but give hints for advances in the quantification of community structure in polar desert ecosystems.

ACKNOWLEDGEMENT

REFERENCES

AG Bodenkunde 1994. Bodenkundliche Kartieranleitung. Schweizerbart'sche Verlagsbuchhandlung, Stuttgart.

Alexandrova, V.D. 1988. Vegetation of Soviet polar deserts. Cambridge University Press, Cambridge.

Bolshiyanov, D.Yu. and H.-W. Hubberten (ed.) 1996. Russian-German Cooperation: The expedition Taimyr 1995. Ber. Polarforsch. 211: 1-208.

Bölter, M. 1992. Environmental conditions and microbiologcial properties from soils and lichens from Antarctica (Casey Station, Wilkes Land). Polar Biol. 11: 591-599.

Bölter, M. 1995. Distribution of bacterial numbers and biomass in soil and on plants from, King George Island (Arctowski Station, Maritime Antarctica). Polar Biol. 15: 115-124.

Bölter, M. 1996. Soil microbiology. Ber. Polarforsch. 211: 72-79.

Bölter, M. and H. Kanda. Preliminary results of botanical and microbiological investigations on Severnaya Zemlya 1995. Proc. NIPR Symp. Polar Biol. 10 (in press).

Bölter, M., R. Möller and W. Dzomla 1993. Determination of bacterial biovolume with epifluorescence microscopy: Comparison of size distributions from image analysis and size classifications. Micron 24, 31-40.

Bornkamm, R. 1987. Allochthonous ecosystems. Landscape Ecol. 1: 119-122.

Bunnell, F.L. 1981. Ecosystem synthesis - a "fairytale". p. 637-646. *In*: Bliss, L.C., O.W. Heal and J.J. Moore (ed.) Tundra ecosystems: a comparative analysis. Cambridge University Press, Cambridge.

Elliot, D. and J. Svoboda 1994. Microecosystems around a large erratic boulder: a high-arctic study. p. 207-213. *In*: Svoboda, J. and B. Freedman (ed.) Ecology of a polar oasis. Captus University Publications, Toronto.

Freedman, B., J. Svoboda and G.H.R. Henry 1994. Alexandra Fiord - An ecological oasis on the polar desert. p. 1-9. *In:* Svoboda, J. and B. Freedman (ed.) Ecology of a polar oasis. Captus University Publications, Toronto.

Holding, A.J. 1981. The microflora of tundra. p. 561-585. In: Bliss, L.C., O.W. Heal and J.J. Moore (ed.) Tundra ecosystems: a comparative study. Cambridge University Press, Cambridge.

Janowiec, M., Z. Andrzejczyk, Z. Jezierska-Anczuków and Z. Jóźwik 1993. Bacterial flora in soils of western Spitsbergen. Polish Pol. Res. 14: 169-175.

Jordan, D.C., M.R. Marshall and P.J. McNicol 1978. Microbiological features of terrestrial sites on the Devon Island Lowland, Canadian Arctic. Can. J. Soil Sci. 58: 113-118.

Munsell Soil Colour Charts 1994. Macbeth Division of Kollmorgen Instruments Corp. New Windsor, New York.

Parinkina, O.M. 1974. Bacterial production in tundra soils. p. 65-77. *In*: Holding, A.J., O.W. Heal, S.F. MacLean and P.W. Flanagan (ed.) Soil organisms and decomposition in tundra. Tundra Biome Steering Committee, Stockholm.

Parinkina, O.M. 1989. Die Mikroflora der Tundraböden. Ökologisch-geografische Besonderheiten und Produktivität. Nauka, Leningrad, 159 p. (in russian).

Pfeiffer, E.M., A. Gundelwein, T. Nöthen, H. Becker and G. Guggenberger 1996. Characterization of the organic matter in permafrost soils and sediments of the Taymyr Peninsula/Siberia and Severnaya Zemlya/Arctic region. Ber. Polarforsch. 211: 46-63.

Schlegel, H.G. 1992. Allgemeine Mikrobiologie. Georg Thieme Verlag, Stuttgart.

Siegert, C. and D.Yu. Bolshiyanov (ed.) 1995. Russian-German Cooperation: The expedition TAYMYR 1994. Ber. Polarforsch. 175:1-91.

Svoboda, J. and G.H.R. Henry 1987. Succession in marginal Arctic environments. Arct. Alpine Res. 19: 373-384.

Effects of Soil Freezing and Thawing on the Bacterial Population in the Wheat Rhizosphere

T. HASHIMOTO[1] AND T. NITTA[2]

ABSTRACT

To clarify any effects of soil freezing and thawing on soil microorganisms, bacterial dynamics was studied in the rhizosphere of winter wheat in field or laboratory conditions. Soil freezing and thawing significantly influenced bacterial viable counts and Adenosine Triphosphate (ATP) content in soil, especially in the surface layers. Fast-growing bacteria, distinguished by analysis of the colony formation rate, showed a more marked increase after soil thawing than slow-growing bacteria. The fluctuation of temperature between +20 °C and -10°C, simulating cycles of a freezing-thawing in the field in April, enhanced the growth of the fast-growing group, the effect being mostly due to the increased contribution of psychrophilic bacteria. Although the numbers of both fast- and slow-growing bacteria were decreased by soil freezing, thawing of soil favors fast-growing, and especially psychrophilic, bacteria, resulting in the significant increase of the bacterial population in the rhizosphere of wheat.

Key words: Plate count, ATP biomass, psychrophilic bacteria, wheat rhizosphere

INTRODUCTION

Soil surfaces freeze every winter in northern Japan. Freezing begins in November. By February the layer of frozen soil may be more than 30 cm thick. In March thawing begins, both from the top and bottom of the frozen layer. By April soil is completely thawed. During the thawing period, the soil surface repeatedly freezes and thaws with daily temperature fluctuations of approximately 8°C.

Several researchers have investigated the effects of soil freezing on microbial CO_2 evolution or mineral nitrogen flush in the laboratory (Ross 1972, Morley et al. 1983, Coxson and Parkinson 1987). It has also been shown that bacterial populations were reduced with soil freezing or drying (Soulides and Allison 1961). There is no doubt that the soil freezing has abiotic effects on microbes. Although such conditions may damage microbes in fields, there has been little research on microbial dynamics during the soil freezing season.

There are several techniques for examining bacterial populations in soil environments. A direct microscopic count gives a number more than 100 times larger than incubation methods. However, if it is necessary to obtain isolates from samples, incubation is the most effective method. Colony forming curve (CFC) analysis has been developed to classify diverse soil bacteria according to their growth velocity on plate (Hashimoto and Hattori 1989). Each group was distinguished by optical media concentrations for their growth and DNA electrophoresis patterns (Kasahara and Hattori 1991, Kasahara et al. 1993). Fast and slow-growing bacteria can be monitored separately using this technique.

The aim of this study was to examine spatial and temporal dynamics of bacterial population with special attention to the contribution of fast and slow-growing bacteria in winter wheat rhizosphere soil during the soil freezing season, especially in the soil thawing period.

[1] Crop Production Division, Ministry of Agriculture Forestry and Fisheries, Chiyodaku, Tokyo 100 Japan
[2] Hokkaido National Agricultural Experiment Station, MAFF, Toyohiraku, Sapporo, 062 Japan

MATERIALS AND METHODS

1 Soil

We used a light-colored Andosols for the experiments. Soil was collected from winter wheat fields in the Hokkaido National Agricultural Experiment Station (43°N, 143°E).

2 Experimental design

(1) First field experiment

Sampling was done once a month from November 1988 to April 1989. Soil samples were collected from different depths of soil layers: 0-2, 2-10, 10-20 and 20-30 cm. Frozen samples were allowed to thaw at room temperature within 3 hours of collection. Worms, insects and discrete pieces of organic matter were removed by hand. Then total viable bacterial count and ATP biomass were examined.

(2) Second field experiment

A field experiment was carried out four replicated microplots (1 m^2) with two treatment: wheat plants(*Triticum aestivum cv. Norin 126*) sown in September 1990 (planted soil) and no plants (bare soil). Soil (0-15 cm) was sampled once a month from November 1990 to May 1991.

(3) Incubation experiments

The incubation experiments were designed to imitate a partial freeze-thaw cycle of the surface soil. A soil sample for the incubation experiment was collected in October 1991. After removing discrete pieces of organic matter by hand, the sample was sieved (5 mm) and stored in plastic bags at 4°C until use. Fifty grams of stored wet soil was put into sterilized test tubes and the soil water content adjusted to 67%. The surfaces of wheat seeds were surface-sterilized and stored on sterilized wet paper overnight at 27°C. Half of the test tubes were inoculated with two germinal seeds. The tubes were sealed with silicon caps and incubated in a climate chamber (LPH-200-RDCT, Nihon Ikakikai Co.) with a 16 hour light (20°C) and an 8 hour dark (15 °C) period. After 12 days, the tubes were divided into three subgroups, (1) nontreated samples, maintained at 20°C, (2) frozen samples, maintained at -10°C, and (3) freeze-thaw samples, alternating between 12 hours at 20°C and 12 hours at -10°C. Samples were harvested after the 0, 10th and 39th day, then viable counts were measured. In a second incubation experiment, viable counts of both mesophilic and psychrophilic fast-growing bacteria were examined. Incubation conditions were similar to the first experiment, but the tubes were incubated in the climate chamber with a 12 hour light (20°C) and a 12 hour dark (15°C) period for 14 days. The three subgroups were then incubated for 30 days.

3. Enumeration of microbes

Viable counts of the bacterial population were determined by colony forming curve (CFC) analysis, i.e., by the plate dilution method with a theoretical model (the FOR model proposed by Hattori 1982). A 0.5 gram sample of fresh soil was dispersed in 50 ml of 1% nutrient broth (DNB) medium (pH 7.1) in a shaker for 30 min at 220 rpm. Ten-fold dilution series were prepared and 0.5 ml of suitably diluted samples were mixed with the DNB medium solidified by 1% Agar Noble (Difco Co.). Plates were incubated at 20°C. Colonies which appeared on plates were counted at suitable time intervals for more than two weeks. The data were analyzed with the FOR model. To estimate the viable counts of psychrophilic bacteria, plates were incubated at 4°C.

4. Assay of ATP concentration

ATP concentration of soil samples collected in the first field experiment were determined by the bioluminescent method (Verstraete et al. 1983). Samples in TEA buffer solution were assayed for ATP concentration using commercially available ATP extract and detection reagents (Lumac). ATP concentration of rhizosphere samples was not determined because ATP extracted from winter wheat roots would influence the results.

## RESULTS

1. Field observations

The viable count in different soil depths varied in relation to the process of soil freezing and thawing (Figure 1). It showed the lowest values in February. In March the viable count began to increase in the surface, the subsurface and the deepest layers, although the effect was less pronounced in the 10-20 cm layer.

489
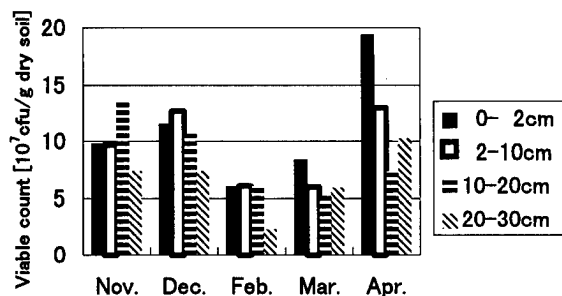
Figure 1. Vertical distribution of heterotrophic soil bacteria.

Soil samples were collected from 0-2, 2-10, 10-20 and 20-30 cm layers on 15 November (prefreezing stage), 20 December (surface freezing stage), 13 February (deepest freezing stage), 24 March (surface thawing stage) and 14 April (post-thawing stage).

To compare with viable count, changes of ATP concentration in different soil depths were observed (Figure 2). In the surface layer, ATP concentration continued to decrease during the period of soil freezing until February. As soil thawed, the ATP concentration increased. In the sub-surface and the deepest layers, although ATP concentration decreased, it did not increase in April. ATP change in the third layer (10-20 cm) showed a pattern different from the other layers.
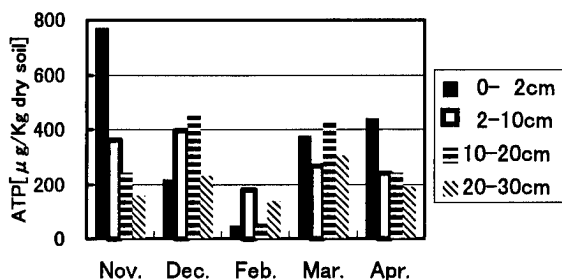
Figure 2. ATP concentration in different soil depths.

Sampling designs are shown in footnote on Figure 1.

In the microplot field experiment, soil bacteria decreased and then increased during the freeze-thaw soil cycle (Figure 3). The total viable count of the planted sample remained higher than that of the bulk soil sample throughout. During thawing, the viable count of the planted sample rapidly increased. The RS ratio, the ratio of the viable count of the planted sample to that of the bulk soil sample, was less than 11 by February, and rapidly increased to 33.6 in April (Table 1).
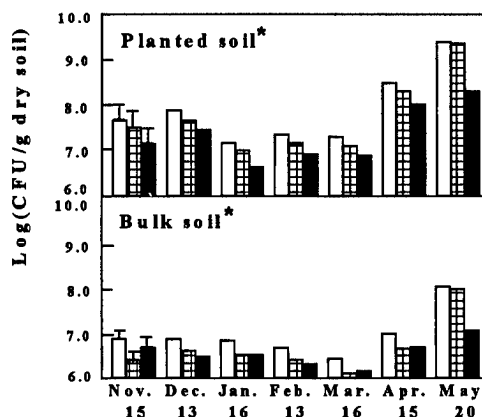
Figure 3. Changes of the bacterial population during the soil freeze-thaw period.

The viable counts of total bacteria (open bars), fast-growing bacteria (checked bars) and slow-growing bacteria (closed bars) are plotted.

*:The vertical lines indicate the least significant differences (P=0.05) by ANOVA for the different sampling times.

Table 1. Changes of RS and FS ratios during a soil freezing-thawing period.

	RS ratio			FS ratio	
	Total	Fasters	Slowers	Planted	Bulk
15 Nov.	6.5 a	12.9 ab	3.2 a	2.4 a	0.6 a
13 Dec.	10.5 a	11.2 ab	9.4 ab	2.2 a	1.4 a
16 Jan.	2.4 a	3.2 ab	1.6 a	2.6 a	1.1 a
13 Feb.	5.3 a	6.2 ab	4.1 a	2.0 a	1.3 a
16 Mar.	7.7 a	9.6 ab	6.1 a	1.5 a	0.9 a
15 Apr.	33.6 b	46.0 c	22.7 b	2.0 a	1.0 a
20 May	24.6 b	24.8 b	21.7 b	14.5 b	9.1 b

Different symbols indicate the least signigicant differences (P=0.05) for the different sampling times.

The FOR model matched the experimental data well. In this experiment, the colony forming curve was constructed from two component curves corresponding to fast- and slow-growing bacteria. The fast- and slow-growing bacteria changed in the process of soil freezing. The fast-growing bacteria remained higher in planted samples than in bulk soil samples. The FS ratio, i.e., the ratio of the viable count of fast-growing bacteria to that of slow-growing bacteria, during the period of soil freezing (December-February) decreased to 1.5-2.6 in the planted, and 0.9-1.3 in bulk soil samples. The fast-growing bacteria responded to soil

490

thawing quicker than the slow-growing ones, the RS ratio in April for fast- and slow-growing bacteria being 46 and 22.7, respectively.

2. Incubation experiment

Viable counts in the sample kept at 20°C continued to increase during incubation (Figure 4, Table 2). The planted sample increased at a higher rate than the bulk soil sample. Thus, the RS ratio rose more than four times after 39 days of incubation. The slow-growing bacteria contributed to an increase in the viable count in the planted sample. Freezing did not alter bacterial population. Samples subjected to a freeze-thaw cycle showed a significant rise in viable count after the 39th day of incubation. The viable count was more than twice as high as the 20°C sample. Both fast and slow-growing bacteria contributed to the increase.
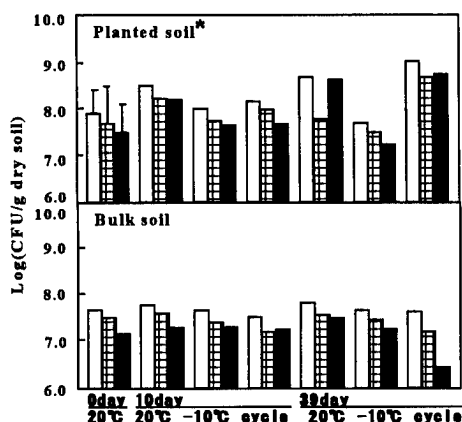
Figure 4. Changes in the bacterial population during the soil freeze-thaw cycle treatment.
See footnote of Figure 3.

Table 2. Changes of RS ratio during a soil freezing-thawing cycle treatment.

		Total	Fasters	Slowers
0day	20°C	1.5	1.3	2.1 a
10day	20°C	4.8	3.8	7.0 ab
10day	−10°C	2.0	1.9	2.0 a
10day	cycle	3.9	5.7	2.3 a
39day	20°C	6.4	1.5	11.9 b
39day	−10°C	0.9	0.9	0.9 a
39day	cycle	28.3	84.1	19.8 c

Different symbols indicate the least significant differences (P=0.05) for the different sampling times.

Similar results were obtained in the second incubation experiment: The cycle incubation promoted the growth of fast-growing bacteria in the planted sample. The viable count of fast-growing psychrophilic bacteria was also analyzed by the CFC method. After a 30 day incubation, the viable counts of both mesophilic and psychrophilic fast-growing bacteria significantly increased in the sample treated with a freeze-thaw cycle. The RS ratio also increased. The ratio of the psychrophilic bacteria to mesophilic fast-growing bacteria was highest in the rhizosphere after cycle incubation (Table 3).

Table 3. Effect of freezing-thawing cycle treatment on fast-growing psychrophilic bacteria.

		Psychrophi-lics (A)	RS ratio	Fasters(B)	A/B
Planted soil					
0day	20°C	7.24E+6 a	2.6 a	2.91E+7 a	0.21 a
30day	20°C	2.13E+6 a	0.9 a	1.99E+7 a	0.11 a
30day	−10°C	3.22E+6 a	1.2 a	1.81E+7 a	0.17 a
30day	cycle	3.42E+7 b	10.2 b	8.73E+7 b	0.44 b
Bulk soil					
0day	20°C	2.86E+6		1.89E+7	0.15
30day	20°C	2.59E+6		1.78E+7	0.15
30day	−10°C	2.97E+6		1.53E+7	0.19
30day	cycle	4.10E+6		1.52E+7	0.27

Different symbols indicate the least significant differences (P=0.05) for the different sampling times.

DISCUSSION

In Hokkaido the temperature of a soil surface layer commonly reaches -10°C or lower from January to February. A survival test of soil microbes at different storage temperatures suggests that the freezing at -10°C is enough for injuring alive cells (Hashimoto et al. 1990). It was observed that water remained unfrozen even at -15°C(Kolaian and Low 1963). Since water is of primary importance to all soil microorganisms, which normally require a water environment for nutrient uptake and cell surface integrity, we propose that in a frozen soil a part of bacterial population survives during the winter period in microsites with unfrozen water. These microsites may be located inside soil aggregates. Further analysis is required to delineate changes of bacteria in soil aggregates during a soil freezing period.

Different effects of temperatures on bacterial dynamics were expected in the incubation experiment. Freezing at -10°C mimics the soil freezing period from November to February. Results showed a tendency for bacterial populations to decrease more in planted soil than in bulk soil. The RS ratio remained lower than 2.0. Samples stored at 20°C were similar to the period of plant growth in May. The bacterial population and RS

491

ratio increased more in planted soil than in bulk soil. The soil subject to freezing and thawing between -10℃ and 20℃ is similar to soil thawing in April; the bacterial population significantly increased. This sample showed a marked increase in the RS ratio. The incubation experiment clarified the role of the freeze-thaw cycle in stimulating the growth of fast-growing bacteria and the relative increase of psychrophilic bacteria in the rhizosphere of wheat. The viable count of the bulk soil sample did not increase significantly.

The soil temperature by the first 10 days of April is approximately 10℃. Such conditions are unsuitable for the growth of mesophilic bacteria. The bacterial viable count of the April sample, however, began increasing, especially in the rhizosphere, displaying a marked increase in the RS ratio. This incubation experiment suggests the role of the fast-growing psychrophilic rhizobium in the sudden increase of viable counts in April.

We therefore propose a model to show the bacterial dynamics during soil thawing. Although both fast and slow-growing bacteria decrease in the process of soil freezing, their response during thawing is distinct. The surface layer of frozen soil repeatedly freezes and thaws. Such drastic changes enhance the growth of fast-growing bacteria, especially of psychlophilic rhizobium, resulting in a sudden increase in the viable count in wheat rhizosphere. Further studies are needed to determine the function of bacteria that multiply or activate during periods of soil thawing and their ecological significance.

REFERENCES

Coxson,D.S. and D.Parkinson. 1987. The pattern of winter respiratory response to temperature, moisture, and freeze-thaw exposure in *Bouteloua gracilis* dominated grassland soils of southwestern Alberta. Can.J.Bot. **65**:1716-1725.

Hashimoto,T. and T.Hattori. 1989. Grouping of soil bacteria by analysis of colony formation on agar plates. Biol.Fertil.Soils **7**:198-201.

Hashimoto,T., T.Nitta and T.Kon. 1990. Effect of freezing and thawing on microbial population in upland soil. Transactions 14th Int.Cong.Soil Sci. Kyoto **III**:277-278.

Hattori,T. 1982. Analysis of plate count data of bacteria in natural environments. J.Gen.Appl.Microbiol. **28**:13-22.

Kasahara,Y. and Hattori,T. 1991. Analysis of bacterial population in a grassland soil according to rates of development on solid media. FEMS Microbiol Ecol. **86**:95-102.

Kasahara,Y., H.Morisaki and T.Hattori. 1993. Hydrophobicity of the cells of fast- and slow-growing bacteria isolated from a grassland soil. J.Gen.Appl.Microbiol. **39**:381-388.

Kolaian,J.H. and P.F.Low. 1963. Calorimetric determination of unfrozen water in montmorillonite pastes. Soil Sci. **95**:376-384.

Morley,C.R., J.A.Trofymow, D.C.Coleman and C.Cambardella. 1983. Effects of freeze-thaw stress on bacterial populations in soil microcosms. Microbial Ecol. **9**:329-340.

Ross,D.J. 1972. Effects of freezing and thawing of some grassland topsoils on oxygen uptakes and dehydrogenase activities. Soil Biol.Biochem. **4**:115-117.

Soulides,D.A. and F.E.Allison. 1961. Effect of drying and freezing soils on carbon dioxide production, available mineral nutrients, aggregation and bacterial population. Soil Sci. **91**:291-298.

Verstraete,W., H.Van de Werf, F.Kucnerowicz and M.Ilaiwi. 1983. Specific measurement of soil microbial ATP. Soil Biol.Biochem. **15**:391-396.

Overwintering of Insect Pathogens

L.C. LEWIS[1]

ABSTRACT

Microorganisms (insect pathogens) that cause diseases in insects, are instrumental in their natural control. Insect pathogens overwinter in soil, crop residue, insects, and insect cadavers. Because these organisms can survive the winter, they remain in the ecosystem and reduce populations of insects in the spring. The relationships between the pathogens, the environment, and insects are presented.

Key Words: Insect pathogens, winter survival, fungi, microsporidia, viruses

INTRODUCTION

Microorganisms (insect pathogens) are important natural regulators of insect pests of agronomic crops. Using modifications of their biology, these pathogens remain viable during the winter months and resume development in the spring in synchrony with the development of their respective insect hosts.

In temperate climates, some pest insects overwinter in a reduced state of activity and resume development in the spring as temperatures begin to increase. The European corn borer, *Ostrinia nubilalis* (Hübner) is such an insect. Its populations are partially regulated by two pathogens, a microsporidium, *Nosema pyrausta* (Paillot) and a fungus, *Beauveria bassiana* (Balsamo) Vuillemin. In this review I use European corn borer and its two pathogens as models to illustrate the relationship between overwintering insect pathogens and the insects. I also discuss these relationships of other pathogens that have slightly different mechanisms of overwintering, however, their impacts are similar, i.e., they kill insects.

THE EUROPEAN CORN BORER

The European corn borer is the primary insect pest of corn and occurs in all but the seven most western continental states. It can cause up to 30% loss in yield per acre (Bergman et al. 1985). In addition to conventional management tools, naturally occurring microorganisms reduce populations of the European corn borer. These natural components overwinter with the host insect. In this paper I define winter survival of the European corn borer, review the life cycle of two of its pathogens, and relate the significance of winter survival of these pathogens to the biology of the European corn borer.

The European corn borer goes through four stages of development: egg, larva, pupa, and adult. These four stages constitute a generation. The larva goes through five instars or larval stages of development. During the fifth instar, all larvae either prepare to pupate and become adults or enter diapause. Diapause, a form of hibernation, is a physiological condition resulting in suspended development. It is controlled by day length, temperature, genetic composition of the population, and, in some instances, by the nutritional quality of host plants. Diapause ensures survival through the fall and winter. The larvae that are in diapause remain in suspended development throughout the winter until spring, when diapause ends, and the larvae resume development and pupate (Mason et al. 1996).

BEAUVERIA BASSIANA

Beauveria bassiana (Balsamo) Vuillemin is a fungus that kills many insects. It is a significant mortality factor of the larval stage of the European corn borer. The fungal/insect cycle begins when a conidium (resting spore) lands on and adheres to the cuticle (skin) of an insect, germinates, penetrates, and grows within the hemocoel (body cavity of the insect). The fungus produces an antibiotic to suppress saprophytes (opportunistic microorganisms) and consumes the body tissues as nutrients. Also, a toxin (beauvericin) may be produced that aids in killing the insect. Once the fungus has consumed the contents of the hemocoel, it grows to the outside where it produces several million conidia which are then available to infect other insects.

NOSEMA PYRAUSTA

Nosema pyrausta (Paillot) is a microsporidium that infects primarily the European corn borer. Many insects are infected with microsporidia; however, they are usually species specific; unlike most fungi that infect many species of insects.

The infection cycle of *N. pyrausta* has a typical pattern: a spore is ingested by a larva, the spore extrudes its polar filament, penetrates a mid-gut cell, and injects the contents of the spore into the midgut cell. The sporoplasm passes through several vegetative stages, ultimately producing many more spores. *Nosema* causes infected midgut cells to slough into the gut lumen. The dead cells, which contain viable *N. pyrausta* spores, are excreted in the frass (fecal material). The frass contaminates plant surfaces where uninfected insects may be feeding. As the insects consume plant tissues, they also eat *Nosema* spores that initiate the infection cycle in the new host. *Nosema pyrausta* also infects the ovarian tissues of females and is passed to the filial generation in the egg. The developing embryo envelopes the spore, and the neonatal larva hatches with an infection of *N. pyrausta*.

NOSEMA PYRAUSTA-EUROPEAN CORN BORER RELATIONSHIPS

For convenience, in this section I discuss the relationship between *N. pyrausta* and the European corn borer at the end of winter. As noted earlier, when temperatures begin to warm, the European corn borer continues its development toward pupation, moth emergence, and eventually egg laying. Some *N. pyrausta* spores remain in the frass within the crop residue. The viability of these spores, however, is nearly zero (Lewis and Cossentine 1986). Some *Nosema*-infected insects die during the winter. Those that do survive have *N. pyrausta* infection in many tissues including the reproductive tissues. The tissues infected and severity of the infection in the insect is dependent on the age of the insect at inoculation and on how many spores were ingested (Sajap and Lewis 1992). Larvae that survive infection early in life with a large number of spores are slower to develop and pass more spores to offspring than do their uninfected counterparts. The direct effect of *Nosema* on reproduction, summarized in Table 1, is a substantial reduction in the number of eggs laid and in the hatch of these eggs.

Table 1. Effect of *Nosema pyrausta* infection on egg production of *Ostrinia nubilalis*.

Msrmnt	Disease status	Zimmack &Brindley (1957)	Lewis & Lynch (1970)	Lewis et. al. (1971)
Egg Mass/♀	infected	14.9	11.3	7.3
	healthy	24.0	17.2	10.2
Eggs/♀	infected	160.2	189.3	-
	healthy	301.2	375.0	-
Eggs/Mass	infected	10.8	-	-
	healthy	12.2	-	-
% Egg Hatch	infected	-	68.7	71.6
	healthy	-	76.6	78.5

Environmental factors are common stresses, i.e., temperature, moisture, availability of host plants, predators, and presence or absence of other disease-causing organisms. *Nosema pyrausta* causes a chronic disease; an infection does not always result in death of the insect. Death is more likely to occur if the *Nosema*-infected insect is confronted with an additional stress.

The following is a scenario that illustrates the effect of temperature on the impact of *N. pyrausta*. European corn borer adults congregate in noncorn refugia or action sites to mate and prepare for egg laying (Showers et al. 1976). If weather conditions are not favorable for flight and egg laying, i.e., cool and wet, moths will remain in the action site and imbibe condensation until weather conditions are favorable for flight and egg laying. In a laboratory experiment to simulate a cold, wet field situation, moths infected with *N. pyrausta* and held at relatively low temperatures (16°C) for one week produced 83% fewer eggs than noninfected moths held at a favorable oviposition temperature (27°C) (Table 2). Also the initiation of significant oviposition was delayed by six days in the 16°C population (Lewis 1995). Models developed by Derrick and Showers (1990) define the relationship between number of adult European corn borers in action sites and the potential for oviposition in adjoining corn fields. The model predicts reaching an economic threshold based

494

on adult counts. If the adults were infected by *N. pyrausta* and were delayed in oviposition by cool temperatures, it is likely the threshold would not be met.

Table 2. Effect of *Nosema pyrausta* and temperature on egg production of *Ostrinia nubilalis*.

	Populations[1]			
	27°C		16°C	
	Non infected	infected	Non infected	infected
♀ per population	472.0	503.0	664.0	488.0
Total egg production (g)	19.8a[2]	6.5c	15.8b	3.4d
Eggs per ♀[3]	661.0	216.0	375.0	117.0

[1]Lewis, L.C. 1995.
[2]27°C populations were placed immediately in the oviposition regime at the beginning of adult emergence; 16°C populations were held at 16°C for 7 days after the beginning of adult emergence.
[3]Means of total egg production followed by the same letter are not significantly different from each other at the 5 percent level (Duncan, 1955).
[4]Eggs per ♀ are calculated values. Noninfected and infected eggs weigh 0.0635 and 0.0598 mg respectively (Saleh et al., 1995).

BEAUVERIA BASSIANA-EUROPEAN CORN BORER RELATIONSHIPS

In this section, the relationship of *B. bassiana* to winter and the European corn borer is examined as was *N. pyrausta*. As the temperature warms, the European corn borer resumes development as previously described, unless it is infected with *B. bassiana* or if viable conidia (spores) are on the insect cuticle.

From the time temperatures begin to increase until moths emerge in March-June, there is substantial mortality of European corn borer larvae from *B. bassiana* (Table 3). There is, however, great variability between years in percentage of larvae killed. Once larval mortality from *B. bassiana* has occurred in the spring, the conidia from cadavers remain viable in plant residue or in the soil.

Table 3. Percentage of overwintering European corn borer larvae killed by *Beauveria bassiana*.

Date of observation	# of larvae collected/# killed by B. bassiana	% of larvae killed by B. bassiana
Spring 1992		
05/22	25/58	44.8
06/02	46/82	56.1
Spring 1993		
03/15	7/19	36.8
04/15	0/6	0.0
05/15	11/71	15.5
Spring 1994		
03/15	17/120	14.2
04/15	17/138	13.0
05/15	13/100	13.0
Winter-Spring 1994-95		
11/15/94	62/132	47.0
03/31/95	69/108	63.9
05/15/95	74/117	63.2
05/25/95	64/86	74.4
06/05/95	49/64	76.7

[a]Bing, L.A., and L.C. Lewis. 1993.

Beauveria bassiana is a soil organism and agronomic practices carried out during the crop season greatly influence the relationship between *B. bassiana* and the European corn borer. Tillage practices greatly influence the amount of inoculum in the soil (Bing and Lewis 1993). In a three-year study in which no-tillage, moldboard plow, and chisel practices were used (Table 4), the no-tillage system had the greatest number of conidia forming units $(CFU)g^{-1}$ of soil over the three-year period. *Beauveria bassiana* occurs in the soil in different tillage systems; the amount of inoculum varies greatly and probably is influenced more by environmental conditions than by tillage practices. Also, this tillage-*B. bassiana* inoculum level influences the number of European corn borers killed (Table 5). In all three systems, *B. bassiana* reduced the number of European corn borer larvae by 31-61 %. The percentage of larvae infected with *B. bassiana* in the crop residue from the no-tillage and moldboard plow systems was twice that in the chisel plow system.

Table 4. Colony forming units (CFU) of Beauveria bassiana per gram of soil for samples collected from no-tillage, moldboard plow, and chisel plow tillage systems in 1988-1990.[a]

Year	No-tillage (CFU g^{-1})	Moldboard Plow (CFU g^{-1})	Chisel (CFU g^{-1})	Sample Dates
1988	162	45	80	13 April, 4 May, 23 May 14 Nov.
1989	51	45	47	27 March, 10 May, 7 June 7 July, 8 Dec.
1990	10	37	25	9 April, 14 May
Mean	74	42	51	

Table 5. Incidence of Beauveria bassiana in Ostrinia nubilalis larvae collected 3 June 1991 that overwintered in different tillage systems.[a]

	No-tillage	Plow	Chisel
O. nubilalis per 100 plants	36	36	26
O. nubilalis with B. bassiana	61*	61*	31*

*Significantly different at $P < 0.01$, $X^2 = 7.1$.
[a]Bing, L.A. and L.C. Lewis. 1993.

Indigenous B. bassiana is extremely important to insect management whether it survives in the soil, in insect cadavers, or in crop residue. Recently, it was discovered that this fungus forms an endophytic relationship with the corn plant. The endophytic Beauveria kills European corn borers that have entered the corn plant (Lewis and Bing 1991, Bing and Lewis 1991). The phenomenon can be initiated by placing B. bassiana on the plant. Once on the . plant, the fungus moves in and colonizes the tissues; thus, B. bassiana is available in the plant to kill any larvae in the plant. The endophytic relationship between the corn plant and B. bassiana at times occurs naturally, i.e., independently of a planned foliar application of the fungus.

This phenomenon in turn provides more inoculum to kill insects. As more crop residue is left on the soil surface, where it remains through the winter, there is more inoculum available to cause direct mortality of European corn borers or to cause an endophytic situation, that will kill European corn borers and keep the inoculum level elevated.

WINTER SURVIVAL OF NOMURAEA RILEYI AND ENTOMOPHTHORA SPP.

Nomuraea rileyi (Farlow) Samson, a fungal pathogen, kills the green cloverworm, Plathypena scabra (F.) a pest of soybean in Iowa (Pedigo et al. 1983). The effectiveness of this fungus in northerly climates, like B. bassiana, is dependent on its ability to survive the winter.

The fungal-insect relationship between N. rileyi and the green cloverworm is different from that between B. bassiana and the European corn borer, i.e., the green cloverworm overwinters as a pupa or an adult not a larva. Structures formed when environmental conditions are unfavorable for conidiogenesis, i.e., thick-walled intra-hyphal hyphae, chlamydospores and intra-larval resting bodies and pseudosclerotia formed during the host prepupal and pupal stages (Pendland 1982, Sutton et al. 1979) facilitate winter survival by N. rileyi. In Iowa N. rileyi mycelia within green cloverworm cadavers produce infective conidia after exposures to surface and subsurface soil conditions for 93 or 105 days, respectively (Thorvilson et al. 1985). These conidia survive the winter independent of a host in the soil or with cadavers. Nomuraea rileyi can survive mild winters in North Carolina as conidia; however, the fungus most likely overwinters as stroma (Sprenkel and Brooks 1977). Conidia from previous seasons remain viable in the soil and initiate epizootics in pest insects the following season in Missouri (Ignoffo et al. 1978).

Fungi in the genus Entomophthora differ from Beauveria sp. and Nomuraea in the production of a resting spore. This "thick-walled" spore is sometimes referred to as the overwintering stage of the fungus. In temperate climates, it allows the fungus to remain viable but dormant and pass through the winter between successive populations of the host insect. For example, Entomophthora aphidis = (Erynia neoaphidis Remaudiere and Hennebert) resting spores can survive winter temperatures of minus 12°C at Sault St. Marie, Ontario, Canada

496

(Terryll et al. 1976). Viability is highest when spores are insulated by snow.

Not all *Entomophthorales* overwinter as resting spores. *Entomophthora planchoniana* Cornu passes the winter as hyphal bodies within cadavers of *Drepanosiphum acerinum* (Walker) an aphid pest of maple trees, *Acer pseudoplantanus* (L.). These hyphal bodies are known to survive temperatures as low as minus 26°C near Zurich, Switzerland (Keller 1987).

Entomophthora floridana Weiser and Numa a fungal pathogen of the twospotted spider mite, *Tetranychus urticae* (Koch) remains viable and infective during the winter months in eastern North Carolina (Brandenburg and Kennedy 1981). Fungal development and infection of the mites occurs at 5°C although reduced from that at higher temperatures. *Entomophthora floridana* however, is believed to form resting spores in more northern climates (Carner 1976).

Insect viruses are also important natural population regulators of some pest insects. *Trichoplusia ni* (Hübner), an important pest of cole crops is suppressed by epizootics of the virus or by applications of it to cabbages. A virus-infected insect produces copious amounts of virus. When the insect dies, it falls to the soil surface, ruptures, and releases the virus. During cultural practices, the virus is mixed with the top few cm of soil where it can overwinter and serve as reservoir to contaminate plants and initiate an epizootic the following growing season (Jaques 1974).

This paper reviews knowledge on efficacy of insect pathogens once they have survived winters in the temperate zone where temperatures reach minus 30°C. It is generally understood that fungi withstand these temperatures by remaining within cadavers, buried as psuedosclerotia and sclerotia, under the protective cover of soil or as endophytes in crop residue. Microsporida, on the other hand, essentially are dependent on host tissue for protection from subfreezing temperatures. Viruses survive under a cover of soil. Little is known about the intricacies of the overwintering mechanisms. Could molecular biology, molecular technology, and molecular genetics be utilized to provide fungi and microsporidia with increased winter survival? If so, these organisms could possibly play an even greater role in managing pest insects.

REFERENCES CITED

Bergman, P.W., R.A. Davis, S.N. Fertig, F. Kuchler, R. McDowell, C. Osteen, A.L. Padula, K.L. Smith, and R.F. Torla. 1985. Pesticide assessment of field corn and soybeans: corn belt states. Nat. Agric. Pesticide Imp. Assess. Prog., USDA-ARS-ERS Staff rep. No. AGES850524A.

Bing, L.A., and L.C. Lewis. 1993. Occurrence of the entomopathogen *Beauveria bassiana* (Balsamo) Vuillemin in different tillage regimes and in *Zea mays* L. and virulence towards *Ostrinia nubilalis* (Hübner). Agriculture, Ecosystems and Environment 45: 147-156.

Bing, L.A., and L.C. Lewis. 1991. Suppression of *Ostrinia nubilalis* (Hübner) (Lepidoptera: Pyralidae) and endophytic *Beauveria bassiana* (Balsamo) Vuillemin. Environ. Entomol. 20: 1207-1211.

Brandenburg, R.L., and G.G. Kennedy. 1981. Overwintering of the pathogen *Entomophthora floridana* and its host, the twospotted spider mite. J. Econ. Entomol. 74:428-431.

Carner, G.R. 1976. A description of the life cycle of *Entomophthora* sp. in the twospotted spider mite. J. Invertebr. Pathol. 28:245-254.

Derrick, M.E., and W.B. Showers. 1990. Relationship of adult European corn borer (Lepidoptera: Pyralidae) in action sites with egg masses in the corn field. Environ. Entomol. 19: 1981-1085.

Duncan, D.B. 1955. Multiple range and multiple F tests. Biometrics 11:1-41.

Ignoffo, C.M., C. Garcia, D.L. Hostetter, and R.E. Pinnell. 1978. Stability of conidia of an entomopathogenic fungus, *Nomuraea rileyi*, in and on soil. Environ. Entomol. 7:724-727.

Jaques, R.P. 1974. Occurrence and accumulation of viruses of *Trichoplusia ni* in treated field plots. J. Invertebr. Pathol. 23:140-152.

Keller, S. 1987. Observations on the overwintering of *Entomophthora planchoniana*. J. Invertebr. Pathol. 50:333-335.

Lewis, L.C. 1995. Effect of *Nosema pyrausta* and temperature on egg production by *Ostrinia nubilalis*. Proceedings of the XVIII Conference of International Working Group on *Ostrinia*, Turda, Romania, September 11-16, 1995, pp. 55-62.

Lewis, L.C., and L.A. Bing. 1991. *Bacillus thuringiensis* Berliner and *Beauveria bassiana* (Balsamo) Vuillemin for European corn borer control: Program for immediate and season long suppression. Can. Entomol. 123: 387-393.

Lewis, L.C., and J.E. Cossentine. 1986. Season long intraplant epizootics of entomopathogens, *Beauveria bassiana* and *Nosema pyrausta* in a corn agroecosystem. Entomophaga 31: 363-369.

Lewis, L.C., and R.E. Lynch. 1970. Treatment of *Ostrinia nubilalis* larvae with Fumidil B to control infections caused by *Perezia pyraustae*. J. Invertebr. Pathol. 15: 43-48.

Lewis, L.C., R.E. Lynch, and W.D. Guthrie. 1971. Biology of European corn borers reared continuously on a diet containing Fumidil B. Ann. Entomol. Soc. 64: 1264-1269.

Mason, C.E., M.E. Rice, D.D. Calvin, J.W. Van Duyn, W.B. Showers, W.D. Hutchison, J.F. Witkowski, R.A. Higgins, D.W. Onstad, and G.P. Dively. 1996. European corn borer: Ecology and management. North Central Regional Extension Publication No. 327, Iowa State University, Ames, Iowa. 57 pp.

Pedigo, L.P., E.J. Bechinski, and R.A. Higgins. 1983. Partial life tables of the green cloverworm (Lepidoptera: Noctuidae) in soybean and a hypothesis of population dynamics in Iowa. Environ. Entomol. 12: 186-195.

Pendland, J.C. 1982. Resistance structures in the entomogenous hyphomycete, *Nomuraea rileyi*: an ultrastructural study. Can. J. Bot. 60: 1569-1576.

Sajap, A.S., and L.C. Lewis. 1992. Chronology of infection of European corn borer (Lepidoptera: Pyralidae) with the microsporidium *Nosema pyrausta*: Effect of development and vertical transmission. Environ. Entomol. 21: 178-182.

Saleh, M.M.E., L.C. Lewis, and J.J. Obrycki. 1995. Selection of *Nosema pyrausta* (Microsporidia: Nosematidae)-infected *Ostrinia nubilalis* (Lepidoptera: Pyralidae) eggs for parasitization by *Trichogramma nubilale* (Hymenoptera: Trichogrammatidae). Crop Protection 14:327.330.

Showers, W.B., G.L. Reed, J.F. Robinson, and M.B. DeRozari. 1976. Flight and sexual activity of the European corn borer. Environ. Entomol. 5: 1099-1104.

Sprenkel, R.K., and W.M. Brooks. 1977. Winter survival of the entomogenous fungus *Nomuraea rileyi* in North Carolina. J. Invertebr. Pathol. 29: 262-266.

Sutton, R.M., W.A. Gardner, D.W. Kraus, and R. Noblet. 1979. Effects of ecdysone, juvenile hormone, and structurally-related compounds on *Nomuraea rileyi*, *Beauveria bassiana*, and *Tritirachium dependens in vitro*. J. Ga. Entomol. Soc. 14: 364-373.

Thorvilson, H.G., L.C. Lewis, and L.P. Pedigo. 1985. Overwintering potential of *Nomuraea rileyi* (Fungi-Deuteromycotina) from (Lepidoptera: Noctuidae) cadavers in central Iowa. J. Kansas Entomol. Soc. 58: 662-667.

Tyrrell, D., D.M. MacLeod, and D.R. Wallace. 1976. Overwintering survival of *Entomophthora aphidis* resting spores. Proceedings of the International Colloquium on Invertebrate Pathology, pg. 430-431, Kingston, Ontario, Canada.

Zimmack, H.L., and T.A. Brindley. 1957. The effect of the protozoan parasite *Perezia pyraustae* Paillot on the European corn borer. J. Econ. Entomol. 50:637-640.

ACKNOWLEDGMENTS

Impact of Freezing and Thawing of Soils on Microbiology and Pesticide Degradation Potential

J. SCHULZE-AURICH[1] AND M. LEHMANN[2]

ABSTRACT

Two soils, a silt loam and a loamy sand, were stored for about 6 months at -20°C. After thawing soil was equilibrated at room temperature and at 4°C until the soil respiration was constant and at the same level as measured for fresh soil. The degradation of a model compound (i.e. extent of mineralization, degradation kinetics and formation of degradates) was compared in fresh and stored soil (after equilibration). The model compound used was proven to be degraded primarily by microbial processes. The microbiology of the soils (fresh and stored) was determined by plate counts and phospho-lipid-fatty-acid analysis (PLFA analysis).

Comparison of the results achieved for fresh and stored soils showed, that freezing did not significantly influence the degradation of the compound. The microbial population in stored soils was reduced for up to 53% compared to fresh soils, but was still analogous to agricultural soils. It is concluded, that storage, including freezing and thawing processes, of the investigated soils did not significantly alter their biological potential for the degradation of pesticides. Therefore it is concluded that storage of soils at -20°C may be a reasonable alternative to storage in the greenhouse or sampling of fresh soils from the field.

Key words: Freezing of soil, biomass, pesticide degradation

INTRODUCTION

The optimum condition for the storage of test soils intended to be used for pesticide degradation studies in the laboratory still is an open question. For the comparison of results of different pesticide soil degradation studies, the major biological, chemical and physical parameters of the soils must either be sufficiently characterized or standardized. Since it is not possible to completely characterize all mechanisms contributing to the fate of a chemical in soil, certain standards are required. The variations of the biological activity of field soil according to season and actual climatic conditions is a permanent process. Therefore the results of laboratory soil metabolism studies conducted with freshly collected soil samples may vary depending on the actual biological state of the collected soil samples. Furthermore the pre-incubation conditions of soil samples, i.e. the acclimatization to the new environment, before application of the chemical to be investigated are also important for the adaptation of the soil biology. One method to overcome the problem of seasonal and weather caused variations is the storage of soils in the greenhouse. This method has been applied at our testing facilities for many years and facilitates the conduct of comparable soil degradation studies all over the year. A further improvement to prevent changes of the soil biology would be the possibility of storage under deep freezing. The question of the feasibility of this storage method without destruction of the biological activity of the soil is still open and was also discussed in the "OECD Workshop on Selection of Soils/Sediments (1995)". In the final report of the workshop the requirement for further investigations concerning this question was pointed out. The results of earlier published studies dealing with this issue are very contradictory. Rugbjerg et al. (1989) investigated the mineralization of Atrazine and TCA. The freezing process was considered not to influence the degradation process. Also Ross et al. (1980) reported the temperature of -20°C to be the most suitable for soil storage. In contrast other authors (Zelles et al. (1991) and Malkomes et al.(1989)) recommend storage at 4°C.

The purpose of the present study was to help clarify uncertainties regarding appropriate storage conditions for soil samples. The degradation of a model compound in fresh and stored (deep frozen at -20°C for 6 months) soil samples was determined. Microbiological characterization of fresh and stored soils was performed

by plate counts and PLFA analysis (Phospho-Lipid-Fatty-Acid).

MATERIALS AND METHODS

Model compound and degradation products

For the determination of the soils pesticide degradation potential a compound (model compound) with the following characteristics was chosen: 1) Short half life time (2-4 days), 2) Well established degradation pathway and major degradates resulting from microbial degradation (Major Pathway [because of confidentiality only a symbolic pathway can be shown]:

Parent Compound → MB1 → MB5 → MB4
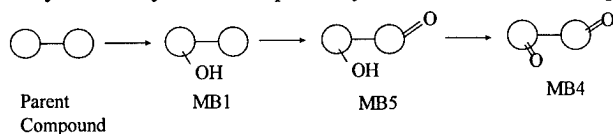
A ^{14}C-labelled Novartis Crop Protection AG compound (recommended field rate: 300 g/ha) was used. Radiopurity: >97.8 %, Specific activity: 2.12 MBq/mg.

Unlabelled model compound was used for dilution of the radioactive material and as reference compound. ^{14}C-labeled degradation products of the model compound generated in an earlier metabolism study were used as reference compounds.

Soil

Soil samples were taken from two locations in Switzerland, their properties, duration and condition of storage are given in Table 1. Before storage or use, the soils were sieved through a 2-mm sieve and adjusted to 40% MWC (Maximum Water-holding Capacity).

Table 1:   Origin, Properties and Storage of Soils

Soil Characteristic	Gartenacker	Collombey
Origin	Les Barges VS, Switzerland	Collombey VS, Switzerland
Classification (USDA)	silt loam	sandy loam
pH	7.25	7.40
C$_{org}$ (%)	2.20	1.70
N total (%)	0.29	0.21
CaCO$_3$ (%)	9.20	7.20
Particle size:		
Clay (%)	9.60	6.20
Silt (%)	49.00	15.20
Sand (%)	41.40	78.60
MWC (g H$_2$O / 100 g Soil)	66.82	46.68
FC (g H$_2$O / 100 g Soil)	48.92	36.15

METHODS AND CONDUCT OF EXPERIMENTS

Soil respiration and biomass determination

The respiration and microbial biomass of soil samples was determined using the method of Anderson et al. (1978). The oxygen consumption was measured with a Voit-Sapromat.

Pre-equilibration of soil

Before conducting the pesticide degradation study the time necessary for equilibration of the soils to ambient conditions after thawing was determined. Soil equilibration was proven by measurement of the soil-respiration. It was proceeded on an assumption that the state of equilibrium was reached at constancy of soil respiration. Soil samples were stored in plastic bags containing 600-800 g soil. For the equilibration experiments the bags were opened and incubated at the appropriate temperatures. In one set of samples respiration of Gartenacker soil was determined before storage and after thawing at ambient temperature (storage conditions: 5 days at -20°C, measurements: 6 h, 1, 3, 10 and 20 days after thawing). In a second set of samples identical soil samples were thawn at 4°C. After 3, 6, 10 and 20 days respiration measurements were conducted. The appropriate soil samples were wormed up to ambient temperature 24 h before measurement. For all samples the soil moisture was adjusted to 40% MWC before start of biomass determination.

Preparation of the radiolabeled model compound

The radiolabelled material was mixed with the unlabelled compound to reduce its radioactivity: Resulting specific activity: 0.7 MBq/mg.

Preparation, treatment and incubation of soils

For the pesticide degradation experiments soil samples (thawing: 24 hours at 20°C, pre-equilibration time: as determined in the pre-equilibration experiments) corresponding to 100 g soil dry weight were placed into open all-glass gas-flow-systems. The systems were continuously ventilated with air at a flow rate of 60 ml/min. The effluent air was passed through two CO$_2$ traps (2 N NaOH; each about 50 ml). Samples were incubated in climatization chambers at 20°C in the dark for up to 50 days.

Extraction of soil samples

The whole content of one incubation flask was three times extracted with about 200 ml acetonitrile:water (80:20, v/v) followed by one extraction with water and a final extraction with 100% acetone (cold extract). The radioactivity in extracts was determined by liquid

scintillation counting (LSC). After extraction at room temperature the soil samples were extracted in a Soxhlet apparatus with acetonitrile for 8 hours (Soxhlet-extract).

HPLC analysis of the extracts

For HPLC analysis (identification and quantification of the parent compound and its degradates) aliquots of the extracts (cold extracts) were concentrated by evaporation of the solvent under reduced pressure.

CO₂ traps

The radioactivity in the trapping solutions (NaOH) was determined by LSC without further preparation of the samples.

Non-extractable Radioactivity

The extracted soil was air-dried, weighed, homogenized and the residual radioactivity determined by combustion of the organic material (radioactive material to $^{14}CO_2$), reabsorption in szintillation cocktail and LSC.

PLFA and plate count analysis

For the characterization and quantification of microorganisms present in the soil samples phospho-lipid-fatty-acid (PLFA) and total-plate-count analysis were performed (by contract lab Solvit, Kriens, Switzerland). For the PLFA analytical method see J. Korner et al. (1992). The total-plate-count method was as follows: 2x5g soil were suspended in 45 ml Ringer's solvent and stirred for 15 min. After soil has precipitated the supernatant was decanted. From the supernatant dilutions between 10^{-3} and 10^{-6} were prepared using Ringer's solvent. Samples of all dilutions were spread on petri plates containing the growth media listed below and incubated at 20 - 22°C in the dark for 7 - 10 days (Environmental Protection Agency).

Plate count growth media:

1) Bacteria Total Plate Count: Plate Count Agar Difco 0479-01-1. 2) Actinomycetes Growth Medium: Actinomycete Isolation Agar Base Difco 1831 17-4; containing Difco Bacto-Glycerol. 3) Fungy Growth Medium: Rose Bengal Base Difco 1831-17-4; containing Chloramphenicol.

High performance liquid chromatography (HPLC)

HPLC analysis was carried out on a *Spectra Physics* Liquid Chromatograph equipped with a Berthold radioactivity monitoring system. Radioactive fractions were quantified using the Berthold evaluation software.

HPLC Running Conditions:

Column: Nucleosil C-18 (*Macherey-Nagel*) length: 25 cm, i.d.: 4.6 mm, particle size: 5 µm. Temperature: 40°C. Mobile Phase: Eluent A:Water, Eluent B: Acetonitrile. Flow rate: 1 ml/min. Detectors: UV/VIS (298 nm), RAM (Berthold, cell volume:150µl)

Calculations

Data were fitted by using the following two compartment model:

$$C_t = C_{01} \bullet e^{-k_1 \bullet t} + C_{02} \bullet e^{-k_2 \bullet t}$$

C_t:	concentration of the test substance at time t.
C_{01}:	average initial concentration of the test substance in compartment 1.
C_{02}:	average initial concentration of the test substance in compartment 2.
k_1:	rate constant of reactions in compartment 1 (fast degradation reactions).
k_2:	rate constant of reactions in compartment 2 (slow degradation reactions).
t:	time.

Data were fitted using the MicroCal Origin 3.5 (MicroCal Software Inc.) software program. The overall disappearance times for 50 % (DT_{50}) and 90% (DT_{90}) of the parent molecule and its major degradate were calculated by iteration.

RESULTS

Pre-equilibration of soil

Gartenacker soil samples stored at -20°C (5 days) were thawn and equilibrated at 20°C or 4°C (stored soils). The respiration (oxygen consumption) of the latter samples was compared with fresh soil (Fig. 1).
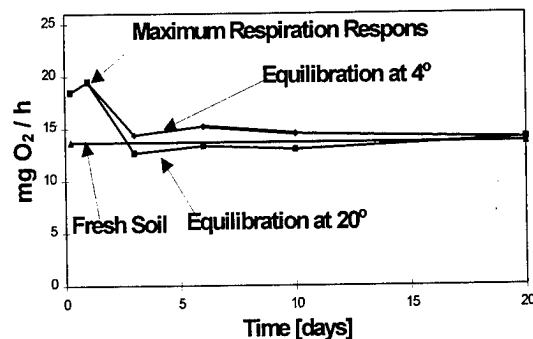
Figure 1: Soil Respiration during Equilibration

For stored soils, independent of the equilibration temperature, respiration reached a maximum within 6 hours after start of equilibration. Thereafter the amount of O_2 consumed decreased and was reaching its equilibrium level after 20 days. At that time the oxygen
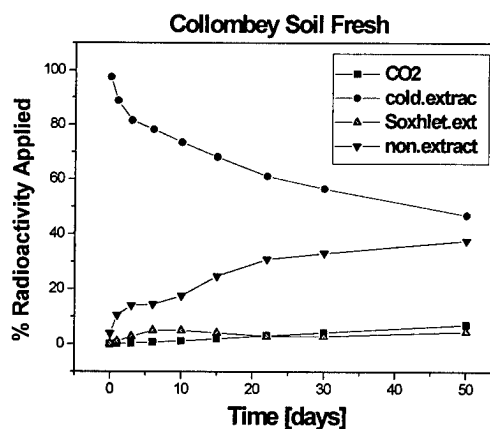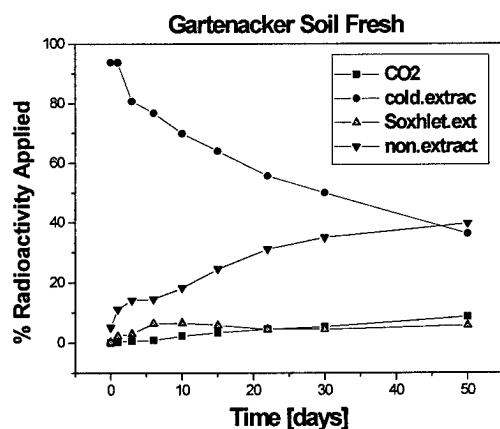
Figure 2: Distribution of radioactivity during degradation of the model compound in fresh and stored Gartenacker soil

Figure 3: Distribution of radioactivity during degradation of the model compound in fresh and stored Collombey soil

consumption of the stored and fresh soils were identical. According to the latter results the stored soils, used for the model compound degradation studies, were equilibrated for 20 hours at 4°C (to prevent loss of water) before application of the model compound.

Degradation of the model compound in fresh and stored non-sterile soils

The degradation studies were performed in Gartenacker and Collombey soil.

Recovery and distribution pattern of radioactivity

The extractable portion of the radioactivity (cold-extract and Soxhlet-extract) was above 90% in all samples at day 0. At the end of the incubation time the extractability was in the range between 42.00 and 52.94% for stored and fresh Gartenacker and Collombey

soils, respectively. Unextractable radioactivity reached values between 33.38 and 39.64% of the totally applied radioactivity after 50 days in the same samples. Rates of mineralization were also very similar for the latter soil samples. At the end of the study, cumulative production of $^{14}CO_2$ reached 6.4 - 8.63% of the total radioactivity in all samples. The kinetic of formation of $^{14}CO_2$ was not different during the 50 days incubation interval between fresh and stored soils (Fig. 2 and 3).

Degradation of the model compound

The compound was degraded to the identical products as found in earlier degradation studies (Gonzalez/Schulze-Aurich 1996, Schulze-Aurich 1996). Besides the unchanged model compound metabolites MB1, MB4 and MB5 were detected as major products (Fig. 4 and 5). Identification of the degradates was performed by HPLC co-chromatography.

502

Gartenacker Soil Fresh

Collombey Soil Fresh

Gartenacker Soil Stored

Collombey Soil Stored
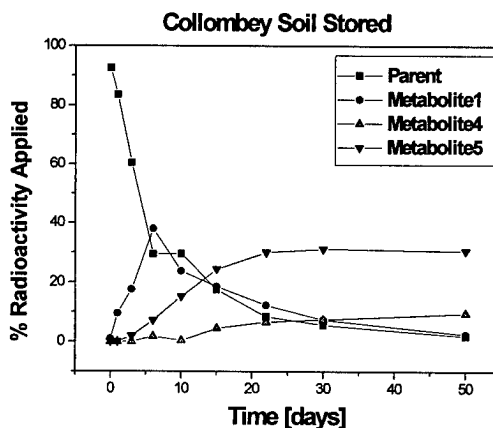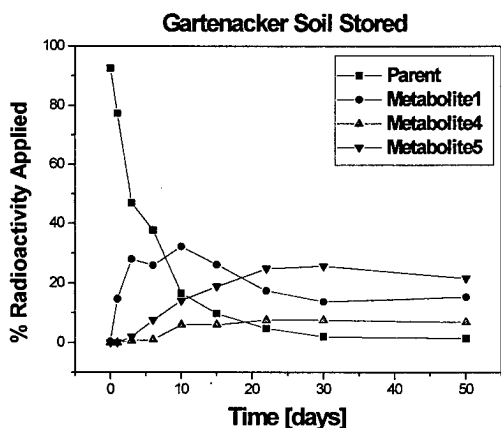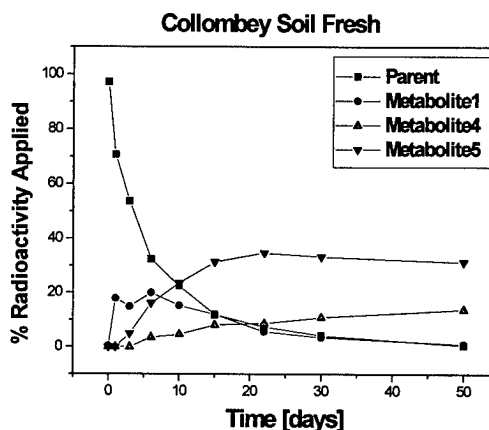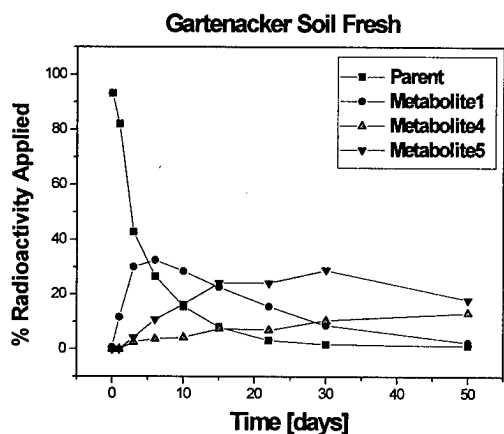
Figure 4: Distribution of the model compound and its metabolites in fresh and stored Gartenacker soil

Figure 5: Distribution of the model compound and its metabolites in fresh and stored Collombey soil

The degradation kinetic of the parent compound was not significantly different in fresh and stored soils. The results are shown in Table 2.

As observed for the parent compound, the degradation kinetic of the primary formed metabolite (MB1) did not significantly differ in stored and fresh soils (see Table 3).

Table 2: Degradation half-life times of the model compound in stored and fresh Gartenacker and Collombey soils

	Kinetics of Degradation of the Model Compound			
	Gartenacker		Collombey	
	fresh	stored	fresh	stored
DT-50	3.2	3.6	3.2	4.5
DT-90	13.0	16.0	19.0	23.0

DT-50: degradation half life time (50% degradation)
DT-90: 90% degradation

Table 3: Degradation half-life times of metabolite MB1 in stored and fresh Gartenacker and Collombey soils

	Kinetics of Degradation of Metabolite MB1			
	Gartenacker		Collombey	
	fresh	stored	fresh	stored
DT-50	13.6	9.0	10.0	7.7
DT-90	14.5	12.0	33.0	42.0

DT-50: degradation half life time (50% degradation)
DT-90: 90% degradation

At the end of the incubation time (50 days) only 1.28 and 1.45% of the model compound were determined in fresh and stored Gartenacker soil, respectively. The same figures were determined for Collombey soil were the model compound was degraded to 0.64 and 1.88% in fresh and stored soil samples, respectively.

In fresh Gartenacker soil MB1 was reaching with 32.50% its maximum at day 6 and decreased to 2.37% after 50 days. In stored Gartenacker soil MB1 was at its maximum within 10 days and accounted for 32.32% at that time. At the end of the study MB1 amounted to 1.45% in the same soil. In Collombey soil similar results

503

were achieved. MB1 was reaching its maximum in fresh and stored soils after 6 days of incubation and accounted for 20.01 and 38.05% in both soils, respectively. After 50 days MB1 accounted for only 1.06 and 2.48% in the same soils, respectively.

All other metabolites formed (MB4 and MB5) were practically not degraded during the incubation time (see Fig. 4 and 5). The amounts of both metabolites formed during the 50 days incubation period were not significantly different in the fresh and stored soils.

Degradation of the model compound in sterile Gartenacker soil

In order to show that the model compound is primarily degraded by microbes, a degradation study in sterilized Gartenacker soil was performed. After 6 days of incubation at 20°C, 88.04% of the radioactivity was extractable. In the extract only the unchanged parent compound was detected. Practically no mineralization (0.03% $^{14}CO_2$) occurred during the incubation time.

Respiration of soils, PLFA-analysis and plate-counts

Respiration of Soils:

The respiration of soil samples used for the degradation study was determined before and after storage at -20°C (after equilibration at 20°C) and before and after incubation of the samples used for the degradation experiment. The results are listed in Table 4.

Table 4:   Biomass (Respiration Method) of the Soils used for the Degradation Study
(mg biomass C/100 g dry soil)

Soil	Before Storage at -20°C	Before Incubation (Degradation Study)	After Incubation (Degradation Study)
Gartenacker fresh		55	38
stored	55	55	47
sterile		0	0
Collombey fresh		38	30
stored	51	53	41

The respiration response of the stored soil samples and therefore the microbial biomass calculated thereof were identical before storage and after thawing (after pre-equilibration). These numbers confirm that the time of pre-equilibration was sufficient. Biomass values for all soils dropped slightly during the incubation time for the degradation study, which usually occurs under laboratory conditions.

Sterilized soils showed no respiration response thus demonstrating the sterility of the samples.

PLFA-analysis and plate-counts before and after storage:

The results of the PLFA- and Plate-Counts analysis are shown in Figure 6.

The number of all PLFA fractions and therefore the number of microorganisms were significantly reduced (Reduction: plate counts: 64-72%, PLFA: 41-51%) in the stored soil samples (after thawing and pre-equilibration). Additionally the microbial community structure was altered, i.e., the relative amount of actinomycetes was increased.

PLFA-analysis and plate-counts before storage and 6 hours after thawing:

An additional experiment was performed to resolve the initial increase of the respiration response determined during the pre-equilibration experiments
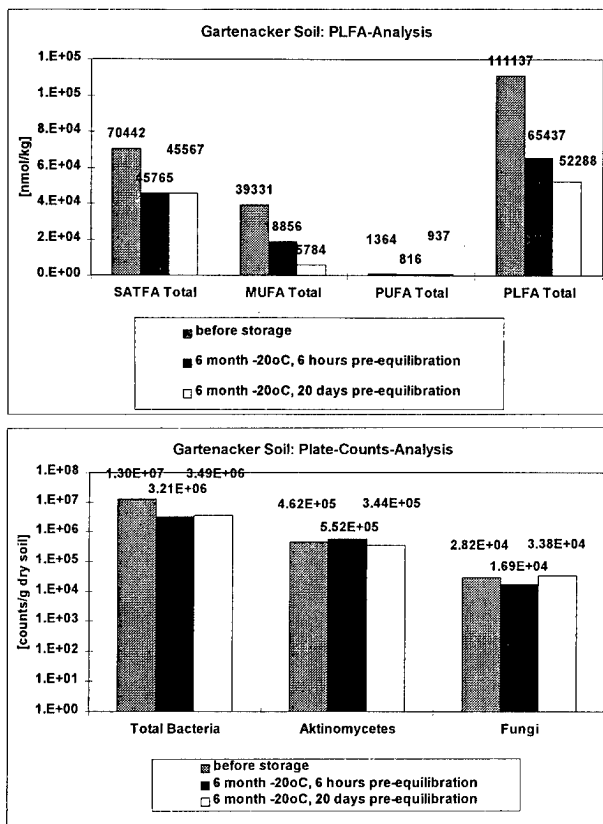
SATFA: Saturated Fatty Acids
MUFA: Mono Unsaturated Fatty Acids
PUFA: Poly Unsaturated Fatty Acids
PLFA: Total Phospho Lipid Fatty Acids

Figure 6:   Plate count and PLFA analysis of Gartenacker and Collombey soil before and after storage
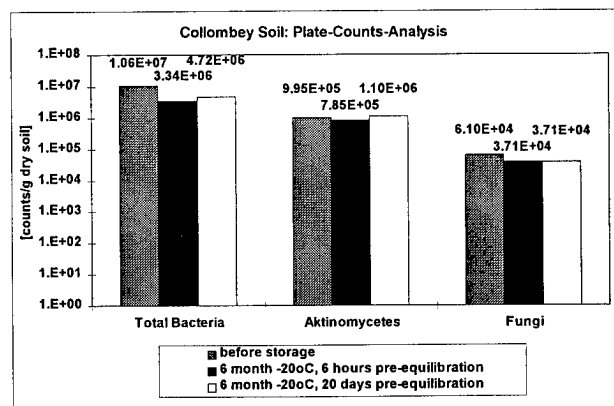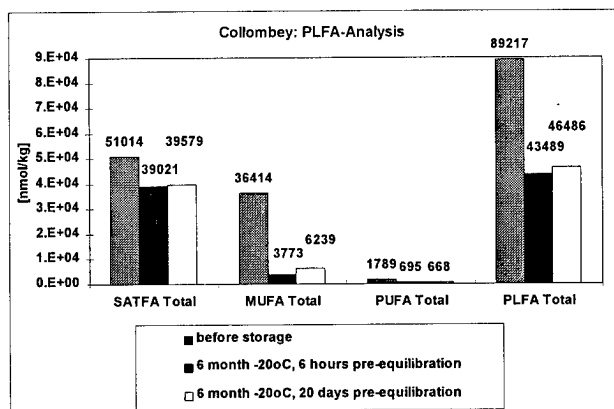
504

Collombey: PLFA-Analysis

Collombey Soil: Plate-Counts-Analysis

SATFA: Saturated Fatty Acids
MUFA: Mono Unsaturated Fatty Acids
PUFA: Poly Unsaturated Fatty Acids
PLFA: Total Phospho Lipid Fatty Acids

Figure 6:   Plate count and PLFA analysis of Gartenacker
(con't.)   and Collombey soil before and after storage

6 hours after thawing of the soils (see Fig. 1 : "maximum respiration response"). As shown in Fig. 6 the values of the plate counts and PLFA analysis were not significantly different for soil samples incubated for 6 hours and 20 days after thawing.

DISCUSSION AND CONCLUSION

To improve the storage conditions of soils used for pesticide degradation studies the pesticide degradation potential and changes of biomass and microbial populations of two soils (a silt loam and a sandy loam) were determined before and after freezing and thawing.

For the degradation study a model compound was used which was primarily degraded by microorganisms (practically no degradation was observed in sterilized soil: justification for its use as test chemical to determine the change of the microbiological degradation potential in soils).

The results of the degradation study were equivalent for fresh and stored Gartenacker and Collombey soils. No significant deviations between the degradation kinetics of the parent compound, the nature and quantity of the metabolites, and the rate of mineralization (formation of $^{14}CO_2$) were determined.

Stored soils, after thawing, were shown to return to the same respiration response after pre-equilibration for 20 days. In contrast the microbial population examined by plate counts and PLFA-analysis was significantly altered after freezing and thawing. The number of microbes per kg soil were decreased by up to 51% (PLFA-analysis) and 72% (plate counts).

Comparing the PLFA amounts of Gartenacker and Collombey soils after storage with published data of agricultural soils (Zelles et al. (1991)) shows that the number of microorganisms was still in the same range as measured in agricultural soils. Therefore the observed decrease in number of microorganisms did obviously not result in a abnormal decrease of the biological activity of the soils. The latter thesis is supported by the results of the pesticide degradation and the respiration response experiments, which were showing no significant influence of the freezing and thawing procedure. The reduction of the number of microorganisms may be compensated by a higher activity of the remaining microbial population as shown by the PLFA and plate-counts analysis 6 hours after thawing (see pre-equilibration experiments Fig.1: "maximum respiration response").

In conclusion, the present study has shown that storage of soils at -20°C had no significant influence on the pesticide degradation capacity of soils, although the number and composition of microorganisms were significantly changed. Therefore storage under these conditions may be a reasonable alternative to storage in the greenhouse or sampling of fresh soils for each experiment. From field soils we know that, depending on the climatic conditions, microbial populations can drop down to 90% of their normal value without loosing its fertility. Even storage under cover (grass, etc.) in the greenhouse does not prevent the soil from losing a part of its microbial biomass. However, if soils are stored at -20°C it is advisable to check, after pre-equilibration (20 days), their biological activity by PLFA analysis and short-term respiration measurements prior to use. However, further investigations with other soils and compounds are needed.

505

REFERENCES

Anderson J.P.E., Domsch K.H.; "A physiological method for the quantitative measurement of microbial biomass in soils", Soil Biol.Biochem. 10, 215-221, [1978].

Environmental Protection Agency recommendation (personal communication).

Gonzalez-Valero J.F., J. Schulze-Aurich; Novartis Crop Protection AG internal Project Report 93GJ01 [1996].

Korner J., Laczko E.; "A new method for assessing soil microorganism diversity and evidence of vitamin deficiency in low diversity communities", Biol Fertil Soils 13, 58-60 [1992].

Malkomes H.-P.; "Identification of herbicide effects on microbial activities in soil samples after storage", Zentralbl. Mikrobiol. 144, 389-398 [1989].

OECD Workshop on Selection of Soils/Sediments, "Final report of the OECD workshop on selection of soil/sediments", Belgirate Italy Final Report; [1995].

Ross D.J., Tate K.R., Cairns A., Meyrick K.F.; "Influence of storage on the microbial biomass estimated by three biochemical procedures", Soil. Biol. Biochem. 12, 369-374 [1980].

Rugbjerg D., Helweg A.; "14C-labelled TCA and Atrazine degradation in soil: Influence of freezing and air-drying", 6th Danish Plant Protection Conference, Side Effects of Pesticides, Weeds, 23-31 [1989].

Schulze-Aurich J.; Novartis Crop Protection AG internal Project Report 94GJ01 [1996].

Zelles L., Adrian P., Bai Q.Y., Stepper K., Adrian M.V., Fischer K., Maier A., Ziegler A.; "Microbial activity measured in soils stored under different temperature and humidity conditions", Soil. Biol. Biochem. 23, 955-962 [1991].

506

Snowmelt Saturation Restricts Scots Pine Growth
on Fine-Grained Tills in Lapland

R. SUTINEN[1], P. HÄNNINEN[2], K. MÄKITALO[3],
S. PENTTINEN[1] AND M.-L. SUTINEN[3]

ABSTRACT

Dielectric properties of till soils in Central Finnish Lapland were determined using time domain reflectometry (TDR) and radar surface arrival detection (RSAD) to study water relations at the growth sites occupied by adult Scots pines and at sites artificially regenerated by pine. It was found that low dielectric values ($\varepsilon < 13$) and water content ($\theta < 0.20$ cm^{3}cm^{-3}) were typical to sites occupied by adult pines and sites where artificial regeneration of pine has succeeded. High dielectric values and water content were observed at the sites, where artificial regeneration of pine has failed. At these sites snowmelt induced soil saturation ($\varepsilon > 30$, $\theta > 0.40$ cm^{3}cm^{-3}) lasted two to five weeks in the early summers 1995 and 1996. A combination of slow water seepage through fine-grained till and slow soil warming in Lapland seem to result in unfavourable growth conditions for Scots pine.

Key words: Scots pine, till soil, dielectric properties, snowmelt.

INTRODUCTION

The nature and distribution of soils determine what trees grow where. Different tree species have their specific requirements for soil moisture, soil acidity and nutrient content. Habitats of tree species are also controlled by temperature, precipitation and topography. The available water, however, may be one of the most important factors in determining the distribution of tree species. Scots pine (*Pinus Silvestris*) is on of the most important species in the Finnish forest industry. Typically pine tend to favor well-drained coarse-textured soils, but artificially regeneration of this species has been tried on a wide variety of sites.

Till is the predominant sediment type on glaciated terrains and in Finland till covers over 75% of the land area. Its textural, mineralogical, geochemical and geophysical and hydraulic properties, however, are highly variable due to the source rock types, sedimentological processes and degree of weathering. Since a major part of Finnish forests are on soils derived from tills, variability of

tills has an crucial effect on selection of natural tree species and, along with temperature, largely determines the forest dynamics near timberline. The spatial variability of tills, geodiversity, forms the framework determining what kind of tree patterns can be developed. Since soil moisture content varies seasonally, it is necessary to know the range limits required and tolerated by the different tree species.

METHODS

Geology and tree species composition

The study sites are located 150-200 km north of the Arctic Circle in Central Lapland, where tills are local in origin and the transport distances are only a few hundreds of meters or even less. Therefore, source rocks have a strong influence on the physical properties of tills. The bedrock outcrops, less than 5% of the land area, are located at the highest and steep-sloped hills. These are composed of erosion-resistant rock types such as quartzites and granites.

Two major geological features can be separated in the study area, the Central Lapland Greenstone Belt in the south, and the granulite complex in the north. The rocks of the greenstone belt are composed of mostly fine-grained basic (albite-amphibole schists) and ultrabasic volcanites (chlorite-amphibole schists) with interlayers of carbonate-rich rocks and mica schists. Relatively small coarse-grained granitic bodies and gabbro complexes occur in the greenstone belt area. Rock types of the granulite complex are highly metamorphosed, garnet-bearing quartz-feldspar gneisses and consequently contain poorly soluble minerals.

Soil dielectric properties and temperature were studied at sites with varying tree species compositions. Scots pine stands are present at sites where till is derived from granulite, gabbro (Hanhilehto site) and on outwash

sand deposits (Liesi site). Norway spruce and pubescent birch are present on till derived from chlorite-amphibole schists (Vaalolehto site) and from intermediate metavolcanic rocks (Äältövittikko site) and rock types associated with komatites (Kuorajoki site).

Dielectric techniques

Time domain reflectometry (TDR) is the technique commonly used for soil moisture determinations (Topp et al. 1980). We used TDR for pointwise dielectric measurements at growth sites of coniferous tree spesies and for monitoring purposes. Radar surface arrival detection (RSAD, Sutinen and Hänninen 1990) with a 100-MHz transmitter and 300-MHz receiver with 3-m TX-RX spacing, was used for continuous dielectric profiling at survey plots 1 ha each. Ten-meter line spacing and an average speed of 4 km/h were used. Both TDR and RSAD, operating in the radio frequency range, measure the travel time (t) of electromagnetic waves along the transmission line inserted into the soil and parent till materials (TDR) and along the soil surface (RSAD). The propagation velocity (v) is dependent on the dielectric coefficient (ε) of the soil such that $v=L/t$ and c/ε, where c is the free space velocity ($3*10^8$meter/second). Hence $\varepsilon=(c*t/L)^2$, where L is the length of the transmission line. Two to three 15-cm-long steel probes were used in TDR measurements. There has been reported by several authors (e.g Topp et al. 1980) that bulk dielectric properties are closely related to volumetric water content. The empirical formula $\theta_v= -0.06+0.024\varepsilon-0.00037\varepsilon^2+0.000003\varepsilon^3$ based on the data from Sutinen (1992) has been used here to calculate water content.

We used a commercial TDR unit (Trase by Soilmoisture Equipment Corp.) for determining dielectric properties at the growth sites of old Scots pines and Norway spruces. Another brand of TDR (Tektronix 1502B metallic cable tester) was used for monitoring purposes at selected sites. Permanent parallel

508

steel probes were installed into soil sequences for manual recording of ε at a weekly basis and automatic recording with TDR and data loggers (Campbell CR10 with SDMX50 multiplexers). SIR-8 and SIR-10 radar units (Geophysical Survey Systems, Inc.) were used for RSAD surveys. Soil and air temperature was recorded manually with Beamex TC 305 temperature calibrator and automatically with Campbell CR10 data loggers using PT-100 temperature sensors (Sensycon).

RESULTS AND DISCUSSION

Dielectric properties of tills

Dielectric properties of the growth sites of Scot pine and Norway spruce differ significantly such that dielectric coefficients of the growth sites of virgin Scots pines predominantly are ε<13 (equivalent to water content θ_v<0.2 cm³cm⁻³, Fig. 1). The growth sites of old spruces, in contrast, show a largedielectric range from ε=6 to ε=36 (0.07<θ_v<0.46 cm³cm⁻³). The bulk dielectric value is primarily determined by the free water content. This is because in the soil dielectric mixture of unfrozen free water (ε=80) dominates over rock particles (ε=6, Hänninen and Sutinen 1994), air (ε=1) and bound water (ε=3.5). The low free water content at the pine sites is an indication of large air/oxygen volume. In contrast, high free water content at spruce sites indicates low air/oxygen volume.

The grain size distribution of the tills are significantly different depending on the source rock types in Lapland. The fine fraction content (d<60 μm) of the till in the greenstone belt, for example, is about 50% (Fig. 2). On the other hand, granulite till contain 30% of fines. The dielectric data collected at the same sites follow similar trend. The mean dielectric value of chloriteamphibole till (at Vaalolehto site measured with RSAD on 6 June 1995 is 22.9, of granulite till 14.2 (RSAD on 10 June 1995) and of
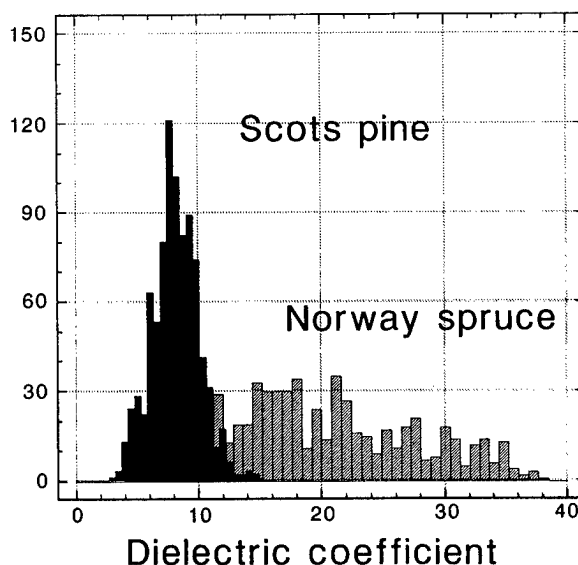
Figure 1. Distribution of dielectric values at the growth sites of adult Scots pines (=870) and Norway spruces (=760) in Central Lapland, measured using TDR with 15 cm-long parallel steel probes inserted vertically into soil.

outwash sand 8.1 (RSAD on 7 June 1995).

The tree species composition follow this trend such that fine-grained till is occupied by Norway spruce and pubescent birch. Scots
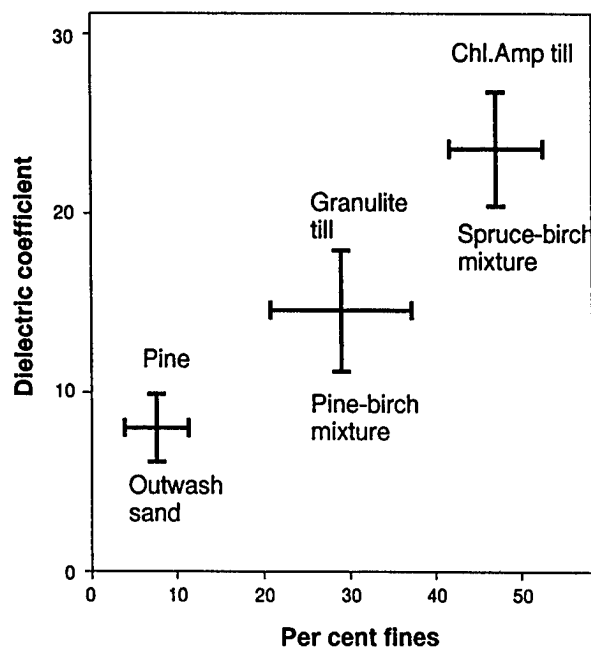
Figure 2. Dielectric properties and fine fraction content (d<60 μm) of two tills and outwash sand deposits in Central Lapland. Dielectric mean +/-std values were measured using RSAD; particle size data represent B horizon.

509

pine typically grows on the granulite till as well as on the outwash sand deposits, whose fine fraction content is only less than 10% (Fig. 2). The undulating morphology at the granulite test site seem have an effect on the vegetation, such that pubescent birch occupies the depressions but silver birch is present along with pine on the topographic highs. Variations in dielectric properties/water content at the growth sites are not due to precipitation but rather due to content of fines of tills. These variations, detected by RSAD under unchangeable weather conditions are less than 50 m according to the semivariogram models.

Seasonal variations

Unfrozen free water content varies seasonally due to snowmelt and precipitation.

Hydraulic properties of soils and parent tills, on the other hand, determine how fast or slow the changes in water content are.

Seasonal variations of dielectric properties of fine-grained till and outwash sediments are significantly different (Fig. 3). The fine-grained till derived from chlorite-amphiblole schist at Vaalelohto tend to be high in moisture through the growing seasons in 1995 and 1996. In 1995 particularly, saturation ($\varepsilon > 30$) lasts roughly from last week of May to first week of July. In contrast, outwash sand stays dry ($\varepsilon < 10$) almost through the monitoring period. The only exception is in mid-June 1996, when sand was temporarily saturated due to the risen groundwater level. The snowmelt rise in dielectric values at the top layers are doubled and the full saturation lasts several weeks in fine-grained till, suggesting low hydraulic conductivity. Presum-
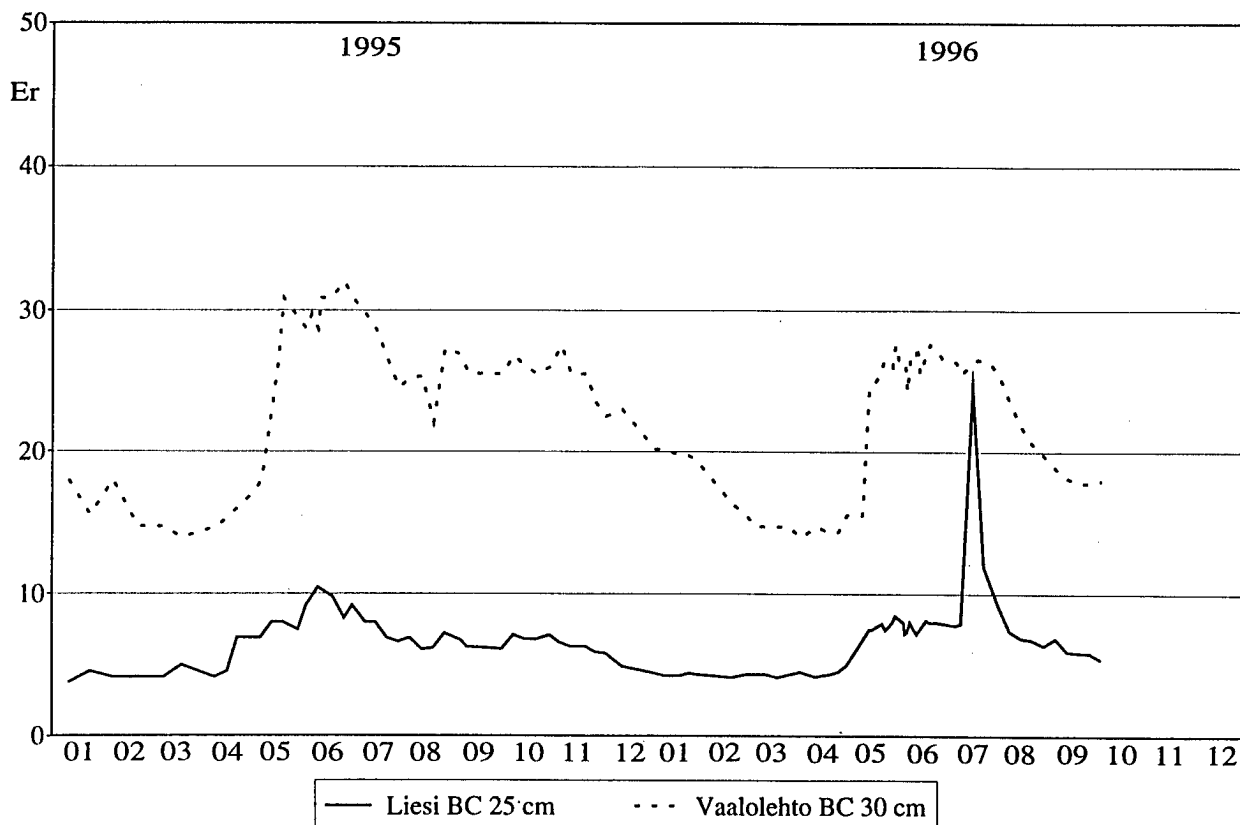
Figure 3. Seasonal variations of dielectric properties of fine-grained till at the Vaalolehto study site and outwash sand at the Liesi study site. The former site was occupied by Norway spruce and pubescent birch and the latter by Scots pine. The 1996 mid-July peak at Liesi is due to temporary rise of ground water level. TDR monitoring was made on a weekly basis with horizontally inserted 15-cm-long steel probes.

510

ably, a similar pattern has also been present in previous years and the high water content may be critical factor in pine seedling dieback in artificial regeneration at Vaalolehto. On the other hand, high water content may cause oxygen deprivation and decrease nutrient uptake and thus subject the seedlings to diseases.

Bulk dielectric properties of the soil sequence from the A0 (5 cm), A (10 cm) to BC (40 cm) horizons of gabbro till (Hanhilehto study site, Fig. 4) stay rather stable not only during winter months, but also during the growing season. On contrast, a snowmelt

effect is clearly visible in black schist till (Fig. 4) next to the gabbro site. Full saturation (ε>30) was reached in all monitored horizons. A very important feature is the slow decrease in water content from the beginning of June through August 1995. This is true especially in the BC 40-cm horizon.

The fine-grained tills at Vaalolehto, Äältövittikko and Kuorajoki sites show a drastic rise in dielectric values due to snowmelt at the beginning of June 1996 (Fig. 5). The till at Äältovittikko is saturated from mid-June through the end of July. Similarly, Kuorajoki till and Vaalolehto tills are saturated or near saturation (ε = 30) from the second week of June through mid-August. Soil temperature rise seems to be coincidental with the decrease in dielectric values at each site. At the time with maximum soil temperatures, 11°C, in mid-August dielectric properties decrease
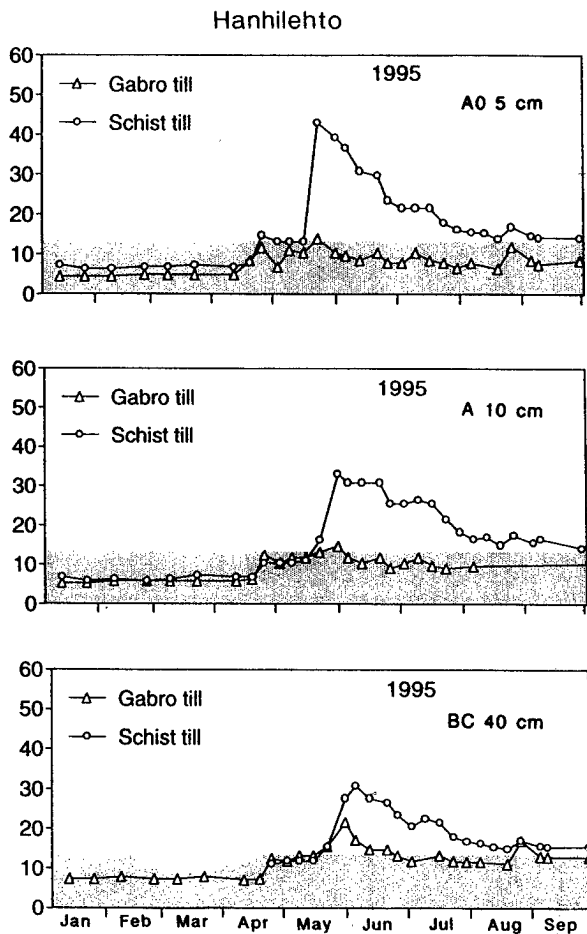
Figure 4. Dielectric variations in gabbro and (black) schist till sequences in 1995 detected by TDR. The artificial regeneration by Scots pine has been succeeded at the gabbro site, whereas artificial regeneration has failed at the schist till site. Both sites were formerly occupied by Norway spruce stands.
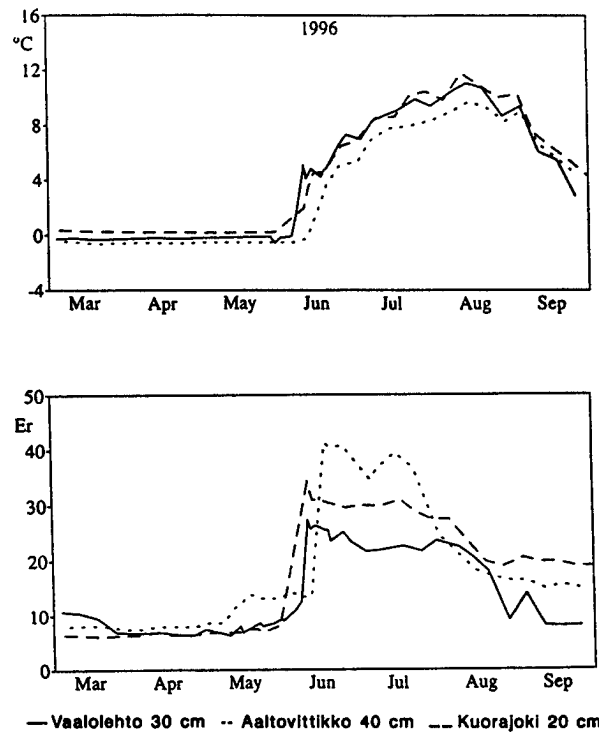
Figure 5. Dielectric and temperature changes in tills associated with chlorite-amphibole schist (Vaalolehto), intermediate metavolcanic rocks (Äältövittkko site) and komatite (Kuorajoki site). Manual dielectric monitoring was made with TDR, temperature with buried PT-100 sensors.

511
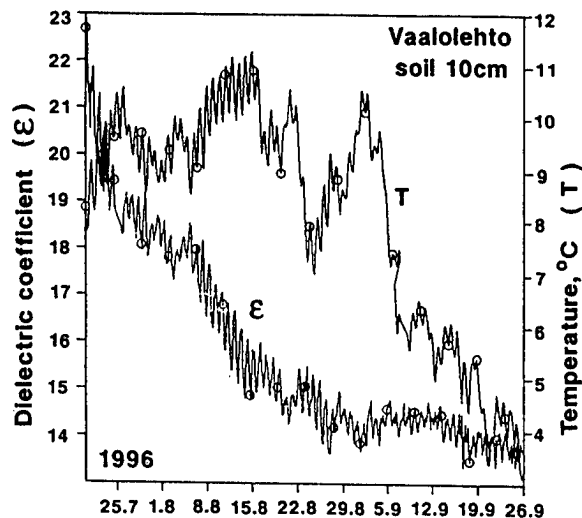
Figure 6. Dielectric and temperature changes at the top of fine-textured till at Vaalolehto site from late July through September 1996 by 1-hour-interval automatic monitoring.

significantly. A very limited amount of rain fell in that period. Automatically monitored data from the Vaalolehto site (Fig. 6) show this phenomenon in more detail. Even daily fluctuations of dielectric coefficients may be seen. In this example, the topsoil temperature rose up to 22°C in mid-August.

The above examples indicate that sites with natural Scots pine stands or sites where artificial Scots pine has succeeded (Hanhilehto case), dielectric values are low. Norway spruce, in contrast, can tolerate sites with high moisture and saturation after snowmelt.

Regional patterns of Scots pine and Norway spruce tend to follow trends, that are largely associated with geologic patterns in Central Lapland. Spruce tends to predominate on tills derived from rocks in the Central Laplands Greenstone Belt. Pine predominates on tills derived from coarse-textured rocks such as granites, gabbros and particularly granulite.

Locally the pine-spruce composition seems to be associated with soil water. According to the present results, the moisture tolerance of pine may be restricted to the dielectric range of $\varepsilon < 13$. This is supported by the dielectric measurements of the sites of adult trees and also the measurements at sites

with artificial pine regeneration. Pine do not naturally occupy moist to wet tills, and also artificial pine regeneration has failed on these tills. Fine-grained tills are derived mostly from basic volcanics and are typically characterized by high nutrient content and incorporated clay minerals. After snowmelt these tills tend to be saturated several weeks, which may be the most important factor restricting Scots pine growth. The present results may also indicate that pine-spruce succession lacks on moist to wet mafic tills and these sites are occupied by repeated (pubescent birch)-spruce generations.

ACKNOWLEDGEMENTS

REFERENCES

Hänninen P. and R. Sutinen. 1994. Dielectric prediction of landslide susceptibility: A model applied to recent sediment flow deposits. 7th IAEG Congress, 137-144.

Sutinen R. and P. Hänninen. 1990. Radar profiling and dielectrical properties of glacial deposits in North Finland. 6th IAEG Congress, 1045-1051.

Sutinen R. 1992. Glacial deposits, their electrical properties and surveying by image interpretation and ground penetrating radar. Bull. Geol. Surv. Finl. 359. 123 p.

Topp G.C., Davis J.L. and A.P. Annan. 1980. Electromagnetic determination of soil water content: Measurements in coaxial transmission lines. Water Resources Research, 16, 3, 574-582.

Seasonal Changes in Soil Temperature and in the Frost Hardiness of Scots Pine Roots Under Subarctic Conditions

M.-L. SUTINEN[1], A. RITARI[1], T. HOLAPPA[2], AND K. KUJALA[2]

ABSTRACT

The survival of conifer roots under subarctic winter conditions is not well understood. The seasonal changes in soil temperature and in the frost-hardiness of adult Scots pine (*Pinus sylvestris* L.) trees was studied between September 1992 and May 1993 in a pine forest growing in dry heathland soil. The study area located in Finnish Lapland (67 °N, 29 °E). Air (2 m above ground) and soil (5-cm depth of mineral soil) temperatures were measured continuously every second hour. The frost-hardiness of the roots in the mineral soil (down to 10 cm) was measured by means of the electrolyte-leakage method. The air temperature was consistently below 0 °C after the first week of October. The coldest month was February with the daily average temperature of -10.3 °C. Snow accumulation started in the first week of October and reached the level of 129 cm in April. The temperatures in the mineral soil varied between +15.4 °C and 0.8 °C. The frost-hardiness of pine roots was at its lowest in September (-6 °C) and at its highest in December (-21 °C). These findings suggest that Scots pine roots have indeed the capacity to sense temperature in such a way that they develop frost-hardiness in advance of a fall in the temperature of the surroundings.

Key words: soil temperature, frost hardiness, seasonal changes, *Pinus sylvestris*, root

INTRODUCTION

Model simulations predict that in the extreme winter conditions of Finnish Lapland, with extremely low and long-lasting low air temperatures and late or little snow cover, the temperature in the upper part of the coarse-textured soil can drop down to -30 °C (Ritari, Kujala, Holappa, unpublished). This has also been experimentally proved (Jalkanen et al. 1995). These findings raise questions about the survival of roots under continued severe freezing temperatures in the soil, and also about the nature of the ameliorating effect of the cover of snow. Freezing damage to roots during the extremely cold winters, with late or little snow cover, has been suggested to be one cause of needle loss by adult Scots pines growing in the coarse-textured soils of Fennoscandia (Kullman and Högberg 1989, Kullman 1991, Tikkanen and Raitio 1990/91, Ritari 1990, Jalkanen et al. 1995). However, the verification of this hypothesis is difficult since there are no data on the seasonal changes in frost-hardiness of the roots of adult Scots pines growing in natural conditions in central and northern Fennoscandia.

Previous studies with Scots pine of more southern Karelian provenances have shown that the roots of adult trees can withstand temperatures down to -28 °C (Korotaev 1994). Containerized Scots pine seedlings grown under natural conditions in a nursery in central Sweden have been shown to

survive temperatures of -25 °C in mid winter (Lindström and Nyström 1987). These findings place the above hypothesis in new light. Since the roots of adult trees, and even of young seedlings, of more southern provenances can withstand temperatures down to -25 °C, one would expect that larger roots of adult Scots pine growing in the subarctic can withstand much lower temperatures. Studies on the freezing-stress resistance of roots of Scots pine seedlings growing in subarctic conditions (Sutinen et al. 1996a), on the other hand, show that roots can withstand even the most extreme freezing soil temperatures that occur in Fennoscandia (Heikinheimo and Fougstedt 1992), but this may be true only in the case of severe freezing of short duration. Tolerance against dehydration stress, caused by prolonged severe freezing, and frequent temperature fluctuation may be critical for the survival of roots Scots pine in the subarctic region and at timberline. Thus, more knowledge on the whole range of frost-hardiness of roots of adult Scots pine growing in natural subarctic conditions is needed.

MATERIALS AND METHODS

Study site

The study site is a naturally regenerated stand of Scots pine (*Pinus sylvestris* L.) in eastern Finnish Lapland (67°30'N, 29°30'E, 270 m a.s.l.). Tree age within the stand varies between 50 and 60 years. The forest site type is *Empetrum-Cladina* type (Cajander 1949) and the soil is sandy. The vegetation is composed of *Cladonia* spp. and various bryophytes, especially *Dicranum* spp. (Väre et al. 1996).

According to the meteorological data of 30 years from a weather station run by the Finnish Meteorological Institute and located at a distance of 25 km from the study site, the mean annual temperature in the area is -6.4 °C, the minimum air temperature ever recorded is -50.4 °C and the record maximum air temperature +30.2 °C.

Temperature and snow recordings

The temperature of the air (2 m above the ground) and in the soil (at depth of 5 cm) were recorded between August 1992 and May 1993 at intervals of two hours using two replications of thermistors coupled to a Squirrel 1200 data logger (Grant Instruments Ltd., Cambridge, England). To make up for missing temperature recordings,

modeling (SOIL-model, Jansson 1996) was employed to generate substitute data.

The freezing temperature sum was calculated by summing the daily mean subzero temperatures. The snow precipitation data is based on data from the weather station of Finnish Meteorological Institute located 25 km from the study site.

Determination of frost-hardiness of roots

Root samples for frost-hardiness analyses were collected at 2-4 week intervals from September 1992 to February 1993. Soil samples for roots were collected by means of 10-cm core auger. Fifteen samples were taken at each time. Samples were placed in plastic bags and kept at +4 °C to await manual separation of roots.

Four replicates per freezing temperature, each 1 g in weight, from each sample were used for the freezing and thawing treatment. The roots were transferred into a test tube measuring 1.5 cm x 10 cm and cooled down in an ethanol bath (Lauda RUK 60). Freezing was initiated at -1.0 °C with ice crystals and tissue then being cooled automatically at the rate of 4 °C/hour. Having reached the desired temperature, the samples were held at that temperature for 30 min and then thawed on ice overnight. Six different freezing treatment temperatures were applied each time.

After the freeze-thaw treatment, the extent of freezing injury was estimated by means of the electrolyte-leakage method, which required the roots to be cut into pieces 0.5 cm in length. The electrolytes were extracted with 4 mL of distilled water using vacuum infiltration and shaking for 20 h. Electrical conductivity (C), (YSI conductivity meter, Model 32, Yellow Springs Instruments) was measured twice, after shaking for 20 h (C_t) and after killing the roots by autoclaving and shaking for 20 h (C_k). The percentage of electrolyte leakage (R) was calculated as follows:

$$R = C_t/C_k \times 100$$
where
C_t = electrical conductivity after freezing
C_k = electrical conductivity after killing

The non-linear, logistic sigmoid function was fitted to the R values vs. freezing temperature (Repo and Lappi 1989). The temperature representing frost-hardiness was estimated from the plot showing percentage electrolyte leakage as follows (Sutinen et al. 1992):

514

frost-hardiness $= (R_1 + R_2)/2$
where
R_1 = percentage electrolyte leakage from
uninjured tissue
R_2 = percentage electrolyte leakage at
highest level of injury

RESULTS

The monthly mean air temperature preceding
the first root sampling in the fall was +9.2 °C and
the air temperature fluctuated during this period
between +14.0 °C and +4.7 °C (Fig. 1A and 1B).
The air temperature was consistently below 0 °C
after the first week of October. The coldest month
was February with the daily average temperature of
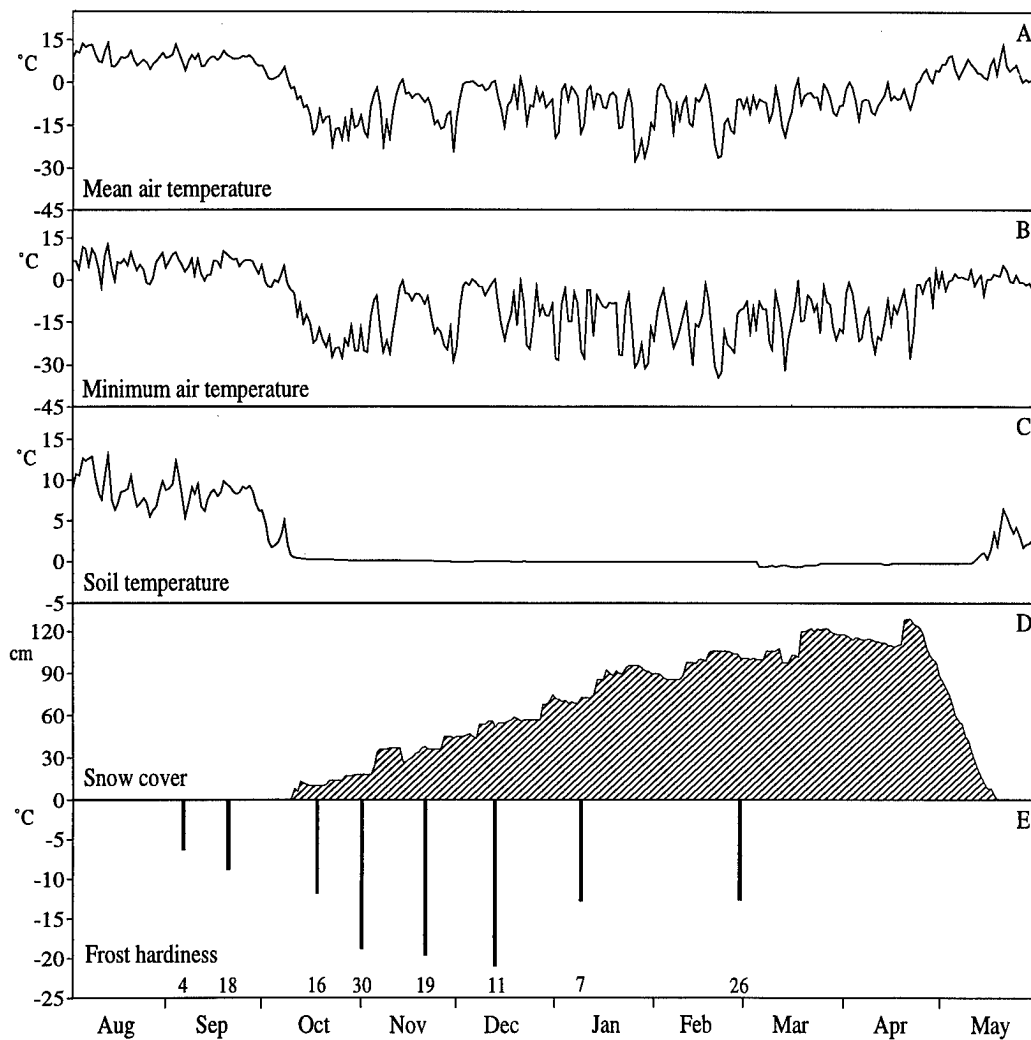
*Figure 1. Meteorological record between August 1992 and May 1993 in the study area. (A) The daily average air
temperature (2 m above ground) (B) Daily minimum air temperature (C) Daily average temperature in the mineral
soil at the depth of 5 cm (G) Daily snow depth values (E) Seasonal changes in the frost-hardiness of Scots pine
roots between September 1992 and February 1993.*

515

-10.3 °C. Snow accumulation started in the first week of October and reached the level of 129 cm in April (Fig. 1D). The freezing air temperature sum of -1700 °C indicates that the winter 1992-1993 represents normal winter when compared to the 30-year average (Meteorological Yearbook of Finland 1992, 1993). The temperatures in the mineral soil varied between +15.4 °C and 0.8 °C (Fig. 1C).

The frost-hardiness of the Scots pine roots was lowest (about -6 °C) in September and was at its maximum of about -20 °C between November and December (Fig. 1E).

DISCUSSION

The study period (August 1992-May 1993) represents normal winter conditions in the study area when compared to the 30-year average (Meteorological Yearbook of Finland 1992, 1993). There were no exceptionally low minimum air temperatures before snow began to accumulate in the fall. The monthly average air temperature in October was nine degrees lower than the 30-year average, but the snow cover was already thick by the time low air temperatures occurred. The average air temperatures of the coldest months (November-February) were slightly milder than the 30-year average. There were no exceptional minimum or maximum air temperatures during these months.

The maximum frost-hardiness of the roots measured in the course of this study was -21 °C (November-December 1992). This is much smaller than has been reported for more southern provenances (Lindström and Nyström 1987, Korotaev 1994). However, the study period represents normal winter conditions without any temperature extremes. It is possible that the roots could have reached a greater level of frost-hardiness had the air temperature and thereby the soil

temperature been lower. This is supported by the finding that the frost-hardiness of roots was -5 °C in September, even though the average soil temperature one month prior to sampling was +9 °C. The question of whether the cold acclimation capacity of Scots pine roots is sufficient in extremely exceptional temperature conditions, such as those generated by late snow cover or disturbed insulation of snow cover due to fodder digging by reindeers, remains unclear. The results obtained concerning young Scots pine seedlings, however, suggest that (in addition to extreme minimum temperatures) we should also consider the time factor (i.e., the duration and frequency of extremely low temperatures [Sutinen et al. 1996a]).

The results obtained in this study indicate that cold acclimation by roots is much slower than that by the aboveground parts of trees. Previous studies conducted on the same study site have shown that during the early phase of cold acclimation (August-September), the frost-hardiness of needles clearly exceeded the lowest minimum air temperatures ever measured on the study site (Sutinen et al. 1996b). Needles survived temperatures of -20 °C even though they had not experienced air temperatures of below 5 °C. Roots attained a similar frost-hardiness level only after experiencing temperatures of 0 °C or below for many weeks. There is also a large difference in the maximum frost-hardiness between needles and roots. The maximum frost-hardiness of roots measured in this study was -21 °C. As is mentioned above, pine roots had experienced temperatures of 0 °C or below for many weeks. The needles survived the temperature of liquid nitrogen after experiencing similar temperature conditions (Sutinen et al. 1996b). Studies focusing on Scots pine seedlings have shown that the frost-hardiness of roots is lower than that of shoots even when the roots are at the same temperature as the aboveground parts of the tree (Sutinen et al. 1996a).

REFERENCES

Cajander, A. K. 1949. Forest types and their significance. Acta Forest. Fenn. 56:1-71.

The Finnish Meteorological Institute, Meteorological Yearbook of Finland 1992. Helsinki, Finland.

The Finnish Meteorological Institute, Meteorological Yearbook of Finland 1993. Helsinki, Finland.

Heikinheimo, M., and B. Fougstedt. 1992. Statistic of soil temperature in Finland 1971-1990. Finnish Meteorological Institute, Meteorological Publications no 22.

Jalkanen, R., T. Aalto, K. Derome, K. Niska, and A.Ritari. 1995. Männyn neulaskatoon 1987 johtaneet tekijät Pohjois-Suomessa. (In Finnish) Metsäntutkimuslaitoksen tiedonantoja 544.

Jansson, P-E. 1996. Simulation model for soil water and heat conditions. Description of the SOIL model. Swedish University of Agricultural Sciences, Uppsala.

Korotaev, A. A. 1994. Untersuchungen zur Frostresistenz von Baumwurzeln. Forstarchiv 65:93-95.

Kullman, L. 1991. Cataclysmic response to recent cooling of a natural boreal pine (*Pinus sylvestris* L.) forest in northern Sweden. New Phytol. 117:351-360.

Kullman, L. and N. Högberg. 1989. Rapid natural decline of upper montane forests in the Swedish scandes. Arctic 42:217-226.

Lindström, A. and C. Nyström. 1987. Seasonal variation in root hardiness of container-grown Scots pine, Norway spruce, and Lodgepole pine seedlings. Can. J. For. Res. 17:787-793.

Repo, T. and J. Lappi. 1989. Estimation of standard error of impedance-estimated frost resistance. Scand. J. For. Res. 4:67-74.

Ritari, A. 1990. Temperature, snow and soil frost conditions in northern Finland during winter 1986-87 p.44-52 *In* K. Kinnunen and M. Varmola (ed.). Effects of air pollutants and acidification in combination with climatic factors on forests, soils and waters in northern Fennoscandia. Report from a workshop held 17-19 October 1988, Rovaniemi, Finland. Nordic Council of Ministers, Miljörapport.

Sutinen, M.L., Palta, J.P. and Reich, P.B. 1992. Seasonal differences in freezing stress resistance in the needles of *Pinus nigra* and *Pinus resinosa*: Evaluation of the electrolyte leakage method. Tree Physiol. 11:241-254.

Sutinen, M-L., K. Mäkitalo, and R. Sutinen. 1996a. Freezing dehydration damages roots of containerized Scots pine (*Pinus sylvestris*) seedlings overwintering under subarctic conditions. Can. J. For. Res. 26:1602-1609.

Sutinen, M-L., H. Raitio, V. Nivala, R. Ollikainen and A. Ritari. 1996b. Effects of emissions from copper-nickel smelters on the frost-hardiness of *Pinus sylvestris* needles in the subarctic region. New Phytol. 132:503-512.

Tikkanen, E., and H. Raitio. 1990/91. Nutrient stress in young Scots pines suffering from needle loss in a dry heath forest. Water, Air, and Soil Poll. 54:281-293.

Väre, H., R. Ohtonen and K. Mikkola. 1996. The effect and extent of heavy grazing by reindeer in oligotrophic pine heaths in northeastern Fennoscandia. Ecography 19:245-253.

IV. MODELING AND REMOTE SENSING
Modeling

Thermal Properties of Seasonally Frozen Soils, and Modeling Soil Freezing or Thawing

D. KURTENER[1] AND P. ROMANOV[2]

ABSTRACT

This paper addresses some problems of soil physical properties and processes, artificial soil freezing or thawing, and land management impacts on soil freezing. In particular, a method for simultaneous measurements of all primary heat properties (SMAPP method) is suggested. This method was tested by experiments. Laboratory calibration illustrated that the experimental equipment measures soil thermal properties with acceptable accuracy.

Thermal properties values of typical seasonally frozen soils in the main regions of the former Soviet Union were considered. We have created a data base of thermal properties of typical seasonally frozen soils.

Modeling of artificial soil freezing or thawing is considered. The model described land management impacts on soil freezing. The model is capable of solving some scientific and applied problems.

Key words: Modeling, land management impact, soil thermal properties, permafrost, frozen soil.

INTRODUCTION

Seasonally frozen soils occur in most of Russia. The northeast regions of Russia contain permafrost.

For regions with seasonally frozen soil or permafrost is very important to know the impact of the land management on soil freezing or thawing. Climate warming will start to destroy these regions.

Current reporting is devoted to information support for prediction of positive or compensation of negative impact of the human activity and climate change. The method is given by Kurtener and Chudnovsky (1979), Kurtener and Romanov (1985), Kurtener and Uskov (1988), Romanov et al. (1990) and includes soil thermal property measurement techniques, information about thermal properties of typical seasonally frozen soils, modeling processes of soil thermal regime and artificial soil freezing or thawing.

METHODS AND DEVICES FOR SOIL THERMAL PROPERTY MEASUREMENTS

The thermal properties of soil affect soil temperature and water regimes, which are very important to biological, ecological, agricultural, and other processes.

The thermal properties of soil that are most familiar are the conductivity λ, the diffusivity a, and volumetric heat capacity c. We call these the primary heat properties.

Traditional experimental method is based on measurements of only one property (the conductivity or the diffusivity) and calculating another two by

$$a = \frac{\lambda}{c} \tag{1}$$

and

$$c = c_s \rho_s v_s + c_w \rho_w v_w + \sum c_a \rho_a v_a, \tag{2}$$

where ρ is bulk density, c_i, $i = s, w, a$, is specific heat

[1] Agrophysical Research Institute,195220 St. Petersburg, Grashdansky av. 14, Russia
[2] Institute of Physics and Technical Problems of the North, 67707 Yakutsk, Oktiabrskia 1, Russia

capacity, v is volume fraction, and subscripts s, w, and a refer to soil solids, water and another components. For example, the ball probe (Kurtener and Semenov 1973) and the pulse method (Taylor and Magic 1984; Ross and Bridge 1987) were used for measurements of only thermal diffusivity. The cylindrical heat probe (Mogilevsky et al. 1974; Sepaskhh and Boersma 1979), ceramic probe (Nakamura and Hibiya 1988), ring probe (Kaganov et al. 1983), and flat probe (Kurtener and Semenov 1973) were used for measurements of only thermal conductivity.

One of the problem of using equation (2) is the need to estimate the particle sizes in the soil. Calculating volumetric heat capacity by equation (2) also requires knowledge of volume faction of soil solid, water, and other components. Because of the difficulty in estimating volume fraction, the equation is applied to soil with well known structure. The problems increase when thermal properties are measured in field conditions. A soil could contain other particles (plant remains, roots, humus, manmade materials) and equation (2) does not account for them. In these cases, volumetric heat capacity must be determined experimentally. But this path is not without flaws. First, it is necessary to organize additional experiments. Second, the main and additional experiments are carried at different times, between which the physical properties can change.

The solution to the problem would be a method enabling simultaneous measurement of all the primary thermal properties using only one sample of soil. The simultaneous measurements of all primary thermal properties (SMAPP method) is based on the heat transfer theory. A solution of the heat flow equation that describes one-dimensional heat transfer in an isotropic medium can be modified as follows:

$$F_3(\lambda, a, T, t) = 0 \qquad (3)$$

The solution (3) can be considered as equation with four unknown roots: λ, a, T, t. If we know the temperature increase from T_1 to T_2 during the time period from t_1 to t_2, we will obtain following system:

$$F_3(\lambda, a, T_1, t_1) = 0, \qquad (4)$$

$$F_3(\lambda, a, T_2, t_2) = 0$$

This system has two equations and only two unknown roots: λ, a. Therefore, the system is defined. The solution of the system with equation (1) reveals full information about all primary thermal properties.

The components of the experimental equipment are: cylindrical heat probe with constant-power generator and controller, temperature sensor and temperature sensor signal amplifier, analogue-to-digital converter, and microcomputer. The cylindrical heat probe is inserted in a soil sample contain in a jars. The jar lid has a hole in the center. The procedure of soil sample preparation is given by Sepaskhah and Boersma (1979). The thermal properties are measured by recording the temperature rate and solving equations (4) with equation (1). The computer makes it many time during a period of experiment and indicates result. The measurement time is sufficiently short: from 90 to 120 seconds.

The simultaneous measurements of all primary soil thermal properties (SMAPP method) was tested by several experiments with samples of different thermal properties. A laboratory calibration study illustrated that the experimental equipment measures the thermal properties with acceptable accuracy. The relative error ranged from 0.052 (for thermal diffusively) to 0.174 (for volumetric heat capacity); the average value was 0.103.

A main benefit of the equipment was the fact that it could measure simultaneously all primary soil thermal properties on one sample.

THERMAL PROPERTIES OF SEASONALLY FROZEN SOILS

Thermal property values of typical seasonally frozen soils for the main regions of the former Soviet Union were investigated a long time of the Agrophysical Research Institute under the direction of Abraham Chudnovsky (Bikis 1958; Osols 1959; Kurtener and Semenov 1973; Sablovskaia 1970; Riabova 1952). All investigations were carried out with traditional experimental equipment that was referred to previously. The thermal conductivity of different kinds of permanently frozen soil for during melting and freezing conditions have been obtained by Feldman. et al. (1988) and Mandarov et al. (1982). A data base of thermal properties of typical seasonally frozen soils has been created.

MATHEMATICAL MODELING OF SOIL FREEZING OR THAWING

The basic idea of the approach is that land management's impact would increase or descries under the influence of natural characteristics of the landscape (geomorphology of landscape, vegetation kinds, soil properties, water regime) and meteorological (climatic) conditions. The models are based on the processes of energy and mass transfer in

the system of soil, plants, active layer of atmosphere, and human impact. In particular, the approach to problem was given by Kurtener et al.(1979a, 1986, 1988, 1995, 1995a), and Chung Sang-Ok and Horton (1987). The model includes:

1. A combination of models describing processes of artificial soil freezing or thawing.

2. A combination of methods for correlating results of modeling with technological parameters.

3. A combination of methods for preparing recommendations.

The scheme of the model is shown in Figure1. It includes four parts. The first part prepares the data. Part two is a complex of models for describing soil freezing or thawing in different isolated cases. The third part includes technical information necessary for preparing recommendations.

Each model describing an isolated case includes a part where human impact is formulated. Also, the cases are distinguished in duration (for short run periods or long-term intervals). The first case describes temperature daily regimes such as low temperature during darkness or warming in day light. The second case studies seasonal processes. Today there are several variants of the model.

For example, Block 2 for one variant describes a system consisting five layers: atmosphere, snow, plant, frozen soil, and melted soil. In winter the plant layer would be considered a combination of snow and plant for some isolated cases. The snow layer could be combination of snow and snow substitute (a material used in the absence of snow to protect crops against freezing). Basis statements includes:

1. Energy and mass transfer in the atmospheric layer, snow layer, and plant layer are considered quasi-steady-state processes.

2. Heat transfer in the frozen soil layers and the melted soil layers is defined as a dynamic process.

3. It is assumed that water transport occurs in the melted soil layer only.

4. Soil water freezes in a narrow range of temperatures.

5. Thicknesses of layers of snow and snow substitute are variable.

6. It is assumed that soil surface is horizontal.

An equation describing one-dimensional conductive heat transfer in soil layers is

$$\lambda \frac{\partial^2 T}{\partial x^2} = C(T) \frac{\partial T}{\partial t}, \qquad (5)$$

$$C(T) = c + L\rho W \frac{di}{dt}$$

where T is temperature, t is time, x is perpendicular distance to the soil surface, λ is soil thermal

conductivity, c is volumetric heat capacity, i is the ratio of ice to water ($0<i<1$), L is latent heat of phase transition. If $i=0$ then eq.(5) describes heat transfer in a melted soil layer.

An equation describing one-dimensional water movement is given below

$$\frac{\partial}{\partial x}(D\frac{\partial W}{\partial x}) - \frac{\partial K}{\partial x} = \frac{\partial W}{\partial t}, \qquad (6)$$

where W is volumetric soil water content, D is soil water diffusivity, and K is hydraulic conductivity. Both D and K vary with water content and thus can vary with depth and time.

Heat transfer and water movement in soil affect each other by model variables. In particular, soil thermal conductivity and volumetric heat capacity are functions of volumetric soil water content. Evaporative flux and latent heat flow by evaporation are functions of soil surface temperature.

A third order boundary condition for eq. (5) is based on theoretical considerations of heat and mass exchange at the soil surface

$$-\lambda \frac{\partial T}{\partial x} = N(T_E - T), x = 0 \qquad (7)$$

where T_E is the equivalent temperature of environment, and N is a generalized heat exchange coefficient. T_E and N are determined by a balance method (Kurtener et al. 1979, 1988) as functions of all model variables (the main meteorological parameters, plant characteristics, snow parameters, agricultural or technical means).

A second order boundary condition for eq. (6) is based on theoretical considerations of heat and mass exchange at the soil surface

$$D\frac{\partial W}{\partial x} - K = G, x = o \qquad (8)$$

where G is determined by balance methods as functions of all model variables. Solution of the system of differential equations has been obtained.

A variants of the model are used in many applications where optimum strategy of agricultural treatments is ought. For example, in regions with a cold climate it is used to improve thermal agricultural treatments. In particular, it is applied to some technologies of snow regulations in winter. Figure 2 is an example of the application of a variant to analyze the consequences of a snow cover substitute to protect winter crops against freeze. Thickness of layer the snow substitute is 10 cm. The properties of snow cover substitute are: bulk density = 50 kg/m^3, soil thermal conductivity = 0.11 W/(mK), soil thermal diffusivity = 1.1*10^{-6} m^2/c.

BLOCK 1
Preparing initial data

BLOCK 2
Complex models for describing processes of soil freezing or thawing

BLOCK 3
Data-base of technological requirements

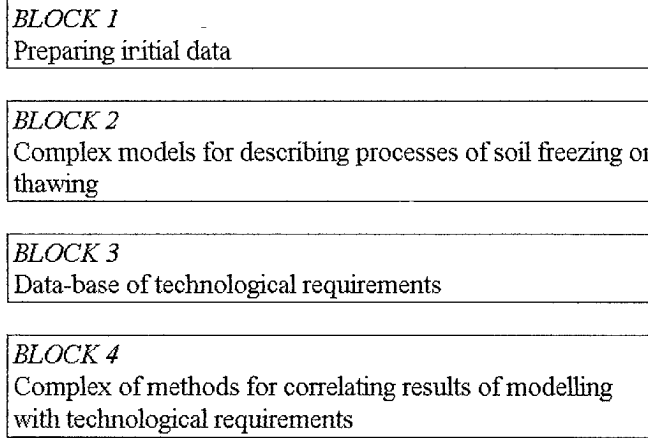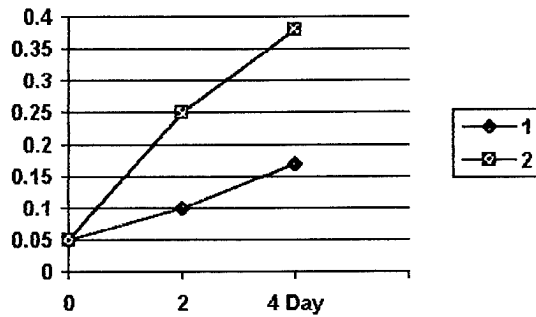| BLOCK 4 |
| --- |
| Complex of methods for correlating results of modelling with technological requirements |

Figure 1. Scheme of the model.

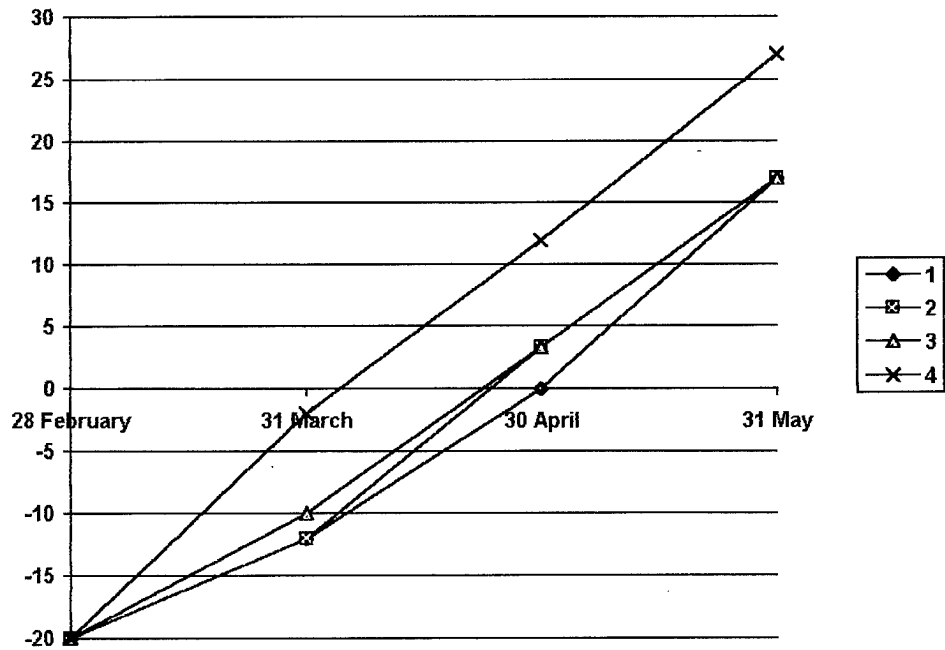*Figure 2. Depth of freeze (in the m) with suddenly very low air temperature (1 is natural conditions, 2 is with using snow substitute).*

Figure 3. Soil temperature at depth 10 cm after different variants of snow cover destruction in spring in Yakutsk area: 1 - natural conditions, 2 - snow removal by use of black paint, 3 - mechanical snow removal, 4 - plastic mulch after mechanical snow removal.

522

Considerable recent attention has been focused on some technologies of snow control in spring, such as transparent plastic mulch after mechanical snow removal against optimum time, only mechanical snow removal against optimum time, and snow removal by use black paint against optimum time. Optimum time is the date which gives maximum of soil heat accumulation and minimum soil heat loss. Kurtener and Romanov (1985) applied a variant of the model to improve these thermal agricultural treatments. Figure 3 shows calculated soil temperature after applying three such treatments. In particular, transparent plastic mulch after mechanical snow removal gives long-term improvement of soil thermal regime. Two other treatments gave only short-term improvements in March and April only.

CONCLUSION

A method for simultaneous measurements of all primary heat properties (SMAPP method) is suggested. The result of a laboratory calibration study shows that the experimental data on the soil thermal properties follows results obtained by using this method with acceptable accuracy.

Thermal properties of typical seasonally frozen soils in the main regions have been considered.

The paper also discusses modeling of artificial soil freezing or thawing. The model describing land management impacts on soil freezing is capable of solving some scientific and applied problems.

REFERENCES

Bikis, L.O. 1958. Influence of soil microrelief on land thermal regime in Latvia conditions. (In Russian.) Review of Ph.D. diss. Latvian Agricultural Academy, Riga.

Chung Sang-Ok, R. Horton. 1987. Soil heat and water flow with partial surface mulch. Water resources research 23:2175-2186.

Feldman, G.M., A.S. Tetl'baum, N.I. Shender, R.I. Gavri'ev. 1988. Handout for prediction of soil thermal regimes of Yakutia. (In Russian.) Publ. Of Siberian Branch of Russian Academy of Sci. Yakutsk.

Horton, R., and P. Wierenga. 1984. The effect of column wetting on soil thermal conductivity. Soil Sci. 138:102-108.

Ivanova, K.F., and V.M. Kozlovskiy. 1992. Measurement of thermal conductivity of unsaturated soils. (In Russian.) Doklady VASHNIL 1:54-57.

Kaganov, M.A., V.M. Kozlovskiy, and M.N. Jakker. 1983. Algorithm of measurement of medium thermal conductivity by ring probe. (In Russian.) Nauchno-tehnicheskii bulleten po agronomicheskoi fizike 46:51-55.

Kurtener, D.A., and M.B. Semenov. 1973. Thermal properties investigation of soil peat after their improvement. (In Russian.) Proc. of Agrophysical Research Institute 31:151-156.

Kurtener, D.A., A.F. Chudnovsky. 1979. Agrimeteorological foundation of thermal melioration of soil. (In Russian.) Hydrometeorolog. Publ., Leningrad.

Kurtener, D.A., G.A. Trubacheva, and M.A. Kusnezov. 1979a. Model of heat and water transfer in soil. (In Russian.) Bull. of Agrophysical Reseach Institute 40:30-34.

Kurtener, D.A., I.B. Uskov. 1982. Climatic factors and the heat transfer in field and controlled environments. (In Russian.) Hydrometeorolog. Publ., Leningrad.

Kurtener, D.A., P.G. Romanov. 1985. Agrometeorological basis of time for beginning snow heat melioration. (In Russian.) Proc. of Agrophysical Reseach Institute 37:65-73.

Kurtener, D.A., M.V. Evtehova, M.T. Bersirov. 1986. Mathematical modeling of thermal and water regime in soil. (In Russian.) p. 139-153 In: I.B. Uskov (ed.) Agriclimate and Crop, Leningrad.

Kurtener, D.A., I.B. Uskov. 1988. Control of agricultural field microclimate. (In Russian.) Hydrometeorolog. Publ., Leningrad.

Kurtener, D.A., F. Hoffmann. 1995. Model of thermal and water regime of soil with inclined surface. (In Russian.) In Intern. Conference of European Geophysical Society, Hamburg, Germany.

Kurtener, D., K. Kunkel. 1995a. Model for prediction of negative impact of climate change on soil microclimate of Middle and East Europe. In All-Russian Conference: Landscape Microclimate, St. Petersburg.

Mandarov, A.A., P.N., Skriabin, I.S. Ugarov. 1982. Condactivity of several kinds of frozen soil for central Yakutia. (In Russian.) In Soil thermal knowledge of cold regions. Publ. Of Siberian Branch of Russian Academy of Sci. Yakutsk.

Mogilevsky, B.M., V.N. Sokolov, and A.F. Chudnovsky. 1974. Resistive method of constant power probe and its use in the measurement of thermal conductivity of

liquid semiconductors. (In Russian.) Inzhenerno-fizicheskii zhurnal 27(6):1033-1040.

Nassar, N., and R. Horton. 1989. Determination of the apparent thermal diffusivity of a nonuniform soil. J. Soil Sci. 147:238-244.

Nakamura, Sh., and T. Hibiya. 1988. Ceramic probe for measuring the thermal conductivity of an electrically conductive liquid by the transient hot wire method. Rev. Sci. Instrum. 59:2600-2603.

Osols, K.V. 1959. Physical conditions of agriculture fields and their influence on the yield. (In Russian.) Review of Ph.D. diss. Agrophysical Research Institute, Leningrad.

Potter, K.N., R.M. Cruse, R. Horton. 1985. Tillage effects on soil thermal properties. Soil Sci. Soc. Am. J. 49:968-973.

Ross, P.J., and B.J. Bridge 1987. Thermal properties of swelling clay soils. Aust. J. Soil Res. 25:29-41.

Riabova, E.P. 1952. Radiation and thermal regime of soil surface. (In Russian.) Review of Ph.D. diss. Agrophysical Research Institute, Leningrad.

Romanov, P.G., D.A. Kurtener, I.B. Uskov (1990). Optimum methods of thermal melioration for climate condition of North. (In Russian.) Trans. of the Congress: Rationalization use of nature in permafrost zone. (In Russian.) Yakutsk.

Sablovskaia, A.G. 1970. Investigation of thermal regime of Latvia soil. (In Russian.) Review of Ph.D. diss. Agrophysical Research Institute, Leningrad.

Sepaskhah, A.R., and L. Boersma 1979. Thermal conductivity of soil as a function of temperature and water content. Soil Sci. Soc. Am. J. 43:439-444.

Taylor, R.J., and K.D. Magic. 1984. Pulse method for thermal measurement. In Compendium of Thermophysical Property Measurement Methods. Plenum Press, New York. p. 305-336.

Extreme-Value Statistics for Maximum Soil Frost Penetration in the Northeastern U.S. Using Air Temperature and Snow Cover Data

A.T. DeGAETANO[1], D.S. WILKS[1], AND M. McKAY[1]

ABSTRACT

Extreme-value statistics for the depth of maximum soil freezing are developed based on model-derived soil freezing estimates. The model used is shown to be quite accurate at estimating the annual maximum depth of soil freezing using only daily air temperature, snow depth and precipitation data. These data are available from a relatively dense network of climatological observing stations, permitting the development of a regional climatology of extreme soil freezing levels based on the Gumbel distribution. This distribution was selected after evaluation of several other candidate distributions. The results suggest that maximum soil freezing depths in the northeastern United States are found across eastern Maine and north-central Pennsylvania. South of these areas, freezing depths decrease because of higher temperatures while, to the north, decreases in the depth of maximum soil freezing can be attributed to deeper and more persistent snow cover.

Keywords: Maximum frost depth, extreme-value analysis, northeastern USA, soil freezing model

INTRODUCTION

Information on the maximum depth of soil freezing is necessary for a variety of climate-sensitive applications ranging from building design to agricultural operations. Given this diversity in applications, requests for soil freezing data are frequently received by the Northeast Regional Climate Center (NRCC). Unfortunately, the only available published source of this information is based on unofficial, undocumented and antiquated (1899–1938) measurements (USDA, 1941). This situation has led us to develop a one-dimensional heat flow model similar to that described by Benoit and Mostaghimi (1985). The resulting physically based model estimates the rate and depth of frost penetration under bare soil and sod using only air temperature, precipitation and snow depth data. Since records of these data extend from the late 19th century to the present, and approximately 8000 stations are in operation nationwide (about 900 are in the northeastern U.S.), model-derived frost depth statistics can be developed for a relatively dense network of sites.

DESCRIPTION OF MODEL

Ideally, the calculation of regional soil freezing statistics should incorporate the features of physically based models to the extent possible (e.g., Flerchinger and Saxton 1989; Guymon et al. 1993; Cary et al. 1978). Given the limitations of meteorological measurements, even from a relatively dense network of stations, the use of such models in this application is not feasible. Alternatively, more empirical models (e.g., Aldrich and Paynter 1953) tend to require less-detailed meteorological data, but incorporate assumptions that make their use unrealistic for applications in which snow cover varies with time. The model that is briefly described in this section combines the desirable features of these two classes of soil freezing models. A more complete description of the model is given in DeGaetano et al. (1996).

---

[1] Northeast Regional Climate Center, Cornell University, Ithaca, New York 14853, USA

The theoretical basis for the model is that frost penetration is driven primarily by thermal diffusion. Figure 1 illustrates this principle. At the lower boundary Z_D, which is set at a depth of 2 m, a daily "deep" temperature T_D is given as a function of the average air temperature from the previous April through March of the current year, the 25th percentile January-through-March snow depth for the current year and the combined thermal diffusivity of the snow and soil. The model assumes that the flux of heat through the lower boundary is negligible.
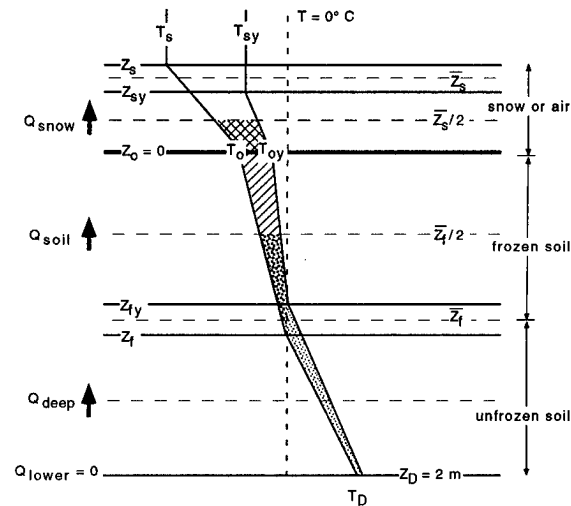
Figure 1. Schematic diagram showing the model's frozen soil state. Depths below or above (in the case of snow and air) the surface are indicated by Z and temperatures are indicated by T. Subscripts indicate snow (s), frozen soil (f), the soil surface (o), and the lower boundary (D). The subscript y refers to the value observed or estimated for the previous day. Heat flux through the center of each layer is indicated by a bold arrow. The stippled area represents the change in energy storage ΔQ_L and the hatched areas represent ΔQ_U.

The upper boundary condition is given by the observed average daily air temperature. Here the assumption is made that the average daily air temperature approximates the temperature of the snow surface. The snow depth Z_s gives the thickness of the first layer in the snow/soil system (Fig. 1). In the absence of snow cover, the air temperature is assumed to equal the temperature at the upper surface of a 1.0×10^{-3}-m laminar layer, the thermal properties of which are characteristic of still air. Progressing downward, soil layers of variable depth are defined by frozen and unfrozen zones, the boundaries of which are at 0°C (Fig. 1). A maximum of three soil layers (one frozen and two unfrozen) is allowed by the model.

Temperature gradients through each layer are assumed to be constant, and thus the heat flux Q_x at the middle of each layer is defined by the difference between the temperatures of the layer boundaries. Imbalances between the resulting vertical heat fluxes (i.e., heat flux convergence or divergence) are rectified by internal temperature changes and, when these changes cross 0°C, by freezing or thawing of soil at an appropriate depth. In this process, the fluxes are balanced by accounting for the heat capacities of soil solids and soil water, and for the latent heat of fusion. This is sketched in Figure 1 and given mathematically for the case when a frozen layer exists at the surface by the governing equation

$$Q_{snow} = Q_{froz} = Q_{deep} \qquad (1)$$

where

$$Q_{snow} = -K_{snow}(T_s - T_0)/Z_s + \Delta Q_U \qquad (2)$$

$$Q_{froz} = K_{froz}(T_0/Z_f) + \Delta Q_L \qquad (3)$$

and

$$Q_{deep} = K_{thaw}T_D/(Z_f - Z_D) + (Z_{fy} - Z_f)(\varepsilon - 0.1)L_f \qquad (4)$$

The variables used in Equations 1–4 are defined in Figure 1 with the exception of the latent heat of freezing L_f soil porosity ε, thermal conductivities of snow K_{snow}, frozen soil K_{froz}, and unfrozen soil K_{deep} and the change in heat storage terms ΔQ. Equations 1–4 are solved numerically for the prognostic variables T_0 and Z_f. Nearly saturated soil is assumed at all times, a valid assumption in the Northeastern U.S. In Figure 1, ΔQ_U is represented by the hatched and cross-hatched areas between the two consecutive daily average temperature profiles. Similarly, ΔQ_L is shown by the speckled and dotted regions.

Only one of three possible soil freezing states is illustrated by Figure 1. In this state a layer of frozen soil extends from the surface to some depth Z_f. The other possible states are that the soil may remain unfrozen from the surface to the lower boundary Z_D, or a layer of frozen soil may exist between two layers of unfrozen soil. In addition, five transition modes are possible, corresponding to the transitions between the three basic states, with the exception of the transition from unfrozen to a buried frozen layer, which is not physically realizable.

The model is initiated in the unfrozen-soil state and continues in this manner until T_0 falls below 0°C. At this point, the transition to frozen-soil mode is activated. Provided the temperature remains below

526

0°C. At this point, the transition to frozen-soil mode is activated. Provided the temperature remains below 0°C on subsequent days, the model operates in the frozen-soil state. In this state, both soil freezing and thawing can occur at the bottom of the frozen layer. When T_o exceeds 0°C the model transitions to either the unfrozen or surface thaw state. In the surface thaw state, the layer of frozen soil is allowed to thaw both from its top and bottom. The temperature throughout the buried frozen layer which results is assumed to be a constant 0°C. For subsequent occurrences of $T_o < 0$°C, freezing occurs at both the top and bottom of the buried frozen layer. Although physically unrealistic in that freezing should initially be allowed to occur only at the top of the surface-thaw layer, this formulation allows a solution without liberal assumptions regarding the temperature profile within a subsurface thawed layer. Given that the purpose of our model is to estimate the depth of maximum frost penetration, the omission of a second frozen layer at the surface is of little consequence.

MODEL VERIFICATION

Validation of the model was possible using frost depth data collected with six Army Corps of Engineers frost depth tubes (Ricard et al. 1976). These gauges were installed at the Ithaca, New York weather observation site, allowing coincident soil freezing and daily meteorological data to be collected. Three gauges were placed under sod. The remaining three gauges were located within a bare soil plot. Frost depth measurements were made on a weekly basis.

Verification of the bare soil case during the

winter of 1995-1996 is presented in Figure 2. Observed maximum frost depths under bare soil ranged from 42 to 26 cm, with a median frost depth of 34 cm (Fig. 2). In all cases, the maximum frost depth occurred between 21 and 29 February. During this winter, the maximum model-derived value of 40 cm occurred on 20 February, indicating exceptional correspondence between the observations and model estimate in both the timing and magnitude of maximum soil freezing. Over the course of the winter the model tracked the timing and progression of soil freezing quite closely (Fig. 2). Over the 15 soil freezing observations shown in Figure 2, the model exhibits a 1.8-cm bias toward overestimation of the observed frost depth, with a mean absolute error of 3.4 cm. Similar validation results were obtained for the sod-covered surface.

FROST DEPTH CLIMATOLOGY

Data

Model-derived annual maximum frost depths were calculated for a set of 306 northeastern U.S. cooperative network stations (Fig. 3). To be included, stations were required to have at least 30 years of non-missing daily climatological data. At all sites serially complete daily temperature data (DeGaetano et al., 1995) were available for one of four periods (1951–1993; 1951–1990, 1961–1993 or 1961–1990). Serially complete snow depth and precipitation data were not available. If missing, these parameters were estimated based on values at neighboring stations. Years were not considered if any data were missing for more than 7 consecutive days during October through April.
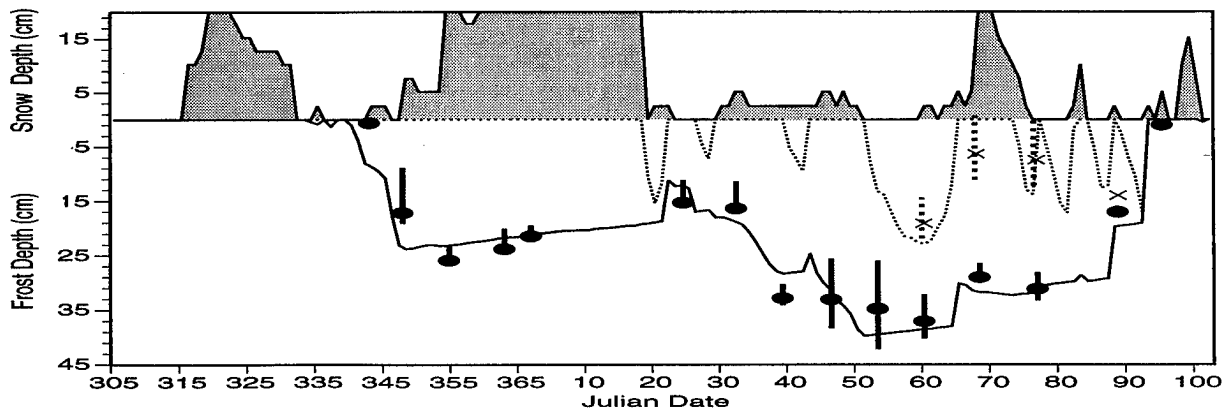
Figure 2. Observed versus estimated frost depths under a bare soil surface at Ithaca, NY for the winter of 1995–96. Modeled frost depths and surface thaw depths are given by the solid and dashed lines, respectively, and correspond to y-axis values ≤ 0. The bars show the range of three frost depth observations, with bold dots identifying the median. Dashed vertical lines and Xs similarly indicate observed thawing. Only two frost depth measurements were available on Julian days 38, 59, 66, 75 and 87. Daily snow depths are indicated by the gray regions at the top of the plot.

Figure 3. Locations of stations used to develop the extreme soil freezing climatology. At least 30 annual maximum frost depth values are available at each site.

Computation of return periods

Smoothing and extrapolation of the modelled annual maximum frost depth data for all stations was accomplished by fitting the Gumbel distribution (Wilks, 1995). This distribution was selected from a pool of 11 candidate distributions using a bootstrap procedure described by DeGaetano et al. (1997) The probability density function for the Gumbel distribution is

$$f(x) = \frac{1}{\beta}\exp\left\{-\exp\left[-\frac{(x-\xi)}{\beta}\right]-\frac{(x-\xi)}{\beta}\right\} \quad (5)$$

where x is the random variable (in this case, annual maximum frost depths). The distribution has two parameters: ξ is a location parameter, and β is a scale parameter. Separate distributions are fit to the data for each station by maximum likelihood. One convenient feature of the Gumbel distribution is that it is analytically integrable, so its cumulative distribution function can be written in closed form. That is, Gumbel probabilities can be obtained using

$$F(x) = \Pr\{X \le x\} = \int_0^x f(x)dx = \exp\left\{-\exp\left[-\frac{(x-\xi)}{\beta}\right]\right\} \quad (6)$$

Average return periods, R, relate to cumulative probabilities F of the distributions of annual maximum data according to

$$R = \frac{1}{\omega[1 - F(x)]} \quad (7)$$

where ω is the average sampling frequency, in this case 1 yr^{-1}. Subsequently, frost depth x, corresponding to a specified return interval is obtained by solving Equation 6 for x and substituting the expression $F(x) = 1 - 1/R$, obtained by rearrangement of Equation 7. These operations yield the expression for frost depth as a function of return period and the parameters of the fitted Gumbel distribution

$$x = \xi - \beta\ln[-\ln(1 - \frac{1}{R})] \quad (8)$$

Thus, it is estimated that frost depths as large or larger than x will be separated, on average, by the number of years given by the return period.

Return period mapping

Maps depicting the spatial distributions of maximum frost depths for specific return intervals were prepared by first gridding the individual station values, and then producing contour maps from the gridded fields by computer. The details of this gridding and contouring procedure are given in DeGaetano et al. (1997). As an example, Figure 4 shows a map of the 100-year return periods for maximum frost depth under bare soil using observed snow cover conditions. Similar maps can be generated for sod-covered and snow-free bare soil conditions. In addition, maps depicting 2-, 5-, 10-, 25- and 50-year return periods for these three surface conditions are available from the authors.
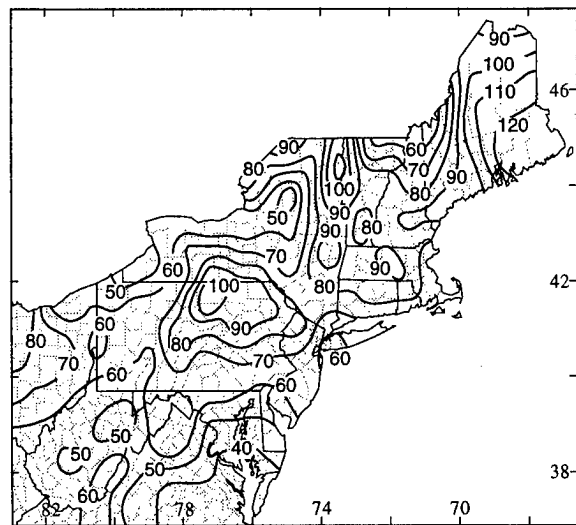
Figure 4. Maximum frost depths (cm) corresponding to the 100-year return period under bare soil.

528

SENSITIVITY TO SOIL PROPERTIES

The frost depths shown in Figure 4 depict results for soils having a clay content of 15% and a porosity of 45%. Non-clay soil particles are assumed to be quartz-based. It is further assumed that air occupies 10% of the available soil volume and that any remaining pore space is filled with water. Although this limits the model's application to wet soil conditions, this restriction is of little consequence over regions such as the northeastern United States, where high levels of soil moisture are typical during the period of soil freezing. In order to quantify the effect of differing clay contents and porosities on maximum frost depths, a geographically representative set of 30 stations was selected. At each of these sites separate frost depths corresponding to the 2-, 5-, 10-, 25-, 50- and 100-year return interval were calculated using soil porosities ranging from 30 to 60% in increments of 5%. Similarly, frost depths were computed for clay contents ranging from 2 to 50%, holding porosity constant at 45%. Separate sensitivity analyses were conducted for bare soil, sod and snow-free bare soil.

Modification of the clay content had little effect on the depth of soil freezing. In general, the difference in maximum soil freezing depth between the standard (15% clay content) and either clay content extreme (2 or 50%) was less than 5%. Given the reference clay percentage, changes in porosity, and thus water content, had a more pronounced effect on the maximum depth of frost penetration. Figure 5 shows these differences in maximum frost penetration as a ratio (multiplied by 100) of the maximum freezing depth based on the given porosity to that which occurred using the 45% standard porosity. Since the station-to-station and return-period-to-return-period differences in these ratios was quite small (generally ≤ 0.03), the values shown in Figure 5 are the medians over the 30 stations and 6 return periods. In application, Figure 5 can be used to adjust the maximum frost depth values presented in Figure 4 to values representative of a site-specific soil porosity. For example, to compute a 100-year return period frost depth for a bare-soil site in New York City having a soil porosity of 55%, the 80-cm value given in Figure 4 is multiplied by 0.89, yielding a depth of 71 cm.
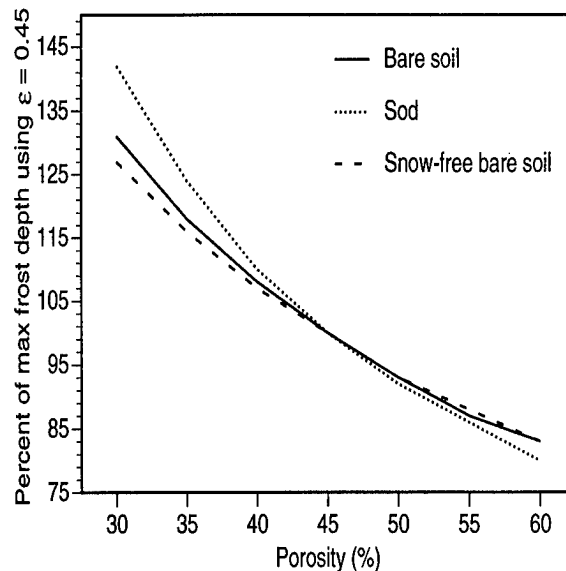
Figure 5. Graph of adjustment factors (percent of the maximum frost depth in a soil with standard porosity of 0.45) used to convert the maximum frost depth values presented in Figure 4 to values representative of a site-specific soil porosity. Adjustment factors are medians over the 30 stations and 6 return periods

SUMMARY

Measured soil freezing depths are not available at a network of stations that is sufficiently dense for most climatological applications. Therefore, a model capable of estimating annual maximum soil freezing depths quite accurately using only those meteorological variables measured by the relatively dense cooperative observer network was used to develop an extreme-value climatology of maximum frost depths in the northeastern United States.

Across the northeastern U.S., maximum frost depths under bare soil tend to be deepest in eastern Maine, where the estimated frost depths associated with the 50- and 100-year return periods exceed 110 cm and 120 cm, respectively. A secondary frost depth maximum occurs in north-central Pennsylvania, where the 50- and 100-year maximum estimated frost depths exceed 90 cm and 100 cm, respectively. This pattern of deepest maximum frost depths is repeated for sod-covered surfaces. However, frost depths are generally 55–75 % shallower under sod.

South of the New York–Pennsylvania border, there is a general decrease in maximum frost depth with latitude. This pattern tends to reverse to the north of that border, as maximum frost depths generally decrease as latitude increases. Maximum

frost depths also decrease toward the coast due to lower elevation and the modifying effect of the Atlantic. Except for Virginia, southern Maryland and Delaware, the shallowest maximum frost depths are found along the shores of the Great Lakes, over the Tug Hill Plateau region of New York (to the east of Lake Ontario) and in extreme northern New Hampshire. Exceptions to this general northward decrease in maximum frost depths occur in the Champlain Valley along the New York-Vermont border and through much of southern New Hampshire. Local variation in insulating snow depth is the likely cause of this spatial pattern of maximum frost depth in the northern part of the domain.

REFERENCES

Aldrich, H.P., and H.M. Paynter. 1953. Analytical studies of freezing and thawing of soils." First interim report. U.S. Army Corps of Engineers, New England Division, Arctic Construction and Frost Effects Laboratory (ACFEL) Technical Report 42.

Benoit, G.R. and S. Mostaghimi. 1985. Modeling soil frost depth under three tillage systems. Trans. ASAE. 28(5)1499-1505.

Cary, J.W., G.S. Campbell and R.I. Papendick. 1978. Is the soil frozen or not? an algorithm using weather records. Water Resour. Res. 14(6)1117-1122.

DeGaetano, A.T., K.L. Eggleston, and W.W. Knapp. 1995. A method to estimate missing daily maximum and minimum temperature observations. J. Appl. Meteor. 34:371–380.

DeGaetano, A.T., D.S. Wilks, and M. McKay. 1996. A physically-based model of soil freezing in humid climates using air temperature and snow cover data. J. Appl. Meteor. 35:1009–1027.

DeGaetano, A.T., D.S.Wilks, and M. McKay. 1997. Extreme-Value Statistics for Frost Penetration Depths in the Northeastern U.S. Journal of Geotechnical Engineering (in press).

Flerchinger, G.N. and K.E. Saxton. 1989. Simultaneous heat and water model of a snow-residue-soil system - I. Theory and development. Trans. ASAE, 32(2) 565-571.

Guymon, G.L., R.L. Berg, and T.V. Hromadka. 1993. Mathematical model of frost heave and thaw settlement in pavements. U.S. Army Corps of Engineers, Cold Regions Research & Engineering Laboratory (CCREL) Report 93-2.

Ricard, J.A., W. Tobiasson, and A. Greatorex. 1976. The field assembled frost gage. U.S. Army Corps of Engineers Cold Regions Research and Engineering Laboratory Technical Note.

USDA. 1941. Climate and man, yearbook of agriculture 1941. U.S. Government Printing Office, Washington, DC.

Wilks, D.S. 1995. Statistical methods in the atmospheric sciences. Academic Press, San Diego, CA.

A Comparison of Three Models
for Predicting Frost in Soils

I. KENNEDY[1] AND B. SHARRATT[1]

ABSTRACT

Three existing soil models capable of simulating soil frost depths and temperatures were evaluated for their ability to predict the depth and timing of soil frost at sites in northern and Midwestern North America. The evaluation was carried out by comparing model simulation results to observed field data. The data used in the comparisons came from two sites, one near Delta Junction, AK, characterized by a Cryaquept soil with grass cover, and the other near Morris, MN, characterized by a Haploboroll soil with corn stubble. Two of the models use a finite difference solution to heat flow in the soil profile, and both predicted frost depth with reasonable accuracy, at least when the simulated snow depth closely matched the recorded snow depth. The third model balances heat fluxes and vastly overpredicted frost depths. The results illustrate the importance of snow cover in controlling soil frost as well as the difficulty in accurately simulating snow cover and soil frost.

Keywords: Modeling, Soil frost depth, SHAW, SOIL

INTRODUCTION

Soil freezing can affect the physical, biological and chemical processes of landscapes. Frost in soil can cause enhanced erosion, flooding, and, as a result of lower infiltration, damage to roads and buildings. Changes in soil physical characteristics are caused by processes more complex than ice formation. Frost heave, for example, is caused by water migrating to a freezing front and thus depends on the hydraulic characteristics of a soil as well as freezing conditions. Frost depth determines to some extent the stability of the soil surface as well as the water storage capacity of the surface. Information about the depth of frost aids state and federal agencies in assessing the potential for flooding and municipalities in determining the depth at which to bury water pipes to prevent freezing. Prediction of frost depths is also useful in regions where probing is incapable of penetrating frozen soil. Thus, an ability to model frost depth can be beneficial to managing resources in communities and watersheds. This study compares three models for assessing frost depth in soils.

A BRIEF DESCRIPTION OF THE MODELS

Three models were tested for their ability to predict frost depths over two winters in west central Minnesota and central Alaska. The simplest model, here called "FROST" (Benoit 1974; Benoit and Mostaghimi 1985) predicts frost depth by balancing heat fluxes in the frozen and unfrozen layers of soil. The other two models "SHAW" (Flerchinger and Saxton 1989a) and "SOIL" (Jansson 1991) use a finite difference method to solve heat and water flow equations for the soil profile.

SHAW has been used successfully to predict frost depths under different tillage systems in the U.S.A. (Flerchinger and Saxton 1989b) and Canada (Hayhoe 1993). Soil temperatures during early winter in Sweden have been underpredicted by SOIL (Thunholm 1990). Benoit and Mostaghimi (1985) reported good results using FROST in central Minnesota, but Van Rooij (1987), in an independent

[1] USDA, Agricultural Research Service, North Central Soil Conservation Research Laboratory, Morris, Minnesota 56267, USA

study, found that FROST overpredicted frost depth in Idaho. This study, however, used a modified version of FROST that included simulation snowmelt (using an energy balance method) and accumulation on the soil surface (Young et al. 1993), rather than reading snow depths directly with other weather data.

EXPERIMENTS

Field data to test the three models were collected in west-central Minnesota during the 1993–1994 and 1994–1995 winters and near Delta Junction, Alaska, during the 1991–1992 and 1992–1993 winters. Microclimatic information was collected at 60-second intervals and averaged hourly at both locations. These data included air temperature, relative humidity, wind speed and direction, solar radiation and liquid precipitation. Frozen precipitation was collected daily at cooperative weather stations 15 km from the Minnesota research site and 20 km from the Alaska research site. Comparison of summertime precipitation between the two Minnesota locations showed nearly identical amounts of rainfall.

were recorded at depths of 0.05, 0.10, 0.20, 0.40, 0.80, 1.60, 2.40 and 3.20 m below a sparse grass canopy. No observations were made of frost depth.

The hourly soil temperatures were averaged to produce daily values for comparison with the models. Temperature isotherms were constructed for both the observed and simulated data. Technical difficulties with datalogging equipment prevented collecting soil temperature data throughout each winter, particularly for the winter of 1991–1992 in Alaska and for the winter of 1994–1995 in Minnesota.

Boundary conditions for the models included a soil temperature of 0.55°C at the bottom of the soil profile in Alaska, and 4.5°C at the bottom of the profile in Minnesota. Initial conditions for the simulations were based on measured soil temperatures and moisture contents near the simulation start date.

Soil types were a Barnes (Udic Haploborolls) loam in Minnesota and a Volkmar (Aquic Cryaquept) loam in Alaska. Selected physical properties of both soils needed for simulations are reported in Table 1.

All parameters in SOIL model were set at default values, except for a parameter dubbed "SMTEM," which the program uses to control how fast snow

Table 1. Selected properties of the soils at the experimental sites

Soil	Organic matter	Bulk density	Sand (%)	Silt (%)	Clay (%)	Saturated conductivity (cm/hr)
Barnes	5.86	1.20	47.7	33.8	18.5	0.5
Volkmar	5.75	1.34	59.8	34.7	5.6	1.5

In Minnesota, experimental plots included corn stalks at heights of 0, 0.3, and 0.6 m, with a corn residue cover of about 60% for all three cases. The corn stalks affected the depth of snow accumulation on the soil surface and thus were a strong influence on frost depth. Frost depths were monitored twice weekly using frost tubes and snow depths were recorded at the same time. Soil temperatures were measured at 60-second intervals and averaged hourly at depths of 0.01, 0.05, 0.10, 0.20, 0.50, 1.0 and 2.0 m in Minnesota. In Alaska soil temperatures

melts in warm air. This parameter was adjusted to prevent complete snow melt during warm periods in the winter. No parameters in FROST or SHAW were adjusted in this study.

RESULTS AND DISCUSSION

Frost depths and soil temperature isotherms simulated by the three models were the basis of comparison to measured data in this study. Overall, in the absence of corn stubble, SHAW estimated frost
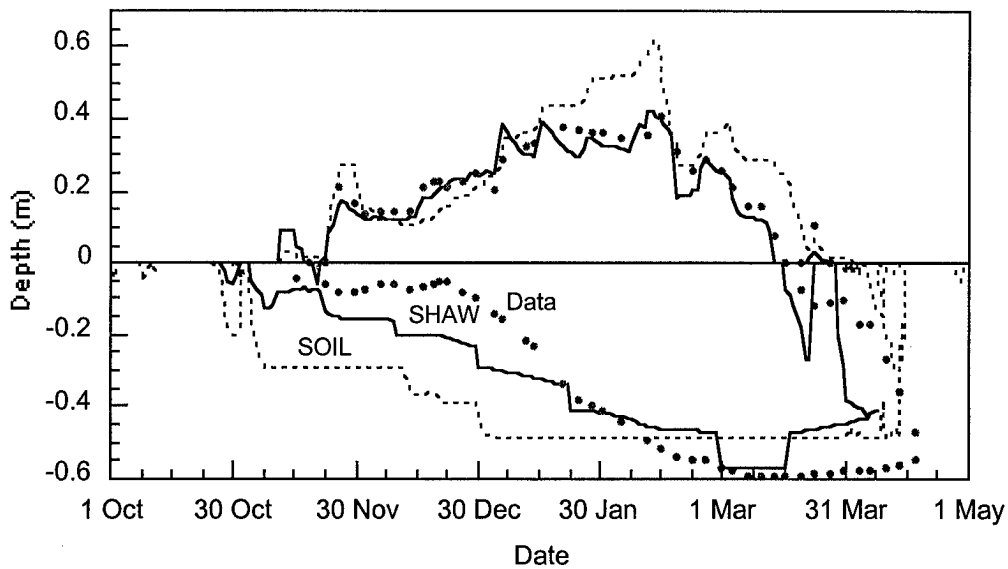
Figure 1. Simulated and measured frost and snow depths near Morris, for the winter of 1993–1994. Unconnected data points represent the data, the solid line represents the SHAW simulation and the dashed line represents the SOIL simulation.
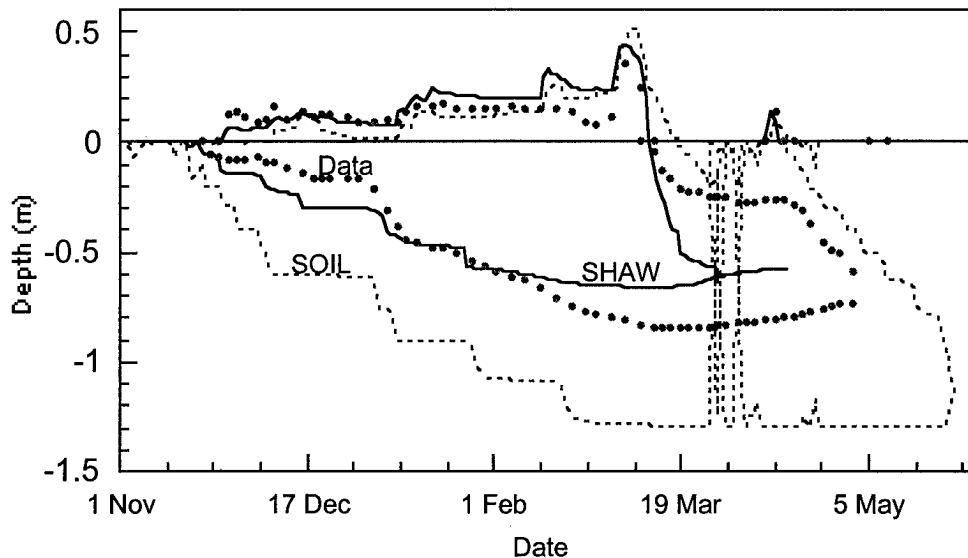
Figure 2. Simulated and measured frost and snow depths near Morris, for the winter of 1994–1995. Unconnected data points represent the data, the solid line represents the SHAW simulation and the dashed line represents the SOIL simulation.

in the absence of corn stubble, SHAW estimated frost depth at Minnesota better than SOIL (Figs. 1 and 2) and FROST (Fig. 3). However, both SOIL and SHAW overestimated the rate of frost penetration as the soil froze in the fall and underestimated the rate later in the season. The faster rate of frost penetration resulted in deeper depths in the season, compared to the measured frost depths. During the 1994-1995 winter, SOIL overestimated the maximum depth of frost by 50% and SHAW underestimated the depth
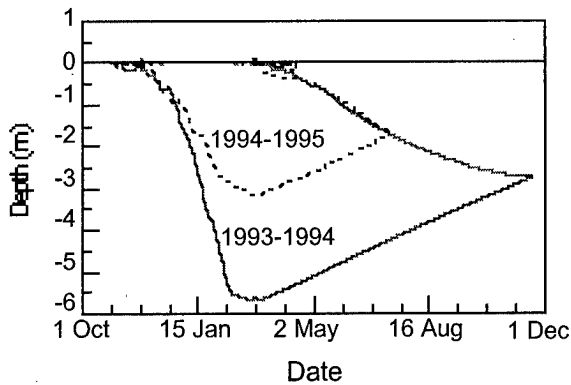
Figure 3. Frost depths near Morris, MN
predicted by FROST for the winters of
1993–1994 (solid line) and 1994–1995 (dashed
line).

by 20%. The cause of overestimation in the SOIL
simulations during the 1994–1995 winter may be due
to underprediction of snow depths. Examination of
Figs. 1 and 2 illustrates that SOIL reasonably
predicted snow depths during the 1993–1994 winter,
but consistently underpredicted snow depth during
the winter of 1994–1995.

Simulated and measured temperature isotherms

(–0.05°C and –0.90°C) are shown in Figs. 4 and 5.
Time series trends in temperature isotherms for
Minnesota during 1993–1994 (Fig. 4) were similar to
trends in frost depth (Fig. 1). In Alaska, differences
between frost depths simulated by SOIL and SHAW
were inconsistent, with SOIL predicting deeper frost
in 1991–1992 and SHAW predicting deeper
penetration in 1992–1993 (Fig. 5). Data below 40 cm
are unavailable for winter 1991–1992, but the data
that are available show that SHAW missed the
timing of the first significant frost penetration by
close to two months, and both SOIL and SHAW
predicted thawing much later than it was observed.
By contrast, the timing is much better for the winter
of 1992-1993 with both models predicting the initial
frost early and the spring thaw a little late.

Snow and frost depths during the winter of
1994–1995 in Minnesota are shown in Fig. 6 (the
previous winter shows similar behavior) and illustrate
the degree to which measured frost depths varied
markedly between the corn stalk height plots. The
taller corn stalks trapped more snow with a snow
depth approximately equal to the stalk height during
the winter. The enhanced snow catch resulted in a
shallower layer of frost. During the 1994–1995
winter, the soil froze only slightly and intermittently
in the 0.6-m stalk plots. None of the models simulate
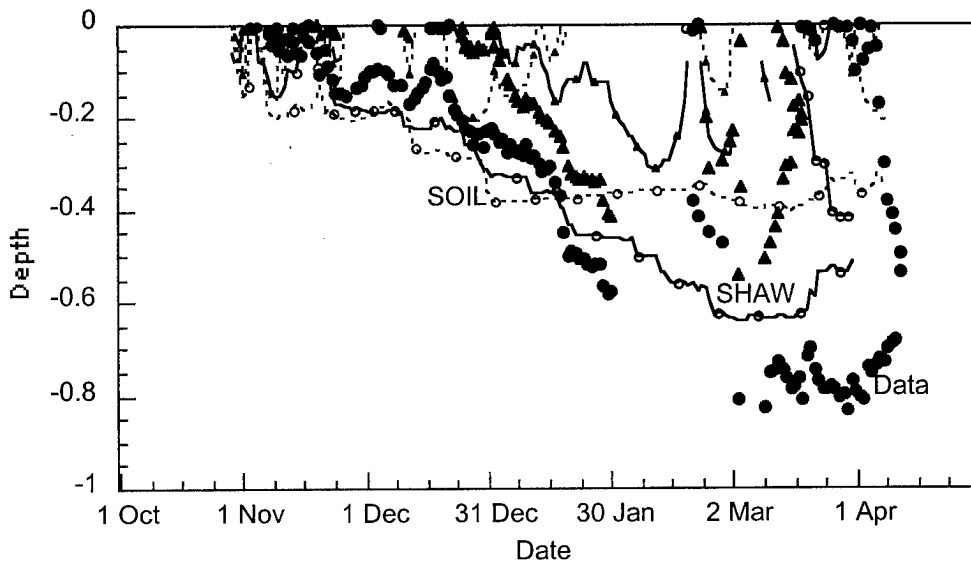
Figure 4. Comparison of temperature isotherms near Morris for the winter of
1993–1994. Circles denote the -0.05°C isotherm while triangles denote the -0.90°C
isotherm Data is denoted by unconnected data points whild simulation by the models
are denoted by lines tagged with symbols representing the temperature. Solid lines
represent SHAW simulation data while dashed lines represent SOIL simulation data.

534
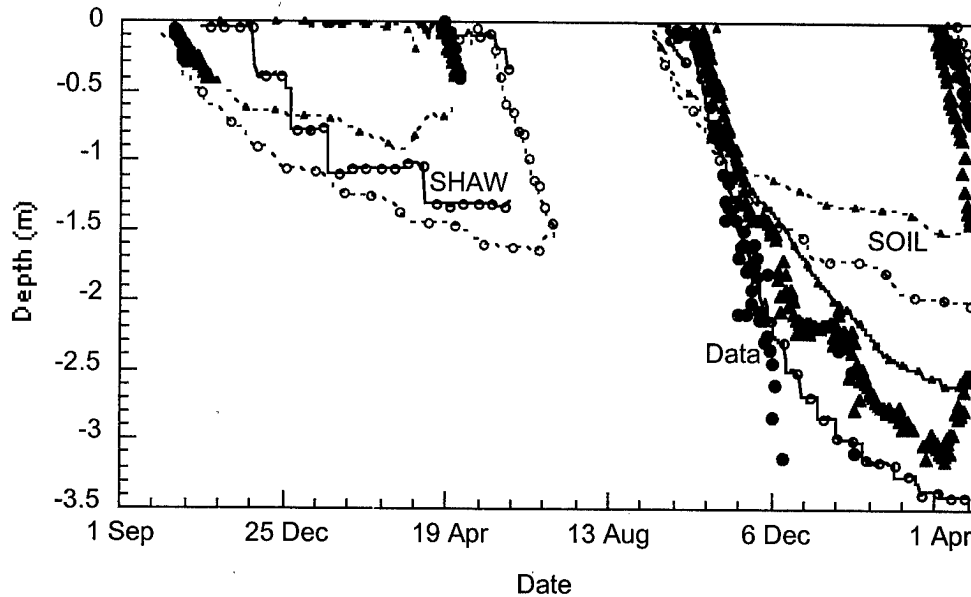
Figure 5. Comparison of temperature isotherms near Delta Junction, AK for fall 1991 to spring 1993. Circles denote the –0.05°C isotherm while triangles denote the –0.90°C isotherm Data is denoted by unconnected data points whild simulation by the models are denoted by lines tagged with symbols representing the temperature. Solid lines represent SHAW simulation data while dashed lines represent SOIL simulation data.

the enhanced snow cover due to trapping and thus cannot account for decreased frost depths in such situations. The FROST model simulates wind-blown snow, but does not account for trapping due to vegetation. Therefore, FROST did not adequately predict snow depth in standing corn stalks.

FROST overestimated the depth of frost in all
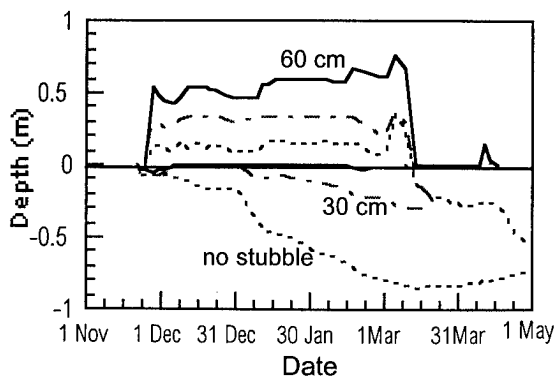
Figure 6. Recorded snow and frost levels near Morris, MN for the winter of 1994-1995. Solid line is for the plot with 0.6 m corn stubble, dot-dash for 0.3 m stubble and dashed line for no corn stubble.

magnitude. This is illustrated in Figs. 3 and 7 for winters at Minnesota and Alaska, respectively. At Minnesota, FROST predicted frozen soil at the 2.5-m depth for the entire summer of 1994. The enhanced depth of freezing simulated by FROST may be due to the inability to track snow depth. FROST predicts a relatively linear rate of thaw from both the top and bottom of the soil profile despite varying environmental conditions. Rates of thaw from the top and bottom of the soil profile were also more nearly equal, whereas measured thaw rates were much faster from the top than from the bottom of the soil profile. The steady rate of thaw predicted by FROST is in contrast to the data and the simulation of the SOIL and SHAW models, all of which predict an accelerating rate of thaw with time in the spring, due to of an increase in daily air temperatures as well as a gradual warming of the frozen portion of the soil.

CONCLUSIONS

The finite difference models (SOIL and SHAW) simulated frost depth and soil temperatures reasonably well under a range of soil and climate conditions. Significant errors were observed between the predictions of these models and measured data,

535
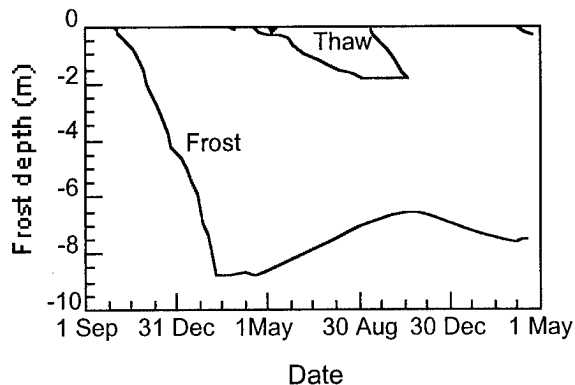
Figure 7. Frost depths near Delta Junction
predicted by FROST for fall 1991 to spring 1993.

but these errors did not portray a general pattern.
Frost depth was at times overpredicted as well as
underpredicted. One weakness in these models
appears to be related to estimating snow depth, which
had a very strong influence on soil freezing. The
capability of SHAW to better simulate snow depth
compared to SOIL and FROST may be one reason
for its overall better performance in estimating frost
depth.

FROST did not predict either frost or snow depth
accurately. Part of the inability to predict frost depth
is due to the inability to predict snow depth.
Nevertheless, the simulation did not predict the rate
of freezing or thawing in a manner consistent with
either SOIL or SHAW, or with observed data.

REFERENCES

Benoit, G. R. 1974. Frost Depth and Distribution
From a Heat Flow Model. Proc. Eastern Snow Conf,
Feb 7-8 1974. pp. 123-144.

Benoit, G. R. and S. Mostaghimi. 1985. Modeling

Soil Frost Depth under three Tillage Systems. Trans
ASAE 28: 1499-1505.

Jansson, P-E., 1991. Soil water and heat model.
Technical description. Division of Agricultural
Hydrotechnics Report 165, Department of Soil
Sciences, Swedish University of Agricultural
Sciences, Uppsala. 72pp.

Flerchinger, G. N. and K. E. Saxton. 1989a.
Simultaneous heat and water model of a freezing
snow-residue-soil system I. Theory and development.
Transactions of the ASAE 32(2):565-571.

Flerchinger, G. N. and K. E. Saxton. 1989b.
Simultaneous heat and water model of a freezing
snow-residue-soil system II. Field verification.
Transactions of the ASAE 32(2):565-571.

Hayhoe, H. N. 1994. Field testing of simulated soil
freezing and thawing by the SHAW model. Canadian
Agricultural Engineering. 36(4):279-2851.

Thunholm, B. 1990. A comparison of measured and
simulated soil temperature using air temperature and
soil surface energy balance as boundary conditions.
Agricultural and Forest Meteorology, 53: 59-72.

van Rooij, C. W. D. M. 1987. Two computer models
to predict the maximum frost penetration in the soil.
Ph.D. University of Idaho.

Young, R. A., G. R. Benoit and D. K McCool. 1993.
Modeling the effects of over-winter processes on soil
erosion and soil erodibility. Proceedings of an
International Workshop on Soil Erosion, Moscow,
Russia, The Center of Technology Transfer and
Pollution Prevention, West Lafayette, IN.

Young, R. A., C. A. Onstad and D. D. Bosch. 1996.
AGNPS: An Agricultural Nonpoint Source Model.
In: Computer models in watershed hydrology, V. J.
Singh (Ed.) Water Resources Publications, Littleton,
CO.

Modeling Soil Freezing and Thawing, and Frozen Soil Runoff With the SHAW Model

G.N. FLERCHINGER[1] AND M.S. SEYFRIED[1]

ABSTRACT

The occurrence of frozen soil can result in significant runoff and erosion events from otherwise mild rainfall or snowmelt events. However, most hydrologic models, including most snowmelt runoff models, include no provisions for soil freezing and thawing, and thus cannot address these extreme, yet common, hydrologic events. The Simultaneous Heat and Water (SHAW) model represents one of the more detailed models of snowmelt and soil freezing and thawing, however the ability of the model to simulate frozen soil runoff has not been evaluated. Thus, the SHAW model was applied to two years of data collected on small (1 m^2) runoff plots on the Reynolds Creek Experimental Watershed in southwest Idaho to demonstrate the ability of the model to simulate freezing-induced moisture migration and to test the ability of the model to simulate frozen soil runoff. Freezing/thawing processes, including liquid water content, were simulated reasonably well. Total runoff simulated from vegetation-covered plots was within the range of measured runoff, but timing was off. Both magnitude and timing of runoff from the bare plots were simulated quite well.

Key words: Moisture migration, unfrozen water content, rangeland

INTRODUCTION

Seasonally frozen soil plays a significant role in the hydrology of northern latitudes. In many areas, rain or snowmelt on seasonally frozen soil is the single leading cause of severe runoff events, but efforts to predict frozen soil runoff have had limited success. Ice blocks the soil pores and greatly diminishes the permeability of the soil when frozen. This is aggravated by the tendency of water to migrate to the freezing front, causing elevated ice contents and frost heave. The Simultaneous Heat and Water model, originally developed by Flerchinger and Saxton (1989) and later updated by Flerchinger and Pierson (1991) and Flerchinger et al. (1996) is capable of simulating the complex wintertime phenomena of snow accumulation and melt, detailed soil freezing and thawing including freezing-induced moisture migration, and associated frozen soil runoff. The objective of this study was to demonstrate the ability of the SHAW model to simulate the processes of soil freezing and thawing and frozen soil runoff. Specifically, this paper demonstrates the ability of the model to simulate soil freezing and thawing processes, particularly with respect to liquid water content, and tests the ability of the model to predict runoff from frozen soil.

THE SHAW MODEL

The SHAW model is a Simultaneous Heat and Water model of a plant-snow-residue-soil system. The system includes a detailed representation of a one-dimensional profile extending from a point in the atmosphere to another within the soil profile. The system may or may not have plant cover or residue and will accumulate and melt snow. The system is represented by integrating detailed physics of heat, water and solute flow through vegetation cover, snow, residue and soil into one simultaneous solution. Weather conditions are used to calculate heat and water flux at the surface boundary, which

consists of absorbed solar radiation, net long-wave radiation exchange, and sensible heat exchange, latent heat exchange and evapotranspiration.

Through an iterative process, flux at the upper boundary is computed concurrently with the interrelated heat, water and solute transfer between nodes down through the system. The equation used for describing heat flow within a partially frozen soil is

$$\frac{\partial}{\partial z}\left(k_s \frac{\partial T}{\partial z}\right) + \rho_l c_l \frac{(\partial q_l T)}{\partial z} + S =$$
$$C_s \frac{\partial T}{\partial t} - \rho_i L_f \frac{\partial \theta_i}{\partial t} + L_v \left(\frac{\partial \rho_v}{\partial t} + \frac{\partial q_v}{\partial z}\right) \tag{1}$$

where z is depth from the soil surface (m), k_s is soil thermal conductivity (W m^{-1} C^{-1}), T is temperature (C), ρ_l and ρ_i are density of water and ice (kg m^{-3}) c_l is heat capacity of water (J kg^{-1}C^{-1}), q_l and q_v are liquid (m/s) and vapor (kg m^{2}s^{-1}) water flow, S is a source/sink term(W m^{-3}) for heat flow, C_s is the volumetric heat capacity of the soil (J m^{-3}C^{-1}), t is time (s), L_f and L_v are latent heat of fusion and vaporization (J kg^{-1}), θ_i and θ_l are volumetric ice and water content (m^{3}m^{-3}), and ρ_v is vapor density (kg m^{-3}). This equation states that the net heat transfer into the layer by conductive and convective transfer is satisfied by a change in temperature, a change in ice content of the soil, and latent heat of vaporization within the layer.

The water flux equation for frozen soil is written as:

$$\frac{\partial}{\partial z}\left[K\left(\frac{\partial \psi}{\partial z} + 1\right)\right] + \frac{1}{\rho_l}\frac{\partial q_v}{\partial z} + U =$$
$$\frac{\partial \theta_l}{\partial t} + \frac{\rho_i}{\rho_l}\frac{\partial \theta_i}{\partial t} \tag{2}$$

where K is unsaturated hydraulic conductivity (m s^{-1}), ψ is soil matric potential (m), and U is a source/sink term for water flux (m^{3}m^{-3} s^{-1}). For the water flux equation, the net liquid and water vapor flux into a layer is equal to a change in ice and water contents of the layer. Here, the relation assumed for the moisture characteristic equation is (Brooks and Corey 1966)

$$\psi = \psi_e \left(\frac{\theta_l}{\theta_s}\right)^{-b} \tag{3}$$

where ψ_e is air entry potential (m), b is a pore size distribution parameter, and θ_s is saturated water content (m^{3}m^{-3}). Unsaturated hydraulic conductivity is computed from

$$K = K_s \left(\frac{\theta_l}{\theta_s}\right)^{(2b + 3)} \tag{4}$$

where K_s is saturated hydraulic conductivity.

Unknowns in equations 1, 2 and 3 are temperature, water content, ice content, and matric potential so an additional equation is needed for a solution. This is provided by the Clausius-Clapeyron equation. When ice is present, and for now neglecting the effects of solutes, total water potential is equal to the matric potential and is related to temperature by (Fuchs et al. 1978):

$$\phi = \psi = \frac{L_f}{g}\left(\frac{T}{T + 273.16}\right) \tag{5}$$

where g is the acceleration of gravity (m s^{-2}). Thus, as the temperature drops, the water potential becomes more negative, creating a gradient in water potential and causing moisture movement toward the freezing front. (An additional term is required in the above equation when the effects of solutes are considered and is included in the model, but is omitted here for simplicity.)

Equations 1 and 2 are solved iteratively and simultaneously by an implicit finite difference scheme using a Newton-Raphson iterative technique. One iteration for the energy flux equation is followed by an iteration of the water flux equation until subsequent iterations are both within a prescribed tolerance. Temperature, water content and soil matric potential are solved for each specified soil depth within the soil profile along with temperature and moisture profiles in the residue, plant canopy and snowpack. Further model details concerning simulation of heat and water transfer for a multi-species plant canopy are given by Flerchinger et al. (1996) and for a snowpack and residue layer by Flerchinger and Saxton (1989).

Infiltration and runoff are simulated using the Green-Ampt infiltration equation and computed at the end of each time step. Effective hydraulic conductivity, K_e, for infiltration is determined by substituting the effective porosity, computed from ($\theta_s - \theta_i$), for θ_l in equation 4. K_e is then reduced linearly depending on ice content and assuming zero

538

conductivity at an available porosity of 0.13 (Bloomsburg and Wang 1969).

SITE DESCRIPTION AND FIELD DATA

The study site was located at the Lower Sheep Creek site, which is a long-term (over 30 years) weather observation site on the Reynolds Creek Experimental Watershed in southwest Idaho. Hourly weather observations of air temperature, wind speed, humidity, and solar radiation are collected at the site along with break point precipitation data. The site is located at an elevation of 1620 m and receives 361 mm of precipitation annually; the area has sparse sagebrush cover with essentially bare ground in the interspace areas between plants

An eight-year study to examine soil freezing processes and frozen soil runoff was initiated in 1989. The study was located on a silt loam soil having a distinctive argillic horizon (40% clay) approximately 25 cm deep. The site had a west-facing slope of 17%. Instrumentation was installed to measure soil water and temperature profiles to a depth a 1 m at four locations, two located under sagebrush plants and two located in the bare interspace area. Soil water was measured hourly using fiberglass moisture blocks calibrated with approximately weekly readings of unfrozen liquid water content using time-domain reflectometry (Seyfried 1993). Runoff was measured from four "miniature" plots approximately 1 m² in size. Two miniature runoff plots were covered by sagebrush and two were located in the bare interspace areas

between sagebrush plants.

MODEL SIMULATIONS

The model was applied to two winter seasons: the 91-92 season which had very little precipitation and snowcover and no runoff; and the 92-93 season which had considerably more precipitation and snow, and the highest runoff measured during the 8-year study. Two separate model runs were conducted for each year: one for the sagebrush areas assuming a leaf area index of 0.5 and modest residue; and one for the bare interspace areas. Results were compared with measured temperatures profiles, water content inferred from the fiberglass soil moisture blocks, and runoff from the miniature runoff plots.

1991-92 Season

The 1991-92 winter season was a particularly dry year with little snowcover and no runoff. Simulated snow and frost depth for the bare interspace are plotted in Figure 1. The lack of significant snowcover and runoff allow us to focus more closely on the freezing processes. Frost during this year linger around 15 cm for much of the winter season. The surface of the bare interspace area experienced several brief thaw cycles.

Simulated total water content and simulated and measured liquid water at the 5, 10, and 20 cm depths under a sagebrush site for the entire winter season are plotted in Figure 2. Measured liquid water contents were inferred from fiberglass blocks, which give only trends in water content. Considerable ice
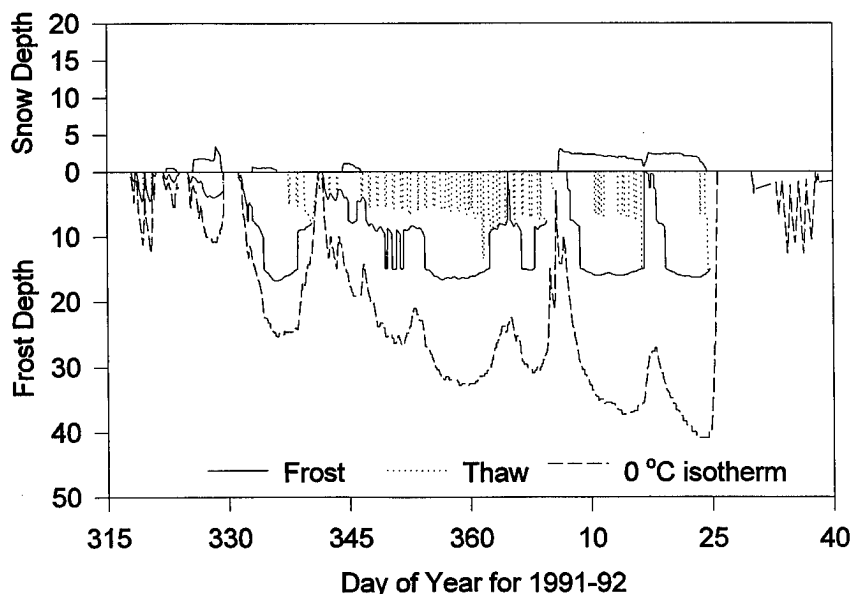
Figure 1. Simulated snow depth, frost depth, thaw depth, and depth of 0°C isotherm for the 1991-92 bare interspace site.

539

accumulation was simulated at the 5-cm layer as water migrated up from the lower depths. The simulated and measured liquid water content dropped in the 5-cm layer as ice formed. An associated drop in liquid water content in the 10-cm layer can be attributed to water migrating up to the 5-cm layer. As the 10-cm layer froze and gradually accumulated water that subsequently froze, there was also a slight decrease in water content at the 20-cm level as water migrated upward.

Simulated and measured water contents for an interspace area plotted in Figure 3 can be compared with those for the sagebrush area in Figure 2. While

simulated liquid water content roughly mimicked the trends measured by the fiberglass blocks, not nearly as much ice accumulated in the interspace simulation as for the sagebrush. We attribute this phenomena partly to the fact that the bare interspace started freezing at a slightly lower water content and, with less cover to insulate it, froze somewhat quicker. Both of these conditions tended to reduce the opportunity for water to migrate up to the freezing front.

1992-93 season

More precipitation fell in the 1992-93 winter
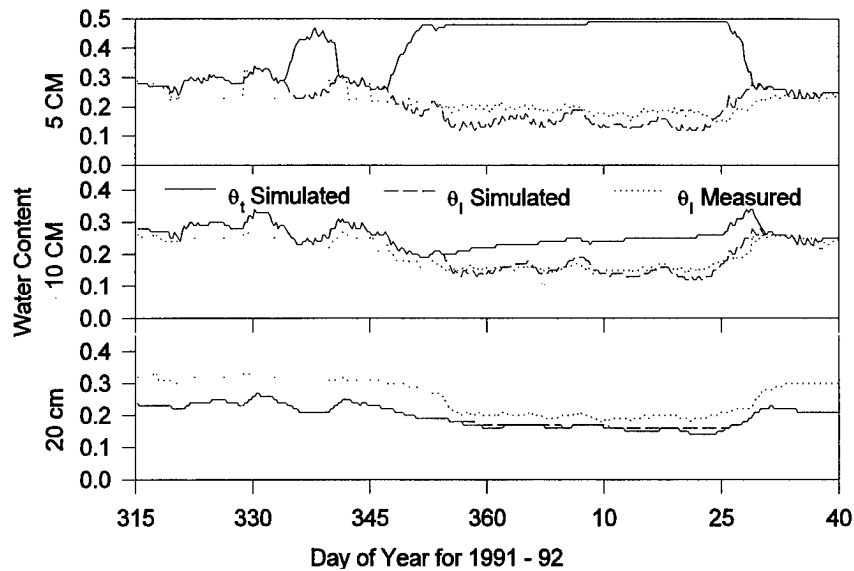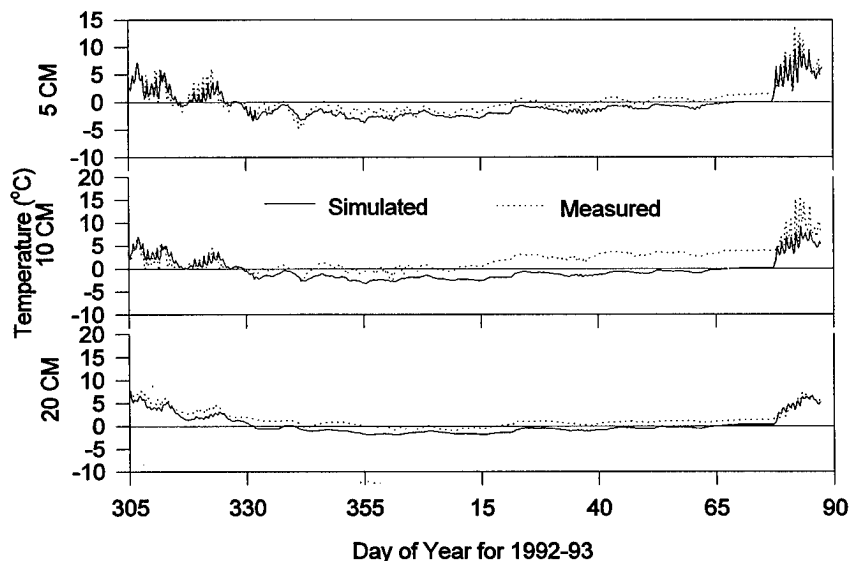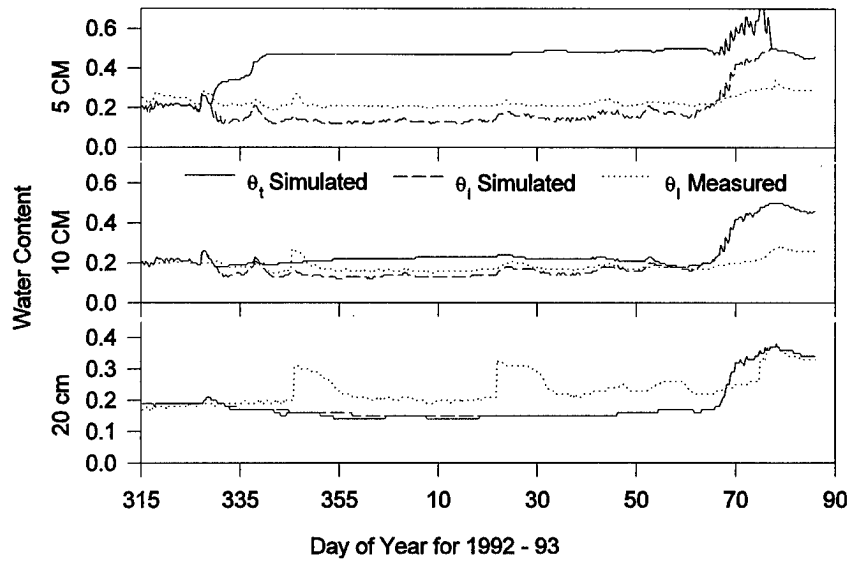

Figure 2. Simulated total water content and simulated and measured liquid water content for the 1991-92 sagebrush site.
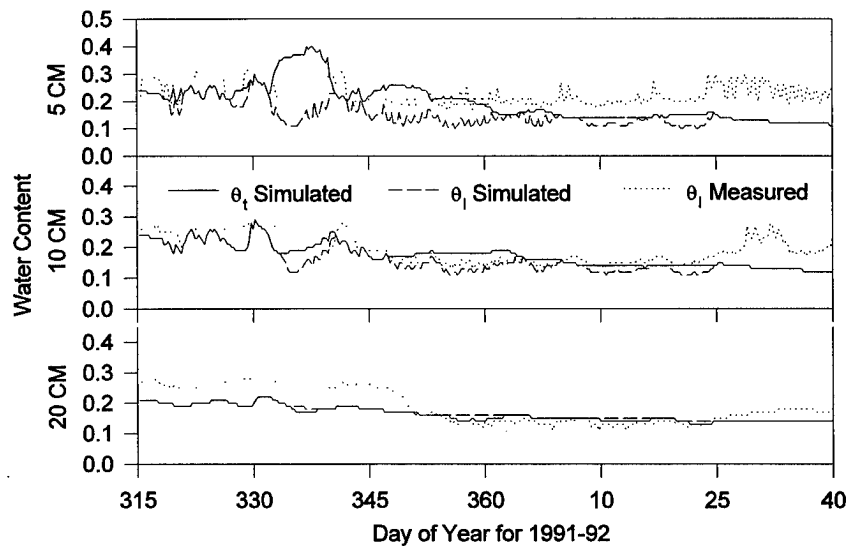
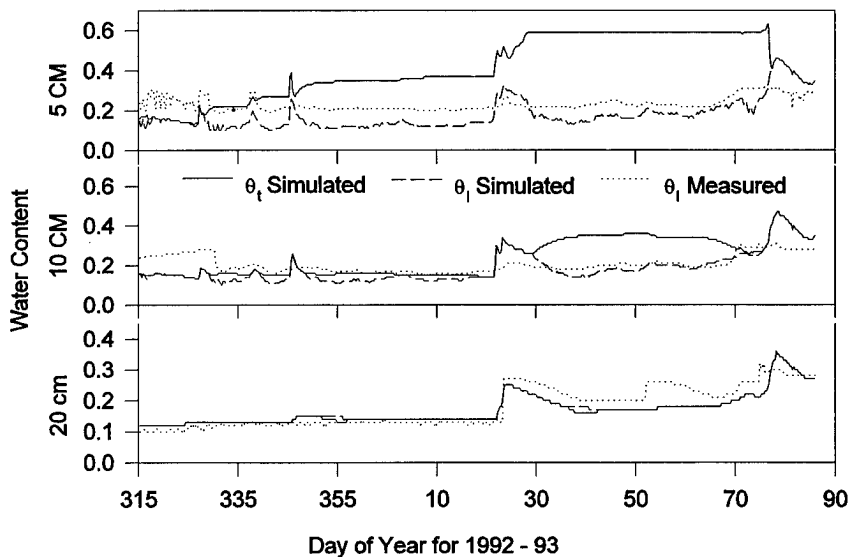*Figure 3. Simulated total water content and simulated and measured liquid water content for the 1991-92 bare interspace site.*

540

season, which had significantly more snowcover and the largest runoff of any of the other years measured during the study. Simulated frost and snow depth for a sagebrush-covered site for this year are plotted in Figure 4. Unlike the 1991-92 season, this year experience very few surface freeze-thaw cycles, due in part to the persistent snow cover.

Simulated and measured hourly temperature for the 5, 10 and 20 cm depths under the sagebrush are plotted in Figure 5. Snow covered the plots for much of the winter, resulting in essentially no diurnal variation in temperature until the snow melted around day 75. Not surprisingly, there was very little

difference between the interspace and sagebrush temperatures due to the large snowcover. At a first glance, it appears that the simulated 10 cm temperature under the sagebrush was consistently underpredicted for much of the winter, but upon closer inspection, the 10 cm temperature sensor apparently drifted somewhat since it measured warmer temperatures than either the 5 or 20 cm temperature sensors for much of the winter.

Simulated and measured water contents for the sagebrush are plotted in Figure 6. Again, we find the simulated liquid water content roughly mimicking the trends in measured water content inferred from the
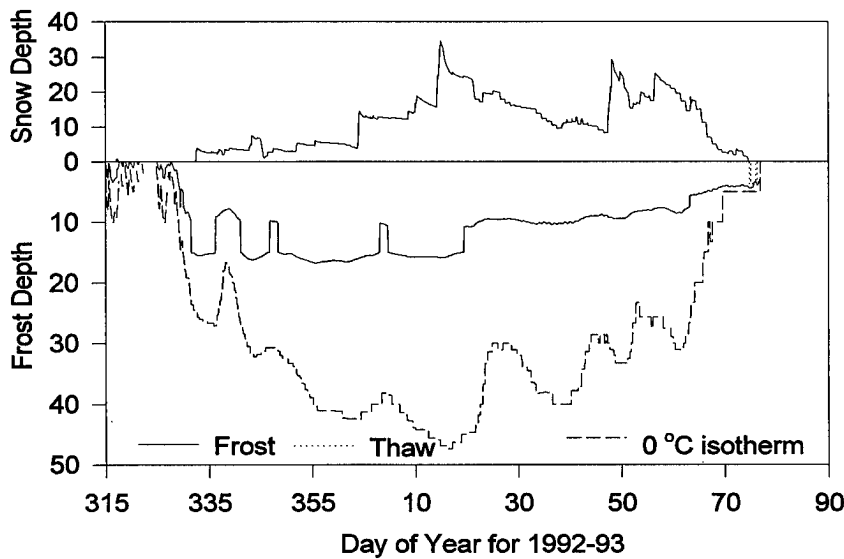
Figure 4. Simulated snow depth, frost depth, thaw depth, and depth of 0°C isotherm for the 1992-93 sagebrush site.

Figure 5. Simulated and measured temperature for the 1992-93 sagebrush site.

541

Figure 6. Simulated total water content and simulated and measured liquid water content for the 1992-93 sagebrush site.

Figure 7. Simulated total water content and simulated and measured liquid water content for the 1992-93 bare interspace site.

fiberglass moisture blocks, and again we find significant ice formation at the 5-cm depth. Since there were no available measurements for total water content, it is difficult to determine whether the ice accumulation at the 5-cm depth is real or not. For comparison, water content under the bare interspace is plotted in Figure 7. The interspace site accumulated water and ice at the 5-cm depth, but not as much early in the season as the sagebrush simulation. The jump in water content in the interspace around day 25 was caused by a brief melt period. The interspace areas were able to absorb the

melt, but the simulated ice content under the sagebrush was sufficiently high that essentially all of the simulated snowmelt resulted in runoff. These contrasts in simulated water contents show their effects in the simulated runoff.

Simulated runoff for the bare interspace is plotted in Figure 8 along with the measured runoff from the two bare interspace runoff plots. A small amount of runoff occurred around day 25 as the soil absorbed much of the melt, and a much larger event occurred around day 75, which was simulated quite well for the interspace. Unfortunately, the high simulated

542

water content for the sagebrush early in the season caused the model to predict a runoff event around day 25 from the brief melt event, which was not observed in the measured runoff for sagebrush (Figure 9); only a small amount of runoff occurred from the interspace plots. (However, this is not as far off as it appears. Field observations indicate that water was ponded and runoff was imminent, but the air temperature suddenly dropped before runoff could occur. Apparently the sagebrush simulation was only slightly ahead of the actual event.)

SUMMARY AND CONCLUSIONS

The Simultaneous Heat and Water (SHAW) model was applied to two years of data for sagebrush-covered and essentially bare ground at the Lower Sheep Creek Watershed located within the Reynolds Creek Experimental Watershed to test the ability of the model to simulate freezing-induced moisture migration, unfrozen water content, and frozen soil runoff. Freezing/thawing processes, including liquid water content, were simulated reasonably well. (Data to check total water content were not available.) Total simulated runoff from the sagebrush plots was within the range of measured runoff, but timing was off possibly due to incorrectly predicting high levels of ice content early in the winter season. However, both magnitude and timing of runoff from the bare interspace plots were simulated quite well.

MODEL AVAILABILITY

The SHAW Model was written by personnel of the USDA Agricultural Research Service and, as such, is public domain software. The model may be obtained by contacting Dr. Gerald N. Flerchinger.

REFERENCES

Bloomsburg, G.L. and S.J. Wang. 1969. Effect of moisture content on permeability of frozen soils. Paper presented at 16th annual meeting of Pacific Northwest Region, American Geophysical Union. 11pp.

Brooks, R.H. and A.T. Corey. 1966. Properties of porous media affecting fluid flow. J. Irrig. and Drain Div., ASCE. 72:61-88.

Flerchinger, G.N., C.L. Hanson and J.R. Wight. 1996. Modeling evapotranspiration and surface energy budgets across a watershed. Water Resour. Res. 32(8):2539-2548.

Flerchinger, G.N. and F.B. Pierson. 1991. Modeling plant canopy effects on variability of soil temperature and water. Agric. and Forest Meteor. 56:227-246.

Flerchinger, G.N. and K.E. Saxton. 1989. Simultaneous heat and water model of a freezing snow-residue-soil system I. Theory and development. Trans. of ASAE 32(2):565-571.

Fuchs, M., G.S. Campbell and R.I. Papendick. 1978. An analysis of sensible and latent heat flow in a partially frozen unsaturated soil. Soil Sci. Soc. Amer. J. 42(3):379-385.

Seyfried, M.S. 1993. Field calibration and monitoring of soil-water content with fiberglass electrical resistance sensors. Soil Sci. Soc. Amer. J. 57(6):1432-1436.
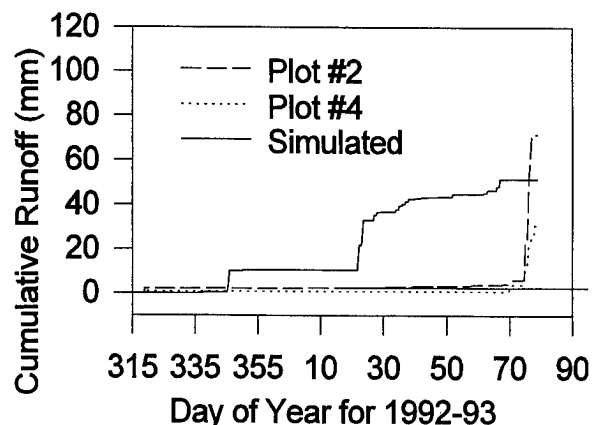
Figure 8. Simulated and measured runoff from the 1992-93 bare interspace site.

Figure 9. Simulated and measured runoff from the 1992-93 sagebrush site.

Remote Sensing

Passive Microwave Detection and Modeling of Frozen Soils in Tundra and Grassland Areas

E.J. KIM[1], Y.-A. LIOU[1], AND A.W. ENGLAND[1]

ABSTRACT

We describe a simple radiometric technique for detecting the presence or absence of snow overlying tussock tundra, and, when snow is absent, for classifying the upper few centimeters of the tundra as frozen or thawed. For more detailed retrievals of the thermal and hydrological conditions, we are developing biophysical land surface process/radiobrightness models for arctic tundra and prairie grass regions. Microwave radiometry is particularly sensitive to temperature and moisture distributions in vegetation canopies and in the underlying soil. By linking such models to satellite radiometric observations, the performance of a model over tundra and grassland regions can be monitored and estimates of near-surface temperature and moisture content with a spatial resolution of ~50 km should be possible.

Field data from our Radiobrightness Energy Balance Experiments on the North Slope of Alaska and in South Dakota are supporting model development.

Key words: Remote sensing, land surface processes, permafrost, tundra, modeling.

INTRODUCTION

Snow cover and a frozen active layer greatly influence the exchange of energy between arctic tundra and the atmosphere. For example, the disappearance of snow cover at the beginning of the summer removes a thermal barrier to the thawing of the active layer, and the simultaneous drop in albedo increases the net insolation available for ground heating and other land-atmosphere exchange processes. Decadal or longer-term warming is apparent in borehole temperature profiles (Lachenbruch 1986), has resulted in a loss of permafrost (Williams 1989; Houghton 1996), and will result in changes in the regional ecosystems (Oechel 1996; Michaelson 1996). These climatic changes, if they represent a trend in regional or global warming, will cause changes in the timing and duration of the snow-free season, and, through their effect upon the freezing and thawing of the active layer (Hinzman 1992), in nearly every aspect of the climatology and ecology of the arctic tundra.

A snow detection and freeze/thaw discrimination technique based on microwave satellite remote sensing observations can provide more consistent observations and more automated retrieval techniques compared with ones based on visible wavelengths. Microwave observations do not depend on solar illumination and can penetrate non-precipitating clouds. The Special Sensor Microwave/Imager (SSM/I) series of polar-orbiting passive microwave sensors, for example, have been operational since 1987, and provide coverage of the entire arctic several times per day. One drawback of satellite microwave radiometers is their relatively coarse spatial resolution; e.g., 43 x 69 km for the 19.35 GHz SSM/I channel. Visible-wavelength sensors can offer higher resolution, but clouds often cover these regions, and bright clouds are similar in appearance to snow. Due to problems such as these, the current NOAA/NESDIS operational snow cover product requires significant manual subjective processing and thus is compiled only on a weekly basis (Grody 1996).

It is worth noting that the spatial resolution of current passive microwave satellite sensors is comparable to that of current climate models. Grid cells for current climate models are hundreds to thousands of square kilometers in area. At these scales, it can be difficult to obtain a meaningful density of point in-situ observations for comparison or assimilation purposes, particularly in regions

like the arctic where access is difficult and expensive.

Satellite-based passive microwave detection of snow and freeze/thaw classification has been the subject of much previous research (Choudhury 1995; Ulaby 1986; Zuerndorfer 1990). The techniques presented here were developed using "ideal" ground-based data from our Radiobrightness Energy Balance Experiment 3 (REBEX-3)–multifrequency, dual-polarization, and multitemporal passive microwave observations with no intervening atmosphere. Using the frequency dependence (spectral gradient) of the microwave brightness (radiobrightness), changes in the spectral gradient on a diurnal time scale, polarization effects, and absolute radiobrightnesses, a technique for classifying the upper few centimeters of tussock tundra as snow-free frozen, snow-free thawed, or snow-covered will be described. This will allow us to estimate sensitivity requirements for successfully applying the classification algorithm using satellite radiobrightness observations. Field measurements of 1-cm and 5-cm subsurface temperatures are used to verify results.

REBEX-3 FIELD EXPERIMENT

REBEX-3 took place at a moist acidic tussock tundra site on the North Slope of Alaska (68 45'47" N, 148 52' 55" W) approximately 160 km south of the Arctic Ocean (Figure 1). The tundra at the site is representative of a large fraction of North Slope tundra areas (Auerbach 1995), typically consisting of sedges, mosses, and lichens overlying Pergelic Cryaquept soils (Michaelson 1996). Continuous permafrost underlies the entire region, and the active-layer depth at the site reached approximately 50 cm.

TTT Continuous Permafrost Line
TTT Discontinuous Permafrost Line
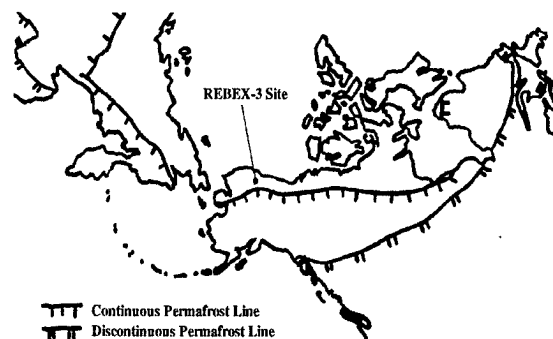
Figure 1. REBEX-3 location.

The field instrument system (Figure 2), the Tower Mounted Radiometer System 2 (TMRS2), was constructed at the University of Michigan, and made automatic observations every 30 minutes. A radiotelephone link provided remote control and

data transfer capabilities. Radiobrightness at 19.35, 37.0, and 85.5 GHz, thermal IR brightness, and wind speed were measured from a 10 m tower. Simultaneous micrometeorological measurements included: upwelling and downwelling shortwave radiation, net radiation, soil and snowpack temperature profiles, soil heat flux, Bowen ratio, soil moisture, 2 m screen air temperature and relative humidity, and liquid precipitation. Coarse snow depth data were provided by a graduated pole and daily video images, which also provided visual verification of site conditions. Data collection spanned one full annual freeze-thaw cycle from September, 1994 until September, 1995 (Kim 1997).

Figure 2. TMRS2 field system installed at the REBEX-3 site.

Apparent ground brightness temperatures T_B, 19- to 37-GHz spectral gradients, the 37-GHz polarization difference, and near-surface ground temperatures for two portions of REBEX-3 are shown in Figure 3 (left-hand column: days 252–268) and Figure 4 (right-hand column: days 501–511). The period shown in Figure 3 includes three snow-free days (254–256) preceding the onset of winter snow accumulation on day 257. The period shown in Figure 4 includes several days with 2 m air temperatures Tair, below freezing (until day 508) which occurred after the disappearance of the winter snowpack at the site. A small amount of snow (< 5 cm) covered the site during days 505–507. The resolution of the video images does not permit a more precise depth estimate. Beginning with day 508, the tundra surface was snow free and thawed except for nighttime refreezing between days 508 and 509.

CLASSIFICATION

The 37-GHz polarization difference, defined as the difference between vertically-polarized (V) and horizontally-polarized (H) 37-GHz brightnesses ("pd37" in Figures 3c and 4c), clearly indicates the onset of winter snow accumulation at
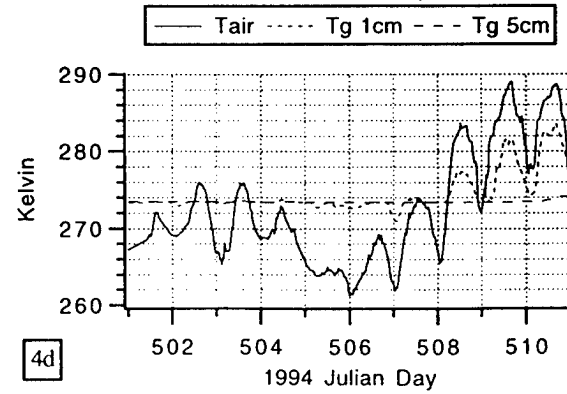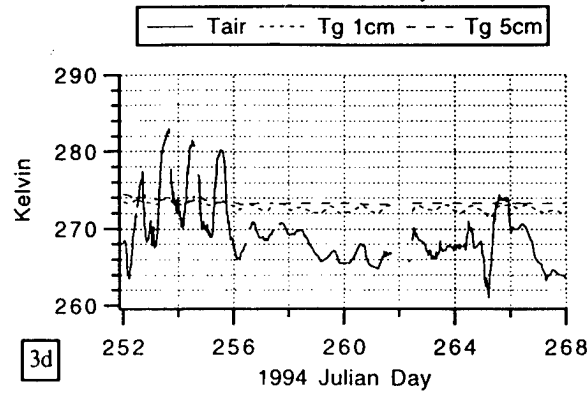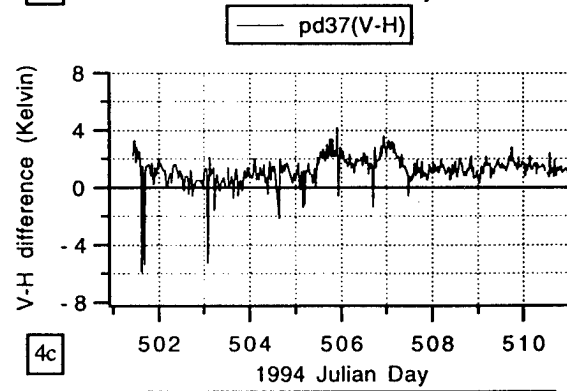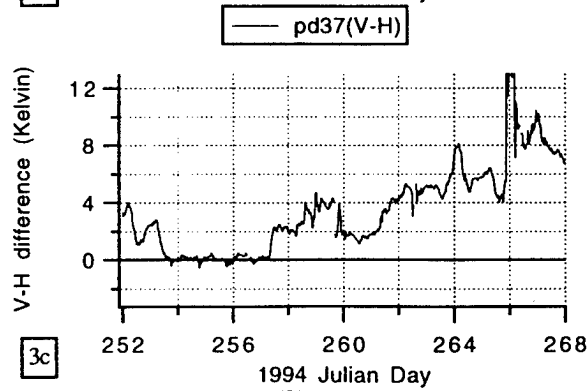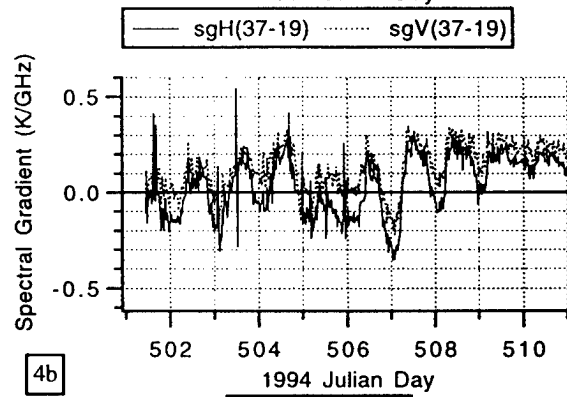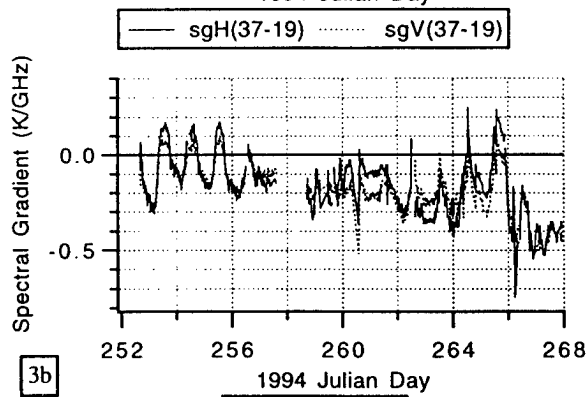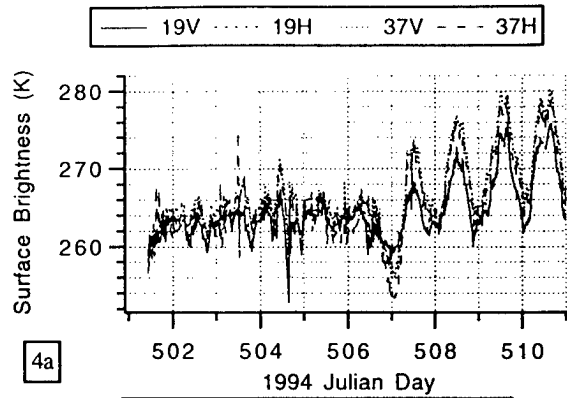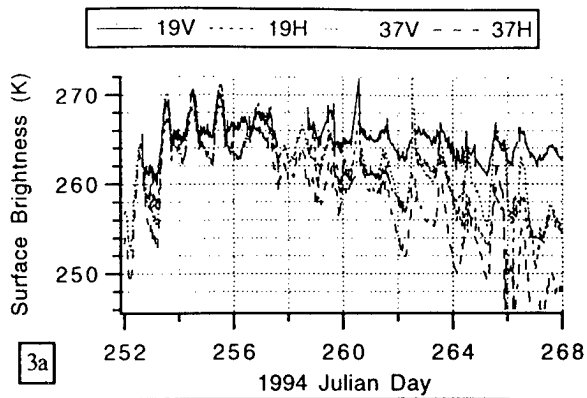
546

Fig. 3. Freeze-up and winter snow arrival.

Fig. 4. Spring cold snap after thaw.

547

day 257.2, and the presence of snow on days 252–253 and 505.5–507.5. Snow-free periods are characterized by polarization differences with nearly constant low values: near zero in the fall (Figure 3) and around 1 K in the spring (Figure 4). Values of 1.5 K or more above these indicate the presence of snow, with an increase of at least 2 K indicating the presence of at least 5 cm of snow.

We believe the sensitivity of the polarization difference to the presence of snow can be explained as follows. At 37 GHz, under snow-free (frozen or thawed) conditions, the observed brightness comes from the upper tundra vegetation which is too rough and too diffuse to act as a planar dielectric boundary with polarization-dependent Fresnel refraction. And, since the tussock vegetation has no preferred orientation, the emission signature has no preferred polarization. Snow, on the other hand, has been shown (Fung 1981; Schanda 1983) to have consistently greater V-polarized emission at the SSM/I incidence angle of 53 degrees for a wide range of snow water equivalent values and snowpack thicknesses. Thus, the presence of even a few centimeters of snow is enough to polarize the signature from tundra. We did not investigate whether thin snow could be differentiated from frost.

The V- and H-polarized spectral gradients, ("sgV" and "sgH" in Figures 3b and 4b) are defined as

$$\frac{\left(T_{B37,p} - T_{B19,p}\right)}{37.0 - 19.35}$$

where $T_{B37,p}$ and $T_{B19,p}$ are the 37 GHz and 19.35 GHz p-polarized brightnesses, respectively. Snow-free tundra which is thawed from the surface to a depth of 5 cm displays a positive V-polarized spectral gradient of approximately 0.2 K/GHz. Snow-free tundra which is frozen from the surface to a depth of 5 cm displays a near-zero or slightly negative V-polarized spectral gradient of 0 to –0.2 K/GHz. When the upper 5 cm were partially thawed, an intermediate spectral gradient was observed. Snow-covered tundra is characterized by negative spectral gradients in general; however, daytime warming can apparently increase the gradient to even positive values as seen on days 262, 264, and 265. These findings are consistent with those of Kunzi (1982) as reported in Ulaby (1986) with the possible exception of positive spectral gradient values when snow was present. If the polarization difference is used first to discriminate between snow-covered and snow-free periods, no ambiguities result.

These radiometric freeze/thaw classification results are fully consistent with the actual 1 cm and 5 cm subsurface temperatures, measured with buried thermistors and plotted in Figures 3d and 4d ("Tg 1cm" and "Tg 5 cm", respectively).

DISCUSSION

In Figures 3a and 4a, we see that the diurnal radiobrightnesses vary by as much as 15 K. The time of measurement must be considered when interpreting an observation. Even then, for a given frequency and polarization, there are multiple combinations of soil and vegetation characteristics, temperature, and moisture which can yield identical values of "instantaneous" radiobrightness. Also, the observed microwave emission is a weighted combination of energy emitted over a range of depths within the vegetation and soil, that is, radiobrightness is an integrated quantity. Thus, a single radiobrightness observation cannot uniquely determine soil temperature and moisture profiles without additional constraints. In the classification technique presented above, multitemporal and multifrequency data were used to address this problem in a limited fashion.

Much more robust remote estimates should be possible through the use of a nonempirical technique such as a land surface process (LSP) model. LSP models provide land-atmosphere boundary conditions and feedback for atmospheric climate models. They are numerical simulations of the response of the soil/vegetation system to diurnal solar and atmospheric forcing. Examples include the Biosphere-Atmosphere Transfer Scheme (Dickinson 1986), the Simple Biosphere model (Sellers 1986), and the Canadian Land Surface Scheme (Verseghy 1991).

REBEX-3 data are supporting development of a land surface process/radiobrightness (LSP/R) model for arctic tundra that is designed to be linked to satellite observations. The tundra LSP/R model is a biophysical representation of the linkage between the observed microwave emission and conditions within the canopy and the soil. Although too computationally intensive to be used as an operational land surface package, it can be run retrospectively for selected regions to obtain much higher fidelity estimates of temperature and moisture profiles within tundra than would be available from any operational LSP model. The choice of a physical model is intended to provide insights into the land surface processes, guidance when developing or improving parameterizations for an operational LSP model, and a better chance of extendibility to regions with different vegetation and conditions than other, less physical approaches.

Note that in order to predict microwave emission, the LSP/R model must first simulate the thermal and moisture regimes. So while observed radiobrightnesses themselves do not directly give us physical temperatures or moistures within the vegetation and soil, the model does estimate these quantities. And, to the extent that the model input data and parameters are accurate and the

548

important processes are adequately represented, the temperature and moisture estimates will also be accurate. The microwave observations are a means of remotely assessing the model's accuracy. Deviations between predicted and observed radiobrightnesses could be used to 'nudge' or otherwise correct the model state in a regular fashion. Current operational numerical weather prediction models routinely assimilate remotely sensed and in-situ observations through such techniques.

By assimilating passive microwave observations made over a period of time to constrain the model, surface fluxes of latent and sensible heat, as well as near-surface and subsurface temperature and moisture conditions may be determinable for areas with relatively thin vegetation, such as tundra and prairie. Again, these estimates will come from the model state, not from a direct inversion of radiobrightness data.

The tundra LSP/R model is based on a prairie grass LSP/R model for which the above approach has been validated (Liou 1996a). The tundra model can be conceptually divided into three modules: a soil thermal module, a vegetation energy balance module, and a radiobrightness module. The overall model's time step is adaptive, but is generally of the order of minutes.

The soil thermal module uses a finite-difference approach to solving coupled partial differential equations which govern the heat and moisture transport within a multilayer (60 layers) soil column, including under freezing and thawing conditions. It is based on the work of Philip (1957) and de Vries (1958), and it computes soil temperature, liquid water content, and ice content for each layer, plus evaporation, condensation, and latent and sensible heat exchange at the top interface. The starting temperature profile and lower boundary conditions are determined from a separate annual model of the soil thermal regime (Liou 1996b). The annual model computes soil temperature profiles using average climatic data (solar radiation, cloud cover, wind speed, etc.) for a site. It is used primarily to reduce the "spin-up time" required by the diurnal LSP/R model (to 1–2 model days in the prairie case).

The vegetation module computes vegetation temperature from an energy balance of shortwave and longwave radiation, and sensible and latent heat exchange with the atmosphere. Plant transpiration is regulated by stomatal resistance, which is computed as a function of soil water availability, air temperature and humidity, solar radiation, and plant temperature. Plant moisture is maintained by water uptake from the soil.

The radiobrightness module uses the temperature and moisture information from the soil and vegetation modules to compute total V- and H-polarized radiobrightnesses for incidence angles from normal through grazing and frequencies throughout the microwave spectrum.

CONCLUSIONS

Changes in the 37-GHz V-H polarization difference have been shown to indicate the presence or absence of snow in tussock tundra regions. To detect snow cover of 5 cm or less, a change in the polarization difference of 1.5 K must be detectable. If this level of precision is not available, then a classifier based on polarization difference can still be applied but the minimum detectable snowpack thickness increases. When used with polarization difference information, the 19.35-GHz–37-GHz spectral gradient can be used to further classify the snow-free tundra as frozen or thawed provided that a spectral gradient accuracy of at least 0.2 K/GHz (ΔT_B of 3.5 K) is available. A positive spectral gradient of up to 0.2 K/GHz is observed for tundra whose upper 5 cm are thawed, and a slightly negative spectral gradient of 0 to − 0.2 K/GHz is observed for snow-free tundra whose upper 5 cm are frozen. A successful satellite-based classifier must meet these accuracy requirements after any effects of spatial scaling and any atmospheric corrections.

Existing SSM/I-based snow detection algorithms can misclassify frozen snow-free ground as snow-covered if only a spectral gradient discriminant is used. Grody (1996) describes a classification method which can remove this ambiguity in some areas using the 19.35 GHz polarization difference. However, the ambiguity remained when this classifier was applied to the REBEX-3 data. We found that the classification tree approach described in this paper, which uses a 37 GHz polarization difference discriminant, was completely successful at distinguishing between snow-covered and snow-free frozen conditions at the REBEX-3 tussock tundra site.

A biophysical land surface process/radiobrightness model is being developed to improve our understanding of and our ability to estimate snow-free land-atmosphere energy and moisture fluxes and near-surface temperature and moisture conditions in arctic tundra regions. The model is similar to one developed for prairie grassland regions and is designed to provide a linkage to satellite radiobrightness observations for remote monitoring and data assimilation applications in climatology and meteorology.

The temporal coverage of major arctic tundra-covered regions provided by the polar-orbiting Defense Meteorological Satellite Program (DMSP) platforms is quite good. For example, each makes at least four sun-synchronous passes per day over points at the latitude of the REBEX-3 site. The spatial resolution of the SSM/I sensors on the DMSP satellites varies from 69 x 43 km for

549

the 19.35-GHz channel to 15 x 13 km for the 85.5 GHz-channel. Spatial resampling techniques can be employed to standardize the resolution and pixel locations to a fixed 25-km grid. SSM/I data for the REBEX-3 time period have been obtained and will be used to test the classification technique using satellite observations.

REFERENCES

Auerbach, N.A., and D.A. Walker. 1995. Preliminary vegetation map, Kuparuk Basin, Alaska: a Landsat-derived classification. Inst. of Arctic and Alpine Res., Univ. of Colorado, Boulder.

Choudhury, B.J., Y.H. Kerr, E.G. Njoku, and P. Pampaloni (Eds). 1995. Passive microwave remote sensing of land-atmosphere interactions. VSP. Utrecht. 227–316.

de Vries, D.A.. 1958. Simultaneous transfer of heat and moisture in porous media. Trans. Am. Geophys. Union. 39: 909–916.

Dickinson, R.E., A. Henderson-Sellers, P.J. Kennedy, and M.F. Wilson. 1986. Biosphere-Atmosphere Transfer Scheme (BATS) for the NCAR Community Climate Model. NCAR Technical Note TN-275+STR. National Center for Atmospheric Research.

Fung, A.K., and H.J. Eom. 1981. Emission from a rayleigh layer with irregular boundaries. J. Quant. Spectrosc. Radiat. Transfer. 26: 397–409.

Grody, N.C., and A.N. Basist. 1996. Global identification of snow cover using SSM/I measurements. IEEE Trans. Geosci. Remote Sensing. 34: 237–249.

Hinzman, L.D., and D.L. Kane. 1992. Potential response of an arctic watershed during a period of global warming. J. Geophys. Res. 97: 2811–2820.

Houghton, J.T., et al, (Eds). 1996. Climate change 1995–the science of climate change. Intergovernmental Panel on Climate Change. Cambridge Univ. Press.

Kim, E.J., and A.W. England. 1997. Field data report for radiobrightness energy balance experiment-3. Univ. of Michigan Radiation Lab. Report RL-918.

Kunzi, K., S. Patil, and H. Rott. 1982. Snow-cover parameters retrieved from Nimbus-7 scanning multichannel microwave radiometer (SMMR) Data. IEEE Trans. Geosci. Remote Sensing. GE-20: 452–467.

Lachenbruch, A.H., and B.V. Marshall. 1986. Changing climate: geothermal evidence from permafrost in the Alaskan arctic. Science. 234: 689–696.

Liou, Y.-A. and A.W. England. 1996a. A land surface process/radiobrightness model with coupled heat and moisture transport for freezing soils. submitted to IEEE Trans. Geosci. Remote Sensing.

Liou, Y.A. and A.W. England. 1996b. Annual temperature and radiobrightness signatures for bare soils. IEEE Trans. Geosci. Remote Sensing. 34: 981–990.

Michaelson, G.J., C.L. Ping, and J.M. Kimble. 1996. Carbon storage and distribution in tundra soils of arctic Alaska, USA. Arctic and Alpine Res. 28: 414–424.

Oechel, W.C.. 1996. presentation at the ARCSS/LAII science meeting. Seattle, WA. Feb. 23–24.

Philip, J.R. and D.A. de Vries. 1957. Moisture movement in porous materials under temperature gradients. Trans. Am. Geophys. Union, 38: 222–232.

Schanda, E.,C. Matzler, and K.Kunzi. 1983. Microwave remote sensing of snow cover. Int. J. Remote Sensing. 4: 149-158.

Sellers, P.J., et al. 1986. A Simple Biosphere Model (SiB) for use within general circulation models. J. of the Atmos. Sci. 43:505–531.

Ulaby, F.T., R.K. Moore, and A.K. Fung. 1986. Microwave remote sensing: active and passive. vol. 3. Artech House. 1603–1634.

Verseghy, D.L. 1991. CLASS–a Canadian land surface scheme for GCMs. I. soil model. Int. J. of Climatology. 11:111–133.

Williams, P.J., and M.W. Smith. 1989. The frozen earth–fundamentals of geocryology. Cambridge Univ. Press. 79-80.

Zuerndorfer, B., A.W. England, and F.T. Ulaby. 1990. An optimized approach to mapping freezing terrain with SMMR Data. Proc. of IGARSS '90.

Monitoring the Effects of Fire on Soil Temperature and Moisture in Boreal Forest Ecosystems Using Satellite Imagery

N.H.F. FRENCH[1], E.S. KASISCHKE[1],
J.L. MICHALEK[1], AND L.L. BOURGEAU-CHAVEZ[1]

ABSTRACT

Fire is a major controlling factor in the ecology of boreal forests. It has been shown that the effects of fire causes dramatic changes in the temperature of the ground layer for 15 to 30 years following fire. Carbon efflux from soils of boreal forest ecosystems is low compared to temperate systems due to cold and often wet soil conditions. Fire can change soil water and temperature conditions, thereby increasing carbon efflux from soil respiration. A set of studies using a variety of remote sensing systems and image processing algorithms is underway to determine the role of remote sensing in estimation of post-fire carbon flux due to increased soil respiration. This paper presents a summary of data, results, and preliminary analyses on the use of remote sensing for the study of factors affecting post-fire biogenic emission of carbon. This effort includes combining field collected data with remote sensing data from three sites in interior Alaska to use as inputs to carbon flux models.

Key words: Boreal forest, carbon flux, remote sensing, thermal infrared, synthetic aperture radar.

INTRODUCTION

The cold climate of the boreal forest region is an important factor in the functioning of the ecosystems of the region (Van Cleve et al. 1991). The climate supports the development of permafrost and is very important in determining the distribution of ecosystems.

Wildfire is another widespread and important factor in the region. The area burned in the North American boreal forest region has averaged 3.3 million ha over the past decade. The effects of these fires on the permafrost and the ground thermal condition is an important consideration when looking at the functioning of ecosystems and when considering the carbon balance within the region.

Fires in the boreal region are often very large and remote. Because of this, ground-based studies of fire-disturbed sites are difficult to perform. For both scientific and management related purposes, devising ways to measure and monitor fire-disturbed sites remotely would be useful. Over the past several years, we have conducted research on using satellite remote sensing instruments to monitor fire-disturbed boreal forests in Alaska and Canada. In this paper, we will review past work and introduce new analyses underway to study post-fire conditions in Alaska using remote sensing technology. After a brief background discussion, we will review some of our previous research, which illustrates how spaceborne imaging radar systems can be used to monitor spatial and temporal variations in soil moisture. Next, we will discuss an approach for using thermal infrared systems for monitoring variations in surface temperature. Finally, we will discuss additional remote sensing analysis techniques and introduce a concept for combining remotely sensed data with field data to derive estimates of post-fire biogenic emissions (emissions from soil respiration) of carbon dioxide (CO_2) across a landscape-scale area.

[1] Earth Sciences Group, Environmental Research Institute of Michigan, P.O. Box 134001, Ann Arbor, Michigan 48113-4001, USA

BACKGROUND

The immediate effects of fire on the ecosystem are obvious. Fire typically kills most of the aboveground vegetation and will often consume much of the forest floor and organic soil. Fire results in a very large immediate release of carbon, in the form of CO_2, CO, and other trace gasses. Post-fire conditions allow for further movement of carbon to the atmosphere because of increases in soil temperature and moisture (Bunnell et al. 1977, Schlentner and Van Cleve 1985). The effect of increased soil moisture and temperature on soil microbial respiration is of particular interest because of its long-term impact on carbon dynamics.

Soil respiration is strongly controlled by temperature and moisture (Bunnell et al. 1977, Schlentner and Van Cleve 1985, Raich and Schlesinger 1992, Raich and Potter 1995). Typically, boreal forest soil respiration rates are slow due to very low temperatures (Van Cleve et al. 1986, Bonan 1990). It has been shown that fire results in dramatic changes in the permafrost and ground layer temperature of boreal forests for 15 to 30 years (Viereck 1982, Viereck personal communication, 1996). The temperature increase is due to several factors, including an increase in direct insolation of the ground due to the loss of the tree canopy, a reduction of the depth of the moss, litter, and organic soil, which serve to insulate the ground, and a decrease in surface albedo. In areas underlain by permafrost, increased ground temperature results in an increase in the depth of the active layer. Changes in the permafrost affect soil moisture which is also important to soil respiration.

The conditions important to soil respiration are highly variable in both space and time. Soil temperature changes diurnally as well as from day-to-day based on air temperature and precipitation. Soil moisture is likewise temporally variable due to precipitation. These two factors also vary spatially in complex ways on very fine scales. Field sampling of sites is inadequate for monitoring variability in soil moisture and temperature. Remote sensing, however, can be used to sample over landscape-scale areas many times during a season. Remote sensing, therefore, provides important inputs for process models to reliably predict carbon flux over landscape-scale areas.

The research presented in this paper is being conducted at sites of various age in order to devise a multiyear analysis approach to the study of fire effects. In this regard, we are substituting space for time, since following one particular burn over many years can be difficult and time-consuming. In addition, studies at one Alaskan site have been on-going for several years, so some information of between-year change is available.

SITE DESCRIPTIONS

Studies are underway at three sites in interior Alaska which burned between 1987 and 1994. By looking at fire scars of different ages, we plan to construct a view of how the age and severity of the burn affects the remote sensing signature and soil carbon efflux. Our initial work with fire scars focused on a site near the town of Tok, Alaska (63°23'N, 142°42'W). A fire in 1990 burned a large area accessible by road. Remote sensing and field data were collected at this site starting in 1992. Current studies involve remote sensing and ground-based measurements from two additional fires located within the same region and about 125 km northwest of the Tok site. Work here began in the summer of 1996. One fire burned in 1987 and the other in 1994. The recent burn is near the Gerstle River along the Alaska Highway (63°52'N, 145°13'W). The older fire mainly burned land within the Fort Greely Military Reservation. Our sites are accessible from the Alaska Highway 20 km east of Delta Junction (63°55'N, 145°21'W).

All three areas lie in the upper Tanana River valley to the north of the Alaska Range. The sites are mainly outside of the recent river floodplain, so river influence is minimal, with flooding from the Tanana not a factor. The topography is flat at all sites, with the exception of a mountainous portion of the Tok burn which was not included in our studies. Soils are derived from glacial outwash in all three areas with loessal deposition also an important source of material at the Gerstle River and Fort Greely sites. Soils are generally heavy textured silt or silty clay at the surface with layers of gravel at varying depths. Drainage is poor to moderately well-drained, depending on the underlying gravel layer. Vegetation at all three sites consists primarily of black spruce (*Picea mariana* (Mill.) BSP) dominated ecosystems. Aspen (*Populus tremuloides* Michx.) and white spruce (*Picea glauca* (Moench) Voss) ecosystems are also present as are areas dominated by shrub willow (*Salix sp.*), but the majority of burned area was black spruce.

The black spruce sites had deep organic soil layers on top of mineral soil before the burn (5 to 20 cm). In some areas this organic material was completely consumed during the burn, while at other locations the surface was only singed. Generally speaking, the fires killed the aboveground trees, sometimes consuming the boles, and it consumed nearly all shrub-layer vegetation. It is important to note, however, that these general statements about the post-burn conditions are not fully accurate because of the high amount of variability in pre-burn condition (e.g., ecosystem type and organic soil depth) and burn severity.

552

DATA DESCRIPTIONS

A variety of remote sensing data were obtained for the three sites over the past six years. Data from before and after the fires have been obtained to asses a variety of factors. First, synthetic aperture radar (SAR) data from the European satellites ERS-1 and 2 were collected to assess the ability to monitor soil water. A detailed analysis of the Tok ERS-1 data has been completed. Further analysis of ERS SAR from the Gerstle River and Fort Greely sites is planned. A Landsat Thematic Mapper (TM) scene of all three sites from September of 1995, and an August 1992 image showing the Tok burn and the site of the 1994 Gerstle River burn have been obtained. And, we are currently in the process of ordering AVHRR imagery to study the temporal variability in the visible, near-infrared, and thermal infrared signatures.

Field data have been collected at the Tok site for five years (1992 to 1996). Data from the Fort Greely burn were collected in 1992 and 1996. The Gerstle River burn was visited in 1992 (before the burn) for aboveground biomass measurements. Since then, the site was visited at the end of 1995 and in the summer of 1996 when extensive data collections were undertaken.

Measurements of soil water content were made for four years at the Tok site by collecting soil samples (French et al. 1996b). A limited number of soil water samples have been collected at the Gerstle River site, but the data have not been analyzed. Vegetation type and biomass, tree density, and burn severity have been collected at 14 sites within the Tok burn (Bourgeau-Chavez 1994). Aboveground vegetation biomass and descriptions and ground-layer organic matter have been collected from burned and adjacent unburned locations at all three sites. In addition to this, surface CO_2 efflux measurements were made during the summer of 1996 in burned and unburned locations at all sites. At some sites, measurements were made several times during the summer to look at the temporal variability in efflux. Field measurements at all sites will continue for the next few years, concentrating on CO_2 efflux measurements and other soil and ground-layer measurements. (See O'Neil et al., this volume, for further information about the CO_2 efflux measurements.)

ERS SAR FOR SOIL WATER MONITORING

Over the last six years, we have conducted a variety of studies to determine the utility of SAR for fire scar studies (Kasischke et al. 1992, Bourgeau-Chavez 1994, French et al. 1996b). Research conducted at the

Tok site has shown that ERS-1 SAR is sensitive to variations in soil moisture in fire-disturbed sites (French et al. 1996b). Results concluded that the brightness of the SAR signature, the SAR backscatter, is related to the volumetric soil water content at several sites within the area burned. It was also shown that the radar signature is closely related to precipitation.

Additional analysis of ERS-1 imagery has revealed bright signatures from many fire-disturbed locations throughout Alaska and Canada (Kasischke et al. 1992, Bourgeau-Chavez et al. 1997, French et al. 1996b). The Gerstle River burn has been the focus of further research in the use of ERS SAR for soil moisture monitoring (Fig. 1). Field measurements of soil water were collected in this burn during the 1996 field season. Comparisons of these data to the radar signature will be made as soon as the SAR data are available. A preliminary look at the ERS-1 imagery of the site shows a relationship between SAR signature and precipitation similar to what was observed at the Tok site. High backscatter is apparent early in May shortly after snowmelt and following large rain events. Low backscatter is seen after several dry days (Fig. 1). Similar signatures are observed on imagery of the 1987 Fort Greely burn. From our original results at Tok and further analysis at these additional sites, we hope to be able to predict soil moisture based on the remote sensing measurement. By doing this, we will be able to measure soil moisture over inaccessible areas. We will also have an ability to monitor soil moisture over time to learn more about the temporal variability in soil moisture. With a knowledge of soil moisture, we will also be able to make more useful inferences regarding temperature anomalies, since moisture and temperature are closely tied.

MEASURING AND MONITORING TEMPERATURE WITH THERMAL INFRARED IMAGERY

Initial analysis of the Tok site using spaceborne thermal infrared remote sensing systems (10-12 μm) has shown increased apparent temperature[1] following

---

1. Apparent temperature is also known as brightness or radiant temperature. It is the actual (kinetic) temperature of a black body which would produce the radiance equivalent to the measured radiant flux. Remote sensing systems measure radiant (apparent) temperature, while thermometers measure kinetic (actual) temperature. In general, radiant temperature is less than kinetic temperature.
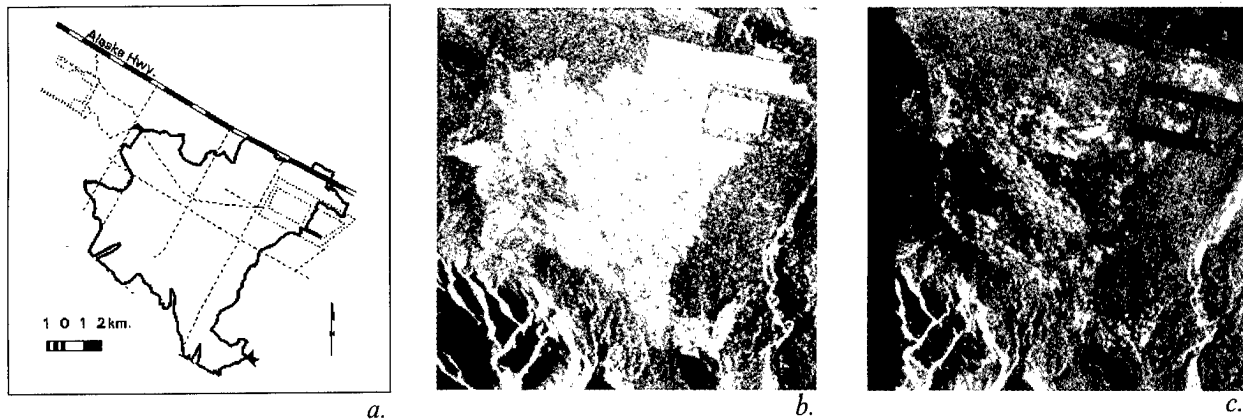
Fig 1: *Synthetic aperture radar imagery of the Gerstle River fire scar. (a) Map showing the extent of the Gerstle River fire scar. (b and c) ERS-1 SAR images from 2 May 1995 and 8 July 1995. Bright backscatter is apparent after snowmelt and heavy rain. Low backscatter is seen after several dry days.*

burning (French et al. 1996a). Using data collected with the Advanced Very High Resolution Radiometer (AVHRR), analysis has shown an increase of as much as 12° C in apparent temperature one year following the burn. This analysis was conducted using composite imagery (Eidenshink 1992) for an initial look at the utility of AVHRR for fire scar detection. Because the data are derived by combining several images over a two-week period, spatial variability in the signature cannot be assessed and calibration of the data is less than optimal (see French et al. 1996a). However, this exercise indicates that the change in apparent temperature at this site due to burning is detectable using the AVHRR band 4 (11-μm wavelength).

Further analysis of single-date AVHRR imagery is underway. The AVHRR sensor collects data over the entire earth twice daily. Therefore, if clouds were not a factor, twice-daily observations of a site would be possible. Due to clouds it is more likely that weekly to monthly observations are possible. However, during cloud-free periods collecting two images in a day is possible, thereby determining the diurnal variation in thermal signature. With AVHRR, therefore, gaining an understanding of temporal dynamics in site temperature will be possible. An initial look at a day/night image pair from a fire scar in Canada has shown that the signature changes dramatically from day to night. This diurnal variation in apparent temperature could be significant in assessing biogenic emission from the soil. By analyzing the diurnal change in temperature, we may be able to learn more about the thermal characteristics of the surface material. The plan for this project includes analysis of AVHRR imagery for monitoring changes in temperature at fire-disturbed sites. This will allow us to determine changes in site conditions, which lead to changes in biogenic emission of CO_2.

The spatial resolution of the AVHRR (1.1 km) limits its utility for looking at fine-scale variability within a burn. Low altitude aerial photos collected one year following the Gerstle River burn show a high amount of spatial heterogeneity due to burning pattern. Spatial heterogeneity is high at the Tok site due to the burning pattern as well as the complex pre-burn vegetation patterns. Therefore, it is desirable to look at these sites with higher resolution systems if possible. The Landsat Thematic Mapper (TM) thermal IR band (10.5-12.5-μm wavelength) has a resolution of 120 m, which allows for spatial discrimination not possible with the AVHRR sensor.

An initial analysis of TM imagery from the Gerstle River fire one year following the burn showed that the apparent temperature within the area burned ranged from 12° to 19°C (Fig. 2). The area burned had a higher apparent temperature (~2-10°C) than the surrounding unburned area, which includes both vegetated (forest and grass field) and non-vegetated (bare agricultural fields) areas. This indicates that Landsat TM data can also be used to delineate burned areas, as demonstrated using AVHRR data but on a much finer scale.

Although the finer resolution of Landsat TM is helpful for spatial analysis, image data are not easy to come by due to the satellite's infrequent orbit return interval and cloud cover. For example, for the years between 1991 and 1995 only two usable images were available over the Alaska study sites. The TM imagery, therefore, cannot be used to monitor thermal variation over time. The utility of the TM sensor, on the other hand, lies in its ability to more finely define within-site variation at a single point in time.

The preliminary analyses we have conducted on AVHRR and TM imagery to date have allowed us to

554

a.
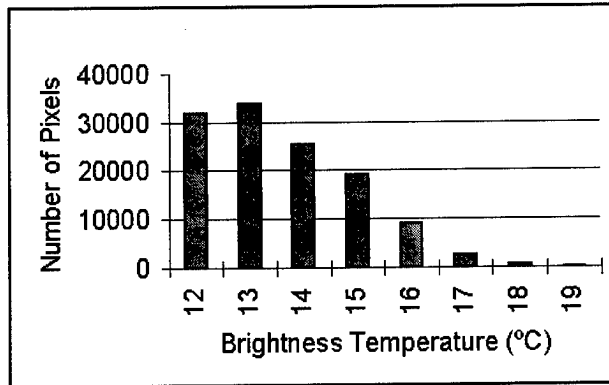
b.

Fig 2: *Thermal image of the Gerstle River fire scar. (a) Landsat TM band 6 image from 18 Sept 1995. (b) Histogram showing the distribution of apparent temperature within the area burned. Higher apparent temperature from areas disturbed by fire has been observed at several sites in the boreal region.*

recognize that fire scars exhibit thermal anomalies, which may aid in fire scar detection and lead to an understanding of thermal properties at the site. These initial studies, however, have not allowed us to determine the cause of the thermal signatures observed. We will be investigating this cause and effect relationship in order to define the utility of thermal sensors for post-fire studies.

Many problems exist in using satellite-based thermal sensors for determination of land surface temperature. Some of these problems are correctable, and algorithms exist for deriving temperature, but inherent factors need to be considered when looking at satellite-derived temperature data (Prata 1993). Some of the important considerations are radiometric calibration, correction for atmospheric effects (haze), and determination of surface characteristics particularly surface emissivity.

Sensor calibration is possible with the AVHRR and TM sensors, and atmospheric effects can be corrected (Prata 1993, François and Ottlé 1996). Differences in the emissivity of materials on the ground need to be considered in determining actual land surface temperature. Spatial differences in surface material emissivity will cause some variability within the burn area. Land surface emissivities can range from 0.90 to 0.99 (Prata 1993). A change in surface emissivity of 0.01 causes a change in apparent temperature of about 0.7°C (at 290°C). In several ways, the range of emissivity with the area of interest can be estimated, so that its effect can be assessed (Becker and Li 1990, Li and Becker 1993). Landsat TM and AVHRR reflective bands can be used with thermal bands to derive emissivity. With day/night images, thermal sensors can help determine properties of the surface material such as thermal inertia. Also, field experiments can be conducted to compare the apparent temperatures measured from a variety of sites within the area of interest to actual temperatures in order to calculate emissivity.

As described above, a variety of tasks are underway to define the utility of AVHRR and TM data for mapping and monitoring surface temperatures within burned areas. To measure actual surface temperature, surface emissivity will need to be determined. Assuming constant emissivity over time, a study of the relative changes in surface temperature (daily, seasonally, or over several years) is possible. The AVHRR can be used for these temporal studies. By knowing more about the fine-scale signature with TM imagery, spatial variation in the signature can be better understood.

ADDITIONAL MEASUREMENTS WITH REMOTE SENSING

As we have discussed previously in this paper, mapping soil moisture and temperature anomalies using remote sensing systems is feasible. Although temperature and moisture are the most important site factors influencing soil respiration, they are not the only drivers determining post-fire biogenic emission of CO_2. Remote sensing may be helpful for two other driving factors, ecosystem type mapping and determination of the amount of organic material left after the burn.

Landsat TM multispectral imagery can be very helpful in mapping cover type and other defining factors to determine ecosystem type. Ecosystem properties learned from ground-based measurements and models can then be used to infer general site conditions in areas not accessible on the ground.

An important factor for post-burn soil respiration

555

is the quantity and quality (nitrogen and lignin concentration) of the organic substrate (Bonan 1990). The composition and amount of organic material left after burning, therefore, would be another factor desirable to measure over the full extent of a fire scar. In this instance, field measurements are needed to determine the quality of the organic material. However, the presence of organic material may be detected using Landsat TM (Colwell et al. 1992). Also, Landsat TM and ERS SAR may be useful in determination of burn severity, which may lead to estimation of the quantity of organic material left after burning. Preliminary results from studies of burn severity are described below. Further investigation is needed, but preliminary analysis shows that these techniques may be useful (Bourgeau-Chavez 1994).

Field data on burn severity were collected during the summer of 1993 at the Tok site to look at its effect on the SAR signature. From this experiment, Bourgeau-Chavez (1994) found a relationship between burn severity and SAR backscatter when soil water was constant. Further analysis at this site is underway that will consider the contribution of surface roughness to the signature, but these initial results are encouraging for using SAR to study burn patterns.

An initial look at Landsat TM multispectral data from the Gerstle River site shows that there is a relationship between within-burn surface characteristics and reflectance properties. Initial field observations indicate that the presence or absence of organic material may be one of the contributors to the variability seen at these wavelengths. A multispectral analysis of the Gerstle River burn is underway to determine if these data are effective for determination of burn severity or detection of the presence or absence of organic material or mineral soil on the surface.

DATA INTEGRATION AND MODELING FOR CARBON EMISSION STUDIES

The importance of soil moisture and temperature in determining CO_2 efflux is generally accepted (Raich and Schlesinger 1992, Raich and Potter 1995). Bunnell et al. (1977) have developed a simple model of the influences of abiotic variables on microbial respiration. The model assumes respiration is a function of temperature and the supply rates of water, oxygen, and nutrients.

We plan to integrate information obtained from Landsat TM, AVHRR, and ERS SAR as well as information obtained from field measurements and modeling efforts. This information will then be introduced into a model to determine the temporal and spatial variability in post-fire soil respiration in a fire-disturbed area.

We are exploring the reasons for bright SAR backscatter, strong reflectance in visible and near IR bands, and high thermal emission. These remote sensing anomalies are due to physical properties of fires scars including soil moisture, albedo, emissivity, and actual surface temperature. The information obtained from analysis of the remote sensing data will be combined to look at a variety of questions. For example, changes in emissivity of the surface can be due to changes in soil moisture. Moisture changes are detectable using SAR, so changes in emissivity due to moisture changes can be accounted for when looking at apparent temperature variation over time. By using one set of data to help understand others, we hope to be able to measure and monitor post-fire conditions which affect biogenic CO_2 emission.

SUMMARY

Carbon flux in the circumpolar boreal region is strongly controlled by the cold climate and by fire. Post-fire warming of a site has an important effect on the functioning of the ecosystem, in particular microbial respiration. Fire, therefore, has an important effect on carbon dynamics long after the fire has occurred.

A set of studies using a variety of remote sensing systems and image processing algorithms is underway to determine the role of remote sensing in estimation of post-fire carbon flux. This effort includes combining field collected data with remote sensing data to use as model inputs.

Analysis of the data has shown that ERS SAR is effective in determination of soil moisture in burned areas. Initial results show that by using Landsat TM and AVHRR imagery, determination of spatial and temporal variations in apparent temperature is possible. Additional information on burn severity and other within-burn variables may be determined using multispectral analysis of Landsat TM imagery. The combination of information from a variety of sensors allows a more complete picture of conditions within burned areas than with one sensor alone. Additionally, field data are incorporated into the analysis in order to measure properties not measurable using remote sensing, and to verify remote sensing results.

Much of the work presented in this paper is incomplete and on-going. Initial assessment, however, points towards a variety of ways to utilize remote sensing data for the study of post-fire carbon dynamics.

REFERENCES

Becker, F. and Z.L. Li. 1990. Temperature independent spectral indices in thermal infrared bands. Remote Sens. Environ. 32:17-33.

Bonan, G.B. 1990. Carbon and nitrogen cycling in North American boreal forests. I. Litter quality and soil thermal effects in interior Alaska. Biogeochemistry 10:1-28.

Bourgeau-Chavez, L.L. 1994. Using ERS-1 SAR Imagery to Monitor Variations in Burn Severity in an Alaskan Fire-Disturbed Boreal Forest Ecosystem, University of Michigan M.S. Thesis, Ann Arbor, MI.

Bourgeau-Chavez, L.L., P.A. Harrell, E.S. Kasischke, and N.H.F. French. 1997. The detection and mapping of Alaskan wildfires using a spaceborne imaging radar system, Int. J. Remote Sensing. 18:355-373.

Bunnell, F.L., D.E.N. Tait, P.W. Flanagan, and K. Van Cleve. 1977. Microbial respiration and substrate weight loss - I: A general model of the influences of abiotic variables, Soil Biol. Biochem. 9:33-40.

Colwell, J.E., R.K. Aggarwala, R.M. Reinhold, C.R. Scwartz, and L. Wood. 1992. Landsat Thematic Mapper measurements of percent crop residue cover. Environmental Research Institute of Michigan, internal report no. 244700-4-F.

Eidenshink, J.C. 1992. The 1990 conterminous U.S. AVHRR data set. Photogramm. Eng. Remote. Sens., 58:809-813.

François, C. and C. Ottlé. 1996. Atmospheric corrections in the thermal infrared: Global and water vapor dependent split-window algorithms - Application to ATSR and AVHRR data. Trans. Geosci. Remote Sens. 34:457-469.

French, N.H.F., E.S. Kasischke, L.L. Bourgeau-Chavez, and P.A. Harrell. 1996a. Sensitivity of ERS-1 SAR to variations in soil water in fire-disturbed boreal forest ecosystems, Int. J. Remote Sensing 17:3037-3053.

French, N.H.F., E.S. Kasischke, R.D. Johnson, L.L Bourgeau-Chavez, and A.L. Frick. 1996b. Estimating fire-related carbon flux in Alaskan boreal forests using multisensor remote-sensing data. In: Biomass Burning and Global Change, Vol. 2, J.S. Levine, ed. MIT Press. pp. 808-826.

Kasischke, E.S., L.L. Bourgeau-Chavez, N.H.F. French, P. Harrell, and N.L. Christensen, Jr. 1992. Initial observations on the use of SAR imagery to monitor wildfires in boreal forests, Intern. J. Remote Sens. 13:3495-3501.

Li, Z.L. and F. Becker. 1993. Feasibility of land surface temperature and emissivity determination from AVHRR data. Remote Sens. Environ. 43:67-85.

Prata, A.J. 1993. Land surface temperatures derived from the Advanced Very High Resolution Radiometer and the Along-Track Scanning Radiometer 1. Theory. J. Geo. Res. 98:16,689-16,702.

Raich, J.W. and C.S. Potter. 1995. Global patterns of carbon dioxide emissions from soils. Global Biogeochemical Cycles 9:23-36.

Raich, J.W. and W.H. Schlesinger. 1992. The global carbon dioxide flux in soil respiration and its relationship to vegetation and climate. Tellus 44B:81-99.

Schlentner, R.E. and K. Van Cleve. 1985. Relationships between CO_2 evolution from soil, substrate temperature, and substrate moisture in four mature forest types in interior Alaska, Can. J. For. Res. 15:97-106.

Van Cleve, K., F.S. Chapin III, C.T. Dyrness, and L.A. Viereck. 1991. Element cycling in taiga forests: State-factor control. BioScience 41:78-88.

Viereck, L.A. 1982. Effects of fire and firelines on active layer thickness and soil temperatures in interior Alaska. Proc. 4th Canadian Permafrost Conference, Calgary, Alberta, March 2-6, 1981. National Research Council of Canada, Ottawa. pp. 123-135.

557

Freeze-Thaw Apparatus and Testing of Time Domain Reflectometry (TDR) and Radio Frequency (RF) Sensors

M.A. KESTLER[1], D. BULL[1], B. WRIGHT[1],
G. HANEK[2], AND M. TRUEBE[3]

ABSTRACT

Time domain reflectometry (TDR) is gaining rapid acceptance in the United States as a nonradioactive technique for measuring volumetric moisture content, and TDR sensors are increasingly being used to determine the effect that fluctuations in moisture content have on pavement systems. Although not as common, radio frequency (RF) sensors can also be used to monitor changes in moisture content in pavement systems. To evaluate the accuracy and repeatability of both TDR and RF moisture sensors installed in pavements experiencing seasonal freezing, the U.S. Army Cold Regions Research and Engineering Laboratory (CRREL) and the U.S. Department of Agriculture Forest Service (USFS) have developed a simple, inexpensive laboratory freeze-thaw moisture sensor testing device. The following paper discusses the test apparatus design and construction, test procedure, and observations resulting from a series of freeze-thaw tests using a sandy-silt.

Key words: Moisture sensors, time domain reflectometry, radio frequency probes, water content, frost heave.

INTRODUCTION

Time domain reflectometry sensors

Time domain reflectometry measures the dielectric constant, which, in turn, is a function of moisture content. The dielectric constants of air, dry soil, and water are approximately 1, 3-5, and 80, respectively. Because the dielectric constant of water is much greater than that of dry soil, the contribution of moisture to the overall dielectric constant of soil-water-air mixtures dominates, and is easily determined.

For measuring volumetric soil moisture content using the TDR method, an electromagnetic pulse is transmitted along a coaxial cable. The reflected wave-form recorded by the TDR readout unit exhibits changes in slope corresponding to changes in the dielectric constant in the surrounding soil. (Changes can also indicate short circuits or open circuits.)

Because the dielectric constant of ice is extremely low, it follows that the dielectric constant reflects the unfrozen moisture content. Two- and three-prong probes (both handmade and commercially produced) are typically used for geotechnical and pavement monitoring applications. For this project, coaxial cables were connected to Trase TDR sensors as shown in Figure 1a. The dielectric constant of the soil-water-air mixture is given by the following equation (Kaya et al. 1994):

$$e = [L_a/L \ V_p]^2$$

where
e = dielectric constant
L_a = apparent length of the probe (Fig. 1b)
L = actual length of the probe
V_p = the propagation velocity setting on the TDR recording device (generally 0.99)

Either Topp's equation (Topp et al. 1994) or a calibration specific to the soil undergoing measurement is typically used to determine volumetric water content. It has been shown by others (Roth et al. 1990 and Schofield et al. 1994) that for most soils, Topp's equation is accurate to within a few percent of the actual water content. Topp's equation is:
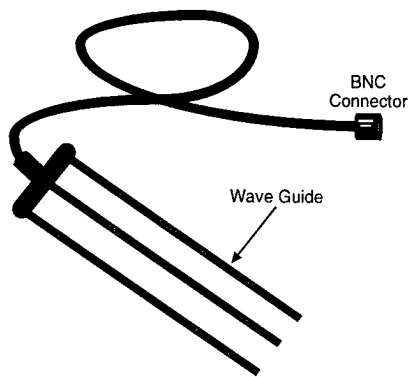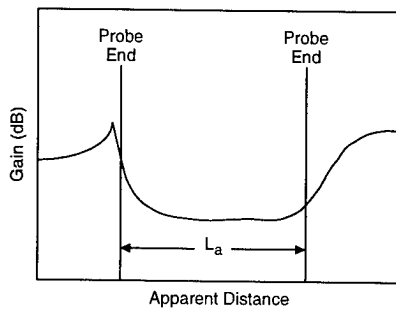
a. TDR probe.   *b. Typical TDR trace.*

Figure 1. Time domain reflectometry (TDR).

$$\theta = -0.053 + 0.0293e - 0.00055e^2$$

$$+ 0.0000043e^3$$

where θ = volumetric water content.

Note that dry density is required to convert from volumetric water content (volume of water/total volume of sample), determined by the TDR and RF sensors, to gravimetric water content (weight of water/weight of soil solids) typically used in pavements engineering.

Radio frequency sensors

Radio frequency (RF) probes, developed by Dartmouth College and CRREL, are now commercially produced as the Vitel moisture sensor. They, too, measure a soil's dielectric constant. The RF probe, shown in Figure 2, consists of a probe head,
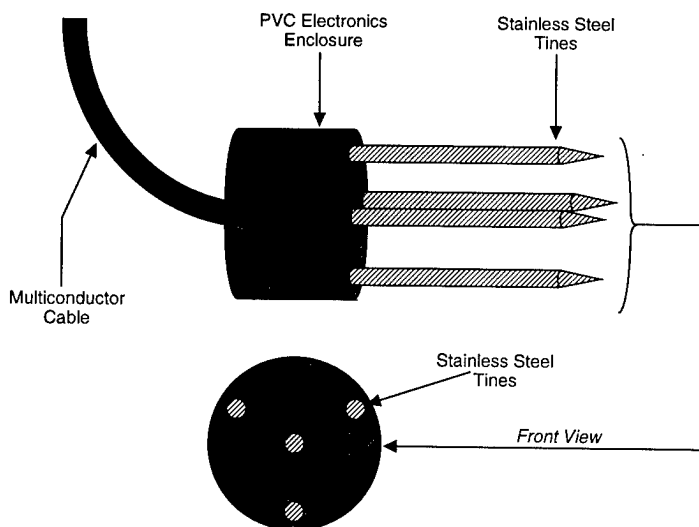
Figure 2. Radio frequency (RF) probe.

four sensing tines, and a multiconductor cable to connect to a soil moisture record-ing device. Electronics within the probe head generate a 50-MHz stimulus, and DC voltages reflect the dielectric constant. The effective volume of soil being sensed is cylindrical (bound by the outer three tines, probe head, and open end of tines—approximately 2.5 cm [1 in.] in diameter × 6.1 cm [2.4 in.] in length).

The probes are either read using a specially manufactured recording device or are hooked up to a commercial data acquisition system. Topp's equation can be applied and an approximate volumetric water content determined. Alternatively, Vitel software includes general calibrations for three soil classifications (sand, silt, and clay). Manufacturer's literature (Vitel 1994) indicates volumetric water content is accurate within ±2%. If soil specific calibrations are performed, the accuracy increases to ±0.5%. If the probes are being used to monitor changes in water content (e.g., monitoring pavements systems), the accuracy is even better because reproducibility is typically ±0.3%.

PAVEMENTS APPLICATIONS

A variety of agencies are currently monitoring seasonal variations in pavement strength. The USFS is interested in developing an affordable, reliable, quantitative method for determining when to suspend and commence hauling timber (to minimize damage to low volume roads during or following midwinter and spring thaw periods). CRREL is interested in developing a thaw weakening model for its mechanistic pavement design procedure for areas of seasonal frost. Based upon these mutually compatible objectives, the USFS and CRREL have been monitoring several pavement test sections in areas of seasonal frost to determine correlations between pavement stiffness (using a falling weight deflectometer) and moisture content (using an affordable moisture sensor monitoring system). TDR/RF calibration tests (in conjunction with this project) have been conducted by Truebe and Hanek (unpublished 1996). This paper discusses basic observations made during freeze-thaw cycling (in a CRREL coldroom) of a 43-cm- (17-in.-) diam.

559

soil sample instrumented with temperature sensors, and three RF and three TDR sensors.

LABORATORY TESTING

The test apparatus and general testing procedure were modeled after CRREL's frost susceptibility laboratory test. Additionally, an attempt was made to closely simulate field conditions.

The TDR/RF testing device consists of a set of 12 clear plastic rings, 43 cm (17 in.) in diameter and approximately 2.8 cm (1.1 in.) high. When fully assembled, the rings form a 14-in.-high vertically expandable cylindrical chamber that houses a soil sample instrumented with temperature and moisture sensors. The cylinder and sample sit atop a porous

plate which itself is on a 2.5-cm (1-in.) thick aluminum base plate. Base plate grooves allow water entry into and through the porous plate. Cold plates at the top and bottom of the sample enable control of the thermal gradient across the soil sample and, therefore, the rate of frost penetration. A constant water table head can be maintained within the soil sample by adding water (to a reservoir) to a height just above the top of the aluminum grooved plate (Fig. 3). Water is added manually and recorded.

Laboratory testing

Sample

The soil used for lab testing was from a USFS road subgrade in Berlin, New Hampshire. The field site is currently being monitored to assess seasonal variations in pavement strength by correlating moisture content and pavement strength. The laboratory sample was constructed at optimal water content. Each of nine lifts was compacted to 90–95% of optimum dry density.

Instrumentation

The sample was instrumented as shown in Table 1 and Figure 4. Changes in elevation of the plastic rings caused by frost heaving were monitored by measuring vertical displacement of screws (drilled into the plastic rings) separated by approximately 120°.

Procedure

The temperature of the sample was first allowed to equilibrate with a thermal gradient of 3.6°F (2°C) applied across the height of the soil sample. The temperatures of both the top and bottom glycol-cooled temperature baths were lowered every 24–48 hours, and the frost line progressed downward until the ma-
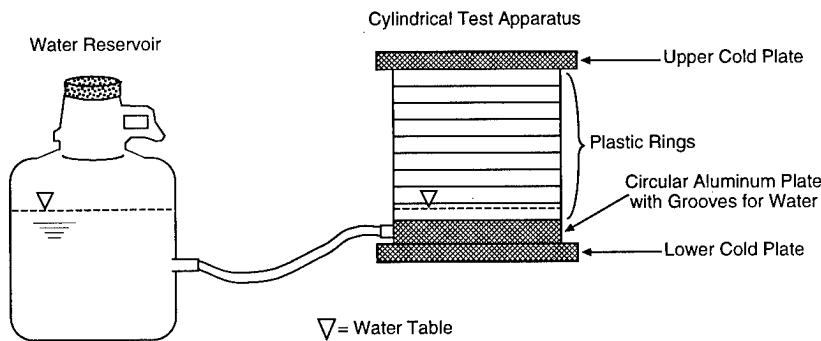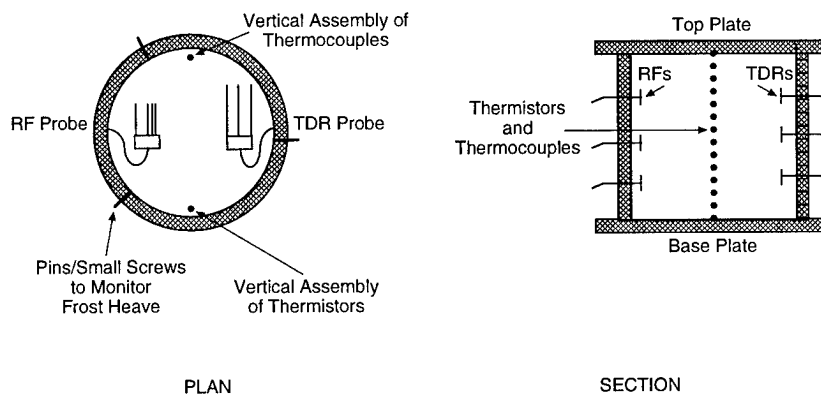

Figure 3. Schematic of test apparatus.

Figure 4. Instrumentation.

Table 1. Instrumentation and monitoring activities.

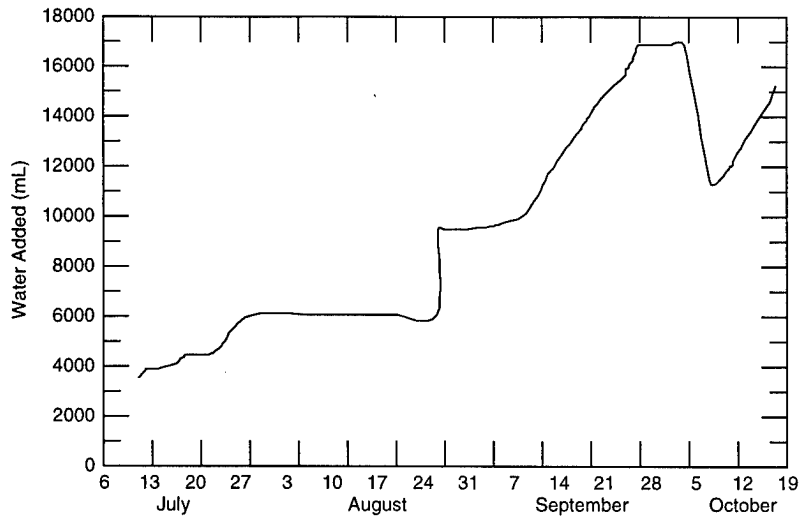| Instrumentation	To measure	Frequency/method
TDR	Volumetric moisture content	Approximately 1–2/ day (manually)
RF	Volumetric moisture content	Approximately 1–2/ day (manually), or hourly (when recorded via datalogger)
Elevation screws	Frost heave	Approximately daily

560

Figure 5. Cumulative water added.

jority of the sample was frozen. The procedure was then reversed to enable thawing from the bottom up. Throughout freezing, water was manually added to the reservoir, recorded, and a constant water table maintained. The freeze cycle was repeated three times. Other than an unknown quantity of water that drained from the system during the second thaw cycle, cumulative water added is shown in Figure 5.

Observations

Temperature and frost penetration

Figure 6a shows the 0°C (32°F) isotherm as a function of time. The figure therefore shows the frozen and thawed sections of the sample through time. The rate of frost penetration was fairly constant.

Frost heave

Frost heave was recorded at 2.6-cm (1-in.) increments throughout the sample by averaging the manual measurements of three points equi-spaced on the circumference of the midsection of each plastic ring. The heave from the base plate to the elevation pins/ screws in each level is shown in Figure 6b. Minimal heave occurred during the first cycle. However, it is believed that the water table was within the 0.64-cm- (0.25-in.-) thick porous plate as opposed to just above it. The water table was raised slightly, for cycles 2 and 3. Total frost heave increased with each cycle. As is also shown by the figure, total consolidation upon completion of thawing did not occur. However, in pavements engineering, traffic generally provides the required overburden pressure to encourage total thaw consolidation.

Water content

Initial volumetric water contents recorded by all three TDR probes immediately following installation were similar to each other. Likewise volumetric water contents recorded by all three RF probes were also similar to each other. However, TDR probe water contents did not exactly match RF probe water contents because initial densities differed: TDRs were installed and compacted in place during construction. Known water contents and densities of each lift enabled calculation of volumetric water content which closely agreed with probe measurements. Because material cannot be compacted between RF probe tines during construction, RF probes were inserted into samples prepared in paper cups, then frozen. The entire frozen RF "popsicle" was placed in the large sample and lifts were constructed around and above it. While this enables material to be compacted in between individual tines, the density of the soil within the popsicle cup was appreciably less than that in the sample. However, calculations showed the RF probes were accurate. If this popsicle technique is used for field installation, the probe should be inserted in a sturdier container than a paper cup so adequate compaction can be obtained. Alternatively, the probes can be inserted either vertically or into a trench wall. These alternative installation methods were impractical for this particular laboratory study because of limited apparatus size.

Figure 6c shows water added to the system at a constant rate while maintaining an almost constant water table. For cycles 2 and 3, water was added at a rate slightly in excess of 400 mL per day. Resulting
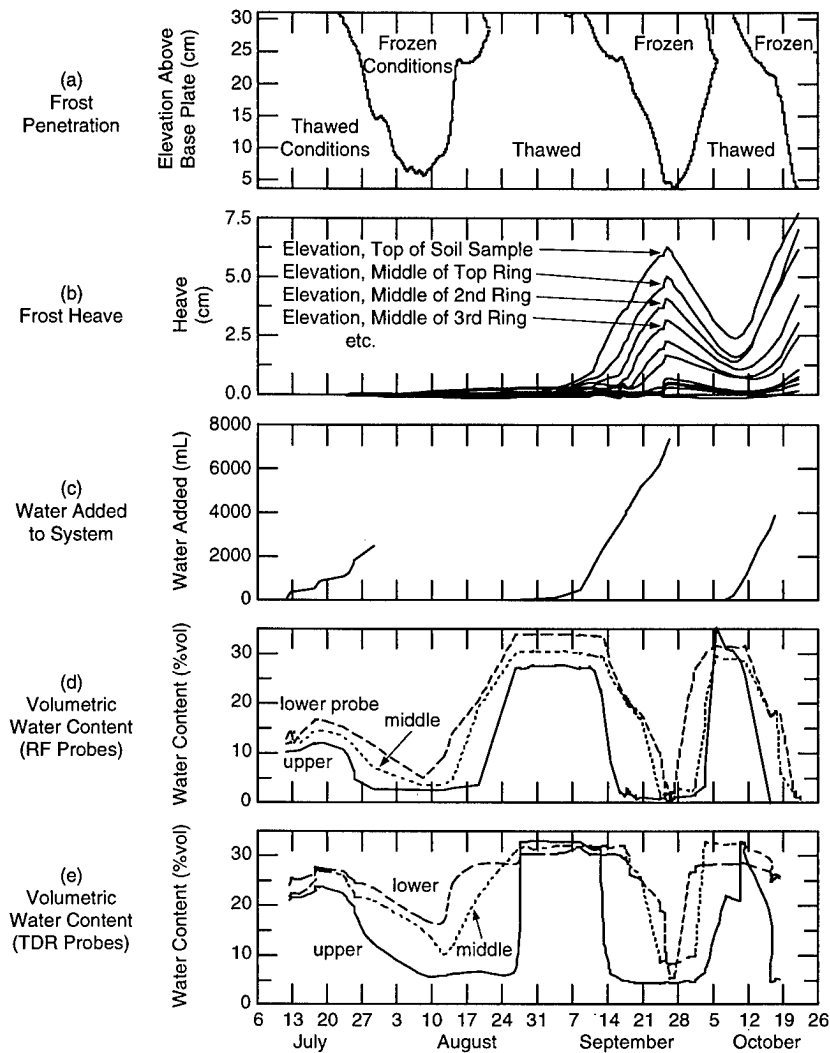
Figure 6. Three freeze cycles.

volumetric water content measured by RF and TDR probes is shown in Figures 6d and 6e. Discrepancy in initial water content has been discussed. However, note that the two water contents measured by the two types of sensors approached one another—as would be expected from freeze-thaw cycling ("working" the density of the sample).

Water on the floor of the laboratory coldroom during the second thaw, indicating a leak in the system, provides a probable explanation of unexpected relative changes in unfrozen water content between the first and second thaws: Upper probes showed an increase in water content between freezes and lower probes showed a decrease — as expected if water had drained from the lower part of the apparatus. Similar increases and decreases recorded by both types of probes actually helps confirm the accuracy of the probes.

Relationships among frost penetration, frost heave, and water content

Relationships among frost penetration, frost heave, and water added into the system were all as anticipated, and are pictorially shown by Figures 6a through 6e. As previously discussed, the rate of frost penetration was relatively constant. Total frost heave (shown by the uppermost curve in Fig. 6b) correlates well to frost penetration and water added into the system. Sharp increases and decreases in volumetric water content recorded by the RF and TDR probes in Figures 6d and 6e also correspond nicely to the progressing freezing front.

Figure 7 shows time frames during which maximum heave rates occurred within each layer. These heave rates and corresponding dates were determined from differences in total heave from the base plate to each of the elevation-pins/screws. The pro-
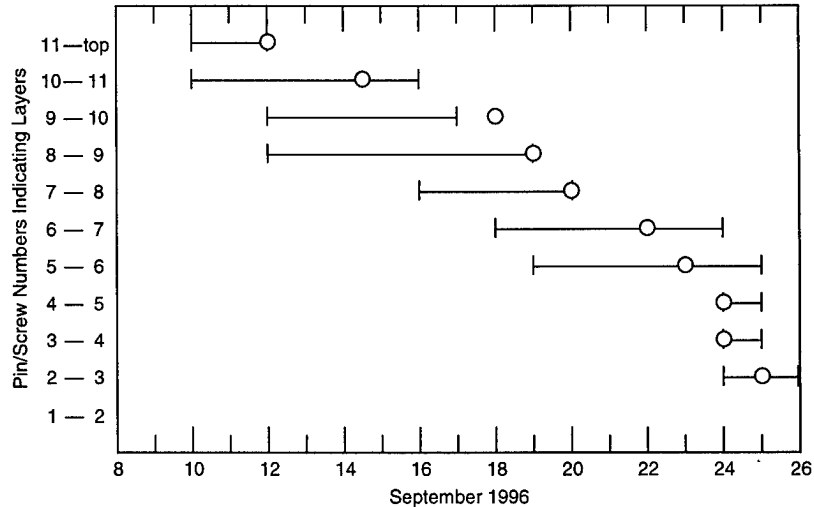
Figure 7. Calendar of dates during which maximum heave rate occurred within various layers—cycle 2.

gression of dates during which maximum heave rate occurred in each underlying layer (as shown by the horizontal offset of Figure 6b curves) closely correlates to each of the measurements discussed above. "Circles" on Figure 7's calendar indicate the dates corresponding to penetration of the 0°C (32°F) isotherm as determined by thermistor readings.

Variations in location of the 0°C (32°F) isotherm within the maximum heave rate ranges could be attributed to a variety of reasons. Planes corresponding to tops and bottoms of adjacent layers were approximated by the horizontal plane running through the centroid of the three averaged elevation pins around

the ring circumference. In reality, heave was not completely uniform. (Note that the sample was generally allowed to thaw before frost had fully penetrated to the bottom. Therefore information from near the bottom of the sample should not be used in the discussion of observations.)

TDR and RF probes can be used to determine frozen and thawed conditions. Frozen and thawed conditions of the silty sand as indicated by sharp increases and decreases in water content very closely coincided with a freezing point of 0°C (32°F) recorded by thermistor and thermocouples. As shown by the very close agreement in freeze and thaw

Table 2. Freeze and thaw dates indicated by temperature and moisture sensors.*

Instrumentation	Cycle 2—Freeze	Cycle 2—Thaw	Cycle 3—Freeze
TDR (upper)	13–14 September 1996	04 October 1996	15 October 1996
RF (upper)	13–14 September 1996	04 October 1996	15 October 1996
Temperature sensors (same location as top moisture sensors)	14–15 September 1996	05 October 1996	14 October 1996
TDR (middle)	21–24 September 1996	03 October 1996	19 October 1996
RF (middle)	17–23 September 1996	03 October 1996	19 October 1996
Temperature sensors (same location as middle moisture sensors)	20 September 1996	03 October 1996	19 October 1996
TDR (lower)	15–24 September 1996	29 September 1996	19–20 October 1996
RF (lower)	20–23 September 1996	29 September 1996	19–21 October 1996
Temperature sensors (same location as bottom moisture sensors)	24 September 1996	30 September 1996	Not Available

*Frequency of moisture sensor readings during cycle one yielded too wide a range of dates to isolate date or short range of dates. Cycle 3 did not include a thaw: the frozen sample was removed from the apparatus for additional testing.

dates indicated by temperature and moisture sensors (Table 2), TDR and RF probes can very reliably indicate freezing and thawing even though probes are subjected to freeze-thaw cycling.

After completion of three freeze-cycles, the sample had heaved approximately 6.4 cm (2.5 in.), or nearly 15%. Surprisingly, the post-test cutting dissection did not reveal any ice lensing. Circular sawblade cut marks on the wall of the sample were visible, but nothing more. However, an appreciable amount of heat was generated during cutting. This could have disguised lensing.

SUMMARY AND CONCLUSIONS

1. Test apparatus: CRREL and the USFS developed a simple, inexpensive laboratory freeze-thaw moisture sensor testing device. A constant water table allows moisture to migrate toward the freezing front as the upper boundary cold plate simulates progressive freezing progressing from the pavement surface in a downward direction. Vertically expandable confining rings form a chamber that allows frost heaving to occur with minimal friction. The test apparatus design enabled a relatively accurate simulation of field conditions in areas of seasonal freezing.

2. Sample observations: A soil sample was prepared, instrumented, and subjected to three freeze thaw cycles. Tight test controls and closely spaced instrumentation enabled a focus on measurements within very thin layers. *Classic relationships* among frost penetration, frost heaving, and water content were all observed. Correlations between data pairs including frost penetration, frost heave, water added to the system, and progression of time corresponding to maximum rate of heave in adjacent underlying layers were as would be expected under (good) field conditions. These observations also, and again, indicate a well designed test apparatus.

3. Moisture sensors: Rapid decreases and increases in water content were observed and shown to be good indicators of freezing and thawing. Freezing and thawing dates indicated by TDR and RF probes correlated closely to those indicated by conventional temperature sensors throughout repeated freeze-thaw cycling. These observations showed that TDR and RF moisture sensors are good indicators of soil conditions.

4. Overall: Laboratory testing showed the TDR and RF probes appear to be a reliable repeatable method for measuring unfrozen water content in soils subject to *freeze-thaw cycling*. Additionally it follows that using the sensors in pavements as a low cost alternative for assessing variations in pavement strength (in pavements that experience seasonal freezing) looks very promising.

REFERENCES

Kaya, A., C.W. Lovell, and A.G. Altschaeffl. 1994. The effective use of time domain reflectometry (TDR) in geotechnical engineering. *In* Proceedings Symposium and Workshop on Time Domain Reflectometry in Environmental, Infrastructure, and Mining Applications, p. 398– 409, Northwestern University, Evanston, Illinois. September.

Roth, K., R. Schulin, H. Fluhler, and W. Attinger. 1990. Calibration of time domain reflectometry for water content measurement using a composite dielectric approach. Water Resources Research, 26(10): p. 2267–2273, October.

Schofield, T.G., G.J. Langhorst, G. Trujllo, K.V. Bostick, and W.R. Hansen. 1994. Comparison of neutron probe and time domain reflectometry techniques of soil moisture analysis. *In* Proceedings Symposium and Workshop on Time Domain Reflectometry in Environmental, Infrastructure, and Mining Applications, p. 130–142, Northwestern University, Evanston, Illinois. September.

Topp, G.C., S.J. Zegelin, and I. White. 1994. Monitoring soil water content using TDR: An overview of Progress, *In* Proceedings Symposium and Workshop on Time Domain Reflectometry in Environmental, Infrastructure, and Mining Applications, pp. 67–80, Northwestern University, Evanston, Illinois. September.

Vitel. 1994. Hydra Soil Moisture Probe User's Manual, Version 1.1, Chantilly, Virginia, February.

Examining the Use of
Time Domain Reflectometry in Frozen Soil

E.J.A. SPAANS[1], J.M. BAKER[2]

ABSTRACT

Time domain reflectometry (TDR) is a powerful technique to simultaneously measure volumetric liquid water content (θ_L) and bulk-soil electrical conductivity (σ_b) in frozen soil. Since TDR detects liquid water indirectly it requires calibration, which is different in frozen than in unfrozen soil because the permittivity for ice is larger than that for air. This hypothesis was confirmed by means of a new procedure to calibrate TDR for θ_L. TDR was applied to monitor θ_L and σ_b in situ in a silt-loam to investigate whether solutes are redistributed when the soil is subject to freezing and thawing cycles. There was no evidence of macroscopic redistribution of solutes, hence it is concluded that solutes were excluded locally into nearby liquid films.

Key words: TDR, liquid water, solutes, instrumentation.

INTRODUCTION

Time domain reflectometry (TDR) is now widely used to measure volumetric water content (θ) in soils, in large part due to its suitability for automation, multiplexing, and in-situ measurements. Also appealing is the fact that commercially available TDR equipment provides ample resolution and reproducibility for most applications in hydrological studies. The method, however, is an indirect measure of water content; it actually measures the travel time of an electromagnetic pulse through soil, which is strongly related to the presence of water. As such, the accuracy of the technique is, in most cases, dependent on the calibration used to convert the measured travel time into volumetric water content. More recently, it was proposed that TDR can be used to measure bulk electrical conductivity (σ_b) in soils as well. The merit, of course, is that θ and σ_b can be measured simultaneously in the same volume of soil using the same equipment.

The TDR technique has drawn considerable attention in frozen-soil research, because the sensitivity of TDR for liquid water is much larger than that for ice. This allows quantitative detection of liquid water in frozen soil, which has historically been a difficult task. Other methods to measure water content that are popular in unfrozen soils, such as neutron moderation and gravimetry, cannot distinguish between liquid water and ice, and thus measure total water content, θ (liquid water content, θ_L, and ice content, θ_i, together). Dilatometry, in which the ice content in a sample is calculated from the expansion of the sample upon freezing, is purely a laboratory method and requires a water-saturated sample. NMR can distinguish between liquid water and ice, but is not amenable to field research. While TDR allows acquisition of data in frozen soil that was previously infeasible, its calibration in frozen soil deserves attention. Application of calibration equations developed for unfrozen soil, where water is exchanged with air, may not apply to frozen soil, where water is exchanged with ice, since the travel time is larger in ice than in air.

The objectives of this paper are to evaluate the use of TDR in frozen-soil research, with special attention to calibration for liquid water content and the measurement of electrical conductivity. A case study in which TDR is applied for in situ monitoring of θ_L and σ_b is presented.

CALIBRATION FOR LIQUID WATER IN FROZEN SOIL

The travel time of the TDR pulse through soil depends on the bulk-soil permittivity (ε_b), the value of which is determined by the permittivity of the individual soil components and their geometric arrangement. In both frozen and unfrozen soil the contribution of the liquid water to the bulk permittivity dominates. However, we expect different TDR calibration curves for unfrozen and frozen soil because permittivity of ice is larger than that of air. Hence, exchanging water with ice will yield smaller changes in ε_b than exchanging water with air. In addition, at identical θ_L, ε_b of frozen soil must be larger than that for the same soil in the unfrozen condition. Likewise, there is no unique calibration for TDR in frozen soil, but rather a family of calibration curves, each curve corresponding to a different total water content. We tested that

hypothesis by comparing TDR calibrations for θ_L in a frozen and unfrozen Waukegan silt-loam (Typic Hapludoll).

The calibration in unfrozen soil was done by wetting, mixing, and repacking a given amount of soil in a container and plotting the measured relative travel time (ratio of the travel times with the probe in soil, t_s, and in air, t_a) against the gravimetrically determined volumetric water. For the calibration in frozen soil we designed a new apparatus, called a gas dilatometer, to independently estimate θ_L. A soil sample was hermetically sealed in the gas dilatometer; subsequent soil freezing reduced total air space and hence increased air pressure inside the gas dilatometer, since ice is less dense than water. The amounts of soil water frozen were computed from measured pressure changes as temperature was incrementally decreased. A relatively wet ($\theta=0.36$) and a relatively dry ($\theta=0.24$) soil were used to examine the significance of total water content on the calibration in frozen soil. More details are provided by Spaans (1994) and Spaans and Baker (1995).

Results of the calibrations are shown in Figure 1; the new method for calibrating TDR in frozen soil shows remarkably little scatter. Table 1 shows the statistical analysis of the calibrations.
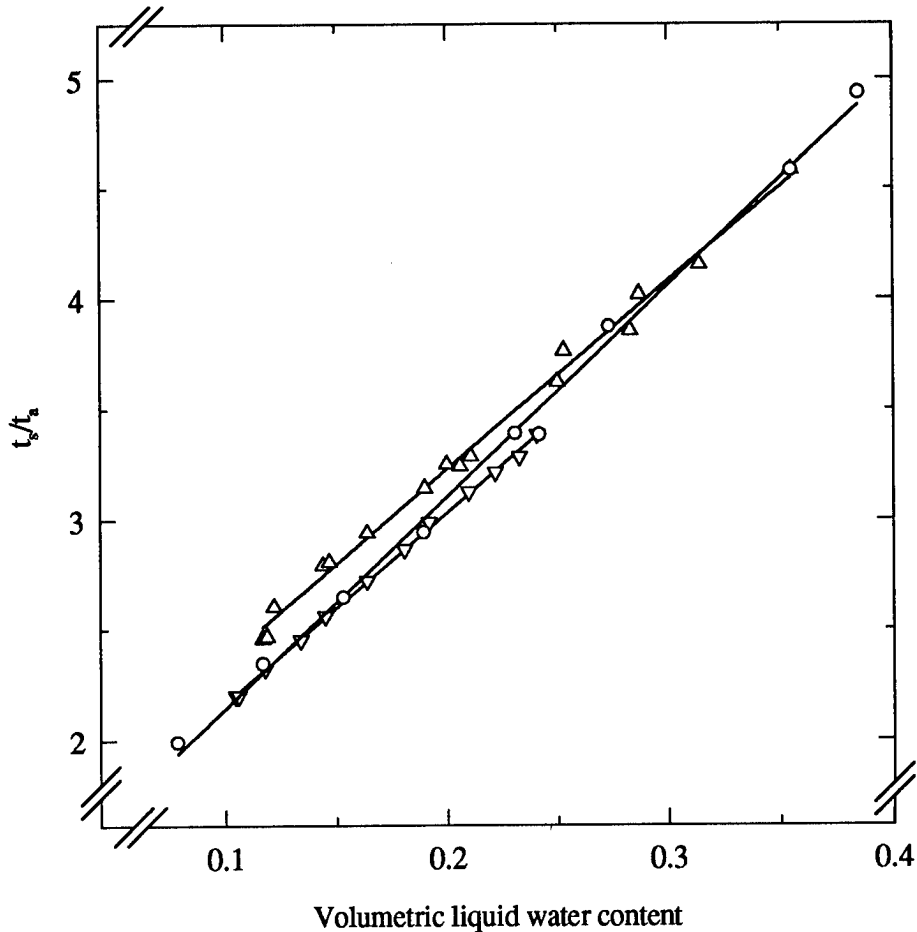

Figure 1. Comparison of different calibrations of TDR for volumetric liquid water content: relatively wet frozen Waukegan silt loam (Δ), relatively dry frozen Waukegan silt loam (∇), and unfrozen Waukegan silt loam (O).

566

Table 1. Statistical analysis on the calibration of TDR for θ_L in frozen and unfrozen soil. Calibration equation is expressed as: θ_L = slope(t_s/t_a) + intercept. SE = standard error. Values with the same index (superscript) are not significantly different at the 1% level.

	slope	intercept	R^2	SE
Wet soil, frozen	0.1161[a]	-0.175[c]	0.994	5.9×10^{-3}
Dry soil, frozen	0.1154[a]	-0.150[d]	0.998	2.1×10^{-3}
Unfrozen soil	0.1039[b]	-0.123[e]	0.996	6.9×10^{-3}

The contribution of the ice to the bulk-soil permittivity is discernible. Consistent with our hypothesis, the change in (liquid) water content needs to be significantly larger in frozen than in unfrozen soil to produce a given change in bulk-soil permittivity. In frozen soil the slopes of the calibration curves for initially wet and dry soils are not significantly different, but the wet frozen soil has a consistently higher permittivity than the dry frozen soil, because it has approximately 12% more ice.

ELECTRICAL CONDUCTIVITY

The TDR signal is partially shorted (attenuated) as it travels through the soil, due to the electrical conductivity of the soil. Several formulations have been proposed to calculate the electrical conductivity from the magnitude of the signal before and after its journey through the soil. The one now most commonly used can be derived from theory of non-ideal transmission lines (Ramo et al. 1984):

$$\sigma_b = K\left(\frac{1+\rho}{1-\rho}\right) = K\left(\frac{2V_0}{V_f}-1\right) \qquad [1]$$

An expression in this form was introduced to soil science by Topp et al. (1988), who cited an article by Giese and Tiemann (1975) as the source of the formulation. That is, by the way, the reason this expression has frequently been named the Giese-Tiemann method. Parameter K depends on the probe configuration, and can be calculated for truly balanced (parallel) or unbalanced (coaxial) probes. For surrogate probes, such as multiwire unbalanced probes, or dual-wire parallel probes without a balun, K needs to be determined empirically (Baker and Spaans 1993). On a Tektronix TDR unit the reflection coefficient, ρ, which is the reflected voltage divided by the incident voltage, can be computed from two points on the TDR trace; the height of the incident pulse, V_0 (height of the trace within about 1 m of the unit), and the height of the trace at very long time, V_f (height of the trace at maximum distance, that is 623 m). The height of the trace is always measured with respect to the baseline, which appears on the screen prior to the pulse generator. Other formulations have been proposed to derive σ_b from a TDR trace, but their lifetimes were brief because they were more complicated and less accurate.

Bulk electrical conductivity in the soil depends on the solute concentration, solute composition, water content, and temperature. Water content primarily determines the path length of the electrical current and the mobility of the ions in the soil water. Temperature affects the viscosity of the water, and thus the ion mobility; solute composition plays a role since ionic conductivity is species dependent. The solute concentration is usually the variable of interest, so if that is derived from σ_b then one has to account for the effects of temperature and water content on σ_b. Since independent measurements on solute composition are usually not readily available, changes in composition are typically assumed irrelevant.

FIELD STUDY

Ice crystals cannot incorporate ions, but can only grow by association with other water molecules. Upon ice crystal formation, solutes are rejected into the remaining unfrozen water, which will become increasingly concentrated. A rapidly penetrating freezing front, however, might enclose particles and solutes which remain as isolated pockets in the ice, which will subsequently migrate out towards warmer regions by thermally induced regelation. Of particular interest is whether the ions are excluded equally in all directions, or pushed ahead of the freezing front, leaving a leached profile behind.

We measured σ_b, θ_L, and temperature in a Waukegan silt-loam (Typic Hapludoll) located in an isolated depression at the Rosemount Experimental Station, MN. Measurements were part of a larger investigation of snow melt hydrology and ponded infiltration into frozen soil (Baker and Spaans, these Proceedings). Two thermistors (YSI 44004, Yellow
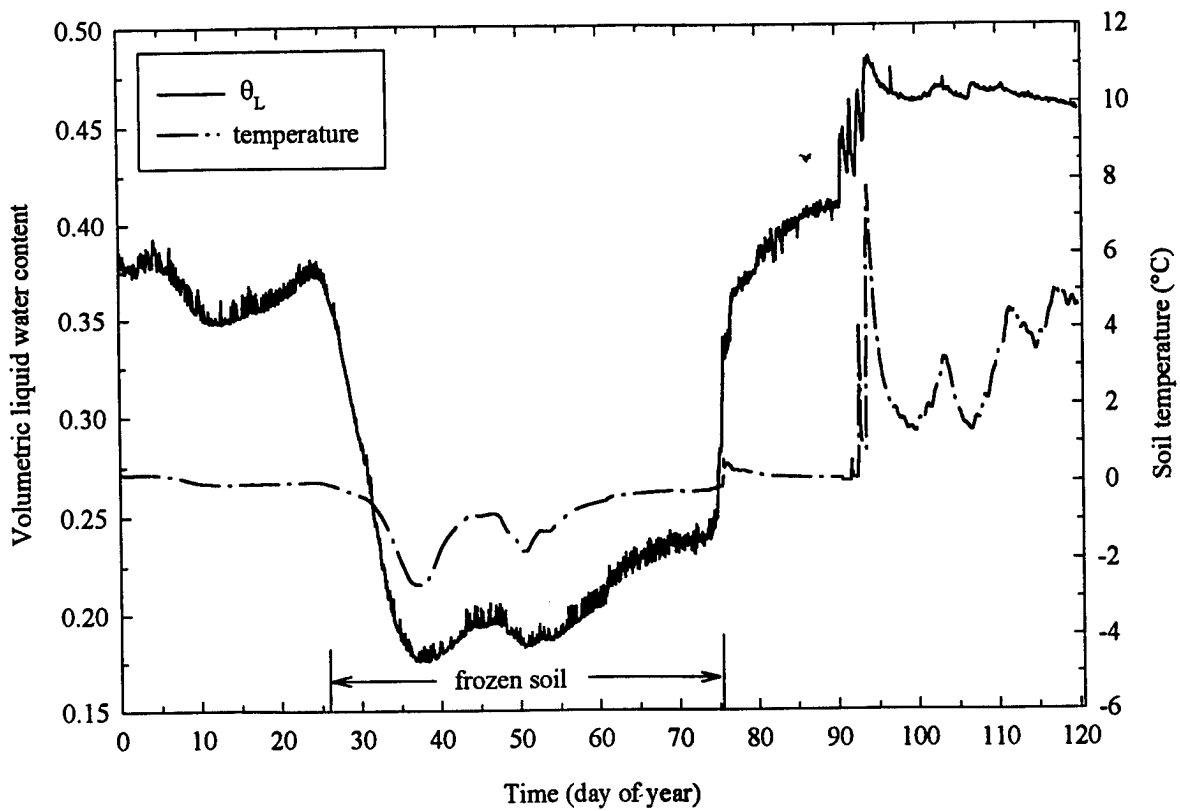
Figure 2. Time series of in situ volumetric liquid water content and temperature in frozen Waukegan silt loam at 0.4 m depth.
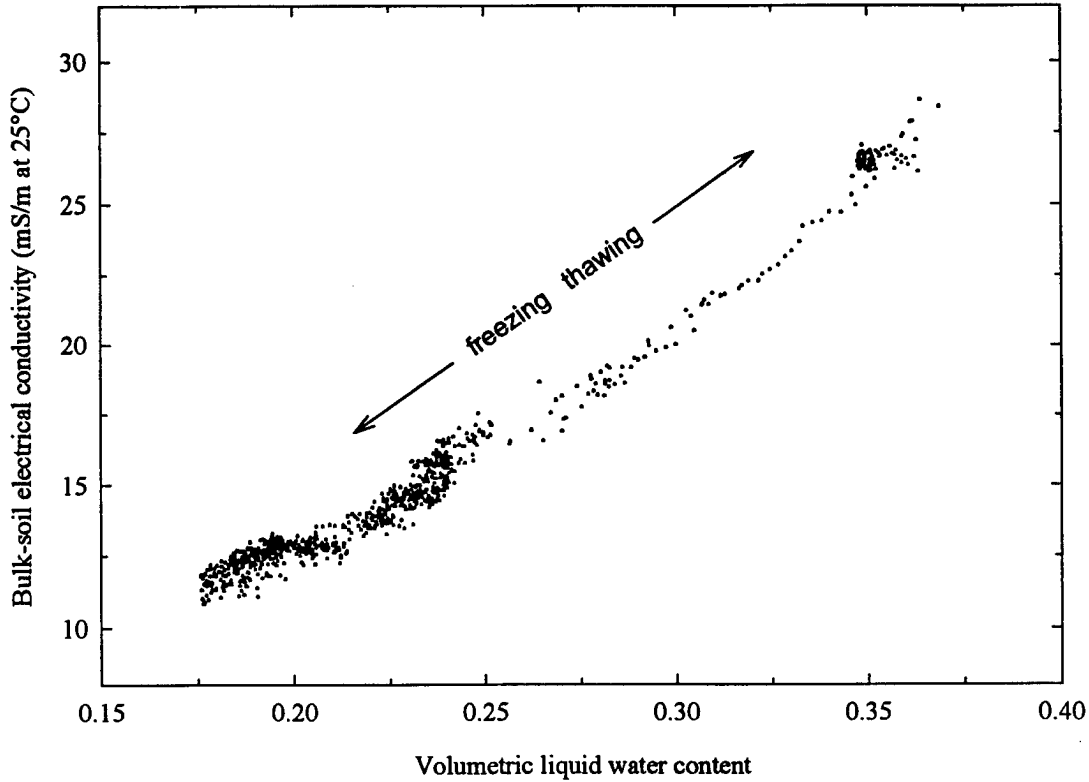

Figure 3. Bulk-soil electrical conductivity, normalized to 25°C, related to volumetric liquid water conten measured in situ in a Waukegan silt loam.

Springs, OH) and one TDR probe (Midwest Special Services, St. Paul, MN) were installed at 17 different depths ranging from 5 to 120 cm. Sensors were multiplexed and measurements automated to allow data acquisition around the clock.

In order to examine the fate of solutes when the soil is subject to freezing and thawing, we first assume that freezing and thawing do not significantly affect the solute composition. Next, we normalize all measurements of σ_b to a common temperature. We used ;

$$\sigma_n = \frac{\sigma_b}{1+0.0185(T-25)} \quad [2]$$

where σ_n is the bulk-soil electrical conductivity normalized to 25°C, and T is the soil temperature (°C). Consequently, comparison of σ_n during freezing and thawing *at equal* θ_L will reveal whether local solute concentration in the profile has changed due to the advancing and retreating freezing front. Figure 2 shows hourly data of σ_n versus θ_L at 0.4 m depth when $T<0$°C. On 26 January 1996, immediately before the soil at this depth froze, $\theta=0.36$ and $\sigma_n=28.6$ mS/m. As the temperature dropped below the freezing point, ice started to form at the expense of θ_L. Simultaneously, σ_n dropped because the resistance of the soil to electrical current rose as the liquid water films narrowed. Temperature reached a minimum of -2.6°C on 6 February, after which the temperature started to rise to -0.8°C one week later. Then another period of cold weather dropped the temperature back to -1.8°C on 20 February, followed by a gradual thaw that was completed, for this depth, on 12 March. Figure 3 demonstrates that σ_n is similar at equal θ_L on both freezing and thawing cycles, indicating that the

solute concentration must have remained intact over the course of the winter. Data from other depths followed similar trends. Consequently, solute redistribution in the winter of 1995/1996, in this soil, was negligible. There is no experimental evidence that solutes were preferentially excluded ahead of the penetrating freezing front, hence we conclude that solutes are excluded locally into the liquid water films.

REFERENCES

Giese, K. and R. Tiemann. 1975. Determination of the complex permittivity from thin-sample time domain reflectometry: Improved analysis of the step response waveform. Adv. Mol. Relaxation Processes 7:45-49.

Baker, J.M. and E.J.A. Spaans. 1993. Comments on "Time domain reflectometry measurements of water content and electrical conductivity of layered soil columns". Soil Sci. Soc. Am. J. 57:1395-1396.

Ramo, S., J.R. Whinnery, and T. van Duzer. 1984. Field and waves in communication electronics. John Wiley & Sons, New York.

Spaans, E.J.A. 1994. The soil freezing characteristic: its measurement and similarity to the soil moisture characteristic. Ph.D. diss. Univ. of Minnesota, St. Paul (Diss. Abstr. 95-01135).

Spaans, E.J.A. and J.M. Baker. 1995. Examining the use of time domain reflectometry for measuring liquid water content in frozen soil. Water Resour. Res. 31:2917-2925.

Topp, G.C., M. Yanuka, W.D. Zebchuk, and S. Zegelin. 1988. Determination of electrical conductivity using time domain reflectometry: soil and water experiments in coaxial lines. Water Resour. Res. 24:945-952.

SUMMARY AND DISCUSSION

Physics, Chemistry, and Ecology of Seasonally Frozen Soils
A Wrap-up Discussion

J.K. RADKE[1], B.S. SHARRATT[2], L.D. HINZMAN[3],
P.H. GROENEVELT[4], AND I.K. ISKANDAR[5]

ABSTRACT

Seasonally frozen soils occur over a large portion of the northern hemisphere and include some of the most productive and also the most fragile soils in the world. Research reported from twelve countries at the International Symposium on Physics, Chemistry, and Ecology of Seasonally Frozen Soils covered a wide range of topics and represented many disciplines. While our knowledge of frozen soils is vast, much remains to be learned. Future frozen soils research needs include: 1) measurement techniques, 2) changes in soil microstructure, 3) adaptation of soil organisms, 4) new simulation models and management tools, 5) interdisciplinary research, and 6) applied research for managing ecosystems. The big task for the future is to integrate knowledge gained through frozen soils research into useful tools for the development of new management systems for our global ecosystems.

INTRODUCTION

Freezing and thawing has a profound influence on the stability, hydrology, and ecology of soils in cold regions. These aspects of frozen soils, along with many others, were discussed at an international Symposium on Physics, Chemistry, and Ecology of Seasonally Frozen Soils held at the University of Alaska in Fairbanks from June 10-12, 1997. The proceedings of the symposium covered recent advancements in the detection and prediction of physical, chemical, and biological processes of cold soils. One objective of the symposium was to provide an opportunity for scientists from around the world to meet and discuss frozen soils phenomena in managed ecosystems. Another objective was to identify knowledge gaps and research needs that will conserve resources while improving productivity of ecosystems in the future.

Approximately 200 abstracts were submitted for oral and poster presentations at the symposium. Almost 80 percent of the submissions were from Russia (40%) and the United States of America (39%). Another eleven percent came from Canada (6%) and Germany (5%). Other countries represented were Japan, Finland, Sweden, China, Israel, England, Switzerland, and Mongolia. About one-half of these contributions are reported in these proceedings. Proceedings papers represented a broad spectrum of research disciplines and topics. Disciplines ranged from earth sciences to social sciences and included such fields as soils, physics, chemistry, biology, ecology, geology, hydrology, engineering, bioremediation, crops, forestry, management, geography, and land use planning. Topics included water and ice phase, carbon dynamics, pedology, tillage, ecosystem processes, nitrogen and phosphorus balance, biology of cryogenic soils, tillage and erosion, climatology, soil-atmosphere gas exchange, modeling, remote sensing, groundwater, frost heave, contaminants, and snow dynamics.

A SYNOPSIS
Keynote Addresses

Dr. Peter J. Williams, distinguished professor at Carleton University (Ottawa, Canada), presented the first keynote address, "The Seasonally Frozen Layer: Geotechnical Significance and Needed Research". He provided a description of freezing processes in porous media and its effects on soil heaving and soil microstructure. Professor Williams suggested further study of freezing effects on soil microstructure with potential applications including contamination containment, remediation, and cold regions agronomy.

Dr. F. Stuart (Terry) Chapin III, distinguished ecologist and professor at the University of California

---

Berkeley, presented the second keynote address, "Influence of Frozen Soils on Ecosystem Processes and their Sensitivity to Climatic Change". He indicated that biological processes occurring during the winter and the freeze-thaw process are critical to understanding the dynamics of high-latitude ecosystems.

Volunteered Papers

Papers presented at the symposium ranged from theoretical and basic to applied and observational. Specific processes were investigated in some papers while procedures and measurement tools for use in frozen soils research were the foci of others.

The soil matrix

Presentations focused on soil physical properties and processes, water and hydrology, heat and thermodynamics, and snow and ice. Some of the topics considered were compaction, erosion, aggregate stability, infiltration, frost heave, frost depth, permafrost depth, waste containment, and engineering aspects. These papers demonstrated that freezing and thawing impact soil properties, at least at the scales above the microstructure. The freeze-thaw process is complex. Soil water does not freeze completely within the realm of ambient temperatures experienced on earth. Soil chemistry and even soil biology influence the phase transition from liquid to solid. The freezing action changes soil structure in ways that are important in agricultural management and construction.

The soil solution phase

The movement of solutes to the freezing zone and the redistribution upon thawing is an important factor in the fate of nutrients and pesticides in agricultural systems. Several papers reported on nitrogen dynamics and others covered phosphorus, carbon, exchangeable cations, and acidity. Remediation of contaminated soils depends on knowledge of chemical movement in frozen soils. Frozen soils may contain or provide channels for the escape of contaminating chemicals. Emissions of soil gases such as carbon dioxide and methane were discussed in several papers. These emissions play roles in environmental quality and nutrient cycling in the soil.

Soil biology

Biological activity under winter conditions was once thought to be suspended when the soil was frozen. We now know that although biological activity is slowed, it does occur in cold and even frozen soil. Isolated pockets within the frozen soil may be hotbeds of activity. Overwinter biological activity and survival are conducive to a healthy and productive soil during the growing season. Biologically aided chemical

transformations and gas emissions do occur during the frozen and especially during the thawing portion of the year. Bioremediation efforts depend on a viable microbial population even under very cold conditions.

Geology and hydrology

Creek flow, ground water recharge, water/rock interaction, solifluction, and soil formation were the focus of many papers. Water quality is a very sensitive issue and spring thaws play a large role in the recharge of streams, lakes, and water tables. Mesoscale freeze-thaw models may help manage and predict the hydrology of snow packs and soils.

Land management

Only a few papers reported on applied research directed at managing soil tillage, crops, trees, and natural resources. The objective of these and similar papers was to assess the impact of management on soil properties or resource allocation (e.g. water infiltration). However, several papers did provide information that will be useful in developing management systems on seasonally frozen lands.

FUTURE DIRECTIONS

Papers presented at the symposium provided state of art information regarding freezing processes and their effects in soils. The depth and broad ranging scope of the papers presented should provide a base for developing new and improved management systems for agriculture, range, forestry, and mining. How to integrate the vast wealth of knowledge into useful forms is a vital step toward enhancing productivity and sustainability of ecosystems.. Simulation models will continue to be important for this effort. Several models have been developed to simulate the simultaneous movement of heat, water, and solutes in soils while undergoing freeze-thaw cycles. These models, however, vary in scale and degree of complexity. Models that are driven by energy and mass transport at the mesoscale lack the testing concerning the fate of chemicals within an ecosystem. Simulations of heat, water, and chemical transport within an ecosystem will aid government and action agencies for future planning, regulation, and management of our natural resources.

Research Needs

Much research remains to be done on seasonally frozen soils to fully understand the processes which affect our land's productivity, environment quality, and the quality of our lives. Specific research needs include:

1. Measurement techniques

New and better research tools are needed to

measure and monitor processes within frozen soils. Time domain reflectometry (TDR), Synthetic Aperture Radar, and other measurement techniques are now widely used in frozen soils research and provide information that was difficult to obtain years ago. Nevertheless, improvements of existing devices and the development of new devices will allow measurements on spatial and temporal time scales which are now impossible.

2. Changes in soil microstructure

Understanding the effects of freeze-thaw on soil microstructure may be key to predicting and modifying soil stability, aggregate strength, pore structure, and other soil properties important to soil quality and productivity.

3. Adaptation of soil organisms

Overwintering of beneficial soil microbes and fauna are necessary for a healthy and dynamic soil. On the other hand, unwanted insects and pathogens degrade soil productivity. Therefore, can soils be managed that will lead to the demise of unwanted pests and favor the beneficial species? Organisms have varying tolerances to freezing stress and identifying the varying degrees of stress under which organisms can survive may aid in managing pests. Pesticide degradation and greenhouse gas emissions are also microbial dependent, thus fate of microbes will affect chemical and gas fluxes in the environment. To what extent the winter climate and frozen soils contribute to these fluxes needs to be better understood over a wide range of ecosystems in cold regions. Organisms also influence soil stability and productivity. More studies are needed on the stability of structural bonds formed by biological processes (exudates or excretions) under freezing and thawing environments.

4. New simulation models and management tools

Complex, data intensive models may be useful in understanding the mechanics of frozen soil processes. However, simpler models are desirable for making management decisions. Such models may need to incorporate economic and other information as well. Models concerned with fate of chemicals in the soil environment still lack development and validation for applications such as management decision-making, land use planning, and political policy making.

5. Interdisciplinary research

Scientists need to develop a broader understanding of global ecosystems by considering other disciplines in their research efforts. While ecologists consider the multidisciplinary aspects of ecosystem processes, many scientists lack the broad perspective in fully understanding complex interactions in soils. The importance of microbial dynamics to soil physical processes such as aggregate stability in environements subject to freezing and thawing is one example.

6. Applied research for managing ecosystems

Despite the vastness of frozen soils, there is little information concerning the spatial extent of soils undergoing annual freezing and thawing throughout the world. The effect of climate and seasonally frozen soils on plants, trees, fish, and wild life needs to be understood to better manage the systems under which these organisms live. Climate and soils largely determine the type of vegetation and the portion of the year during which it can be grown. Sustainable and environmentally safe management systems are needed to ensure an adequate food supply for the world population. Knowledge gained and shared at this symposium regarding seasonally frozen soils must be utilized in planning and development of new management systems for agriculture, forestry, and natural resources. This may be our biggest challenge of all.

Future symposia

Knowledge gained from this international symposium will stimulate research within the frozen soil community. New acquaintances made at the symposium will undoubtedly lead to increased cooperation and collaboration across international boundaries. With the escalating awareness of environmental quality, new research results will be forthcoming. Thus, another international symposium should be planned for early in the next century. Perhaps this future symposium would be most beneficial to the international community if held in Russia where interest and research in frozen soil processes is widespread.